The 18th International Symposium on District Heating and Cooling (DHC2023)

Conference Proceedings

HOST 主办单位：

China District Heating Association (CDHA)

中国城镇供热协会

CO-ORGANIZER 协办单位：

Tsinghua University Building Energy Research Center (THUBERC)

清华大学建筑节能研究中心

SPONSOR 支持单位

Tangshan Xingbang Pipeline Engineering Equipment Co., Ltd.

唐山兴邦管道工程设备有限公司

Huntsman Polyurethanes Shanghai Ltd.

上海亨斯迈聚氨酯有限公司

REVOHEAT (Tianjin) New Energy Technology Co., Ltd.

乐沃（天津）新能源技术有限公司

SHANDONG LCARBO ENERGY TECHNOLOGY CO., LTD.

山东琅卡博能源科技股份有限公司

Danfoss (China) Investment Co.,Ltd.

丹佛斯 (中国) 投资有限公司

Beijing Huayuan Taimeng Energy Saving Equipment Co., Ltd.

北京华源泰盟节能设备有限公司

RUNA Smart Equipment Co., Ltd.

瑞纳智能设备股份有限公司

Nanfang Pump Industry Co., Ltd.

南方泵业股份有限公司

Xinxing Cathay International Group Co., Ltd.

新兴铸管股份有限公司

AutoHeat Tech Co.,Ltd

北京圣法瑞特热工科技有限公司

Contents

RES & Waste Heat

Research on urban energy planning using industrial waste heat for district heating: A case study in Tangshan

Ying Kong[a], Xu Luo[a], Jiayang Chen[a], Zhaoyang Liu[a], Jianjun Xia[a*]

[a] *Building Energy Research Center, Tsinghua University, Beijing, 100084, China*

[*] *Corresponding author. xiajianjun@tsinghua.edu.cn*

ABSTRACT

Winter heating demand is growing rapidly in northern China, while existing heat sources based on fossil energy are facing being shut down and the new ones are difficult to get approved as China aims to carbon peaking and neutrality. Under both pressures, there is an urgent need to develop new low-carbon heat sources for district heating (DH) in northern China to replace conventional heating methods and fulfill the new heating demand. In cities with abundant industrial waste heat (IWH) resources, IWH can be used as a kind of high-quality heat source for DH system, optimizing the energy structure of DH system and effectively reducing local coal consumption. Tangshan, Hebei Province is dominated by heavy industry with large scale of high-energy consumption industries such as steel and cement. IWH resources here are abundant, but not fully used. This paper presents a planning scheme to maximize the use of IWH for DH in Tangshan. IWH potentials of 15 districts/counties in Tangshan are compared with their DH demands in 2035 respectively. According to the geographical location and the balance situation between supply and demand, the 15 districts/counties are divided into four heating regions. The IWH is preferentially used to undertake the heating base load, and the heating structure of each region in 2035 is planned. Finally, the consumption of fossil energy is calculated and economic analysis is conducted. The planning scheme results show that the IWH in four heating regions can meet 85%-100% of the heating load and 99%-100% of the heating demand, which has obvious energy saving, carbon reduction, and economic benefits. Therefore, using IWH for DH is a feasible way to achieve low-carbon development of industrial cities.

Keywords: District heating; Industrial waste heat; Low-carbon development; Urban energy planning

1. INTRODUCTION

Recently, the demand for space heating in northern China is growing rapidly. The area of DH has increased from 11 billion m^2 in 2016 to 13.8 billion m^2 in 2020. The heating source structure of DH in northern China is shown in Figure 1 [1], with coal-fired heat source accounting for up to 70% of the total, generating a large amount of pollutants and carbon emissions [2]. Under the background of China's dual-carbon development goal, the DH system in northern China is facing the double pressure of increasing demand and insufficient clean heat source. Replacing traditional coal-fired heat sources with low-carbon and economical heat sources on a large scale is the key to the low-carbon transformation of DH system in China [3].

Clean, low-carbon heating models have received a lot of scholarly attention. Lund et al., proposed the fourth generation of European DH system, which is based on extensive use of cogeneration, recovery and utilization of waste heat resources, and integration of other heat sources such as geothermal and solar energy [4]. D. Connolly redesigned new heating routes for the EU's strategy to achieve the 2050 energy target [5]. Fu Lin et al. proposed a new district heating model suitable for China, in which low-grade waste heat from power plants/factories is fully recovered and utilized [6]-[11]. It can be found that in the low-carbon heating routes in Europe and China, the utilization of waste heat resources is becoming more and more important.

Studies have shown that there are a lot of waste heat resources in the industrial field [12]. To make full use of waste heat resources, it is necessary to estimate the heat scale first, and there have been many studies in this regard [13]- [17]. Johannes Pelda used stoichiometric methods to determine the theoretical potential of IWH in 10 German cities in 2030 and 2050 [13]. Pia Manz estimated the IWH of energy-intensive industries in 28 EU countries based on the spatial matching method [14]. Ao Luo et al. estimated that the recyclable potential of IWH in northern China is about 100 Mtce (2.93EJ) [17]. These IWH are mainly flue gases below 200°C or liquids below 100°C [17], which is an ideal heat source for DH.

At present, there have been relevant studies on the use of IWH for heating [18]- [25]. Jelena Ziemele studied the use of IWH in DH system and calculated the economic rationality of the project [19]-[20]. In practical engineering application, Li Yemao et al. planned to integrate the IWH from two steel mills into the DH system of a county seat, and the economic cost and carbon emissions were significantly reduced compared with traditional heating schemes [21].

The industrial cities in northern China have abundant IWH resources and high coverage of DH network, thus they have adequate advantages in implementing IWH for heating. In Tangshan, for example, the DH area is 194 million m^2 in 2021, and the heating load is 6909MW, with coal cogeneration accounting for 74%. With the transformation of China's energy structure, the scale of coal-fired thermal power will gradually decrease [1]. In this context, Tangshan's heat supply mode, which relies heavily on coal-fired cogeneration, will face challenges. Meanwhile, Tangshan has a large scale of energy-consuming industries. In 2021, the city has produced 131.11 million tons of crude steel, 18.5 million tons of coke and 31.41 million tons of cement. These industrial products are accompanied by a large amount of IWH release in the production process. The use of IWH for heating may be an important way to solve the problem of low carbon heating in Tangshan in the future.

In this study, Tangshan City, which is rich in steel IWH resources, was used as the subject, and the plan to maximize the use of IWH for DH in 2035 was proposed. This study estimated the environmental and economic benefits of the planning options, thus proving the feasibility of IWH as the main heat source for DH.

The specific research framework was shown in Figure 2. Firstly, based on the development trend of population and heating in Tangshan, the heating demand in 2035 was predicted. Then, we conducted field research on the IWH resources in Tangshan's key industrial plants, then the IWH resources were matched with the heating demand. The surplus area of IWH resources is integrated with the shortage area, and this study divided Tangshan into different heat supply zones. The IWH industrial plants in each heat supply zone are screened according to certain standards to determine the plants that actually undertake waste heat supply. Finally, the scale of waste heat supply and peak load of each zone are determined, so as to obtain the heat source structure and fossil energy consumption of each heat supply zone.

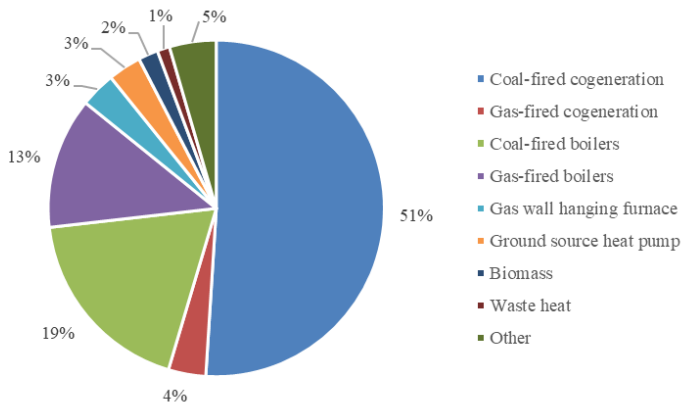

Figure 1. The heating source structure of DH in northern China (2020)

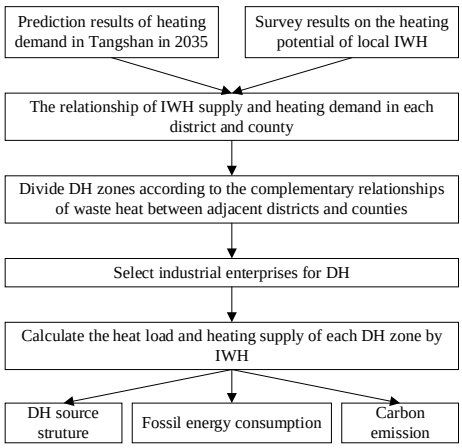

Figure 2. Research framework

2. METHODOLOGY

2.1. Forecasting methods for heating demand

This study used the index method to forecast the heat load and heat demand of each district and county in 2035.

Heating load is calculated according to Formula (1):

$$Q_h = q_h \times \bar{A} \times P \times 10^{-3} \tag{1}$$

Where Q_h is the heating load (kW), q_h is the heating index of unit building area (W/m^2), $\bar{A}$ is the per capita building area (m^2/person), and P is the population. The $\bar{A}$ and P of each district/county in Tangshan in 2035 are based on the research results [26], and $\bar{A}$ is 50 m^2/person. Considering the increase of the proportion of new buildings in the future, the improvement of the energy-saving characteristics of the building envelope and the improvement of the operation and management level of the heating system, the q_h in 2035 is set at 29W/m^2 in this study.

After the Q_h is obtained, the daily average temperature parameters of the local heating season should be combined to calculate the heat demand during the whole heating season, as shown in Formula (2).

$$Q_h^a = Q_h \times \sum_d \frac{t_d - t_i}{t_o - t_i} \times \frac{3600 \times 24}{10^9} \tag{2}$$

Where Q_h^a is the annual heat demand (GJ), d is the number of heating days, t_d is the average daily outdoor temperature (℃), t_i is the designed room temperature for heating (℃), t_o is the outdoor temperature on the coldest day.

Then, the results of Q_h and Q_h^a of each district and county in Tangshan are obtained, as shown in Table 1.

Table 1. Forecast results of heating load and heat demand of each district and county in Tangshan in 2035

District / County	Heating Load (MW)	Heat Demand (million GJ)	District / County	Heating Load (MW)	Heat Demand (million GJ)
Central Downtown	3122	26.53	Qian'an	915	7.78
Guye	446	3.79	Luanzhou	232	1.97
Fengrun	481	4.09	Zunhua	435	3.7
Fengnan	478	4.06	Qianxi	197	1.68
Haigang	98	0.83	Yutian	290	2.47
Caofeidian	669	5.69	Laoting	174	1.48
Lutai	117	0.99	Luannan	212	1.8
Hangu	124	1.05	**Sum**	**7990**	**67.91**

2.2 Investigation of industrial waste heat potential

To find out the potential IWH resources in Tangshan, this study investigated and analyzed 41 industrial plants through field investigation and questionnaire survey, including 20 steel mills, 11 cement factories, 5 chemical plants and 5 other light industry plants. It basically covers all districts and counties of Tangshan and most plants with IWH. The distribution of plants is shown in Figure 3.

The results show that there are four main types of media carrying IWH in these plants: flue gas, exhaust air, steam, and circulating cooling water. The conditions for calculating the theoretical waste heat potential are shown in Table 2, and the theoretical IWH potential of these industrial plants can be calculated by combining the research data of temperature and flow of these media. Through calculation, the total theoretical IWH potential of the surveyed industrial plants is 10226 MW, and the available heat supply in the heating season is 120 million GJ. The IWH potential of different industrial sectors is shown in Table 3. It can be found that the IWH potential of Tangshan is nearly 1.5 times of the current heat demand, which can provide enough low-carbon heat source for Tangshan.

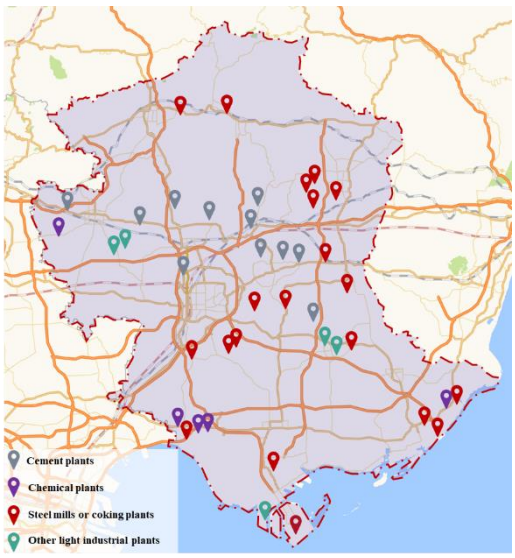

Figure 3. Location map of the IWH plants

Table 2. Conditions for calculating the theoretical waste heat potential

Flue gas	Lower limit temperature after heat extraction is set to 80℃
Exhaust air	Lower limit temperature after heat extraction is set to 60℃
circulating cooling water	The actual difference temperature between supply and return water
Exhaust steam	Latent heat released by isothermal condensation

Table 3. Theoretical waste heat potential of enterprises in different industries

Industries	The theoretical waste heat potential (MW)	Available heat in heating season (million GJ)
Cement plant	435	5.1
Steel or coking plant	8401	99.1
Chemical plant	1133	13.4
Other light industries	257	3.0
Sum	**10226**	**120.6**

2.3 Supply and demand matching and heating zoning

Although the total IWH potential in Tangshan is much greater than the heat demand, the geographical distribution of industrial enterprises is not uniform, so it is necessary to analyze the balances of heat supply and demand of heat by regions. By comparing the heating load and IWH potential of each district and county, as shown in Figure 4, it can be seen that IWH is lacking in the main urban area, Guye, Fengrun, Lutai, Hangu, Yutian, Luannan and Laoting, where IWH needs to be imported from outside regions.

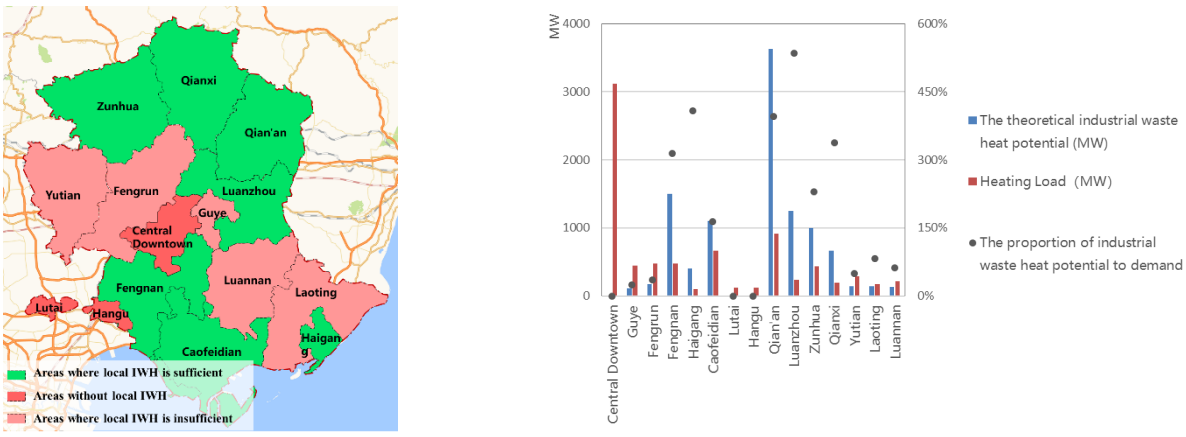

Figure 4. Matching IWH supply and heat demand by districts or counties in Tangshan

Comprehensively considering the IWH supply and demand matching situation and geographical location of each district and county, Tangshan is divided into 4 DH zones ——I, II, III and IV. In these zones, the surplus districts or counties can provide supplementary IWH to the neighboring districts or counties with insufficient IWH, so as to maximize the proportion of IWH supply in each heat supply zone. Based on the load demand of each zone, IWH resource and environmental protection grade of each industrial plant, 41 industrial plants were screened, and finally this study determined 17 plants as the main heat source for each zone. The specific zoning scheme and the distribution of selected heat supply plants are shown in Figure 5.

Figure 6 shows the matching between heating load and IWH supply in each heating zone. The heat supply of IWH in each zone can be basically realized by cross-regional combined heat supply.

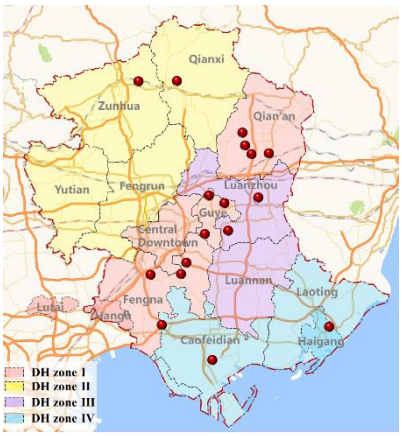

Figure 5. DH zones and selected heat supply plants distribution

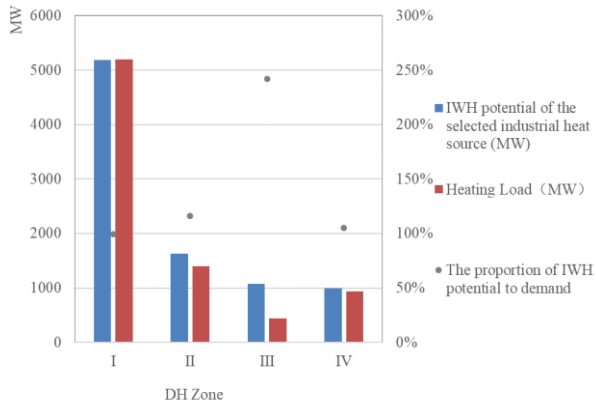

Figure 6. Heat supply and demand matching of each DH zone

3. RESULTS

According to the heating load prediction results and the IWH sources in each DH zone, the specific heating scheme is formulated for the 4 zones, and economic and environmental benefit analyses are conducted.

3.1 Planning heating scheme

As shown in Figure 7, the maps of DH network are planned for each DH zone. By building cross-regional pipeline networks with multi-heat sources cogeneration, it is achieved that heat demand of each district and county in Tangshan can be satisfied by industrial low-grade waste heat as much as possible, then the whole city's low-carbon heating transformation would be realized.

In the specific scheme, IWH is set to bear the base heating load preferentially, and if IWH power is insufficient in extreme cold period, the local CPH will be used for peaking. The heating load and heat supply by the selected industrial plants are listed in Table 4, and the corresponding structures are shown in Figure 8 and Figure 9.

In DH zone I, the IWH resources of Fengnan and Qian'an are extremely abundant, and other districts and counties are insufficient. It is planned that one of the selected industrial plants in Qian'an bear all heat demand of this county, and the IWH of other three local selected enterprises is transported to the central downtown, Guye, Fengnan, Lutai and Hangu through the long-distance pipeline network, and heat these areas jointly with the other selected enterprises. Under this scheme, industrial heating enterprises shares the zone's 85% of heating load and 99% of heat supply. The heat supply of IWH is 43.6 million GJ in the whole heating season, and the local CHP only supple 0.6 million GJ heat during the extreme cold period.

A total of 27.9 million GJ of low-grade waste heat is recovered throughout the heating season, with consuming 15.7 million GJ extracted steam of internal generator sets (decreasing power generation by 872.1 million kWh) and using 5.1 million kWh (equal to 18.5 thousand GJ) electricity due to electric heat pump, thus the comprehensive heating COP of waste heat recovery is 13.8. Therefore, the heating efficiency of IWH is much higher than that of conventional CHP and electric heat pumps.

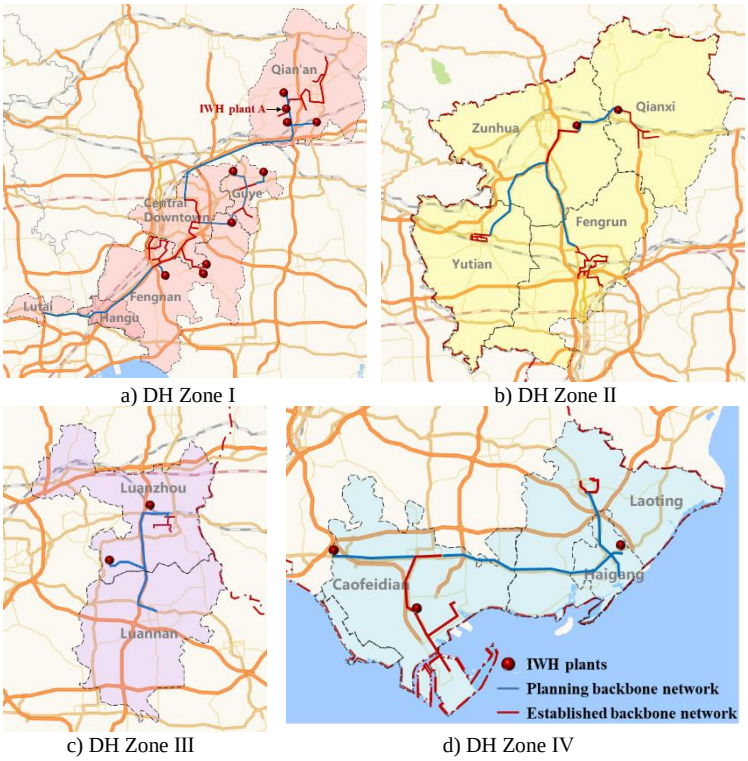

a) DH Zone I b) DH Zone II

c) DH Zone III d) DH Zone IV

Figure 7. Heating network planning maps of four DH zones

Table 4. The heating load and heat supply of different heat sources in each DH zone in the planning scheme

DH Zone	Industrial waste heat recovery and heating system			Heating by CHP
	Low grade industrial waste heat	Generator set extraction steam for low grade waste heat recovery	Electricity consumption for low grade waste heat recovery	
Heating load (Unit: MW)				
Ⅰ	2613.4	1822.9	9.8	754.6
Ⅱ	833.9	569.8	0.0	0.0
Ⅲ	283.5	160.6	0.0	0.0
Ⅳ	441.7	383.9	0.0	116.3
Sum	4172.4	2937.3	9.8	870.9
Heat supply (Unit: million GJ)				
Ⅰ	27.9	15.7	0.02	0.6
Ⅱ	8.2	3.7	0.0	0.0
Ⅲ	2.8	0.9	0.0	0.0
Ⅳ	4.6	3.4	0.0	0.1
Sum	43.6	23.7	0.02	0.6

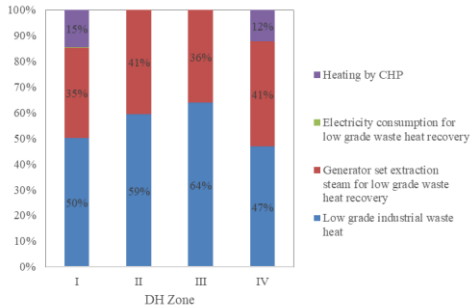

Figure 8. Heating load structure of 4 DH zones

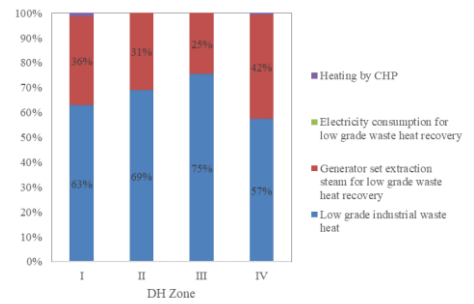

Figure 9. Heat supple structure of 4 DH zones

In DH zone II, heat demand of the whole zone is supplied by IWH of two industrial enterprises in Zunhua and Qian'an. The total heat supply from IWH is 11.9 million GJ, of which 8.2 million GJ is from recovered low-grade waste heat and 3.7 million GJ is given through consuming internal generator sets extracted steam.

Similarly, DH zone III also achieves 100% IWH heating. However, because the IWH in DH zone IV has a high percentage of low-temperature waste heat, which cannot be fully recovered, the industrial plants cannot meet the full heat demand, and requires a local CHP to supplement 12% of the heating load.

Overall, in this IWH heating scheme, the waste heat recovery and heating system will take up 89% of the total heating load (7990MW) and 99% of the total heat demand (67.9 million GJ) in 2035 in Tangshan, with recovering a total of 43.6 million GJ of low-grade waste heat and achieving a comprehensive heating COP 14.1.

3.2 Economic analysis

Comprehensive heating cost includes heat source side heating cost and heat network transmission cost, and includes equipment depreciation cost and operation cost respectively. The result of economic analysis of planning scheme is shown in Table 5.

On the heat source side, the investment includes heat exchanger (0.05 yuan /W), absorption heat exchanger (0.5 yuan /W) and electric heat pump (0.3 yuan /W), and the operation cost is mainly the energy consumption cost, that is, the direct electricity consumption of the electric heat pump and the power loss of the generator set caused by the pumping steam of the generator set in the plant.

On the heat network transmission side, the investment is the construction costs of the pipe network from IWH plants to the urban primary network. The unit investment of DN800, DN1000, DN1200 and DN1400 is 7 million, 9 million, 12 million and 15 million yuan/km respectively, and the investment in pumps and relay pumping stations is taken as 1.2 yuan/W. The operating cost is mainly the electricity consumption of water pump.

The investment in equipment is depreciated over 15 years in this study, and the economic analysis of this scheme is shown in Table 6. The total initial investment is 6.55 billion yuan, of which 2.52 billion yuan is invested in heat-source equipment and 4.02 billion yuan is invested in pipe network. The average heating cost of the heat source side is 13.4 yuan/GJ, which has better economic benefits compared with the general heat source selling price of 29.6 yuan/GJ in Tangshan. The scheme's average comprehensive heating cost is 19.4 yuan /GJ, and the unit area heating cost is 4.85 yuan/m^2 (heat demand per unit area is 0.25GJ/m^2), which has a better cost advantage compared with the current heating price 20 yuan/m^2.

Table 5. Economic analysis of planning scheme

DH Zone	**Heat source side**				**Network**			**Comprehensive heating costs (yuan/GJ)**
	Heat supply of IWH (million GJ)	Initial investment (million yuan)	Operating cost (million yuan / a)	Heating costs of heat source side (yuan / GJ)	Planning backbone network investment (million yuan)	Operating costs of network (million yuan / a)	Heating costs of network side (yuan / GJ)	
Ⅰ	43.6	1593.9	456.7	12.9	2322.4	110.7	6.1	19.0
Ⅱ	11.9	499.6	116.7	12.6	719.8	10.6	4.9	17.5
Ⅲ	3.8	138.9	32.5	11.1	316.0	4.0	6.6	17.7
Ⅳ	8.0	291.6	125.4	18.2	666.3	9.7	6.8	25.0
Sum / Average	67.3	2524.0	731.3	13.4	4024.6	135.0	6.0	19.4

3.3 Scheme comparison

The waste heat heating scheme is compared with the traditional heating scheme. As shown in Table 6, two comparison schemes are set. On the basis of giving priority to existing heat sources such as coal-fired cogeneration, gas-fired boilers and other heat sources (including all kinds of electric heat pumps, biomass boilers and biomass cogeneration), the heat supply gap in 2035 is solved by gas-fired boilers in comparison scheme 1. In contrast, scheme 2 is assumed by air source heat pump (COP 3).

The three schemes are compared in terms of operation energy consumption, heating cost and carbon emission. The results are shown in Table 7.

In terms of operational energy consumption and carbon emission, due to huge heating capacity of IWH, the planning scheme can replace most coal-fired CHPs and gas boilers, and reduce a large amount of fossil energy consumption (more than 800 thousand tce per year) and decrease CO_2 emission by 2.4 million tons per year compared with the comparison solution. In addition, the national average coal consumption factors and the national carbon emission factor for power generation in 2019 are 300 gce / kWh and 600 gCO_2 / kWh, respectively. However, as the proportion of renewable power in the overall power generation structure in China continuously rising, the two factor values will also fall, thus the advantages of the IWH heating scheme and comparison scheme 2 with electricity consumption will be further expanded. In the long run, gas-fired boilers for heating are not worth widespread promotion and construction. From the viewpoint of heat supply cost on the heat source side, although the IWH heating scheme requires a large amount of new IWH recovery equipment and initial investment is higher, the annual operation cost is much lower than the two comparison schemes, thus the heat supply cost is pulled down,

which is only less than 50% compared with comparison schemes. As a result, IWH enterprises involved in DH can be provided a better economic profit space.

Table 6. Compare the heating load undertaken by various heat sources in the scheme (unit: MW)

The type of heat source	IWH heating scheme	Comparison Scheme 1	Comparison Scheme 2
IWH	7127	-	-
Coal-fired CHP	863	6626	6626
Gas-fired boilers	-	1219	223
Air source heat pumps	-	-	996
Other	-	145	145

Table 7. Comparison results

Comparison Items		IWH heating scheme	Comparison Scheme 1	Comparison Scheme 2
Energy consumption	Coal（thousand tce)	11	946	946
	Natural gas (million Nm^3)	-	279.8	51.2
	Electricity（million kWh)	1405.7	-	784.1
	Sum（thousand tce)	432	1318	1249
Heat source side	Initial investment of new equipment（million yuan)	2524.0	59.8	298.9
	Operating cost (million yuan / a)	746.5	2275.9	1906.7
	Heating costs of heat source side (yuan / GJ)	13.4	33.6	28.4
CO_2 emissions（thousand tCO_2)		865	3282	3254

4. DISCUSSION AND CONCLUSION

The feasibility of this scheme is mainly determined by the survival status of the waste heat supply plants by 2035 and the technical feasibility involved in the scheme. The stability of survival of IWH plants has been fully considered in this scheme. The possibility of future survival of plants is investigated from the aspects of plants waste heat scale, plants environmental protection grade and so on. Large-scale plants have stronger anti-risk ability to the market, and plants with high environmental protection grade are not easy to be restricted by environmental protection policies. In addition, Tangshan has started the optimization and integration of steel enterprises around the main urban area and the removal of steel enterprises from the urban since 2019. At present, steel mills in the main urban area of Tangshan have basically moved out, and there is no possibility of large-scale relocation again. For other areas, plants with relocation plans have been avoided in this scheme. The local cogeneration unit can be used as the backup heat source in case of unforeseeable production reduction risk in the long run. In terms of technical feasibility, it mainly involves low-grade waste heat recovery technology and long-distance pipeline heating technology. These technologies have been relatively mature at present, and there are also application cases.

This study explored the feasibility of maximizing the use of IWH resources to meet the urban heating demand in the industrial cities of northern China in the future, to achieve the goal of low-carbon heating.

The final planning scheme shows that two of the four heating zones can meet all their heating needs entirely from IWH, while the remaining two zones only require very small amounts of heat from combined power plants to supplement the heating gap during extreme cold periods. In general, the IWH recovery system can bear 89% of the heating load and 99% of the heat demand in Tangshan, and 43.57 million GJ of low-grade waste heat can be recovered in the whole heating season, and the COP of comprehensive heating can reach 14.1. The proposed solution will reduce fossil energy consumption by at least 800 thousand tce and CO_2 emissions by 2.4 million tons, compared with conventional solutions using gas-fired boilers and air source heat pumps to meet increased heating demand.

In addition, the planning scheme is economically sound. The initial investment of the whole scheme is 6.55 billion yuan. According to the depreciation life of 15 years, the average heating cost of the heat source side is 13.4 yuan/GJ, which has better economic benefits compared with the current heat source selling price of 29.6 yuan/GJ in Tangshan.

IWH heating scheme

ACKNOWLEDGEMENT

This work was supported by the 14th Five-Year National Key R&D Plan of China (Grant No. 2022YFC3802401) and Ministry of Housing and Urban-Rural Development R&D Project of China (Grant No. K20220771).

REFERENCES

[1] Building Energy Conservation Research Center. Annual report on China building energy efficiency 2023 [M]. Beijing, China: Architecture and Building Press; 2023.

[2] Chen J , Shan M, Xia J, et al. Effects of space heating on the pollutant emission intensities in "2+26" cities[J]. Building and Environment 2020;175:106817.

[3] Lin W, Xu X, Ge B, Liu X. Gaseous pollutants in Beijing urban area during the heating period 2007-2008: variability, sources, meteorological, and chemical impacts [J]. Atmos Chem Phys 2011;11(15):8157-70.

[4] Lund H, Werner S, Wiltshire R, Svendsen S, Thorsen J, Hvelplund F, Mathiesen B. 4th Generation District Heating (4GDH) Integrating smart thermal grids into future sustainable energy systems [J]. Energy 2014;68:1e11.

[5] Connolly D, Lund H, Mathiesen B V, et al. Heat Roadmap Europe: Combining district heating with heat savings to decarbonise the EU energy system[J].Energy Policy, 2014, 65(feb.):475-489.

[6] Sun Jian, Fu Lin, Zhang Shigang. Experimental study of heat exchanger basing on absorption cycle for CHP system [J]. Appl Therm Eng 2016;102:1280-6.

[7] Li Wentao, Zhao Jingquan, Fu Lin, et al. Energy efficiency analysis of condensed waste heat recovery ways in cogeneration plant [J]. Energy Convers Manag 2015;101:616-25.

[8] Zhao Xiling, Fu Lin, Wang Xiaoyin, Sun Tao, et al. Flue gas recovery system for natural gas combined heat and power plant with distributed peak-shaving heat pumps [J]. Appl Therm Eng 2017;111:599-607.

[9] Wei Maolin, Zhao Xiling, Fu Lin, Zhang Shigang. Performance study and application of new coal-fired boiler flue gas heat recovery system [J]. Appl Energy 2017;188:121-9.

[10] Wu Y, Fu L, Zhang S, et al. Study on a novel co-operated heat and power system for improving energy efficiency and flexibility of cogeneration plants [J]. Appl Therm Eng 2019;163:114429.

[11] Fu L , Li Y , Wu Y ,et al. Low Carbon District Heating in China in 2025- a District Heating Mode with Low Grade Waste Heat as Heat Source[J].Energy 2021;230(2):120765.

[12] Jouhara H, Olabi A.G. Editorial: industrial waste heat recovery[J]. Energy,2018,160:1-2.

[13] Pelda J, Stelter F, Holler S. Potential of integrating industrial waste heat and solar thermal energy into district heating networks in Germany [J]. Energy 2020;203:117812.

[14] Manz P, Kermeli K, Persson U, et al. Decarbonizing District Heating in EU-27 + UK: How Much Excess Heat Is Available from Industrial Sites?[J].Sustainability 2021;13(3):1439.

[15] Nielsen S, Hansen K, Lund R, Moreno D. Unconventional excess heat sources for district heating in a national energy system context [J]. Energies 2020;13(19):5068.

[16] Brueckner S, Miro L, Cabeza L F, et al. Methods to estimate the industrial waste heat potential of regions – A categorization and literature review[J]. Renewable & Sustainable Energy Reviews 2014;38(oct.):164-171.

[17] Luo A , Fang H , Xia J ,et al.Mapping potentials of low-grade industrial waste heat in Northern China[J].Resources Conservation and Recycling 2017;125:335-348.

[18] Fang Hao, Li Yemao, Xia Jianjun, Zhao Haifeng.Key issues and solutions of low-grade industrial waste heat applied to urban centralized heating systems[J]. Heating Ventilating & Air Conditioning 2016;46(12):15-22. (in Chinese)

[19] Drysdale D, Mathiesen B, Lund H. From carbon calculators to energy system Analysis in cities [J]. Energies 2019;12(12):2307.

[20] Ziemele J , Dace E .An analytical framework for assessing the integration of the waste heat into a district heating system: Case of the city of Riga[J].Energy 2022;254:124285.

[21] Jelena, Ziemele, Roberts, et al. Evaluation of the industrial waste heat potential for its recovery and integration into a fourth generation district heating system - ScienceDirect[J]. Energy Procedia 2018;147:315-321.

[22] Li Y, Xia J, Fang H, et al. Case study on industrial surplus heat of steel plants for district heating in Northern China[J]. Energy 2016;102:397-405.

[23] Xia J, Zhu K , Jiang Y .Method for integrating low-grade industrial waste heat into district heating network[J].Building Simulation 2016;9(2): 153-163.

[24] Gao, Junwei, Sun, et al. New low temperature industrial waste heat district heating system based on natural gas fired boilers with absorption heat exchangers[J]. Applied thermal engineering: Design, processes, equipment, economics 2017;125:1437-1445.

[25] Wahlroos, Mikko, Parssinen, et al. Future views on waste heat utilization - Case of data centers in Northern Europe[J].Renewable & sustainable energy reviews 2018;82:1749-1764.

[26] Zheng Wen. Research on clean heating roadmap for Northern Chinese: potentials and regional balances[D].Tsinghua University,2021. (in Chinese)

The 18th International Symposium on District Heating and Cooling, September 3–6, 2023, Beijing, China

WASTE HEAT RECOVERY FROM DATA CENTERS FOR DECARBONIZATION OF HEAT SUPPLY IN DISTRICT HEATING SYSTEMS

Benjamin Ott[a*], Peter Radgen[a]

[a] *University of Stuttgart, Institute of Energy Economics and Rational Energy Use, Stuttgart, 70565, Germany*
[*] *Corresponding author. benjamin.ott@ier.uni-stuttgart.de*

ABSTRACT

Achieving decarbonization goals in heat supply requires the use of suitable defossilized heat sources, such as producers of unavoidable waste heat. Data centers can be a suitable source of waste heat, since they are in continuous operation and can provide a largely constant amount of waste heat throughout the year. In general, the waste heat temperature in traditional air-cooled data centers is around 30 °C, which is mostly dissipated to the environment unused. In order to monetize and utilize this waste heat for integration into a district heating network, the use of heat pumps is required. In order to analyze the technological and economic impact of the different concepts, a mathematical model was created comprising of data center, heat pump, heat path and end consumers.

All components of the value chain are mathematically modelled in Python. In addition, three technology concepts are compared. Temperature upgrading can take place both centrally in the data center and externally in a power house with large heat pumps. In addition, there is the possibility of using a decentralized water-to-water heat pump in combination with a low exergy heat distribution system. Technical parameters as well as the respective economic parameters are determined for the three cases and compared from the perspective of the different business actors (data center, contractor and energy supply company). In addition, an economical comparison is made with a selection of benchmark technologies (gas condensing boiler and individual air-to-water heat pump) for heat supply from an end-user perspective.

Depending on the scenario and technology concept, waste heat recovery from data centers can be an economical alternative to other heat supply concepts; both for the business actors and end users.

Keywords: Data Center, Waste Heat, Decarbonization, Circular economy, Heat Pump

1. INTRODUCTION

More than 55% of the world's population lives in urban areas and, according to an UN estimate, this figure is expected to rise to 68% by 2050 [1]. These areas were responsible for 64% of global primary energy consumption in 2013 [2]. In 2020, 62.8% of the final energy demand of the residential sector was used for heating houses in Europe [3]. Thereby, the share of renewable energy in the space heating sector was 26.8% [3]. Globally, renewables accounted for only 12% in the heating sector in 2021 [4]. In contrast, the share of renewables in the electricity sector was 28% in 2021 [5]. In order to meet the requirements of the Paris Agreement (COP21), their share will have to increase further in the future. The increase in energy prices for fossil fuels is another driving factor for the need to decarbonize and transform the heat supply [6]. Among other things, the commodity price for natural gas in Europe is estimated to increase six-fold from 2020 to 2023 despite a recovery [7]. For this reason, the search for suitable and low-greenhouse gas heat sources is intensifying.

A potentially suitable and so far not extensively used waste heat source are data centres. Data centres are the backbone of digitization and are necessary for a large number of today's digital application. With digital transformation, a high growth rate can be observed in this dynamic sector. Global data centre electricity consumption in 2021 was estimated at 220 to 320 TWh/a, or about 0.9 to 1.3% of the world's total electricity consumption [8–10]. Depending on the scenario, there may be an increase to up to 500 TWh/a by 2030 [11]. This supplied electrical energy is completely converted into heat and usually dissipated unused to the environment. The advantages of supplying waste heat via data centres include the fact that they are often located in metropolitan areas near a large number of potential heat consumers [12]. In addition, due to the high availability requirements of their customers for digital services, they are in continuous operation all year round and can thus reliably and constantly supply heat at an attractive temperature level [12]. Compared to conventional environmental heat sources such as ambient air (winter 2022/2023 in Germany: 2,9 °C) or shallow geothermal energy (all year round 7 – 12 °C), waste heat temperatures of 20 to 35 °C can be achieved in standard air-cooled data centres, which are particularly suitable in combination with heat pumps [12–15]. Using direct water cooling, on the other hand, waste heat temperatures of 50 to

60 °C can be achieved and direct use may be possible. Households, industrial companies or even heating networks can then be potential consumers.

Despite all these advantages, the waste heat is rarely used. There are various reasons for this, such as poor and insufficient communication between the necessary stakeholders, the relatively low temperature level of waste heat (especially compared to industrial waste heat), concerns about dependencies and legal and fiscal disadvantages, and the potentially high investment requirements for the necessary infrastructure [12,15,16]. To counter these prejudices, more transparency and open communication are needed to achieve sustainable business models and requirements [12,17]. In previous economic/technical analyses (for instance [18]), the focus was primarily on the system as a whole, whereby the situation of the individual stakeholders was not considered in detail. This work aims to look at the cost structure for the relevant actors in relation to different scenarios. In addition, the perspective of the end consumers in the form of households will also be considered in comparison to the conventional heating concepts (e.g. gas heating or air-water heat pump).

2. METHODOLOGY

2.1. Technical and organisational structure of a waste heat recovery project

In an air-cooled data centre, air circulates in the server room and is heated as it flows through the servers (see Figure 1, System I.). According to the ASHRAE guidelines, the recommended supply air temperature is in the range of 18 to 27 °C [19]. Typically, the temperature increase is in the range of 10 to 15 K [20]. The heated air is then cooled by a heat exchanger and transfers its heat to the water circuit (e. g. **C**omputer **R**oom **A**ir **H**andler (CRAH) or **R**ear **D**oor **H**eat e**X**changer (RDHX)). Then, depending on the cooling strategy, the cooling water is cooled down directly by means of free cooling (see Figure 3, dashed line) via a recooler or by interposing a mechanical chiller (see Figure 3, System II.). Both the circulating air and the chilled (Heat Exchanger A) and chilling water (Heat Exchanger B) can be the source of waste heat extraction. In this study, however, the waste heat is extracted from the water circuit because most of the waste heat is supplied centrally and extraction is easier. In addition, only extraction option A will be considered here, because in this way the load for the mechanical chiller is reduced, resulting in an economic advantage for the data centre. At the same time, however, this reduces the removable waste heat temperature ($t_1 < t_3$), which means that a temperature increase may be necessary depending on the end application.

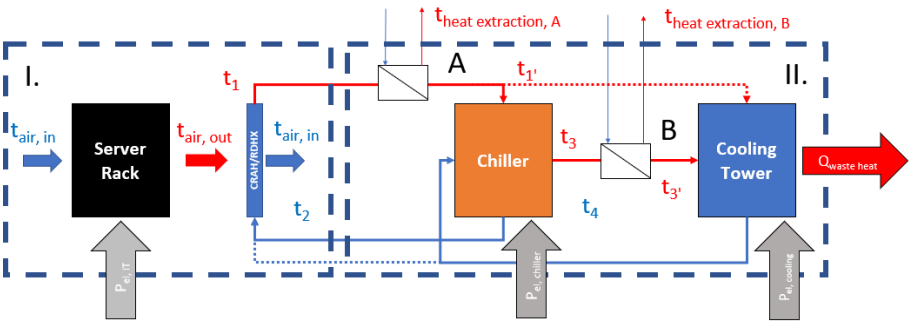

Figure 1. Hydraulic design of the data centre with regard to the cooling system and waste heat extraction (based on [16])

Many possibilities are conceivable with regard to the heat consumer and the hydraulic connection. In the case of heat distribution via a heating network and the integration of a heat pump to raise the temperature, three different scenarios are conceivable (see Figure 2). Waste heat upgrading can take place centrally both in the data centre (*Opt. 1*) and in an energy station (*Opt. 2*). In the second case, there is a cold network section, which should reduce investment costs and heat losses. The same applies to the decentralised variant (*Opt. 3*), where the heat pump is located at the end user's premises. In general, the waste heat can be utilised with open or closed local heating networks or by feeding it into a district heating network. In the case of the stand-alone solution, a backup for the heat supply must be kept available. This figure also shows all the necessary main components that are modelled in the calculation model. The relevant technical modules are the data centre, the heat exchangers, the heat pump(s), the energy centre, the heating network and the district heating transfer station at the end user's premises. All these components interact and influence each other. If, for example, the waste heat temperature is increased by modifying the cooling system, the required temperature lift over the heat pump is reduced and it achieves a more energy-efficient COP.

A waste heat recovery project with a data centre as the waste heat source will rarely be implemented and operated by one stakeholder. Often, in addition to the data centre operator, an energy supplier and/or contractor could be involved who is responsible for heat upgrading and distribution. As a result, ownership and responsibility for the technologies may differ depending on the project. Typically, the data centre's area of responsibility ends at the heat exchanger for waste heat

extraction and from there an energy supplier is responsible. This can result in an uneven distribution of financial and technological expenditure. In addition, the end user influences the technical concept with its requirements (e. g. temperature etc.) for heat supply. Since the heat sink here is to be private households, the temperature and performance requirements are largely influenced by the building age class, the type of house and the living space.

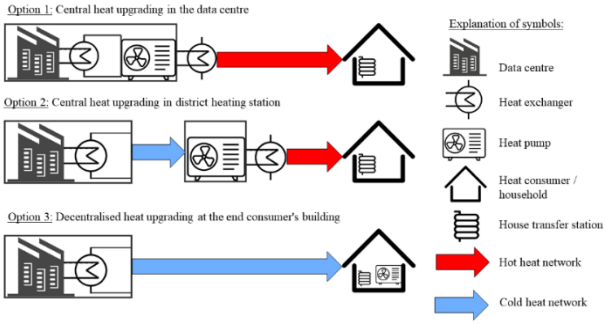

Figure 2. Options for placing the heat pump and type of heating network (based on [21])

2.2. Calculation basis for the economic evaluation of a waste heat recovery project

All relevant technologies and actors listed above are transferred into an object-oriented model in Python. The overall structure of all modules is shown in Figure 3. The main components are the data center (see Figure 1), the heat network, the heat pump, the heat exchangers and the households as end users. In addition, one module calculates the energy prices for electric power and natural gas, which are relevant for the calculation of heat prices and the comparative calculation at the household level.

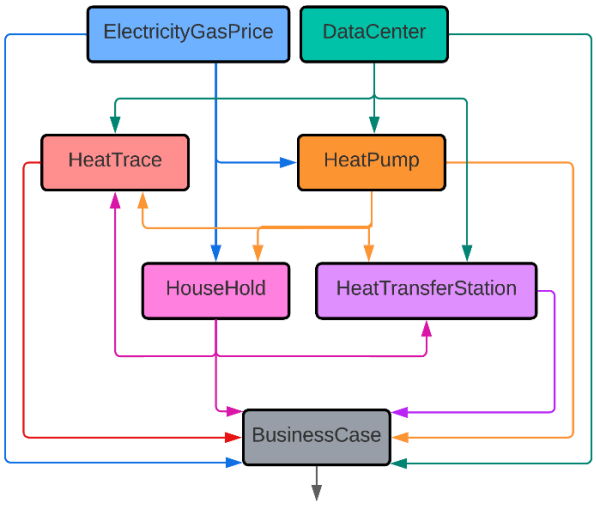

Figure 3. Module structure and connections of the calculation model (Python) (based on [21])

The module "*ElectricityGasPrice*" contains data sets for energy prices (electric power and natural gas) for different types of consumers (industrial, commercial, household, etc.), the development of which can be extrapolated for the future [22–24]. In addition, CO_2 prices are added based on the targets of the German Emissions Trading Authority of the Federal Environment Agency, with a target corridor of between 55 and 65 $€/t_{CO_2}$ applying from 2026 onwards [25]. For this reason, the developments of the specific CO_2 emission factors are included in addition to the energy prices. While the emission factor for natural gas remains constant, it approaches zero for electricity by 2050, in line with the decarbonisation target.

The "*DataCenter*" module contains the mathematical model of the cooling system of a data centre (see Figure 1). In the first step, the waste heat output is calculated on the basis of information on the theoretical IT power, the utilisation and the proportion of usable waste heat. Since the load is usually almost constant throughout the year and only fluctuates slightly, it is assumed that the waste heat power is permanently available. The waste heat temperature recovered is then calculated, which depends on the location of the heat extraction. For this purpose, the respective temperature gradients and the heat absorption capacity of the corresponding components are taken into account. The costs for the cooling system as well as the energetic and economic advantages for the data centre are not considered in detail for reasons of simplification. For example, systems that can achieve a higher waste heat temperature (e. g. RDHX) are more expensive (CapEx) than standard solutions (e. g. CRAH).

The module "*HeatPump*" calculates the investment, operating and maintenance costs and the upgraded heat. The size, position and number of heat pumps are determined depending on the application scenario (see Figure 2). For the central application case, the COP map of the *Viessmann VITOCAL 350-HT PRO* is available [26]. In contrast, there is currently no commercial water-to-water heat pump for domestic customers, which is why the COP map was only calculated theoretically with a correction factor. The energy costs result from the COP map and the energy prices.

The "*HeatTransferStation*" module provides the investment and maintenance costs of the heat exchanger (HX) within the data centre, the district heating station and the house transfer station.

Table 1. Overview of a selection of technical and economic assumptions

	Technical Assumptions		Economic Assumptions
Data centre (DC)	IT power = 5 MW	**Data centre (DC)**	Calculatory interest rate = 5 %
	Load DC = 80 % (30 % usable waste heat)		Depreciation time (only HX) = 15 a
	Air cooled DC $t_{server,out} = 33\ °C$		Annual interest rate for loans = 1 %
	Extraction duration = 2000 h/a		Repayment period = 15 a
Heating network	Network length = 1 km		Debt ratio = 80 %
	Share of cold network (option 2) = 10 %		Return factor (only HX) = 1 %
	Laying under a paved surface	**Energy supplier/Contractor**	Calculatory interest rate = 5 %
End consumer	Building type = multi-family house, 1998		Depreciation time (HP) = 15 a Depreciation time (HN) = 25 a
	Required heat for space heating without hot water supply		Annual interest rate for loans = 1 %
	Year of construction 1998 (flow temperature = 55 °C)		Repayment period = 15 a
Heat Pump (HP)	Water/water large HP (central) [26] Heating power = 206,2 kW (26/55 °C; COP = 5,60)		Debt ratio = 80 %
	Water/water large HP (decentral) Heating power = 10 kW (26/55 °C; COP = 5,60)		Return factor = 3 %
	Air/water HP (decentral/individual) Heating power = 6 kW (9,2/55 °C; COP = 3,58) [27]	**End consumer**	Energy price = 120 €/MWh
Gas condensing boiler	Heating power = 11 kW [28]		Base price = 200 €/a
			Service price = 150 €/a
		Subvention	Climate Protection Plus funding programme (German/BW)

The module "*HeatTrace*" is used to design the pipelines of the heating networks (HN) and to determine the usable amount of heat that is supplied to the end user. The configuration is done depending on the selected scenario, because there can be "cold" and "hot" network sections. The required diameter is calculated as a result of a minimization problem with the input variables of the nominal pipe sizes (DN), the associated maximum flow velocity and cross-sectional area as well as the flow and return temperature of the transport medium as well as the power to be transmitted. In addition, the heat losses over the transport route are also calculated. For cold heat networks, barely insulated plastic casing pipes ($\lambda_{cold} = 0.4\ W/(mK)$) are used. The hot heat networks, on the contrary, have thermal insulation ($\lambda_{hot} = 0.03\ W/(mK)$). Moreover, the investment and operating costs are calculated. Here, only underground networks are taken into account in the initial costs, with a differentiation being made between paved (e. g. in cities) and unpaved ground (e. g. green field) [29].

The module "*BusinessCase*" is the main element of the calculation model. This involves the calculation of the profit and cost structures of the stakeholders. First, the ownership of the technologies is divided among the stakeholders. This determines which technology component of the waste heat recovery project is operated by the stakeholder and what are the investment costs. In addition, (German) subsidy amounts can be calculated and credited to the stakeholders, which reduces the necessary investment. Furthermore, the stakeholder-specific heat prices, revenues and profits are calculated to determine the cost and profit structure. In addition to the economic consideration, the ecological ones are also considered by calculating the greenhouse gas emissions.

The last module "*HouseHold*" is used to evaluate the economic and ecological impact and competitiveness of waste heat recovery in comparison with standard heating systems (natural gas heating and air-to-water heat pump) on the basis of end consumers in the form of private households (e. g. single-family house, apartment house etc.). Based on the building type, the building age class, the living space and the provision of space heating and hot water, the heating capacity and the heat demand are calculated. For the modeling of the decentralized heating systems, an existing heating cost comparison calculator is used [30].

2.3. Overview of data sources and assumptions made for the scenarios

In order to determine the specific investment costs and maintenance costs, the technology profiles from [31] were used. In this case, Scenario 1, 2 and 3 are compared, assuming a local district heating network where the backup heating is covered by a district heating network. The associated costs are not considered here. An overview of a selection of the most important parameters for the model calculation are included in Table 1. For energy prices, the heat pump is operated with industrial electricity, while household tariffs for electricity and natural gas are applied. The participants are the data centre, to which only the heat exchanger in the data centre is assigned, a contractor responsible for the heat pump and the energy supplier, to which all components from the heating network to the household connection are assigned. The household in turn owns the household transfer station.

3. RESULTS

Figure 4 shows the annual operating profits of the individual stakeholders over an estimated project duration of 30 years for three different cases. The profit for the data centre does not differ in any of the three cases, as the amount of waste heat extracted is always the same and the temperature does not change. This is another reason why the amortisation periods are the same in all cases and amount to 7 years. The situation is different for the other two stakeholders. The contractor tends to account for the majority of the value added via the temperature upgrade by means of the heat pump. The profit reductions in cases 1 and 3 result from the assumption that a full reinvestment in the heat pump is required at the end of its useful life. When looking at the cost structure of the contractor in Figure 5, it can be seen that in case 2 the total costs barely change. Although a modernisation of the heat pump is also necessary here, this additional burden is compensated by the assumption that the financing and depreciation costs for the building envelope of the energy centre no longer apply, because no new building has to be constructed. The total costs are higher for the contractor in case 3 because the specific costs for the compact decentralised heat pumps are higher than those for the central heat pump. This leads to more than twice the costs of reinvestment compared to the central option. For the contractor, the amortization period of the project in case 1 is around 7 years. This is due to the fact that in this case the heat losses through the hot heat network are the highest and in order to ensure the supply of the end users with the required amount of heat, the heat pump has to increase its heating power. However, the higher energy costs are more than compensated by the heat price.

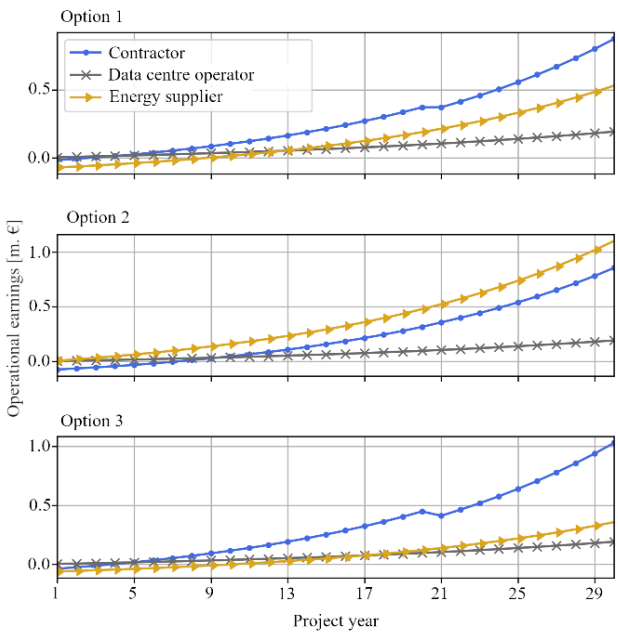

Figure 4. Operational earnings of stakeholders

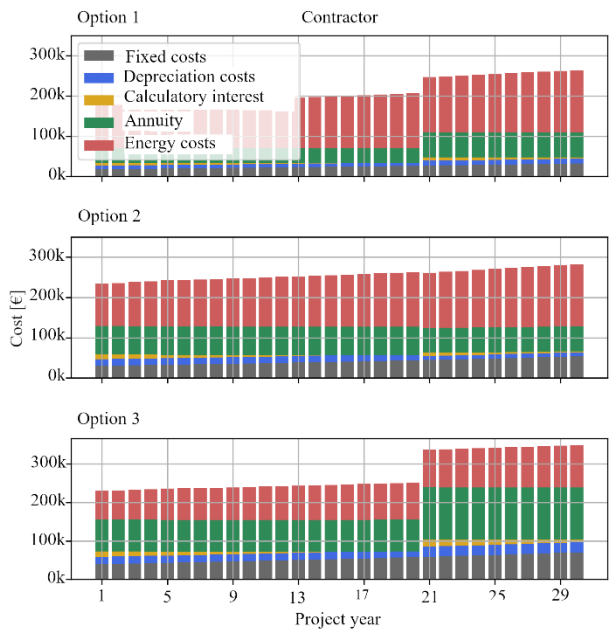

Figure 5. Cost breakdown of the contractor

The energy supplier in turn only operates the heat networks and heat exchangers, assuming that no reinvestment in the installed hardware is required. This leads to the result that the cost structure for the energy supplier is similar in all cases.

However, since in case 3 only low-cost plastic casing pipes are installed without an additional thermal insulation layer, the annual costs are lowest there. However, when considering the gains, this does not have a positive effect, as the total amount of heat transferred is the lowest (1,441 MWh/a). In contrast, 2,966 MWh/a are transported in case 1 and a total of 5,177 MWh/a in case 2 via the two subnetworks. This then also leads to the highest profits at similar heat prices in case 2. This also has a positive effect on amortization, which is achieved after about 6 years. Overall, the largest cost factors are the investment costs for the heat pump and the heating network as well as the energy costs.

Depending on the scenario, there are different financial implications for end users. Figure 6 shows the cumulative total after-tax costs over a 30-year period for an apartment building connected to the heating network, which draws its heat from the data centre. The classic fossil-based district heating supply with standard market conditions and gas heating as well as air-to-water heat pumps are used as comparative technologies. In both case 1 and case 2, waste heat recovery can compete with district heating and gas heating from the perspective of end users. To a certain extent, waste heat recovery benefits from the assumption that fossil energy prices will rise faster than electricity prices and that the effects of rising CO_2 prices can be compensated by a progressive decarbonization of electricity generation.

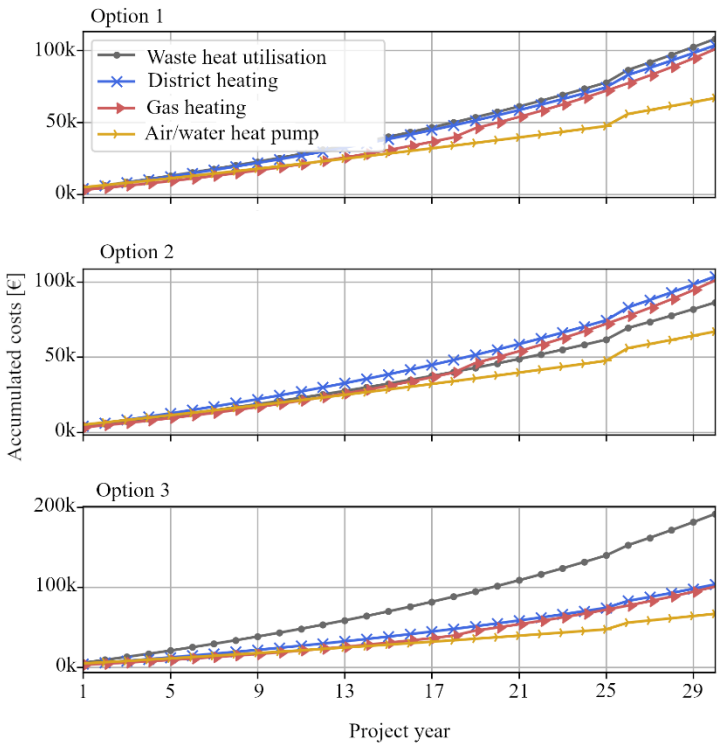

Figure 6. Comparison of the cumulative costs of different heating systems

The significantly higher costs in the case of decentralized upgrading are based on the assumption that a comparable water/water heat pump is about 30% more expensive than an air/water heat pump. These additional costs on the investment side cannot currently be compensated by a theoretically higher COP with lower associated energy costs. In contrast to the economic comparative analysis, the ecological comparison shows significant advantages of waste heat utilization compared to the fossil-based technologies and a slight advantage over the air/water heat pump (see Figure 7). By using waste heat with low greenhouse gas emissions and upgrading it with a relatively small amount of electricity, whose greenhouse gas emissions should decline in the future, a positive contribution to the decarbonization of the heat supply can be made.

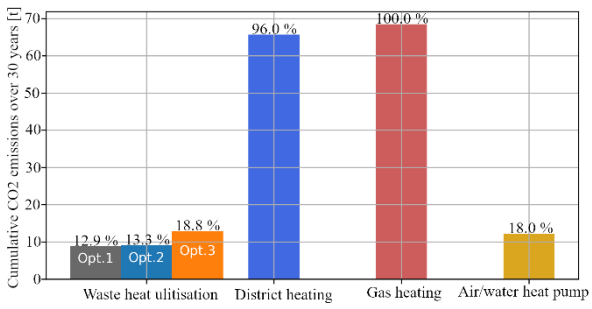

Figure 7. Cumulative CO_2 emissions by end-user heating technology

Compared to the air/water heat pump, it is primarily the heat source and the annual performance factor that have an impact on greenhouse gas emissions. This is because in both cases the same electricity is used with comparable specific emission factors.

4. DISCUSSION

This model is based on a number of assumptions and cannot necessarily be applied to every scenario. For example, underground construction costs can differ significantly depending on the region. This is particularly relevant in regions that do not yet have a well-developed heating network. The results of this model calculation depend to a large extent on further developments in the fields of energy and politics. It is the relation of fossil energy prices to that of renewable electricity that is of greatest importance. At this point, there are currently large uncertainties with regard to future developments and an accurate forecast is not feasible. However, a large number of steps are necessary to achieve the climate targets set out in the agreements. In order to achieve progress in terms of greenhouse gas emission savings in the heating sector, which has been less decarbonized to date, an increase in the overall economic energy efficiency can be achieved via sector coupling. In particular, waste heat from the increasing number of data centres worldwide can be utilised for this purpose.

The calculated cases are mainly applicable to regions that have a modern building stock with a high energy standard and tend to have low grid temperatures. As soon as it comes to supplying heat to older, uninsulated buildings, waste heat utilisation quickly reaches its limits due to the increased electricity demand for upgrading to higher temperatures.

5. CONCLUSION

Within the framework of this modelling study, it could be shown that, depending on the scenario, the use of waste heat from data centres can make sense both economically and ecologically for the stakeholders involved as well as for the end consumers. Depending on further developments, especially on the energy markets and in the field of power generation and heat distribution as well as the political framework conditions, the conditions for waste heat utilization can be influenced both positively and negatively. The great advantage of this method is that it makes the cost structure transparent for all stakeholders and shows the relevant levers for optimising economic efficiency and environmental compatibility. It can be used for an initial economic assessment of potential waste heat utilisation projects.

ACKNOWLEDGEMENT

This work was carried out as part of the research project "Bytes2Heat" and was financially supported by the German Federal Ministry for Economic Affairs and Climate Action. Many thanks in particular to Mr. Phillip Riegger, who actively supported the implementation as part of his student research work at the Institute of Energy Economics and Rational Energy Use, University of Stuttgart.

REFERENCES

[1] United Nations, 68% of the world population projected to live in urban areas by 2050, says UN. https://www.un.org/en/desa/68-world-population-projected-live-urban-areas-2050-says-un (accessed 31 May 2023).

[2] International Energy Agency, Cities are at the frontline of the energy transition, 2016. https://www.iea.org/news/cities-are-at-the-frontline-of-the-energy-transition (accessed 31 May 2023).

[3] Eurostat Statistics Explained, Energy consumption in households, 2022. https://ec.europa.eu/eurostat/statistics-explained/index.php?title=Energy_consumption_in_households (accessed 31 May 2023).

[4] International Energy Agency, Renewable heat, in: Renewables 2022, Paris, 2022.

[5] International Energy Agency, Renewable electricity, in: Renewables 2022, Paris, 2022.

[6] Statistisches Bundesamt, Daten zur Energiepreisentwicklung - Lange Reihen bis Januar 2023, Wiesbaden, 2023.

[7] World Bank Group, Commodity Markets Outlook: Lower Prices, Little Relief, Washington, DC, 2023.

[8] International Energy Agency, Data Centres and Data Transmission Networks, 2022. https://www.iea.org/reports/data-centres-and-data-transmission-networks (accessed 31 May 2023).

[9] E. Masanet, A. Shehabi, N. Lei, S. Smith, J. Koomey, Recalibrating global data center energy-use estimates, 2020.

[10] R. Hintemann, S. Hinterholzer, Data center boom in Germany continues: Cloud computing drives the growth of the data center industry and its energy consumption, 2022.

[11] D. Turek, P. Radgen, Drivers for future data centre demand – historical trends and prospects for 2030: Final Report,

Stuttgart, 2021.

[12] B. Ott, M. Weber, M. Bornholdt, P. Radgen, Mit Bits und Bytes gegen die Gaskrise. Wärmewende cool meistern, e|m|w (2022).

[13] Deutscher Wetterdienst, Deutschlandwetter im Winter 2022/2023, 2023. https://www.dwd.de/DE/presse/pressemitteilungen/DE/2023/20230227_deutschlandwetter_winter22-23_news.html (accessed 31 May 2023).

[14] Bayerisches Landesamt für Umwelt, Oberflächennahe Geothermie, Augsburg, 2013.

[15] B. Ott, M. Weber, P. Radgen, C. Noll, C. Scherz, T. Pauthner, Mit Bytes2Heat die Wärmewende vorantreiben, in: Datacenter Insider (Ed.), Nachhaltigkeit im Rechenzentrum, Augsburg, 2021, pp. 28–32.

[16] B. Ott, M. Weber, P. Radgen, Wie Abwärme aus Rechenzentren die Wärmewende in Deutschland voranbringen kann, in: 17. Symposium Energieinnovation, Graz, Graz, 2022, pp. 1–13.

[17] M. Uddin, R. Alsaqour, A. Shah, T. Saba, Power Usage Effectiveness Metrics to Measure Efficiency and Performance of Data Centers, in: Applied Mathematics & Information Sciences, 2014, pp. 2207–2216.

[18] M. Pärssinen, M. Wahlroos, J. Manner, S. Syri, Waste heat from data centers: An investment analysis, Sustainable Cities and Society 44 (2019) 428–444. https://doi.org/10.1016/j.scs.2018.10.023.

[19] ASHRAE, 2021 Equipment Thermal Guidelines for Data Processing Environments: ASHRAE TC 9.9 Reference Card.

[20] K. Ebrahimi, G.F. Jones, A.S. Fleischer, A review of data center cooling technology, operating conditions and the corresponding low-grade waste heat recovery opportunities, Renewable and Sustainable Energy Reviews 31 (2014) 622–638. https://doi.org/10.1016/j.rser.2013.12.007.

[21] P. Riegger, Technoökonomische Analyse der Abwärmenutzung aus Rechenzentren. Forschungsarbeit, Stuttgart, 2023.

[22] Bundesnetzagentur, Strompreise für Gewerbe- und Industriekunden in Deutschland in den Jahren 2012 bis 2022, 2023. https://de.statista.com/statistik/daten/studie/154902/umfrage/strompreise-fuer-industrie-und-gewerbe-seit-2006/ (accessed 9 June 2023).

[23] Bundesnetzagentur, Strompreise für Haushaltskunden in Deutschland in den Jahren 2012 bis 2022, 2023. https://de.statista.com/statistik/daten/studie/154908/umfrage/strompreise-fuer-haushaltskunden-seit-2006/ (accessed 9 June 2023).

[24] Bundesnetzagentur, Gaspreis nach Verbrauchergruppen in Deutschland in den Jahren 2011 bis 2022, 2023. https://de.statista.com/statistik/daten/studie/154961/umfrage/gaspreis-nach-verbrauchergruppe-seit-2006/ (accessed 9 June 2023).

[25] Presse und Informationsamt der Bundesregierung, Anreiz für weniger CO2-Emissionen. https://www.bundesregierung.de/breg-de/themen/ (accessed 29 March 2023).

[26] Viessmann, Planungsanleitung: VITOCAL 350-HT PRO, 2017.

[27] Umweltbundesamt, Trends der Lufttemperatur, 2023. https://www.umweltbundesamt.de/daten/klima/trends-der-lufttemperatur#steigende-durchschnittstemperaturen-weltweit (accessed 11 June 2023).

[28] Viessmann, Datenblatt Vitodens 200-W, 2015.

[29] P. Konstantin, Investitionsrechnung, Kosten und Preisbildung, in: P. Konstantin (Ed.), Praxisbuch der Fernwärmeversorgung: Systeme, Netzaufbauvarianten, Kraft- Wärme-Kopplung, Kostenstrukturen und Preisbildung, Springer Berlin Heidelberg, Berlin, Heidelberg, 2018, pp. 137–157.

[30] L. Eltrop, Heizkostenvergleichsrechner V07, 2022.

[31] S. Ortner, M. Pehnt, Analyse des wirtschaftlichen Potenzials für eine effiziente Wärme- und Kälteversorgung: Beitrag zur Berichtspflicht EnEff-RL, Artikel 14 Anhang VIII, 2021. https://www.umweltbundesamt.de/sites/default/files/medien/1410/publikationen/2021-08-05_cc_54-2021_effiziente_waerme-kaelteversorgung.pdf (accessed 9 June 2023).

The 18th International Symposium on District Heating and Cooling, September 3–6, 2023, Beijing, China

CASE STUDY ON COMBINED HEAT AND WATER SYSTEM FOR DISTRICT HEATING IN BEIJING BY RECOVERING INDUSTRIAL WASTE HEAT IN TANGSHAN

Xiaolin Yang[a], Zhaoyang Liu[a], Jianjun Xia [a*]

[a] *Building Energy Research Center, Beijing, 100084, China*
[*] *Corresponding author. xiajianjun@tsinghua.edu.cn (J. Xia). China*

ABSTRACT

With the proposal of China's dual-carbon goal, recovering industrial waste heat (IWH) for district heating has gained more attention. Due to the obvious geographical correlation between water demand and heat demand in urban areas of northern China, some scholars have proposed that combined heat and water (CHW) system is more economical to transport water and heat to the city simultaneously, compared with separate heat supply and separate water supply. In this study, Beijing lacks desalinated water (DW) resources and clean low-carbon heat sources, while Tangshan, Hebei is rich in IWH near the sea. Combining the multi-effect distillation (MED) CHW system with the seasonal pit heat storage, a case of long-distance transport of hot DW from Tangshan to Beijing is planned and the costs, energy consumption and feasibility of the case are analyzed. In result, the heat from various waste heat (WH) sources of the three major iron and steel plants near the sea in Tangshan can be recovered throughout the year to produce 95 °C hot DW and transported to Beijing, which can supply 271.2 million tons of DW and 91.5 million GJ of heat annually, satisfying 10% and 41% of the demand in Beijing, respectively. Compared with the current gas-based heating solution in Beijing, the introduction of IWH from Tangshan can save 2.68 billion Nm^3 of natural gas per year, which has obvious energy-saving, environmental and economic benefits.

Keywords: Industrial waste heat; District heating; Combined heat and water; Seasonal thermal storage

INTRODUCTION

With the rapid urbanization and the improvement of residents' living standards, the district heating (DH) area in urban areas of northern China has maintained an average annual growth rate of 8.7% from 2011 to 2020. According to Tsinghua Building Energy Research Center, it reached 15.63 billion m^2 in 2020, which was mainly met by coal-fired cogeneration, followed by coal-fired and gas-fired boilers, with industrial waste heat (IWH) accounting for only about 1%. However, in 2020, the industrial energy consumption accounting for 65% of the total national energy consumption was about 3.2 billion tce, of which 70% was used in metallurgical, chemical, cement, fuel and other production industries. The comprehensive energy utilization efficiency of these industries is less than 50%, and the IWH temperature is concentrated at 30-100 °C, which is more suitable for DH rather than industrial applications[1].

There have been many case studies on recovering low-grade IWH for DH at home and abroad[2,3]. Fang et al.[4] proposed a comprehensive method for efficient utilization and benefit evaluation of low-grade IWH, and used this method to recover 122MW of heat from a steel plant and a copper plant in Chifeng City, China for DH. Li et al.[5] proposed a theoretical method for using three types of IWH from steel plants for DH, and applied this method to recover 225MW of heat from two major steel plants. However, IWH is generally not close to heat users, which requires long-distance transportation (LDT). As the LDT distance increases, the energy consumption and pipe material cost will increase. Considering the obvious geographical correlation between water and heat demand in northern urban areas, Li et al.[6] first proposed the combined heat and water (CHW) system in 2019, which can directly produce hot desalinated water (DW) at the required temperature and transport it to users through a single pipe. Compared with separate water supply and heat supply, the CHW system is more economical due to lower LDT costs. Chen et al.[7] conducted a case study on CHW for recovering waste heat (WH) from Haiyang Nuclear Power Plant in 2021. Li et al.[8] tested the operation effect of CHW in Haiyang Nuclear Power Plant and confirmed its economy and feasibility. However, since CHW is a new topic, there is no research on the combination of IWH and CHW.

IWH is generated throughout the year and is mainly related to production process, while building heating load only exists during the heating season and is greatly affected by meteorological parameters. In order to further improve the economy of CHW, it may be necessary to recycle IWH throughout the year, which requires selecting an economical and reasonable seasonal thermal storage (STS) method. Among the widely used sensible thermal storage (TS) technologies, the construction scale of tank TS is generally small, aquifer TS has high geological requirements, and buried pipe TS is mainly at medium to low temperatures. In contrast, pit TS has the advantages of high TS temperature and density, short construction

period, no special geological requirements, and good economy[9]. Therefore, it is suitable for recovering IWH.

The urban heating area in Beijing, China in 2022 is 927 million m^2, with gas boilers and gas-fired wall-mounted boilers accounting for up to 74% and non-fossil fuels accounting for only 2.6%. This requires the urgent development of clean and low-carbon heating. Beijing also lacks DW. In 2020, the production and domestic water consumption was about 2.6 billion m^3, and the DW resources were unable to make ends meet for a long time. After the South-to-North Water Diversion Project entered Beijing, the per capita DW increased to 150m^3, but it was still significantly lower than the international extreme water shortage warning line (500 m^3). Tangshan City, Hebei Province is a major steel city, and some factories are near the seaside and have good desalination conditions. Through on-the-spot investigation and questionnaire survey of 49 enterprises with high environmental protection rating and large production capacity in Tangshan City, the total amount of WH in winter is 280 million GJ, of which IWH of power plants is 110 million GJ and that except power plants is 170 million GJ. It is estimated that the total building heating demand in winter in Tangshan in 2035 will be 70 million GJ. Therefore, the IWH in Tangshan is enough to meet the local heating demand, and there is at least 100 million GJ of heat surplus. It can be considered to recover IWH through the CHW system to provide clean and low-carbon heat sources and DW for Beijing.

METHODOLOGY

Technical Principles

If IWH is recovered throughout the year, the CHW system can be divided into four parts: heat-water co-production (HW-CoP), LDT, STS, and end heat release (EHR), as shown in Figure 1. The principle of HW-CoP is to combine seawater desalination and WH utilization methods to generate DW while heating it to about 100 °C. The principle of LDT is to use an insulated water pipe to transport high-temperature DW from the factory side to the city side. Due to the direct supply of DW to urban users, the LDT system is a single-pipe system and does not require a return water pipeline. Pressurized pumping stations are built along the way to ensure the pressure in the pipe and prevent vaporization and water hammer. The principle of STS is that in the non-heating season, the hot DW is stored and the replaced low-temperature DW is supplied to urban users. In the heating season, the stored hot DW is used for DH, and the low-temperature DW after heat exchange returns to the STS device. The EHR is to extract heat from hot DW to the circulating water of urban heat network, and the DW cooled to below 20 °C is sent to water treatment plants for subsequent treatment for municipal water supply.

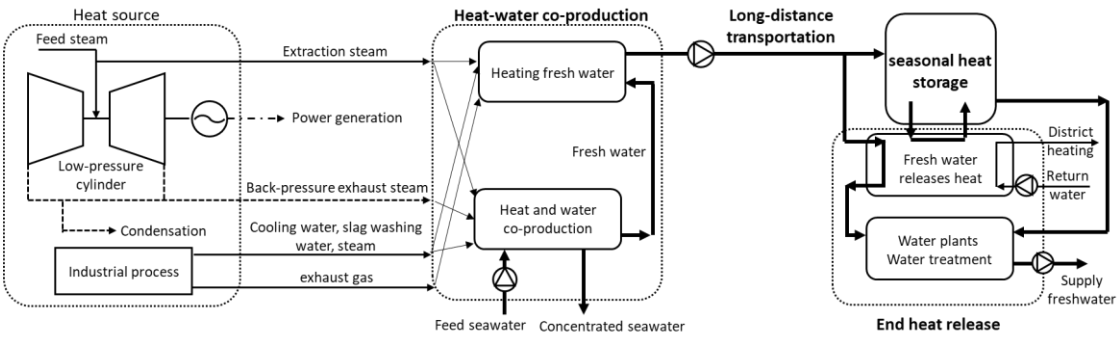

Figure 1. Overall technical schematic of the CHW system

Waste Heat Resources Statistics

There are three major steel plants located in Caofeidian District along the coast of Tangshan. The annual iron production of plant B is about 13 million tons, and that of plant A and C is both about 7 million tons. The types of IWH mainly include steam, flue gas, dusty air, circulating cooling water and slag washing water. After deducting the self-recovered IWH, the remaining available IWH is counted. Considering that the recovery rate of slag washing water and slag washing steam is 80%, and that of other IWH is 100%. The specific calculation method of the average heat power of various IWH is as follows.

$$\boldsymbol{P_{fg}} = \frac{\boldsymbol{q_{fg}}}{\boldsymbol{3600}} \times \left(\boldsymbol{c^h_{p\_fg} t^h_{fg} - c^l_{p\_fg} t^l_{fg}}\right), \tag{1}$$

where P_{fg} is gas thermal power (MW), q_{fg} is gas flow (Nm^3/h), t^h_{fg} and t^l_{fg} are the upper and lower limits of gas temperature, respectively (°C), and $c^h_{p\_fg}$ and $c^l_{p\_fg}$ are the average volume constant pressure specific heat capacities corresponding to the upper and lower limits of gas temperature, respectively (kJ/(Nm^3·°C)). Considering the factors such as space limitation and corrosion at low temperature, the lower recovery temperature limit of flue gas is 80 °C[10] and that of dusty air is 60 °C[11]. The calculation method of specific heat capacity of flue gas refers to a relevant standard[12].

$$\boldsymbol{P_{cw}} = \frac{\boldsymbol{q_w}}{\boldsymbol{3600}} \times \left(\boldsymbol{h^h_w - h^l_w}\right), \tag{2}$$

where P_{cw} is the thermal power of circulating cooling water (MW), q_w is the circulating cooling water flow (t/h), and h^h_w

and h_w^l are the upper and lower limits of the enthalpy of circulating cooling water, respectively (kJ/kg).

$$\boldsymbol{P_s} = \frac{\boldsymbol{q_s}}{\boldsymbol{3600}} \times \left(\boldsymbol{h_s^h} - \boldsymbol{h_s^l}\right), \tag{3}$$

where P_s is the steam thermal power (MW), q_s is the steam flow rate (t/h), and h_s^h and h_s^l are the enthalpy of saturated steam and the enthalpy of saturated water under steam pressure, respectively (kJ/kg).

$$P_{sw} = \frac{[187+1.96\times(t_{sw}^h - t_{sw}^l)]\times m_{sw}}{330\times24\times3600} \times \frac{2}{3}, \tag{4}$$

where P_{sw} is the thermal power of slag washing water (MW), t_{sw}^h and t_{sw}^l are the temperature of iron slag before and after cooling, respectively (K), m_{sw} is the annual output of iron slag (t/a), 330 is the annual running days of the factory (days), 187 is the latent heat of iron slag (kJ/kg), 1.96 is the sensible heat of iron slag (kJ/(kg·K)), 2/3 is the ratio of the heat of slag washing water to the total heat of slag washing process, and the remaining 1/3 is the heat of slag washing steam.

$$\boldsymbol{P_{sp}} = \frac{\boldsymbol{1.25\times m_{sp}\times(t_{sp}^h - t_{sp}^l)}}{\boldsymbol{330\times24\times3600}}, \tag{5}$$

where P_{sp} is the thermal power of steam generated by steel slag stuffy tank (MW), t_{sp}^h and t_{sp}^l are the temperature of steel slag before and after cooling, respectively (K), m_{sp} is the annual output of steel slag (t/a), 330 is the annual running days of the factory (days), 1.25 is the specific heat capacity of steel slag at constant pressure (kJ/(kg·K)).

The T-Q diagrams of IWH from the three steel plants are shown in Figure 2, Figure 3 and Figure 4 respectively.

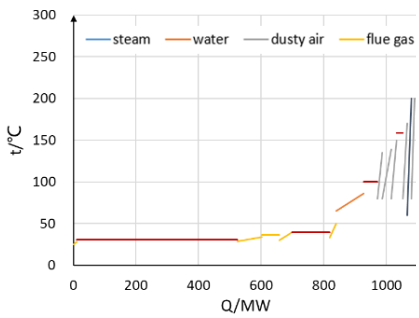

Figure 2. T-Q diagram of plant A

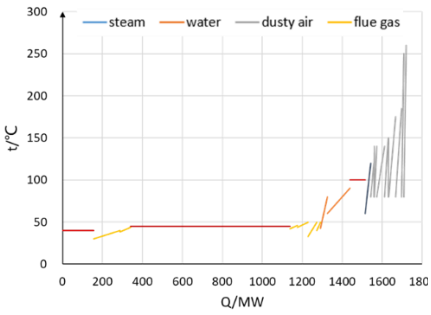

Figure 3. T-Q diagram of plant B

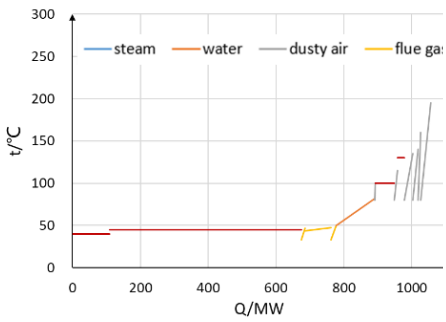

Figure 4. T-Q diagram of plant C

Heat-water Co-production (HW-CoP)

The maximum temperature of the pit TS is 90-100 °C, and the HW-CoP is set to produce 95 °C DW. Commonly used thermal seawater desalination methods include low-temperature multi-effect distillation (LT-MED) and multi-stage flash (MSF). If MSF is used, a large amount of extraction steam is needed as the driving heat source, and the WH of exhaust gas cannot be utilized. Therefore, LT-MED is adopted. The specific process of LT-MED is referred to the previous research[13]. The seawater temperature of Tangshan in winter and other seasons is set to 3 °C and 15 °C respectively, and the concentration of raw seawater is set to 3%. According to the previous optimization results[13], the heat source temperature and effect number of LT-MED are 70 °C and 10, respectively. LT-MED produces DW at about 65 °C and DW is further heated to 95 °C through exhaust gas heat exchangers. When the exhaust gas heat is not enough, it is necessary to extract steam from existing generator sets and set up heat exchangers. In order to reduce the entransy loss caused by the extraction steam heat exchanger, an absorption heat pump (AHP) driven by the extraction steam is set up before the heat exchanger to initially heat the 65 °C DW. The heat exchange end difference of the exhaust gas-water heat exchanger is 10 °C. The heat exchange end difference of each heat exchanger in AHP is 3 °C and the COP is 1.7.

For circulating cooling water, its WH is recovered by an AHP driven by extraction steam. One part of the cooling water is used to produce 70 °C steam as the heat source of LT-MED, and the other part is used to heat DW. For slag washing water, 70 °C steam is generated by vacuum flash evaporation and thermal compression, which is also used as the heat source of LT-MED. In order to maximize the utilization of WH, after the reasonable matching of extraction steam and exhaust steam, the gas generator sets of plant A and C need to be transformed into back pressure units, and 70 °C exhaust steam is used as the heat source of LT-MED.

The schematic diagram of the overall heat extraction process is shown in Figure 5. Throughout the year, the WH from three steel plants was almost fully utilized, and the entransy efficiency reaches about 40%, as shown in Table 1.

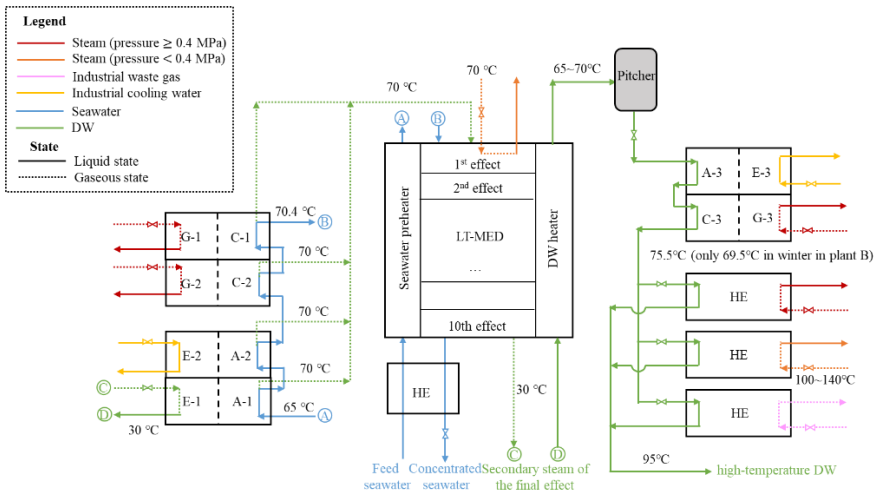

Figure 5. Schematic diagram of HW-CoP. A: absorber; E: evaporator; G: generator; C: condenser; HE: heat exchanger.

Table 1. Specific parameters of HW-CoP in the three plants

Plant	A		B		C	
Period	Winter	Other seasons	Winter	Other seasons	Winter	Other seasons
70 °C heat source steam flow rate (t/h)	1183	1244	1800	1842	1156	1221
Desalinated water flow rate (t/h)	9434	10118	14737	15084	9112	9844
Gained output ratio (GOR)	8.0	8.1	8.2	8.2	7.9	8.1
Heat generation power of fresh water when cooled to 10 °C (MW)	931	999	1454	1489	899	972
Waste heat recovery efficiency (%)	100	94.7	100	90.1	100	95.5
Entransy efficiency (%)	43.2	36.5	40.5	36.5	42.9	39.7

Long-distance Transportation (LDT)

In order to facilitate the construction, it is preliminarily planned to lay pipelines along the existing highway, and a total of three parallel water pipelines will be built to Beijing South Sixth Ring, which can be constructed in stages. The planned route is shown in Figure 6.

When designing the pipe diameter, it is necessary to comprehensively consider the initial pipeline investment and the electricity cost of water pumps. The calculation method of specific frictional resistance R, water pump power W, and transport heat loss P_{loss} refers to previous literature[7]. The conventional heating system has two pipelines: water supply pipeline and return water pipeline, and the economic R range is 30-70 Pa/m[7]. In contrast, the CHW system operates throughout the year and requires only a single pipe. Therefore, compared with the initial pipeline investment, the impact of pump power consumption on the total annual cost is more dominant, so the economic R is also smaller than that of the conventional heating system. In this project, it is 15-20Pa/m, and the economic flow velocity is 1.7-2.2m/s. When the pipe diameters of line A, B and C are 1400 mm, 1600 mm and 1400 mm respectively, the overall economy of the system is the best. The main parameters of LDT are shown in Table 2. When the transport distance exceeds 200 km, the heat loss ratio can be controlled below 3%, and the temperature drop of hot DW can be controlled below 2.5 °C.

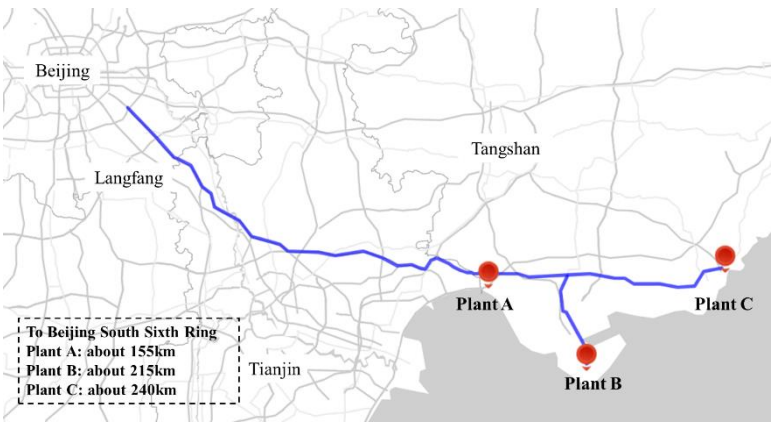

Figure 6. Planned route for LDT

Table 2. Main parameters of LDT

Line	A		B		C	
Pipe length (km)	155		215		240	
Pipe number	1		1		1	
Pipe inner diameter (mm)	1400		1600		1400	
Period	Winter	Other seasons	Winter	Other seasons	Winter	Other seasons
Flow G (t/h)	9434	10118	14737	15084	9112	9844
Specific frictional resistance R (Pa/m)	16.3	18.8	19.7	20.7	15.2	17.8
Pump power W (kW)	10596	13071	27792	29801	14783	18639
Transport heat loss P_{loss} (MW)	16.0	14.3	25.0	22.4	24.8	22.2
Heat generation power (MW)	931	999	1454	1489	899	972
Heat loss ratio (%)	1.7	1.4	1.7	1.5	2.7	2.3
Temperature drop Δt (K)	1.5	1.2	1.5	1.3	2.3	1.9

Seasonal Thermal Storage (STS) and End heat release (EHR)

The heating season in Beijing is 121 days, while the three plants in Tangshan run for 151 days in winter and 179 days in other seasons. Therefore, when Beijing is in the heating season, plants run every day to ensure heating, and when Beijing is in the non-heating season, plants run for 30 days in winter and 179 days in other seasons. A total of 209 days of 95 °C DW needs to be stored. The pit TS is adopted, and the TS efficiency can reach up to 95%[9]. The specific process is shown in Figure 7 and Figure 8. During the heating season, both the long-distance transported hot DW and the stored hot DW enter the EHR to transfer the heat to the primary network circulating water, and at the end of the heating season, all the water in reservoir is low-temperature DW. The long-distance transported hot DW meets the basic heat load, and the STS can flexibly adjust the heat supply to meet the peak heat load and some basic heat load. During the non-heating season, the long-distance transported hot DW is channeled into the top layer of the large STS pit, while low-temperature DW is replaced from the bottom. At the end of the non-heating season, all the water in the reservoir is high-temperature DW. For EHR, in order to fully tap the heating capacity of hot DW, the temperature after heating should be as low as possible. Since the absorption heat exchanger and electric heat pump in the substation are designed to further extract sensible heat, Li et al.[6] proposed that hot DW can be cooled to below 10 °C. The specific process is shown in Figure 9. The heat exchange end difference of the evaporator and condenser of the electric heat pump is 3 °C, the thermodynamic perfection is 60 %, and the calculated COP is about 4.7. Temporarily considering the uniform temperature distribution of the hot DW in the STS pit, the design parameters of STS are shown in Table 3. The three lines need 175 million m^3 of equivalent water volume.

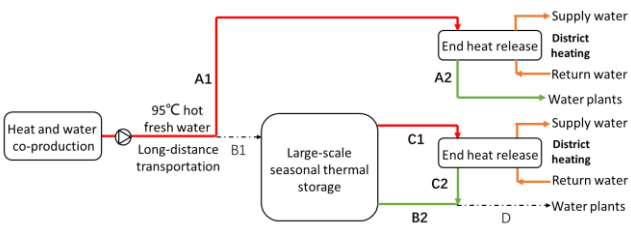

Figure 7. STS process in the heating season

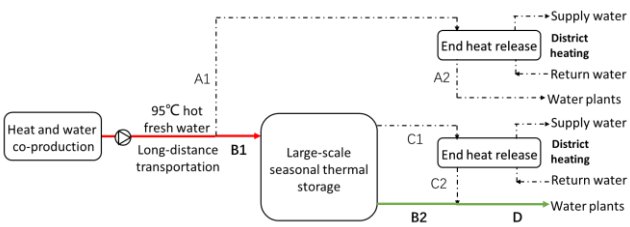

Figure 8. STS process in the non-heating season

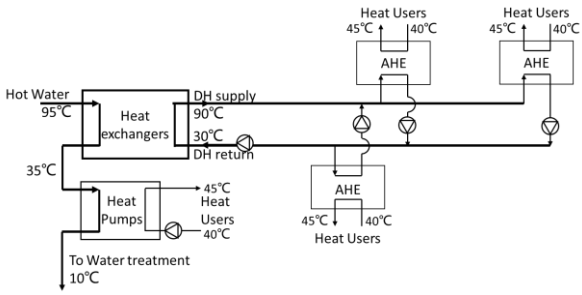

Figure 9. Process diagram of EHR. AHE: absorption heat exchanger.

Table 3. Design parameters of STS

Line	A		B		C	
Period	Winter	Other seasons	Winter	Other seasons	Winter	Other seasons
Flow of desalinated water (DW) into pits G (t/h)	9434	9357	14737	13633	9112	8931
Temperature of DW into pits $t_{hw} - \Delta t$ (°C)	93.5	93.8	93.5	93.7	92.7	93.1
Temperature of DW out of pits $t_{supply,hs}$ (°C)	89.4	89.6	89.4	89.5	88.5	88.9
Equivalent water volume (10^4 m^3)	679.2	4346.7	1061.1	6480.1	656.1	4229.0
Total (10^4 m^3)	5025.9		7541.2		4885.0	

RESULTS

Total Heat and Desalinated Water (DW) Supply

From the perspective of heat source, the annual heat and DW supply is shown in Table 4. From the perspective of end users, the annual heat and DW distribution is shown in Table 5. Finally, 270 million tons of DW (820000 tons/day) can be produced throughout the year, meeting 10% of Beijing's current annual DW demand. An annual total of 91.54 million GJ of IWH is used, of which 33.7 million GJ is directly supplied and 57.9 million GJ is stored. According to the building heating demand of 0.25 GJ/m^2, it can supply about 370 million m^2, accounting for 40% of the current urban heating area in Beijing. Moreover, the heat extracted is less than 20% of the annual IWH discharged by the industrial and power plants in Tangshan, and the remaining part can fully meet the local heating demand in the heating season.

Table 4. Annual supply of heat and DW

Line	A		B		C		Total	
Period	Winter	Other seasons	Winter	Other seasons	Winter	Other seasons	Winter	Other seasons
95 °C desalinated water output (10^4 t)	3419	4347	5341	6480	3302	4229	12062	15056
Heat production (10^4 GJ)	1215	1544	1898	2302	1173	1503	4286	5349
Heat loss during long-distance transportation (10^4 GJ)	21	22	33	35	32	34	86	91
Heat loss of seasonal thermal storage (10^4 GJ)	12	76	19	113	11	73	42	263
End released heat (10^4 GJ)	2628	——	4001	——	2525	——	9154	——

Table 5. Annual distribution of heat and DW

Line		A		B		C		Total	
Period		Winter	Other seasons	Winter	Other seasons	Winter	Other seasons	Winter	Other seasons
End released heat (10^4 GJ)	Long-distance transportation	957	——	1495	——	914	——	3366	——
	Seasonal thermal storage	1671	——	2506	——	1611	——	5788	——
10 °C desalinated water supply (10^4 t)		2740	5026	4280	7541	2646	4885	9665	17452

Environmental analysis of energy consumption

Under the same heating capacity, compared to current gas heating, if calculated based on calorific value of 36MJ/Nm^3 and combustion efficiency of 95%, the CHW system can save 2.68 billion Nm^3 of natural gas annually, with an energy saving rate of 33%, and can also provide 270 million tons of DW annually. The CO_2 emission reduction rate is 33% and main pollutant emission reduction rate reaches 28%. The specific results are shown in Figure 10, Figure 11and Figure 12.

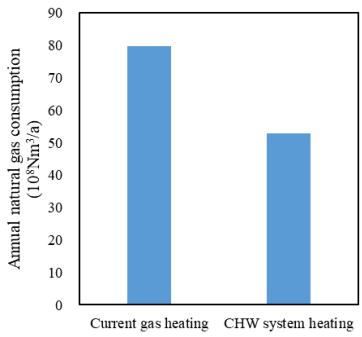

Figure 10. Comparison of gas consumption

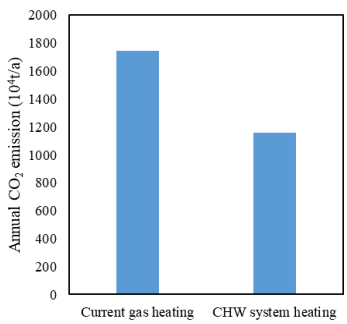

Figure 11. Comparison of CO2 emission

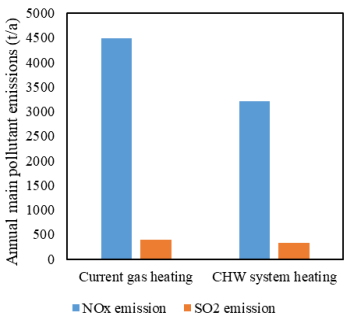

Figure 12. Comparison of main pollutant emissions

Economic analysis

The entire system needs to increase initial investment by 45.3 billion yuan, including STS of 17.5 billion yuan, HW-CoP of 12 billion yuan, LDT of 9 billion yuan, EHR of 3.2 billion yuan, and engineering construction of 4.6 billion yuan. The annual electricity consumption is 2.4 billion kWh, which is mostly the reduced power generation caused by extraction. The specific calculation results of initial investment and operating costs are shown in Table 6 and Table 7, respectively.

The current DW cost of LT-MED is about 6-8 yuan/t. When the heat price is set at 50 yuan/GJ, the static investment payback periods corresponding to water prices of 6 yuan/t and 8 yuan/t are 11.1 years and 9.8 years, respectively. Even if the natural gas price in Beijing is 2 yuan/Nm^3, the fuel cost for natural gas heating still reaches 60 yuan/GJ. If it is used as the heat price and the water price is 6 yuan/t, the static investment payback period is 9.1 years. The equipment lifespan is generally over 15 years, and it of LDT and STS is longer, so all three scenarios are economically feasible. The detailed

analysis is shown in Table 8.

Table 6. Specific calculation results of initial investment

Part	Key equipment	Key design parameter		initial investment (10^8 yuan)
Source	Low-temperature multi-effect distillation (LT-MED)	Desalinated water (DW) flow	33283 t/h (winter) 35046 t/h (other seasons)	111.61
	Absorption heat pump (AHP) for LT-MED	Heating capacity	1376 MW	6.88
	AHP for heating DW	Heating capacity	240 MW	1.20
	Heat exchangers	Heat exchange area	15500 m^2	0.31
Transport	A single pipe	Hot DW temperature	95 °C	89.70
	Pump and relay pumping station	Total power	61512 kW	0.70
End	Heat exchangers	Heat exchange area	890571 m^2	17.24
	Electricity heat pump	Heating capacity	4939MW	14.81
Storage	Thermal storage pit	Equivalent water volume	175 million m^3	174.52
Construction	/	/	/	46.33
Entire system	Terminal heating power		9153 MW	463.29
	DW flow		33283 t/h (winter) 35046 t/h (other seasons)	

Table 7. Specific calculation results of operating costs

Part		Parameter	Operating costs (10^8 yuan/a)
Reduced power generation caused by extraction steam		1.23 billion kWh	5.54
Low-temperature multi-effect distillation (LT-MED)	Power consumption	0.68 billion kWh	3.05
	Pretreatment drugs		0.73
Long-distance transportation		0.46 billion kWh	2.06
Operation and maintenance			4.17
Heat payment to the factory			4.58
Total annual cost			20.13

Table 8. Economic analysis of the CHW system

	Water price (yuan/t)	Heat price (yuan/GJ)	Total annual income (10^8 yuan)	Annual net income (10^8 yuan)	Static investment payback period (year)
Scenario 1	50	6	62.04	41.91	11.1
Scenario 2	50	8	67.46	47.33	9.8
Scenario 3	60	6	71.19	51.06	9.1

DISCUSSION

Feasibility analysis

In terms of technology, the terrain along the way from Tangshan to Beijing South Sixth Ring is relatively flat and the construction is less difficult. The new type of pipe has good heat insulation performance and long lifespan. The temperature drop of LDT does not exceed 2.5 °C. The single pipe supplies hot DW, so the pipe is easily maintained. The STS efficiency can be as high as 95%. In terms of water quality, all 15 conventional water quality parameters of LT-MED meet China's drinking water standards and are significantly superior to the membrane method. Because the CHW system transports high-temperature DW, it can kill residual microorganisms in water and further ensure water quality. The stainless-steel lining of the new pipe can ensure that the water quality meets the food grade requirements, the direct buried pipe does not affect the ecological environment, and there is no evaporation loss and pollution. The safety of water delivery is better than that of open channel. In terms of economy, the CHW system can achieve “one medium, two purposes”, combining one DW pipe and two heating pipes into one, making LDT more economical. In addition, the water price for LT-MED is usually 6-8 yuan/t, and the current gas heating price in Beijing is 80-100 yuan/GJ, indicating that this system has obvious economic advantages.

Potential in Northern China

The total annual IWH of steel plants within 200 km of the coastline in northern China are estimated to be at least 1 billion GJ, mainly concentrated in the Beijing-Tianjin-Hebei region, and also distributed in Shandong and Liaoning provinces. If the CHW system is used to recover these IWH throughout the year, calculated based on a heating demand of 0.25GJ/m^2 during the heating season, it can meet approximately 4 billion m^2 of building heating, accounting for 25% of the DH area in northern cities and towns. Simultaneously, the annual production of about 3 billion tons of DW accounts for 6% of the north industrial and domestic DW demand. The coastal areas of northern China are densely populated and lack clean and low-carbon heat sources and DW, with a heating scale of 5 billion m^2 and an annual DW consumption of 1.7 billion

tons[8]. If all the above IWH is supplied to the northern coastal areas, 80% of the building heating can be satisfied, and the remaining half of DW can be transported to other areas. Compared with gas-fired boilers, assuming a thermal efficiency of 95% and a calorific value of 36MJ/Nm^3, the annual natural gas consumption can be reduced by 29.2 billion Nm^3, and the annual emissions of CO_2, NO_X, and SO_2 can be reduced by 64 million tons, 14000 tons, and 700 tons, respectively.

CONCLUSION

This study first proposed the technical scheme of using CHW system to recover IWH throughout the year, and planned the scheme of recovering IWH from three major steel plants in the coastal area of Tangshan City to supply heat and DW to Beijing. The main purpose is to provide a preliminary attempt and reference for the future promotion of the combination of CHW and IWH through this case. The main conclusions are as follows:

1. Without affecting local heating in Tangshan, the three steel plants can provide 91.54 million GJ of heat to Beijing during the heating season and 270 million tons of DW throughout the year. Compared with the current gas heating in Beijing, the energy saving rate, CO_2 emission reduction rate and main pollutant emission reduction rate are 33%, 33% and 28% respectively, and the thermal pollution caused by IWH in Tangshan can also be reduced.
2. The CHW system adopts a single pipe, greatly increasing the economic transportation distance. This case verifies that it still has good economic benefits even if the transmission distance is more than 200 km, but this is related to its annual operation. If it only runs during the heating season, the economic distance may be reduced. STS plays a dual role of heat storage and heat peak shaving, and is expected to develop on a large scale in northern China.
3. Although the CHW system is a new topic, it has been continuously studied in recent years. If it is used to recover IWH of iron and steel plants along the coast of northern China throughout the year, it can meet 4 billion m^2 of building heating and 3 billion tons of DW, and has a good application prospect.

ACKNOWLEDGEMENT

This work was supported by the 14th Five-Year National Key R&D Plan of China (Grant No. 2022YFC3802401).

REFERENCES

[1] F. Guo, X. Zhu, P. Li, et al. Low-grade industrial waste heat utilization in urban district heating: Simulation-based performance assessment of a seasonal thermal energy storage system. Energy 2022; 239(PE): 122345.
[2] J. Xia, Y. Jiang. Key issues and solutions in a district heating system using low-grade industrial waste heat. Energy 2015; 86: 589-602.
[3] J. Ziemele, E. Dace. An analytical framework for assessing the integration of the waste heat into a district heating system: Case of the city of Riga. Energy 2022; 254(PB): 124285.
[4] H. Fang, J. Xia, K. Zhu, et al. Industrial waste heat utilization for low temperature district heating. Energy Policy 2013; 62: 236-246.
[5] Y. Li, J. Xia, H. Fang, et al. Case study on industrial surplus heat of steel plants for district heating in Northern China. Energy 2016; 102: 397-405.
[6] Y. Li, W. Pan, J. Xia, et al. Combined heat and water system for long-distance heat transportation. Energy 2019; 172: 401-408.
[7] J. Chen, W. Zheng, Y. Kong, et al. Case study on combined heat and water system for nuclear district heating in Jiaodong Peninsula. Energy 2021; 218: 119546.
[8] Z. Li, L. Fu, H. Liu. A novel combined heat and water (CHW) technology applied in China northern coastal regions: Actual demonstration project towards promoting. Energy Conversation and Management 2022; 257: 115409.
[9] H. Mahon, D. O'Connor, D. Friedrich, et al. A review of thermal energy storage technologies for seasonal loops. Energy 2022; 239: 122207.
[10] H. Fang, C. Wang, B. Lin. Current Situation of Clean Heating Using Surplus Heat from Iron and Steel Industry and Prediction on the Future Potential of the Surplus Heat. Building Energy Efficiency 2019; 47(06): 106-111. (in Chinese)
[11] B. Zhang. Modeling and Simulation of Hot Water Heating System for Bathing Using Waste Heat from Cement Plant Waste Gas. Wuhan University of Technology 2012. (in Chinese)
[12] General Administration of Quality Supervision, Inspection and Quarantine of the People's Republic of China. Calculation method and utilization guides for waste heat resource's quantity of industrial boiler's and flame heating furnace's exhaust gas 2009. (in Chinese)
[13] X. Yang, Z. Liu, J. Xia. Optimization and analysis of combined heat and water production system based on a coal-fired power plant. Energy 2023; 262 (PB): 125611.

ANNEX TS5: RES DHC TECHNOLOGY AND APPLICATION FACT SHEETS

Komoszynska M.a*, Rasmussen A. b, Guddat M.G.A c, Sørensen P.A. d, Borup L. e

a Magdalena Komoszynska, PlanEnergi, Skørping, 9520, Denmark
b Allan Rasmussen, PlanEnergi, Skørping, 9520, Denmark
c Max Gunnar Ansas Guddat, PlanEnergi, Skørping, 9520, Denmark
d Per Alex Sørensen, PlanEnergi, Skørping, 9520, Denmark
e Line Borup, PlanEnergi, Skørping, 9520, Denmark

ABSTRACT

The research focus of the IEA DHC Annex TS5 project is the integration of Renewable Energy Sources into existing District Heating and Cooling systems (RES DHC) using large-scale solar thermal, central heat pumps, renewable Power to Heat (P2H)-systems, biomass, geothermal and large heat storages in combination with Combined Heat and Power (CHP) and surplus heat. The work is performed using the experience, market knowledge and good practices from a multinational, technical specialist environment across the globe. One key result of the work is RES DHC technology and application factsheets summarizing reliable knowledge about the existing enhanced solutions for the technical and operational integration of RES plants into existing traditional and modern DHC systems. This gives an overview of RES DHC technologies such as seasonal thermal storage, geothermal energy, solar district heating, wind turbine, large-scale heat pump, photovoltaics, and biomass heat plant. biomass combined heat and power and technology applications including fluctuating energy coupled with heat pump and thermal storage, solar thermal combined with long term storage, excess heat from data centre used as a heat source for heat pump and control systems for district heating cooling. The collected information includes technology description, status of technology readiness level, investment and maintenance costs (price standards from Northern, Europe, Southern Europe, North America and Asia), regulation capacity and velocity, temperatures and capacities, list of suppliers and demo examples. This research addresses Research and Development (R&D) challenges related to the integration of RES in DHC systems and should contribute to establishing renewable heat sources as environmentally friendly and emission-free heat generation technologies for the DHC sector.

Keywords: RES; DHC; factsheets; energy systems integration

1. INTRODUCTION

IEA DHC Annex TS5 project has been conducted over the period 2019-2024 and targets all aspects related to the integration of high shares of renewable energy sources (RES) into existing urban District Heating and Cooling (DHC) systems. The work scope was grouped into four subtasks:

Subtask A. RES technologies for DHC – gaining up-to-date knowledge about the current status of the energy transition per participating in the project country and the recently developed or enhanced solutions for the technical and operational integration of RES plants into existing and modern DHC systems,

Subtask B. Transformation of large DHC systems to higher shares of RES – providing practical knowledge on transformation processes of centralised DHC to a high share of RES including bottlenecks, challenges and key enablers, planning tools and review of case studies,

Subtask C. Decentral integration of RES into DHC systems – compiling handbooks, guidelines and reviews of technical and non-technical aspects for the decentralised RES integrated into DHC systems, including planning criteria, integrational and operational challenges, simulation tools,

Subtask D. Non-technical framework – developing advanced instruments addressing non-technical market barriers and opportunities.

The overview of the subtasks and the relation between them is shown in Figure 1.

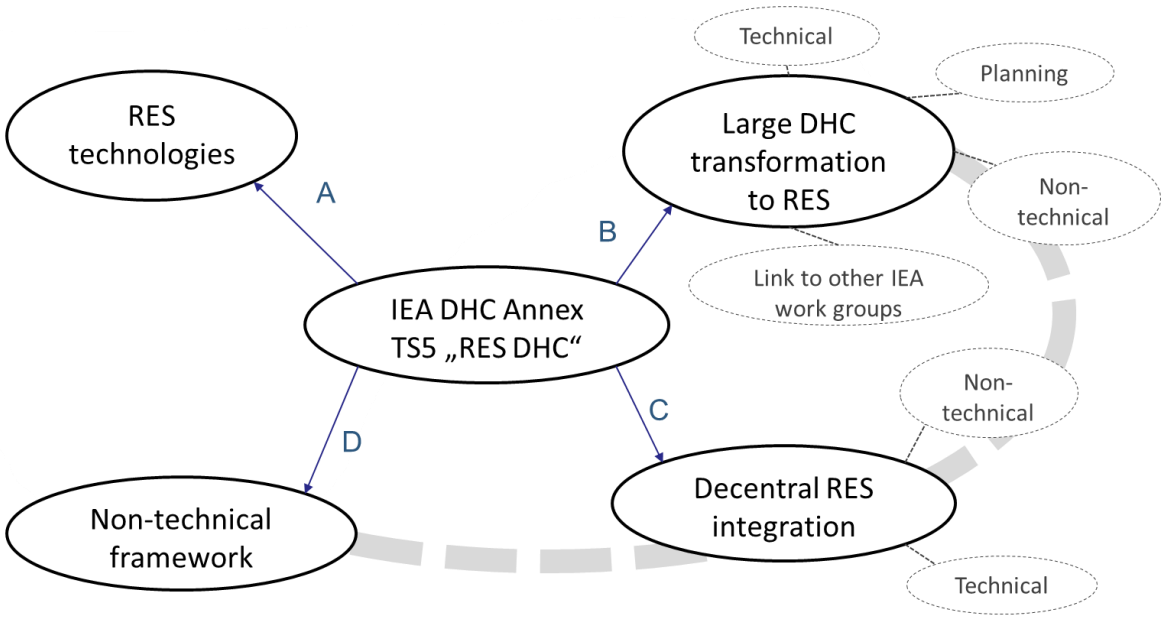

Figure 1. Work plan of the IEA DHC Annex TS5.

The project focuses on collecting and organising knowledge about the innovative application of both well-known and developing RES technologies. This includes large-scale solar thermal, central heat pumps, renewable Power-to-Heat (P2H)-systems, biomass, geothermal and large heat storages in combination with Combined Heat and Power (CHP) and surplus heat.

The achievement of the work from Subtask A is the key topic of this paper. This includes technology and application factsheets which give an overview of the current knowledge on RES technologies analysed individually and integrated in combination with others in more sophisticated systems, so-called applications. As part of the subtask, the current (2021) transition status for the participating countries along with the existing examples of integration of RES technologies and applications for transition have been reported in State-of-the-art.

A reliant information source for the energy technology and cost data worldwide is still a challenging point, given intensive decarbonisation programmes across the countries. There is plenty of ongoing or recently completed transition projects for the DHC systems integrating high proportion of the RES. The similar planning, design and implementation problems are encountered by many national and regional authorities, heat suppliers, DHC operators, energy consultants, engineers and also end-users. This experience is, however, not distributed in a common platform, neither the key and up-to-date technology parameters are collated and shared to facilitate future similar projects. Technological factsheets and applications, developed as part of the IEA DHC Annex TS5 project are “a drop in the ocean” of data management needs, however, a significant step in facilitating energy transitions of DHC systems, uptake of RES-solutions and security of reliable energy supplies.

2. METHODOLOGY

2.1. Topic selection and data acquisition

The work in Subtask A has begun with identifying and quantifying the current RES development status in the DHC in each country which was represented by a project partner or project participant. The report was completed for nine countries using the contributions of the corresponding representing company (Table 1).

Table 1 Authors and countries presented in the State-of-the-art report.

Country	Author	Company
Austria	Salzmann M., Leusbrock I.	AEE - Institut für Nachhaltige Technologien
Canada	Boulter R.	CanmetENERGY - Natural Resources Canada
China	Rong L.	Beijing District Heating Group - China District Heating Association
Denmark	Sørensen P.-A.	PlanEnergi
France	Bourdon D.	CEA | The French Alternative Energies and Atomic Energy Commission
Germany	Hay S.	AGFW | Energy Efficiency Association for Heating, Cooling and CHP
Italy	Spirito G., Dénarié A., Caputo P.	Politecnico di Milano & Giannetti D., GSE, AIRU

Sweden	Lind J., Sanchéz-García L., Persson U.	HU | Halmstad University
Switzerland	Chevillat Y., Deschaintre L., Planair. Caputo P.	Politecnico di Milano. Belliardi M. SUPSI

The technology topics for factsheets (ID "F" in Table 2) and applications (ID "A" in Table 2) have been identified based on the most popular DHC development projects applying RES, and common needs raised by the project participants. Basic information on technologies was sourced using existing knowledge of RES technologies from the Danish "Technology Data Catalogue" issued by the Danish Energy Agency and IEA and European technology catalogues. The main text was developed by individual authors specialising in technology. The investment and operation cost sections were differentiated by a global region which was provided by the cost data contributor listed in Table 3. The documents have been reviewed and approved by independent readers as per the Reviewer column in Table 2.

Table 2 Authors and topics of the factsheets and applications.

ID	Topic	Author(s), PlanEnergi	Issue date	Reviewers
F1	Thermal Energy Storages	Rasmussen A. (PlanEnergi)	2022	Gunnar Ansas Guddat M. (PlanEnergi) Thomas Schmidt (Solites) Vivian J. (University of Padova) Pauschinger T. (AGFW)
F2	Geothermal Energy	Rasmussen A. (PlanEnergi)	2021	Gunnar Ansas Guddat M. (PlanEnergi) Sanchez Garzia L. (Halmstad University) Pauschinger T. (AGFW), Rasmussen A. (PlanEnergi)
F3	Solar Thermal	Borup L. (PlanEnergi)	2021	Gunnar Ansas Guddat M. (PlanEnergi) Feike F. (TU Darmstadt) Lennermo G. (Energianalys) Pauschinger T. (AGFW) Pauschinger T. (AGFW), Borup L. (PlanEnergi), Sørensen P.A. (PlanEnergi)
F4	Wind Power	Borup L. (PlanEnergi)	2021	Gunnar Ansas Guddat M. (PlanEnergi) N/A Pauschinger T. (AGFW)
F5	DH Grids	Rasmussen A. (PlanEnergi)	2021	Gunnar Ansas Guddat M. (PlanEnergi) Hay S. (AGFW) Pauschinger T. (AGFW), Rasmussen A. (PlanEnergi); Sørensen P.A. (PlanEnergi)
F6	Large Scale Heat Pumps	Komoszynska M. (PlanEnergi)	2022	Gunnar Ansas Guddat M. (PlanEnergi) Sorknaes P. (AAU) Pauschinger T. (AGFW)
7	PV	Borup L. (PlanEnergi)	2021	Gunnar Ansas Guddat M. (PlanEnergi) N/A Pauschinger T. (AGFW)
F8	Biomass Heat (HOB)	Borup L. (PlanEnergi)	2021	Gunnar Ansas Guddat M. (PlanEnergi) Salzmann M. (AEE) Ferla G. (POLIMI) Pauschinger T. (AGFW)
F9	Biomass (CHP)	Borup L. (PlanEnergi)	2021	Gunnar Ansas Guddat M. (PlanEnergi) Salzmann M. (AEE) Ferla G. (POLIMI) Pauschinger T. (AGFW)
A1	Fluctuating Energy Coupled with a Heat Pump and Seasonal Thermal Storage	Borup L. (PlanEnergi)	2021	Komoszynska M. (PlanEnergi) Schmidt T. (Solites) Vivian J. (University of Padova) Pauschinger T. (AGFW)
A2	Solar Thermal Combined with Long Term Storage	Borup L. (PlanEnergi)	2022	Komoszynska M. (PlanEnergi) Feike F. (TU Darmstadt) Lennermo G. (Energianalys) Pauschinger T. (AGFW) Pauschinger T. (AGFW), Sørensen P.A. (PlanEnergi)
A3	Excess Heat from Data Center Utilized as Heat Source for Heat Pump	Gunnar Ansas Guddat M. (PlanEnergi)	2021	Komoszynska M. (PlanEnergi) Sorknaes P. (AAU) Pauschinger T. (AGFW)
A4	Energy Management Systems / Control Systems for DHC with many Producers	Borup L. (PlanEnergi)	2021	Komoszynska M. (PlanEnergi) Hay S. (AGFW) Pauschinger T. (AGFW)

Table 3 Contributors to the cost data.

Cost data region	Contributor
Northern Europe	Denmark, PlanEnergi
Southern Europe	Italy, Politecnico di Milano
North America	Canada, CanmetENERGY - Natural Resources Canada
Asia	Korea, Seok Mann Yoon Ph.D, Korea District Heating Corp.,

3. RESULTS

3.1. State-of-the-art

The state-of-art task aims to report the transition status for the participating in the RES-DHC Annex TS5 countries in the DHC sector towards the RES technologies. This also should identify existing examples of integration of RES technologies and applications for transition. The document (Figure 2) is to elaborate on the following topics according to the existing knowledge in each country:

- ✓ The DHC history in the country.
- ✓ Political objectives.
- ✓ Status of shares of RES divided in fuels: biomass, solar thermal, heat pumps, geothermal heat, waste incineration, surplus heat from industries, etc.
- ✓ Obstacles and opportunities for RES transition.
- ✓ Status for sector coupling (power to heat, integration of electricity in the heating sector).

The key findings regarding the status and perspectives for the development of RE systems have been also summarised and compared between the individual countries. This provides a brief overview of the current situation in the energy sector and the country's position in implementing 'green' technologies in the DHC supply. The objectives, motivation techniques and encountered obstacles show a better understanding of how advanced each nationality is in realising its own goals and aims set by the international policy, such as EU climate targets to tackle climate change. Moreover, an approach for integrating sector coupling in the energy transition strategy is given, as this plays a crucial role in utilising fluctuating RE to reach carbon neutrality.

Figure 2. State-of-the-art review on RES DHC – paper cover.

3.2. Factsheets

Factsheet's structure consists of the following chapters (the front page of the published documents is shown in Figure 3):

- ✓ Technology description – a general description of the technology, types, materials, heat source, most common units, construction, efficiencies, and heat losses.
- ✓ Status of Technology Readiness Level (TRL) – technology maturity on the energy market and in application with DH systems.
- ✓ Investment and maintenance costs - price standards from Northern, Europe, Southern Europe, North America and Asia expressed in Euros (€) per installed thermal capacity (MW_{th}), heat production output (MWh) depending on

size, type, and operating temperatures.

- ✓ Regulation capacity and velocity – flexibility and time of regulating the load.
- ✓ Temperatures and capacities - operating temperatures for the heat source and heating medium, typically available size and capacity range.
- ✓ List of Suppliers – the list of the largest and most popular corresponding technology suppliers.
- ✓ Demo examples – case studies for 1-3 examples of project realisation with the discussed technology.

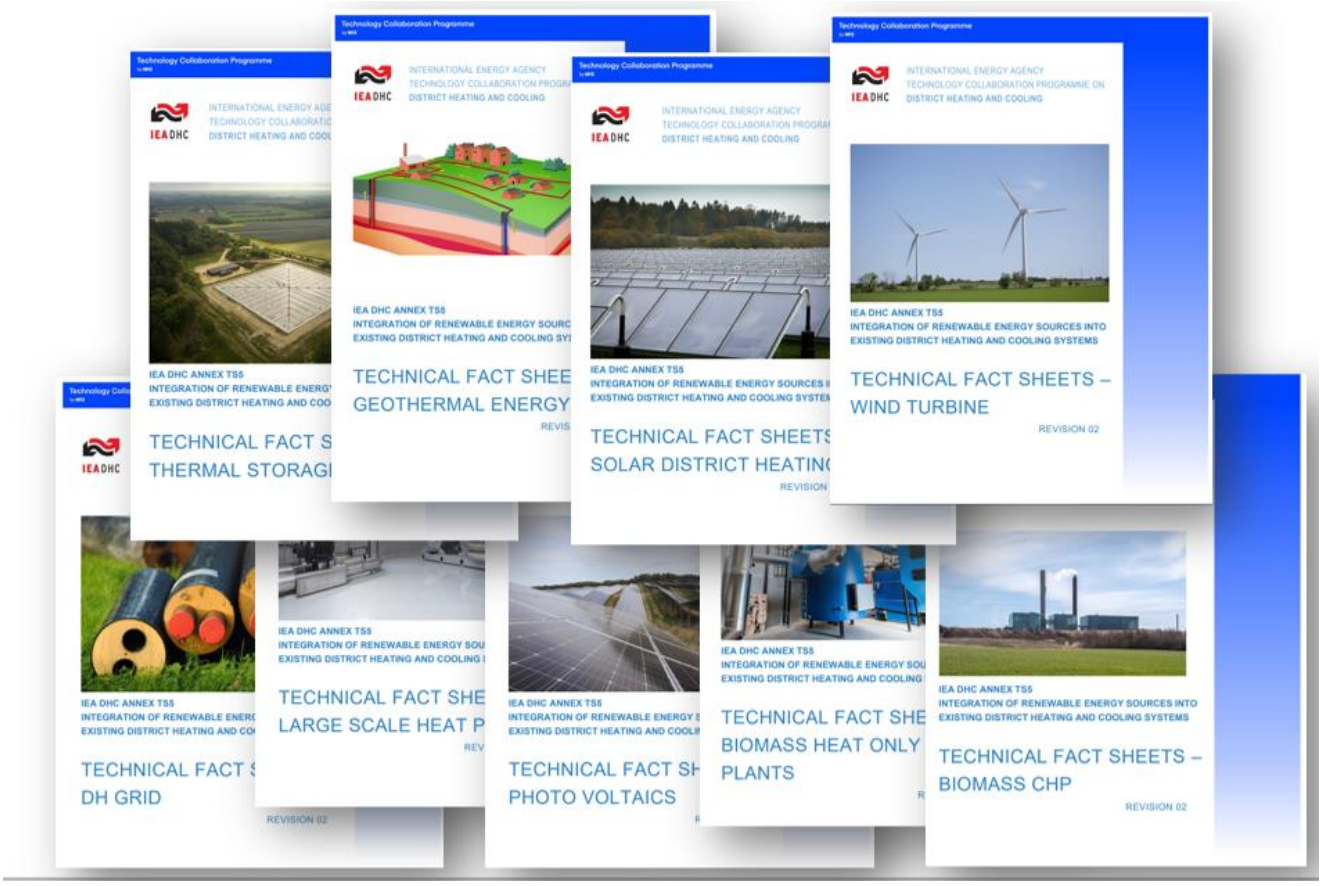

Figure 3. Factsheets – paper cover.

3.3. Applications

Application is a form of a factsheet where a system consisting of more than one RES technology is described (the front page of the published documents is shown in Figure 4). These focus on the integration, storage or management of a fluctuating energy source and its effective application in the DHC systems. The structure of the documents is similar to the standard factsheets, however, the applications are based specifically on a case study and present the main story along with key parameters and challenges of the corresponding projects.

Figure 4. Applications – paper cover.

3.4. Dissemination and future development

A combined State-of-the-art report along with nine factsheets and four applications has been issued and published on the project website [1] in January 2023. The documents are intended to be updated before the project end in 2024.

The next edition should also include new topics such as:

- ✓ High-temperature heat pumps
- ✓ Excess heat
- ✓ New fact sheet proposals

4. DISCUSSION

The documents developed in Subtask A aim to supplement the energy planning process and aid the green energy transition of the DHC systems worldwide. The format of the factsheets is concise and information references are indicated to expand knowledge and find detailed data sources. This is the first step in the unification and consolidation of base parameters for the RES technologies and requires regular updates for the factsheets to remain a value.

ACKNOWLEDGEMENT

The work on Subtask A has succeeded with the help of several engaged project partners and participants, both from the scientific and industrial sectors. The name of the authors and reviewers are indicated in **Table 1**. The State-of-the-art, factsheets and applications have been edited by the author of this paper and approved by project leader Pauschinger T. (AGFW), and task leader Sørensen P.A. (PlanEnergi).

REFERENCES

[1] IEA DHC Annex TS5 project website www: Link: https://www.iea-dhc.org/2019-2024-annex-ts5

RESEARCH ON ENERGY SAVING AND CARBON REDUCTION PATHS FOR WASTE HEAT HEATING IN INNER MONGOLIA INDUSTRIAL PARK

Yanhe Li [ab],Chunlin Wang[a*],Hao Fang[ab],Qingwei Zhao[b],Mingyu Li[a]

[a] *Chifeng University, Chifeng, 024000, China*

[b] *Inner Mongolia Fulong Heating Engineering Technology Co., LTD, Chifeng, 024000, China*

[*] *Chunlin Wang. 12404535@qq.com*

ABSTRACT

This article is guided by the goal of "energy-saving and carbon reduction path for industrial waste heat heating in Inner Mongolia Industrial Park", taking the contradiction between the production side and the heat transmission and distribution side of industrial waste heat heating as the source of the problem, and integrating existing literature and data to clarify the research progress and basic indicators related to industrial waste heat heating in Inner Mongolia. Based on the literature and yearbook combined with the actual situation of Inner Mongolia, the "Evaluation Index System for the Total Industrial Waste Heat Status in Inner Mongolia" for industrial enterprises and heating enterprises was selected and constructed Using management methods to establish a comprehensive evaluation function, it is proposed to use decision-making methods to calculate the weight of evaluation indicators, and use multiple hierarchical analysis and entropy method to analyze the characteristics of industrial waste heat heating supply and demand indicators in Inner Mongolia; Exploring the influencing factors of industrial waste heat heating from the perspective of indicator explanatory power; Finally, the design conforms to the energy-saving and carbon reduction path of industrial waste heat heating in Inner Mongolia, thereby achieving the goal of serving the reality.

Keywords: Carbon reduction; Waste heat sources; Heating system；

1. INTRODUCTION

The green development and low-carbon operation mode of industry is a common problem faced by all countries in the world. The total amount of waste heat in winter in China's process industry is 1 billion GJ, and the total amount of waste heat in winter in data centers is 600 million GJ. Industries above the provincial level contribute more than 1/2 of the industrial output and 1/3 of the carbon emissions in the country. The outline of the 14th Five-Year Plan proposes to optimize the layout of regional industrial chains, guide key links of industrial chains to stay at home, and strengthen the capacity building of central and western and northeastern regions to undertake industrial transfer. From 2001 to 2020, the share of industrial added value in the central and western regions will increase from 31.58 percent to 41.54 percent. Therefore, the integrated utilization of the total amount of industrial waste heat in Inner Mongolia is an important way to implement the national greenhouse gas emission reduction plan.

1.1FOREIGN RESEARCH PROGRESS

In terms of relevant foreign research, Kaya Yoichi believes that population and population-related measurement factors (such as per capita GDP) are the fundamental factors affecting the total carbon emissions of a country or region. This view is also accepted by most experts in China. Per capita GDP and per capita energy consumption have become the basis for carbon index calculation in most industries in China. However, there are also different views on the influencing factors of total carbon emissions in foreign countries. By collecting carbon emission data of OECD member countries from 1982 to 1997, Hamilton et al. found that the biggest factor affecting the total carbon emission was energy intensity.

In terms of field research abroad, Lu Ruixu investigated three eco-industrial parks in Kalenburg, Denmark, Kitakyushu, Japan, and Chattanooga, USA, and analyzed the utilization of circular economy to improve resource utilization and the proportion of renewable energy use in foreign countries. Skole R and others conducted research and analysis on the scale of industrial waste heat heating in Sweden, which believes that the rapid development of waste heat heating in Sweden and the extensive use of waste heat are inseparable from the government's strong support for industrial waste heat heating. Based on the international experience of studying carbon peak, Yu Li concluded that the establishment of carbon system cannot be separated from the formulation of laws and bills, the promotion of policy tools, the setting of organizations and the setting of cooperation mechanisms.

Globally, the minimum carbon emission price set by the Paris Agreement is $40 / ton. China's ferrous and non-ferrous metal exports play an important role in driving GDP. In terms of carbon emissions, considering the waste heat recovery of the metallurgical industry can reduce the energy consumption per unit GDP and reduce the total carbon emissions. With the

global rise in energy prices, countries around the world have increased investment in research and development and application of industrial waste heat recovery. Before 1975, the number of patents of "six countries and two organizations" in the field of waste heat recovery was almost zero; From 1975 to 1981, driven by some developed countries, the number of patents increased rapidly. From 1981 to 2010, this technology was still valued by all countries, and although the number of patent registrations fluctuated, it was still at a stage of steady increase. In the aspect of low temperature waste heat recovery, compared with foreign advanced industrial technology, China still has a big gap. Adding the carbon emission dimension to the traditional waste heat heating evaluation index, and analyzing the driving factors of the index, is conducive to the new technology to be discovered and paid attention to faster. The above research has well revealed the influencing factors of carbon emissions and the experience of reducing carbon emissions, and laid a good foundation for China to carry out energy saving and consumption reduction of industrial waste heat heating.

1.2 DOMESTIC RESEARCH PROGRESS

Domestic research on the path of energy saving and carbon reduction of industrial waste heat heating draws on foreign research models, which are usually analyzed from the perspective of carbon emission and industrial waste heat heating, and only analyze the evaluation methods of carbon emission of industrial enterprises, lacking industrial waste heat heating and other aspects for evaluation and analysis. Xia Jianjun et al. found by studying the path of building carbon peaking that indirect emissions related to heating heat in northern China accounted for 1/4 of building carbon emissions, while industrial waste heat in northern China will account for more than 1/5 of the total urban heating supply in the future, which is similar to the proportion of thermal power waste heat. In the middle and late period of the "13th Five-Year Plan", China's industrial energy use and carbon emissions have entered a "new cycle of growth", the energy consumption and carbon emissions of the traditional "two high" industries have not decreased but increased, and the explosive growth of emerging industries has made the rebound trend of industrial energy use and carbon emissions more and more obvious. Xu Liping et al. pointed out that Inner Mongolia not only faces the problem of improving people's living standards and rapid economic development, but also needs to achieve the goal of carbon peak in less than 10 years. Time is pressing and the task is arduous. The 14th Five-Year Plan for Circular Economy Development issued by the National Development and Reform Commission pointed out that enterprises in the park should be organized to implement cleaner production transformation; Actively utilize waste heat and pressure resources, promote the application of cogeneration, distributed energy and photovoltaic energy storage integrated system, and promote the cascade utilization of energy. Suo Chao and others suggested formulating carbon emission accounting standards and evaluation systems for industrial parks, carrying out the construction of carbon peaking demonstration industrial parks, and exploring the path of "carbon peaking and carbon neutrality" for industrial parks in line with China's national conditions. Wang Shen et al. used the multi-objective model to explore the path of low-cost carbon peaking and carbon neutrality in China, and found that the contribution of heat supply transition to carbon peaking is greater, but the feasibility of industrial transformation such as steel is low. Fei Weiliang et al. analyzed the problems faced by the collaborative promotion of pollution reduction and carbon reduction in China's industrial parks, and put forward the path of pollution reduction and carbon reduction in China's industrial parks. Yan Kun et al. built an evaluation index system for low-carbon development of industrial parks by analyzing the relationship between carbon emission accounting at different levels, such as enterprises, parks and cities. Yang Ruupu et al. studied the evaluation method of pollution reduction, carbon reduction and efficiency improvement of industrial parks by constructing the Collaborative Development index (IPSR). Yu Guangbin et al. proposed measures such as data sharing and management of pollutants and greenhouse gas emissions, and strengthening park construction, in order to improve the level of ecological civilization and build a good ecological culture. After defining and defining low-grade industrial waste heat, Fang Hao points out that urban central heating is a suitable place for the application of low-grade industrial waste heat from the perspective of "quality" and "quantity" of heat. Ouyang Zhiyuan and others made multidimensional efforts from the three levels of technology, economy and system, and made breakthroughs one by one to promote the comprehensive green and low-carbon transformation of the economic and social system. In summary, this field is mostly based on the simple quantitative analysis of industrial waste heat energy saving and carbon reduction research, and has not yet established the evaluation system of industrial waste heat heating under the dual-carbon target.

1.3 RESEARCH OBJECTIVES

Based on the climate governance issue of carbon emission reduction, taking industrial waste heat heating project as the research object, the research on carbon emission measurement in industry and heating industry is expanded. Looking at the current research status of carbon emissions in the heating industry in China, there is little attention to industrial waste heat, and most of the current research focuses more on carbon emissions in light industry and human life. In this paper, the carbon calculation method of industrial waste heat heating project and the carbon emission calculation method of the project are introduced. In the specific cases from the reference, data processing, data calculation, result verification to the conclusion were elaborated, and then according to the conclusions obtained by the specific project to improve the current project plan, finally, the design in line with the Inner Mongolia industrial waste heat heating energy saving and carbon reduction path, so as to achieve the realistic goal.

2.CARBON EMISSION CALCULATION METHOD

The basic idea of carbon emission calculation method of waste heat heating in industrial parks is to fully consider the characteristics of carbon emissions of industrial parks and heating. Based on the 2006 IPCC Guidelines for National

Greenhouse Gas Inventories, Guidelines for Calculating Greenhouse Gas Emissions Caused by Energy Consumption, General Principles for Comprehensive Energy Consumption Calculation (GB2589-81) and previous relevant studies, a set of methods for carbon emissions accounting for waste heat heating in industrial parks is formed. The method system should at least include the determination of the accounting scope, carbon emission measurement model and formula, and use the actual case to calculate and verify the method.

2.1 ACCOUNTING SCOPE

Carbon emissions of waste heat heating in industrial parks mainly include two parts: fossil energy use and power consumption. Fossil energy consumption mainly includes supplementary heating and recovery of low-temperature waste heat. Power consumption mainly includes recovery of low-temperature waste heat and waste heat heating system. The heating system going to the park and the system supplying to the city will be divided into two sets of transmission and distribution systems, and it is necessary to comprehensively calculate the carbon emissions of this part.

2.2 CALCULATION METHOD OF CARBON EMISSION

Based on the above analysis, the calculation method and formula for carbon emission of waste heat heating in industrial parks can be proposed as follows:

$$E=E1+E2+E3$$

Where, E is the total carbon emission of waste heat heating in the industrial park, and E1 is the carbon emission of low temperature waste heat; E2 is the carbon emission of supplementing fossil energy heating; E3 is the process carbon emissions generated by the waste heat heating system. The low temperature waste heat carbon emission of E1 is not calculated if there is no low temperature heat recovery technology.

$$E1=ADEJ\times EFci+ADEh\times EFcj$$

Where, ADEJ is the fossil fuel consumption of the low-temperature heat source to assist recovery, EFci is the CO2 emission coefficient of the corresponding energy combustion, ADEh is the power consumption of the low-temperature heat source to assist recovery, and EFcj is the CO2 emission coefficient of the purchased power of the corresponding region.

$$E2=ADEg\times EFci$$

Where, ADEg is the consumption of supplementary heating fossil energy, and EFci is the CO2 emission coefficient of corresponding energy combustion.

$$E3=ADEk\times EFcj$$

Where, ADEk is the power consumption of the waste heat heating system, and EFcj is the CO2 emission coefficient of the purchased power in the corresponding area.

As part of the waste heat of industrial enterprises is heated in the form of steam, this part of steam is calculated as standard coal by using the general principle of comprehensive energy consumption calculation (GB2589-81); Among them, the "heat unit, symbol and conversion" clearly stipulates that the low calorific value is equal to 29271 kilojoules (or 7000 kcal) of solid fuel, called 1 kg of standard coal. The calculation formula is as follows:

Coal consumption method for power generation: standard coal consumption = standard coal consumption for power generation × low calorific value of standard coal

The relevant table is as follows:

Table 2-1Carbon emission coefficient of direct combustion of energy

Emission coefficient of energy combustion	CO2 emission factor
Natural gas	21.84
Diesel oil	3.159
Raw coal	2.009
Pulverized coal	2.01
Coke	3.044
Coke oven gas	7.699
Blast furnace gas	9.874
Liquefied natural gas	2.889
Gasoline	2.985
kerosene	3.095

Fuel oil	3.235
Liquefied petroleum gas	3.165

Unit of CO2 emission factor: t•t -1 or t•(104 m3)-1;

Source: Climate Change 1995: Climate Change Science, IPCC Working Group I, 1996.

Table 2-2Carbon emission coefficient of regional power grid

Outsourced Power	CO2 emission factor
North China Regional Power Grid	11.232
East China Regional Power Grid	8.238
Northeast Regional Power Grid	11.716
Central China Regional Power Grid	6.887

Unit of CO2 emission factor: t•(104 kwh-)

Source: Guide to Instruments for Calculating Greenhouse Gas Emissions from Energy Consumption, World Resources Institute, 2011.

3.PRACTICAL CASE STUDIES

The steel plant is located in a county of a city in North China, with an annual output of more than 6 million tons of iron and 6.5 million tons of steel. The plant has a large amount of industrial waste heat in the production process, and the grade of this waste heat varies. This project mainly recycles industrial waste heat from two iron and steel plants. This paper takes one of them to calculate the carbon emission of heat supply project. The industrial waste heat mainly used in this steel plant is blast furnace slag water, and other high-temperature steam in other sites is used as supplementary heat to carry out peak heating in the cold period. The main heat sources are shown in the following table:

3.1 RESIDUAL HEAT PARAMETERS

Table 3-1Low temperature waste heat of the plant

Type of heat source	Recyclable residual heat	Temperature range
	/MW	/ ℃
1# blast-furnace slagging water	34.5	62/50
2# Blast-furnace slugging water	34.5	62/50
3# Blast-furnace slugging water	5	62/50
4# Blast-furnace slugging water	12.5	62/50
5# Blast-furnace slugging water	12.5	62/50
1, 2# blast-furnace wall cooling of circulating water	65	45/35
3, 4# blast furnace wall cooling circulating water	34	45/35
5# blast-furnace wall cooling circulating water	17	45/35
Sintering furnace exhaust waste heat	83.3	143
Sensible heat of sinter	61.2	110/80

Table 3-2Waste heat from high temperature in the plant

Steam source	Heat	Steam temperature	Steam pressure	Steam flow
	MW	℃	Mpa	t/h
12MW soda water heat exchange station	40	150	0.5	75
15MW soda water heat exchange station	26	150	0.5	75
Sintering waste heat boiler	18	330	1.4	70
Blast-furnace converter gas generator set	50	530	530	8.8

3.2 CALCULATION OF CARBON EMISSIONS

Calculate the total carbon emission of waste heat heating in the steel mill based on the carbon emission calculation method introduced above:

$$E2 = 4.86 * 9.874 + 6405 * 2.009 = 12916 \text{ tco}$$

In the formula, the consumption of blast furnace gas is 40000m3, and the CO2 emission coefficient is 9.874 t•(104 m3)-1. The steam consumption is equivalent to 5323tce of standard coal, and the CO2 emission coefficient is 2.009 t•t-1.

$$E3 = 840 * 11.232 = 9435 \text{ tco}$$

In the formula, the total power consumption of waste heat heating system in heating period is 1046MWh, and the CO2 emission coefficient is 11.232.

$$E=12916+9435=22351tCO2$$

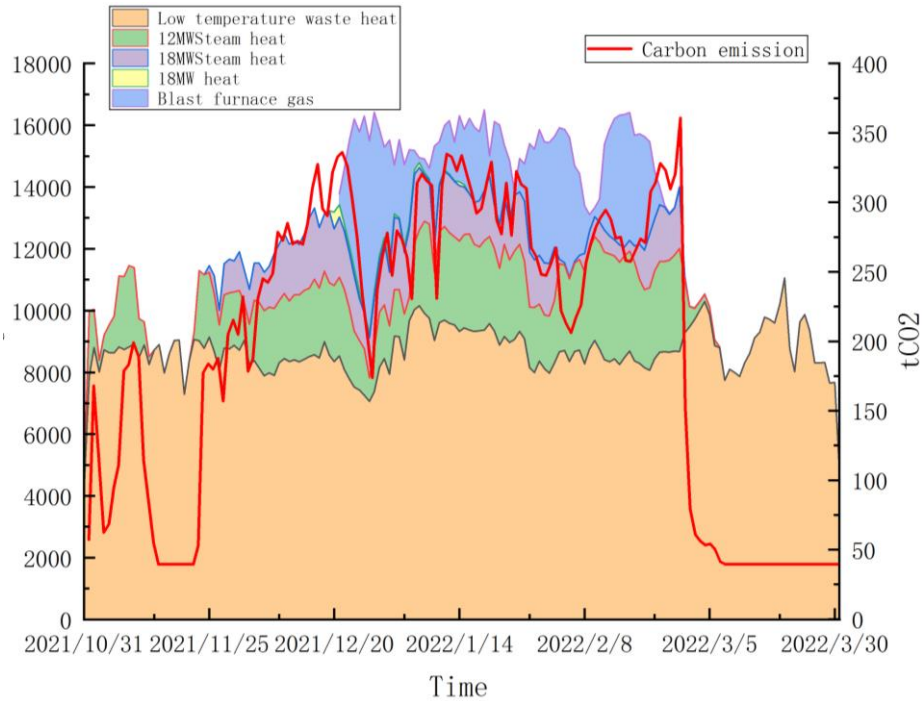

Figure 3-1 Heating accumulation diagram and carbon emission curve

The carbon emission without low temperature waste heat in the formula, the total carbon emission is 22351 tCO

From the figure above, we can see that the industrial waste heat heating in the park is mainly affected by the use of steam and less by the use of blast furnace gas, and the carbon emission is higher in the cold period due to more supplementary heat sources.

3.3 METHODS FOR REDUCING CARBON EMISSIONS FROM INDUSTRIAL WASTE HEAT UTILIZATION IN THE PARK

According to the investigation and statistics, the waste heat of industrial enterprises is mainly concentrated below 60℃, and the high temperature heat source is less. The specific situation is shown in the following table:

Table 3-3Surplus heat of different industrial enterprises

Name	Low temperature waste heat MW (below 60 ° C)	High temperature waste heat MW (above 60 ° C)
A Copper plant	267.27	102.03
B Copper Works	238.01	82.53
A Steelworks	359.5	134

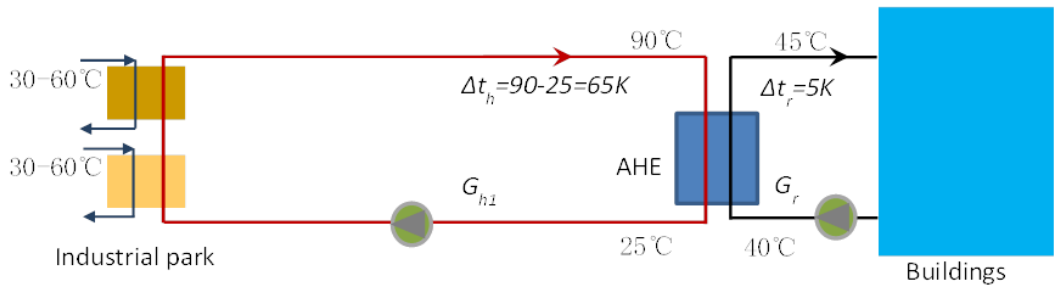

Figure 3-2 Absorption heat exchanger heating technology

In order to recover as much low-temperature waste heat as possible, absorption heat transfer technology is introduced below.

Use common heat exchanger, low temperature waste heat than: (60-45)/(90-45) = 33.3% using low temperature waste heat of absorption heat exchanger (60-25)/(90-25) = 63.6%. The recovery capacity of low temperature waste heat is 1.9 times that of ordinary heat exchangers.

4.SUMMARY

Through the analysis of specific cases, the effective measures to reduce the carbon emissions of industrial waste heat heating are obtained:

1. By reducing the use of fossil energy and the use of cleaner fuels for heating can effectively reduce the carbon emissions of supplementary fossil energy heating.

2. Combined with the use of absorption heat exchangers to reduce the return water temperature to improve the recovery ratio of low-grade waste heat, to avoid low-grade waste heat can not be fully utilized;

3. By using the absorption heat exchanger to increase the temperature difference reduces the flow rate, effectively reducing the power consumption of long-distance transmission.

According to the above suggestions on reducing carbon emissions for industrial waste heat heating, it can effectively reduce carbon emissions for our waste heat heating project to the maximum extent, so as to reduce greenhouse gas output and protect the environment, and then reveal the feasibility of saving energy and reducing carbon for industrial waste heat heating, and enrich the existing research on the path of saving energy and reducing carbon for industrial waste heat heating. To provide reference for the path of energy saving and carbon reduction of industrial waste heat heating in Inner Mongolia.

REFERENCES

[1]Jin Jing, Ma Jiping, Li Shuibao, Ji Huixiang. Research on the Carbon Emission Accounting Method System for Industrial Parks - Taking a National Industrial Park in Ningxia as an Example [A]. Yinchuan, Ningxia: Information Center of the Development and Reform Commission of the Ningxia Hui Autonomous Region, Ningxia Bairun Environmental Protection Technology Co., Ltd., 2019.

[2]Yan Kun, Lv Yizheng, Guo Yang, Tian Jinping, Chen Lujun. Research on greenhouse gas accounting methods for industrial parks [A]. Beijing: School of Environment, Tsinghua University, Tsinghua University Ecological Civilization Research Center, 2021.

[3]Zhang Yanfei, Wang Xiaofei, Yu Fei, Cui Zhaojie. Accounting Methods and Empirical Research on Carbon Emissions in Industrial Parks [A]. Jinan, Shandong: School of Environmental Science and Engineering, Shandong University, 2013.

[4]Shi Xijie, Li Xiao. Comparison and inspiration for the development of energy-saving and low-carbon buildings at home and abroad [A]. 2023.

[5]Zhang Liang. Research on Recycling Industrial Waste Heat for Central Heating [C]. Shandong: Shandong University of Architecture, 2012.

[6]Cui Ke, Ma Changming, Tan Zhiheng, Jiang Kai, Xie Ruoyi. Research on the Application of Data Center Waste Heat in Urban Heating [A]. Hangzhou: Alibaba Group, 2023.

[7]Tan Wenyi, Liu Lili, Ma Huan, Xu Yanhua. Research on PM10 Capacity Accounting Method for Industrial Parks in Jincheng City [A]. Nanjing, Jiangsu: Department of Environmental Engineering, Nanjing University of Engineering, 2008.

[8] Tian Jinping, Sangjing, Chen Yalin, Chen Lvjun. Current Situation, Challenges, and Prospects for Improving Comprehensive Energy Efficiency in Industrial Parks [A]. Beijing: School of Environment, Tsinghua University, 2022.

[9] Yang Rupu, Wang Min, Hu Jingtao, Lv Yanli, Zhao Mengxue, Li Liping, Feng Xiangzhao. Evaluation Method and Empirical Study on Synergistic Efficiency of Industrial Park Pollution Reduction and Carbon Reduction [A]. Beijing: Environmental and Economic Policy Research Center of the Ministry of Ecology and Environment, Hohhot, Inner Mongolia: Inner Mongolia Autonomous Region Ecological Environment Low Carbon Development Center, 2023.

[10] Yang Kaiyu, Mao Zhixin. Research on the Green Development Path of Industrial Parks under the Dual Carbon Goal [B]. Nanchang, Jiangxi: China Power Construction Group Jiangxi Electric Power Construction Co., Ltd., Carbon Neutrality Research Institute, 2023.

Large-scale district heating systems utilizing multi-stage electric heat pumps and heat storage to discharge data center waste heat

Yang Jing, Xiaoyun Xie*, Yi Jiang

Building Energy Research Center, Tsinghua University, Beijing 100084, People's Republic of China

* *Corresponding author. xiexiaoyun@tsinghua.edu.cn, China*

ABSTRACT

Global data center electricity consumption accounts for around 0.9-1.3% of final demand, promoting energy saving and waste heat recovery from data centers becoming important. The waste heat capacity of data centers exceeds 2 kW/m^2 and liquid-cooled data centers even exceed 10 kW/m^2, while heating load of users is only about 50 W/m^2. Characteristics of gaps in heat capacity and geographical location make district heating systems large-scale and long-distance. This paper presents a system utilizing multistage electric heat pumps and heat storage for data center waste heat heating application. Multistage heat pumps at the data center side and the user side are used to raise supplied temperature and lower returned temperature respectively, improving the efficiency of long-distance district heating. It is economical for system using reasonable heat storage only meeting the demand of peak regulation, and the recommended heat storage size is about 5% of district heating capacity. Appropriate district heating parameters and multistage heat pump settings should be selected according to the actual data center and secondary network operation. Case study shows that the total coefficient of performance (COP) of multistage heat pumps of the district heating system is 5.67, among which the COP of data center side is 8.815 and the user side is 14.1. The energy consumption of this system per heating load using recommended heat storage size is 52.15 kWh/GJ, and the initial investment per heating area of which is 63.07 CNY/m^2. The static payback period is 6.59 years considering the district heating price is 50 CNY/GJ, and this system reduces CO_2 emission of 59.06 kgCO_2/GJ and 125.16 kgCO_2/GJ compared with coal-fired and gas-fired district heating systems, respectively.

Keywords: Data center; District heating; Waste heat recovery; Heat storage; Multistage heat pump

NOMENCLATURE

Symbols	
A	transfer area (m^2)
c_{pw}	specific heat of water (kJ/(kg·K))
COP	coefficient of performance
G_w	inlet water mass flow rate (kg/s)
IT	information technology
K	heat transfer coefficient (kW/ K/m^2)
Q	heat capacity (kW)

t	temperature (℃)
T	degree kelvin (K)
ΔT	temperature difference (K)
W	power (kW)
Greek symbols	
η	efficiency
ρ	density (kg/m^3)
τ	time
Subscripts and superscript	
con	condenser
eva	evaporator
hw	heating water
in	inlet
out	outlet
w	water

1. **INTRODUCTION**

The amount of heat consumed for district heating network globally was nearly 16EJ in 2021, about 10% more than a decade earlier, which still accounted for 8% of total final heat consumption. Nearly 90% of district heat globally was produced from fossil fuels, predominantly coal (over 45%), natural gas (about 40%) and oil (3.5%), and renewables represented less than 8% of global district heat supplies.[1] Aligning with the Net Zero Emissions requires significant efforts to improve the energy efficiency of existing networks, switch them to renewable and waste heat sources (such as bioenergy, solar thermal, geothermal, and waste heat from industrial installations and data centers).

With the demand for digital services growing rapidly, energy demand from data centers accounted for 1-1.5% of global electricity use and around 300 $MtCO_2$ in 2020[2]. The waste heat temperature level of data centers varies from 10 to 60 ℃ depending on different cooling system settings such as air-cooled or liquid-cooled, which is ideal for district heating to meet the thermal comfort demand of residential and commercial buildings. Recovering data center waste heat improves energy efficiency of data centers and reduces energy consumption of district heating system.

There have been some studies of district heating system discharging data center waste heat, for instance, system design, performance analysis and new heat pump technologies. Liu et al.[3] proposed an integrated system with carbon dioxide heat pump, mechanical subcooling cycle and lithium bromide-water absorption refrigeration cycle, and the payback period of developed system is 2.04-2.46 years. Six cogeneration system with different configurations are investigated to better harvest the low-grade thermal energy in data centers, and the unit cost of district heating is 4.25 $/GJ[4]. Pan et al.[5] built an adsorption refrigeration system for solar and data center waste heat utilization. Results show that data center waste heat recovery by adsorption chiller has very short payback period and this application has greater economic potential and brighter prospect in the future than solar cooling application. Li et al.[6] introduced thermal energy storages to avoid the mismatch between data centers' heat supply and district heating systems' heat demands. The water tank could shave the peak load by 31% and save the annual energy cost by 5% with a payback period of 15 years. Feike et al.[7] developed a district heating system (60-75℃) to utilize waste heat from a high performance computer (40-45℃) via a heat pump at the Technical University of Darmstadt, and the heat pump operated very efficiently with an average COP of 5. Previous studies have

demonstrated that district heating systems recovering data center waste heat have excellent benefits in terms of energy, technical, economic and environmental analysis.

Some literatures have studied the performance of different thermal devices to improve the temperature grade of data center waste heat. Al-Sayyab et al.[8] presented a compound ejector-heat pump with low GWP refrigerants driven by photovoltaic thermal waste heat for simultaneous data center cooling and waste heat recovery for district heating network. Regarding the energy and exergy analysis, the cooling coefficient of performance enhancement ranges from 15% to 54% compared with a traditional R134a heat pump. Li et al.[9] used CO2 transcritical heat pumps to recover waste heat from data centers for district heating, which reduced energy cost by 23.0-75.0% compared with common direct electric-heating, coal-heating, gas-heating, air source heat pump, and ground source heat pump. Amiri et al.[10] proposed a techno-economic analysis of waste heat utilization in data centers applying absorption chillers, and absorption chiller system enabled saving electricity for the value of 4.34-13.025 million kWh/year for the data centers with power consumption range of 4.5-13.5 MW. In most application scenarios, there is a lack of high temperature heat drive absorption or adsorption refrigeration to recover data center from data centers for district heating, so the application of electric heat pump to raise temperature is more extensive.

The waste heat capacity of data increases rapidly with the denser installation of servers inside racks, for example, common cooling system is designed for racks with 10-15 kW and blade servers can even dissipate more than 60 kW heat[11]. The disparity between the waste heat capacity and the heat load of users promotes future data center district heating systems to be long-distance and large-scale. Meanwhile, the economics of data center district heating system are related to scales, and the medium and large scales can be considered profitable business opportunities[12]. This paper presents a large-scale district heating system utilizing multistage electric heat pumps and heat storage to discharge waste heat from data centers. Multistage heat pumps are used to raise supplied temperature and lower returned temperature respectively, improving the efficiency of long-distance district heating. Thermal storage is introduced to avoid the mismatch between data centers' heat supply and district heating systems' heat demands.

2. SYSTEM DESCRIPTION

The schematic diagram of the large-scale district heating system discharging waste heat from a single or multiple data centers is shown in Fig.1, containing mainly multistage electric heat pumps, sensible heat exchangers (SHE), heat storage (thermal reservoirs) and long-distance heating network. Returned heating water is heated stepwise to the supplied temperature on the data center side by SHE and multistage heat pumps, in the same vein, heating water is cooled to returned temperature and supplies enough heat to users. Thermal reservoirs store both hot and cold water for peak regulation of heating network and security of data centers. Large temperature difference of heating network lowers pump energy consumption and improves economy, and also increases heat capacity stored in the thermal reservoirs. In this scenario, multistage series electric heat pumps are required on both the heat source side and user side due to the large temperature difference of heating network. Multistage heat pumps outperform a single-stage heat pump in terms of combined COP because of the closer similarity between evaporation and condensation temperature in each stage.

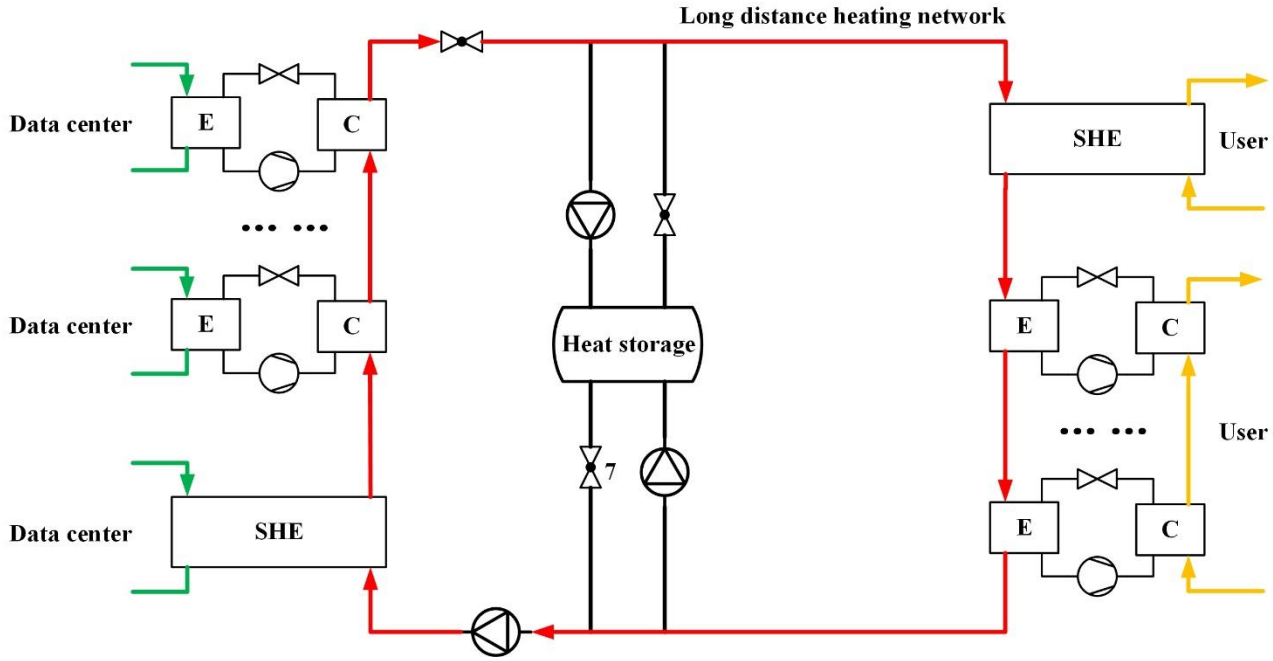

Fig. 1 Principle of large-scale district heating system recovering waste heat from data centers.

Recycled waste heat cones from a single or multiple data centers with different temperatures, which needs to be connected to the district heating system in order of temperature level. Thermal users adjust the series of multistage heat pumps at the user side according to required temperature and heating load. At the data center side, large centralized centrifugal heat pumps are applied in series, and small screw heat pumps are used at thermal user side to ensure the same returned heating water temperature. The volume of thermal storage is determined by waste heat capacity of data centers, thermal users' demand, as well as the temperature difference between supplied and returned heating water. It is also necessary to consider the form of data center cooling system, geographical conditions and the existing district heating network.

3. MODEL DEVELOPMENT AND OPERATING MODES

A mathematical model is presented to verify the technical performance of this district heating system recovering waste heat from data centers. The main equipment sub-models include electric heat pumps, sensible heat exchangers and heat storage. This section describes detailed equations and reasonable system operating modes, to simplify the simulation process, the following assumptions are also made.

(1) The system operates under steady-state flow conditions.
(2) Each component could be treated as a control volume for energy and exergy balances.
(3) The variable condition regulation of this system is ideal.
(4) The power consumption and waste heat capacity of data centers remain unchanged.
(5) The thermal efficiency of the heat storage is 100%, and there is no mixing between stored cold water and hot water.

Sensible heat exchanger adopts logarithmic mean temperature difference module, where Q_{SHE} is the transferred heat capacity of SHE. K and A represent heat transfer coefficient and area, which can be calculated by designed conditions. t_h and t_c respectively represent the hot and cold fluids on both side of the heat exchanger, the subscripts of in and out are inlet and outlet of components. The main function of SHEs is to make full use of low-temperature cooling and high-temperature heating of district heating water.

$$Q_{SHE} = KA\frac{\left(t_{h,in}-t_{c,out}\right)-\left(t_{h,out}-t_{c,in}\right)}{\ln\left[\left(t_{h,in}-t_{c,out}\right)/\left(t_{h,out}-t_{c,in}\right)\right]} \tag{1}$$

Electric heat pumps are applied to raise supplied temperature and lower returned temperature of heating water, which can efficiently improve the transmission capacity of network and reduce energy consumption of pumps. The configuration of multistage electric heat pumps can increase evaporating temperature and lower the condensing temperature, boosting energy utilization efficiency of whole system. To simplify calculation, the thermodynamic perfection model is used to coupling the relationship between temperature and energy as equation (2). Q_{con} and W represent the heat production and power consumption, $G_{w,con}$ and η are mass flow rate flowing through the condenser and the thermodynamic perfection. $T_{con,out}$ and $T_{eva,out}$ are the absolute temperature of the outlet water of the condenser and evaporator, in unit K, c_{pw} is the specific heat capacity of water and ΔT represents minimum temperature difference of heat exchangers.

$$COP = \frac{Q_{con}}{W} = \frac{G_{w,con}c_{pw}\left(t_{con,out}-t_{con,in}\right)}{W} = \eta\frac{T_{con}}{T_{con}-T_{eva}} = \eta\frac{T_{con,out}+\Delta T}{T_{con,out}-T_{eva,out}+2\Delta T} \tag{2}$$

Combining sensible heat exchanger and electric heat pump modules and energy and mass conservation law, a simple mathematic model of district heating system discharging waste heat from data centers can be established. Thermal reservoirs are used to store hot and cold water, and the volume of hot and cold water in the reservoirs need to be recorded assuming that the heat storage efficiency is 100% and there is no mixing. Equation (3) is the calculation formula of the variation of the volume of hot water stored in thermal reservoirs versus time, and equation (4) is the average heating load of thermal users.

$$V(\tau) = \frac{\int\left[\dot{Q}(\tau)-\dot{Q}_0(\tau)\right]d\tau}{\rho c_{pw}\left(t_{hw,in}-t_{hw,out}\right)} \tag{3}$$

$$Q = \int\dot{Q}(\tau)d\tau = \int k\left(t_0-t_a(\tau)\right)d\tau \tag{4}$$

Where Q and Q_0 represent heating load of thermal users and supplied heating capacity of data centers, V is the volume of hot water stored in reservoirs. ρ is the density of water, and $t_{hw,in}$ and $t_{hw,out}$ represent supplied and returned heating water temperatures. k is the average heat leakage coefficient for thermal users, expressed in W/K, t_0 and t_a represent respectively average indoor temperature of thermal users and ambient temperature.

In this paper, EES software is used to establish the steady-state model of the complex system, and the performance parameters such as heat load and power consumption of each part are calculated with one hour as the time step. Based on hypothesis 5, the model only calculates the volume of remaining hot water in the heat storage reservoir at each time point to evaluate the heat storage and the volume of the heat storage device.

According to above two equations, the variation curve of heating load in the period with district heating can be obtained as shown in Fig. 2, when the total heating capacity of network, the designed indoor temperature of thermal users and ambient temperature are known. The curve in Fig.2 is calculated based on the conditions that the total heating load per area in the period with district heating is 0.4 GJ/m^2, the average designed indoor temperature of thermal users is 24℃, and meteorological parameters of Zhangjiakou, Hebei Province in 2020-2021 are adopted.

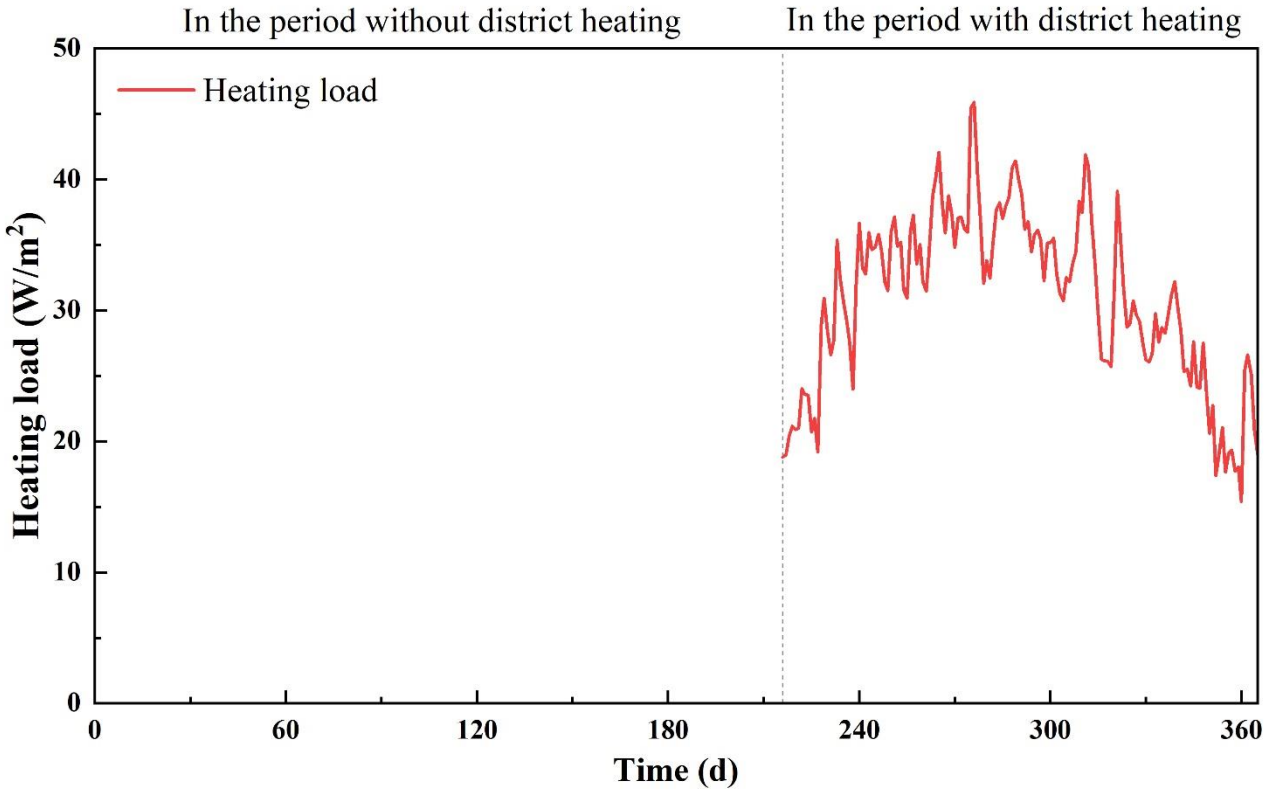

Fig. 2 Heating load per area of thermal users versus time.

Therefore, the district heating system recovering data center waste heat has different operating modes under various scales of thermal storage. This paper assumes that waste heat capacity of data centers does not change with time. When the volume of thermal reservoirs is relatively large, the waste heat capacity of data centers in the period without district heating can be stored and recovered as Fig. 3. If the thermal reservoir is small, the heat storage device can only peak regulation from early period to cold period as Fig. 4. Other operating modes all fall somewhere between above two modes, and the following district heating system all use data centers with waste heat capacity of 10MW as heat source.

Fig. 3 shows the schematic diagram of operating mode using large-scale thermal storage (System I), it can operate in three different ways throughout whole year. In the period without district heating, system uses multistage heat pumps in data centers to raise all the waste heat to supplied temperature and stores waste heat in thermal reservoirs (Mode 1). In the district heating period, both data centers and heat storage provide heat for thermal users, and the multistage heat pumps in user side lower returned temperature of heating water (Mode 2 and 3). For such a system, the operating conditions of data centers remain unchanged throughout the year, and the regulation of system only needs to control the heat storage and release. Large-scale thermal reservoirs ensure that data centers and district heating network have sufficient cold and hot water backup, greatly improving security.

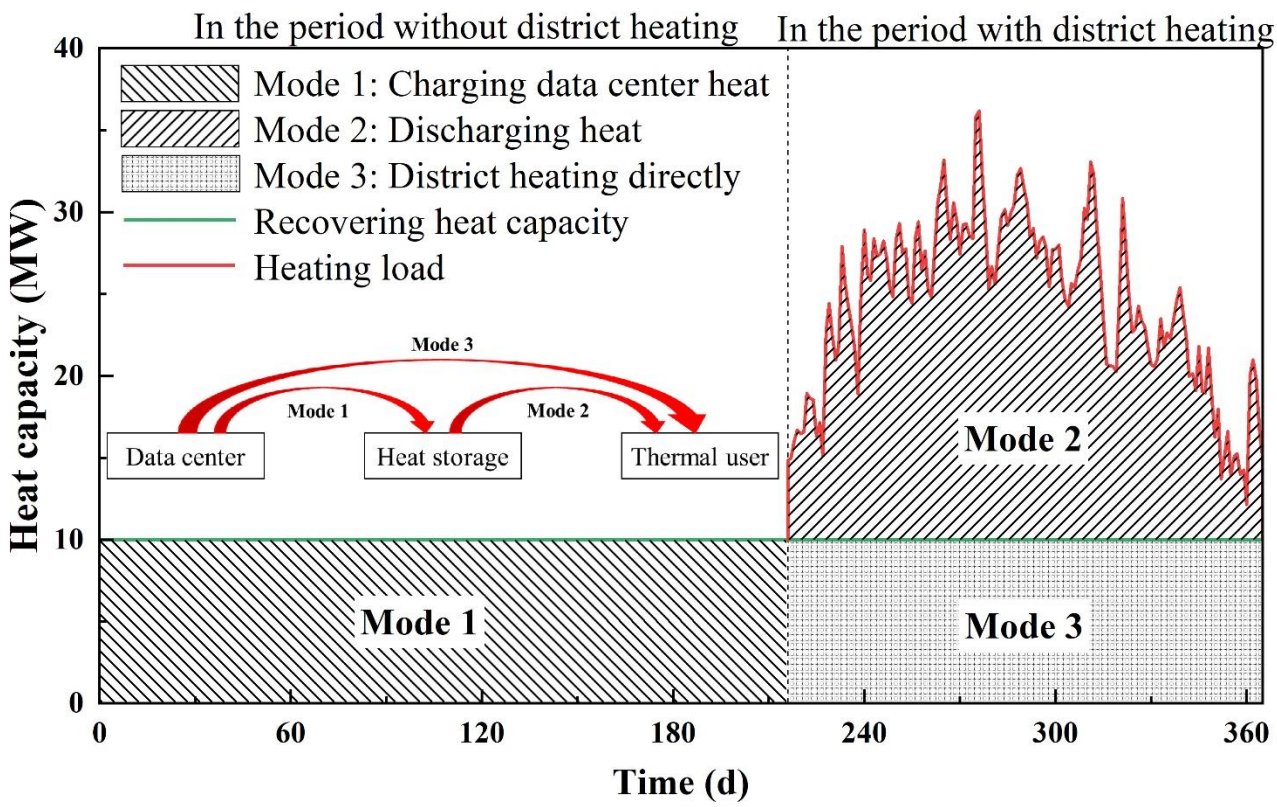

Fig. 3 Schematic diagram of operating mode of district heating system using large-scale thermal storage.

Operating modes of district heating system using small-scale thermal storage (System II) is proposed in Fig. 4, which only charges and discharges waste heat in the district heating season. Thermal reservoirs cannot store supernumerary waste heat when network does not work, this part of data center waste heat should be released to environment by evaporative cooling or other equipment (Mode 4). In early cold season, as outdoor temperature is higher and heating load us smaller, the excess waste heat of data centers will be heated and stored in thermal reservoirs (Mode 1) for harsh cold season (Mode 2). In last cold season, waste heat of data centers exceeds heating load and the excess has no value of utilization, data centers should discharge part waste heat to environment (Mode 4) and provide district heating meanwhile (Mode 3).

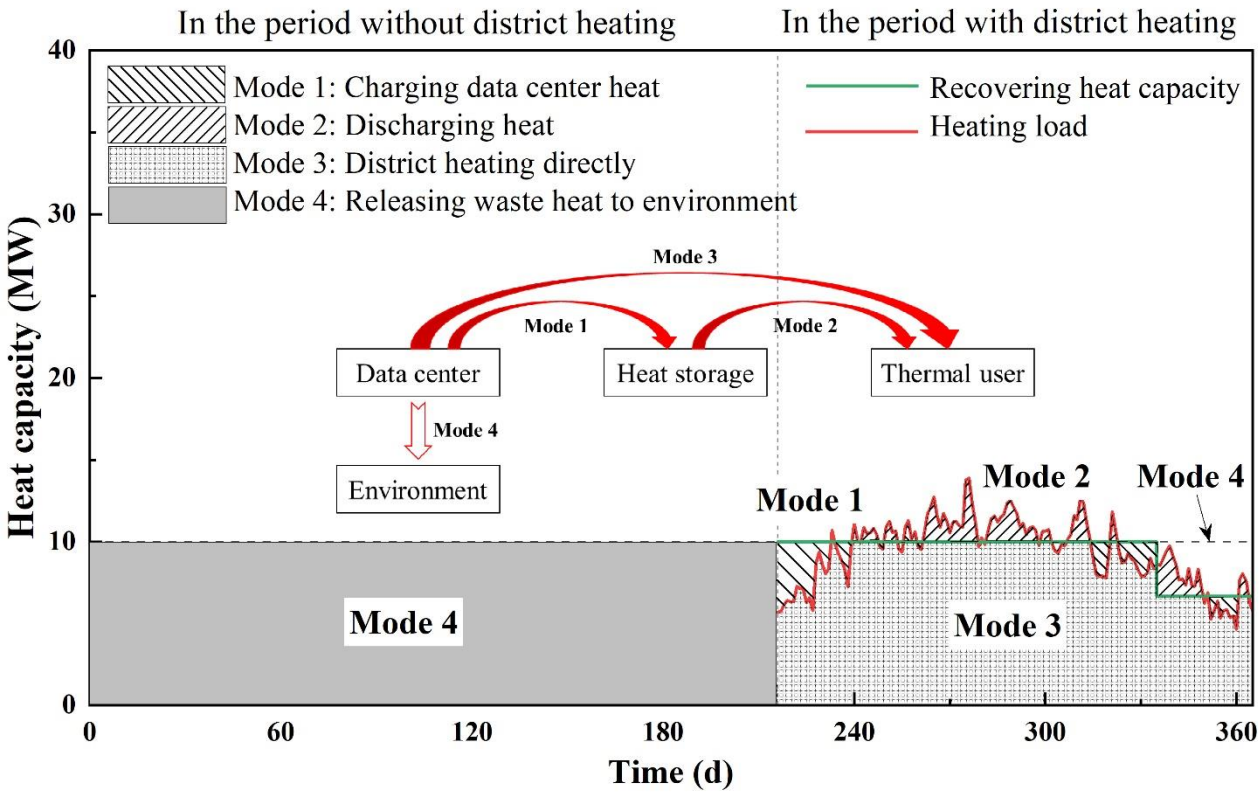

Fig. 4 Schematic diagram of operating mode of district heating system using small-scale thermal storage.

The above two operating modes cover almost all district heating systems recovering waste heat from data centers, among which System II are the most complex and these of System I are simplest. Other system forms are all related to the above two, for instance, some systems store only part of waste heat in non-district heating season, some systems discharge partial waste heat in district heating season and the volume of thermal reservoirs is smaller than system of Fig. 4, and some systems are not equipped with heat storage. Comparing the two systems, it can be found that operating modes of System I are simpler and the recovered heating capacity of data centers is larger, but System I requires more volume and expense of thermal reservoirs.

4. CASE STUDY

This section provides a case study of district heating systems to analyze the technical and economic performance of recovering waste heat from data centers. For designs of district heating network, heating load of thermal users and upper limit of supplied heating capacity are known. In this case, the selection of appropriate volume of thermal reservoirs in proposed system becomes the primary problem, considering energy efficiency and economy.

In this case study, waste heat is reclaimed from multiple data centers and supplied to thermal users, and it is assumed that chilled water temperature of data centers is 17/30℃, secondary heating water temperature of thermal users is 40/50℃, heating water temperature of network and thermal reservoirs are 15/65℃. For a 10MW data center, as the volume of thermal reservoir increases, so does the number of thermal users it can handle. When the price of thermal reservoir is 100 CNY/m^3, the initial investment of the reservoir per unit heating area is shown in Fig. 5(a). Taking technical and economic considerations into account, the recommended volume range of thermal reservoir in figure should be selected if waste heat of data centers is sufficient. In this recommended range, a less investment in thermal reservoirs can significantly increase heating area handled by a known data center. The recommended volume is about 5% of total heating load, in this situation, thermal reservoirs is only responsible for recovering waste heat from data centers in the period with district heating, carrying out peak regulation of network and ensuring the security of data centers.

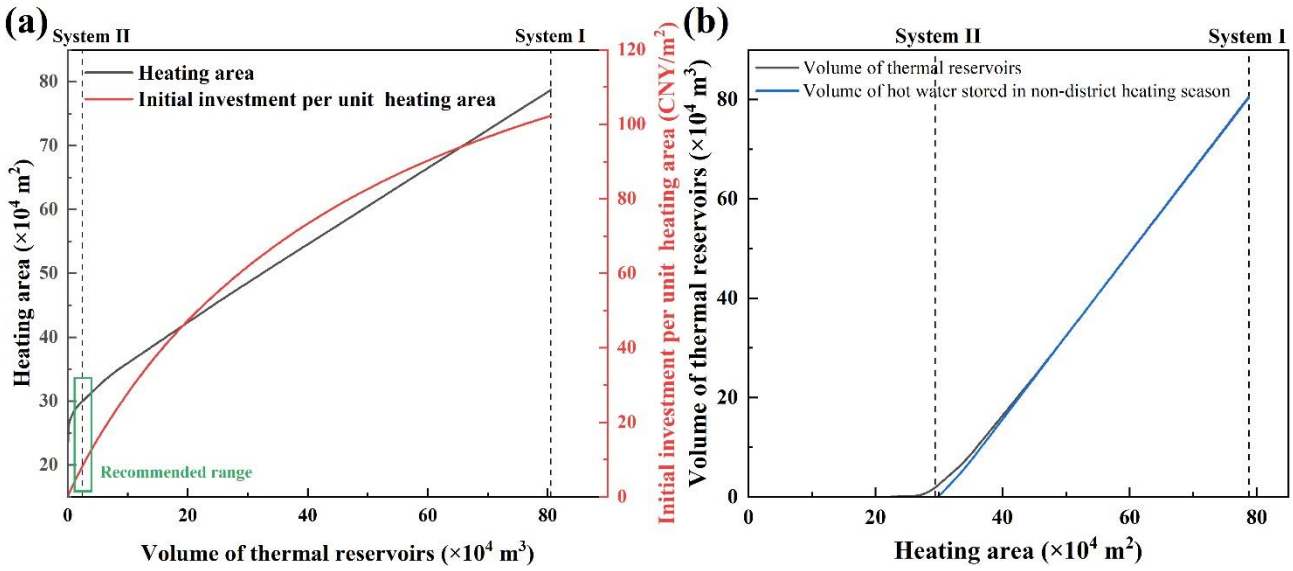

Fig. 5 The performance of various scale thermal reservoirs for a 10MW data center. (a) Heating area and initial investment; (b) Volumes of thermal reservoir and hot water stored before district heating season.

Fig. 5(b) describes volumes of thermal reservoir and hot water stored before district heating season under different scales. When heating area is relatively small (less than 22.22×10^4 m^2), which is also the most common situation in current practice, the supplied heating capacity by 10MW data centers has exceeded the maximum heating load (45.89 W/m^2) of thermal users and there is no requirement for heat storage, so the excess waste heat needs to be discharged into the environment. With the increase of heating area (22.22×10^4~29.41×10^4 m^2), the data center has been unable to match the maximum heating load and needs to build thermal reservoirs for peak regulation in the period with district heating. When the heating area is further expanded (29.41×10^4~78.74×10^4 m^2), storing heat only in district heating season has not met the demand for total heating load, so it is necessary to store waste heat in non-district heating season. In addition, the increase of thermal users promotes the increase of heating capacity stored in advance, until the heating area is 78.74×10^4 m^2, all waste heat in non-district heating season has been stored.

Based on above analysis, the volume of thermal reservoirs chosen in this case is 0.1025 m^3/m^2 and about 5.36% of total heating load, among which 45% of the volume is used for peak regulation of network and 55% of the volume is applied to ensure the security of data centers. The operating mode adopts System II in Fig. 4, which can save initial investment but adjustment of data center cooling system is more complex.

Sensible heat exchangers and 8-stage electric heat pumps work together on the data center side to recover waste heat from cooling water (17/30℃) and heat heating water from returned temperature (15℃) to supplied temperature (65℃). Similarly, sensible heat exchangers and 6-stage electric heat pumps on the thermal user side transfer heat from network (15/65℃) to secondary network (40/50℃). Multiple heat pumps consist of multiple heat pumps in series, large centralized centrifugal heat pumps and small screw heat pumps are used in the data center and thermal user side respectively.

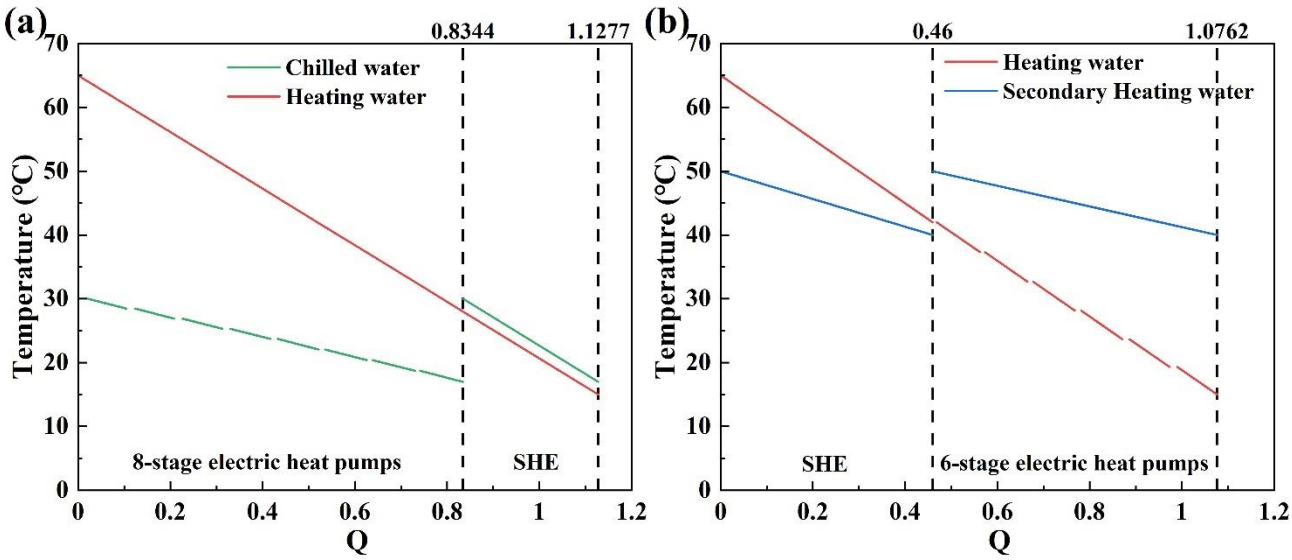

Fig. 6 Schematic of T-Q figure in data center and user side. (a) data center; (b) thermal user.

Fig. 6 shows the heat transfer process in the data center and thermal user side, including heat capacity and temperatures of each component. In the data center side, 26% of heat capacity obtained by network is transferred directly using sensible heat exchangers, and the remaining 74% needs to be raised by 8-stage electric heat pumps. Meanwhile, 42.74% of heat capacity obtained by thermal users is exchanged and 57.26% is heated in 6-stage electric heat pumps in user side.

Table 1 Technical performance of district heating system.

	Data center side		Thermal user side	
Heat capacity of SHE	26%		42.74%	
COP of multiple electric heat pump	Stage	COP	Stage	COP
	1	5.035	1	11.68
	2	5.372	2	9.879
	3	5.765	3	8.575
	4	6.23	4	7.59
	5	6.787	5	6.818
	6	7.468	6	6.199
	7	8.318		
	8	9.41		
	Average	6.523	Average	8.074
Combined COP of SHE and multiple heat pumps	8.815		14.1	
Total COP	5.67			

Table 1 shows the technical and energy performance of the proposed case study, and the total COP of whole district system is 5.67 without considering the energy consumption of pumps and thermal reservoirs. Average COPs of multiple electric heat pumps in data center and thermal user side are 6.523 and 8.074 respectively, and combined COPs of SHE and heat pumps are 8.815 and 14.1.

In this case, four data centers with a total IT power consumption of 245MW are planned to provide heat for the surrounding communities with a total heating area of 8.18 million m^2 and a total rated heating load of 338.29MW. The designed volume of thermal reservoirs is 838.1 thousand m^3, and Table 2 and Table 3 show initial investment and energy consumption of proposed system, gas-fired and coal-fired system. Prices of electric heat pumps, sensible heat exchangers, thermal reservoirs,

gas-fired and coal-fired boilers are 0.5 CNY/W, 800 CNY per heat transfer area, 100 CNY/m^3, 0.3 CNY/W and 0.2 CNY/W. On the basis of the above prices, the installation cost of each component should be considered at 15% of the initial investment. It is assumed that energy prices of electricity, gas and coal are 0.5 CNY/kWh, 2.5 CNY/m^3 and 1 CNY/kg, and the price supplied to thermal users is 50 CNY/GJ.

Table 2 Economic performance of district heating system.

Investment	Proposed system	Gas-fired system	Coal-fire system
Network (million CNY)	121.95	121.95	121.95
Pump (million CNY)	10.26	10.26	10.26
User side (million CNY)	163.77	12.88	12.88
Data center (million CNY)	123.61	0	0
Boiler (million CNY)	0	115.06	70.71
Heat storage (million CNY)	96.33	0	0
Total (million CNY)	515.92	260.15	215.8
Average (CNY/m^2)	63.07	31.8	26.38

Table 3 Energy consumption of district heating system

Energy consumption	Proposed system	Gas-fired system	Coal-fire system
Pump (kWh/GJ)	1	1	1
User side (kWh/GJ)	22.06	0	0
Data center side (kWh/GJ)	28.74	0	0
Heat storage	0.35	0	0
Boiler	0	31.25 m^3 gas/GJ	47.77 kg coal/GJ
Operating cost (CNY/GJ)	26.08	78.63	48.27
CO_2 emission (kg/GJ)	0	59.06	125.16
Static payback period	6.59 years	/	38.14 years

The expensiveness of electric heat pumps and thermal reservoirs make the total initial investment of proposed system highest than that of gas-fired and coal-fired boilers, and average investments are 63.07 CNY/m^2, 31.8 CNY/m^2 and 26.38 CNY/m^2. The operating energy consumption of above three district heating system is 52.15 kWh/GJ, 1 kWh/GJ+31.25 m^3 gas/GJ and 1 kWh/GJ+47.77 kg coal/GJ, and the operating cost is 26.08 CNY/GJ, 78.63 CNY/GJ and 48.27 CNY/GJ, respectively. When the price of district heating obtained by thermal users is 50 CNY/GJ, static payback periods of proposed system and coal-fired system are 6.59 years and 38.14 years, and the gas-fired system cannot recover the initial investment. This system reduces CO_2 emission of 59.06 kgCO_2/GJ and 125.16 kgCO_2/GJ compared with gas-fired and coal-fired district heating systems when all electricity is generated from renewable energy in future, respectively. The existence of thermal reservoirs can better embrace unstable renewable energy electricity.

The proposed district heating system recovering waste heat from data centers utilizing multi-stage electric heat pumps and thermal storage is more efficient, environmentally friendly and less expensive to operate, however, has a higher initial investment in electric heat pumps and heat storage. The energetic performance of proposed system is definitely better than gas-fired and coal-fired system, but its economics are heavily influenced by the price of various energy and equipment. The instability of data center waste heat capacity, the large-volume heat storage technology and the operating regulation of multistage heat pumps are the main obstacles to the application of the data center district heating system.

5. CONCLUSION

This work presents a large-scale district heating system discharging waste heat from data centers, and the energetic and economic analysis of which utilizing multi-stage electric heat pumps and various scales heat storage are evaluated. Main conclusions are summarized as below:

(1) The data center district heating system with peak regulation using heat storage is more efficient, environmentally friendly and less expensive to operate, but has a higher investment in multistage VCR heat pumps and heat storage units. It is economical for system using small-scale heat storage only meeting the demand of peak regulation, and the recommended heat storage size is 5.36% of heating load.

(2) The energy consumption of proposed system using recommended heat storage size is 52.15 kWh/GJ, and the initial investment per heating area of which is 63.07 CNY/m^2 with a static payback period of 6.59 years.

ACKNOWLEDGEMENT

The authors gratefully acknowledge the support from National key research and development program of China (key projects of international cooperation in science and technology innovation) (Grant number 2019YFE0102700).

REFERENCES

[1]. Delmastro, C., District Heating. 2021, IEA.
[2]. IEA, Data Centres and Data Transmission Networks. 2022, IEA: Paris.
[3]. Lin, X., et al., An idea to efficiently recover the waste heat of Data Centers by constructing an integrated system with carbon dioxide heat pump, mechanical subcooling cycle and lithium bromide-water absorption refrigeration cycle. Energy Conversion and Management, 2022. 256: p. 115398.
[4]. Chen, X., et al., Multi-mode operation and thermo-economic analyses of combined cooling and power systems for recovering waste heat from data centers. Energy Conversion and Management, 2022. 266: p. 115820.
[5]. Pan, Q., J. Peng and R. Wang, Application analysis of adsorption refrigeration system for solar and data center waste heat utilization. Energy Conversion and Management, 2021. 228: p. 113564.
[6]. Li, H., et al., Energy, economic, and environmental analysis of integration of thermal energy storage into district heating systems using waste heat from data centres. Energy, 2021. 219: p. 119582.
[7]. Feike, F., et al., Evaluation of the waste heat utilization from a hot-water-cooled high performance computer via a heat pump. Energy Reports, 2021. 7: p. 70-78.
[8]. Al-Sayyab, A.K.S., J. Navarro-Esbrí and A. Mota-Babiloni, Energy, exergy, and environmental (3E) analysis of a compound ejector-heat pump with low GWP refrigerants for simultaneous data center cooling and district heating. International Journal of Refrigeration, 2022. 133: p. 61-72.
[9]. Li, J., et al., Optimal schemes and benefits of recovering waste heat from data center for district heating by CO2 transcritical heat pumps. Energy Conversion and Management, 2021. 245: p. 114591.
[10]. Amiri, L., et al., Techno-Economic Analysis of Waste Heat Utilization in Data Centers: Application of Absorption Chiller Systems. Energies, 2021. 14(9): p. 2433.
[11]. Habibi Khalaj, A. and S.K. Halgamuge, A Review on efficient thermal management of air- and liquid-cooled data centers: From chip to the cooling system. Applied Energy, 2017. 205: p. 1165-1188.
[12]. Pärssinen, M., et al., Waste heat from data centers: An investment analysis. Sustainable Cities and Society, 2019. 44: p. 428-444.7

The 18th International Symposium on District Heating and Cooling,
September 3-6, 2023, Beijing, China

THERMOECONOMIC ANALYSIS OF COKING WASTE HEAT DISTRICT HEATING AND COOLING BASED ON MULTIPLE HETEROGENEOUS HEAT FLOWS RECONFIGURATION

Fangtian Sun[a*], Xiaoqing Zhao[a], Yali Zhang[a], Rui Li[a]

[a] *Beijing University of Civil Engineering and Architecture, Beijing, 100044, China*
[*] *Corresponding author. sunfangtian@bucea.edu.cn*

ABSTRACT

Annual coke production of the coking plants in Northern China accounts for about 47% of China's annual total coke production. There is a great deal of waste heat characterized by wide temperature range and multiple heat flows in the coking plant. Recovering coking waste heat for space heating and cooling contributes to achieving goals of carbon emission peak and carbon neutrality. However, conventional coking waste heat recovery methods results in greater irreversible loss and lower ratio of waste heat utilization. To efficiently recover low temperature coking waste heat, a novel coking waste heat district heating and cooling system based on multiple heterogeneous heat flows reconfiguration is proposed and analyzed from the perspective of thermodynamics and economics. Results show that waste heat utilization ratio, annual system coefficient of performance, and annual product exergy efficiency are about 65.1%, 7.56 and 30.3%, respectively for the proposed coking waste heat district heating and cooling system with waste heat transportation distance at 30 kilometers. Compared with the conventional heating and cooling systems, the proposed district heating and cooling system can save natural gas by 23.3 Nm^3 by utilizing waste heat of one-ton coke production, and its potential of carbon emission reduction by 95.4%.

Keywords: District heating and cooling; Coking waste heat recovery; Waste heat flows reconfiguration; Waste heat utilization ratio; Annual product exergy efficiency; Payback period

1. INTRODUCTION

The amount of China's coking production is the largest in the world, and amount of coking production in Northern China is about 47% of the total production amount [1]. The coking process discharges a great deal of waste heat, which is featured by weak viscosity, strong corrosiveness, multiple heat fluxes and large temperature difference among different type waste heat flux. The waste heat distribution of coking process is illustrated in Fig.1.

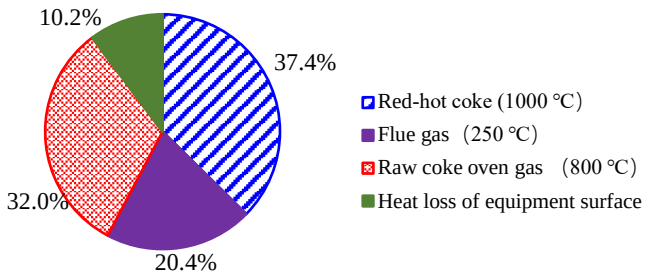

Fig.1. Waste heat distribution of coking process

Recovering coking waste heat for district heating and cooling contributes to achieving the goal of carbon peak emissions and carbon neutrality [2]. For waste heat of the red-hot coke, dry quenching technology is adopted for waste-heat power generation [3]. With regard to raw coke oven gas, the heat pipe heat exchanger is currently used for generating high-pressure steam [4]. As for waste heat of flue gas, coal moisture control technology is usually taken [5]. Besides, For the conventional methods of coking waste heat recovery, there are larger loss in the process of waste heat utilization and smaller efficiency of waste heat, and a great deal of low-temperature waste heat is discharged into ambient atmosphere [6]-[7]. By using the existing technologies of coking waste heat recovery, distribution of waste heat flux in temperature and quantity for the coking process is shown in Fig.2.

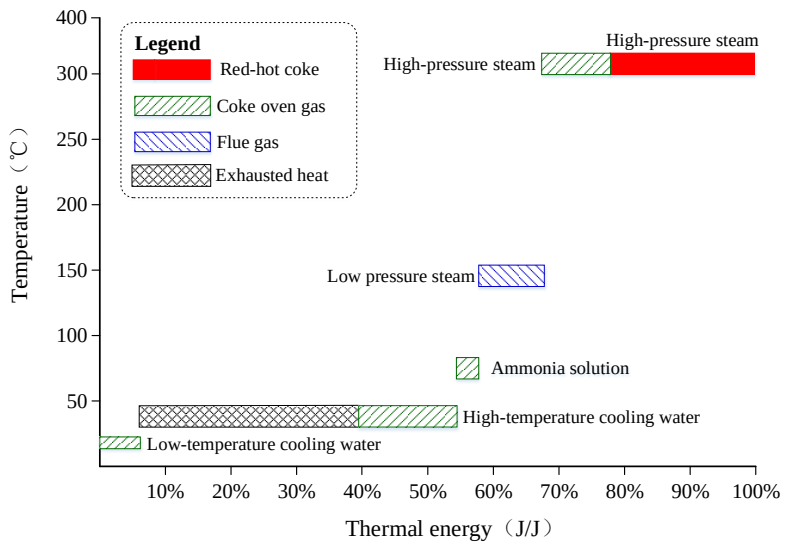

Fig.2. Distribution of waste heat flux in temperature and quantity for current coking process

In addition, the coking plant is generally situated far away from the center of end-consumers because of great emission of atmospheric pollutants. The long distance for transporting waste heat would result in large investment capital of the primary network and high electricity consumption of circulating water pumps for the primary network. Thus, the economic distance for transporting waste heat has become the key to the development of coking waste heat recovery and utilization. To solve the problem, F.T Sun et al [8] proposed a new high-temperature district heating and cooling system for recovering waste heat of flue gas in a coking plant. In the energy station of the proposed district heating and cooling system, the absorption heat exchangers [9]-[10] are adopted to enlarge temperature difference between supply and return of the primary network for longer economic waste heat transportation distance. However, other type waste heat does not be considered, especially for low temperature waste heat in cooling water.

To efficiently recover and utilize waste heat of the coking process, a new coking waste heat district heating and cooling system based on multiple heterogeneous heat flows reconfiguration is put forward according to the principle of energy cascade utilization.

2. OPERATIONAL PRINCIPLE OF THE PROPOSED DISTRICT AND COOLING SYSTEM

The proposed district heating and cooling system is designed by principle of heating as the main object and cooling as the auxiliary object. During a cooling period, cold energy from the proposed district heating and cooling system only provides for the public buildings with high density cooling load. Sketch of the proposed district heating and cooling system is shown in Fig.3.

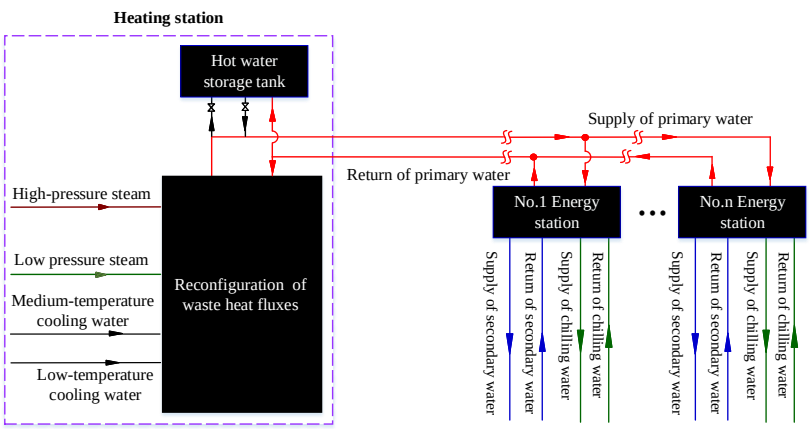

Fig.3. Sketch of the proposed district heating and cooling system

2.1. Heating station

The heating station subsystem consists of the waste heat fluxes reconfiguration system and a hot water storage tank, and its sketch is illustrated in Fig.4.

During the heating period, waste of the low-temperature cooling water is upgraded to 40 ℃, and converged with both waste

heat of high-temperature cooling water and waste heat from the condenser. The low temperature waste heat about 40 ℃ is split into four parts. The water-to-water heat exchanger -1 is used to recover one part of low temperature waste heat, and heat return water of the primary network. The double-effect absorption heat pump -2 is used to recover another part of low temperature waste heat, and heat circulating water in the primary network from the heat exchanger- 1. The single-effect absorption heat pump is used to the third part of low temperature waste heat, and heat the circulating water in the primary network. The fourth part comes into the cooling water, and discharge low temperature waste heat. The heated circulating water in the primary network from the single-effect absorption heat pump flows into heat exchanger -2 and -3, and is heated by medium temperature hot water from red-hot coke and flue gas, and low-pressure steam, respectively. Finally, the heated circulating water in the primary network from the heat exchanger -3 is severed as supply water of the primary network. The hot water storage tank is used to take in surplus waste heat and discharge heat to cover the regulating demand of heat load. With the decrease of heat load demand, the heat exchanger-3 and -2 get out of operation step by step.

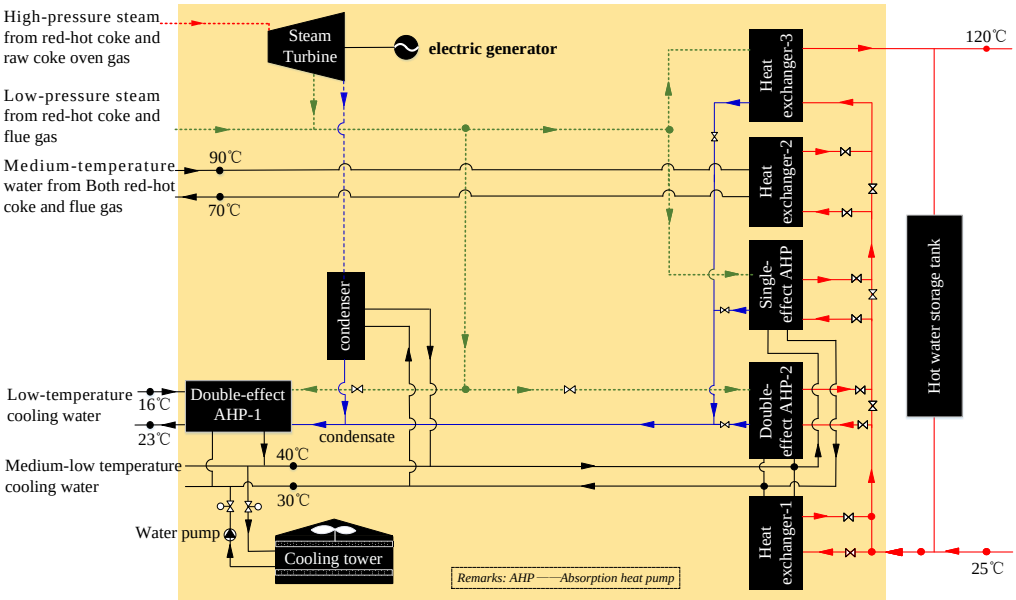

Fig.4. Sketch of heating station subsystem based on multiple heterogeneous heat flows reconfiguration

During the transitional period, the hot water storage tank is used to store high-temperature within the range from 70 ℃ to 120 ℃.

During the cooling period, the heat exchanger -1, double-effect absorption heat pump -2 and single-effect absorption heat pump are shut off, and hot water storage tank, the heat exchanger -2 and -3 are put into operation. With the increase of the cooling load demand, the heat exchanger -2 and -3 would be put into operation.

2.2. Energy station

The energy station subsystem mainly comprises a single-effect absorption heat pump, a heat exchanger, an ice thermal energy storage tank, a cooling tower and two electric compression chillers, and its sketch is shown in Fig.5.

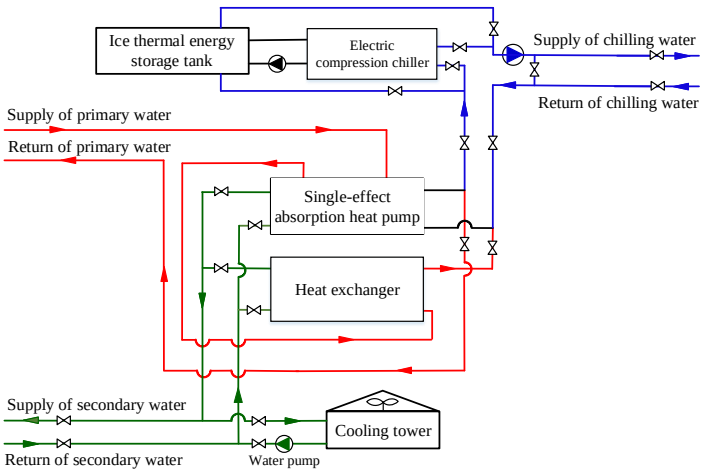

Fig.5. Sketch of the energy station subsystem

During the heating period, the single-effect absorption heat pump is coupled with the heat exchanger for transmitting heat from the circulating water in the primary network to that of the secondary network, and lower the temperature of the return water for the primary network to 25 ℃, which is much lower than that of the secondary network. It is emphasized that the ice thermal energy storage tank and two electric compression chiller are shut off during the whole heating period.

During the cooling period, the single-effect absorption heat pump is decoupled with the heat exchanger, and works together with other equipment. In the day time, with the increase of the cold load, the ice thermal energy storage tank would be put into operation in turn. At night, the electric compression chiller is opened for generating ice thermal energy. It needs to be pointed out that the single-effect absorption heat pump works day and night, and the chilling water of the single-effect absorption heat pump severs as cooling water of the electric compression chiller, which has smaller pressure ratio of outlet pressure of refrigerant to inlet pressure of refrigerant for the compressor. Thus coefficient of performance of electric compression chiller located in the energy station is big.

It needs to emphasized that the operation modes of the primary network, secondary network and chilling water network adopt the mode of constant mass flow rate.

3. ANALYSIS OF CASE

3.1 Main information of case

The case located in the northern China, and its heat load and cooling load are 67,350 kW and 37,647 kW. The studied coking plant can produce coke by 1000,000 tons per year, and the distance between the coking plant and the center of end-consumers is 30 kilometers. The prices of cold energy, thermal energy, electricity and waste heat are 0.74 ¥/kWh, 30 ¥/kWh, 0.7405 ¥/kWh and 0.054 ¥/kWh. The annual interest of bank is 4.8%.

The main thermal parameters of the proposed district heating and cooling system are listed into Table 1.

Table 1. Main parameters of the proposed district heating and cooling system

Subsystem	Equipment	Inlet / Outlet temperature for PN (℃)		Capacity (kW)		COP (W/W)	
		Space heating	Space cooling	Space heating	Space cooling	Space heating	Space cooling
Heating station	Heat exchanger-1	25 / 37	——	8,356	——	——	
	Double-effect AHP-2	37 / 55	——	12,523	——	1.375	——
	Single-effect AHP	55 / 65	——	6,959	——	0.880	——
	Heat exchanger-2	65 / 80	65 / 80	10,670	10,670	——	
	Heat exchanger-3	80 / 120	85 / 120	27,856	27,856	——	
	Double-effect AHP-1	——		13,244		1.476	
	Condenser	——		3,826		——	
	Electricity generator	——		2,861		——	
	Cooling tower	——		9844	29515	——	
	Hot water storage tank	——		768,000 m^3		——	
Energy station	Single-effect AHP	120 / 25	120 / 65	32,185	21,170	0.789	0.738
	Heat exchanger	94.7 / 45	——	35,165	——	——	
	Electric compression chiller	——	12 / 7	——	7906	——	8.520
	Cooling tower	——	37 / 32	——	8197	——	
	Ice thermal energy storage tank	——	7 / 3	——	10855 m^3	——	

Remarks: PN—primary network

3.2 Thermodynamic performance

With the increase of the demand of heat or cold load, the system coefficient of performance would vary to a certain extent, and the system coefficient of performance for space heating is significantly different from that for space cooling. Besides, exergy efficiency is generally used to evaluate energy conversion and transfer process [11]. Therefore, the proposed district heating and cooling system should be assessed from the aspect of one year, and annual system coefficient of performance

and annual product exergy efficiency are presented.

Annual system coefficient of performance (ASCOP) is defined as the ratio of output load to electricity consumption for one year, and it is computed as follows:

$$ASCOP = \frac{\int q_h d\tau + \int q_c d\tau}{\int q_e d\tau} \quad (1)$$

Annual system product exergy efficiency (ASPEE) is defined as the ratio of output exergy for the secondary network and chilling network to input exergy for one year, and it is calculated as follows:

$$ASPEE = \frac{\int Ex_{h,out} d\tau + \int Ex_{c,out} d\tau}{\int Ex_{in} d\tau} \quad (2)$$

The proposed district heating and cooling system is compared with the conventional heating and cooling systems [8], and their ASCOPs and ASPEEs are shown in Fig.6.

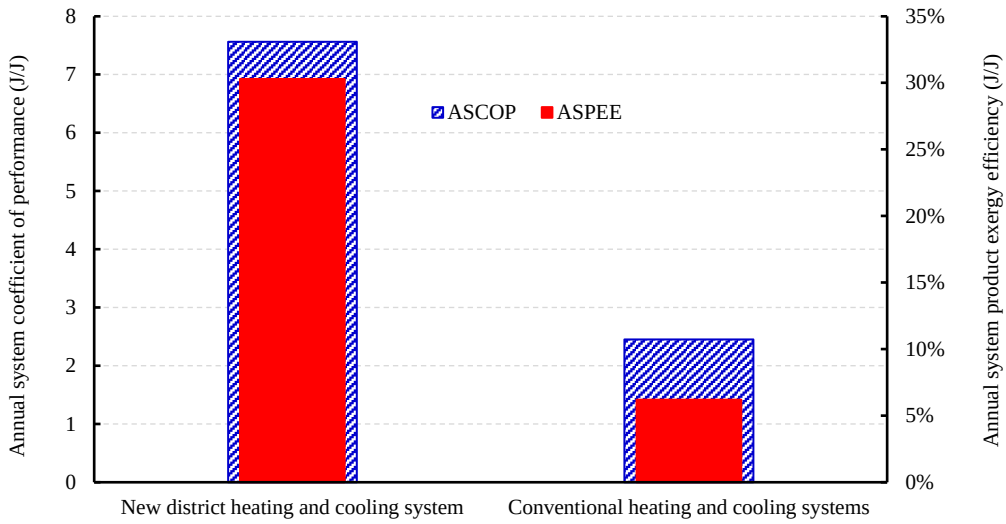

Fig.6. ASCOP and ASPEE of two type heating and cooling systems

As can be seen from the Fig.6 that ASCOP of the proposed district heating and cooling system is about 3.1 times of that of the conventional heating and cooling systems. It is caused by the fact that the proposed district heating and cooling system could recover a great deal of coking waste heat for saving natural gas and electricity. Besides, ASPEE of the proposed district heating and cooling system is larger 24.1% than that of the conventional heating and cooling systems. For the proposed district heating and cooling system, waste heat utilization ratio is about 65.1% during a year, and recovering waste heat of one ton of coke production would save natural gas by about 23.3 Nm^3.

Thus, compared with the conventional heating and cooling systems, the proposed district heating and cooling system has a more advanced energy conversion and transfer process.

3.3 Economic benefit

The first costs of equipment are computed according to average value of current market price for the same equipment, and other cost are calculated according to China's current investment estimation in public works [12]. The initial investment capital of the proposed district heating and cooling system is given in Table 2.

Table 2. Initial investment capital of the proposed district heating and cooling system

Subsystem	Item			
	Equipment cost (¥)	Construction cost (¥)	Installment cost (¥)	Other cost (¥)
Heating station	681,190,000	102,180,000	136,240,000	102,180,000
Primary network	17,610,000	38,040,000	3,520,000	2,640,000
Energy station	67,740,000	10,160,000	13,550,000	10,160,000

Compared with the conventional heating and cooling systems, the proposed district heating and cooling system has larger initial investment capital, which would have an impact on the economic benefit of the proposed district heating and cooling system. Investment recovery period is an indicator of economic benefit, and it is usually used to assess feasibility of the district heating and cooling systems.

At present, considering great reduction potential of carbon emission-reduction, China's central and local government generally provide an extra financial subsidy for construction of the low-carbon district heating and cooling system. The relationships between subsidy ratio and investment recovery period are exhibited in Fig.7.

Fig.7 shows that investment recovery period becomes shorter with the increase of financial subsidy ratio. As for benchmark of investment recovery period in the section of district heating at 10 years, the fair financial subsidy ratio is about 31.5% for the proposed district heating and cooling system. Compared with investment recovery period of the conventional heating and cooling systems at about 8.5 years, the proposed district heating and cooling system has longer investment recovery period, but its potentials of energy-saving and emission-reduction are greater.

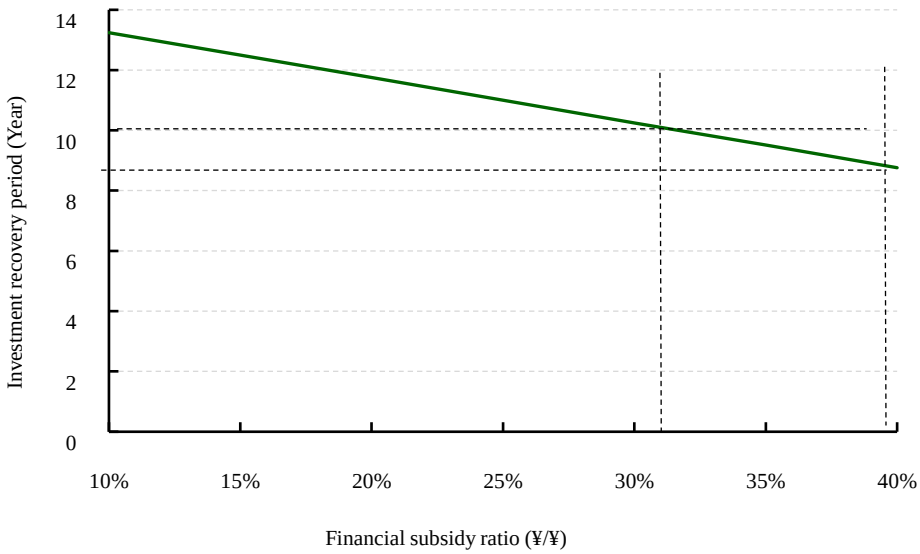

Fig.7. variation curve of investment recovery period with the rising of subsidy ratio

4. CONCLUSION

The proposed district heating and cooling system is analyzed from the perspectives of thermodynamics and economics, some important conclusions are made as follows:

(1) Reconfiguring the multiple heterogeneous waste heat flows contributes to decreasing irreversible loss and increasing waste heat utilization rate for low carbon district heating and cooling.

(2) For the proposed district heating and cooling system with waste heat transportation distance at 30 kilometers, annual system coefficient of performance, annual system product exergy efficiency, and annual waste heat utilization rate are 7.56, 30.3, and 65.1%, respectively.

(3) The proposed district heating and cooling system has large initial investment capital, and it subsidy at is helpful to encourage development of the coking waste heat district heating and cooling.

ACKNOWLEDGEMENTS

The authors acknowledge the financial support from both Beijing Natural Science Foundation (3222027).

REFERENCE

[1] Energy Statistics Department of the Bureau of Statistics of the People's Republic of China. China Energy Statistics Yearbook 2021. Beijing: China Statistical Publishing House, 2022.
[2] State Council of the People's Republic of China. Notice on the Action Plan for Carbon Peak before 2030, October 21, 202 (in Chinese). https://www.gov.cn/zhengce/content/2021-10/26/content_5644984.htm
[3] Kai Sun, Chen-Ting Tseng, David Shan-Hill Wong, Shyan-Shu Shieh, Shi-Shang Jang, Jia-Lin Kang, Wei-Dong Hsieh. Model predictive control for improving waste heat recovery in coke dry quenching processes. Energy, 2015, 80: 275-283.
[4] Shaojie Zhang. Pilot study on ascension-pipe heat exchanger used for waste heat recovery of coke oven gas. Energy Procedia, 2019,158:26-31.
[5] MATZ, JIANG Z Y. Heat pipe research and development in China. Tsukuba, Japan: Proc. Int. Heat Pipe Conf., 2002: 128-432.

[6] YIN Hengyu, FAN Junjie, DENG Jiaxiao, DU Meifang, CHEN Shixuan. Analysis and optimization of waste heat recovery system in coke oven. Chemical Industry and Engineering progress, 2020, 39(03): 1181-1186.
[7] Shiyue Qin, Shiyan Chang. Modeling, thermodynamic and techno-economic analysis of coke production process with waste heat recovery. Energy, 2017,141: 435-450.
[8] Fangtian Sun, Junlong Li, Lin Fu, Yonghong Li, Ruixiang Wang, Shigang Zhang. New configurations of district heating and cooling system based on absorption and compression chillers driven by waste heat of flue gas from coke ovens. Energy, 2020, 193:116707.
[9] Lin Fu, Yonghong Li, Yanting Wu, Xiaoyin Wang, Yi Jiang. Low carbon district heating in China in 2025- a district heating mode with low grade waste heat as heat source. Energy, 2021, 230 :120765.
[10] Xiaoyun Xie, Yi Jiang. Absorption heat exchangers for long-distance heat transportation. Energy, 2017, 141:2242-2250.
[11] Mengxiao Yu, Xiaobin Liu, Zhiqiang Liu, Sheng Yang. Energy, exergy, economic and environmental (4E) analysis of a novel power/refrigeration cascade system to recover low-grade waste heat at 90–150 °C. Journal of Cleaner Production 2022, 363:132353.
[12] Standard fixed institute of Ministry of Housing and Urban-Rural Development of the People's Republic of China. Indicators of investment in public works estimates. Beijing, China: China’s Planning Press, 2007. (in Chinese).

The 18th International Symposium on District Heating and Cooling, September 3–6, 2023, Beijing, China

Transformation of DHC systems to higher shares of RES – Technical and organizational solutions of six European regions

Carina Seidnitzer-Gallien[a], Michael Salzmann[a*], Ingo Leusbrock [a*], Stefan Hay[b*], Riccardo Battisti[c*], Giulia Crespi[d*], Giulio Buffo[d*], Enrico Pochettino[d*], Laure Deschaintre[e*], Stefan Thalmann[f*], Lilli Wolny[g*], Dirk Mangold[h], Nicolas Picou[i], Paula Möhring[j], Per Alex Sørensen[k], Laura Junasová[l]

[a] *AEE – Institute for Sustainable Technologies, Gleisdorf, 8200, Austria*
[b] *AGFW e.V., Frankfurt/Main, 60596, Germany*
[c] *Ambiente Italia SRL, Milano, 20129, Italy*
[d] *IREN S.p.A., Torino, 10143, Italy*
[e] *Planair SA, Yverdon-les-bains, 1400, Switzerland*
[f] *Verenum AG, Zürich, 8006, Switzerland*
[g] *SEC, Szczecin, 70-653, Poland*
[h] *SIG Solites, Stuttgart, 70563, Germany*
[i] *Auvergne Rhone-Alpes, Villeurbanne, 69100, France*
[j] *Hamburg Institut, Hamburg, 22765, Germany*
[k] *PlanEnergi, Skørping, 9520, Denmark*
[l] *DHC+ Technology Platform c/o Euroheat & Power, Brussels, 1200, Belgium*

[*] *Corresponding author.* c.seidnitzer-gallien@aee.at

ABSTRACT

The EU's ambitious targets for reducing greenhouse gas emissions by 55 % until 2030 can be achieved by improving energy efficiency and by a consistent and sustainable replacement of the fossil energy sources used today, with renewable alternatives. The activities in the project RES-DHC stands for a wider introduction of Renewable Energy Sources (RES) in District Heating and Cooling (DHC) sector to actively support the transformation to climate neutrality. The main objective of RES-DHC is to support the transformation of existing urban DHC systems to RES in six participating regions and thereby to derive – from these practical cases – technical and organizational solutions for such transformation processes. Therefore, the project is based on two key approaches. A market-oriented implementation process with concrete measures and actions in the six participating regions (Austria, Germany, Italy, Poland, France, Switzerland) is pursued through the implementation of regional stakeholder advisory group. To ensure a sustainable implementation process, strategy and action planning by the regional stakeholder advisory group was used to trigger the realization of measures at an early stage. The measures range from technical feasibility studies on the integration of waste heat sources, geothermal energy, storage technologies, large-scale solar thermal plants, and supply options from the district heating return flow to legal framework improvements, market support and awareness raising for investments in RES DHC. Overall, it can be underlined in a very positive way to bring all crucial stakeholders of a region together and to work jointly on solution strategies.

Keywords: Renewables, DHC, Transformation, Stakeholder

Abbreviation meaning	
RES	Renewables
DHC	District heating and cooling
CAPEX	Capital expenditure
RSAG	Regional stakeholder advisory group
CHP	Combined heat and power plant

1. INTRODUCTION

1.1 Framework conditions for district heating and cooling

Decarbonization is one of the greatest challenges of our time, not only due to advancing climate change, but also due to a

geopolitical crisis. The importance of moving away from fossil fuels does not only relate to the reduction of energy consumption, the increase of energy efficiency and the production of renewable energies, but mainly concerns the reduction of dependency on single energy sources with the increase of diversification [1] to achieve the ambitious targets for reducing greenhouse gas emissions by 55 % until 2030 [2]. The district heating and cooling sector covers more than 50 % of the total energy consumption in Europe [3] and the existing district heating and cooling grids offer a great potential to supply urban regions with heat or cold. About 60 million people in the EU benefit from district heating at present, so that the degree of supply with district heating ranges from 20 % in Central Europe to more than 50 % in Northern Europe [3]. In Austria, an economic potential of up to 50 % is achievable, which means almost a doubling in district heating supply [4]. The Heat Road Map Europe defines the share of district heating for a smart energy system with sector integration at about 50 % [5]. The share of renewables in district heating is led by Sweden with 70 % and already achieves more than 50 % in e.g., Denmark, Lithuania, Switzerland, France, or Spain. Still, there is a high potential for further development and especially for full decarbonization of the district heating sector. **Figure 1** presents the share of district heating and cooling in European regions and the share of renewables in DHC.

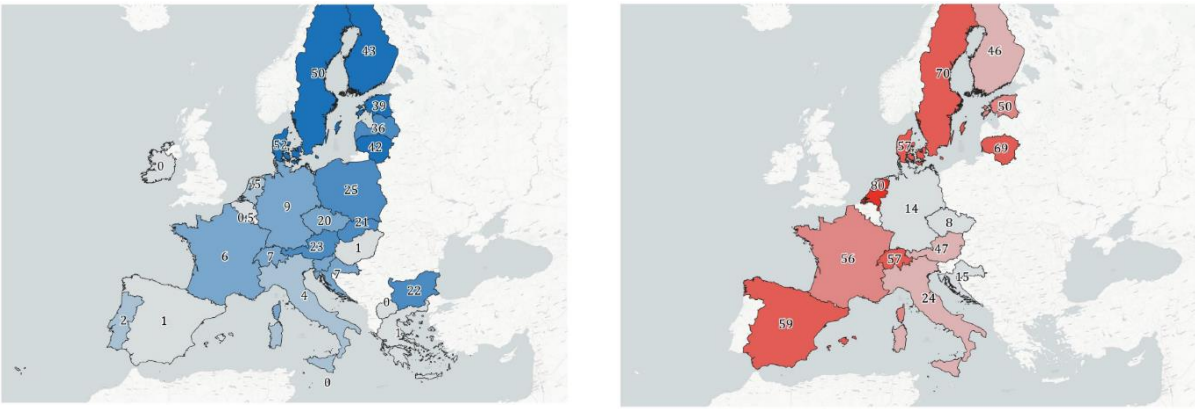

Figure 1: Ratio of district heating to heat market in % (left) and ratio of renewable energy sources to district heating in % (right). Image source: Hamburg Institut [3]

1.1 District heating and cooling – current heat production scenario

At present, most of the heat in DHC required is provided by centralized systems with a small number of production plants. Sustainable solutions make it possible to utilize local resources with a high share of renewable energy sources and to integrate them into existing heating and cooling grids in a sustained transformation process, therefore good examples are found in Scandinavian and Baltic countries [3, 6, 7, 8]. In combination with heat storage systems [9], fluctuating energy sources can also be used reliably in the heat supply. Available energy carriers such as solar thermal energy [10], geothermal energy [11, 12], ambient heat, or industrial waste heat can be combined via heating networks and continuously integrated into the regional heat supply. Heat pump technologies increase the use of low temperature sources, increase efficiency in heating networks, enable fluctuating renewable electricity generation to be converted into usable heat for utilization in heating grids.[13, 14] In parallel to the right combination of technical solutions, the necessary regulatory and organizational barriers need to be addressed through active stakeholder integration, innovation and business models, sustainable financing options and legal-political frameworks [15, 16, 17, 18].

1.2 Challenges and barriers for RES in district heating and cooling in European regions

The barriers for a realization a high share of RES in DHC often depends on country specific boundary conditions, due to political and legal regulations, energy planning and building renovation aspects, over-reliance on fossil fuels and a lack of awareness. **Table 1** presents a summarized overview of the consulted barriers and challenges.

Table 1: Challenges and barriers for RES in DHC in European regions [3, 19]

Technical Barriers	• Retrofitting of existing networks by lowering the supply temperatures or increasing the heat density • Integrate and plan decentralized renewable sources e.g., solar thermal energy or industrial waste heat (e.g. space requirements) • Lack of experience with new generation and storage technologies as well as technologies to couple the different sectors • Compatibility of building stock with the low operating temperatures required for 4th or 5th generation of DHC
Political and regulatory	• Political action and decarbonization targets tend to focus mainly on the

barriers	electricity sector. • Numerous laws and policies at EU and national level that address DHC • Lack of financial support and no clear regulation for financial investors • Negative boundary conditions e.g., fossil fuel subsidies, mis-regulated heat prices
Financial and economic barriers	• High CAPEX and long payback periods make it difficult to attract investors • Lack of reliable funding schemes • Lack of clear and reliable business models to have secure political and financial interests
Social barriers	• Lack of involvement of citizens and stakeholders in the development of DHC projects • Awareness for social benefits • Unrealistic expectations about cost savings delivered by DHC
Knowledge and perception barriers	• Poor reputation of RES and DHC • Not offer the appropriate individual heating solution for customers • Lack of awareness of different stakeholders, e.g., politicians, building owners, installers • Lack of specialists and skilled employees e. g. in heating, ventilation, and air conditioning as well as underground construction

The activities of the EU project RES DHC address these multiple challenges of market acceptance to achieve a higher share of renewable energy sources in urban district heating and cooling grids and to deal with the development of solutions and instruments for the implementation of projects.

2. METHODOLOGY

The main methodological approach of the project integrates a vertical pillar that includes the close to market implementation process of concrete actions and measures, supported by the development of regional stakeholder groups. The phases of the implementation process range from strategy development, action planning, consultation with the regional stakeholder group, to the realization of actions to improve the legal and policy framework, increase stakeholder engagement, and promote investments in renewable energy while considering environmental, economic, and social impacts. The horizontal pillar of the project is the transnational support and cooperation within the regional stakeholder groups together with selected experts.

2.1. Stakeholder analysis and engagement

To identify, analyze and manage the relevant stakeholders in the development of reliable measures to increase the share of RES in DHC of the participating regions, a four-step stakeholder integration process [20] was initiated. First, the relevant stakeholders in the region were identified; then, the importance of the stakeholders was explained; and third, the needs and expectations were collected and compared with the relevant value proposition. In the fourth step, key stakeholders were consolidated, and a working group (RSAG) was organized to support and guide the action and implementation process in each region.

2.2. Decarbonization mapping and guidelines

The analysis process of decarbonization road mapping addresses a five step-by-step plan for the development of climate neutrality for district heating networks. The aim is to identify, coordinate and systematically plan the relevant renewable technologies, energy sources and regional resources to implement target-oriented measures and projects. Based on the analysis of the initial situation, it is necessary to define in the next step the system boundaries, targets until 2035 and 2050. In the third step, measures and their potentials are identified, and their techno-economic capabilities are determined. The fourth step aims at implementing scenarios for the future heat supply with the identified measures and mapping the reduction paths. In the fifth step, the most realistic reduction path is selected, and implementation is planned with concrete projects.

2.3 Content analysis for decision-making

Is the analysis of the implicit or explicit content of communicated material by classifying, tabulating, and evaluating the essential elements and issues to determine their importance, and preparing them for policy and decision makers [21]. The aim is to support the legal and political approaches to achieving climate neutrality in the DHC sector with a structured content analysis, to assess the effectiveness of funding programs, to examine taxes, fees, and other incentive systems and to provide them as a basis for decision-making.

2.4 Capacity building and information campaigns

Capacity building and knowledge transfer in the decarbonization of district heating systems as well as increasing the share of renewable energies and their technical, economic, and social aspects are a key issue in this context for the relevant stakeholders. Online events, study tours, face-to-face workshops, coachings or individual trainings provide a valuable way to increase awareness and know-how to selected stakeholder groups such as energy and municipal utilities, planning agencies, local governments and municipalities, energy cooperatives, research intstitutions and interested citizens.

2.5 Feasibility studies

Using feasibility analysis, the measures will be analyzed for their applicability under the given regional framework conditions. Possible implementation difficulties can thus be identified at an early stage and considered in further project development. Analysis of selected implementation projects regarding their technical, economic, ecological, and social effects.

2.6 Consulting in bilateral workshops

Offering tailored consulting to energy and municipal utilities, workshops were held with interested applicants. The topics of the workshops were the transformation of existing DHC from fossil based to renewable generation and the options for setting up new DHC systems running on renewable heating sources. The workshops were prepared in a preparatory meeting with the client and then held online or on the ground with the utilities.

3. RESULTS

Six European regions are involved in the RES DHC project. The heat supplier-based regions Graz (AT), Szczecin and Westpommern (PL), and some areas within North-West of Italy (IT) are dealing on implementation-related issues and concrete case studies to increase the share of renewables in DHC. The authority-based regions Baden-Württemberg (DE), Auvergne-Rhône-Alpes (FR), and Swiss Cantons (CH) focus on the development of legal and policy framework conditions and their market support actions. Selected results from the regions will be highlighted below.

3.1 Formation of regional stakeholder advisory groups

The aim of setting up regional working groups was to promote decarbonization in district heating with targeted measures, workshops, and activities in the region and to optimally support decision-makers. The selected working groups in the six regions connect the key stakeholders who can contribute to the implementation of measures and knowledge providers for decisions. These range from energy suppliers, heat grid operators and district heating associations, regional authorities, municipalities, energy agencies and research institutions. Depending on the region, the working groups have intensified different measures and activities, including addressing the technological integration of RES, improving the regulatory and political framework, working on funding models, developing decarbonizations strategies or stimulating knowledge exchange and transfer between operators, citizens, and experts. The regional stakeholder groups formed the basis for the development of further implementation. The set-up of the RSAG, the open exchange within the group, the identification of ideas and the realization of measures are a key success factor for the participating regions towards a decarbonized district heating supply. The RSAGs are also a good example for the acceleration of implementations and valued communication with the community. In the long term, the RSAGs will collaborate after the end of the project.

3.2 Decarbonization mapping for the City of Graz

The urban district heating supply of the city of Graz with an average heat production of about 1,100 - 1,200 GWh/a and a grid length of about 450 km (status 2022) has developed a road map for the decarbonization of the heat supply and focuses on the use of renewable energy sources with concrete projects in order to strengthen the city and the surrounding region in the long term in achieving the climate targets, to guarantee the security of supply and to increase the added value. The specific projects (**Figure 2**), with a heat production capacity of around 660 GWh by 2030, focus on the intensive integration of waste heat from commerce and industry (~240 GWh), heat based on non-recyclable waste (~185 GWh), the energetic utilization of sewage sludge and waste heat from the sewage treatment plant (~36 GWh), and biomass plants in combination with solar thermal and storage technologies (~200 GWh). In addition, intensive efforts are being made to increase efficiency in existing urban buildings and heating systems, as well as in the network densification of the existing urban district heating area and the grid expansion to newly developed urban districts. Reduction paths until 2040 to achieve fully renewable district heating in Graz have also been developed but are not yet backed up with concrete projects and implementations. The energy savings of the concrete implementations (**Figure 2**) manage to increase the share of renewable energy from 22 % in 2022 to approximately 65 % in 2030. In the development of the concrete projects for the interim goal by 2030 [28], it has become clear that bringing together the key decision-makers is the essential success factor for realizing implementations and identifying new ideas through cooperation with experts.

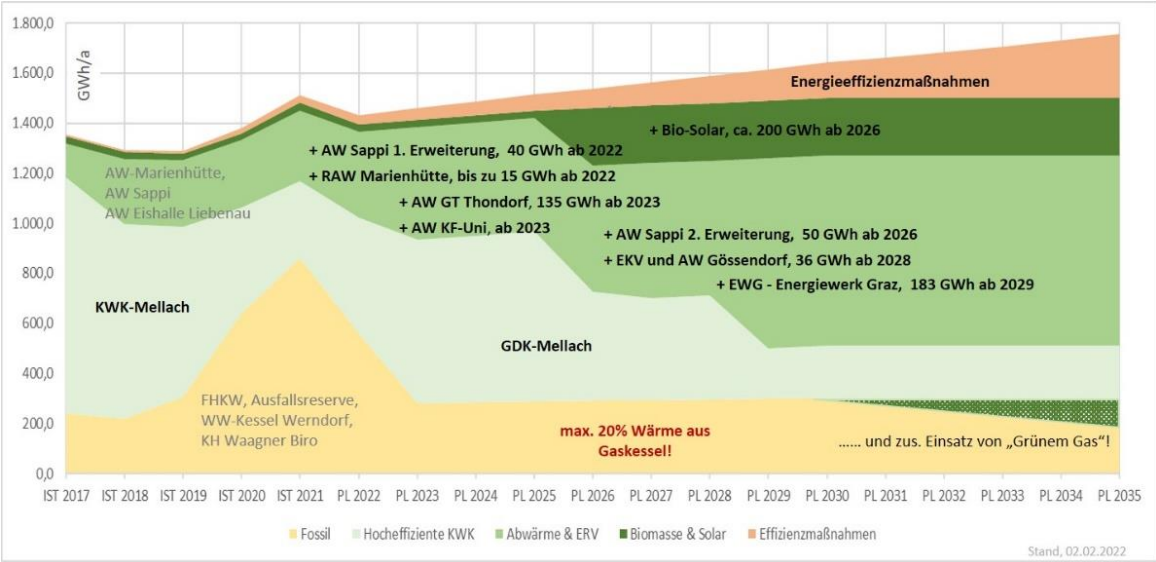

Figure 2: Decarbonisation strategy 05/2022 of district heating in the wider region of Graz with concrete projects up to 2035. Hocheffiziente KWK = high-efficient CHP, Abwärme & ERV = waste heat & energetic recycling of residual materials, Effizienzmaßnahmen = efficiency measures, Bio-Solar = biomass with solar thermal plant, AW = waste heat, RAW = residual waste heat utilisation, EKV = energetic sewage sludge utilistion, GDK = gas combined power plant. Image source: Energie Graz [28]

3.3 Guideline to temporary solutions for the expansion of DH in Swiss regions

The supply of heat in Switzerland is responsible for an energy consumption of around 100 TWh per year and is about half of the total energy consumption (as of 2020). More than 60 % of this, or over 60 TWh per year, is currently generated using fossil fuels. Since fossil energies must be reduced to achieve the climate targets, Switzerland's "heat strategy" focuses on increasing efficiency, with a forecast reduction to 70 to 80 TWh/a. The remaining energy demand is to be decarbonized as far as possible through the expansion of DH grids supplied with waste heat and renewable energies as well as decentralized individual solutions. Coordinating the expansion and new construction of DH grids in line with the overall municipal energy planning is a complex, time-consuming, and lengthy process. Therefore, it is important to involve potential heat customers in the planning process at an early stage so that they are informed about the possibility of connecting to a thermal network when renewing their energy production or building new ones. At the same time, it is also necessary to offer clever and approvable temporary heat supply solutions, so-called temporary solutions, so that the time (**Figure 3**) until the customer is connected to the thermal network can be covered. The guideline [26] describes these possibilities from a technical, economic, operational, and legal point of view. The information supports the optimal planning and valuable implementation and helps to improve the economic efficiency and expansion of thermal networks.

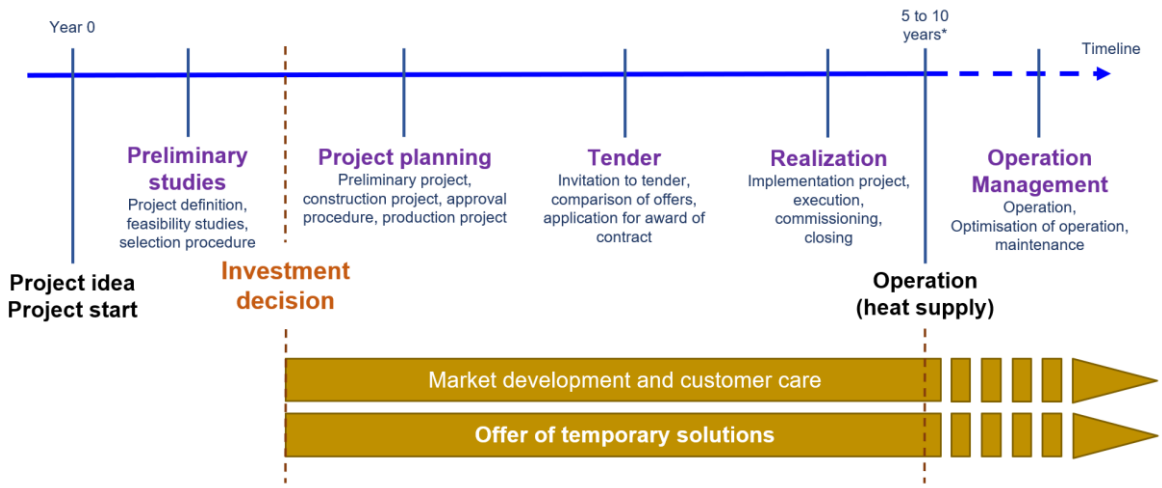

Figure 3: Timeline of the offer of temporary solutions in the planning and operation of a DH based on the SIA phases according to SIA 108 (Image source: Verenum AG). *Estimation, depending on the situation may be shorter or longer [26]

3.4. Feasibility study on energy storage technologies – investigations in Graz and Italy

A feasibility study on cavern storage technologies was conducted in urban area of Graz. Hydraulic engineering and rock mechanics criteria were defined, which are useful for the construction of caverns, and were compared with the geological

conditions in the urban area of Graz. Therefore, possible locations could be identified in the West and Northwest of the city of Graz. These are in solid rock and offer the necessary topographical and logistical conditions for the for the construction of cavern storage systems. For two sites, a possible concept with different storage volumes was elaborated, based on the principle of individual storage shafts. The initial analysis has shown that there are potential areas of application for cavern storage in Graz, although technical questions regarding casting, thermal insulation and charging cycles still need to be clarified in further detailed analyses. [22]

A study on the possibility of integrating thermal storage solutions in district heating systems was also investigated in an existing DH network in Italy. The scope of the action includes the analysis of different scenarios of alternative heat supply solutions aiming at increasing the share of RES in the heat supply mix and reducing the dependance on heat production from CHP and gas boilers, also considering future expansions of the system and existing hydraulic constraints of the network. This preliminary study will be useful for the DH network operator to carry out further investigations and assessments for the improvement of its asset.

The studies on storage technologies clearly show the necessity of integrating fluctuating renewable energy sources into the district heating supply and that, despite the high investment costs, the consideration of the regional framework conditions and differences, further detailed planning and research work is still necessary.

3.5 Spatial planning aspects for RES locations in Poland

In Poland, only 24% of heat is produced in DH, and over 70% of energy production is based on coal. According to KOBiZE (National Center for Balancing and Managing the Emissions) biggest RES potential in Poland in the nearest future will be solar collectors, heat pumps and pellet boilers. SEC group conducted an internal project on decarbonization mapping for the E.ON based assets with more than 280 MW installed capacity in Poland. Due to current development of decarbonization concepts for DH systems, an inventory of existing and planned actions regarding urban development has been planned and implemented. This action showed, where it is possible to locate e.g., solar thermal solutions or heat pumps using wastewater or rivers as heat source. All the investments in DH require a formal procedure, that ensures, that new installations safe for environment and citizens and fulfils necessary requirements regarding safety of the technology. Once a DH company has identified relevant areas for renewables, there are three possible scenarios to check availability. (1) There is no spatial planning available: In this case construction conditions are required, sometimes additional investigations based on national regulations are necessary. (2) Spatial management plan will be developed: In this case, DH company can apply to the municipality to put appropriate regulations in the planning process. (3) Spatial management plan exists: The use of RES in the area is possible, then the building permit is necessary, or the use of RES is not foreseen, then construction is normally excluded, although amendment can be applied at the municipality. For the development of further spatial energy planning the communication with the municipality is essential.

The results from Poland demonstrate that only viable spatial planning can enable the increase of renewable technologies to be utilized in a meaningful way and can significantly accelerate the decarbonization process by reducing the period from approval to implementation.

3.6. Methodological guide for decarbonization to support decision-making in Baden-Württemberg

The overall climate goal in the model region Baden-Württemberg is to have 45% of renewable heat for the district heating (DH) generation by 2030 and to be climate neutral by 2040 [23]. In 2018 round about 10% of the energy consumption for heating purposes in Baden-Württemberg was supplied by DH systems [24]. The implementation of the political goals to achieve a climate-neutral heat supply by 2040 in Baden-Württemberg poses enormous challenges for utilities, planners, investors, and cities. Successful measures to increase the RES share in DHC require adjustments of the system components heat generation, heat distribution and heat consumption in individual DH systems based on available local RES. A methodical approach was developed to identify and to unlock local potentials and support the decision-making process. Concrete in two demo cases the methodological approach supported the municipalities on their way towards a higher share of RES in DHC. In these demo cases the current state of the local heat consumption as well as the available renewable energy sources were analyzed. It became obvious, that individual DH systems has specific needs to increase RES in DHC. Besides that, the evaluation of the actual state of existing DH systems and the analysis of local potentials to improve the share of RES are easier than the implementation of concrete measures based on the results gained: In both demo cases the measures discussed leads to further technical challenges that needs to be investigated before starting the decision making and implementation process. Based on the results, further steps for the elaboration of an individual transformation plan and specific measures for the implementation were discussed in certain stakeholder workshops. The methodological approach elaborated during the project is in line with the national founding program (BEW) in Germany [27].

3.7 Standardization on permitting process and improvement of the incentive framework in Italy

In Italy, in 2021, the building stock connected to district heating networks has reached a volume of approximately

382 million m^3 and the extension of the urban district heating networks is of approximately 4,800 km [25]. Considering the mix of primary energy sources used in production systems, fossil fuels (mostly natural gas) represent 73% of the total, while the remaining quota is covered by solar, geothermal, biomass, wastes and heat recovered from industrial processes [25]. To support the expansion of renewable technologies and district heating and to achieve the climate targets, it is necessary to work on the regulatory framework. The simplification and standardization of the permitting procedures for the project development of district heating networks run on renewables is an essential approach in Italy; allowing to reduce time and costs while increasing the probability of project success and local acceptability. Specific factsheet on different RES technologies were prepared together with the key market stakeholders, including the Italian DH Association (AIRU), debugging false myths about such technologies and proposing concrete actions for simplifying their adoption. Another measure was to provide suggestions for improving the current incentive framework, since district heating from renewables is not adequately represented in the many incentive opportunities available in Italy. This action, therefore, aimed to bridge this gap by proposing practical solutions for its correction in different fields and at different levels, including incentives for buildings, White Certificates, reduced VAT, etc., thus also making projects more bankable. One of the concrete results of this action was the adoption of a 4% lower VAT regime for DHC at the beginning of 2023.

3.8 Capacity building workshops and webinars on knowledge transfer

To overcome with the lack of knowledge and awareness for RES in DHC, information campaigns, with webinars, face-to-face workshops, capacity building activities and study tours for targeting local authorities, end users and utilities were addressed to adequately inform about the real potential, costs, and benefits of renewables in district heating. In total, more than 40 events were organized in the six regions. Concrete capacity building workshops on renewable technologies, including large scale heat pumps, solar thermal, biomass, storage technologies, deep geothermal potential, approaches to reduce grid temperatures as well as spatial planning were addressed. Events on financing, marketing green DHC with certificates of origin and business models, and energy communities have tried to highlight the financial added value of the efforts towards more renewable DHC. Furthermore, the provision of information for consumers on participation models (cooperatives, crowdfunding, collective shares, energy communities, etc.), focusing on the role that district heating can have in thermal energy communities in the future were developed and disseminated. The intensive awareness work has trained relevant stakeholders in the regions in terms of technical and organizational skills and prepared them for the steps towards decarbonization.

A widespread impact has been demonstrated the Auvergne Rhône Alpes region of eastern France by a conducted webinar series. The region accounts for 900 km of district heating network with heat production of about 4,000 GWh. Between 2020 and 2022, the production of renewable heat in DH networks rose from 65% to 70%. The region's partners have put their faith in the development of digital tools to help local authorities estimate the development potential of heating networks and renewable energy production (terristory.fr, by AURA-EE) and design offices to size installations (ENRSim by the CEA). Funding for solar installations and thermal storage has also been boosted by the Regional Council ERDF. The impact of the webinars on solar thermal energy for DH with more than 130 participants has been viewed almost 10,000 times.

4. DISCUSSION AND CONCLUSION

The structured methodological approach of the RES DHC project as well as the different implementations on the technological, structural, and regulatory-financial level in the six regions demonstrated concrete examples of how the decarbonizations of DHC can be advanced and the transformation towards climate-neutral heat supply can be promoted in a sustainable way. The project indicates that the analysis of technical parameters and local potentials for renewable energy is much easier to design compared to the decision-making and implementation process since all barriers, including the technological barriers, have to be addressed by regulation at European, national, regional and local level. Thus, uncertainties in the development of the transformation strategy, such as the heat demand forecast or cost estimates, can lead to barriers in the decision-making process. To overcome these barriers, the decarbonizations scenarios usually need to be backed up with technical studies as well as economic analyses to be best prepared for targeted decision-making.

A total of 38 measures to increase RES in DHC and support the market acceptance were identified by the partners and their implementation started. The selected measures have shown that starting with a functioning RSAG, ideas, measures and realizations are tackled faster, more efficiently and effectively. That concrete reduction scenarios for DH grids with structured measures and accurate target paths can considerably speed up decarbonization. That new funding schemes, work on faster permitting processes and spatial energy planning measures were realized only through the collaboration in the project and a high impact was reached through the numerous trainings and awareness raising. Furthermore, the frequent exchange of knowledge between the project partners, e.g., regarding the transnational coaching activities and various project meetings enhanced the creativity for developing and implementing the measures. With six model region countries as well as two more supporting countries (Denmark and Belgium), the project enabled comparisons of the current status quo as well as the targets and visions for RES in DHC. This increased the ideas and range of solutions that were applied in the measures. Therefore,

the consistent implementation of emission-reducing measures, DH grids and their urban areas of the participating regions can take on a pioneering role in climate protection and at the same time improve the quality of life and sustainability for their inhabitants.

ACKNOWLEDGEMENT

This project has received funding from the European Union's Horizon 2020 research and innovation program under grant agreement No. 952873

REFERENCES

[1] European Commission. REPowerEU. 2022. https://commission.europa.eu/strategy-and-policy/priorities-2019-2024/european-green-deal/repowereu-affordable-secure-and-sustainable-energy-europe_en#timeline
[2] Europäische Kommission 2021: Overview of District Heating and Cooling Markets and Regulatory Frameworks under the Revised Renewable Energy Directive, Report, Brüssel, https://energy.ec.europa.eu/publications/district-heating-and-cooling-european-union_en
[3] Corscadden, J., Möhring, P., Krasatsenka, A. 2021: Renewable Energy Sources in District heating and Cooling, EU Level Survey, RES-DHC Project https://www.res-dhc.com/wp-content/uploads/2021/05/RES-DHC_WP2_Task_2.1_D2.1_Survey_EU-Level_FINAL_UPDATED_202104.pdf
[4] Büchele, R., et.al. 2021: Potenzial für eine effiziente Wärme- und Kälteversorgung, Wien.
[5] Persson, U., Wiechers, E. Möller, B. et.al. 2019. Heat Roadmap Europe: Heat distribution costs, Energy, Volume 176, p. 604-622 https://doi.org/10.1016/j.energy.2019.03.189
[6] Sorknaes, P., Alberg Østergaard, P, Zinck, J. et.al. 2020. The benefits of 4th generation district heating in a 100 % renewable energy system, Energy, Volume 213. https://doi.org/10.1016/j.energy.2020.119030
[7] Zhang, Y., Johansson, P. et.al. 2022. Assessment of district heating and cooling systems transition with respect to future changes in demand profiles and renewable energy supplies, Energy Conversation and Management, Volume 268, https://doi.org/10.1016/j.enconman.2022.116038
[8] He, X., Toan Tran, C. et. al. 2021. Production planning for district heating networks: A sequential method to consider share of renewables in annual heat production, Energy Reports, Volume 7, p. 237-243, https://doi.org/10.1016/j.egyr.2021.08.151
[9] Reisenbichler, M., Van Helden, W., Leusbrock, I. et.al. 2020. Großwärmespeicher – Ein Weg zur vollständigen Erneuerbaren Wärmeversorgung von Städten. 16. Symposium Energieinnovation, Graz. https://www.gigates.at/images/Artikel/200131_AEE-giga_TES_EnInnov20_LF-v10_final.pdf
[10] Tian, Z., Zhang, S., Deng, L. et.al. Large-scale solar district heating plants in Danish smart thermal grid: Developments and recent trends, Energy Conversation and Management, Volume 189, p. 67-80. https://doi.org/10.1016/j.enconman.2019.03.071
[11] Lund, J.W., Toth, A.N. 2021 Direct utilization of geothermal energy 2020 worldwide review. Geothermics, Volume 90, https://doi.org/10.1016/j.geothermics.2020.101915
[12] Tissen, C., Menberg, K., Benz, S.A. 2021. Identifying key locations for shallow geothermal use in Vienna, Renewable Energy, Volume 167, p. 1-19. https://doi.org/10.1016/j.renene.2020.11.024
[13] Yuan, M., Thellufsen, J., Sorknaes, P. et.al. 2021. District heating in 100 % renewable energy systems: Combining industrial excess heat and heat pumps, Energy Conversion and Management, Volume 244. https://doi.org/10.1016/j.enconman.2021.114527
[14] Monie, S.W.M., Åberg, M. 2023. Potential to balance load variability, induced by renewable power, using rock cavern, thermal energy storage, heat pumps, and combined heat and power in Sweden, Applied Energy, Volume 343. https://doi.org/10.1016/j.apenergy.2023.121210
[15] Lygnerud, K., Popovic, T., Schultze, S. et.al. 2023. District heating in the future – thoughts on the business model, Energy, Volume 278, https://doi.org/10.1016/j.energy.2023.127714
[16] Selvakkumaran, S., Eriksson, L., Ottosson, J. et.al. 2021. How are business models capturing flexibility in the District Energy (DE) grid? Energy Reports, Volume 7, p. 263-272. https://doi.org/10.1016/j.egyr.2021.08.146
[17] Johannsen, R.M., Sorknaes, P., et. al. 2023, Energy communities' flexibility in different tax and tariffs structures, Energy Conversion and Management, Volume 288, https://doi.org/10.1016/j.enconman.2023.117112#
[18] Ma, Z., Knotzer, A., et.al. 2020. A literature review of energy flexibility in district heating with a survey of the stakeholders' participation, Renewable and Sustainable Energy Reviews, Volume 123, https://doi.org/10.1016/j.rser.2020.109750
[19] Riccardo, B., 2021, Baseline surveys in the 6 participating regios, RES-DHC Project, https://www.res-dhc.com/wp-content/uploads/2021/05/RES-DHC_WP2_Task2.1_D2.2_SummaryOfSurveys_FINAL.pdf
[20] Müller-Stewens, G., Lechner, C. 2016. Strategisches Management – Wie strategische Initiativen zum Wandel führen, 5. Auflage, Schäffer, Poeschl Verlag, Stuttgart.
[21] Krippendorff, K. 2004. Content Analysis: An Introduction to Its Methodology. 4th Edition, London, SAGE Publications.
[22] Geisler, T., Dax, F., et.al. 2022. Machbarkeit von Untertage-Wärmespeichern (Kavernenspeicher -CTES) im Nahbereich der Stadt Graz, RES DHC Projekt. Graz. https://www.res-dhc.com/at/2023/04/04/geologische-machbarkeit-von-kavernenspeicher-ctes-im-nahbereich-der-stadt-graz-wurde-untersucht/
[23] Ministerium für Umwelt, Klima und Energiewirtschaft Baden-Württemberg (Hrsg.): Klimaschutzgesetz Baden-Württemberg, https://um.baden-wuerttemberg.de/de/klima/klima-schutz-in-baden-wuerttemberg/klimaschutzgesetz/ ; [22.02.2021].
[24] Ministerium für Umwelt, Klima und Energiewirtschaft Baden-Württemberg (Hrsg.): Energiebericht 2020, [15.02.2021].
[25] AIRU. La crescita del Teleriscaldamento in Italia, https://www.airu.it/italia/ [30.05.2023]
[26] Thalmann, S.; Deschaintre, L.: Leitfaden zu Übergangslösungen beim Ausbau thermischer Netze, Verenum AG und Planair SA für das Projekt RES-DHC, Zürich und Yverdon-les-Bains 2023
[27] Bundesministerium für Wirtschaft und Klimaschutz. Richtlinie für die Bundesförderung für effiziente Wärmenetze „BEW". Vom 1. August 2022. https://www.bundesanzeiger.de/pub/de/amtliche-veroeffentlichung?1 [04.07.2023]
[28] Götzhaber, W., Meißner, E., Moravi, G. et.al. 2022. Wärmeversorgung Graz 2030/2040 – Wärmebereitstellung für die fernwärmeversorgten Objekte im Großraum Graz. https://www.umwelt.graz.at/cms/dokumente/10084666_7301688/c4df10ce/AU22-05243_Grazer-Energieagentur-Broschuere_.pdf [04.07.2023]

ANALYSIS OF CARBON EMISSIONS USING BIOMASS ENERGY TO REPLACE COAL IN RURAL BUILDINGS HEATING SECTOR

Cun wei[a], Zhigang Zhou[a*], Mingyang Cong[a], Yaling Wu[a], Dayi Yang[b], Jing Liu[a], Shi Huang[a]

[a] *School of Architecture, Harbin Institute of Technology, Key Laboratory of Cold Region Urban and Rural Human Settlement Environment Science and Technology, Ministry of Industry and Information Technology, Harbin, 150000, China.*

[b] *Faculty of Computing, Harbin Institute of Technology, Harbin,150000, China.*

**Corresponding Author: Zhigang Zhou, E-mail address: hit_zzg@163.com*

Abstract

China requires reducing greenhouse gas emissions, increasing the use of renewable energy, and achieves carbon neutrality by 2060. Biomass is a significant renewable energy source that has several advantages over conventional fossil fuels. This paper develops a new model for the evaluation of the implementation of biomass as a fuel to replace coal for heating in rural buildings. Following the new model proposed in this paper a case study was conducted in Heilongjiang province of China. Then, we calculate the amount of crop straws that can be collected from 2005 to 2020, and analyze coal consumption and carbon dioxide emission of heating in rural buildings from 2011 to 2020. Considering China's carbon neutral target requirements, we analyzed the changes in coal consumption, biomass demand, carbon reduction using the biomass to replace coal for heating in rural areas from 2021 to 2060. We can conclude that coal consumption and carbon dioxide emissions show a fluctuating trend in the past decade with an average value of about 1,100,000 tons and 2,090,000 tons, respectively. Through the use of biomass, carbon dioxide emissions gradually decrease from the initial baseline value to 0, and carbon neutrality can be achieved in rural building heating. The demand for biomass to replace coal accounts for a small portion of the current collectible biomass, with the highest proportion accounting for about 1.7% of the collectable biomass straw.

Keywords: Carbon emissions, Biomass energy, Crop straw, Rural buildings, Heating

EVALUATION OF WASTE HEAT RESOURCES IN TANGSHAN

Zhaoyang Liu[a], Xiaolin Yang[a], Xu Luo[a], Jianjun Xia[a*]

[a] *Building Energy Research Center, Tsinghua University, Beijing, 100084, China*
[*] *Corresponding author. xiajiajun@tsinghua.edu.cn*

ABSTRACT

Waste heat is an important low-carbon heat source for energy systems dedicated to carbon neutrality, attracting the attention of researchers worldwide. In order to promote the utilization of industrial low-grade waste heat resources, it is necessary to investigate and evaluate its potential. Assessments of different waste heat resources have been carried out, mostly in Europe, and many of the research data used in these assessments are outdated. Waste heat assessment for China is focused on industrial plants and power plants, usually through a top-down approach. There is a lack of assessment at the city level and few data on waste heat studies. Therefore, this paper selects Tangshan, an important industrial city, as the evaluation target and conducts an evaluation of waste heat resources. By distributing questionnaires to factories and making field visits, we collected and analyzed information on energy consumption, waste heat resources and the current status of waste heat utilization in key industrial enterprises, based on which we studied the industrial distribution characteristics, temperature distribution characteristics and geographical distribution characteristics of waste heat. It is found that there are 846PJ of key low-grade waste heat resources in Tangshan area, mainly concentrated in the iron and steel industry and the electric power industry. Among them, power plants and steel plants have larger heat sources available, with 539PJ of waste heat in steel plants and 221PJ in power plants.

Keywords: Industrial waste heat, Estimation, Low-grade waste heat

Zhaoyang Liu: Carbon reduction of district heating and industrial heating
Xiaolin Yang: District heating, technical research of industrial waste heat recovery and the optimization research of combined heat and water (CHW) system.
Xu Luo: Industrial energy system, and low-carbon heating technology.
Jianjun Xia: Building energy conservation, energy planning, heating planning and district heating

1. INTRODUCTION

In order to cope with climate change and solve the problem of resource and environmental constraints, China has proposed the goal of zero carbon in 2020. The heat-using sector is an important component of carbon emissions, and how to achieve thermal decarbonization has become a key topic in carbon neutral research. The heat sector consumed 50% of global end-use energy consumption and produced 40% of carbon emissions in 2018[1]. The heat sector in China mainly includes the supply of heat for urban building heating and light industrial production in northern areas, with 57% of the majority of heat sources currently being coal-fired boilers and thermal media cogeneration plants, and the rest mainly coming from natural gas boilers and a small amount of gas-fired cogeneration[2]. Fossil energy sources such as coal and natural gas are still the main heat sources for heating in China. In order to achieve the goal of carbon reduction in the field of heating, low-carbon must be found for heat demand.

Low temperature waste heat discharged from power plants, factories, data centers, waste incineration, wastewater treatment plants, etc. can transform traditional fossil energy-based heat sources. Waste heat recovery requires consideration of various factors, such as the amount of available waste heat, temperature levels, and geographic location, and these variables can affect the feasibility and economics of recovering waste heat, so a thorough evaluation of waste heat can help facilitate the recovery of waste heat.

Waste heat resources have been estimated at the national level in various European countries, the United States, China, and India, and in some countries, waste heat temperature levels in different sectors have been analyzed and waste heat maps have been conducted. Zuberi[7] assessed the techno-economic waste heat recovery potential of the Swiss industry. [11] conducted a bottom-up estimation of waste heat in key energy-using industries in the US manufacturing sector and found that about 20-50% of industrial energy inputs are lost in the form of waste heat. [12] estimated the waste heat potential of five energy-intensive industrial sectors in India. Luo [13] estimated the low-grade industrial waste heat potential in northern China and found that about 100 Mtc of industrial waste heat could be recovered in northern China during the heating season.

Temperature distribution is also an important area for waste heat assessment. Bühler[3] estimated the recoverable waste heat for three sectors in Denmark to be 266 PJ, about 13% of the end-use energy, but only the temperature of the heat was mapped, not the geographic location of the waste heat. Luberti [8] estimated waste heat by sector and temperature for the power generation and industrial sectors in the EU, and the analysis showed a total waste heat of 2880 TWh, of which 81.1% was below 80°C. The United States has 43 × 109 GJ of waste heat above 30°C and can reduce 12% of U.S. primary energy consumption and 13% of carbon emissions by recovering waste heat[9].

The geographic distribution of waste heat resources has an important impact on the availability of waste heat, and spatial modeling of waste heat resources and conducting waste heat mapping can promote the utilization of waste heat. Lund[4] performed a detailed spatial analysis for eight categories of heat sources in Denmark, which showed that potential waste heat sources existed near almost all central heating areas. Alice [5] estimated the total heat demand for the residential sector in Italy at 329 TWh and the amount of WH and renewable heat that can be used for DH at 156 TWh, and developed a GIS map containing heat sources and DH demand. Max[6] mapped the waste heat from the power generation and industrial sectors in the UK, which was estimated to be 391,000 GWh in 2018, with waste heat concentrated in areas of high population density and traditionally strong industrial base. Waste heat resources in the energy and industrial sectors were quantified and mapped in 27 European countries and found that 46% of the waste heat resources were concentrated in 63 strategic thermal synergy regions[10]. Zheng [14] surveyed and mapped the power plant, industrial waste heat, biomass and waste resources in 1047 administrative regions in northern China and analyzed the regional heat balance.

Waste heat assessments at the national level are usually obtained by estimation. Some studies derive energy consumption data from carbon emission data or obtain energy consumption data directly from metering facilities[10], and then draw on existing waste heat recovery factors to derive waste heat resources for different temperatures and industries, while other scholars derive waste heat resources from waste heat per unit of product and product yield. Both rely heavily on waste heat resource information from previous scholars, which is generally obtained through waste heat resource survey at the provincial and municipal level [14].For example, the theoretical waste heat potential of 290 industrial enterprises in the Basque Country was evaluated by analyzing an industrial database[15]. Luo[13] has conducted a detailed study of waste heat in 80 steel and cement plants in Hebei Province, combining questionnaire research and field research, in which the total amount of waste heat, the heat source medium, the temperature and geographical distribution of waste heat were analyzed. Other regional waste heat resource assessments at the provincial and municipal level are also generally analyzed using estimated methods. Dénarié[16] evaluated the industrial waste heat potential of the city of Milan, Italy, by applying heat recovery factors. In [17], the potential for industrial and commercial waste heat supply was estimated for the community of Lokstedt, Hamburg, Germany, using a method that estimates the energy demand by the energy demand per unit of personnel

and the number of employees, and then obtains the waste heat potential based on the percentage that can be recovered as waste heat. In [18], the industrial waste heat in the Basque Country of Spain was estimated by industry and temperature, and the method used was to obtain the waste heat potential by multiplying the plant energy use data by key recovery factors.

In addition to power plants and factories, several studies have analyzed other potential sources of waste heat. Wilson [19] estimated the waste heat recovery potential of wastewater in the UK to be about 18.3 TWh. Davies [20]analyzed the feasibility of using waste heat from data centers for central heating in the UK. Persson [21] analyzed the waste heat potential of various types of urban waste heat sources in Europe, including data centers and wastewater treatment plants.

There are relatively few existing surveys on waste heat resources, especially in China. The survey[13] that have been conducted also focus on two industrial sectors, steel and cement, neglecting other waste heat sources. Therefore, this study selects an important manufacturing city (Tangshan City) as a case study to conducting surveys of waste heat resources and add to those not covered by the research by estimating. This research combines research and estimation methods to conduct a bottom-up assessment of total waste heat resources, temperature analysis, and geographic mapping of plants, power plants, waste-to-energy plants, and data centers in Tangshan City.

2. METHODOLOGY

2.1 overall methodology

- Survey: In view of the key energy-using industries in Tangshan City, 49 factories and power plants were selected for investigation, mainly in steel plants, cement plants and power plants. The waste heat potential, temperature and location of key waste heat sources were investigated through field investigation and questionnaire.
- Estimation: In order to improve the assessment results, the potential of other 128 waste heat sources is estimated by product output or carbon dioxide. The data comes from the government 's mandatory report or statistical data.

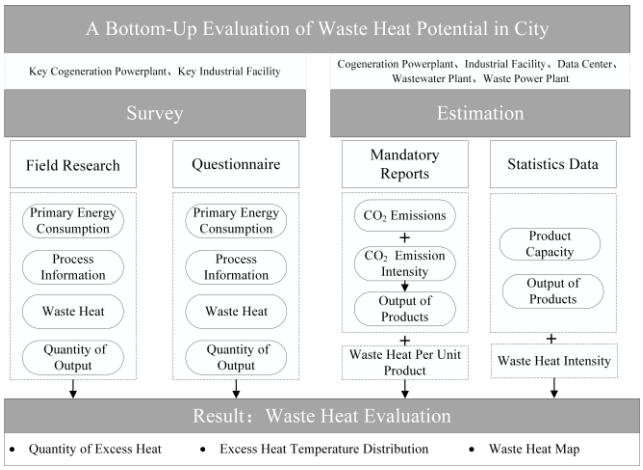

Figure 1 Methods for evaluating waste heat

2.2 waste heat survey

This study investigates and analyzes the heat source medium, total amount and temperature of low-grade waste heat through questionnaire distribution and field visits, and estimates the recoverable amount of low-grade industrial waste heat by combining the current feasible low-grade waste heat utilization technology. The recovery of waste heat is constrained by various factors, and when investigating the potential of waste heat recovery in Tangshan iron and steel enterprises, it is necessary to combine the current level of technology to select waste heat resources that have a high recovery potential and can be achieved with existing technology, therefore the following assumptions were applied in the investigation :

- For the waste heat carried by solid finished products, it is difficult to recover, and it is also difficult to install waste heat recovery equipment at the site, so it is not considered as a recoverable waste heat resource for the time being.
- For flue gas waste heat, considering its complex composition, if the recovery temperature is too low often condenses out corrosive substances, in order to avoid excessive investment in anti-corrosion costs, only the waste heat above 80℃ is considered in the calculation of waste heat potential, and the waste heat below 80℃ is not considered. Taking into account the characteristics of the flue gas, the recoverable proportion of flue gas waste heat is taken to be 0.8.
- For the low-pressure saturated steam generated by the gasification cooler, heat supply will produce greater economic and energy-saving benefits than power generation due to the low efficiency of power generation, so it is also considered

as a waste heat source for statistical purposes.

2.3 waste heat estimation

2.3.1 Industrial Waste Heat Estimation

The estimation of industrial waste heat includes three industries: steel manufacturing, metal processing and cement manufacturing. The data source is the greenhouse gas emission disclosure form for key emission units published by the Tangshan ecological environment department in 2019. The estimation method is shown in Equation 1, using the total annual carbon emissions of the enterprise divided by the carbon emissions per unit product to obtain the annual production, and using the average waste heat per product and temperature distribution coefficient obtained in the survey to obtain the estimated waste heat.

$$Q = \frac{M_{CO_2}}{f_{CO_2}} * \mathrm{q} \tag{1}$$

Where M_{CO_2} represents the total annual carbon emission published by the plant, f_{CO_2} represents the carbon emission per ton of product published by the plant, q represents the average waste heat per ton of product obtained by survey.

2.3.2 Waste-to-Energy Plants and Power Plants

The data source for waste-to-energy plants is the installed power generation capacity published in China's automatic monitoring platform for domestic waste-to-energy plants. The data source for power plants is the installed capacity published in the National Carbon Emission Data Public Platform. The estimation is shown in Equation 2, using the Heat-to-Power Ratio from the previous study[22] multiplied by the power generation capacity to obtain the potential waste heat.

$$Q = P_{power\ plant} * r * \mathrm{h} \tag{2}$$

Where $P_{power\ plant}$ represents the power generation, r represents the Heat-to-Power Ratio, r is taken as 2.5 for waste-to-energy plants and 1.5 for power plants, h represents the running time of the power plant and is taken as 6000 hours.

2.3.3 Data Center

The waste heat of the data center is estimated by its power consumption, which is derived from the number of racks and the average power consumption of the racks and the load factor, as shown in Equation 3

$$Q = p_{data\ center} * N * \eta * \mathrm{h} \tag{3}$$

Where P represents the power of a single server, N represents the number of racks, η represents the load factor, and h represents the operating time of the server and is taken as 8760 hours.

2.3.4 Wastewater Treatment Plant

The total amount of annual wastewater treatment is derived from the national list of wastewater treatment facilities made public by the Ministry of Ecology and Environment, and the waste heat is calculated as in Equation 4

$$Q = c * \Delta t * V \tag{3}$$

Where c represents the effluent heat capacity, assumed to be equal to 4.2 kJ/kg*°C, Δt represents the heat extraction temperature difference, taken as 5°C, and V represents the annual treated effluent volume.

3. RESULTS

3.1 Waste Heat Resources Evaluated by Survey

49 key waste heat sources were investigated, including 16 steel manufacturing plants, 11 cement plants, 7 power plants, 6 chemical plants, 4 coke plants and 5 other plants, which have extremely rich waste heat resources with a heating capacity of 23.4 GW and annual waste heat of 668.5 PJ. Among the investigated companies, steel plants and power plants are the most important waste heat sources, and these two types of waste sources account for the highest percentage of the investigated plants, 55% and 35%, respectively (**Figure 4**). Exhaust steam is the most important waste heat medium, because the waste heat from power plants and captive plants of steel plants is cooled by air or water in the form of exhaust steam (**Figure 2**). Waste heat is mainly concentrated in the low temperature range, with 81% of the waste heat below 60°C (**Figure 3**)

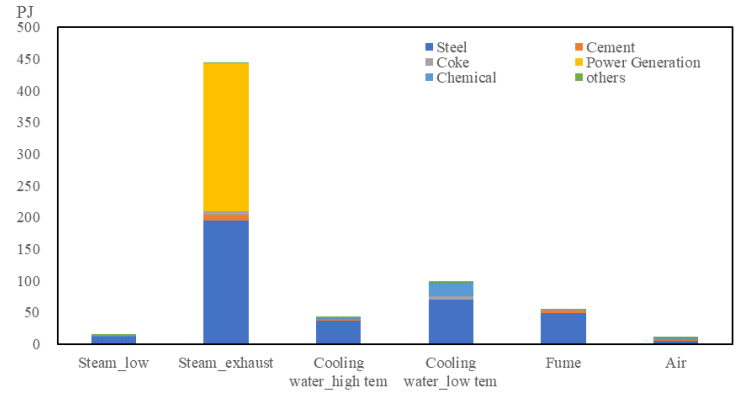

Figure 2 Media distribution of the investigated waste heat (Steam_low is the saturated steam below 1.6 MPa, Steam_exhaust is the spent steam removed from the turbine, Cooling water_high tem is the cooling water above 60°C, Cooling water_low tem is the cooling water below 60°C)

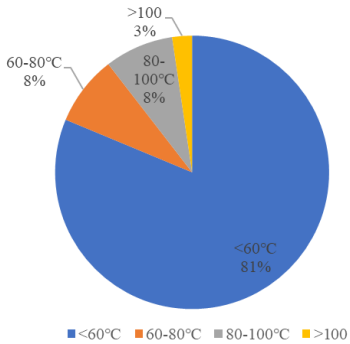

Figure 3 Temperature distribution of the investigated waste heat

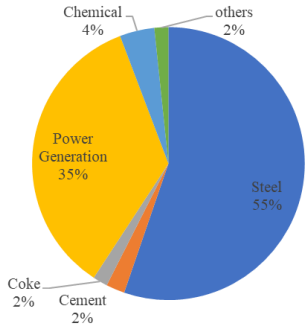

Figure 4 Distribution of waste heat sources in different plants

3.1.2 Waste heat analysis in steel plants

One of the steel plants in the survey was chosen as a case study to present its internal waste heat resources, with an annual production of 7.5Mt of crude steel. The steel plant has a high proportion of low temperature waste heat, with approximately 75% of the waste heat below 60°C and approximately 66% of the waste heat contained in exhaust steam (**Figure 5**). Ironmaking and gas power generation are the largest waste heat generating processes, accounting for approximately 25% and 54% of the total respectively (**Figure 6**).

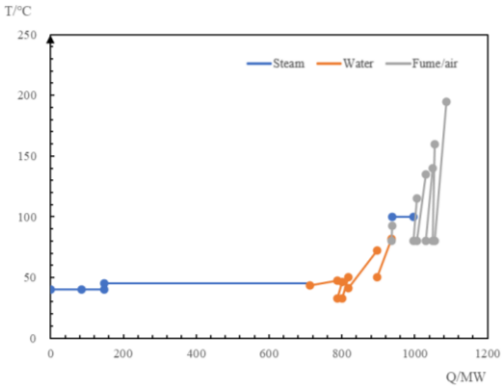

Figure 5 Temperature and media distribution of waste heat in case steel plant

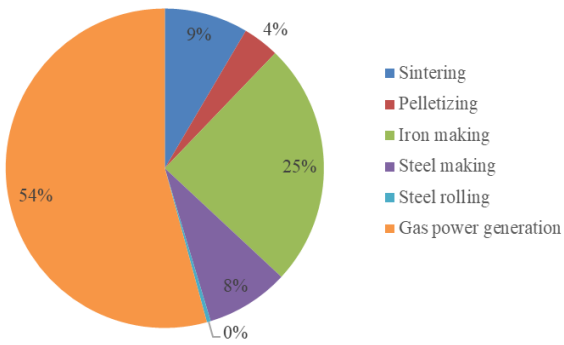

Figure 6 Waste heat from various processes in case steel plant

Using the data obtained from the survey of these 16 steel plants, an average total waste heat of 3601MJ/t crude steel was obtained, with the media distribution as shown in Table 1, to be used in the estimation of waste heat resources of other steel plants in Tangshan (**Table 1**).

Table 1. Waste heat of each medium per unit of crude steel in a steel plant (MJ/t)

	Steam_low	Steam_exhaust	Cooling	Cooling	Fume	Air	Total

			water(>60°C)	water(<60°C)			
Steel Manufacturing	121	1904	361	683	478	55	3601

In addition to this, the average value of the waste heat per unit of product in the steel processing process of the steel plants surveyed was also calculated (**Table 2**) to estimate the metal treatment plant where the steel processing takes place.

Table 2. Waste heat of each medium per unit of crude steel in a metal processing plant (MJ/t)

	Steam_exhaust	Fume	Total
Metal processing	66	48	114

3.1.3 Waste heat analysis in cement plants

A cement plant with an annual production capacity of 4.4 million tonnes was also selected as a case study to look at its internal waste heat resources. The waste heat in the cement plant is also concentrated below 60°C, accounting for approximately 82%. Exhaust steam and rotary kilns are the two largest processes in the cement plant in terms of waste heat, accounting for 82% and 11% respectively.

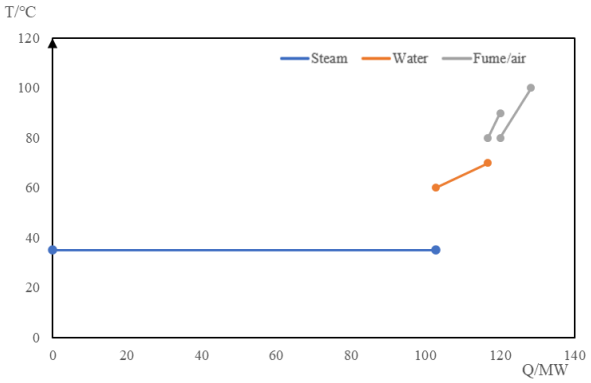

Figure 7 Temperature and media distribution of waste heat in case cement plant

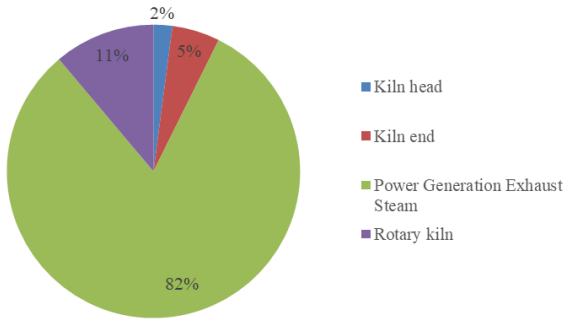

Figure 8 Waste heat from various processes in case cement plant

The average unit cement waste heat of the 11 cement plants is 724 MJ/t, and its distribution in different media is shown in **Table 3**, which can serve to estimate the waste heat resources of other cement plants

Table 3. Waste heat of each medium per unit of crude steel in a metal processing plant (MJ/t)

	Steam_low	Steam_exhaust	Cooling water(>60°C)	Cooling water(<60°C)	Fume	Air	Total
Cement	0	441	89	0	172	22	724

3.2 Waste heat resource evaluation in Tangshan

The total waste heat resources in Tangshan City are evaluated at 846 PJ, with a heating capacity of 32.1 GW. Waste heat from steel plants and power plants accounts for the vast majority, with about 539 PJ, or 64%, from steel plants and 221 PJ, or 26%, from power plants (**Figure 10**(c)). Waste heat resources are mainly concentrated in Caofeidian and Leting counties on the coast, as well as in Fengnan and Fengrun districts near the city center, and in Qian'an, where there are many large steel plants (**Figure 10**(a)). Waste heat resources in Tangshan City are mainly concentrated within low temperatures, with less than 60°C accounting for approximately 80% of the waste heat (**Figure 10**(b)), since the main waste heat from power plants and steel plants is spent steam from power generation (**Figure 9**).

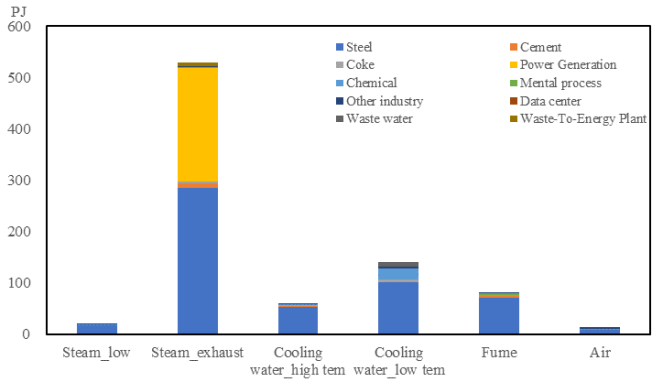

Figure 9 Media distribution of the investigated waste heat

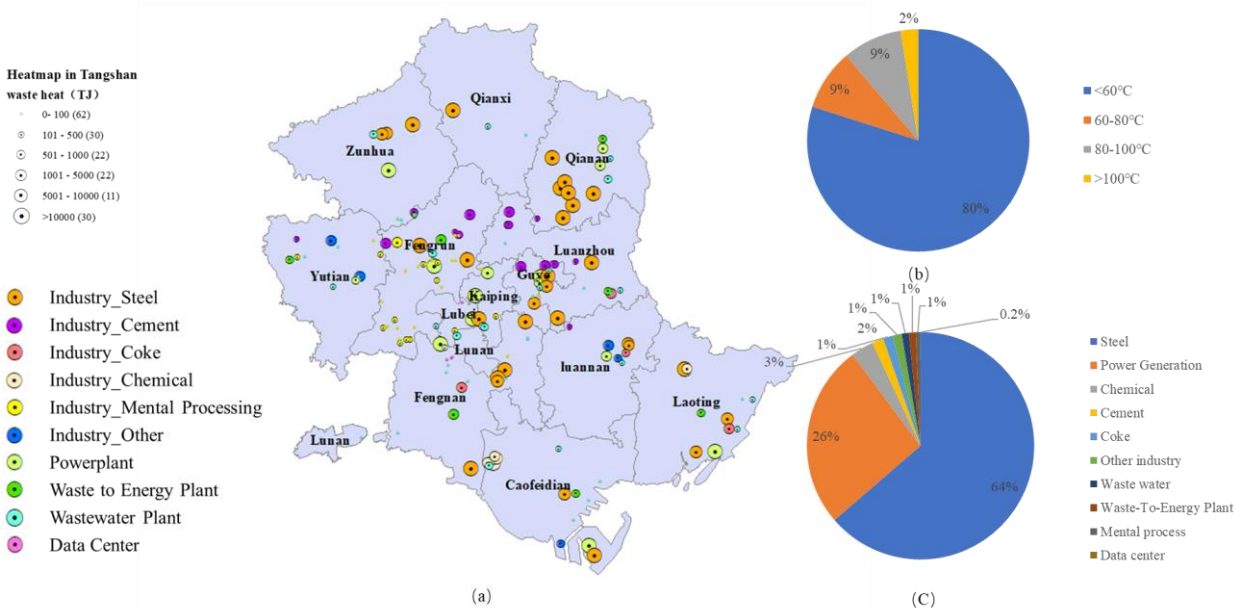

Figure 10 (a) Geographical distribution of waste heat resources (b) Temperature distribution of waste heat resources (c) Distribution of waste heat resources by heat source type

4. DISCUSSION

The previous analysis has shown that Tangshan City has an abundance and relatively even distribution of waste heat resources, which have great potential for supplying heat. It is worth noting that the vast majority of this waste heat is below 60°C and cannot be utilized directly for the existing heat demand in Tangshan, especially for industrial use, and requires a heat pump to raise the temperature.

In addition, the spatial analysis of waste heat resources generally needs to be accompanied by an analysis of heating demand[13][14]. District heating demand and industrial heating demand have been estimated for each district and county in Tangshan. The district heating demand was obtained by multiplying the heat demand per unit of floor area with the heat supply area, while the industrial heat demand was obtained by consulting the environmental assessment reports of key heat-using enterprises. Although the total amount of waste heat resources in Tangshan is abundant, there are still four districts and counties where the waste heat supply capacity is less than the heat demand, and the problem of insufficient heat sources can be solved by using the rich waste heat resources in the surrounding areas.

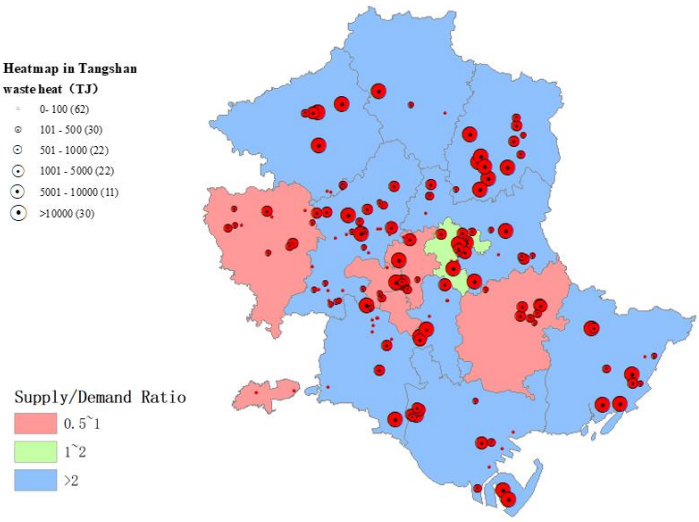

Figure 11 Heat balance map of Tangshan

5. CONCLUSION

In this paper, a bottom-up evaluation method combining survey and estimation is used. The base data for the estimation of waste heat resources in the industrial sector is derived from the survey of local plants of the same type and is therefore more reliable than a simple estimation. The study identified a wide range of waste heat resources in the Tangshan area, with a heating capacity of approximately 32.1 GW and a waste heat capacity of approximately 846 PJ, and the results of the evaluation showed that most of the waste heat resources come from steel plants or power plants. The analysis found that about 80% of the waste heat resources in Tangshan City are below 60°C, which poses a challenge for the utilization of waste heat. The heat demand in Tangshan City can be fully met by waste heat in total, but after considering the spatial distribution there are four districts and counties that need to introduce waste heat resources from the surrounding areas.

ACKNOWLEDGEMENT

This study was supported by 14th Five-Year National Key R&D Plan of China (Grant No.2022YFC3802401) and Ministry of Housing and Urban-Rural Development R&D Project of China (Grant No. K20220771).

REFERENCES

[1] International Energy Agency. Renewables 2019 market analysis and forecast from 2019 to 2024. 2019. https://www.iea.org/reports/renewables-2019.
[2] Building Energy Conservation Research Center. Annual Report on China Building Energy Efficiency 2023. Beijing: China Architecture & Building Press; 2023, 110.
[3] Bühler, Fabian, Fridolin. "Mapping of low temperature heat sources in Denmark." 28th International Conference on Efficiency, Cost, Optimization, Simulation and Environmental Impact of Energy Systems 2015.
[4] Lund, Rasmus , U. Persson . "Mapping of potential heat sources for heat pumps for district heating in Denmark." Energy.2016,129-138.
[5] Alice Dénarié a, A F F , A G S ,et al. Assessment of waste and renewable heat recovery in DH through GIS mapping: The national potential in Italy. Smart Energy, 2023.1.
[6] Max D.A. Albert, Katherine O. Bennett, Charlotte A. Adams, Jon G. Gluyas, Waste heat mapping: A UK study,Renewable and Sustainable Energy Reviews,2022, 1364-0321,
[7] Zuberi M J S ,Bless Frédéric, Jonathan C ,et al.Excess heat recovery: An invisible energy resource for the Swiss industry sector[J].Applied Energy, 2018, 228:390-408.
[8] Luberti M , Gowans R , Finn P ,et al.An estimate of the ultralow waste heat available in the European Union[J].Energy, 2022, 238.
[9] Rattner A S , Garimella S .Energy harvesting, reuse and upgrade to reduce primary energy usage in the USA[J].Energy, 2011, 6172-6183.
[10] Persson U , Mller B , Werner S .Heat Roadmap Europe: Identifying strategic heat synergy regions[J].Energy Policy, 2014, 663-681
[11] Johnson, Ilona, Choate, William T., & Davidson, Amber. Waste Heat Recovery. Technology and Opportunities in U.S. Industry. United States. https://doi.org/10.2172/1218716
[12] Saha B K , Chakraborty B , Dutta R .Estimation of waste heat and its recovery potential from energy-intensive

industries[J].Clean Technologies and Environmental Policy, 2020, 22(9).
[13] Luo A , Fang H , Xia J ,et al.Mapping potentials of low-grade industrial waste heat in Northern China[J].Resources Conservation and Recycling, 2017, 125:335-348.
[14] Wen Zheng,Yichi Zhang,Jianjun Xia,Yi Jiang. Cleaner heating in Northern China: potentials and regional balances[J]. Resources, Conservation & Recycling,2020,160(C).
[15] L. López,J.M. Blanco,J.J. Bonilla,S. Bacza,J.M. Sala. Determination of energy and exergy of waste heat in the industry of the Basque country[J]. Applied Thermal Engineering,1998,18(3).
[16] A. Dénarié,M. Muscherà,M. Calderoni,M. Motta. Industrial excess heat recovery in district heating: Data assessment methodology and application to a real case study in Milano, Italy[J]. Energy,2019,166.
[17] S. Brückner,H. Schäfers,I. Peters,E. Lävemann. Using industrial and commercial waste heat for residential heat supply: A case study from Hamburg, Germany[J]. Sustainable Cities and Society,2014,13.
[18] Larrinaga Pello,Campos-Celador Álvaro,Legarreta Jon,Diarce Gonzalo. Evaluation of the theoretical, technical and economic potential of industrial waste heat recovery in the Basque Country[J]. Journal of Cleaner Production,2021,312.
[19] Wilson M P , Worrall F .The heat recovery potential of 'wastewater': a national analysis of sewage effluent discharge temperatures[J].Environmental Science: Water Research & Technology, 2021, 7.
[20] Davies G , Maidment G , Tozer R .Opportunities for Combined Heating and Cooling Using Data Centres[J]. 2015.
[21] Persson, U., Averfalk, H., Nielsen, S., & Moreno, D. (2020). ReUseHeat project - Accessible urban waste heat (Revised version). https://www.reuseheat.eu/wp-content/uploads/2021/02/D1.4-Accessible-urban-waste-heat_revised-compressed.pdf
[22] Yin S, Xia J, Jiang Y. characteristics analysis of the heat-to-power ratio from the supply and demand sides of cities in northern China. Energies, 2020, 13(1):242

The 18th International Symposium on District Heating and Cooling, September 3–6, 2023, Beijing, China

UTILIZING WASTE HEAT FROM DATA CENTERS TO SUPPLY RESIDENTIAL QUARTERS: A SIMULATION STUDY

Maximilian Stahlhut[a], Dimitri Nefodov[a], Thorsten Urbaneck[a*]

[a] *Chemnitz University of Technology, Chemnitz, 09111, Chemnitz*

[*] *Corresponding author. thorsten.urbaneck@mb.tu-chemnitz.de*

ABSTRACT

Data centers (DCs) and their electrical/electronic components require permanent cooling. Most of the cooling demand in DCs is caused by the servers. Direct liquid server cooling enables an efficient heat removal of the server waste heat. With this technology, the cooling medium (water) leaves the rack with a maximum outlet temperature between $T_{\mathrm{IT,out,max}}$ = 50...60 °C. Consequently, free cooling with dry coolers is feasible throughout the year. At the same time, waste heat recovery is conceivable for various applications while also necessary for ecological reasons. This paper therefore investigates the heat utilization of DCs with direct liquid server cooling to supply a representative residential quarter with a peak load of 1855 kW and an annual heat load of 5078 MWh. Raising the temperature level of the DC waste heat to the temperature level of the local heating grid $T_{\mathrm{grid,s}}$ = 75 °C is done with two heat pumps including two compressors each (refrigerant R1234ze(E)). This study uses transient simulation software TRNSYS to analyze the effect of different DC sizes on the coverage of the heating load of a residential quarter as well as the proportion of reused energy of the DC (*ERF*, Energy Reuse Factor). The results show that for an IT power capacity $P_{\mathrm{el,IT,max}}$ = 2200 kW the heating load of the grid is fully covered with an *ERF* = 0.38 $\mathrm{MWh_{th}/MWh_{el}}$ (web load profile). A further increase in DC size reduces the *ERF* value. A ratio bigger than $P_{\mathrm{el,IT,max}}/Q_{\mathrm{grid,a}}$ = 0.83 $\mathrm{kW_{el}/(MWh_{th}/a)}$ causes an *ERF* ≤ 0.2 $\mathrm{MWh_{th}/MWh_{el}}$. With regard to discussions on legal obligations for waste heat recovery from DCs (e.g. Energy Efficiency Act in Germany), the ratio of DC size and annual heat load plays a decisive role. Additionally, a simplified economic analysis complements the findings of this study.

Keywords: waste heat recovery; data center; heat pump; district heating; simulation

1. INTRODUCTION

The global demand for computing power is constantly increasing. Reason for this is, among other things, the increase in online services, streaming or professional applications (simulations, artificial intelligence, etc.) [1]. A large part of the world's computing power is generated in data centers (DCs). These are responsible for about 1% of the global energy electricity demand with an increasing trend [2]. Servers have the highest electricity demand in DCs [3]. The energy demand of the servers is caused by IT loads (running programs on the server) which is then dissipated into heat. To avoid overheating of the electrical/electronic components, cooling must be provided. Various cooling technologies [4] and technical implementations [5],[6] are available. Direct liquid-cooling enables efficient heat dissipation for servers in the high-performance computing (HPC) sector. Copper coils on the mainboard lead the cooling medium (water) directly to the installed components (CPU, RAM, etc.). This allows relatively high outlet temperatures $T_{\mathrm{IT,out,max}}$ = 50…60 °C (in comparison cooling with air $T_{\mathrm{IT,out,max}}$ = 30…40 °C). Therefore, heat recovery is conceivable for various application and, in some cases, politically required. In Germany, for example, a legally binding Energy Reuse Factor *ERF* (ratio of reused energy and total DC energy demand) of at least 20% is being demanded for DCs [7].

The various possibilities for waste heat recovery from DCs are already discussed in the literature [8]. One way to use the waste heat is to integrate it into local heating grids to supply heat to buildings. Especially the integration of DC waste heat in heating grids at university campuses has been investigated exemplarily [9]-[11]. Due to a trend towards an increase in power-intensive loads and thus liquid-cooled systems [12], waste heat utilization in heating grids becomes possible for different areas of application. One promising field is supplying residential quarters with DC waste heat. However, a study investigating the suitability of DC waste heat for covering the heat load of a residential quarter depending on the DC and grid size is not known to the authors. In particular, statements on the *ERF* value to meet policy requirements are relevant for DC planning.

Therefore, this paper uses transient system simulation with TRNSYS simulation program [13] to investigate the coverage of the heating load of a typical residential quarter with waste heat from a DC with direct liquid-cooling. Influence of different DC sizes on heating load coverage and *ERF* value are included in the study. A simplified economic analysis complements

the investigation.

2. METHODOLOGY

Modelling the Heating Grid

In this study a typical residential quarter is modeled in TRNSYS. Load data (domestic hot water and heating) from a real residential quarter (Brühl in Chemnitz, Germany [14]) with a peak load of $\dot{Q}_{\mathrm{grid}}$ = 1855 kW and an annual heat demand of $Q_{\mathrm{grid,a}}$ = 5078 MWh/a are integrated into the simulation program. Figure 1 shows the load duration curve and the grid temperature for one year. To ensure comparability to other residential quarters with different heating loads, Figure 1 plots the normalized heating load $\dot{Q}_{\mathrm{grid}}/\dot{Q}_{\mathrm{grid,max}}$. The supply temperature in the grid is $T_{\mathrm{grid,s}}$ = 75 °C and the return temperature varies over the year $T_{\mathrm{grid,r}}$ = 50…62 °C. $T_{\mathrm{grid,s}}$ and $T_{\mathrm{grid,r}}$ are also based on monitoring data [14] and aim to represent a modern heating grid with relatively low temperatures.

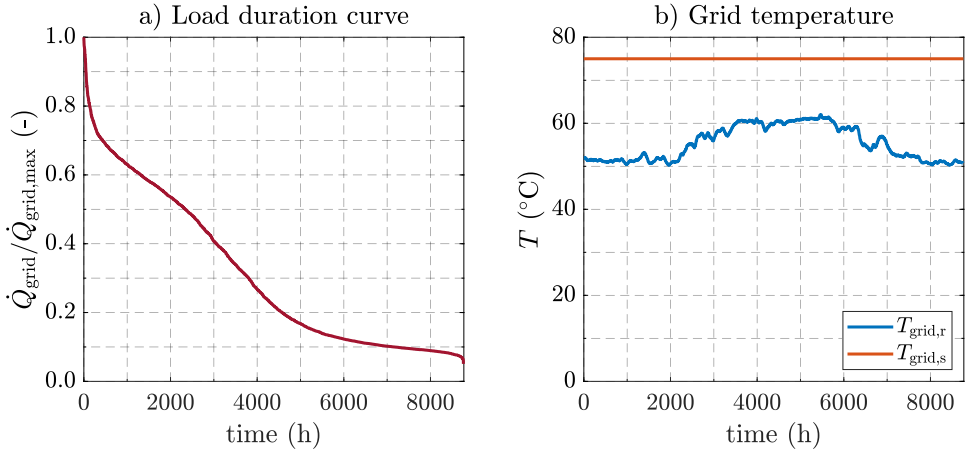

Figure 1. Load duration curve and grid temperature over one year of the investigated residential quarter (Brühl in Chemnitz, Germany [14])

The heat supply of the residential quarter is provided by two heat pumps and a hot water tank (detailed presentation and evaluation of the concept by *Nefodov* et al. in [15], [16]). Both heat pumps (refrigerant R1234ze(E)) have a nominal capacity of 750 kW and consist of two stages with own compressor each stage. Table 1 summarizes the key assumptions for the two heat pumps.

Table 1. Model assumptions for the two heat pumps (refrigerant R1234ze(E))

Heat pumps – power rating	
$\dot{Q}_{\mathrm{HP,rated}}$	750 kW
$\dot{Q}_{\mathrm{HP,con1,max}}$, $\dot{Q}_{\mathrm{HP,con3,max}}$	372 kW
$\dot{Q}_{\mathrm{HP,con2,max}}$, $\dot{Q}_{\mathrm{HP,con4,max}}$	378 kW
COP	4.1…5.05
$\dot{Q}_{\mathrm{HP,con}}/\dot{Q}_{\mathrm{HP,con,max}}$	0.75…1
Heat pumps – evaporator	
$\dot{m}_{\mathrm{eva1}}$, $\dot{m}_{\mathrm{eva2}}$	31,970 kg/h
$\Delta T_{\mathrm{HP,eva}}$	8…16 K
$T_{\mathrm{HP,eva,in}}$	51…53 °C
Heat pumps – condenser	
$\dot{m}_{\mathrm{con1}}$, $\dot{m}_{\mathrm{con3}}$	19,963…26,618 kg/h
$\dot{m}_{\mathrm{con2}}$, $\dot{m}_{\mathrm{con4}}$	20,311…27,082 kg/h
$\Delta T_{\mathrm{HP,con}}$	12 K
$T_{\mathrm{HP,con,in}}$	65 °C

Table 2. Relevant parameters of the system equipment

Hot water tank – TRNSYS Type 534	
Storage volume	1,600 m^3
Height	12 m
Medium	water
Dry cooler – TRNSYS Type 511	
$\dot{Q}_{\mathrm{cool,des}}$	253 kW
$T_{\mathrm{cool,in,des}}$	50 °C
$T_{\mathrm{cool,out,des}}$	40 °C
$P_{\mathrm{cool,fan,des}}$	8.8 kW
$T_{\mathrm{amb,des}}$	32 °C
Medium	water-glycol

An integration of the two heat pumps into the supply system takes place according to the diagram in Figure 2. Waste heat from the liquid-cooled DC is raised to the required temperature level of 75 °C of the heating grid by the two heat pumps (HP1, HP2). The heat provided by the heat pumps can vary between $\dot{Q}_{\mathrm{HP,con}}/\dot{Q}_{\mathrm{HP,con,max}}$ = 0.75…1. A *COP* is calculated based on the utilization of each heat pump. The mass flow in the evaporator $\dot{m}_{\mathrm{eva}}$ is set constant while the mass flow in the condenser $\dot{m}_{\mathrm{con}}$ varies to achieve a constant temperature lift of $\Delta T_{\mathrm{HP,con}}$ = 12 K. Through the integration of the three way valves the input temperature in the condenser is set to a constant value $T_{\mathrm{HP,con,in}}$ = 65 °C ($T_{\mathrm{HP,con,out}} = T_{\mathrm{grid,s}}$ + 2 K to

compensate heat losses).

In order to harmonize the waste heat loads from the DC and the heat load of the residential quarter, a tank storage (flat-bottom tank) with 1600 m^3 storage volume and a dry cooler are integrated into the system. Table 2 lists the relevant parameters. The cooling power of the dry cooler is adjusted automatically in the simulation model according to the DC size. In principle, the heat supply is also possible with smaller storage volumes [15]. The high storage volume ensures more supply security.

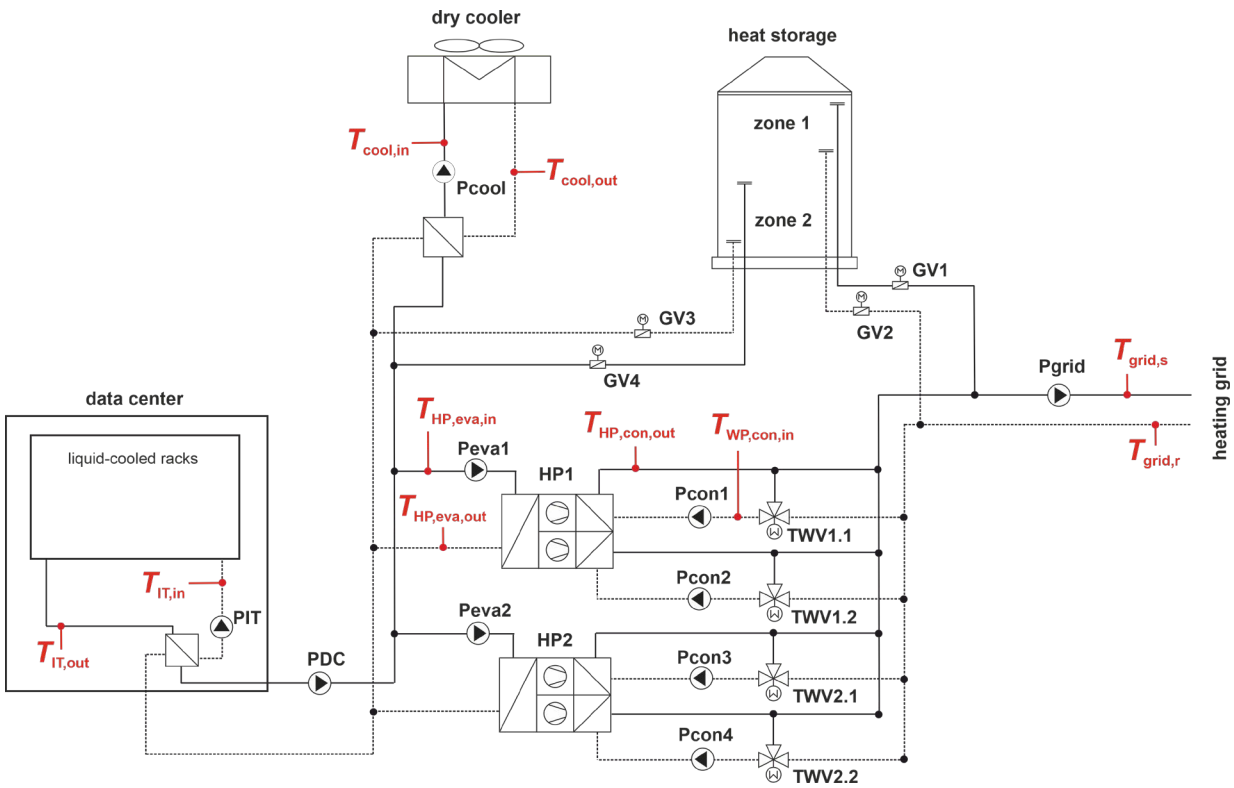

Figure 2. Simplified system scheme for supplying the heating grid with DC waste heat

The heat storage included in the system according to Figure 2 is divided into two zones. Zone 1 has the temperature level of the supply side ($T_{\mathrm{grid,r}}$ to $T_{\mathrm{HP,con,out}}$) and zone 2 the temperature level of the waste heat side ($T_{\mathrm{HP,eva,out}}$ to $T_{\mathrm{HP,eva,in}}$). Charging and discharging of the zone 1 of the storage tank (GV1 and GV2 open) and zone 2 (GV3 and GV4 open) takes place depending on the waste heat load of the DC and the heating load of the residential quarter. The main functions of the hot water storage can be summarized as follows:

- Covering the peak load of the heating grid with zone 1,
- Covering low loads of the heating grid (below the minimum operating point of the heat pumps) with zone 1,
- Cooling the waste heat of the DC with zone 2.

In the simulation model the DC size and thus the waste heat load of the DC is varied while the heating load of the residential quarter remains constant. The fraction of the heating load which is covered by the heat pumps is described by the ratio f_{HP} (Equation 1).

$$f_{\mathrm{HP}} = \frac{Q_{\mathrm{HP,con,a}} - Q_{\mathrm{los,a}}}{Q_{\mathrm{grid,a}}} = \frac{Q_{\mathrm{HPsys,a}}}{Q_{\mathrm{grid,a}}} \tag{1}$$

$Q_{\mathrm{HPsys,a}}$ describes the annual heat provided by the heat pump system to the heating grid and $Q_{\mathrm{grid,a}}$ represents the annual heat load of the heating grid. A ratio of $f_{\mathrm{HP}} = 1$ corresponds to a complete coverage of the heat load by the heat pumps while $f_{\mathrm{HP}} < 1$ means an undersupply.

Modelling the data center

In addition to information technology (IT) (servers, storage systems, network technology), DCs also consist of a cooling system, a power supply and other small consumers (see Figure 3). The power distribution between IT and facility systems can be evaluated using the Power Usage Effectiveness (*PUE*). The *PUE* (Equation 2) represents the ratio of the annual energy demand of the entire DC $P_{\mathrm{el,DC,a}}$ to the annual energy demand of the IT components $P_{\mathrm{el,IT,a}}$.

$$PUE = \frac{P_{\mathrm{el,DC,a}}}{P_{\mathrm{el,IT,a}}} \tag{2}$$

In principle, almost the entire electrical energy demand in a DC is converted into heat. However, for heat recovery purposes, the heat generated by the IT components is primarily relevant. In the investigated direct liquid-cooling system, heat dissipation from the servers occurs using water as the cooling medium. The remaining IT components (network equipment and storage systems) are mostly air-cooled due to their lower power consumptions (heat dissipation through room air conditioning). In this analysis, those components are not relevant for heat recovery. In the simulation, a ratio of water-cooled IT components to all IT components is assumed to be 90%, resulting in $\dot{Q}_{\mathrm{IT,w}}/\dot{Q}_{\mathrm{IT}} = 0.9$.

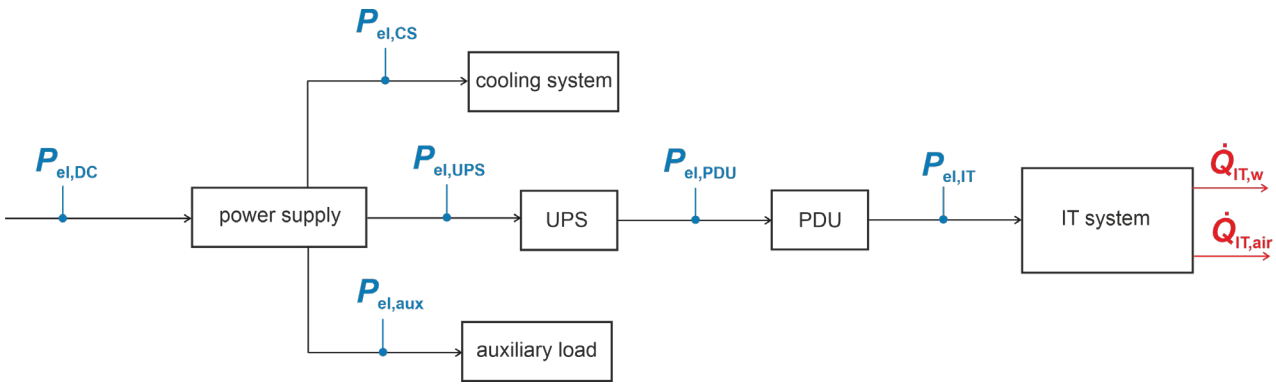

Figure 3. Simplified energy flow in a data center

The simulation model in TRNSYS focuses on representing the IT system (starting from the power distribution unit, as shown in Figure 3) and its heat dissipation. Relation between the IT inlet temperature $T_{\mathrm{IT,in}}$ and IT outlet temperature $T_{\mathrm{IT,out}}$ is described with the lumped capacitance model assuming the IT racks to have a single constant temperature (validated in [17],[18]). In the simulation model, a capacitance of each rack C_{rack} = 14.7 kJ/K with $P_{\mathrm{el,IT,rack}}$ = 50 kW and an effectiveness of $\varepsilon = 0.9$ is assumed. With increasing DC size, the number of racks increase in the simulation model. Through the control of the pump PIT (Figure 2) the output temperature of the liquid-cooled racks is set to $T_{\mathrm{IT,out}} = 55$ °C. The IT inlet temperature varies between $T_{\mathrm{IT,in}} = 40\ldots50$ °C depending on the outlet temperature of the heat pump evaporator $T_{\mathrm{HP,eva,out}}$ as well as the return temperature of the hot water storage (zone 2).

The energy demand of the other consumers (UPS, room air conditioning, etc.) is considered with a constant *PUE* value of 1.2, aiming to represent a state-of-the-art performance of a water-cooled DC. In comparison, the Climate Neutral Data Centre Pact [19] sets a *PUE* value of 1.3 for predominantly air-cooled DCs.

IT components and, consequently, the heat dissipation in a DC show part load performance. Depending on the usage profile, these loads fluctuate throughout the day and/or week. *Salom* et al. [20] categorized typical load profile for DCs. One possible classification can be made based on data loads, web loads and high-performance computing (HPC) loads (detailed explanation in [20]). Figure 4 illustrates these three load profiles.

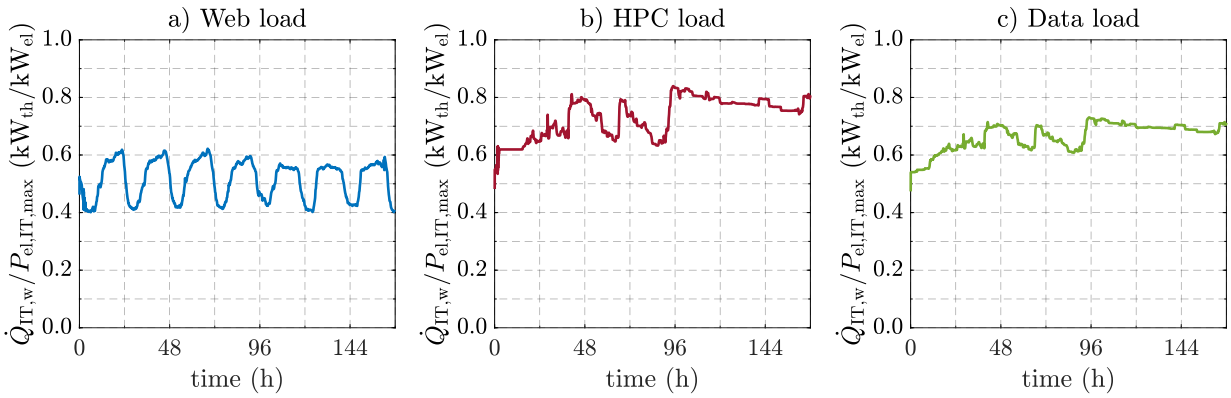

Figure 4. Heat dissipation to the cooling medium water $\dot{Q}_{\mathrm{IT,w}}$ relative to the IT power capacity $P_{\mathrm{el,IT,max}}$ for the three load profiles: a) Web load, b) HPC load, c) Data load (assuming 90% of the IT components are liquid-cooled)

An assessment of the heat recovery from DCs can be accomplished using the Energy Reuse Factor (*ERF*) (Equation 3). This value represents the ratio of energy being reused divided by the sum of the total energy demand in a DC $P_{\mathrm{el,DC,a}}$. In the context of this study, the energy being reused refers to the heat supplied to the heat pump evaporators $Q_{\mathrm{eva,a}}$.

$$ERF = \frac{Q_{\mathrm{eva,a}}}{P_{\mathrm{el,DC,a}}} \tag{3}$$

3. RESULTS

Supply of the heating grid

Figure 5 depicts the two metrics, *ERF* and f_{HP}, as a function of DC size and annual grid load. To facilitate the applicability of the results to various DCs and heating grid loads, the reference value $P_{\mathrm{el,IT,max}}/Q_{\mathrm{grid,a}}$ is introduced. Assuming an equal load duration curve, same DC configuration as well as the same supply concept, the metrics *ERF* and f_{HP} can be extrapolated to different DC and heating grid sizes.

In Figure 5, it can be observed that the two metrics, *ERF* and f_{HP}, exhibit contrasting trends. *ERF* initially increases and reaches a maximum value of $ERF_{\max} = 0.8$ $\mathrm{MWh_{th}/MWh_{el}}$ at $P_{\mathrm{el,IT,max}}/Q_{\mathrm{grid,a}} = 0.06$ $\mathrm{kW_{el}/(MWh_{th}/a)}$. As the DC size increases while keeping the grid load constant, the *ERF* decreases. Complete coverage of the grid load (assumption $f_{\mathrm{HP}} \geq 0.99$) is attained at $P_{\mathrm{el,IT,max}}/Q_{\mathrm{grid,a}} = 0.43$ $\mathrm{kW_{el}/(MWh_{th}/a)}$.

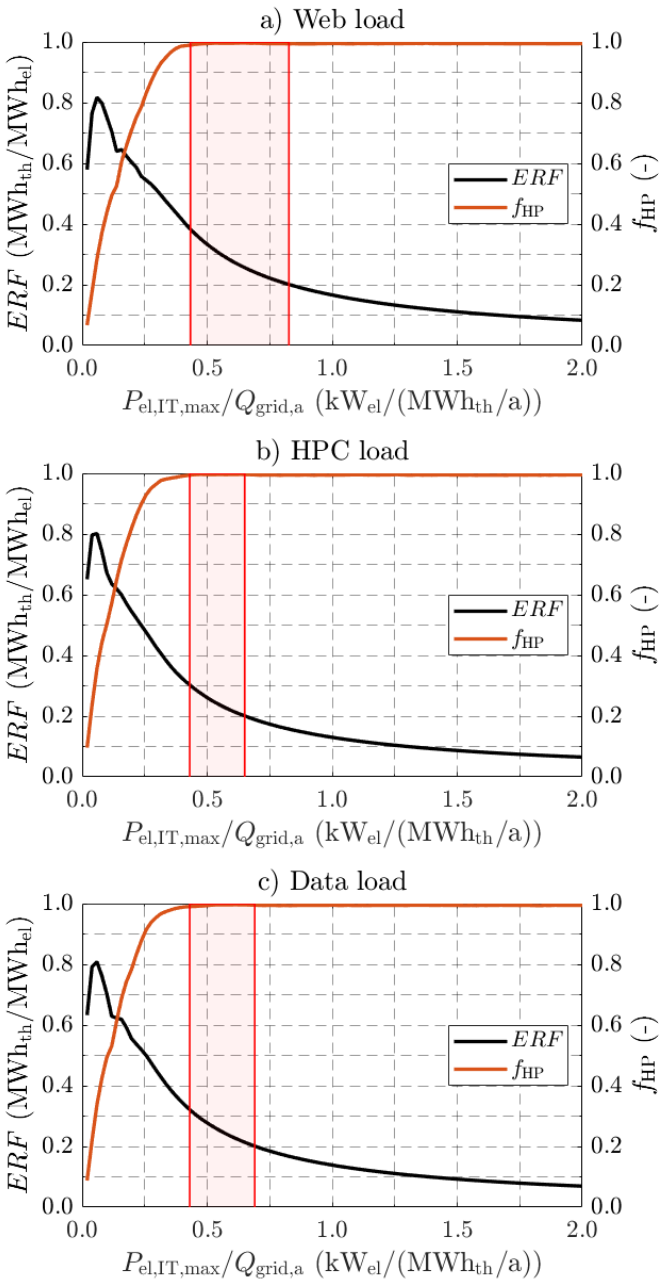

Figure 5. *ERF* and f_{HP} for the three load types a) Web load, b) HPC load, c) Data load as a function of $P_{\mathrm{el,IT,max}}$ / $Q_{\mathrm{grid,a}}$ – highlighted red area shows region where $f_{\mathrm{HP}} \geq 0.99$ and $ERF \geq 0.2$

Economic evaluation

Based on the assessed electricity and heat demands, it is possible to determine the demand-related costs for the heat supply system. The following cost analysis does not include capital costs, operating costs and other expenses. Based on this simplification, the marginal costs k_{mar} (in €/MWh) for providing heat can be calculated (assuming complete coverage of the heating load with the heat pumps, $f_{\mathrm{HP}} \geq 0.99$). Equation 4 illustrates the assumptions for calculating the marginal costs.

$$k_{\mathrm{mar}} = \frac{k_{\mathrm{h}} \cdot Q_{\mathrm{eva,a}} + k_{\mathrm{el}} \cdot (P_{\mathrm{el,pump,a}} + P_{\mathrm{el,HP,a}})}{Q_{\mathrm{HPsys,a}}} \tag{4}$$

$P_{\mathrm{el,pump,a}}$ represents the annual electricity demand of the pumps exclusively required for the heat supply of the heating grid ($P_{\mathrm{el,Peva,a}}$, $P_{\mathrm{el,Pcon,a}}$, $P_{\mathrm{el,Pgrid,a}}$). k_{h} symbolizes the heating costs, k_{el} the electricity costs and $P_{\mathrm{el,HP,a}}$ the annual electricity demand of the heat pumps. Figure 6 shows the marginal costs k_{mar} as a function of k_{el} and k_{h}.

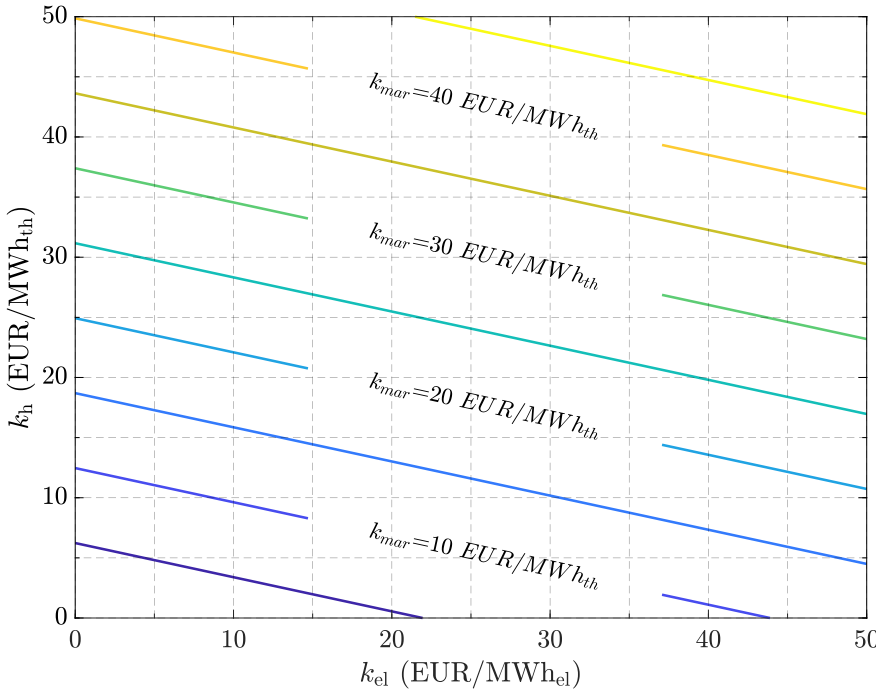

Figure 6. Marginal costs k_{mar} depending on the cost of electricity k_{el} and the heat supply cost k_{h}

4. DISCUSSION

The results of this study demonstrate (under the defined assumptions) that achieving an *ERF* greater than 0.38 is not feasible when fully meeting the heating demand of the residential quarter. This is attributed to the different load profiles between the IT system's heat dissipation and the heat demand in the grid. The heat demand exhibits strong seasonal variations, while the heat loads from the DC undergo only minor fluctuations throughout the year. Consequently, fully covering the grid load during the winter months through the proposed supply system leads to a significant portion of the DC waste heat requiring cooling during the summer months. From the perspective of the DC, increasing the *ERF* value can be achieved by under-supplying the heating grid. In this case, grid operators would need to plan additional supply technologies to fully cover the grid load during the winter months. The proportion of reused energy reaches its maximum when the dissipated heat from the DC matches the minimum heating load in the residential quarter. In this scenario, there is no need for cooling the DC waste heat. DC operators can thus save investment costs as well as operating costs for the cooling infrastructure.

The *ERF* value is influenced not only by the amount of heat dissipated into the supply system but also by the design of the DC. Depending on the type of DC usage, the composition of IT components (servers, network equipment, storage system) and therefore the proportion of waste heat provided at a sufficiently high temperature level for heat recovery can vary. Additionally, the *PUE* value (Equation 2) has an impact on the *ERF* value. Increasing the *PUE* value (e.g., due to an inefficient cooling system or more conversion losses at the UPS) while leaving the proportion of utilized waste heat constant, decreases the *ERF* value.

The demand-related costs for the proposed heat supply system are primarily dependent on the energy cost for operating the heat pump and the heat supply cost. The heat supply cost has a greater influence on the demand-related costs. An increase of 10% in heat supply cost leads to 7.8% increase in the marginal costs, whereas the same increase in electricity prices results

in a 2.2% increase in the marginal costs. Therefore, the economic viability of the heat supply system is significantly dependent on the heat supply cost for the DC waste heat.

5. CONCLUSION

The heating load of the presented residential quarter with an annual heat demand of $Q_{\mathrm{grid,a}}$ = 5078 MWh/a and a peak load of $\dot{Q}_{\mathrm{grid}}$= 1855 kW is completely covered with a DC size of $P_{\mathrm{el,IT,max}}$ = 2200 kW (under the defined assumptions). The proportion of the reused energy is *ERF* = 0.38 MWh_{th}/MWh_{el} for this DC size while using the web load profile (HPC load *ERF* = 0.3 MWh_{th}/MWh_{el}, data load *ERF* = 0.32 MWh_{th}/MWh_{el}). As the DC size increases while maintaining a constant grid load, the *ERF* decreases. For the web load a ratio $P_{\mathrm{el,IT,max}}/Q_{\mathrm{grid,a}}$ greater than 0.83 $kW_{el}/(MWh_{th}/a)$ leads to an *ERF* smaller than 0.2 MWh_{th}/MWh_{el} (HPC load 0.65 $kW_{el}/(MWh_{th}/a)$, data load 0.69 $kW_{el}/(MWh_{th}/a)$).

The results demonstrate that it is possible to fully supply a residential quarter with DC waste heat. If a certain proportion of reused energy for DCs is required by policy-makers, the ratio of DC size to annual grid load needs to be considered in the planning of both the DC and the heating grid. If the DCs contribute only partially to the heat supply of the heating grid, larger *ERF* values are generally achievable. In order to meet the heating demand, additional supply technologies would then be necessary in the winter period to meet the grid's peak load.

The design of the DC has a significant impact on the presented results. Both the proportion of usable waste heat from the DC and the energy demand of the DC infrastructure affect the *ERF* value. For further analysis, it is conceivable to account for this impact by looking at different types of DC configurations. This would allow a more comprehensive assessment of the *ERF* value and therefore the heat recovery potential for liquid-cooled DCs.

ACKNOWLEDGEMENT

The research work is funded by the German Federal Ministry of Education and Research under the reference 03SF0623A/B/C based on a resolution of the German Bundestag. Project management is carried out by Projektträger Jülich (PtJ). The authors would like to express their sincere thanks for the funding, support and cooperation.

REFERENCES

[1] Jones N. How to stop data centres from gobbling up the world's electricity. Nature. 2018 Sep; 561 (7722): 163-166. doi: 10.1038/d41586-018-06610-y PMID: 30209383.

[2] Cozzi L. et al. Digitalization and Energy. OECD, 2017. https://www.iea.org/reports/digitalisation-and-energy [last accessed 08.05.2023]

[3] Hintemann R., Hinterholzer S. Data centers 2021: Data center boom in Germany continues - Cloud computing drives the growth of the data center industry and its energy consumption. Borderstep Institute for Innovation and Sustainability. doi: 10.13140/RG.2.2.31826.43207

[4] Li Z., Kandlikar, S. G. Current status and future trends in data-center cooling technologies. Heat Transfer Engineering 2015; 36(6): 523-538. doi: 10.1080/01457632.2014.939032

[5] Gavaldà O., Depoorter V., Oppelt T., van Ginderdeuren K.: Report of different options for renewable energy supply in Data Centres in Europe. Deliverable D4.1, 2014. http://www.renewit-project.eu/documents/deliverable/ [last accessed 08.05.2023]

[6] VDI Verein Deutscher Ingenieure. VDI 2054 Ventilation and air conditioning Data processing. 2019 Aug.

[7] Federal Ministry for Economic Affairs and Climate Action. Press Release. https://www.bmwk.de/Redaktion/DE/Pressemitteilungen/2023/04/20230419-kabinett-beschliesst-energieeffizienzgesetz.html [last accessed 08.05.2023]

[8] Ebrahimi K., Jones G. F., Fleischer A. S. A review of data center cooling technology, operating conditions and the corresponding low-grade waste heat recovery opportunities. Renewable and Sustainable Energy Reviews. 2014; 31: 622-638. doi: 10.1016/j.rser.2013.12.007

[9] Oltmanns J., Sauerwein D., Dammel F., Stephan P., Kuhn C. Potential for waste heat utilization of hot-water-cooled data centers: A case study. Energy Science & Engineering. 2020; 8(5): 1793-1810. doi: 10.1002/ese3.633

[10] Feike F., Oltmanns J., Dammel F., Stephan P. Evaluation of the waste heat utilization from a hot-water-cooled high performance computer via a heat pump. Energy Reports. 2021; 7: 70-78. doi: 10.1016/j.egyr.2021.09.038

[11] Dvorak V., Zavrel V., Torrens Galdiz J. I., Hensen J. L. Simulation-based assessment of data center waste heat utilization using aquifer thermal energy storage of a university campus. Building Simulation. 2020; Vol. 13: 823-836. doi: 10.1007/s12273-020-0629-y

[12] Statista Search Department. Data Center 2021. Statista. https://www.statista.com/study/107178/data-center/ [last accessed 08.05.2023]

[13] Klein S. A. et al. TRNSYS 18: A Transient System Simulation Program. Solar Energy Laboratory, University of

Wisconsin, Madison, USA. 2017. http://sel.me.wisc.edu/trnsys [last accessed 08.05.2023]
[14] Urbaneck T., Shrestha N. Lal, Oppelt T., Frotscher O., Göschel T., Uhlig U., Frey H. Solare Fernwärme für das Quartier Brühl in Chemnitz – Begleitforschung (SolFW). Technische Universität Chemnitz, Fakultät für Maschinenbau, Professur Technische Thermodynamik (Ed.), inetz GmbH (Ed.). 2020 - ISBN: 987-3-9812586-5-3, Open Access: https://nbn-resolving.org/urn:nbn:de:bsz:ch1-qucosa2-390452
[15] Nefodov D., Xiao S., Richter M., Urbaneck T. Optimal Design of a Heat Pump System with Hot Water Storage and Approach for Evaluating the Flexibility. EuroHeat&Power. 2022; Vol. 1 (51): 20-29 - ISSN 1613-0200-22698
[16] Nefodov D., Xiao S., Richter M., Urbaneck T. Optimising Operations of a Heat Pump System with Hot Water Storage. 2022; Vol. 2 (51): 34-43 - ISSN 1613-0200-22698
[17] Carbó A., Oró E., Salom J., Canuto M., Macías M., Guitart J. Experimental and numerical analysis for potential heat reuse in liquid cooled data centres. Energy Conversion and Management. 2016; Vol. 112: 135-145. doi: 10.1016/j.enconman.2016.01.003
[18] Pardey Z., Demetriou D., Erden H., Vangilder J., Khalifa H., Schmidt R. Proposal for Standard Compact Server Model for Transient Data Center Simulations. ASHRAE Transactions. 2015; Vol. 121: 358-370
[19] Climate Neutral Data Centre Pact (CNDCP). Self Regulatory Initiative. https://www.climateneutraldatacentre.net/ [last accessed 15.05.2023]
[20] Salom J., Urbaneck T., Oró E. Advanced Concepts for Renewable Energy Supply of Data Centres. Gistrup (Denmark): River; 2017, 334. ISBN: 978-87-93519-42-8 (Hardback) 978-87-93519-41-1 (E-Book)

ABBREVIATIOS

CPU	Central processing unit
GV	Gate valve
HP	Heat pump
HPC	High performance computing
IT	Information technology
Pcon	Pump condenser
Pcool	Pump dry cooler
PDC	Pump data center
PDU	Power distribution unit
Peva	Pump evaporator
Pgrid	Pump heating grid
PIT	Pump information technology
RAM	Random access memory
TWV	Three way valve

NOMENCLATURE

Quantities

COP	Coefficient of Performance	kW_{th} / kW_{el}
ERF	Energy Reuse Factor	MWh_{th} / MWh_{el}
f_{HP}	Fraction heat pump	-
k_{el}	Electric energy cost	€/MWh_{el}
k_h	Heat supply cost	€/MWh_{th}
k_{mar}	Marginal cost	€/MWh_{th}
$\dot{m}$	Mass flow rate	kg/s, kg/h
P	Electric Power	kW, MW
PUE	Power Usage Effectiveness	-
Q	Heat quantity	kWh, MWh
$\dot{Q}$	Heat	kW, MW
T	Temperature	°C

Subscripts

a	Year	grid	Heating grid	rated	Rated power
amb	ambient	HP	Heat pump	s	Supply
air	Air	HPsys	Heat pump system	th	Thermal
aux	Auxiliary	in	In	UPS	Uninterrupted power supply
con	Condenser	IT	Information technology		
cool	Dry Cooler	los	Losses	w	Water
CS	Cooling system	max	Maximum		
DC	Data center	out	Out		
des	Design mode	pump	Pump		
el	Electric	PDU	Power distribution unit		
eva	Evaporator	r	Return		
fan	Fan	rack	Rack		

APPLICATION ANALYSIS OF DATA CENTERS AS DISTRICT HEATING SOURCES

Liu Junhong*, Zhang Xiucheng, Xu Zhenhong, Yuan Jingjing, Han Chang

School of Thermal Energy Engineering, Shandong Jianzhu University, Jinan 250101, China
** ljhruby@sdjzu.edu.cn*

ABSTRACT

The rapid development and popularization of information technology have led to the rapid development of data centers. A large amount of energy is consumed by uninterruptible power supply data centers, and is converted into thermal energy through IT equipment within the data center to dissipate into the atmosphere, which accelerates global warming and energy waste, and greatly increases the water consumption, even may damage the ecological balance of water bodies. Based on the supplied temperature and heat, and connection to district heating network, the applicability of using data centers as heat source for the fourth generation of district heating (4GDH) and the fifth generation of district heating and cooling (5GDHC) was analyzed. When data centers are used as heat sources, priority should be given to the utilization of the chilled water side. The series or parallel connection method should be determined based on the heat consumption scale, and the annual heat production and consumption balance should be matched.

Keywords: Data Centers, 4GDH, 5GDHC, exhaust heat recovery

1. INTRODUCTION

A data center (DC) is a building that provides an operating environment for centrally placed electronic information devices [1]. With the widespread application of such as information technologies, cloud computing, and big data, data centers have rapidly developed and brought huge energy consumption at the same time, which is a major challenge faced by global data centers.

The total number of global data centers exceeds 3 million at the end of 2021, and its total power consumption accounts for approximately 1.3% of the global total power consumption [2]. There are over 550000 data centers in China, with an annual total power consumption of approximately 202.8 billion kWh, accounting for 2.7% of the country's total power consumption. It is predicted that the electricity consumption of China's data centers will exceed 400 billion kWh by 2030, accounting for 3.7% of the total electricity consumption in society [3]. With the further promotion of China's "carbon peak, carbon neutrality" strategy, the data center needs green and low-carbon development with energy conservation and consumption reduction.

A large amount of energy is consumed by data centers that operate continuously throughout the year, and electrical energy is converted into thermal energy through servers and network transmission equipment within the data center. In order to ensure the normal operation of IT equipment, a refrigeration and air conditioning system is required to continuously cool the data center whole year. The energy consumption of the refrigeration and air conditioning system in the data center accounts for 30-50% of the total energy consumption in the data center [4]. Therefore, the energy-saving of the refrigeration and air conditioning system is the key to energy conservation and consumption reduction in the data center.

In addition, data centers using chillers consume a significant amount of water through cooling towers. The refrigeration system emits heat from data centers into the surrounding environment to maintain the normal operating temperature of IT equipment when using chillers. This has accelerated global warming and energy waste, and greatly increased the annual water consumption for cooling tower water replenishment. For example, a data center in Beijing with an IT equipment capacity of 6000kW consumes a maximum daily water consumption of 744.04 tons, and the cooling tower make-up water volume of 615.6 tons [5]. A Grade A data center in the suburbs of Shanghai uses a water-cooling system, with an annual cooling circulating water replenishment of 1.314 million tons, accounting for about 99% of the base's annual water consumption [6]. With the intensification of the global freshwater crisis in recent years, problems such as uneven distribution of freshwater resources and excessive development of groundwater have gradually emerged [7]. More and more people are paying attention to the conservation and utilization of water resources. How to reduce water consumption in data centers has become a major research topic in data centers [8].

Free cooling technology which is currently recognized as one of the important energy-saving measures for data centers at home and abroad also exacerbate global warming, and may damage the ecological balance of water bodies. Free cooling

technology uses natural cold air [9] or low-temperature water [10],[11] to cool the DC room. However, the use of natural cold air releases a huge amount of heat that can be utilized into the atmosphere, exacerbating global warming. Using low-temperature water sources discharges heat from the data center into rivers, lakes, and seawater, which can cause the water around the heat exchanger to warm up, resulting in changes in the water environment of the water body, such as a decrease in dissolved oxygen content [12], eutrophication [13], and affecting the growth of aquatic organisms [14], thereby disrupting the ecological balance of the water. These impacts require close monitoring to obtain more accurate data.

The heat production in data centers is stable and significant. If this heat can be utilized, it will effectively reduce global warming and energy waste caused by heat emissions, improve energy efficiency in data centers, and significantly reduce water consumption in data centers. Although research on exhaust heat recovery in data centers has been conducted from various aspects and has been applied in fields such as heating [15],[16], greenhouses [17], swimming pools [18], and absorption refrigeration [19], most people hasn't enough knowledge of exhaust heat in data centers and paid insufficient attention to it.

The supply and return water temperature, heating capacity, and connection methods with the heating network that data centers can provide are introduced. And issues when using data centers as district heating and cooling sources are proposed. This will expand people's understanding of data centers as heat sources and provide development ideas for large-scale exhaust heat recovery and utilization in data centers.

2. 4GDH and 5GDHC

District heating (DC) uses steam or hot water as the medium, supplying domestic and production heat to users in a certain area through the heating network from a centralized heat source. At present, district heating technology has developed from the first generation of steam heating to the fourth generation of district heating (4GDH) [20], until the latest stage of development: the fifth generation of district heating and cooling (5GDHC) [21]. The required heat source temperature has become lower and lower, from the first generation of steam less than 200°C to 4GDH of low hot water at 30°C-70°C, until 5GDHC of 5°C-30°C [22].

4GDH has lower grid losses because of its better utilization of low-temperature heat sources, can improve efficiency in the production system – heat pumps, CHP units and boilers. 4GDH can form an integration of overall smart energy systems based on renewable energy including a sustainable use of biomass [23].

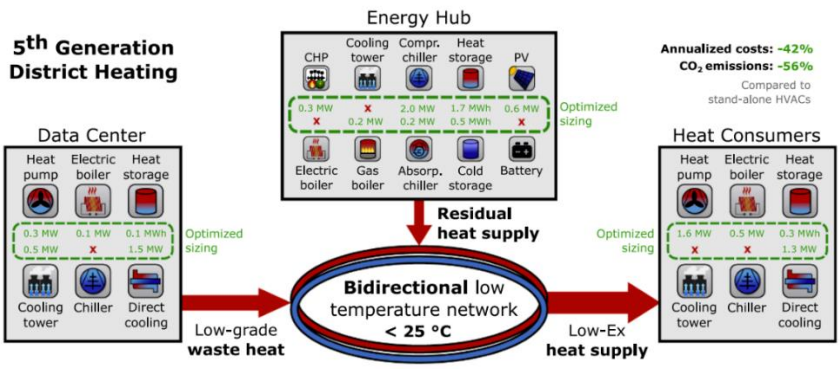

Figure 1. Illustration of the concept of 5GDHC [22]

While the heating network of 5GDHC consists of a warm and a cold pipe as shown in Figure 1. The temperature of the fluid in the warm pipe is around 5-10°C higher than the temperature in the cold pipe. The temperatures in both pipes are close to the surrounding, which keeps heat losses to a minimum. In order to raise the temperature level for space heating (SH) or domestic hot water (DHW), heat pumps are equipped. Heat pumps use water from the warm pipe as heat source, discharge cooled water from the evaporator into the cold pipe. Likewise, chillers use the network as heat sink. They take water from the cold pipe and discharge the heated fluid into the warm pipe. Thus, the flow direction of the water in the network can change over time in each segment of the network and only depends on the operation of the decentralized pumps needed by the heat consumer. Long Weiding et al. [24] think that 5GDHC is energy bus (Ebus) which is proposed in 2008 in China. The water temperature of the Ebus pipeline network is as low as 12°C-30°C, and uninsulated plastic pipelines can be used with longer transportation distances. For circular heating networks, the delivery pump can be exempted.

The data center has exhaust heat all year round and is a supplier in the district heating network, but it is both a user and a supplier in the district energy system, so it is a prosumer [25]. Under a certain business model, these prosumers can benefit by contributing heat to the heating network. 5GDHC and the active distribution network form a complex new scenario of tight coupling of electricity-heat-cooling, heat prosumers and bi-directional transfer, forming a multi-energy flow of prosumer-based integrated energy system [26]. The prosumer integrated energy system driven by 5GDHC has attracted

attention and research both at home and abroad.

3. Feasibility analysis as heat resources

Although the heat and temperature within IT servers is different, and even local high temperatures of 115°C may occur[27] However, due to its heat is taken away through the refrigeration and air conditioning system (RACS), as shown in Figure2, the temperature of the medium that can be utilized in the RACS is directly considered when recovering the exhaust heat.

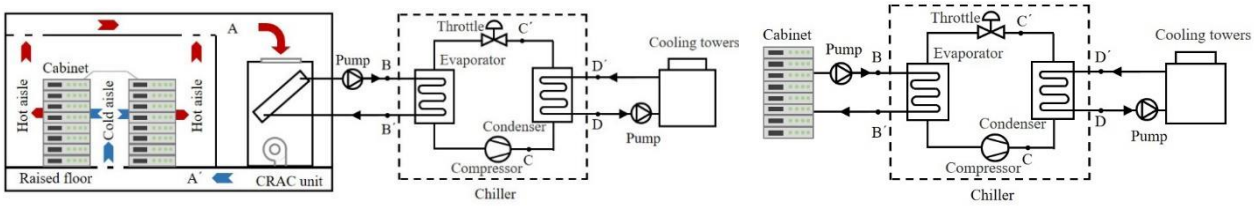

a. air cooling b. liquid cooling

Figure 2. Schematic diagrams of RACS for data centers

Chillers are often used to prepare cold air for cooling IT equipment in DC equipped with low-power density cabinets, as shown in Figure 2a. Returned hot air is cooled through computer room air conditioning (CRAC) unit before sent to the raised floor. With the development of server technology, the power density of data center cabinets is gradually increasing. Traditional cold air cooling methods cannot meet the demand, so liquid cooling with larger heat capacity is needed to meet the heat dissipation needs of IT equipment. Liquid cooling is the process of releasing heat from IT equipment to the liquid cooling medium through direct immersion or indirect contact with the cooling plate, as shown in Figure 2b.

In Figure 2, the medium in loop A is air, loop B is chilled water, loop C is refrigerant, and loop D is cooling water. The chiller can be configured according to the cooling needs of the data center. When a chiller is not needed, the chilled water directly exchanges heat with the cooling water in the outdoor cooling tower through a replaced heat exchanger.

3.1. Supplied temperature

Air cooling DCs often adopt traditional primary return centralized air conditioning systems, which mix fresh air (Omitted in the figure 2 for simplicity) and return air through CRAC units. Because the mixed air needs to be cooled and dehumidified, it is generally equipped with a 7/12°C chiller. In order to reduce the energy consumption of the air conditioning system, the fresh air is treated separately for dehumidification now. Therefore, CRAC units only undertakes the cooling function, which can maximize the inlet and outlet water temperature of the chilled water and improve the efficiency of the chillers.

18°C-27°C is currently a common inlet temperature requirement for electronic information equipment in production enterprises around the world. Considering a temperature difference (TD) of 6°C between the suppled air temperature and the cold water supplied, the supply water temperature range for chilled water is 12°C-21°C. At present, the supply/return water temperatures for chilled water are 12/17°C [28], 12/18°C [29], 13/19°C [30], 14°C/20°C [31], 15/22°C [32], and 18/28°C [33] etc., with a water TD between 5°C-10°C. While the temperature of the cooling water supply and return in summer is generally set at 32/37°C, and will decrease in other seasons, the minimum inlet temperature is considered to be 15°C. If the design TD of the cooling water is within 5°C-8°C, the return water temperature range of the cooling water is 7°C-32°C.

If the air in the computer room is directly utilized, the supply air temperature is between 18°C-27°C, and the return air temperature range is between 26°C-42°C when the supply and return air TD is between 8°C-15°C. For rack mounted servers that can accept an environment with a supply air temperature of 10°C-35°C, or even more wide (5°C-40°C) [34], the return air temperature will correspondingly increase.

Liquids have higher heat carrying capacity and convective heat transfer coefficient than air, especially in boiling situations. Therefore, direct contact with server components can generate higher heat transfer rates. Liquid cooled servers can increase the supply temperature, such as 30/35°C [35], and can use large TD, such as 40°C/55°C [36], even 45/60°C [37], and the supply temperature difference between 5°C-15°C. The supply temperature varies with the different liquid cooling methods, server types, and media, and ranges from 14°C-62°C in the literature based on Xiao statistics [38]. Although a temperature difference of 15°C between liquid cooled coolant and electronic components can meet the heat dissipation needs, the power consumption of servers increases with the increase of coolant inlet temperature [39]. Therefore, the supply temperature is mostly between 30°C-40°C, which accounts for 2/3 of the statistical literature by Xiao.

According to the different medium temperatures, the matching degree of DH in the data center is shown in Table 1. In addition, if a chiller with heat recovery is used, the heat exchanger is connected in series at point C in Figure 2 or in parallel at point CC '. The C-point series heat exchanger is a partial heat (sensible) recovery heat exchanger that can provide hot water at 40°C-45°C [40], while the CC 'point parallel heat exchanger is a total heat recovery heat exchanger that can provide hot water at 40°C-48°C [41] for 4GDH.

Table 1. Supplied temperature in DC and matched DH

Cooling method	classify	medium	Inlet temp	Outlet temp	TD	Matched DH
Air cooling	chiller	Chilled water	7℃～21℃	12℃～28℃	5～10℃	5GDHC
		Chilling water	15℃～37℃	7℃～32℃	5～8℃	4GDH &5GDHC
	air directly	Air	18℃～27℃	26℃～42℃	8℃～15℃	4GDH &5GDHC
Liquid cooling	single-phase	Coolant	30℃～60℃	35℃～75℃	5℃～15℃	4GDH &5GDHC
	two-phase	Coolant	14℃～62℃	19℃～77℃	5℃～15℃	4GDH &5GDHC

3.2. Heating scale

If the DC scale is divided by area [42], the heat generation of data centers with the same area will vary depending on the power of the cabinets. Therefore, according to the Ministry of Industry and Information Technology of the People's Republic of China, the scale of the data center is defined based on the number of standard racks. Due to the uninterrupted operation of IT equipment for 8760 hours throughout the year, and the conversion of 97% of electricity consumption into heat, the heat generation of different data centers is shown in Table 2.

Table 2. Heating Capacity of Data Centers of Different Scales

Data center scale	type	Standard rack quantity (a/ piece)	Power(kW)	Heat(kW)
micro data center	micro	a＜100	＜250	＜242.5
small data center	small	100≤a＜500	250～1250	242.5～1212.5
midsize data center	midsize	500≤a＜3000	1250～7500	1212.5～7275
large data center	large	3000≤a＜10000	7500～25000	7275～24250
	supersize	a≥10000	≥25000	≥24250

The actual power consumption of data centers depends on the load rate of servers, which varies depending on the type and rate of server load.

3.3. Connection to district heating network

Heat of data centers used as district heating sources can directly and indirectly release heat to the heating network.

Heat direct utilization only requires heat exchanger and water pump connected in series or parallel with the pipelines of its RACS, which increases less investment but may limit its applicability due to the low temperature. When connected in series, the heat exchangers of the heat recovery system can be arranged at points A, B, C, and D as shown in Figure 2. When connected in parallel, the heat exchangers can be connected at points AA ', BB', CC ', and DD', respectively.

In order to increase the applicability of exhaust heat recovery, heat indirect utilization is by connecting heat pump (HP) in series or parallel on the pipeline to increase the temperature connecting to the heating network. That is to say, through indirect utilization, heat is absorbed from the air in the computer room, the chilled water and the cooling water of the chiller through a heat pump, and then heated and transported to the heating network.

Mahdi et al. [43] used an air source heat pump in a data center in Iran to directly recover exhaust heat of the return air of the computer room, thereby reducing the temperature of the return air and the cooling load of the RACS. Zhang et al. [44] used plate heat exchanger on the chilled water side of 12℃/18℃ in the data center first, and then used centrifugal heat pump units to provide 45℃/40℃ hot water for space heating. Li Peng'an [45] used a screw heat pump to raise the temperature of 22℃/17℃ cooling water in parallel with the cooling tower to prepare 50℃/45℃ hot water for 2000m^2 space heating, saving an annual cost of ￥192600; Li Jinyi [46] used the same method to prepare 50℃/40℃ hot water from 28℃/20℃ cooling water using a centrifugal water source heat pump for heating 500000m^2. The water source heat pump unit can be connected in series with the cooling tower to prepare hot water for heating at 45℃/40℃ [47], also suppress the risk of water freezing during the heating season [48].

4. RESULTS AND DISCUSSION

Based on the above lists of temperature, heat production and utilization of data centers, it's obvious that data center can be good district heating sources. The economy of a data center exhaust heat recovery system is closely related to its heat recovery rate. When the recovery rate is relatively low, the economy is corresponding poor [44]. When data centers are used as district heating sources, the followings should be considered.

4.1. Priority for the use of chilled water

As shown in Figure 2, the chilled water with closed cycle which does not come into contact with the outside world has better water quality than the cooling water that contacts with the outside through cooling tower. Furthermore, utilization of the chilled water side can reduce the capacity of the chiller. The pressure control requirements in the exhaust heat recovery

system are low, and the system initial investment and maintenance cost are low.

4.2. Selection of series and parallel connection

When the heat recovery system is parallel connection with the loop of chilled water, the resistance is small, but its fluctuation of water temperature can affect the temperature fluctuation of chilled water supply and return. Therefore, when the heat recovery load is relatively large, it is recommended to use a heat recovery system in parallel with the data center, and set up a heat recovery variable frequency water pump and plate heat exchanger to ensure stable operation of the hot return water temperature. When the heat recovery load is relatively small, it is recommended to use a heat recovery system in series with the data center cold source [44].

4.3. Annual heat production and consumption balance

Since the data center's annual heat production is relatively stable, if it is used as a district heat source, the thermal equilibrium of its heat users must be considered (that is, the matching between the). If the heat is only used for space heating in winter, the heat from other seasons is still nowhere to be used, which is not conducive to the development of data centers as heat sources. Even for data centers that use liquid cooling, absorption refrigerator can be used to utilize waste heat in summer. Data center's heat production and heat users' heat consumption should match throughout the year. Therefore, the range of users who can use heat of low temperature in the data center should be expanded.

Space Heating in winter has different temperature requirements for different heating modes. For example, the water supply temperature for hot water floor radiation heating systems should be between 35°C-45°C, and should not exceed 60°C; The TD between supply and return water should be between 5°C-10°C; The capillary network radiation system arranged on the ceiling and wall should have a water supply temperature of 25°C-35°C, and a water supply and return temperature difference of 3°C-6°C. Even with the use of radiators for heating, a large amount of low-temperature hot water below 60°C is now used.

When the full year domestic hot water supply system is not equipped with sterilization and disinfection facilities, the outlet temperature of water heating equipment in hospitals, sanatoriums should be between 60°C-65°C, while in other buildings should be between 55°C-60°C [50].

The design water temperature of the swimming pool is between 25°C-28°C, so the water supply temperature does not exceed 40°C all year round.

Controlling root zone temperature is more important than controlling air temperature for greenhouses. The temperature range required for the Greenhouse root zone is relatively narrow (15°C-25°C) [51]. Root zone heating can reduce the greenhouse environment required for crop growth by 5°C-15°C compared to traditional heating air, and save energy by 28%. Cooling down the root zone helps the greenhouse weather through summer. So low temperature in the data center is very useful for greenhouses root zone all year around.

Appropriate temperature helps to promote the healthy development of animals. Excessive or low temperature can lead to various adverse reactions, even leading to animal death. According to the Environmental Quality Standards for Livestock and Poultry Farms [52], the temperature inside young poultry houses is 21°C-27°C, while the temperature inside adult poultry houses is 10°C-24°C, and the temperature inside cattle houses is 10°C-15°C. Water temperature is an important environmental condition for aquaculture, and different varieties of aquatic products have different requirements for water temperature. Sea cucumber breeding requires a water temperature of 16°C-23°C, marine fish (such as turbot) cultivation generally requires a water temperature of 12°C-20°C, and shrimp and shellfish cultivation requires a water temperature of 22°C-25°C [53].

Commercial linen washing and drying requires heat throughout the year. For medical linen, the washing temperature should be below 38°C in the early stage, and the water temperature should be around 60°C during bleaching [54]. The drying should be done with hot air not exceeding 65°C.

While drying of herbs, fruits, vegetables also need heat. Because most of these plants are generated outside of winter, they can greatly consume the exhaust heat of non-heating seasons. Herb has the characteristics of heat sensitivity, volatility, and high viscosity. It is necessary to consider drying in a low-temperature environment. For example, for rhizome type traditional Chinese medicine with a slice thickness of 0.4cm, the drying rate is highest and quality is best when the hot air temperature is between 50°C-65°C [55]. The optimal temperature range for yam variable temperature drying is 45°C-65°C [56], and the optimal hot air supply temperature for apple slice drying is 50°C [57].

Due to the mutual heat exchange between heat users, annual heat production and consumption balance of DC should consider matching in the district heating network as shown if figure 3. In figure 3, others can represent heat storage, Absorption refrigerator and other methods that can balance heat throughout the year.

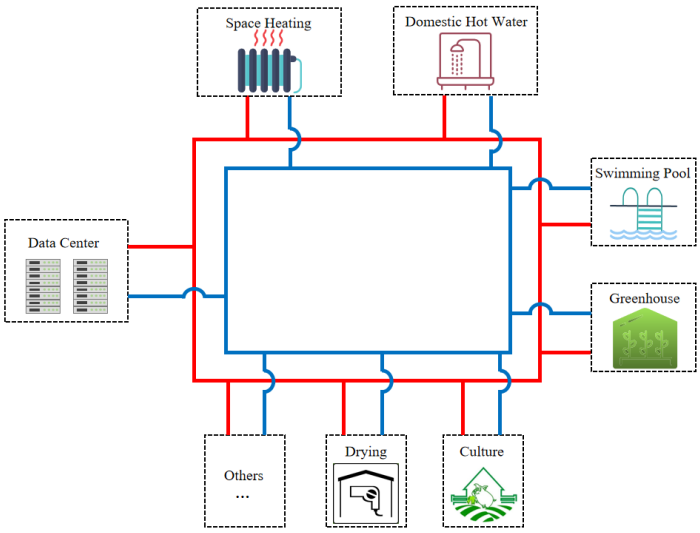

Figure 3. Schematic diagram of annual heat production and consumption balance of DC in DH network

5. CONCLUSION

In this work data centers used as district heating sources are discussed and are perfect for exhaust heat recovery to slow down global warming and reduce water consumption. When data centers are used as heat sources for district heating, priority should be given to the utilization of the chilled water side. The series or parallel connection method should be determined based on the heat consumption scale, and the annual heat production and consumption balance should be matched.

At present, only how to use data centers as heating sources for 4GDH and 5GDHC has been proposed, providing different options for exhaust heat utilization and annual heat production and consumption balance. However, more research and exploration are needed to specifically combine this huge potential heat source with surrounding district heating applications. In terms of practical engineering, currently data centers are mostly constructed through contracting, and their affiliated units are responsible for operation and maintenance management. Data centers and municipal heating belong to different industries and units. How to coordinate and promote the construction and renovation of heating pipelines and other facilities is a major issue in reality. In terms of theoretical research, the design and automatic control of these exhaust heat reuse solutions will be the key to achieving heat production and consumption balance, and their specific implementation methods still need further research.

ACKNOWLEDGEMENT

This work is supported by Shandong Province Science and Technology Small and Medium Enterprises Innovation Ability Enhancement Project(2022TSGC2566).

REFERENCES

[1] China Electronics Engineering Design Institute. Code for Design of Data Centers: GB50174-2017. Beijing:China Planning Press;2017.
[2] Cheng H D, Chen H X, Shao S Q, et al. Comprehensive COP Evaluation System for Energy Efficiency of Data Center Cooling System. Journal of Refrigeration 2020;41(6):77-84.
[3] Zhao Z Y. A lot of exhaust heat in data centers is being wasted. China Energy News;2021-06-14(002).
[4] Zhang H N, Shao S Q, Tian C Q. Research advances in free cooling technology of data centers. Journal of Refrigeration 2016;37(4):46-57.
[5] Zhang M L, Chu J. Annual water consumption analysis of a data center in Beijing. Water & Wastewater Engineering 2021;57(S2):257-260.
[6] Zhang G B. Experience of cooling circulating water system in A data center. Green Environmental Protection Building 2017;(11):35.
[7] Chen E L. The global freshwater resource crisis is intensifying. Ecological Economy 2022;38(10):5-8.
[8] Yin P. Data center research (8): water resource utilization. Heating Ventilating & Air Conditioning 2018;48(03):1-7.
[9] Chen Y, Zhang Y F, Meng Q L. Study of ventilation cooling technology for telecommunication base stations in Guangzhou. Energy and Buildings 2009;41:738–744.
[10] Niu X R, Xia C H, Sun G L, et al. A data center in Qiandao Lake is designed with an air-conditioning system using lake water cooling technology. Heating Ventilating & Air Conditioning 2016;46(10):14-17.
[11] Elahee K, Jugoo S. Ocean thermal energy for air-conditioning: case study of a green data center. Energy Sources

2013;35(7):679-684.
[12] Castro M J, Garc1A-Rodr1Guez J A, González-Vida J M, et al. Numerical simulation of two-layer shallow water flows through channels with irregular geometry. Journal of Computational Physics 2004;195(1): 202-235.
[13] Takamura N, Iwakuma T, Yasuno M. Photosynthesis and primary production of Microcystis aeruginosa Kütz. in Lake Kasumigaura. Journal of Plankton Research 1985;7(3): 303-312.
[14] Wang Y B. Tissue-specific expression and stress response of Hsp 70 in carp under thermal influence. Northeast Normal University 2008.
[15] Cao L. Design and case analysis of exhaust heat recovery system in data center. District Heating 2022;221 (06):140-144.
[16] Jang Y, Lee D, Kim J, et al. Performance characteristics of a waste-heat recovery water-source heat pump system designed for data centers and residential area in the heating dominated region. Journal of Building Engineering 2022;62:105416.
[17] Ljungqvist H M, Mattsson L, Risberg M, et al. Data center heated greenhouses, a matter for enhanced food self-sufficiency in sub-arctic regions. Energy 2021;215:119169.
[18] Oro E, Allepuz R, Martorell I, Salom J. Design and economic analysis of liquid cooled data centres for exhaust heat recovery: a case study for an indoor swimming pool. Sustainable Cities and Society 2018;36:185-203.
[19] Ebrahimi K, Jones G F, Fleischer A S. Thermo-economic analysis of steady state exhaust heat recovery in data centers using absorption refrigeration. Applied Energy 2015;139:384–397.
[20] Lund H, Werner S, Wiltshire R, Svendsen S, Thorsen J E, Hvelplund F, et al. 4th Generation District Heating (4GDH) Integrating smart thermal grids into future sustainable energy systems. Energy 2014;68:1–11.
[21] Buffa S, Cozzini M, Dantoni M, et al. 5th generation district heating and cooling systems: a review of existing cases in Europe. Renewable and Sustainable Energy Reviews 2019;(6):504-522.
[22] Wirtz M, Kivilip L, Remmen P, et al. 5th Generation District Heating: A novel design approach based on mathematical optimization. Applied Energy 2020;260:114158.
[23] Lund H, Alberg P, et al. The status of 4th generation district heating: Research and results. Energy 2018;164.
[24] Long W D, Bai W, Fan R, et al. After the outbreak: the development of the energy bus and the fifth-generation district heating and cooling system. Heating Ventilating & Air Conditioning 2020;50(10):1-13.
[25] Huang P, Copertaro B, Zhang X, et al. A review of data centers as prosumers in district energy systems: Renewable energy integration and exhaust heat reuse for district heating. Applied Energy 2020;258:114109.
[26] Liu X Z, Zhang P C, Yan Z. Analysis on multi-energy flow of prosumer-based integrated energy system driven by the fifth generation district heating and cooling network. Automation of Electric Power Systems 2023;47(04):78-90.
[27] Davies G F, Maidment G G, Tozer R M. Using data centres for combined heating and cooling: an investigation for London. Applied Thermal Engineering 2016;94:296-304.
[28] Su Z. Study on the refrigeration system optimization of a data center based on PUE analysis. Refrigeration & Air Conditioning 2021;35(02):162-168.
[29] Wang Y H, Wang X L, Wan C Y, et al. Design of air-conditioning cold source system in a data center in Shenzhen. Heating Ventilating & Air Conditioning 2021;51(S2):225-230.
[30] Zhang Y N, Li B, Li L L, et al. Air-conditioning system design of a data center in Xi'an. Refrigeration and Air-Conditioning 2022;22(11):92-101.
[31] Pan D H, Wang Y L, Yang Y, et al. HVAC design of a large scientific research complex. Heating Ventilating & Air Conditioning 2022;52(10):124-128.
[32] Shao H X. Energy-saving design of the data center air-conditioning system of a financial institution. Shanghai Energy Saving 2022;(04):527-531.
[33] Zhao L, Li H P. Design of an air-conditioning system for a data center in the Yangtze River Delta region. Heating Ventilating & Air Conditioning 2020;50(01):86-91.
[34] An Z, Fei Z F, Qi P C. Analysis of the influence of increasing the air supply temperature on the data center. Heating Ventilating & Air Conditioning 2023;53(03):67-69+36.
[35] Wu X F. Application of energy-saving technology of liquid-gas dual-channel refrigeration system in a data center. Building Energy & Environment 2019;38(06):33-35+6.
[36] Xiao X W, Zheng W J, Zeng C L. Design of a liquid cooling system for a performance test bench of a liquid cooling server. Refrigeration & Air Conditioning 2021;35(05):706-712.
[37] Chen J Q. Research on energy saving of refrigeration technology of highly efficient cloud computing Center. Refrigeration and Air-Conditioning 2019;19(06):7-9+37.
[38] Xiao X W. Application progress of liquid cooling technology in data center. Heating Ventilating & Air Conditioning 2022;52(01):52-65.
[39] Zimmermann S, Meijer I, Tiwari M K, et al. Aquasar: A hot water cooled data center with direct energy reuse. Energy 2012;43(1):237-245.

[40] Ye Q L. The application of condensing heat recovery type chiller in hotel building. Fujian Construction Science & Technology 2021;179(04):86-89.
[41] Ma X Q, Wang F, Chen R. Application analysis of condensing heat recovery system for hotel buildings in Shanghai area. Green Building 2016;8(01):23-27.
[42] Yang X P. Status quo and development trend of data center construction. Intelligent Building 2017;203(07):20-24.
[43] Deymi-Dashtebayaz M, Valipour-Namanlo S. Thermoeconomic and environmental feasibility of exhaust heat recovery of a data center using air source heat pump. Journal of Cleaner Production 2019;219:117-126.
[44] Zhang F, He X, Cheng X, et al. Application research of exhaust heat recovery system in data center. Designing Techniques of Posts and Telecommunications 2022;562(12):80-83.
[45] Li P A. Condensation heat recovery and heating of a chiller in a data center in Langfang, Hebei. Intelligent City 2016;2(12):109-110.
[46] Li J Y. Discussion on the heating method of utilizing the exhaust heat of a data center in Jinan. Building Energy & Environment 2021;40(09):64-67.
[47] Zhang G H, Zhang P L, Shi W X, et al. Analysis of the effect of recovering condensing heat from data center for heating in northern China. Heating Ventilating & Air Conditioning 2016;46(12):28-33.
[48] Jang Y, Lee D, Kim J, et al. Performance characteristics of a waste-heat recovery water-source heat pump system designed for data centers and residential area in the heating dominated region. Journal of Building Engineering 2022;62:105416.
[49] China Academy of Building Research.Design code for heating ventilation and air conditioning of civil buildings: GB50736-2012. Beijing:China Planning Press;2012.
[50] East China Construction Group Co., LTD. Standard for design of building water supply and drainage:GB50015-2019. Beijing:China Planning Press;2019.
[51] He F, Ding X M, Si C Q. Current situation and development trend of root zone temperature control technology of greenhouse crops. Agricultural Engineering Technology 2022;42(31):12-16.
[52] Liu G C, Bian X J, Tang J L, et al. Environmental quality standard for the livestock and poultry farm:NT/T388-1999. Beijing:Standards Press of China;1999.
[53] Jiang Y L, Cui X L, Cui C M. Study on exhaust heat recovery and utilization technology of aquaculture wastewater. Journal of Aquaculture 2020;41(12):60-63.
[54] Niu J G. Scientific washing of Medical linen (III). China Cleaning Industry 2016;(11):22-25.
[55] Li K. Study on hydrodynamic model and characteristic mechanism of hot-air drying of rhizome Chinese medicinal materials. Yunnan Normal University 2020.
[56] Jiu M. Study on the hot-air drying characteristics of Chinese yam. Zhongyuan University of Technology 2018.
[57] Zhang D P, Jia B G, Liu F, et al. Optimization of hot air drying temperature in apple slices. Journal of Shandong Jianzhu University 2021;36(01):67-74.

Pipeline & Network

The 18th International Symposium on District Heating and Cooling, September 3–6, 2023, Beijing, China

DATA-DRIVEN FAULT DETECTION AND DIAGNOSIS FOR SECONDRY DISTRICT HEATING NETWORKS

Hui Gao[a*], Shi Huang[b,c], Ying Shi[a], Haiyang Geng[a], Mingdi Chen[a], Zhongbo Li[d], Peng Sun[d], Wenxiao Shan[b,c], Zhigang Zhou[b,c]

[a] *Smart Heating Technology, Beijing District Heating Project Design Co. Ltd, Beijing, 100071, China*
[b] *School of Architecture, Harbin Institute of Technology, Harbin, 150090, China*
[c] *Key Laboratory of Cold Region Urban and Rural Human Settlement Environment Science and Technology, Ministry of Industry and Information Technology, China*
[d] *Smart Heating Technology, Beijing District Heating Group Co. Ltd, Beijing, 100028, China*
[*]*Hui Gao. caugao@163.com*

ABSTRACT

The heating pipe networks has a significant influence on the stability and reliability of the district heating system. With the increase of pipelines' service life, the fault problems such as leakage, caused by aging and corrosion, have appeared gradually. Hence, the importance of Fault Detection and Diagnosis (FDD) for the District Heating Network (DHN) has become prominent. Meanwhile, the quantity of the flow, temperature and pressure sensors in DHNs is being enhanced due to the rapid development of smart heating technology, which provides fundamental conditions for using data-driven methods to diagnose leakage faults of the DHN. In this work, the dynamic thermal model based on an actual DHN is established with the identification of key parameters, and the dataset of the system dynamic response is obtained by simulating multiple fault conditions. An FDD method is proposed based on Long Short-Term Memory (LSTM) neural network and both hydraulic and thermal data, and the FDD model is constructed. Eventually the model is tested and verified in an actual project case, which provides a feasible solution to improving the timeliness and the accuracy of FDD for DHN.

Keywords: district heating networks; dynamic thermal simulation; fault detection and diagnosis; LSTM

1. INTRODUCTION

The efficiency and stability of the district heating system relies on the reliability of the heating pipe network, which can be compromised by the disruption of components. Heating pipe network are mainly affected by hydraulic faults (water leakages and increased pressure losses) and thermal faults (i.e. anomalous heat losses)[1]. Such faults reduce the heating quality of district heating system, increase energy consumption as well as economic losses[2].

According to research[3,4], water leakage is the most common fault that causes approximately 33 % of district heating networks failures. Thus,timely and accurate detection of leakage faults is extremely important for the reliability and economy of district heating system[5].

Nowadays, temperature, pressure, and flow sensors are usually installed in each heat source, substation, and even customer building. Operational data can be monitored and recorded in real time through supervisory control and data acquisition (SCADA) systems,thus supporting the operation maintenance of district heating system[6–8].It provides fundamental conditions for using data-driven methods to diagnose faults of the district heating system.

The analysis of system operating conditions is the foundation for fault diagnosis problems.The operating conditions of the district heating system can be divided into hydraulic conditions and thermal conditions.Persis et al.[9,10] established a dynamic hydraulic response model for pipeline networks based on graph theory methods.The thermal condition of district heating system should be based on the hydraulic condition model. Chertkov et al.[11] provided detailed calculation formulas for the transient thermal diffusion process of fluid turbulent flow in heating pipelines. Zheng et al.[12] proposed a new function method to solve the dynamic variation relationship of inlet and outlet temperatures of heating pipelines. Based on the established dynamic thermal simulation model, Qiu et al.[13] analyzed the thermal response of the heating networks under two fault conditions: insulation layer detachment and sudden change in heat source water supply temperature.

Based on thermal and hydraulic conditions simulation, the leakage can be located by comparing the simulated pressures and flow rates with measured values at the upstream end, the downstream end or any other location along the pipe[5,14]. Compared with other fault detection and diagnosis methods,data-driven methods are much faster, as they train models based on existing data containing faults and their symptoms[15].Refs.[16–20] have demonstrated that data-driven methods can

successfully detect leakage faults in oil and gas pipe networks.

Xue et al.[1] uses a delayed alarm algorithm based on the amount of water replenished by the heat source to determine whether the pipeline network is in a leakage fault state, and trains a fault diagnosis model based on limit gradient enhancement (XGBoost) using the change rate data of node pressure in the fault state and normal state. Zhou et al.[21] construct and train a BP (Back Propagation) heating pipe-network leakage diagnosis model (HPLDM) which is used to LD towards the single heat-source branch pipe-network and the double heat-sources with double loops pipe-network. Kai Vahldieka et al.[22]developed three model- and data-based approachesto to localize leakages in real time.

Based on the above research, it can be seen that fault diagnosis of heating networks mainly focus on the primary networks fault, and the research on secondary networks is not sufficient. At the same time, most data-driven research on fault diagnosis identifies fault characteristics through hydraulic operating conditions such as pipe flow or node pressure, and lacks attention to thermal operating conditions such as supply and return water temperature and indoor temperature in secondary heating networks.

According to the actual engineering application of the heating system, the monitoring data of the secondary pipe network is complete. This paper is aim to establish the fault diagnosis model of the secondary heating network based on data-driven methods,which can make full use of rich data in district heating system.

2. Hydraulic and thermal simulation of District Heating Networks

2.1. steady-state hydraulic simulation model

According to the concept and method of graph theory, District Heating Networks can be abstracted as a connected graph composed of two basic elements: pipes and nodes; The secondary District Heating Networks is usually a branch form pipe network, so it can be abstracted as a directed connected graph which can express the flow direction in the pipe.

In order to simplify hydraulic conditions, the following assumptions are made for the model:

（1）The distribution of flow velocity, pressure at any cross-section of the pipeline is uniform,which simplifies the fluid flow inside the pipeline into a one-dimensional process;

（2）The fluid inside the pipe is incompressible fluid

Simplify according to the above conditions,the steady-state hydraulic calculation mode can be express in the form of matrix equations

$$\begin{cases} \mathbf{AG} = \mathbf{Q} \\ \mathbf{B}_{\mathrm{f}} \Delta \mathbf{H} = \mathbf{0} \\ \Delta \mathbf{H} = \mathbf{S}|\mathbf{G}|\mathbf{G} + \mathbf{Z} - \Delta \mathbf{H}_{\mathrm{pump}} \\ \Delta \mathbf{H}_{\mathrm{pump}} = \mathbf{C}_0 + \mathbf{C}_1 \mathbf{G} + \mathbf{C}_2 |\mathbf{G}|\mathbf{G} \end{cases} \tag{1}$$

where $\mathbf{A}$ is incidence matrix, $\mathbf{G}$ is the flow column vector, $\mathbf{Q}$ is node net inflow column vector, $\mathbf{B}_{\mathrm{f}}$ is Basic circuit matrix $\Delta\mathbf{H}$ is pipe pressure drop column vector, $\mathbf{S}$ is pipeline impedance coefficient matrix, $\Delta\mathbf{H}_{\mathrm{pump}}$ is pump head column vector,and $\mathbf{C}_0$、$\mathbf{C}_1$、$\mathbf{C}_2$ are water pump characteristic parameters Diagonal matrix

2.2. Dynamic thermal simulation model

The Dynamic thermal model in this paper simulates the distribution process of hot water in the secondry pipeline network, focusing on the two physical quantities: flow and temperature.

In order to simplify the problem, some assumptions are made for the model:

（1）Neglecting the heat capacity of thermal conductors such as pipe walls, insulation layers, and soil;

（2）The temperature distribution of any cross section in the pipe is uniform, which means that there is no radial heat transfer in the fluid

（3）Neglecting the axial thermal conductivity of the fluid

（4）The thermal resistance between the fluid and the external environment is evenly distributed along the axial direction of the pipeline

The specific model is divided into two parts,first one is the simulation of pipelines as follows:

According to the law of conservation of energy, the temperature change during fluid flow can be represented by the following equation:

$$\rho c_{\mathrm{p}} A_{\mathrm{c}} \frac{\partial T}{\partial t} \mathrm{d}x = \frac{\partial}{\partial x}\left(\lambda \frac{\partial T}{\partial x}\right) - c_{\mathrm{p}} G \frac{\partial T}{\partial x} \mathrm{d}x - \frac{T - T_{\mathrm{env}}}{R} \mathrm{d}x \tag{2}$$

where ρ is the fluid density in the pipeline, A_{c} is Cross-sectional area of pipeline, λ is thermal conductivity of fluid, R is equivalent heat transfer thermal resistance of the pipeline,and T_{env} is ambient temperature

Adopting backward differentiation for the time term and first-order upwind differentiation for the spatial term, discrete equation of dynamic thermal simulation can be modified as follows:

$$T_i^{(n)} = \frac{T_i^{(n-1)} + \frac{\Delta t}{\rho c_{\mathrm{p}} A_{\mathrm{c}} R} T_{\mathrm{env}}^{(n)} - u^{(n)} \frac{\Delta t}{\Delta x} T_{i-1}^{(n)}}{1 - u^{(n)} \frac{\Delta t}{\Delta x} + \frac{\Delta t}{\rho c_{\mathrm{p}} A_{\mathrm{c}} R}} \tag{3}$$

The second part of dynamic thermal simulation model is about heat buildings.This paper simplifies the heating building as a lumped parameter particle,dynamic heat balance equation of the equivalent building is as follows:

$$C_{\mathrm{b}} \frac{\mathrm{d}T_{\mathrm{n}}}{\mathrm{d}t} = Q_{\mathrm{rad}} - K_{\mathrm{b}}\left(T_{\mathrm{n}} - T_{\mathrm{env}}\right) \tag{4}$$

where C_{b} is the equivalent total heat capacity of buildings, T_{n} is indoor temperature of buildings, Q_{rad} is heat dissipation of radiator, and K_{b} is the thermal conductivity of the buildings.

To simulate the dynamic thermal process of buildings, backward differentiation is adopted for time terms:

$$T_{\mathrm{n}}^{(n)} = \frac{C_{\mathrm{b}}}{C_{\mathrm{b}} + K_{\mathrm{b}} \Delta t} T_{\mathrm{n}}^{(n-1)} + \frac{K_{\mathrm{b}} \Delta t}{C_{\mathrm{b}} + K_{\mathrm{b}} \Delta t} T_{\mathrm{env}}^{(n)} + \frac{\Delta t}{C_{\mathrm{b}} + K_{\mathrm{b}} \Delta t} Q_{\mathrm{rad}}^{(n)} \tag{5}$$

$$Q_{\mathrm{rad}}^{(n)} = c_{\mathrm{p}} G_{\mathrm{rad}}^{(n)}\left(T_{\mathrm{su}}^{(n-\eta_{\mathrm{rad}})} - T_{\mathrm{re}}^{(n)}\right) = K_{\mathrm{rad}}\left(\frac{T_{\mathrm{su}}^{(n-\eta_{\mathrm{rad}})} + T_{\mathrm{re}}^{(n)}}{2} - T_{\mathrm{n}}^{(n)}\right) \tag{6}$$

where K_{rad} is the equivalent heat transfer coefficient of radiator, η_{rad} is flow time of fluid in the radiator, T_{re} is return water temperature of radiator, and T_{su} is the supply water temperature of radiator.

2.3. Dynamic simulation analysis of district heating system

This paper selects a typical secondary heating system in Beijing as the research object, and the parameters are shown in Table 1.

Table 1. Secondry heating system parameters

total heating area(m2)	Heating buildings	Indoor design temperature(℃)	design supply/return water temperature(℃)	circulating flow rate(kg/s)
181700	12	20	50/40	82.135

The district heating network consists of 23 supply pipes,23 return pipes and 48 nodes as show in figure 1.Among them, the maximum pipe diameter is DN400 and the minimum pipe diameter is DN100.Equivalent the heat source to a pipe segment in the heating pipeline network,numbered n1'- n1.The system sets up a water replenishment and constant pressure device at node n1',which maintains a constant pressure of 0.2MPa under design conditions.

Figure 2 shows the dynamic temperature simulation of heating system for 7 days from January 1 to January 7 in the middle heating period, taking n11 as an example. It can be seen that the heat exchange station adjusts the water supply temperature with changes in environmental temperature, and the water supply temperature of user n11 is close to the water supply temperature of the heating station. The indoor temperature fluctuates around 20 ℃, slightly lagging behind the ambient temperature.

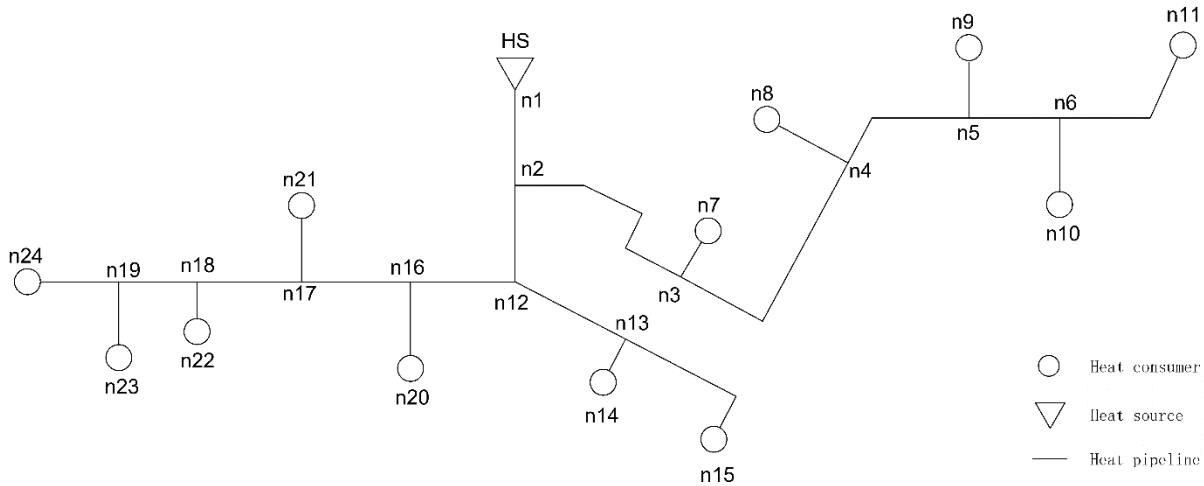

Figure 1. Plan of the heating networks

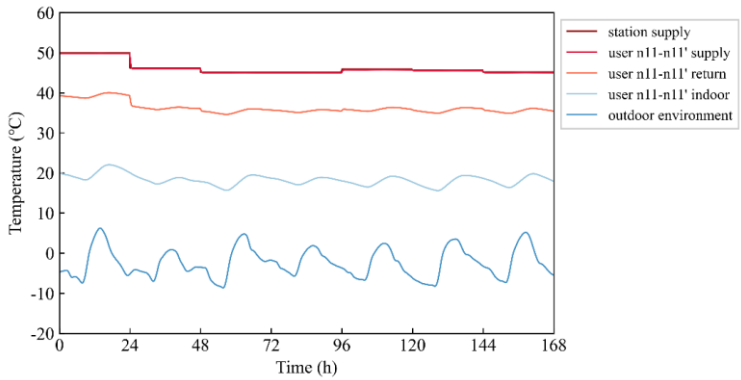

Figure 2. Dynamic temperature change curve of heat user n11-n11'

To study the influnce of leakage conditions, a simulation time of 24 hours was set, and the outdoor parameters were selected as the temperature on January 1st. The pipeline section n3-n4 was set to leak at t=12 hours, with the leakage location at the midpoint of the pipeline section and a leakage flow rate of 3.28Kg/s. Select heat users n7-n7' located in front of the leaking pipe section (closer to the heat source), n11-n11' located behind the leaking pipe section (further away from the heat source), and n24-n24' located at the end of the main water supply pipe adjacent to the leaking pipe section for research.

Obviously, flow and pressure will vary with leakage, which is also the basis of most fault diagnosis research. At the same time, we can observe that the return water temperature of heat users will significantly decrease , indicating the possibility of using sequential data of temperature for leakage diagnosis.

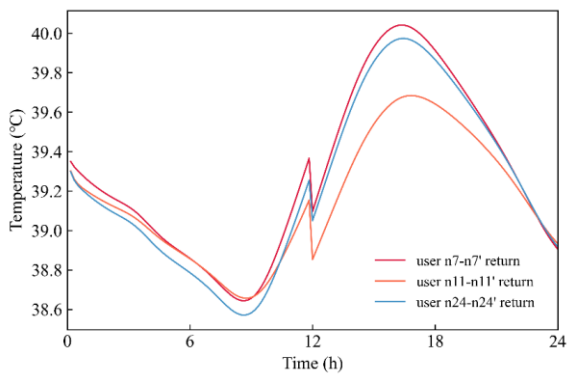

Figure 3. Temperature curve of return water for heat users under leakage conditions

3. Data-driven fault diagnosis model for heating pipeline networks

3.1. Construction of Pipeline Leakage Dataset

Due to the huge number of parameters and the complexity of the heating system, it is necessary to mine the potential value of these data through machine learning methods.To achieve this, it is necessary to construct a dataset containing types of fault conditions.

Assuming leakage occurs in pipeline section n2-n4, the networks should add a new node nleak at the location of the leak, as shown in Figure 4. At the same time, the original pipeline n2-n4 should be split into two new pipelines, n2-nleak and nleak-n4, while the other pipelines remain unchanged.

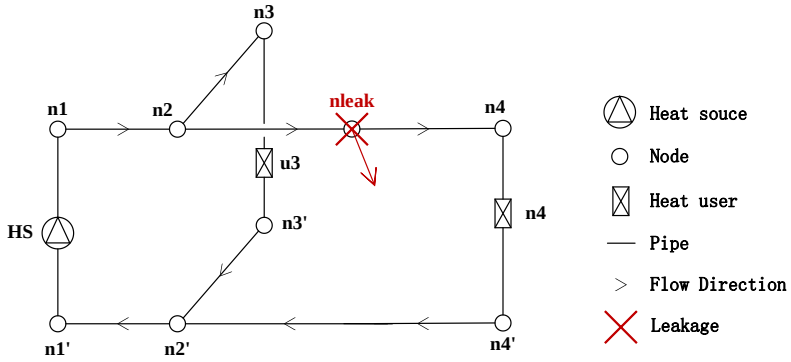

Figure 4. Schematic diagram of pipeline leakage

3.2. Fault Diagnosis Model Based on Pressure Data

This paper uses the PyTorch framework to build and train a pipeline fault diagnosis model based on BP neural network, which is shown in Figure 5.In practical engineering, pressure sensors have different measurement accuracy due to different models, which has a certain impact on the quality of data. Common pressure sensor accuracies include 0.01MPa, 0.001MPa, etc. Set the measurement accuracy of the pressure sensor to 0.001MPa. Randomly divide the stress dataset into training, validation, and test sets, accounting for 60%, 20%, and 20% of the dataset.

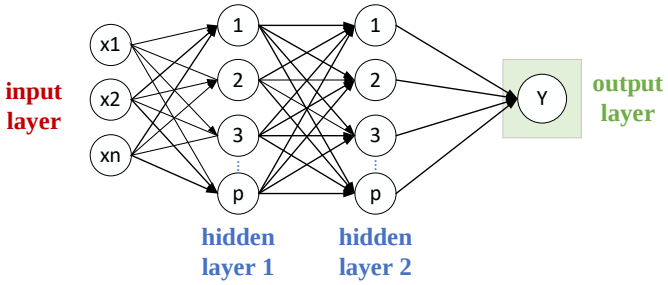

Figure 5. Schematic diagram of Bp neural network

As the accuracy of sensors decreases, the accuracy of model fault diagnosis gradually decreases. In practical engineering, the data accuracy obtained by pressure sensors is relatively low, which may lead to a decrease in model efficiency. So it is necessary to diagnose based on high-precision temperature data.

3.3. Fault Diagnosis Model Based on sequential data of temperature

To explore the potential value of sequential data of temperature in heating system, a neural network model based on time series is necessary. Therefore, this paper build and train a pipeline fault diagnosis model based on LSTM neural network, which is shown in Figure 6.

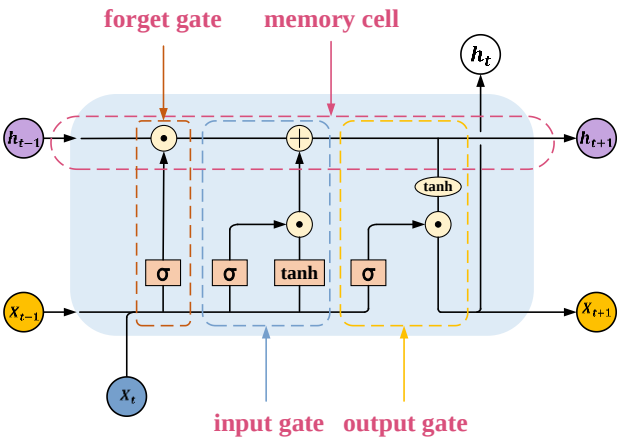

Figure 6. Schematic diagram of LSTM neural network

4. RESULTS

Train the BP neural network fault diagnosis model for 5000 generations, and the training process is shown in the left part of Figure 7. The model with the highest accuracy rate on the verification set is taken as the final model obtained through training. At this time, the accuracy rate of the model on the test set is 86.23%, and the confusion matrix of its diagnosis results is shown in Figure 8.

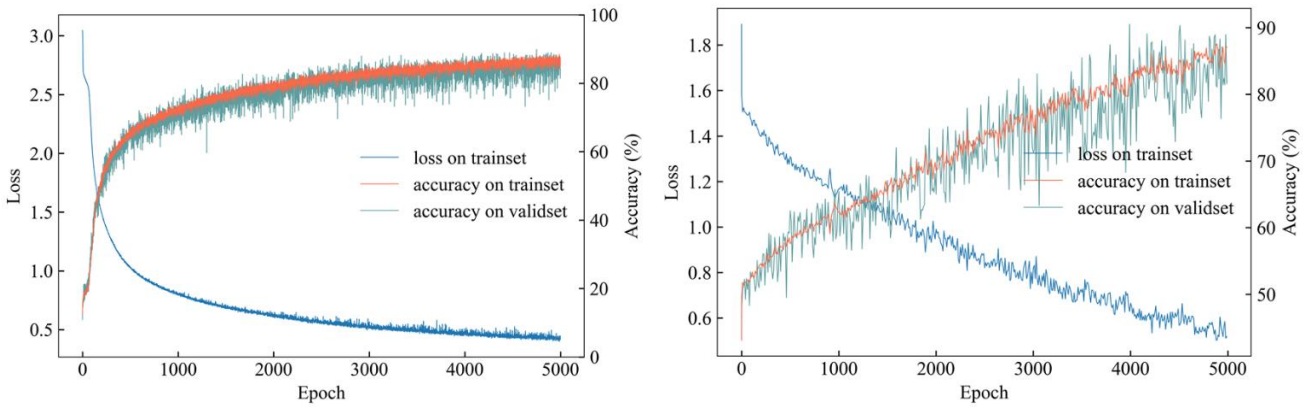

Figure 7. BP and LSTM Fault Diagnosis Model Training Process

The training results of the BP fault diagnosis model under different pressure sensor accuracies show that as the sensor accuracy decreases, the accuracy of the model's fault diagnosis gradually decreases. When the sensor accuracy is 0.001MPa and 0.01MPa, the diagnostic accuracy significantly decreases to 62.42% and 42.72%, and the pressure data has lost the main hidden information, making the model ineffective. The measurement accuracy of pressure sensors has a significant impact on the accuracy of pipeline network fault diagnosis models driven by pressure data.

Train the LSTM model for 5000 generations, and the training process is shown in the right part of Figure 7. Figure 9 shows the performance of the optimal model on the test set. It can be seen from the figure that the model can accurately diagnose the faulty pipeline segment under most fault conditions, while the accuracy of diagnosis has decreased on individual pipeline segments such as n6 and n10, but still maintains a certain level of effectiveness. Overall, the diagnostic accuracy reaches 90.62%, which can meet the actual engineering requirements.

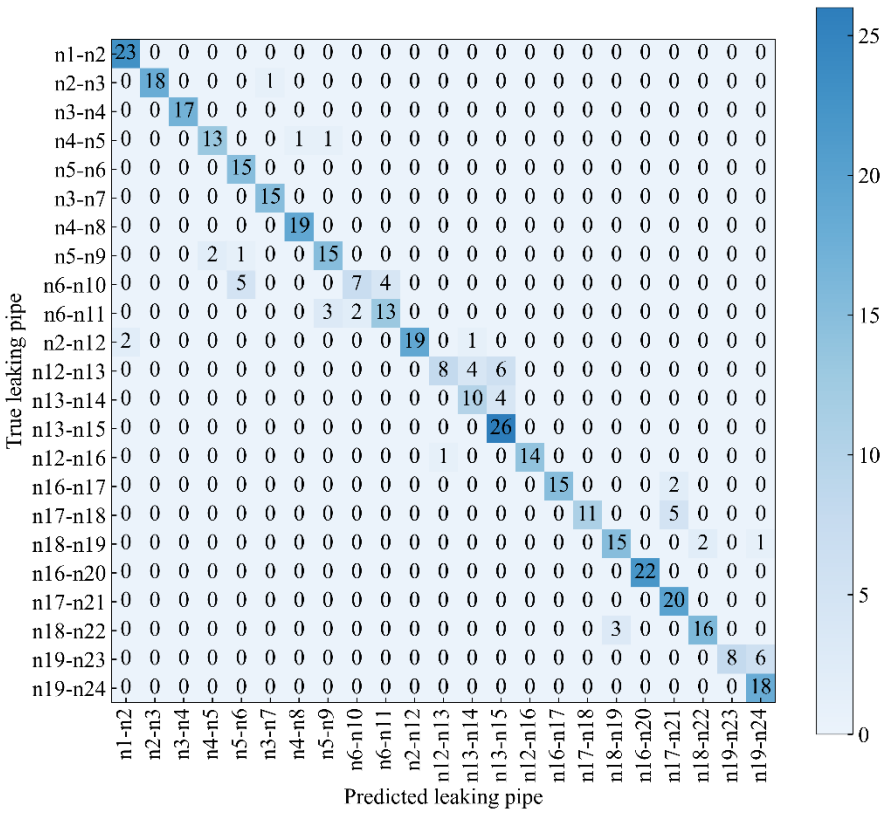

Figure 8. Confusion matrix of BP Fault Diagnosis Model on Test Set

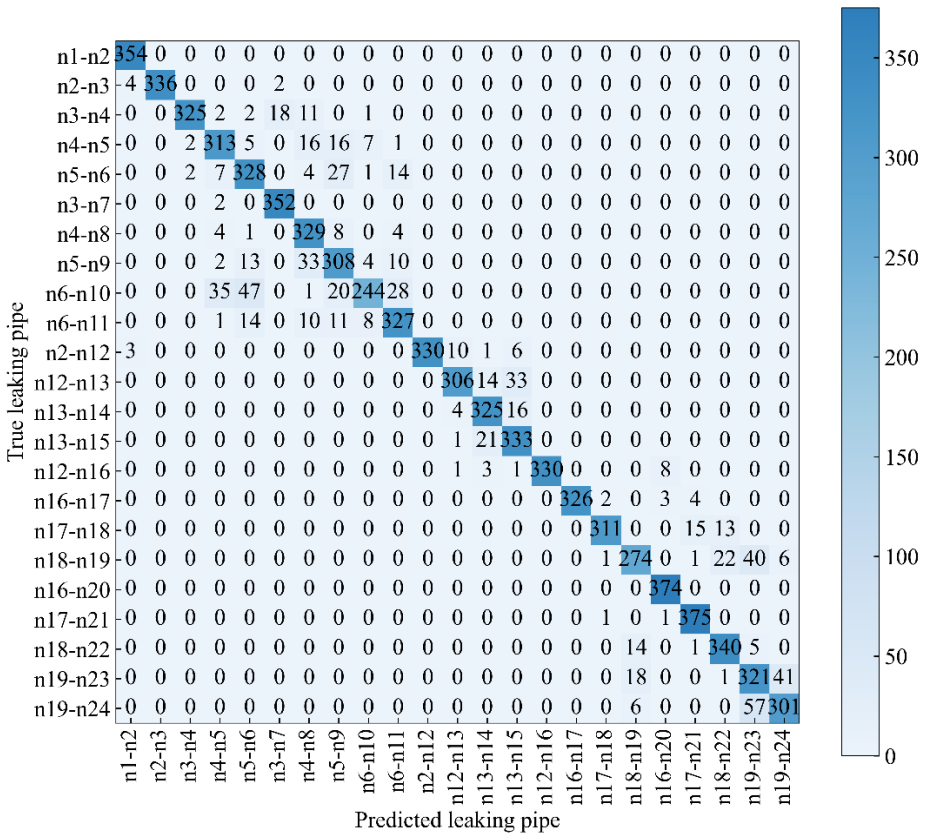

Figure 9. Confusion matrix of LSTM Fault Diagnosis Model on Test Set

5. DISCUSSION

Compared with most heating network leakage diagnosis models,this paper not only utilizes common pressure data for fault diagnosis, but also constructs a fault diagnosis model based on sequential data of temperature.

The dynamic thermal simulation model in the article equates a heating building to a particle with lumped parameters. Further refinement of the thermal process modeling of heating buildings can be studied to make the simulation model more accurate.

The fault diagnosis model based on sequential data of temperature not only can diagnose pipeline leakage faults, but also has the possibility of diagnosing various fault conditions such as pipeline blockage and insulation layer damage. In the future, it can further enrich the types of pipeline fault diagnosis.

6. CONCLUSION

Conclusion may include advantages, limitations, and possible applications.

This paper studies the modeling and calculation methods of the secondary heating networks, simulation and dataset construction for various operating conditions, and fault diagnosis models based on dynamic thermal data. A relatively complete theoretical method for data-driven fault diagnosis of the secondary heating pipe network is established.

This paper demonstrates the effectiveness of the data-driven fault diagnosis method in the case study.The results show that the diagnostic accuracy of the fault diagnosis model based on pressure data can reach 86.23%. The diagnostic accuracy of the fault diagnosis model based on temperature time series data is 90.62%, which can complement the fault diagnosis model based on pressure data and meet practical engineering needs.

REFERENCES

[1] Xue P, Jiang Y, Zhou Z, Chen X, Fang X, X., J. Liu. Machine learning-based leakage fault detection for district heating Networks. Energy & Buildings 2020;233:110161.

[2] M. Li, W. Deng, K. Xiahou, T. Ji, Q. Wu. A Data-Driven Method for Fault Detection and Isolation of the Integrated Energy-Based District Heating System. IEEE Access;8: 23787-23801

[3] Buffa S, Fouladfar MH, Franchini G, Gabarre IL, Chicote MA. Advanced Control and Fault Detection Strategies for District Heating and Cooling Systems—A Review.Applied Sciences-Basel 2021;11(1):455

[4] Månsson S, Kallioniemi POJ, Thern M, Van Oevelen T, Sernhed K. Faults in district heating customer installations and

ways to approach them: Experiences from Swedish utilities. Energy 2019;180:163–74.
[5] S. Zhou, Z. O'Neill, C. O'Neill. A review of leakage detection methods for district heating networks. Applied Thermal Engineerin 2018;137:567–574
[6] P. Xue, Z. Zhou, X. Fang, X. Chen, L. Liu, Y. Liu, J. Liu. Fault detection and operation optimization in district heating substations based on data mining techniques. Applied Energy 2017;205: 926–940
[7] Y. Lu, Z. Tian, P. Peng, J. Niu, J. Dai. Identification and evaluation of operation regulation strategies in district heating substations based on an unsupervised data mining method. Energy and Buildings 2019;202:109324,
[8] P. Xue, Y. Jiang, Z. Zhou, X. Chen, X. Fang, J. Liu. Multi-step ahead forecasting of heat load in district heating systems using machine learning algorithms. Energy 2019;188:116085
[9] De Persis C, Kallesøe C S. Pressure regulation in nonlinear hydraulic networks by positive controls 2009 European Control Conference (ECC). IEEE, 2009:4102-4107.
[10] De Persis C, Jensen T N, Ortega R et al. Output Regulation of Large-Scale Hydraulic Networks. IEEE Transactions on Control Systems Technology. 2014;22:238-245.
[11] Chertkov M, Novitsky N N. Thermal Transients in District Heating Systems. Energy 2019;184: 22-33.
[12] Zheng J, Zhou Z, Zhao J, et al. Function method for dynamic temperature simulation of district heating network. Applied Thermal Engineering 2017;123:682-688. .
[13] Qiu Y, Li G, Wei L, et al. Dynamic thermal performance of district heating network under typical safety accidents. Journal of Building Performance Simulation 2022;15: 678-690.
[14] A. Abdulshaheed, F. Mustapha, A. Ghavamian. A pressure-based method for monitoring leaks in a pipe distribution system: A Review. Renewable and Sustainable Energy Reviews 2017;69:902–911
[15] Mirnaghi M S, Haghighat F. Fault detection and diagnosis of large-scale HVAC systems in buildings using data-driven methods: A comprehensive review. Energy and Buildings;2020:229:110492.
[16] Z. Qu, H. Feng, Z. Zeng, J. Zhuge, S. Jin. A SVM-based pipeline leakage detection and pre-warning system. Measurement.2010;43(4):513–519,
[17] S.K. Mandal, F.T.S. Chan, M.K. Tiwari. Leak detection of pipeline: An integrated approach of rough set theory and artificial bee colony trained SVM. Expert Systems with Applications.2012;39: 3071–3080
[18] M.B. Abdulla, R. Herzallah. Probabilistic multiple model neural network based leak detection system: Experimental study.Journal of Loss Prevention in the Process Industries.2015;36:30–38
[19] M. Zadkarami, M. Shahbazian, K. Salahshoor. Pipeline leakage detection and isolation: An integrated approach of statistical and wavelet feature extraction with multi-layer perceptron neural network (MLPNN). Journal of Loss Prevention in the Process Industries 2016;43: 479–487
[20] R. Xiao, Q. Hu, J. Li. Leak detection of gas pipelines using acoustic signals based on wavelet transform and Support Vector Machine. Measurement 2019;146:479–489
[21] Shoujun Zhou, Chen Liu, Youen Zhao, Guozheng Zhang, Yaling Zhang.Leakage diagnosis of heating pipe-network based on BP neural network.Sustainable Energy, Grids and Networks 2022;23:100869
[22] Kai Vahldiek, Julia Koltermann, Dennis Pierl.Leakage Localization in District Heating Networks Based on Real Network and Measurement Data. Energy Reports 2021;7:508-516

The 18th International Symposium on District Heating and Cooling, September 3–6, 2023, Beijing, China

Numerical Analysis of Complex Network Hydraulics in Cold District Heating Networks: A Simulation Study of a District from a German Living Lab Project

Rahul M Karuvingal [a*], Kai Droste [a], Thomas Schreiber [a], Dirk Müller [a]

[a] *Institute for Energy Efficient Buildings and Indoor Climate - RWTH Aachen University, Aachen, Germany*
[*] *Corresponding author. rahul.karuvingal@eonerc.rwth-aachen.de*

ABSTRACT

The successful transition to renewable energy sources requires innovative decarbonization energy concepts for community heating and cooling supply. A district in this study is an example of this, with a planned cold district heating network utilizing CO2-free heat generation technologies such as geothermal and waste heat recovery from sewage systems. The network topology is structured in a ring configuration with two pipes, one for the supply line planned to be at 46 °C and one for the return line at 28 °C. Dynamic thermo-hydraulic simulations are a promising method to investigate low-temperature networks and are used in this study to analyze network hydraulic interactions. Models are built using a Modelica-based simulation framework using the well-tested AixLib system library. Two different simulation models are developed, each with two scenarios: a full district simulation model with centralized and decentralized network pumps and a simulation model of only the first construction section with the same two scenarios. The full district simulation model incorporates three supply stations, while the simulation for the first construction section has only one. The results indicate that when using centralized pumps, both full district and first construction phase area, energy demands are either over or under-met for certain buildings. However, decentralized pump systems appear to efficiently meet demands. In full district simulations, we observe the hydraulic interactions between the centralized supply stations are different than in the decentralized scenario. The findings highlight hydraulic inconsistencies of centralized pumping schemes and the effectiveness of decentralized control strategies in meeting mass flow demands for heating. Decentralized pumping offers a promising solution, but in the case of multiple supply stations careful allocation of mass flow and advanced control systems are necessary to prevent overloading and thus ensuring efficient resource distribution in network. Numerical analysis shows the importance of evaluating hydraulic interactions in optimizing energy usage, enhancing comfort, and implementing effective pump control strategies.

Keywords: Cold heating networks, Simulation, Modelica, Dynamic thermo-hydraulic model

1. INTRODUCTION

In its report, the Intergovernmental Panel on Climate Change (IPCC) highlights that severe and irreversible consequences for the planet's ecosystem and human societies are anticipated if greenhouse gas (GHG) emissions continue at their current rate. The report emphasizes the urgent need to promptly implement ambitious mitigation strategies and enhance climate resilience [1]. The energy sector is a significant contributor to GHG emissions. In 2020, global energy production by fossil fuel amounted to 14.155 millions of tonnes of oil equivalent (Mtoe), with the European Union (EU) accounting for 565 Mtoe. The EU has implemented stringent measures to reduce energy consumption and increase the share of renewable energy in the sector. As of 2020, the share of renewable energy in total energy usage stands at 22 %, with a target set for 2030 to reach 32 % [2]. The primary objective of this transition is to decrease reliance on fossil fuels within Europe. Hence, it is crucial to reduce overall energy demand through efficient energy distribution and consumption. Approximately half of the energy used in Europe is allocated to heating and cooling buildings [3],[4], with the residential building sector accounting for 40 % of this consumption. Consequently, the building sector's energy consumption represents a substantial portion of the total energy usage. Urbanization trends and the projected increase in cooling demand [5] pose significant challenges to further reducing energy consumption in the building sector, due to growing building stock and energy infrastructure constraints. Therefore, developing an efficient energy supply method that encompasses the entire process from the energy supply system to the building itself will be crucial in the future. District heating and cooling (DHC) networks are widely recognized as a prominent solution for decreasing primary energy consumption and reducing GHG emissions [6].

Lund et al. [7] provide a comprehensive overview of different classifications and technological advancements in district heating systems. The work describes the classification up to the 4th-generation district heating (4GDH) and discusses various challenges associated with achieving sustainable integration of different energy systems, implementing smart energy systems, and improving energy efficiency in buildings for 4GDH. The pioneering 4GDH technology focuses on the integration of

renewable energy sources and the recovery of excess heat within the district heating network.

Buffa et al. [8] present the latest state-of-the-art technology in district heating and cooling, referred to as the 5th generation district heating and cooling (5GDHC). This advanced system is also known as anergy networks, cold district heating networks, ambient loops, or balanced energy networks. Wirtz et al. [9],[10] delve into the concept of 5GDHC in detail and address uncertainties and research gaps based on a survey of 53 5GDHC networks in Germany. The concept of 5GDHC represents a supply approach for districts that enables the integration of diverse renewable energy technologies due to the low-temperature requirements. It also facilitates the coupling of electricity, heating, and cooling through the operation of decentralized heat pumps and chillers [11]-[14].

There remains a comparative lack of practical experience in designing and operating these hydraulically complex low-temperature networks [15]. Dynamic simulation techniques present an opportunity to gain detailed insights into the behavior of such systems, thereby offering new possibilities for their design and evaluation [13]. In this regard, the utilization of dynamic thermo-hydraulic simulation models offers a valuable means to comprehend the dynamic processes occurring within DHC networks. While several demonstrations have already been realized for complex DHC networks incorporating high shares of renewable energy sources [4], and dynamic models have been employed for thermal network design [16], the use of dynamic modeling in the design and operation of DHC networks remains uncommon.

This study presents an analysis of dynamic thermo-hydraulic simulations conducted to plan a district within Germany's Living Lab project TransUrban.NRW[1]. During the planning phase, we developed two different simulation models, each with two scenarios: a full district simulation model with centralized and decentralized network pumps and a simulation model of the first construction section with the same two scenarios. The full district was planned with 43 buildings and 3 supply stations. The network topology follows a ring structure and comprises two pipelines: the supply pipeline (hot) and the return pipeline (cold). The supply line maintains a temperature of 46 °C, while the return line is intended to be at 28 °C. The first construction phase area of the district is planned with 4 buildings and 1 supply station, with the same temperature maintained in the supply and return line for the network. Based on existing literature definitions, this network does not align precisely with 4GDH and 5GDHC. For the remainder of this paper, we will refer to it as a cold district heating network.

The paper is organized as follows: Section 2 presents the methodology, including the various open-source tools and simulation models employed. Section 3 elaborates on and discusses the results obtained from the simulations. In Section 4, we derive conclusions and outline future research directions.

2. METHODOLOGY

In this section, we discuss various simulation models that were constructed during the planning phase of the district. We elaborate on the software tools employed and the specific model setup. We start by elaborating on how we create simulation models for different individual components using the modeling language Modelica and the different packages used. Then, we explain the workflow of designing the entire models for a specific district using different open-source tools. Finally, we analyze the different simulation models, their variations, and the boundary conditions associated with each model.

2.1 Building simulation models for individual components.

The construction of the district system model necessitates the incorporation of key components, namely, heating medium carriers in the form of network pipes, substations representing buildings with heating demands, hydraulic components, and control systems, and central supply stations comprising heat sources. We adopt the Modelica language to model these individual components, utilizing the AixLib[2] open-source Modelica library [17]. For modeling the pipe elements, a dynamic and equation-based thermo-hydraulic pipe model, known as the plug-flow pipe model [18], is employed. This model is specifically designed for simulating long pipes within district heating and cooling systems, considering transport delay, heat loss, insulation, storage effects, and temperature propagation along the pipe length, idealized as plug-flow.

The plug-flow pipe model (refer to Figure 1 and Figure 3) precisely handles fluctuating inlet temperatures, varying mass flows (including stopping or reversing flows), and complex network layouts that encompass branching and meshed systems. To enhance the accuracy of pressure loss representation in a pipe segment, the plug-flow pipe model incorporates a parameter called "fac," which enables the consideration of flow resistances associated with bends, thermal expansion joints, and other specific pipe sections.

For a more precise simulation of heat losses, we have integrated a model that represents the surrounding soil as a combination of cylindrical thermal resistors (R) and capacitances (C). These RC combinations effectively capture cylindrical heat transfer

[1] https://reallabor-transurban-nrw.de/
[2] https://github.com/RWTH-EBC/AixLib

and thermal storage effects occurring in both the pipe and the adjacent soil. Thermal connectors establish connections between the pipes and the inner surfaces of the cylindrical thermal capacities. For heat loss calculations, the undisturbed soil temperature is utilized for the outer surface of the pipes. Furthermore, these pipe models can be seamlessly linked with ground temperatures, enabling dynamic heat gain or loss calculations in conjunction with the ground.

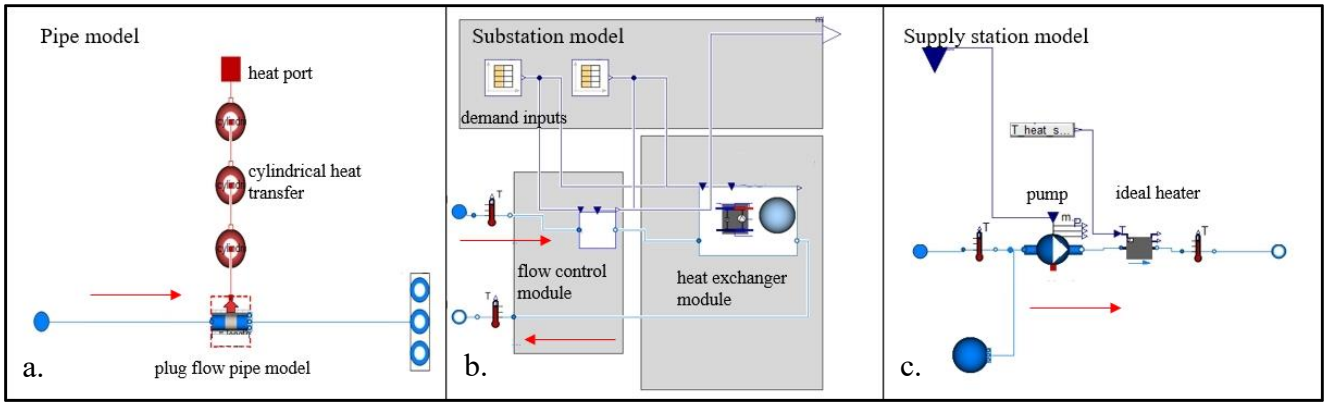

Figure 1. Centralized pumping component models: a. pipe model, b. substation model, and c. supply station model

We have developed three substation models to accommodate various simulation scenarios. The first model (refer to Figure 1), tailored for simulations involving centralized pumping, encompasses a heat exchanger module, heat demand input tables, a valve, and temperature sensors. The heat exchanger consists of primary and secondary sides, with the primary side connected to the network and the secondary side linked to the building. The second model (refer to Figure 2) is designed to simulate scenarios with a centralized pumping network. It integrates a flow control unit that regulates the mass flow according to the building's demand. This model comprises a motorized control valve and a PI control unit that adjusts the valve based on the temperature sensor on the primary side of the heat exchanger. The third model (refer to Figure 3) addresses simulations featuring decentralized pumping. It incorporates a decentralized pump unit that is controlled by the calculated mass flow derived from heat demands, the heat exchanger, and temperature sensors. These substation models facilitate the evaluation of different pumping configurations and control strategies within their respective scenarios.

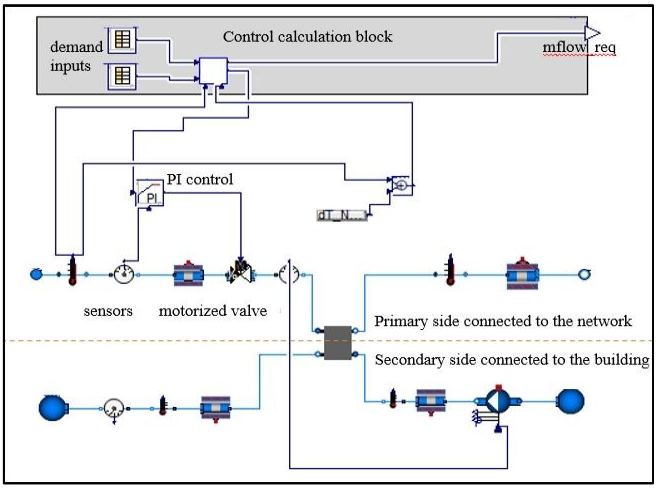

Figure 2. Substation model with PI control unit for centralized pumping cold heating network

Additionally, we have developed two supply station models to be employed in two distinct simulation scenarios. The first model (refer to Figure 1) incorporates an ideal heating source and a centralized pump controlled by the mass flow determined from the total demand in the network. The second model (refer to Figure 3) features an ideal heating source without any pump. The heating medium can be adjusted as required for the network. These two models serve as the primary energy sources for the district in all the simulation variants detailed in this paper.

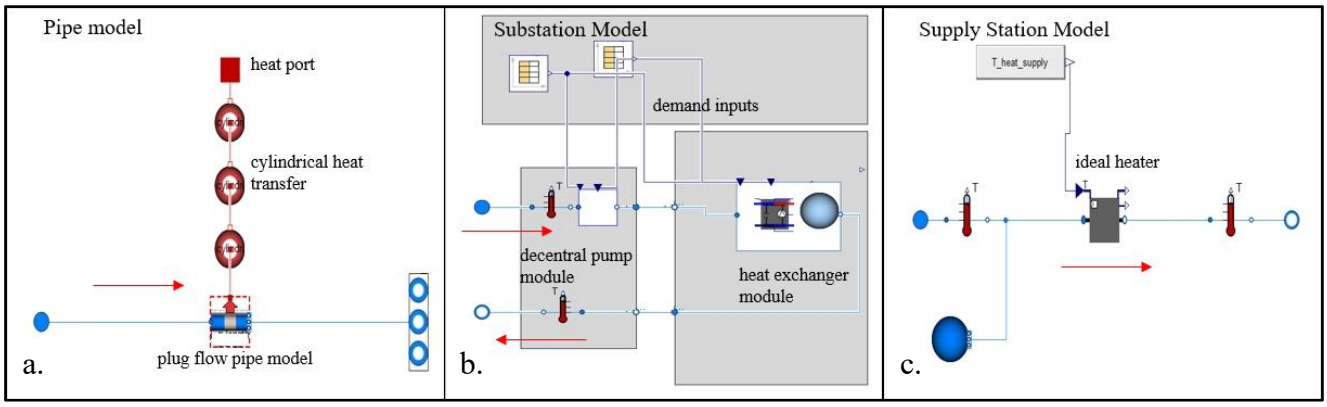

Figure 3. Decentralized pumping component models: a. pipe model, b. substation model, and c. supply station mode

2.2 Workflow for designing entire network models

To construct the model for the cold heating network, we utilize a self-developed toolchain comprising a series of open-source tools. This toolchain enables the automated generation of models, optimization of energy supply, forecasting of demand, and analysis of complex network simulations. For a more comprehensive understanding of the toolchain, we refer to the work conducted by T. Schreiber et al. [19].

For this study, a tool called TEASER[3] is used to estimate demands for the buildings within the district. This tool generates individual reduced-order dynamic simulation models, derived from building archetypes, for each building in the district. The demands are calculated based on these models, which employ the analogy of circuits to describe the processes of heat transfer and storage, following the principles outlined in the German guideline VDI 6007 [20]. These generated demands serve as the basis for the initial design of supply stations and pipe networks. Subsequently, the network structure is visualized using the software QGIS, employing three primary layers: building or substations, network or pipes, and supply stations. This approach facilitates the generation of Geographical Information System (GIS) data for each layer, and the resulting data files are exported in the geojson format.

Once the demands and GIS data have been generated, the uesgraphs[4] [21] tool is employed to automatically generate the network model. Currently, an advanced version of this tool is under development at the institute, incorporating notable features described in the work by Mans et al. [22]. The tool utilizes the demand files, ground temperature simulation files, GIS data files, and individual component simulation files.

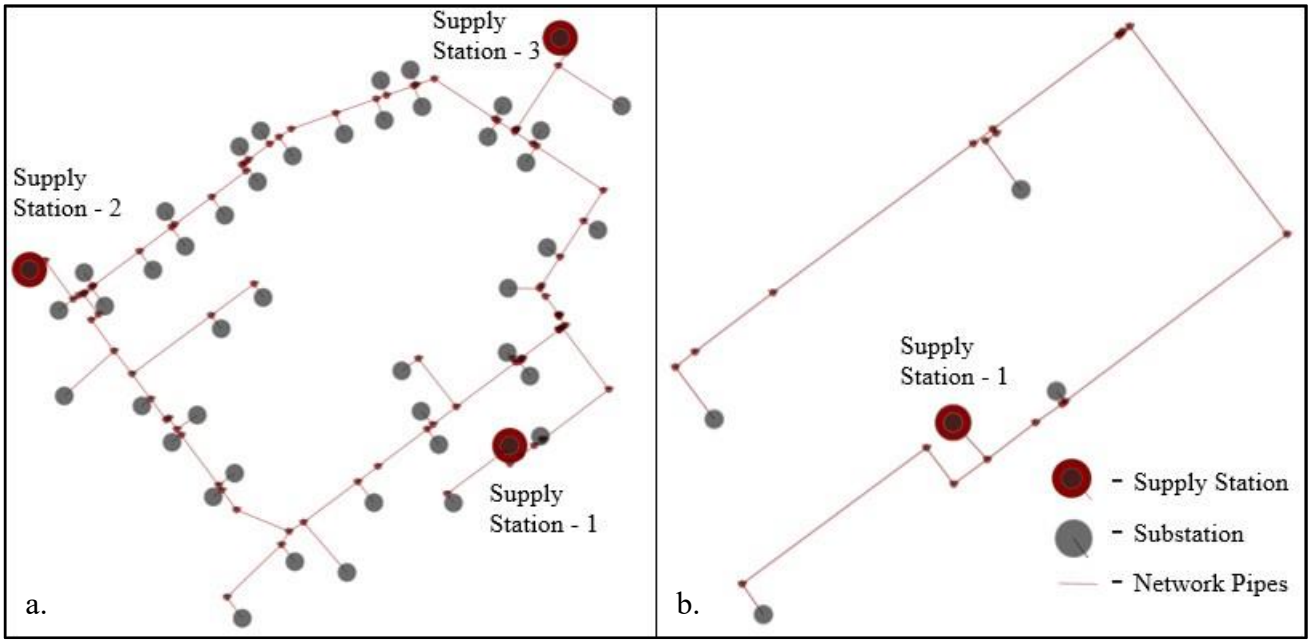

Figure 4. Uesgraph generated simulation model layout: a. full district and b. construction phase 1

[3] https://github.com/RWTH-EBC/TEASER
[4] https://github.com/RWTH-EBC/uesgraphs

By combining these input files, the tool generates simulation models for the entire district executable via software environments supporting the Modelica language, such as Dymola or OpenModelica.

2.3 Different simulation variants and their boundary conditions

In this study, we describe different simulation variants and their associated boundary condition. The heat-carrying medium in the network is water and all the demands for each building are calculated over the course of a year. The supply temperature is 46°C, while the planned return temperature is 28°C, resulting in a temperature difference (dT) for the entire network of 18 K. The specific heat capacity of the carrying medium water is taken as 4.187 kJ/kgK to calculate the required mass flows from the pre-simulated demands. The pipes are insulated in the network and the calculations for the thermal resistance are done with the heat conductivity of the pipe insulation as 0.021 W/(m K).

To gain a comprehensive understanding of the impact of both decentralized and centralized pumping systems on the district, we have developed and analyzed the simulation variants described in Table 1. The simulations are categorized based on the project's scope, encompassing either the construction phase 1 or the entire district. In simulations covering the entire district, the network incorporates three supply stations.

The pump configurations consist of two options: a centralized pumping scenario where each supply station is equipped with a dedicated pumping unit or a decentralized pumping scenario where each substation possesses its own pump.

In the case of centralized pumping, the substation model incorporates a valve that is either non-controlled, mechanically set to an open position, or a controlled motorized valve that can be adjusted using a proportional-integral (PI) controller. The estimation of mass flow is performed by considering the input demands provided for each individual building.

For simulations involving the centralized pumping scenario, the centralized pump situated in the supply station is regulated based on the cumulative mass flow required for all buildings within the network.

Table 1. Simulation variants: a comparative overview.

Variant	Scope	Pump configuration	Substation model	Supply Station (SS)
1	Construction phase 1	Centralized	non-controlled valve	1 ideal SS with pump
2	Construction phase 1	Centralized	PI controlled motorized valve	1 ideal SS with pump
3	Construction phase 1	Decentralized	controlled pump unit	1 ideal SS without pump
4	Full district	Centralized	non-controlled valve	3 ideal SS with pump
5	Full district	Decentralized	controlled pump unit	3 ideal SS without pump

Figure 5 illustrates the generated simulation models representing Variant 4 and Variant 1, developed for the centralized pumping scenario for the full district and construction phase 1 case.

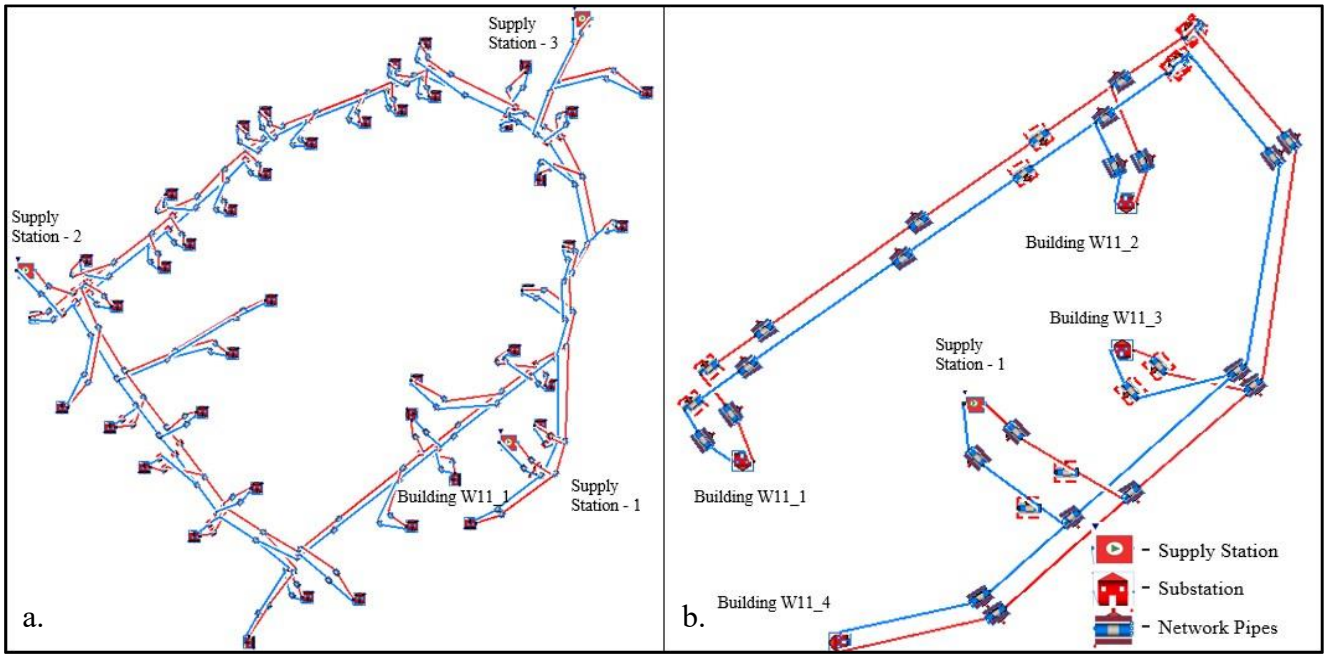

Figure 5. Auto-generated Modelica simulation model: a. full district and b. construction phase 1

The simulation duration for all the variants is one year. The heat demands during the summer consist of domestic hot water, while for the remaining time, it includes both space heating and domestic hot water. The simulation interval spans from 0 seconds to 31,536,000 seconds, with a timestep of 3600 seconds. During the simulation, data is collected at regular intervals, specifically every 3,600 seconds (equivalent to 1 hour), constituting the output interval length. The solver employs the Cvode-variable order integration algorithm to solve the system equations.

3. RESULTS & DISCUSSION

Numerous results are generated through each simulation; however, only the relevant outcomes are presented within this paper. For the purposes of this study, building 11_1 (shown in Figure 5) was selected as the reference building, given its position as the furthest structure in construction phase 1. The temperature plot for the supply and return in the supply station, ground temperatures throughout the year, as well as the supply and return for the substation at building 11_1, are illustrated in Figure 6.

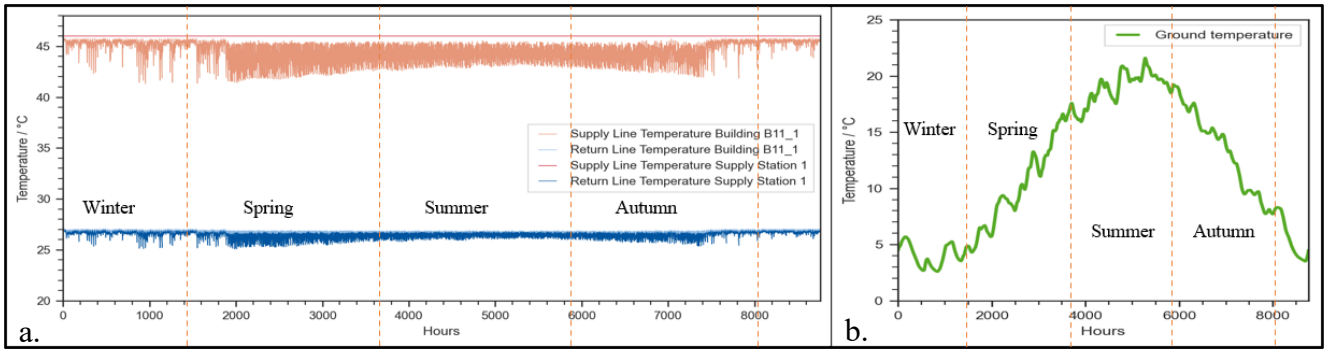

Figure 6. Temperature plot from the simulations for building 11_1: a. network temperatures and b. ground temperatures

Figure 7 and Figure 8 depicts the results of the required and delivered mass flow for building 11_1 obtained from variant 1, variant 2, and variant 3 which utilizes centralized pumping in the network. The graphs in Figure 7 reveal instances where the demands are either underserved or overserved, resulting in hydraulic inconsistencies.

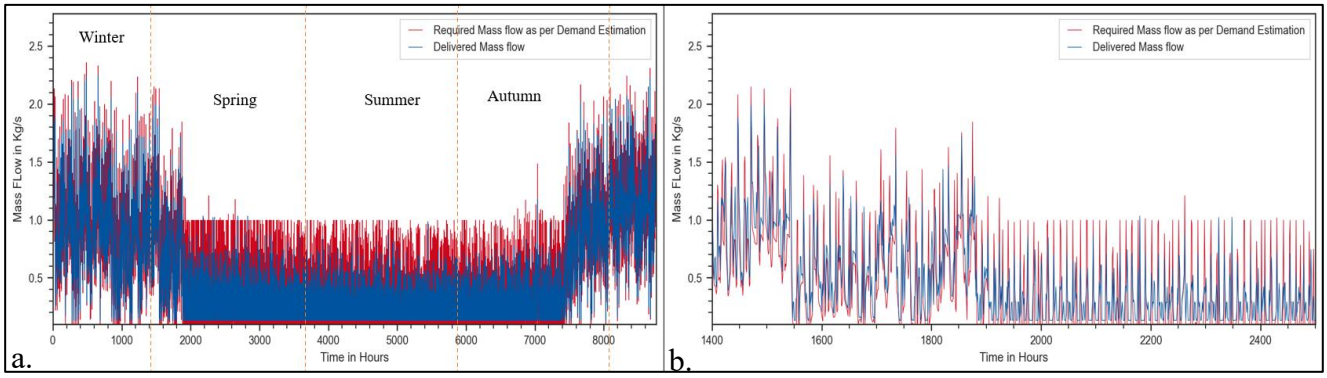

Figure 7. Variant 1 mass flow for building 11_1: a. full year and b. spring period

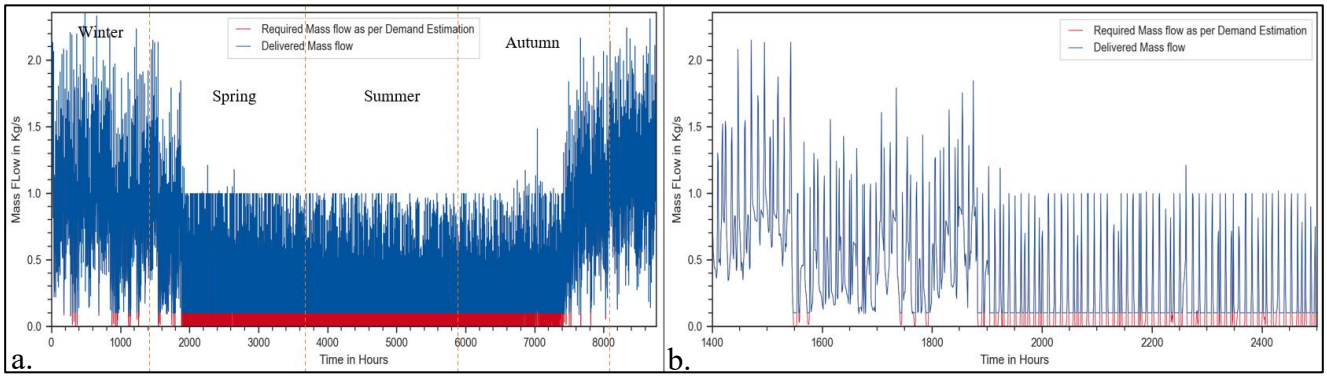

Figure 8. Variant 2 and variant 3 mass flow for building 11_1: a. full year and b. spring period

Figure 9a presents the outcomes of the total mass flow extraction from individual supply stations in the centralized pumping scenario for variant 4. Conversely, Figure 9b demonstrates the results for variant 5, depicting the total mass flow acquisition

from each supply station in the decentralized pumping scenario.

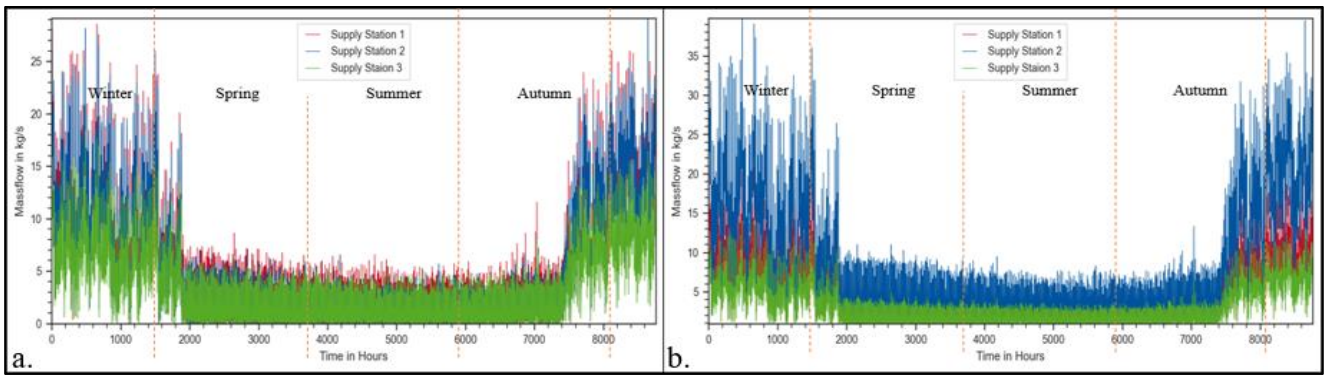

Figure 9. Mass flow from the supply stations: a. variant 4 and b. variant 5

In variant 2, the required mass flow is successfully achieved by adding a control block for the substation motorized valve, yielding comparable results to those depicted in Figure 8 for the centralized pumping station. The PI control utilizes a mass flow sensor and a calculation block constructed using the temperature sensor at the inlet to regulate the motorized valve. This implementation ensures the appropriate supply of mass flow necessary to meet the building's heating demands.

Table 2 presents a summary of results for different variants highlighting hydraulic inconsistencies. These inconsistencies resulting from centralized pumping have significant implications. They contribute to operational inefficiencies, suboptimal performance, increased energy consumption, and higher operating costs. Inadequate mass flow can negatively impact building heating or cooling, affecting occupants' comfort levels. Conversely, an excessive supply of mass flow can result in wasteful energy usage and unnecessary equipment wear and tear.

Table 2. Summary of Simulation Results: a comparative overview of different variants.

Variant	Duration of Undersupply (threshold: 0.1 kg/s)	Successful Achievement of Required mass flow	Temperature Fluctuations in supply and return line	Mass flow distribution with multiple supply stations
1	3829 hours (43.7% of total simulation time)	no, over or underserved	2-4 K	not applicable (NA)
2	0 hours	yes	2-4 K	NA
3	0 hours	yes	2-4 K	NA
4	3752 hours (42.8 % of total simulation time)	no, over or under served	2-4 K	aligned and distributed mass flow from each supply station
5	0 hours	yes	2-4 K	major distribution from supply station 2 further investigation needed

5. CONCLUSION

The results outlined in the preceding section yield several important conclusions. Firstly, centralized pumping schemes demonstrate hydraulic inconsistencies and deviations in meeting mass flow demands. These inconsistencies can result in operational inefficiencies, increased energy consumption, and potential comfort issues for building occupants. Mechanical adjustment of simple valves poses challenges in dynamically satisfying demands. However, by implementing decentralized control strategies and incorporating features such as PI control and motorized valves, the required mass flow can be effectively achieved, ensuring the satisfaction of heating demands in buildings. Secondly, decentralized pumping strategies offer a promising solution to address these challenges. Moreover, the results indicate that in decentralized pumping scenarios, mass flow extraction predominantly occurs from specific supply stations. Further investigation is required to evaluate the implications of this phenomenon in cases involving multiple active supply stations. Advanced control systems are necessary for the allocation of mass flow among substations and should be optimized to prevent the overloading of a particular supply station within the decentralized system. In conclusion, the study emphasizes the advantages of decentralized pump control in enhancing the efficiency and reliability of mass flow delivery. Careful design and implementation of decentralized strategies are crucial for optimizing energy usage, improving comfort levels, and ensuring a balanced distribution of resources throughout the district. These findings contribute to advancing the understanding and implementation of effective pump control strategies while planning a cold district heating network. Future work should explore advanced control strategies and robust simulation models, scalability of decentralized strategies in larger district heating networks, integration of renewable energy sources and storage technologies, and economic viability of decentralized pumping solutions.

ACKNOWLEDGEMENT

We gratefully acknowledge the financial support provided by the BMWK (Federal Ministry for Economic Affairs and Climate Action), promotional reference 03EWR020E.

REFERENCES

[1] Climate change 2014: Synthesis Report. Contribution of Working Groups I, II and III to the Fifth Assessment Report of the Intergovernmental Panel on Climate Change. IPCC, Geneva, Switzerland; 2014, 151pp.
[2] EU energy in figures: statistical pocketbook 2022. Luxembourg: Publications Office of the European Union; 2022, 263pp.
[3] European Commission. An EU Strategy on Heating and Coolin. Brussels, 16.2.2016 COM (2016) 51 Fina; Belgium, Brussels, 2016, 13pp.
[4] Bertelsen, N., Vad Mathiesen, B., 2020. EU-28 Residential Heat Supply and Consumption: Historical Development and Status, link: https://www.mdpi.com/1996-1073/13/8/1894 ; 2020 [accessed in June 2023]
[5] Sanner, B., Kalf, R., Land, A., Mutka, K., Papillon, P., Stryi-Hipp, G., Weiss, W.,2011. 2020-2030-2050. Common Vision for the Renewable Heating and Cooling Sector in Europe. Publications Office of the European Union: Luxembourg, 2011, 44pp.
[6] Rezaie, B., Rosen, M.A.,2012. District heating and cooling: Review of technology and potential enhancements. Applied Energy; vol. 93, pp. 2–10.
[7] Lund, H., Werner, S., Wiltshire, R., Svendsen, S., Thorsen, J.E., Hvelplund, F., Mathiesen, B.V., 2014. 4th Generation District Heating (4GDH). Energy 2014; vol.68, 1–11.
[8] Buffa, S., Cozzini, M., D'Antoni, M., Baratieri, M., Fedrizzi, R., 2019. 5th generation district heating and cooling systems: A review of existing cases in Europe. Renewable and Sustainable Energy Reviews; vol.104, 504–522.
[9] Wirtz, M., Kivilip, L., Remmen, P., Müller, D., 2020. 5th Generation District Heating: A novel design approach based on mathematical optimization. Applied Energy; vol.260, 114-158.
[10] Wirtz, M., Schreiber, T., Müller, D., 2022. Survey of 53 Fifth-Generation District Heating and Cooling 5GDHC Networks in Germany, link: https://onlinelibrary.wiley.com/doi/pdf/10.1002/ente.202200749 ; 2022[accessed in June 2023]
[11] Lund, H., Østergaard, P.A., Chang, M., Werner, S., Svendsen, S., Sorknæs, P., Thorsen, J.E., Hvelplund, F., Mortensen, B.O.G., Mathiesen, B.V., 2018. The status of 4th generation district heating: Research and results. Energy 2018; vol.164, 147–159.
[12] Lund, H., Duic, N., Østergaard, P.A., Mathiesen, B.V., 2018. Future district heating systems and technologies: On the role of smart energy systems and 4th generation district heating. Energy 2018, 165, 614–619.
[13] Blacha, T., Mans, M., Remmen, P., Müller, D., 2019. Dynamic Simulation of Bidirectional Low-Temperature Networks - A Case Study to Facilitate The Integration Of Renewable Energies. Building Simulation 2019; Rome, Italy, pp. 3491.
[14] Boesten, S., Ivens, W., Dekker, S.C., Eijdems, H.,2019. 5th generation district heating and cooling systems as a solution for renewable urban thermal energy supply. Adv. Geosci. 2019; vol. 49, 129–136.
[15] Sulzer, M., Hangartner, D., 2014. Kalte Fernwärme (Anergienetze)-Grundlagen-/Thesenpapier, link: https://www.researchgate.net/publication/262418798_Grundlagen-Thesen_Kalte_Fernwarme_Anergienetze ; 2014[accessed in June 2023]
[16] Schweiger, G., Larsson, P.O., Magnusson, F., Lauenburg, P., Velut, S.,2017. District heating and cooling systems-Framework for Modelica-based simulation and dynamic optimization. Energy 2017; vol.137, 566 – 578.
[17] Müller, D., Lauster, M., Constantin, A., Fuchs, M., Remmen, P., 2016. AIXLIB – An Open-Source Modelica Library within the IEA-EBC ANNEX 60 Framework, link: http://www.ibpsa.org/proceedings/bausimPapers/2016/A-02-3.pdf [accessed in June 2023]
[18] van der Heijde, B., Fuchs, M., Ribas Tugores, C., Schweiger, G., Sartor, K., Basciotti, D., Müller, D., Nytsch-Geusen, C., Wetter, M., Helsen, L., 2017. Dynamic equation-based thermo-hydraulic pipe model for district heating and cooling systems. Energy Conversion and Management; vol.151, 158–169.
[19] Schreiber, T., Beckhölter, T., Derzsi, K., Droste, K., Karuvingal, R., Wackerbauer, D., Wirtz, M., Welter, S., Zhang, Y., Muller, D., 2023. Planning the Design and Operation of Urban Energy Systems with Limited Data Availability: A Holistic Open-Source Tool Chain (under review)," CISBAT 2023.
[20] Lauster, M., Mans, M., Remmen, P., Fuchs, M., Müller, D., 2016. Scalable design-driven parameterization of reduced order models using archetype buildings with teaser, link: https://publications.ibpsa.org/conference/paper/?id=bausim2016_E-01-1 [accessed in June 2023]
[21] Fuchs, M., Teichmann, J., Lauster, M., Remmen, P., Streblow, R., Müller, D., 2016. Workflow automation for combined modeling of buildings and district energy systems. Energy; vol.117, 478–484.
[22] Mans, M., Blacha, T., Schreiber, T., Müller, D., 2022. Development and Application of an Open-Source Framework for Automated Thermal Network Generation and Simulations in Modelica. Energies; 15, 4372.

The 18th International Symposium on District Heating and Cooling, September 3–6, 2023, Beijing, China

SAFETY EVALUATION OF DISTRICT HEATING PIPELINE NETWORK BASED ON CORROSION FAILURE PROBABILITY ANALYSIS

Ang Wang[a,b], Yan Li [a*], Xiao Dong[c], Huiling An[a], Xingqiao Jia[a]

[a] *Hebei Province Low-Carbon and Clean Building Heating Technology Innovation Center, Yanshan University, 066004, PR China*
[b] *Tianjin Land Resources and House Vocational College, Tianjin, 300270, PR China*
[c] *XINXING DUCTILE IRON PIPES CO., LTD, Wuan, 056300, PR China*
[*] *Corresponding author. 35476149@qq.com*

ABSTRACT

To improve the mechanical stability of centralized heating pipelines and ensure their safety and reliability, the author's team proposed a new mode of socket-type connecting ductile iron thermal pipelines. Based on the corrosion characteristics of pipelines and using the Jinan-Laiwu long-distance heating project as an example, this study utilized the MC method to establish a calculation model of mechanical failure probability for thermal pipelines from both strength and stability perspectives. The study found that under the 30-year service life limit, the mechanical failure probability of ductile iron pipelines was much lower than that of steel pipelines, which means ductile iron pipes still have large safety margin. therefore, the service life of ductile iron pipelines is determined as the age when the mechanical failure probability reaches 0.60. Under this condition, the service life of ductile iron pipes is 50 years, which is 20 years longer than that of steel pipes. By comparing the probabilities of two mechanical failure modes, it was found that steel pipelines and ductile iron pipelines have different main failure modes. Sensitivity analysis was then conducted on the parameters, revealing that factors such as corrosion resistance, wall thickness, elastic modulus, and allowable stress were highly correlated with the pipeline mechanical failure probability. Ductile iron pipes have more advantages in the above parameters, resulting in better mechanical stability. The study found that the temperature sensitivity coefficient of steel pipelines was 0.31, which is much higher than the temperature sensitivity parameter of ductile iron pipelines (0.03). This indicates that steel pipelines are more temperature-sensitive, which means steel pipelines are more prone to mechanical failure in the early stages of heating. After analysis, it has been confirmed that under the same usage environment, ductile iron pipelines have a higher level of safety and longer service life.

Keywords: Thermal Insulation Pipeline, Ductile Iron Thermal Pipeline, Safety Evaluation, Mechanical Failure Probability

1. INTRODUCTION

Thermal pipelines commonly use carbon steel as the base material, which is buried underground after welded. There are the following shortcomings in this model during construction and usage: (1) The production process, construction method, and usage environment result in poor corrosion resistance of steel pipelines during usage [1-3]. (2) The heating pipes are welded as a whole, which will transfer and accumulate thermal expansion displacement during temperature changes, that will causing significant displacement in the pipes and weakening the pipes' ability to resist temperature changes. Therefore, natural compensation, installation of compensators, and preheating should be taken to reduce the thermal expansion displacement of heating pipes. (3) Due to the properties of the base material and the effects of welding, the allowable stress of steel thermal pipes decreases as corrosion progresses [4]. These shortcomings of steel thermal pipes will affect pipeline safety and service life.

In response to the shortcomings of thermal pipelines, the research team author belongs to proposed a new model of ductile iron thermal pipeline for heating projects, as shown in Figure 1. This thermal pipe is based on ductile iron and has the following main features: (1) The inner lining surface is polished, and the outer lining surface is coated with a zinc layer to slow down the corrosion rate of pipeline, which is effectively improve the pipeline's corrosion resistance. (2) The pipe segments are connected with the socket joint. At the socket joint, there is a 10-15mm gap between the socket and the spigot, which can fully adapt to the axial thermal expansion of the pipeline caused by temperature changes. Therefore, there is no need to set natural compensation or install compensators along the pipeline, which enhanced the pipeline's ability to cope with thermal expansion. (3) The base material of the pipeline has a higher allowable stress, and there is no need for welding during the installation process, reducing the impact of high-temperature welding on the pipeline material. The research team has verified its good economic feasibility [5]. By conducting engineering practices and experiments, they have confirmed the feasibility of using ductile iron thermal pipelines [6].

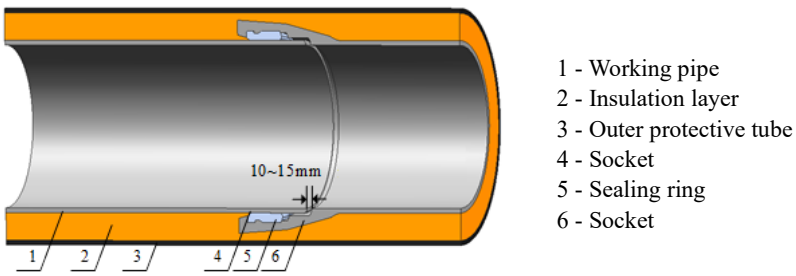

Figure 1. Schematic diagram of ductile iron heating pipeline

Many scholars have conducted research on the methods of safety evaluation for thermal pipelines, such as analytic hierarchy process[7], fuzzy evaluation method combining safety assessment [8], GIS and comprehensive evaluation method combining accident tree analysis method and analytic hierarchy process[9]. These studies provide a good research foundation for the safety evaluation of thermal pipelines. In order to study the characteristics of ductile iron thermal pipelines in mechanical stability and service life, this article takes the Jinan-Laiwu long-distance heating project as an example and uses the Monte Carlo method (MC) to establish a mechanical failure probability calculation model for the cumulative corrosion of thermal pipelines.

2. MECHANICAL FAILURE TYPES OF HEATING PIPELINE

Based on common mechanical failure cases of thermal pipelines, mechanical failures of thermal pipelines can be categorized into two types: pipeline strength failure and pipeline stability failure. Pipeline stability failure can further be classified into three types: vertical instability, radial instability, and local buckling.

2.1 Pipeline strength failure

The reasons for the strength failure of the heating pipeline underground can be attributed to the increase of the loading effect, the decline of the structural resistance, or a combination of them. When the loading effect on the pipeline is less than the structural resistance of the pipeline, the pipeline is safe, otherwise, it will be damaged.

2.2 Pipeline stability failure

(1) Vertical instability: When the temperature of the thermal pipeline increases, the pipeline undergoes axial expansion. If both ends of the pipeline are fixed, the pipeline may experience vertical instability as shown in Figure 2 (a). In severe cases, the thermal pipeline will be arched squeezed out of the ground.

(2) Radial instability: Under external circumferential pressure, the thermal pipeline may experience elliptical deformation. When the deformation exceeds the critical value, the thermal pipeline may undergo radial instability as shown in Figure 2(b).

(3) Local buckling: the buried thermal pipeline can be considered as a rod system from an overall perspective, but for a small section of the pipeline, it belongs to a thin-walled shell, especially for pipes with large diameters. For buried pipelines with large diameter, high temperature, and high pressure, significant local deformation may occur when the maximum compressive strain reaches a critical value. This can result in axial bending, buckling, and wrinkling of the pipeline, referred to as local buckling as shown in Figure 2(c) [10].

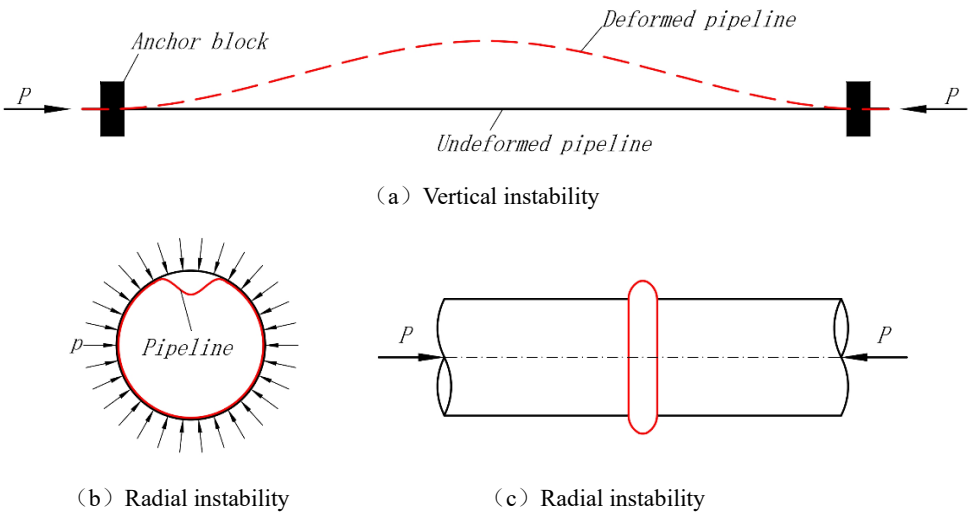

Figure 2. Schematic diagram of pipeline stability failure

3. MECHANICAL FAILURE STATE EQUATION OF THERMAL PIPELINES

3.1 Corrosion model of thermal pipeline

According to recent statistical data, corrosion is responsible for 66% of the total failures in thermal pipelines of central heating networks, making it the primary reason for the failure of such networks [11]. Numerous studies have shown that the power function corrosion model can accurately simulate the corrosion changes in pipelines:

$$\delta(\tau)= \delta_0-\Delta\delta(\tau)= \delta_0-k[365(\tau-\tau_0)]^n \tag{1}$$

Where $\delta(\tau)$ —wall thickness of the pipeline after τ years， mm；δ_0——Initial wall thickness of the pipeline， mm；$\Delta\delta(\tau)$ ——corrosion depth，mm；τ_0——starting corrosion time，year；τ——pipeline usage time, years；k、n——corrosion parameters.

Guo Hao et al[12]. conducted internal wall corrosion tests and accelerated soil corrosion simulation tests. Through experiments and data fitting, they proposed the recommended values for k of the inner and outer walls of carbon steel pipes are 0.037 and 0.111, respectively, and the recommended values for n are 0.430 and 1.851, respectively. The recommended values for k of the inner and outer walls of ductile iron pipes are 0.029 and 0.104, respectively, and the recommended values for n are 0.396 and 1.840, respectively. This study referred to the fitting values of the corrosion parameters obtained by Guo Hao et al.

3.2 Stress calculation of thermal pipeline

The reason for pipeline strength failure is that the stress on the pipeline exceeds its allowable stress. The stress generated in the pipeline can be decomposed into hoop stress σ_t, axial stress σ_{ax} and radial stress σ_r along the circumference, length, and diameter directions of the pipeline, respectively.

The Iowa formula is the theoretical basis for calculating the circumferential stress caused by external loads on buried flexible pipelines. Spangler proposed a formula to calculate the hoop stress σ_t based on the Iowa formula, which considers the simultaneous action of internal and external pressures [13]. The axial stress σ_{ax} consists of the axial stress σ_{ax}^{t} generated by temperature changes and the Poisson stress σ_{ax}^{p}that is associated with σ_t. It is generally believed that the working pipes of thermal pipelines are thin-walled metal pipes, the radial stress σ_r is approximately zero in theory, which can be ignored. According to the third strength theory, the external equivalent load σ_{eq} of the thermal pipeline under the combined action of circumferential and axial stresses can be calculated. The detailed stress calculation formula is shown in Table 1.

Table 1. Calculation formula for pipeline stress

Strain mode	**Formula**	**Description**
Hoop stress σ_t	$\frac{3k_bW_vE_p\delta D_{po}}{E_p\delta^3+3k_zpD_{po}^3+0.0915E_{soil}D_{po}^3}+\frac{p\left(D_{po}-2\delta\right)}{2\delta}$ （2）	k_b—bending coefficient of soil; E_p—Elastic modulus of pipes, MPa;W_v—vertical distributive load, N/m; δ—pipe wall thickness, mm; α_p—Linear expansion coefficient of pipes，℃$^{-1}$； D_{po}—pipe outer diameter, mm; k_z—Deformation coefficients of pipe; E_{soil}—Soil deformation modulus, MPa; p—Pipeline internal pressure, MPa; t_w—water temperature inside the pipe，℃; v_p—Poisson ratio; t_0—initial temperature of thermal pipe，℃。
Axial stress σ_{ax}	$\nu_p\left[\frac{3k_bW_vE_p\delta D_{po}}{E_p\delta^3+3k_zpD_{po}^3+0.0915E_{soil}D_{po}^3}+\frac{p\left(D_{po}-2\delta\right)}{2\delta}\right]-\alpha_pE_p\left(t_w-t_0\right)$ （3）	
External equivalent load σ_{eq}	$\left(1-\nu_p\right)\left[\frac{3k_bW_vE_p\delta D_{po}}{E_p\delta^3+3k_zpD_{po}^3+0.0915E_{soil}D_{po}^3}+\frac{p\left(D_{po}-2\delta\right)}{2\delta}\right]-\alpha_pE_p\left(t_w-t_0\right)$ （4）	

3.3 Mechanical failure state equation of thermal pipeline

The mechanical failure state equation of thermal pipeline can be expressed as:

$$G(S，R)=S-R \tag{5}$$

Where S——The beneficial effects of thermal pipeline stability; R——Critical action of thermal pipeline stability.

When $G(S,R)>0$, the thermal pipeline does not fail; When $G(S,R)<0$, the thermal pipeline fails; When $G(S,R)=0$, the thermal pipeline is in a critical state.

In the strength failure state equation of thermal pipeline, S represents the allowable stress of thermal pipeline (σ_{cr}), R represents the external equivalent load (σ_{eq}); In the vertical instability state equation of thermal pipeline, S represents the vertical distributed load of the thermal pipeline (W_v), R represents the critical load for vertical instability of the thermal pipeline ($W_{v,cr}$); In the vertical instability state equation of thermal pipeline, S represents the critical deformation of thermal pipeline(ΔX_{cr}), R represents the deformation of thermal pipeline(ΔX); In the local buckling state equation of thermal pipeline, S represents the critical buckling stress of thermal pipeline($\sigma_{f,cr}$), R represents the axial stress of thermal pipeline(σ_{ax}). The failure state equations of thermal pipelines under different failure modes are shown in Table 2.

Table 2. The failure state equations of thermal pipelines

Failure mode	State equation	Description
Strength failure	$G_1=\sigma_{cr}-\sigma_{eq}=3[\sigma]-\sigma_{eq}$ （6）	$[\sigma]$—Permissible stress，MPa；γ_{soil} — volume weight of backfilling soil，kN/m^3；h— Buried depth of pipeline top，m；μ_D—coefficient of vehicle dynamic load；D_{mo}—Outer diameter of thermal pipeline outer protection pipe，m； F — Vehicle standard load，kN；A — Thermal pipeline cross-sectional area，m^2；I_p — Cross-section moment of inertia，m^4；D_L — Lag coefficient of deformation.
Vertical instability	$G_2=\gamma_{soil}hD_{mo}+\frac{\mu_D FD_{mo}}{(0.2+2h\tan 30^\circ)(0.6+2h\tan 30^\circ)}-\frac{1.1\sigma_{ax}A}{E_pI_p}\max\left(10,\frac{\pi}{200}\sqrt{\frac{E_pI_p\times 10^3}{\sigma_{ax}A}}\right)$ （7）	
Radial instability	$G_3=0.03D_{po}-\frac{1.5D_Lk_zW_vD_{po}^3}{E_p\delta^3+3k_zpD_{po}^3+0.0915E_{soil}D_{po}^3}$ （8）	
Local buckling	$G_4=0.1254E_p\frac{\delta}{D_{po}}-\sigma_{ax}$ （9）	

4. Mechanical Failure Probability of Thermal Pipeline Based on Monte Carlo (MC)

4.1 Monte Carlo method (MC method)

Monte Carlo simulation (MC) is a method to solve theoretically possible deterministic problems through randomness. This method is based on a probability distribution model of random variables, using random simulation technology to conduct a large number of random sampling simulations. It replaces event probability with simulation frequency and uses simulation results as the basis for project risk assessment. With the development of computer technology, its application in pipeline stability assessment has become increasingly widespread, and many methods for calculating pipeline failure probability have been derived based on it[14,15].These studies also demonstrate the unique advantages of the MC method in pipeline failure probability assessment. Therefore, this paper will also use this method to evaluate the mechanical failure probability of a thermal pipeline.

When calculating the failure probability of thermal pipeline in this paper, first, it is assumed that the eigenvalues of each random variable follow a normal distribution and are independent of each other. Then, based on the mean μ_i and coefficient of variation CV_i of random variable i, a simple random sampling method is used to sample each random variable, and pseudo-random numbers are generated based on its distribution pattern. Subsequently, the obtained sampled values x_i are substituted into the limit state equation G_i. If G_i <0, the failure count under this mode will increase by one time. Otherwise, the failure count remains unchanged. Repeat this steps until all of the sampled samples are used up. The failure probability $P_{f,i}$ can be obtained based on the ratio of the failure frequency and sampling number of each of the four failure modes, and the mechanical failure probability of the pipeline can be derived accordingly.

4.2. Mechanical failure probability of pipeline inJinan-Laiwu long distance heating project

Taking a DN700 pipeline section in the Jinan-Laiwu long-distance heating project as an example, the failure probability of the steel thermal pipeline and ductile iron thermal pipeline at different service life spans is calculated. The interval estimation method is used to process the involved parameters. When the confidence level is set to 95%, the mean values μ_i and coefficient of variation CVi of each parameter are shown in Table 3. The relevant parameters are input into the corresponding limit state equation Gi of the mechanical failure mode, and the MC method is used to calculate the failure probability $P_{f,i}$ and the mechanical failure probability P_f of the thermal pipeline.

Table 3. Parameter values related to mechanical failure of two types of thermal pipelines

Symbol/Unit	μ_i of steel pipes	μ_i of ductile iron pipes	CV_i	Symbol/Unit	μ_i of steel pipes	μ_i of ductile iron pipes	CV_i
D_{po}/mm	720	738	0.01	p/MPa	1.6	1.6	0.10
D_{mo}/mm	850	870	0.01	F/kN	70	70	0.10
δ/mm	9.0	10.8	0.05	k_I/—	2.891	2.761	0.05
h/m	1	1	0.01	n_I/—	0.430	0.396	0.05
$[\sigma]$/MPa	125	140	0.01	k_O/—	0.002	0.002	0.05
α_p/1/°C	0.0000124	0.000011	0.01	n_O/—	1.528	1.506	0.05
E_p/MPa	206000	165000	0.04	k_b/—	0.157	0.157	0.15
v_p/—	0.30	0.28	0.02	k_z/—	0.096	0.096	0.15
D_L/—	1.5	1.5	0.20	γ_{soil}/kN/m^3	17.6	17.6	0.10
t_w/°C	120	120	0.01	E_{soil}/MPa	3.5	3.5	0.10

(1) Mechanical failure probability of steel thermal pipeline

Through MC method simulation, the variation of mechanical failure probability P_f of DN700 steel thermal pipeline with age is shown in Figure 3. From Figure 3, it can be seen that:

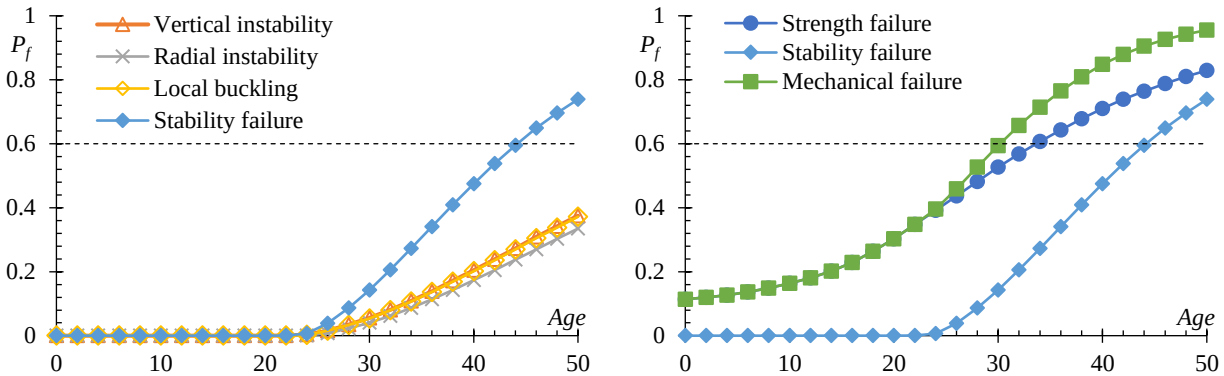

(a) Stability failure probability (b) Mechanical failure probability

Figure 3. Failure probability of steel thermal pipeline

1) The design service life of steel thermal pipeline is 30 years [16], and the corresponding mechanical failure probability of it is 0.59, which is close to 0.60. Therefore, the mechanical failure probability of 0.60 can be used as the standard to determine the design service life of the thermal pipeline.

2) The stability failure probability of steel heating pipeline during the initial 20 years is 0. After 20 years of pipeline use, the probability of vertical instability, radial instability, and local buckling increases year by year, but the difference is not significant. As of the design service life of 30 years, the maximum difference among the three is 0.015.

3) The strength failure probability of the steel thermal pipeline during its service life span is higher than the stability failure probability, and the difference in probability between the two reaches the maximum value of 0.40 in the 26th year. At 30 years, the mechanical failure probability in pipeline is 0.59, and the strength failure probability is 0.53, which is 0.38 higher than the stability failure probability. This fully demonstrates that strength failure is the main failure mode of steel thermal pipeline.

(2) Mechanical failure probability of ductile iron thermal pipeline

Through MC method simulation, the variation of mechanical failure probability P_f of DN700 steel thermal pipeline with age is shown in Figure 3. From Figure 4, it can be seen that:

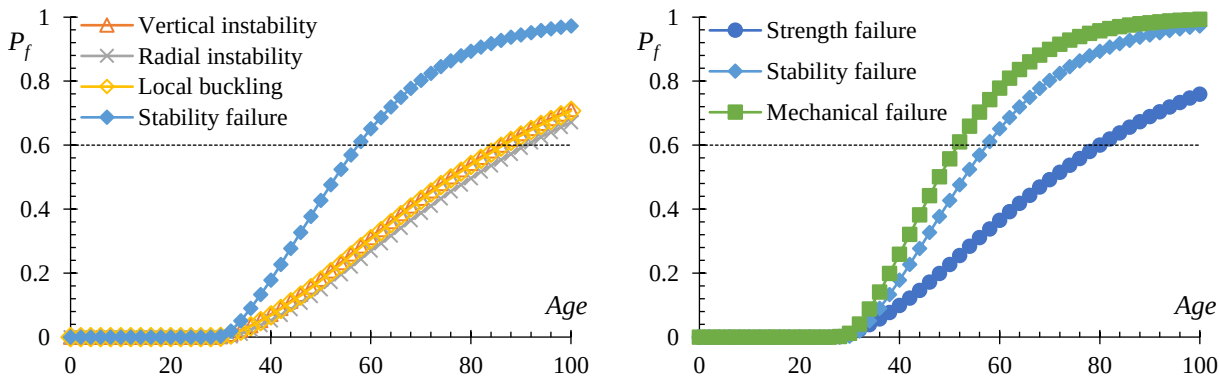

(a) Stability failure probability (b) Mechanical failure probability

Figure 4. Failure probability of ductile iron thermal pipeline

1) Based on the mechanical failure probability of 0.60 as the basis for the design service life of thermal pipeline, the mechanical failure probability of ductile iron thermal pipeline at 51 years is 0.59, close to 0.60.

2) The stability failure probability of ductile iron thermal pipeline during the initial 26 years is 0. the probability of vertical instability, radial instability, and local buckling began to increase year by year after the 26th year, but the difference was not significant. The stability failure probability in the 58th year is 0.61, exceeding 0.60 for the first time, while the strength failure probability first reaches 0.60 is the 80th year (0.601), which is 22 years later than the stability failure probability.

3) The stability failure probability of ductile iron thermal pipeline is higher than the strength failure probability after 34 years, and the difference in probability between the two reaches the maximum value of 0.31 in the 70th year. This indicates that stability failure is the main failure mode of ductile iron thermal pipeline.

(3) Comparison of failure probabilities between two types of thermal pipelines

The comparison of failure probability between steel thermal pipeline and ductile iron thermal pipeline is shown in Figure 5. it can be seen that:

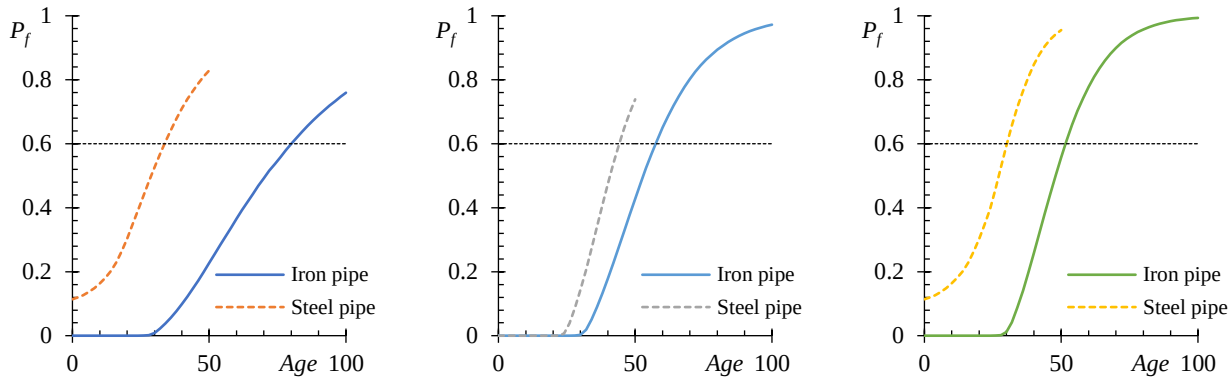

(a) Strength failure probability (b)Stability failure probability (c) Mechanical failure probability

Figure 5. Failure probability comparison of thermal pipelines

1) Due to the superior anti-corrosion performance of ductile iron thermal pipelines compared to steel thermal pipelines, and the fact that the wall thickness of ductile iron thermal pipelines is 1.8 mm thicker than that of steel pipelines of the same nominal diameter, the strength failure probability of ductile iron thermal pipelines is 0.52 lower than the steel thermal pipelines when the design service life is 30 years. At the 30th year, the strength failure probability of steel thermal pipelines is 0.53, while ductile iron thermal pipelines require approximately 72 years to achieve this strength failure probability, with a difference of 42 years. Therefore, ductile iron thermal pipelines have greater advantages in preventing strength failure of pipelines.

2) The stability failure probability of ductile iron thermal pipelines is lower than that of steel thermal pipelines. At the designed service life span of 30 years, the difference between the two is 0.14, which is smaller than the difference in strength failure probability between them.

3) At the designed service life span of 30 years, the mechanical failure probability of steel thermal pipelines is 0.59, while the mechanical failure probability of ductile iron thermal pipelines is only 0.01, with a difference of 0.58 between the two. The low mechanical failure probability of ductile iron thermal pipelines indicates that the pipeline still has abundant safety reserves, and a service life span of 30 years is not suitable for such pipelines. Therefore, referring to the relationship between the mechanical failure probability of steel thermal pipelines and the designed service life span, the year corresponding to mechanical failure probability exceeding 0.60 can be used as the design service life span for ductile iron thermal pipelines. At the 51th year, the mechanical failure probability of ductile iron thermal pipelines is 0.59, close to 0.60, and its service life span is 21 years longer than that of steel pipelines. Therefore, it is recommended to increase the service life span of ductile iron thermal pipelines from 30 years to 50 years when the usage conditions are similar.

(4) Sensitivity analysis of thermal pipelines

Sensitivity analysis can calculate the rate of change in failure probability P caused by changes in sensitive factor X, reflecting the degree of influence of sensitive factor X on failure probability P. Wu et al. [17] proposed a dimensionless sensitivity coefficient S_a for the influence of sensitivity factor X on sensitivity, which can better compare the relative impact of each sensitive factor X on the failure probability P. This article draws inspiration from its sensitivity coefficient calculation criteria to conduct sensitivity analysis on the 20 parameters involved in mechanical failure probability analysis, and selects the top 5 sensitive factors that are positively correlated with the sensitivity of thermal pipeline mechanical stability and the top 3 sensitive factors that are negatively correlated, as shown in Figure 6. it can be seen that:

1) The most sensitive positive correlation factor with the mechanical failure probability of steel thermal pipelines is the elastic modulus E_p, which is also positively correlated with the mechanical failure probability of ductile iron thermal pipelines. Therefore, using materials with higher elastic modulus as thermal pipelines is not conducive to the mechanical stability of thermal pipelines. Elastic modulus of ductile iron pipeline (1.65×10^5MPa) is less than the elastic modulus of steel pipes (2.06×10^5MPa), therefore, ductile iron thermal pipelines have a lower probability of mechanical failure.

2) The permissible stress $[\sigma]$ is negatively correlated with the mechanical failure probabilities P_f of both types of thermal pipelines. The permissible stress of ductile iron thermal pipelines (140 MPa) is slightly larger than that of steel thermal pipelines (125 MPa). Therefore, ductile iron thermal pipelines have a lower mechanical failure probability.

3) The temperature of water inside the pipeline (t_w) is positively correlated with the mechanical failure probability of steel

thermal pipelines, while it has a relatively small impact on ductile iron thermal pipelines. Therefore, it can be inferred that the mechanical failure probability of steel pipelines in the early stage of heating is higher than that of ductile iron thermal pipelines.

4) The sensitivity coefficient between wall thickness δ and the mechanical failure probability P_f of ductile iron thermal pipelines is -0.928, but it has a sensitivity coefficient of only 0.003 for the mechanical failure probability of steel thermal pipelines. When the nominal diameter is DN700, the wall thickness of ductile iron pipelines is 1.8mm thicker than that of steel thermal pipelines. Therefore, the mechanical failure probability of ductile iron thermal pipelines is smaller.

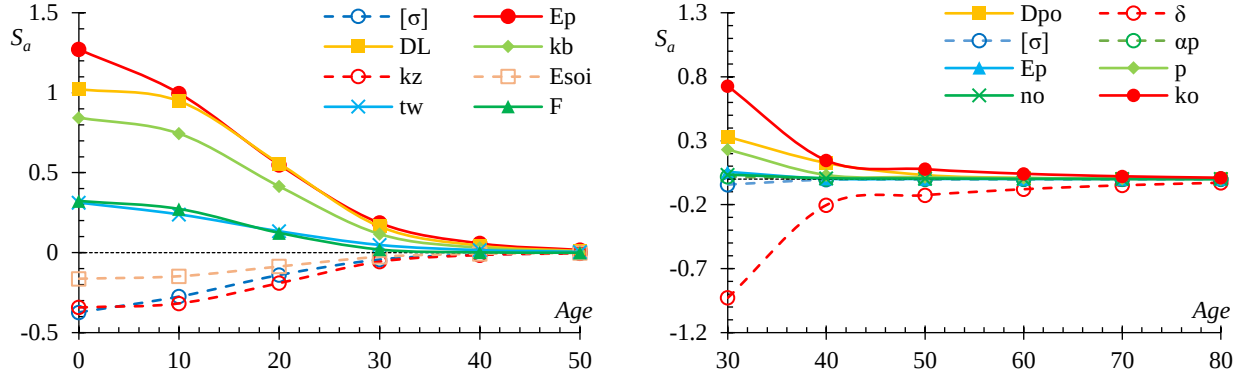

(a) S_a of steel thermal pipelines (b) S_a of ductile iron thermal pipelines

Figure 6. Sensitivity coefficient comparison of thermal pipelines

5. CONCLUSION

Based on the case study of the Jinan-Laiwu long-distance heating project, the mechanical stability of thermal pipes was evaluated using the Monte Carlo method, and sensitivity analysis was conducted on the parameters involved. The main conclusions of this paper are as follows:

(1) The anti-corrosion performance of ductile iron thermal pipelines is better than that of steel thermal pipelines, and the wall thickness of ductile iron thermal pipelines is 1.8mm thicker than that of the steel thermal pipelines at the same nominal diameter. This results in a mechanical failure probability of only 0.01 for ductile iron thermal pipelines after 30 years of use, which is much lower than the mechanical failure probability of 0.59 for the steel thermal pipelines. Therefore, a design service life of 30 years is not suitable for this type of pipeline. The relationship between the mechanical failure probability of steel thermal pipelines and the design service life can be used as a reference to determine the design service life for pipelines with a mechanical failure probability exceeding 0.60. The probability of mechanical failure of ductile iron after 51 years of use is 0.59, close to 0.60. Therefore, the design service life of ductile iron pipelines can be limited to 50 years, which is 20 years longer than steel pipelines and increases the service life of pipelines by 67%.

(2) Within the design service life, the strength failure probability of steel thermal pipelines is greater than the stability failure probability by 0.38 (30-year service life), while the stability failure probability of ductile iron thermal pipelines is greater than the strength failure probability by 0.38 (50-year service life). This indicates that strength failure is the primary failure mode for steel thermal pipes, while stability failure is the primary failure mode for ductile iron thermal pipes. The reason for the different failure modes is due to the different mechanical failure sensitivity parameters of the two types of pipes. Steel pipes are most sensitive to the elastic modulus E_p (S_a=1.27), while ductile iron pipes are most sensitive to the pipe wall thickness δ (S_a =-0.93).Steel thermal pipelines have a larger E_p(2.06 × 10^5MPa vs 1.65 × 10^5MPa) and a smaller δ (9.0mm vs 10.8mm) than ductile iron thermal pipes, so when facing similar usage environments, ductile iron pipes have a higher level of safety. In addition, the sensitivity coefficient of steel thermal pipelines to temperature is 0.31, higher than that of ductile iron pipelines, which is 0.03.This means the mechanical failure probability of steel thermal pipelines during the beginning of the heating period is higher than that of ductile iron thermal pipelines.

(3) The sensitivity coefficients of allowable stress [σ] for the two types of pipes are -0.37 (steel pipes) and -0.04 (ductile iron pipes), both of which belong to the negative correlation factors that have a significant impact on the mechanical failure probability of their respective pipeline modes. Ductile iron thermal pipes have a higher allowable stress (140 MPa vs 125 MPa) and therefore have a lower mechanical failure probability.

After analysis and comparison, it has been determined that ductile iron thermal pipelines have advantages over steel pipes in terms of corrosion resistance, wall thickness, elastic modulus, and allowable stress. These parameters are highly correlated with the mechanical stability of thermal pipelines. As a result, under the same use environment, ductile iron thermal pipes have better mechanical stability, higher safety, and better prospects for application in heating engineering.

ACKNOWLEDGEMENT

The authors would like to acknowledge for the financial support from Hebei Province Key Research and Development Project (20374505D) to the research work.

REFERENCES

[1] Feng Xingfa, Yang, Xian, Li, Yongsuo. Influence Of Underground Tunnel Excavation On Upper-Level Existing Pipelines. Advances In Civil Engineering 2022;2022-04-17
[2] Shen Hui, Bi Jinfeng, Luo Xianqi. Impact Assessment Of Common Supported Excavation Of Double Foundation Pits On The Adjacent Tunnel Progress In Civil Engineering, Pts 1-4 [C] 2012;170-173:1524-527
[3] Gao Feng, Zhao Tuanzhi, Zhu Xuebin. Land Subsidence Characteristics And Numerical Analysis Of The Impact On Major Infrastructure In Ningbo, China. Sustainability[J] 2023;15:2023-01-26
[4] Zhao Zuo Peng,Xu Kai,Xu Peng Fei,Wang Bin. Co2 Corrosion Behavior Of Simulated Heat-Affected Zones For X80 Pipeline Steel[J]. Materials Characterization, 2020(Prepublish).
[5] Wei Xitao. Study On Technical Economy Of Application Of Ductile Iron Pipe In Heating Engineering. A Dissertation In Architecture And Civil Engineering 2021
[6] Song Xiangyu. Thermal Dynamic Heat Transfer Characteristics And Thermal Insulation Optimization Of Directly Buried Ductile Iron Heat Pipe . A Dissertation In Architecture And Civil Engineering 2021
[7] Yin Shuo, Hao Xuejun, Tang Qingguo. Safety Evaluation Of Heat Exchange Stations Based On Analytic Hierarchy Process . Regional Heating 2014;(01): 16-20+33
[8] Zhen Xing Research On The Safety Assessment System Of Central Heating Pipeline Based On Gis . Handan: Hebei University Of Engineering, 2016: 9-11
[9] Wang Xueping. Research On Leakage Risk Assessment Of Directly Buried Pipeline In A Central Heating Project . Beijing: Beijing Jiaotong University, 2020
[10] Yu Maohong, Qiang Hongfu, Zan Yuewen. Development And Prospects Of Equal Strength Theory. Applied Mechanics 2004;21(6): 1-20
[11] Zhen Xing. Research On The Safety Assessment System Of Central Heating Pipeline Based On Gis .Handan: Hebei University Of Engineering, 2016: 9-11
[12] Guo Hao. Research On Electrochemical Corrosion Mechanism Of Water Supply Pipeline . Tianjin: Tianjin University, 2017
[13] Watkins R K, Spangler M G. Some Characteristics Of The Modulus Of Passive Resistance Of Soil: A Study In Similitude[C]//Highway Research Board Proceedings. 1958, 37.
[14] Singh M ,Markeset T. Hybrid Models For Handling Variability And Uncertainty In Probabilistic And Possibilistic Failure Analysis Of Corroded Pipes. Engineering Failure Analysis Jul 2014; 42 :197-209
[15] Application Of Markov Modelling And Monte Carlo Simulation Technique In Failure Probability Estimation - A Consideration Of Corrosion Defects Of Internally Corroded Pipelines. Ossai Ci,Boswell B, Davies, Ij. Engineering Failure Analysis Oct 2016; 68:159-171
[16] Ministry Of Housing And Urban Rural Development Of The People's Republic Of China. Projectcode For Heating Engineering. Beijing; 2021,10
[17] Wu Y T, Mohanty S. Variable Screening And Ranking Using Sampling-Based Sensitivity Measures[J]. Reliability Engineering & System Safety, 2006, 91(6): 634-647.

The 18th International Symposium on District Heating and Cooling, September 3–6, 2023, Beijing, China

INSTANDHALTUNG-FW: PREPARING THE GROUND ON THE PATHWAY TO PREDICTIVE MAINTENANCE IN DISTRICT HEATING

Hay S.[a*], Huther H.[a], Langroudi P.[b], Weidlich I.[b] Kropp, I.[c]

[a] *AGFW | Der Energieeffizienzverband für Wärme, Kälte und KWK e.V., Frankfurt, 60596, Germany*
[b] *HafenCity University Hamburg, Hamburg, 20457, Germany*
[c] *3S Consult GmbH, Dresden, 01309, Germany*
[*] *Corresponding author. s.hay@agfw.de*

ABSTRACT

District Heating (DH) utilities require focused maintenance strategies for their networks to ensure both security of supply and economic efficiency. Moreover, implementing optimized maintenance practices not only enhances resource efficiency but also plays a crucial role in national and international climate protection efforts. Requirements for maintenance strategies are meaningful inventory, accurate damage statistics, and comprehensive operating data as well as reliable simulation results from asset management tools. Scarce existing data in combination with the numerous influences on the service life of a DH pipes result great uncertainties in asset management. To reduce these uncertainties and to improve maintenance strategies, an ageing model was developed in the "Instandhaltung-FW" (engl. “Maintenance-DH”) project that increases the reliability of the results of asset management simulations by combining statistical ageing models and material-based service life models. The combined ageing model was validated using data from four DH utilities. The results show that the use of the combined ageing model can increase the forecast accuracy of the simulation. In addition to the aforementioned factors, the importance of relying on databases becomes evident. As a result, an artificial dataset has been created to address the scarcity of data and mitigate privacy/confidentiality concerns. This helps researchers to use the data for development and simulation purposes. Due to the developing technical possibilities and political requirements, e. g. for the remote readability of heat consumption data in Germany, the number of remotely readable data points in DH networks will increase significantly in the next years. The digitalization of DH networks should promote predictive maintenance strategies in DH.

The path to implement predictive maintenance in DH starts with the improvement of inventory and damage statistics. In addition, research for adaptions on asset management tools and aging models of DH pipes is required. DH companies and Researchers will address these tasks in the future, for example in the upcoming national research project Sustainable Asset Management District Heating.

Keywords: **District Heating networks; Predictive maintenance; Transformation.**

NOMENCLATURE

n_i	is cycles at i^{th} stress level during service	k	reaction rate
N_i	is cycles at i^{th} stress level on SN-curve	R	gas constant (8.31 J/mol·K)
E_a	Arrhenius activation energy (kJ/mol)	A	frequency factor
t_1	service life at temperature T_1 (K)	t_2	service life at temperature T_2 (K)
T	absolute temperature		
D	is the fraction of life consumed by exposure to the cycles at the different stress levels.		

1. INTRODUCTION

When maintaining heating networks, for technical, economical, and ecological reasons it is highly recommended to exploit the service life of the pipelines completely. The service life of pipelines in heating networks is influenced by various factors, such as the quality of the pipelines supplied, the quality of the workmanship during the construction of the heating network and the operational loads. Since the reliability of the heat supply in district heating systems is influenced by the operational capability of the pipelines of the heating network, maintenance strategies aim at limiting the risk of failure of the pipelines to a level defined by the utility [1].

Basically, maintenance strategies can be divided into reactive, proactive, and risk-oriented strategies [2]. Reliable inventory, damage, and operating data, in conjunction with an increase in the number of measuring points in heating networks for recording operating parameters and the use of artificial intelligence, will make it possible to use predictive maintenance

strategies in the future [3]. Since the listed requirements for predictive maintenance are not yet fulfilled in many district heating systems today, the estimation of the service life of pipelines in heating networks, using commercially available software tools in asset management, often forms the basis for the development of the company-specific maintenance strategy. These asset management software programmes usually use statistical ageing models, among other things, to forecast damage rates, failure probabilities and to determine investments in renovation measures. Compared to other infrastructures such as water supply, the statistical data basis for the use of these ageing models for district heating pipes is small. In connection with the multiple factors affecting the service life of district heating pipes, the uncertainty of the simulation result increases when using statistical ageing models due to the limited data availability. In addition to statistical ageing models, material-based service life models and methods for condition assessment can be used to estimate the service life of the pipes of the heating network [4]. The further development of material-based service life models for mapping ageing processes based on complex material stress in situ continues to be the subject of research projects [5].

The aim of the research project "Maintenance-DH" is to develop a combined ageing model by linking statistical ageing models and material-based service life models, which increases the reliability of forecasts on the service life of district heating pipes. In addition, the exchange with district heating supply companies during the project aims to use previous data bases and approaches to identify practice-oriented recommendations and measures for improved maintenance strategies in the future. These activities to improve asset management have so far run parallel to plans for the decarbonisation, transformation, and digitalisation of district heating systems: The decarbonisation and transformation of existing systems towards a higher share of renewable energy sources requires, among other things, the substitution of fossil heat generation plants, the reduction of heat consumption and will probably lead to more decentralised DH systems. These measures require a further digitalisation of existing networks due to the parallel increasing complexity of existing systems. This will lead to an increase in the digital recording of operating parameters in existing DH networks [6]. In addition, the number of digital data points in district heating systems in Germany will increase by the end of 2026 due to the legal requirement for consumption recording and remote readout of customer systems [7]. If network operators record operating parameters such as pressure and temperatures in addition to pure consumption data, this legal regulation can generate valuable data for operational optimisation and predictive maintenance strategies. Based on the results of the research project "Maintenance-DH", the following paper shows the path to predictive maintenance in district heating systems.

2. DATA BASIS, COMBINED AGEING MODEL AND SIMULATIONS SCENARIOS

2.1. Data from four utilities and damage rate from AGFW statistics

Available inventory, damage and operating data were provided by four different district heating supply companies (abbreviated here as network A-D) for the development of the combined ageing model. The inventory data included georeferenced network plans with identification numbers for individual pipe sections of the heating network, the year of construction, the length and nominal diameter of the pipelines and the pipe system used. Figure 1 summarises the percentage shares of the different pipe systems in the four district heating systems.

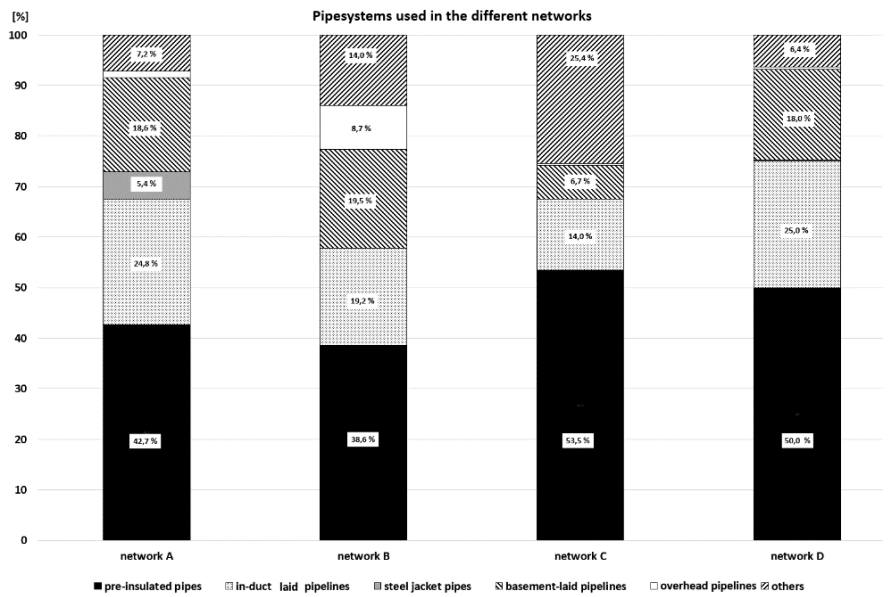

Figure 1. Pipe systems used in the four networks A-D, source: AGFW

Based on the percentage shares of different pipe systems shown, it can be assumed that various pipe systems with different materials are installed in today's district heating systems. The pipe system of buried pre-insulated bonded pipes has the largest share in all district heating systems and therefore forms the focus in the development of the combined ageing model. In addition to pre-insulated pipes, other pipe systems with a steel service pipe, such as in-duct laid pipeline, overhead pipes and basement-laid pipes, are used due to the design temperatures of the district heating networks under consideration. In table 1 additional information on the networks like the length in kilometres trench, the average age of all pipes and the number of collected damages on all pipes of the systems are given. It should be noted that the percentages for the pipe systems of network D in Figure 1 refer to the entire system with more than 300 kilometres length trench. For the simulations in the project, data of a subnetwork was provided by the utility (see Table 1).

Table 1. Additional data form the four DH networks

network	length in [km trench]	average age in [a]	number of damages [-]
A	328.4	30.1	186
B	102.8	37.6	12
C	184	30.7	667
D	13.6	26.0	35

For the further development of the combined ageing model, the damage data of the pipe system pre-insulated pipes were used. Figure 2 shows the ageing distribution of the pipelines with damage events for networks A, C and D for the pre-insulated pipe system. The low number of recorded damages as well as the missing allocation to the pipe ID in the data of network B has led to the fact that the data basis of the practice partner could not be used in the investigations. Overall, the number of damage events and the age of the pre-insulated pipes of the four network operators are low. According to the European standards for quality and design, buried pre-insulated bonded pipes are designed for a minimum service life of 30 years [8, 9]. As shown in figure 2, most of the pipelines of the four utilities have not yet reached the minimum service life according to the design.

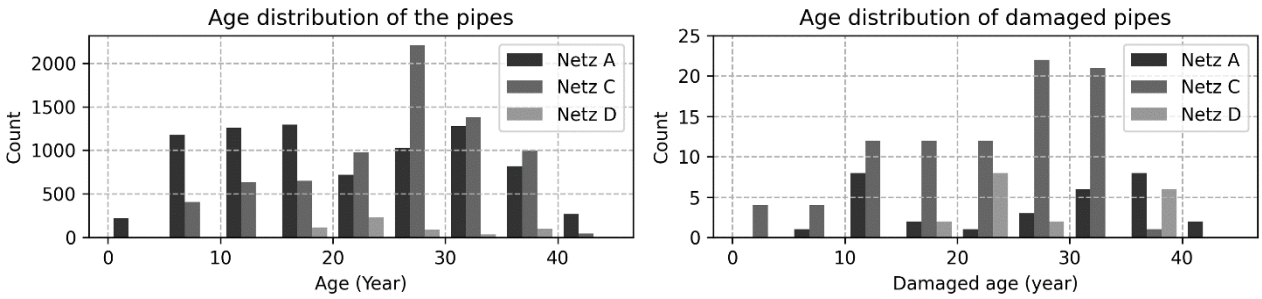

Figure 2. Age distribution of pre-insulated pipes and damaged pre-insulated pipes in the networks A, C and D, source: HCU

By setting up an "inventory and damage database" on a national level, AGFW is aiming to overcome data shortage for asset management of district heating pipes. By the end of the project, 54 of a total of 196 district heating network operators had participated in the statistics [10]. Regarding the length trench of district heating networks in Germany, inventory data of 9490 kilometres trench (44.5 % in relation to the total length for district heating networks in Germany based on [11]) have been submitted by the network operators to the statistics. 25 of the participating utilities entered a total of 2267 damages for different pipe systems into the database. In the process, the option of a detailed description of the damage was rarely used by utilities. Figure 3 shows the resulting damage rates for pre-insulated pipes, basement-laid pipes and in duct laid pipes that could be used for the simulations in the project. This is based on 4279 km trench with 651 damage events for pre-insulated pipes, 1138 km trench with 34 damage events for basement-laid pipelines and 1478 km of route with 192 damage events for in duct laid pipes that could be evaluated [10].

For the use of material-based service life models, the in-situ stresses that result from the operation of the heating network and lead to the fatigue of the materials are essential. None of the four practical partners could provide complete, historical operating modes of the heating network over the service life of the pipelines. Therefore, an algorithm for the simulation of historical temperature modes was developed in the project and integrated into the combined ageing model [3].

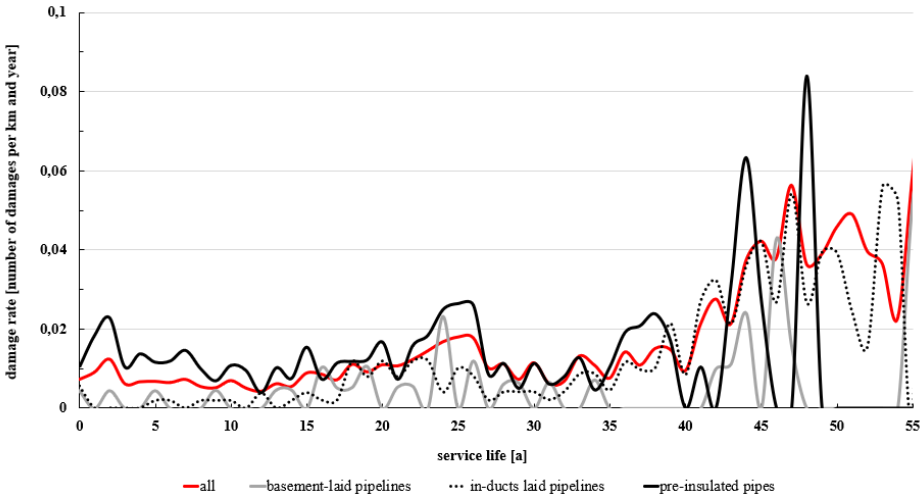

Figure 3. Damage rate of different pipe systems in numbers of damages per kilometres and year, source: AGFW

2.2. Design and structure of the combined ageing model

The implemented combined model consists of 3 main components:

- Backwards simulation for historical load collectives.
- Material specific ageing models.
- Condition prediction and derivation of artificial data points for ageing.

To have a proper predictive approach, it is important to have the loading history on pipes. This data mostly is not available specially for the pipes which are more than 10 years in operation. Therefore, a backward simulation model has been developed to enable to understand the loading history based on the availability of the weather data where the pipe is located. This was explained was explained extensively in our previous work [15]. For this model the temperature and non-temperature variables have been used.

Regarding material specific ageing models there are two models, which are broadly being used in district heating for pipes. Palmgren-Miner's rule for fatigue estimation and Arrhenius equation for thermo-oxidation of the PUR foam. But before diving to the equations, it is worth noting that rainflow-counting algorithm is used to prepare the backward simulation results for further calculations [16].

For calculation of damage accumulation of the steel medium pipe Palmgren-Miner's rule is used as follows:

$$D = \sum_{i=1}^{k} \frac{n_i}{N_i} \tag{1}$$

In general, when the damage fraction reaches to unity, failure occurs. This is critical to monitor in DH pipes because they are continuously subjected to temperature fluctuations that will cause thermal fatigue. However, while this may be the first damage accumulation model, it is highly recommended according to EN 13941-1:2019 [17].

The temperature changes not only cause damage to the steel pipes but also impact the partial pressure on the foam cells. This leads to increased oxygen ingress into the cells, ultimately resulting in foam oxidation. The Arrhenius law relates the rate of a chemical reaction to the temperature and activation energy of the reaction. The Arrhenius equation suggests that an increase in temperature leads to an exponential increase in the rate of a reaction. The equation is given as:

$$k = Ae^{\frac{-Ea}{RT}} \tag{2}$$

According to EN 253, a derivation of the previous equation the Arrhenius law for thermo-oxidative aging of polyurethane insulation materials applies in DH pipes relative to accelerated ageing of the foam. The equation is as follows:

$$\log_{10}\left(\frac{t_2}{t_1}\right) = \left(\frac{1}{T_1} - \frac{1}{T_2}\right) \cdot \frac{E_a}{(2{,}303 \cdot R)} \tag{3}$$

Correspondingly, it is possible to calculate the foam oxidation of the pipes by considering the condition of service life of the fresh pipes and incorporating it into the model.

Finally, the statistical data on failures will be compared with the actual data from operational pipes, enabling a conditional assessment to predict potential failures. The following figure illustrates the principal flow of the entire algorithm of the combi-model that was used for the implementation. The basic elements of flow-chart symbols are used to describe the combi-model in figure 4 [12].

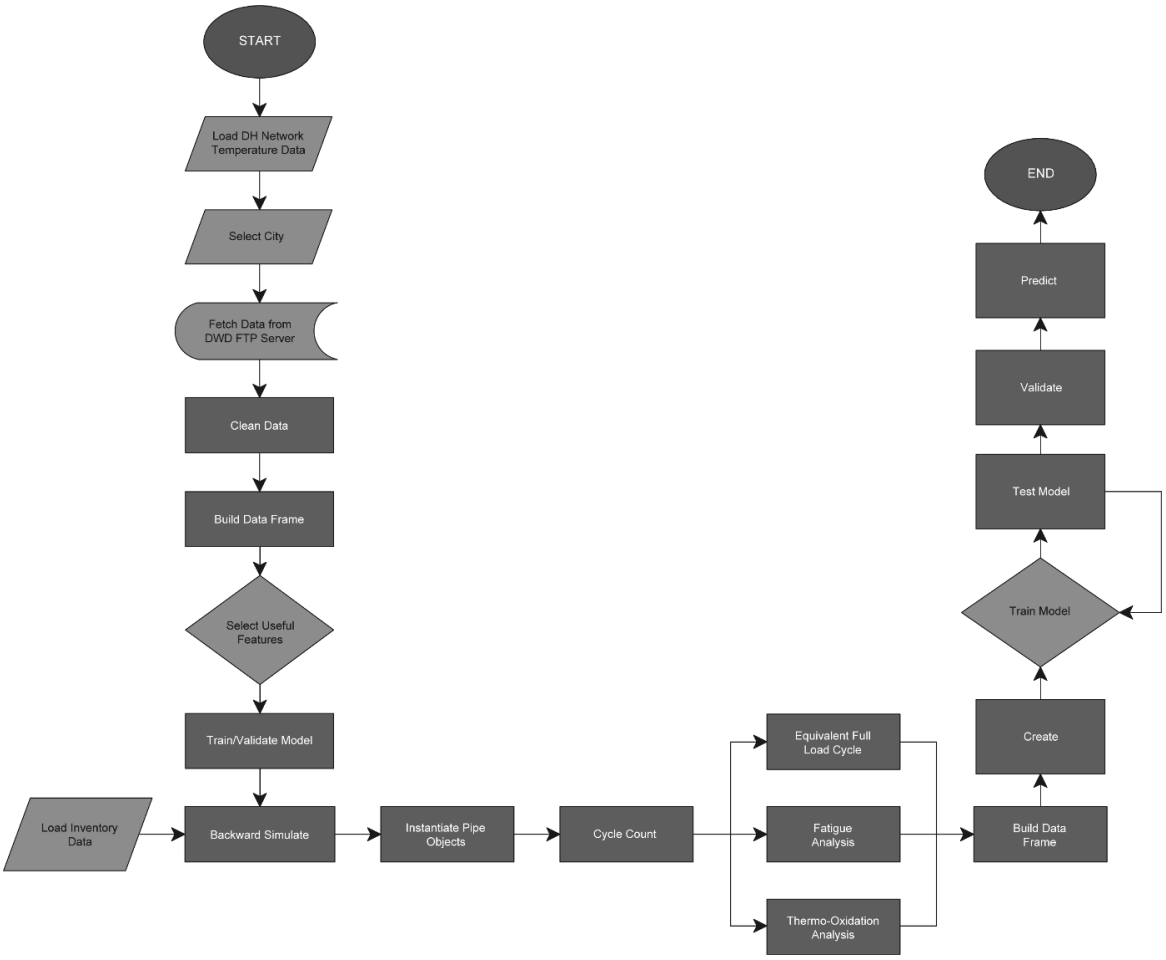

Figure 4. Flow chart diagram of the combi model based on flow-chart symbols, source: HCU

The vertical line on the left describes the backwards simulation. This is followed horizontally at the bottom by the material-specific ageing models. Finally, the right vertical thread describes the part of the condition prognosis with derivation of artificial data points for ageing. Following the backward simulation, the material-specific ageing values can be calculated for all pipes to be considered. These are, among others, the equivalent full load cycles, the activation rate, and the fatigue index. The prototypically implemented combination model can be used to derive service lives for ageing modelling. In the context of risk modelling, various condition-based assessment factors are available for the pipeline sections, e.g.

- Age, absolute [years].
- Remaining service life, absolute [years].
- Reserve of service life, 0-100 [%].
- Predicted damage rate, absolute [p./km.a]
- Predicted damage number, absolute [No.]

A detailed description of the algorithm is documented in the final project report [10]. In addition, the code of the algorithm and essential instructions for its use are published in a freely accessible form [13].

The factors listed above are parameters that can be changed over time. Up to now, the usual risk modelling has focused on static observations at a specific point in time. The software has been extended to support dynamic risk modelling. Finally, by implementing the algorithm presented here in the asset management software KANEW 3S® [14], the combination of statistical ageing models with material-based service life models was established using backwards simulation.

2.3 Asset simulations with the data of the network operators

For a comparative asset simulation with the data sets of the three network operators, 3 scenarios were defined and simulated:

- Scenario 1 - Analysis based on own damage statistics (S1)
- Scenario 2 - Analysis based on own damage statistics and combination with data from AGFW inventory and damage statistics (S2)
- Scenario 3 - Analysis based on own damage statistics, combination with data from AGFW inventory and damage statistics and application of material-based analyses (S3).

For each scenario, damage analyses and service life estimates were carried out as a basis for further risk analyses and strategy simulations. A very simplified risk analysis was carried out to demonstrate the benefits of using the combined model, as no comprehensive assessment criteria were available for the networks.

Condition criteria (with equal weighting among them):

- Remaining useful life.
- Damage rate.

Criteria for significance/importance

- Nominal size.

The complete results are published in the project final report [10]. In the further analysis of the simulation results, the focus is on the development of the damage rate and the derivation of the service life.

3. RESULTS OF THE SIMULATIONS

Figure 5 shows the simulation results for the three scenarios (S1-S3) for networks A, C and D based on the damage rates of pre-insulated pipes. To determine the average service life, the damage rate is set at 0.1 damage per kilometre of pipe per year. This is common in other sectors, such as water supply, and was confirmed in a workshop with the utility companies.

In network A, the damage rate of 0.1 damage per kilometre of pipeline per year is reached after 69 years. Including the damage data of the previous AGFW statistics in S2, the useful life increases to 88 years. In S3, the average service life is reduced by 4 years by applying the material-based service life models.

In the simulations for network C, the district heating pipes reach a mean service life of 155 years in S1, even more than 200 years in S2 and 178 years in S3. The damage functions are due to a low number of damages and the relatively low average age of the pre-insulated pipe system in the heating network.

The simulated damage function increases in network D for S1 already at the beginning to 0.08 damage per km pipe and year and remains const. afterwards. Since an increasing renewal of the pipes in the heating network is necessary in this context, the damage function in S1 does not reach the defined limit damage rate. In the further simulations, the marginal damage rate and thus also an average service life of the pipelines is reached. It is 81 years for S2 and 78 years for S3.

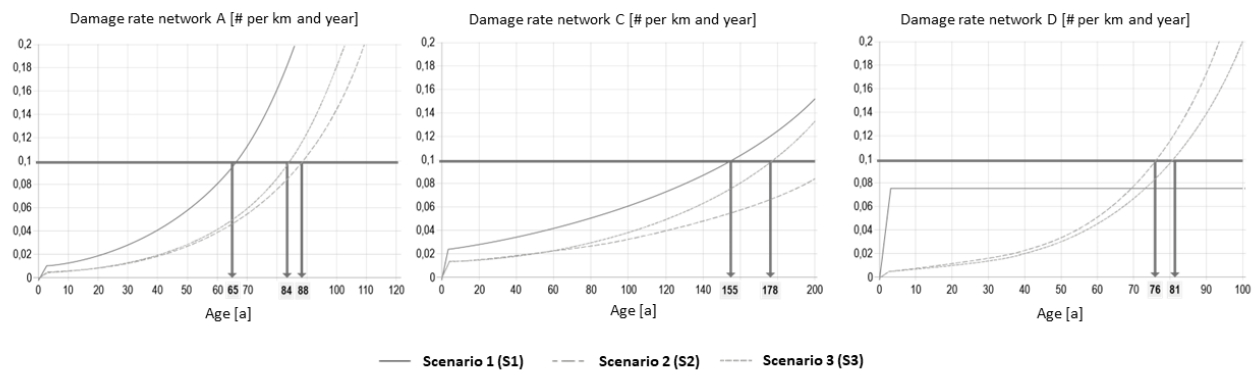

Figure 5. Results of the simulation of the three scenarios with KANEW 3S® for the three district heating systems, source: 3S Consult

4. DISCUSSION OF RESULTS

Based on the data and simulation results, it is clear that a large proportion of the utilities' district heating pipes have not yet reached the end of their service life. For an asset management simulation, complete inventory, damage, and operating data form the basis for reliable results. The development and application of a combined ageing model based on statistical ageing models and material-based service life models shows in the three practical examples that the validity of the simulation results can be increased in principle. It was necessary to develop the algorithm for the backward simulation for the use of material-based service life models to compensate for the lack of historical operating data from the utilities. In summary, the data from the four practice partners showed that the databases for reliable asset simulations needs to be improved. Similarly, the AGFW's inventory and damage database is still under development at the national level, but in the long term it can help to increase the reliability of asset simulations by providing a larger statistical data set.

The results for estimating the remaining service life of pre-insulated pipes aged due to real life application as well as the experience of utility companies in Germany show that the pipe system can achieve service lives of over 50 years [4]. Since numerous, different influences affect the service life of the pipe systems and a large proportion of the district heating pipes have not yet reached the minimum service life according to the design, there is a further need to validate the simulation results. In addition, improvements based on further research results, e.g., for material-based service life models [5], will be incorporated into existing asset simulations in the future. In parallel, political framework conditions and technological developments to increase overall efficiency will increase the number of remotely readable measuring points for recording operating parameters in district heating networks. This operating data will also enable improved forecasts and even predictive maintenance strategies in asset management using artificial intelligence. In order to be able to use these improved asset simulation models, companies should:

- Completely collect and document inventory, damage and operational data and process historical data as best as possible.
- Investigate causes of damage where possible, assign failure causes to the different materials of the pipe system and categorise the damaged pipe.
- Check and document the material properties of the pipeline before construction (e.g., quality control according to [8]).
- Record, categorise and document the condition of existing pipelines in the case of network extensions, connection compaction in the network or rehabilitation measures.
- Carefully document maintenance activities, failures of recording devices, etc. in the record of operational data.

Similarly, by implementing these recommendations, utilities contribute to supporting scientific work, e.g., in the development of Artificial Intelligence algorithms to quantify complex ageing processes of materials due to stresses acting in situ. These contributions from practice are necessary to enable long-term predictive maintenance strategies in the field of district heating.

5. CONCLUSION

Predictive maintenance requires reliable inventory, damage, and operating data as well as information on the condition of the pipes of the heating network, which can be used to identify ageing processes using artificial intelligence.

An incomplete database only offers district heating operators the possibility to apply proactive maintenance strategies with a high risk for an early replacement of the pipelines or reactive maintenance strategies. In the research project "Maintenance-DH", a combined ageing model and an algorithm for the generation of historical operational data were developed, which can improve the prediction of asset simulations. After the implementation of the developed algorithms in a market-available asset simulation software, the simulations with the data of the three practice partners show the potential for reducing the uncertainty in the simulation result, but at the same time also illustrate the necessity for improving the database. Based on the simulation results in connection with the work in the “Maintenance-FW” project, recommendations for improving the data basis were developed and presented in this paper.

Based on the status regarding inventory, damage and operational data, predictive maintenance can represent a long-term goal of district heating utilities, which utilities can get a step closer to by applying the project results "Maintenance-DH". It is expected that further steps towards predictive maintenance will be achieved in the future through research results related to ageing models, data processing of asset simulation software and artificial intelligence algorithms. As the results of the project show, the close cooperation between research and practice is a promising approach to enable improved maintenance strategies.

ACKNOWLEDGEMENT

The authors acknowledge the financial support by the Federal Ministry for Economic Affairs and Climate Action of Germany in the project Instandhaltung-FW (project number 03ET1625). Besides that, the authors acknowledge the four district heating operators for providing data.

AUTHOR CONTRIBUTION

S. Hay contributed as the coordinator of the research project as well as previous research results in the field of maintenance of DH networks and chiefly responsible for preparing the manuscript. P. Pourbozorgi Langroudi was responsible for designing and conceptualizing the study, collecting and analyzing the data, and developing the model. H. Huther and I. Weidlich provided scientific supervision of the study. I. Kropp contributed with the experience in asset management of district heating pipes and was responsible for the simulations in KANEW 3S™. All authors contributed with the critical discussion of the results and editing of the manuscript.

REFERENCES

[1] AGFW FW 113. Quality of supply in district heating. Frankfurt am Main, AGFW, 2017. (in German)
[2] AGFW FW 114. Strategies for maintenance and planning of rehabilitation. Frankfurt am Main, AGFW, 2013. (in German)
[3] Langroudi P., Weidlich I., Hay S. Backward Simulation of Temperature Changes of District Heating Networks for Enabling Loading History in Predictive Maintenance. Energy Reports 2021:Volume 7 (Supplement 4): Pages 119-127 https://doi.org/10.1016/j.egyr.2021.09.031.
[4] Hay S., Leuteritz A., Morgenthum M. Remaining service life of preinsulated bonded pipes—A key element of transformation strategies and future district heating systems in Germany. Energy Reports 2021:Volume 7 (Supplement 4):Pages 440-448, https://doi.org/10.1016/j.egyr.2021.08.084.
[5] IEA DHC. IEA DHC Annex TS 6 – Status Assessment, Ageing, Lifetime Prediction and Asset Management of DH Pipes - Annex Text. https://www.iea-dhc.org/the-research/2021-2025-annex-ts6/downloads, 2023 [7th June 2023].
[6] Hay S., Kallert A. M., Lottis D., Ziegler R., Weidlich I., Dollhopf S.. Existing District Heating Networks in Context of German Climate Goals: Potentials for "UrbanTurn". Conference Proceedings ISEC 2nd Sustainable Energy Conference 2022, Congress Graz Austria, Pages 196-203.
[7] Bundesministerium der Justiz. Verordnung über die Verbrauchserfassung und Abrechnung bei der Versorgung mit Fernwärme oder Fernkälte, https://www.gesetze-im-internet.de/ffvav/BJNR459110021.html, 2021 [31st May 2023]
[8] EN 253 (2018). District heating pipes - Preinsulated bonded pipe systems for directly buried hot water networks - Pipe assembly of steel service pipe, polyurethane thermal insulation and outer casing of polyethylene. European CEN, Brussels.
[9] EN 13941-1 (2018). District heating pipes – Design and installation of thermal insulated bonded single and twin pipe systems for directly buried hot water networks: Part 1: Design. European CEN, Brussels.
[10] Hay S., Huther H., Langroudi P., Weidlich I., Kropp, I. EnEff: Wärme Entwicklung von neuen und verbesserten Instandhaltungsstrategien für kleine und große Wärmeverteilnetze durch Kombination statistischer Alterungsmodelle mit materialbasierten Nutzungsdauermodellen. Frankfurt am Main: AGFW, 2022, 167. (in German)
[11] AGFW. AGFW Hauptbericht 2020. Frankfurt am Main, AGFW, 2021. (in German)
[12] International Organization for Standardization. ISO 5807:1985. Information processing - Documentation symbols and conventions for data, program and system flowcharts, program network charts and system resources charts. https://www.iso.org/standard/11955.html, 2019 [6th June 2023]
[13] Langroudi P., Weidlich I. Dhc-maintenance, https://github.com/pakdad/dhc-maintenance, 2022 [31st May 2023].
[14] 3S Consult. KANEW 3S®. https://www.3sconsult.de/en/kanew-3s/,2022. [6th June 2023]
[15] Pourbozorgi Langroudi, Pakdad; Weidlich, Ingo; Hay, Stefan (2021): Backward simulation of temperature changes of District Heating networks for enabling loading history in predictive maintenance. In: Energy Reports 7, S. 119–127. DOI: 10.1016/j.egyr.2021.09.031.
[16] Murakami, Y. (Ed.) (1992): The rainflow method in fatigue. The Tatsuo Endo memorial volume : the papers presented at the International Symposium on Fatigue Damage Measurement and Evaluation Under Complex Loadings in memory of Prof. Tatsuo Endo, the inventor of the rainbow method, Fukuoka, Japan, July 25-26, 1991, supported by ONO SOKKI Co. Ltd. International Symposium on Fatigue Damage Measurement and Evaluation under Complex Loadings. Oxford, England: Butterworth-Heinemann. Available online at https://permalink.obvsg.at/.
[17] EN 13941-1 (2021): District heating pipes – Design and installation of thermal insulated bonded single and twin pipe systems for directly buried hot water networks: Part 1: Design. European CEN, Brussels.

RESEARCH AND APPLICATION OF NEW TECHNOLOGY FOR DUCTILE IRON THERMAL PIPES

Yifeng Ma[a], Junqiang Xu[b], Xiao Dong[c], Yan Li [a*], Xingqiao Jia[a], Peiyuan Mi[a]

[a] *Hebei Province Low-Carbon and Clean Building Heating Technology Innovation Center, Yanshan University, Qinhuangdao, 066004, China*

[b] *CHINA ELECTRIC INTERCONTINENTAL ENVIRONMENTAL PROTECTION TECHNOLOGY CO.,LTD, Handan, 056000, China*

[c] *XINXING DUCTILE IRON PIPES CO.,LTD, Wuan, 056300, China*

[*] *Corresponding author. 35476149@qq.com*

ABSTRACT

In the context of the carbon peak and carbon neutrality, urban district heating has been developing rapidly. Currently, the widely used welded steel heating pipes was generally suffering rapid corrosion rate of conveying pipes, low installation efficiency of manual welding, and poor axial adaptability of rigid joints. In that case, the author's research team has completed theoretical analysis, model establishment and laboratory research, and then proposed a new pattern of ductile iron thermal pipes with flexible joint: 1) Ductile iron materials had strong corrosion resistance, which could extend the service life of working pipes to 50 years. 2) The flexible interface had a high sealing guarantee rate, and the sealing ring had the same service life as the working pipe under thermal operating conditions. 3) The overall mechanical stability of the pipeline was high, and flexible socket connections could naturally compensate for axial thermal elongation, which could effectively reduce the probability of pipeline mechanical failure. In view of the urgent need to improve the economy of heat transmission in long-distance heat supply pipelines, this paper proposed to paint high adhesion Aluminate cement inorganic drag reduction coating on the inner wall of the pipeline based on the new pipeline model, which could reduce the specific friction resistance of the pipeline by 35%. Taking the DN1600 long-distance heat supply pipeline in Laiwu District as an example, the economy of welded steel heating pipes and the new pattern of ductile iron thermal pipes with resistance reducing and anti-corrosion coating was compared and analyzed. The results showed that the unit heat transfer cost throughout the entire life cycle of the new pattern could be reduced by 28.5%, which had excellent economic performance.

Keywords: district heating, ductile iron thermal pipes, improve service life, ensure security, improve economy

1. Introduction

The carbon emissions from winter building heating in northern China were enormous.As of the end of 2020, the total heating area in the northern region has reached 21.8 billion square meters, and annual heating energy consumption was equivalent to 369 million tons of standard coal[1]. With the proposal of "carbon neutrality and the carbon peaking", the heating structure was facing major changes, and cogeneration and other low-carbon clean heat sources would have huge development space to achieve long-distance centralized heating[2]. As a key link in heat transportation, the scale of heating pipelines was increasing rapidly. Currently, the maximum specifications of pipelines have developed to DN1400 or even DN1600, and the maximum length has reached over 40 kilometers. However, the slow progress of pipeline technology has hindered the further development of centralized heating.With the increase of pipeline scale, the total investment cost of comprehensive pipeline materials, civil engineering, and installation engineering was high. The theoretical service life of the steel heating pipeline currently used was only 30 years, and the cost of pipeline investment allocated to the entire life cycle accounts for over 25% of the total heating cost.

1) With the increase of pipeline scale, the total investment cost of comprehensive pipeline materials, civil engineering, and installation engineering was high[3]. The theoretical service life of the steel heating pipes currently used was only 30 years, and the cost of pipeline investment allocated to the entire life cycle accounted for over 25% of the total heating cost.

2) Due to the distance between low-carbon clean heat sources (such as large thermal power plants) and urban heat load centers, the power consumption of circulating water pumps was high during long-distance heat transmission, resulting in a significant increase in heating energy costs.

3) Owing to unfavorable control of dissolved oxygen concentration during the heating period and neglect of maintenance during non-heating periods, severe corrosion occurred on the inner wall of the heating pipeline, leading to an

accelerated thinning rate of the pipeline and further shortening its service life. At the same time, the accumulation of corrosion products has led to an increasing resistance to pipeline operation year by year[4,5].

Therefore, improving the economy and safety of heating pipelines has become one of the important tasks for achieving low-carbon and clean heating in northern China.

2. Problems existing in the mode of prefabricated thermal insulation steel heat pipe

At present, the commonly used mode of directly buried prefabricated insulated steel heating pipelines in China was shown in Figure 1: The working pipe was made of Q235B, 10# or 20# steel and other carbon steel materials, the insulation layer was made of rigid polyurethane foam plastic materials, the outer protective pipe was made of high-density polyethylene materials, and the interface mode was manual welding of the working pipe, and the outer protective pipe was made of hot-melt patching process.After 30 years of comprehensive promotion and use, it was found that this pipeline model has certain limitations.

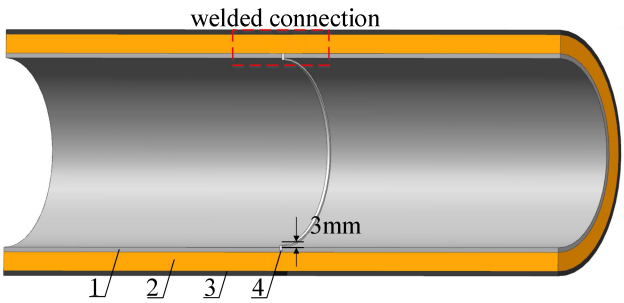

1-steel working pipe, 2-insulation layer, 3-outer protective pipe, 4-weld bead remaining-height

Figure 1. Structure of prefabricated insulated steel heating pipes

1) Poor corrosion resistance of carbon steel working pipes under operating conditions of thermal pipelines：Due to unfavorable control of dissolved oxygen concentration during the heating period and neglect of maintenance with water during non-heating periods, significant electrochemical corrosion has occurred on the inner wall of the pipeline. On the one hand, accelerating the thinning rate of the pipe wall greatly shortened the actual service life of the working pipe, making it difficult to achieve a theoretical lifespan of 30 years. On the other hand, it caused the accumulation of corrosion products on the inner wall, and the roughness of the pipeline increases year by year, significantly increasing the pipeline resistance and water pump power consumption throughout the entire life cycle.

2) Significant shortcomings in the efficiency and quality of manual welding processes: The welding process of thermal pipelines required a large amount of labor, and the construction speed and efficiency were at a low level, resulting in high construction costs. Besides, the quality of the welding process was also constrained by construction conditions such as labor quality and weather conditions. In addition, during the manual welding process, a weld reinforcement of about 3mm would be generated, which would increase the resistance of the pipeline and power consumption of the water pump to a certain extent.With the large-scale construction of heating networks, this excessive reliance on manual installation methods has become a bottleneck that restricts the efficiency and quality improvement of pipeline construction.

3) The rigid interface formed by welding lacks axial adaptability: The working temperature difference of thermal pipelines was large, and the primary network water supply pipeline would be 100 ℃ or even higher than the normal temperature during severe cold periods. For welded steel thermal pipelines, compensators or curved pipe sections were usually used to compensate for the axial thermal elongation caused by temperature rise. In that case, the initial investment of the pipeline and the local resistance of the pipeline were both increased.

Therefore, the prefabricated insulation steel heating pipeline model has shown drawbacks in ensuring service life, improving installation efficiency and improving economy.

3. A new model of prefabricated insulated ductile iron heating pipeline

In 2018, the author's research team first proposed a new model of ductile iron thermal pipelines using flexible socket connections[6], as shown in Figure 2.

1) The working pipe was manufactured using the centrifugal casting process of ductile iron, the outer surface coated with a metal zinc coating, and the inner surface polished or coated with a drag reducing and anti-corrosion coating.

2) The outer protective pipe was made of high-density polyethylene material, and the thermal insulation layer was made of rigid polyurethane foam plastic material. The straight or allotype thermal insulation structure process could be selected according to the engineering requirements.

3) The work pipe adopted flexible socket connection, the interface insulation adopted the non-hot melt patching process, and the gasket adopted the modified rubber material that is resistant to high temperature and aging.

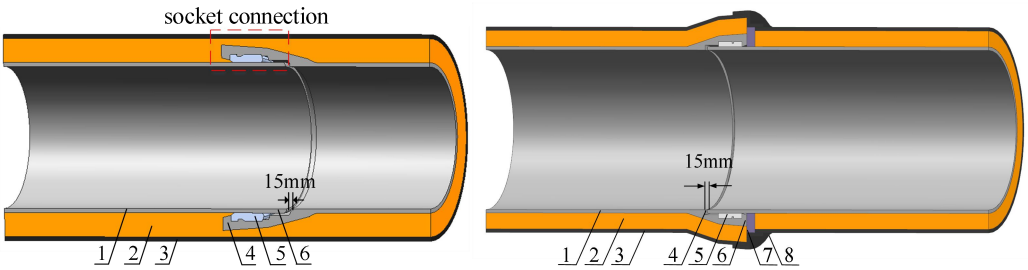

1-ductile iron working pipe, 2-insulation layer, 3-outer protective pipe, 4-socket, 5-gasket
6-spigot, 7-rubber plastic expansion pad, 8-heat shrinkable polyethylene sleeve
(a) flat thermal insulation structure (b) allotype thermal insulation structure

Figure 2. Structure of prefabricated insulated ductile iron thermal pipes

4. Advantages of prefabricated insulated ductile iron thermal pipes

4.1 Strong corrosion resistance of work pipes

In the new pipeline mode, the corrosion resistance of the working pipe was a pivotal parameter that affects the overall service life and operating resistance of the pipeline.By using weight loss method and electrochemical test method, the basic corrosion laws and mechanisms of ductile iron hanging pieces and Q235B carbon steel hanging pieces under different hot water temperature conditions were tested[7], as shown in Figure 3, and an analysis model for the corrosion rate of pipeline inner walls was established[8].Through mutual verification of experimental data and analytical models, the corrosion rate changes of ductile iron pipes and steel pipes were determined, as shown in Figure 4.

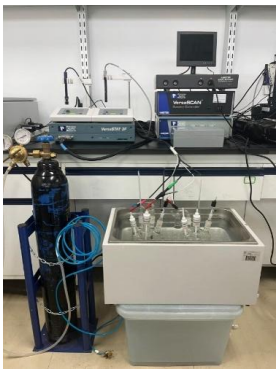

(a) electrochemical tester

(b) ductile iron sample

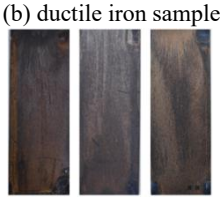

(c) Q235B steel sample

Figure 3. Corrosion rate of pipeline inner wall changed with temperature

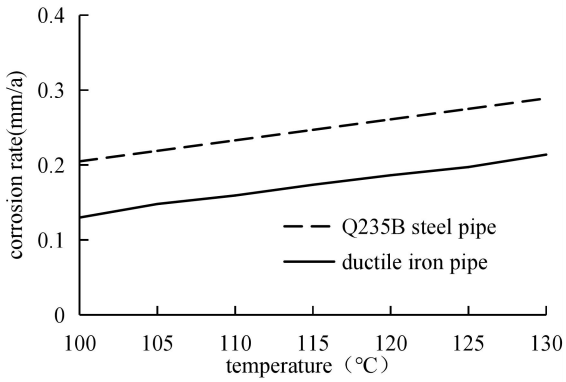

Figure 4. Corrosion rate of pipeline inner wall changed with temperature

The inner wall corrosion rate of carbon steel pipes and ductile iron pipes was positively correlated with temperature, mainly because increasing temperature changed ion activity, thereby accelerating the inner wall corrosion rate of pipelines.The corrosion resistance of ductile iron pipes under operating conditions of thermal pipelines has significantly improved, only 70% of that of carbon steel pipes. Therefore, it could slow down the corrosion of the inner and outer walls, effectively reduced the thinning rate of the pipe wall, and extended the service life of the pipeline to 50 years. In addition, it could also reduce the annual increase rate of inner wall roughness, further reducing the resistance of pipeline operation throughout its entire life cycle.

4.2 High sealing guarantee rate of socket joint

The sealing performance of socket joints was a pivotal parameter affecting the safety of pipeline operation.As the internal pressure of the pipeline increased, the contact pressure between the socket type interface sealing ring and the warehouse wall gradually increased, and the interface sealing performance became stronger, which could satisfy the pressure bearing technical requirements of 2.5MPa for thermal pipelines.

The service life of gasket was also a focus of research. Based on the Arrhenius life prediction theory, this paper conducted accelerated aging experiments on modified special rubber under thermal operating conditions[9,10]. Firstly, the changes in permanent compression deformation of the gasket with time under different hot water temperature conditions (90℃~130℃) were detected, as shown in Figure 5.Furthermore, based on the Arrhenius curve, the continuous service life of the sealing ring in 130℃ hot water environment was estimated to 33 years, as shown in Figure 6. Besides, the expected

service life would reach 50 years under heating conditions.

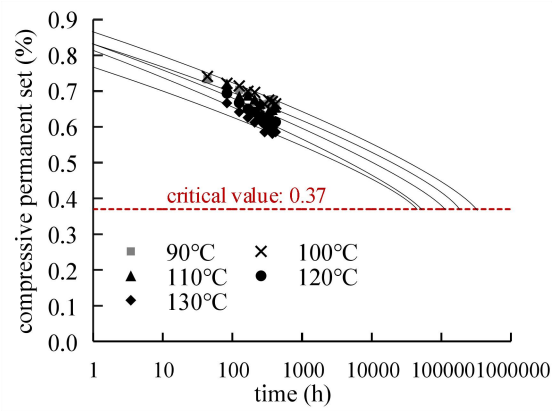

Figure 5. Relationship between permanent compression deformation rate and aging time at different temperatures

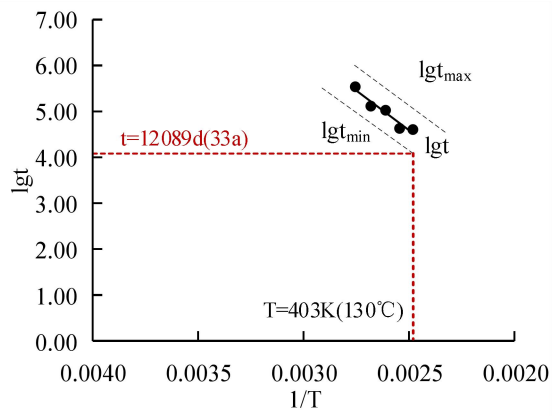

Figure 6. Arrhenius curve

4.3 Excellent mechanical stability of pipelines

At the joint of ductile iron pipes, the installation gap of 10-15mm between the socket and the spigot was sufficient to absorb the axial thermal elongation with a temperature difference of 120 ℃, which greatly reducing the secondary stress generated by temperature changes. In addition, the socket joint had a deflection capacity of 1.5 °~3.5 °, which could adapt to a certain degree of foundation settlement[11].

In order to accurately evaluate the mechanical stability characteristics of nodular cast iron thermal pipes, this paper established a mechanical failure model of thermal pipes[12,13], and adopted the Monte Carlo method to solve the failure probability of pipes. Taking DN700 pipeline as an example, the impact of corrosion occurrence and temperature changed on the probability of pipeline mechanical failure was analyzed, as shown in Figure 7 and Figure 8(SP is the abbreviation of steel pipes, DIP is the abbreviation of ductile iron pipes).

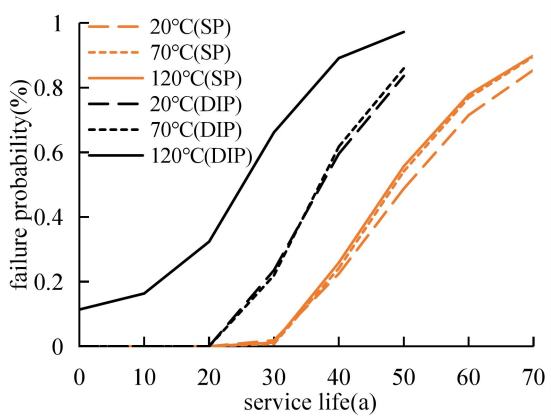

Figure 7. Mechanical failure probability of thermal pipelines at different temperatures

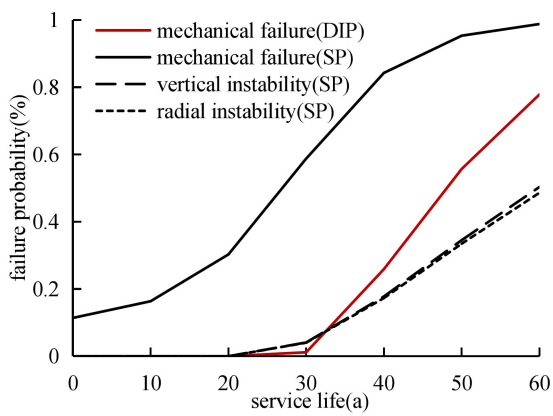

Figure 8. The Influence of corrosion on the mechanical failure probability of Thermal Pipeline

1) With the increase of hot water temperature, the mechanical failure probability of ductile iron thermal pipelines and steel thermal pipelines increased. Due to the stronger adaptability of ductile iron pipeline socket joints to axial thermal elongation and radial thermal expansion, the negative impact of temperature changed on pipeline stability would be largely eliminated. Therefore, the mechanical failure probability of ductile iron thermal pipelines was always lower than that of steel thermal pipelines under different hot water temperatures.

2) The probability of mechanical failure of ductile iron thermal pipelines and steel thermal pipelines under corrosion was increasing year by year. After 20 years of use, steel heating pipelines would gradually experience problems such as vertical instability and radial instability. However, ductile iron had better corrosion resistance, which could better cope with the thinning of pipeline wall thickness and stress decline, and could reduce or even eliminate the negative impact of pipeline wall corrosion on pipeline stability. Therefore, the probability of mechanical failure in ductile iron thermal pipelines due to corrosion was much lower than that in steel thermal pipelines.

5. Optimization design of drag reducing and anti-corrosion coating

Long distance heating pipelines had long and large flow rates, resulting in high operational resistance for heat transfer

and high-power consumption of circulating water pumps.In addition, due to corrosion on the inner wall of the pipeline, the roughness of the inner wall of the pipeline was increasing year by year, further increasing the operational resistance of the pipeline and the power consumption of the circulating water pump.The author's team proposed a method of spraying drag reducing and anti-corrosion coating on the inner wall of prefabricated insulated ductile iron pipes.

The drag reducing and anti-corrosion coating was made of Aluminate cement mortar inorganic material, which had good resistance to high temperature, bending and corrosion, and could have a high adaptability to the axial and radial deformation of the pipeline when the temperature of the thermal pipeline changed.This paper established a mathematical model for thermal pipeline analysis, analyzed and compared the resistance characteristics of ductile iron pipelines with drag reducing and anti-corrosion coating and bare pipe wall schemes under DN1200, DN1400, and DN1600 pipeline specifications, as well as steel pipelines with bare pipe schemes. The results were shown in Table 1.

Table 1. Comparison of specific frictional resistance of different heating pipeline

Diameter	Ductile iron pipelines with drag reducing and anti-corrosion coating Specific frictional resistance(Pa/m)	Ductile iron pipelines with bare pipe Specific frictional resistance(Pa/m)	Steel pipelines with bare pipe Specific frictional resistance(Pa/m)
DN1200	135.37	176.58	268.84
DN1400	71.32	79.50	118.56
DN1600	37.15	39.59	57.18

Compared to bare walled steel pipelines, the resistance reduction of DN1200, DN1400, and DN1600 bare walled ductile iron pipelines was 34.3%, 32.9%, and 30.8%, respectively.After applying drag reducing and anti-corrosion coating on ductile iron pipelines, the pipeline resistance further decreased by 23.3%, 10.3%, and 6.2%.Therefore, anti-corrosion and drag reducing coatings could effectively reduce the roughness of the inner wall of the pipeline, thereby reducing the resistance along the pipeline and the power consumption of the circulating water pump throughout the entire operating cycle.

6. Economic analysis of prefabricated insulated ductile iron heating pipes

Taking the long-distance heating project from Laiwu Industrial Zone to Jinan City as an example, the pipeline system was designed with a length of 78 kilometers and a pipeline specification of 2 × DN1600, and the heat source heating capacity 3276MW. Paper compared and analyzed the economic performance of steel thermal pipelines (Scheme 1) and ductile iron thermal pipelines coated with anti-corrosion and drag reducing internal coatings (Scheme 2).

6.1 Analysis of investment costs for pipeline construction

The investment cost for pipeline construction included the cost of working pipes, insulation and external protection pipes, drag reduction and anti-corrosion coating costs, pipeline installation costs, and civil engineering costs. This paper calculated the construction investment costs for both schemes, as shown in Figure 9.

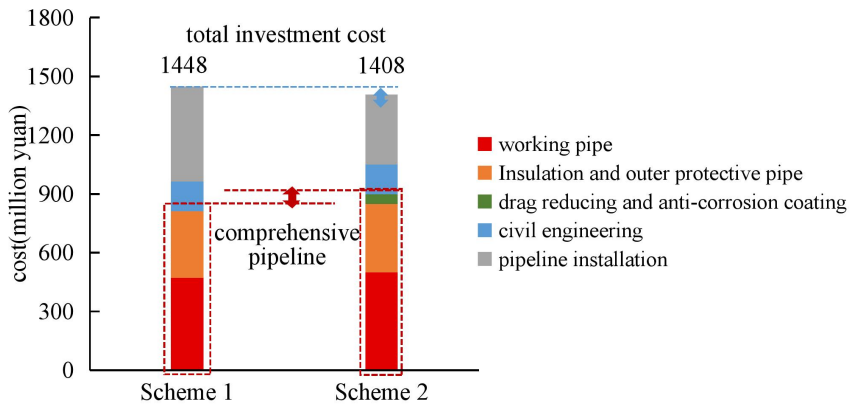

Figure 9. Composition of construction investment costs for Scheme 1 and Scheme 2

Compared with steel heating pipelines, the investment cost of ductile iron heating pipeline pipes is 10.7% higher, mainly due to the increase in pipeline investment cost caused by internal coating of drag reducing and anti-corrosion coatings.Compared with Scheme 1, the Scheme 2 had a 10.7% higher investment cost in pipe materials, mainly due to the increase in pipeline investment cost caused by the internal coating of ductile iron pipes with drag reducing and anti-corrosion coatings. The installation cost was 26.3% lower, mainly due to the fact that the socket connection method increases the speed by 5-10 times compared to the welding method, greatly improving the efficiency and quality of pipeline installation, and thereby reducing pipeline installation costs. The total investment cost for pipeline construction was equivalent to that of steel thermal pipelines.

6.2 Analysis of annual cost for pipeline operation

The annual cost of pipeline operation included heat dissipation loss cost, water pump power consumption cost, water replenishment cost, and maintenance cost. This paper calculated the annual operating costs of the two schemes separately, as shown in Figure 10.

Compared with Scheme 1, the operating cost of the Scheme 2 decreased by 34.5%, mainly due to the effective reduction of pipeline specific friction and the reduction of water pump power consumption cost through drag reduction and anti-corrosion coating. In addition, the ductile iron thermal pipelines did not require the installation of compensators or natural compensation, which could effectively reduce local resistance and further reduce operating costs.

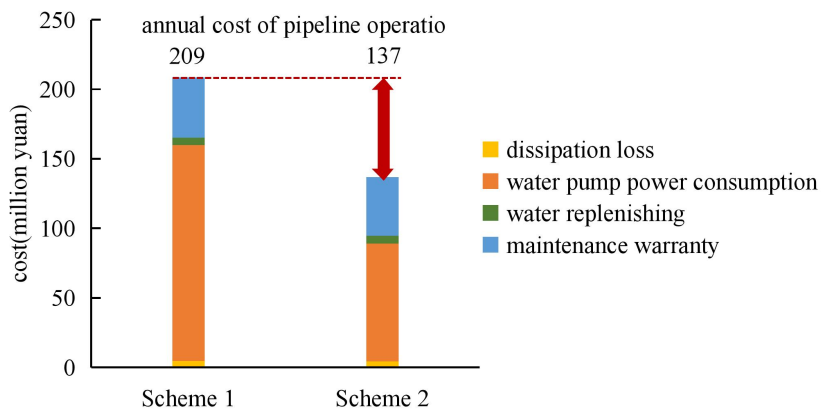

Figure 10. Composition of annual cost of pipeline operation for Scheme 1 and Scheme 2

6.3 Analysis of unit heat transfer cost throughout the entire life cycle

The unit heat transfer cost throughout the entire life cycle was composed of the cost of unit heat construction investment allocation and the operating cost of unit heat supply, as shown in Equation 1.

$$c = c_j + c_y = \frac{C_j}{nQ} + \frac{C_y}{Q} \tag{1}$$

where c is unit heat transfer cost throughout the entire life cycle, yuan/GJ. c_j is cost sharing of unit heat construction investment, yuan/GJ. c_y is investment cost for pipeline construction, yuan. C_y is annual cost of pipeline operation, yuan/a. n is service life of the pipeline, a. Q is system heating capacity, GJ/a.

This paper calculated the full life cycle unit heat transfer cost of two schemes, as shown in Table 2. Compared to Scheme 1, the unit heat transfer cost throughout the entire life cycle of the Scheme 2 was 7.46 yuan/GJ, with a decrease of approximately 28.5%. Due to the fact that the service life of ductile iron heating pipelines could reach 50 years, which could significantly reduce the cost of construction investment per unit of heat, and at the same time, the operating resistance of pipelines could be significantly reduced, which could reduce the operating cost per unit of heat supply. Therefore, using a ductile iron heating pipeline model coated with anti-corrosion and drag reducing lining could significantly improve the economy of long-distance heating pipelines.

Table 2. Comparison of unit heat transfer cost throughout the entire life cycle

Evaluating indicator	Scheme 1	Scheme 2
c_j（yuan/GJ）	1.96	1.14
c_y（yuan/GJ）	8.48	5.56
c（yuan/GJ）	10.44	7.46

7. CONCLUSION

To improve the economy and safety of thermal pipelines, this paper proposed a new model of ductile iron thermal pipelines with flexible socket joint, which had significant advantages compared to steel thermal pipelines.

1) Excellent corrosion resistance, the corrosion resistance of ductile iron pipes was three times that of carbon steel pipes. In this case, the service life of the pipeline could be extended to 50 years, while the problem of increased inner wall roughness caused by the accumulation of corrosion products could be alleviated and the operating resistance of the entire life cycle of the pipeline could be reduced.

2) Reliable flexible socket joint, and the gasket made of modified rubber material had a continuous service life of up to 33 years, which could have the same lifespan as the pipeline under heating conditions. In addition, the socket connection

method could significantly improve the efficiency and quality of pipeline installation, and reduced the cost of pipeline engineering.

3) Remarkable mechanical stability, the probability of stress failure due to corrosion and temperature changes of ductile iron thermal pipelines was much lower than steel thermal pipelines.

4) Lower specific friction of pipelines, the use of drag reducing and anti-corrosion coating on ductile iron thermal pipelines could reduce the specific friction of pipelines by more than 35%, which had great significance for reducing pipeline resistance and operating costs.

5) Favorable economic performance, the total investment cost for the construction of ductile iron pipelines was similar to that of steel pipelines. Due to the improvement of pipeline life and the application of anti-corrosion coatings, the unit heat transfer cost throughout the entire life cycle could be reduced by 28.5%.

ACKNOWLEDGEMENT

The authors would like to acknowledge for the financial support from Hebei Province Key Research and Development Project (20374505D) to the research work.

REFERENCES

[1] Clean Heating Industry Committee(CHIC). Report on the Development of Chinese Clean Heating Industry(2020). 2020.
[2] Yan Li, Weqin Wang, Yifeng Ma, et al. Study of New Cascade Heating System With Multi-Heat Sources Based On Exhausted Steam Waste Heat Utilization In Power Plant. Applied Thermal Engineering, 2018, 136: 475-483.
[3] Yongpeng Yan, Huai Wang, Huizhong Zhao. Discussion on the installation method of large diameter long-distance heating pipelines. District Heating, 2020(05): 87-93.
[4] Shoujun Zhou, Zheng O'Neill, Charles O'Neill. A Review of Leakage Detection Methods for District Heating Networks. Applied Thermal Engineering, 2018, 137: 567-574.
[5] Min-sung Hong, Yoon-Sik So, Jeong-Min Lim, et al. Evaluation of Internal Corrosion Property in District Heating Pipeline Using Fracture Mechanics And Electrochemical Acceleration Kinetics-Sciencedirect. Journal of Industrial and Engineering Chemistry, 2020.
[6] He Qishu, Wei Xitao, Zhao Zhicheng, et al. Discussion on Feasibility of Application of Ductile Iron Pipe in District Heating System. Building Science, 2022,38(02): 125-130+137.
[7] Mcneil L S, Edwards M. The Importance of Temperature in Assessing Iron Pipe Corriosion in Water Distribution System. Environmental Monitoring & Assessment, 2002, 77(3): 229-242.
[8] Zhijian Tang, Seungkwan Hong, Weizhong Xiao, et al. Characteristics of Iron Corrosion Scales Established Under Blending of Ground, Surface, and Saline Waters and Their Impacts on Iron Release in the Pipe Distribution System. Corrosion Science, 2006a, 48: 322-342.
[9] Junfeng Duan, Yang Han, Chenxi Xue,et al. Experimental Research on Bending of Flexible Interface of Ductile Iron Pipeline Rubber Ring. Water & Wastewater Engineering, 2016, 52(03): 103-106.
[10] Wang Jun. Study on Thermal-oxidative Aging and Life Assessment of Rubber Sealing Material. Harbin Institute of Technology. 2011.
[11] Kenneth T. Gillen, Mathew Celina, Robert Bernstein. Validation of improved methods for predicting long-term elastomeric seal lifetimes from compression stress-relaxation and oxygen consumption techniques. Polym. Degrad. Stab, 2003, 82: 25-35.
[12] Linlin Lu, Wei Liang, Laibin Zhang, et al. A Comprehensive Risk Evaluation Method for Natural Gas Pipelines by Combining a Risk Matrix with a Bow-tie Model. Journal of Natural Gas Science and Engineering, 2015, 25: 124-133.
[13] Oleg Shabarchin, Solomon Tesfamariam. Risk Assessment of Oil and Gas Pipelines With consideration of Induced Seismicity and Internal Corrosion. Journal of Loss Prevention in the Process Industries, 2017, 47: 85-94.

The 18th International Symposium on District Heating and Cooling, September 3–6, 2023, Beijing, China

STATUS ASSESSMENT, AGEING, LIFETIME PREDICTION AND ASSET MANAGEMENT OF DISTRICT HEATING PIPES

Hay S.[a]*, Yarahmadi N.[b], Sällström J. H.[b], Jakubowicz I.[b], Vega A.[b], Langroudi P.[c], Kropp, I.[d], Leuteritz A.[e], Below H.[f], Cadenbach A.[g]

[a] *AGFW | Der Energieeffizienzverband für Wärme, Kälte und KWK e.V., Frankfurt, 60596, Germany*
[b] *RISE Research Institutes of Sweden, Gothenburg, 41279, Sweden*
[c] *HafenCity University Hamburg, Hamburg, 20457, Germany*
[d] *3S Consult GmbH, Dresden, 01309, Germany*
[e] *Leibniz-Institut für Polymerforschung Dresden e.V., Dresden, 01069, Germany*
[f] *IMA Materialforschung und Anwendungstechnik GmbH, Dresden, 01099, Germany*
[g] *Fraunhofer-Institut für Energiewirtschaft und Energiesystemtechnik IEE, Kassel, 34117, Germany*
[*] *Corresponding author. s.hay@agfw.de*

ABSTRACT

Today District Heating (DH) utilities have to work on status assessments and lifetime predictions while many pipes in the DH systems are close to the expected service lifetime according to the design criteria. Consequently, they have to think about suitable maintenance strategies. Additionally, they must also work on the transformation of their DH systems towards the increased use of renewable energy sources.

Because the ageing of DH pipes consists of several different processes the results of available lifetime prediction models show a large variation, so that reliable predictions require many researchers working on this topic. Therefore, researchers started an international research collaboration platform under the supervision of IEA DHC, where the experience of international researchers and research results from national research projects are being compiled and consolidated. The overall goals of the annex task shared 6 “Status assessment, ageing, lifetime prediction and asset management of district heating pipes” are to improve existing methodology of accelerated ageing, lifetime prediction, status assessment and asset management of district heating pipeline systems to provide district heating companies with valuable knowledge on how to treat their pipe network optimally. Besides the tasks to improve the knowledge of ageing processes and lifetime prediction, there is a need to revise the current standards to gain more realistic results. Asset management tools based on this enable utilities to develop targeted strategies for decarbonizing district heating systems in addition to predictive maintenance. The TS 6 project as well as the scientific approach are presented in this contribution.

Keywords: **District Heating pipes; ageing; asset management.**

1. INTRODUCTION

In the planning of heating networks, the pipe systems are designed in accordance with the relevant standards, depending on the stresses acting on them. The material properties of the pipelines of a heating network deteriorate over time due to ageing processes taking place during service. To ensure the security of supply in district heating systems, asset management simulations are used to develop suitable maintenance strategies based on statistical ageing models. Besides that, material based ageing models are used to predict the service life of DH pipes based on acting loads in situ. These material ageing models are described in the relevant standards for each type of pipe. Regarding pre-insulated bonded pipes status assessment, accelerated ageing and lifetime predictions of buried pipes are described in EN 253 [1], EN 448[2] and EN 13941 [3]. The findings of Swedish and German research have led to the complete deletion of the previous relation of lifetime at operative temperature and time of accelerated ageing tests of DH pipes in the European Standard [1]. A verified replacement of this testing method is currently not available.

A reliable asset management simulation of DH networks is a strong tool to meet the requirements of high security of supply. When the average age of existing DH networks is increasing, the asset management is becoming more important to ensure the security of supply. Besides that, as described in Reference [4] on the example of a case study in Germany, the remaining service life of DH pipes is important to develop a suitable transformation strategy to fulfil the climate goals in existing DH systems. To improve the existing methods and models for asset management of DH pipes, further investigations in status assessment and ageing mechanisms of DH pipes are needed. Based on the results of these investigations, models for lifetime predictions must be improved as well as to be evaluated through further testing in the field. The future perspective of the

DH system and the piping technologies used, need to be considered for managing the assets from a system-oriented point of view. The TS 6 project is collecting relevant findings and results from researchers to address the described approach. The overall goal of the project is to identify holistic and innovative approaches to improve ageing methodology and calculations for lifetime predictions of DH pipes. To manage the requirements on the pathway to improve the security, economic and sustainability of DH systems the findings of the TS 6 project needs to be migrated in the relevant standards, so that DH operators can use them. project needs to be migrated in the relevant standards, so that DH operators can use them.

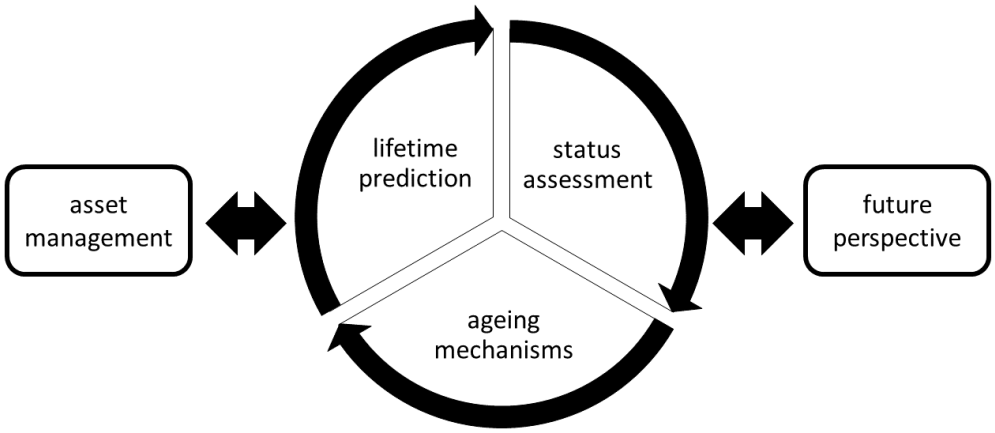

Figure 1. Approach of the TS 6 project to improve asset management in DH based on the needs of DH operators, source: AGFW.

Based on the approach described, the TS 6 project is divided into five work packages. The different work packages as well as the current results are presented in the following paragraphs.

2. STATUS ASSESSMENT OF DH PIPES - SUBTASK A

The status of a DH-pipeline depends on the local load spectrum and the involved material of the system. This includes the pipe materials and the bedding situation in the trench (e.g., presence of groundwater). The overall objectives of Subtask A are to improve the knowledge concerning the status of DH networks in participating countries, status assessment methods and failure modes of DH networks.

To achieve these goals, there is a need to investigate which types of pipe failures occur in the district heating networks and their frequency. Therefore, network owners have to improve their existing data set and statistics. Failure registers should include a categorization of the failures related to reason of the failure installation, operation, design, or site conditions. Besides that, it is recommended to identify the causes behind the failures and if they are age related.

Identified available technologies for status assessment based on different approaches to evaluate status of the pipes are summarized as follows:

- Surveillance system for leakage detection: Measuring the electrical conductivity between alarm wires and service pipes indicating water leakage by increased conductivity due to humidity in the DH pipe.
- Thermographic check: By airplanes or drones, to show under defined weather conditions the increase of heat losses of existing DH pipes. An increased heat conductivity is used to make ageing processes visible.
- Visual inspection: Visual condition assessment by experts in freely accessible pipelines as well as camera inspections in non-accessible district heating culvert systems
- Material testing in the lab: Test removed pieces of buried pipes from the field to the lab according to [1], chemical and physic-chemical test methods (thermogravimetry, infra-red spectroscopy, Raman spectroscopy, dynamic mechanical analysis, etc.)
- Investigation and evaluation of the status for the pipe in the field: using the Pipeopsy method (use the RISE (SP) Plug Method in the field, examine the plug in the laboratory and restore of the pipe) [5] or on-site testing of axial shear strength with mobile test rig [6].

- Evaluation of measurement data: Analysis of operational as well as conditional data of the pipes via measurement equipment using simulation models and material ageing models (e. g., fatigue analysis according to [3]).

Figure 2 shows three different ways of determining the actual adhesion strength of a pipe by measuring of shear strength. From the left to the right image in Figure 2, the amount of interference on the pipe decreases as the specimen is removed. Similarly, the cost of removing the specimen decreases. In Subtask A of the TS 6 project, it is planned to present scientific results and practical experience of the different methods for condition assessment in a comparative manner.

Figure 2. Different methods to measure the adhesion between steel pipe, PUR and PE-casing: In the laboratory (left picture, source FFI Hannover) and the field (middle, source: IMA Dresden) and (right picture, source: RISE)

3. AGEING OF DH PIPES - SUBTASK B

The ageing of a DH pipeline depends on the pipe system and the materials themselves, the operational load spectrum, and the local boundary conditions. The scope of the project includes pre-insulated pipes, concrete duct DH systems and alternative pipe materials. Ageing processes of the materials used based on single ageing mechanisms are well known. For example, if steel is used as the service pipe material, corrosion is a mechanism that affects the service life. Besides that, damage accumulations in the area of low cycles fatigue are used to estimate the ageing of the service pipe based on thermal stresses [3]. Until the amendment of EN 253 in 2018, the axial shear strength due to artificial or operational thermal ageing was an essential criterion for ensuring the quality, describing the actual status and predicting the remaining service life of pre-insulated DH pipes. Evidence that the change in axial strength occurs in three phases - thermal ageing, plateau, thermo-oxidative ageing - has led to the deletion of the Continuous Operating Temperature Test in EN 253. For the degradation of the PUR foam thermal ageing and thermal oxidative ageing are well known [7, 8, 9, 10, 12].

As different ageing mechanisms (e.g., chemical, thermal, mechanical) sometimes occur simultaneously in different materials (e.g., steel, PUR foam and PE coating) as a result of operational stresses on the pipelines, the results of tests of the actual condition and service life predictions with simulation models can differ. Therefore, the overall objective of Subtask B is to improve knowledge on ageing processes taking place in real applications under operational load conditions. Here, the main question is, when are pipes obsolete? Besides that, the crucial and dominated ageing mechanisms especially for each material in pipe design and generally for status assessment and life-time prediction of DH pipe needs to be elucidated. Another important topic is to define reliable accelerated ageing test methods for different materials and pipes systems considering elevated temperature and mechanical load, etc. Especially for the PUR-foam of pre-insulated DH pipes, there are current findings gained in national research projects available that needs to be discussed and harmonized in the TS 6 project [6, 7, 8, 9, 10, 13, 14].

4. LIFETIME PREDICTION MODELS - SUBTASK C

Prediction of service life for materials expected to perform reliably for many decades, is a challenge. Lifetime prediction of a district heating system has to consider different time dependent phenomena. The deterioration of individual properties can mostly be explained, but this does not describe the performance of the design. A wide range of mechanisms for the degradation of polymer-based materials, metals and concrete includes thermal degradation, mechanical degradation, oxidation, chemical attack, creep, and fatigue. Some of them are already considered in the design process of the DH pipes, f. e. the fatigue of the steel pipe caused by temperature changes of the DH system [3].

To allow extrapolation of short-time data to predict long-term performance, an appropriate mathematical model must be applied through which the short-term values obtained at elevated temperatures and/or higher stresses can be recalculated to conditions in service. Methodologies that make a combined approach possible are needed. Considering the diverse range of piping systems utilized in DH networks, including post-insulated steel pipes in concrete ducts and buried pre-insulated bonded pipes, it is essential to examine each system individually when making predictions regarding their lifespan.

Pre-insulated bonded pipes are nowadays the most used system of piping in DH systems and the most used model to predict lifetime of a product is the so-called Arrhenius approach which is based on assumption that an overall degradation process has a rate of deterioration proportional to $\exp(-E_a/RT)$ where E_a is the activation energy, R is the gas constant and T is the absolute temperature. Data is produced under accelerated aging conditions to estimate the value of E_a. This value of E_a is then assumed to be constant in the entire temperature range below the level of accelerated temperature, allowing extrapolation to predict lifetime at a lower service temperature.

There are two crucial requirements for a relevant accelerated ageing test:

1. degradation processes are speeded up without being changed.
2. all factors which might contribute to degradation in the intended end-use environment are considered in the ageing test.

In a previous investigation degradation of DH pipes at different temperatures (130 – 170 °C) were studied. The outcome of the study was that results from accelerated aging at temperatures ≥150 °C follow a different trend than from temperatures below 150 °C [9]. The key conclusion was that one degradation process is dominant over a temperature regime ≥150 °C and another one is dominant below 150 °C. Consequently, accelerated tests at temperatures ≥150 °C cannot be used for the prediction of lifetime at service temperatures because they do not follow the Arrhenius relationship. However, through optimization techniques, the networks are able to maintain a temperature equivalent to a constant value that remains below 90°C [19]. During operating conditions, DH pipes undergo significant temperature variations due to variations in customer demands, soil-pipe interaction, and weather conditions. The temperature fluctuations lead to expansion and contraction of the steel service pipe, which give rise to alternating axial shear stress due to the restrain of the pipe by the surrounding soil. Because a relevant accelerated ageing test must include all factors which might affect the rate of degradation, significance of a repetitive axial shear stress on the rate of thermal degradation of DH pipes were investigated. The main conclusion from this study was that the mechanically stressed pipes degrade significantly more rapidly than non-loaded pipes aged at the same temperature [18]. Other research results show that the mechanical load has a minor influence on the ageing behaviour of PUR foam and thus on the service life of the district heating pipes [10, 12]. The exchange and discussion of these previous research results is necessary in order to compare the results of the laboratory tests with the actual loads in the field and the resulting ageing effects.

Furthermore, the FTIR analyses of the aged samples provided a strong indication that the effect of combined mechanical and thermal ageing was not due to fatigue but due to a faster chemical degradation of the PUR foam. These results in total suggest that a combine mechanical and thermal exposure should be adopted in accelerated ageing tests to avoid overestimation of the lifetime of DH pipes and to reproduce better the ageing characteristics of mechanically stressed DH pipes, especially those intended for use in the fourth-generation district heating networks. This in turn means that there is a need to develop another calculation model that considers the effect of both temperature and repetitive axial shear stresses.

For prediction of service life of different materials and components, associated input data and different models are also needed. The overall objective of Subtask C is to elaborate appropriate mathematical models that can allow extrapolation of short-time data to predict long-term performance of DH pipes. To achieve this goal existing as well as improved models for ageing processes must be compiled. Of course, the prediction models must be evaluated by studying the results of simulations and the results of the status assessment of naturally aged pipes.

5. ASSET MANAGEMNT (AM) - SUBTASK D

According to the Institute of Asset Management, there are six areas in an AM framework: Strategy & Planning, Asset Management Decision Making, Lifecycle Delivery, Asset Information, Organization & People, Risk & Review [15].

An asset management strategy combining re-active and proactive views based on the importance or the risk of assets, is recommended. Supply reliability and economic restrictions should be considered as well. In order to improve asset management strategies a better documentation of network operational conditions is needed. If historical operational data is not available new approaches like artificial intelligence can be used to enable load history in asset management [16]. Besides that, there is a need to build up reliable failure statistics that can be used for risk-based inspections methods.

Current software programs support asset strategy simulations considering ageing models and a risk-based assessment of single assets. For getting an improved asset management procedure an intelligent status assessment is necessary. The existing wire technology or an implemented (light-)fibre technology could be used to determine changes arising from ageing processes aside from leakage detection. The intelligent use of such a (already existing) surveillance technology might push the asset management to a much higher level. In any case "big data" statistics also improve the Asset Management. Using hydraulic models will help to assess supply reliability (overall and for each customer) based on condition (status assessment, ageing behavior) and also to improve risk assessment of the system and support decisions about maintenance activities.

As shown in Figure 1, the improvement of asset management is a closed loop approach running status assessment test in the field, improving ageing models as well as accelerated ageing test in the laboratory and the validation of the lifetime prediction models based on improved mathematical models to describe ageing processes in DH pipes. So, the overall objective of Subtask D is to establish an AM framework for the other four subtasks in TS 6 project, enabling effective and sustainable AM decisions in short- and long-term.

The work areas in this subtask cover a comprehensive description of asset management processes/activities and their relationships/interfaces including a state-of-the-art review on data requirements, available technologies/tools, inputs, and outputs. Existing examples from the DH sector should be given, but also experiences from other infrastructure sectors.

Furthermore, a KPI (key performance indicators) system should be established in order to evaluate DH pipe systems related to technical, economic and ecological aspects. The focus should be here on KPIs related to status assessment, ageing and lifetime prediction as well as rehabilitation related indicators.

Since ecological aspects become more and more important, the carbon footprint over the lifetime of DH pipes should be assessed to support rehabilitation and/or re-investment decisions of network operators.

Another important aspect in DH pipe network operation and asset management is the knowledge about current and future supply reliability for various supply scenarios. The influence of decentralized renewable energy sources on network operations should be investigated.

The findings of the other subtasks will improve asset management. New or further developed methodologies will be implemented in the existing asset simulation tool KANEW 3S. A practical demonstration with data from various network operators will show these benefits.

6. FUTURE PERSPECTIVE OF DH PIPES - SUBTASK E

For future heating networks, the reduction of the operating temperatures will determine the developments. Design technology and DH pipe systems will change with new requirements and different load spectra of future DH-systems. New materials, joining methods and backfilling will be used, which lead in combination with different loads to different ageing phenomena, changes in lifetime and the subsequent predictions and asset management.

It can be assumed that the reduction of the operating temperature will have a positive effect on the service life of existing pipelines. Similarly, the changes in operating temperature will have a similar effect on the future pipe materials to be used [17].

How the transformation process of the heating networks to a larger number of decentralized and fluctuating renewable energies will affect the life span of existing pipelines cannot be estimated at present. Further investigations are necessary to avoid endangering existing networks as the backbone of the heat supply and as a component of a successful decarbonization of the district heating systems. The work in subtask E will contribute to these requirements.

Regarding the status assessment, ageing and lifetime prediction, the development of the digitalization of the district heating system is expected to have further positive effects. The availability of real time data will allow an improved and precise life cycle assessment. Currently, the possibilities and the degree of digitalization of future heating networks are difficult to estimate. However, it can be assumed that existing networks without digital elements will continue to be operated and will require greater attention from the perspective of remaining service life estimation. In a more digitalized DH system, the heat and temperature losses along the pipes could be used for status assessment.

The transferability of the gained experience from the 3rd gen DH networks will be one central key point to make future networks more secure, more reliable, and easy to maintain. Therefore, a knowledge transform framework will be advantageous to be planned for future developments.

Another very important but also central point in the context of futures perspectives is circular economy. It is a future research area, and it is important to determinate the quality of different recycled material which has potential to use in DH system.

The subtask E will contribute to this future research area by collecting the available findings as well as to prepare key performance indicators for the implementation in asset management simulation tools.

7. CONCLUDING REMARKS

District heating can contribute to improve the environment. To this end, there is a need to assess the status of the district heating networks, predict service lifetime, and develop methods for asset management of the networks including maintenance. There is also need to have improved product standards for the district heating network components to manufacture optimal components with the current knowledge. The present networks must be improved by selective replacement of obsolete parts, since replacing entire networks would be too costly in economic and environmental aspects. When building new or expanding existing networks, it is essential that optimal components are used. Hence, the lifetime and the environmental impact from manufacturing are essential.

The IEA DHC TS 6 Project have been created to improve the methodology of asset management of district heating networks. The main objectives of the project are

- Collection of research results available
- Harmonize latest results and make proposals for the improvement of related standards/recommendations
- Make research results available for DH utilities
- Identify and close knowledge gabs
- Involve the international DH community (researchers, experts, municipalities, etc.).

ACKNOWLEDGEMENT

The authors would like to thank the International Energy Agency Technology Collaboration Programme on District Heating and Cooling as well as the members of the executive committee for supporting the TS 6 research project.

REFERENCES

[1] EN 253 (2023). District heating pipes - Preinsulated bonded pipe systems for directly buried hot water networks - Pipe assembly of steel service pipe, polyurethane thermal insulation and outer casing of polyethylene. European CEN, Brussels.

[2] EN 448 (2023). EN 489 District heating pipes - Preinsulated bonded pipe systems for directly buried hot water networks - Fitting assemblies of steel service pipes, polyurethane thermal insulation and outer casing of polyethylene. European CEN, Brussels.

[3] EN 13941-1 (2023). District heating pipes – Design and installation of thermal insulated bonded single and twin pipe systems for directly buried hot water networks: Part 1: Design. European CEN, Brussels.

[4] Hay S., Leuteritz A., Morgenthum M. Remaining service life of preinsulated bonded pipes—A key element of transformation strategies and future district heating systems in Germany. Energy Reports 2021. Volume 7. Pages 440-448. https://doi.org/10.1016/j.egyr.2021.08.084.

[5] Yarahmadi, N. Sällström J. H. Improved Maintenance Strategies for District Heating Pipe-Lines. The 14th International Symposium on District Heating and Cooling. https://ri.diva-portal.org/smash/record.jsf?pid=diva2%3A1559716&dswid=7313. 2014 [11th May 2023].

[6] GEF Chemnitz GmbH, IMA Materialforschung und Anwendungstechnik GmbH, IPF Leibniz-Institut für Polymerforschung Dresden e. V. (2011). Zeitstandfestigkeit von Kunststoffmantelrohren - Permeations- und Degradationsverhalten, Wechselbeanspruchung, Alterungsgradient, Muffenbewertung, Versagensverhalten. Forschung & Entwicklung, Heft 17, ISBN: 3-89999-026-9. AGFW, Frankfurt am Main (in German).

[7] Leuteritz A., Döring K.-D., Lampke T., Kuehnert I. Accelerated aging of plastic jacket pipes for district heating. Polynm. Test. 51. 2016. p. 142-147.

[8] N. Yarahmadi, A. Vega, I. Jakubowicz. Accelerated ageing and degradation characteristics of rigid polyurethane foam. Polymer Degradation and Stability 138 (2017), p. 192 – 200.

[9] N. Yarahmadi, A. Vega, I. Jakubowicz. Determination of the long-term performance of district heating pipes through accelerated ageing. Polymer Degradation and Stability 153 (2018), p. 15 – 22.

[10] GEF Chemnitz GmbH, IMA Materialforschung und Anwendungstechnik GmbH, IPF Leibniz-Institut für Polymerforschung Dresden e. V. (2016). Qualitätssicherung für zukünftige Kunststoffmantelrohrsysteme in der Fernwärmeversorgung. Forschung & Entwicklung, Heft 39, ISBN: 3-89999-062-5. AGFW, Frankfurt am Main (in German).

[11] CHANG W. L. Decomposition Behavior of Polyurethanes via Mathematical Simulation. Journal of Applied Polymer Science. 1994 Vol. 53. p. 1759-1769.

[12] AGFW et al. (2020). EnEff: Wärme Technische Gebrauchsdaueranalyse von Wärmenetzen unter Berücksichtigung volatiler erneuerbarer Energien - Teil I: Untersuchungsergebnisse zur Materialdegradation. Forschung & Entwicklung, Heft 55, ISBN: 3-89999-080-3. AGFW, Frankfurt am Main (in German).

[13] Kim J., Kim Y. S., Kim H.-J., Yoon J. Effect of operating temperature conditions in 21-year-old insulated pipe for a district heating network. Case Studies in Thermal Engineering 27. https://doi.org/10.1016/j.csite.2021.101265, 2021 [7th June 2023].

[14] Kim J., Kim Y. S., Kim H.-J., Yoon J. Shear strength distribution of district heating pipe under accelerated aging condition with respect to PU foam density. Polymer Testing 110. https://doi.org/10.1016/j.polymertesting.2022.107567, 2022 [7th June 2023].

[15] Institute of Asset Management. Asset Management - An Anatomy Version 3. https://theiam.org/media/1486/iam_anatomy_ver3_web-3.pdf, 2015 [11th May 2023].

[16] Langroudi P. P., Weidlich I., Hay S. Backward simulation of temperature changes of District Heating networks for enabling loading history in predictive maintenance. Energy Reports 2021. Volume 7. Pages 119-127. https://doi.org/10.1016/j.egyr.2021.09.031.

[17] Weidlich I., Banushi G., Yarahmadi N. et al. Effects of Loads on Asset Management of the 4th Generation District Heating Networks. IEA DHC Project - Annex XII final report. https://www.iea-dhc.org/the-research/annexes/annex-xii/annex-xii-project-01, 2020 [11th May 2023].

[18] Vega, Alberto; Yarahmadi, Nazdaneh; Sällström, Jan Henrik; Jakubowicz, Ignacy (2020): Effects of cyclic mechanical loads and thermal ageing on district heating pipes. In Polymer Degradation and Stability 182, p. 109385. DOI: 10.1016/j.polymdegradstab.2020.109385.

[19] Pourbozorgi Langroudi, Pakdad (2022): An Analysis of the most Frequent Operational Temperature of four District Heating Networks of Germany: HafenCity Universität Hamburg.

The 18th International Symposium on District Heating and Cooling,
September 3–6, 2023, Beijing, China

EVALUATION OF HEAT TRANSFERRED BETWEEN FACILITIES VIA AN UNINSULATED-PIPE NETWORK ON A HEAT-SOURCE WATER NETWORK

Jincheng Dai[a], Minako Nabeshima[b*], Masaki Nakao[c]

[a] *Graduate school of Engineering, Osaka City University, Osaka, 558-8585, Japan*
[b] *Graduate school of Engineering, Osaka Metropolitan University, Osaka, 558-8585, Japan*
[c] *Urban Resilience Research Center, Osaka Metropolitan University, Osaka, 558-8585, Japan*
[*] *Corresponding author.nabeshima@omu.ac.jp*

ABSTRACT

A single-loop heat-source water network system that utilizes hot spring and wastewater heat for the hot-water-supply heat pump has been planned for hotel facilities as a system to utilize hot spring heat from the district. Although previous studies have confirmed that the heat-source water network system saves more energy than conventional systems, it is necessary to consider whether insulation is necessary for low-temperature heat-source water pipes to reduce the initial costs associated with buried piping during installation. In this study, to simulate a system consisting of a pipeline and a heat pump, a simple unsteady lumped-parameter model for heat loss from a buried pipe was proposed instead of the conventional finite element method model. This model showed that the steady-state characteristics were equal to the heat transfer analysis values, and the heat loss from the pipe was a good approximation with the results of the FEM model. Finally, the unsteady buried piping model in a heat-source water network system was simulated using Dymola to calculate heat transfer between facilities with varying soil conditions and burial depths. In the case study, the effect of soil conditions on the amount of heat obtained from the heat-source network was found to be significant for small-scale facilities, which tend to lack hot spring heat, and the effect of the burial depth was found to be small within a realistic range of burial depths. When the heat demand of the small-scale facilities increased without heat recovery equipment, the calculated heat loss of the network piping system decreased as the obtained heat of the small-scale facilities from the uninsulated buried piping system increased and the heat source temperature decreased. The obtained heat from the uninsulated buried piping system was estimated to be almost the same as that from the insulated-pipe system. The overall system coefficient of performance (COP) decreased by 0.02, compared to that of the system with insulated pipes.

Keywords: *Hot spring heat utilization; District Heat Supply System; Unsteady Heat Transfer*

1. INTRODUCTION

1.1. Background and motivation

The effective utilization of renewable energy, such as solar power, wind power, hydropower, geothermal energy, solar thermal energy, and other naturally occurring heat sources, is attracting growing interest as untapped sources of energy. Japan, a nation renowned for its hot springs, has over 27,000 hot spring sources distributed throughout its territory. Of these sources, approximately 52% have temperatures of 42 °C or higher, making the potential for utilizing the untapped energy from hot springs or wastewater heat high. Multiple hot spring facilities are clustered in hot spring towns, but these facilities often inefficiently use their high-temperature hot spring water by releasing heat into rivers or lowering the temperature to levels suitable for bathing through dilution with cold water. However, there exists a current situation in which both hot spring facility operators with excess heat and those who purchased heat but do not have enough coexist in hot spring towns. Consequently, the attempt to promote the effective use of region-wide renewable heat has failed.

Nabeshima et al.[1] proposed heat source water network system (HWNS), a single-loop decentralized heat source system that assumed the installation of a heat-pump hot-water supply unit at each facility and calculated the effects of the system energy saving. This is a unidirectional low-temperature network for district hot water supply but with only a single-loop pipe, which differs from the fourth-generation district heating and cooling (DHC) system with two pipes.

The HWNS connects multiple hot spring facilities with a primary network pipeline in hot spring regions and circulates heat-source water that has undergone thermal exchange with hot springs and wastewater, acting as a heat source for each facility. The calculation results confirmed that the HWNS has a higher energy-saving potential than conventional systems. However, the HWNS is a regional heat supply system that suffers from increased heat loss owing to long buried pipes, and the exchange of heat between facilities becomes more complex. In particular, the insulation materials required for long

buried pipes can impact initial costs, thus, complicating the implementation of the system. Dai et al. [2] have demonstrated that the insulation of buried pipes has almost no effect on the heat acquisition of facilities but does impact the heat supply facility. Although the heat exchange (heat sales) between facilities is expected to accelerate the recovery of initial costs to some extent, it is difficult to calculate its value.

1.2. The purpose of this study

Although previous research has provided an overall evaluation of the HWNS, it is necessary to examine whether insulation is necessary for low-temperature-source water pipelines to suppress the initial cost of regional piping during an actual implementation. Moreover, the detailed heat balance between facilities due to heat transfer is still unclear. In this study, we investigate the heat utilization between hotel facilities of the HWNS. The proposed system was evaluated through a dynamic one-dimensional (1D) simulation using Dymola.

Therefore, this study uses uninsulated buried pipes as a premise and investigates their impact on the heat transfer and thermal balance of facilities within the system under different soil conditions to effectively utilize hot spring heat and promote cost savings.

1.3 Previous works

In a recent study, Abugabbara et al.[3], introduced the latest district heating and cooling systems, which are characterized by low network temperatures achieved through the use of uninsulated pipes, decentralized heat pumps and chillers for modulating the network temperature; they shared energy flows between interconnected buildings. This study presents a simulation model for designing and analyzing such systems that are developed using the Modelica language and consisting of component models from thermal, fluid, and control domains. The model was used to simulate and analyze the first existing Swedish district system with simultaneous heating and cooling demands and bidirectional energy flows, connecting nine buildings with total respective annual heating and cooling demands. A detailed analysis of the heat conduction between buried double pipes without insulation was also performed. Simulation results revealed a 28% reduction in distribution losses, compared to traditional networks with insulated pipes. In this study, the primary focus lies on the examination of the steady-state heat transfer occurring between the double buried pipes and surrounding ground surface. The investigation does not delve into the discussion of unsteady-state heat transfer that may arise between the buried pipes and the soil.

Van Der Heijde et al. [4] proposed an open-source pipe model for thermal networks, which assumed the case of unsteady-state heat losses. This study presents the mathematical derivation and software implementation of a thermo-hydraulic model for thermal networks, which adheres to the aforementioned requirements, and compares it to both experimental data and a commonly used model. A good correlation between experimental data from a controlled test set-up and simulations using the presented model was found. Compared to measurement data from a district heating network, the simulation results led to a larger error than in the controlled test set-up, but the general trend was still closely approximated, and the model yielded results similar to those obtained by a pipe model from the Modelica Standard Library. However, the presented model simulated 1.7 (for low number of volumes) to 68 (for highly discretized pipes) times faster than the conventional model for a realistic test case. Nevertheless, the unsteady heat transfer model presented in this study primarily relies on the thermal delay characteristics of the pipeline under various conditions. This model does not adequately capture the real-time heat transfer dynamics between the buried pipeline and the surrounding soil.

Jakubek, et al. [5] conducted a study on the cost of burying pipelines and analyzed the heat losses in pre-insulated and double pipes in a heating system network. The study involved comparing the heat losses in the ground calculated by an analytical 1D model with measurements obtained from a dedicated experimental setup. The laboratory measurements and analytical models had a good agreement, with an error level of approximately 8%, depending on the type of district heating pipe. An economic analysis showed that twin-pipe systems were expected to provide a return on investment after five years when compared to single-pipe pre-insulated heating networks.

In our study, the main premise to save the construction cost of the system is through the use of uninsulated buried pipelines. Previous studies did not consider soil properties as they focused on pre-insulated pipes. However, for uninsulated pipes, soil characteristics such as moisture content have a significant impact on the heat conduction between the buried pipes and the soil. Therefore, it is believed that a pipe model that considers soil properties is necessary. A model is developed to determine whether the heat exchanged between the facilities is consistent in systems employing insulated and uninsulated pipelines.

2. METHODOLOGY

2.1. Details of the system

Ten facilities, five large-scale and five small-scale, are connected by a single-loop heat-source water network piping. Components other than the pipe model (such as heat pumps, heat exchangers, tanks, etc.) utilize components from the Modelica library, and overall system planning and heating and cooling loads are the same as in the study by Nabeshima et

al. [1]. Each facility is equipped with facility piping that circulates hot spring water and wastewater that has undergone heat exchange. The surplus heat is transferred to other facilities through a core network piping system that spans 3.5 km, connecting multiple facilities via heat exchangers and is utilized as a heat source for heat-pump-type water heaters (hereafter referred to as HP water heaters) (Figure 1). The system in large-scale facilities (Figure 2) consists of heat exchangers for wastewater, hot springs, water-source HP water heaters, system for preheating tap water, and a single-loop network piping for heat exchange. The system in small-scale facilities (Figure 3) is the same as the system in large hot spring facilities, except for the hot spring-source heat exchanger. The hot spring heat is primarily used within the facility, with any surplus heat transferred to the network piping system via heat exchange.

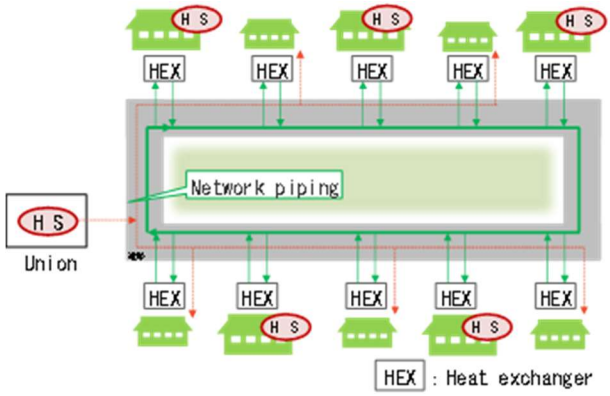

Figure 1. Block heat-source water network system: ten facilities, five large-scale and five small-scale, connected by a single-loop heat-source water network piping. Union is in charge of supplying hot spring-source water to small-scale facilities.

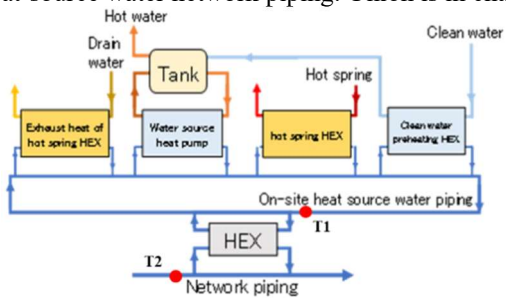

Figure 2. System diagram of the large-scale facility. The control of heat exchangers is performed based on the temperature difference between T1 and T2.

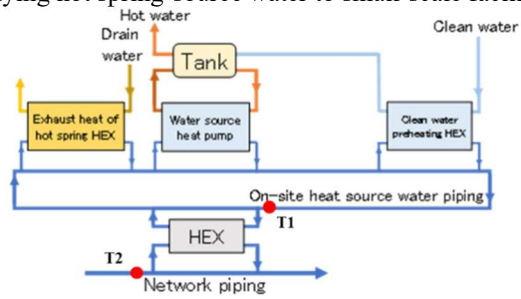

Figure 3. System diagram of the small-scale facility. The control of heat exchangers is performed based on the temperature difference between T1 and T2.

2.2 Piping Model for simulation

The piping models existing in the Modelica Library [7], such as Modelica.Fluid.Pipes.DynamicPipe,consider heat loss through the insulation material of the pipes, but they cannot calculate the convective heat loss of buried pipes considering the soil thermal capacity. To calculate the heat loss of uninsulated buried pipes and reproduce the thermal properties of the soil, unsteady-state calculations are necessary. The finite element method is commonly used for non-steady-state heat transfer calculations, but such complex calculations are difficult to implement along HWNS pipelines. To simplify the calculations, a cylindrical model is assumed for a certain depth of buried pipes, and the heat resistance and heat capacity of the soil thickness around the pipes are considered for calculations.

$$R_s = ln\left\{\frac{2h_1}{d} + \sqrt{\left(\frac{2h_1}{d}\right)^2 - 1}\right\} \times \frac{1}{2\pi\lambda_s} \tag{1}$$

$$R_s = \frac{ln\left(\frac{d+\Delta r}{d}\right)}{2\pi L\lambda_s} \tag{2}$$

$$\Delta r = e^{[2\pi L\lambda_s R + ln(d)]} - d \tag{3}$$

The thermal resistance of the soil from the outer surface of buried piping to the ground surface (Figure 4) is calculated using Equation 1. In this study, to simplify the calculations, the cylindrical model shown in Figure 5 was used, which considers only the thermal resistance and thermal capacity of the soil thickness surrounding the piping. The thermal resistance value obtained from Equation 1 is substituted into Equation 2, and the corresponding soil thickness Δr is

determined such that the thermal resistance values are equal according to Equation(3). Therefore, the steady-state characteristics of this cylindrical model are in agreement with the buried piping. The cylindrical model was described in Modelica language and integrated into the facility system simulation that had already been constructed. Consequently, it became possible to investigate the changes in the source water temperature due to the unsteady thermal characteristics of the soil more easily than when using conventional unsteady calculation methods (such as the thermal response factor method [8]). The cylindrical model limits the calculation range of the soil around the piping to the corresponding soil thickness and considers the soil surface temperature boundary, which results in high accuracy in the unsteady heat transfer near the piping but is expected to have larger unsteady errors than conventional methods.

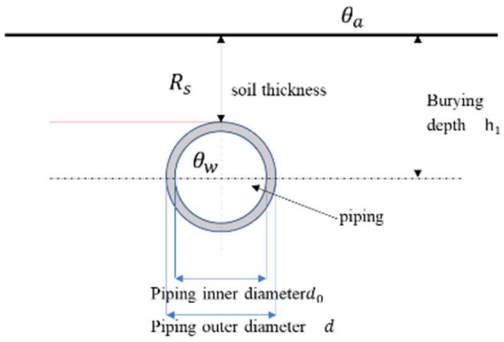

Figure 4. Buried piping

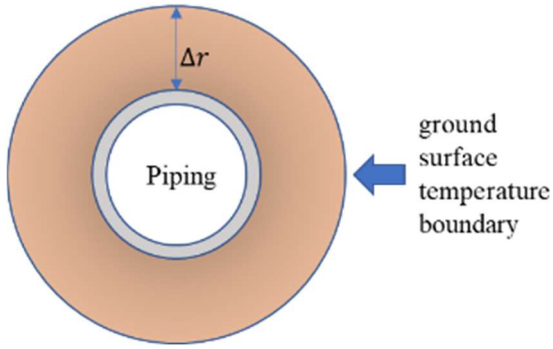

Figure 5. Equivalent soil thickness

The soil division model is divided into three parts as shown in Figure 6: (1) the surface temperature boundary, (2) the soil division, and (3) the pipe boundary. An overview of each of these three parts is described below:

(1) The surface temperature boundary is defined by Equation (4). This is the upper boundary condition of the soil division model, where the surface temperature is specified.

(2) The soil division is represented by Equation (5), and it is used to perform convergence calculations of the soil temperature using a distributed constant-system division model by receiving temperature or a heat flow set as a boundary condition.

(3) The pipe boundary sets the hot water temperature inside the pipe as the lower boundary condition of the soil division model. The insulation owing to the thermal resistance of the pipe material is also calculated in this part using Equation (6).

$$c_\rho V_n \rho \frac{dT_{n+1}}{dt} = \frac{1}{R_n}(T_n - T_{n+1}) + Qflow_{air} \tag{4}$$

$$c_\rho V_i \rho \frac{dT_i}{dt} = \frac{1}{R_{i-1}}(T_{i-1} - T_i) + \frac{1}{R_i}(T_{i+1} - T_i), \quad i \in (2{:}n) \tag{5}$$

$$c_\rho V_n \rho \frac{dT_1}{dt} = Qflow_{water} + \frac{1}{R_1}(T_2 - T_1) \tag{6}$$

Table 1

Parameter	Definition	Unit	Parameter	Definition	Unit
$\boldsymbol{R_s}$	Soil heat resistance	K/W	$\boldsymbol{\lambda}$	thermal conductivity	W/(mK)
$\boldsymbol{\lambda_s}$	Soil thermal conductivity	W/K	$\boldsymbol{air}$	ground boundary	-
$\boldsymbol{\Delta r}$	Equivalent soil thickness	M	$\boldsymbol{\rho}$	density	kg/ m³
$\boldsymbol{h_1}$	Burying depth	M	$\boldsymbol{Qflow}$	heat flow	W
$\boldsymbol{L}$	Piping length	M	$\boldsymbol{n}$	division number	-
$\boldsymbol{d}$	piping radius	M	$\boldsymbol{V}$	volume	m³
$\boldsymbol{T}$	temperature	°C	$\boldsymbol{r_p}$	piping radius	m
$\boldsymbol{water}$	water boundary	-	$\boldsymbol{L}$	longitudinal length	m
$\boldsymbol{c_\rho}$	specific heat	J/(kgK)	$\boldsymbol{R}$	thermal resistance	K/W
$\boldsymbol{\Delta r}$	small radius	M			

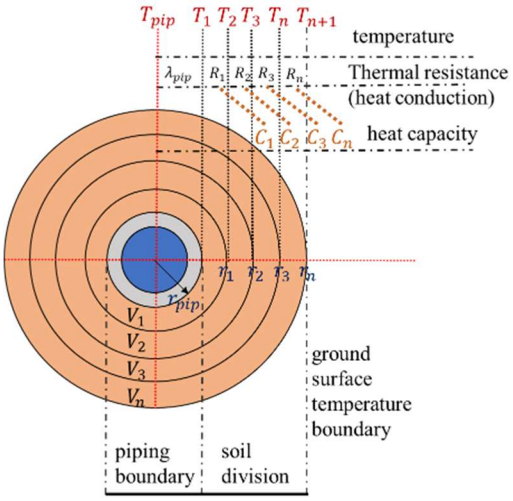

Figure 6. soil division model

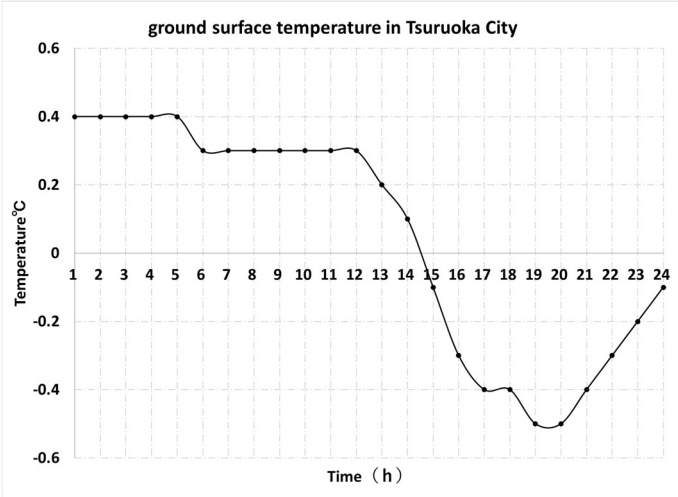

Figure 7. Winter ground surface temperature in Tsuruoka City.

2.3 Model verification

The thermal response factor method, which is used for transient heat load calculations of buildings, was employed to perform non-transient heat transfer calculations of buried pipelines and evaluate the modeling errors due to different soil conditions. Tables 3 and 4 show the root-mean-square error (RMSE) and coefficient of variation of RMSE (CVRMSE) (Equations 7 and 8) of sensible and heat flux at ground surface, respectively. The error in the heat flux at the pipe surface is small, whereas at the ground surface response is relatively large. However, in Tsuruoka City, Japan, where a change in the maximum daily ground-surface temperature boundary condition of approximately 1 ℃ (Figure 7) due to snow on the ground, and a maximum temperature change of the buried pipeline of up to 10 ℃ due to the introduction of the heat source water temperature is expected, the impact of the error in the heat flux at the ground surface response is considered small.

$$RMSE(x,y) = \sqrt{\frac{1}{m}\sum_{i=1}^{m}(x_i - y_i)^2} \tag{7}$$

$$CVRMSE(x,y) = \sqrt{\frac{1}{m}\sum_{i=1}^{m}(x_i - y_i)^2} \Big/ \frac{1}{m}\sum_{i=1}^{m}|y_i| \tag{8}$$

Table 2

Parameter	Definition	Unit
$\boldsymbol{m}$	Number of samples	-
$\boldsymbol{x}$	Calculated value of the soil division model	-
$\boldsymbol{y}$	Calculated response	-

Table 3. 24-hour RMSE, CVRMSE (heat flux at the pipe surface)

Sand	**Moisture content 0%**	**Moisture content 23.3%**	**Moisture content 0 %**	**Moisture content 0 %**
depth	0.33m	0.33m	1m	1.5m
RMSE	0.06693	0.03325	0.01513	0.01818
CVRMSE	4.89%	0.48%	1.11%	1.33%

Table 4. 24-hour RMSE, CVRMSE (heat flux at the ground surface)

Sand	**Moisture content 0%**	**Moisture content 23.3%**	**Moisture content 23.3%**
depth	0.33m	0.33m	1m
RMSE	0.13880	1.27693	0.79496
CVRMSE	29.35%	32.07%	35.88%

3. CASE STUDY

Using the thermal response simulation test, the impact of different soil conditions on directly buried uninsulated pipelines in the HWNS was evaluated. The soil division model was implemented in the HWNS to conduct a comparative analysis of the change in heat transfer between facilities. The assumed conditions of each case are shown in Table 5. The standard yearly data for Tsuruoka City, Yamagata Prefecture, is used as the outdoor conditions for cold regions, based on the reference weather year created from the expanded AMeDAS meteorological data for 2001～2010 [9].

Table 5. Soil conditions

No.	Substance	Moisture content%	Thermal diffusivity m^2/s	Burying depth m
S1	sand	0	0.0002	0.33
S2	sand	0	0.0002	1
S3	sand	0	0.0002	1.5
S4	sand	23.3	0.0008	1
S5	sand + clay	21.6	0.0009	1
S6	loam	36.6	0.0003	1

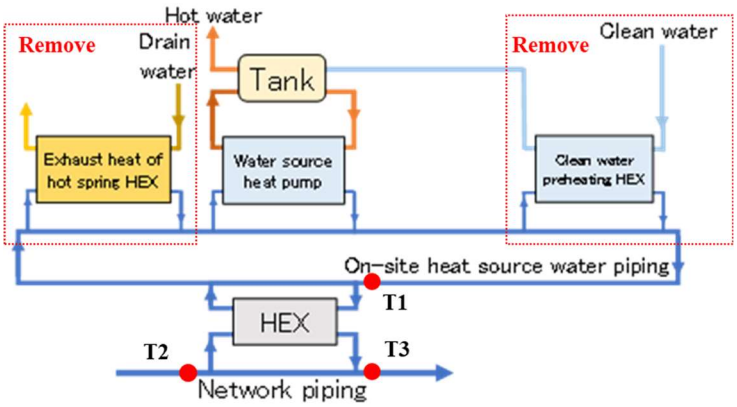

Figure 8. Small-scale facility with temperature measuring points: the heat exchanger marked "Remove" means that they are removed in the case with no heat recovery at a small-scale facility.

4. RESULTS

The daily heat balance (Table 7) for large-scale accommodations, small-scale accommodations, and the network pipelines during the period is calculated, and the results of the case studies shown in Table 5 are examined. The system's coefficient of performance (SCOP), which evaluates heat generation and power consumption in the overall system is calculated from Equation 9.

(1) Influence of Soil Conditions

As shown in Figure 9, the SCOP is 1.17 for all S1, S2, and S3 conditions, with approximately the same amount of heat exchanged throughout the day. The burial depth is considered to have a weak effect on the overall heat exchange. For S4, S5, and S6, the SCOP is 1.12, 1.11, and 1.15, respectively. Thus, the differences in soil conditions affect the SCOP. Regarding the change in the daily heat exchange, the heat loss caused by the network pipeline is significant under the conditions of S4, S5, and S6, and small-scale accommodations can hardly receive any heat. From the viewpoint of soil conditions, heat loss increases with an increase in thermal diffusivity. Thus, soil conditions have a significant impact on the heat-source water network system in cold regions.

(2) Presence of Heat Recovery Equipment for Small-Scale Accommodations

This study investigated whether the heat gain of small-scale accommodations increases when the heat recovery equipment is removed, as shown in Figure 8, and the daily integral values of heat exchange are shown in Figure 10. When the heat recovery equipment is removed, the SCOP for S3–S6 became 1.30, 1.08, 1.08, and 1.11, respectively. In S3, where the soil thermal diffusivity is low, the SCOP was higher than when the heat recovery equipment was present. Otherwise, it decreased by approximately 0.3 to 0.4. However, the heat loss caused by the network pipeline decreased, and the heat exchange for small-scale facilities increased overall.

Figure 8 shows the temperature measurement points for the main network pipeline and small-scale facilities. The temperature difference between the facilities and the network pipeline is shown in Figure 11, and the temperature difference

between the network pipeline before and after passing through the small-scale facility is shown in Figure 12. According to Figure 11, the temperature difference between the small-scale facility and the network pipeline is only up to 2 ℃ when there is a heat recovery device in the small-scale hostel, indicating that the heat recovery in the small-scale hostel is small. In the case where there is no heat recovery device, the temperature of the heat-source water in the small-scale hostel decreases, and the temperature difference between T1 in the small-scale hostel and T2 in the network pipeline increases up to 6 ℃. The increase in the heat recovery in the small-scale hostel results in a larger temperature difference between T2 and T3 in the small-scale hostel and a greater decrease in the water temperature of the network pipeline (Figure 12), resulting in a decrease in the temperature difference between T3 and the surface of the soil (Figure 13). By removing the heat recovery device in the small-scale hostel, the heat recovery in the small-scale hostel increased to the same level as that with insulation (S4), and the heat loss from the pipeline also decreased. In the case of an uninsulated network pipeline, the heat dissipation from the large hostel to the network pipeline increased, but it was confirmed that it could transfer heat to the small-scale hostel in the same way as the insulated pipeline.

$$SCOP = \frac{Q_{con,sys}}{E_{sys}} \tag{9}$$

Table 6

$Q_{con,sys}$: system generated heat	GJ
$SCOP$: System COP	-
E_{sys} : System power consumption (includes all HPs and Pumps)	GJ

Table 7 Character definition

QNW	Amount of heat from facilities to the network for 24 h (positive) Amount of heat from the network to facilities for 24 h (negative)
Enthalpy diff.	Pipe heat loss and change in the internal energy by water temperature change (negative)

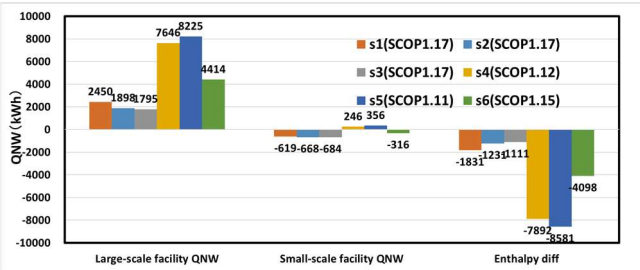

Figure 9 Daily integral value in S1~S6: enthalpy variation and the SCOP of large-scale facilities, small-scale facilities, and buried pipes throughout the day in each case.

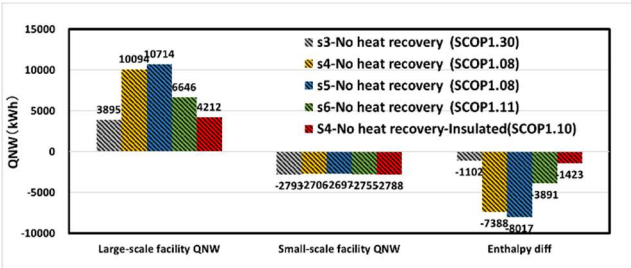

Figure 10 Daily integral value in S3~S6: enthalpy variation and the SCOP of large-scale facilities, small-scale facilities, and buried pipes throughout the day in each case with no heat recovery.

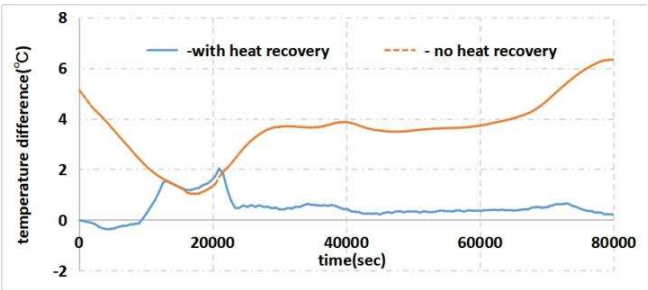

Figure 11 Temperature difference in T2-T1; the temperature difference between temperature measurement points, where a larger difference corresponds to a higher heat exchange rate.

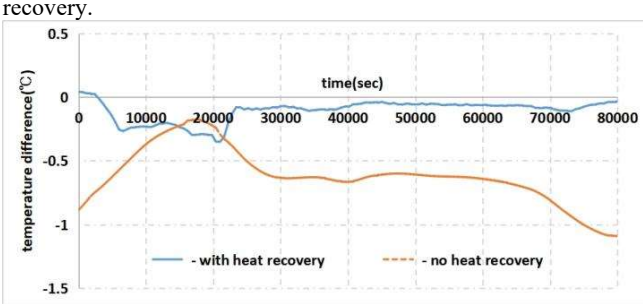

Figure 12 Temperature difference in T3-T2; the temperature difference between temperature measurement points, where a larger difference corresponds to a higher heat exchange rate.

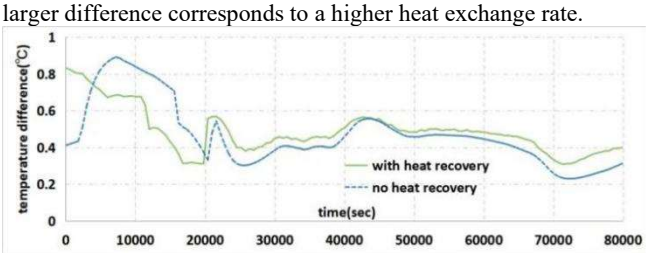

Figure 13 Temperature difference between T3 and the inner surface of the soil.

5. CONCLUSION

The findings obtained in this study are summarized as follows:

(1) We proposed an unsteady-state heat transfer model for pipelines, ensuring the preservation of steady-state heat transfer characteristics. Furthermore, we demonstrated the model's capability to accurately compute the heat flux at the surface of the pipeline.

(2) Based on a comparison under different insulation conditions, there was a small correlation between the insulation of the network pipes and the amount of heat recovered by small-scale facilities, and they achieved almost the same amount of heat acquisition. When the heat recovery equipment of the small-scale hot spring inn was removed, the amount of heat exchange exceeded the amount of heat transferred, and the decrease in the system COP of the entire heat source water NW was only 0.03.

(3) Soil conditions significantly affected the heat acquisition of small-scale facilities in uninsulated piping systems. The insulation status of the network piping had minimal influence on the heat acquisition of small-scale facilities. However, it is important to consider that the insulation of buried pipes can impact the heat input to the system.

(4) When the heat recovery equipment in small-scale facilities was removed, the amount of heat released from large-scale facilities to the HWNS and the amount of heat acquired from the HWNS by small-scale facilities both increased, and even with uninsulated piping, the amount of heat acquired was equivalent to that acquired with insulated piping.

ACKNOWLEDGEMENT

This study reports the results of research conducted after the completion of the NEDO subsidy project "Cost reduction technology development for renewable energy heat utilization: Total cost reduction technology development for a heat source water network system using dispersed heat sources utilizing renewable energy heat such as hot spring heat (November 2020 to July 2022)".

REFERENCES

[1] Nabeshima, M., Koh, N., Nakao, M., Mike, M., 2018. Estimation of the energy-saving effect of introducing a heat source water network system with single-loop piping utilizing hot spring heat. Energy Procedia 149, 519–528.

[2] Jincheng, D., Nabeshima, M., Nishioka, M., Nakao, M., Mike, M., Sawabe, K. "Study on area-wide Hot Spring Heatutilization system- Confirmation of heat balance in Heat Source Water Network System and Heat Source Plant System - " (In Japanese)

[3] Abugabbara, M., Javed, S., Johansson, D., 2022. A simulation model for the design and analysis of district systems with simultaneous heating and cooling demands. Energy 261, 125245.

[4] Van Der Heijde, B., Fuchs, M., Ribas Tugores, C., Schweiger, G., Sartor, K., Basciotti, D., Müller, D., Nytsch-Geusen, C., Wetter, M., Helsen, L., 2017. Dynamic equation-based thermo-hydraulic pipe model for district heating and cooling systems. Energy Conversion and Management 151, 158–169.

[5] Jakubek, D., Ocłoń, P., Nowak-Ocłoń, M., Sułowicz, M., Varbanov, P.S., Klemeš, J.J., 2023. Mathematical modelling and model validation of the heat losses in district heating networks. Energy 267, 126460.

[6] Arabkoohsar, A., Alsagri, A.S., 2020. Thermodynamic analysis of ultralow-temperature district heating system with shared power heat pumps and triple-pipes. Energy 194, 116918.

[7] Modelica Buildings library <https://simulationresearch.lbl.gov/modelica/> [accessed on: 01-10-2023]

[8] Mitalas, G.P., Stephenson,D.G.,1967. Transactions American Society of Heating. Refrigerating, And Air - Conditioning Engineers Vol. 73. Part 1.

[9] AMeDAS - Japan Meteorological Agency< https://www.jma.go.jp/jma/en/Activities/amedas/amedas.html >

STUDY ON THE EFFECT OF LARGE THRUST ON LINING OF HEATING SHIELD TUNNEL

Liu Yangpeng

Beijing District Heating Project Design Company, 100078，China
lyp@bhpd.cn.

ABSTRACT

In order to study the effect of large thrust of heat pipe on shield lining, actual measurement and analysis at different locations in heating tunnel were carried out in different stages based on first heating shield tunnel in China. The results showed that the segments were greatly affected in the stages of concrete pouring in bottom and heating operation. The segments near the fixing supports were affected most by the large longitudinal thrust, and the range of influence reached 14 segment rings. In order to further study the influence range of large thrust on tunnel lining, heating shield tunnel with fixing supports under different thrust and soil friction was simulated, and the relationship between thrust, friction coefficient and influence range was obtained. Based on the analysis of measurements and numerical simulation, the formula for estimating the influence range of longitudinal thrust on shield segment were obtained by improving calculation formula of frictional resistance in shield construction and combining the principle of structure against sliding. The formula can provide some reference for the design of heating shield tunnel in the future.

Keywords: Thermal shield tunnel; Longitudinal thrust; prototype test; simulation analysis

1. INTRODUCTION

Thermal shield tunnel, as compared to other municipal engineering projects, faces the design challenge of a large thrust on the supporting structure inside the tunnel, in addition to the characteristic of high temperature and humidity. The thrust on the supporting structure is generated mainly by two factors: the thermal expansion and contraction of the thermal pipes due to temperature changes, and the pressure from the fluid medium inside the pipes. Taking the Northeast Thermal Power Shield Tunnel as an example, the designed thrust for its fixing support structure is 400kN.

The reason for such a large thrust is due to the thermal expansion and contraction of the pipes. Although the change in length for a 1-meter pipe is extremely small, the impact on kilometer-scale pipelines is enormous. The length change caused by temperature is absorbed by the thermal compensators, and the resulting huge force is constrained by the fixing supports. In addition, due to the constraints of the thermal process requirements, only one fixing support can be set up, and the thrust cannot be dispersed by increasing the number of supports.

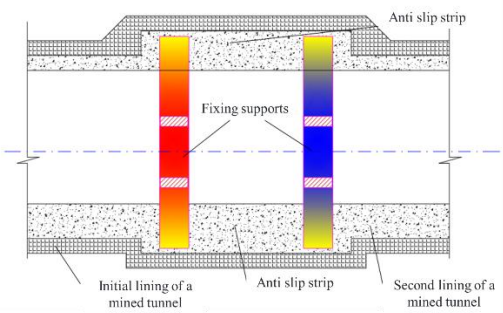

Figure 1. Sketch of Anti slip strip

Usually, the frictional force between the structure and the soil is utilized to resist the thrust force. In the past, the construction of thermal tunnels mainly involved open-cut trenches and tunneling methods, and the lining structure was basically cast in situ. In the design, the lining is locally thickened (setting anti-slip strip) [1] to use the lateral soil pressure to resist the large thrust force, as shown in Figure 1. This construction measure shortens the length of the tunnel that relies on frictional force as resistance, and also reduces the range of the tunnel affected by the large thrust force [2].

For shield tunnels, the lining segments are all prefabricated. Due to the limitations of the construction process, it is difficult

to set anti-slip strip by locally increasing the thickness of the segments. Therefore, it is necessary to rely entirely on the frictional force between the outer wall of the structure and the soil to resist the thrust force, which puts higher demands on the structural lining's resistance. This requires a better understanding of the stress distribution of the lining structure under large thrust.

Regarding the study of the stress of shield tunnel segments, Dong Xinping [3] analyzed the failure process of single-ring lining in shield tunnels using the incremental method. He Chuan et al. [4] conducted a study of the mechanical characteristics of segmental lining structures under different geological conditions through model experiments. In addition, regarding the study of the transverse stiffness of lining segments, Huang Hongwei et al. [5] conducted model experiments on the effective rate of transverse stiffness of shield tunnels. Feng Kun et al. [6] conducted prototype experiments on transverse stiffness. Regarding the longitudinal stress of tunnels, Liao Shaoming et al. [7] analyzed the relaxation law of longitudinal stress in soft soil shield tunnels through field measurements, while Li Jianqiang [8] explored the effect of shield attitude on the lining segments during construction. Li Xiaojun et al. [9] analyzed the longitudinal stress deformation of the lining structure of a shield tunnel using the flexibility method beam model and calculated the deformation. These studies mainly focus on highway and railway tunnels, and the thrust force experienced during segment placement. However, in thermal shield tunnels, the longitudinal thrust force is caused by the thrust of the pipes during operation. Therefore, it is necessary to study the stress of the segments under the long-term thrust force of the pipes.

This paper is based on the Northeast Thermal Shield Tunnel Project in Beijing. Field measurements of the concrete strain and steel reinforcement force at different stages and locations of the lining segments were conducted. The results were analyzed in depth. Finally, based on the field measurements and numerical analysis results, combined with the principle of resistance to slip, the formula for frictional force in the thrust of the shield machine was used to propose a method for estimating the range of the longitudinal thrust force. The method can provide a reference and guidance for the design of future thermal shield tunnels.

2. PROJECT OVERVIEW

The North Line Project of the Beijing Northeast Thermal Power Center's Supporting Heat Network (Dongba Middle Road to Jinyu Road) is a 6.2 km-long pipeline constructed using a 6.44 m-diameter earth pressure balance (EPB) tunnel boring machine. It is the first thermally insulated shield tunnel in China, and also the first large-section thermal shield tunnel in the world with a cross-section diameter exceeding 4 m. The external diameter of the tunnel is 6 m, the internal diameter is 5.4 m, and the thickness of the lining pipe segments is 300 mm. The width of each pipe ring segment is 1.2 m, and the specific form is "3+2+1", which includes three pieces of type A segments, two pieces of type B segments, and one piece of type C segment in each ring. The lining pipe segments at the support locations consist of special segments containing embedded steel plates. The main cross-section forms include four sections: standard pipeline tunnel cross-section, fixing support location cross-section, orienting support cross-section, and sliding support pier cross-section, as shown in Figure 2.

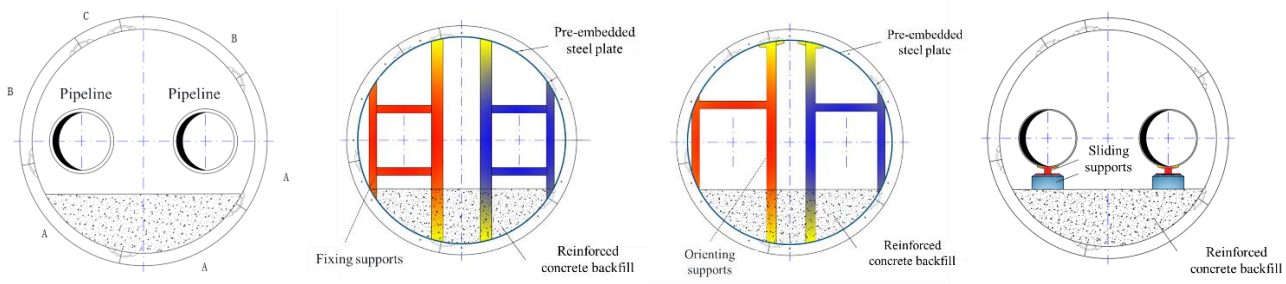

a.Standard section **b.** Section at fixing supports **c.** Section at orienting supports **d.** Section at sliding supports

Figure 2. Main section form

The supports are welded to the embedded steel plates and the lining pipe segments to form an integral structure [10,11], and the designed thrust for each support is shown in Table 1. The fixing supports in the same group are spaced apart from the return water supports by one ring of pipe segments, which is 2.4 m apart, and the sliding support piers are also spaced apart by 2.4 m. The adjacent pipe rings are installed in the same group of orienting supports, which are spaced 1.2 m apart.

The average soil cover thickness of the tunnel for the entire project is 6.5 m. The strata that the shield tunnel passes through are mainly composed of fine-grained clay and medium-fine sand.

Table 1. Pipe thrust of different types of supports（unit:kN）

Force	Types of supports		
	Fixing supports	Orienting supports	Sliding supports

Longitudinal force Fy	400	70	0
Lateral force Fx	100	220	0
Vertical force Fz	0	0	320

Note: The longitudinal force is in the direction of the tunnel, the lateral force is perpendicular to the direction of the tunnel, and the vertical force is in the same direction as gravity.

3 ON-SITE MEASUREMENT PLAN

The monitoring elements such as the reinforcement meter and concrete strain gauge in the test pipe ring were embedded during the pouring of the pipe segments on site. They were buried at the bottom, side walls, and top of the tunnel, with the steel bar counter arranged longitudinally along the tunnel. The specific layout of the measuring points is shown in Figure 3.

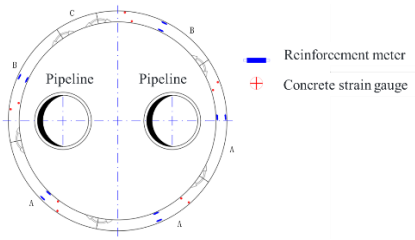

Figure 3. Test element layout

Figure 4. Installation of test elements and data acquisition

The testing period started from the installation of the pipe segments in July 2014 and continued until the entire thermal system was fully operational in January 2016. The main stages of the testing period include: (I) shield tunnel construction and pipe segment installation stage (July 2014-October 2014), (II) bottom concrete pouring and pipeline equipment installation stage (October 2014-June 2015), (III) pipeline hydrostatic pressure testing stage (June 2015-October 2015), and (IV) heating operation stage (October 2015-March 2016).

For the fixing supports, testing was conducted in pipe segments 2636-2668, with testing points set up in every third pipe segment on both sides as well as on the pipe segments three, six, nine, twelve, and fifteen segments away from the fixing support. However, no testing was conducted on the pipe segments where the fixing supports are located (2651-2653).

For the orienting supports, testing was conducted in the western sections at pipe segments 1752 and 1753 and in the eastern sections at pipe segments 1125 and 1126.

For the sliding support piers, testing was conducted in the western sections at pipe segments 2455-2459 (with sliding support piers located on segments 2456 and 2458) and in the eastern sections at pipe segments 2191-2195 (with sliding support piers located on segments 2192 and 2194).

4 MEASURED RESULTS AND ANALYSIS

4.1 Temperature test results and analysis of tunnel lining curved segments.

Figure 5 shows the results of temperature testing for the pipe segments at different stages (obtained using the temperature measurement system of the sensor inside pipe segment 2652). The purpose of the temperature testing is to prevent temperature anomalies caused by leaks of high-temperature hot water inside the pipes during operation, so that these abnormal test results can be eliminated.

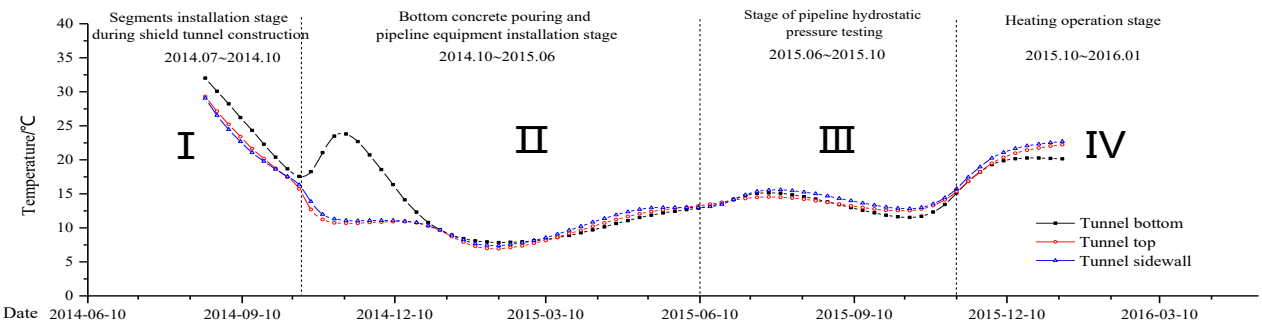

Figure 5. Segment temperature of NO.2652

The initial temperature of the pipe segments was the highest, which was caused by outdoor storage before installation. In the second stage, the temperature of the pipe segments was generally maintained between 10℃ and 15℃. The sudden temperature change at the bottom of the tunnel was caused by the exothermic reaction of the hydration after the bottom

concrete was poured. After normal heating operations commenced, the temperature of the pipe segments rose to over 20℃ and remained stable. From the test results, it can be seen that the temperature change of the pipe segments was stable, and the influence of abnormal temperatures on the test results can be ruled out.

4.2 Internal force test results and analysis of tunnel lining segments at different positions.

The cumulative results of concrete strain and internal force testing for pipe segments at different locations are shown in Tables 2 and 3. Figures 6, 7, and 8 depict the changes in test results at different locations during different stages.

Table 2. Test value of concrete strain

Location		Top			Side Wall			Bottom		
		Initial Value (με)	Stable Value (με)	Maximum value occurrence stage.	Initial Value (με)	Stable Value (με)	Maximum value occurrence stage.	Initial Value (με)	Stable Value(με)	Maximum value occurrence stage.
Fixing supports	Inner Side	-331	-444	Ⅳ	-332	-431	Ⅳ	-474	-557	Ⅳ
	Outer Side	-450	-498	Ⅳ	-412	-489	Ⅳ	-449	-512	Ⅳ
orienting supports	Inner Side	-267	-409	Ⅱ	-202	-214	Ⅳ	-197	-206	Ⅱ
	Outer Side	-159	-140	Ⅱ	-249	-422	Ⅳ	-204	-174	Ⅱ
sliding supports	Inner Side	-185	-243	Ⅳ	-199	-163	Ⅱ	-271	-187	Ⅱ
	Outer Side	-283	-159	Ⅳ	-195	-326	Ⅱ	-481	-452	Ⅱ

Table 3. Test value of internal force of steel bar

Location	Top			Side Wall			Bottom		
	Initial Value（kN）	Stable Value（kN）	Maximum value occurrence stage.	Initial Value（kN）	Stable Value（kN）	Maximum value occurrence stage.	Initial Value（kN）	Stable Value（kN）	Maximum value occurrence stage.
Fixing supports	27.04	38.02	Ⅳ	22.42	26.12	Ⅳ	18.88	41.96	Ⅳ
orienting supports	16.19	18.16	Ⅱ	17.76	31.29	Ⅳ	17.60	19.42	Ⅱ
sliding supports	19.88	27.08	Ⅳ	22.03	21.04	Ⅱ	21.16	13.07	Ⅱ

From the on-site test results, it can be observed that the maximum internal force value at the fixing support occurs during the IV stage. This is because during this stage, the pipeline generates the largest thrust, which causes changes in internal forces in the connected pipe segments. From the results of the internal force testing of the reinforcement, the internal force values of the pipe segments at the top and bottom of the fixing support are relatively large, with a maximum change of 23.08kN at the bottom. The internal force value of the lateral wall is the smallest, and the change is also the least.

At the orienting support, the largest change in internal force occurs in the lateral wall during the IV stage. This is because the function of the orienting support is to constrain the left and right displacement of the pipeline in the tunnel, and the horizontal force acting on the support from the pipeline is ultimately transmitted to the pipe segments after heating.

The main characteristic of the change in internal force at the sliding support is that the internal force of the bottom pipe segments gradually increases. This is because after the construction stage, the concrete base of the sliding support is subjected to increased load due to the added bottom lining, and the load on the bottom is further increased after the pipeline is filled with water during operation.

In summary, the internal force of the pipe segments remained stable before assembly, but experienced sudden changes after assembly due to the effect of the surrounding soil on the internal force redistribution of the lining. During the II and IV stage, the internal force of the pipe segments was fluctuating, but gradually stabilized after heating. The maximum change in axial force during this stage was 15kN, and the strain changed between 100με and 200με, equivalent to a stress range of 2.6MPa to 3.3MPa, all of which are within the safe range.

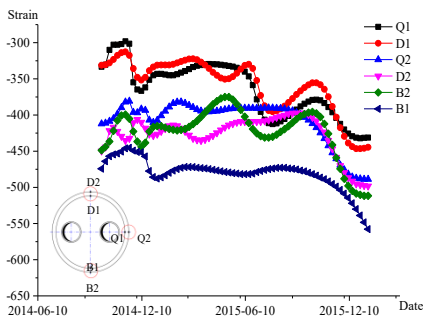

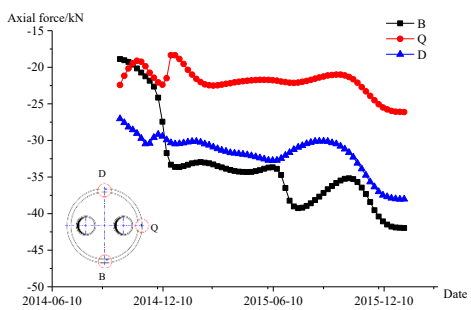

a.Strain **b.** Axial force

Figure 6. Test value of fixing supports

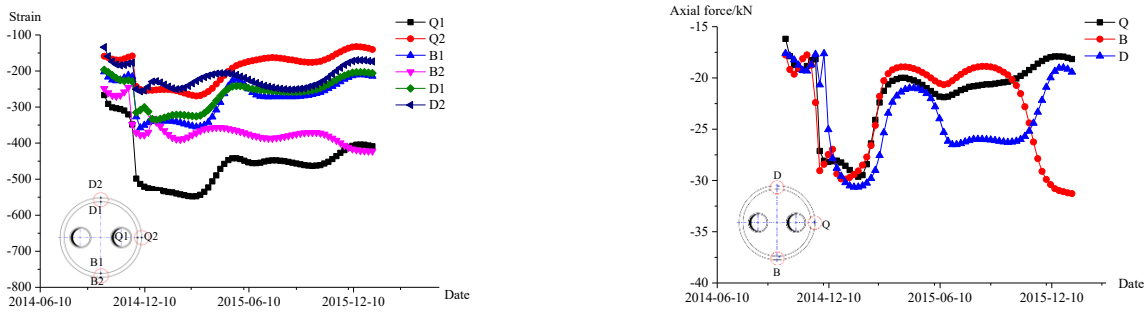

a.Strain **b.** axial force

Figure 7. Test value of orienting supports

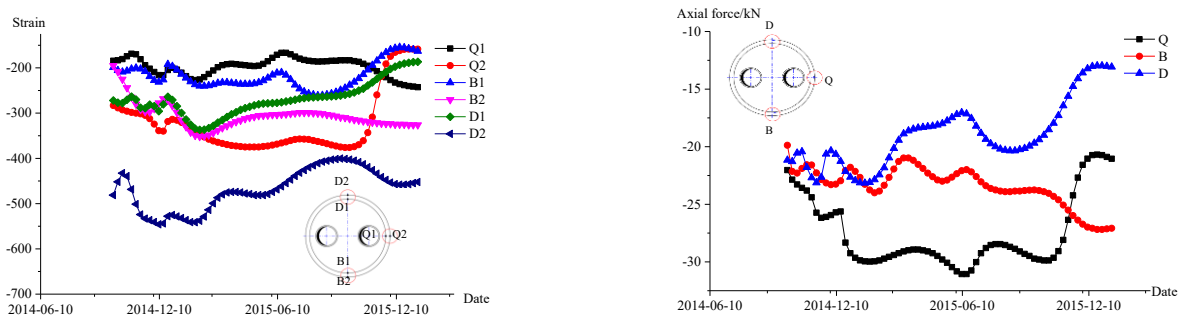

a.Strain **b.** axial force

Figure 8. Test value of sliding supports

Indeed, from the test results, the impact of the large thrust faced by the fixing support during operation has the greatest safety impact on the tunnel structure. Therefore, it is necessary to understand the internal force distribution of the surrounding pipe segments.

4.3 Results and analysis of internal force testing in the surrounding segments of the pipeline under longitudinal thrust

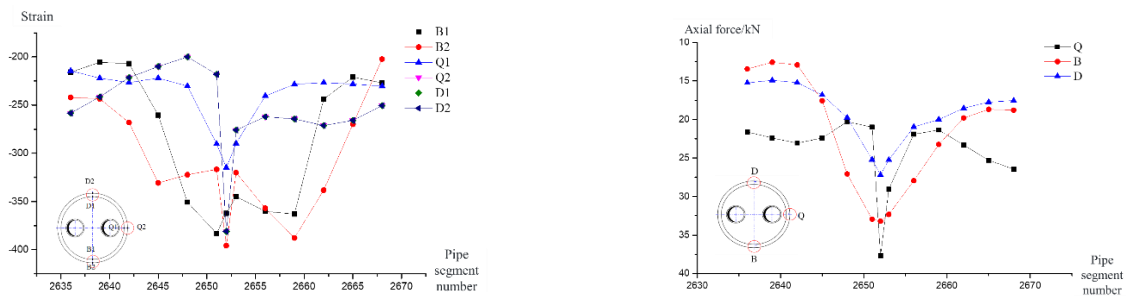

a.Strain **b.** axial force

Figure 9. Test value of shield segment near fixing supports

By analyzing the test results of the pipe segments within a range of 35 rings on both sides of the fixing support after the stable operation of the pipeline network, the maximum internal force was found to be at the fixing support location, and the internal force on the pipe segments tended to flatten out as the distance from the support increased, as shown in Figure 9. In addition, the axial stress of the pipe segments at different locations in the tunnel showed different variation patterns.

As seen from the trend analysis of the stress test results, the attenuation at the fixing support location was relatively rapid, and there was no significant change in axial force starting from the 6th ring. However, due to the influence of the sliding supports on both sides of the support, the effect of the bottom extended to the 12th ring.

The monitoring results of the steel bars show that the axial forces of the three rings near the fixing support are close, and the axial force test results within the first three rings before the fixing support show obvious attenuation, which extends the impact to between the 6th and 9th rings.

Through the analysis of the test results, the range of influence of the fixing support is about 14 rings on both sides, with each pipe ring being 1.2m wide. Therefore, it can be considered that the range of impact of pipeline thrust during normal operation is about 16.8m.

5 STUDY ON THE EFFECT RANGE OF LONGITUDINAL THRUST ON SHIELD TUNNEL SEGMENTS

The test results show that the longitudinal thrust transmitted to the pipe segment at the fixing support has the greatest impact on the structure. Therefore, further numerical analysis and research need to be carried out.

5.1 Model and parameters

Based on the Beijing Northeast Thermal Power Shield Tunnel as an example, we use numerical simulation software to establish a thermal shield tunnel model with a fixing support (as shown in Figure 10). The left and right boundaries of the model are 5 times the radius of the tunnel, the lower boundary is 3 times the radius of the tunnel, the longitudinal length is 36m, and the length of the 30 pipe segments is a total of 6.5m deep. The boundary conditions of the calculation model are the top free surface, and the other directions are constrained along the vertical coordinate direction of each surface. The Mohr-Coulomb criteria are used, and the average density of the soil is 1750kg/m^3. The friction angle is selected according to the friction coefficient under different working conditions, as shown in Table 4.

Table 4. List of different cases

cases	1	2	3	4	5
Thrust.F/kN	100	250	500	750	1000
Friction coefficientμ	0.1	0.25	0.5	0.75	1

Note: The friction coefficient is calculated as the tangent of 2/3 of the angle of friction at the contact surface.

The fixing support is tightly combined with the steel plate embedded in the pipe segment, and the thrust is acted on the fixing support. The frictional forces between the pipe segments and the soil are simulated by defining contact surfaces. The simulation is carried out for shield tunnels under different thrust and different contact surface friction coefficients.

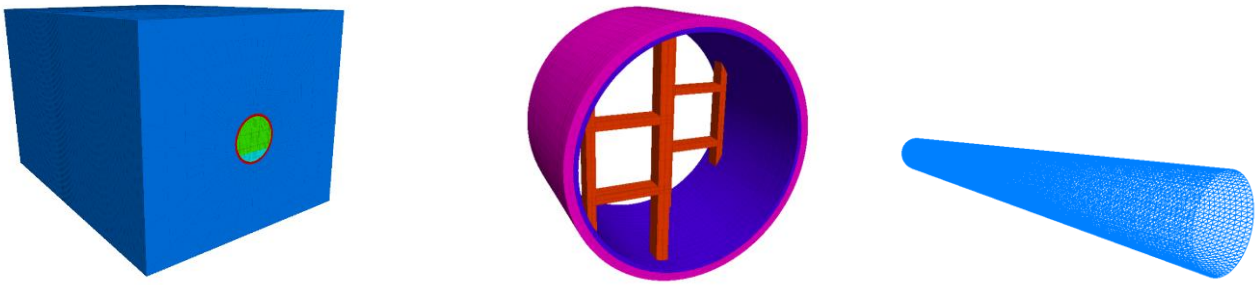

a.Soil model **b.** fixing supports model **c.** interface model

Figure 10. Calculation model

5.2 Results and analysis

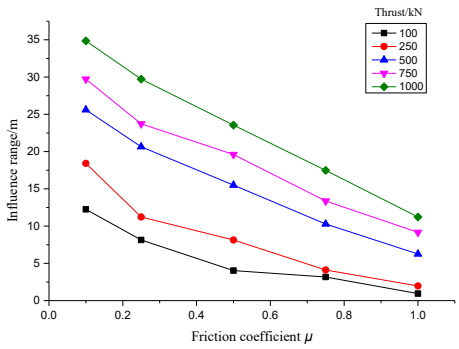

Figure 11. Relationship between thrust, friction coefficient and influence range

By simulating different operating conditions under different friction coefficient conditions and different thrusts, the resulting impact range is calculated and analyzed. The statistical results are shown in Figure 11. From the changes in the curve, we can conclude that under the same thrust, the range of thrust impact gradually decreases with the increase of the friction coefficient. At the same friction coefficient, the smaller the thrust, the smaller the range of influence on the pipe ring.

5.3 Estimation of the influence range of tunnel segments.

According to the analysis results, the range of thrust impact on the pipe segment is closely related to the frictional force between the soil and the pipe segment. Therefore, if this range can be determined at the initial design, the corresponding pipe segments can be specially treated.

In the calculation of shield tunneling jacking force, the formula for friction resistance is derived based on the balance of thrust and frictional force. Since the shield tunnel cannot be equipped with anti-slip bars like a mined tunnel, the resistance to the large thrust generated by the pipeline is entirely dependent on the frictional force between the structure and the soil, and the principles of the two are the same.

Zhu Hehua et al. [12] studied the calculation of frictional resistance based on the top thrust model experiment of shield tunnel construction. They proposed a simplified calculation method, which involves multiplying the frictional stress f (kPa) per unit area by the total outer surface area, i.e.:

$$F = L\pi Df \tag{1}$$

$$f = \mu\left(\frac{W}{\pi D} + \frac{P_v + P_h}{2}\right) \tag{2}$$

$$P_v = \gamma H \tag{3}$$

$$P_h = \gamma\left(H + D/2\right)\tan^2\left(45° - \varphi/2\right) \tag{4}$$

In the equation, F is the thrust transferred to the pipe segment (kN); D is the outer diameter of the shield tunnel (m); W is the unit length self-weight of the shield tunnel (kN/m); L is the length of the shield machine (m); γ is the unit weight of soil (kN/m3); H is the burial depth (m); φ is the angle of friction between the soil and the pipe segment; P_v and Ph are the vertical and horizontal soil pressures exerted on the outside of the shield structure, respectively. μ is the friction coefficient, which is the tangent value of the friction angle between the soil and the shield structure. However, this angle is difficult to determine, and the upper limit is usually φ, while the lower limit is $\varphi/2$ or $\varphi/3$ [12]. Stein [13] suggested that the friction angle considering the grouting effect should be between 6º and 17º. Unlike the top thrust process of the shield machine, in the operation of the engineering project, the shield segments are no longer affected by the grouting, but the soil has been disturbed. Therefore, it is recommended that $2\varphi/3$ be taken (the angle of friction between the soil and the shield casing is the arithmetic mean between the upper and lower limits).

If the thrust F is known, the length of the shield tunnel can be estimated using Equation 1. Similarly, in the case of known thrust T, the range of pipe segments affected by the thrust can be calculated. However, unlike concrete pipe segments, shield tunnels have much larger differences in stiffness and integrity. Therefore, the range of influence on the shield tunnel is greater than that of concrete pipes. To calculate the range of influence on the pipe segment, a magnification factor α needs to be multiplied to the thrust T.

$$L' = \frac{\alpha T}{\pi Df} \tag{5}$$

The value of α can be obtained by comparing the numerical simulation results with the calculation results from Equation 1. Figure 12 shows the histogram of the ratio of simulated thrust to calculated frictional resistance using Equation 1 for the same conditions (i.e., the frequency of occurrence of α values that result in the same ratio).

The ratio was found to conform well to a normal distribution through a residual Q-Q (Sample Quantiles-Theoretical Quantiles) test (Figure 13), with a mean of 22.15057 and a variance of 10.26. Therefore, the magnification factor can be determined to be 22.15.

Taking the thermal shield tunnel of Beijing Northeast Thermal Power Center as an example, at the location of ring number 2651, with an outer diameter of 6m and an average burial depth of 6.5m, the main soil is sandy soil with an average density of 1750kg/m^3 and a friction angle of 30°. Considering the effect of grouting on the surrounding soil during shield construction, 2/3 of the friction angle ($2\varphi/3$) is taken. The unit length weight of the pipe segment is 42.75kN/m, and the thrust is taken as the normal heating stage thrust value of 400kN, and is substituted into Equations (2), (3), (4), and (5). The calculated range of influence is 14.87m, which is close to the measured range of influence (16.8m).

The reason why the calculated value is smaller is because there are sliding supports set at both sides of the fixing support at

a distance of about 6m, which leads to the enlargement of the measured range of influence.

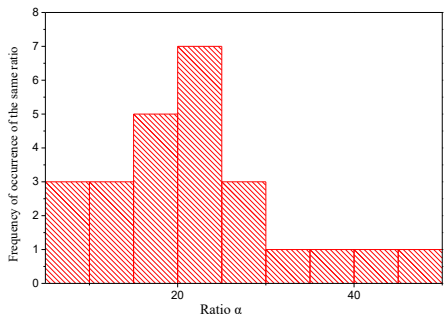

Figure 12. Histogram of frequency distribution

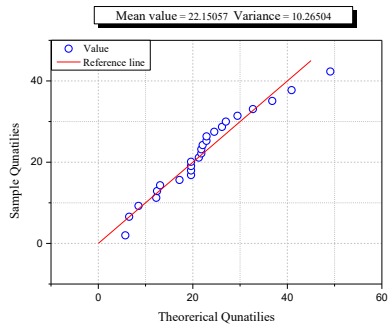

Figure 13. Q-Q figure test

6 CONCLUSION

This paper combines with the first domestic thermal shield tunnel project in the North Line of the supporting heating network of the Beijing Northeast Thermal Power Center. From the construction of the shield tunnel to the heating operation stage, internal force tests were carried out on the pipe segments at different positions (fixing support and adjacent pipe segments, orienting support, and sliding support) of the tunnel top, sidewall, and bottom. Through the analysis of the measured data and combined with numerical simulation, the following conclusions were obtained.

1. The internal forces of the pipe segments in the thermal shield tunnel are affected by the thermal pipeline, mainly in two stages: the bottom installation stage and the operation stage of the pipeline. The maximum stress of the pipe segments at the fixing support is in the operating process, which is due to the influence of the large thrust of the pipeline in the operation process.

2. In addition to the longitudinal thrust of the pipeline affecting the pipe segments at the fixing support, its range of influence also extends to the surrounding pipe segments. Through testing of the surrounding pipe segments, its range of influence on the pipe segments in this project is 14 rings.

3. Combining with engineering examples, numerical simulations were carried out on the scope of the tunnel affected by different thrust and friction coefficients. It was found that under the same thrust, the greater the friction coefficient between the pipe segments and the soil, the smaller the range of influence; under the same friction coefficient, the smaller the thrust, the smaller the range of influence.

4. Based on the relationship between the simulated friction coefficient, thrust, and range of influence and the principle of structural anti-sliding, the calculation formula of the frictional resistance in the shield thrust force was used to convert the shield length parameter, and the magnification factor was combined with the numerical simulation results. Thus, the estimation formula of the range of influence of the tunnel under the longitudinal large thrust was obtained. This formula was used to estimate the range of influence of the large thrust in the engineering example, and the result was close to the measured data, proving that the formula can provide a reference for the design of thermal shield tunnel pipe segments.

REFERENCES

[1] CJJ200-2014，Technical specification for city heat-supplying pipe net constructed by mining method[S].

[2] Dong Shu-mian. Mechanical mechanisms and design calculation methods for fixing supports of thermal pipes under huge pushing forces[J].Tunnel Consruction, 2013, 33(1):45-53

[3] Dong Xin-ping, Incermental analytical solution for failure history of a single ring of segmented tunnel lining[J]. Chinese Journal of Geotechnical Engineering, 2015, 37(1):119-125

[4] HE Chuan, ZHANG Jiang-gang, YANG Zheng. Model tests on mechanical characteristics of segment lining structure under multi-layered strata[J]. Chinese Journal of Geotechnical Engineering, 2008, 30(10):1537-1543.

[5] HUANG Hong-wei, XU Ling, YAN Jia-lu, et al. Study on transverse effective rigidity ratio of shield tunnels[J]. Chinese Journal of Geotechnical Engineering, 2006, 28(1):11-18.

[6] FENG Kun, HE Chuan, XIA Song-ling. Prototype tests on effective bending rigidity ratios of segmental lining structure for shiled tunnel with large cross-section[J]. Chinese Journal of Geotechnical Engineering, 2011, 33(11):1750-1758.

[7] LIAO Shao-ming, MEN Yan-qing, XIAO Ming-qing, et al. Field tests on longitudinal stress relaxation along shield tunnel in soft ground [J]. Chinese Journal of Geotechnical Engineering, 2017, 39(5):795-803.

[8] LI Jian-qiang. Research on the influence of shielding postures to tunnel segment force[D]. Northeastern University

[9] LI Xiao-jun, HUANG Bai-lin, ZHU He-hua, et al. Centrifugal model test of pile foundation for wind power unit under cyclic lateral

loading[J]. Engineering Mechanics,2016, 33(4):157-165.
[10] DONG Shu-mian, NIU Xiao-hua, DONG Le-yi, et al. One kind of fixing supports in thermal shield tunnel, CN104033162A [P]. 2014.
[11] DONG Shu-mian, NIU Xiao-hua, DONG Le-yi, et al. One kind of orienting supports in thermal shield tunnel, CN104033162A [P]. 2014.
[12] ZHU He-hua, XU Qian-wei, LIAO Shao-ming, et al. Experimental study on thrust force during tunnel excavation with earth pressure balance shield machine[J]. Rock and Soil Mechanics 2007, 28(8):1587-1594.
[13] Stein D, Mollers K, Bielecki R. Microtunneling[M].Berlin: Verlag Ernst & Sohn, 1989

The 18th International Symposium on District Heating and Cooling, September 3–6, 2023, Beijing, China

ACCURATE MODELING OF THERMAL LOSSES IN HEATING NETWORKS FOR EFFICIENT OPERATIONAL PLANNING

Pascal Friedrich[a*], Stefan Niessen[b], Thanh Huynh[b]

[a] *Technische Universität Darmstadt, 64289, Germany*
[b] *Siemens AG, Erlangen, 91058, Germany*
[*] *Corresponding author. pascal.friedrich@mmes.tu-darmstadt.de*

ABSTRACT

In this paper we present a simplified nonlinear modeling approach for thermal losses in heating pipes that closely approximates the behavior of models with exponential heat loss function throughout the entire operational range. Our approach enables accurate modeling of part-load operation as well as nonlinear modeling without the need to fix the direction of flow. Our approach is suited for use in district heating system models with multiple suppliers at different locations in the grid, where flow directions are not necessarily known beforehand. It can be solved with modern standard optimization algorithms. We compare our model to different common approaches using an illustrative case and discuss model quality.

Keywords: district heating, operation, thermal losses, nonlinear optimization, bidirectional flow, decentral heat supply

1. INTRODUCTION

The heating sector stands for more than half the global energy consumption while being dominated by fossil fuels [1]. Hence decarbonizing the heating sector is the major challenge towards carbon free energy supply. For densely populated areas, increasingly decentralized district heating networks (DHN) are expected to play a key role in providing emission free heat efficiently [2,3].

Efficient operation can be greatly supported by operational planning with numerical optimization [4]. The behavior of DHN can be described by nonlinear models, which often find use in system analysis with simulation environments [5–9]. For the use in operational planning, nonlinear models remain difficult to solve and are often approximated by simplified approaches [10–12]. In part-load operation, e.g. in summer, thermal losses in DHN account for up to 60% [13]. With energetic renovation of supplied buildings, network heat losses become even more important [13]. Nonlinear effects are particularly strong in part-load operation, so that optimization with linearized models becomes a challenge.

In decentral operated heating systems with flexible operation scheduling, water does not necessarily flow through every pipe at every point in time and so modeling temporary standstill of water becomes relevant. In models with decentral supply, the flow direction in a pipe might not always be known, as shown in Figure 1. Modelling a pipe in such a way that it realistically represents bidirectional flows as well as hydraulic and thermal behavior can be a major challenge.

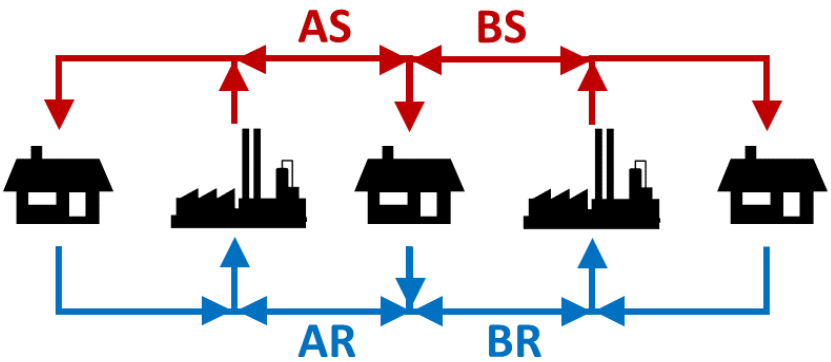

Figure 1: Small example network with decentral supply. Flow direction in pipes AS, BS, AR and BR are not known prior to an optimization of the operation.

In this paper we discuss different approaches to model thermal losses in DHN concerning model errors in both full load and part load operation. We show that standstill of water can lead to problems in some cases and introduce an approach that closely approximates the nonlinear properties over the whole operating range. In our approach, standstill can be modeled without risking infeasibility, enabling bidirectional modelling.

Our approach works with modern off-the-shelf optimization algorithms. Neither expert knowledge about likely operation points nor tight variable bounds are needed prior to the optimization.

The paper is structured as follows: In the second section of the paper, we explain the requirements of bidirectional thermal pipe modeling for decentral district heating systems. In the third section, we briefly introduce the standard exponential modeling approach and two approximations discussed in literature. In part four, we introduce our new approach. We then discuss the quality and restrictions of different approaches using a simple illustrative case in Section 5 and conclude in Section 6.

2. THERMAL MODELLING OF BIDIRECTIONAL PIPES

Temperature drops over the course of a thermal pipe depend on the flow direction. A possible approach to model this physical property is by splitting one bidirectional pipe p into two unidirectional pipes i and j.

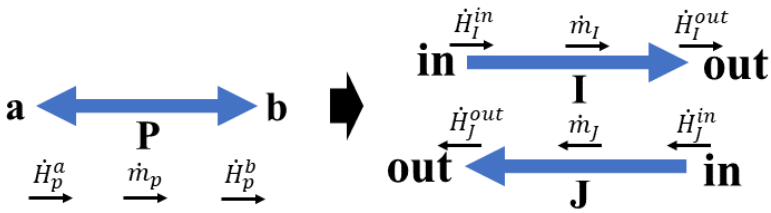

Figure 2: Modeling one bidirectional pipe P by splitting it into two unidirectional pipes I and J. Black arrows under $\dot{m}$ and $\dot{H}$ indicate direction of positive flow. Blue arrows indicate possible flow direction.

Both I and J are via a big-M approach with two binary variables b_i, indicating activity of one unidirectional pipe. Only one of both pipes can be active at a time, forcing a standstill in the counterpart. Both pipes allow mass flow $\dot{m}$ in only one direction.

$$0 \leq \dot{m}_i \leq b_i M \quad \forall\, i \in \{I, J\}, b \in \{0,1\}, M \gg \dot{m}_i \tag{1}$$

$$b_J + b_I = 1 \tag{2}$$

For mass flow, a simple balance holds:

$$\dot{m}_p = \dot{m}_I - \dot{m}_J \tag{3}$$

Energy flowing through of a pipe can be modeled by introducing a flow of enthalpy $\dot{H}$, coupling $\dot{m}$ and temperature T via thermal capacity c_p of the fluid:

$$\dot{H} = c_p \dot{m}\, T \tag{4}$$

Note that c_p is assumed to be constant.
The energy balance of the bidirectional pipe can be calculated by combining enthalpy flows of the two unidirectional pipes:

$$\dot{H}_p^a = \dot{H}_I^{in} - \dot{H}_J^{out} \tag{5}$$

$$\dot{H}_p^b = \dot{H}_I^{out} - \dot{H}_J^{in} \tag{6}$$

T^a and T^b are given by combining (3), (4) and (5) resp. (6).
We now want to find a function $T_i^{out} = f(\dot{m}_i, T_i^{in})$ that satisfies following requirements:

- Closely approximating nonlinear behavior over the whole range of $\dot{m}_i$, including 0
- Not causing numerical problems e.g. by divergence, for any possible value of $\dot{m}_i$, including 0
- Solvability to global optimum with reliable standard solvers

3. COMMON MODELLING APPROACHES OF THERMAL LOSSES

In this Section, we present different modeling approaches provided in the literature. In the following, the thermal loss coefficient of the pipe U, the pipe length L, the ambient temperature T^a and the specific heat capacity of water c_p are assumed to be constant.

2.1. Multi variate exponential approach

A standard approach to model heat losses of a fluid flowing through in insulated pipe is given by (22) by modeling outlet temperature T^{out} as a function of the inlet temperature T^{in} and mass flow $\dot{m}$. T^{out} depends on the T^a, c_p, as well as U and L.

$$T^{out} = (T^{in} - T^a)e^{\frac{\dot{m}^{char}}{\dot{m}}} + T^a \tag{7}$$

$$\text{with } \dot{m}^{char} = \frac{LU}{c_p} \tag{8}$$

This is a multi-variate exponential term, which is a great challenge to for standard optimization solvers if global optimality is requested. Nonetheless, similar approaches find frequent use in simulation frameworks such as Modelica [9]. This approach is referred to in the following as *EXP*.

With (7) heat loss $\dot{Q}^{loss}$ can be calculated as

$$\dot{Q}^{loss} = c_p \dot{m}(T^{in} - T^{out}). \tag{9}$$

2.2. Linear approximation via first order Taylor series

(7) can be linearized by a Taylor series of first order. The assumption $\dot{m} \gg \dot{m}^{char}$ [12,14–16] leads to the expression as shown in (22). This approach is referred to in the following as *APRXA*.

$$T^{out} \approx T^{in} - \frac{\dot{m}^{char}}{\dot{m}_0^2}(T^{in} - T^a)(\dot{m} - \dot{m}_0) \tag{10}$$

2.2. Approximation via simplifying exponential term

Under the assumption $\dot{m} \gg \dot{m}^{char}$, we approximate the exponential term in (7) following

$$\lim_{x \to x_0} \exp(-x) = 1 - x. \tag{11}$$

(7) becomes

$$T^{out} \approx T^{in}\left(1 - \frac{\dot{m}^{char}}{\dot{m}}\right) + \mathrm{T}^{\mathrm{a}}\frac{\dot{m}^{char}}{\dot{m}}. \tag{12}$$

This approximation leads to the approach proposed in [12]. The authors develop an optimization model for operational planning in district heating networks. Mixing of water flows at junctions of multiple pipes and thermal losses are considered in the model, for details consider [12]. The authors aim to minimize the number of bilinear terms (terms of the form $z =$

$x * y$) in the model to speed up computation time, by using enthalpy flow $\dot{H}$.

By inserting (4) and (8) in (12), we can transform (12) to the approximation of thermal losses presented by [12]:

$$\dot{H}^{out} = \dot{H}^{in} - \mathrm{U\,L}\,(T^{in} - T^{a}). \tag{13}$$

(22) depicts an energy balance over the pipe, so that losses can easily be calculated:

$$\dot{Q}^{loss} = \dot{H}^{in} - \dot{H}^{out} = UL(T^{in} - T^{a}). \tag{14}$$

Physically speaking, this approach supposes that the temperature difference between the fluid and the ambient, causing heat losses, is constant across the pipe length. The approach is equal to that used in the classic design of district heating networks [17,18], where constant water temperature is the main assumption while approximating heat losses.

This approach is referred to in the following as *APRXB*.

2.2. Neglecting influence of ambient temperature

Further simplification of (12) is possible by neglecting the influence of T^{a}:

$$T^{out} \approx T^{in}\left(1 - \frac{\dot{m}^{char}}{\dot{m}}\right). \tag{15}$$

We can show that this leads to the approach to model thermal losses that has been presented by [10], which has been adapted in following works such as [11,19]. We introduce transit time τ and τ^{char}, which can be used to substitute $\dot{m}$ and $\dot{m}^{char}$ considering pipe cross-Section A and water density ρ:

$$\tau = \frac{\rho L A}{\dot{m}} \tag{16}$$

$$\tau^{char} = \frac{A \rho c_p}{U} \tag{17}$$

$$\frac{\tau}{\tau^{char}} = \frac{\dot{m}^{char}}{\dot{m}} \tag{18}$$

(15) can therefore be written as follows, equivalent to the approach by [10]:

$$T^{out} \approx T^{in}\left(1 - \frac{\tau}{\tau^{char}}\right). \tag{19}$$

This approach is referred to in the following as *APRXC.*

4. PROPOSED MODELLING APPROACH

In this Section, our new approach is presented. First, we analyze the results of outlet temperatures for all models shown in Section 2. We then develop the new modeling approach.

4.1. Analysis of outlet temperatures and thermal losses

With approaches *EXP*, *APRXA*, *APRXB* and *APRXC*, outflowing temperatures can be calculated. For *APRXA*, a point of interest $\dot{m}_0$ must be chosen, around which the linearization takes place.

Figure 3 shows that the upper bound of $\dot{m}$ should be chosen as $\dot{m}_0$: Otherwise, for mass flows $\dot{m} > \dot{m}_0$, the resulting tangent of a Taylor approximation T^{out} would exceed T^{in}, which would represent a nonphysical energy gain. With a high $\dot{m}_0$ thermal losses are heavily underestimated, see Figure 3 and Figure 5.

If no tight boundaries for $\dot{m}$ are known in operational planning, *APRXA* results in nearly constant T^{out} and very low energy losses.

APRXB and *APRXC* show a much better approximation to the reference model *EXP*, see Figure 4. Both approaches result in

diverging T^{out} for $\dot{m}$ close to zero, which can lead to problems in numerical optimization:

$$\lim_{\dot{m}\to 0} T^{in}\left(1-\frac{\dot{m}^{char}}{\dot{m}}\right)+\mathrm{T}^{\mathrm{a}}\frac{\dot{m}^{char}}{\dot{m}}=-\infty\ \forall\, T^{in}>T^{a} \tag{20}$$

$$\lim_{\dot{m}\to 0} T^{in}\left(1-\frac{\dot{m}^{char}}{\dot{m}}\right)+\mathrm{T}^{\mathrm{a}}\frac{\dot{m}^{char}}{\dot{m}}=\infty\quad \forall\, T^{in}<T^{a} \tag{21}$$

$$\lim_{\dot{m}\to 0} T^{in}\left(1-\frac{\dot{m}^{char}}{\dot{m}}\right)=-\infty \tag{22}$$

This might lead to problems in some model formulations: Standstill in a sub-pipe i of a bidirectional pipe p modeled with *APRXB* or *APRXC* as introduced in Section 2 would cause an unbounded variable T_i^{out}.

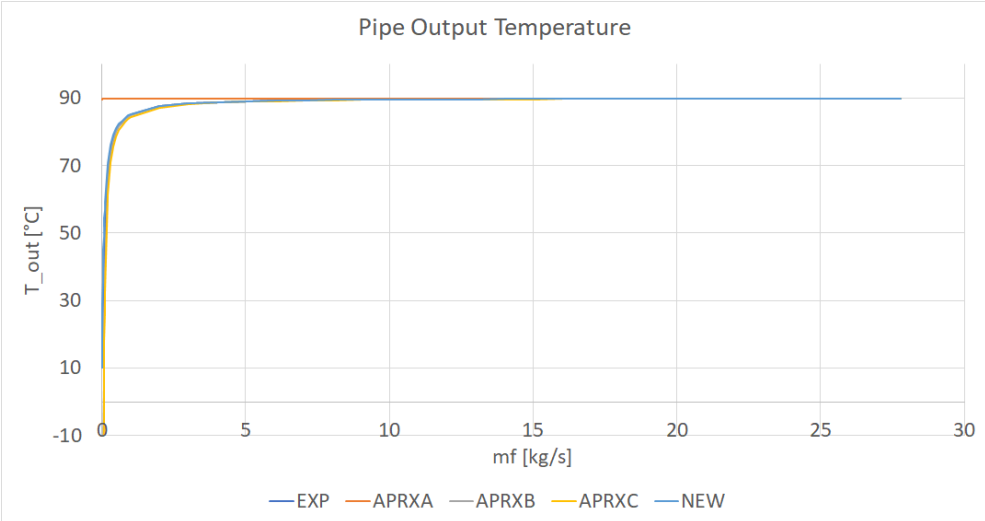

Figure 3: Output temperature of an exemplary district heating pipe with different modeling approaches. $T^{in} = 90°C$, $T^{a} = 10\ °C$. Pipe specifications in annex.

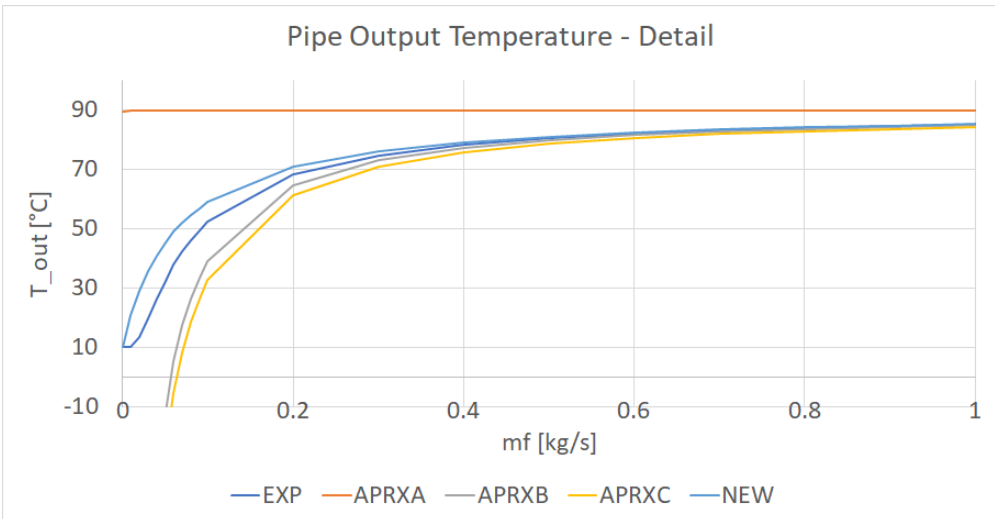

Figure 4: Detailed view for small mass flow of output temperature of an exemplary district heating pipe with different modeling approaches. $T_{in} = 90°C$, $T_a = 10°C$. Pipe specifications in annex.

Figure 5 shows that some approaches result in constant heat losses, while *APRXC* significantly overestimates the losses over the whole operation range. Constant heat losses explain the resulting negative temperatures at low mass flow in Figure 4.

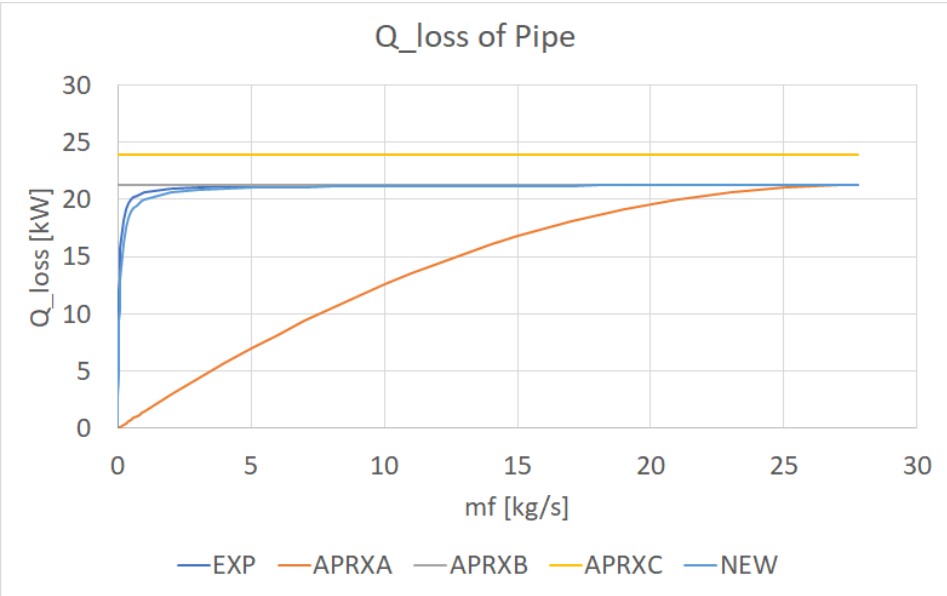

Figure 5: Thermal losses of an exemplary district heating pipe with different modeling approaches. $T_{in} = 90°C$, $T_a = 10°C$. Pipe specifications in annex.

4.2. New modeling approach

APRXB and *APRXC* show very similar behavior, with better approximation than *APRXA*. As the difference in both approaches is a computationally inexpensive linear term, *APRXB* forms the starting point for further developments.

Comparing *APRCB* and *EXP* in Figure 3, T^{out} has an almost horizontal course for high mass flow, and significant underestimation for low mass flow. At mass flow of $\dot{m}^{krit}$ and lower, T^{out} falls to non-physical negative values. An approach to correct T^{out} is to shift the curve associated with *APRXB* to the left by the value of $\dot{m}^{krit}$. To calculate $\dot{m}^{krit}$, we set T^{out} to T^a in (9) and (14) and equate both expressions, which leads to:

$$\dot{m}^{krit} = \frac{T^{earth} - T^{in}}{T^{earth} - T^{in}} * \frac{UL}{c_p} = \frac{UL}{c_p} = \dot{m}^{char} \tag{23}$$

It shows that $\dot{m}^{krit}$ equals $\dot{m}^{char}$, a term constant for all $T^{in}$and $\dot{m}$. (14) and (12) can now be corrected, which result in model *NEW*:

$$\dot{H}^{in} - \dot{H}^{out} = U\,L\,(T^{in} - T^a) + c_p\,\dot{m}^{char}(T^{in} - T^{out}) \tag{24}$$

With (4), this leads to a closed expression for T^{out}:

$$T^{out} = \frac{T^{in}\frac{\dot{m}}{\dot{m}^{char}} + T^a}{1 + \frac{\dot{m}}{\dot{m}^{char}}}. \tag{25}$$

This approximation closely follows *EXP* over the whole operation range and results in $T^{out} = T^a$ for $\dot{m} = 0$, see Figure 4. When both $\dot{m}$ and T^{in} are variables, (24) is of bilinear type. This type of equation can be solved by modern solvers such as *Gurobi 10.0.0* [20] to global optimality without dependency on starting points. (24) can be used to refine the optimization model proposed by [12]. For further speed up, [12,14,21] describe iterative solution methods for bilinear models.

5. MODEL ERROR ANALYSIS IN AN ILLUSTRATIVE CASE

In this Section, we compare the results obtained with the approaches presented in Section 3 and 4 when applied to a small use case. We discuss the results with regard to energetic efficiency and compliance with temperature requirements of consumers both for a full-load and part-load operation as well as an effect of standstill in pipes. We only analyze model errors, so a system with known mass flow direction is used. All temperatures are restricted to positive values.

We use SCIP 6.0.0 to solve systems using approach *EXP,* which can find a solution of with a well estimated starting point. For all other discussed approaches, we use Gurobi 10.0.0., which can solve quadratic and bilinear systems as well as treating binary variables [20].

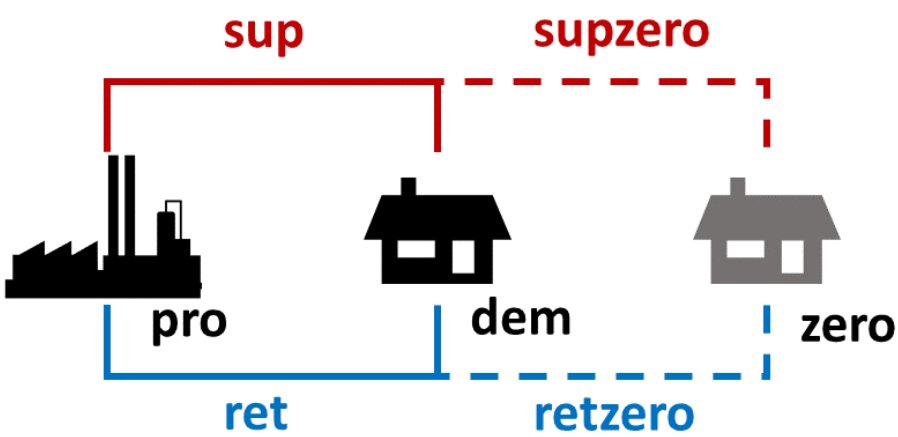

Figure 6: Small use case with one producer *pro*, one active consumer *dem* and one optional consumer without demand *zero*. Note that pipes *supzero* and *retzero* and consumer *zero* only occur in Section 4.2

5.1. Model errors in operation

First, we evaluate a case where one consumer *dem* is supplied by one heat station *pro*. Both are connected via a pair of pipes, as shown in Figure 6. First, we analyze a high load scenario *Winter* and a partial load scenario *Summer*. Detailed specifications are found in the annex. Target temperatures for both seasons are chosen according to the analysis of a real district heating network presented in [13]. Demand $\dot{Q}_{dem}$ is chosen so that following constraints are fulfilled:

- Winter: The resulting mass flow meets exactly nominal mass flow $\dot{m}^{nom}$ specified by the pipe vendor (Table 8) with model EXP.
- *Summer*: Cumulated heat losses amount to 60% of produced heat with model *EXP*.

Table 1: *Winter* scenario specifications

$\dot{m}_{dem}$ $(\frac{kg}{s})$ with *EXP*	$\dot{Q}_{dem}$ (kW)	$T_{dem}^{in,min}$ $(°C)$	T_{dem}^{out} $(°C)$	T^{a} $(°C)$
23.61	3422	90	55	7

Table 2: *Summer* scenario specifications

$\dot{Q}^{loss}/\dot{Q}_{pro}$ with *EXP*	$\dot{Q}_{dem}$ (kW)	$T_{dem}^{in,min}$ $(°C)$	T_{dem}^{out} $(°C)$	T^{a} $(°C)$
0.6	19.36	78.23[a]	70.23[a]	7

We use each model approach discussed in Sections 3 and 4 to calculate produced heat and output temperatures at production so that the constraints defined in Table 1 and Table 2 are met, see Table 3 and Table 4, and heat production is minimized for *Winter* and maximized for *Summer* (to avoid a trivial solution). To evaluate whether temperature requirements of each schedule would be met in the reference system *EXP*, we recompute the system and check actual input temperature at *dem* $T_{dem,act}^{in}$ with model *EXP* with the determined operation points, see Table 5 and Table 6.

Comparing $\dot{Q}_{pro}$ for all approximate approaches with approach *EXP*, we can see that all modeling approaches except *APRXA* manage to schedule a sufficient amount of heat production, with a minor overproduction by approach *APRC* (Table 3, Table 4). This behavior matches the observations made in Section 4, with *APRXA* underestimating and *APRXC* overestimating thermal losses. Table 5 shows a corresponding temperature deviation for *APRXA*.

In *Summer*, model errors become more significant. *APRXA* and *APRXC* show significant deviations in $\dot{Q}_{pro}$ (Table 4) and T_{dem}^{in} (Table 6).

[a] Calculated with model EXP according to temperatures at production $T_{pro}^{in} = 65°C$ resp. $T_{pro}^{out} = 85°C$, as presented in [13]

Table 3: Operation points in *Winter*

Value	*APRXA*	*APRXB*	*APRXC*	*NEW*	*EXP*
$\dot{Q}_{pro}$ (kW)	3460	3492	3495	3492	3492
T_{pro}^{out} $(°C)$	90.03	90.22	90.24	90.22	90.22
T_{pro}^{in} $(°C)$	54.98	54.87	54.85	54.87	54.87

Table 4: Operation points in *Summer*

Value	*APRXA*	*APRXB*	*APRXC*	*NEW*	*EXP*
$\dot{Q}_{pro}$ (kW)	19.96	50.14	61.45	46.9	48.4
T_{pro}^{out} $(°C)$	78.36	85.43	87.9	84.63	85
T_{pro}^{in} $(°C)$	70.12	64.71	62.51	65.25	65

5.2. Model errors at standstill

The effect of stand still is demonstrated in case *Standstill*. It is an extended version of scenario *Winter*.

Two consumers *dem* and *zero* are supplied by one heating station, see Figure 6. Temperatures are constrained to non-negative values to avoid divergence. Consumer *zero* has no heat demand at the evaluated timestep. Mixing at junctions is modeled via enthalpy- and mass-balance as described in [12]. Temperature propagation at junctions is explicitly modeled as well, see [12].

Table 5: Temperature validation in *Winter*

Value	*APRXA*	*APRXB*	*APRXC*	*NEW*	*EXP*
$T_{dem,act}^{in}$	89.8	90	90.02	90	90

Table 6: Temperature validation in *Summer*

Value	*APRXA*	*APRXB*	*APRXC*	*NEW*	*EXP*
$T_{dem,act}^{in}$	72.29	78.61	80.83	77.9	78.23

With approaches *APRXB* and *APRXC*, a small mass flow must flow through pipe *supzero* and *retzero* to avoid negative temperatures and therefore infeasibility. To fulfill the condition of no heat power at consumer *zero*, either no temperature difference or no mass flow over the edge *zero* must occur. Both *APRXB* and *APRXC* result in the smallest feasible mass flow over *supzero* and *retzero* to minimize losses over the pipes. A modelling of true standstill not possible with approaches *APRXB* and *APRXC*. Still, this leaking mass flow causes additional losses of about $35\,kW$ to $39\,kW$ in both models, on top of the model errors discussed in 5.1. *NEW* allows to compute a realistic system state. At standstill, water temperature mus fall to ambient temperature: $T_0^{in} = 7°C$. A modelling of true standstill necessary for bidirectional models as stated in Section 2 is not possible with approaches *APRXB* and *APRXC*.

Table 7: System state at consumer *zero* in scenario *Standstill*

Value	*APRXA*	*APRXB*	*APRXC*	*NEW*	*EXP*
T_{zero}^{in} $(°C)$	89.83	55	55	7	7
T_{zero}^{out} $(°C)$	55	55	55	55	55
$\dot{m}_{zero}$ (kg/s)	0	0.0636	0.0636	0	0
$\dot{Q}_{supzero}^{loss}$ (kW)	0	22.15	24.02	0	0
$\dot{Q}_{retzero}^{loss}$ (kW)	0	12.77	14.64	0	0
$\dot{Q}_{pro}$ (kW)	3460.69	3526.47	3533.94	3491.45	3491.5

7. CONCLUSION AND OUTLOOK

We have discussed several approaches to model heat losses in operational optimization models. We could show that linear modeling of losses *APRXA* show significant deviations from the reference model *EXP*. We showed that bilinear approximations of show satisfying results to schedule heat production and meet temperature requirements at customers, while being less challenging so solve than the original multi variate exponential approach. We introduced a new bilinear approach *NEW*, which allows accurate modeling, so that realistic system states can be calculated even for pipes with no mass flow, enabling accurate bidirectional nonlinear modeling for numerical optimization with standard solvers such as Gurobi 10.0.0.

ACKNOWLEDGEMENT

This paper was written as part of the project EnEffWärme:MeFlexWärme, funded by the Federal Ministry of Economics and Climate Protection of the Federal Republic of Germany (Bundesministerium für Wirtschaft und Klimaschutz).

Special thanks go to my colleagues at the Energy Information Networks & Systems Lab of the Technical University of Darmstadt, especially to Andreas Bott and Julia Barbosa for fruitful exchanges on just about every topic.

ANNEX

Table 8: Pipe specifications

Nominal Diameter	$\boldsymbol{U}$ $(\boldsymbol{W/m.K})$[b]	$\boldsymbol{L}$ $(\boldsymbol{m})$	$\dot{\boldsymbol{m}}^{\boldsymbol{max}}(\boldsymbol{kg/s})$[b]	$\dot{\boldsymbol{m}}^{\boldsymbol{nom}}$ $(\boldsymbol{kg/s})$[b]
DN150	0.3369	790	27.29	23.61

REFERENCES

[1] IEA, Renewables 2022, IEA, Paris, 2022.

[2] H. Lund, B. Möller, B.V. Mathiesen, A. Dyrelund, The role of district heating in future renewable energy systems, Energy 35 (2010) 1381–1390. https://doi.org/10.1016/j.energy.2009.11.023.

[3] J. Burchardt, Klimapfade 2.0: Ein Wirtschaftsprogramm für Klima und Zukunft Gutachten für den BDI [Bundesverband der Deutschen Industrie, Boston Consulting Group GmbH, München, 2021.

[4] Optimization in the energy industry, Springer, Berlin, 2009.

[5] Michael Wetter, Christoph van Treeck, IEA EBC Annex 60: New Generation Computing Tools for Building and Community Energy Systems, 2017.

[6] K. Hinkelman, S. Anbarasu, M. Wetter, A. Gautier, W. Zuo, A fast and accurate modeling approach for water and

[b] Taken from [18], standard insulated pipe

steam thermodynamics with practical applications in district heating system simulation, Energy 254 (2022) 124227. https://doi.org/10.1016/j.energy.2022.124227.

[7] K. Hinkelman, J. Wang, W. Zuo, A. Gautier, M. Wetter, C. Fan, N. Long, Modelica-based modeling and simulation of district cooling systems: A case study, Applied Energy 311 (2022) 118654. https://doi.org/10.1016/j.apenergy.2022.118654.

[8] A. Maccarini, A. Sotnikov, T. Sommer, M. Wetter, M. Sulzer, A. Afshari, Influence of building heat distribution temperatures on the energy performance and sizing of 5th generation district heating and cooling networks, Energy 275 (2023) 127457. https://doi.org/10.1016/j.energy.2023.127457.

[9] Rickard Hägg, Dynamic Simulation of District Heating Networks in Dymola, Department of Energy Science, Lund, 2016.

[10] G. Sandou, S. Font, S. Tebbani, A. Hiret, C. Mondon, Predictive Control of a Complex District Heating Network, in: Proceedings of the 44th IEEE Conference on Decision and Control, IEEE, 2005, pp. 7372–7377.

[11] L. Mitridati, J.A. Taylor, Power Systems Flexibility from District Heating Networks, in: 20th Power Systems Computation Conference, IEEE, Piscataway, NJ, 2018, pp. 1–7.

[12] L. Deng, H. Sun, B. Li, Y. Sun, T. Yang, X. Zhang, Optimal Operation of Integrated Heat and Electricity Systems: A Tightening McCormick Approach, Engineering 7 (2021) 1076–1086. https://doi.org/10.1016/j.eng.2021.06.006.

[13] J.J. Oltmanns, Analysis and Improvement of an Existing University District Energy System, Universitäts- und Landesbibliothek, Darmstadt, 2021.

[14] P.M. Castro, Tightening piecewise McCormick relaxations for bilinear problems, Computers & Chemical Engineering 72 (2015) 300–311. https://doi.org/10.1016/j.compchemeng.2014.03.025.

[15] S. Lu, W. Gu, C. Zhang, K. Meng, Z. Dong, Hydraulic-Thermal Cooperative Optimization of Integrated Energy Systems: A Convex Optimization Approach, IEEE Transactions on Smart Grid 11 (2020) 4818–4832. https://doi.org/10.1109/TSG.2020.3003399.

[16] S. Huang, W. Tang, Q. Wu, C. Li, Network constrained economic dispatch of integrated heat and electricity systems through mixed integer conic programming, Energy 179 (2019) 464–474. https://doi.org/10.1016/j.energy.2019.05.041.

[17] QM Fernwärme, Planungshandbuch Fernwärme, 1st ed., EnergieSchweiz Bundesamt für Energie BFE, Ittigen, 2021.

[18] isoplus Fernwärmetechnik GmbH, Planungshandbuch, 6th ed., Sondershausen, 2011.

[19] Anna Schwele, Integration of Electricity, Natural Gas and Heat Systems With Market-based Coordination. Dissertation % This file was created with Citavi 6.4.0.35, 2020.

[20] H. Nagarajan, M. Lu, E. Yamangil, R. Bent, Tightening McCormick Relaxations for Nonlinear Programs via Dynamic Multivariate Partitioning, in: M. Rueher (Ed.), Principles and Practice of Constraint Programming, Springer International Publishing, Cham, 2016, pp. 369–387.

[21] L.L.C. Gurobi Optimization, Gurobi Optimizer Reference Manual: Version 10.0, https://www.gurobi.com/documentation/10.0/refman/refman.html.

The 18th International Symposium on District Heating and Cooling, September 3–6, 2023, Beijing, China

ASSESSING MACHINE LEARNING ALGORITHMS FOR LEAK DETECTION IN SMART DISTRICT HEATING NETWORKS

Mohammed Ali Jallal[a*], Mathieu Vallée[a], Yacine Gaoua[a], Thibaut Wissocq[a], Nicolas Lamaison[a]

[a] *Univ. Grenoble Alpes, CEA, Liten, Campus Ines, 73375 Le Bourget du Lac, France*

[*] *Corresponding author. mohammed-ali.jallal@cea.fr*

ABSTRACT

This paper presents a comprehensive evaluation of six machine learning algorithms, including artificial neural network (ANN), support vector machines (SVM), decision trees (DT), random forests (RF), Extreme Gradient Boosting (XGboost), and Naïve Bayes (NB), for detecting small and large leaks in district heating networks (DHN). The methodology employed in this study utilizes a comprehensive dataset encompassing network topology, temperatures, consumer demands, and pressure differentials. This dataset consists of 23 features, and it boasts an impressive number of samples, with a total of 9,009,630 samples for each feature. A simple network model from the CEA internal DistrictHeating library is utilized to simulate network faults, incorporating hydraulic fluid loss and insulation degradation. The results indicate that the random forests algorithm achieved remarkable accuracy rates of 98.38% during training and 97.99% during testing, demonstrating high precision and recall. Decision trees exhibited high accuracy but a slight potential for overlearning. The ANN algorithm demonstrated consistent and balanced performance across all metrics. XGBoost showed potential overlearning but maintained good recall rates. SVM and NB had lower overall performance. The findings highlight the random forests algorithm as the top performer, aiding in the selection of suitable machine learning algorithms for leak detection in DHN. Automating leak detection using these algorithms minimizes heat loss, improves energy efficiency, and reduces maintenance costs. Continuous monitoring and real-time detection enable proactive maintenance strategies, preventing heat supply disruptions and optimizing system performance.

Keywords: District heating networks, leak detection, machine learning algorithms, district heating system simulation.

1. INTRODUCTION

District heating and cooling systems, also referred to as district energy systems, efficiently distribute thermal energy for heating and/or cooling purposes across multiple buildings or sites within a district using insulated pipes. These systems are designed to be energy-efficient by utilizing waste heat from various sources, such as industrial processes, power production, or renewable energy sources. However, these complex systems may encounter a variety of issues that compromise their reliability and efficiency, including pipe leaks, heat exchanger failures, energy supply interruptions, and more. Therefore, regular monitoring, maintenance, and troubleshooting are necessary to ensure dependable and efficient operation.

Among these issues, pipe leaks are a significant concern in district heating and cooling systems and can occur due to various factors, such as corrosion, wear and tear, ground movement, joint failures, material degradation, and external damage [1]. These leaks can cause heat or cooling loss, decreased efficiency, increased energy consumption, and service disruptions. To mitigate the risk of pipe leaks, regular inspections, preventive maintenance, and prompt repair or replacement of damaged pipes are necessary.

To detect and address pipe leaks in district energy systems, two methods are commonly used, hardware-based and software-based. Hardware-based methods use sensors or meters to monitor flow rates, pressure levels, temperature profiles, abnormal sounds, or vibrations [2]. In contrast, software-based methods use data analytics, modeling, and simulation to predict system behavior and remote control and monitoring platforms for real-time information dissemination and triggering of alerts or notifications [3]. However, these methods have some limitations, such as false alarms, data interpretation challenges, and cost concerns. To address these gaps, several measures are recommended, including improvements in sensor technology, algorithm refinement, expansion of sensor coverage, utilization of automated decision-making algorithms, integration of expert knowledge, and meticulous planning, and technology selection. Furthermore, regular monitoring, maintenance, and continuous improvement of leak detection methods are essential in optimizing their performance and effectiveness in identifying pipe leaks in district energy systems.

A limited number of studies have investigated the detection and localization of leakage faults in district heating systems,

utilizing different approaches and sources of data. One approach is based on the propagation of pressure waves that occur as an initial reaction to the occurrence of a leakage [4]. This approach involves recognizing the leakage entry based on measurement data, evaluating pressure measurement data to find the time at which pressures dropped due to leakage, and using theoretical wave propagation calculations to attribute the leakage to the exclusion area where the wave propagation fits best. Another approach is a machine learning-based method that uses simulated network models and training data to train machine learning models for leakage localization [5]. This approach utilizes operational data such as pressure and flow rate measurements for training and can provide real-time results for leakage localization. Pierl et al. proposed a method that combines model-based numeric-analytical techniques with sensor data from the actual network to locate leaks [6]. This approach involves comparing and contrasting three different methods, including pressure wave detection, model-based numeric-analytical, and machine learning approaches, to exploit different properties of simulation models and sensor information for leakage localization. Manservigi et al. [7] and Bahlawan et al. [8] both describe an approach that couples a DHN simulation model with an optimization algorithm for detecting and identifying thermal and hydraulic faults. This approach provides outstanding performance on the presented case study, however it is limited by the availability and accuracy of the model input parameters. Additionally, some studies investigate optimal sensor placement and the influence of noise on pressure wave evaluation for leakage localization in district heating networks (DHNs) [9]. These studies focus on identifying the optimal locations for sensors in the network and evaluating the impact of measurement noise on the accuracy of pressure wave-based leakage localization.

Other studies have utilized sensors and observation data, data analytics tools, and remote sensing techniques for leakage fault detection in district heating systems. One study proposed a machine learning-based leakage fault detection (LFD) method that utilized variation rates of observation data from installed flowmeters and pressure sensors [3]. Another study focused on developing methods for district heating leakage measurement, which included pressure measurements and direct measurement of water loss using fixed metering devices [2]. One study used an object-oriented program to construct a DHN representation and combined it with sensor data to calculate residual values, and Bayesian Network was then used to determine the possibility of different operating outcomes [10]. In another study, a saliency analysis method was proposed for leakage detection in district heating systems using remotely sensed infrared imagery, visible imagery, and geographic information system (GIS) data [11]. A different approach was proposed in a study that used unmanned aerial vehicle (UAV) image analysis for leakage detection in district heating systems [12].

These studies highlight the importance of fast and accurate leakage detection and localization in DHNs to prevent energy losses, maintain network stability, and minimize shutdowns. Different approaches, including pressure wave detection, model-based numeric-analytical methods, and machine learning, are being explored and evaluated using real network data to improve the effectiveness and efficiency of leakage detection and localization in DHNs. Further research and development in this area may lead to improved methods for identifying and localizing leaks in real-time, resulting in more reliable and efficient operation of district heating networks. It is worth mentioning that while some of the studies mentioned in both sections have used machine learning (ML) and other forms of artificial intelligence (AI), there does not seem to be any large-scale research specifically focused on using AI for pipeline leak detection in heating and cooling networks. This could be an area for future research and development, as AI has shown great promise in other industries and could potentially improve the accuracy and efficiency of leak detection in district heating and cooling systems.

The objective of this study is to evaluate the efficiency of prominent ML algorithms, namely deep neural network, decision trees, random forests, extreme gradient boosting, naïve bias, and support vector machine, in detecting leakages in DHNs. These algorithms have demonstrated remarkable performance across various industries, making their evaluation in the context of district heating and cooling systems significant. The outcomes of this research contribute to the knowledge base of academic researchers and industrial engineers specializing in the digitalization of district heating and cooling systems. The findings provide valuable insights into the effectiveness of different ML algorithms for detecting leakage faults. This information guides the development of cost-effective smart detection techniques, offering practical solutions to identify and address leakages in heating and cooling networks.

Academic researchers can leverage the insights from this study to advance their understanding of the applicability of machine learning algorithms in district heating and cooling systems. Industrial engineers can utilize the research findings to inform their decision-making processes and develop efficient strategies for implementing leak detection technologies in real-world scenarios. Ultimately, the aim is to enhance the reliability and sustainability of district heating and cooling systems by effectively detecting and mitigating leakage faults using state-of-the-art machine learning approaches.

2. METHODOLOGY

2.1. District Heating Network Model Presentation

For a representative yet not too complex simulation of DHN faults, we used a linear network model available in the DistrictHeating library [13], developed internally at CEA. Figure 1 presents a schematic view of this model. It is composed of a thermal plant providing heat to a number of consumer N_c, placed linearly along the network (no branches, equal distance between consumers). The plant and consumer 1 are considered to be connected at the same location. The diameters for the different sections are calculated so that the nominal velocity is 2m/s and the pressure gradient is constant. The DHN supply temperature $T_{s,DHN}$ is calculated based on an expert law as a function of the external temperature. The plant pump imposes a differential pressure ΔP so that consumer N_c always has a local differential pressure $\Delta P[N_c]$ equal to a given setpoint ΔP_{sp}. The secondary side return temperature $T_{IN,s}[c]$ and supply temperature set point $T_{OUT,s,SP}[c]$ at each consumer are considered known. The demand at each consumer $Q_{dem}[c]$ is defined by distributing a global demand $Q_{dem,DHN}$ among all consumers. The normalized distribution weights w_c, defined in Equation (1), can be fixed or computed randomly dynamically.

$$Q_{dem}[c] = w_c \cdot Q_{dem,DHN}, \forall \ c \in [1: N_c], \tag{1}$$

The desired mass flow rate $\dot{m}_{dem}[c]$ at each consumer is calculated so that the local demand $Q_{dem}[c]$ is satisfied depending on the secondary side temperatures, the local primary side supply temperature $T_s[c]$ (affected by heat losses) and the local differential pressure $\Delta P[N_c]$ (affected by charge losses). Depending on the heat exchanger and valve characteristics, the required mass flow rate is either achieved $(\dot{m}_{dem}[c] = \dot{m}[c])$ or not. In the former case, the valve opening $O[c]$ is calculated to ensure this flow depending on its characteristic curve. In the latter case, the valve is fully open and the resulting secondary supply temperature $T_{OUT,s}[c]$ and primary mass flow rate are calculated $(\dot{m}[c] < \dot{m}_{dem}[c])$.

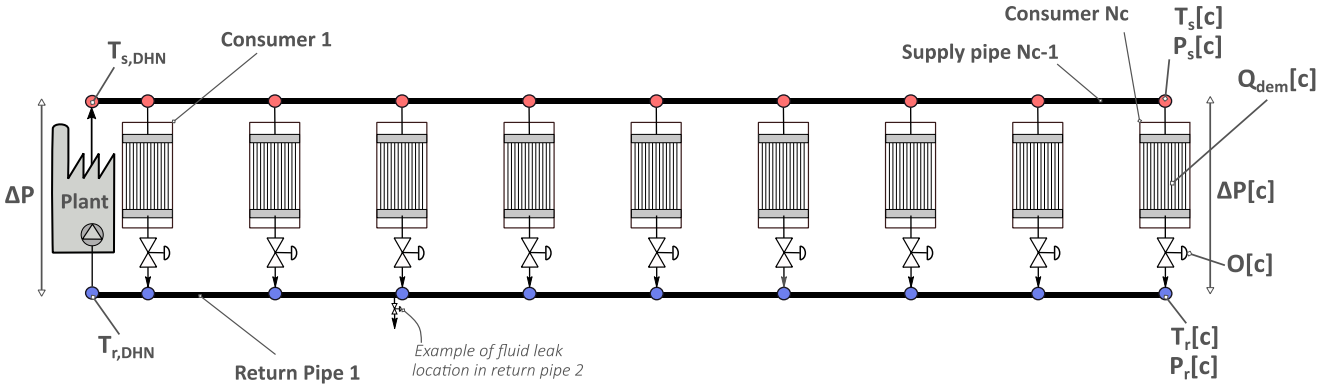

Figure 1. Schematic representation of the linear network model used for hydraulic leaks modeling

For fault simulation, we extended the model to include the option of introducing hydraulic fluid loss at the beginning of each pipe ($N_c - 1$ possible locations). This was accomplished by incorporating hydraulic valves connected to the entrance of each pipe (supply or/and return), with one side connected to ambient air. Figure 1 illustrates this arrangement. The unfaulty opening f_{leak} of this valve is set to zero. The characteristic curve of the valve is linear with a nominal point calculated with a flow rate calculated as shown in Equation (2) for a differential pressure of $\Delta P_{v,nom}$ with $\dot{m}_{nom,DHN}$ the DHN flow rate for peak sizing demand $Q_{dem,DHN,nom}$ and nominal supply $T_{s,DHN,nom}$ and return $T_{r,DHN,nom}$ temperatures.

$$\dot{m}_{v,nom}[p] = \dot{m}_{nom,DHN} \cdot \left(1 - \frac{p}{N_c}\right), \forall p \in [1: N_c - 1] \tag{2}$$

With such a model, the leaked flow rate depends on the local network pressure. Moreover, for a similar value of f_{leak}, the leaked flow rate value will depend on the location along the linear network. It is worth mentioning that no new fluid is added at the main plant into the network when a leak occurs. The assumption is thus made that a compressor group with a membrane can hold the pressure in the network without the need of backup fluid injection.

2.2. Considered DHN and performed simulations

The DHN considered in this study has the following characteristics:

- A nominal sizing demand $Q_{dem,DHN,nom}$ of 6MW;
- A yearly demand of 28 GWh and a linear density of 4.3 $MWh.mL^{-1}.yr^{-1}$ leading to a supply line length of 6.5km (same for return line);
- 10 customers distributed equally along these 6.5km with the first one at the same location as the central plant;

- The external temperature observed by the piping is the one of the gallery and is set constant at 15°C;
- All piping have a base insulation thickness of 15cm with a conductivity of the insulation material considered to be $0.04 W.m^{-1}.K^{-1}$;
- All the substations are sized for 0.6MW, primary supply and return temperatures of 90 and 55°C, and secondary supply and return temperatures of 70 and 50°C.

The operating conditions common to all the simulations are the following:

- The set point for differential pressure at customer 10 is 1.5bar;
- The fixed absolute pressure at the entrance of the thermal plant is set to 5bar;
- The secondary return temperature $T_{IN,s}[c]$ at each consumer is set to 48°C while the set point for secondary supply temperature $T_{OUT,s,SP}[c]$ is set constant at 70°C.

The specific operating conditions for the performed simulations are the following:

- Each simulation is performed over 4 weeks, with predefined boundary conditions for external temperature T_{ext}, thermal load $Q_{dem,DHN}$, and supply temperature $T_{sup,DHN}$;
- Six different time series are used for boundary conditions, corresponding to the first 6 periods of 4 weeks of a typical year (January 1st to June 18th);
- For each of the nine possible locations, a leak is imposed on the return line with a random start time (between hours 0 and hours 672) and a random intensity $f_{leaks} \in [0-1]$ (an intensity of 1 corresponds to 10% of the opening for the valve representing the leak, see section 2.1);
- One reference simulation (without fault) is performed for each possible location and boundary condition (54 references in total);
- A total of 1134 simulations is obtained. Each simulation yields a dataset of 8065 recorded instant (every 5 minutes) with more than 30 recorded variables each.

More details on the simulation methodology and produced data set can be found in [14]. The produced dataset itself is available online as Open Data [15].

Only part of the recorded data is used for the machine-learning algorithms. In particular, the following variables are used:

- Boundary conditions for the whole system (T_{ext}, $Q_{dem,DHN}$, $T_{sup,DHN}$);
- Pressure in the return line at each substation ($P_{ret,1}$ to $P_{ret,10}$);
- Temperature in the return line nearby each substation ($T_{ret,1}$ to $T_{ret,10}$).

It should be noted that the pressure and temperature at the substations is not measured in general, and would require installing additional sensors. However, they are considered in a first approach before trying to reduce the amount of information required.

2.3. Machine learning algorithms presentation

2.3.1. Artificial neural network

The fully connected artificial neural network (ANN) is a widely used machine learning model consisting of interconnected layers of neurons [16], [17]. Each neuron computes a weighted sum of inputs from the previous layer, which is then passed through a non-linear activation function [16]. The output of a neuron in a given layer is determined by the weights and biases associated with its connections to the previous layer. During training, the ANN adjusts these weights and biases to minimize the error between predicted and target outputs [18]. The process involves updating the weights and biases based on the calculated partial derivatives of the loss function [19]. Once the network is trained, it can be used to predict outcomes for new inputs by propagating the inputs through the network and generating the corresponding output vector. For a more detailed understanding of the ANN model, please refer to the references [16], [19].

2.3.2. Support vector machines

Support vector machines (SVMs) are supervised learning algorithms used for classification and regression tasks. They aim to find a hyperplane that can effectively separate data points while maximizing the margin between different classes [20]. This hyperplane is described by a linear equation, where the input vector is denoted as x, the output label as y, and the normal vector to the hyperplane as w. SVMs solve an optimization problem that strikes a balance between maximizing the margin and allowing for classification errors. This trade-off is controlled by a parameter C, which determines the importance of margin maximization versus the tolerance for misclassified points, represented by variables ξ_i [20]. In cases where the data is not linearly separable, SVMs employ a technique known as the kernel trick. By mapping the input vectors to a higher-dimensional feature space using a kernel function, SVMs can effectively separate the data using a linear hyperplane in the transformed space. The decision function of SVMs involves the dot product of the weight vector, Lagrange multipliers α_i, output labels y, and the kernel function $K(x,x')$ [20]. For more detailed information about SVMs, please refer to the associated reference [20].

2.3.3. Decision trees

The decision tree technique is a versatile algorithm used for classification and regression tasks. It builds a model by making sequential decisions based on input variables to estimate the target variable [21]. The mathematical aspect of decision trees involves determining the ideal split by computing purity or error measures at each algorithmic step. The choice of measure depends on whether the task is classification or regression. For classification tasks, two popular purity measures are the Gini index and entropy. The Gini index can be calculated using the formula $1 - \sum_{j=1}^{n}(p_j)^2$, where p_j is the proportion of data points in a subset that belong to class j. On the other hand, entropy can be expressed as $-\sum_{j=1}^{c} -p_j log_2(p_j)$, where p_j is the proportion of data points in a subset that belong to class j [21]. For regression tasks, the common error measure is mean squared error, defined in [18].

2.3.4. Random forests

Random Forest is an ensemble learning algorithm that combines the predictions of multiple decision trees to make accurate predictions. It constructs a "forest" of decision trees by selecting random subsets of the training data through bootstrapping. This diverse sampling allows each tree to learn from a different portion of the dataset. Random Forest also introduces randomness in feature selection, considering only a subset of features at each split, which promotes diversity and reduces overfitting. The trees are built independently using impurity measures like Gini impurity or error metrics like mean squared error. Predictions are made by aggregating the predictions of all trees, with the majority vote (classification) or average (regression) determining the final prediction. Random Forest is advantageous for its robustness, feature importance estimation, and capability to handle high-dimensional data. Overall, Random Forest is a powerful algorithm that leverages multiple decision trees to deliver accurate predictions while addressing overfitting through random sampling and feature selection [22], [23].

2.3.5. Extreme Gradient Boosting

Extreme Gradient Boosting (XGBoost) is a high-performance algorithm that combines weak models, typically decision trees, into a strong ensemble. It optimizes an objective function $Obj(\Theta)$, Equation (3), which consists of a loss term $\mathcal{L}(\Theta)$ and a regularization term $\Omega(\Theta)$ [24]. By iteratively adding trees and utilizing gradient descent, XGBoost minimizes the loss function to improve predictions.

$$Obj(\Theta) = \mathcal{L}(\Theta) + \Omega(\Theta) \tag{3}$$

Mathematically, XGBoost updates the ensemble predictions by fitting new trees based on the negative gradient of the loss function. The learning rate determines the contribution of each new tree. The algorithm continues until a stopping criterion is met [24].

2.3.6. Naive Bayes

Naive Bayes is a classification algorithm that applies Bayes' theorem and makes the naive assumption of feature independence [25]. Bayes' theorem allows us to calculate the posterior probability of a class given the features. The algorithm assumes that the features are conditionally independent of each other given the class [25]. To predict the class of a new sample, we calculate the probabilities of each class based on the observed features and select the class with the highest probability. This is done using the argmax function, which returns the value of the class that maximizes the expression [25]. Laplace smoothing is often employed to handle unseen feature values and ensure non-zero probabilities. To gain a more in-depth understanding of Naive Bayes, it is recommended to consult the relevant references [25], [26] for detailed information.

3. RESULTS AND DISCUSSION

In this study, a comprehensive evaluation of six machine learning algorithms was conducted to detect both small and large leaks in DHNs. The algorithms assessed included artificial neural network (ANN), support vector machines (SVM), decision trees (DT), random forests (RF), XGboost, and Naïve Bayes (NB). These algorithms were trained, validated, and tested using a substantial dataset consisting of a total of 9,009,630 samples for each feature. This dataset covered a wide range of leak prevalence, ranging from 0% to 10% of the considered pipe nominal flow. With a diverse set of 23 features, the algorithms' ability to detect leaks was thoroughly evaluated across various scenarios.

To create the training, validation, and testing datasets, the data was initially grouped based on the intensity level of each leak. Then, each resulting dataset was divided into three portions: 60% for training, 20% for validation, and 20% for testing. This splitting process ensured that the training, validation, and testing datasets had a balanced distribution of leak intensities. After the initial split, the datasets were grouped again to form distinct training, validation, and testing sets.

To ensure optimal performance, a randomized search cross-validation (CV) approach was employed to identify the most suitable hyperparameters for each algorithm. The randomized search CV technique played a crucial role in optimizing the

performance of the machine learning algorithms.

For the ANN, we explored various combinations of hyperparameters, including hidden layer sizes, activation functions, dropout rates, and learning rates for the Adam optimizer. The Adam optimizer, known for its efficiency according to previous literature, was chosen for training the ANN weights and biases. Through this process, we identified the optimal hyperparameters for the ANN, comprising two hidden layer size of {91, 89}, a sigmoid activation functions in both hidden layers, dropout rates {0.2, 0.2}, and a learning rate of 0.01. In the SVM experiments, different combinations of kernel types, regularization parameter values, and gamma values were tested. It was determined that a linear SVM achieved the best performance, considering the complexity increase caused by nonlinear kernels in the presence of large datasets. As a result, a linear SVM with a regularization parameter value of 8.76 was adopted based on the findings. In the case of the DT algorithm, a thorough exploration of diverse combinations of maximum tree depth and minimum sample split values was conducted. This process enabled the identification of optimal hyperparameters for the DT, which were determined to be a maximum tree depth of 298, a minimum sample split value of 14, and a minimum sample split value per leaf of 7.

Furthermore, the RF algorithm was subjected to experimentation involving various combinations of the number of trees and maximum tree depth. Through this process, it was ascertained that the RF model with 386 trees and a maximum tree depth of 272 yielded the best results. Additionally, the optimal hyperparameters for the RF model were determined to be a minimum sample split value of 6 and a minimum sample split value per leaf of 3.

In the case of XGboost, combinations of hyperparameters such as learning rate, maximum depth of trees, and subsample ratio were explored. After careful evaluation, the optimal hyperparameters for XGboost were determined to be: colsample_bytree: 0.783, gamma: 0.415, learning_rate: 0.273, max_depth: 9, min_child_weight: 7, and subsample: 0.755. Regarding NB algorithm, Gaussian NB was selected as the most suitable variant with a var_smoothing value of $1.59\ 10^{-4}$, based on the characteristics of the dataset and the leak detection problem in DHNs.

By employing the randomized search CV approach, a comprehensive assessment of numerous hyperparameters for each algorithm was efficiently conducted, leading to the identification and implementation of optimal configurations.

During the comprehensive analysis of various machine learning algorithms in the training and testing phases, the effectiveness of these algorithms in detecting leaks was evaluated using multiple evaluation metrics. To compare their performance and identify potential overlearning, evaluation metrics such as accuracy, precision, recall, and the F1 score were considered.

Upon examining the results, the random forests algorithm emerged as a standout performer. It achieved remarkable accuracy rates of 98.38% during training and 97.99% during testing, showcasing its ability to make highly accurate predictions. Moreover, the precision rates of 99.72% during training and 99.34% during testing demonstrated its capability to correctly identify positive instances. The recall rates of 96.84% during training and 96.41% during testing further indicated its effectiveness in capturing actual positive instances. These exceptional performance metrics position the random forests algorithm as a top contender for leak detection tasks.

In comparison, while other algorithms also demonstrated strong performance in certain aspects, they showcased varying degrees of limitations. The decision trees algorithm displayed high accuracy rates of 98.70% during training and 94.87% during testing, and precision rates of 99.90% during training and 92.91% during testing. However, it exhibited a slight decline in performance during testing, suggesting a potential for overlearning. The ANN algorithm consistently performed well across both training and testing phases, exhibiting accuracy rates of 83.44% during training and 83.45% during testing, precision rates of 96.72% during training and 96.53% during testing, recall rates of 67.23% during training and 67.59% during testing, and F1 scores of 79.33% during training and 79.51% during testing. This suggests that the ANN algorithm is less prone to overlearning and provides reliable performance for leak detection tasks.

XGBoost demonstrated relatively high accuracy rates of 89.09% during training and 61.78% during testing. However, its performance noticeably dropped during testing, indicating a potential for overlearning during the training phase. Its precision rates were 91.73% during training and 55.66% during testing, recall rates were 84.54% during training and 96.07% during testing, and F1 scores were 87.99% during training and 70.48% during testing, highlighting its effectiveness in accurately detecting positive instances. On the other hand, SVM and NB exhibited lower overall performance compared to other algorithms, with accuracy rates of 54.92% during training and 54.85% during testing for SVM, and 55.46% during training and 55.31% during testing for Naïve Bayes. Their precision, recall, and F1 scores were also comparatively lower, indicating their limitations in effectively detecting leaks.

Figure 2 presents the performance metrics of the developed machine learning algorithms for leak detection in DHN, highlighting their accuracy, precision, recall, and F1 scores.

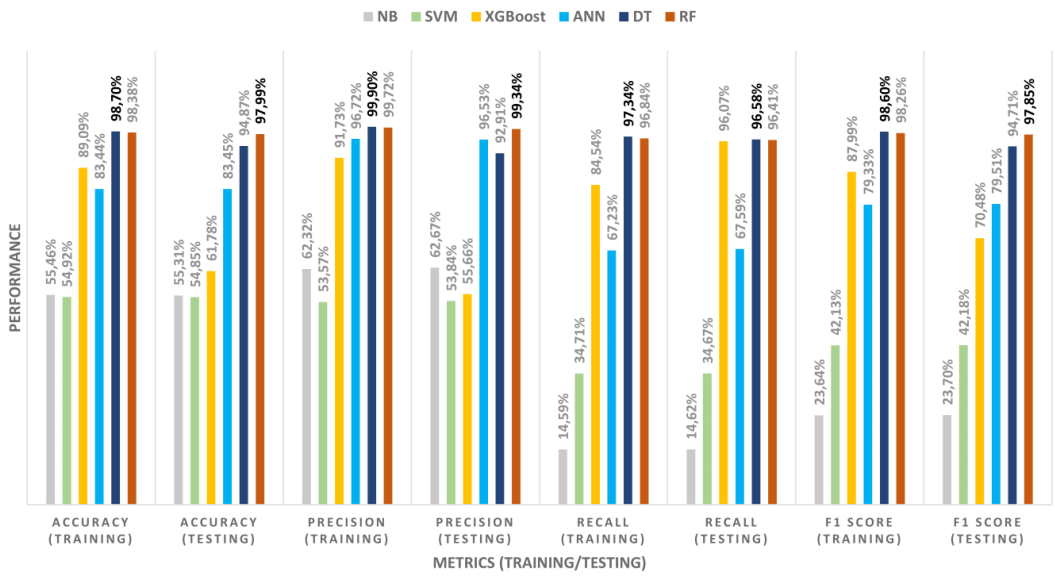

Figure 2. Comparative analysis of machine learning algorithms for leak detection in DHN

In conclusion, the analysis highlights the random forests algorithm as the top-performing algorithm, demonstrating exceptional accuracy, precision, recall, and F1 scores. The decision trees algorithm showed a slight tendency for overlearning, while the ANN algorithm exhibited consistent and balanced performance. XGBoost displayed potential overlearning during training but maintained good recall rates. On the other hand, SVM and NB showed lower overall performance in leak detection. These findings offer valuable insights for selecting the most suitable machine learning algorithm for leak detection tasks, with random forests standing out for its robust performance.

4. CONCLUSION

The present study highlights the effectiveness of machine learning algorithms in detecting leaks in district heating networks. Through the evaluation of various algorithms, such as artificial neural networks, support vector machines, decision trees, random forests, XGBoost, and Naïve Bayes, valuable insights have been gained regarding their performance in detecting both small and large leaks. Notably, random forests demonstrated the highest accuracy and precision during testing, indicating its effectiveness in accurately identifying leaks. The potential for further improvement lies in adopting hybrid machine-learning approaches that leverage the strengths of different algorithms or incorporate ensemble methods. These hybrid approaches can enhance leak detection performance by improving accuracy, reducing false positives and false negatives, and increasing overall system efficiency. In addition, the performance of these approaches should be evaluated using more diverse data from real systems and simulation, in particular, using tools for large-scale simulation of DHN [27]. In conclusion, the adoption of machine learning algorithms, particularly through hybrid approaches, can revolutionize leak detection in district heating networks. By utilizing data and advanced analytics, engineers can enhance accuracy, efficiency, and reliability, resulting in reduced energy losses, improved operational performance, and increased sustainability. The ongoing advancement of machine learning in this field holds promising prospects for the future of district heating systems, driving improvements in energy efficiency and supporting the transition to more sustainable heating solutions.

ACKNOWLEDGEMENT

The preparation of the dataset used for this work was financially supported by the IEA DHC Annex XIII program, in the frame of the project “AI for Forecasting and Fault Detection in DHN” (contract n° XIII-3) https://www.iea-dhc.org/the-research/annexes/annex-xiii/annex-xiii-project-03.

REFERENCES

[1] S. Zhou, Z. O’Neill, and C. O’Neill, “A review of leakage detection methods for district heating networks,” Appl. Therm. Eng., vol. 137, no. January, pp. 567–574, 2018, doi: 10.1016/j.applthermaleng.2018.04.010.

[2] E. Filippini, I. Marini, M. Ongari, and E. Pedretti, “District heating leakage measurement: Development of methods,” Energy Procedia, vol. 149, pp. 297–306, 2018, doi: 10.1016/j.egypro.2018.08.193.

[3] P. Xue, Y. Jiang, Z. Zhou, X. Chen, X. Fang, and J. Liu, “Machine learning-based leakage fault detection for district heating networks,” Energy Build., vol. 223, 2020, doi: 10.1016/j.enbuild.2020.110161.

[4] B. Rüger et al., “Online Leakage Attribution to Exclusion Areas Prototype Application,” Energy Procedia, vol. 149, pp. 575–584, 2018, doi: 10.1016/j.egypro.2018.08.222.

[5] K. Vahldiek, B. Rüger, and F. Klawonn, “Leakages in District Heating Networks—Model-Based Data Set Quality

Assessment and Localization," Sensors, vol. 22, no. 14, 2022, doi: 10.3390/s22145300.
[6] D. Pierl et al., "Online model- and data-based leakage localization in district heating networks - Impact of random measurement errors," Conf. Proc. - IEEE Int. Conf. Syst. Man Cybern., vol. 2020-October, pp. 2331–2338, 2020, doi: 10.1109/SMC42975.2020.9283233.
[7] L. Manservigi, H. Bahlawan, E. Losi, M. Morini, P. R. Spina, and M. Venturini, "A diagnostic approach for fault detection and identification in district heating networks," Energy, vol. 251, p. 123988, 2022, doi: 10.1016/j.energy.2022.123988.
[8] H. Bahlawan et al., "Detection and identification of faults in a District Heating Network," Energy Convers. Manag., vol. 266, no. March, 2022, doi: 10.1016/j.enconman.2022.115837.
[9] K. Vahldiek, B. Rüger, and F. Klawonn, "Optimal Sensor Placement and Influence of Noise on Pressure Wave Evaluation for Leakage Localization in a District Heating Network," Sustain. Energy, Grids Networks, vol. 30, p. 100672, 2022, doi: 10.1016/j.segan.2022.100672.
[10] N. Zimmerman, E. Dahlquist, and K. Kyprianidis, "Towards On-line Fault Detection and Diagnostics in District Heating Systems," Energy Procedia, vol. 105, pp. 1960–1966, 2017, doi: 10.1016/j.egypro.2017.03.567.
[11] Y. Zhong et al., "Pipeline leakage detection for district heating systems using multisource data in mid- and high-latitude regions," ISPRS J. Photogramm. Remote Sens., vol. 151, no. March, pp. 207–222, 2019, doi: 10.1016/j.isprsjprs.2019.02.021.
[12] K. Hossain, F. Villebro, and S. Forchhammer, "UAV image analysis for leakage detection in district heating systems using machine learning," Pattern Recognit. Lett., vol. 140, pp. 158–164, 2020, doi: 10.1016/j.patrec.2020.05.024.
[13] L. Giraud, R. Baviere, M. Vallée, and C. Paulus, "Presentation, Validation and Application of the DistrictHeating Modelica Library," Proc. 11th Int. Model. Conf. Versailles, Fr. Sept. 21-23, 2015, vol. 118, pp. 79–88, 2015, doi: 10.3384/ecp1511879.
[14] M. Vallee, N. Lamaison, and T. Wissocq, "Report on Fault Data and Fault Simulation Models for Components of a DHC system," 2022. [Online]. Available: https://www.iea-dhc.org/the-research/annexes/annex-xiii/annex-xiii-project-03.
[15] M. Vallee, "[dataset] Fault Detection and Diagnosis in District Heating." 2022. [Online]. Available: https://www.kaggle.com/datasets/mathieuvallee/ai-dhc
[16] M. A. Jallal, S. Chabaa, and A. Zeroual, "A novel deep neural network based on randomly occurring distributed delayed PSO algorithm for monitoring the energy produced by four dual-axis solar trackers," Renew. Energy, vol. 149, pp. 1182–1196, 2020, doi: 10.1016/j.renene.2019.10.117.
[17] M. A. Jallal, A. El Yassini, S. Chabaa, A. Zeroual, and S. Ibnyaich, "A deep learning algorithm for solar radiation time series forecasting: A case study of el kelaa des sraghna city," Rev. d'Intelligence Artif., vol. 34, no. 5, pp. 563–569, 2020, doi: 10.18280/ria.340505.
[18] M. A. Jallal, A. González-Vidal, A. F. Skarmeta, S. Chabaa, and A. Zeroual, "A hybrid neuro-fuzzy inference system-based algorithm for time series forecasting applied to energy consumption prediction," Appl. Energy, vol. 268, no. January, p. 114977, 2020, doi: 10.1016/j.apenergy.2020.114977.
[19] M. A. Jallal, A. El Yassini, S. Chabaa, A. Zeroual, and S. Ibnyaich, "AI data driven approach-based endogenous inputs for global solar radiation forecasting," Ing. des Syst. d'Information, vol. 25, no. 1, pp. 27–34, 2020, doi: 10.18280/isi.250104.
[20] J. Cervantes, F. Garcia-Lamont, L. Rodríguez-Mazahua, and A. Lopez, "A comprehensive survey on support vector machine classification: Applications, challenges and trends," Neurocomputing, vol. 408, pp. 189–215, 2020, doi: 10.1016/j.neucom.2019.10.118.
[21] M. Badarna and I. Shimshoni, "Selective sampling for trees and forests," Neurocomputing, vol. 358, pp. 93–108, 2019, doi: 10.1016/j.neucom.2019.04.071.
[22] X. Ma et al., "Predicting the utilization factor of blasthole in rock roadways by random forest," Undergr. Sp., vol. 11, pp. 232–245, 2023, doi: 10.1016/j.undsp.2023.01.006.
[23] T. Vadcard, A. Batailly, and F. Thouverez, "Evidential Random Forests," Expert Syst. Appl., p. 116950, 2022, doi: 10.1016/j.eswa.2023.120652.
[24] R. Sarkhani Benemaran, "Application of extreme gradient boosting method for evaluating the properties of episodic failure of borehole breakout," Geoenergy Sci. Eng., vol. 226, no. April, p. 211837, 2023, doi: 10.1016/j.geoen.2023.211837.
[25] M. Vishwakarma and N. Kesswani, "A new two-phase intrusion detection system with Naïve Bayes machine learning for data classification and elliptic envelop method for anomaly detection," Decis. Anal. J., vol. 7, no. April, p. 100233, 2023, doi: 10.1016/j.dajour.2023.100233.
[26] L. Li et al., "Naive Bayes classifier based on memristor nonlinear conductance," Microelectronics J., vol. 129, no. July, 2022, doi: 10.1016/j.mejo.2022.105574.
[27] R. Bavière, M. Vallée, S. Crevon, N. Vasset, N. Lamaison, "DISTRICTLAB-H: a new tool to optimize the design and operation of district heating and cooling networks," DHC Symposium (submitted), 2023.

Digitalization of DH

The 18th International Symposium on District Heating and Cooling,

September 3–6, 2023, Beijing, China

The Simulation Test Bed Of Multi-Family Buildings With Hydraulic Radiator Heating System

Zhikai Liu , Yanran Wang *

School of Environmental Science and Engineering, Tianjin University, Tianjin, 300350, PR China

** Corresponding author. yaran_wang@tju.edu.cn*

ABSTRACT

For hydraulic radiator district heating system (DHS) of multi-family buildings in China, heating enterprises hesitate to implement new regulation strategy, as they are worried about the heat imbalance between supply and demand after adopting the new control strategy. It may cause end-users to complaint about the government. And the lack of pre-simulation platform of the new strategies makes their practical application more difficult. Besides that, there were many issues during the test period, such as the lack of the consumer cooperations and the damage of the temperature sensors or flow rate meters. Therefore, it is necessary to establish a simulation test bed of the secondary DHS and create a digital twinning, which can simulate and analyze the performances of multi-family buildings with hydraulic radiator heating system under various control strategies and operation modes. In this study, a digital DHS is established by co-simulation of the EnergyPlus and the Matlab, where the multi-family buildings system is simulated by EnergyPlus and the mathematic descript of radiator and hydraulic network is constructed by Matlab. The simulation test bed was validated by measured data and used as a simulated test bed. A series of analyzes are being performed on this platform, such as the effect of hydraulic coupling and the different control strategy. Result shows that efficient terminal flow rate control can save 8.4% - 13% energy, which indicates that the installation of terminal control devices in existing communities is of great significance.

Keywords: digital twinning, district heating system, thermal-hydraulic couple

1. INTRODUCTION

In China, the energy consumption of district heating systems (DHS) accounts for 40% of the building sector. With the acceleration of urbanization, the proportion is still increasing [1]. According to survey statistics, the overheating problem of end users is prominent due to the lack of effective control measures for the secondary network, which accounts for 23% of the total heat consumption, and has great potential for energy saving [2]. Compared with countries of advanced heating technology in Europe, such as Denmark, there is still much space of Chines space heating for improvement [3]. However, the forms of DHS in two countries are not the same, which leads to some mature technologies in Europe may not be applicable in China [4]. The scale of Chinese secondary DHS is more complex with larger heat substation, and the typical of end users are mostly high-rise multi-family buildings, which brings new problems [5],[6]. On the other hand, heating enterprises are hesitant to easily implement advanced control strategy for flow rate regulation and supply temperature regulation, although most secondary networks have achieved the intelligent transformation. This is because they are worried about the imbalance between heat supply and demand after adopting the new regulation strategy, which will lead to complaints from users. Besides that, there were many issues during the test period, such as the lack of the consumer cooperations and the damage of the temperature sensors. Therefore, it is necessary to establish a simulation test bed of the secondary DHS and create a digital twinning. However, there is still a lack of simulation methods considering both the network hydraulic coupling performances and multi-family building thermal dynamics to analyze the radiator heating system performances under various control strategies and operation modes.

Researches on modeling and simulation methods for the multi-family building thermal dynamics are sufficient. Jiang et al. obtained an analytical solution using the state space method [7]. The thermal-electrical analogy approach, namely the RC network method is widely adopted to model the building thermal dynamics, in which resistances and capacitances were used to describe the heat dissipation and heat storage effect of the wall, emitter, and the indoor air [8],[9]. System identification method was also adopted to regress the unknown parameters by measured data. The effectiveness of such type of modeling methods have been proved by several researches [10],[11]. Besides that, there are also many commercial software that can simulate the dynamic thermal process of buildings, EnergyPlus (EP) is one of them and has been proved by several research [12],[13]. However, the hydraulic coupling effects of the network are not fully considered in the modeling of the building thermal dynamic process, especially for radiator heat dissipation, which depends on the supply temperature and flow rate distributions. There are many studies on hydraulic simulation of network and has been proved by many cases

[14-17]. Guelpa et al. described the hydraulic performances of the DH pipelines using the mass and momentum conservation equations to construct the SIMPLE hydraulic simulation algorithm for the DH network [18]. Wang et al. established a meshed DH network hydraulic model, which adopts the Newton-Raphson iteration algorithm to solve the equations [19]. Combined simulation of the network hydraulics and the thermal dynamics of multi-family buildings is essential for analyzing the operation performances of the radiator heating system. Xu et al. developed a thermostatic radiator valve (TRV) controlled radiator space heating system [20] with a simplified topology of the network. Huang et al. proposed a modeling method considering both the network hydraulic and building thermal dynamics to analyze the energy consumption of the heating system [21]. But neither of them can test the different control strategies, and the topology of network has been too simplified to reflect the influence of the topology on the hydraulic distribution.

The current advanced control methods mainly focus on the temperature control and terminal flow control strategies. Regarding the temperature control strategy, the regulation frequency [22] and supply water temperature [23],[24] can be optimized to reduce operating costs and accommodate more renewable energy or low temperature waste heat. Yuan et al. used room temperature as an indicator to regulate the supply temperature and achieved 5.8% energy saving rate [25]. Zwan et al. proposed a control strategy for temperature-constrained renewable energy sources and considered the thermal inertia of buildings as well as acceptable indoor temperature when regulating the heat supply [26]. For the terminal flow rate control strategy, Liu et al. adopted a wireless on-off strategy for adjusting [27], results show that energy consumption can be reduced about 30% compared with an uncontrolled system. Dan et al. used the model predictive control (MPC) as an adjustment method to regulate the flow rate and achieved a better tracking effect on the set point [28]. However, there is still a lack of simulation methods considering both the network hydraulic coupling performances and multi-room thermal dynamics to analyze the radiator heating system performances under various control strategies and operation modes.

As the hydraulic coupling effects of the valves cannot be ignored in the hydraulic heating system, when the valve opening of a room radiator reduces, the flow rate of the adjacent room will increase, which leads to a rise of its air temperature. As the temperature difference between the two rooms increases, the heat transfer through inner wall will cause the temperature of adjacent rooms to decrease. Analysis of such effects need effective thermal-hydraulic coupling simulation model. For a hydraulic radiator heating system, all the following factors need to be fully considered: the temperature distribution of the radiator; the heat capacity of the envelope; the heat transfer between adjacent rooms; the hydraulic coupling effects of the network and the effect of the control valves on the flow rates.

In this paper, a digital twinning of secondary district heating system (DHS) is created, which considers both thermal dynamitic of multi-family buildings and hydraulic radiator characteristics. It can be used to simulate and analyze the performances of multi-family buildings with hydraulic radiator heating system under various control strategies and operation modes, which enables the pre-simulation of different strategies before the practical application. The multi-family buildings are simulated by EnergyPlus, whose environment can not only simulate the building thermal inertia, but also can simulate the influence of occupant behavior on indoor temperatures. The mathematic description of hydraulic radiator heating systems is established by Matlab. Both software exchange data through Ptolemy II for co-simulation [29]. A case study of multi-family building with hydraulic radiator heating system is conducted using the proposed method. Performances of the one layer of constructed building under different operation strategies are analyzed.

2. METHODOLOGY

2.1. Radiator model

As the thermal capacity of water is about more than 10 times larger than that of the steel radiator shell, the thermal capacity of the shell is neglected. The temperature distribution of the radiator is uniform along the horizon and varies with the vertical direction [30]. Therefore, the dynamic heat transfer of the radiator is considered as a one-dimensional heat transfer process, as shown in Fig. 1. The equation of radiator heat transfer process can be fully described by partial differential equation (PDE), which is written as Eq. (1).

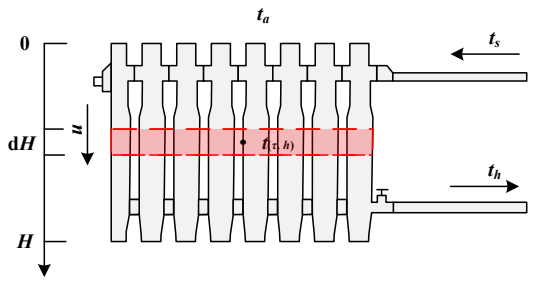

Figure 1. Radiator heat transfer model

$$\frac{\partial t(\tau,h)}{\partial \tau}+u\frac{\partial t(\tau,h)}{\partial x}=\frac{k_{\mathrm{r}}F}{c_{\mathrm{w}}\rho_{\mathrm{w}}V}\left[t_{\mathrm{a}}(\tau)-t(\tau,h)\right] \tag{1}$$

where $t(\tau, h)$ (°C) represents the temperature distribution along the vertical direction of the radiator; τ (s) denotes the time; h (m) represents the vertical location of the radiator; F (m^2) is the heat transfer area of the radiator; k_{r} [W/(m^2·K)] is the heat transfer coefficient of the radiator; c_{w} [J/(kg·K)] denotes the heat capacity of water; V (m^3) is the volume of the radiator; ρ_{w} (kg/m^3) is the density of the water; t_{a} (°C) is the indoor air temperature; u (m/s) represents the speed of the water in the radiator, which can be derived according to the following formula,

$$u=\frac{H}{V/q} \tag{2}$$

where q (m^3/s) represents the volume flow rate, H (m) is the height of the radiator.

Along the vertical direction, the Eq. (1) is discretized into "M" segments by first-order upwind scheme, which yields the following ordinary differential equation (ODE):

$$\frac{dt(\tau,i\Delta h)}{d\tau}=Kt_{\mathrm{a}}(\tau)-\left(K+\frac{u}{\Delta h}\right)t(\tau,i\Delta h)+\frac{u}{\Delta h}t\left[\tau,(i-1)\Delta h\right] \tag{3}$$

where K equals to $k_{\mathrm{r}}F/(c_{\mathrm{w}\rho\mathrm{w}}V)$; Δh denotes the spatial step size, which is related to the number of discrete segments; i is the control volume nu*mber*. And t (τ,0) is considered to be equal to the supply temperature t_{s} (°C).

After obtaining the temperature distribution of the radiator, the heat dissipation from the radiator to the indoor air can be calculated by the following formula:

$$Q=\sum k_{\mathrm{r}}f_{\mathrm{r}}\left[t_{\mathrm{r}}(i)-t_{\mathrm{a}}\right] \tag{4}$$

where f_{r} (m^2) denotes the area of the discrete radiator parts.

The fourth order Runge-Kutta method [30] is adopted to solve these equations in Matlab and the inputs are the indoor air temperature, supply temperature and flow rate of the radiator, which can be obtained form EP, different supply temperature control strategies and hydraulic modules respectively.

2.2. Hydraulic model

The topology of the network can be described by graph theory, which can be regarded as a directed graph [32]. The DH topology can be described by the basic incidence matrix **A**. Element a_{ij} represents the relationship between the ith node and j^{th} branch. If the node and branch are adjacent, a_{ij} equals 0. For the jth branch, if the water flows into the ith node, the a_{ij} is 1. If the water flows out of the ith node, a_{ij} is -1. According to the Kirchhoff's first law, the net flow of a node can be written as the Eq. (5).

$$\mathbf{AG}=\mathbf{0} \tag{5}$$

where **A** is the basic incidence matrix, The elements of vector **G** (kg/s) represents the flow rate of each pipeline.

According to the Kirchhoff's second laws, the algebraic sum of the pressure drops equals to zero along the clockwise of the loop and can be written as follows.

$$\mathbf{C_f}\left(\mathbf{\Delta P}-\mathbf{H_p}\right)=\mathbf{0} \tag{6}$$

where $\mathbf{C_f}$ is the independent loop matrix whose rows represent the independent loops and columns represent the branches. The element c_{ij} of the matrix $\mathbf{C_f}$ equals 0 when the jth branch is not on the ith loop. If the flow direction of water within the jth branch is the same as the direction of ith loop, the c^{ij} is 1. On the contrary, the c^{ij} is -1, when the flow direction is inverse. The element of vector **ΔP** (Pa) equals the sum of pressure drop of the pipeline, radiator and programmable electric control valve, which can be written in the form of Eq. (7). **Hp** (Pa) is the vector of pressure difference provided by pump, whose element equals 0 if there is no pump on the jth branch.

$$\Delta p_j=\Delta p_{\mathrm{p},j}+\Delta p_{\mathrm{r},j}+\Delta p_{\mathrm{v},j} \tag{7}$$

where the subscript 'j' denotes the number of branches; $\Delta p_{\mathrm{p},j}$ is the pressure drop of jth pipeline, which can be calculated according to the Darcy-Weisbach formula as the form of Eq. (8); $\Delta p_{\mathrm{r},j}$ is the pressure drop of radiator and $\Delta p_{\mathrm{v},j}$ represents the pressure drop of valves, which equals 0 if there is no radiator or CRV on the jth branch.

$$\Delta p_{\mathrm{p},j} = s_j \cdot \left| g_j \right| \cdot g_j \tag{8}$$

where s_j (s^2/m^5) is the hydraulic impedance, g_j (kg/s) is the flow rate of jth branch.

The relationship between the pressure drops and valve opening of the valve adopted in this paper can be depicted by Eq. (9).

$$\Delta p_{\mathrm{v},j} = s_{\mathrm{v},j} R^{2(1-x)} g_j^2 \tag{9}$$

where $s_{\mathrm{v},j}$ (s^2/m^5) is the hydraulic impedance of the jth valve with the degree fully open; R denotes the rangeability of the valve; x is the valve opening, which varies from 0 to 1.

As the hydraulic questions of the network is nonlinear, the Newton-Raphson iteration method is adopted to solve the equations in Matlab. The inputs are the opening degree of each valve, which can be obtained according to different terminal flow rate control strategies. The outputs are the radiator flow rates.

2.3. Building model

The Sketchup is used to build physical model of the building and divide each room into one single thermal zone. Then some specific details are needed to set in the EP, such as lighting schedule, equipment schedule and occupant behavior. Especially for the radiator system, it is also necessary to set the radiator distribution ratio of convection and radiation in EP. The inputs are radiator heat dissipations and the outputs are temperatures of outdoor air and indoor air.

2.4. Development of simulation test bed

The integrated model of multi-family building with hydraulic radiator heating system is formed by connecting the radiator model, hydraulic model and building model. The radiator and hydraulic model are constructed and solved in Matlab and the building model is simulated by EP. Implementation of co-simulation required correctness to handling the exchange data between two software and configuring the integrated environment, which is listed in Table 1.

Table 1. The exchange data between two software through BCVTB

	Matlab to EP	EP to Matlab
ExternalInterface:Actuator	HeatPower	----------
Output:Variable	----------	Site Outdoor Air Drybulb Temperature
	----------	Zone Mean Air Temperature

Matlab obtained the temperatures of outdoor and indoor air from BCVTB, which are provided by EP. The outdoor temperature is used to calculate the supply temperature by different source strategies. The valve opening degrees are calculated by different terminal strategies according to the indoor air temperature. Once the supply temperature and the radiator flow rate are obtained, the heat powers of the radiator can be calculated according to equation (4). Then the calculated heat powers are transferred from Matlab to the EP through BCVTB. From the above analysis, the BCVTB is essentially a platform with global simulation parameters (begin time, end time, time step) for transmitting data between different software, so the configuration file (*.cfg) must be set correctly to guide what data could be transmitted. The Fig. 2. shows the process of how it works.

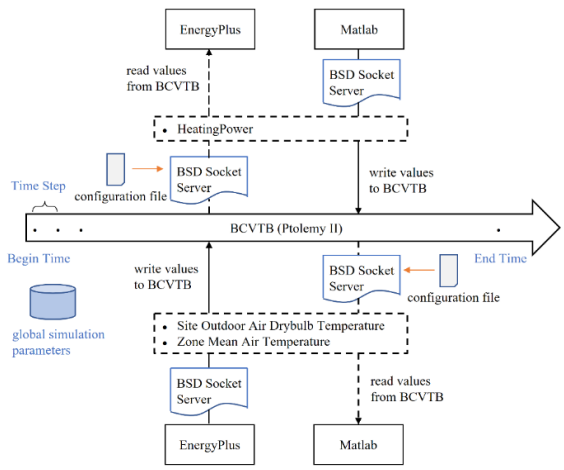

Figure 2. Simulation process of the co-simulation between Matlab and EnergyPlus

3. Model validation

The surveyed building is located in Tianjin, China with total floor area of 1420 m^2. Radiator systems are used for heating during the winter period, and the building physical model is shown in figure 3. Temperature sensors were installed in 4 typical spaces which were selected from 12 households to record indoor temperature, and intelligent control valve was installed at heating inlet of the building to record supply and return temperature. The areas of three arow pointed rooms in are 14.4 m^2, 14.4 m^2, and 58.79 m^2, respectively and the orientation of the building are plotted in the Fig. 3.

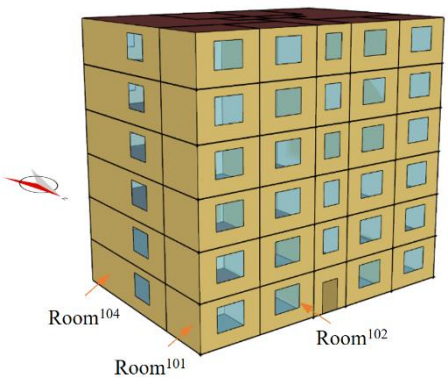

Figure 3. Building physical model

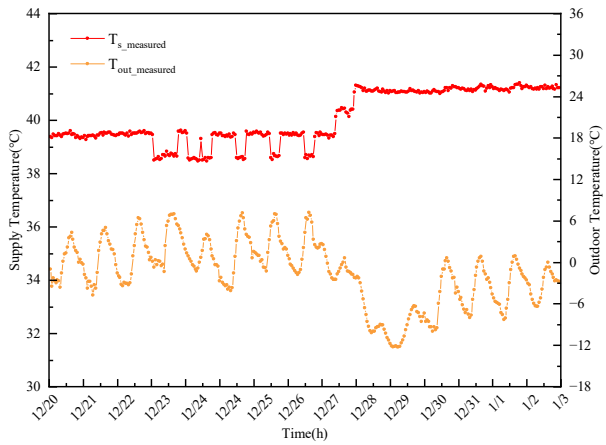

Figure 4. The measured supply temperature during the test period

The constructed model was validated using the average indoor air temperature and return temperature from the four typical users, which were measured hourly between December 20th and January 3rd. The supply temperature and outdoor temperature during the tested are shown in the Fig. 4. And the Fig. 5 shows the comparison between the average indoor temperature and the simulated values, while the Fig. 6 shows the comparison between the average return temperature and the simulated values.

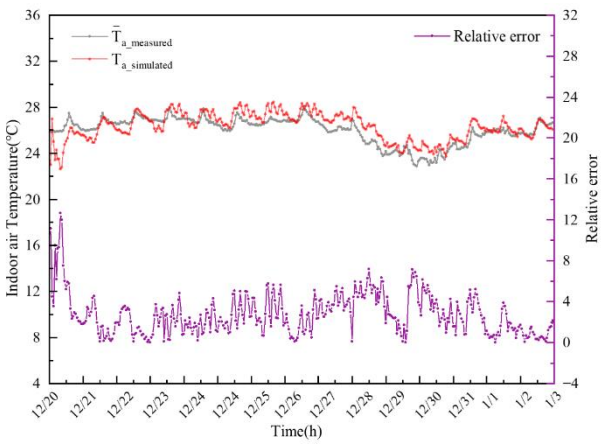

Figure 5. Comparison of the indoor air temperature

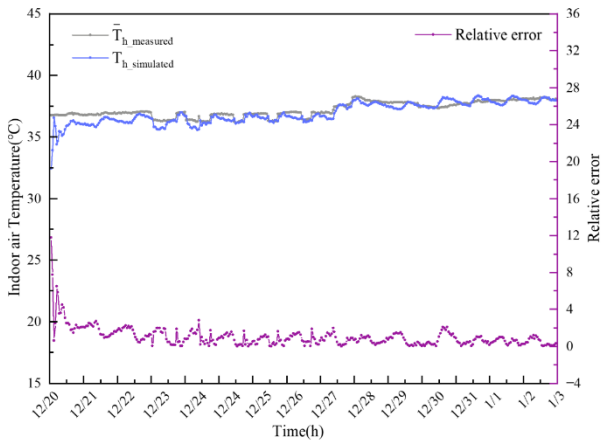

Figure 6. Comparison of the return temperature

The average relative error of indoor air temperature and return temperature are 2.74% and 1.13% respectively, which indicates the simulation test bed of multi-family building with hydraulic radiator heating system is accurate.

4. Results and discussion

4.1. Analysis of the coupling effect

To analyze the coupling effects of the radiator valves, certain condition was considered. The openings of all the radiator valve were maintained 100% at first, and at the 8th hour the valve opening of $Room^{101}$ was set to 0, with the outdoor temperature and supply temperature remaining unchanged at -7℃ and 65℃, respectively. The simulated flow rates and indoor temperatures of $Room^{101}$, $Room^{102}$ and $Room^{104}$ were displayed in Fig. 7.

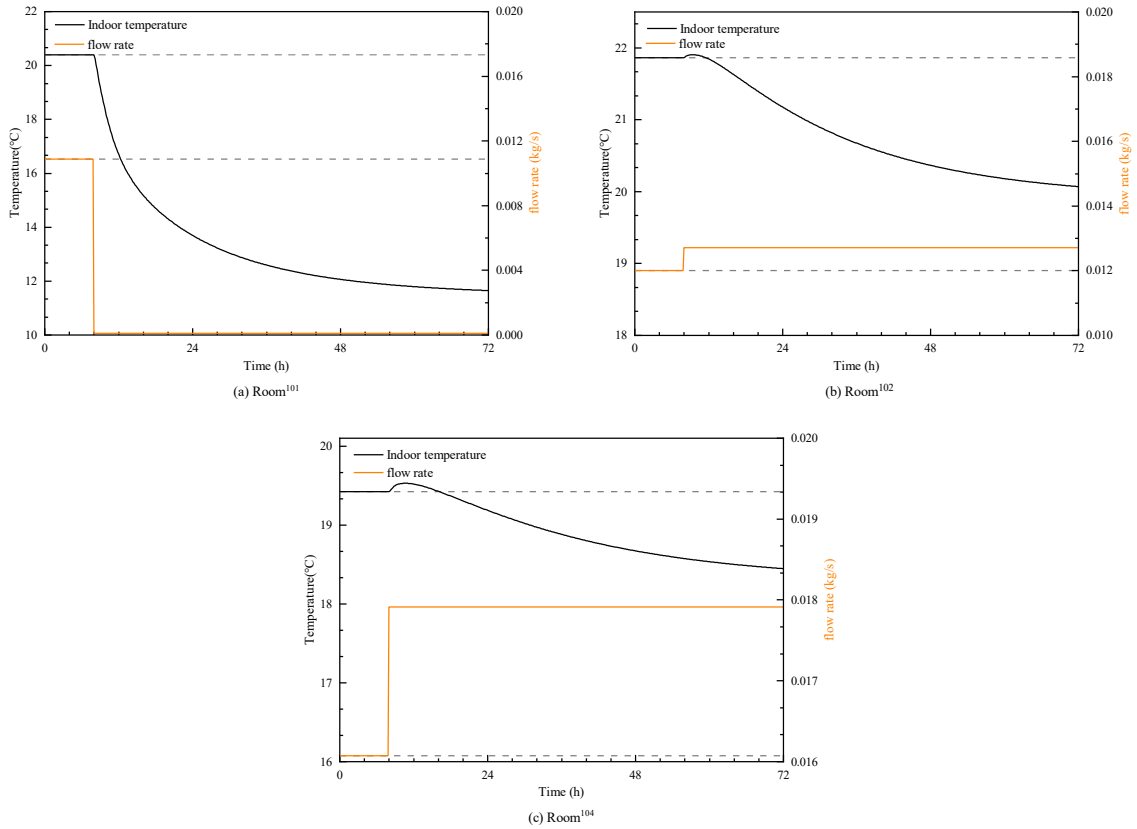

Figure 7. Calculate flow rate and temperature of ROOM^{101}, ROOM^{102}, and ROOM^{104}

The flow rates of the adjacent Room^{102} and Room^{104} increase by 6.0% and 11.4%, respectively, as the valve of ROOM^{101} is closed. As a result, the temperatures of Room^{102} and Room^{104} increase in a short time, which was displayed as the solid line in Fig 7. However, the temperature decreases again after 4-8 hours due to the heat transfer through inner wall. 64 hours later, the temperatures of Room^{101}, Room^{102} and Room^{104} become 11.6 °C, 20 °C and 18.4 °C respectively. The average declines are 43%, 9.1% and 5.3%. Results show that the hydraulic coupling effect is stronger than that of the heat transfer effect between neighboring rooms in a short time. But from a long-term view, the influence of the heat transfer through adjacent rooms is dominant.

4.2. Energy consumption of different control strategies

Since the simulation platform can freely set the control strategies, the following common scenarios were selected for simulation: (1) weather compensator without terminal control; (2) weather compensator plus on/off control; (3) weather compensator plus proportion control with frequency 10min; (4) weather compensator plus proportion control with frequency 30min. The Fig. 8 shows the total energy consumption of each heated room on the first floor under the above control strategies during the whole heating period. The layout of each layer is depicted in figure (9).

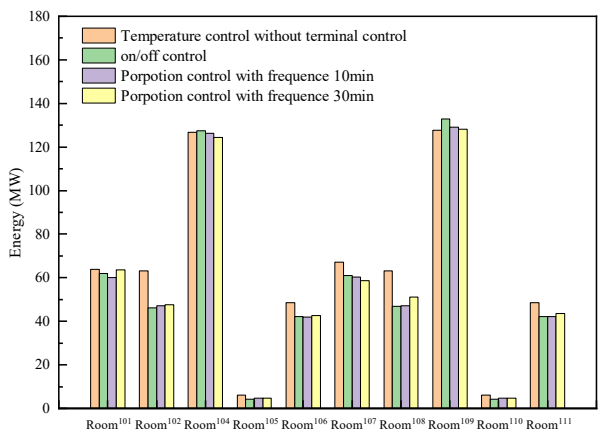

Figure 8. The energy consumption histogram

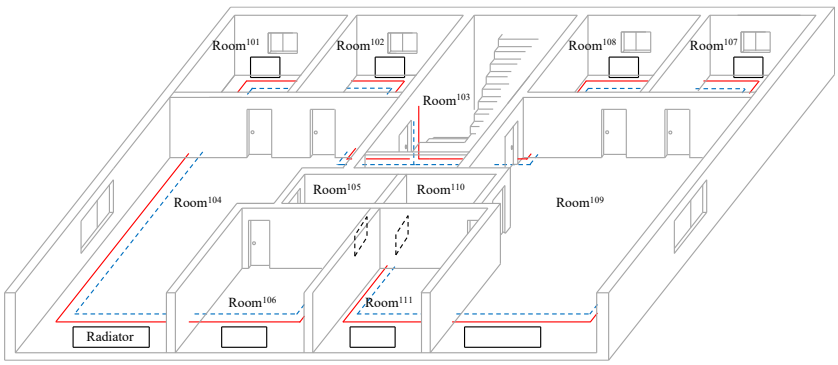

Figure 9. Each layer layout in multi-family building

Fig. 8 shows the energy consumption of each heated room under the above control algorithm during the whole heating period. No matter which terminal flow rate control was adopted, the heated room has a reduction of energy consumption compared with supply temperature regulation. The implementation of terminal flow rate control could save about 8.4%-13% energy compared with weather compensator. Therefore, it is meaningful for the existing communities to install terminal control devices.

5. CONCLUSION

A novel simulation platform of secondary DHS is proposed by co-simulation of EnergyPlus and the Matlab, where the multi-family building is simulated by EnergyPlus, and the mathematic description of radiator dynamic performances and network hydraulic characteristics are established in Matlab. The fourth order Runge-Kutta and Newton-Raphson iteration numerical method are adopted to solve the constructed model in Matlab. The proposed test bed can be used to simulate and analyze different control strategies. The advanced control strategies did not test or develop in this paper and only Four common operation modes are compared. The results showed that energy saving rate is 8.4%-13% after adopting the terminal flow rate control.

ACKNOWLEDGEMENT

This work is supported by the National Natural Science Foundation of China (No. 52008290).

REFERENCES

[1] L. Zhang, X. Ma, Y. Wang. The increasing district heating energy consumption of the building sector in China: Decomposition and decoupling analysis. Journal of Cleaner Production 2020;271:122696.

[2] Y. Zhang, J. Xia, H. Fang. Field tests on the operational energy consumption of Chinese district heating systems and evaluation of typical associated problems. Energy and Buildings 2020;224:110269.

[3] Zhang L, Gudmundsson O, Li H. Comparison of district heating systems used in China and Denmark. International Journal of Sustainable and Green Energy 2015;4(3):102-116.

[4] Østergaard D S, Tunzi M, Svendsen S. What does a well-functioning heating system look like? Investigation of ten Danish buildings that utilize district heating efficiently. Energy 2021;227:120250.

[5] Liu L, Fu L, Jiang Y. Major issues and solutions in the heat-metering reform in China. Renewable and Sustainable Energy Reviews 2011;15(1):673-680.

[6] Zhang Y, Xia J, Fang H. Field tests on the operational energy consumption of Chinese district heating systems and evaluation of typical associated problems. Energy and Buildings 2020;224:110269.

[7] Y. Jiang. State-space method for the calculation of air conditioning loads and the simulation of thermal behavior of the room. ASHRAE Transactions 1982;88:122–132.

[8] A. Li, Y. Sun, X. Xu. Development of a Simplified Resistance and Capacitance (RC)-network Model for Pipe-embedded Concrete Radiant Floors. Energy and Buildings 2017;150:353-375.

[9] O.M. Brastein, A. Ghaderi, C.F. Pfeiffer. Analysing uncertainty in parameter estimation and prediction for grey-box building thermal behaviour models. Energy and Buildings 2020;110236.

[10] S. Wang, X. Xu. Parameter estimation of internal thermal mass of building dynamic models using genetic algorithm. Energy Conversion and Management 2006;47(13-14):1927-1941.

[11] Q. Chen, N. Li, W. Feng. Model predictive control optimization for rapid response and energy efficiency based on the state-space model of a radiant floor heating system. Energy and Buildings 2021;238:110832.

[12] Hong T, Sun K, Zhang R. Development and validation of a new variable refrigerant flow system model in EnergyPlus. Energy and Buildings 2016;117:399-411.

[13] Yu T, Heiselberg P, Lei B. Validation and modification of modeling thermally activated building systems (TABS) using EnergyPlus, Building Simulation. Springer Berlin Heidelberg 2014;7:615-627.

[14] Stevanovic V D, Prica S, Maslovaric B. Efficient numerical method for district heating system hydraulics[J]. Energy Conversion and Management 2007;48(5):1536-1543.

[15] S. Zhou, H. Li, P. Gong. Hydraulic modeling of double-source and ring-shaped heating networks. Applied Thermal Engineering 2017;119:215-221.

[16] Zheng X, Sun Q, Wang Y. Thermo-hydraulic coupled simulation and analysis of a real large-scale complex district heating network in Tianjin. Energy 2021;236:121389.

[17] Liu Z, Zhang H, Wang Y. An adaptive double-Newton-iteration hydraulic calculation method for optimal operation of the meshed district heating network. Energy 2023;272:127132.

[18] Guelpa E, Toro C, Sciacovelli A. Optimal operation of large district heating networks through fast fluid-dynamic simulation. Energy 2016;102:586-595.

[19] Wang Y, You S, Zhang H. Hydraulic performance optimization of meshed district heating network with multiple heat sources. Energy 2017;126:603-621.

[20] B. Xu, F. Lin, H. Di. Dynamic simulation of space heating systems with radiators controlled by TRVs in buildings. Energy and Buildings 2008;40(9):1755-1764.

[21] J. Huang, Y. Xu, P. Jones. Building Energy and Thermo-Hydraulic Simulation (BETHS) for District Heat System in Residential Communities: A Case of Shenyang, China. Energy and Buildings 2021;247:111114.

[22] K.C.B. Steer, A. Wirth, S.K. Halgamuge. Control period selection for improved operating performance in district heating networks. Energy and Buildings 2011;43(2-3):605-613.

[23] D. Hering, M.E. Cansev, E. Tamassia. Temperature control of a low-temperature district heating network with Model Predictive Control and Mixed-Integer Quadratically Constrained Programming. Energy 2021;224:120140.

[24] N. Aoun, R. Baviere, M. Vallee. Modelling and flexible predictive control of buildings space-heating demand in district heating systems. Energy 2019;116042.

[25] Yuan J, Huang K, Han Z. A new feedback predictive model for improving the operation efficiency of heating station based on indoor temperature. Energy 2021;222:119961.

[26] van der Zwan S, Pothof I. Operational optimization of district heating systems with temperature limited sources. Energy and Buildings 2020;226:110347.

[27] L. Liu, L. Fu, Y. Jiang. A new "wireless on-off control" technique for adjusting and metering household heat in district heating system. Applied Thermal Engineering 2012;36:202-209.

[28] D. Rogers, M. Foster, C. Bingham. A recursive modelling technique applied to the model predictive control of fluid filled heat emitters. Building and Environment 2013;62:33-44.

[29] Wetter M. Co-simulation of building energy and control systems with the Building Controls Virtual Test Bed. Journal of Building Performance Simulation 2011;4(3):185-203.

[30] T.H. Pedersen, R.E. Hedegaard, K.F. Kristensen, B. Gadgaard, S. Petersen. The effect of including hydronic radiator dynamics in model predictive control of space heating. Energy and Buildings 2018;183:772-784.

[31] J.R. Dormand, P.J. Prince. A family of embedded Runge-Kutta formulae. Journal of Computational and Applied Mathematics 1980;6(1):19–26.

[32] Fu Xiangzhao, Wang Yueren, Wang Yuan. Fluid distribution network. Third ed. Beijing: China Architecture & Building Press; 2010 [In chinese]

The 18th International Symposium on District Heating and Cooling, September 3–6, 2023, Beijing, China

Construction of Information Model Framework for Centralized Heating System Oriented to Digital Twin

Wang Zhihao [a] Shu Haiwen [a*] Qi Jianwei [a] Wang Haichao [a] Shu Jingji [a]

[a] *Dalian University of Technology, Dalian, 116000, China*

[*] *Shu Haiwen. Shwshw313@sina.com*

ABSTRACT

With the deepening of digital transformation and the continuous development of new generation information technology, applying the "digital twin" technology to heating systems is an important approach to achieve intelligent heating. Information data is a key component of the entire digital twin and serves as the driving force for the proper operation of the whole heating system. Therefore, a universal information model for heating systems based on the Open Platform Communications unified architecture (OPC UA) is proposed for digital twin-oriented heating systems. By adopting the core technologies of OPC UA specification, nodes, and references, an information model framework for the heating network is presented. Furthermore, an information model design method for the facility level is proposed using pipeline component as an example, and the standardized definition of the information involved in the model is addressed to provide complete information for more accurate hydraulic and thermodynamic reflection of the actual system in the digital twin. This approach aims to effectively address the problems of lack of standardization and comprehensiveness of information required for digital twin development in heating systems. The UaModeler is used to output visualized information models and XML description files. Additionally, an OPC UA server is developed to test the established information model, validating the correctness and feasibility of instantiating the information model for the heating network system based on the OPC UA standard.

Keywords: Central heating; Digital twin; OPC UA; Information model

0. PREFACE

Currently, new generation information technologies such as industrial Internet and cloud computing have demonstrated powerful capabilities in the operation management and scheduling control of complex production systems. The construction of smart cities has become an important task and goal for local economy and social development in China[1]. Developing smart heating has become a consensus in China's heating industry[2]. "Digital twin" as an emerging concept, is gradually becoming a research hotspot in various fields and is considered a technological pathway for achieving smart heating in the heating domain. The core element of a Digital Twin is the twin data, which drives the operation of different components and serves as the "lifeblood" of Digital Twin applications[3]. Therefore, the design of an OPC UA information model is crucial as it provides standardized data exchange and communication interfaces necessary for implementing digital twins. This model forms the foundation for the construction and realization of digital twin platforms, enabling seamless integration of different devices and subsystems from centralized heating systems into the digital twin environment, facilitating comprehensive management and intelligent control of physical systems.

1. FUNDAMENTALS OF INFORMATION MODELING FOR CENTRALIZED HEATING SYSTEMS

1.1. Digital Twin

The concept of Digital Twin was initially proposed by Professor Grieves in 2003 and defined as a three-dimensional model composed of a physical product in the real space, a virtual product in the virtual space, and the connection between them[4]. A Digital Twin system involves creating a digital replica of a physical object and simulating its various processes through the collection of node information. In the case of heating systems, the development of each process in the Digital Twin relies on the exchange of information data. Therefore, in order to meet the requirements of Digital Twin, it is necessary to establish a relatively universal information model for multi-level centralized heating systems. This will enable unified data representation, strengthen application development and resource integration, and address the challenge of connecting " information isolation islands" in the system.

1.2. OPC UA information model

In order to meet the information transmission needs of Digital Twin, this paper establishes an Open Platform

Communications unified architecture (OPC UA) information model for heating systems. OPC UA is the latest generation of data exchange technology standard for industrial communication, created by the OPC Foundation. It is independent of manufacturers and platforms, enabling horizontal information integration such as data collection and device interoperability at the device level across different domains[5].

According to the concept of the OPC UA information model, real-world entities and their related information can be mapped as nodes. Nodes have different categories based on their purposes, such as object types, objects, and variables. Nodes are described by attributes such as name, data type, and data value, and their relationships are established through references. Therefore, the modeling process involves defining node attributes and node relationships.

According to the OPC UA modeling specification, this paper presents the information modeling process for centralized heating systems oriented to Digital Twin. The process consists of four stages: requirements analysis, type model creation, model instantiation, and document export, as shown in Figure 1.

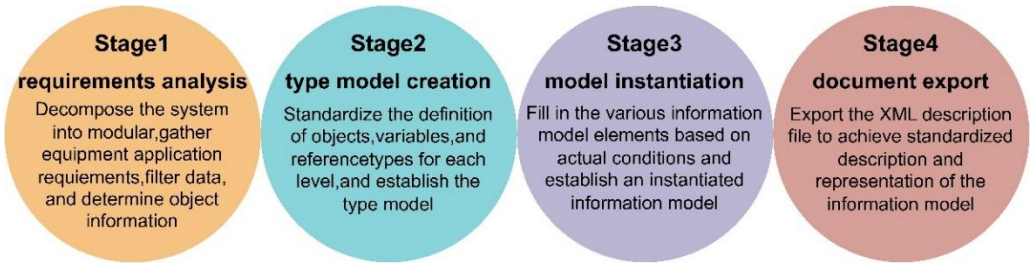

Figure 1. Modeling process

2. REQUIREMENTS ANALYSIS FOR INFORMATION MODELING OF CENTRALIZED HEATING SYSTEMS

This section will focus on the application of digital twin technology in heating systems and systematically analyze the requirements for information modeling in heating systems. Specifically, the requirements will be obtained from the following aspects:

Firstly, analyze the operational characteristics and processes of the heating system, divide the centralized heating system into different levels, and determine the types of objects that need to be modeled.

Secondly, gather relevant operational data, mathematical modeling parameters, and descriptive information for each device based on their functional requirements in the digital twin system.

2.1. Composition and division of centralized heating systems

Based on the digital twin demonstration project "Huanghua Centralized Heating System" shown in Figure 2, the system has been divided. At the system-level, the centralized heating system is divided into the heat source system, heating network system, intermediate station system, and heat user system. In the Huanghua Centralized Heating System, the pressure isolation heat exchange stations and heat exchange stations share similarities in their operational processes and equipment composition. Therefore, they are classified as the "intermediate station system" level. At the equipment-level, an object-oriented approach is adopted to establish object types for the main equipment components of each system. For example, in the heating network system, object types such as pipe section, pipe connectors, and valves are established. Based on the requirements, further refinements can be made under each object type. For example, the valve object type can be further refined into categories such as shut-off valves, control valves, and safety valves. These components and subsystems coordinate with each other to achieve the efficient and safe operation of the heating system.

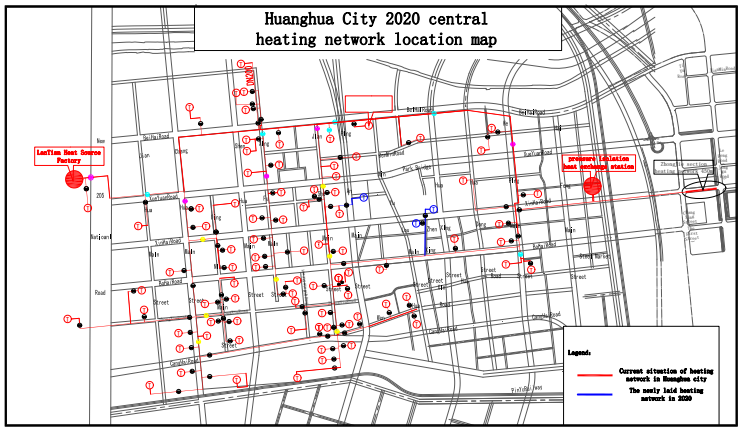

Figure 2. Location map of the centralized heating network in Huanghua City

2.2. Acquisition of requirements of information model oriented to Digital Twin

The comprehensiveness of information is crucial for an information model as it impacts the accurate representation of the physical world and the proper functioning of digital twin systems. This paper focuses on the analysis of pipe-section objects within a centralized heating system to fulfill the requirements of acquiring a pipe-section information model. In this paper, a pipe is defined as a straight conduit that does not exhibit changes in diameter, branching, or redirection, and possesses identical specifications and materials. The utilization requirements of pipe information can be considered from the following four aspects：

（1）Design Information: In order to accurately position objects in the actual physical world for digital twin systems, it is necessary to obtain location information such as number, start location, and end location. Additionally, equipment descriptive information such as pipe outer diameter and wall thickness is essential for pipe thermal calculations. All of these details can be acquired from design documents, which encompass the aforementioned information.

（2）Pipe Heat Loss: To fulfill the requirements of pipe heat loss calculations, an analysis of the mathematical model for heat dissipation per unit length of centralized heating pipelines[6] reveals that the information model should include details such as the thermal conductivity of the pipe material, soil surface temperature, and the distance between supply and return pipes' centers.

（3）Hydraulic Calculation: Hydraulic calculation is a fundamental aspect of the design and operation of centralized heating systems, and it is an essential component of a digital twin system. An analysis of the mathematical model for hydraulic conditions in heating pipe networks[7] indicates that the information model should encompass data such as the flow velocity of the heat transfer medium and the dynamic viscosity coefficient of the medium.

（4）Dynamic Simulation: To achieve online simulation of the centralized heating pipe network in a digital twin system and determine the optimal operation of the heating system, an analysis of the mathematical model for dynamic simulation of the pipe network[8] reveals that the pipe segment information should also include parameters such as the density of the pipe material, specific heat capacity of the pipe material, and specific heat capacity of the heat transfer medium.

Through the requirement analysis for pipe-section oriented to digital twin, comprehensive acquisition of object information can be achieved. This enables the model to better describe and depict the attributes, methods, behaviors, and other characteristics of physical objects. It facilitates combination and expansion of different object information models within the centralized heating system.

3. INFORMATION MODELING OF CENTRALIZED HEATING NETWORK SYSTEM

In the digital twin implementation of centralized heating systems in other projects, the time constraints of the projects often limit the information models to specific projects, in order to avoid any impact on subsequent digital twin modeling of heating systems. Although information models have been applied for some centralized heating digital twin systems, the information is often incomplete and lacks generality. This paper aims to establish a more generic information model that can serve as a basis for establishing information models for digital twin systems of all heating systems. It can integrate various data sets from existing centralized heating systems, forming a comprehensive and systematic heating information model to support real-time monitoring, analysis, and optimization of the heating system.

In this section, we will focus on constructing an overall information model framework for the centralized heating system and provide a detailed introduction to the information modeling of the heating network system. By establishing a rational information model, we can effectively describe the diverse data and information pertaining to the heating network.

3.1. Overall information model

The information model should comprise both the basic descriptive information of the heating system and the digital twin's required parameters. In terms of extensibility, the information should be open and modifiable. Following the OPC UA information modeling principles and specifications, an abstract analysis of the constitution and operation process of the centralized heating system is conducted to establish the overall information model, as depicted in Figure 3. It primarily consists of the static information set, the dynamic total parameter set, and the component set.

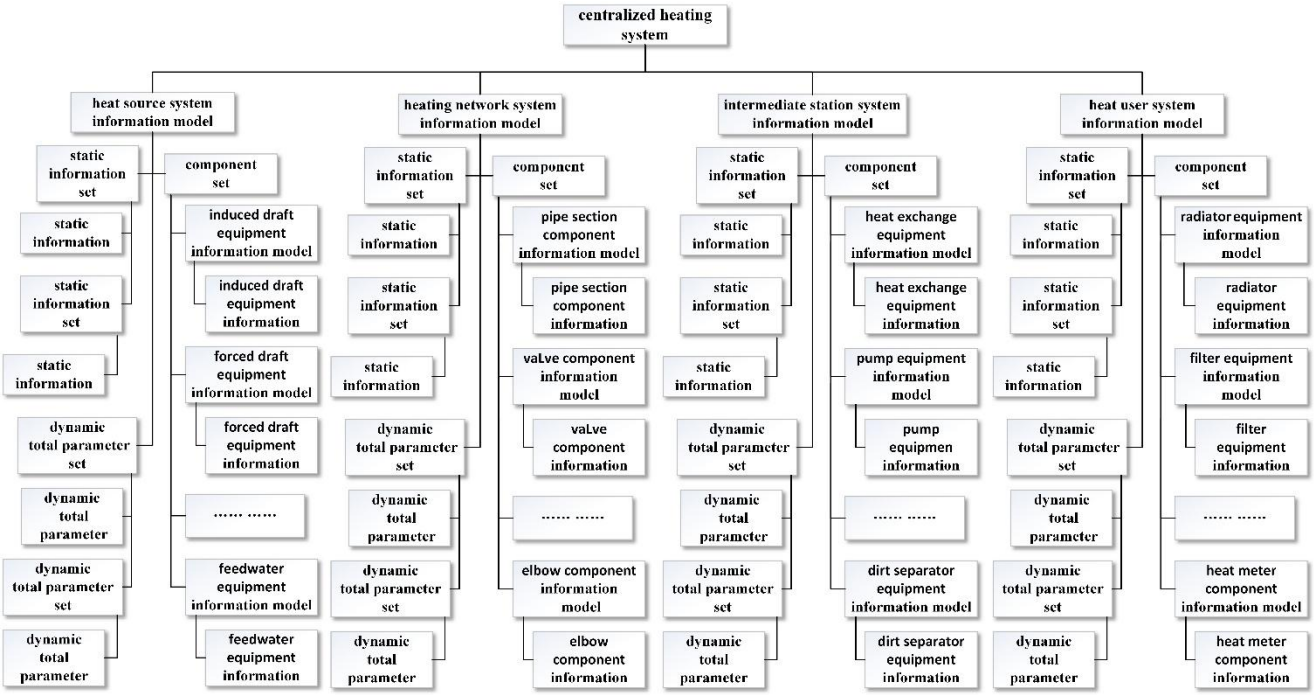

Figure 3. Overall information model framework

The static information set is a collection of static attribute data for each system. Static data refers to information that does not change or changes infrequently, such as number, name, type, etc. It reflects the inherent properties of each system. The dynamic total parameter set is defined as the collected data that undergoes changes during the overall operation of the system, reflecting the variations occurring throughout the operational process. It includes information such as supply water temperature, return water temperature, etc. The component set consists of equipment component objects owned by each system. These objects are also constructed by information models that describe their own attributes.

Within this framework, subsets can be nested within sets, and components can also have a similar nesting structure, allowing for extensibility[9]. Following the information modeling rules and based on the aforementioned information model framework, the centralized heating system can be effectively modeled. This model can comprehensively cover the information related to centralized heating projects.

3.2. Establishment of type model

Based on the overall information model framework for the centralized heating system, in addition to establishing a system-level information model for the heating network, an information model for the equipment-level included in the heat network system should also be created.

Mapping the system-level information model of the heating network to OPC UA object node types is shown in Table 1. The modeling rule "M" indicates that it is mandatory, meaning that this node must be present during the modeling process and cannot be omitted.

Table 1. System-level object node types in the heating network

Node Class	Node DisplayName	Node BrowseName	TypeDefinition	ModelllingRule
ObjectType	热网类型	HeatingNetworkType	BaseObjectType	M
Object	静态信息集	StaticInformationSet	FolderType	M
	动态总参数集	DynamicTotalParameterSet	FolderType	M
	组件集	ComponentSet	FolderType	M

The heating network system has an object type named " HeatingNetworkType " derived from the BaseObjectType in the OPC UA standard. Under this object type, objects, variables, and methods can be established. Therefore, under the HeatingNetworkType, three objects– StaticInformationSet, DynamicTotalParameterSet, and ComponentSet - are created, with their types defined as FolderType in the OPC UA standard. After analyzing the information and parameter requirements in the heating network information model, variables, methods, or objects can be further established under the respective sets. The OPC UA graphical representation of HeatingNetworkType in system-level is depicted in Figure 4. The reference relationships between nodes are represented by different arrows.

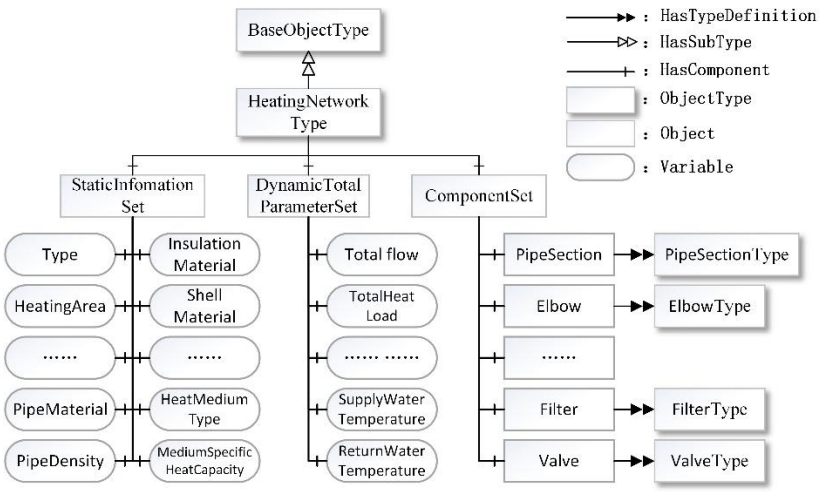

Figure 4. OPC UA graphical representation of HeatingNetworkType in system-level

The Static Information Set of the heating network includes data that does not change over time, such as the network type, heating area, and heat medium type. These data are used to describe the fundamental characteristics and performance of the heating network.

The Dynamic Total Parameter Set of the heating network includes overall data that changes over time, such as the total flow and total heat load of the heating network. These data are used to describe the operational status and efficiency of the heating network.

Taking the example of the Static Information Set object under the HeatNetworkType, the established variables include pipe material, pipe density, heat medium type, etc. The standardized definitions for some variables are provided in Table 2.

Table 2. Standardized definitions of some variables in the static information set

Node Class	Node DisplayName	Node BrowseName	DataType	Description
variable	管网类型	Type	String	Does the heating network belong to the primary network or the secondary network
	供热区域	HeatingArea	String	The scope of the heating network's operation
	热媒种类	HeatMediumType	String	The medium for heat transfer
	热媒比热容	MediumSpecificHeatCapacity	Float	Specific heat capacity of the fluid in the pipeline
	管道材料	PipeMaterial	String	Materials used for the heating network pipelines
	管道密度	PipeDensity	Float	Density of the heating network pipelines
	管道比热容	PipeSpecificHeatCapacity	Float	Specific heat capacity of the heating network pipelines

The Component Set encompasses the components of the heating network, such as pipe sections, valves, and others. These components are also treated as objects and derived from the corresponding equipment-level information models that have been created. The mapping of some equipment-level information model for the heating network to OPC UA object node types is shown in Table 3.

Table 3. Equipment -level object node types in the heating network

Node Class	Node DisplayName	Node BrowseName	TypeDefinition	ModelllingRule
ObjectType	管段类型	PipesectionType	BaseObjectType	M
	三通类型	TeeType	BaseObjectType	M
	弯头类型	ElbowType	BaseObjectType	M
	过滤器类型	FilterType	BaseObjectType	M
	阀门类型	ValveType	BaseObjectType	M
Object	动态参数集	DynamiclParameterSet	FolderType	O

Due to the excessive amount of information in the PipeSection object information model and the fact that not every pipe section requires monitoring of dynamic parameters, the dynamic parameter set object is established under the PipeSectionType. The dynamic information of the pipe sections is created within this set. Its modeling rule is set as Optional, meaning that by default, the DynamicParameterSet is not created when a pipe section is established. It is only created for pipe sections that have monitoring requirements.

As an example, the OPC UA graphical representation of PipeSectionType in equipment-level is shown in Figure 5. The object type is derived from BaseObjectType, and it defines the characteristic variables of a pipe section, including position, number, nominal diameter, and others. The reference relationships between nodes are represented by different arrows.

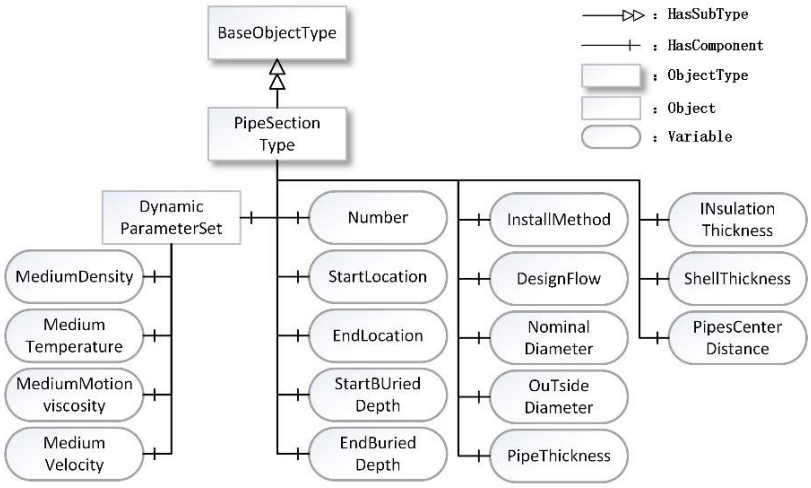

Figure 5. OPC UA graphical representation of PipeSection types in equipment-level

3.3. Instantiation of the information model

Instantiation refers to converting the abstract device information model into specific object information that represents the actual functioning heating system. Taking the valve as an example, a partial instantiation information model for the Valve Type is shown in Figure 6. Since the valve belongs to the control device category, the definition of the valve type is divided into two parts: attributes and methods. The attributes include the number, type, and others, while the methods include start and stop operations. For method nodes, the information model only defines the nodes, and the method functions are written during application development. The initial value for a readable variable like the degree of opening is set to 0.0 during instantiation. Once the variable node is bound to a data source, the readable variable will be updated with the actual value.

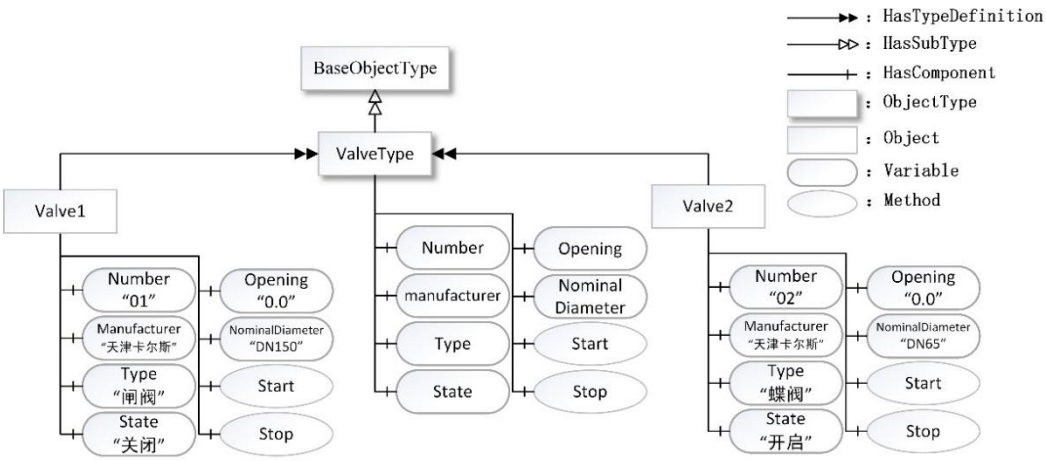

Figure 6. Instantiation of VavleType

4. DESCRIPTION OF THE INFORMATION MODEL FOR CENTRALIZED HEATING NETWORK SYSTEM

For information model design, graphical representation is the most intuitive and easy-to-understand approach. However, computers cannot interpret the meaning of graphical representations. Therefore, it is necessary to use XML files to provide a standardized description of the established centralized heating network information model, representing it in a format that can be understood and parsed by computers.

4.1. Generation of the information model

After the instantiation of the information model, the UaModeler tool can be used to create the information model for the heating network system. UaModeler is a visual modeling generator for OPC UA that can parse custom information models and output them as XML files compliant with the OPC UA specification. Figure 7 illustrates the visual model of the heating network system under the functional requirements using UaModeler.

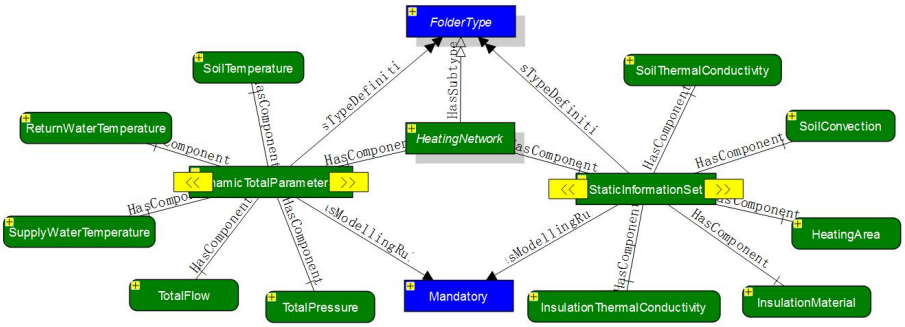

Figure 7. UaModeler model of the heating network system

4.2. XML description of the information model

The provided XML snippet in Figure 8 depicts the textual description of the heating network system information model. It is evident that using XML files for structuring the information model enables a standardized description and representation of the components and devices within the heating network system. This facilitates compatibility and interoperability of the information model across different systems and platforms[10].

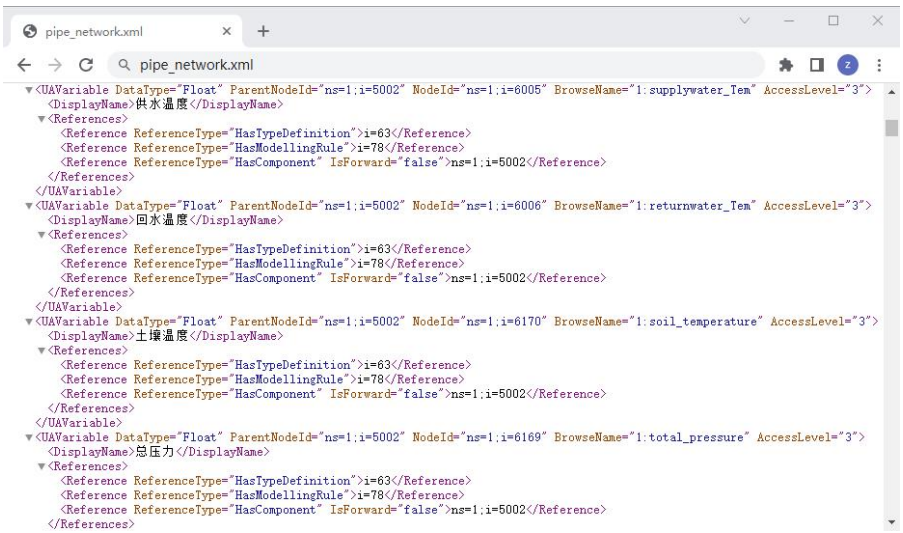

Figure 8. XML file

5. VALIDATION OF THE INFORMATION MODEL FOR THE CENTRALIZED HEATING SYSTEM

The compiled result of parsing the heating network system XML file into OPC UA server-readable code using tools such as Python, Open62541, and Cmake is illustrated in Figure 9.

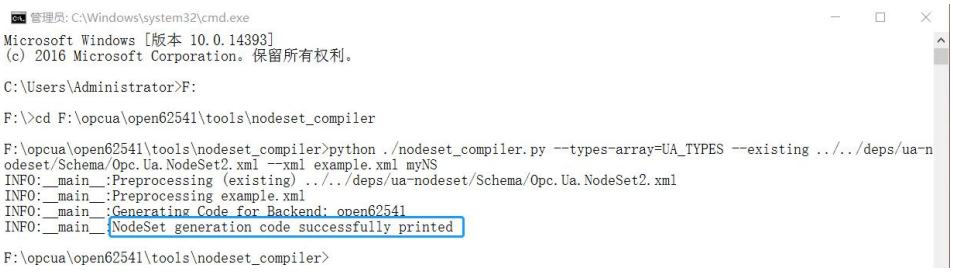

Figure 9. Model compilation

After successfully running the OPC UA server in a C++ environment using the open-source library Open62541, the OPC UA client software UaExpert is used to establish a connection with the OPC UA server. The server's address space node types are obtained, and the success of the information model creation is determined based on the changes in the nodes. The test result is shown in Figure 10.

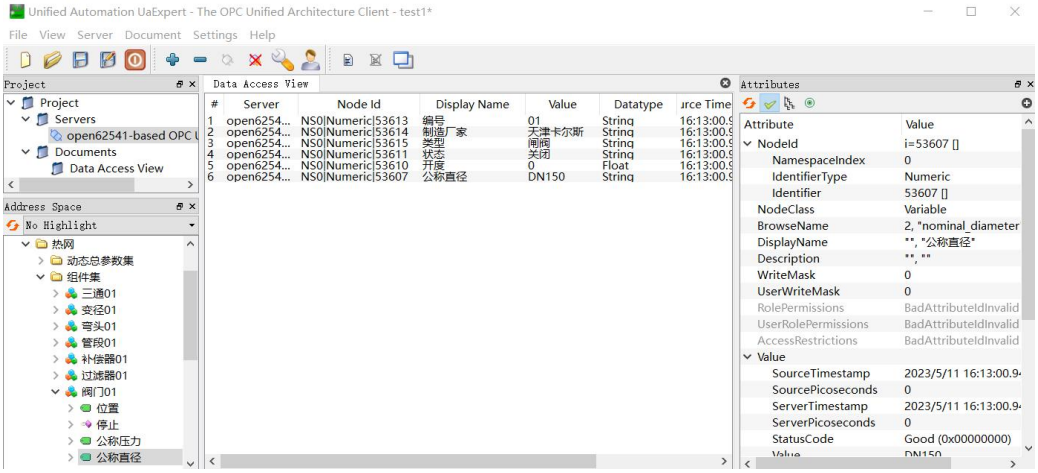

Figure 10. UaExpert test result

The provided figure displays the instantiated information model of the heating network system. The node browsing area successfully shows the valve 's properties, such as its number, type, and status. The test results indicate that the created information model can be mapped to the OPC UA server's address space. It enables access to the server's address space through an OPC UA client, allowing retrieval of the properties of any object within the heating network system.

6. CONCLUSION

This paper presents a general information model for heating systems, designed specifically for their operational characteristics and digital twin requirements. The information model is developed using the OPC UA modeling approach, encompassing both the system-level and equipment-level models for heating networks. The model defines standardized representations of the included information, ensuring scalability and comprehensive description of the heating system. The proposed information model framework offers a viable technical solution for applying digital twin technology in heating systems, addressing the lack of standardized and comprehensive information required for digital twin development. It serves as a valuable reference for instantiating and standardizing information models for different heating systems.

7. ACKNOWLEDGMENTS

This work is supported by China National 14th Five-Year Plan of Key Research and Development Program “Development of the digital-twin for a district heating system and the smart control based on dynamic simulation towards a low-carbon energy sector” (2021YFE0116200).

REFERENCES

[1] GE Junbo, FAN Xin, GUO Weiguo. State of Intelligent Heating in China's Heating Industry and its Development Trends [J]. District Heating;2022(04):118-122.
[2] ZHONG Wei, LU Shuowei, LIU Rong. The concept, technology, and value of intelligent heating [J]. District Heating;2018(02):1-5.
[3] TAO Fei, LIU Weiran, LIU Jianhua, LIU Xiaojun, LIU Qiang, QU Ting, HU Tianliang, ZHANG Zhinan, XIANG Feng, XU Wenjun, ZHANG Yingfeng, LIU Zhenyu, LI Hao, CHENG Jiangfeng, QI Qinglin, ZHANG Meng, ZHANG He, SUI Fangyuan, HE Lirong, YI Wangmin, CHENG Hui. Digital twin and its potential application exploration[J]. Computer Integrated Manufacturing Systems;2018,24(01):1-18.
[4] Grieves M. Digital twin: Manufacturing excellence through virtual factory replication[J]. White paper;2014: 1-7.
[5] HOU Xiaopeng, WU Zhihui, LIU Haibo, GUO Yipeng, AN Yuan, LI Bo. Information Interconnection and Intercommunication Method for Woodworking Equipment Based on Open Platform Communications Unified Architecture (OPC UA). Chinese Journal of Wood Science and Technology;2022,36(06):95-102.
[6] CJJ/T 81-2013, Technical specification for directly buried hot-water heating pipeline in city[S].
[7] SUN Wei. Modeling analysis and hydraulic balance regulation on heat supply network[D]. Beijing University of Chemical Technology;2008.
[8] CHEN Changming. Urban heating system of the secondary network modeling and dynamic analysis[D]. Zhejiang University;2017.
[9] HU Fei, XU Yun, LIAO Yinghua, HOU Peng, YANG Ming. Research on Information Modeling and Communication of CNC Machine Tool Based on OPC UA. Machine Tool & Hydraulics;2021,49(20):53-58.
[10] WANG Xiaoyou, LIAO Yinghua, WANG Hua. Information model of extrusion line monitoring system based on OPC UA. Manufacturing Technology & Machine Tool; 2023(04):141-147.

The 18th International Symposium on District Heating and Cooling, September 3–6, 2023, Beijing, China

DISTRICTLAB-H: A NEW TOOL TO OPTIMIZE THE DESIGN AND OPERATION OF DISTRICT HEATING AND COOLING NETWORKS

Roland Bavière[a,b*], Mathieu Vallée[c], Stéphanie Crevon[b], Nicolas Vasset[c], Nicolas Lamaison[c]

[a] *DistrictLab, 38000 Grenoble, France*
[b] *Univ. Grenoble Alpes, CEA, Liten, DTCH, 38000 Grenoble, France*
[c] *Univ. Grenoble Alpes, CEA, Liten, Campus Ines, 73375 Le Bourget du Lac, France*
[*] *Corresponding author. roland.baviere@districtlab.eu*

ABSTRACT

This article introduces a new scalable thermal-hydraulic modeling framework for dynamic simulation of small to large-scale District Heating (DH) and Cooling (DC) networks. The roots of this new development are to be found in the need for a more efficient solver including an accurate substation model. Following a comprehensive literature review, the solver is presented and validated using existing dynamic experimental data for a straight pipe. In a following step, a real large DH network, from the city of Metz (FR), is modeled and simulated, with results showing good consistency with field data. The numerical efficiency of the proposed approach is then assessed, leading to a quasi-linear scaling of the algorithm up to sizes comparable to the largest DH systems in Europe and to performances that compares very favorably to other models described in the literature. This work opens pathways towards the definition of advanced network architecture and the optimization of design and control strategies. To illustrate these new possibilities, the last section briefly presents real life use cases addressed with the tool such as the evaluation of an innovative 3-tubes architecture, the network resizing for lowering the temperature and the real time control optimization of the supply temperature.

Keywords: District Heating, Dynamic simulation, Thermal-hydraulic solver, innovative District Heating concept

1. INTRODUCTION AND STATE-OF-THE-ART

Due to their inherent ability to integrate waste heat and renewable energy, District Heating (DH) networks are cost efficient systems for any policy targeting a reduction of greenhouse gas emissions [1]. Defining transition scenarios for DH networks towards higher generation systems [2], designing and refining new networks as well as optimizing the operation of existing systems are crucial tasks to meet the ambitions associated to the deployment of these DH technologies. Thermal-hydraulic simulation and more specifically predictive simulation should play a key-role in those processes. By predictive, we mean the ability to simulate accurately situations and arrangements that go beyond those already characterized by existing operational data. Among various methodological options, physical models relying on an explicit representation of every component are particularly relevant. Brange *et al.* [3] showed how network simulation could help to identify and solve bottlenecks issues. Tol and Svendsen [4] proposed a simulation-based methodology for improving the dimensioning of piping networks and network layout. Wang [5] and Hirsch *et al.* [6] both relied on heuristic optimization approaches combined with network simulation capabilities for the appropriate selection of relevant design and operating parameters. In all these approaches, the obtained results are sensible to the accuracy of the underlying network model, as evidenced by Guelpa [7] for district heating networks and Yliruka *et al.* [8] in the more general context of energy systems models. Our contributions consist in presenting and evaluating a scalable and precise thermal-hydraulic model for dynamic simulation of fully described DH networks.

The models related to the present work are of 1-D nature and of the pseudo-dynamic type, an approach combining steady-state simulation of the hydraulic part and transient simulation of the temperature and passive flow tracers transport problems. Three main difficulties characterize the current research efforts for obtaining accurate models of this kind: a fine resolution of the transportation problem, a consistent and predictive description of substation operation, and a good scalability and CPU performances for full representation of large-scale DH networks.

On the temperature transport problems, we can group available methodologies in two main categories, depending on whether the computational grid remains at the node level, i.e. the pipe extremities, or meshes the pipe. The former category groups smart plug-flow models, sometimes labeled node methods, which compute transportation times between pipe extremities for modeling temperature profiles. Heat storage in the solid part of the pipe is accounted for by lumping a mass related to a pipe and modeling it at one extremity [9]. Some of the schemes proposed can be unconditionally stable ([10], [11]). However, the

lack of a computational grid inside the pipe decouples the internal temperature profile from other parts of the system. This is quite limiting when significant heat flow can occur between pipes, such as in the twin-pipe arrangement. Concerning methodologies equipped with in-pipe computational grids, the main issue mentioned in the literature concerns numerical stability; many proposed schemes can ensure a contained numerical diffusion, but are limited in regions where a suitably defined Courant number is lower than one ([12], [13], [14], [15]). On the opposite, an unconditionally stable, but quite diffusive stable implicit first-order upwind Finite Volume scheme (hereafter denoted UFV), has been described [16].

On the substations side (assumed here as indirectly-connected type substations), the primary outlet temperature at the substation level, hereafter denoted $T_{out,p}$, is of prime order on the thermal-hydraulic behavior of a DH network. Many tools available today ([17], [18], [19]) will rely on the setting of this $T_{out,p}$ variable in one way or another by the user; this, in particular in order to ease the numerical process of solving a thermal-hydraulic state. Another possibility consists in relying on a heat exchanger model to evaluate $T_{out,p}$. Benonysson *et al.* [20] and Giraud *et al.* [21] followed a grey-box modelling approach and proposed various forms of explicit empirical models linking inflow/outflow temperatures and flow variables. First principles models relying on the ε-NTU (i.e. effectiveness-number of transfer units) formulation or the mean logarithmic temperature difference formulation have been also proposed ([22], [7]). However, the integration of such models in a thermal-hydraulic simulation engine suitable for large-scale systems, comprising several hundreds or even thousands of substations, remains undone.

Finally, concerning scalability, several authors have developed DH simulation models at the district-scale using general-purpose environments. The equation-based Modelica language and the Dymola platform have been extensively used ([23], [21], [24]). A meshed DH network simulator in MATLAB/Simulink [25] and a plug-flow model for the TRNSYS software [26] have been developed. However, to simulate large-scale systems, a tool specifically crafted for this task is required. Guelpa *et al.* [27] proposed a dedicated thermo-fluid model to this end but the obtained computational costs were too high for the direct simulation of the DH system of the city of Turin, which is the largest in Italy. Omitting the imposed $T_{out,p}$ issue mentioned in the previous paragraph, existing commercial software could be used, but they additionally are limited by their capacity to handle dynamical scenarios [19] or architectures beyond the classical two-tube designs ([17], [18]).

The present paper reports on our work to design, implement, validate and demonstrate the usage of DistrictLab-H, a new software targeting predictive thermal-hydraulic simulation of small to large-scale DH systems. The main design options for DistrictLab-H are the preference for "first principle" models, i.e. mass, momentum and energy balances, over empirical models, the use of unconditionally stable calculation schemes and the formulation of a compact yet generic modeling language. The key strengths and novelties of the tool are its abilities i) to model innovative architectures that go beyond the classical 2-tubes configuration, ii) to solve efficiently large-scale and meshed systems and iii) to compute accurately the primary outlet temperature at the substation.

The following sections of the paper are structured as follows. In section 2, the thermal-hydraulic models and equations are presented together with the solving strategy. In section 3, the temperature transport solver is validated and the model scalability is studied. In section 4, real-life case studies are presented. Finally, section 5 summarizes the obtained results and concludes the paper.

2. OVERVIEW OF DISTRICTLAB-H™

The present section presents the core equations of the models. Although, these are described from a District Heating network point of view, similar equations are used when dealing with District Cooling networks.

2.1. Model structure and definitions

The DH network model is structured using an oriented graph in which a node acts as a thermal-hydraulic connector and an edge represents either a distribution pipe or a substation. This formalism allows expressing the governing equations in matrix form. In this context, the connectivity matrix between two ensembles, say U and V, respectively of cardinality N_U and N_V, is defined as the $N_U \times N_V$ matrix whose non-zero entries all equal 1 and correspond to (i, j) pairs where element # i of U is "linked" to element # j of V. The exact meaning of the "link" is case dependent.

In this approach, several edges are connectable to a unique node but each edge must be connected to exactly one "inlet" and one "outlet" node. A "fixed grade" node is a point of known head or pressure, i.e. a node connected to a Boundary Condition of the Pressure Imposed type (BCPI), where flow can enter or exit the network. To increase expressivity of the formalism, distribution pipes can host modeling gadgets (e.g. pumps, heat generators, valves etc.) and a variant exists to represent substations. These elements allow modeling classical two-tube networks and more innovative architectures, as the one presented in Figure 1.

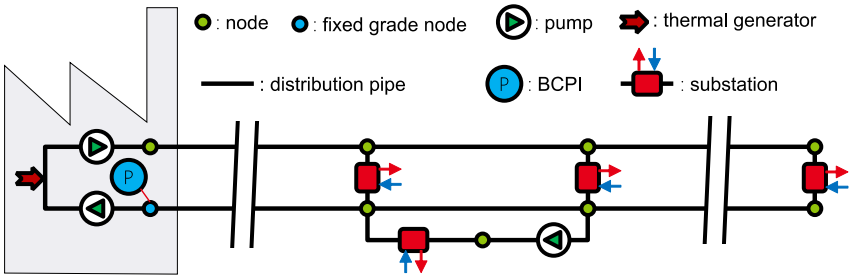

Figure 1. Schematic side-view of a model comprising a production unit, a 2-tube network and distributed consumers of various connection types.

The thermal-hydraulic kernel is built to treat 1D models of the pseudo-dynamic type, an approach combining steady-state simulation of the hydraulic part and transient simulation of the temperature transportation problem. This assumption is applicable for liquid water networks in which hydraulic wave travel several orders of magnitude faster than temperature and tracers waves and for problems where pressure transients can be discarded. Benonysson [9] and Boulos *et al.* [28] both demonstrated its efficiency respectively for DH dynamic simulation and contaminant propagation in water networks. A node is treated as an infinitesimal fluid volume hosting both a pressure and a temperature state whereas an edge is seen as a one-dimensional fluid element hosting a mass flow-rate state and an axially distributed set of temperature states.

2.2. Mass and energy balances at the node level

Let $\mathbb{A}_+$ (respectively $\mathbb{A}_-$) be the (node - edge) connectivity matrix where the "link" (as defined beforehand) means "is the inlet node of" (respectively "is the outlet node of"). Let $\mathbb{B}$ be the (node - BCPI) connectivity matrix where the "link" stands for "is connected to". With $\overrightarrow{\dot{m}_e}$ and $\overrightarrow{\dot{m}_{BCPI}}$ respectively the edge and BCPI mass flow-rate vectors, mass conservation for all the nodes in the network reads in the matrix form as shown in Equation (1).

$$(\mathbb{A}_+ - \mathbb{A}_-) \cdot \overrightarrow{\dot{m}_e} + \mathbb{B} \cdot \overrightarrow{\dot{m}_{BCPI}} = \vec{0} \tag{1}$$

Pressure is imposed with Equation (2) in all fixed-grade nodes (BCPI ensemble), where $\overrightarrow{P_{st}}$ and $\overrightarrow{P_{st,BCPI}}$ respectively stand for the node and BCPI stagnation pressure vectors.

$$\mathbb{B}^T \cdot \overrightarrow{P_{st}} - \overrightarrow{P_{st,BCPI}} = \vec{0} \tag{2}$$

To derive the energy balance equations at the node level, let $\overline{\mathbb{A}_+}$ (respectively $\overline{\mathbb{A}_-}$) be the (node - edge) flow dependent connectivity matrix where the "link" means "is the upstream node of" (respectively "is the downstream node of"). Similarly, let $\overline{\mathbb{B}_+}$ and $\overline{\mathbb{B}_-}$ be the equivalent matrixes for the (node - BCPI) ensembles. Energy conservation for all the nodes in the network reads as shown in Equation (3) with $T_{f,edge,out}$, $T_{f,BCPI,ext}$, $T_{f,node}$ and $\mathbb{D}(\ )$ standing for the edge outlet temperature, the BCPI external temperature, the node temperature and the operator transforming a vector to the corresponding diagonal matrix respectively.

$$\mathbb{D}\left(\overrightarrow{T_{f,node}}\right) \cdot \left(\overline{\mathbb{A}_+} \cdot \overrightarrow{|\dot{m}_e|} + \overline{\mathbb{B}_+} \cdot \overrightarrow{|\dot{m}_{BCPI}|}\right) = \overline{\mathbb{A}_-} \cdot \overrightarrow{|\dot{m}_e \cdot T_{f,edge,out}|} + \overline{\mathbb{B}_-} \cdot \overrightarrow{|\dot{m}_{BCPI} \cdot T_{f,BCPI,ext}|} \tag{3}$$

2.3. Momentum and energy balance for a distribution pipe

In matrix form, the momentum balance equation written for the distribution pipes is shown in Equation (4), with g, ρ_f, z, D, A_f, and $\overrightarrow{\Delta H_s}$ standing for the gravity constant, the fluid density, the node altitude, the pipe diameter, the pipe cross-sectional area and the momentum source associated to pumping elements, respectively and ξ and f are non-dimensional factors respectively representing singular and regular friction losses.

$$\left(\mathbb{A}_{pipe,+} - \mathbb{A}_{pipe,-}\right)^T \cdot \left(\overrightarrow{P_{st}} + g \cdot \overrightarrow{\rho_f \cdot z}\right) - \frac{1}{2} \cdot \mathbb{D}\left(\overrightarrow{\left(\xi + f \cdot \frac{L}{D}\right) \cdot \frac{|\overrightarrow{\dot{m}_{pipe}}|}{\rho \cdot A_f^2}}\right) \cdot \overrightarrow{\dot{m}_{pipe}} + \overrightarrow{\Delta H_s} = \vec{0} \tag{4}$$

In the laminar regime, f is computed using the classical $64/Re$ law where Re corresponds to the Reynolds number. In the turbulent regime, f is evaluated using the law formulated by Swamee and Jain [29] as a function of Re, pipe diameter and roughness. Finally, the transition regime is approximated using a cubic polynomial designed such that the first derivative of

f remains continuous. Hydraulic singularities (e.g. bend, elbow …) are accounted for considering constant singular pressure loss coefficients cumulated in the ξ factor.

To model temperature transportation, concentric "fluid" and "pipe wall" domains are included, surrounded by an insulation layer submitted to a user-defined external temperature. The model considers a convective heat transfer coefficient at the fluid-wall interface (denoted h_{fw}) and a user defined heat loss coefficient representing the insulation layer (denoted h_{ins}) but neglects the thermal resistances through the pipe wall. The h_{fw} coefficient is derived from correlations defining the Nusselt number ($Nu = h_{fw} \cdot D/\lambda$) as a function of the flow regime. A standard value of 4.36 is chosen for the laminar regime while in the turbulent regime, Nu is evaluated through an improved version of the original correlation [30], described in [31], and depends on Prandtl and Reynolds non-dimensional numbers.

The 1D energy balance equation along the x coordinate for the fluid domain follows the classical formulation, shown in Equation (5), with Cp_f, χ_{fw} and S_f respectively standing for the specific heat capacity, the heating perimeter and a conditional source term used to model the effect of a heat generator. The 'w' and 'f' indices respectively relate quantities relative to the wall and fluid domains.

$$\frac{\partial}{\partial t}\left(A_f \cdot \rho_f \cdot Cp_f \cdot T_f\right) + \frac{\partial}{\partial x}\left(A_f \cdot \rho_f \cdot Cp_f \cdot u \cdot T_f\right) = \chi_{fw} \cdot h_{fw} \cdot \left(T_w - T_f\right) + S_f \tag{5}$$

Similarly, the 1D energy balance equation along the x coordinate for the wall domain is shown in Equation (6).

$$\frac{\partial}{\partial t}\left(A_w \cdot \rho_w \cdot Cp_w \cdot T_w\right) = \chi_{fw} \cdot h_{fw} \cdot \left(T_f - T_w\right) \tag{6}$$

2.4. Momentum and energy balance for a substation

The model considered here represents a substation of the indirectly connected type composed of a service pipe and an ensemble consisting of a counter-current plate heat exchanger, a secondary temperature controller and an active two-way valve positioned on the primary side (see Figure 2).

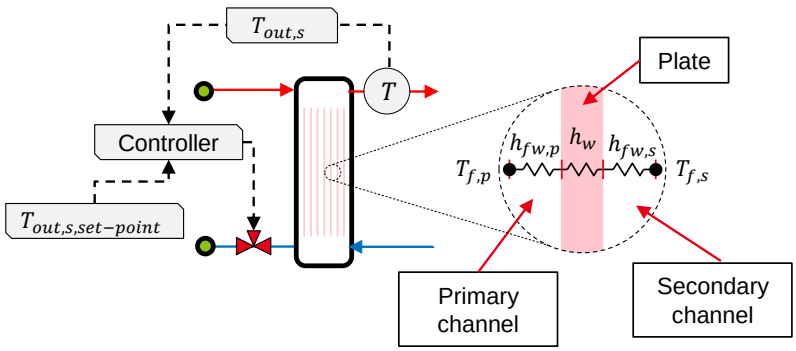

Figure 2. Schematic of the substation model.

From the hydraulic viewpoint, the model is similar to that of a distribution pipe so the corresponding equations set is similar to that already presented in Equation (4), with 'pipe' replaced by 'sst', $\overrightarrow{\Delta H_s}$ removed and the ξ factor representing the presences of the two-way valve and heat exchanger.

From the thermal viewpoint, 1D energy balance equations are written for both the primary and the secondary fluid streams within the heat exchanger. These streams are thermally coupled through a series of heat transfer coefficients accounting for conduction through the plate (h_w) and fluid-wall convection (hereafter denoted $h_{fw,p}$ and $h_{fw,s}$). Equation (7) shows this balance for the primary stream. The same equation is written for the secondary stream with index 'p' replaced by 's'.

$$\frac{\partial}{\partial t}\left(A_{f,p} \cdot \rho_{f,p} \cdot Cp_{f,p} \cdot T_{f,p}\right) + \frac{\partial}{\partial x}\left(A_{f,p} \cdot \rho_{f,p} \cdot Cp_{f,p} \cdot u_p \cdot T_{f,p}\right) = \chi_{fw} \cdot \frac{1}{1/h_{fw,p} + 1/h_w + 1/h_{fw,s}} \cdot \left(T_{f,s} - T_{f,p}\right) \tag{7}$$

The present model relies on a parametric law to estimate the fluid-wall heat transfer coefficients ($h_{fw,p}$ and $h_{fw,s}$) where the parameters are inferable from the values provided in typical heat exchanger data sheet. A two-coefficient power law with respect to the Reynolds number is therefore considered, as shown in Equation (8) with e, K and q respectively standing for the channel height, the constant and the power exponent of the law and the index 'j' is an alias for either 'p' or 's'. This equation can be viewed as a simplified version of the laws proposed by [32] and [33], discarding some dependencies to the plate geometry and Prandtl number. Typical values for q fall within the 0.6 – 0.8 range.

$$\frac{h_{fw,j} \cdot (2 \cdot e_j)}{\lambda} = max(8; K_j \cdot Re^{q_j}) \tag{8}$$

2.5. Solving strategy

The global thermal-hydraulic model is computed relying on a hydraulic solver and a temperature transport solver, as shown in Figure 3. On the one hand, the hydraulic problem, which expresses mass and momentum conservation throughout the network, is a non-linear static problem and solves the pressure in the nodes and mass flow rates in the edges. On the other hand, the temperature transport problem, which expresses energy conservation throughout the network, is a quasi linear-problem and solves the temperature in the nodes, edges and substations.

Specifically, for each time-step, DistrictLab-H™ triggers several resolutions of the aforementioned two sub-problems in order to obtain a converged thermal-hydraulic solution. Optionally and after convergence of the thermal-hydraulic problem, DistrictLab-H™ can solve a scalar field linear dynamic transportation problem (transportation time, influence zone, etc.).

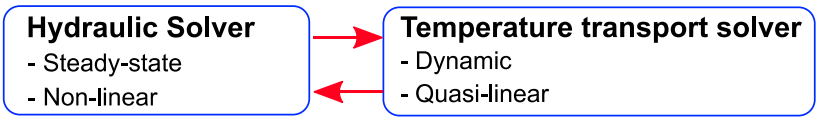

Figure 3. Main computation steps within the thermal-hydraulic solver

3. VALIDATION AND SCALABILITY

3.1. Transient temperature transport validation

The present section focuses on the error analysis for the temperature transport inside a single pipe submitted to varying inlet temperature. The main objectives here are i) to validate the temperature transport solver and ii) to evaluate an innovative discretization scheme based on donor-cell classical finite volume approach combined with a cell profile assumed as bilinear, coherent with what is expected in DH systems. The experimental data used for this validation were first presented by Sartor and Dewalef [34], and generously provided by one of the authors. Appendix A described the specific dataset used here.

Figure 4 (left) presents the results for Dataset 1 for which 2 steps are applied to the incoming water temperature. It highlights in the upper panel, the envelopes related to the imposed mass flow rate accuracy (+/- 3%) and in the lower panel, the uncertainty range for temperature measurement (0.9 K). The results are obtained for a converged mesh and a time step of 1s. A very satisfactory match between simulation and experimental results is proven with an instantaneous error remaining within the measurement system uncertainty range. It is worth emphasizing here that the transportation time is accurate even though the operating conditions simulated are extreme in terms of temperature ramp (about 90°C/min) with respect to normal operating conditions of heating grid production units (typically 5°C/min).

In order to compare the classical discretization scheme, denoted UFV, and the innovative one introduced above, denoted UFVbl, a mesh convergence analysis was conducted for different datasets and time steps. The resulting graphs are shown in Figure 4 (right) for both calculation schemes. Results show clearly that mesh convergence is attained for a Courant number (respectively cell size) one order of magnitude lower (respectively larger) for the UFVbl scheme. The latter results show the decisive advantage of the UFVbl scheme when dealing with large numbers of edges, since only a rather coarse grid is needed to obtain convergence. For both schemes, the error is shown to be the highest for the highest velocity dataset (Dataset 3), which is expected with finite volume schemes subjected to numerical diffusion. In Figure 4 (right), numerical diffusion clearly saturates the attainable accuracy, however, we believe that this accuracy is sufficient to conduct real-case studies on large-scale DH networks, as will be presented in the following section.

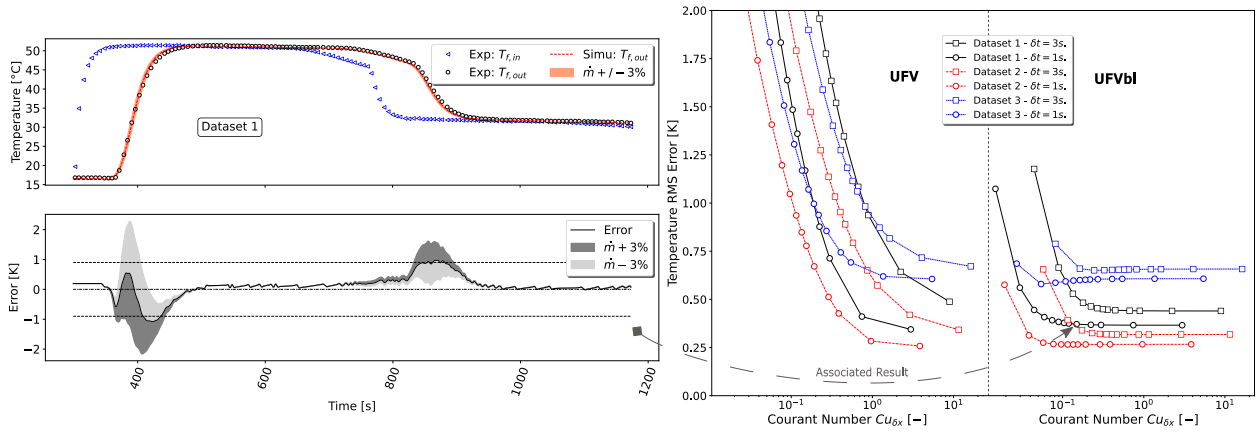

Figure 4. Left: Simulation results for Dataset 1 using the UFVbl scheme. Right: RMS error on the outlet pipe temperature for UFV and UFVbl calculation schemes as a function of the Courant number $Cu_{\delta x} = u \cdot \delta_t / \delta_x$, for 2 integration time steps (δ_t) and 3 datasets.

3.2. Large scale performances

The city of Metz, France, hosts a 2nd generation two-tube DH system with a yearly heat production of 450 GWh and 366 substations. Figure 5 (left) shows the layout of the Metz High Pressure Network (HPN) along with the position of the two supply units, namely SU1 and SU2, and five important substations, namely HPBP1 to HPBP5. Appendix B presents additional details of the HPN and describes the developed validation methodology.

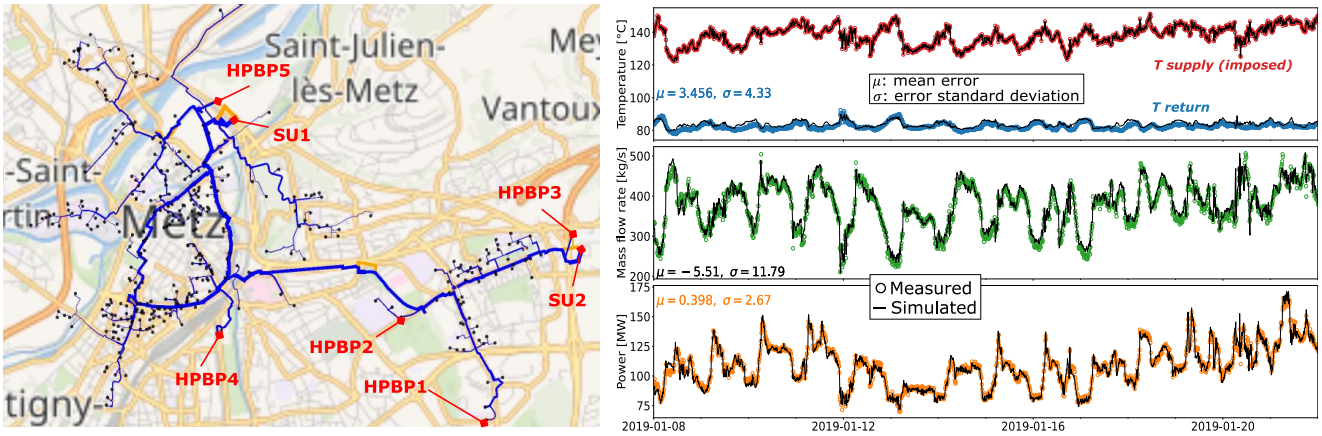

Figure 5. Left: HPN model for the DH system of Metz (base map from OpenStreetMap and OpenStreetMap Foundation, see www.openstreetmap.org). Right: Temperatures and mass flow rate at the main supply unit SU1 and total delivered power.

To verify the model, the numerical and experimental data were compared at the production level (see Figure 5 right) and at the consumer level (see Table 1) where the mean and standard deviation of a set of errors are denoted μ and σ respectively. These elements show that reasonable accuracy is obtained for such a large scale DH system. On-going work such as local pressure drop calibration helps to reduce the model uncertainties and will lead to a fully representative simulator.

Table 1. Error indicators obtained at the substation level for a two-week simulation of the Metz HP network.

	$\mu\{T_{in,pr}\}$ $[K]$	$\sigma\{T_{in,pr}\}$ $[K]$	$\mu\{T_{out,pr}\}$ $[K]$	$\sigma\{T_{out,pr}\}$ $[K]$	$\mu\{\Delta H\}$ $[bar]$	$\sigma\{\Delta H\}$ $[bar]$
HPBP 1	−2.44	1.31	−0.01	0.88	−0.06	0.42
HPBP 2	−2.24	1.88	+0.91	1.0	−0.46	0.48
HPBP 3	+1.47	3.06	+0.09	1.67	+0.19	0.43
HPBP 4	+1.00	1.35	−0.00	1.6	−0.44	0.18
HPBP 5	+1.74	0.82	+0.09	0.39	+0.02	0.05

3.3 Scalability

The scalability of the tool is now evaluated. Similarly to [27], the number of nodes N_n is used to quantify the problem size.

Figure ***6*** presents first the results obtained with the tool on a single core of an Intel i7@2.11GHz processor for a 10 minutes time-step. The number of nodes was artificially increased using replication of the Metz DH system (see section 3.2) with the replicas connected to nodes located close to the main production unit of this DH system. Interestingly, the proposed model scales quasi-linearly with N_n, at least up to $N_n = 6.5 \cdot 10^4$, which is the highest value tested. For illustration, this figure exceeds the size required to model the DH system of the city of Turin, which is among the largest in Europe.

The present results are also compared to available simulators and models published in the open literature.

Figure ***6*** plots the results obtained with the model described in Giraud et al. [35] and its larger-scale variants produced using the same method as previously, programmed using the Modelica language and simulated with the Dymola® simulation engine. In this case, the simulation time scales as $\propto N_n^2$.

Figure ***6*** also presents the CPU times reported in Guelpa et al. [27]. In this case, the execution time corresponds to a single iteration of a dynamic thermo-fluid model programmed and executed in Matlab®, using a 3.3 GHz CPU. Again, the CPU time scales as $\propto N_n^2$ and the results exhibit a cliff effect for N_n greater or equal to 2.10^4. It can therefore be concluded that for a given problem size, the execution of the present model is several orders of magnitude faster than with the other assessed tools.

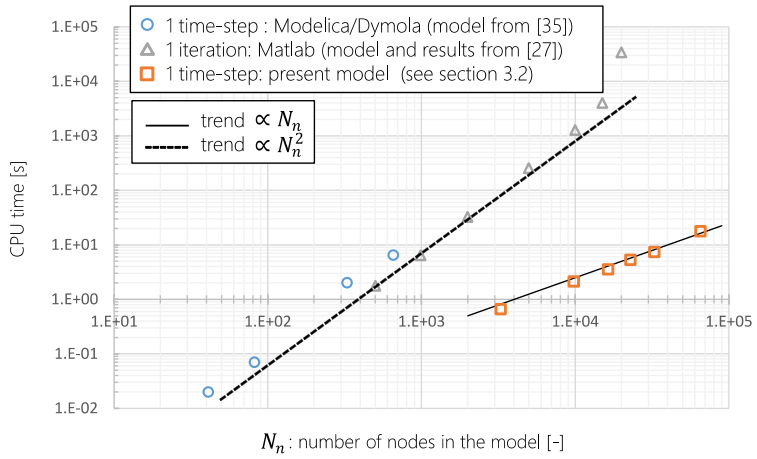

Figure 6. Influence of the problem size on CPU time for dynamic DH network simulation. The results concerning the Modelica and the present model have been obtained on the same computer using a 10 minutes time-step.

4. USE CASES

This last section illustrates the main use cases of DistrictLab-H™ with existing projects as example, pointing out the practical impact of the tool on the field. The following use cases share the common goal of improving energy efficiency of foreseen or existing DH systems by numerical means. These cases all rely on the development of a numerical model of the system. In practical terms, we relied on the tool's automatic model builder allowing to set-up a network layout based on Geographical Information System (GIS) and to parametrize the consumers' and substations' models from energy consumptions. A few days of work is generally required to bring the model to a suitable readiness level. For each use case, the objectives and the approach are described, followed by the presentation of the main outcomes.

• ***Use case 1: Assessing an innovative three-tube architecture to ease surplus heat integration***. District Heating networks have historically been designed to work in a context where energy sources where both abundant and flexible. These systems now face the challenge of abating carbon emissions of existing material. The "CADOuest" company [36], in cooperation with the "Services Industriels de Lausanne" [37], recently proposed an innovative concept based on an architecture allowing to connect new low temperature sources and consumers between the return line of an existing two-tube high temperature network (130 - 70) and a new third tube. Thanks to its versatility, DistrictLab-H™ was used to assess this architecture, to reveal and correct its potential weaknesses and establish its control rules. The project aims to deliver annually 11 GWh of low temperature heat, with a 90 % share of renewable energy [38].

• ***Use case 2: Network resizing to lower operational temperature.*** A large share of existing DH networks have been sized to operate at high temperature levels. However, in some cases, limited investments can be sufficient to ensure a transition towards lower network temperatures. The DistrictLab-H™ simulation engine is equipped with a resizing module allowing to automatically prescribe piping diameters required to satisfy local hydraulic design rules (velocity, pressure drop), in a multi-scenario context. This feature was recently applied to study the transition between an existing high temperature network to a lower temperature system for a French system. The results showed the techno and economic feasibility of the transition and helped to plan the project over a several years period.

• ***Use case 3: Optimize the evolution of an existing network with respect to a temperature reduction target.*** In the same context of a technical retrofit for existing, earlier generation DH networks, a methodology has been developed in order to tackle the design problem with a constraint in the network operating temperature target. Joint modifications of several elements at once (substations, pipes, hydraulic pumps) are assessed. This multi-asset perspective generalizes the approach of network resizing described above. With an objective set for the operating temperature, a multi-objective optimization problem is formulated for simultaneous minimization of investment costs and operation. This kind of study, implemented

through metaheuristics and using DistrictLab-H™ for evaluating operation costs of a solution candidate, takes advantage of the great performance of the simulator for its use in a typically costly optimization procedure (here an implementation of the NSGA2 algorithm [39]). After a thorough evaluation of the approach [40], a study in real, dynamical operating conditions for a DH network [41] showed its capacity to help decision makers on performing needed investment choices, by proposing sets of solution at different investment and operational costs.

• ***Use case 4: Optimizing real-time supply temperature control.*** Most two-tube DH Networks are operated relying on both variable supply temperature and differential pressure setpoints. These degrees of freedom are useful to secure the energy delivery to the consumers but can be very hard to set in practical situations. We developed and deployed two real-time supply temperature controllers on the DH systems equipping the French cities of Metz and Grenoble respectively [42]. These are based on the DistrictLab-H™ on-line module. As shown in Figure 7, in the Grenoble case, the systems works in tight connection with the Energy Optima 3™ production planner [43] (provided by Energy Opticon company) and targets a global production and distribution optimization. The installation of the system on the field to aid the decision of the operator revealed temperature reduction potentials of 15 degrees in some portions of the network.

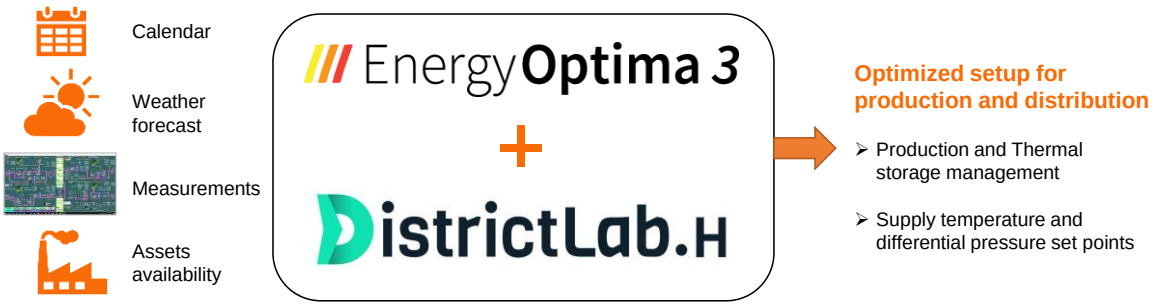

Figure 7. Optimizing real-time supply temperature control combining DistrictLab-H™ and Energy-Optima™

5. CONCLUSION AND PERSPECTIVES

In this paper, we present a new tool, i.e. DistrictLab-H™, for the predictive simulation of district thermal networks. After reviewing the relevant scientific literature and available tools, the proposed thermal-hydraulic models and solver are detailed. In the present approach, the main models being of the first principle type, their validity is expected to go beyond situations and arrangements already characterized by existing operational data.

The innovative discretization scheme for the temperature transport solver is then validated and shown to behave favorably with respect to the classical first-order upwind finite volume scheme. The large scale performances of the solver are then evaluated with the modeling of the Metz (FR) DH network, which is the 3rd largest such system in France. The good accuracy of the model for the prediction of return temperatures, a crucial advantage, is shown. The quasi-linearity of the solver execution time with respect to the number of nodes in the model is demonstrated up to $6.5 \cdot 10^4$ nodes, which is the range for the largest DH systems in Europe. These performances compare very favorably to other models described in the literature.

To illustrate the new possibilities offered by the tool, the last section briefly introduced several real life use cases. An assessment for an innovative 3-tubes architecture for low temperature heat surplus integration has been performed. Additionally, network resizing for lowering the temperature could be tackled using a meta-heuristics approach with DistrictLab-H™ positioned as simulator. Finally, the predictive capabilities of the simulator allowed to perform real-time optimization of production supply temperature for two large DH networks; operational margins up to 15K were found in some portions of the networks.

On-going research efforts include further validation of systems including thermal energy storage and pairs of pre insulated pipes buried directly into the ground. Also, a methodology for automatic hydraulic calibration of pipes roughness based on field data is under development. Regarding the application, the meta-heuristics approach for network resizing will be extended with the integration of distributed storages as additional operation assets.

REMARK

All the models and the solver described in this article have been implemented in the commercial DistrictLab-H™ software tool dedicated to dynamic simulation of large scale thermal networks [44].

ACKNOWLEDGEMENTS

We acknowledge the financial support of the UEM and CCIAG operating companies in the research program that has led to the development of DistrictLab-H™. We also thank Nicolas SCHOENACKER and Loic GIRAUD, respectively from UEM and CCIAG, for the many fruitful discussions we had during the development of the tool. The authors are also grateful to Kevin SARTOR for providing the data and technical details relative to the experiments conducted in University of Liège.

REFERENCES

[1] D. Connolly *et al.*, "Heat Roadmap Europe: Combining district heating with heat savings to decarbonize the EU energy system"," *Energy Policy*, vol. 65, pp. 475–489, 2014, doi: 10.1016/j.enpol.2013.10.035.

[2] H. Lund, "4th Generation District Heating (4GDH). Integrating smart thermal grids into future sustainable energy systems," *Energy*, vol. 68, pp. 1–11, 2014, doi: 10.1016/j.energy.2014.02.089.

[3] L. Brange, J. Englund, K. Sernhed, M. Thern, and P. Lauenburg, "Bottlenecks in district heating systems and how to address them," *Energy Procedia*, vol. 116, pp. 249–259, Jun. 2017, doi: 10.1016/j.egypro.2017.05.072.

[4] H. Tol and S. Svendsen, "Improving the dimensioning of piping networks and network layouts in low-energy district heating systems connected to low-energy buildings: A case study in Roskilde, Denmark," *Energy*, vol. 38, pp. 276–290, 2012, doi: 10.1016/j.energy.2011.12.002.

[5] N. Wang, "Hydraulic resistance identification and optimal pressure control of district heating network," *Energy Build*, vol. 170, pp. 83–94, 2018, doi: 10.1016/j.enbuild.2018.04.003.

[6] P. Hirsch, M. Grochowski, and K. Duzinkiewicz, "Decision support for design of long distance heat transportation system," *Energy & Buildings*, vol. 173, pp. 378–388, 2018, doi: 10.1016/j.enbuild.2018.05.010.

[7] E. Guelpa, "Impact of network modelling in the analysis of district heating systems," *Energy*, vol. 213, p. 118393, 2020, doi: 10.1016/j.energy.2020.118393.

[8] M. Yliruka, S. Moret, and N. Shah, "Detail or uncertainty? Applying global sensitivity analysis to strike a balance in energy system models," *Computers & Chemical Engineering*, p. 108287, May 2023, doi: 10.1016/j.compchemeng.2023.108287.

[9] A. Benonysson, "Dynamic Modelling and Operational Optimization od District Heating Systems," PhD thesis, Laboratory of Heating and Air Conditionning, Technical University of Denmark, 1991.

[10] I. Gabrielaitiene, B. Bohm, and B. Sunden, "Modelling temperature dynamics of a district heating system in Naestved, Denmark –A case study," *Energy Conversion and Management*, vol. 48, pp. 78–86, 2007, doi: 10.1016/j.enconman.2006.05.011.

[11] I. Gabrielaitiene, B. Bohm, and B. Sunden, "Evaluation of Approaches for Modeling Temperature Wave Propagation in District Heating Pipelines," *Heat Transfer Engineering*, vol. 29, no. 1, pp. 45–56, 2011, doi: 10.1080/01457630701677130.

[12] V. D. Stevanovic, Z. B., S. Prica, B. Maslovaric, V. Karamarkovic, and V. Trkulja, "Prediction of thermal transients in district heating systems"," *Energy Conversion and Management*, vol. 50, 2009, doi: 10.1016/j.enconman.2009.04.034.

[13] A. Dénarié, M. Aprile, and M. Motta, "Heat transmission over long pipes: New model for fast and accurate district heating simulations"," *Energy*, vol. 166, pp. 267–276, 2019, doi: 10.1016/j.energy.2018.09.186.

[14] M. Betancourt Schwartz, M. Tahar Mabrouk, C. Santo Silva, P. Haurant, and B. Lacarrière, "Modified finite volume method for the simulation of dynamic district heating networks"," *Energy*, vol. 182, pp. 954–964, 2019, doi: 10.1016/j.energy.2019.06.038.

[15] H. Wang and H. Meng, "Improved thermal transient modelling with new 3-order numerical solution for a district heating network with consideration of the pipe wall's thermal inertia," *Energy*, vol. 160, pp. 171–183, 2018, doi: 10.1016/j.energy.2018.06.214.

[16] Y. Wang *et al.*, "Thermal transient prediction of district heating pipeline: Optimal selection of the time and spatial steps for fast and accurate calculation," *Applied Energy*, vol. 206, pp. 900–910, 2017, doi: 10.1016/j.apenergy.2017.08.061.

[17] "TERMIS user Guide – Version 5.0" Schneider Electric released Q4." 2012.

[18] "The Netsim Manual – Netsim release 3.5" Vitec Feb." 2017. [Online]. Available: http://doc.energy.vitec.net/ManualData/ve/en/netsim/pdf/NetSim.pdf

[19] "PICALOR – Manuel d'utilisation version 3.97" Gfi Progiciels released Oct." 2018.

[20] A. Benonysson, B. Bohm, and H. F. Ravn, "Operational Optimization in a District Heating System," *Energy Convers. Mgmt*, vol. 36, no. 5, pp. 297–314, 1995, doi: 10.1016/0196-8904(95)98895-T.

[21] L. Giraud, R. Bavière, C. Paulus, M. Vallée, and J.-F. Robin, "Dynamic Modelling , Experimental Validation and Simulation of a Virtual District Heating Network," *28th Int. Conf. Effic. Cost*, pp. 2845–2856, 2015.

[22] S. L. Lazarević, V. D. Čongradac, A. S. Andjelkovic, M. V. Kljajić, and Ž. S. Kanović, "District heating substation elements modeling for the development of the real-time model," *Thermal Science*, vol. 23–3b, 2019, doi: 10.2298/TSCI181226031L.

[23] B. Heijde *et al.*, "Dynamic equation-based thermohydraulic pipe model for district heating and cooling systems"," *Energy Conversion and Management*, vol. 151, pp. 158–169, 2017, doi: 10.1016/j.enconman.2017.08.072.

[24] I. Hoyo Arce, S. H. Lopez, S. L. Perez, M. Rama, K. Klobut, and J. A. Febres, "Models for fast modelling of district heating and cooling networks," *Renewable and Sustainable Energy Reviews*, vol. 82, pp. 1863–1873, 2018, doi: 10.1016/j.rser.2017.06.109.

[25] M. Vesterlund, A. Toffolo, and J. Dahl, "Simulation and analysis of a meshed district heating network," *Energy Conversion and Management*, vol. 122, pp. 63–73, 2016, doi: 10.1016/J.enconman.2016.05.060.

[26] S. A. Klein *et al.*, "TRNSYS 17 a Transient System Simulation program," vol. 4. 2009.

[27] E. Guelpa, A. Sciacovelli, and V. Verda, "Thermo-fluid dynamic model of large district heating networks for the analysis of primary energy savings," *Energy*, vol. 184, pp. 34–44, 2019, doi: 10.1016/j.energy.2017.07.177.

[28] P. F. Boulos, T. Altman, P.-A. Jarrige, and F. Collevati, "An event-driven method for modelling contaminant propagation in water networks," *Appl. Math. Modelling*, vol. 18, pp. 84–92, 1994.

[29] P. K. Swamee and A. K. Jain, "Explicit equations for pipe-flow problems" Proc," *ASCE, J. Hydraul. Div*, vol. 102, no. Y5, pp. 657–664, 1976.

[30] B. S. Pethukov, "Heat transfer and friction in turbulent pipe flow with variable physical properties," *Advances in Heat Transfer*, vol. 6, no. 504, 1970.

[31] V. Gnielinsky, "New equations for heat transfer in turbulent pipe and channel flow," *Int. Chemical Engineering*, vol. 16, pp. 359–368, 1976.

[32] W. W. Focke, J. Zachariades, and I. Olivier, "The effect of the corrugation inclination angle on the thermohydraulic

performance of plate heat exchangers," *Int. J. Heat Mass Transf*, vol. 28, pp. 1469–1479, 1985, doi: 10.1016/0017-9310(85)90249-2.

[33] A. C. Talik, L. S. Fletcher, N. K. Anand, and L. W. Swanson, "Heat transfer and pressure drop characteristics of a plate heat exchanger," in *Proceedings of the ASME/JSME Thermal Engineering Conference*, New York, USA, 1995, pp. 321–329.

[34] K. Sartor and P. Dewalef, "Experimental validation of heat transport modelling in district heating networks"," *Energy*, vol. 137, pp. 961–968, 2017, doi: 10.1016/j.energy.2017.02.161.

[35] L. Giraud, R. Bavière, M. Vallée, and C. Paulus, "Presentation, Validation and Application of the DistrictHeating Modelica Library," in *Proc. of the 11th International Modelica Conference September*, Versailles, France, 2015, pp. 21–23. doi: 10.3384/ecp1511879.

[36] "CADOuest company website." Accessed: Jun. 05, 2023. [Online]. Available: https://cadouest.ch/

[37] "Services Industriels de Lausanne website." Accessed: Jun. 05, 2023. [Online]. Available: https://www.lausanne.ch/vie-pratique/energies-et-eau/services-industriels.html

[38] "RES DHC Project website." [Online]. Available: https://www.res-dhc.com/

[39] F.-A. Fortin, F.-M. D. Rainville, M.-A. Gardner, M. Parizeau, and C. Gagné, "DEAP: Evolutionary Algorithms Made Easy," *Journal of Machine Learning Research*, vol. 13, no. 70, pp. 2171–2175, 2012.

[40] Y. Merlet, R. Baviere, and N. Vasset, "Formulation and assessment of multi-objective optimal sizing of district heating network," *Energy*, vol. 252, p. 123997, Aug. 2022, doi: 10.1016/j.energy.2022.123997.

[41] Y. Merlet, N. Vasset, and R. Bavière, "Optimal retrofit of district heating networks to lower temperature levels," *Energy (to appear)*, 2023.

[42] R. Bavière and M. Vallée, "Optimal Temperature Control of Large Scale District Heating Networks," *Energy Procedia*, vol. 149, pp. 69–78, Sep. 2018, doi: 10.1016/j.egypro.2018.08.170.

[43] "Energy Optima website." [Online]. Available: https://fr.energyopticon.com/energy-optima-3/

[44] "DistrictLab | Track 100% of energy losses in thermal grids." Accessed: Nov. 29, 2022. [Online]. Available: https://www.districtlab.eu/

[45] D. Tenchine and P. Gauthé, "Occurrence of thermal stratification in sodium cooled fast reactor piping," *Nucl. Eng. Des*, vol. 274, pp. 1–9, 2014.

APPENDIX A – Experimental data description

The test rig, built in the Thermodynamics laboratory of the University of Liège for the characterization of temperature transportation in water networks, consists in an insulated steel pipe of 39m long for an internal diameter of 52.48mm. The liquid is introduced at a constant mass flow rate and temperature steps are applied. All details on the apparatus are provided in [34].

We choose to present here results on three specific datasets of the original paper for which velocities (u), Reynolds (Re) and Peclet (Pe) numbers range from 0.58 to 1.06 m/s, $4.8 \cdot 10^4$ to $8.2 \cdot 10^4$ and $2.0 \cdot 10^5$ to $3.7 \cdot 10^5$, respectively. For these operational values, the flow is always turbulent and axial thermal diffusion is negligible. Moreover, the specific Richardson number, denoted Ri_s, accounting for the dynamic of the applied temperature step, remains very low, which according to Tenchine and Gauthé [45] rules out thermal stratification effects. Table 2 summarizes the information about these 3 datasets.

Table 2. Mean figures regarding the dataset considered.

	Reference name in [46]	$\boldsymbol{u}$ $[\boldsymbol{m/s}]$	$\boldsymbol{T_f}[°\boldsymbol{C}]$	$\boldsymbol{Re}$ $[-]$	$\boldsymbol{Pe}$ $[-]$	$\boldsymbol{Ri_s}$ $[-]$	$\boldsymbol{Pr}$ $[-]$
Dataset 1	PipeDataULg150801	0.58	41.4	$4.8 \cdot 10^4$	$2.0 \cdot 10^5$	$6.3 \cdot 10^{-5}$	4.22
Dataset 2	PipeDataULg151204_1	0.75	29.5	$4.9 \cdot 10^4$	$2.7 \cdot 10^5$	$1.1 \cdot 10^{-5}$	5.48
Dataset 3	PipeDataULg160118_1	1.06	38.1	$8.2 \cdot 10^4$	$3.7 \cdot 10^5$	$8.6 \cdot 10^{-5}$	4.51

APPENDIX B – Metz DH Network presentation and validation methodology

The Metz DH consists of a High-Pressure Network (HPN) feeding customers and 7 secondary low-pressure networks. In the present work, we modeled the HPN, i.e. a pressurized water two-tube meshed network comprising two supply units and a booster pumping station. The HPN is operated with forward temperatures in the 105 to 160 °C range, relies on distribution pipes laid in concrete ducts and hosts substations of the indirectly connected type. The simulator was obtained by an automatic translation of a pre-existing model derived for a static simulation program comprising 3270 nodes, 3658 distribution pipes and 366 substations.

The formal validation of such large-scale simulator, affected by many sources of uncertainty including imprecisions on the network geometry and lack of experimental data at the consumer level, exceeds the scope of the present paper. However, for verification purposes, the model was simulated on a two weeks winter period using a time step of 10 min, which coincided with the measured data resolution. Based on the findings of section 3.1, the UFVbl computational scheme was used together with a maximum mesh size of 40 m, leading to $Cu_{\delta x}$ numbers greater or equal to one for velocities greater or equal to 0.06 m/s. When possible, time series provided by the operating company were used as boundary conditions for the simulation. This is the case for the set-point temperature of the supply units, for the head gain or mass flow-rate across the pumps and for the $\{T_{in,s}, T_{out,s,set-point}, \dot{Q}\}$ triplet of the monitored consumers (5 out of 366). For the other consumers, default laws

provided by the operating company to model $T_{in,s}$ and $T_{out,s,set-point}$ were used and the heating load $\dot{Q}$ was deduced from the energy consumption provided by the billing system and a top down mechanism based on the total heating power of the production units.

The 18th International Symposium on District Heating and Cooling,
September 3–6, 2023, Beijing, China

Application and Energy analysis of AI-based digitalization of district heating system

He Le[a*], Du Yanhui[b]

a Beijing Shuoren Times technology Co., Ltd, Beijing, 100085, China
b Beijing Chengshuo Qizhi technology company, Beijing, 100085, China
** HE LE. hlswjtu@126.com*

ABSTRACT

Implementation of Dual Carbon policy and requirements in the reduction of CO_2 emissions raise an awareness of improving the operational flexibility and energy efficiency of district heating. Digitalization of district heating systems plays important role in the energy sector, as it provides a reliable and cost-effective way to provide heat for buildings and end users. This paper reviews the digitalization history of district heating in China, and assesses the current condition of district heating systems. District heating in China is complicated because of its vast territory and climate diversity. By examining the key components of digital systems, such as sensors, controllers, software, and communication networks, and how they interact with each other, the challenge and problems faced was addressed. With analyzing how digital technologies such as big data, artificial intelligence, digital twins, and Internet of Things (IoT) can be applied to improve efficiency, this paper provides the latest technical application such as intelligence heat load forecasting, large-scale network hydronic balance, and accurate heating control. The conclusions obtained from case study and data analyzed show that district heating systems have strong potentials to be more efficient with digital technology in future. However, more efforts are required for assessment and optimization of these potentials in order to achieve benefits.

Keywords: Digitalization; District heating; Heating load; Artificial intelligence

1. INTRODUCTION

In September 2020, China proposed the goals of "peak carbon emissions by 2030" and "carbon neutrality by 2060"(Dual carbon goals) which have placed higher demands on China's response to climate change, promotion of ecological civilization, and the development of high-quality energy [1]. In 2021, the total energy consumption for building in China was 1.11 billion tce, accounting for approximately 21% of the country's total energy consumption. The energy consumption for heating in northern China was approximately 212 million tce, making energy-saving and emission reduction in heating crucial for achieving the dual carbon goals [2]. From 2001 to 2021, the district heating area in northern China increased from 5 billion m^2 to 16.2 billion m^2, while the total energy consumption increased by less than double, mainly due to the development of building energy-saving technologies [2]. The digitalization of district heating system (DHS) has played a crucial role in energy-saving and emission reduction.

2. DIGITALLIZATION DEVELOPMENT OF CHINA DHS

The digital upgrade of DHS in China has accompanied the development of centralized heating systems. The earliest commercial cases of DHS can be traced back to Lockport in 1870 and New York in 1880 worldwide. China introduced centralized heating systems for the first time in 1950 [3]. In 1976, the Beijing Municipal Utilities Bureau collaborated with the 502nd Institute of the Ministry of Aerospace to develop a centralized system based on integrated circuits for monitoring the heating network in Beijing [4]. In 1986, the thermal plant companies in China began using computer to monitor heating networks. Since then, different computer systems were installed for control and management in several cities, such as Beijing, Shenyang, and Hohhot [5]. Most district heating companies adopted distributed SCADA systems at that time and public telephone lines for dial-up internet or radio stations was utilized for remote monitoring of heat stations because of the inadequacies of wireless communication [6][7].

Domestic research has been conducted on the application of computer-based automatic monitoring in DHS, and five functions were summarized as follows [8]: real-time parameter detection to understand system conditions; uniform flow regulation to eliminate hydronic imbalances; proper matching of operating conditions to ensure demand-based heating; timely fault diagnosis to ensure operational safety; sound operational records for quantitative management. In early 2000, to improve the computer applications level in DHS, certain heating planning was implemented to synchronize the design and implementation of computer monitoring systems for DHS companies with more than one million m^2 area [4]. In 1989, the Chifeng Gas and Heating Company cooperated with Tsinghua University, developed and implemented a microcomputer-

based monitoring system for the district heating network in Chifeng city [9]. Zhang Tao utilized computer distributed control systems, microcomputers, and programmable logic controllers (PLC) to control and optimize the thermal power plant's heating system, and the software developed had a certain degree of versatility for operating on Windows [10].

With the development of 2G and 3G communication, heating monitoring systems based on GPRS and PLC control have been applied. The stability and cost performance of GPRS allowed it to become an ideal communication for remote monitoring in heating system and encouraged more establishment [11]. Shi Dengfeng has studied the system architecture and function requirements of local controls, raised that temperature and pressure were key aspects of heating system control, and proposed a control strategy based on temperature and pressure. A four-part architecture of remote monitoring system for DHS was formulated consisting of monitoring center, communication network, on-site monitoring equipment, and primary instruments [12][13].

The development of automation in the secondary network of DHS has been slow due to various factors such as economic development, technological level, communications, installation and ownership [14]. Until 2017, manual balancing valves were primarily used for building balance and control. In 2017, intelligent building balance systems with remote control began to be applied. Electrical controlled valves were utilized and data such as water flow rates, temperatures, pressures, and other parameters were uploaded into the cloud for analysis. Algorithms embedded in cloud were implemented to regulate and control valve with precision remotely [14].

In 1995, scholars analyzed three methods of heat metering allocation used in foreign countries [15], and summarized the suitable forms of heating systems for heat metering [16]. In 2010, the Ministry of Housing and Urban-Rural Development of China (MOHURD) issued the "Opinions on Further Advancing the Reform of Heating Metering", which required that during the 12th Five-Year Plan period, existing buildings in northern cities at or above the prefectural level should complete heating metering renovations to meet the mandatory energy-saving standard of 50%. The five methods of heat metering mentioned in the document were: heat meters method, on-off method, heat distribution meter method, flow-temperature method, and temperature-area method. Data such as flow rates, water temperatures, and heat consumption of end users was able to be collected into the monitoring system, improving the transparency of heating.

Providing users with suitable room temperature is the core objective of DHS. However, collecting room temperature for a large number of users has always been a challenge. Traditional manual sampling is unable to provide real-time feedback and often has significant errors. Some scholars have designed devices that utilize public telephone networks as a transmission medium to remotely collect user room temperature data, which has partially solved the problem [17]. Wireless temperature collection devices based on GPRS or 3G have limitations in terms of cost and power consumption, making it difficult to promote on a large scale. While room temperature collection devices based on low power consumption NB-IoT meet the requirements, providing conditions for large-scale collection of users' room temperature. Therefore, the complete digitization of the heating system, from heat source, heat exchange stations, heating networks to end-users, has become feasible.

Table1. Development of DHS digitalization

Phase	Time	Basic Function	Typical technic
Early age of automation	1980-2000	Localized control Attended station	Local control Station Computer based Local data collection Telephone network
Remote Control	2000-2010	Heating net monitoring Unattended Station Remote dispatch Failure diagnosis	Monitoring Center GPRS、3G PLC Field devices
Digitalization	2010-2018	Heat Source, network, station, user monitoring End user heating metering Auto balance of Secondary network Digitalized Dispatch center	4G, Optical fiber SCADA Cloud based Whole network balance
Intelligent District heating	2018-	Whole net intelligent control Room temperature collection Accurate control self-aware, self-analyzing, self-diagnosing, self-optimizing, self-regulating, and self-adaptable [18]	Big Data Artificial intelligence Digital Twins Modeling & Simulation

The management of DHS is transitioning from digitization to intelligentization. The "Blue Book of heating in China 2019-Smart Urban Heating" was released, providing an elaboration on smart heating and offering guidance for the digitization for DHS [18]. The book states that "smart heating is based on heating informationalization and automation, and adopts the route of deep integration of information technology and physical systems. It utilizes Internet of Things, spatial

positioning, cloud computing, information security, and other "Internet+" technologies to perceive and connect various elements in the "source-network-load-storage" process of the heating system. It employs big data, artificial intelligence, modeling and simulation, and other technologies to comprehensively analyze and optimize various resources in the system. It utilizes advanced control technologies such as prediction model to precisely regulate objects at various levels and stages of the system based on demand. The goal is to create an intelligent heating system that is self-aware, self-analyzing, self-diagnosing, self-optimizing, self-regulating, and self-adaptable. "

The digitalization process for China's DHS can be summarized into four stages, as shown in Table 1. It is accompanied by the development of technologies such as big data, Internet of Things (IoT), and artificial intelligence (AI), progressing from local automation, remote monitoring to digitalization and intelligentization.

3. KEY TECHNOLIGIES FOR THE DIGITALIZAITON OF DHS

3.1 IoT Balance Valve

Hydronic balancing of the secondary network often relies on manual balancing valves, requiring personnel to regulate on site with special instruments, and real-time remote control is not supported. The new type of (Internet of Things) IoT smart balancing valve combines balancing control and data acquisition, as shown in Figure 1. The valve is equipped with a PT1000 sensor to collect water temperatures of the secondary network. The data is uploaded to the cloud through NB-IoT, LORA, CAT.1, etc., and receives instructions from the cloud. The cloud-embedded algorithm can perform real-time analysis based on parameters such as water temperatures, flow rates, etc., and send instructions to the valve with more accuracy.

Figure 1. IoT balance valve

3.2 IoT Room temperature collector

Traditional heating control method focuses on regulating supply or return water temperature, lacking direct control over room temperature. Due to communication cost, large-scale room temperature acquisition systems were difficult to promote before 2018. With NB-IoT, room temperature collectors can be installed in conjunction with users' switches and sockets, as shown in Figure 2. With stable power supply, the fixed installation prevents users' movement from disturbing the temperature data. The room temperature can be collected every 10 minutes, providing a basis for temperature-based control algorithms.

Figure2. NB-IoT Room temperature collector

3.3 Programmable Logic Controller (PLC)

PLC (Programmable Logic Controller) serves as the "brain" for the control of heat exchange stations and is a core device for local control. Through RS485 interface, the PLC communicates with field devices such as heat meters, valves, flow meters, and pumps. It collects real-time data such as supply and return water temperatures, pressures, flow rates, valve positions, and pump frequencies. With PID algorithms, the PLC can set the supply water temperature by controlling the valves or pump [19]. The domestically developed PLC controllers have been widely applied in the heating industry, as shown in Figure 3. Some researchers have used soft-PLC for distributed control of boiler systems, achieving automatic control and combustion optimization [20].

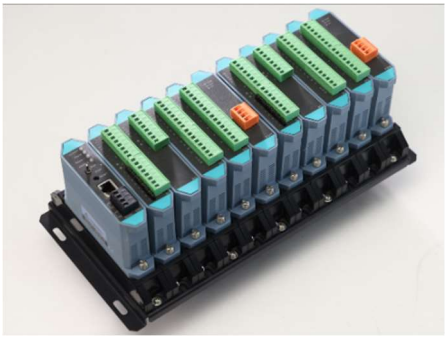

Figure 3. Domestic developed PLC (Type- STEC1800)

3.4 Monitoring software for DHS

In the 1990s, the computer monitoring software and hardware used for district heating systems in China were mainly imported, with software solutions provided by countries such as Finland and Germany [6][21][22]. The development of domestic software started relatively late, and early automation software focused on self-control of boilers or optimization of certain stations [23]. However, for large-scale district heating networks with large area and numerous parameters, the coupled control between heat exchange stations and coordination between multiple stations and heat source scheduling were significant challenges to address. Tsinghua University proposed the concept of whole-network balance for automatic control of DHS, and the software developed has been successfully applied in some projects [24]. By combining whole-network balance with heat source optimization and adjustment of secondary circulation pumps, energy-saving effects have been achieved [25]. Considering the thermal storage capacity and thermal inertia of large-scale heating networks, researchers have proposed whole-network balance algorithms based on heat consistency. These algorithms have been used for real-time control of 1,500 heat exchange stations in Chengde DHS, stabilizing room temperature within an acceptable deviation and improving energy efficiency [26][27].

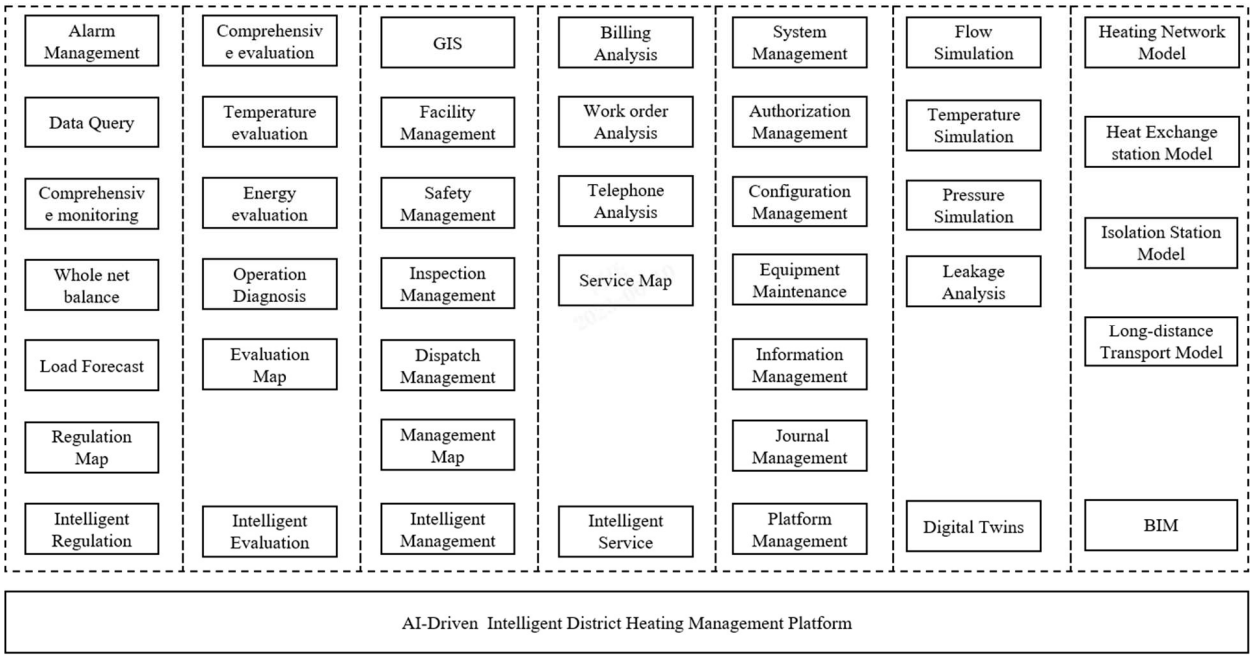

Figure 4. Intelligent Software structure for DHS

Most functions of smart heating software have been domestically developed and implemented, such as load forecasting, whole-network balance, energy analysis, fault alarms, billing service, digital twins, etc., as shown in Figure 4. However, significant challenges are posed when heating companies want to upgrade their systems. Due to varying scales and diverse demands, the automation implementation in district heating company is often complex in history. A heating company may be served by several software vendors, and a single module may involve 3 to 5 brands. The digital upgrade needs to be carried out in stages and should not affect normal operation, ensuring a certain level of compatibility with existing software. Innovative software architecture is needed and approaches are required in terms of database design, data integration. Software based on distributed systems, data middleware, which shows high scalability is favored in the market.

3.5 Summary

New communication technologies have changed the form of sensors and field instruments. As the components for

underlaying data collection and execution, sensors are the physical foundation of digitalizing, while programmable logic controllers (PLCs) serve as the core of local control. Lower instruments are connected to upper computer through communication. Upper computer analyzes the state of the heating and issue instructions as a brain, enabling centralized monitoring and local control to meet the requirements. Specialized algorithm has been developed for load forecasting and whole-network balance in large-scale DHS networks, enabling centralized control and unified scheduling. Local instruments, controllers, communications, and software mutually support and constrain each other. The operation of algorithm relies on the support of field devices, and well-designed algorithms can optimize the performance of the equipment and extend the system's lifespan. In the process of digitization, the harmonious integration of software and hardware is crucial for the smooth operation of the system.

4. FRONTIER DIGITALIZATION TECHNOLOGIES IN DHS

4.1 IoT and Big Data

The concept of the Internet of Things (IoT) was proposed in 1999. It was defined as connecting all objects, including people, to the Internet through information sensing devices such as radio frequency identification (RFID), enabling intelligent identification and management [28]. The IoT has been predicted to be the next technological and economic wave in the global information industry after the Internet and Its core was to enable information exchange and communication between objects [29]. In 2010, China identified the IoT as a strategic emerging industry and placed emphasis on its development, the research on the architecture and standardization of the IoT has been gradually advancing [30]. On May 7, 2020, the Ministry of Industry and Information Technology issued a notice on promoting the comprehensive development of mobile IoT. It called for deepening the coverage of 4G networks and accelerating the construction of 5G networks. NB-IoT was identified to meet the demands of most low-rate scenarios, while LTE-Cat.1 was designated for medium-rate IoT requirements. Low-rate applications constitute the largest proportion of IoT, and LTE-Cat.1 and NB-IoT have become the mainstream technologies for the future development of the IoT.

Table2. Comparison of CAT.1 and NB-IoT

Comparison	**CAT.1**	**NB-IoT**
Upper speed	5M/s	60kb/s
Download speed	10M/s	27kb/s
Scenario	Wearable devices, ATMs, POS, Retail kiosks, consumer electronics devices, smart metering	Intelligent Gas meters, water meters, Industry monitor, agricultural irrigation, street lights
Battery Powered	Yes	Yes

The collection of environmental temperature and pressure in heating is suitable for the application of IoT. Although Cat.1 and NB-IoT differ in key technical parameters such as bandwidth, speed and coverage enhancement, as shown in Table 2, their application scenarios are not conflicting [31]. Both technologies belong to low-power communication and are suitable for battery-powered scenarios. NB-IoT has longer communication delays and smaller data sizes, making it suitable for scenarios with longer waiting times and lower real-time requirements, such as room temperature collection. On the other hand, Cat.1 supports larger data sizes and provides better real-time performance, making it suitable for valve control. Research has shown that the signal strength coverage of both technologies is similar [32], and varies because of the distribution of base stations. In some areas, balance valves based on CAT.1 have been applied in well, as shown in Figure 5. By adding external antennas inside the well, the valves with communication boxes and battery can be installed underground. This low-cost approach eliminates the need for electric wiring and reduces impact on residents.

Figure 5. In-well installation of IoT balance valve with CAT.1 external antenna

4.2 Artificial Intelligence and Edge Computing

Artificial Intelligence (AI) is a discipline that focuses on the research and development of intelligent machines capable of simulating and extending human intelligence. In the early applications of AI technology in HVAC systems, neural network techniques were primarily used for load prediction. Researchers have utilized neural networks to study the cooling and heating loads of a specific area, analyzing different load patterns over the past 24 hours or a week to predict the load for each time period in the future 24 hours [33]. The previous heat load prediction methods can be grouped into two main groups, including physical energy and data-driven approaches. The physical energy approach relies entirely on analyzing functional correlations of building parameters to build the heat load profile. While the data-based approaches construct prediction models by learning the underlying relations of heat usage and other influential factors based on the DH historical data [34]. Due to the rapid development in Machine Learning, a substantial amount of work was found using ML algorithms for energy predictions in the investigated period, and it can be observed that ML algorithms in general produce more accurate predictions than traditional regression methods [35].

With the rapid increase in data generated by network, there is a higher demand for data transmission and real-time data processing. It was projected that by 2020, the global data volume will exceed 40 zettabytes (ZB), and 45% of the data generated by the Internet of Things (IoT) will be processed at the network edge, which is known as edge computing [36]. Edge computing can greatly alleviate the pressure on network bandwidth and data centers, reduce system latency, and lower the risk of user data leakage. Therefore, it is well-suited for applications in industrial IoT, virtual reality, smart cities, and other similar scenarios [36]. With the advancement of computer technology and sensors, as well as the improvement of data collection such as room temperature, it has become a reality to utilize room temperature to optimize the supply water temperature of heating stations or boilers. Some study in China have combined AI technology with edge computing to learn and analyze data from heat exchange stations, and directly guide the heating operation based on room temperature [37], as shown in Figure 6, and stable room temperature and energy-saving effects were achieved. Deploying AI algorithms on edge devices enables local data processing and decision-making, reducing reliance on cloud computing and minimizing data transmission delays. The application of edge computing devices can simplify the installation and debugging process, suitable for the intelligent transformation and enhancement of heating systems.

Figure 6. AI edge computing device for heat control [37]

4.3 Digital Twins

Digital Twins refer to dynamic virtual models of physical entities that are established in a digitized manner, encompassing multiple dimensions, timescales, disciplines, and physical quantities. They simulate and depict the attributes, behaviors, rules, and other aspects of physical entities in their real environment. The concept of Digital Twins was initially proposed by Professor Grieves in 2003 during a product lifecycle management course at the University of Michigan. It was primarily applied in the fields of military and aerospace industries [38]. Since then, it has found extensive applications in various domains such as satellite/space communication networks, ships, vehicles, power plants, aircraft, complex electromechanical equipment, warehouses, healthcare, manufacturing workshops, and smart cities. Tao Fei has proposed a five-dimension model for Digital Twins and conducted studies on its compositional framework and application guidelines, which is applicable to different fields and various applications. Some companies have implemented Digital Twin-based intelligent health management systems for power plant generators, and has completely transformed the traditional "black box" operational mode of generator units, enabling realistic and transparent monitoring and accurate fault prediction based on multidimensional features [39].

In the heating industry, the primary application of Digital Twins is for hydraulic simulation, network scheduling and leakage analysis. It allows the visualization of underground pipeline operations and scheduling through Digital Twin techniques. Research has proposed an industrial heating scheduling platform based on a Digital Twin model, combining the

steam pipeline network in an industrial park with GIS map data, and optimizes the scheduling of the steam pipeline network to meet the steam pressure requirements at the user end [40]. The closed environment within pipeline networks often poses challenges for direct problem-solving, and large-scale network scheduling lacks intuitive information representation. Beijing Shuoren Times technology Co., Ltd has released a Digital Twins application (ARH) in 2023 China International Trade Fair for Heating, Ventilation, Air-conditioning, Sanitation & Home Comfort systems (ISH), providing multidimensional data visualization and display for heating systems, enabling people to make informed decisions and conduct analysis in a more comprehensive manner, as shown in Figure 7.

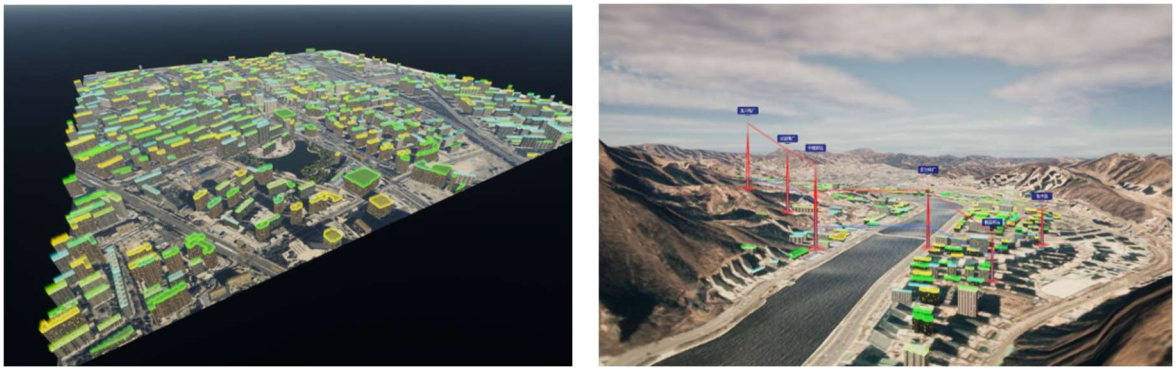

Figure 7. Artificial Reality for Heating industry (ARH) in energy analysis and hydronic simulation by Beijing Shuoren Times technology Co., Ltd

5. CASE STUDY

Chengde Thermal Power Group has a large-scale heating system with total area of over 76 million m^2. At the end of 2019, the heating system underwent digital transformation with the implementation of functions such as load prediction, network balancing, and comprehensive monitoring. Precise load prediction, automatic network balancing, and coordinated operation between heat sources, networks, and users were achieved. More than 1,500 heating stations were automatically controlled and operated after the transformation. Automatic optimization of the entire network was realized, system faults can be diagnosed automatically, energy consumption was controlled with comprehensive benchmarking, system operation can be evaluated comprehensively, and entire heating process was managed digitally while providing personalized heating for end users. The software architecture was based on a multi-heat source network and distributed system, ensuring the integrity of underlying data and stability of communication. With AI algorithms, the system has achieved 5.8% reduction in heat consumption, 13% reduction in water consumption, 10% reduction in electricity consumption, 20% reduction in system failure rate, and 12% reduction in user complaint rate.

6. CONCLUSION AND PROSPECT

Digitalization of DHS faces several issues. First, the digitalization of heating requires a comprehensive review and upgrade of the existing equipment, a deployment of software based on needs, which require significant financial investment. Secondly, certain DH companies do not have sufficient understanding of the heating digitalization, and unclear about demand, which causes some digital cases failed for not effectively fulfilling the intended purpose. Thirdly, relevant technologies for DHS digitalization are still under continuous development, and their effectiveness needs further verification in practice.

The urban DHS is trending with more complexity and intelligence, posing challenge for control. The digitalization of DHS is important for energy-saving and carbon emission reduction. The digital development of DHS in China has been accompanied by the advancements in communication, software, and algorithm models. It has evolved from local control to intelligent heating that encompass the entire process of heating production and operation. The stability of underlying sensors provides reliable data, while advanced communication methods enable data collection from every aspect of the network. Cloud and distributed software architecture allow heating companies to apply the intelligent transformation step by step. With edge computing, artificial intelligence and digital twins, the operation of large-scale district heating scheduling become more precise.

REFERENCES

[1] Tong Guangyi. Construction of Smart Energy System Based on Dual Carbon Goal. Smart Power 2021; Vol.49:No.5.

[2] THUBERC.2023 Annual Report on China Building Energy Efficiency. Beijing: China Architecture & Building Press; 2023, Page14.

[3] Sven Werner. International review of district heating and cooling. Energy 2017; Vol 137: Page 617~631.

[4] 曾享麟,李先瑞,项恩田,赵金璋.中国城镇集中供热 2000 年技术进步发展规划(讨论稿). District Heating1995; No.1.

[5] 江亿. 城市集中供热网的计算机控制和管理. District Heating 1995; No.5.
[6] 原贺新,刘海英,马卫华. SCADA 系统在热网中的应用.Urban Management and Science & Technology 1999; Vol.1:No.2.
[7] 董志国.集中供热管网的监控系统. Gas & Heat 2005; Vol.25: No.10.
[8] 石兆玉.供热系统运行与调控.Beijing: Tsinghua University Press;1995, Page307.
[9] 刘豫峰.热网微机监控系统开发成功. Gas & Heat 1990; Vol. 4.
[10] Zhang Tao,Xu Xiangdong,Lü Zehua, Zhang Yongzhe. State monitoring control and optimizing management system of heat networks using computer. Journal of Tsinghua University (Sci&Tech) 1996; Vol.36:No.7 Page92~96.
[11] 吴云峰,周龙军.基于 GPRS 技术 PLC 远程通信应用于城市热网监控. District Heating 2004; No.4.
[12] Dong Weixiu,Lv Yaojun,Shi Dengfeng,Gan Chunhong. Energy-saving Control Technology in Heating System. Building Energy & Environment 2005; Vol.24:No.5 Page73~76.
[13] 史登峰,戴斌文,邓宇春.集中供热系统监控技术. District Heating 2007; No.5.
[14] 何乐.智能楼栋平衡系统在供热二次网上的应用. District Heating 2018; No.2.
[15] Wu Yuanwei. Technical means of heat measurement and charge apportionment in multi-family residential buildings. Journal of HV&AC 1995; No.5.
[16] 涂光备,冀英,贺克瑾,李松深.适合热计量的室内采暖系统.Gas & Heat 1999; No.6.
[17] Zhao Naibo, Liu Haishan, Wang Lifeng, Fan Shengwen. Indoor Temperature Gathering Telephone in Automatic Heating Control. Industry Control Computer 2008; Vol.21: No. 4.
[18] China District Heating Association. Blue Book of Heating in China2019-Smart Urban Heating. Beijing: China Architecture &Building Press;2019, Page17.
[19] 江亿.集中供热网控制调节策略的探讨. District Heating 1997; No.2.
[20] Zhao Yongsheng, Wang Siyuan, Zhu Jiling,Zhang Wei,Gong Cheng. Design on Distributed boiler control system based on soft PLC. Microcomputer Information 2003; Vol.19: No.7.
[21] 赵红平,王兆霖. 芬兰 AFORA 公司提供的热网监控系统简介. District Heating 1989; No.10.
[22] 冯鑫,刘宜兵.德国纽伦堡市(Nuremberg) 区域集中供热网自动监控系统. District Heating 1997; No.2.
[23] 吕泽华,徐向东,曹仁风,张涛,王点宏,李明,蒋灰力.采暖锅炉计算机监控管理系统. Journal of Engineering for Thermal Energy and Power 1998; Vol.13: No.76.
[24] 崔耀华.城市集中供热全网平衡软件介绍. District Heating 2006; No.3.
[25] Zhang Yuzhong, Liu Xiaomin, Qin Bin. Energy saving operation optimization in urban district heating system: a case study. Journal of HV&AC 2015; Vol.45: No.6.
[26] 庞印成.基于热量平衡的全网平衡调节模式探索与实践.第三届中国供热学术年会 2020.
[27] 王少驰,刘玉侠,马东亮,李爽.供热系统热负荷预测分析及应用. District Heating 2023; No.2.
[28] Wang Baoyun. Review on internet of things. Journal of Electronic Measurement and Instrument2009; Vol. 23: No.12.
[29] Zhu Hongbo, Yang Longxiang, Zhu Qi. Survey on the Internet of Things. Journal of Nanjing University of Posts and Telecommunications (Natural Science) 2011; Vol.31: No.1.
[30] Sun Qibo, Liu Jie, Li Shan, Fan Xiaochun, Sun Juanjuan. Internet of Things: Summarize on Concepts, Architecture and Key Technology Problem. Journal of Beijing University of Posts and Telecommunications 2010; Vol.33: No.3.
[31] Zhao Jing. The Status and Trend of Low Rate Cellular Communication Technology for IoT. Mobile Communications 2016; Vol.40:No.7.
[32] Chen Bo, Gan Zhihui. Analysis on the Coverage Capability of NB-IoT and CAT1. Mobile Communications 2017; Vol.41:No.22.
[33] 王波,蒋鹏,卿晓霞. 人工智能技术及其在建筑行业中的应用. Cyber Security and Data Governance 2004; Vol.8.
[34] L. Minh Dang, Sujin Lee, Yanfen Li, Chanmi Oh, Tan N.Nguyen, Hyoung-Kyu Song, Hyeonjoon Moon. Daily and seasonal heat usage patterns analysis in heat networks. Scientifc Reports 2022; Vol.12.
[35] Mengting Jiang, Camilo Rindt, David M.J. Smeulders. Optimal Planning of Future District Heating Systems—A Review. Energies 2022; Vol.15.
[36] Shi Weisong, Zhang Xingzhou, Wang Yifan, Zhang Qingyang. Edge Computing: State-of-the-Art and Future Directions. Journal of Computer Research and Development 2019; Vol 56: No.1.
[37] 何乐,李琳,王振功.基于人工智能以室温为目标的换热站调控方式浅析. District Heating 2023; No.2.
[38] Tao Fei, Liu Weiran, Zhang Meng. Five-dimension digital twin model and its ten applications. Computer Integrated Manufacturing System 2019; Vol.25: No.1.
[39] Tao Fei, Liu Weiran, Liu Jianhua. Digital Twin and its potential application exploration. Computer Integrated Manufacturing System 2018; Vol.24: No.1.
[40] 洪方驰,王叶飞,孙海龙,林小杰,钟崴.基于数字孪生模型的工业供热系统调度平台.Gas & Heat 2020; Vol.40: No.5.

A DIGITAL TWIN PLATFORM DESIGN OF A CENTRAL HEATING SYSTEM IN NORTHERN CHINA

Qi Jianwei[a] Shu Haiwen[a] Wang Zhihao[a] Wang Haichao[a] Shu Jingji[a]

[a] *Dalian University of Technology, Dalian, 116000, China*
[*] *Shu Haiwen. Shwshw313@sina.com*

ABSTRACT

In the northern region of China, centralized heating is the primary method of supplying heat during the winter months, supplemented by new energy sources heating systems. The energy consumption of centralized heating accounts for as much as 57% of the total energy consumption of the whole society. However, traditional centralized heating systems suffer from low levels of information technology and intelligence, poor network coordination, significant waste of thermal resources, slow emergency response times and other issues. To address these concerns in Huanghua City's central heating system in Hebei Province, the authors propose a digital twin platform construction plan that applies digital twin technology to data acquisition and analysis; creation of digital models; prediction analytics; intelligent decision-making and optimization. This research designs specific functions such as operation monitoring, equipment management, energy consumption analysis and fault handling through coordinated optimization based on the digital twin platform. The paper also elaborates on how this platform deeply integrates physical systems with information systems by leveraging its advantages in data perception and human-computer interaction to achieve comprehensive management and intelligent control over the entire centralized heating system. Ultimately, this study aims to improve operational efficiency while reducing energy wasted and enhancing reliability and environmental protection for the centralized heating system. The proposed construction plan for a digital twin platform provides an effective solution to addressing current challenges faced by traditional centralized heating methods, and truly realizing transformation towards smart-heating.

Keywords: Intelligent heating; Digital twin; Digitalization of DHC systems; Industrial heating system;

1. Introduction

The northern region's frigid climate necessitates significant heating to sustain both human livelihoods and industrial production. Centralized heating remains the principal method of meeting this demand. However, traditional centralized heating systems face several challenges, including lengthy heating pipelines, high rates of leakage, and aging equipment, as illustrated in Figure 1.

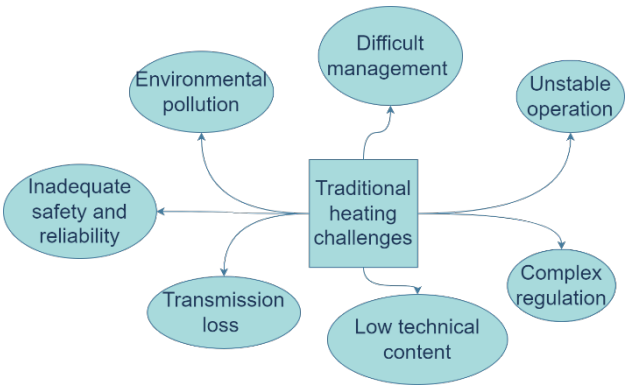

Figure 1. Challenges faced by traditional centralized heating systems

Specifically, traditional heating system regulation techniques are relatively outdated, lacking coordination [1] and exhibiting significant lag. Some heating stations still rely on manual experience to adjust, resulting in an imbalanced pipeline network and unstable heating for residents [2]. Heating data collection is incomplete and susceptible to data loss or leakage [3]. Aging and corrosion issues plague heating pipelines and equipment, with a lack of effective risk management and emergency response plans leading to potential safety hazards such as leaks and explosions [4], posing a threat to personal and property security. Additionally, fixed heating temperatures and heat supply provided, by traditional centralized heating system cannot meet the personalized needs of different users [5].

To address the above issues, achieving a "clean, low-carbon, safe, and efficient" transformation of the heating system has become a hot topic in the contemporary energy field. Digital Twin technology, as an emerging technology, offers bidirectional interaction between the actual system and the digital twin body, enabling real-time monitoring, fault diagnosis, intelligent control, and optimized decision-making support [6]. Designing a Digital Twin platform for a centralized heating system in northern China has significant research and practical application value.

2. OVERVIEW OF A CENTRALIZED HEATING SYSTEM IN NORTHERN REGION

As shown in Figure 2, the centralized heating system covers the entire Huanghua city area with a heating area of 7.5145 million square meters. It includes a total of 5.3982 million square meters for centralized heating and 0.6835 million square meters for clean energy heating. The heat source comprises three 70MW coal-fired hot water boilers and a 200MW pressure-isolation heat exchange station, with 82 block heat exchange stations and a primary heating network of 51 kilometers and a secondary heating network of 131 kilometers. Clean heating mainly involves air-source gas engine-driven heat pump energy stations and shallow geothermal water-source heat pump energy stations.

Figure 2. Heating status of a centralized heating system in the northern region

3. DESIGN FRAMEWORK OF CENTRALIZED HEATING PLATFORM BASED ON DIGITAL TWIN

The design framework of the centralized heating platform based on digital twin is shown in Figure 3, comprising four layers: data, model, simulation, and application.

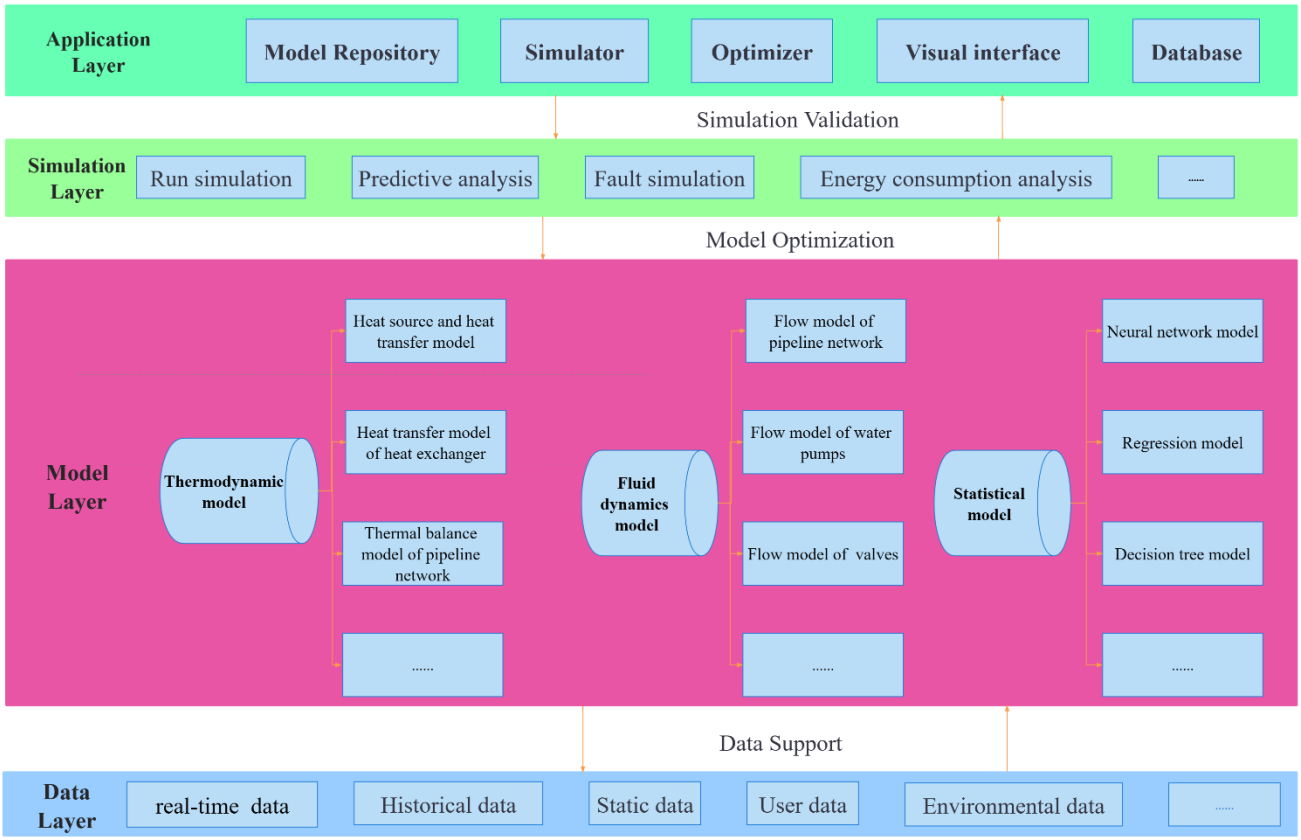

Figure 3. Design Framework of Digital Twin Platform for Centralized Heating System

3.1. Data Layer

The data layer serves as the foundation of a digital twin platform, aiming to provide comprehensive, accurate, and real-time data support. For a district heating system, the data that needs to be collected includes real-time monitoring data, system equipment parameters, user information, environmental temperature, and so on.

Data collection for centralized heating systems primarily involves the deployment of sensors, actuators, and controllers. The frequency of data collection is defined based on data type and characteristics to ensure real-time data acquisition. For this system, the following steps are taken:

Heat source station: a sampling interval of 2-5 seconds can be chosen to achieve high-precision monitoring of heating parameters, while at the energy station, a sampling interval of 10-30 seconds can be chosen to save energy and extend the sensor's lifespan.

Pipe network: different nodes such as pipe connections, branch points, and elbows can be selected for data collection. The sampling frequency can be adjusted according to the characteristics and operating conditions of the pipe network. Usually, data can be collected once every hour or half an hour.

For equipment such as boilers, heat exchangers, and pumps, sensors and intelligent controllers can be installed to collect data on the equipment's operating status and energy consumption. The sampling frequency can be adjusted according to the characteristics and operating conditions of the equipment. Data can be collected once every minute or ten minutes.

User data collection: smart thermostats, smart meters, and other devices can be installed at the user end to collect data on energy consumption and indoor temperature. Different types of users such as residential, commercial, and industrial can be selected for data collection. The sampling frequency can be adjusted according to the user's characteristics and energy use. Usually, data can be collected once every hour or half an hour.

3.2. Model Layer

The data for the model layer mainly comes from the data layer, and the operation status of the centralized heating system is simulated by establishing mathematical and physical models. Meanwhile, the application layer can optimize and adjust the system based on the predictive results of the model layer. Specifically, the model layer of the centralized heating system digital twin platform includes the following aspects:

Thermodynamic model: Used to describe the thermodynamic characteristics of the heating system, including models of heat

transfer of heat source and heat exchanger, and heat balance of pipeline system. These models are based on the design and operation parameters of the actual system and are simulated using modeling software to achieve a digital description and simulation analysis of the physical system.

Fluid dynamics model: Used to describe the fluid characteristics of the heating system, including flow models of pipeline, heat exchanger, water pump, valve, etc. The model takes into account factors such as equipment geometry, material properties, and fluid flow state to predict parameters such as fluid velocity, flow rate, pressure, etc.

Statistical model: Used to describe the data characteristics and behavioral patterns of the heating system, including models of data distribution, trends, periodicity, correlation, etc. Examples of such models include feedforward neural network models and recurrent neural network models, which enable digital monitoring and analysis of the heating system's performance.

3.3. Simulation Layer

In the simulation layer, the first step is to create a model that considers the unique characteristics of the northern centralized heating system, such as the length, diameter, material, and heat dissipation of the heating pipeline, as well as the performance parameters of various equipment. Simulation tools and algorithms, such as OpenModelica and EnergyPlus, are commonly used for modeling and simulation experiments. After the model is established, simulation experiments and analysis are conducted using historical or real-time data to verify its accuracy and reliability. If the model does not match actual data, it is calibrated for increased accuracy and reliability. Simulation experiments are used to test different control strategies and optimization algorithms to find the best approach.

Overall, the simulation layer is an extension of the digital twin platform that creates simulation models and conducts experiments to provide accurate data and analysis for the model layer, which is essential for optimizing the digital twin model.

3.4. Application Layer

The application layer is the top layer of the digital twin platform and serves as the carrier of digital twin technology, providing users with a visual, interactive platform for simulation, prediction, and optimization. For the digital twin platform plan of a northern centralized heating system, the application layer utilizes a model library, simulator, and optimizer to achieve real-time monitoring, fault diagnosis, decision optimization, and other application functions.

4. FUNCTION DESIGN

Considering the need for smart and coordinated heating network intelligence, and based on the digital twin framework for the centralized heating system, the digital twin platform for centralized heating is designed with the following functions for the application scenario of smart heating:

4.1. Real-time Monitoring

Real-time monitoring function is shown in Figure 4, which achieves real-time dynamic parameter display, fault alarm, historical data retrieval, and data access control. The specific design strategies are as follows:

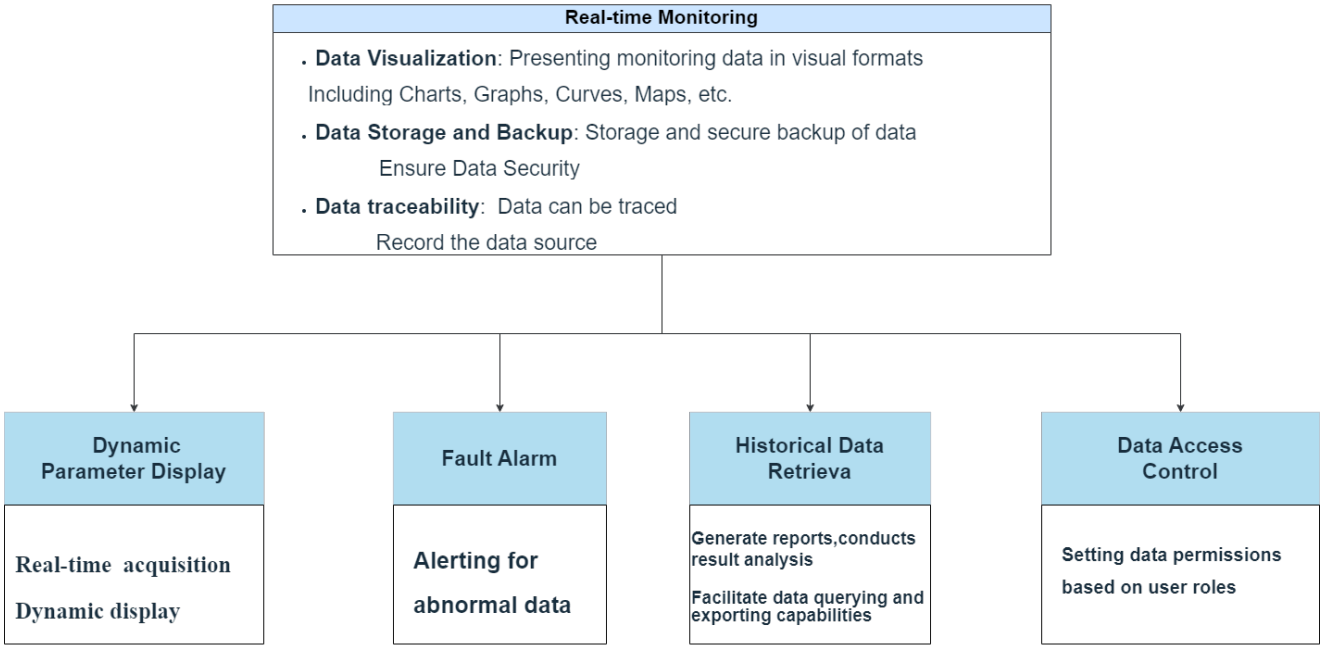

Figure 4. Demonstration of Real-time Monitoring Functionality

Data Collection: Different strategies can be used, for example, the pipeline network adopts a timed collection strategy of every hour or half an hour, while the equipment adopts a strategy of automatic triggered collection when faults or abnormalities occur.

Data Transmission and Storage: The heat source and district heating exchange stations use wired transmission and local storage methods to achieve fast access and processing of data, while the energy station uses wireless transmission to monitor the decentralized clean energy heating system in real-time. In the dispatch center, cloud storage is chosen to facilitate remote access and sharing of data.

Visualization Display: Real-time data is displayed in the form of charts or curves to show the real-time data of temperature, pressure, flow rate, and other equipment. At the same time, the pipeline network is simulated to display its structure, flow rate, and other information, allowing users to discover problems in a timely manner by simulating the operation of the pipeline network.

4.2. Equipment Management

The equipment management function achieves comprehensive information management of equipment, and the functional design of the equipment management system is shown in Figure 5.

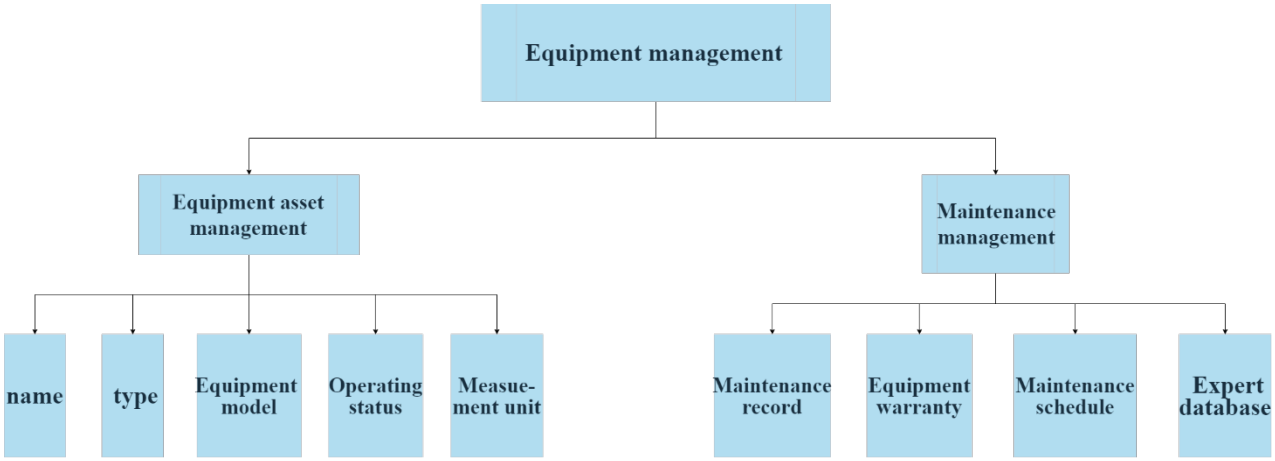

Figure 5. Functional Design of Equipment Management System

The equipment management function provides a list of all equipment, including valves, water pumps, heat exchangers, and other types of equipment, with their names, technical parameters, and other details. In addition, equipment can be grouped and viewed based on different loops, categories, and operating statuses, which clarifies the composition and real-time status of equipment on the pipeline network loops.

It also has the ability to record maintenance records, including information such as maintenance time, content, results, personnel, and historical records of inspections and failures. Operators can view and add fault records and maintenance records at any time. When it is time for equipment maintenance, the system can automatically prompt and develop an annual maintenance plan, generate an annual fault statistics report, and other related functions.

4.3. Energy Analysis

As shown in Figure 6, the energy analysis function processes energy consumption data such as heat, electricity, and water consumption at various points in the heating system, and establishes an energy consumption model for the heating system. Through overall energy consumption levels, energy consumption structure analysis, energy consumption trend analysis, and energy consumption efficiency evaluation, a comprehensive evaluation of the energy consumption of the heating network can be achieved.

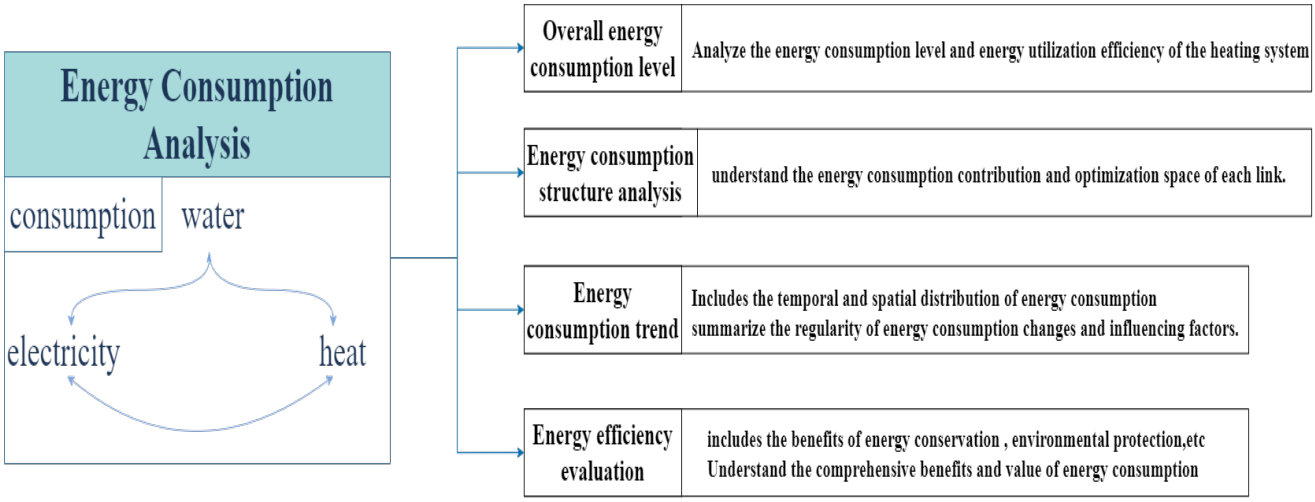

Figure 6. Energy Analysis

4.4. Intelligent Control

The intelligent control function refers to the use of artificial intelligence-related technologies to control the heating system intelligently. The intelligent control function includes the following features (as shown in Figure 7):

Temperature / pressure / flow regulation: The heating system's temperature is automatically or manually adjusted based on real-time data of temperature, pressure, and flow.

Load forecasting: Through data analysis and machine learning technologies of the digital twin platform, the heating system's load can be predicted and analyzed to adjust the system's operating parameters in advance.

Pump / valve control: The digital twin model is used to analyze the usage of pumps and valves, and to automatically adjust the working status of the pumps and the opening and closing of the valves.

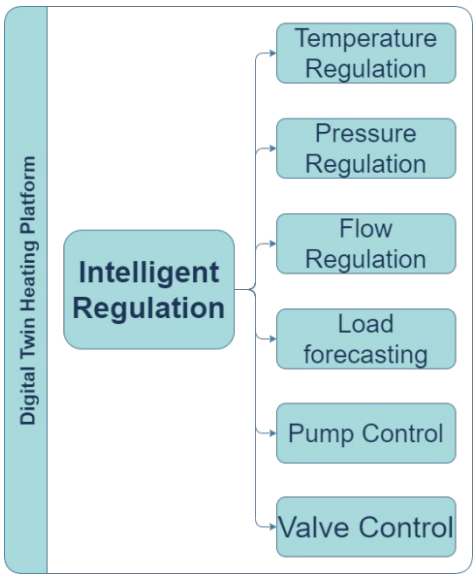

Figure 7. Functional Design of Intelligent Control System

4.5. Fault Handling

Compared with traditional emergency fault handling, the digital twin platform comprehensively manages sudden events, including fault diagnosis, recording and statistical analysis of fault logs, intelligent recommendation of components, and a fault diagnosis knowledge base, as shown in Figure 8.

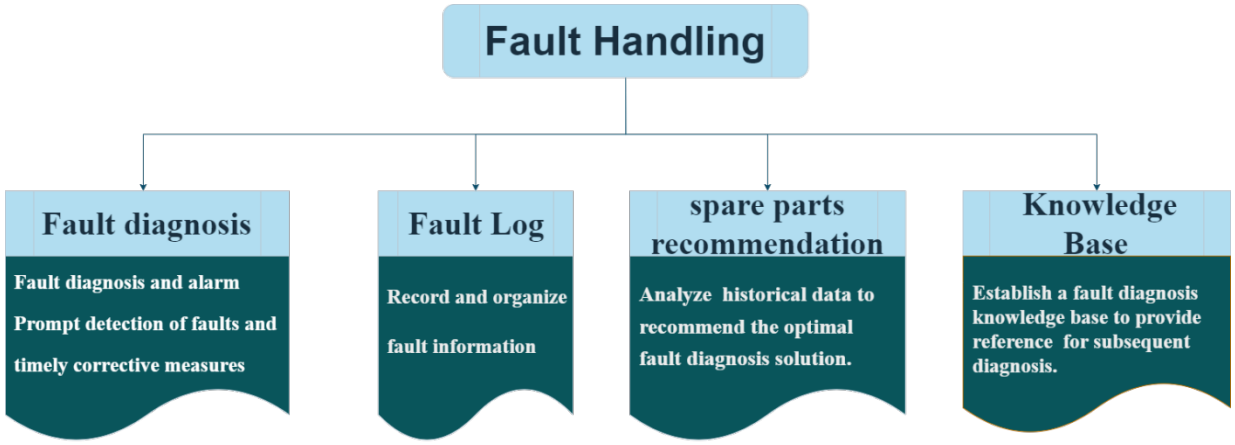

Figure 8. Functional Design of Fault Handling System

The fault diagnosis process, as shown in Figure 9, includes finding the cause of the fault, determining the fault type by the digital twin fault model, and locating the fault by a fault diagnosis algorithm. If the fault cannot be located, an alarm will be issued and professional assistance will be requested. Once the fault area is identified, the fault will be repaired based on the expert database, and the fault log will be recorded.

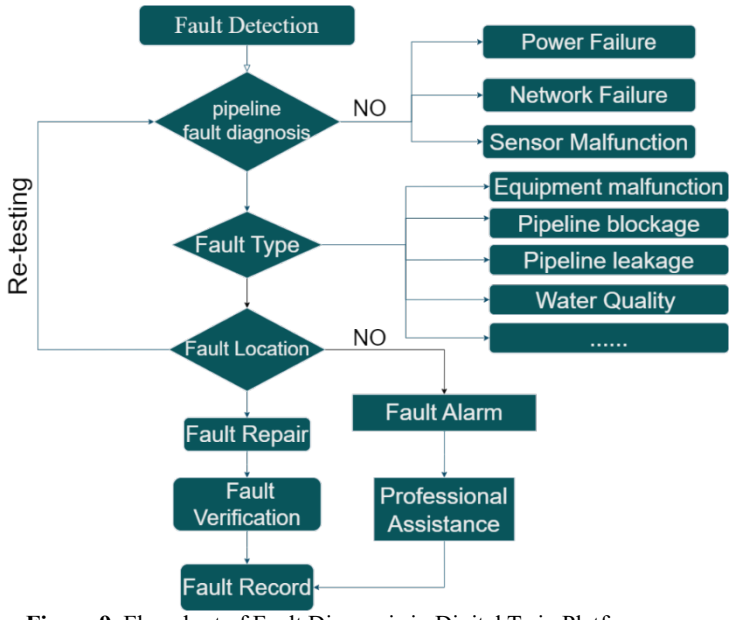

Figure 9. Flowchart of Fault Diagnosis in Digital Twin Platform

5. ANALYSIS OF APPLICATION PROSPECTS

The digital twin platform for heating systems enables real-time monitoring, prediction, and optimization, leading to improved heating efficiency, cost reduction, enhanced user experience, and sustainable development. It comprehensively monitors and intelligently controls the heating system, achieving precise heating, avoiding waste and irrational investment. Additionally, it can personalize heating according to user needs, providing real-time heating information and services. It also monitors and diagnoses the operating status of the heating system, promptly detecting problems. After the construction of the digital twin platform for centralized heating in northern China, its application prospects are extremely broad, supporting the transformation of centralized heating systems towards intelligent heating modes.

6. CONCLUSION

(1) In response to the transformation of centralized heating towards intelligent and information-based systems, this paper

proposes a general design scheme for a centralized heating platform based on digital twin technology, which provides a new approach for intelligent heating in centralized heating projects.

(2) This paper analyzes the key technologies of the digital twin platform for heating supply, discusses the main functional modules of the platform implementation, and constructs a centralized heating digital twin platform that helps improve the safety of the heating system, enhance the dynamic perception ability of heating supply, and improve the user's thermal comfort experience.

(3) The establishment of physical models for each component of the digital twin system for heating supply involves a significant workload, given the large-scale and multi-level coupling characteristics of the heating network. Therefore, the next research focus will be on optimizing the digital twin model by creating a more precise heating twin model.

ACKNOWLEDGEMENT

This work is supported by China National 14th Five-Year Plan of Key Research and Development Program “Development of the digital-twin for a district heating system and the smart control based on dynamic simulation towards a low-carbon energy sector” (2021YFE0116200).

References

[1] YUAN Shanshan. Research on Dynamic Performance of Centralized Heat-supply System [D]. Tianjin University,2010.
[2] JIANG Miao. Study on influencing factors and forecasting methods of heating load in central heating system [D]. Harbin Institute of Technology,2021.
[3] Zhong Wei, ZHENG Lijun, Yu Zitao; LIN Xiaojie; Smart heat-supply roadmap based on digital twin [J]. Water Conservancy & Electric Power Machinery,2020(11).
[4] LI Dachuan. Urban heating network security evaluation and incident management research[D]. Tianjin University,2014.
[5] HAN Boyi. Research on balance adjustment and optimal operation of the secondary network in centralized heating system [D]. Harbin Institute of Technology,2021.
[6] SHEN Chen, JIA Mengshuo, CHEN Ying, et al. Digital Twin of the Energy Internet and its Application[J]. Global Energy Interconnection,2020,3(01):1-13.

The 18th International Symposium on District Heating and Cooling,
September 3-6, 2023, Beijing, China

DYNAMIC TRANSPORT PROCESS ANALYSIS OF DISTRICT HEATING SYSTEMS CONSIDERING SOURCE-LOAD UNCERTAINTY

Xiaojie Lin[a*], Yihui Mao[a], Tianyue Qiu[b]

[a] *College of Energy Engineering, Zhejiang University, Hangzhou, 310027, China*
[b] *Zhejiang Engipower Technology Co., LTD, Hangzhou, 311100, China*
[*] *Corresponding author. Xiaojie.lin@zju.edu.cn*

Abstract

District heating systems (DHS) are essential platforms for coordinating renewable energy with traditional energy sources and achieving flexible integration of renewable energy. However, the uncertainties in the output of renewable energy units and the total heat load of user clusters can impact the transport process of DHS. It is necessary to quantitatively analyze the thermal characteristics and the temperature response of nodes in the DHS under uncertainties in both the source and load sides. This paper presents a method for calculating the dynamic temperature response of nodes in a DHS under source-load uncertainty scenarios. It proposes prediction and combination methods for the supply-demand probability intervals of source and load nodes under different credible levels and analyzes the influence of source-load uncertainty boundary conditions on the transport process of the DHS. The dynamic DHS model is constructed to calculate the temperature response of each node under multiple source-load uncertainty scenarios. A case study and analysis were conducted on a Beijing DHS consisting of 90 nodes and 109 pipes. The simulation results demonstrate that the proposed model and algorithm can effectively quantify the probability intervals of thermal power at source and load nodes and analyze the dynamic temperature response of nodes under source load uncertainty.

Keywords: District heating system, Dynamic model, Uncertainty quantification

RESEARCH ON HEATING LOAD FORECASTING BASED ON MULTIPLE METEOROLOGICAL ELEMENTS

Dawei Zou [a,b], **Jie Liu** [a,b*], **Rongmeng Deng** [a]

[a] *Key Laboratory of Meteorological Disaster Prevention and Mitigation of Shandong Jinan, 250031, China,*
[b] *Tai'an Meteorological Bureau Tai'an, 271000, China*
[*] *Corresponding author. liujie00821@163.com*

Abstract

Urban central heating is the main way of heating in the northern region during winter. However, there is excessive energy consumption and resource waste in the actual operation of central heating systems. Accurate prediction and control of heat load for urban central heating systems is a prerequisite for better operation and regulation. Meteorological factors have great research value as the main influencing factors in the prediction of heat load. Traditional heat load prediction calculations generally only use temperature as a variable, neglecting the influence of other meteorological elements outside of outdoor temperature on heat load, resulting in mismatch between predicted and actual heat load. Validated calculations show that the error between the traditional heat load model calculation value and the actual heat load is close to 15%. Especially when encountering abrupt weather changes, mismatched heat loads caused by sudden changes in meteorological factors can cause significant energy waste. In this pa per, daily meteorological data and actual heat load data for Tai'an City from 2018 to 2022 were used. Through correlation analysis, five meteorological elements, including daily average temperature, daily maximum temperature, daily minimum temperature, daily maximum wind speed, and daily total sunshine hours showed a significant correlation with the daily heat load. They can be used as parameters for optimizing heat load calculation. Multiple regression was used to establish a regression model for the five meteorological elements and heat load. Using data from the 2022 2022-2023 heating season for testing, the prediction error of the new model was reduced by 6.9% compared to the traditional model, especially improving the prediction accuracy in situations where heat load predictions were underestimated, with an error reduction of 9.1%. It effectively improves the accuracy of heat load forecasting.

Keywords: Energy saving of heat supply, Meteorological Forecast, Heating load forecast

The 18th International Symposium on District Heating and Cooling, September 3–6, 2023, Beijing, China

OPTIMIZATION OF THE CONTROL STRATEGY OF THE LOW-TEMPERATURE DISTRICT HEATING SYSTEM WITH THE SEWAGE HEAT PUMP BASED ON DIGITAL TWIN MODELING

Zhonghui Lu [a], Zhe Tian[a], Xiaochen Yang[a*], Yakai Lu[b]

a Tianjin Key Laboratory of Built Environment and Energy Application, School of Environmental Science and Engineering, Tianjin University, Tianjin 300072, China

b School of Energy and Environmental Engineering, Hebei University of Technology, Tianjin, 300401, China

** Corresponding author. E-mail address: xiaochen.yang@tju.edu.cn*

ABSTRACT

The operational phase of buildings consumes large amount of energy. The traditional district heating system management, which relies on experienced maintenance personnel, is difficult to meet more and more strict energy-saving requirements currently. However, by integrating the optimal control strategy on the demand side based on digital twin modeling, the overall energy efficiency of the whole system can be effectively reduced. A digital twin model, obtained through the modeling simulation and system identification algorithms, can simulate the system performance under the actual operating conditions. Based on the digital twin model, the optimization algorithm such as particle swarm algorithm, is applied to conduct the multi-objective optimization of the district heating system operation. The optimized operation and control strategy is extracted into rules, forming a two-level operation and control mode architecture that combines upper-level supervisory control with lower-level local control. The two-layer control strategy is then applied to guide the subsequent operations in engineering. In this study, the proposed method was applied to a case study in Tianjin, which uses the sewage source heat pump as the heat source. The scale of the heating area is 480,000 m^2. The heat users are residential buildings with a design heat load of 11,571kW and the heating form is radiant floor heating. The design temperature of supply and return water is 50/40℃ for the primary loop, and 45/35℃ for the secondary loop. The signal of the temperature, flow rate, equipment start-stop status, energy consumption data and meteorological data were collected, so to establish the digital twin model with high accuracy. Combined with the optimization algorithm, the operation strategy can be optimized to reduce the system energy consumption.

Keywords: Low-temperature district heating; Digital twin; Operation optimization; sewage heat pump; Building energy efficiency

1. INTRODUCTION

The heating, ventilation and air conditioning (HVAC) system consumes great amount of energy in building sector, which ranges from 30% to 50% [1]. The energy-saving of HVAC system is achieved by two aspects: improving equipment performance and optimizing system operation strategy [2]. For existing systems, the improvement of equipment performance, e.g. replacing an high-efficiency heat pump, is usually costly. However, the traditional district heating system management, which relies on the experiences and knowledge of the maintenance engineer, is find to be more and more difficult to meet increasingly strict energy-saving requirements at present. Therefore, optimizing the existing operation strategy of the system is a feasible and low-cost way to save energy. In the previous research, there are two basic approaches to optimize the operation strategy: model-based method and data-driven method [3].

Data-driven method can efficiently analyze the hidden knowledge from data. Li et al. [4] searched for the optimal fan speed of the cooling tower through extreme value search control. Xue et al. [5] applied the unsupervised data mining to analyze operation data of district heating substations. Awan et al. [6] used Conditional Reasoning Tree, Aggregate Hierarchical clustering and association rule mining to analyze the chiller system. The results showed that the practical performance of chiller is strongly influenced by the temperature difference of evaporator. However, the performance of data-driven model depends on the quantity and quality of historical operation data of the system [7]. When the data is incomplete, the energy-saving effect of the data-based method will be much limited due to the poor performances of the control.

With the development of intelligent algorithms and simulation software, model-based optimization methods are gradually used. Generally, in the study of operation optimization using model-based methods, the simulation models of each

equipment are developed first, followed by an optimization model built with different goals, such as lower cost, better indoor comfort, higher system efficiency and etc., which can be conducted by finding the optimal set values of operation parameters. Fan et al. [8] developed a detailed simulation model of an airport building with its HVAC system by TRNSYS. The operating performance of HVAC system and the maximal potential of each equipment are analyzed. Karami et al [9] developed the dynamic simulation model with Modelica and the model is calibrated with actual data. The optimal control strategy is find using the particle swarm optimization search algorithm. Huang et al [10] used model library in Modelica to simulate the HAVC system and optimized it based on Hooke Jeeves algorithm. Niu et al. [11] built a full-performance simulation chiller plant model based on Modelica language and then hierarchically calibrated the model using the measured data. An optimization framework based on GenOpt-Dymola was established for the holistic optimization problem. Although the model-based method has shown the ability to improve the system operation, there are few studies conducted the calibrated digital twin model of the low-temperature central heating system with sewage heat pump as the heat source. The main difficulties include: (1) the configuration parameters of simulation model are usually difficult to obtain accurately due to the limited data measures and the difficult of parameter estimation [12]; (2) Optimization variables may not be controllable in engineering, which makes the optimization results difficult to apply. For example, due to the difficulty of sewage discharge, the sewage heat exchanger cannot be started and stopped frequently.

In this paper, a model-based optimization method of the operation strategy of a case LTDH (low-temperature district heating) supplied by the sewage heat is proposed. Dymola/Modelica, which can couple the hydraulic, thermal and control logic of the system, is selected as the modeling and simulation tool. The digital twin model is calibrated by the measurements of the case system. According to the characteristics of the system, the optimization variables and the constraints are determined to ensure that the optimization results can guide the actual operation.

2. METHODOLOGY

The proposed method is shown in Figure 1, which includes four processes: data preprocessing, construction of digital twin model, model calibration and optimization of operation strategies. The digital twin model can simulate the operation state of thermal, hydraulic and electrical parameters of the system under different operating conditions. The optimization method can find the optimal solution under certain objectives. By combining their advantages, the optimal operation strategy of the system can be obtained.

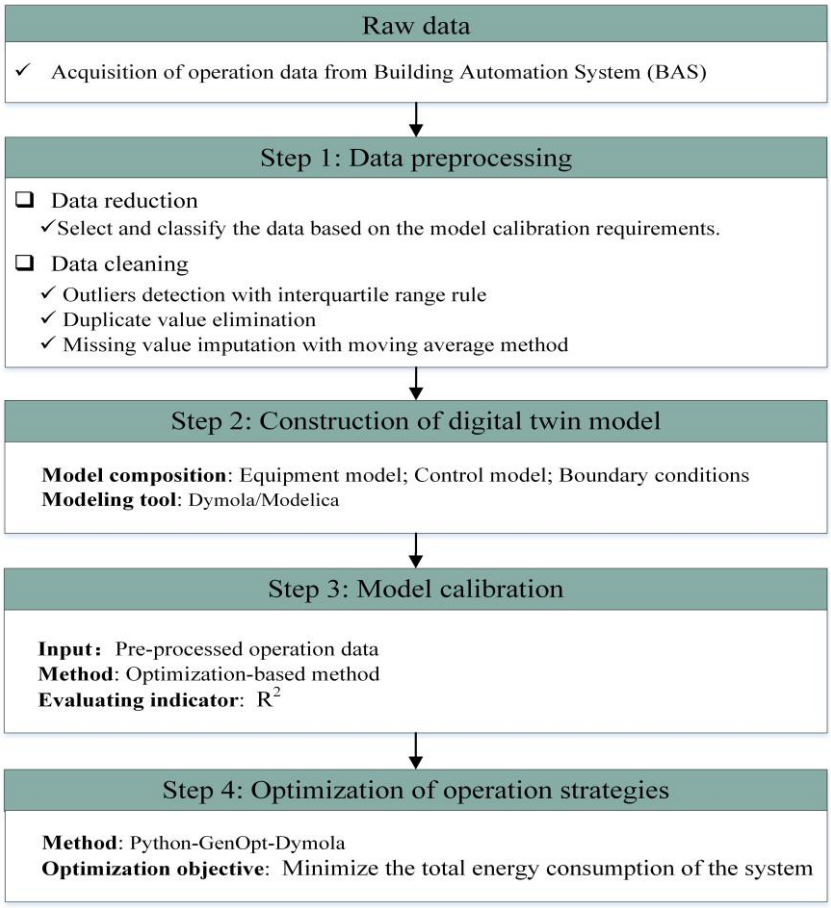

Figure 1. Framework of the model-based optimization of system operation strategy

2.1. Data preprocessing

Data reduction: Building automation system will collect many kinds of data. Based on the parameters needed for model calibration, data are classified and selected to reduce the workload of data preprocessing.

Data cleaning: Due to the failure of sensors and communication equipment, abnormal values and missing values always appear in the data set. Data cleaning is to clean up lost values, detect and delete abnormal values. In this study, missing values are handled using a simple moving average method with a window size of 5 samples. Moving average method takes the values in a rolling period before or after the occurrence of missing values and calculates their average or median to fill in the missing values. Duplicate value refers to the value that remains unchanged in continuous operation time. This paper will delete all the objects with duplicate values. Outliers will be detected using a simple filter, namely the quartile range rule.

2.2. Establishment of digital twin model

The digital twin model is established using the Modelica language of the Dymola platform. Modelica language can be used for unified modeling in multiple fields and collaborative simulation. Dymola is based on Modelica language, which not only provides a general platform for cross-domain modeling, but also provides convenience for multi-domain simulation modeling. Dymola platform has a variety of model libraries, which greatly reduces the difficulty of modeling. Another advantage of Dymola is that it can quickly solve complex multidisciplinary system modeling problems. Because Dymola uses nonlinear equations to describe the model, it is more robust and efficient. Its optimized parameter processing operation generates less codes for large data tables, so the speed of model conversion, simulation and post-processing will be improved.

The whole model can be divided into three parts: equipment model, control model and boundary conditions. The idea of hierarchical modeling is adopted to build the model, which can find the deviation and error in the modeling process more quickly. The system is divided into multiple loops, and the main equipment in the loop is modeled and tested first. Then the devices are connected into a loop and control logic is added. Finally, the multi-loop is connected into a whole model, and the boundary of the model is constructed.

2.3. Model calibration

In order to further ensure that the operating conditions and the energy consumption of the model were consistent with those of the actual system, model calibration was carried out based on measured data. In this paper, energy (e.g. power) and state (e.g. temperature) variables are calibrated to ensure that the model is consistent with the actual system in terms of energy consumption and operating conditions. In this way, the optimal control strategy obtained by model optimization is applicable in practice.

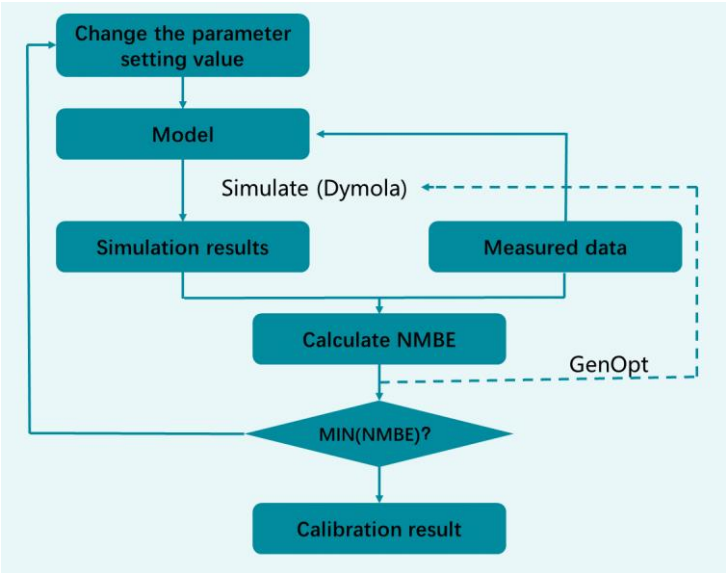

Figure 2. Model calibration process

The calibration process is shown in Figure 2. The calibration process can be considered as an optimization process. By adjusting the model parameters, the difference between the simulation results and the actual data is minimized. Therefore, the optimization-based method can be used to calibrate the model. In this paper, Dymola and GenOpt are used for joint simulation to optimize model parameters, which is more suitable for models that only need to identify nominal parameters and have complex internal mechanism and structure. Because this method does not pay attention to the specific form of the

model, it has strong universality. It can be used to calibrate not only a single equipment model, but also a system model. The normalized mean deviation error (NMBE) between simulation data and measured data is taken as the optimization objective.

$$J = min(NMBE) = min\left(\frac{\sum_{i=1}^{m}|s_i - m_i|}{\sum_{i=1}^{m} m_i}\right) \tag{1}$$

Where: J is the calibration objective; s_i is the simulated value; m_i is the measured value; m is the number of data points.

In addition, relying solely on error indicators is not sufficient to fully demonstrate the consistency between simulation results and actual results. It is also necessary to evaluate the similarity between the simulation result curve and the actual result curve through the square of the Pearson correlation coefficient (R^2):

$$R^2 = \left(\frac{\sum_{i=1}^{m}(m_i - \overline{m}) \cdot (s_i - \overline{s})}{\sqrt{\sum_{i=1}^{m}(m_i - \overline{m})^2 \cdot \sum_{i=1}^{m}(s_i - \overline{s})^2}}\right)^2 \tag{2}$$

Where: $\overline{m}$ is the mean of measured values; $\overline{s}$ is the mean of simulated values.

2.4. Optimization of operation strategies

Optimization variable selection principle: (1) The coupling between variables should be considered to achieve global optimization. (2) The controllability of variables and ease of deployment of optimized results should be considered. For the manual control part of the system, the reset of the set-point and the start/stop of the equipment are directly manually operated by the operation engineers. Therefore, the value of set-point, the number of running equipment and the serial number of running equipment can be used as optimization variables.

This paper takes the total energy consumption of the system as the optimization goal, which can be expressed as follows:

$$J = minE = min\left(\int_{t_1}^{t_2} P_{ttl}(t)dt + \mu \cdot max(0, \Delta\Phi)^2\right) \tag{3}$$

Where: E is the total energy consumption (kWh) of the system, t_1 and t_2 are the starting and ending time (h) of optimization respectively, $P_{ttl}(t)$ is the total power (kW) of the system at time t, μ is the penalty factor and $\Delta\Phi$ is the penalty function. The penalty function uses the secondary side return water temperature as a constraint to avoid failing to meet the demand of heat users.

$$\Delta\Phi = \int_{t_1}^{t_2} (T_{re} - T_{re,lim})\, dt \tag{4}$$

Where: T_{re} is the secondary side return water temperature (℃), $T_{re,lim}$ is the minimum value of secondary side return water temperature, which is set according to the measured data. $T_{re,lim}$ is set to 30 ℃ in this paper.

The model and the objective function are highly non-linear. The GenOpt optimization program was adopted in this paper. GenOpt is an optimization program, which can be coupled with external simulation software such as TRNSYS, EnergyPlus and Dymola to minimize the cost function or other objective functions. In GenOpt, there is a library with local and global multi-dimensional and one-dimensional optimization algorithms. In this paper, the GPS-PSO algorithm was used to optimize the variables for minimizing energy consumption and identifying the optimal solution. As shown in figure 3, the framework consists of an optimization layer and a simulation layer. In the optimization layer, the GenOpt calls for Dymola for optimization, and continuously generates feasible solutions of all the optimal variables. Then in the simulation layer, Dymola receives the feasible solutions from GenOpt, and carry out simulation. During the whole process, Python is employed as the tool for connecting the two layers and linking adjacent optimization/simulation periods.

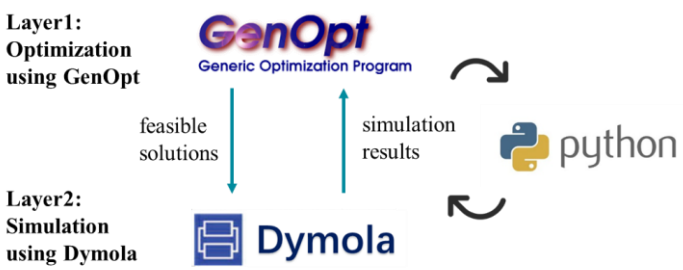

Figure 3. The Python-GenOpt-Dymola optimization framework

3. DESCRIPTION OF THE LOW-TEMPERATURE DISTRICT HEATING SYSTEM

In this study, the proposed method was applied to a case study in Tianjin, which uses the sewage source heat pump as the heat source. The scale of the heating area is 480,000 m2. The heat users are residential buildings with a design heat load of 11,571kW and the heating form is radiant floor heating. The design temperature of supply and return water is 50/40℃ for the primary loop, and 45/35℃ for the secondary loop. The main equipment parameters in the system are shown in Table 1. It is worth noting that there are 20 sewage heat exchangers, which are divided into four groups.

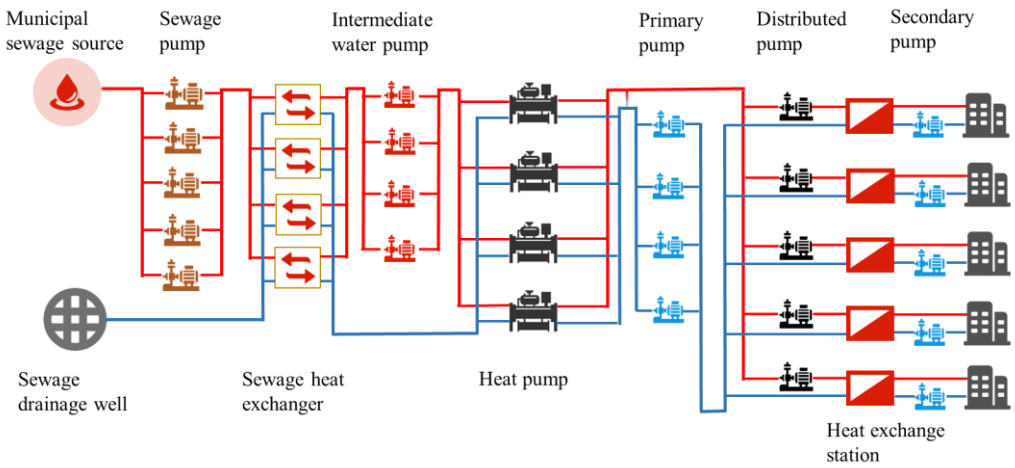

Figure 4. The schematic diagram of the system

Table 1. Technical specifications of the system

Equipment	Quantity	Technical specifications
Sewage pump	5	Rated power 55 kW, rated flow 450 m3/h, rated head 25 m
Sewage heat exchanger	20	Rated heat exchange capacity 720kW
Intermediate water pump	4	Rated power 75 kW, rated flow 781 m3/h, rated head 25 m
Heat pump	4	Rated capacity 4000kW, power 907.8kW, Rated chilled water flow 530m3/h, Rated cooling water flow 350m3/h
Primary pump	4	Rated power 37 kW, rated flow 484 m3/h, rated head 18 m
Distributed pump	10	Rated power 24.8 kW, rated flow 200 m3/h, rated head 18.5 m
Heat exchange station	5	Rated heat exchange capacity 2400kW
Secondary pump	10	Rated power 20 kW, rated flow 210 m3/h, rated head 15 m

The system is equipped with a monitoring platform. The monitoring variables are shown in Table 2. The available monitoring data range is from November 1, 2022 to March 15, 2023, and the data acquisition interval is 5 minutes.

Table 2. Data acquisition of the system

Data acquisition location	Type
Primary water main pipe	Supply and return water temperature, flow, pressure, quantity of heat
Intermediate water main pipe	Supply and return water temperature, flow, pressure, quantity of heat
Sewage main pipe	Supply and return water temperature, flow, pressure
All pumps in the system	Start-stop state, operating frequency, current, power voltage, frequency setting value, circulating pressure difference setting, fault alarm signal
Sewage heat exchange	Temperature, pressure, start-stop state
Heat pump	Start-stop status, chilled water supply and return water temperature, cooling water supply and return water temperature, condensation pressure, evaporation pressure, current percentage, power, guide vane valve opening, chilled water inlet and outlet pressure, cooling water inlet and outlet pressure, fault alarm signal
Heat exchange station	Supply and return water temperature, flow, pressure, quantity of heat

4. RESULTS

4. 1 Model calibration results

The result of model calibration is shown in Figure 5-8. According to the suggested hourly level value of R^2 given in ASHRAE Guide 14[13], when R^2 is not less than 0.75, the model meets the requirements.

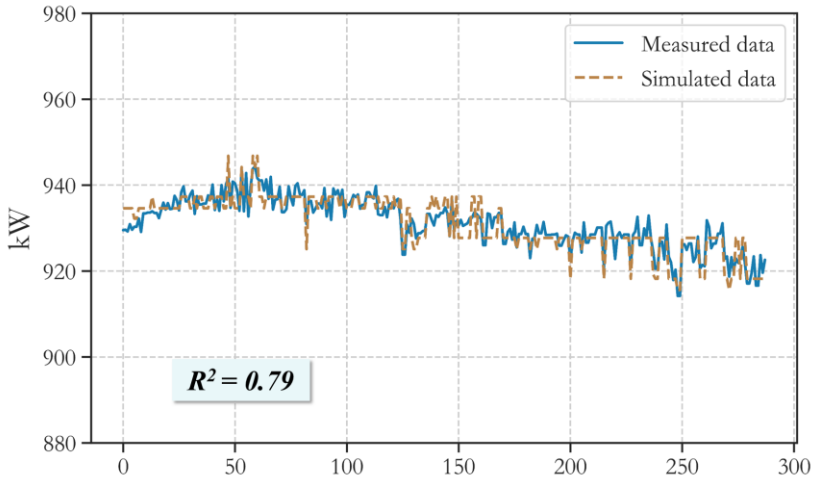

Figure 5. Comparison between simulation data and measured data of heat pump electric power

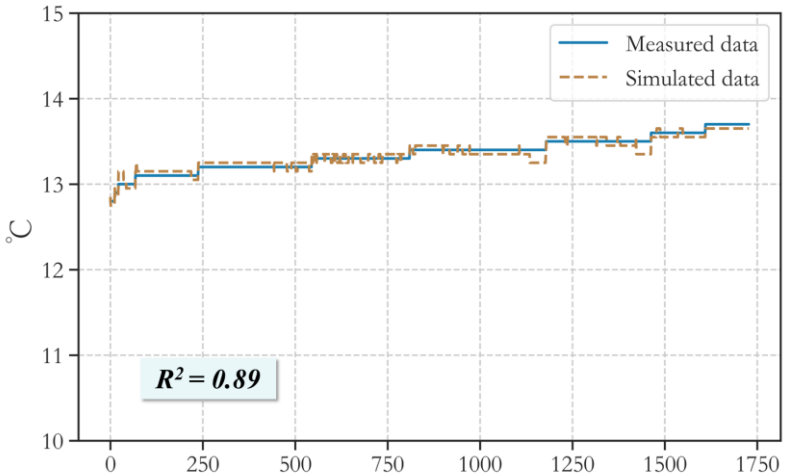

Figure 6. Comparison between simulated data and measured data of water outlet temperature in sewage heat exchanger

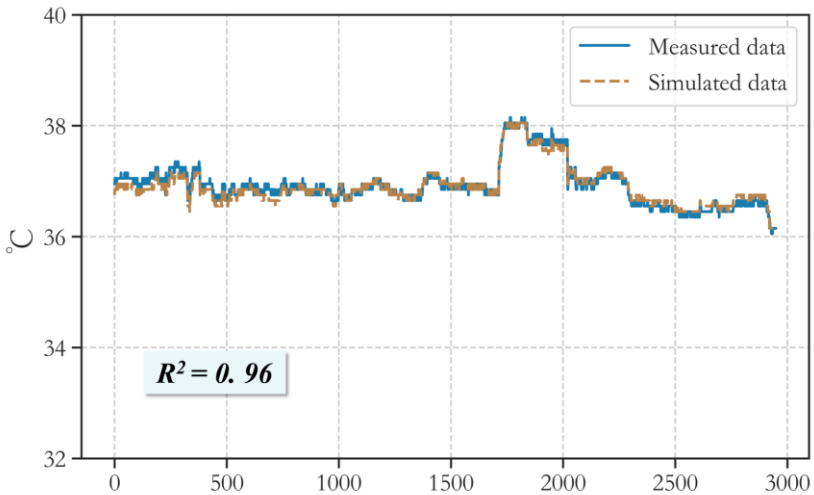

Figure 7. Comparison between simulated data and measured data of secondary water supply temperature in heat exchange station

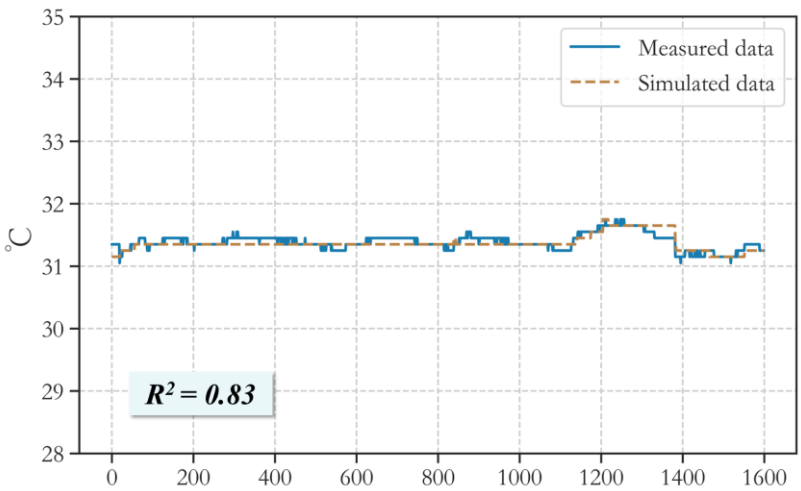

Figure 8. Comparison between simulated data and measured data of return water temperature of radiator

4. 2 Optimization results

The optimization variables selected in this paper are as follows: the number and frequency of sewage pumps, the number and frequency of intermediate water pumps; the number of sewage heat exchangers; the number of heat pumps, the number and frequency of primary pumps, primary water supply temperature. Other equipment, such as distributed pumps, are not optimized because they are in the heat exchange station instead of the energy station and have different control platforms.

The system operation strategy of November 2, 2022 was optimized. The comparison of daily energy consumption before and after optimization is shown in Figure 9.

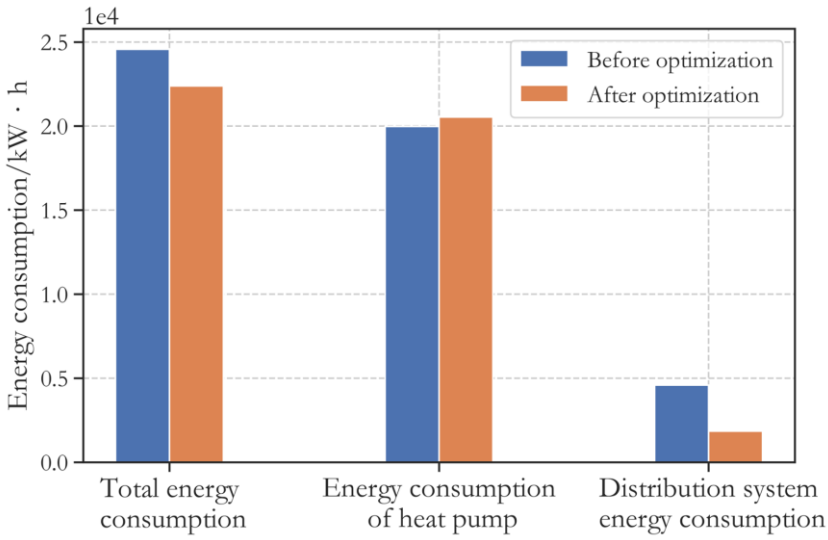

Figure 9. Comparison of daily energy consumption before and after optimization

Because of the small fluctuation of daytime load in the early heating period, there is no optimization of the number of equipment. In the original operation strategy, the water pump keeps the maximum operating frequency to ensure the efficient operation of the heat pump. The optimization results show that by reducing the operating frequency of the pump and the supply temperature of the primary water, although the energy consumption of the heat pump is slightly increased, the total energy consumption is reduced, which can be reduced from 24,565 kWh to 22,386 kWh. The energy saving rate is 8.9%.

5. CONCLUSION

In this paper, a model-based optimization method is proposed to optimize the operation strategy of sewage heat pump system. The model is calibrated by the measured data to improve the accuracy. Considering the deployment of the operation strategy, the optimization variables are selected according to the system characteristics. Based on Python-GenOpt-Dymola, an optimization framework is constructed to solve the optimal operation strategy. After optimization, the energy consumption of the system can be significantly reduced.

ACKNOWLEDGEMENT

This work is supported by Tianjin key R&D projects "R&D and application of key technologies for the digital twin and efficient operation of green low-carbon building energy", (22YFZCSN00180).

REFERENCES

[1] Yang B, Melikov A K, Kabanshi A, et al. A review of advanced air distribution methods-theory, practice, limitations and solutions[J]. Energy and Buildings, 2019, 202:109359. DOI: 10.1016/j.enbuild.2019.109359

[2] Arie Taal, Laure Itard, Wim Zeiler. A reference architecture for the integration of automated energy performance fault diagnosis into HVAC systems. Energy & Buildings 179 (2018) 144–155. DOI: 10.1016/j.enbuild.2018.08.031

[3] Wang Y, Jin X, Fang X. Rapid evaluation of operation performance of multi-chiller system based on history data analysis[J]. Energy & Buildings, 2017, 134(JAN.):162-170. DOI: 10.1016/j.enbuild.2016.10.041

[4] Li, X., et al., Dynamic modeling and self-optimizing operation of chilled water systems using extremum seeking control. Energy and Buildings, 2013. 58: p. 172-182.

[5] Xue P, Zhou Z, Fang X, et al. Fault detection and operation optimization in district heating substations based on data mining techniques[J]. Applied Energy, 2017, 205:926-940. DOI： 10.1016/j.apenergy.2017.08.035

[6] Awan M B, Li K, Li Z, et al. A data driven performance assessment strategy for centralized chiller systems using data mining techniques and domain knowledge[J]. Journal of Building Engineering, 2021, 41:102751. DOI： 10.1016/j.jobe.2021.102751

[7] Guo, Y., et al., Deep learning-based fault diagnosis of variable refrigerant flow air-conditioning system for building energy saving. Applied Energy, 2018. 225: p. 732-745.

[8] Bo, Fan, Xinqiao, et al. The method of evaluating operation performance of HVAC system based on exergy analysis[J]. Energy & Buildings, 2014. DOI： 10.1016/j.enbuild.2014.03.059

[9] Karami, Majid, Wang, et al. Particle Swarm optimization for control operation of an all-variable speed water-cooled chiller plant[J]. Applied Thermal Engineering Design Processes Equipment Economics, 2018. DOI: 10.1016/j.applthermaleng.2017.11.037

[10] Huang S, Zuo W, MD Sohn. Amelioration of the cooling load based chiller sequencing control[J]. Applied Energy, 2016, 168(apr.15):204-215. DOI: 10.1016/j.apenergy.2016.01.035

[11] Niu J, Zhou R, Tian Z, et al. Energy-saving potential analysis for a 24-hour operating chiller plant using the model-based global optimization method[J]. Journal of Building Engineering, 2023: 106213

[12] Jang Y E, Kim Y J, Catalao J. Optimal HVAC System Operation Using Online Learning of Interconnected Neural Networks[J]. IEEE Transactions on Smart Grid, 2021, PP (99):1-1. DOI: 10.1109/TSG.2021.3051564

[13] R.a.A.-C.E, ASHRAE Guideline. Measurement of Energy and Demand Savings, American Society of Heating, INC., 2002.

The 18th International Symposium on District Heating and Cooling,

September 3-6, 2023, Beijing, China

Predicting Heat Demand for Efficient District Heating Systems Using Deep Learning Algorithms

Kevin Naik[a,b,*], Anton Ianakiev[a], Appu Ulahannan Mathew[a], Ming Sun[a]

[a] *Nottingham Trent University, Nottingham, UK*
[b] *Ecolibrium, London, UK*
[*] *Corresponding author: kevin.naik@ntu.ac.uk*

Abstract

The International Energy Agency states that in 2018, buildings and construction were responsible for 36% of energy use and 39% of carbon dioxide emissions. As people spend more time indoors, significant amounts of energy are required to maintain a comfortable temperature. District Heating Systems (DHS) are a safe and efficient way to provide heat to buildings. To reduce energy loss, it is essential to accurately predict and control the operations of DHS. Predicting a building's heat requirement in advance enables DHS operators to adjust the supply temperature and flow rate accordingly. Therefore, accurate heat demand prediction is crucial for improving energy efficiency. With the rise in deep learning's popularity, numerous new algorithms have been proposed for time-series predictions. This work aims to evaluate the performance of deep learning-based methods such as DeepAR, Temporal Fusion Transformer (TFT), and N-Beats, along with traditional sequence models such as Recurrent Neural Network (RNN), Gated Recurrent Unit (GRU), and Long Short-Term Memory (LSTM), in predicting heat loads. The study also seeks to explore the impact of seasonality on prediction accuracy.

Keywords: District Heating Systems; energy efficiency; deep learning; time-series predictions; Temporal Fusion Transformer (TFT); Recurrent Neural Network (RNN); Gated Recurrent Unit (GRU); Long Short-Term Memory (LSTM); heat load

1. INTRODUCTION

This research builds upon the authors' previous studies in heat demand prediction and optimization. It references two published papers comparing real-life data models with simulated data models and exploring multi-energy system optimization software using hypernetworks and a micro-service architecture. Additionally, the authors have conducted research on optimizing heat consumption at a micro-level using a user-centric data-driven model. Drawing from this foundation, the present study aims to further explore and assess the potential of deep learning algorithms for accurate heat demand prediction [1,2,3].

The building and construction sectors are recognized as major contributors to global energy consumption, accounting for approximately one-third of total energy consumption and nearly 15% of direct carbon dioxide emissions. With urbanization and population growth accelerating, these figures are projected to rise even further. Consequently, there is an increasing need for sustainable and efficient heating solutions to maintain comfortable indoor temperatures. Heating, Ventilation, and Air Conditioning (HVAC) systems are crucial for achieving optimal indoor conditions but contribute significantly to overall energy consumption. To improve energy efficiency, accurate prediction, and control of District Heating Systems (DHS) operations are essential. By accurately forecasting a building's heat demand in advance, DHS operators can proactively adjust supply temperature and flow rate, thereby enhancing energy efficiency and sustainability.

Energy consumption prediction can be approached through physics-based models or data-driven methods. Physics-based models require detailed system information and expert knowledge, making them costly and time-consuming. In contrast, data-driven models, leveraging deep learning techniques, have gained popularity as an alternative solution. These models have demonstrated promising results in various domains, including time-series prediction.

In this research, our objective is to investigate the effectiveness of different deep learning algorithms for time-series prediction, specifically focusing on heat consumption prediction. The primary aim is to contribute to the reduction of energy consumption and CO2 emissions by exploring the potential of deep learning algorithms. We will employ advanced models such as Temporal Fusion Transformers, DeepAR, and NBeats to identify the most suitable model for accurately predicting heat demand in buildings. Furthermore, we will establish baseline scores for performance comparison by utilizing traditional models such as RNN, LSTM, and GRU.

This study will utilize heat and weather data to evaluate the performance of the selected deep learning models. We will

employ suitable evaluation metrics, including mean absolute error (MAE), root mean square error (RMSE), and mean absolute percentage error (MAPE), to assess the effectiveness of the models. The outcomes of the best-performing model will be visually presented, facilitating easier interpretation, and understanding of the results. Ultimately, the research aims to contribute to improved energy efficiency and sustainability in the building sector through accurate heat demand prediction.

The findings of this research carry immense significance for practitioners in the field. Accurate heat demand prediction achieved through deep learning algorithms offers a transformative potential for energy management and building operations. It enables practitioners to optimize heating systems, resulting in improved energy efficiency, cost savings, and sustainability. With precise predictions at their disposal, practitioners can make informed decisions regarding retrofitting strategies, enhance resource allocation, reduce carbon emissions, and elevate overall operational effectiveness. By leveraging the outcomes of this study, practitioners can embrace data-driven approaches, optimize energy usage, and contribute to a more sustainable and efficient building sector.

2. Literature Review

This section reviews techniques for heat and energy prediction in district heating systems. It emphasizes the importance of the building industry's energy consumption and the need for renewable sources. The following literature works are discussed.

In [4], a coordinated energy management method using LSTM and DRL is proposed. It reduces power costs and peak consumption while maintaining temperature regulation. SDS [5] presents a short-term heating load prediction algorithm using a feature fusion LSTM model. It achieves improved accuracy compared to other methods. [6] compares machine learning algorithms for district heating value prediction, finding that linear regression and decision trees perform best depending on the dataset.

[7] explores deep learning models for energy usage forecasting, highlighting their potential but noting the lack of comparative studies. [8] focuses on load forecasting in district heating systems using the informers model, which shows stable and consistent forecasting. To improve efficiency, [9] introduces LGBM for return temperature prediction, reducing heat loss.

[10] proposes an SVR-based model for heat load prediction, outperforming other methods. Additional meteorological parameters are suggested for improvement. [11] presents a quantum weighted GRU model for short-term multiple load forecasting, demonstrating enhanced accuracy.

These works contribute to understanding heat and energy prediction, showcasing effective techniques, and identifying areas for further research.

3. METHODOLOGY

3.1 Models

3.1.1. RNNs [15] are suitable for sequential data like time series and language data. They possess a memory that retains information from previous inputs, allowing them to capture temporal dependencies. RNNs employ the backpropagation through time (BPTT) algorithm for training, and different configurations such as one-to-one, one-to-many, many-to-many, and many-to-one are utilized.

3.1.2. LSTM [5] addresses the issue of long-term dependencies in traditional RNNs. It consists of four parts within each recurring structure: forget gate, input gate, cell state, and output gate. The forget gate determines the retention or discarding of previous information, while the input gate measures the relevance of fresh input. The cell state stores information, and the output gate determines the next hidden state.

3.1.3. GRUs [9] are newer variations of RNNs that address the problems of vanishing and exploding gradients. They employ two gates: reset gate and update gate. The update gate determines the information to be passed from previous time steps, while the reset gate controls the amount of previous data to forget. GRUs combine the use of tanh and sigmoid functions for information addition and discarding.

3.1.4. DeepAR [12] is a time series model that combines deep learning and autoregressive modeling. It excels in handling multiple time series with slightly different distributions. DeepAR builds a global model using the multiple time series, incorporating historical data and extra static features. It eliminates the need for explicit preprocessing steps like scaling, as the model internally scales the autoregressive input.

3.1.5. N-BEATS [13] is a modular deep learning architecture composed of stacked ensembled feed-forward networks. It leverages meta-learning to generalize across multiple time series datasets. Each N-Beats block consists of two residual branches: backcast and forecast. The forecast is updated based on the residual error from the reconstruction of the backcast, allowing for improved approximation of the backcast signal.

3.1.6. TFT [14] is a transformer-based time series forecasting model developed by Google. It supports multiple, heterogeneous time series and three types of features: temporal data with known inputs into the future, temporal data known only up to the present, and categorical data. TFT prioritizes interpretability and incorporates a Variable

Selection component to measure the influence of each feature. It also employs an interpretable Multi-Head Attention mechanism for emphasizing important past time-series steps.

3.2 Evaluation Metrics

In evaluating the performance of the forecasting models, the Mean Absolute Error (MAE) was chosen as the scale-dependent error metric. MAE is a commonly used metric as it is simple to understand and calculate. Since the evaluation focuses on forecasting a single variable, MAE is suitable for measuring the accuracy of the predictions. The MAE is computed by taking the mean of the absolute differences between the actual values and the predicted values. By using MAE, the forecasting models can be assessed based on the average absolute deviation from the actual values, providing insights into the accuracy of the predictions. Overall, the selection of MAE as the evaluation metric offers a straightforward and interpretable measure to assess the forecasting performance of the models.

3.3 Preprocessing

Two preprocessing steps were applied to the data before training the forecasting models. The first step involved normalizing the data using min-max scaling. By normalizing the data, the range of values was transformed to a standardized range of 0 to 1. This normalization ensures that variables with different scales do not bias the model fitting and learning processes. Additionally, min-max scaling aids in stabilizing and accelerating the backpropagation during the learning phase.

The second preprocessing step involved resampling the data to a daily basis. The original dataset contained 24 data points for each day, corresponding to hourly measurements. To simplify the data and increase the efficiency of training and testing, the values were averaged to obtain a single data point for each day. This resampling technique significantly reduced the size of the dataset while preserving the daily trends and patterns. Resampling the data on a daily basis facilitated smoother training and testing cycles for the forecasting models.

3.4 Training

The training phase involved comparing different representations of seasonality data, including one-hot encoding and numerical value encoding, and evaluating the impact of including or excluding monthly and day-of-week information. Hyperparameter tuning was also performed to optimize the models by adjusting key parameters. These steps were crucial in determining the most effective encoding methods and fine-tuning the models for improved performance.

3.5 Data Analysis:

The temperature values in the dataset range from a minimum of -10 to a maximum of 30, while the load values range from a minimum of 19 to a maximum of 383. Based on the range of load values, it is suspected that the data may contain some anomalies or outliers. To validate this assumption, a boxplot was generated for the load variable (Figure 2 Load Boxplot), revealing no outliers in the dataset.

However, to further verify the presence of outliers, a boxplot was also created for the temperature variable (Figure 3 Temperature Boxplot). The boxplot indicates the existence of outliers for the temperature variable, suggesting the presence of unusual or extreme temperature values.

Another aspect examined in the data analysis is the normality of the data distribution. This was evaluated by constructing histograms for both the temperature and load variables. The histogram for the temperature variable (Figure 4 Temperature Histogram) displays a bell-shaped curve, indicating that the temperature data follows a normal distribution.

Conversely, the histogram for the load variable (Figure 3 Load Histogram) does not exhibit a normal distribution pattern. This suggests that the load data does not conform to a standard Gaussian distribution.

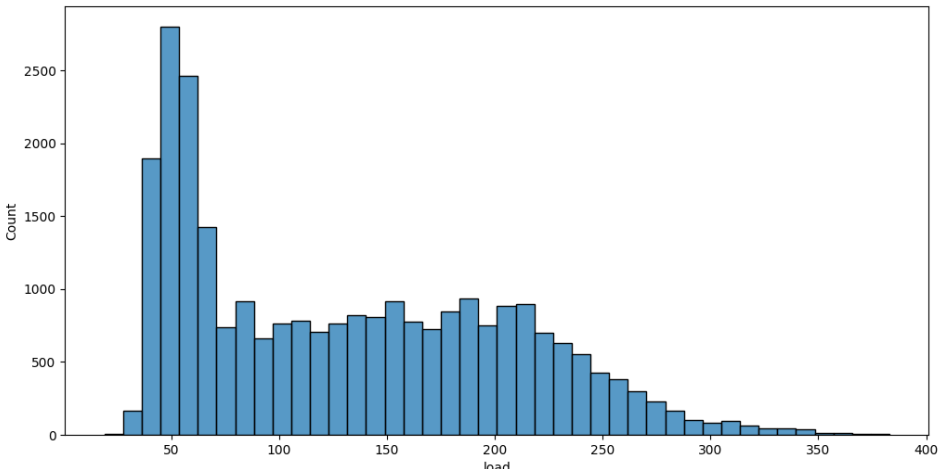

Figure 1 Load Histogram

These findings regarding outliers and data distribution characteristics are important considerations for further pre-processing and modelling steps. They help in identifying any potential data anomalies, determining appropriate pre-processing techniques, and selecting suitable models for predicting the heat load based on temperature and time variables.

Stationarity refers to the property of a time series where its statistical characteristics remain constant over time. There are different types of stationarities, including strict stationarity, first-order stationarity, second-order stationarity, trend stationary models, and difference-stationary models. However, strict stationarity is often too stringent for real-world models.

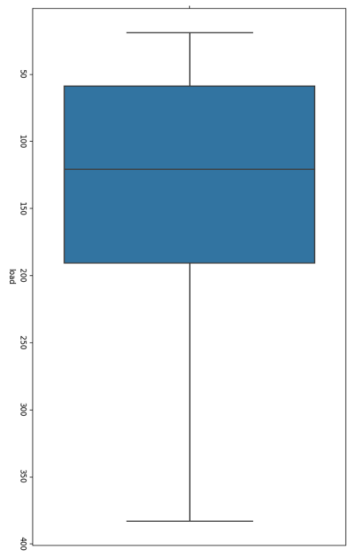

Figure 2 Load Boxplot

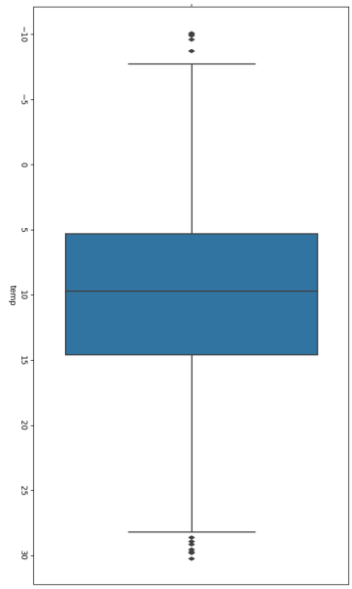

Figure 3 Temperature Boxplot

In first-order stationarity, the means of the time series remain constant over time, while other statistical properties like variance can vary. Second-order stationarity extends this concept by having a constant mean, variance, and autocovariance over time, allowing other statistics to evolve.

Trend-stationary models incorporate a deterministic trend, where the series mean changes over time, but the amplitudes of fluctuations remain constant. Difference-stationary models require differencing to achieve stationarity.

The importance of stationarity lies in the ease of analysis it offers. Many time series analysis tools and techniques rely on stationarity, allowing for straightforward application. Moreover, certain models require the absence of stationarity in the data, making it essential to check for stationarity.

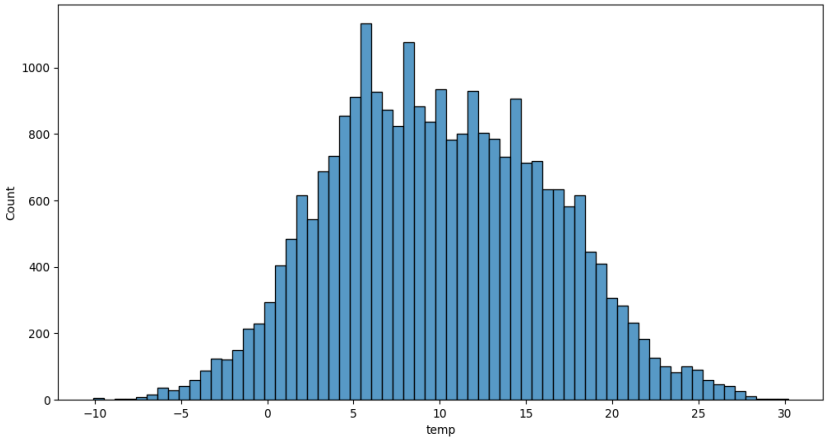

Figure 4 Temperature Histogram

To assess stationarity in our dataset, we can use the Augmented Dickey Fuller Test (ADF), which is a unit root test. A unit root signifies a stochastic trend in a time series, making its pattern unpredictable. The ADF test helps determine stationarity by testing for the presence of a unit root. The test involves formulating null and alternative hypotheses and checking if the p-value is less than a significance level (typically 0.05).

After conducting the ADF test on our dataset, we obtained a p-value of 0.079. Since the p-value is greater than 0.05, we fail to reject the null hypothesis. Therefore, we conclude that there is some degree of stationarity present in our dataset.

Seasonality in a time series refers to predictable and recurring patterns or variations that occur within a specific period, typically a year. It represents the regular cycles and changes in specific sectors or phenomena that are dependent on seasons or specific calendar periods. Seasonality can manifest in various forms, such as daily, weekly, monthly, or yearly patterns.

When examining seasonality, it is important to distinguish between additive and multiplicative seasonality. In additive seasonality, the amplitude of the seasonal pattern remains relatively constant, while in multiplicative seasonality, the amplitude of the seasonal pattern changes based on trends.

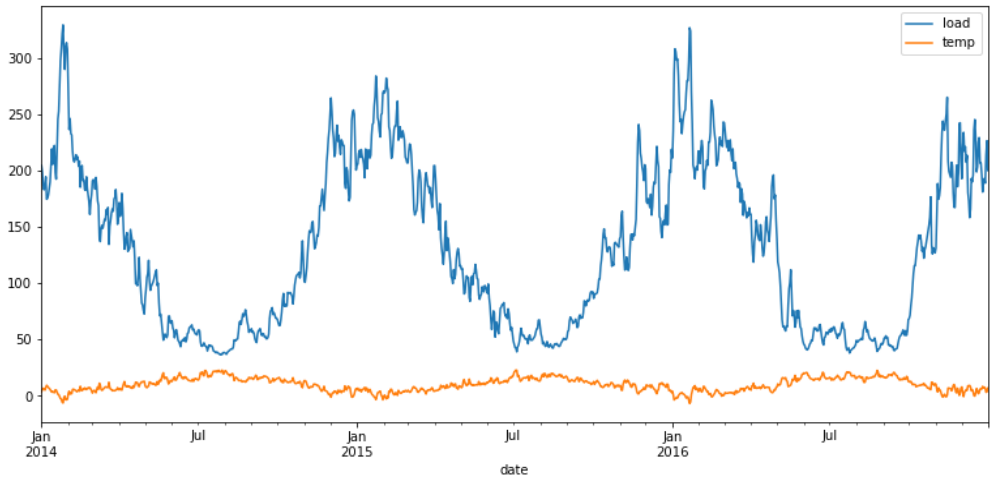

Figure 5 Load and Temperature Patterns Across Months

In the given dataset, two types of seasonality have been identified: monthly seasonality and day-of-week seasonality. By plotting the load and temperature columns over time, it becomes evident that during the summer season, the temperature increases while the load decreases (Figure 5 Load and Temperature Patterns Across Months). Conversely, during the winter season, the temperature decreases and the load increases. This indicates a monthly seasonality pattern. Additionally, considering the amount of time people spend at home on weekdays versus weekends, it is logical to assume that there is a possibility of higher load on weekends compared to weekdays, suggesting day-of-week seasonality.

To represent this seasonality in the dataset, two encoding methods have been tried: one-hot encoding and ordinal encoding. In one-hot encoding, the monthly and day-of-week data are represented by columns, where the selected column has a value of one and the remaining columns have a value of zero. In ordinal encoding, the month and day-of-week are represented by numerical values within a specific range (e.g., 1 to 12 for months and 1 to 7 for days of the week).

By incorporating this seasonality into the dataset using different encoding methods, it is expected that the models will be able to capture and utilize this information to improve their performance.

4. DISCUSSION and RESULTS

The focus of this work was to evaluate different neural network-based time-series forecasting algorithms for heat load prediction. We compared the performance of well-known models such as RNN, LSTM, and GRU, which served as our baseline models. Additionally, we explored advanced models including DeepAR, Temporal Fusion Transformers, and NBeats.

To assess the performance of each model, we conducted experiments with various configurations and parameters. We investigated the impact of incorporating daily and monthly data to improve predictive accuracy. Hyperparameter tuning was also performed to identify the optimal model configuration. Our goal was to evaluate the effectiveness of state-of-the-art time-series models and compare them against the baseline models.

The Mean Absolute Error (MAE) was employed as the evaluation metric to assess the accuracy of the predictions. To evaluate the model performance, we compared the predicted heat load values for the last two months of 2016 with the actual values. This comparison allowed us to gauge the models' performance and determine the most effective approach for heat load prediction.

We initially experimented with three baseline models: RNN, LSTM, and GRU, using a common configuration. The RNN model had a hidden state size of 64 and a batch size of 16. We trained the model for 20 epochs without applying any dropout. The achieved MAE score for the RNN model was 0.0348. It is worth noting that the small MAE score was primarily due to the range of the predicted data being between 0 and 1, rather than solely reflecting the model's performance.

Next, we applied the same configuration to the LSTM and GRU models. The LSTM model achieved an MAE score of 0.0325, while the GRU model obtained an MAE score of 0.144.

Figure 6 and Figure 7 illustrate the predictions made by the LSTM and GRU models, respectively.

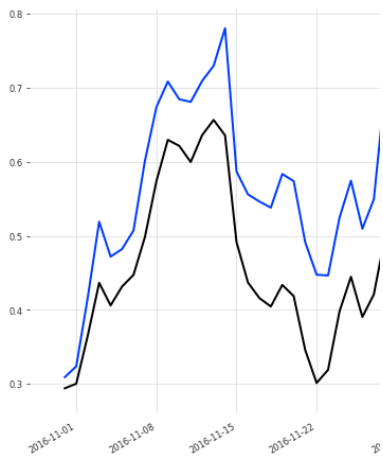

Figure 6 GRU Result

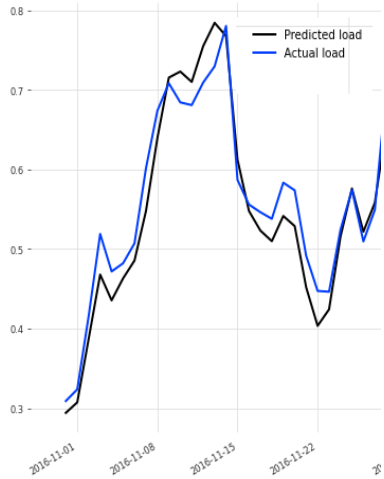

Figure 7 GRU Result Fine Tuned

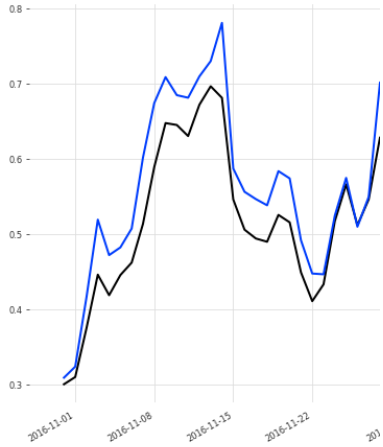

Figure 8 LSTM Result

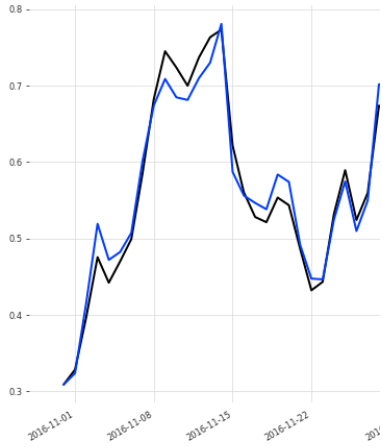

Figure 9 LSTM Result Fine Tuned

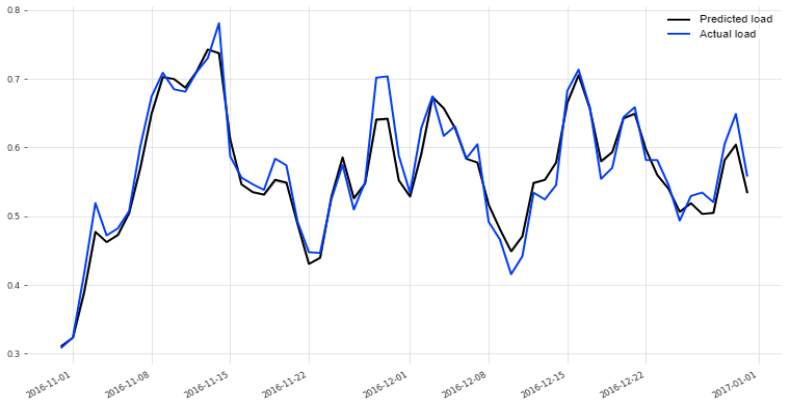

Figure 10 DeepAR Result

To improve the baseline models' performance, we explored two strategies: adding monthly data and conducting hyperparameter tuning. By incorporating monthly data and optimizing the hyperparameters, we observed significant improvements in the MAE scores.

For the RNN model, incorporating monthly data and conducting hyperparameter tuning resulted in an improved MAE score of 0.028. Similarly, for the LSTM model, the best performance was achieved when both monthly and day-of-week

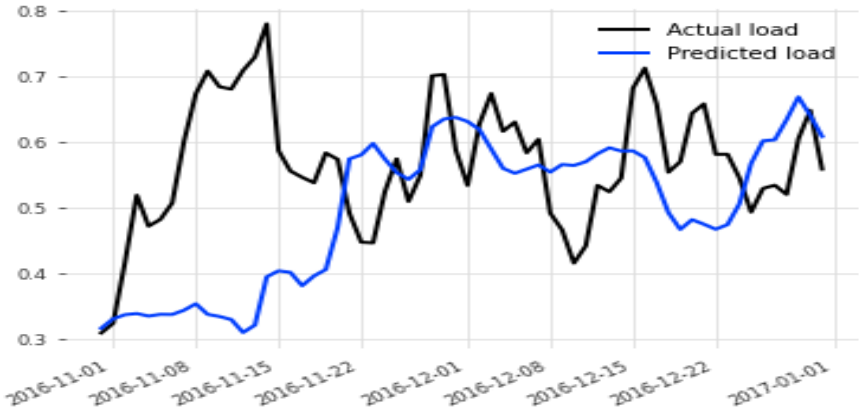

Figure 11 Prediction using NBeats

data were added, yielding an impressive MAE score of 0.021. In the case of the GRU model, incorporating monthly data during training led to a notable improvement, reducing the MAE score from 0.144 to 0.026.

Out of the three baseline models and their different configurations, the LSTM model with both monthly and day-of-week data exhibited the best performance, achieving an MAE score of 0.021. The prediction results of the best baseline model can be seen in Figure 9.

DeepAR is a powerful time series model that combines deep learning and autoregressive characteristics. With a two-layer architecture and a hidden dimension of 16, the initial DeepAR model achieved an MAE score of 0.0212. Through hyperparameter tuning and incorporating both monthly and day-of-week data, we improved the model's performance, reducing the MAE score to 0.018. The predictions made by the optimized DeepAR model are depicted in Figure 10.

NBeats is a deep learning architecture that utilizes a stacked ensemble of feed-forward networks interconnected through backcast and forecast links. Initially, when considering only the temperature as a feature, the NBeats model achieved an MAE score of 0.274 after training for 20 epochs. However, by incorporating the monthly data as an additional input, we observed a significant improvement in performance, reducing the MAE score to 0.124. The prediction generated by the optimized NBeats model can be seen in Figure 11.

Temporal Fusion Transformer (TFT) is a transformer-based time series forecasting model developed by Google. It represents an advancement over the DeepAR model. In our experiments, the TFT model with a single hidden layer and a hidden state size of 64 achieved an MAE score of 0.08525. However, after incorporating the monthly data as an additional input, we observed a slight improvement in performance, reducing the MAE score to 0.084. Figure 12 displays the predictions generated by the optimized TFT model.

In this experiment, we evaluated and compared various time series forecasting models including RNN, LSTM, GRU, DeepAR, NBeats, and TFT. The RNN-based models served as the baseline for comparison. Initially, predictions were made using only temperature as a feature. Subsequently, we enhanced the models by incorporating seasonal information such as month and day of the week data. Additionally, we performed hyperparameter tuning to optimize the models by adjusting parameters like layer size, hidden state size, and applying dropout.

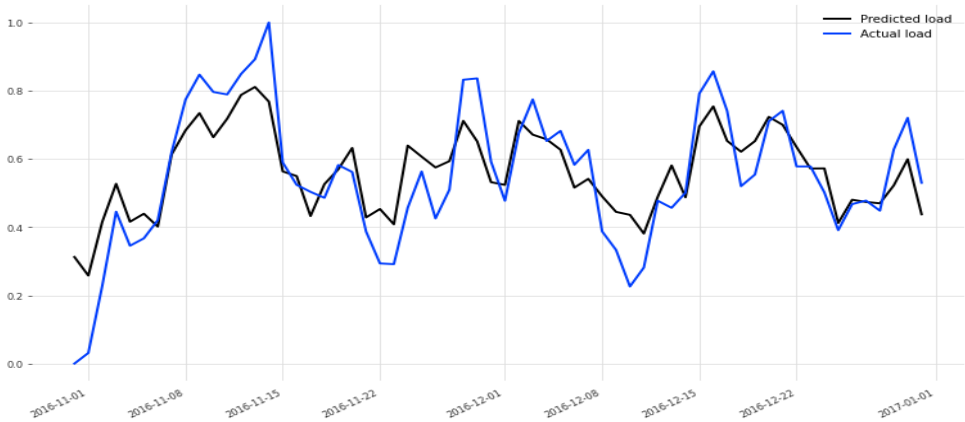

Figure 12 Prediction of TFT model

The best performing model in terms of Mean Absolute Error (MAE) was DeepAR with an MAE score of 0.018, followed closely by LSTM. The table below summarizes the MAE scores of the base models and the fine-tuned models for each

approach:

Model	Base Model Performance	Fine-Tuned Model Performance
RNN	0.0348	0.028
LSTM	0.032	0.021
GRU	0.144	0.026
NBeats	0.274	0.124
TFT	0.852	0.084
DeepAR	0.021	0.018

Based on our comparison study, DeepAR emerged as the best model for predicting the heat load. The fine-tuned models consistently outperformed their respective base models, demonstrating the importance of incorporating seasonal information and optimizing model parameters.

6. CONCLUSION

In conclusion, this research paper aimed to address the crucial task of heat load prediction in the context of building energy efficiency. With the buildings and construction sector being one of the largest energy consumers and contributors to carbon dioxide emissions, accurate heat load prediction becomes vital for improving energy efficiency and reducing environmental impact.

Throughout the study, we explored and compared several time series forecasting models, including RNN, LSTM, GRU, DeepAR, NBeats, and TFT. These models were evaluated based on their ability to predict the heat load given parameters such as time and temperature. The baseline models provided initial insights, and subsequent enhancements were made by incorporating seasonal information and performing hyperparameter tuning.

The findings of this research revealed notable improvements in model performance through the addition of seasonal data and fine-tuning. The DeepAR model emerged as the best-performing model, achieving an impressive Mean Absolute Error (MAE) score of 0.018. This model demonstrated its capability to accurately predict heat load, which is essential for optimizing the operation of district heating systems and improving overall energy efficiency.

The significance of incorporating seasonal information, such as monthly and day-of-week data, was evident in enhancing the predictive accuracy of the models. Furthermore, hyperparameter tuning played a crucial role in optimizing the models, allowing for adjustments in layer size, hidden state size, and other parameters to achieve better performance.

The results of this research highlight the potential of advanced time series forecasting models in accurately predicting heat load, thereby enabling more efficient and sustainable energy management in buildings. The application of these models can assist HVAC system operators, district heating systems, and building managers in making informed decisions related to heat supply and energy consumption.

As future work, further exploration can be done to evaluate the models on larger datasets and expand the scope to include other factors that influence heat load, such as weather conditions and occupancy patterns. Additionally, the integration of real-time data and the development of an automated system for heat load prediction could be valuable for proactive energy management in buildings.

The research findings hold significant importance for practitioners in the field of energy management and building operations. Accurate heat demand prediction using deep learning algorithms can lead to improved energy efficiency, cost savings, and sustainability. It empowers practitioners to optimize heating systems, reduce carbon emissions, make informed retrofitting decisions, enhance resource allocation, and improve overall operational effectiveness.

REFERENCES

[1] K. Naik and A. Ianakiev, "Heat demand prediction: A real-life data model vs simulated data model comparison," *Energy Reports*, vol. 7, pp. 380–388, Oct. 2021, doi: https://doi.org/10.1016/j.egyr.2021.08.093.
[2] S. Jones *et al.*, "A multi-energy system optimisation software for advanced process control using hypernetworks and a micro-service architecture," *Energy Reports*, vol. 7, pp. 167–175, Oct. 2021, doi: https://doi.org/10.1016/j.egyr.2021.08.159.
[3] K. Naik and A. Ianakiev, "Optimising Heat Consumption at Micro-Level Using User-Centric Data-Driven Model," *SSRN Electronic Journal*, 2022, doi: https://doi.org/10.2139/ssrn.4108849.
[4] G. Pinto, D. Deltetto, and A. Capozzoli, "Data-driven district energy management with surrogate models and deep reinforcement learning," *Applied Energy*, vol. 304, p. 117642, Dec. 2021, doi: https://doi.org/10.1016/j.apenergy.2021.117642.
[5] G. Xue, Y. Pan, T. Lin, J. Song, C. Qi, and Z. Wang, "District Heating Load Prediction Algorithm Based on Feature Fusion LSTM Model," *Energies*, vol. 12, no. 11, p. 2122, Jun. 2019, doi: https://doi.org/10.3390/en12112122.
[6] J. Runge and R. Zmeureanu, "A Review of Deep Learning Techniques for Forecasting Energy Use in Buildings," *Energies*, vol. 14, no. 3, p. 608, Jan. 2021, doi: https://doi.org/10.3390/en14030608.
[7] K. Svensson and F. Wernstedt, "Evaluation of a Machine Learning Approach To Heat Prediction," 2002. Available: https://www.diva-portal.org/smash/get/diva2:830045/FULLTEXT01.pdf
[8] M. Gong, Y. Zhao, J. Sun, C. Han, G. Sun, and B. Yan, "Load forecasting of district heating system based on informer," *Energy*, p. 124179, May 2022, doi: https://doi.org/10.1016/j.energy.2022.124179.
[9] M. Gong, Y. Bai, J. Qin, J. Wang, P. Yang, and S. Wang, "Gradient boosting machine for predicting return temperature of district heating system: A case study for residential buildings in Tianjin," *Journal of Building Engineering*, vol. 27, p. 100950, Jan. 2020, doi:

https://doi.org/10.1016/j.jobe.2019.100950.
[10] F. Dalipi, S. Yildirim Yayilgan, and A. Gebremedhin, "Data-Driven Machine-Learning Model in District Heating System for Heat Load Prediction: A Comparison Study," *Applied Computational Intelligence and Soft Computing*, vol. 2016, pp. 1–11, 2016, doi: https://doi.org/10.1155/2016/3403150.
[11] S. Wang and Z. Zhang, "Short-Term Multiple Load Forecasting Model of Regional Integrated Energy System Based on QWGRU-MTL," *Energies*, vol. 14, no. 20, p. 6555, Jan. 2021, doi: https://doi.org/10.3390/en14206555.
[12] D. Salinas, V. Flunkert, J. Gasthaus, and T. Januschowski, "DeepAR: Probabilistic forecasting with autoregressive recurrent networks," *International Journal of Forecasting*, vol. 36, no. 3, Oct. 2019, doi: https://doi.org/10.1016/j.ijforecast.2019.07.001.
[13] B. N. Oreshkin, D. Carpov, N. Chapados, and Y. Bengio, "N-BEATS: Neural basis expansion analysis for interpretable time series forecasting," *arXiv:1905.10437 [cs, stat]*, Feb. 2020, Available: https://arxiv.org/abs/1905.10437
[14] B. Lim, S. Ö. Arık, N. Loeff, and T. Pfister, "Temporal Fusion Transformers for interpretable multi-horizon time series forecasting," *International Journal of Forecasting*, vol. 37, no. 4, pp. 1748–1764, Oct. 2021, doi: https://doi.org/10.1016/j.ijforecast.2021.03.012.
[15] K. Cho *et al.*, "Learning Phrase Representations using RNN Encoder–Decoder for Statistical Machine Translation," *Proceedings of the 2014 Conference on Empirical Methods in Natural Language Processing (EMNLP)*, 2014, doi: https://doi.org/10.3115/v1/d14-1179.

The 18th International Symposium on District Heating and Cooling, September 3–6, 2023, Beijing, China

Realization of the large-scale smart district heating based on effective digitalization process

Xiaochen Yang[a*], Zhe Tian[a], Rui Zhao[b], Miao Sun[c], Wenze Guan[a], Dingzhou Liu[a]

[a] *Tianjin Key Laboratory of Built Environment and Energy Application, School of Environmental Science and Engineering, Tianjin University, Tianjin 300072, China*

[b] *Tianjin Thermal Power Company Limited, Tianjin, 300041, China*

[c] *Tianjin Energy IoT Technology Company Limited, Tianjin, 300450, China*

[*] *Corresponding author. xiaochen.yang@tju.edu.cn*

ABSTRACT

District heating(DH) is experiencing fast development in China with the expanding rate of 9% annually in the past 10 years. It has become the main heating method for the northern cities, while the worries of the huge energy consumption and CO2 emission force the current DH system to be upgraded towards smarter operated type. Concerning the very large scale of DH network in China in general, it can be labor intensive and costly to fully implement the digital facilities in the whole grid. Therefore, this study presents the optimal digitalization process of the case DH system with the complex layout and high heat density. We investigate the impacts of the amount and location of the smart meters on the control performances. Dynamic models of the case study are established by Modelica. Setting the indoor temperature as the control parameter, parametric analyses of the supplied heat, the supply temperature and the supply flowrate are conducted by varying the sampling time, the smart meter location in the thermal grid, and the selections of the indoor temperature as feedback signal. Moreover, in order to further simplify the installation of the indoor temperature sensors, a data-driven method to predict the indoor temperature is developed based on Multilayer Perceptron(MLP). By applying the control method to different heating cases, the system performances are compared, and the possible factors are characterized and discussed.

Keywords: Digitalization of district heating; Smart control technologies; Indoor temperature prediction; Smart meters

1. INTRODUCTION

The district heating industry in China is developed with high speed at present. During the past decade, the average expanding rate of the DH area is around 9% annually. In 2020, the heating area in northern cities of China has reached 15.6 billion m^2, along with an overall energy consumption of 214 million tons of standard coal equivalents (tce, where 1 tce= 29.307 GJ)[1]. Nowadays, transition from the fossil intensive type to the more sustainable type is promoted for the DH of China, so to achieve the goals of reaching carbon neutral in 2060[2].Consequently, the digitalization of the DH system also progresses concerning the huge scale and the complex layout of the Chinese DH network.

Since the concept of the 4th generation DH was launched[3], more and more attention has been put into the digitalization and automation of the old labor intensive DH system. The data collection and transmission play an important role in the system upgrading process. Some EU countries has made relevant standards that require the smart meters to be installed at the DH consumer side with the coverage no less than 27% by 2025[4]. So far, the district heating system in China is still under the process from the 3rd generation to the 4th generation. The overall digitalization degree still needs to be developed. Moreover, as most DH company is mainly owned by the state, the promotion of digitalized DH strongly depends on the local policy.

Another issue that hinders the fast development of the digitalized DH in China is the economy and complexity of implement the facilities that required by the modern data collection and control system. From a recent survey of 85 DH companies in China (the heating area of the 85 DH companies covers 35% of the overall heating area of China), the scale of the Chinese DH network can be as much as tens of billion m^2.

Table 1 Survey of 85 DH companies in China in 2019

no.	Bussiness scale (heating area)	Amount	Share[%]
1	>100 million m²	5	6%
2	50-100 million m²	12	14%
3	30-50 million m²	17	20%
4	10-30 million m²	33	39%
5	<10 million m²	18	21%

Therefore, it is hard to equip every end user with smart meters and local controller. How to establish effective management and control system with just necessary amount of the devices is of great value to be investigated.

In this study, we investigate the possible factors that would restrict the arrangement of the smart meters for the data collection and the system control. A case study model was built by Modelica. Parametric analyses were performed on the metering time step, the installation location in the network, and the selection of the appropriate consumer for the representative indoor temperature as feedback signal. Moreover, a data-driven method of the indoor temperature forecast was developed. The method was applied to improve the heating control for four case communities, and the energy saving performances in practice were demonstrated.

2. METHODOLOGY

2.1 Modelica model for the parametric analyses

In order to investigate the impact from different parameters of the data collection and processing on the DH digitalization, this study establishes a Modelica model for conducting the parametric analyses. The model include the primary side, the distribution network, and the residential multi-storey building as the demand side. The building and the heat supply are connected by the indirect form with the heat exchanger. The properties of the building envelope follow the standard of the "Thermal design code for civil building"[5] and "Design standard for energy efficiency of residential buildings in severe cold and cold zones"[6]. The reference design heat load is shown in Table 2:

Table 2 Heating parameters of the case study

Design outdoor T for heating [°C]	Heating duration [days]	Accumulated heat load [kW•h/(m^2•year)]	Total supplied heat [kW•h/(m^2•year)]
-9	125	30.4	37.5

According to the actual condition, the primary side and secondary side are indirectly connected. The supply/return temperatures of the primary and secondary sides are 95/70°C and 45/35°C respectively. The weather compensation is considered to regulate the primary side supply temperature. Correspondingly, the flowrate on the secondary side is adjusted according to the changes on the primary side.

Table 3 Adjustment of the DH flowrate on the secondary side

Outdoor temperature [°C]	-10~-5	-5~0	0~5	5~10
Flowrate (kg/h•m^2)	3.0	2.8	2.6	2.4

The baseline DH system is built by the Modelica language. The schematic diagram of the system is shown in the following figure.

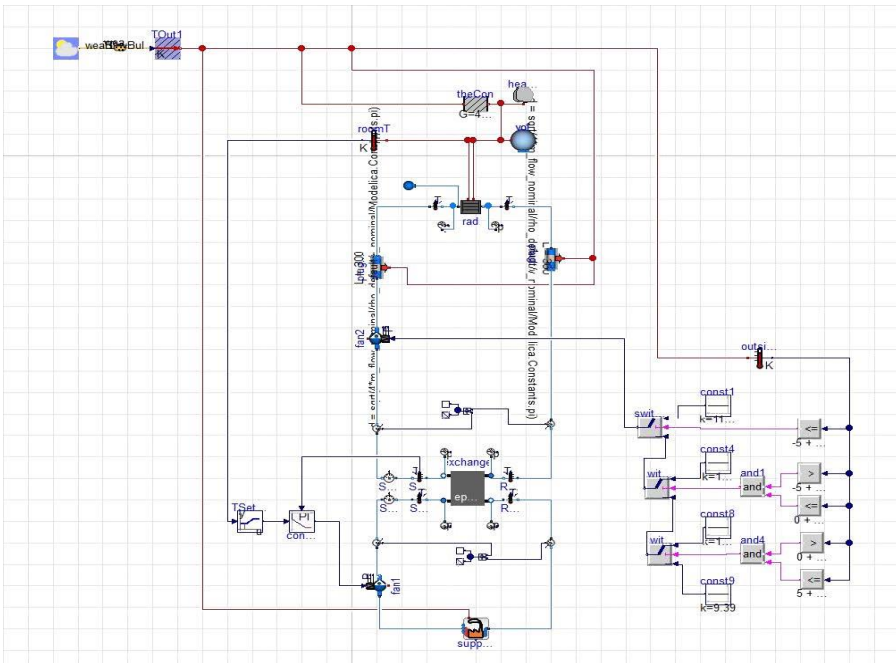

Figure 1 Modelica model of the baseline heating system

The parametric analyses such as the time step, the location of the sensors, can be conducted by changing the component properties and the simulation settings.

2.2 Parametric investigations of the data collection and processing of digitalized DH system

2.2.1 Impact of the time step

The time step of the smart meters is of great importance for the control of the digitalized DH system. The small enough time step is helpful to identify the fluctuation in the system, while too small time step might catch the meaningless oscillation and result in redundant computation cost. The investigation of the time-step impact has been carried out regarding the electric load calculation, and found that the maximal power rate measured with the time step of 10 min is 6 times as much as that with the time step of 1 hour, while the minimal power rate is half of that of the 1-hour time step measurement[7].

In terms of the large scale DH network, the mismatch between the time step of the data collection and the transportation time of the heating media is of great importance for the control precision. Therefore, we performed parametric simulations of the primary supply temperature and transient flowrate by seven time lengths, including 4 hours, 2 hours, 1 hour, 30 min, 15 min, 5 min, 2 min, so that to quantify the differences.

2.2.2 Impact of the sensor location in the network

For large scale DH network, it is hard to install the sensor to every heat consumer, therefore, in most cases, the sensor is equipped at the heating entrance. However, such arrangement might result in the deviation of the DH supply properties along the distribution line. The deviation can be significant if the end user is far from the heat entrance. In order to investigate the of the sensor location in the DH network, the distances of 100 m, 500 m, 1000 m, and 2000m are tested by the models. The flowrate of the supply water is assumed to 1 m/s concerning the general operation, the heat conductivity was assumed to 0.0387 W/(m·K), and the simulation time step was set to 30 min.

2.2.2 Impact of the temperature feedback

As an important element for the automatic control, the feedback signal from the consumer side needs to be implemented as the input to the controller. In general, the indoor temperature is most widely used the feedback variable. However, for large scale DH network, it is complicated and costly to install the temperature sensors in every end consumer side. Therefore, most DH companies use the representative demand side temperature for simplification. It means, several consumers on the special locations are selected as the representative consumer, and the mean value of their indoor temperatures is utilized as the feedback signal. Such strategy is feasible for the cases that the operation principal is to guarantee the minimal indoor temperature. For example, in China, the DH regulation requires the indoor temperature to be at least 18 °C. So the consumers at the most severe locations, such as the top floor, the bottom floor, and the corner, are usually selected as the critical consumer for estimating the representative temperature. However, such estimation cannot demonstrate the actual indoor temperature in all relevant consumers, and it is possible to result in over heating or insufficient heating. Thus, we investigate the impact from the different estimation of the representative temperature on the actual amount of heat supply. The corner consumer with three external envelopes (04) and the middle consumer with only one external envelope (02) are chosen for comparison. The indoor temperature measurements of the flat 04 and flat 02, as well as the weighted temperature are applied as the input to the DH model. The corresponding flowrates and overall supply heat are simulated and compared.

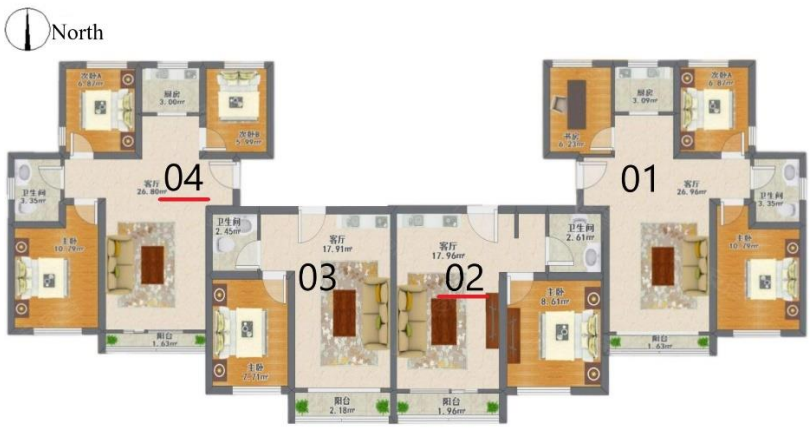

Figure 2 Floor plan of the measured case study

2.3 Estimation of indoor temperature with Multilayer Perceptron

Multilayer Perceptron (MLP) is one kind of artificial neural network (ANN), which can be used for forecast for different

purposes in the building energy field based on historical data. In order to minimize the installation of temperature sensors in the demand side and reduce the corresponding expenses, we investigate the possibility of estimating the indoor temperature by MLP with the measurements of the other parameters, such as the weather, the physical information of the building, the occupancy and etc. The architecture of the MLP estimation model for the indoor temperature is shown in Figure 3.

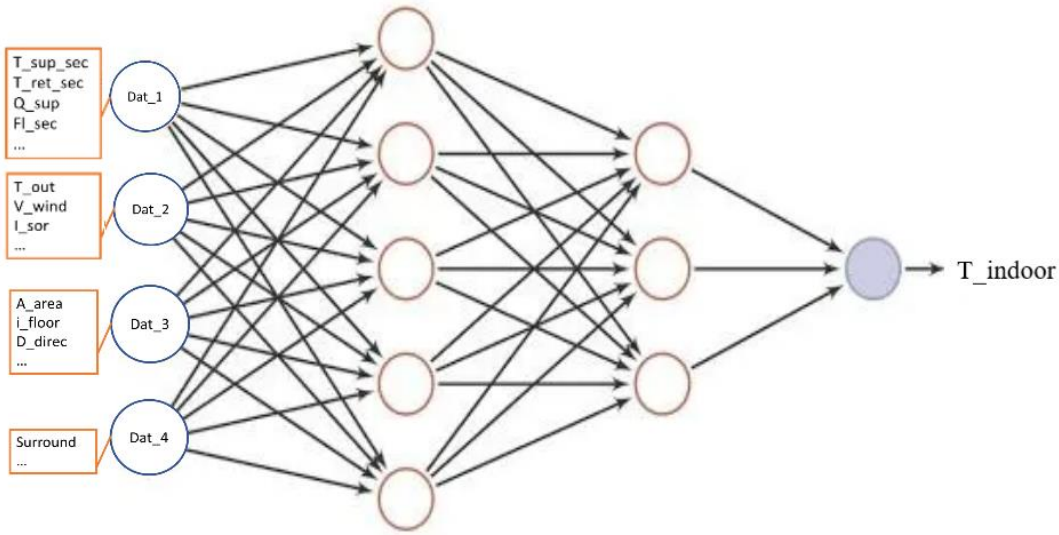

Figure 3 Architecture of the MLP model for the indoor temperature estimation

Four sets of input data are considered. Dat_1 represents the measured data from the primary side including the DH substation, such as the supply water temperature (T_sup_sec), the return water temperature (T_ret_sec), the supplied heat (Q_sup), the flowrate (Fl_sec). Dat_2 represents for the climate data, which plays an important role in the final heat consumption. Dat_2 includes the outdoor dry bulb temperature (T_out), the wind speed and direction (V_wind) and the solar radiation (I_sor). Dat_3 are basically physical information of the heated building, such as the heating area (A_area), the floor level (i_floor) and the orientation (D_direc). Dat_4 are the characteristic information of the heat consumer, such as the neighbors uses/ not uses heating.

3. RESULTS

3.1 Simulated system performances with different time step

The same case study model was repeated by only regulating the settings of the time step. The comparisons of the crucial parameters are shown in the following figures.

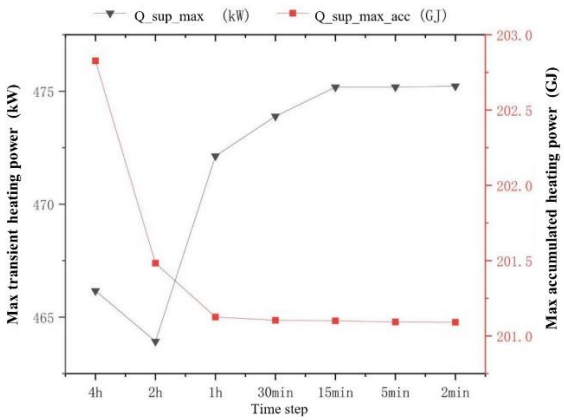

Figure 4a Maximal heat supply with different time steps

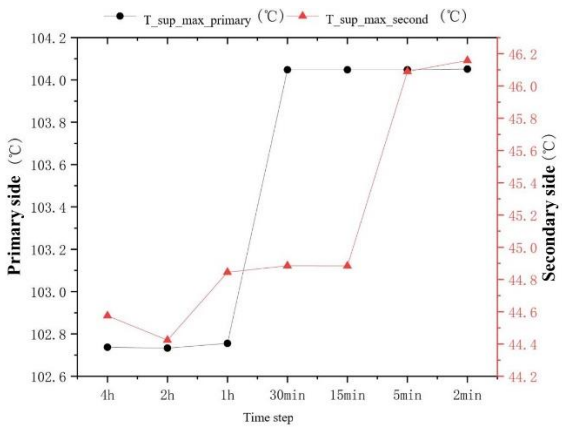

Figure 5b Maximal DH supply T with different time steps

It is significant that the finer time step can capture more variated features of the parameters. While the computation cost also surges with the shorter sampling period, it is important to find the trade off time step with sufficient accuracy and fast simulation speed. From Fig 4a, the two curves of the heating energy reach the elbow at the time step of 1 hour and 30 min. Afterwards, neither the transient heating power nor the accumulated heating energy change insignificantly. Similarly, in terms of the maximal supply temperature which is affected by the weather compensation and the heat demand, the simulated values with the time step greater than 1 hour are apparently smaller compared to those with shorter time steps. It is because

the transient maximal temperature is efficiently even out by the longer sampling duration, which sometimes results in dropout of the necessary feature and insufficient dimension of the heat supply facilities. Based on the comparison results, the optimal time step can be 1 hour or 30 minutes.

3.2 Comparison of different meter locations in the network

By simulating the meter located by the distances of 100m, 500m, 1000m and 2000m away from the heat distributor site (either directly from the heat plant or from the DH substation), the results of the simulated secondary side supply temperatures are shown in the following figure.

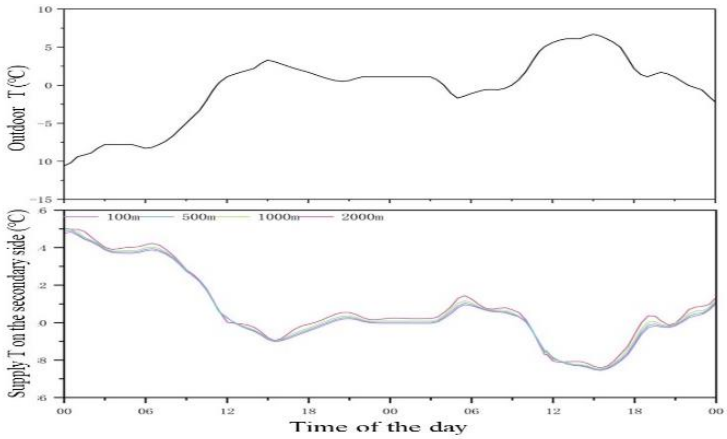

Figure 6 Supply temperature variations

Due to the weather compensation settings, the secondary supply temperature correlates to the outdoor temperature strongly. Along with the decrease of the outdoor temperature, the sensor located farthest from the heat distributor requires the highest temperature to maintain the same level indoor temperature. It means, when the scale of the heat demand side is large, the proper location of the feedback sensor in the network is important. Too close distance might result in insufficient heating for the rest of the heat consumers, while too far distance can result in overheating for the heat consumers before the sensor in the same distribution line.

3.3 Comparison of different meter locations for the representative room temperature

Long-term performance was performed in the case building. The weather data and the actual indoor temperature measurements of a whole heating season from 2020/11/1-2021/4/1 were used as the input to model. By varying the different indoor temperature measurements as the feedback to the heat supply, the corresponding heating consumption of the whole building was simulated. Consequently, the impact of using the representative temperatures by different locations can be characterized by comparing the total heat supplied and the operation temperatures. Figure 7 and Figure8 illustrate the results of using three different representative temperatures mentioned above as the feedback for control.

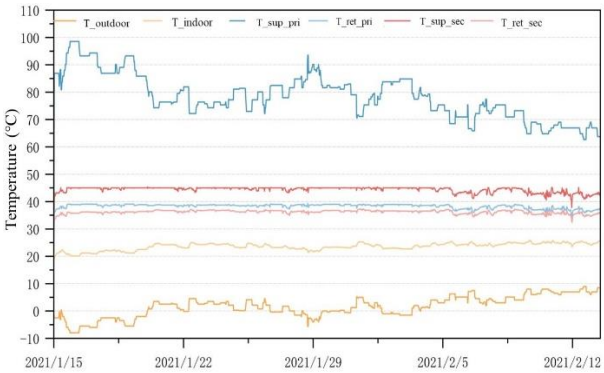

(a) Representative temperature from the corner consumer

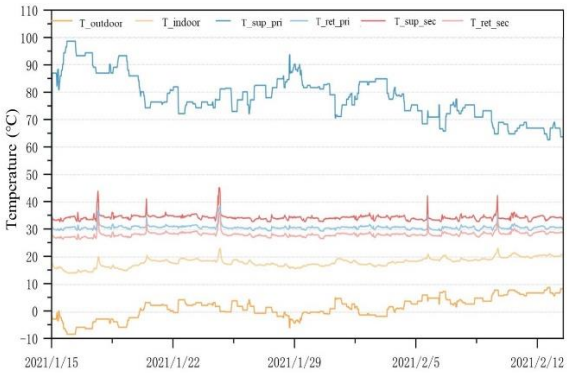

(b) Representative temperature from the middle consumer

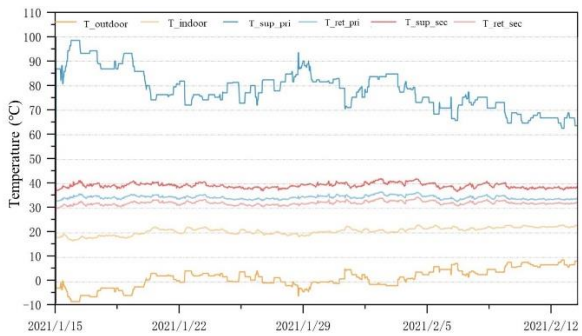

(c) Representative temperature of the weighted mean from the corner consumers and low-temperature consumers
Figure 7 Temperature levels using different representative temperature as feedback

In general, the thermostat maintains the indoor temperature above the setpoint by regulating the heat supply valve. The lower the feedback of the representative indoor temperature, the more heat is required to be supplied. From Figure 7, the required supply temperatures are higher than the other two scenarios. The reason is because the corner consumer theoretically requires more heat to maintain the same indoor temperature levels due to the more heat loss from the envelope. While for the scenario that uses the representative temperature from the middle consumer, the supply temperature levels are the lowest. However, the feedback from either the corner consumer or the middle consumer can result in overestimate or underestimate of the actual heat demand of other consumers who share the same distribution line. The effective weighted mean representative temperature is helpful to alleviate such deviation. As shown in Figure 7c, the DH supply temperature levels are between those of the side corner and middle corner, and are more stable. The comparisons of the energy consumptions of different scenarios are shown in

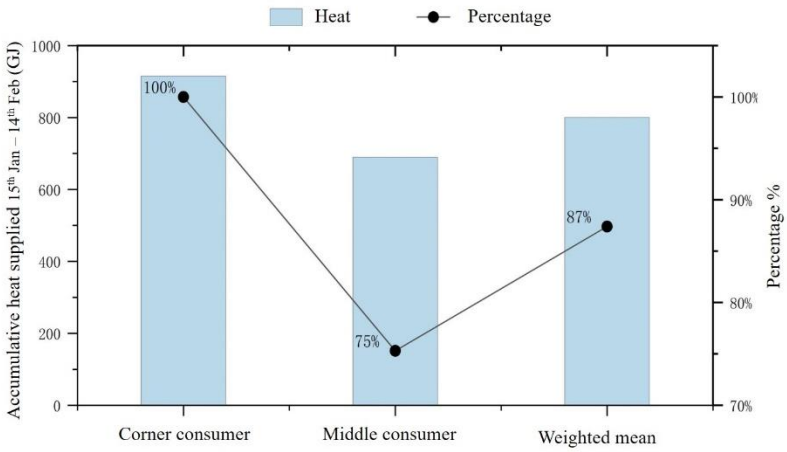

Figure 8 Energy consumptions using different representative temperature as feedback

Taking the corner consumer scenarios as the reference, the middle scenario consumes the least energy to maintain the same indoor temperature settings, which only accounts for 75% of the corner scenario. However, such operation is risky to induce insufficient heat supply to other consumers. While the weighted mean scenario reduces the 13% energy consumption compared to the corner consumer scenario, but the supply safety as well as the stability are guaranteed.

3.4 data-driven forecast of the indoor temperature and the system improvement

The MLP model was applied to predict the indoor temperature for one month period, which was from 2nd Feb 2022 to 2nd Apr. 2022. The results of the prediction is shown in Figure 9 together with the measurements. It can be seen that the two curves are close to each other.

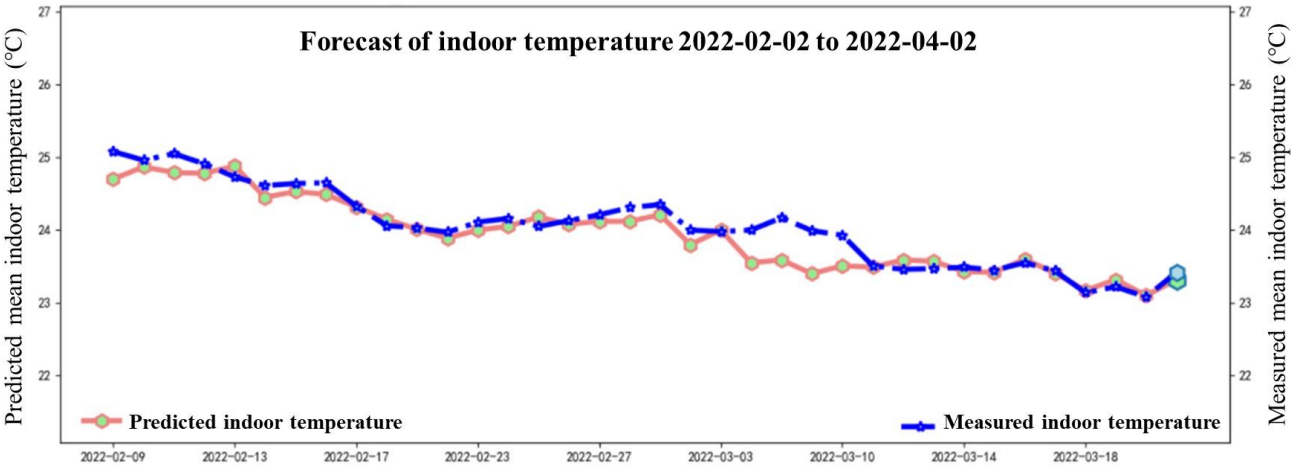

Figure 9 MLP prediction of the indoor temperature

From the error analysis in Table 4, the error between the prediction and the measurements are tiny. While the R^2 value is close to 1, which means the shape of the prediction curve is similar to the measured temperature curve. Therefore, it is reliable to use the predicted indoor temperature as the feedback signal for the control of the DH supply.

Table 4 Analyses of the MLP forecast of the indoor temperature

Model	MSE	RMSE	MAE	R^2
MLP model	0.62	0.79	0.50	0.88

We have applied the proposed indoor temperature forecast method to improve the DH supply in four case residential communities in Tianjin, the results are shown in the following table.

Table 5 Energy saving effect by using the indoor temperature forecast as feedback

Number	Period	Heating Area (10^4 m^2)	Energy Saving Ratio (%)
1	5th Mar-31st Mar	7.5	12.14%
2	5th Mar-31st Mar	7.8	19.18%
3	5th Mar-31st Mar	6.25	6.64%
4	25th Jan – 31st Mar	4.3	3.86%

The energy saving ratio by using the MLP indoor temperature forecast as feedback ranges from 3.86-19.18% during the test period, which proves the efficacy of the DH digitalization method. Case4 shows relatively less energy savings compared to the other cases. The reason is due to the large vacancy rate of the case building.

4. CONCLUSION

In this study, we investigate the possible factors that would affection the installation of the smart meters for the digitalization of large scale DH in China. A Modelica model of a case DH system was established for the parametric analyses. The main conclusion of the study can be drawn as follows:

1. Comparing 7 different lengths of time steps of the data acquisition, 30 minutes and 1hour are found to be sufficient to capture the significant behavior of the DH dynamics.
2. The locations of the heat meters in the network needs to be well planned, especially for the large scale network, otherwise overheating or underheating would occur.
3. Applying the representative indoor temperature from the corner consumer as the feedback signal to the DH supply would probably leads to overheating to other consumers that share the same distribution line, while representative indoor temperature from the middle consumer would leads to opposite results. Considering both the comfort and energy consumption, the weighted indoor temperature is recommended.
4. The MLP forecast of the indoor temperature can predict the indoor temperature with small error, and it helps to reduce up to 19.18% of the heating energy in the cases in Tianjin.

ACKNOWLEDGEMENT

This study obtained great support and inspiration from the IEA TS4 working group, we would like to thank them sincerely.

REFERENCES

[1] BERC (Building Energy Research Center Tsinghua University). Annual Report on the Development of Building Energy Saving in China 2022. Beijing China: 2022.
[2] Fu L, Li Y, Wu Y, Wang X, Jiang Y. Low carbon district heating in China in 2025- a district heating mode with low grade waste heat as heat source. Energy 2021;230:120765. https://doi.org/10.1016/j.energy.2021.120765.
[3] Lund H, Werner S, Wiltshire R, Svendsen S, Thorsen JE, Hvelplund F, et al. 4th Generation District Heating (4GDH). Integrating smart thermal grids into future sustainable energy systems. Energy 2014;68:1–11. https://doi.org/10.1016/j.energy.2014.02.089.
[4] EU(2012). Directive 2012/27/EU of the European Parliament and of the Council of 25 October 2012 on energy efficiency. Strasbourg: 2012.
[5] China Academy of Building Research. Thermal design code for civil building (GBT50176-2016) 2016.
[6] China Academy of Building Research. Design standard for energy efficiency of residential buildings in severe cold and cold zones (JGJ26-2018) 2018.
[7] Widén J, Wäckelgård E, Paatero J, Lund P. Impacts of different data averaging times on statistical analysis of distributed domestic photovoltaic systems. Sol Energy 2010;84:492–500. https://doi.org/10.1016/J.SOLENER.2010.01.011.

MODEL-BASED OPERATION OPTIMIZATION OF A GEOTHERMAL CASCADE UTILIZATION HEATING SYSTEM

Xinyuan Chen[a], Zhe Tian[a], Xiaochen Yang[a*], Yakai Lu[b]

[a] *Tianjin Key Laboratory of Built Environment and Energy Application, School of Environmental Science and Engineering, Tianjin University, Tianjin 300072, China*

[b] *School of Energy and Environmental Engineering, Hebei University of Technology, Tianjin, 300401, China*

[*] *Corresponding author. xiaochen.yang@tju.edu.cn*

ABSTRACT

80% of China's urban building heat demand is provided by the district heating systems. The rapid development of digital district heating in China has solved the problems of low heating efficiency and low user comfort to some extent. This paper analyzes and studies the operation control strategy of a digital geothermal cascade utilization heating system in Tianjin. The system is divided into high and low zones for heating, with the supply and return water temperatures of 70/50 ℃ and 45/35 ℃ respectively. The heating forms of users in high and low zones are radiators and radiant panels, which use the geothermal water for heating directly. In case of the insufficient heat supply, the users in low zones also use heat pump to heat up the geothermal water, with a three-way valve regulating the proportion of direct heating and indirect heating. This study built the digital simulation model of geothermal cascade utilization heating system by Modelica. The model is calibrated based on the collected power, flow, temperature and pressure data of each equipment from the case study. The combined optimal values of the geothermal water flow, the opening of the three-way valve, the outlet temperature and operating number of the heat pumps were optimized by Genopt, so to maximize the energy utilization efficiency of the cascade heating system. The results show that the optimized operation control strategy can save energy and improve the utilization rate of geothermal water compared with the original strategy.

Keywords: Geothermal energy, Cascade utilization, Operation strategy, Model simulation

1. INTRODUCTION

All activities in human society are inseparable from energy. Currently, building sector accounts for nearly 40% of the world's annual energy consumption and 40% of the total direct and indirect carbon dioxide emissions [1]. The increase in global greenhouse gas emissions has led to a series of environmental problems such as the climate change. Therefore, it is necessary to improve the energy efficiency in building energy supply system.

District heating supplies heat to large regions by one or more energy stations. Compared with decentralized heating, district heating can adopt some environment-friendly and efficient large-scale equipment. The heat source is centrally dispatched according to user demand and aggregate the low-grade heat that would be otherwise wasted, so to effectively improve the energy utilization. District heating systems has provided heat for 80% of urban buildings in China [2]. Despite the rapid development of China's heating industry, the overall efficiency of district heating systems is relatively low, which is reflected by unnecessarily wasting a large amount of energy to ensure indoor comfort [3]. With the development of science and technology, the emergence of digital district heating has played an important role in solving this problem. A grey-box model of end-users of large-scale district heating networks is developed, which is scale-free and suitable for district heating real-time control [4].

The geothermal cascade utilization heating system utilizes the heat of geothermal fluids by several stages to meet the temperature requirements of different heat exchange equipment, ensuring that the geothermal tail water temperature is within a reasonable range so as to avoid serious environmental pollution to the ground. Wu et al. [5] studied the performance impact of changing different parameters on geothermal cascade utilization heating systems, and conducted economic analysis and multi-objective optimization based on the TOPSIS decision-making method. Although geothermal cascade utilization systems can reduce carbon dioxide emissions and effectively reduce energy costs, the maximization of the systems' energy-saving potential can only be achieved by adopting appropriate operating strategies. In the existing research, Ref. [6] determines the water supply temperature from the perspective of ensuring users' thermal demand when analyzing the operation strategy of geothermal cascade utilization heating systems. The energy saving potential was not

completely reached since the impact of optimizing water supply temperature from the heat source side was not considered. To achieve the maximal energy-saving in geothermal cascade utilization heating systems, it is necessary to evaluate various operating strategies of the system with sufficient historical data, and finally characterize the optimal operating strategy. However, the data acquisition of actual engineering is difficult because of the lack of sufficient material and financial resources, and may be constrained by time and space. Therefore, the development of the accurate digital simulation systems is essential. The purpose of this study is to develop and establish a virtual digital simulation model based on the actual cascade geothermal heating system. Multi-scenario simulation is conducted, the system performances are analyzed and evaluated by different operating strategies, which is helpful to provide effective methodology of optimizing the operation strategies for practical engineering.

2. SYSTEM DESCRIPTION

This article selects the geothermal cascade utilization heating system (GCUHS) of a residential community in Tianjin as the reference case. The system layout is shown Figure 1, which includes the centralized energy station, heat exchange station and heat inlet. The heat exchange station is equipped with the plate heat exchangers for secondary heating. The total heating area supplied by the system is about 400000 square meters.

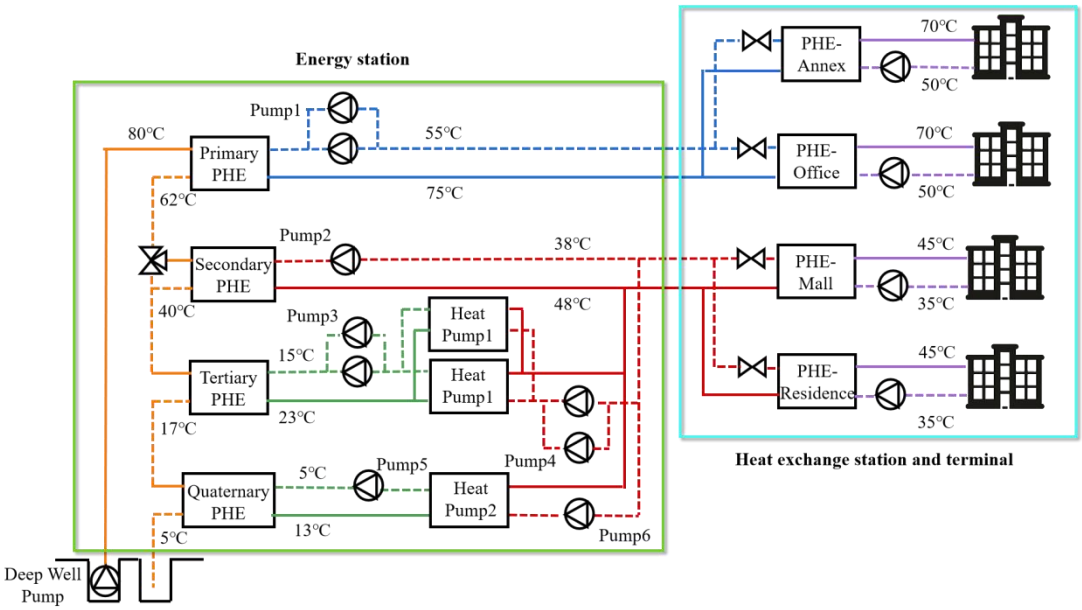

Figure 1. System flowchart of GCUHS

Table 1. The parameters of main equipment in the GCUHS.

	Heating capacity (kW)	Shaft power (kW)	Design flow rate (m^3/h)	Head (m)
Primary PHE	1500	/	/	/
Secondary PHE	3000	/	/	/
Tertiary PHE	2000	/	/	/
Quaternary PHE	2000	/	/	/
Heat Pump1	2200	400	/	/
Heat Pump2	2200	485	/	/
Deep Well Pump	/	150	120	130
Pump1	/	7.5	55	25
Pump2	/	37	290	35
Pump3	/	45	205	25
Pump4	/	37	200	35
Pump5	/	37	210	25
Pump6	/	30	220	35

The heat source of this system is the geothermal water with a temperature around 80 ℃. The cascade utilization of geothermal water is achieved through the series connection of four stage plate heat exchangers. According to the different water supply temperatures, it can be divided into high zones and low zones for heating. The high zones for heating include annexes and office buildings, with a designed supply and return water temperature of 70/50 ℃ and a designed heat load of 2450kW. The heating terminals of the users in high zones are radiators. The heat is supplied directly from the geothermal water through the primary plate heat exchanger. The low zones for heating include the commercial and residential buildings radiant heating from the radiation panels. The design supply and return water temperature is 45/35 ℃ and the design heat load is 8913kW. In case of the insufficient heat supply, the users in low zones also use the heat pump to heat up the geothermal water, with a three-way valve regulating the proportion of direct heating and indirect heating. The main equipment parameters of GCUHS are shown in Table 1.

3. METHODOLOGY

The purpose of this study is to establish a digital simulation model to simulate the operating states of thermal, hydraulic, and electrical parameters of the geothermal cascade utilization heating system under different operating conditions, so to find the optimal operating strategies to maximize energy savings. The overview of the entire research process is shown in Figure 2. The following sections are arranged according to the steps of this methodology.

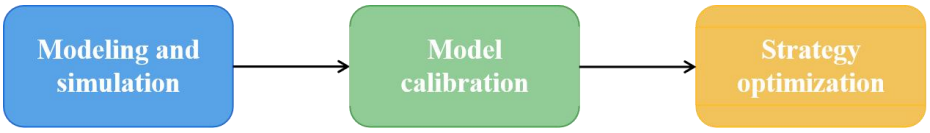

Figure 2. Outline of the workflow

3.1. Modeling and simulation

The digital simulation model of the geothermal cascade utilization heating system is constructed using the Modelica language of the Dymola platform. Modelica is a special language for describing physical systems. It adopts graphical object-oriented modeling, which can span different fields and disciplines and easily realize the unified modeling of complex systems. Modelica's modeling libraries are very large, including both the Standard Library for basic modeling and the Building Library specially developed for HVAC systems, which is convenient to use in modeling and simulation.

Hierarchical modeling is to decompose the modeling problems of multiple inputs and outputs into a series of modeling problems of single input and multiple outputs. The Dymola platform provides great convenience for hierarchical modeling. When the system structure is relatively complex, hierarchical modeling can make the model structure clearer, which is conducive to quickly identifying and resolving errors in the modeling process. Due to the existence of a large number of device models in the Building Library, the modeling process mainly starts from the device layer. The overall system construction plan is divided into three stages: the first stage is the selection and improvement of device models, and the control logic of the device layer is designed. The second stage is the connection of various devices in a single loop, as well as the design of loop layer control logic. The third stage is to construct a complete digital simulation model of the cascade geothermal heating system through the connection of various loops and the design of the overall control strategy, as shown in Figure 3.

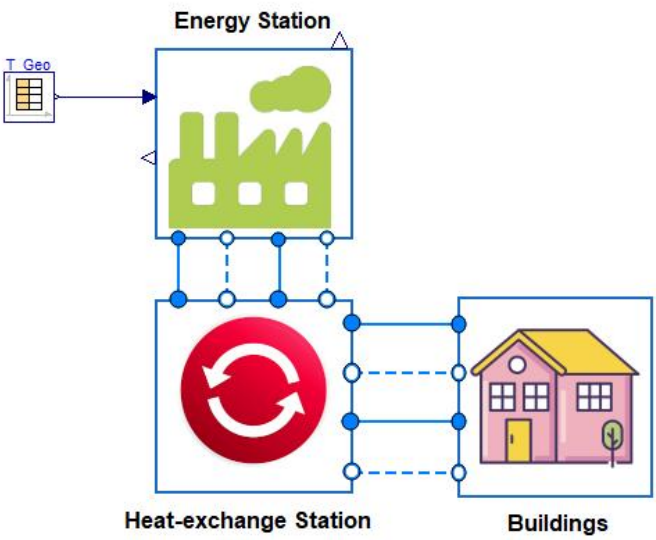

Figure 3. Top level diagram of Modelica model for GCUHS

3.2. Model calibration

The model calibration is the process of reducing model uncertainty by comparing the predicted output of the model under specific conditions with measured data under the same conditions. Due to the impact of changes in equipment performance during design, construction, and operation, if the parameters in the model are only defined based on the sample data of the equipment during modeling, there will be a significant deviation between the simulation results and the actual system operation results. Therefore, it is necessary to calibrate the simulation model through the actual operating data of the system to improve the accuracy of the simulation model.

In fact, calibration can be understood as an optimization process that continuously optimizes parameter values to calibrate the model. The calibration method adopts an optimization method based on the joint simulation of Dymola and Genopt. In the Genopt optimization program, a set of initial values of model parameters are customized, and the boundary of the simulation model is built using the measured data. The optimization algorithm continuously optimizes and inputs the optimized calibration values into the model for calculation until the difference between the measured and simulated values is minimized.

There are different stopping criteria for calibrating different objects in digital simulation models. In terms of energy consumption, the normalized mean bias error (NMBE) is used for evaluation:

$$NMBE = \frac{\sum_{i=1}^{n}(m_i - s_i)}{\sum_{i=1}^{n} m_i} \cdot 100\% \#(1)$$

Due to NMBE being a relative error indicator, errors may be offset when calculating temperature. Therefore, the root mean square error (RMSE) is used for evaluation in terms of temperature:

$$RMSE = \sqrt{\frac{\sum_{i=1}^{n}(m_i - s_i)^2}{n}} \#(2)$$

In addition, relying solely on error indicators is not sufficient to fully demonstrate the consistency between simulation results and actual results. It is also necessary to evaluate the similarity between the simulation result curve and the actual result curve through the square of the Pearson correlation coefficient (R^2):

$$R^2 = \left(\frac{\sum_{i=1}^{n}(m_i - \overline{m}) \cdot (s_i - \overline{s})}{\sqrt{\sum_{i=1}^{n}(m_i - \overline{m})^2 \cdot \sum_{i=1}^{n}(s_i - \overline{s})^2}} \right)^2 \#(3)$$

Where:
$\overline{m}$: the mean of measured values
$\overline{s}$: the mean of simulated values
m_i: the measured value
s_i: the simulated value
n: the number of data points

The recommended hourly level values for the above indicators are given in ASHRAE Guidelines 14[7], as shown in Table 2. When the calculated evaluation indicators are within the allowable range, it is considered that the model calibration work has been completed.

Table 2. Recommended error range for calibration errors

	Hourly criteria
NMBE	≤ ±10%
RMSE	≤ 1.5℃
R^2	≥ 75%

3.3. Strategy optimization

This study selected four variables as optimization variables: geothermal water flow rate, the opening of the three-way valve, the outlet temperature and operating number of the heat pumps. First of all, the flow rate of geothermal water not only affects the energy consumption of the deep well pump, but also affects the utilization rate of geothermal energy, so it is necessary to optimize the flow rate of geothermal water under different working conditions. Secondly, the opening of the three-way valve determines the distribution ratio of flow between secondary PHE and tertiary PHE, namely the ratio of direct heating by geothermal water and indirect heating by heat pumps, thereby affecting the energy consumption of the

geothermal cascade heating system. Finally, heat pumps are the main power equipment of the geothermal cascade heating system, responsible for the majority of the energy consumption of the entire system. Optimizing the outlet temperature and operating number of heat pumps under different operating conditions can maximize the energy-saving potential of the system.

For the geothermal cascade utilization heating system in this study, the main energy consumption comes from heat pumps and water pumps. The cumulative time-varying total power consumption can be expressed as:

$$P_{tot}(t) = \sum_{i=1}^{3} \left(P_{hp,i}(t) + P_{conp,i}(t) + P_{evap,i}(t)\right) + \sum_{j=1}^{3} P_{prip,j}(t) + \sum_{k=1}^{4} P_{secp,k}(t) + P_{dwp}(t) \#(4)$$

Where:
P_{tot}: Total power consumption (kW)
$P_{hp,i}$: Power of heat pump (kW)
$P_{conp,i}$: Power of condenser water pump (kW)
$P_{evap,i}$: Power of evaporator water pump (kW)
$P_{prip,j}$: Power of primary loop pump (kW)
$P_{secp,k}$: Power of secondary loop pump (kW)
P_{dwp}: Power of deep well pump (kW)
As mentioned earlier, the purpose of this study is to minimize the energy consumption of the geothermal cascade heating system. The objective function for this optimization problem is:

$$J = min\left(\int_{t_0}^{t_0+\Delta t} P_{tot}(t)dt + \mu \cdot max(0, \Delta\emptyset)^2\right)$$

$$= min\left(\int_{t_0}^{t_0+\Delta t} f\left(N_{hp}, N_{prip}, N_{secp}, T_{hpw,set}, T_{w,sup}, Q_{load}\right) dt + \mu\left(max\left(0, \int_{t_0}^{t_0+\Delta t} \left(T_{re} - T_{re,lim}\right) dt\right)\right)^2\right) \#(5)$$

Where:
μ: Penalty coefficient
$\Delta\emptyset$: Penalty function
N_{hp}: Operating number of heat pumps
N_{prip}: Operating number of primary pumps
N_{secp}: Operating number of secondary pumps
$T_{hpw,set}$: Outlet temperature set point of heat pumps (℃)
$T_{w,sup}$: Supply water temperature of terminals (℃)
Q_{load}: Heat load (kW)
T_{re}: Secondary loop returned water temperature (℃)
$T_{re,lim}$: Lower limit value of secondary loop returned water temperature (℃)
In this study, the thermal load is used as the boundary of the optimization. The static optimization method is used to optimize and calculate in the time section of a single working condition, obtaining the optimal set point value during this time period. Compared with dynamic optimization that considers the temporal changes of working conditions, static optimization is beneficial for reducing optimization time and difficulty. In addition, the thermal inertia of buildings ensures that using static optimization methods in a short period of time does not result in significant errors.
The implementation of the optimization framework involves calling Genopt and using the built-in GPS-PSO algorithm to find the optimal value of the optimization variables. Afterwards, the relationship between the optimization results and other variables are analyzed, so as to summarize rules for engineering embedding.

4. RESULTS

4.1. Calibration results

The electric power, flow rate, temperature and pressure data of each equipment during the heating season in 2022-2023 were collected in a 5-minute step. The data from January to February were selected for model calibration. The calibration results of some equipment is shown in Figure 4-6. Ideally, if the results of the simulation model can perfectly match the measured data, the resulting cloud of points cloud will form a 45° behavior line. As can be seen from Figure 4-6, the results of the calibration model are concentrated near the 45° line and show small dispersion. Therefore, the results indicate that the constructed digital simulation model can well reflect the actual behavior of the geothermal cascade utilization heating system.

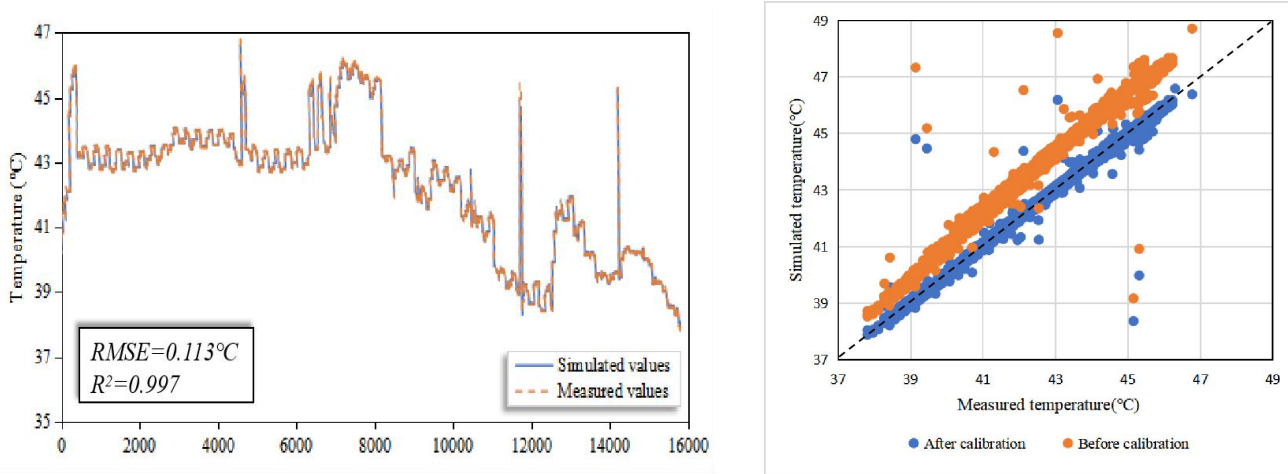

Figure 4. Results comparison for primary side outlet temperature of secondary PHE

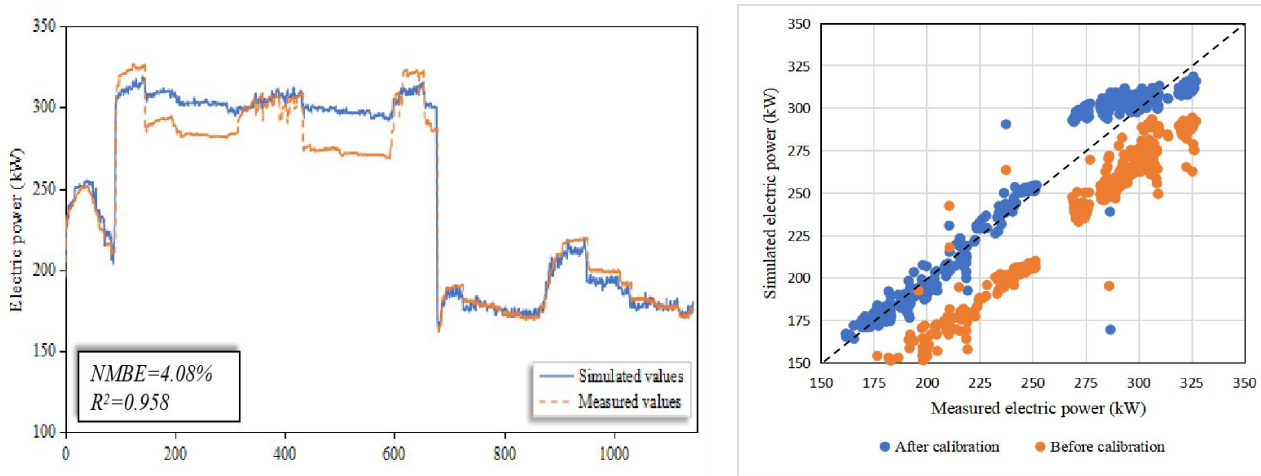

Figure 5. Results comparison for electric power of Heat Pump1

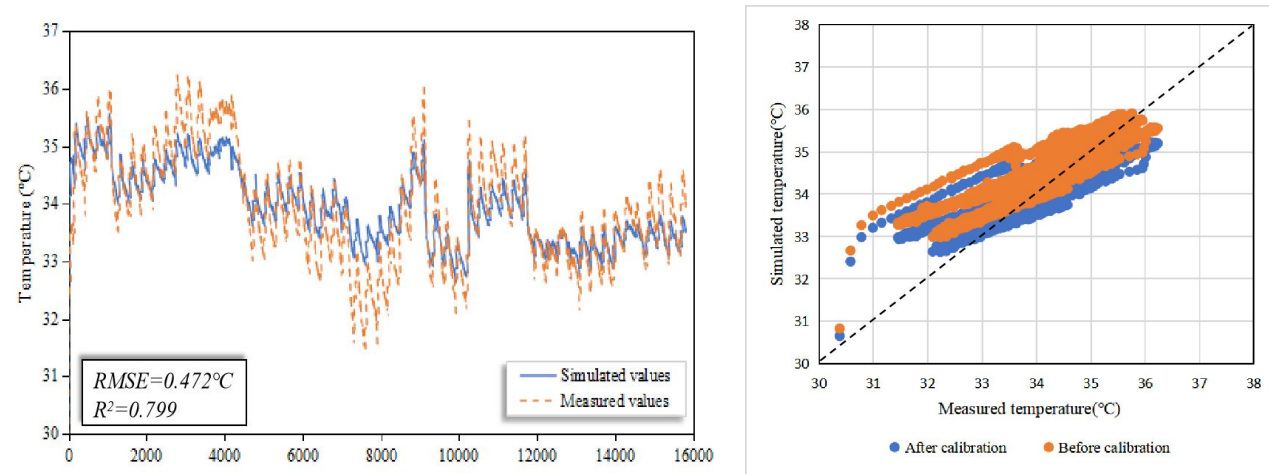

Figure 6. Results comparison for outlet temperature of terminals in high zones for heating

4.2. Optimization results

The calibrated model can be used for full operating condition simulation of the geothermal cascade utilization heating systems. This article optimizes the operating strategies for load rates of 25%, 50%, 75%, and 100% respectively. From Figure 7, it can be seen that the total energy consumption of the system after optimization is lower than that before optimization, with a maximum energy saving rate of 15% and an average energy saving rate of 7.14%. Taking the working condition at the load rate of 50% as an example to analyze the reasons of energy savings, where heat pumps account for 60% of the contribution to energy conservation. This is because only one heat pump is turned on before optimization, with the heat pump's partial load rate of 90%. After optimization, two heat pumps are turned on. Due to the same type of heat pumps, the partial load rate of each heat pump is 45%. As can be seen from Figure 8, heat pumps have better COP after

optimization, thus resulting in energy conservation.

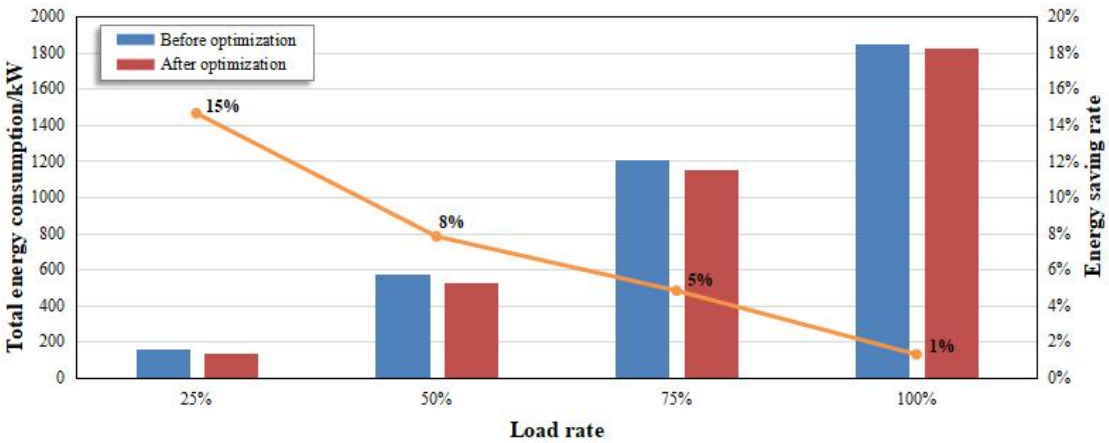

Figure 7. Comparison of energy consumption before and after optimization

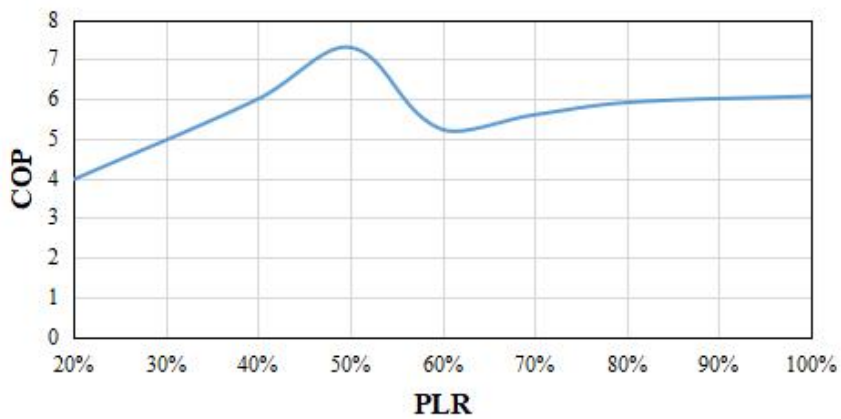

Figure 8. Heat pump coefficient of performance (COP) vs part load ratio (PLR) in the case study

In addition, the utilization efficiency of geothermal energy is used to evaluate the utilization effect of geothermal energy, which is defined as:

$$\varepsilon = \frac{t_g - t_h}{t_g - t_{h,d}} \#(6)$$

Where:
ε: Utilization efficiency of geothermal energy
t_g: Outlet temperature of geothermal water (℃)
t_h: Reinjection temperature of geothermal water (℃)
$t_{h,d}$: Design reinjection temperature of geothermal water (℃)

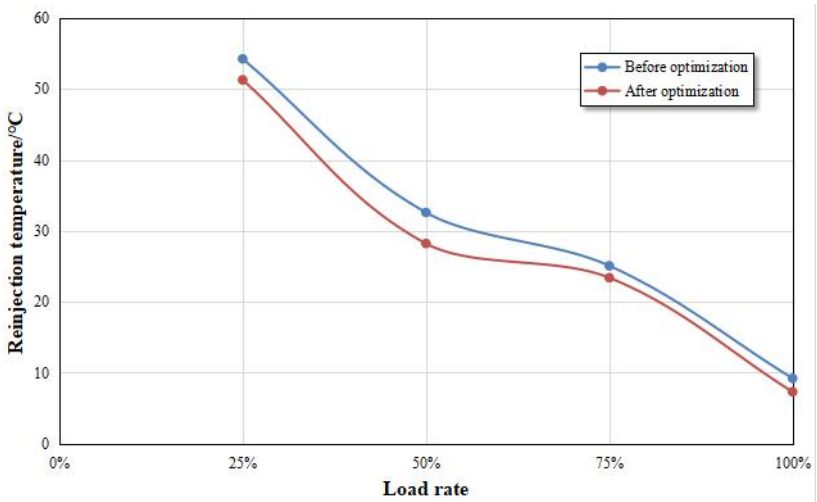

Figure 9. Comparison of reinjection temperature before and after optimization

After optimization, the average utilization efficiency of geothermal energy has increased from 66% to 70%.

5. CONCLUSION

This article takes a geothermal cascade utilization heating system in Tianjin as a case study, builds a digital simulation model and calibrates the model to conduct research on the optimization of operation strategies. The optimal set point values of geothermal water flow rate, the opening of the three-way valve, the outlet temperature and operating number of the heat pumps under different operating conditions constitute the optimal operation strategy of the system. Compared with the original strategy, the optimized operation strategy can save energy and improve the utilization efficiency of geothermal energy.

Some equipment is not able to perform calibration work due to the lack of actual operating data, which may have some deviation from the actual system. In future work, model calibration work can be further carried out by collecting more measured data.

ACKNOWLEDGEMENT

This work is supported by Tianjin key R&D projects "R&D and application of key technologies for the digital twin and efficient operation of green low-carbon building energy", (22YFZCSN00180).

REFERENCES

[1] Ala'raj, M.; Radi, M.; Abbod, M. F.; Majdalawieh, M.; Parodi, M. Data-driven based HVAC optimisation approaches: A Systematic Literature Review. Journal of Building Engineering. 2022, 46, 103678.

[2] Zhang, L.; Li, Y.; Zhang, H.; Xu, X.; Yang, Z.; Xu, W. A review of the potential of district heating system in Northern China. Applied Thermal Engineering. 2021, 188, 116605.

[3] Liu, L.; Zhang, H.; Liu, Y. A smart and transparent district heating mode based on industrial Internet of things. International Journal of Energy Research. 2021, 45(1), 824-840.

[4] Saletti, C.; Zimmerman, N.; Morini, M.; Kyprianidis, K.; Gambarotta, A. A control-oriented scalable model for demand side management in district heating aggregated communities. Applied Thermal Engineering. 2022, 201, 117681.

[5] Wu, Z.; Wang, Y.; You, S.; Zhang, H.; Zheng, X.; Guo, J.; Wei, S. Thermo-economic analysis of composite district heating substation with absorption heat pump. Applied thermal engineering. 2020, 166, 114659.

[6] Zheng, G.; Li, F.; Tian, Z.; Zhu, N.; Li, Q.; Zhu, H. Operation strategy analysis of a geothermal step utilization heating system. Energy. 2012, 44(1), 458-468.

[7] R.a.A.-C.E, ASHRAE Guideline. Measurement of Energy and Demand Savings, American Society of Heating, INC., 2002.

The 18th International Symposium on District Heating and Cooling, September 3–6, 2023, Beijing, China

RESEARCH ON THE BUILDING COMPLEX HEAT LOAD PREDICTION AND HISTORICAL-DATA DEPENDENCY BASED ON SUBSPACE IDENTIFICATION METHOD

Wei Jiang[a,b], Peng Wang[a,b*], Yaxiao Liu[a,b], Yifei Zhang[a,b*]

[a] *School of Architecture, Harbin Institute of Technology, 2651#, the 2nd Campus of Harbin Institute of Technology, 73 Huanghe Road, Nangang, Harbin, Heilongjiang 150090, China*

[b] *Key Laboratory of Cold Region Urban and Rural Human Settlement Environment Science and Technology, Ministry of Industry and Information Technology, Harbin, Heilongjiang, 150001, China*

[*] *Corresponding author. cahnburg@hit.edu.cn (P. Wang), 29598757@qq.com (Y. Zhang)*

ABSTRACT

Both the intelligent energy system defined by 4GDH and 5GDH, and the construction of smart cities proposed in China's 14th Five-Year Plan have demanded the transformation of traditional heat supply to intelligent and digital heat supply, and building heat load prediction is one of its basic functions. In this paper, the heat load of the building complex under the group substation is predicted by the subspace identification method, and the prediction results of the heat load and the average indoor temperature are verified using a group substation in a district of Harbin city as an example, and the dependence of the model on historical data in the short- term and medium-term prediction is discussed. The results show that the larger the training sample size the better the prediction results, but the improvement will be limited after the sample size reaches a certain scale; the difference between the MAPE (mean absolute percentage error) values of medium-term and short-term heat load prediction is 0.20%, and the difference between the RSME (root mean square error) values is 0.0401 MW, i.e., the length of the training period is less significant on the heat load prediction results; the optimal rolling periods for short-term and medium-term prediction in this case are 48–72h, 26–30d.

Keywords: Heating system, Heat load prediction, Group substation, State space model, Subspace identification

1. INTRODUCTION

With the development of renewable energy and intelligent management technology, Danish scholars Lund[1] et al. defined the concept of the 4GDH (4th generation district heating) system and proposed the intelligent energy system, and then the 5GDH (5th generation district heating) system continued the goal of the smart urban energy system[2]. In China's 14th Five-Year Plan, the construction of smart cities has been included in the important tasks and targets of national economic and social development, and the development requirements of improving energy utilization efficiency and realizing low-carbon heating and clean heating have been put forward for the heating industry, and the traditional heating has ushered in a critical period of transformation to smart digital heating. Heilongjiang Province, Hebei Province, and Beijing Municipality have successively introduced local construction standards for smart heating, which have gradually radiated to the whole country. In the process of digitalization of heat supply realization, building heat load prediction is one of the basic functions. Only with more accurate prediction of heat load in hourly, daily, and weekly cycles can the heating parameters be actively adjusted in various parts of the heating system to adapt to the changing patterns of heat load, thus realizing intelligent operation of the heating system.

Prediction models are mainly classified into white box models[3], black box models[4], and gray box models[5]. The white box model is a forward modeling method with a clear explanation of the load generation process[6], but due to the complexity of the load generation process, the large number of assumptions and idealization in the modeling process makes the model easy to mismatch with the actual situation[7]; the black box model is built without acquiring the physical characteristics of the system, and the model can be calibrated by historical data to obtain high prediction accuracy, but its disadvantage is also that it relies too much on historical data, and its ability to cope with abnormal operating conditions and generalization is poor[8]; while the gray box model combines the white box model with the black box model, which has the advantages of both, and can not only explain the process of load generation, but also correct the model through historical data[9].

At present, the gray box model has been widely used by domestic and foreign scholars to predict building heat load. For example, Ding[10], Wang[11], Berthou[12], and Bumelt[13] used the resistive capacity model (RC model) to establish a gray box prediction model for building heat load, which is also a common building heat load prediction model[14]. In addition, there are also studies on predicting building heat load using or improving the RC model. Wei[15] et al. proposed a two-step identification method based on the RC model with reasonable identification of the thermal characteristics of the building

with higher accuracy compared with the results of the conventional RC model. Cui[16] et al. used an improved RC model to predict the average temperature of each floor of a freestanding two-story house. The results obtained have acceptable accuracy. Lv[17] et al. modeled the thermal zone system using RC model and reduced the thermal zone energy consumption by 22% and improved indoor comfort by updating the model parameters weekly. Cholewa[18] et al. proposed a widely applicable and simple short-term thermal load prediction method based on the energy model of the building, which helps to reduce the building heating energy consumption. Asgari[19] et al. developed a gray box model by combining machine learning with physical processes to predict server temperature, which exhibited better performance compared to traditional zone temperature prediction models and advanced black box models based on nonlinear autoregressive exogenous models.Hu[20] et al. proposed an improved gray box room thermal model to study the demand response of residential air conditioning in Hong Kong potential, which can be integrated into a smart home energy management system to control energy consumption. Thilker[21] et al. proposed a nonlinear gray box model based on stochastic differential equations to accurately predict indoor air temperature, return water temperature, and heat load in a school building, which can serve to control indoor air temperature or provide flexibility. Based on the RC model, a state-space model is established through the physical structure to conveniently describe the multidimensional system. Based on the state-space description of linear invariant systems in modern automatic control theory, Jiang Y.[22] from Tsinghua University proposed to introduce the state-space approach into the simulation of dynamic thermal processes in buildings and established the dynamic thermal process model of buildings with the state space model as the core algorithm.

Identification and prediction with subspace identification method have been widely used in the field of control. This method does not require parameterization and is suitable for MIMO (multiple-input multiple-output) system identification, which has the advantages of good stability and robustness[23]. The common three-subspace identification methods are CVA (canonical variate analysis)[24], MOESP (multivariable output-error state space)[25] and N4SID (numerical algorithms for subspace state space system identification) [26], where CVA is established based on statistical theory and MOSEP and N4SID are proposed based on linear algebra and ensembles. Overschee and Moor[27] introduced the unification theorem and proposed that state sequences can be derived using orthogonal and oblique projections, and then using least squares method to find the system matrix. Some scholars applied the subspace discrimination method to predict the residuals of neural network models[28] and to identify the model parameters after reconfiguring the displacement[29], etc. In the field of heating, some scholars also used the subspace discrimination method to predict and verify the secondary network return water temperature of a heat station in Tianjin[30].

Research on building heat load prediction have shown that the state-space model is a favorable form to describe the multidimensional system of building thermal processes and is also the basic model that fits the subspace discrimination. Therefore, this paper establishes the research idea of estimating model parameters based on the state-space model of building thermal processes and using subspace discrimination methods to predict heat load. In addition, due to the high degree of residential agglomeration in China and the distribution conditions of the control equipment, the heating regulation is mostly performed at group substations, so this paper takes the building complex covered by group substation as the research object. The applicability of the method is discussed through the application in a group substation in Harbin city, error analysis of the prediction results and the dependence study of historical data.

2. METHOD

2.1. Framework

In this paper, the state space model describing the thermal process of the building is used as the base model, and the historical data of heat supply and indoor and outdoor temperature of the group substation are used to identify the parameters to be determined in the state space model by the N4SID subspace identification method, and the heat load prediction model of the building complex is formed based on the identified parameters, and research the training strategy and prediction duration, and the error analysis is performed to obtain the dependence of the heat load prediction results on the historical heat supply data. The research framework is shown in **Figure 1**.

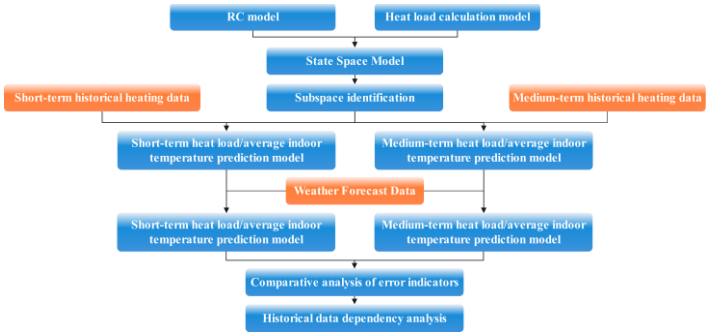

Figure 1. Research frame diagram

2.2. State Space Model

In view of the large number of buildings under the jurisdiction of the group substation, and the historical data from the parameters monitored in the group substation and a small number of indoor air temperature measurement points, the group of buildings under the jurisdiction of the group substation are considered as an equivalent building, and the state space model consisting of a single mass point is used to describe the thermal processes of the group of buildings, as follows:

$$I\frac{dt_{in}}{d\tau} = Q + W(t_{out} - t_{in}) \tag{1}$$

Where I is the heat capacity of the building complex, including the heat capacity of indoor air, envelope structure and household equipment, etc., J/K; t_{in} is the average indoor temperature of the building complex, °C; τ is time, s; Q is the heat supply per unit time of the building complex, W; t_{out} is the outdoor temperature, °C; W is the net heat loss per unit time of the building complex under the unit temperature difference between indoor and outdoor, including heat transfer from the envelope structure, heat consumption by cold air infiltration and heat gain from solar radiation, etc., W.

The equivalent building heat load is calculated based on the indoor-outdoor temperature difference, as follows:

$$H = h_s(t_{in} - t_{out}) \tag{2}$$

Where H is the heat load of buildings, W; h_s is the heat load of a building complex per temperature difference between indoor and outdoor, W/K.

Let t_{in} be the state variable $\mathbf{x}$, $[H_l\ t_{out}]^T$ be the input variable $\mathbf{u}$, H be the output variable $\mathbf{y}$, the above equations describing indoor temperature change and building heat load are written in the form of a state space model, as follows:

$$\begin{cases} \dot{\mathbf{x}} = \mathbf{A_0}\mathbf{x} + \mathbf{B_0}\mathbf{u} \\ \mathbf{y} = \mathbf{C_0}\mathbf{x} + \mathbf{D_0}\mathbf{u} \end{cases} \tag{3}$$

Where $\mathbf{A_0} = -\frac{W}{I}$, $\mathbf{B_0} = \begin{bmatrix} \frac{1}{I} & \frac{W}{I} \end{bmatrix}$, $\mathbf{C_0} = h_s$, $\mathbf{D_0} = \begin{bmatrix} 0 & -h_s \end{bmatrix}$ are coefficient matrix, where W, I as well as h_s can be obtained from the coefficient matrix above.

This model is a continuous state space model in a multiple-input single-output system, which needs to be discretized and then identified by a subspace identification method[27], so the above model is discretized using Euler's method to obtain the following equation:

$$\begin{cases} \mathbf{x}(k+1) = \mathbf{A}\mathbf{x}(k) + \mathbf{B}\mathbf{u}(k) \\ \mathbf{y}(k+1) = \mathbf{C}\mathbf{x}(k+1) + \mathbf{D}\mathbf{u}(k+1) \end{cases} \tag{4}$$

Where $\mathbf{A}=\mathbf{E}+T\mathbf{A_0}$, $\mathbf{B}=T\mathbf{B_0}$, $\mathbf{C}=\mathbf{C_0}$, $\mathbf{D}=\mathbf{D_0}$; T is the sampling period; E is the unit matrix; k is the current moment, $(k+1)$ is the predicted future moment; and the prediction duration $t = T$.

2.3. Subspace Identification Method

Different state variables can be transformed with non-singular linear transformations[32], and according to this property and the state space model (4), the historical time-series data of input $\mathbf{u}$ and output $\mathbf{y}$ are used as known quantities, including: heat supply per unit time of the building complex Q, outdoor temperature t_{out}, and heat load of the building complex H. the coefficient matrix characterizing the equivalent building thermal process and building heat transfer is identified in the following steps:

1) Reconstruct the state space model (4) based on the state space model (5), where the state variable $\mathbf{x}'$ is the identification state variable of the reconstructed model and the system output $\mathbf{y}'$ is the average indoor temperature and heat load of the building complex, i.e. $\mathbf{y}' = [\mathbf{x}\ \mathbf{y}]^T$, as follows:

$$\begin{cases} \mathbf{x}'(k+1) = \mathbf{A}_1\mathbf{x}'(k) + \mathbf{B}_1\mathbf{u}(k) \\ \mathbf{y}'(k+1) = \mathbf{C}_1\mathbf{x}'(k+1) + \mathbf{D}_1\mathbf{u}(k+1) \end{cases} \tag{5}$$

Where $\mathbf{A}_1$, $\mathbf{B}_1$, $\mathbf{C}_1$, $\mathbf{D}_1$ is the coefficient matrix of the new state space model (5).

2) The generalized observable matrix $\mathbf{\Gamma}_M$ and the lower triangular Toeplitz matrix $\mathbf{H}_M$[33] are constructed from the matrix coefficients $\mathbf{A}_1$, $\mathbf{B}_1$, $\mathbf{C}_1$, and $\mathbf{D}_1$, where the number of rows M of the matrix equation should be at least greater than the order of the system[27], and since equation (1) is a first-order differential equation, $M = 2$ is taken in this paper. the $M \times N$-

dimensional Hankel matrices $\mathbf{Y}_p$, $\mathbf{U}_p$, $\mathbf{Y}_f$, and $\mathbf{U}_f$ are constructed from the input $\mathbf{u}$ and output $\mathbf{y}$[33], where the parameter N can be determined according to the training sample capacity, $\mathbf{U}_p$ and $\mathbf{Y}_p$ are past inputs and outputs, and $\mathbf{U}_f$ and $\mathbf{Y}_f$ are future inputs and outputs.

$$\mathbf{Y}_f = \mathbf{\Gamma}_M \mathbf{X}_f + \mathbf{H}_M \mathbf{U}_f \tag{6}$$

3) Let $\mathbf{W}_p = \begin{bmatrix} \mathbf{U}_p & \mathbf{Y}_p \end{bmatrix}^T$, the LQ decomposition of $\mathbf{U}_p$, $\mathbf{Y}_p$, $\mathbf{U}_f$ and $\mathbf{Y}_f$ is as follows:

$$\begin{bmatrix} \mathbf{U}_f \\ \mathbf{W}_p \\ \mathbf{Y}_f \end{bmatrix} = \begin{bmatrix} \mathbf{R}_{11} & \mathbf{0} & \mathbf{0} \\ \mathbf{R}_{21} & \mathbf{R}_{22} & \mathbf{0} \\ \mathbf{R}_{31} & \mathbf{R}_{32} & \mathbf{R}_{33} \end{bmatrix} \begin{bmatrix} \mathbf{Q}_1^T \\ \mathbf{Q}_2^T \\ \mathbf{Q}_3^T \end{bmatrix} \tag{7}$$

According to Katayama's subspace system identification method[33], $\mathbf{R}_{33}$=0. Thus, from eq. (7), it follows that:

$$\mathbf{Y}_f = \mathbf{R}_{32}\mathbf{R}_{22}^{+}\mathbf{W}_p + (\mathbf{R}_{31} - \mathbf{R}_{32}\mathbf{R}_{22}^{+}\mathbf{R}_{21})\mathbf{R}_{11}^{-1}\mathbf{U}_f \tag{8}$$

where the superscript + is the Moore-Penrose generalized inverse of the matrix.

The formula for $\mathbf{X}_f$ is obtained by combining eqs. (6) and (8):

$$\mathbf{X}_f = \mathbf{\Gamma}_M^{+}\mathbf{R}_{32}\mathbf{R}_{22}^{+}\mathbf{W}_p \tag{9}$$

4) The SVD decomposition of $\mathbf{R}_{32}$[34] gives $\mathbf{R}_{32} = \mathbf{U}_1\mathbf{\Sigma}_1\mathbf{V}_1^T$, the derivation yields $\mathbf{\Gamma}_M = \mathbf{U}_1$. According to eq.(9), the calculation gives $\mathbf{X}_f = [\mathbf{x}(M) \ldots \mathbf{x}(M+N-1)]$. Let $\mathbf{X}_{f,M+1} = [\mathbf{x}(M+1) \ldots \mathbf{x}(M+N-2)]$, $\mathbf{U}_M = [\mathbf{u}(M) \ldots \mathbf{u}(M+N-2)]$, $\mathbf{X}_{f,M}$, $\mathbf{U}_{M+1}$, $\mathbf{Y}_{M+1}$ in the same way.Based on the state space model (4), it is written in the form of a matrix equation as follows:

$$\begin{cases} \mathbf{X}_{f,M+1} = \begin{bmatrix} \mathbf{A} & \mathbf{B} \end{bmatrix} \begin{bmatrix} \mathbf{X}_{f,M} \\ \mathbf{U}_M \end{bmatrix} \\ \mathbf{Y}_{M+1} = \begin{bmatrix} \mathbf{C} & -h_s \end{bmatrix} \begin{bmatrix} \mathbf{X}_{f,M+1} \\ \mathbf{U}_{2,M+1} \end{bmatrix} \end{cases} \tag{10}$$

Eq. (10) is then solved using the least squares method to obtain the coefficient matrix $\hat{\mathbf{A}}_1, \hat{\mathbf{B}}_1, \hat{\mathbf{C}}_1, \hat{\mathbf{D}}_1$ and the identified state variables $\mathbf{x}'$. The state variables $\mathbf{x}$ and $\mathbf{x}'$ in the state space models (4) and (5) can be transformed by a non-singular linear transformation to calculate the non-singular constant transformation matrix $\mathbf{P}$. That is:

$$\mathbf{x}' = \mathbf{P}\mathbf{x} \tag{11}$$

5) Substitute the non-singular constant transformation matrix P into the state space model (5) as follows:

$$\begin{cases} \mathbf{x}'(k+1) = \mathbf{P}\mathbf{x}(k+1) = \hat{\mathbf{A}}_1\mathbf{P}\mathbf{x}(k) + \hat{\mathbf{B}}_1\mathbf{u}(k) \\ \mathbf{y}'(k+1) = \begin{bmatrix} \mathbf{x}(k+1) \\ \mathbf{y}(k+1) \end{bmatrix} = \hat{\mathbf{C}}_1\mathbf{P}\mathbf{x}(k+1) + \hat{\mathbf{D}}_1\mathbf{u}(k+1) = \begin{bmatrix} \hat{\mathbf{C}}_{1,1}\mathbf{P} \\ \hat{\mathbf{C}}_{1,2}\mathbf{P} \end{bmatrix}\mathbf{x}(k+1) + \begin{bmatrix} \hat{\mathbf{D}}_{1,1} \\ \hat{\mathbf{D}}_{1,2} \end{bmatrix}\mathbf{u}(k+1) \end{cases} \tag{12}$$

Combine eq. (4) and (12) to obtain the coefficient matrix: $\hat{\mathbf{A}} = \mathbf{P}^{-1}\hat{\mathbf{A}}_1\mathbf{P}$, $\hat{\mathbf{B}} = \mathbf{P}^{-1}\hat{\mathbf{B}}_1$, $\hat{\mathbf{C}} = \hat{\mathbf{C}}_{1,2}\mathbf{P}$, $\hat{\mathbf{D}} = \hat{\mathbf{D}}_{1,2}$.

6) Substitute the coefficient matrix $\hat{\mathbf{A}}$, $\hat{\mathbf{B}}$, $\hat{\mathbf{C}}$, $\hat{\mathbf{D}}$ into eq. (4) to obtain the average indoor temperature and heat load prediction model for the building complex as follows:

$$\begin{cases} \text{State Equation:} \ \mathbf{x}(k+1) = \hat{\mathbf{A}}\mathbf{x}(k) + \hat{\mathbf{B}}\mathbf{u}(k) \\ \text{Output Equation:} \ \mathbf{y}(k+1) = \hat{\mathbf{C}}\mathbf{x}(k+1) + \hat{\mathbf{D}}\mathbf{u}(k+1) \end{cases} \tag{13}$$

Based on the current state variable $\mathbf{x}(2M+N-2)$ and the input $\mathbf{u}(2M+N-2)$, the average indoor temperature $\mathbf{x}(2M+N-1)$ for the next cycle is predicted by the state equation, and the heat load of the building complex $\mathbf{y}(2M+N-1)$ for the next cycle is predicted by the output equation. This cyclic iteration can obtain the average indoor temperature and heat load of the building complex for the next i cycles.

2.4. Historical Data Input Strategy

Since buildings are thermally inert, historical heat supply affects the current heat load, i.e., the building heat consumption

has a temporal genetic property. To investigate the dependence of heat load prediction on historical heat supply data, two training strategies, rolling training and accumulative training, are proposed in this paper.

The rolling training sample volumes are divided into different lengths to verify their effects on the heat load prediction results of building clusters. The prediction types are divided into two categories according to the prediction length: firstly, short-term prediction, with hourly scale, the training samples are divided into rolling 20h, 24h, 28h, 32h, 36h, 48h, 60h and 72h to predict the heat load for the next 1h, 6h, 12h, 18h and 24h; secondly, medium-term prediction with day scale, the training samples are divided into rolling 20d, 22d , 24d, 26d, 28d and 30d to predict the next 2-10d.Since the current heat load is not easily determined by the period of historical heat load and heating condition, accumulated training prediction is proposed, i.e., all the existing historical data are used as training samples to predict the heat load of the building complex. Taking the rolling training 20d and accumulation training prediction for the next 3d as an example, comparing the two prediction strategies is shown in **Figure 2**.

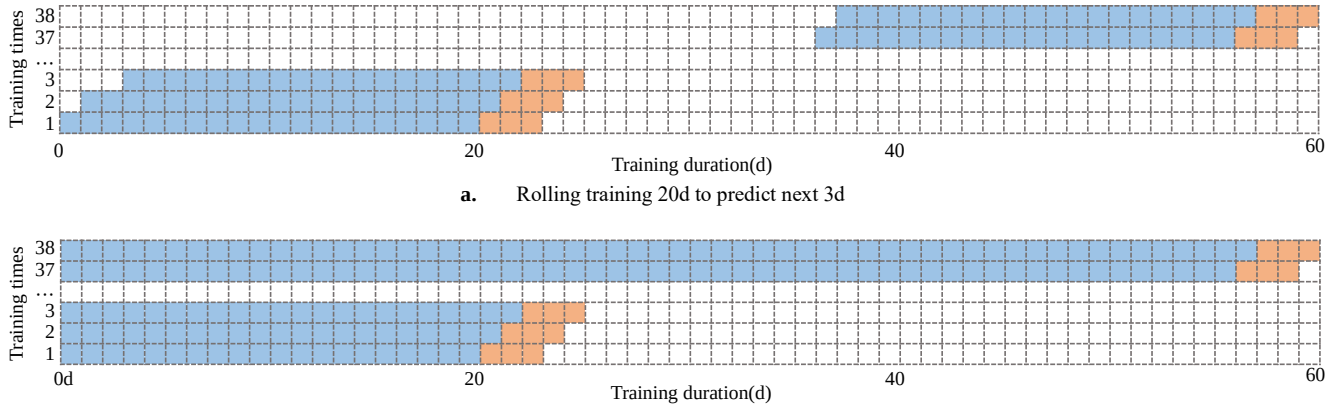

a. Rolling training 20d to predict next 3d

b. Accumulated training to predict next 3d

Figure 2. Example of historical data input strategy

3. CASE STUDY

3.1. Case Overview

The research object of this paper is a group substation in a residential area of Harbin city, and there are 18 heating buildings in the area of the group substation, with a construction area of about 259,200 m^2, and temperature measurement points are set in 52 households respectively, and the percentage of measurement points is 1.60%. The data collected in the experiment include heat supply of the group substation, indoor and outdoor air temperature of some rooms of the building. The sampling period is 1h, containing a total of 1488h of operational data from 00:00 on December 1, 2019 to 23:00 on January 31, 2020.

Abnormal data were generated due to the influence of data collection, transmission process and human factors[35], and the outliers were judged by using the criterion that the average value of two adjacent data sets was used to replace the outliers; for data missing up to 3h, polynomial fitting smoothing was used; for data missing more than 3h, they were directly rejected. The time series diagram of outdoor temperature and heat supply variation of the building complex is drawn as in **Figure 3**.

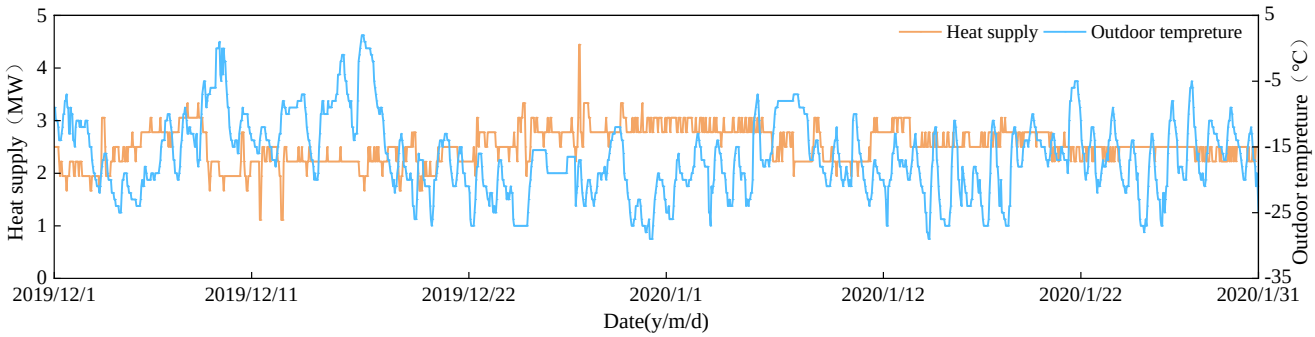

Figure 3. Timing diagram of heat supply and outdoor temperature change of building complex

The indoor air temperature of each measurement point is weighted and averaged by the area of the household to obtain the average indoor temperature:

$$\bar{t} = \frac{1}{\sum_{i=1}^{52} A_i} \sum_{i=1}^{52} (t_i \cdot A_i) \tag{14}$$

where $\bar{t}$ is the average indoor temperature, °C; t_i is the measured indoor air temperature of the i-th measurement point, °C; A_i is the floor area of the room where the i-th measurement point is set, m^2; i is the number of measurement points.

The following is the data after pre-processing, the light blue area consists of the measured values of all temperature measurement points, and the dark blue line is the calculated average indoor temperature at each moment, as in **Figure 4**.

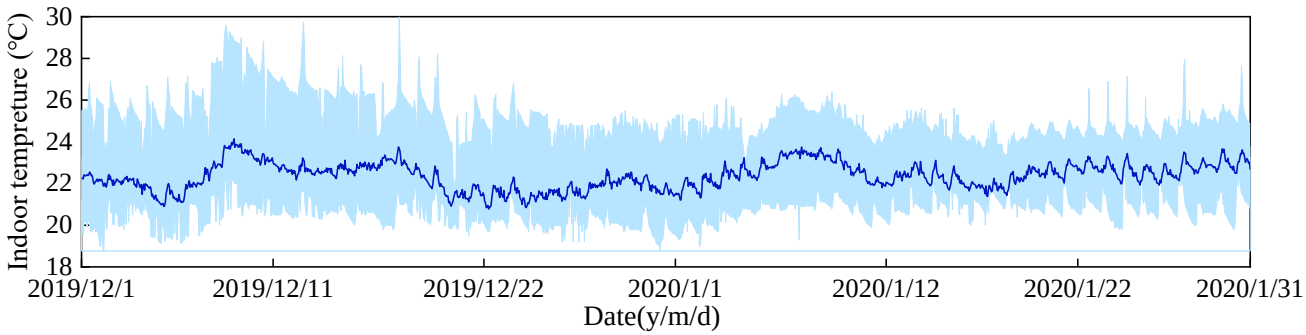

Figure 4. Timing diagram of indoor temperature change in the building complex

3.2. Evaluation Indicators for Prediction

In this research, two evaluation metrics commonly used in the prediction model are used to evaluate the prediction results, which are MAPE (mean absolute percentage error) and RMSE (root mean square error). The smaller the value of these two indicators, the better the prediction results of the model, as follows:

MAPE: a statistical indicator commonly used to measure predict accuracy, reflecting the average magnitude of predict error.

$$\text{MAPE} = \left(\frac{1}{n}\sum_{i=1}^{n}\frac{|\hat{y}_i - y_i|}{y_i}\right) \cdot 100\% \tag{15}$$

Where y_i is the actual processing values of heat load, MW; n is the number of predictions.

RMSE: consistent with the original data magnitude, reflecting the deviation of the predicted value from the true value.

$$\text{RMSE} = \sqrt{\frac{1}{n}\sum_{i=1}^{n}(\hat{y}_i - y_i)^2} \tag{16}$$

4. PREDICTION RESULTS AND ANALYSIS

4.1. Short-term and medium-term prediction results of heat load and indoor temperature

Combined with the historical data input strategy, the inputs are selected from a total of 1488h of operational data, and the state space model is used to identify different training data and predict the heat load and average indoor temperature of the building complex for different future durations. **Figure 5** shows the prediction results of rolling training 30d to predict the next 6d compared with the actual data:

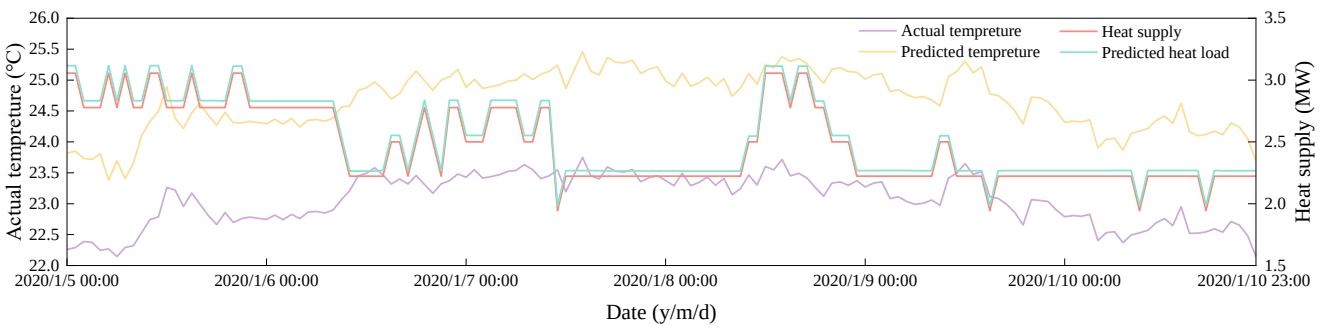

Figure 5. Prediction results of rolling training 30d for next 6d vs. actual data

4.2. Historical data dependency analysis

Based on the historical data input strategy shown in **Figure 2**, the subspace identification method was used to predict the

heat load at short-term and medium-term duration, and the MAPE and RSME results are shown in **Figure 6**.

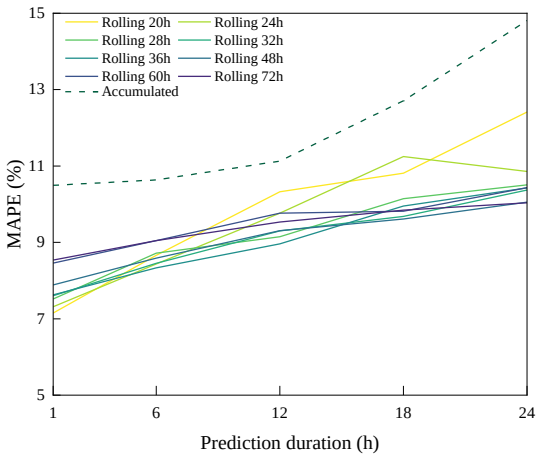

a. MAPE values of short-term building complex heat load prediction

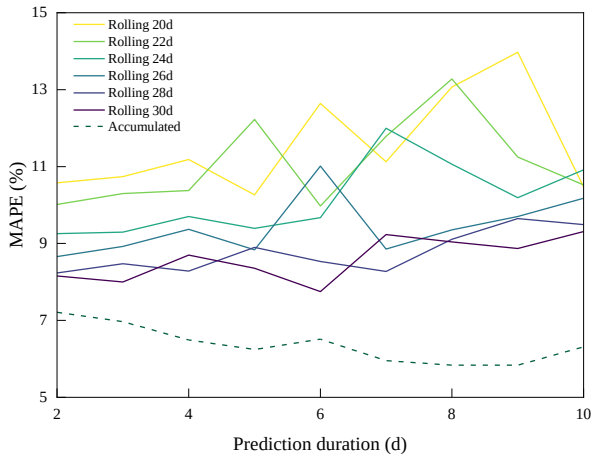

b. MAPE values of medium-term building complex heat load prediction

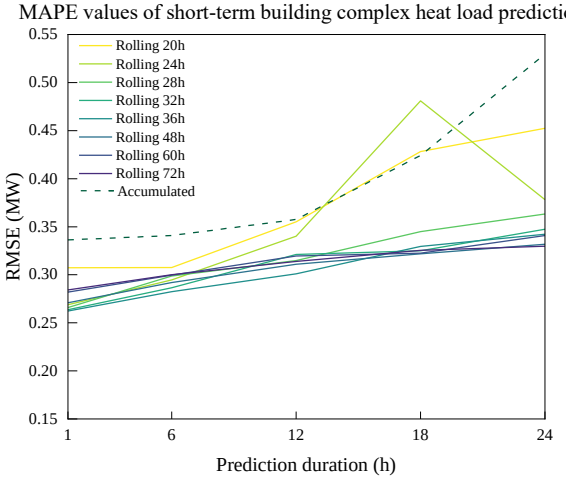

c. RMSE values of short-term building complex heat load prediction

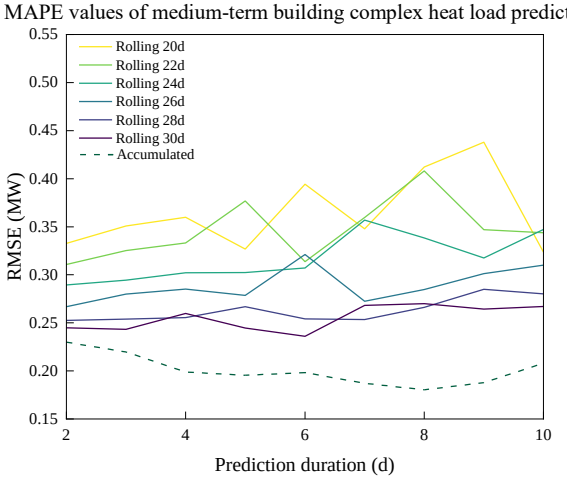

d. RMSE values of medium-term building complex heat load prediction

Figure 6. Short-term and medium-term building complex prediction heat load error

In the short-term heat load prediction, the rolling training 28–48h is better and less volatile, with MAPE difference range of 0.35–0.53% and RMSE difference range of 0.01–0.03MW. In the medium-term prediction, the accumulated prediction has the lowest error, with MAPE lowest to 5.83% and RMSE lowest to 0.18MW, and the stability is also better. Comparing the medium-term prediction with the short-term, the difference between the two is not significant, with a difference of 0.20% in MAPE value and 0.04MW in RSME value, i.e., in terms of the length of the prediction duration, the heat load prediction in this case is less dependent on the historical heating data.

While predicting the heat load of the building complex, its average indoor temperature can be predicted, and the evaluation index of temperature prediction under different training strategies is calculated, and the results obtained are shown in **Figure 7**, where the dashed lines indicate the error values generated when using the accumulated training strategy.

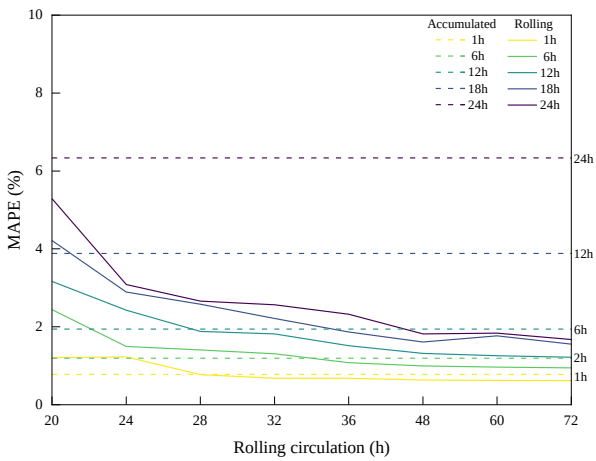

a. MAPE values of short-term average indoor temperature prediction

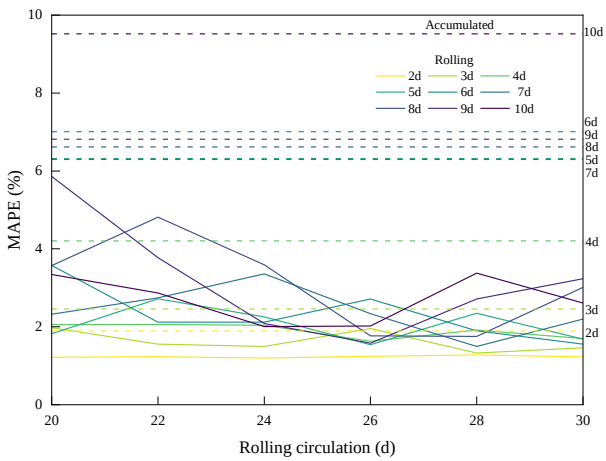

b. MAPE values of medium-term average indoor temperature prediction

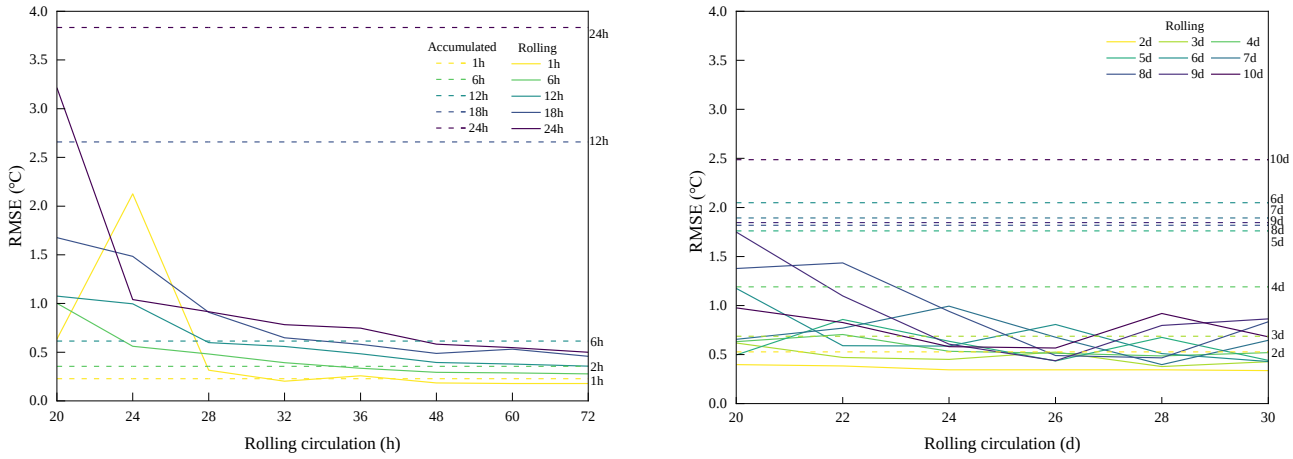

c. RMSE values of short-term average indoor temperature prediction d. RMSE values of medium-term average indoor temperature prediction

Figure 7. Short-term and medium-term average indoor temperature load error

When predicting short-term average indoor temperature, the prediction errors of rolling training 48–72 h were small and similar, with MAPE differences of 0.02–0.21% and RMSE differences of 0.01–0.09°C. The prediction error increased with the increase of prediction duration; the error of accumulated prediction increased rapidly when the prediction duration was longer than 12h.

The prediction results of each training sample fluctuated greatly in the medium-term prediction, and the prediction error became less stable with the increase of the prediction target length. When the prediction target length was 2d, the rolling effect prediction was the best, with MAPE values between 1.20–1.27% and RMSE values between 0.34–0.53°C; when the prediction length was 1–4d, the prediction result of rolling training 24–30d was close to the real data. The above data variation can be interpreted as the prediction results have their optimal dependence period on the historical data, and the data beyond this dependence period no longer play a positive role in the prediction result.

In summary, for this case, the optimal rolling circulation for short-term prediction is between 48–72h, and the optimal rolling circulation for medium-term prediction is between 26–30d, as shown in the following **Figure 8**.

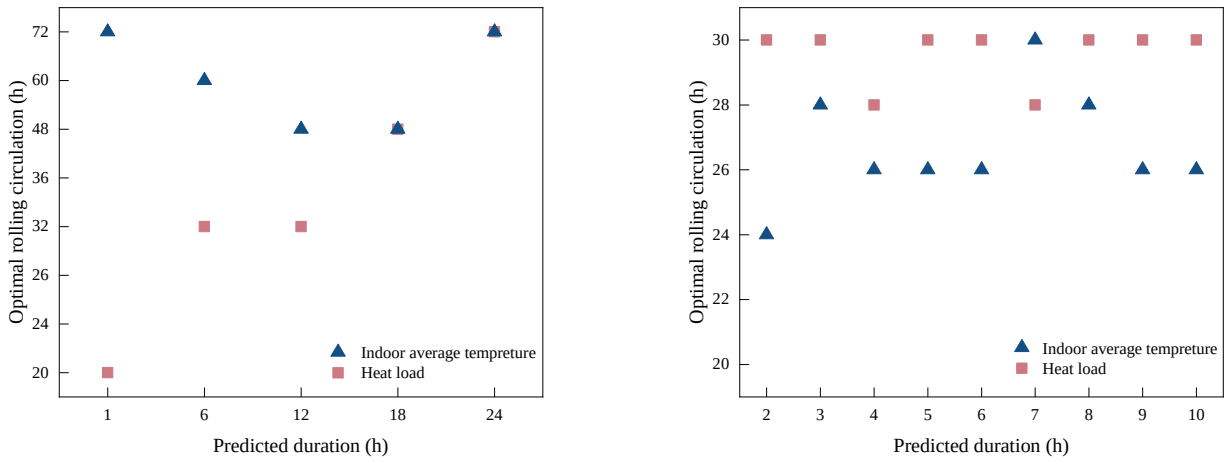

a. Short-term prediction optimal rolling circulation b. Medium-term prediction optimal rolling circulation

Figure 8. Optimal rolling circulation for different prediction targets in the short and medium term

5. CONCLUSION

In this paper, a subspace identification method based on the state space model of building thermal process is proposed to predict the heat load of the building complex under the group substation, and the heat load prediction results are verified by taking a group substation in a district of Harbin city as an example, and the dependence of the model on historical data in short- and medium-term prediction is discussed, and the following conclusions are obtained:

(1) In predicting the short-term heat load, the prediction result of rolling training 28–48h is better and not much different, with the difference range of MAPE 0.35–0.53% and RMSE 0.01–0.03MW. For the heat load prediction and heating regulation of the residential district in this case, the above errors are within the acceptable range;

(2) Short-term prediction has smoother error variation and more stable prediction results compared with medium-term prediction. When predicting indoor temperature, the minimum MAPE value of short-term prediction is 0.62%, which is only 30% of the minimum MAPE value of 2.00% of the medium-term prediction; when predicting heat load, although the results

of medium-term prediction fluctuate more, the medium-term prediction gets lower error values: the lowest MAPE is 5.83% and the lowest RMSE is 0.18MW.

(3) The prediction results are closest to the actual values when the rolling training strategy is used to predict the short-term average indoor temperature, with the best rolling period rolling at 48–72h, MAPE values between 0.02–0.21%, and RMSE values between 0.01–0.09°C. The cumulated training strategy is more suitable for heat load prediction for medium-term time lengths, with MAPE values between 5.83–7.21% and RMSE values between 0.18–0.23MW.

ACKNOWLEDGEMENT

This work was supported by the National Key R&D Program of China (No. 2021YFE0116100).

REFERENCES

[1] Lund H, Werner S, Wiltshire R, Svendsen S, Thorsen JE, Hvelplund F, et al. 4th eneration District Heating (4GDH): integrating smart thermal grids into future sustainable energy systems. Energy, 2014; 68: 1–11.
[2] Buffa S, Cozzini M, D'Antoni M, Baratieri M, Fedrizzi R. 5th generation district heating and cooling systems: A review of existing cases in Europe. Renewable and Sustainable Energy Reviews, 2019; 104: 504–522.
[3] Aparicio-Fernández C, Vivancos J L, Cosar-Jorda P, et al. Energy modelling and calibration of building simulations: A case study of a domestic building with natural ventilation[J]. Energies, 2019, 12(17): 3360.
[4] Wei Y, Zhang X, Shi Y, et al. A review of data-driven approaches for prediction and classification of building energy consumption[J]. Renewable and Sustainable Energy Reviews, 2018, 82: 1027–1047.
[5] Bacher P, Madsen H. Identifying suitable models for the heat dynamics of buildings[J]. Energy and buildings, 2011, 43(7): 1511–1522.
[6] Afram A, Janabi-Sharifi F. Theory and applications of HVAC control systems–A review of model predictive control (MPC)[J]. Building and Environment, 2014, 72: 343–355.
[7] Zhao H, Magoulès F. A review on the prediction of building energy consumption[J]. Renewable and Sustainable Energy Reviews, 2012, 16(6): 3586–3592.
[8] Abdul Afram, Farrokh Janabi-Sharifi. Black-box modeling of residential HVAC system and comparison of gray-box and black-box modeling methods[J]. Energy & Buildings, 2015, 94.
[9] Afroz Z, Shafiullah G M, Urmee T, et al. Modeling techniques used in building HVAC control systems: A review[J]. Renewable and sustainable energy reviews, 2018, 83: 64–84.
[10] Ding Y, Lyu Y, Lu S, et al. Load shifting potential assessment of building thermal storage performance for building design[J]. Energy, 2022, 243: 123036.
[11] Wang J, Jiang Y, Tang C Y, et al. Development and validation of a second-order thermal network model for residential buildings[J]. Applied Energy, 2022, 306: 118124.
[12] Berthou T, Stabat P, Salvazet R, et al. Development and validation of a gray box model to predict thermal behavior of occupied office buildings[J]. Energy and Buildings, 2014, 74: 91–100.
[13] Bumelt T , J Dostál. Distributed agent-based building grey-box model identification[J]. Control Engineering Practice, 2020, 101: 104427.
[14] Dimitriou V, Firth S K, Hassan T M, et al. The applicability of Lumped Parameter modelling in houses using in-situ measurements[J]. Energy and Buildings, 2020, 223: 110068.
[15] Wei, Z , Ren, F , Zhu, Y . Data-driven two-step identification of building thermal characteristics: A case study of office building[J]. Applied Energy, 2022, 326: 119949.
[16] Cui B, Fan C, Munk J, et al. A hybrid building thermal modeling approach for predicting temperatures in typical, detached, two-story houses[J]. Applied energy, 2019, 236: 101–116.
[17] Lv R, Yuan Z, Lei B, et al. Model predictive control with adaptive building model for heating using the hybrid air-conditioning system in a railway station[J]. Energies, 2021, 14(7): 1996.
[18] Cholewa T, Siuta-Olcha A, Smolarz A, et al. On the short term forecasting of heat power for heating of building[J]. Journal of Cleaner Production, 2021, 307: 127232.
[19] Asgari S, MirhoseiniNejad S M, Moazamigoodarzi H, et al. A gray-box model for real-time transient temperature predictions in data centers[J]. Applied Thermal Engineering, 2021, 185: 116319.
[20] Hu M, Xiao F, Wang L. Investigation of demand response potentials of residential air conditioners in smart grids using grey-box room thermal model[J]. Applied energy, 2017, 207: 324–335.
[21] Thilker C A, Bacher P, Bergsteinsson H G, et al. Non-linear grey-box modelling for heat dynamics of buildings[J]. Energy and Buildings, 2021, 252: 111457.
[22] Jiang Y. State space method for analysis of the thermal behavior of room and calculation of air conditioning load. ASHRAE Trans, 1981, 88: 122–132.
[23] Hachicha S, Kharrat M, Chaari A. N4SID and MOESP algorithms to highlight the ill-conditioning into subspace

identification[J]. International Journal of Automation and Computing, 2014, 11(1): 30–38.
[24] Larimore, W. E. Canonical variate analysis in identification, filtering, and adaptive control[C]. IEEE Conference on Decision & Control. IEEE, 1990: 596–604 vol.2.
[25] Verhaegen M, Dewilde P. Subspace model identification Part 1. The output-error state-space model identification class of algorithms[J]. International Journal of Control, 1992, 56(5): 1187–1210.
[26] Overschee P V, Moor B D. N4SID: Two subspace algorithms for the identification of combined deterministic-stochastic systems[C]. IEEE Conference on Decision & Control. IEEE, 1994. DOI:10.1109/CDC.1992.371682.
[27] Overschee P V, Moor B D. A unifying theorem for three subspace system identification algorithms[J]. Automatica, 1995, 31(12):1853–1864.
[28] Hassanpour H, Mhaskar P, Risbeck M J.A hybrid machine learning approach integrating recurrent neural networks with subspace identification for modelling HVAC systems. The Canadian Journal of Chemical Engineering 100. 12(2022). DOI: 10.1002.
[29] Guo X, Li C, Luo Z, Cao D. Modal Parameter Identification of Structures Using Reconstructed Displacements and Stochastic Subspace Identification[J]. Applied Sciences, 2021, 11(23). DOI: 10.3390.
[30] Lu G, Wang Y, You S. Study on dynamic modeling and system identification of district heating system[J]. District Heating, 2021, (01): 16–22.
[31] Huang C. A combined invariant-subspace and subspace identification method for continuous-time state–space models using slowly sampled multi-sine-wave data[J]. Automatica, 2022, 140:110261.
[32] Jiang W. Foundation of modern control theory[M]. Beijing: Chemical Industry Press, 2018.
[33] Katayama T. Subspace methods for system identification[M]. London: Springer, 2005:149–161.
[34] Verhaegen M, Dewilde P. Subspace model identification Part 1. The output-error state-space model identification class of algorithms[J]. International Journal of Control, 1992, 56(5):1187–1210.
[35] Yu X, Gu J, Qi C, et al. Comparison of several centralized heating load forecasting models[J]. HV&AC, 2019, 49(02): 96–99.

4GDH & 5GDHC

The 18th International Symposium on District Heating and Cooling,
September 3–6, 2023, Beijing, China

Numerical Analysis of Possible Heat Gains from the Soil for a Cold District Heating and Cooling Network in Germany

Kai Droste[a*], Rahul M Karuvingal[a], Thomas Schreiber[a], Dirk Müller[a]

[a]*Institute for Energy Efficient Buildings and inddoor Climate - RWTH Aachen University, Aachen, Germany*
[*] *Corresponding author. kai.droste@eonerc.rwth-aachen.de*

ABSTRACT

Fifth-generation District Heating and Cooling (5GDHC) networks use low-temperature energy sources like geothermal or industrial waste heat. These networks are characterized by low operation temperatures between -5 °C and 35 °C, allowing uninsulated pipes in the distribution network. Uninsulated pipes can use soil as an energy source, providing thermal gains by absorbing heat in winter or dissipating heat in summer. Within the buildings connected to the network, the heating demand is fulfilled by decentralized heat pumps, which utilize the available temperature for heating purposes. The district studied in this paper is part of Germany's first "Living Lab of the Energy Transition" project (TransUrban.NRW), which realizes four districts with low-temperature heating and cooling networks. The specified district consists of 36 single-family houses, which will be built with varying move-in times for residents. Therefore, it is conducted if the supply station can be built after the first residents have moved in. The results give valuable insides for projects with comparable scope. A Modelica model, utilizing the well-tested AixLib library, has been developed to evaluate the thermal performance of the connected 5GDHC network comprising the first three buildings in the district. This model enables the investigation of whether the thermal gains obtained by uninsulated pipes are sufficient to meet the heating and cooling demands. It simulates the temperatures of the glycol-water mixture inside the pipe, depending on the buildings' demand, the soil temperature, and the ambient temperature in a high resolution. Further, to evaluate the system's thermal performance, the ground temperature is considered via a variable in the calculations. The simulation results show that the minimum temperature of the 5GDHC pipes is about 0°C from April to November, sufficient to meet the heating demand, via the heat pumps, of the connected buildings without a supplementary heating supply. Therefore, supplementary heating sources may not be required for the district heating network during this period. In future work, we are planning to validate our simulations against real-world measurements from the considered district.

Keywords: 5GDHC networks; Simulation; Shallow Geothermal Energy

1. INTRODUCTION

To fulfill the climate goals of the EU [1] and reduce the carbon footprint of various sectors, including the buildings and construction sector, the utilization of district heating (DH) networks is crucial. This sector currently accounts for 34% of the total energy demand [2], with residential buildings alone consuming 21%[2]. These networks can make use of decentralized heat sources, such as geothermal heat or waste heat, to supply heat to connected buildings. To minimize losses in the DH network and enable the use of renewable energy sources, the fluid temperature is lowered. The latest generation, known as 5GDHC (5th generation of district heating and cooling), achieves the lowest temperatures ranging from -5 to 30 °C [3]–[5]. Furthermore, in order to make use of these low temperatures within buildings, water-water heat pumps are utilized to raise the temperature to the desired level.

The use of uninsulated pipes in 5GDHC networks enables heat gains and losses through the surrounding soil, utilizing them as shallow geothermal collectors. This approach can optimize the energy efficiency of the system and reduces reliance on fossil fuels. Studies have indicated that these low-temperature district heating and cooling networks with uninsulated PE pipes can achieve significant heat gains, with up to 50% obtained from the soil [6].

In this study, a simulation is conducted to analyze a section of a 5GDHC network with uninsulated Pipes. The objective is to validate whether the heat gains from the soil are sufficient to meet the heating and cooling demands of three interconnected buildings within the district.

The paper is organized as follows. Chapter 2 outlines the methodology employed for the simulation, starting with a description of the district under investigation. Additionally, the toolchain used to construct the simulation model is explained in more detail. In Chapter 3, the simulation results are presented and discussed, focusing on the visualization of pipe temperature variations throughout the year. Therefore, a potential use case scenario is demonstrated to provide practical insights. Finally, Chapter 4 provides a comprehensive conclusion based on the findings of this study, summarizing the key outcomes and implications.

By following this structure, the paper provides a comprehensive analysis of the simulation study, offering valuable insights into the performance and feasibility of utilizing uninsulated pipes in the 5GDHC network for meeting the heating and cooling demands of the interconnected buildings.

Furthermore, by adopting 5GDHC networks and incorporating decentralized heat sources, the building sector, especially residential buildings, can make substantial progress in reducing their carbon footprint and dependence on fossil fuels. These innovative systems offer a sustainable and efficient solution for heating and cooling, contributing to the overall climate goals of the EU.

2. METHODOLOGY

2.1. The investigated District

This study is conducted within the framework of the research project TransUrban.NRW[1], which aims to implement low-temperature heating and cooling networks in former coal mining regions in Germany. The project encompasses the development of four districts, each with distinct characteristics such as pipe temperatures, insulation, building types, and heating/cooling sources.

For the purpose of this study, the focus is on the district "Wohnen am Stadteilpark." This district consists of various building types, including single-family houses, multi-family houses, and non-residential buildings. The district comprises a total of 36 buildings, with the first construction phase primarily involving single-family houses, which are specifically examined in this study. These buildings are constructed according to the latest KFW 40 insulation standard and are located in an area with a climate typical of Germany.

The DH network within "Wohnen am Stadteilpark" operates at temperatures ranging from -2 °C to 15 °C. To accommodate the lower temperatures, a glycol-water mixture is used. The pipes in the network are uninsulated, taking advantage of the proximity to ambient temperature and enabling heat gains or losses from the surrounding soil. Additionally, the pipes serve as horizontal geothermal collectors.

Given the varying building types and staggered move-in times, this study investigates whether the heating and cooling demands of the district's diverse buildings, including single-family houses, multi-family houses, and non-residential buildings, can be adequately fulfilled using the network as a horizontal collector. To simulate this scenario, the heating and cooling equipment in the energy hub (EH) is disabled, allowing for a direct connection between the warm and cold pipes.

2.2. Overall Workflow

To analyze the connectivity of the three investigated buildings through the District Heating and Cooling (DHC)-Network, a toolchain has been presented in earlier work **[7]** and is used in this study. This toolchain is specifically designed for modeling, simulating, and designing DHC-Networks and their supply and substations.

For the district modeling and simulation, the modeling language Modelica is employed. Modelica offers an object-oriented construct that facilitates model reuse. Additionally, Modelica enables dynamic simulation of heat transfer and mass flow for buildings and pipes. Furthermore, the employed toolchain seamlessly integrates with modules and packages from Modelica.

[1] https://www.reallabor-transurban-nrw.de/

The first step is creating a district layout using QGIS, an OpenStreetMap (osm) based geoinformation system (GIS) editor. The district layout included the network layout, pipe length and diameter, as well as the geographic position of the buildings. Additionally, information such as building layout, number of stories, usage, construction year, and orientation for solar gains was added to the QGIS drawing.

The data from the QGIS drawing was then exported as a GEOJSON file. This file was imported into uesgraphs **[8]**, open source project, that utilizes the Python package NetworkX**[9]**. Uesgraphs automatically generates a Modelica simulation model based on the provided GEOJSON data.

The generated simulation model incorporates a basic building and pipe model, as well as a model for the EH. Figure 1 illustrates the resulting graph and node model generated by uesgraphs. Each line section in the model is assigned a corresponding pipe model template, with the diameter and length specified based on the values set in QGIS and imported from the GEOJSON file. The simulation model integrates the building and technical central models, which act as nodes within the overall model, based on the graph model.

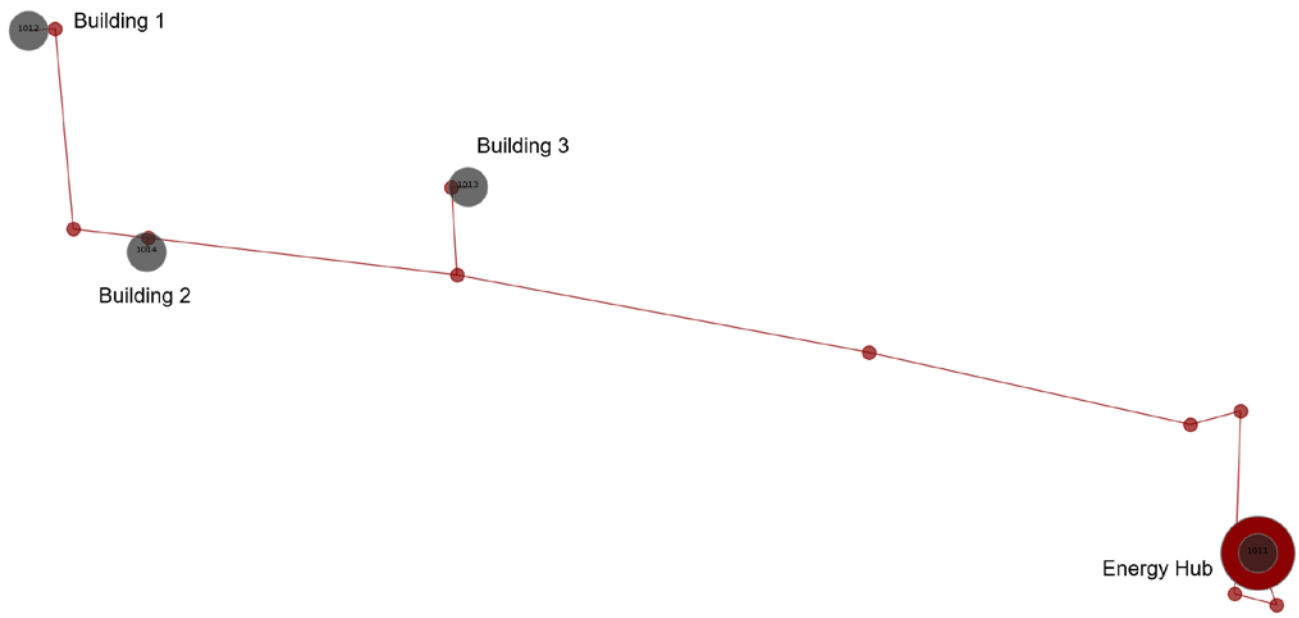

Figure 1: Graph and node model of the district generated with uesgraphs

Figure 2 provides a simplified illustration of the specific part of the district under investigation. For this purpose, the models were developed using the Aixlib library**[10]**, which is an open library employing the Modelica modeling language. This library is developed over the last years and was used in many projects. The Aixlib library offers a range of models specifically designed for modeling building energy systems (BES) within the Modelica framework.

Network modelling

The network infrastructure connecting the buildings and the EH comprises pipe connection sections and temperature sensors. For modeling these pipe connection sections, we utilize the Aixlib model "PlugFlowPipeEmbeddedDis" [11]. This model extends the functionality of a standard pipe model by incorporating the simulation of the surrounding soil. The soil parameters are determined based on sandy soil with clay content, as referenced in [12]. Additionally, the soil temperature varies throughout the year in response to ambient temperature changes. The ground temperature profile is depicted by the green line in Figure 4 in Chapter 3.

The length of each pipe segment is determined according to the development plan of the district. The cumulative length of both the warm and cold pipe sections amount to 553 meters. The Pipe diameter is varying between DN 225 and DN 60. To enable heat gains from the surrounding soil, the pipes in the DHC network are uninsulated and buried at a depth of one meter below the ground surface. Furthermore, a temperature sensor is placed adjacent to each pipe segment.

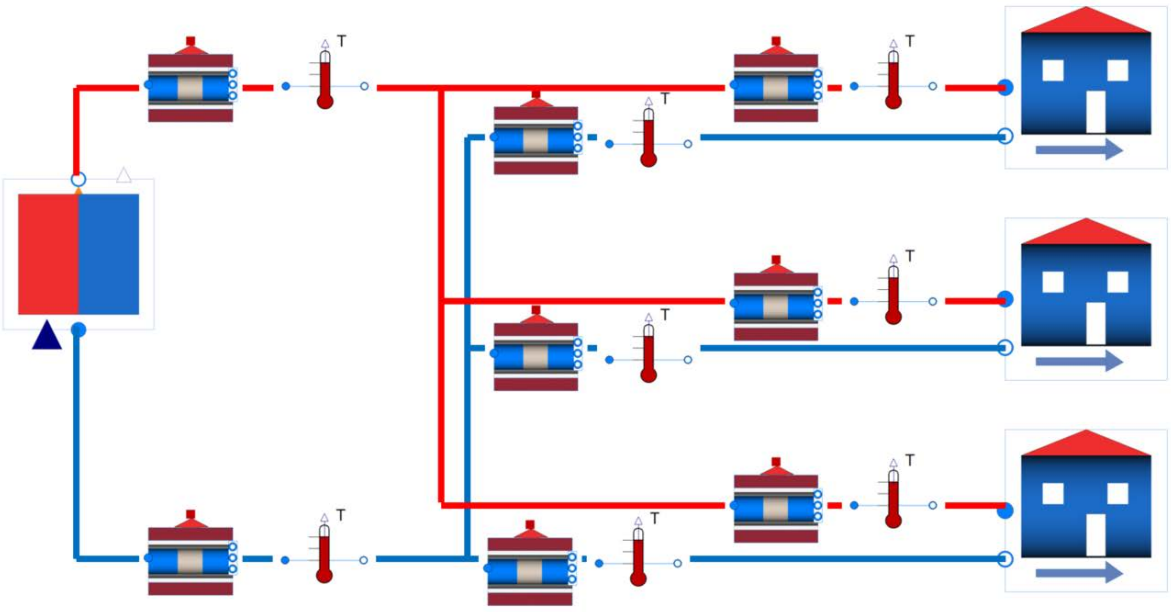

Figure 2: Simplified illustration of the Modelica model for the three buildings connected through the DHC network

Modeling the Buildings

In Figure 2, the three building models representing the substations of the single-family houses are positioned on the right side. Figure 3 provides a detailed view of the substation, illustrating the components within. Each substation consists of a circulation pump for the primary side of the DHC network and a heat pump model responsible for meeting the building's heating and domestic hot water (DHW) demands. An input table is connected to both pumps to set them to the appropriate mode based on the demand. Furthermore, the heat pump set temperature for heating is 35 °C and for DHW 60 °C. Since the footprint of the three investigated buildings differ, two buildings are equipped with 7.7 kW heat pump (Building 2 and 3), and one building es equipped with a 22 kW heat pump (Building 1).

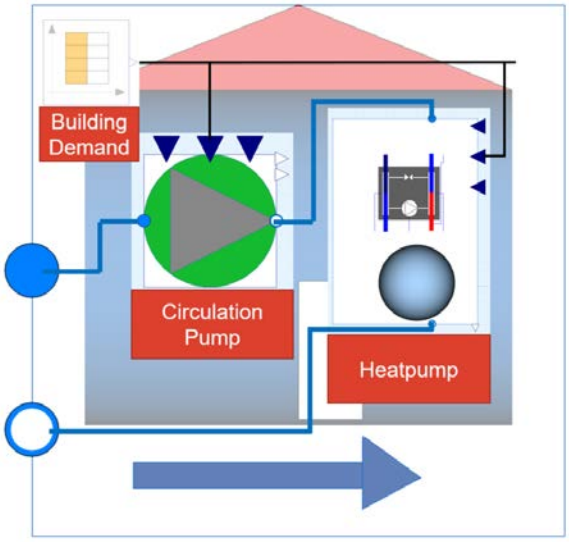

Figure 3: Detailed view of a substation within a building

On the primary side of the heat pump, a temperature difference of 5 K between the cold and warm pipe is set. Additionally, an electric heating booster can be employed within the substations if the temperature of the 5GDHC network is too low to meet the heating demand. Furthermore, the substations are able to supply cooling, at a set temperature of 20 °C, for the buildings. Therefore, direct cooling is used without a fixed temperature difference on the primary side.

To determine the specific demands of the buildings, calculations, and simulations are performed in a preceding step using TEASER *[13]*, another open-source development over the last years. TEASER is using a model of resistances and capacities based on VDI 6007 Part 1*[14]*. The course of the demand profiles of a building over one year are shown in *Figure 4* in Chapter 3. Additionally, to prevent the fluid in the pipes or the surrounding soil from freezing, a Boolean variable is incorporated. When the supply temperature drops below -3 °C, this variable triggers the shutdown of the primary pump. In such cases, the heating demand can only be met through the use of the electric heating booster within the heat pump.

Technical Central

On the left side of Figure 2, the red and blue icon represents the model of the EH. In this configuration, the heating and cooling equipment within the EH is disabled, and the warm and cold pipes are directly connected. As a result, no additional pump is required inside the EH since single family houses already have pumps on the primary side. Furthermore, this approach allows for direct coupling of buildings, enabling a building with a heating demand to fulfill the cooling demand of the adjacent building.

3. RESULTS AND DISCUSSION

Figure 4 illustrates the temperature profiles of the warm and cold pipes of the substation in building 1, as well as the ground temperature, and the buildings heat, cool, and DHW demand throughout the year. The ground temperature, represented by the green line, serves as input data for the simulation as well as the buildings demands, which are represented by the light red, blue, and green lines in the background of the plot. Since the DHC network pipes are uninsulated, as explained in Chapter 2.2, the heating network temperature closely follows the ground temperature. The heat pumps in the buildings are set to maintain a constant temperature difference of 5 K on the primary side, resulting in spikes in the temperature of the cold pipe (blue line) as shown in Figure 4. The frequency of the spikes in the temperature plots is higher during the colder winter months, reflecting the increased heat demand. This can be observed by the higher frequency of the light red lines in the background, which represents the heating demand of building 1. The gray dashed horizontal line represents the temperature at which the pumps on the primary side of the substation are shut off (-3 °C) to prevent freezing of the soil surrounding the pipe. During these periods, the heating demand is met by the electric heating booster. The minimum temperature observed during the simulation is approximately -3.7 °C.

In addition to the winter heating demand, there is also a heat demand during the summer months primarily for DHW (light green line). During winter, the temperature of the warm pipe (red line) is lower than the ground temperature due to insufficient heat gains from the soil to the DHC pipes. Moreover, since the substations are capable of cooling the buildings, there are spikes in the temperature of the warm pipe during the summer months. These spikes are a result of direct cooling (light blue line) using heat exchangers in the buildings, and their magnitude varies depending on the cooling demand of each building.

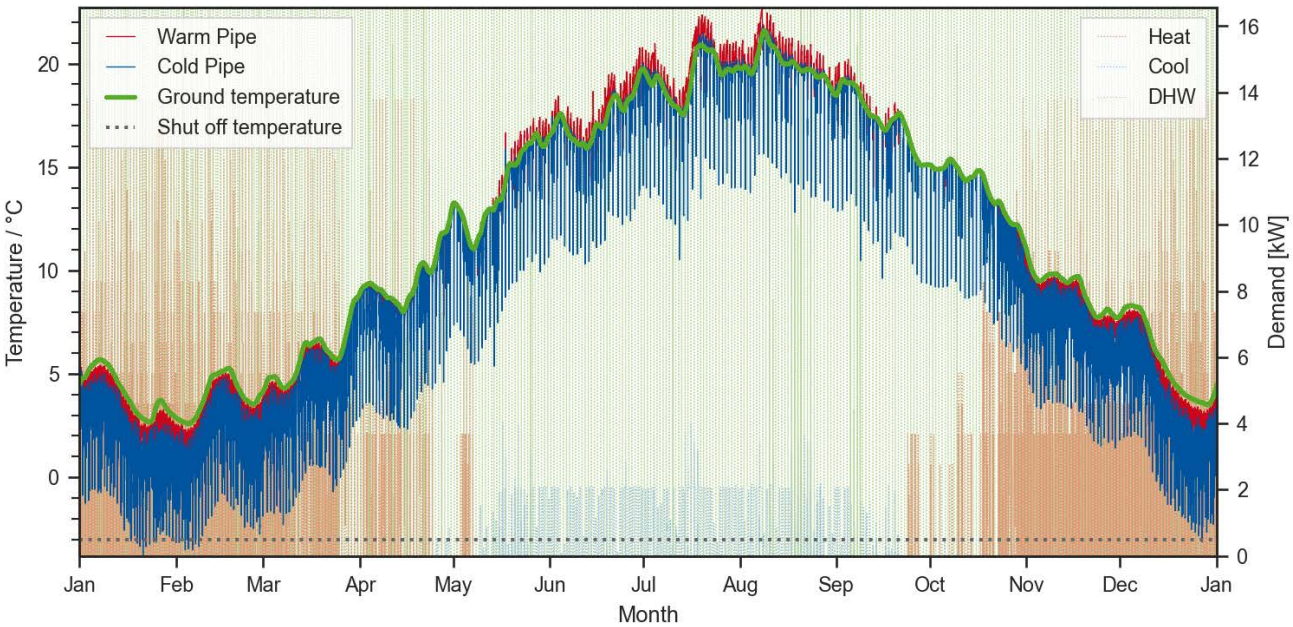

Figure 4: Plot of the temperatures of the pipe in front of building 1 during the year. In the background the specific heat, cool, and DHW demands are depicted.

Furthermore, it is important to analyze the temperature variations in the different pipe sections. By examining the temperature profile of each section, we can identify areas with significant heat gains or losses within the DHC network. This information allows us to optimize the network design and identify potential areas for improvement.Figure 5 presents plots of the DHC network temperatures for three hours on two specific days, one during winter and one during summer, with a one-hour resolution. For each plot the three buildings are on the left side and the EH on the right side. The color gradient represents the temperature within the pipes, and the line thickness indicates the mass flow. Furthermore, the dot next to the building name represents the heat pump mode. There are three different modes available heating, cooling, and off. Each plot represents one hour of time. The two selected days were randomly chosen to depict the temperature variations within the pipe.

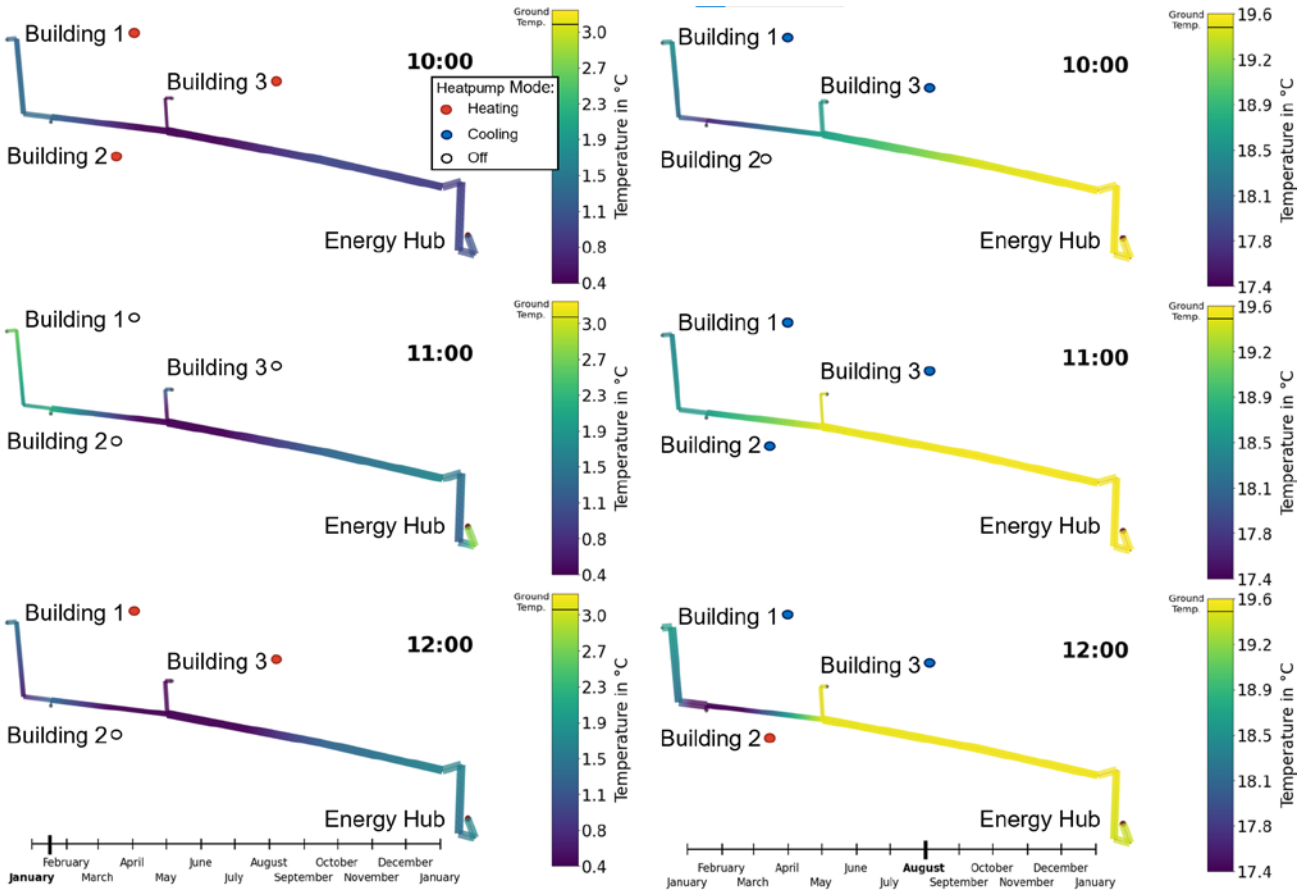

Figure 5: Temperature of the DHC network on a winter and summer day

On the selected winter day (January 16th), the DHC network exhibits a relatively uniform temperature at each point, with the surrounding soil temperature at approximately 3.2 °C. As the heat pump in the first building starts, the mass flow increases, causing the network temperature to decrease. The farther away the piping is from the building, the higher the temperature, as it benefits from heat gains from the ground. In the second plot at 11:00 o'clock, all heat pumps are turned off , resulting in a slight increase in pipe temperature. The last plot depicts a heat demand from the first and third building while the second one has no demand, resulting in decreased temperature in the pipes leading to buildings one and three.

On the right side of Figure 5, three hours of a summer day (August 1st) are displayed. The surrounding soil temperature is approximately 19.4 °C. During summer, there is also a heat demand for DHW, as indicated by the presence of blue spikes in the cold pipe throughout the year in Figure 4. Additionally, as the substations provide cooling capabilities, a cooling demand for buildings one and three can be observed in the plot. Furthermore, at 12:00 o'clock, Building two exhibits a heating demand, resulting in a decrease in pipe temperature in the vicinity of Building two.

These simulation results provide valuable insights for reevaluating the planning and construction process of a district equipped with uninsulated pipes and a DHC network operating at ground temperature level. It suggests that if the DHC

network is built as a first step, the initial buildings can utilize the network as a horizontal geothermal collector. Consequently, there is no need to build the EH before the first residents move in. Furthermore, it could also be possible, if the pipes are long enough, that no additional EH is needed.

4. CONCLUSION

In this study, a part of a district in the real laboratory TransUrban.NRW was analyzed. The investigation focused on a specific section of the district, consisting of three buildings, which were modeled and simulated for one year using the Modelica simulation language. The primary heat source utilized in the simulation was the surrounding soil of the uninsulated pipes of the DHC network.

The simulation results consistently demonstrated that the temperature of the heat transfer medium within the pipe remained above a defined threshold throughout the year.

Overall, the simulation confirmed that it is feasible to meet the heating demand of three single-family houses using the heat gains from an uninsulated DHC network, with the electrical heaters of the heat pumps serving as a temporary backup during extreme cold periods. This finding suggests that in district developments, the EH can be constructed after the initial buildings are completed or is not needed for very small districts.

Furthermore, these results open up new possibilities for planning very shallow geothermal fields for neighborhood use. For example, connecting 3-5 buildings to a single shallow geothermal field could significantly reduce costs as only one geothermal field needs to be planned and built.

In addition, the results of this study will be validated in the real laboratory. The completion of the first buildings and the EH is scheduled for the summer of 2023. The real laboratory nature of this project allows for experimentation and validation, such as demonstrating that certain buildings can operate without additional heat from the EH, relying solely on heat gains from the soil.

Funding: We gratefully acknowledge the financial support provided by the BMWK (Federal Ministry for Economic Affairs and Climate Action), promotional reference 03EWR020E.

REFERENCES

[1] European Commision, Ed., “establishing the framework for achieving climate neutrality and amending Regulations (EC) No 401/2009 and (EU) 2018/1999 (‘European Climate Law’),” vol. L243, no. 1, Jun. 2021.

[2] Global ABC, “2022 GLOBAL STATUS REPORT FOR BUILDINGS AND CONSTRUCTION,” *2022 GLOBAL STATUS REPORT FOR BUILDINGS AND CONSTRUCTION*. https://globalabc.org/our-work/tracking-progress-global-status-report (accessed May 31, 2023).

[3] H. Lund *et al.*, “The status of 4th generation district heating: Research and results,” *Energy*, vol. 164, pp. 147–159, Dec. 2018, doi: 10.1016/j.energy.2018.08.206.

[4] T. Blacha, M. Mans, P. Remmen, and D. Müller, “Dynamic Simulation Of Bidirectional Low-Temperature Networks - A Case Study To Facilitate The Integration Of Renewable Energies,” presented at the Building Simulation 2019, Rome, Italy, pp. 3491–3498. doi: 10.26868/25222708.2019.210670.

[5] M. Wirtz, L. Kivilip, P. Remmen, and D. Müller, “5th Generation District Heating: A novel design approach based on mathematical optimization,” *Applied Energy*, vol. 260, p. 114158, Feb. 2020, doi: 10.1016/j.apenergy.2019.114158.

[6] R. Zeh *et al.*, “Large-Scale Geothermal Collector Systems for 5th Generation District Heating and Cooling Networks,” *Sustainability*, vol. 13, no. 11, Art. no. 11, Jan. 2021, doi: 10.3390/su13116035.

[7] T. Schreiber *et al.*, “Planning the Design and Operation of Urban Energy Systems with Limited Data Availability: A Holistic Open-Source Tool Chain (under review),” *CISBAT 20232*, 2023.

[8] M. Mans, T. Blacha, T. Schreiber, and D. Müller, “Development and Application of an Open-Source Framework for Automated Thermal Network Generation and Simulations in Modelica,” *Energies*, vol. 15, no. 12, p. 4372, Jun. 2022, doi: 10.3390/en15124372.

[9] A. A. Hagberg, D. A. Schult, and P. J. Swart, “Exploring Network Structure, Dynamics, and Function using NetworkX,” 2008.

[10] D. Müller, M. Lauster, A. Constantin, M. Fuchs, and P. Remmen, “AIXLIB – AN OPEN-SOURCE MODELICA LIBRARY WITHIN THE IEA-EBC ANNEX 60 FRAMEWORK”.

[11] B. Van Der Heijde *et al.*, “Dynamic equation-based thermo-hydraulic pipe model for district heating and cooling systems,” *Energy Conversion and Management*, vol. 151, pp. 158–169, Nov. 2017, doi: 10.1016/j.enconman.2017.08.072.

[12] B. Glück, *Simulationsmodell “Erdwärmekollektor” zur wärmetechnischen Beurteilung von Wärmequellen, Wärmesenken und Wärme-/Kältespeichern*. 2008. [Online]. Available: http://www.berndglueck.de/Erdwaermekollektor

[13] P. Remmen, M. Lauster, M. Mans, M. Fuchs, T. Osterhage, and D. Müller, “TEASER: an open tool for urban energy modelling of building stocks,” *Journal of Building Performance Simulation*, vol. 11, no. 1, pp. 84–98, Jan. 2018, doi: 10.1080/19401493.2017.1283539.
[14] German Association of Engineers., Ed., “VDI 6007-1: Calculation of Transient Thermal Response of Rooms and Buildings – Modelling of Rooms.” Jun. 2015.

The 18th International Symposium on District Heating and Cooling, September 3–6, 2023, Beijing, China

4TH GENERATION DISTRICT HEATING MODEL BASED ON ENERGY PROSUMER BEING CONNECTED TO 3RD GENERATION DISTRICT HEATING NETWORK

Jaejoon Choi[a*], Young Jik Youn[a], Sae Byul Kang[a], Hyun Hee Lee[a], Kyung Min Kim[b]

[a] *Korea Institute of Energy Research, Daejeon, 34129, South Korea*
[b] *Korea District Heating Cooperation, Seongnam, 13487, South Korea*

[*] *Corresponding author. jjchoi@kier.re.kr*

ABSTRACT

Decarbonization or zero-carbonization is recognized as a global trend and a direction that all mankind should pursue. District heating sector is similarly being demanded to be decarbonized. In South Korea, about 6% of total heat consumption is generated by district heating sector, so efficient decarbonization is essential for national carbon reduction. It is hoped that the medium-temperature (near 120°C) thermal network, which is currently adopted to effectively transport large-scale heat at district heating sector, will be replaced with a low-temperature (near 60°C) thermal network suitable for micro thermal grids. In this study, several renewable prosumer-based low-temperature thermal network models were established. In this model, it shows the new direction of the new micro thermal network by utilizing the thermal network currently configured in South Korea. In conclusion, heat consumers will no longer be simple heat consumers, but will be active in supply as prosumers, which are expected to contribute to efficient use of heat energy, easy inflow of renewable heat energy, and reduction of carbon dioxide by using lower temperature heat energy.

Keywords: District Heating Model, Prosumer, 4DHC

1. INTRODUCTION

The Conference of Parties (COP21), held in Glasgow, England in 2021, drew worldwide attention and interest to go to a zero-carbon society. In response, Korea has set a goal of reducing greenhouse gas emissions by 40% by 2030 compared to 2018 and creating a carbon-neutral society by 2050[1].

Accordingly, Europe is paying attention not only to electricity but also to thermal energy production and consumption, making efforts to supply renewable heat energy based on Renewable Heat Obligation (RHO) or Renewable Heat Incentive (RHI) policies that encourage carbon-neutral thermal energy production and consumption.

In the case of the Republic of Korea, the Ministry of Trade, Industry and Energy determined that it was necessary to establish a production and consumption system in the region through the establishment of a microgrid base in the 2021 <Strategy for Activating Distributed Energy[2]>, and accordingly, it was deemed necessary to enhance the ability to operate and manage the independent and autonomous energy network at the village level. In addition, it tried to expand self-consumption through incentives for self-generation of renewable energy, and to establish a production and consumption system in the region based on prosumers by establishing a microgrid base.

The 5th Basic Supply Plan for District Heating[3] enacted by the Ministry of Trade, Industry and Energy mentioned the growing interest in the environment, such as fine dust and climate change response, and the increasing demand for eco-friendly energy facilities. Also, in order to improve regional acceptance and expand the role of distributed energy, it was decided to induce LNG cogeneration plants for district heating near demand areas (metropolitan areas, large cities), and induce decentralization of thermal energy such as low-temperature heat supply networks and unused heat. In addition, technical standards are prepared to establish a basis for the utilization of the 4G district heating system and a heat trading system is prepared. In order to expand the supply of renewable heat (geothermal heat, solar heat, water heat), when promoting energy conversion, consider ways to expand the use of renewable thermal energy such as establishing a basis for utilizing the 4th generation district heating system.

Until now, the energy supply method has maintained a centralized power method in which power is generated using a large-scale power plant at the center and distributed to each region. Based on a very large grid, the energy supply stability is excellent, and the urban living environment is improved by not installing energy supply facilities in populated cities and

installing energy supply facilities in sparsely populated countryside. Since large-scale power plants are concentrated and operated, the unit cost of power generation is low and maintenance is simple. Since it is operated centrally, the unit cost of power generation is low and maintenance is easy.

Also, as the production of new and renewable energy such as solar power, wind power, and geothermal power increases, problems arise in accessing power and hot water grids. Irregular and poor power quality hindered the stability of the power grids, and in the case of new and renewable heat energy, there was a problem in that it was produced at a temperature (above 100 ° C) that was not suitable for mid- to long-distance heat transport.

In addition, as the production of renewable energy, such as solar power, wind power, and geothermal heat, increases, problems arise in accessing power and hot water systems. Irregular and poor quality renewable energy hinders the stability of the power system. However, in the case of new and renewable thermal energy, a problem has arisen that it is produced at a temperature (100 ° C or higher) that is not suitable for mid- to long-distance heat transport.

In district heating, 3GDH (3rd Generation District Heating) is defined as the connection between cogeneration and large-scale consumers for mid- to long-distance transportation. Considering that the basic pipe network temperature of third-generation district heating is around 100℃, it is not easy to utilize renewable heat energy such as solar heat, geothermal heat, water heat, and fuel cell heat, which generally generate heat below 100℃. Accordingly, low temperature district heating (LTDH), which is operated as 4GDH (4th Generation District Heating) using a pipe network temperature of around 60℃, is attracting attention. This is being researched and demonstrated in many countries around the world, including Korea.

Renewable energy has a low energy density and a large installation site area, so not only the device but also the site where it is installed is very important. There is a way to install and operate these in large quantities on an idle site where no one lives. However, since it is best to install and produce in a location close to the consumer due to the nature of energy transportation and microgrids, it is reasonable and reasonable to utilize the land resources of the energy consumer as well. Therefore, consumers can directly operate renewable energy such as solar heat, geothermal heat, and fuel cells using land resources in houses, buildings, and sites. This concept is called energy prosumer(Producer+Consumer=Prosumer). However, when installation, sales, and maintenance are considered, it can be effective to have a professional organization manage them.

2. 4G DISTRICT HEATING MODEL

As a premise of the 4th generation district heating model to be applied in Korea, it was considered that it should be a model that can be realized with a slight modification rather than a fundamental change in concept, which can make the most of the currently operating district heating resources. In Korea, since the 3rd generation district heating network is currently widely distributed nationwide, it was considered that it should be fully utilized, and furthermore, a separate model is also considered possible.

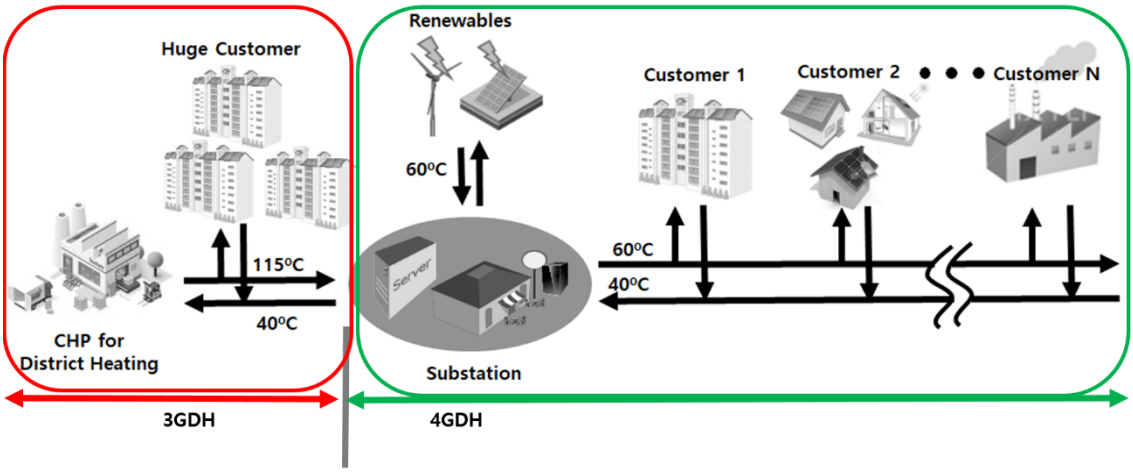

Figure 1. Distinction between 3GDH and 4GDH

2.1. SUBSTATION

Korean district heating is operated with 3G(district heating network temperature of 100℃ or higher). In order to change this to around 60℃ of district heating network temperature, which is the 4th generation, various models can be considered. Among these options, a substation is placed at the end of the 3G network to utilize the thermal energy used in the 3G network. The return water temperature of the 3G network is generally above 60 °C, so it can be a good supply temperature and supply energy for the 4G district heating network. The following figure shows the concept of 4G district heating in connection with 3G district heating.

Basically, the substation should play the role of maintaining the net temperature of the 4GDH network. The network temperature of the 4GDH network does not have to be a set temperature, but all customers must be able to use district heating supply water, and the network temperature must be maintained enough to connect and supply renewable heat energy from substations and prosumers.

The substation should be able to access renewable heat energy, which is the basic facility of the network operator, and should include a small cogeneration system, heat pump, heat-only boiler, and heat storage device.

In order to maintain the temperature of the district heating supply chain, the balance between the heat energy produced and the heat energy consumed must be considered, and digitalization is necessary for this. Digitalization is a tool that can calculate all constants and variables so that the entire system can be predicted and simulated for the energy produced and consumed.

When substations and renewable prosumers continuously produce heat, a device for proper consumption is also required to prevent the 4G district heating network temperature from continuously increasing. The ORC (Organic Rankine Cycle) system is an excellent device for this. While a steam turbine converts high-temperature heat into electricity, the ORC system efficiently converts low-temperature heat (80°C to 400°C) into electricity. Therefore, it can be said that it is a key device that is essential for Substation.

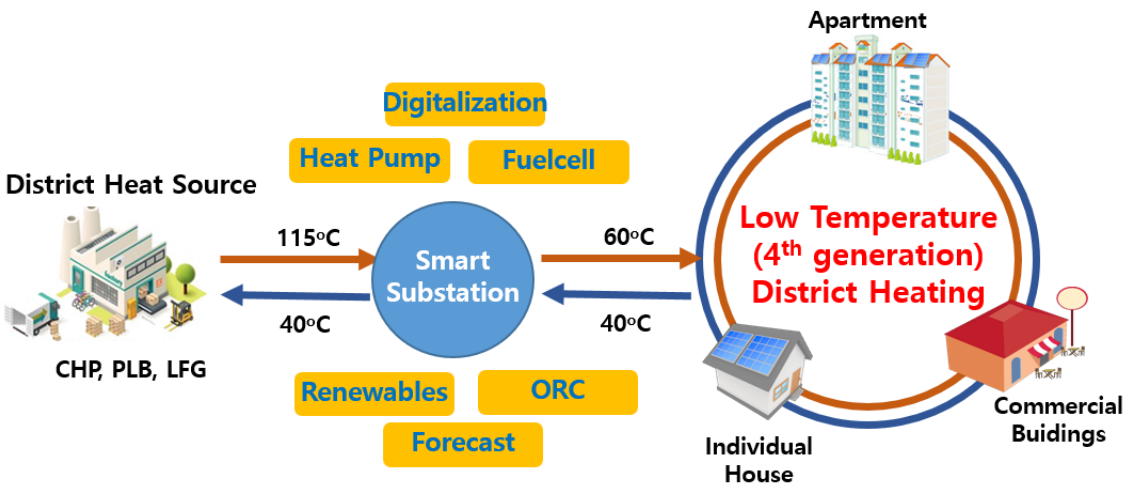

Figure 2. Roles and Functions of Substation

2.2. 2-LINE LTDH PIPING MODEL

2-line LTDH is a method in which district heating water from the customer's heat exchanger is directly injected into the return line. Due to the nature of LTDH where consumers are connected in series, the temperature of district heating water supplied from the 1st consumer to the Nth consumer is the same. However, since the amount of heat required by the consumer changes every moment, the change of the district heating water supply temperature in the substation is essential, and load prediction and temperature control are necessary.

In this concept, since heating water is transferred to the return line while passing through the consumer, the flow rate on the main pipe side decreases, so that the diameter of the pipe can be reduced whenever it passes through the consumer, and in general, less pumping power can be consumed.

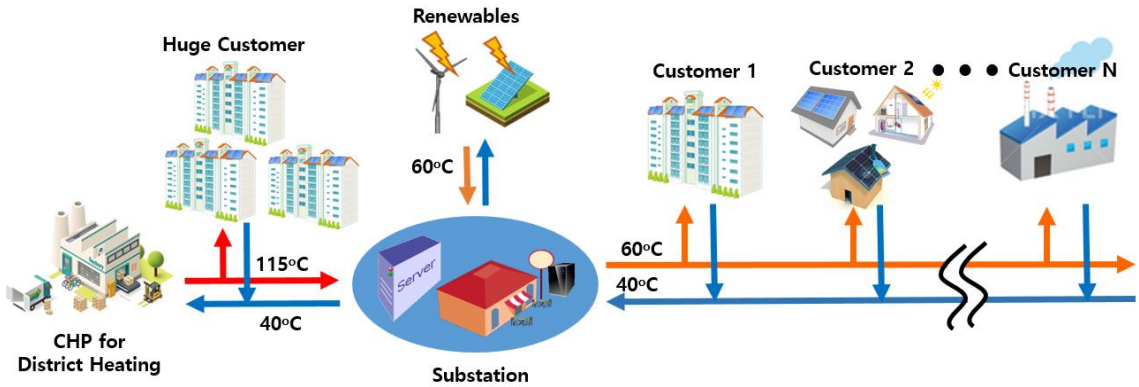

Figure 3. Two-Line LTDH Piping Model

2.3. ENERGY PROSUMER

The supply of new and renewable energy such as solar heat, geothermal heat, and fuel cells poses problems in installation and operation costs, but space, area, and location for installation can also become problems. For distributed installation of energy devices, not relying on central facilities operated by network operators, but actively utilizing land and location resources on the consumer side affects not only the spread of renewable energy, but also reasonable consumption of energy and energy loss. Therefore, consumers are encouraged to play a role as a prosumer, not just as a consumer any longer. In 4GDH, the act of constructing a new renewable energy or own power plant (heat-only power plant) on the customer side and consuming it on the customer side or connecting it to the district heating pipe to participate in the district heating network becomes indispensable in 4GDH. The (thermal) power generation resources held by the customer can be handled by the network operator from installation to operation, or the customer can directly operate them.

If the consumer-side resource is owned by the prosumer, the energy produced from the consumer-side resource can be preferentially used by the prosumer. Prosumers can first consume energy produced from their resources and then transfer heat to district heating pipes if they have extra energy, but district heating network operators need to recognize such prosumer's energy production and consumption patterns first, and prepare and take countermeasures accordingly. A prosumer can estimate the heat to be produced at the substation by receiving a forecast report on when and how much heat is needed and when and how much heat can be left and delivered to the district heating pipe, and can cope with slightly changing values at any time.

Basically, when a prosumer sells thermal energy to a network operator, it is set at a lower price than the unit price of the thermal energy produced by the network operator. Energy prices can be set differently in consideration of the time, time, and surrounding situation (such as when prosumers are flocking to supply energy at once), and prosumers can also choose whether it is advantageous to consume the energy produced themselves or to supply it to district heating pipes.

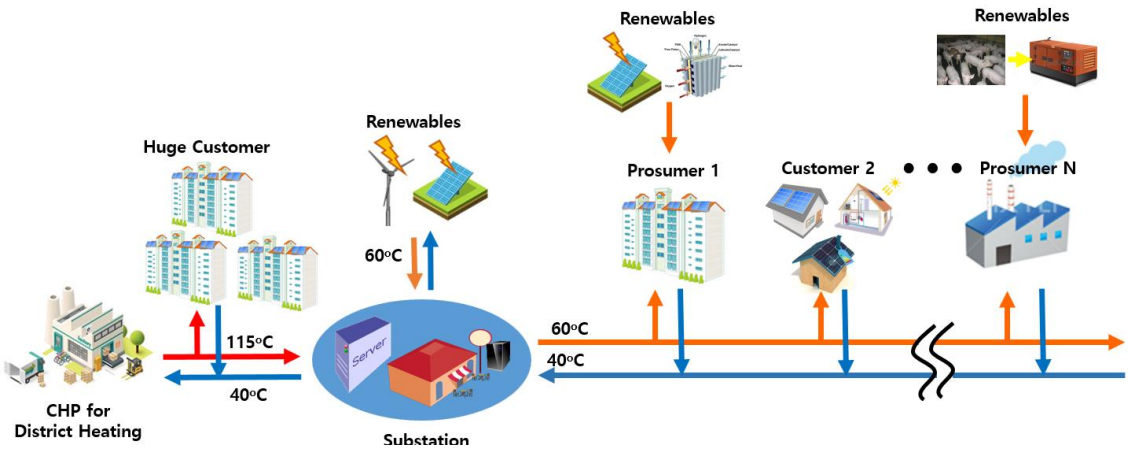

Figure 4. Energy Prosumer Concept in 4GDH Model

2.4. 4G DISTRICT HEATING AND COOLING

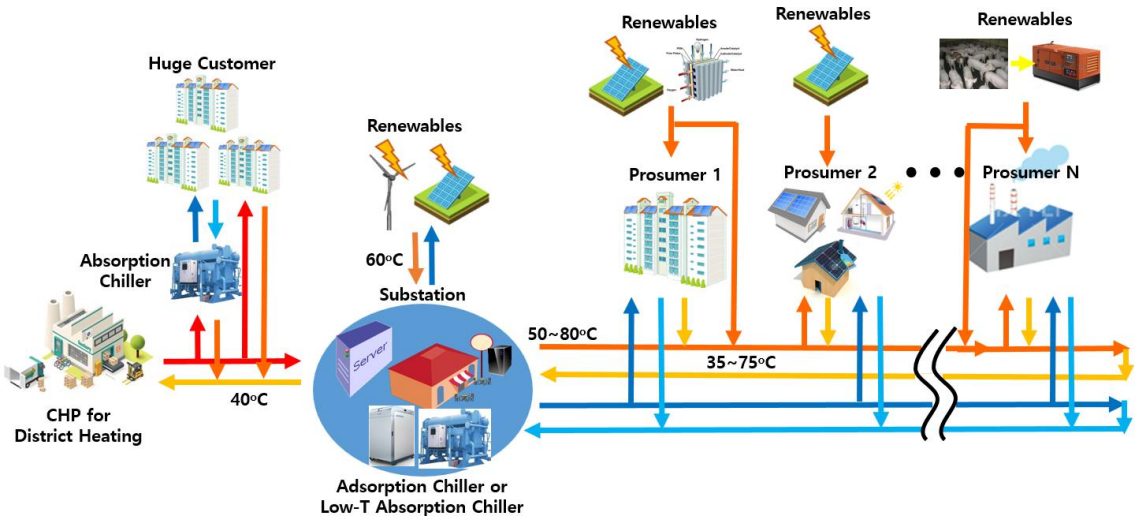

Figure 5. 4G District Heating and Cooling Model

In Korea, district cooling is realized by using an absorption chiller inside the site using high-temperature water of 95℃ or higher of the 3GDH. In the 4GDH network, the concept is a bit more complicated because prosumers use or supply energy throughout the DH pipe network. Basically, the substation for 4GDHC can make cold water with an adsorption chiller or a low-temperature absorption chiller that can produce cold water with low-temperature thermal energy (hot water around 60℃) or an absorption chiller, which is the conventional method. In the 4GDHC concept, DH pipes consist of a pair of heating pipes and a pair of cooling pipes, and a heating network and a cooling network are configured at the same time.

Prosumers can raise the temperature of the return water entering the substation by transferring thermal energy from the heating network, and the substation can operate the cooling network by making cold water using hot water and a refrigerator. The influx of prosumers is desirable because the more heat produced by prosumers, the less heat energy production for cold water production the substation bears.

If the district heating pipe temperature rises above the value considering the cooling and heating demand, the overall energy balance may be displaced, so the pipe temperature must be properly maintained using a refrigerator and ORC system. Prosumers can contribute to the cooling network with their own air conditioners, but considering the limited renewable energy and the prosumer site itself is not very large, it is not easy for prosumers to directly contribute to the cooling network. There may be a way for prosumers to generate cooling energy from fuel cells or other non-renewable energy sources and contribute to the cooling network, but the pricing policy for cooling energy produced from non-renewable sources should be severely considered.

3. CONCLUSION

A 4th generation district heating network that can be connected to a 3rd generation district heating network in Korea was modeled.

A substation concept is required to connect the 3rd generation district heating network to the 4th generation district heating network. The substation plays a role not only in connecting district heating households, but also in controlling connected renewable energy and controlling consumers and prosumers.

2-line piping was considered, and a model was developed in which thermal energy prosumers intervened in 4th generation district heating to buy and sell thermal energy.

The 4th generation district heating and cooling model, which even considers cooling, is also being considered.

ACKNOWLEDGEMENT

This research was conducted with the research fund support from the Korea District Heating Corporation.

REFERENCES

[1] Carbon Neutral Green Growth National Strategy and 1st National Basic Plan, Korea Government, 2023
[2] Distributed Energy Activation Strategy, Ministry of Trade, Industry and Energy, 2021
[3] The 5th Basic Supply Plan for District Heating, Ministry of Trade, Industry and Energy, 2020

The 18th International Symposium on District Heating and Cooling, September 3-6, 2023, Beijing, China

Economic comparison of heating and cooling supply systems in warm climates – using a case study

Oddgeir Gudmundsson[a*] and Irene Aiello[a]

[a] *Danfoss A/S, Climate Solutions, Nordborg, 6430, Denmark*
[*] *Corresponding author. og@danfoss.com*

Abstract

District energy systems are widely recognized as a sustainable and future proof solution for fulfilling urban heating demands in cold climates. However, the question remains on their applicability in climates requiring both heating and cooling of buildings. While district energy systems are traditionally designed for fulfilling either heating or cooling demands the latest system designs offer the possibility for integrating both heating and cooling demands into the same system. The commonality with these systems is low operating temperatures, which offers the possibility for end-user to use the network as a heat source, or heat sink, for their own heat pumps. These end-users are commonly referred to as prosumers, as they can both take, and delivery, thermal energy at useful temperature levels to the district energy system. This paper compares the levelized cost of heating and cooling for fulfilling space heating, space cooling and domestic hot water demands of a neighborhood with a mixture of new and old buildings in Rome, Italy, when applying low temperature district heating (4GDHC), ultra-low temperature district heating (5GDHC) and building level heating and cooling solutions. The results indicate that 4GDHC is the most competitive heating and cooling supply solution for the considered case.

Keywords: 4GDH, 4GDHC, 5GDHC, Economics

Urban Energy System

The 18th International Symposium on District Heating and Cooling, September 3–6, 2023, Beijing, China

EQ-City – PRE-PLANNING APPROACH FOR AN EFFICIENT AND ENVIRONMENTALLY FRIENDLY HEAT SUPPLY OF QUARTERS AND CITIES

Anna Marie Cadenbach[a*], Nermina Abdurahmanovic[a], Tarek Anwarzai[a], Alexander Jahn[a], Alwina Kaiser[a,b]

[a] *Fraunhofer Institute for Energy Economics and Energy System Technology IEE, Kassel, 34117, Germany*
[b] *University of Kassel, Kassel, 34127, Germany*
[*] *Corresponding author. anna.cadenbach@iee.fraunhofer.de*

ABSTRACT

Especially low temperature district heating is recognized as a key technology for the (cost-) efficient integration of renewable energy and waste heat sources in our energy systems. To achieve the goals of the energy transition, new innovative concepts are needed for district heating-based supply of neighborhoods and cities. However, the limited availability of information and data in the pre-planning phase pose a challenge to the development of viable supply concepts. To address this issue, Fraunhofer IEE has developed EQ-City, an Excel-based planning tool that streamlines the development and evaluation of heat supply concepts, even with limited data. This paper provides a comprehensive overview of the functionalities and capabilities of EQ-City. It begins by highlighting the motivation and importance of low temperature district heating systems in the context of the energy transition and the need for sustainable energy solutions. The challenges encountered during the pre-planning phase are discussed, emphasizing the key role of EQ-City in overcoming these challenges. The technical intricacies of EQ-City are explained, including its energy conversion chain methodology. The step-by-step process of using the tool is described, covering aspects such as building energy demand analysis, heating network design, and the selection of suitable supply technologies. The ability of EQ-City to consider both district heating supply and individual building heat supply is emphasized, enabling a holistic evaluation of low temperature DH concepts. A key strength of EQ-City lies in its extensive database of technologies and supply options for sector coupling, providing diverse possibilities for heat supply. The tool facilitates multi-criteria analysis, allowing users to evaluate different supply options based on economic, technical, ecological, regulatory, and soft factors. The flexibility of the tool is underscored, enabling stakeholders to assign custom weights to criteria based on their specific interests. To demonstrate the practical application of EQ-City, several case studies showcasing innovative concepts developed and evaluated using the tool are presented. The outcomes of these evaluations, including economic feasibility, technical viability, and environmental benefits, are thoroughly discussed. In conclusion, this paper summarizes the contributions and benefits of EQ-City in the development of sustainable supply concepts for low temperature district heating. It emphasizes the importance of informed decision-making during the pre-planning phase and highlights how EQ-City empowers stakeholders, including municipal utilities, municipalities, and component manufacturers, to make sustainable and efficient supply concept decisions. Overall, this paper provides a comprehensive understanding of EQ-City, its functionalities, and its application in the pre-planning phase of low temperature district heating projects. EQ-City plays a crucial role in advancing sustainable energy systems and facilitating the integration of renewable energy sources.

Keywords: Pre-planning; Low temperature district heating; Heat supply concepts; Sustainable energy systems; Multi-criteria analysis.

1. INTRODUCTION

The global shift towards sustainable energy systems has prompted various countries to implement comprehensive strategies to mitigate climate change and reduce dependence on fossil fuels. Germany, in particular, has taken significant steps towards achieving its energy transition goals. The German energy transition plan, also known as "Energiewende," aims to transition the country's energy sector from conventional sources to a more sustainable and renewable energy mix. As part of the Energiewende, the development of new innovative district heating (DH) concepts based on renewable and climate-friendly sources has become a crucial focus for various sectors and stakeholders throughout German society. These DH concepts play a vital role in achieving the ambitious targets set by the energy transition plan, including substantial reductions in greenhouse gas emissions and the integration of a higher share of renewable energy sources into the heating sector.

Simultaneously, municipal heat planning has gained significant importance in Germany as a central instrument of the energy transition. It is now mandatory for municipal utilities and decision-makers to devise cost-effective and climate-friendly solutions for meeting the heating demands of communities. This obligation, coupled with the need to align with the broader energy transition goals, poses significant challenges for stakeholders involved in heat planning and decision-making

processes. In this political atmosphere and mindset, the Fraunhofer IEE has identified the important steps of an energy transition concept starting from the status quo identification and the pre planning phase, through the implementation and the validation phase. Based on these different planning phases, scientific models were developed to support the achievement of the political requirements. In this case the excel-based planning tool EQ-City is intended to support the pre-planning phase by identifying the status quo of heat demand and supply for a defined district and comparing it with different variants of alternative supply structures such as renewable-based DH supply. The different supply variants and strategies are not only compared based on technical or energetic parameters but also from an economic perspective based on the equivalent annual cost method based on VDI 2067 [1]. Furthermore EQ-City also includes an automated multi-criteria analysis which supports decision makers, energy supplies etc. to identify the most appropriate supply solution due to the automatic generated outlay of the comparison results but also in identifying key performance indicators (KPI). These KPI can be weighted based on the results of e.g., first stakeholder assemblies and drawn out to the different heat supply variants for further comparison. Finally, the user receives a clearer picture of possible alternative heat supply structures and strategies with a solid path for further system specific research while highlighting necessary adaptations and cost orientation.

As a result of the urgent need to transform the heating sector, including the DHC sector, several tools have been developed. To assess where EQ City stands in relation to these tools and understand its unique features, a review of existing tools has been conducted. One of these tools is THERMOS [2], which specializes in planning and optimizing district heating and cooling systems. It provides valuable insights to stakeholders, enables feasibility assessment, evaluates energy supply scenarios, and optimizes system configurations. Another tool called ESyOpt [3,4], developed by Fraunhofer UMSICHT, offers model-based planning of energy systems. It allows for comprehensive analysis, optimization, and decision-making in the development of sustainable energy systems. It provides features for modeling, simulating, and evaluating various scenarios. Similarly, the nPro [5] District energy planning tool focuses on planning and sizing district energy systems, with an emphasis on renewable energy sources. It enables cross-sectoral analysis and facilitates the integration of renewable energy into the system. Additionally, EnergyPLAN [6] assists in designing sustainable energy solutions by considering renewable energy integration and cross-sector interactions. While all the tools are an aid for planning energy systems of districts, EQ City stands out for its libraries of predefined building and district types, automated sizing of system components and cost functions. These enable EQ-City to quickly validate the existing real data set, but also provide a qualitative and effective way to fill information gaps. One design principle of EQ-City is to reduce the amount of input data required, while keeping the ability to add detailed information for fine-tuning. This is a great advantage in the pre-planning phase, as it allows the user to get a first impression of possible results. By conducting a thorough review and comparison of existing tools, this paper aims to position EQ City within the landscape of energy transition planning tools, highlighting its unique contributions and showcasing its potential to support decision-makers, municipal utilities, and municipalities in making effective and efficient sustainable supply concept decisions. EQ-City offers a comprehensive profitability calculation also taking funding options into account and an add-on, for coupling the electricity and heat sectors.

However, there are several open questions surrounding the significance and uniqueness of such a tool. This paper aims to identify and answer some of these questions, which include:

- How does EQ-City help overcome challenges in the pre-planning phase of district heating-based supply concepts?
- What technologies and supply options are available using the EQ-City database, especially for sector coupled systems?
- How are the different supply variants evaluated using multi-criteria analysis in EQ-City?

And finally,

- How can EQ-City be utilized by municipal utilities, municipalities and decision makers to make sustainable supply concept decisions effectively and efficiently?

In response to these questions, the paper highlights the basic functionality of the EQ-City tool (see chapter 2) and possible applications (see chapter 3).

2. A TOOL-BASED APPROACH FOR DEVELOPING AND EVALUATING LOW TEMPERATURE DISTRICT HEATING SUPPLY CONCEPTS

The calculation and evaluation process for the heat and electricity sectors involves several steps as part of a process chain for energy balancing of quarters and cities. These consecutive steps encompass characterizing the urban area, selecting buildings with different uses, selecting system technology, conducting a multi-criteria analysis (also known as utility value analysis) based on KPI, and considering integration options for photovoltaic (PV) systems (see **Figure 1)**. This comprehensive process allows users of the tool to evaluate parameters such as energy flows, efficiency, CO_2 emissions and costs, ultimately generating a detailed automatically generated report summarizing district characteristics and evaluation results. The tool was designed as an Excel-based instrument and implemented using VBA code.

Figure 1. Simplified process flow of the program [7]

The initial step of the process is the characterization of the urban area and the selection of various default building types for heat demand calculation (see section 2.1). Based on the calculated demand and requirements a supply set comprising centralized and decentralized energy sources can be assembled in the second step (see section 2.2). The modelling of the energy system is supported by plausibility checks and a comprehensive database of system components. For the electricity sector, a Python plug-in provides options for integrating PV systems with battery storage or e-mobility options, considering climate data and household numbers. In the third step (see section 2.3), a multi-criteria analysis takes place. It allows the user to select and weigh hard evaluation factors like efficiency or profitability and individual soft evaluation factors for decision making. Finally, an automatically generated report provides an overview of district characteristics, evaluation results, and a concise summary of findings.

2.1. Heat Demand Calculation

The calculation of the heat demand takes place by defining energetic district types (EDT) [8] and single buildings using a simplified building typology (BT) derived from [9]. Established default values are available as part of the tool by a drop down-menu. The default values can be easily adjusted by the user. If more detailed data (e.g., measurement data) is available, it can be used by the tool (e.g., through files in csv format) for describing the urban space and building types. However, detailed information about construction details and planned development measures is seldom available in an early stage of urban planning and development. The calculation of the heat demand depends on the quality of the available data or information (see **Table 1**). Accordingly, the calculation results vary in their level of detail.

Table 1. Quality of the available data or information for calculation of the heat demand

	Data base	**Available date**	**Calculation basis**	**Results**
Option 1	Low	District type, building age class, refurbishment status	Energetic district types (EDT) based on[8]	Annual heating demand
Option 2	Average	Climate zone, number of buildings, building use, building age class	Pre-simulated load profiles of representative buildings based on [9]	Time-resolved load profiles
Option 3	High	Measurement data	Measurement data (e.g. files in csv format or other formats readable by excel)	Time-resolved load profiles

The EDT and the BT allow a rough estimation of heating demand for central district heating or decentralized building supply. This step is a central prerequisite to estimate properties of the supply network and calculate economic efficiency. One way to address these requirements is through the definition and use of an urban typology. This approach with energetic district types (EDT) is used in EQ city. The EDT are an urban typology [8] linking urban energy needs and potential. The eight urban space types with predominantly residential and mixed use already contain important energy information and data of typical building geometry and construction details based on building age and renovation status. These EDT also contain a lot of information about energy potential regarding various sources. The EDT are subdivided into ten building age classes based on building standards, heat insulation and energy saving regulations [8]. Each age class has four states for the renovation status of the buildings with associated heat transfer coefficients and simulated heating requirements. The EDT specifies the number of buildings and their composition based on a building typology [8]. The building types include a

typical length of the street frontage per building and number of flats and inhabitants. After entering EDT and building types, heating and domestic hot water requirements as well as heating loads and annual duration curves are determined. This information is furthermore necessary for the calculation of the network length.

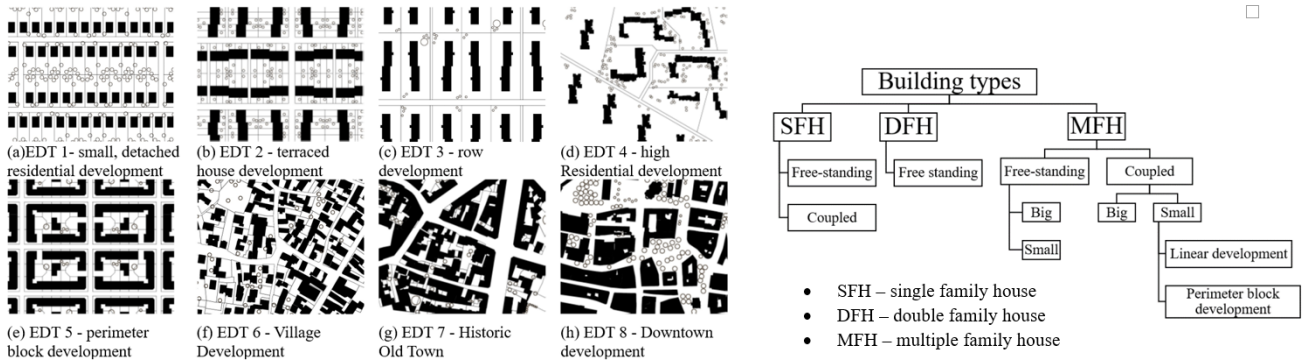

Figure 2. Energetic urban typology (left) and implemented building types (right)

In addition to the urban area types, individual energy-related properties such as schools or hospitals are also incorporated in EQ-City to link energy demand of neighborhoods. It is possible to add, edit or delete energetic single objects or more EDT to the area of interest. The district area can be specified as a number in hectares of net building land and will be multiplied by the number of buildings per hectare defined by EDT to output an average number of buildings. If the number is known, it can also be adjusted. Once the district is defined, one to four occurring building types are defined as well (see **Figure 2)**.

Furthermore, the ratio of the buildings can be adjusted. For each building type there are characteristic parameters available as well as specific annual heating requirement in kilowatt hours per year and square meter. Finally, when building types and corresponding parameters are chosen or defined heating demand and domestic hot water requirements are calculated as sum of individual absolute heat demands for each building. The building data was expanded by integrating an Access database, which was populated with specific annual duration curves generated through individual simulations for each building in different climate zones with TRNSYS [10]. The output sheet presents the cumulative annual duration curves, representing the entire district.

2.2. Composition of heat supply options for buildings

The second part of the tool is based on the demand estimations. Depending on the number of heat consumers, the coincidence factor for the maximum heating load is additionally calculated. This calculation includes upper and lower deviations for the degree of simultaneity. This is intended to reduce the effort to calculate numerous scenarios in detail by eliminating inefficient or expensive supply structures in the beginning. The focus is on the energy requirements and potentials of different building types and the combination of technical systems, rather than the specific details of individual buildings and consumers. This forms the basis for the automated design of the selected system technology. Once the heat demand of the buildings as part of the district or city has been identified, the status quo of the supply structure should be reproduced with the tool to compare it with various supply options. Requirements of the building types are placed on the supply technology such as needed temperature levels or the heating and domestic hot water profiles.

Supply scenarios are modelled based on EDT and demand assessment. To facilitate this process, uniform object classes are defined for technical system components. The analysis focuses on different components, with particular attention paid to small local heating networks. Users can select and link these objects using a drop-down menu. First the components used inside the building types must be defined. To streamline the user experience, the software automatically sizes each component using pre-stored information, minimizing the need for additional information and manual interaction. In the case of a bivalent heating system, a dwelling's coverage rate and building type details define the amount and temperature levels of heat. EQ-City offers a set of common decentralized heating units in its libraries, based on fossil fuels or biomass, but also heat pumps, solar thermal collectors and photovoltaic power plants. Some components can be used as centralized supply technology for a district heating grid and also as decentralized heat supply as individual heating units inside buildings. For a domestic heating network, the amount of heat required would be determined based on the amount and information about the building types and how much heat they need. Based on the details of the building types within the grid area, the flow temperatures, mean pipe diameter and grid length will be sized automatically and can be adjusted manually. The network must be supplied with the required amount of heat also considering network losses and the required level of heat based on renewable and climate-friendly heat sources. The distribution of the proportional supply to the grid and the resulting emissions are defined by the coverage rate of each heating device in the system and their specified emission factor.

Heat networks offers also potential for sector coupling as they offer the possibility to use surplus energy, especially from renewable sources such as PV, to heat buildings and domestic hot water. For this purpose, a PV plug-in has been integrated to take these costs into account. EQ-City generates load profiles for household electricity usage based on various household parameters and photovoltaic electricity generation based on selected weather data. It enables the calculation of profitability for photovoltaic systems. The resulting costs are added to the overall cost of each heat supply variant. It is essential for determining the operating costs within the framework of the economic efficiency calculation, as it provides information on the profitability and economic viability of such projects. Especially to house owners, the usage of photovoltaic electricity in their own appliances is important to save energy costs.

When creating the heating supply setup of a variant additional components like pumps, storages and heat exchangers can be implemented too. Because EQ-City does not do a detailed planning of each system those system elements are mostly considered in terms of costs and less in detail of thermos-hydraulic plausibility. The main impact of these additional technologies is to receive a better statement about the investments. All technical and economical details of components can be customized as information becomes available. New or extraordinary devices, which cannot be found in the EQ-City libraries or with different parameters, could be added to the system. Based on the annuity methodology and system component data of VDI 2067 [1] in addition with cost functions different cost types like investment costs, operating costs or heat generation costs are calculated and shown for each defined variant in the result paper.

Figure 3 shows schematically different examples of heat supply structures and their components, which can be further analyzed or adjusted by the operator of the tool.

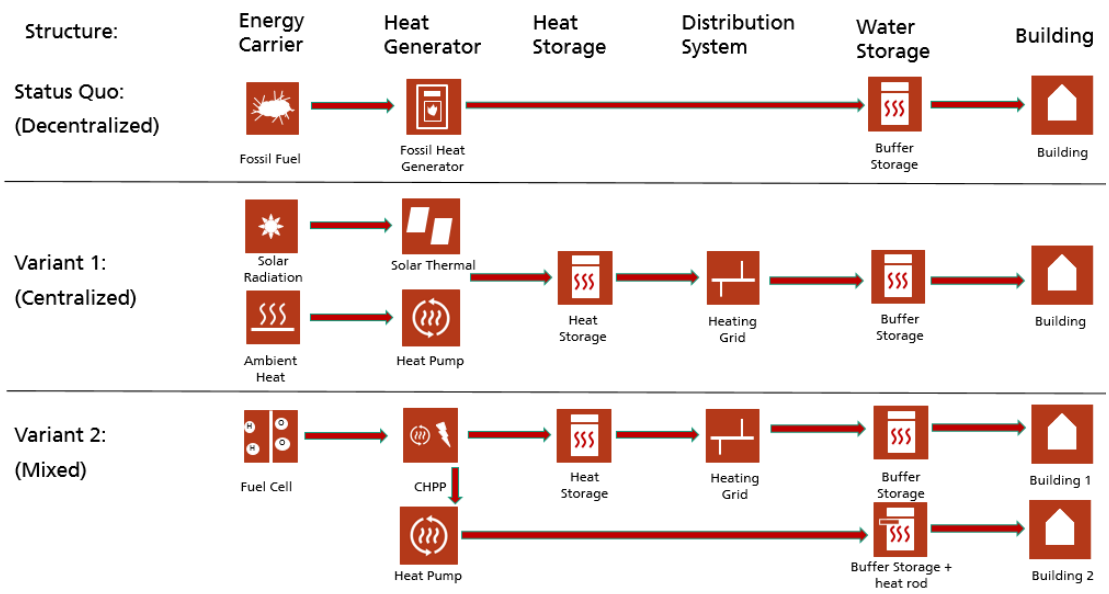

Figure 3. Examples of heat supply structures and their components

2.3. Multi Criteria Analysis

The individual supply options are evaluated based on the utility analysis. The utility value analysis is a method of the multi criteria analysis for evaluating sustainable heat supply options, enabling decision-makers to systematically consider various criteria and make informed decisions to identify a sustainable heat supply option. After the various sustainable heat sources are identified and the desired supply options are defined, the evaluation criteria relevant to the analysis are determined. Encompassing both hard evaluation factors (HEF) [11] like economic viability, primary energy demand, CO_2 equivalents, and space requirements, as well as soft evaluation factors (SEF) [11] like acceptance, user-friendliness, complexity (control depth), innovation content, price stability, and contract design (see **Figure 4**). Additionally, stakeholder dialogue can contribute additional criteria that align with decision objectives and represent important aspects of the issue.

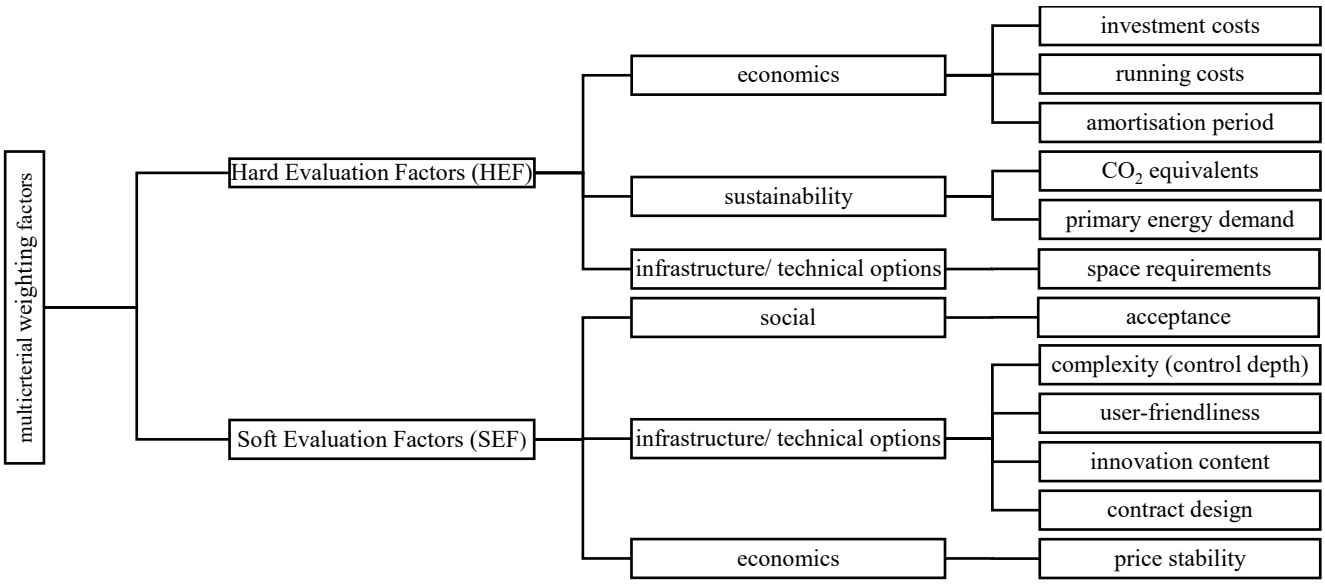

Figure 4. Criteria hierarchy for the choice of a heat supply system

The tool is already flexible designed so that both HEF and SEF can be added, removed and defined by the decision-maker, and assigned their own weighting factors accordingly. Default settings are also stored as a definition aid. A specially designed report sheet, which is automatically generated by the tool, is used to present the results. Once the criteria are defined, they are weighted to determine their relative importance, considering the preferences and goals of the decision-makers. The next step involves assessing the heat supply options based on the established criteria. Each option is evaluated for each criterion, using different rating scales. For example, a numerical 10-point scale can be used for the evaluation. Weighting factors can also be applied to consider the relative importance of criteria within an option. The aggregated ratings are then used to calculate an overall utility value or score for each heat supply option, employing mathematical formulas or decision rules that multiply the ratings by the weights and sum the results. This comprehensive assessment provides insights into the utility and performance of each option in relation to the defined criteria.

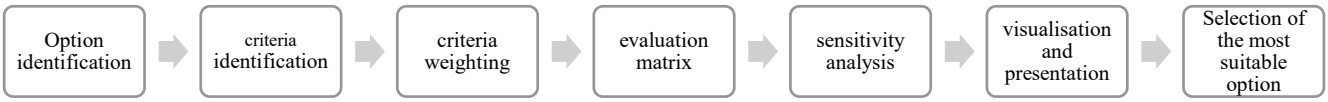

Figure 5. Process of the utility value analysis

Analyzing and comparing the results of the utility value analysis allows decision-makers to understand the advantages and disadvantages of the different heat supply options. Sensitivity analyses can be conducted to examine the effects of variations in weights or ratings and verify the stability of the decision. The results can be visually presented using bar charts to depict the ranking of the various supply options. This systematic and structured evaluation process (see **Figure 5**) empowers decision-makers to make well-informed choices regarding sustainable heat supply options. Furthermore, by considering multiple criteria, the utility value analysis captures the strengths and weaknesses of the options in a transparent manner, providing a clear framework for discussion and communication among stakeholders.

3. APPLICATION EXAMPLE – DEVELOPMENT OF AN INNOVATIVE ENERGY CONCEPT WITH EQ-CITY

To illustrate the potential applications an example[1] of a new innovative concept developed and evaluated using the pre-planning tool EQ-City is presented. This example shows the conversion of an area from a sports field to a residential area. The size of the planning area is 2.5 ha. The new buildings (EnEV 2016 energy standard) are 17 detached and terraced houses and 8 apartment buildings. The aim is to develop affordable housing. The buildings are created in the tool and the maximum heating load is calculated as 277 kW. An efficient local heating system is to be developed and integrated into the new building structure. Together with the local supplier, a centralized low temperature district heating (LTDH) supply option and two semi-centralized supply options based on ultra-low temperature district heating (U-LTDH) are developed and analyzed with EQ-City to achieve this goal.

[1] This example is intended to illustrate how EQ-City works. The example is based on a real use case but has been simplified for clarity.

- **1. LTDH (80 °C):** The centralized option involves the use of a heating network with a flow temperature of 80 °C and connected CHP and gas boiler (peak load) supply units.
- **2.a U-LTDH (9 °C):** The first semi-centralized variant involves the use of a cold network at a temperature level of 10 °C which is connected to a geothermal collector. The buildings are equipped with decentralized heat pumps. The heat pumps are powered by locally installed photovoltaic panels. A heating rod is used to provide domestic hot water.
- **2.b U-LTDH (9 °C):** The semi-centralized supply units differ in the use of a wood pellet boiler (peak load).

To meet the targets, evaluation criteria were defined together with the energy supplier and weighted accordingly. In the case of HEF, factors related to economic efficiency were weighted at 40% and those related to sustainability at 30 %. For the SEF, system flexibility and complexity were rated at 10% and social aspects at 20 %. This is just a simplified example, as there are many different factors in each category. Economic factors can be heat generation costs or planning uncertainties. Regarding environmental aspects there can be criteria like greenhouse gas emissions, renewables coverage or land usage. The SEF are highly individual and can be created by the user of the tool. These are especially helpful for decision making when there are solutions that are otherwise very close (like 2.a and 2.b).

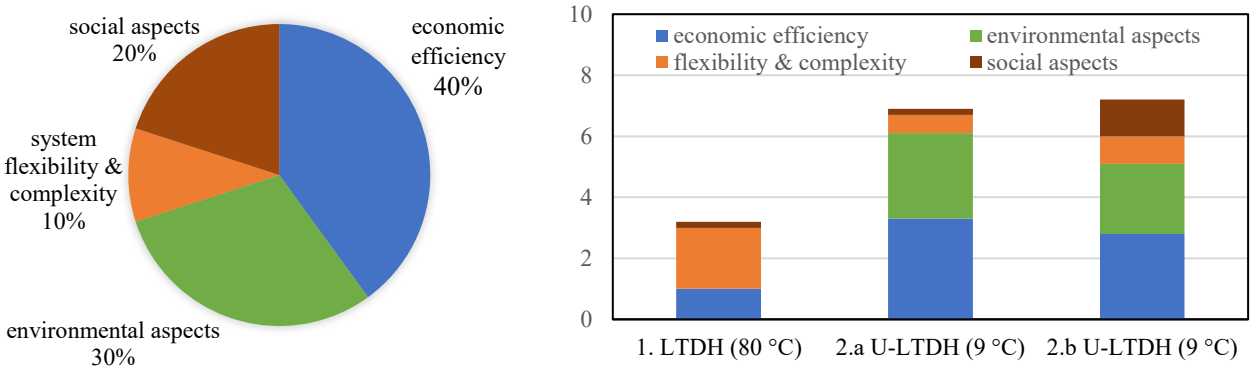

a) Weighting of factors

b) evaluation of weighted factors for the considered variants

Figure 6. Example evaluation of district energy supply options

EQ-City's key advantage is its ability to offer a comprehensive and easily understandable overview of essential information, empowering efficient decision-making and analysis for a deeper understanding of a district's energy needs. This is particularly valuable in the early planning stage when little data is available. By representing the buildings using the building types and EDT, and utilizing the tool's procedures for dimensioning the piping network and supply systems, accurate estimations can be made. Additionally, EQ-City enables a comprehensive comparison of total costs, primary energy consumption, CO2 emissions, and annual heat demand. This can be achieved by employing predefined cost functions or specific cost inputs. By consolidating economic and sustainability factors into a score presented through a visual bar chart, the tool empowers users to assess scenarios, make adjustments, and enables decision-makers to swiftly and effectively evaluate and optimize their energy concepts (see **Figure 6 b)**).

The evaluation of the analysis has shown that variant 2.a performs best in terms of economic efficiency. The reason is that subsidies and a separate heat pump tariff are advantageous, while fuel costs for gas and wood pellets are disadvantageous. Furthermore, 2.a also scores best in terms of sustainability since the lowest emissions are generated due to the low supply temperatures and the combined use of HP and PV. Considering the technical options, variant 1 is preferred due to its simplicity and minimal operational management requirements. However, when taking all factors into account, variant 2.b emerges as the preferred choice, aligning closely with the objective of developing affordable housing. In addition to the application in district projects with new buildings, the tool was also used for transformation projects in existing districts, for district projects with mixed development (residential, commercial and schools) and for campus redevelopments. Through these various applications, a good level of verification has already been achieved.

4. CONCLUSIONS AND OUTLOOK

The EQ-City tool, with its comprehensive functionalities, proves to be an invaluable resource during the preliminary planning phase of energy transition projects. It offers a holistic approach to assessing heat demand and supply scenarios, incorporating technical, energetic, economic, and multi-criteria considerations. By leveraging pre-existing building and heat generator data libraries, EQ-City allows for the swift validation of real data sets and efficient filling of information gaps. The tool facilitates the comparison of various supply options and strategies, enabling the identification of key performance indicators and their evaluation through stakeholder assemblies. Notably, EQ-City sets itself apart from existing tools with

its extensive database and ability to integrate the electricity and heat sectors, offering a more integrated perspective on system development. Through its calculation and evaluation processes, as well as automatically generated reports, the tool provides detailed insights into neighborhood characteristics and evaluation outcomes.

In the presented application example, the use of the EQ-City pre-planning tool proved instrumental. Its comprehensive functionality facilitated the evaluation and comparison of different heating options, considering multiple criteria such as economic efficiency, sustainability, technical complexity, and social aspects. This systematic and data-driven approach allowed for evidence-based decision-making in assessing the feasibility and performance of various heating systems within the context of housing retrofitting. Consequently, valuable insights were gained to determine the most suitable option for the affordable housing development's specific objectives. Thus, the EQ-City tool establishes itself as a reliable and efficient resource for energy system analysis and planning.

Looking ahead, the EQ-City tool holds promising prospects for further research and application in the field of energy transition. Future studies can focus on expanding its capabilities to encompass larger-scale energy systems, such as city quarters or entire districts, by incorporating additional urban area types and building typologies. Efforts can also be directed towards enhancing the tool's flexibility and customization options to cater to specific regional or contextual requirements. Integrating advanced modeling and simulation techniques can improve the accuracy and reliability of heat demand and supply predictions. Additionally, incorporating emerging technologies and energy storage solutions into EQ-City can enable a more comprehensive analysis of sustainable heat supply options. The tool can further benefit from ongoing developments in renewable energy sources, smart grids, and demand-response strategies, supporting the exploration of innovative system configurations and optimized energy flows. As part of future plans, the existing Excel tool is intended to be ported into Python, aiming to achieve greater flexibility, improved performance, and long-term sustainability. Furthermore, collaboration with stakeholders can provide valuable feedback and contribute to the continuous improvement of the tool. In summary, the EQ-City tool serves as a solid foundation for future research endeavors in energy transition planning. It not only addresses the present challenges but also opens doors for sustainable and efficient heat supply systems.

ACKNOWLEDGEMENT

The results presented in this paper have been funded by the Hessian Ministry of Higher Education, Research and the Arts. The authors responsible for the content of this paper acknowledge the funding received.

REFERENCES

[1] Technical rule VDI 2067 Blatt 1:2012-09, 2012. Economic efficiency of building installations - Fundamentals and economic calculation, 44 pp.

[2] THERMOS Tool, 2021. What is THERMOS? https://www.thermos-project.eu/ro/thermos-tool/what-is-thermos/. Accessed 11 May 2023.

[3] Hunstock, B., Kanngießer, A., 2021. Modellbasierte Planung von Energiesystemen. Fraunhofer UMSICHT, 2 pp.

[4] Schneeloch, J., Rosin, L. Environomic optimisation of local energy concepts for utility companies under the influence of increased energy prices. IEWT 2023.

[5] Wirtz, M., 2023. nPro: A web-based planning tool for designing district energy systems and thermal networks. https://www.sciencedirect.com/science/article/pii/S0360544222034624.

[6] Lund, H., Thellufsen, J.Z., Østergaard, P.A., Sorknæs, P., Skov, I.R., Mathiesen, B.V. EnergyPLAN – Advanced analysis of smart energy systems, 16 pp.

[7] Fraunhofer-Institut für Energiewirtschaft und Energiesystemtechnik (IEE). EQ-City - Planung der Wärmeversorgung für Quartiere und Städte. https://www.iee.fraunhofer.de/de/geschaeftsfelder/analyse-und-beratung/eq-city.html. Accessed 30 May 2023.

[8] Hegger, M., Dettmar, J., Martin, A., et al., 2012. Schlussbericht UrbanReNet. EnEff:Stadt - Verbundprojekt Netzoptimierung - Teilprojekt: Vernetzte regenerative Energiekonzepte im Siedlungs- und Landschaftsraum: Abschlussbericht 0327832D, 273 pp.

[9] Diefenbach, N., Cischinsky, H., Clausnitzer, K.-D., et al., 2010. Datenbasis Gebäudebestand: Datenerhebung zur energetischen Qualität und zu den Modernisierungstrends im deutschen Wohngebäudebestand. Institut Wohnen und Umwelt; Bremer Energie-Institut, Darmstadt, Bremen, 150 pp.

[10]Hesse, S., 2021. Entwicklung von synthetischen Wärmelastprofilen für Quartiere. B. Sc., 52 pp.

[11]Kallert, A.M. Modelling and simulation of lowtemperature district heating systems for the development of an exergy-based assessment method, München, 131 pp.

The 18th International Symposium on District Heating and Cooling, September 3–6, 2023, Beijing, China

TRANSFORMATION AND OPTIMIZATION OF THERMAL GRIDS FOR THE DEVELOPMENT OF HYBRID GRID STRUCTURES

Anna Marie Cadenbach[a*], Lina Wett[a], Frank Marten[a], Mike Vogt[a], Erik Prade[a], Daniel Ackermann[a], Bernd Wagner[b], Stefan Adldinger[c], Andreas Fiegl[d], Lina Taube[e], Lioba Thomalla[f]

[a] *Fraunhofer Institute for Energy Economics and Energy System Technology IEE, Kassel, 34117, Germany*
[b] *AGFW Project Company for Rationalization, Information and Standardization mbH, Frankfurt Main, 60596, Germany*
[c] *Municipal utilities Neuburg on the Danube., Neuburg on the Danube, 86633, Germany*
[d] *ENERPIPE GmbH, Hilpoltstein, 91355, Germany*
[e] *BBH Consulting AG, Berlin, 10179, Germany*
[f] *Institute for Climate Protection, Energy and Mobility – Law, Economics and Policy e.V., Berlin, 10179, Germany*

[*] *Corresponding author. anna.cadenbach@iee.fraunhofer.de*

ABSTRACT

In the heating sector, district heating (DH) is a key element of the energy supply. To meet the climate targets, a transformation of existing thermal grids is needed. Challenges arise from decreasing heat demands and increasing integration of power-to-heat applications. However, this integration leads to a wider range of control and operation management requirements.

Against this background, the transformation and optimization of DH for the development of hybrid grid structures (HGS) are illuminated. The focus is on the development of a generation-oriented operation of two separated energy systems, electrical energy systems (EES) and thermal energy systems (TES). To achieve this goal, approaches for optimized and integrated operation are developed, tested, evaluated and implemented, considering technical, economic and regulatory framework conditions. Initially, the simulation-based development of operating strategies for HGS are conducted. The aim is to show how a flexibilization of existing DH systems in the context of HGS must be designed to meet future demands of DH system. The developed operating strategies will be tested on a coupled test bed for power and heat grids in order to identify synergy potentials for increasing the efficiency and flexibility of HGS. Finally, the developed operating strategy will be implemented in a neighborhood of the city of Neuburg on the Danube in Bavaria, Gemany.

The investigations focus on lowering grid temperatures in the context of the operation-optimized interaction of EES and TES. Based on a low-temperature DH supply, heat pumps (HP) as an interface between EES and TES, offer the possibility of efficiently integrating renewable energies into the heating network. Decentralized storage potentials, also represent a local supply option for the HP and, with possible access to building-side storage, can contribute to increasing the flexibility of the electricity grid.

The paper presents an overview of the work currently being conducted and highlights the potential of HGS.

Keywords: district heating; operational optimization; hybrid grid structures; flexibilization, sector coupling

1. INTRODUCTION

1.1. BACKGROUND AND MOTIVATION

The Energiewende sets clear targets for reducing greenhouse gas (GHG) emissions and energy consumption. GHG emissions are to be reduced by 40 % by 2020 compared to 1990 levels, and by 2050 the target is up to 95 %. [1] Against this background, the heating sector is of critical importance, accounting for around 58 % of total energy consumption and around 40 % of energy-related greenhouse gas emissions in Germany. [2] In the heating sector in Germany, DH is an important component of the energy supply system, as approx. 14 % of the building heat demand is currently covered by DH. [3] In order to decarbonize the energy supply a paradigm shift in existing DH systems towards hybrid energy systems (HES) is taking place and sets new requirements on flexible operation [4]. Against this background, the research project "EnEff:Wärme: HybridBOT_FW" [5] aims to implement a hybrid network structure in a model neighborhood in Neuburg on the Danube in Germany. The investigation focusses on lowering grid temperatures in the context of the operation-optimized interaction of EES and TES. To achieve this goal, co-simulation and experimental approaches for optimized and integrated operation by

combining electrical distribution networks and district heating networks are being developed, tested and implemented in practice, taking into account technical, economic and regulatory framework conditions [6]. This paper gives an overview of the current work and first results of the project in the case of co-simulation and the development of control strategy, that provides the prerequisite for practical implementation. In addition, definitions of terms are introduced and the supply area is presented.

1.2. DEFINITIONS

When dealing with Hybrid Energy Systems (HES), various terms like HES itself, hybrid grid structure (HGS) or Grid-supportiveness are of importance. A clear and common understanding of the content scope of the terms, their hierarchy, interaction and dependencies is required in general and in regard to the project-specific conditions and investigations. An appropriate means to meet the above requirements is the development of definitions. Therefore, a multi-phase-process was carried out, selecting the relevant terms, deciding their hierarchy and working out a representative, consensus and useful understanding of the terms as definitions in the project-specific context. Figure 1 shows the hierarchical relation and provides a keyword-like reference to the respective terms as a result.

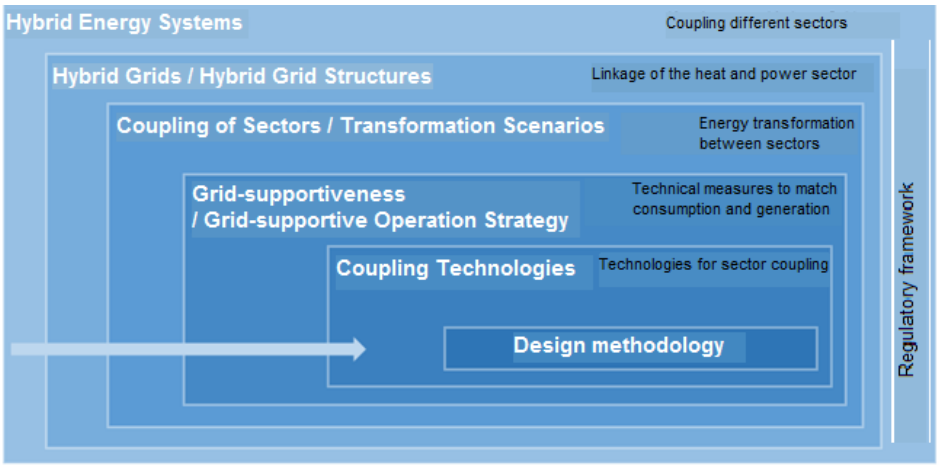

Figure 1. Hierarchical terms [7]

The output of the multi-phase-process has been summarized in a document "Key definitions of the project" [7]. It is available online to the sector as an introduction and basis for discussion on the topic of hybrid energy systems, but also for reflection and feedback on the document and its content.

2. HYBRID SUPPLY CONCEPT

2.1. DESCRIPTION OF THE SUPPLY CONCEPT

The innovative supply concepts to be investigated in the project “HybridBOT_FW” presented as part of this paper focus on the possibilities of reducing grid temperatures particularly related to highly variable-constant district heating operation in the context of the operation-optimized and grid-oriented interaction of the electricity and heat sector. In this context, raising (winter months) or lowering (summer months) the grid temperature can meet a power demand that fluctuates throughout the year and minimize heat losses in the distribution grid. The HGS is implemented by a combined heat supply via a DHG and decentralized coupling technology in the buildings for feeding into thermal storages. The supply area consists mainly of new and existing residential buildings and a few existing and newbuild commercial buildings. The residential buildings are many single-family and two-family houses as well as fewer small and large multi-family buildings. The heating network includes flexible polyethylene pipelines with a length of about 4,134 m to supply 130 buildings and a heat output 1,110 kW. Further details of the dimensioning can be found in Table 1. In deviation from this the municipal utility will implement plastic jacket pipes.

Table 1. Design parameters of the DHG

Description	Value
Grid temperatures (supply / return)	80 / 50 °C
Route length DHG	4,134 m
Number of connected parties	130
Thermal power	1,110 kW th.
Annual heat demand	2,977 MWh/a
Total pressure drop	3.68 bar
Operating pressure	1 bar
Volume DHG	9,808 l

2.2. DERIVATION OF THE SUPPLY CONCEPT

In relation to the focus described in 2.1, three innovative supply solutions, referred to as energy routes in Figure 2, have been developed. The innovative regenerative supply simultaneously considers the requirements of new housing districts as well as the transformation of existing districts, which are part of the investigated district. The basic concept of the energy routes is identical, they vary in the division of the DHG, the heat generation plant and the supply temperatures. The consensus is that all buildings are connected to the DHG. And further, in the context of a hybrid grid structure, decentralized thermal storages are installed in the buildings in combination with coupling technologies. Electricity gained from photovoltaic (PV) modules on the building roofs is used in heating applications via electric heating elements in smaller buildings and heat pumps in apartment buildings. This, in combination with the DHG, allows flexible operation of sector coupling technologies and thus purchase from the power grids. The sector coupling technologies are dimensioned in relation to the domestic hot water (DHW) load in consideration of the thermal storage volume.

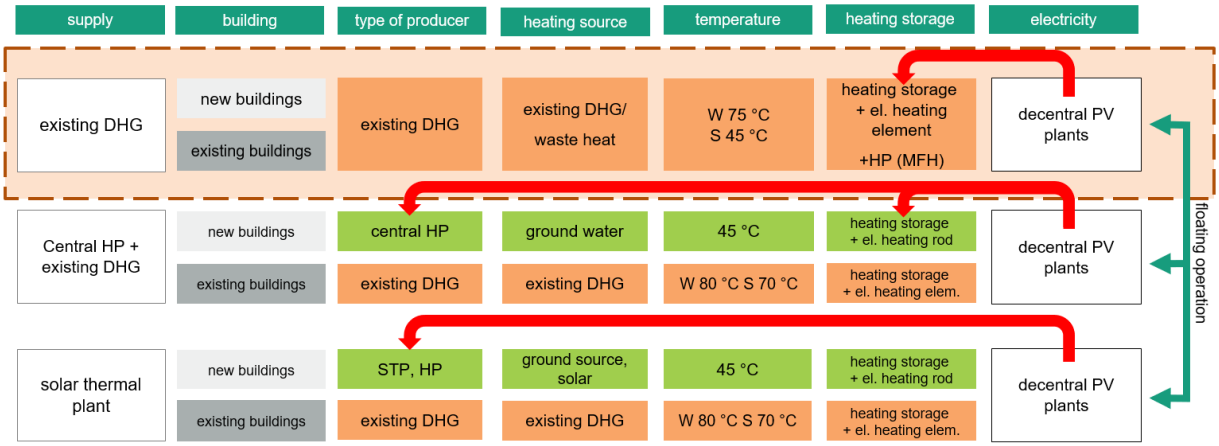

Figure 2. developed supply solutions, referred to as energy routes

In the first energy route in Figure 2 the investigated DHG of the district is supplied by an existing DHG. Due to the presence of high-temperature industry in the city of Neuburg on the Danube, the existing DHG is supplied with industrial waste heat as its main energy source. The investigated DHG is hydraulically separated via a head-end station which enables a flexible supply in terms of temperature and heating power. Through a highly variable-constant district heating operation the supply temperature varies between 45 °C in summer and 75 °C in winter to reduce heat losses. In contrast, the new housing district in the second energy route contains a separate low-temperature DHG, which is supplied by a groundwater heat pump. Accordingly, the flow temperature is 45 °C and the DHW is reheated by the decentralized coupling technologies in the buildings. In the third energy route, the new housing district is supplied by a ground source heat pump. Part of the summer load as well as the regeneration of the ground is covered by a solar thermal plant. Due to the available waste heat through the existing DHG, the first energy route in Figure 2 is selected for further investigation as part of this paper.

3. CO-SIMULATION OF A HYBRID NETWORK

To investigate the impact of district control strategies on both the electric and heating grid, a co-simulation of the new housing district in Neuburg on the Danube was created, which is a part of the investigated district described in chapter 2.

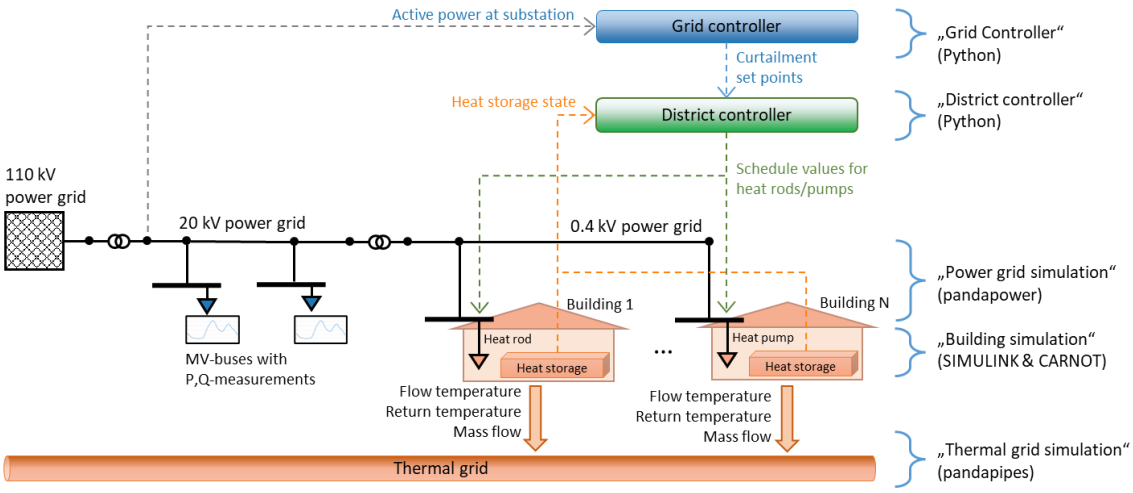

Figure 3. Co-simulation of the investigated district in Neuburg on the Danube.

Alongside models of the physical electric and thermal grid with buildings and coupling technologies, two controller algorithms were included to emulate decisions from the district energy management and the distribution system operator (DSO). A schematic view of the co-simulation is shown in Figure 3. The coupling of different simulators was enabled through the OpSim-environment [8], while individual simulation components were implemented in Python and MATLAB [9]. The following sections explain the simulation components in more detail, as well as first results from testing a grid control strategy.

3.1. POWER GRID SIMULATION

The electricity network model consists of a medium voltage (MV; 20 kV) feeder supplying various low voltage (LV; 0,4 kV) grids in the city of Neuburg on the Danube. Only the two LV-grids serving the new housing district are modelled in detail. All other LV-grids and directly connected MV-consumers/producers are modelled as (re)active power (P, Q) time series, measured by the DSO in 2021. The simulation software used is the open-source Python library "pandapower" [10]. The MV-topology was obtained directly from the DSO as a GIS-shapefile and converted to pandapower via QGIS. The LV-grids were created in QGIS, based on the DSO's building location plans of the new districts. The new housing district contains 25 buildings, and as some of them have multiple grid connections, they are represented by 30 LV-loads.

In the co-simulation, the "power grid simulation" receives active power consumption values every 15 minutes from the heat elements and heat pumps in the "building simulation" as input for its calculation. The resulting electrical power flow value at the substation is sent to the "Grid controller" component (see Figure 3).

3.2. THERMAL GRID SIMULATION

The thermal grid is modelled in the "pandapipes" [11] network calculation program. Pandapipes is also an open-source Python library for modeling, analysis and optimization of district heating and gas systems. The model in pandapipes consists of several components: pipes with pressure loss and heat loss to the surroundings, a circulation pump depicting the supply of the specified flow temperature and pressure lift, flow controls and heat exchangers, which together represent the heat consumers. The flow control component is responsible for defining the mass flow the customer receives, while the heat exchanger extracts a specific amount of heat from the system.

In the co-simulation, building mass flow and temperature values (flow and return) are received from the "building simulation" every 15 minutes, to calculate pressure and heat loss statically along the thermal grid in pandapipes (see Figure 3).

3.3. BUILDING SIMULATION

The building simulation model contains the charging and discharging of the decentralized thermal storages. The discharge is based on time series of the heat demand for DHW and heating and the supply is provided by DHG and coupling technologies. The latter are controlled by the "district controller" and turned off when a maximum temperature is reached, while the supply by the DHG is only based on the storage temperature level. When the upper and lower storage temperatures fall three and four Kelvins below the set target value, storage charging begins. The charging continues until the lower storage target temperature is exceeded.

In the co-simulation, the "building simulation" receives every 15 minutes on/off values for the heat pumps and for the heating elements from the "district controller", as input for its calculation. The resulting electric power consumptions of the buildings are sent to the "power grid simulation" component, whereas mass flow and temperature results are sent to the previously described "thermal grid simulation" component (see Figure 3).

3.4. GRID- AND DISTRICT CONTROLLER

The co-simulation includes two controller algorithms; the "District controller" emulates decisions from the foreseen district energy management, whereas the "Grid controller" emulates the DSO's actions, as shown in Figure 3. During the creation of this paper, the "District controller" algorithm is still under development; a first prototype is shown in chapter 4 below. In this work, the "Grid controller" has a straightforward decision logic: When the active power consumption at the HV/MV-transformer reaches a pre-set threshold, the heat elements and heat pumps in the district receive an "off" signal. In this condition the district buildings are only supplied by the DHG. In all other cases, a permanent "on" signal is sent to the heating elements and heat pumps. Hence, the "District controller" will encompass market-based decisions and possibly, planned congestion time windows from the DSO, whereas the "Grid controller" would only become active when unwanted load peaks occur at the substation to the HV-grid. The reason for the latter decision logic is, that the HV-grid is operated by another DSO and increased power consumption into the MV grid is costly.

3.5. RESULTS OF THE CO-SIMULATION

Figure 4 shows the active power consumption at the HV/MV-transformer in the electricity network, with and without the Grid control algorithm (the latter being the "base case"). Whenever this consumption exceeds a threshold (in this case, an

arbitrary value of 12,7 MW was chosen), the "Grid control" algorithm sends an "off" signal to all heat elements and heat pumps in the district "building simulation". This reduces the power flow along the MV-feeder and causes a small (but noticeable) reduction of active power at the HV/MV-transformer. Even though the active power consumption cannot be brought below its threshold, it demonstrates that the modeled smart district can support its electricity network through flexible load shifts. Figure 5 (a) shows the difference between the two power curves from Figure 4, to study this effect in more detail. As expected, the activation of the grid controller reduces the power flow by about 150 kW, corresponding to 30 heat elements and heat pumps in 25 district buildings, with an average electric power around 5 kW. A rebound effect can be seen after the Grid control's active period ends: the power difference becomes positive, meaning that after they are switched back on, some heat pumps and heat elements compensate for the power they did not provide during the "off" period. Figure 5 (b) shows the heat demand P[kW] supplied by the DHG over the same modeled time period. The first demand peaks in the early morning hours are equal for the simulation with and without Grid Controller. In this time frame the Grid controller is not intervening and the heat demand in the district cannot be fully covered by the other heat sources and requires heat supply by the DHG, which leads to peaks independent from whether the Grid controller is active. In the following time periods a substantial difference in heat extraction between the simulation with and without Grid controller can be seen. A shutdown of heating elements results in a shift of heat consumption from the heating elements to the DHG and thus in higher peaks of extracted heat.

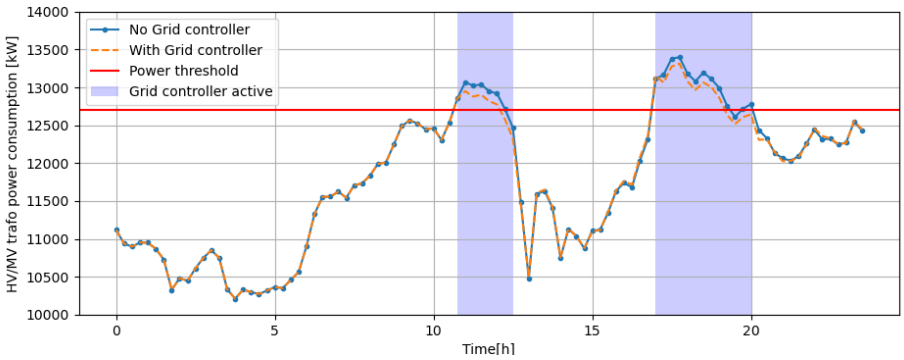

Figure 4. Change of active power flow at HV/MV trafo in the electricity network, due to actions of the Grid Controller "DSO".

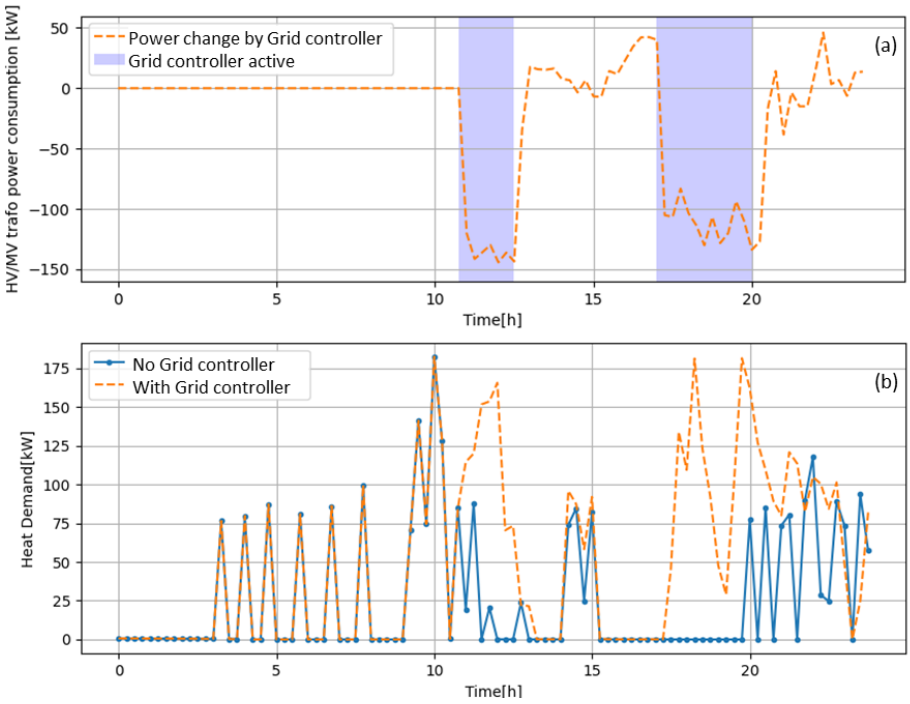

Figure 5. Effect of the Grid Controller "DSO" on the district building power consumption in (a) the electricity network and (b) the thermal grid.

These results show the interplay and tradeoff between using flexibility between the electric and thermal district grid: a load reduction in the electricity network causes additional load in the thermal grid, hence, relieving one network causes additional stress in the other. This motivates the development of smart district control strategies, explained in the following chapter 4, which consider the most cost-efficient tradeoff when possible.

4. OPERATING STRATEGY

4.1. CONCEPT OF A DISTRICT CONTROLLER

The purpose of this chapter is to explain why it makes sense to use a district controller when implementing neighborhood concepts regarding sector coupling. The background to this is the barriers that arise when several actors want to implement a HES together. These barriers arise because, in practice, the actors still operate very much separately from one another and, accordingly, their economic goals are also aligned with the respective sector. The actors (using Germany as an example) involved in most HES are listed below:

DSO: Has the goal that the energy should remain in the neighborhood, i.e., back feeding should be avoided and the demand peaks should be reduced. In the long term, this reduces the pipe diameter and thus the investment costs.

Heat Producer and Heat Grid Operator: Have the goal of a full supply of heat to the buildings, so they want to supply as much heat as possible to the district and as efficient as possible. For them, only the heat price of an economical energy production of the own plants is of interest. No consideration of the decentralized generation.

Electricity Supplier: Has the goal of selling as much electricity as possible to the neighborhood. For the electricity supplier, only the electricity price counts to ensure economic electricity marketing. He would like to achieve economies of scale and quantity in energy trading. No interest in purchasing heat from the DHG but would consider operating the decentralized PtH plants.

Consumer: Would like to be always supplied with heat and electricity at the lowest possible price.

It is therefore consequent to say that there must be one actor, the "district supplier", who considers the goals of all mentioned actors and optimizes the central as well as the decentralized energy portfolio. In each situation, he decides on the energy supply in the district based on a detailed economic analysis and ensures the most favorable possible full supply of electricity and heat to the buildings. To fulfill this task, the district supplier needs a suitable tool, accordingly, the district controller should be mentioned here. The role of the district supplier can in turn be assigned to the local energy supplier, the public utility. Figure 6 shows the concept of the district controller from the perspective of a public utility.

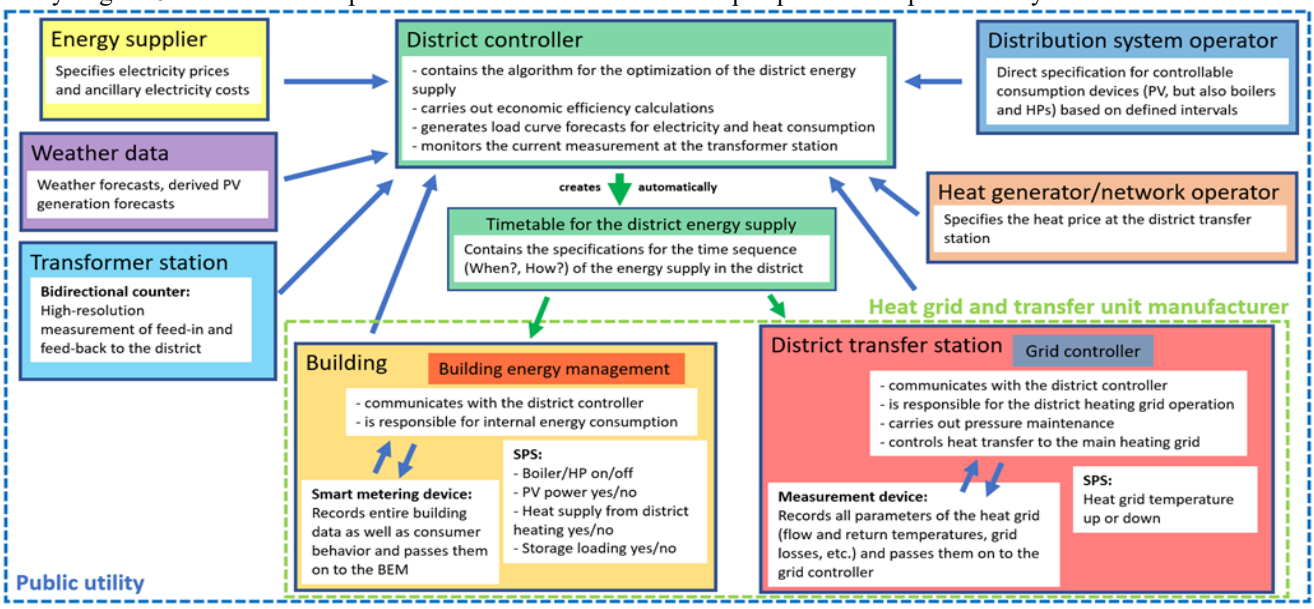

Figure 6. Concept of the district controller with all participants

The district controller can be located, for example, in the control room of the public utility and represents the central control unit of the district. The district controller receives all information and data that arise in its control area and essentially contains an optimization algorithm, which is described in more detail in the following chapter.

4.2. DEVELOPMENT OF AN ALGORITHM

To obtain the optimal solution to the question when to use which type of energy while satisfying the demand and minimizing the costs, mixed-integer linear programs (MILP) are commonly used [12]. The problem at hand exists of three fixed time series: The power and heat demand and the PV production. Each house has a battery, a thermal energy storage (TES) and a heat pump or a heating element. The MILP is used to calculate optimal values for all connections between these components (see Figure 7) For the MILP problem the objective function consists of three parts, as in Equation (1):

$$Cost_{total} = \min_{\forall t} \sum C_{elec} * P_{buy} - C_{sell} * P_{sell} + C_{Heat} * P_{heat} \quad (1)$$

These three parts are the price for purchasing electricity, the price for selling electricity and the price for obtaining heat for every time step. Currently modelled in detail, as in Equation (2):

$$C_{total} = \min_{\forall t} \sum C_{elec}\left(P_{stor} + P_{demand,el} + P_{Heater} + P_{HP}\right) - C_{sell}\left(P_{PV} + P_{stor}\right) + C_{Heat} * P_{demand,heat} \quad (2)$$

The TES is implemented as a capacity model with homogeneously distributed temperature as in [12]. The battery is implemented with losses for charging/discharging and self-discharge. Upper bounds for the charging/discharging current are also applied [13]. As in this example the heat pump cannot be regulated and is only able to produce water up to 70˚C, it is simply a fixed efficiency-factor for the electric energy flowing to the TES [14]. Additionally, some extra rules are applied, like that the heat pump must be switched on for at least 30 minutes to extend the durability.

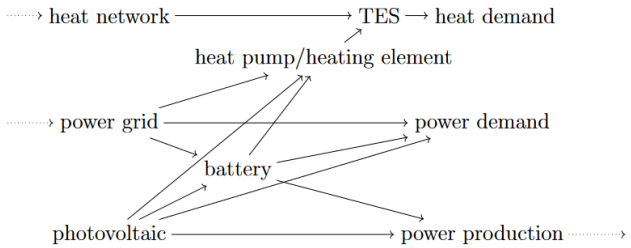

Figure 7. Shows the components and the optimized connections of the MILP. The flow through the dotted lines is minimized after multiplying with the corresponding energy prices.

Right now, the algorithm is only capable to optimize single houses and not yet the whole district. The result of such an optimization for a single-family house with an auxiliary heater is shown in Figure 8. In the upper graph the electricity demand is plotted along with how it is satisfied. For the PV revenue, is in the second graph shown how it's optimally used. The third and fourth graph shows the state of the energy storages: On the left you see how much energy is stored (positive values) or requested (negative values), on the right you see the state of charge or the temperature. The last two graphs show the energy purchased from the energy grids. Looking at the second plot, it is visible that as soon the power demand is satisfied (light blue), power is used to charge the storages (green and purple) and the remaining part sold (orange). The main part of the heat demand is satisfied using the energy from the heat network and only remaining power from the PV is used to heat up the storage.

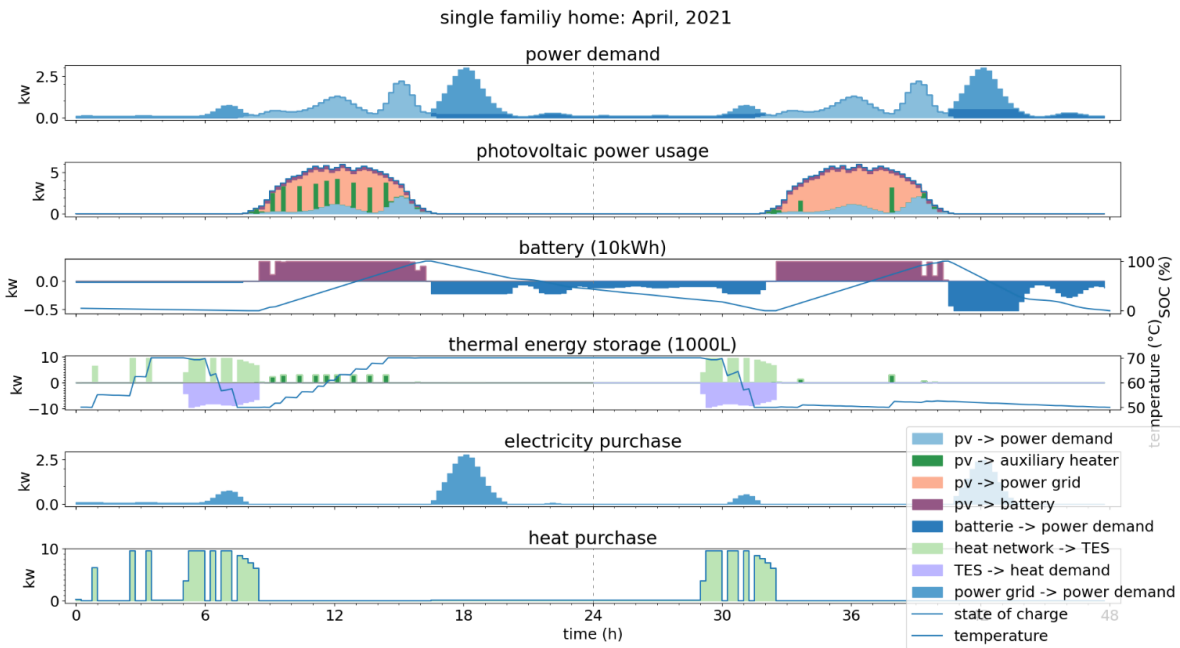

Figure 8. Optimization results: Although the optimization is only requested for one day, it is calculated on two times the same day to avoid the situation that the storages are emptied by the end of the first day. Caused by the cost-function an optimization usually ends with empty storages.

5. CONCLUSION

The hybrid network structure implemented in the district requires an optimized operation strategy. Due to the combined heat supply of the buildings by DHG and sector coupling technologies, the heat demand of the buildings is reflected in both the electricity and the heating sector. The co-simulation shows that flexible load shifting in the new housing district has a positive effect on the utilization of transformers in the electricity grid. A power grid overload can be counteracted by switching off

the sector coupling technologies in an electric grid-oriented manner. Furthermore, the shutdown of the coupling technologies results in a load shift from the electricity grid to higher peak loads in the DHG. The load shift within the hybrid network structure leads to an interplay in which reduction of the load in one sector leads to more stress in the other. An optimized operation strategy can reduce the respective load peaks in the whole.

Stakeholders associated with energy supply and consumption in a district have conflicting interests. This results in the position of a district supplier, who takes over the neighborhood supply of electricity and heat at the same time. In this way, the interest of an overall cost-efficient energy supply is ensured. The tool of a district supplier is the district controller, which minimizes the costs of energy supply by taking multiple information into account.

6. OUTLOOK

The investigation has shown that the application of flexible load shifting in one district has little effect on higher voltage levels. Scaling up the results to other parts of the city can show at what point significant effects on the higher voltage levels start to occur. An implementation of transient modeling, regarding the DHG model in panda pipes, is currently in development and will be implemented in the simulation. Future scope also includes a comparison and validation between the CARNOT and pandapipes models. By simulating different type days or longer periods of the DHG models, further conclusions about effects on heat losses in the DHG can be made.

The additional installation of decentralized coupling technologies in combination with PV modules has the potential to decarbonize the heat supply, especially in existing DHG. The practical implementation of such a supply solution depends to a large extent on economic conditions. In the further course of the research project, a result is reached on whether advantages can be achieved in terms of economy and energy efficiency.

ACKNOWLEDGEMENT

The results presented in the paper are part of the national research project “EnEff:Wärme: HybridBOT_FW” funded by the Federal Ministry for Economic Affairs and Climate Action based on a resolution of the German Bundestag (FKZ: 03EN3041). The authors responsible for the content of this paper highly acknowledge received funding.

REFERENCES

[1] Graichen, Patrick, Peter, Frank und Litz, Philipp. Das Klimaschutzziele von - 40 Prozent bis 2020: Wo landen wir ohne weitere Maßnahmen? Berlin, Germany: Agora Energiewende, 2017.
[2] Bundesverband der Energie- und Wasserwirtschaft e.V. BDEW. Entwicklung des Wärmeverbrauchs in Deutschland – Basisdaten und Einflussfaktoren. Berlin, Germany: BDEW, 2022.
[3] AGFW - Der Energieeffizienzverband für Wärme, Kälte und KWK e. V. AGFW-Hauptbericht 2021. Frankfurt am Main, Germany: AGFW, 2022.
[4] Cadenbach, Anna, et al. Neubau und Transformation hocheffizienter Wärmenetze im Kontext der Dekarbonisierung und Flexibilisierung unserer Energiesysteme. Berlin, Germany: FVEE, 2022.
[5] Projektträger Jülich; BMWK. Enargus, https://www.enargus.de/detail/?id=3799940; 2021. [Access 12. June 2023].
[6] AGFW. HybridBOT_FW. https://www.agfw.de/forschung/hybridbot; 2022 [Access 22. May 2023].
[7] AGFW, BBH Consulting AG, ENERPIPE GmbH, Fraunhofer IEE, IKEM, Stadtwerke Neuburg a. d. Donau. EnEff:Wärme:HybridBOT_FW - Transformation of the urban district heating supply, Key definitions of the project. Frankfurt on the Main, Germany : AGFW, 2022.
[8] OpSim: test- and simulation-environment for grid control and aggregation strategies, http://opsim.net/en; 2023. [Access 1. June 2023].
[9] MATLAB. Version 9.11.0.1809720 (R2021b) Update 1. Natick, USA : The MathWorks Inc., 2021.
[10] Thurner, Leon, et al. pandapower - an Open Source Python Tool for Convenient Modeling, Analysis and Optimization of Electric Power Systems 2018; Bd. 33.
[11] pandapipes: An easy to use open source tool for fluid system modeling, analysis and optimization with a high degree of automation, https://www.pandapipes.org; 2023. [Access 10. May 2023].
[12] Schütz, Thomas, Streblow, Rita und Müller, Dirk. A comparison of thermal energy storage models for building energy system optimization 2015; Bd. 93, S. 23-31.
[13] Liu, Chunyang, et al. A MILP-Based Battery Degradation Model for Economic Scheduling of Power System 2023; Bd. 14.
[14] Krützfeldt, Hannah, et al. MILP design optimization of heat pump systems in German residential buildings 2021; Bd. 249.
[15] Forschungszentrum Jülich GmbH. CARNOT Toolbox. Jülich, Germany: Fachhochschule Aachen, Solarinstitut Jülich, 2021.

Research on the Low-carbon Transformation Path of Inner Mongolia Rural House Heating System

Xinyang Li *, Chunlin Wang , Yuhang Jiang

Chifeng Academy, Chifeng Inner Mongolia, 024000, China

ABSTRACT

With the increasing demand for a better life, the requirements for indoor thermal environment are gradually increasing. Improving the winter thermal environment of rural houses in northern China has become an important issue in the field of building energy conservation. Research on the application of "active+passive" clean heating technology has significant potential. It not only contains indoor heating demand and the comprehensive utilization of renewable energy, but also provides technical support for exploring the transformation path of rural residential carbon reduction, promoting rural construction, accelerating the low-carbon transformation of rural energy, and assisting rural revitalization. This paper carried out from three aspects: investigating residents' thermal habits, conducting environmental parameter testing, assisting infrared temperature measurement technology to analyze the energy saving potential of typical residential buildings, and exploring key indicators that affect the carbon reduction transformation of typical agricultural houses in Inner Mongolia; Couple measured data and calculation models to analyze the optimal scheme of active and passive combined heating and system operation adjustment strategy; Through the method of multi-objective optimization, a technical path for achieving low-carbon reconstruction of buildings that combines carbon emissions and economic indicators is proposed. The research results of the project will improve the thermal environment of rural residential buildings, accelerate the application process of renewable energy heating, and have important significance for energy conservation and carbon reduction of rural residential buildings.

Keywords: Rural house; Indoor thermal environment; Renewable energy; Heating system

1. INTRODUCTION

With the continuous development of China's economy, the form of energy is becoming increasingly severe. As the world's largest energy consumer, our per capita energy consumption is only one-third of that of developed countries, and our future energy demand will increase significantly. Therefore, it is urgent to save energy and improve energy efficiency. In the northeast and other cold areas heating cycle is long, the vast number of rural and pastoral areas heating demand is also very large, while agricultural and pastoral areas heating is still mostly coal-fired, coupled with rural heating methods are relatively backward, resulting in lower energy efficiency. The 20th National Congress of the Communist Party of China clearly pointed out the need to "promote green development and accelerate the green

transformation of development mode". There are plans to implement the carbon peaking action step by step, further promote the energy revolution, strengthen the clean and efficient use of coal, accelerate the planning and construction of a new energy system, and actively participate in the global governance in response to climate change.

Since China has clearly stipulated the goal of "striving to peak carbon dioxide emissions before 2030 and achieve carbon neutrality before 2060", it has become an inevitable trend for the energy model to shift to a green and low-carbon model. Guided by the concept of sustainable development, this paper aims to promote the construction of a moderately prosperous society in agricultural and pastoral areas of Inner Mongolia, and with the support of the theoretical system of green building, this paper conducts research on low-energy residential building mode for rural areas with the weakest building energy efficiency in Inner Mongolia, which is in line with China's energy development strategy and the concept of green development strongly advocated.

At present, most of the problems related to rural heating are research on the current situation of energy consumption and research on the form and equipment of heating systems. Because the demand habits of heat users in agricultural and pastoral areas are different from urban heating, the heating system is relatively independent, and it is always difficult to obtain first-hand information on the heat demand statistics in agricultural and pastoral buildings. At the same time, the habits of opening windows and doors in buildings cannot be analyzed, and data can usually only be obtained in the form of survey interviews, which is costly and difficult to collect. Therefore, through field research, computer simulation analysis, theoretical calculation, on-site measurement and other research methods, this paper conducts research on a series of key issues affecting the heating energy consumption and thermal comfort of rural residential buildings, and analyzes the improvement of clean heating on rural houses.

2. INVESTIGATION ON THE GENERAL SITUATION OF TYPICAL RURAL BUILDINGS IN INNER MONGOLIA AND THE CHARACTERISTICS OF WINTER HEATING ENERGY

The selected area of typical farmhouses is a farmhouse in Wengniuteqi, Chifeng City, built in 2003, with no other houses close to it, and independent courtyards. In terms of exterior, the farmhouse uses 37 brick walls plus 50 mm expanded polyphenylene board for insulation. There are 10 rooms including bedroom 1, bedroom 2, bedroom 3, kitchen, living room, dining room, bathroom, toilet, sun room 1 and sun room 2. The room area is 130.575 m2 and the heating area is 130.575 m2. The permanent household size is 4 people, 1 elderly person lives in 2 bedrooms all year round, 2 adults go out to work and do not often stay at home, and 1 young person goes to school and does not often stay at home. The exterior windows are double-layer plastic steel windows. Construction of the Sun Room in early 2023. The detailed table is shown in Table 1, and the floor plan and the official plan of the farm house are shown in Figures 1 and 2. The typical heating period of a farm house is from October 15 to April 15 of the following year, and the main heating method is to heat the kang and earth heating together, using lump coal as heating material, and the price is between 1100-1300 yuan. The annual coal consumption is about 5 tons.

Figure1 Front view of the farmhouse

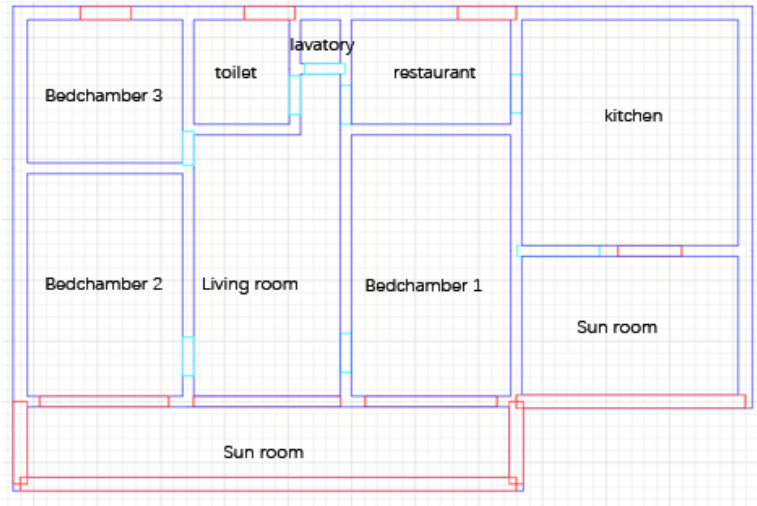

Figure2 Floor plan of the farmhouse

Table 1 Basic information about farmhouses

East-west length	North-south length	Facades	Interior walls	Not near the exterior windows of the sun room
14.25m	8m	8mm plastering + 50mm expanded polystyrene board + 370mm clay solid brick + 8mm plastering + 7mm wall panel	8mm plastering + 120mm clay solid brick + 8mm plastering + 7mm wall panel	Double glazed windows, made of plastic steel, 1.2m high and 0.9m above the ground,

Table2 Basic information on farmhouses

Close to the sun room exterior window	Sun room roof	Room roof	Exterior doors	Sun room glass
Double glazed window, material is plastic steel, height is 2.1m, height is 0.4m,	Single slope color steel roof, ceiling material 10mm PVC board	Double slope tile roof, 60% slope, horizontal distance 4 meters, elevation difference 2.4m	It is an aluminum alloy frame glass exterior door, 2.1m high and 2m wide	Three-layer glass windows, the material is aluminum alloy

3 MEASURED DATA AND SIMULATION ANALYSIS OF TYPICAL FARMHOUSES

3.1 Instrument distribution location

The green dot represents the position of the thermograph, the red dot represents the position of the heat flux densitometer, and the blue dot represents the position of the CO2 autographer.

1. Indoor temperature

Master bedroom, second bedroom, kitchen. The living room, bathroom, and boiler room are each arranged, and the change of indoor temperature in each room is tested, and the recording time is 4 days.

2. Heat transfer coefficient of the envelope

The measurement of the envelope mainly includes: internal wall, inner door, roof, ground 3 items, heat flux density meter arrangement for internal wall, inner door, roof, ground 4 items. The location is shown below.

3. Dots in the sun

Because the depth of the sunlight room is not very large, there is no need to consider the longitudinal temperature fluctuation, but the length of the bay is still very long, so it is necessary to arrange three points to record the temperature change, and then the second is to record the temperature change inside and outside the wall of the sun room. and temperature changes on the outside of the sun room on three sides of the glass and the roof and ground. (Green represents a thermometer arranged on the surface, yellow represents a thermometer arranged on the ground, and orange represents a thermometer arranged on the roof, one on the ground and two on the roof). As shown in Figure 3 below:

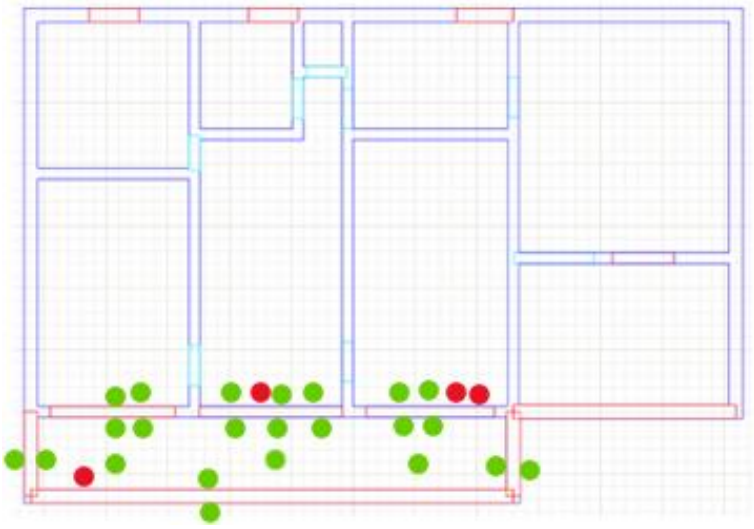

Figure 3. Location of sunlight dots

4. CO2 self-recorder placement

Place it in the center of the house, record the amount of cold air penetration in the room and the sunlight room.

5. Outdoor temperature measurement

A temperature self-recorder is arranged outdoors to record the change of outdoor temperature within 4 days.

3.2 Analysis of room temperature in a typical farmhouse

The fluctuation chart of each room is shown in Figure 4, as can be seen from the figure, except for the sun room, the temperature fluctuation of each room is relatively small, and most of the time is at 18 °

C, but the indoor temperature fluctuation of the sunlight room is more severe, which is due to the characteristics of the sunlight room, and the outdoor temperature fluctuation within 4 days of measurement is large, and the outdoor temperature change is also roughly in line with the outdoor temperature change in Wutun Taohai Town. Therefore, according to the change of the indoor temperature of the room, the indoor temperature can be taken at 18 ° C during the simulation to a large extent to replace the indoor temperature change of the room, and it can be seen that the maximum temperature is reached from 3 pm to 5 pm every day, because bedroom 1, living room, bedroom 2 are close to the solar room, so the amplitude of temperature fluctuations is roughly consistent with the amplitude of solar room fluctuations, and the delay is about 1 hour. And because the dining room, bedroom 3, toilet, and bathroom are close to bedroom 1, living room, and bedroom 2, the temperature fluctuation is delayed by about an hour, but the amplitude is consistent with the fluctuation between the sun.

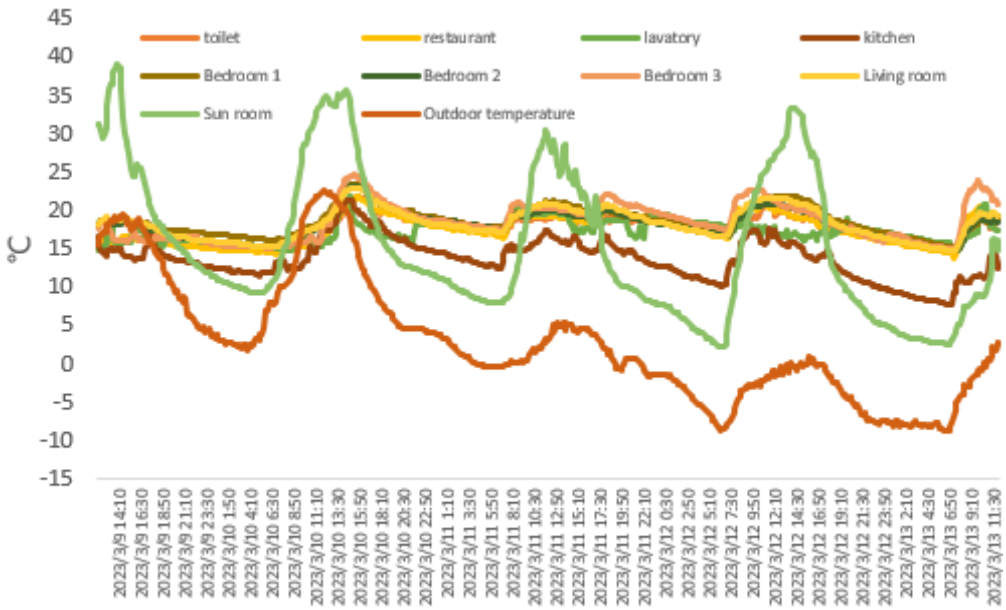

Figure 4. Table of indoor temperature changes in farmhouses

3.2.1 Thermal environment assessment of typical farmhouses

According to the thermal comfort calculation tool (ASHRAE-55), the PMV-PPD value of each room of a typical farm house can be known, and it can be known that except for the heat feeling in bedroom 1 of a typical farm house, people in other rooms will have a cold sensation such as cold, slightly cold, cool, and slightly cooler. It can be seen that the comfort of the rooms in a typical farmhouse is poor. According to the indoor thermal and humid environment evaluation standard of civil buildings (GB/T 50785-2012), the thermal environment rating of the room is carried out. The rating levels are shown in Table 3 below

Table3. APMV evaluation indicators

grade	Evaluation indicator APMV
Class I	-0.5⩽APMV⩾0.5
Class II	-1⩽APMV<-0.5 or 0.5<APMV⩽1
Grade III	APMV<-1 or APMV>1

The thermal sensation of a typical farmhouse is rated according to the APMV evaluation index table, as shown in Table 4 below:

Table4 Thermal environment assessment table of farmhouses

name	Average outdoor temperature (6 am)	Average temperature	Average humidity	Metabolic rate	Garment thermal resistance	PMV	PPD	Hot feeling	grade
Bedroom 1	-2.5	18.7	37.9	1.6	0.9	-0.06	5%	neuter	Class I
Bedroom 2	-2.5	18.1	37.9	0.7	0.9	-3.57	100 %	cold	Grade III
Bedroom 3	-2.5	18.6	37.9	1.1	0.9	-1.22	36%	Slightly cooler	Grade III
Living room	-2.5	18.3	39.2	1.2	0.9	-2.26	87%	cold	Grade III
kitchen	-2.5	13.7	32.0	1.2	0.9	-1.99	76%	cool	Grade III
lavatory	-2.5	17.3	38.2	1.2	0.9	-2.58	95%	cold	Grade III
toilet	-2.5	17.5	41.3	1.2	0.9	-2.5	93%	cold	Grade III
restaurant	-2.5	17.5	35.2	1.2	0.9	-2.54	94%	cold	Grade III

3.3 Heat load of a typical farm house envelope

3.3.1 Heat transfer coefficient

Since the heat flux density value and the temperature difference between the inside and outside of the envelope have been measured, the heat transfer formula is as follows, and the calculation formula of the heat transfer coefficient inside the envelope is as follows:λ

$$\lambda = \frac{q\delta}{(t_i - t_e)} \tag{3.1}$$

In the formula:

λ: Internal heat transfer coefficient of the envelope;

δ: Wall thickness, mm;

t_i: Temperature of the inner surface of the envelope, K;

t_e: Temperature of the outer surface of the envelope, K.

The heat transfer coefficient of the inner surface of the envelope is calculated as follows:

$$h_1 = \frac{q}{(t_n - t_i)} \tag{3.2}$$

In the formula:

h_1: Heat transfer coefficient of the inner surface of the envelope;

t_n: Room room temperature, K;

q: Heat flux density value, W/m2.

The heat transfer coefficient of the outer surface of the envelope is calculated as follows:

$$h_2 = \frac{q}{(t_e - t_w)} \tag{3.3}$$

In the formula:

t_w: Outdoor air temperature, k.

$$\mathrm{K} = \frac{1}{\frac{1}{h_1} + \frac{\delta}{\lambda} + \frac{1}{h_2}} \tag{3.4}$$

In the formula:

K: Heat transfer coefficient of the envelope, W/(m2•K).

The calculation results are shown in Table 5 below:

Table 5. Heat transfer coefficient of each enclosure

name	Heat transfer coefficient (W/(m2•k)
Facades	0.51
Exterior windows	3.11
Interior walls	1.53
Main room roof	0.27
Sun room roof	0.58
Sun glassSun glass	0.66
door	0.60
ground	0.47

3.3.2 Number of air changes

Since changes in CO2 concentration have been measured in the room. Average is obtained based on area weighting. The core of the analysis of room CO2 is that the gas satisfies the law of conservation of mass. The formula is as follows:

$$V[C_{in}(k) - C_{in}(k-1)] = \Delta\tau Q[C_{out} - C_{in}(k-1)] + \Delta\tau FR \tag{3.5}$$

In the formula:

C_{in}: CO2 concentration, ml/m3;

C_{out}: Outdoor CO2 concentration, ml/m3;

Q: Ventilation capacity, m3/s; $\tau$for time, s;

FR: CO2 release from personnel, ml/s;

V: Room volume, m3.

During the test, the outdoor CO2 concentration can be considered stable, and the measurement results are converted to about 300 ppm.

The number of air changes n is:

$$\mathrm{n} = \frac{Q}{V} \tag{3.6}$$

It can be calculated by the formula, and the number of air changes is 0.55 times/h.

3.3.3 Thermal load analysis of typical farm house envelope

The heat load of the terminal building is determined by the heat gain and loss of the building. However, when maintaining the temperature of the room, it can be approximately considered that the heat gain and heat loss are equal, so this paper uses the heat loss of the building load as the heat load of the envelope.

The heat loss of the envelope mainly includes: 1. Heat transfer and heat dissipation of the envelope;

$Q_1$2. Heating infiltrates cold air from the gap between doors and windows to the room to consume heat, which is called cold air penetration heat consumption; 3. Heating consumes heat fromQ_2 doors, holes and invading cold air adjacent to the roomQ_3 , called cold air intrusion heat consumption. In summary, the hourly load of each room in a typical farm house is statistically shown in Figure 5. Comparing the load data of each room, it can be found that the heat dissipation of the sunlight room is positive at all times, which is due to the architectural characteristics of its sunlight room, its room temperature is very high, much higher than the room temperature of the adjacent room, so it needs to transfer heat to other rooms, and the heat transfer reaches the highest value at about 2 pm. And because bedroom 1, living room, bedroom 2 are close to bedroom 3, bathroom, toilet, dining room, they will also be affected, obviously and the impact amplitude is less than the load of the room next to the sun.

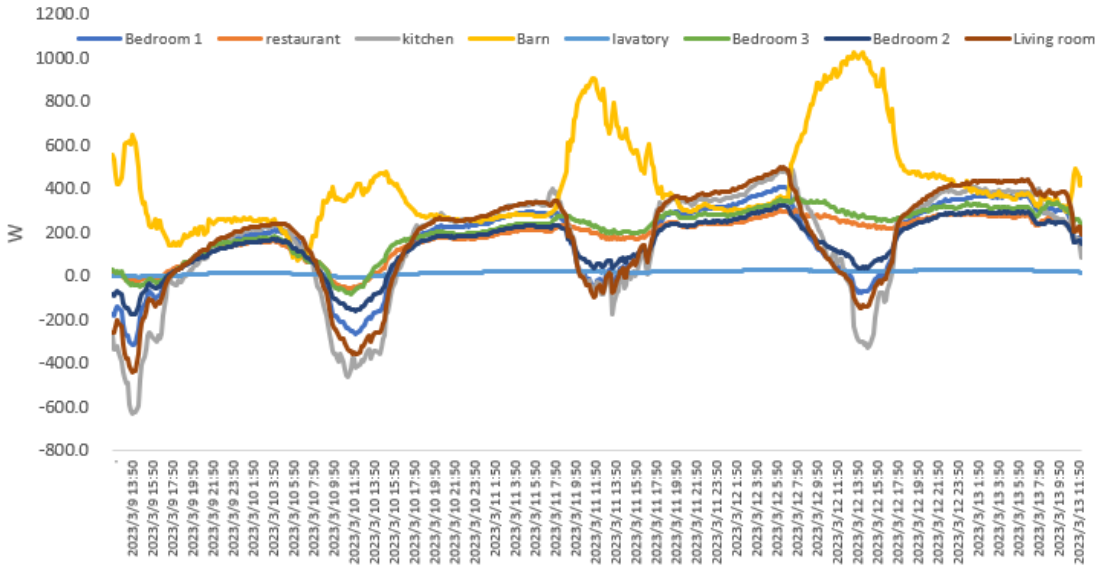

Figure 5. Changes in load in each room

It can be seen from Figure 9 that the load change between the sunlight is the most obvious, compared with the impact of the sun room on other rooms in the figure below, you can know that the impact of the sun room on the room load, the other heat dissipation of the room is almost unchanged can be regarded as a fixed value, so it can be known that the load change of the room is mainly affected by the heat dissipation in the sunlight.

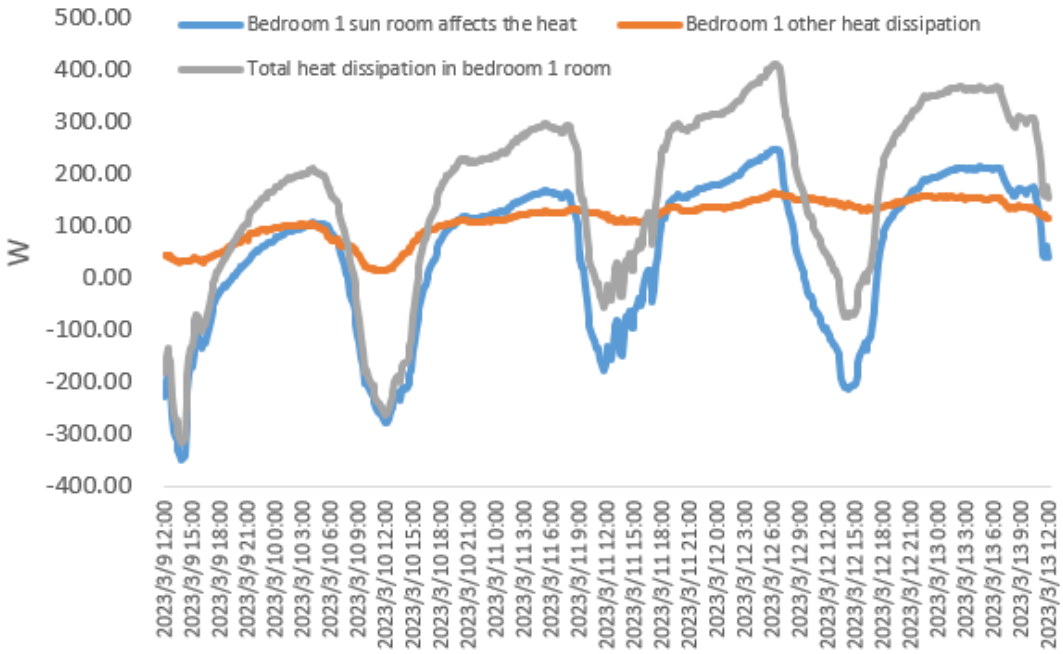

Figure 6. Bedroom 1 is affected by the load of the sunlight room

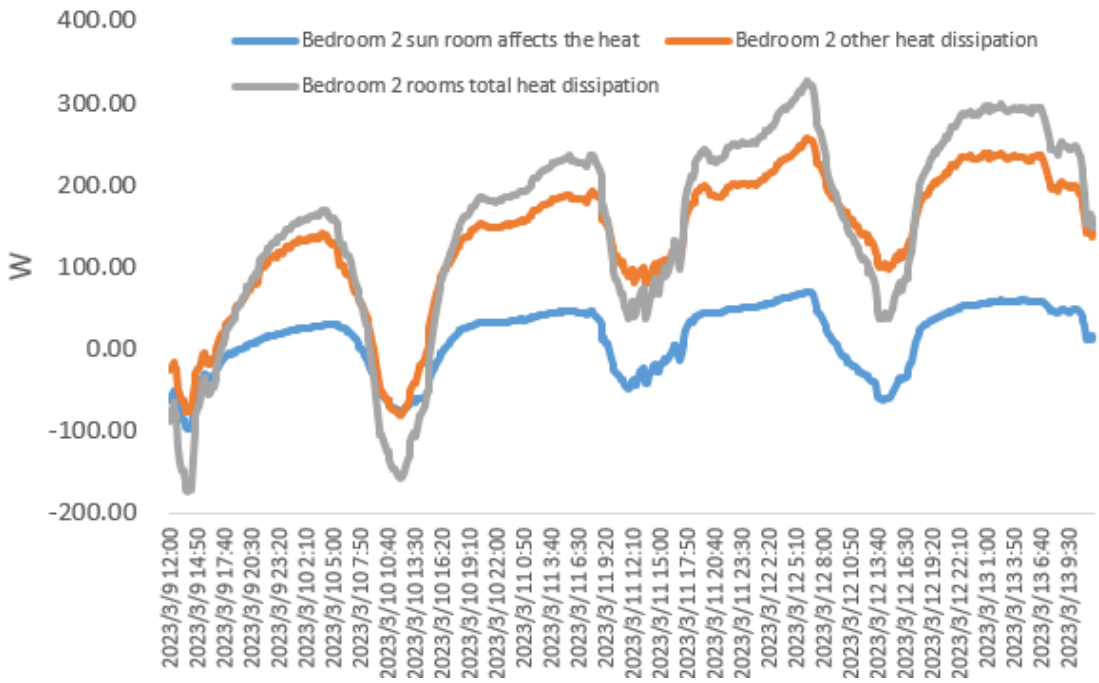

Figure 7. Bedroom 2 is affected by the load of sunlight

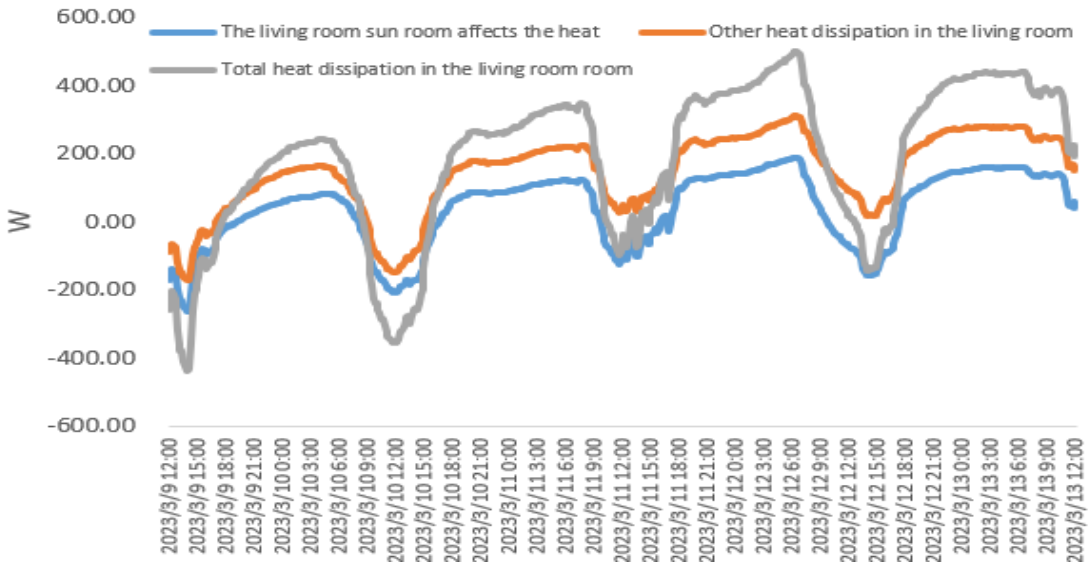

Figure 8. Living room affected by the load of sunlight

According to the above analysis, the room is mainly affected by the sun room load, so it is necessary to analyze the impact of the sun room load on the room, the impact of bedroom 1 is shown in the following table, it can be seen that on March 9, the total heat dissipation of the sun room is greater than the heat absorption of the sun room in a day of bedroom 1, bedroom 2, living room, so it can be judged that on March 9, the sun room can be used as a room heat source, providing 5480.9 W, 1516.4 W, 3910.5 W heat for the room respectively, However, in the following days, due to the low outdoor temperature, the heat dissipation of the room by the sun room is much smaller than the load of the room, so that the sunlight room cannot be used as a heat source to provide heat for the room, and heating equipment is still needed to heat the room. The specific values are shown in the following table:

Table6. Bedroom 1: Variation in solar room load

Time	2023/3/9	2023/3/10	2023/3/11	2023/3/12
Sunlight absorbs heat	5233.00	12485.40	16546.48	18901.85
Heat dissipation between sunlight	10713.95	6447.20	3346.22	4930.17

Table7. Bedroom 2 is affected by the load of the sun room

Time	2023/3/9	2023/3/10	2023/3/11	2023/3/12
Sunlight absorbs heat	1451.07	3469.28	4604.82	5242.97
Heat dissipation between sunlight	2967.49	1800.46	935.89	1409.82

Table8 Living room affected by the load of the sun room

Time	2023/3/9	2023/3/10	2023/3/11	2023/3/12
Sunlight absorbs heat	4019.58	9153.78	12976.84	14581.47
Heat dissipation between sunlight	7930.08	4893.10	2183.80	3514.86

Through the analysis of the above typical building loads, it can be known that the room is greatly affected by the sun room, and to a certain extent, even the sun room can be used as a heat source for the house instead of traditional heating. However, the specific extent of the room affected by the solar room load and the clean heating renovation still need to be simulated by TRNSYS, as shown in the following

section.

3.4 TRNSYS simulation of a typical farmhouse

3.4.1 Sketch up modeling of a typical farmhouse

Sketch up modeling can be imported into the TRNSYS 3D plug-in to generate a simulation system, which can be adjusted to achieve TRNSY simulation of rural houses. After Sketch up is imported by the TRNSYS 3D plug-in, first draw the zone, that is, the building hot area, according to the floor plan of a typical farmer, build a model according to the size of the measured room and the position of doors and windows, etc., set the height of the 2nd floor of the warehouse to 2.9 m, in addition to the floor height of other rooms 3 m, bedroom 1, bedroom 2 window height 2.1 m, The remaining rooms have windows 1.2 m high, outer doors 2 m wide and 2 m high, inner doors 2 m high and 0.8 m wide. Figure 9 below:

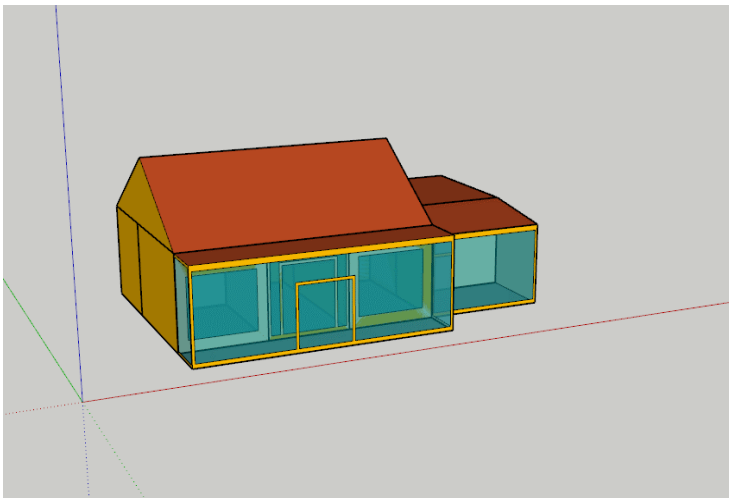

Figure 9. Sketch up modeling

3.4.2 METEONORM weather files

METEONORM is a global meteorological calculation software and database for solar energy and applied meteorology established by the Swiss Federal Ministry of Energy. After entering the latitude and longitude of the location of a typical farmhouse, the program will simulate the month, day and hour weather data in the specified area through relevant calculation rules and plug-ins based on the meteorological data in the area. The software will produce a suffix TM2, which has a typical meteorological annual file. and use it as a TRNSYS weather module reference file when calculating building loads.

3.4.3 TRNSYS simulation module settings

The diagram of a typical farmer's TRNSYS simulation system is shown in Figure 10 below, and the module model and function description are shown in Table 9 below:

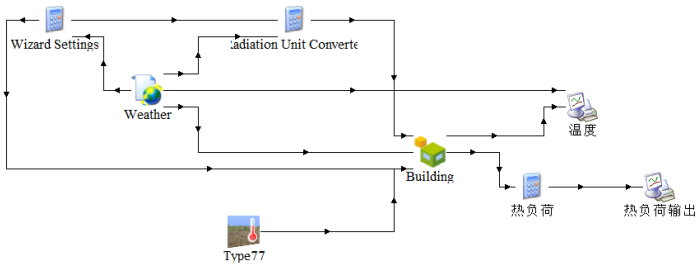

Figure 10. A typical TRNSYS farmhouse

Table9 TRNSYS modules

Module model	Feature description
Type109-TMY2	Associate a weather data file and read weather data from the file
Type65c	It is mainly used for graphics rendering to output data online.
equation	Implement variable data calculation between modules
Type77	Simulate soil temperature

After setting the parameters, running TRNSYS yields the annual load change of a typical farm house as shown in Figure 11. It can be seen that the maximum heat load in a typical farm area is 3.44 kW, which occurs in the 8433rd hour, and the cumulative heat dissipation of the building during the heating period is 4746.03 kWh. (In the figure, positive values are heating loads, negative values are cooling loads).

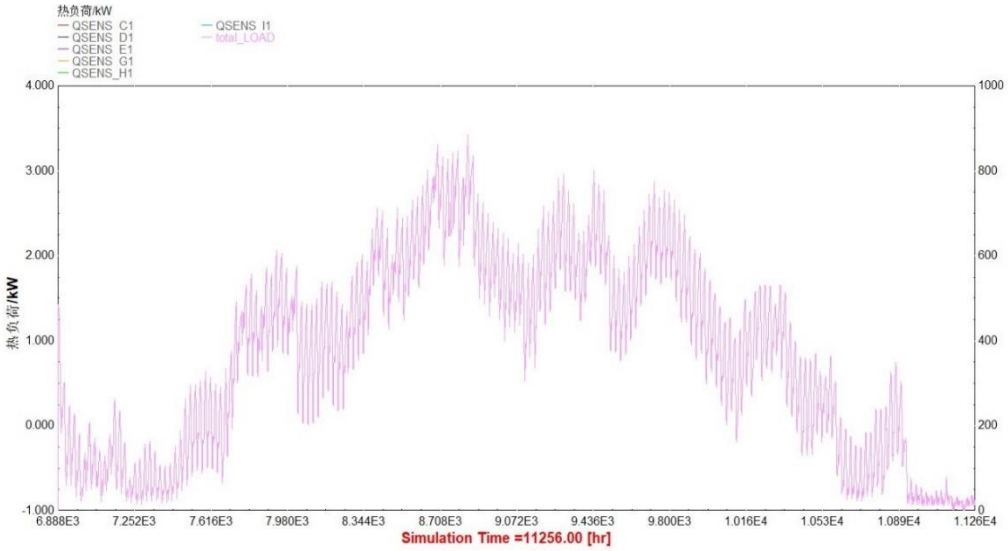

Figure 11. TRNSYS load simulation

3.5 Typical Building DeST Simulation

3.5.1 DeST modeling

The DeST model is drawn according to the floor plan of a typical building, and the renderings are shown in Figure 12 below. Due to the setting of the DeST system, the air conditioning system is used as the radiator to maintain the required temperature in each room. The simulated time is the same as the TRNSYS time.

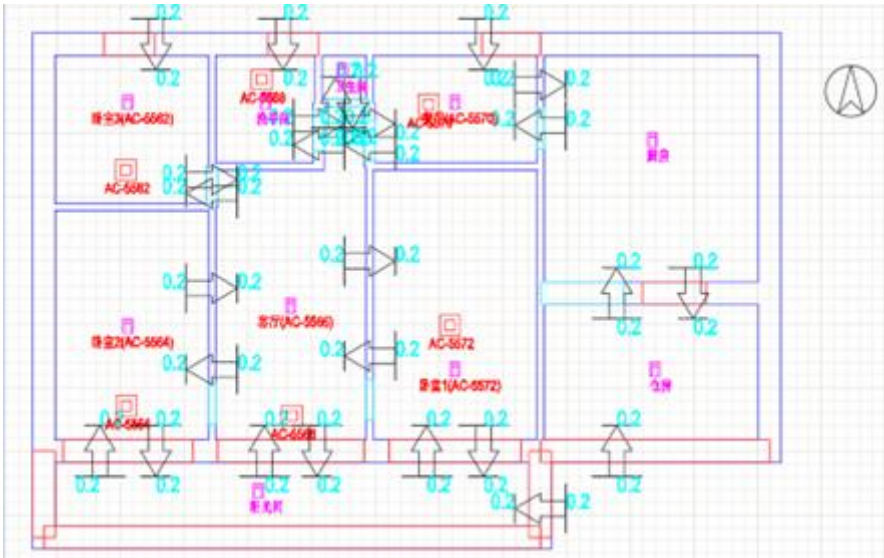

Figure 12 typical DeST farmhouse

3.5.2 DeST parameter settings

1. Choice of location and outdoor temperature

Since the outdoor temperature selected by DeST needs to be accurate, the selected area is Chifeng City.

2. Indoor temperature

DeST simulation needs to set the indoor temperature data in advance, so it needs the maximum and minimum indoor temperature data of the heating season, but there is a simple algorithm, that is, to measure the indoor temperature change of the day, according to this copy and paste the indoor temperature change of the entire heating season, taking the living room as an example as shown in the figure below:

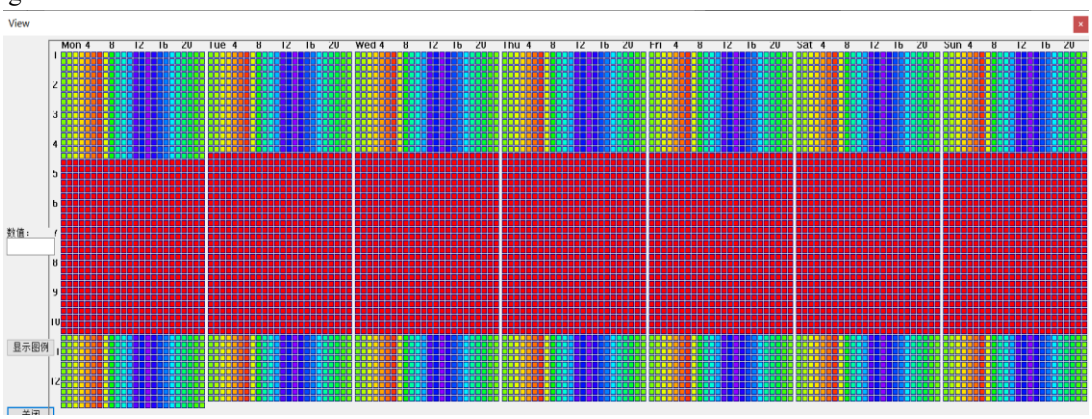

Figure 13 Maximum temperature of living room design

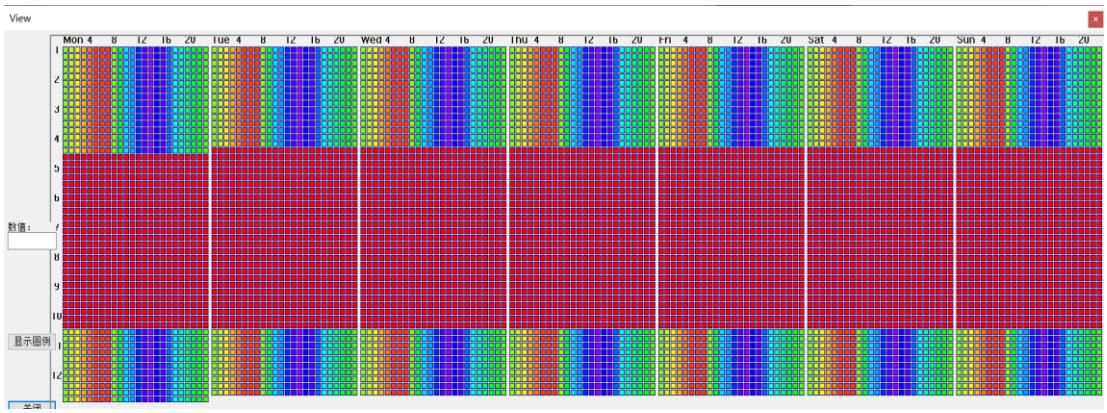

Figure 14 Minimum temperature of living room design

3. Envelope parameters

According to the actual investigation situation, the material composition of the surveyed envelope structure can be imported into DeST, and the simulation diagram of the corresponding enclosure structure can be obtained, including: exterior wall, exterior door, inner door, exterior window, solar window, solar door and other parameters.

4. Schedule settings

According to the actual situation, the settings include parameters such as personnel heat disturbance, lighting heat disturbance, heat backup heat disturbance, and air conditioning start and stop. Personnel heat disturbance is set to 6:00-11:00; 15:00-21:00 is mild interference, 11:00-14:00 is severe interference; Lighting heat disturbance set to 18:00-20:00; The device thermal disturbance settings are the same as the lights; Air conditioning start-stop setting time is 7:00-0:00.

3.6 DeST simulation

The simulation values are shown in Figure 3.30 below, and the load change of a typical farm house is obtained by running DeST, and it can be seen that the maximum heat load of DeST simulating the load of a typical farm house area is 4 kW, which occurs at the 9299th hour.

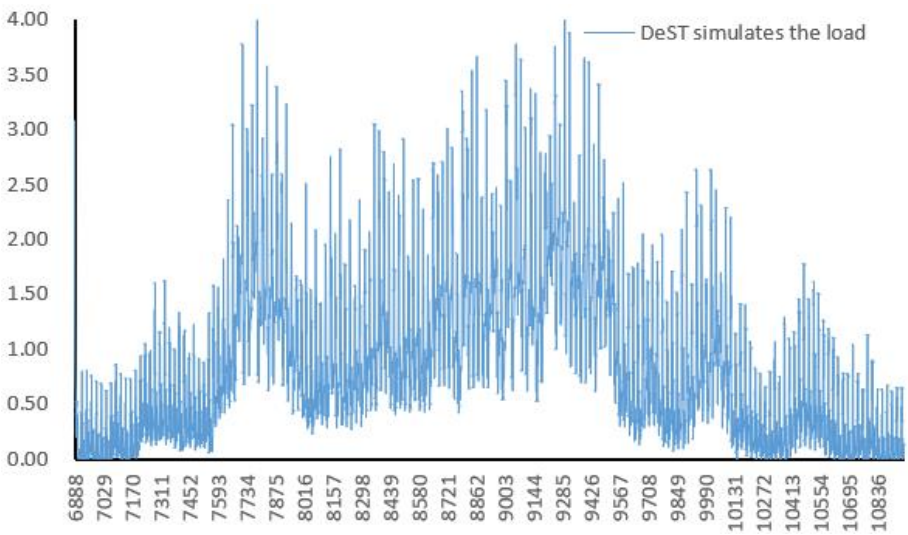

Figure 15. DeST load simulation

3.7 DeST vs. TRNSYS

According to the comparison of the simulated measured data on March 9 with the simulated data on March 9, it can be concluded that the difference between the simulated data and the actual data is very large, as shown in Figure 32 below, which is due to the large temperature fluctuation within four days of obtaining the actual temperature, and the outdoor temperature of the simulated data is the weather station Satellite data simulations will produce large fluctuations under specific weather conditions, and the inevitable interference of human activities will also have a great impact on the measured data, and the above reasons lead to a large load difference. Although the difference between the simulated load and the actual load is very large, comparing the load simulation values of DeST and TRNSYS, it can be found that the load change of TRNSYS is more relevant to the actual load than that of DeST.

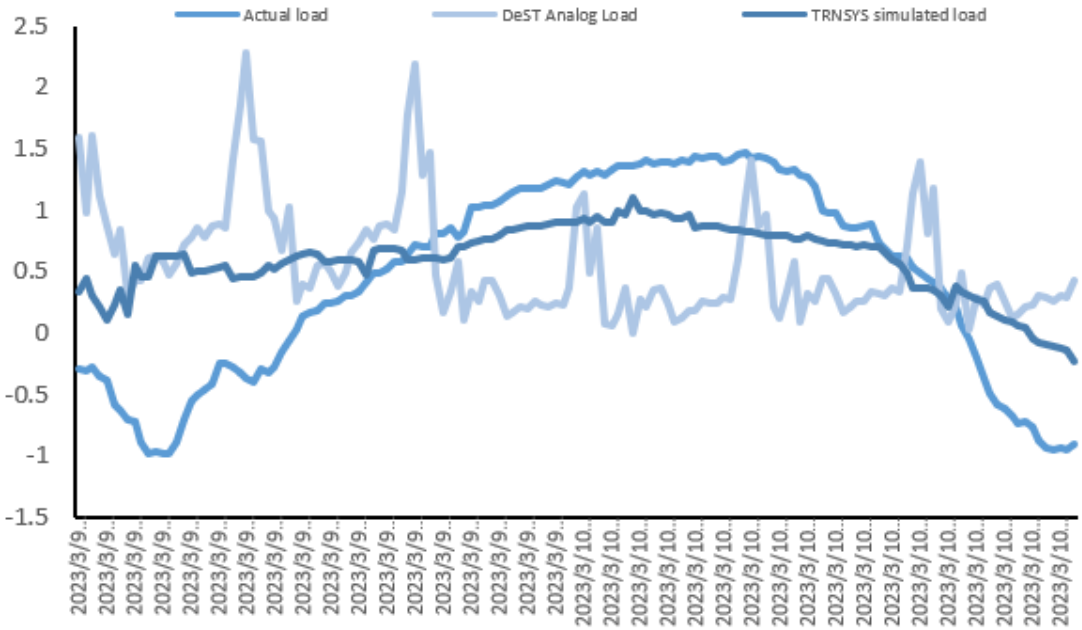

Figure 16. Comparison of simulated load and actual load

4. TYPICAL FARM HOUSE CLEANING HEATING RENOVATION AND SIMULATION SOFTWARE ADAPTABILITY ANALYSIS

The clean heating transformation analyzed in this paper is passive solar room heating, because typical farmhouses have their own sunshine room, if you want to achieve the effect of analyzing the solar heating transformation, you need to simulate the operation results of typical farmhouses without sun.

4.1 TRNSYS simulation

4.1.1 Sketch up modeling of a typical farmhouse without sunlight

After removing the sunlight, the resulting Sketch up is modeled as shown in Figure 17 below. The parameter settings of the room are shown in Section 3.4.1.

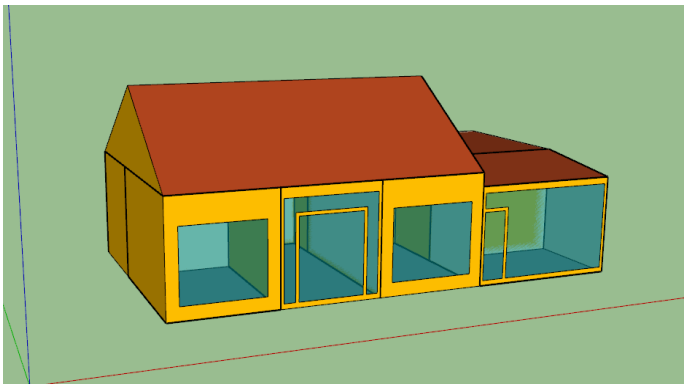

Figure 17. Typical building without sunlight

4.1.2 TRNSYS simulation and analysis

The system parameter settings are shown in Section 3.4.3 and are unchanged except for deleting the sun room. The year-round load change of a solar-free farm house running TRNSYS is shown in Figure 18 below

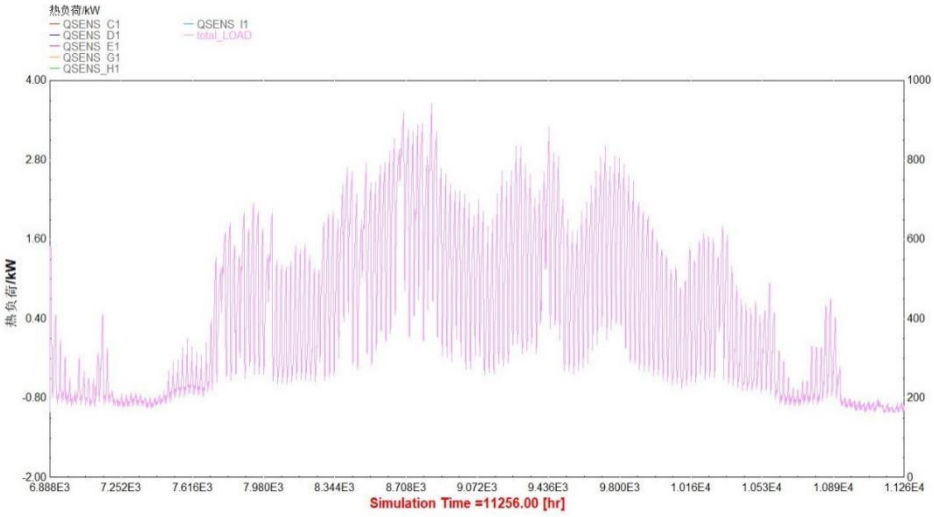

Figure18. TRNSYS load simulation

It can be seen that the maximum heat load in the absence of solar is 3.65 kW, which occurs at the 8840th hour. (In the figure, positive values are heating loads, negative values are cooling loads).

4.2 DeST simulation

4.2.1 DeST modeling

No other building parameters were modified except for the deletion of the solar room, as shown in Figure 19 below:

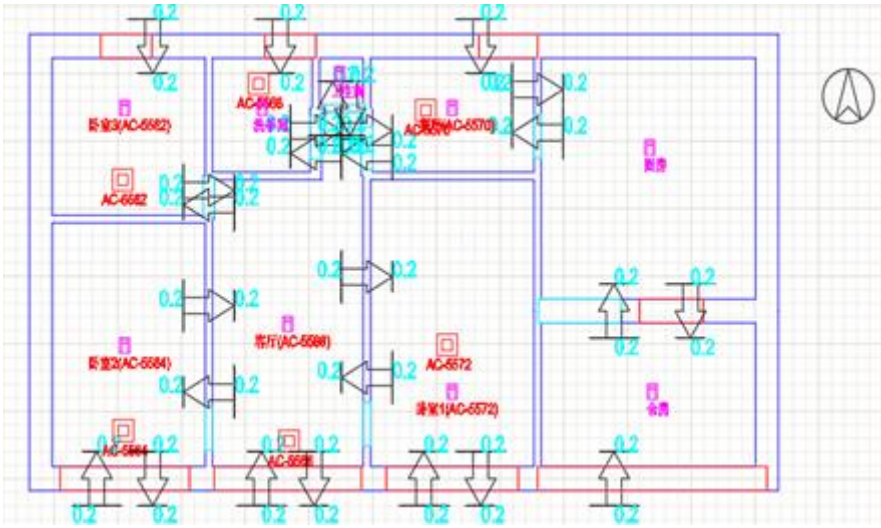

Figure 19. DeST load simulation

4.2.2 DeST simulation

From the DeST simulation analysis shown in Figure 36 below, the maximum heat load simulated by DeST in the absence of solar is 7.42 kW, which occurs at the 7762nd hour. (In the figure, positive values are heating loads, negative values are cooling loads).

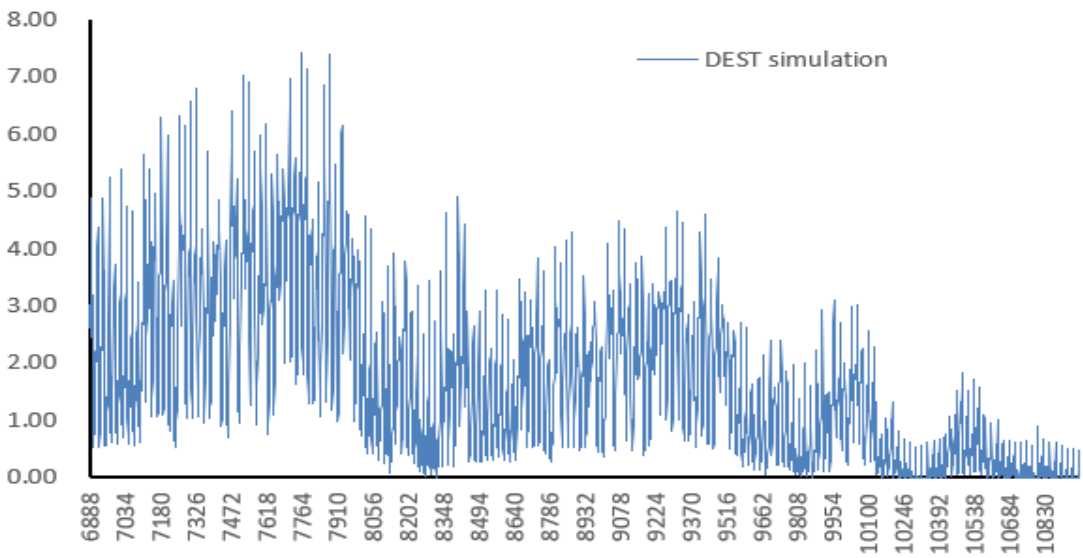

Figure 20. DeST load simulation

4.3 DeST and TRNSYS pair fit analysis

Since there is no measured data of typical farmhouses without solar rooms, it is necessary to compare the two software, and the simulation analysis of the two software can be seen that the load value of the non-solar room is simulated according to the measured data of the solar room, and the DeST is obviously too large, so the comprehensive comparison of typical farm house simulation and clean heating renovation analysis can conclude that TRNSYS is more suitable for the clean heating renovation simulation of this article.

5 DISCUSSION

5.1 Comparison of PMV-PPD indicators

The following table shows the PMV-PDD values of the sunless room, and the comparative analysis with Table 4 shows that the renovation of the sun room does improve the comfort of the room to a certain extent. The thermal feeling of bedroom 1 has changed from slightly cool to neutral, and other houses close to the sun have a smaller PMV-PPD value to a certain extent, which can have a certain effect on the composite rural clean heating transformation.

Table10. Analysis of clean heating effect

name	Average outdoor temperature (6 am)	Average temperature	Average humidity	Metabolic rate	Garment thermal resistance	PMV	PPD	Hot feeling
Bedroom 1	-2.50	18.20	38.86	1.60	0.91	-0.91	23%	Slightly cooler
Bedroom 2	-2.50	17.90	38.56	0.70	0.91	-6.57	100 %	cold
Bedroom 3	-2.50	18.10	39.16	1.08	0.91	-1.34	42%	Slightly cooler
Living room	-2.50	17.90	39.65	1.20	0.91	-1.00	26%	Slightly cooler
kitchen	-2.50	11.20	33.20	1.20	0.91	-2.55	95%	cold
lavatory	-2.50	15.50	39.01	1.20	0.91	-1.56	54%	cold
toilet	-2.50	17.30	41.65	1.20	0.91	-1.13	32%	Slightly cooler
restaurant	-2.50	17.20	35.77	1.20	0.91	-1.18	34%	Slightly cooler

6. CONCLUSION

This paper investigates the envelope parameters of typical farmers and the basic situation of typical farmhouses through field research, and calculates the temperature changes and load changes of typical farmers through survey data and measured data. The load change situation due to the actual measurement of the existence of the sunlight so the overall change law and the load change between the sunlight has a great relationship, after calculation can be obtained on March 9, the heat dissipation between the sunlight is the total heat dissipation of bedroom 1, bedroom 2, living room in a day is greater than the heat absorption between the sun, so it can be judged that on March 9, the sun room can be used as a room heat source, providing 5480.9 W, 1516.4 W, 3910.5 W heat for the room respectively, However, in the following days, due to the low outdoor temperature, the heat dissipation of the room by the sun room is much smaller than the load of the room, so that the sunlight room cannot be used as a heat source to provide heat for the room, and heating equipment is still needed to heat the room. After analyzing typical farmers, DeST and TRNSYS software simulations are carried out on typical farmers, although the deviation of analog values is large, which may be due to large temperature fluctuations within four days

of obtaining the actual temperature, and the outdoor temperature of the simulation data is simulated by weather stations and satellite data, so there will be large fluctuations in specific weather conditions, and the inevitable interference of human activities will also have a great impact on the measured data. And according to the comparison of DeST and TRNSYS two software load simulation analysis, it can be known that DeST is more suitable for the simulation of building load, TRNSYS is more suitable for clean heating renovation analysis and simulation, both software have different degrees of adaptability, but compared to this article, TRNSYS is more suitable.

REFERENCES

[1]ZHAO Yan,YE Jiandong,XING Yongjie. Energy-saving renovation of existing residential buildings in rural areas of northern China[J].Construction Science and Technology,2010,No.166(05):43-46.)

[2]WU Runqi. Research on ecological design of office building envelope based on data analysis and evaluation[D].North China University of Technology,2022.

The 18th International Symposium on District Heating and Cooling, September 3–6, 2023, Beijing, China

Uncertainty and Sensitivity Analysis for Urban Energy System Planning

Amedeo Ceruti[a*], Hartmut Spliethoff[a]

[a] *Technical University of Munich, Garching b. München, Germany*
[*] *Corresponding author. amedeo.ceruti@tum.de*

ABSTRACT

The European Union has ambitious goals to reduce greenhouse gas emissions. A fundamental energy system transformation is needed to achieve them and limit climate change impacts. District heating is a valuable technology to supply densely populated urban areas with renewable energy. However, increasing sector coupling and the fluctuating nature of renewable energy sources make efficiently planning these systems challenging. Mixed-integer linear programming (MILP) is an optimization method that can aid the energy system planning process in its early stages. However, uncertainty can significantly impact the optimization results and, therefore, the decision-making process. A methodology to assess parameter uncertainty and model sensitivity is applied to urban districts with different temporal and spatial resolutions. First, the uncertainty of the model parameters is characterized. Then, a quasi-Monte Carlo Simulation of the model using Saltelli's sampling scheme is used to analyze the impact of uncertainty in the model outputs, and a global sensitivity analysis with Morris' method identifies the most impactful parameters. Finally, the identified parameters are included in a stochastic programming formulation of the original MILP model to derive a more robust decision. Dealing with parameter uncertainty is often neglected in energy system optimization and can impact optimal decision-making. Under uncertainty, the investigated method assesses and provides optimal decisions for urban district energy system planning. Precise uncertainty characterizations, their validation, and high computational demands are identified as bottlenecks that should be addressed.

Keywords: Energy System Optimization, Optimization under Uncertainty, Sensitivity Analysis

1. INTRODUCTION

The European Union has set ambitious goals for greenhouse gas emission reductions, including reaching net zero by 2050. It is imperative to quickly transition from fossil fuel-based to completely renewable energy systems to achieve those goals. However, systems with high shares of inherently fluctuating renewable energy sources, like wind and solar, are complex to design. Parameter uncertainty, inherent to energy system planning because it always requires dealing with unknown future trends and intermittent energy sources, must be holistically addressed. Mixed-integer linear programming (MILP) energy systems optimization models (ESOMs) are a valuable tool to deal with these arising challenges.

Pfenninger et al. highlighted the uncertainty in ESOM parameters as an open challenge [1]. Addressing it can additionally lead to more transparency and confidence in the models. Uncertainty can be understood as lacking knowledge about a given outcome and can be classified as parametric and structural. The first term refers to a "lack of empirical knowledge to calibrate model parameters to their "true" value", while the latter arises from an imperfect model structure [2]. Uncertainty in ESOMs at the district scale needs to be assessed to plan robust and sustainable energy systems effectively.

In this paper, a framework to make energy systems planning decisions under uncertainty is presented in Section 2. This method has four distinct steps: uncertainty characterization; uncertainty assessment; global sensitivity analysis; and optimization under uncertainty. Then, the framework is applied to a case study in an exemplary fashion in Section 3. Conclusions and an outlook are presented in Section 4.

2. METHODOLOGY

2.1. Model

A MILP model based on Sameti and Haghighat [3] is formulated for a district-scale urban energy system. The objective is to minimize net-present value system costs (Equation 1). The optimization selects cost-optimal investment decision variables, mainly G_i, the installed capacity of technology i in kW or kWh and the binary decision y to build a district heating network (DHN). Investment costs are annualized with the capital recovery factor (CRF_i) to account for depreciation during technology-dependent lifetime (Eq. 2). Operational costs mainly include energy carrier, electricity grid, and CO_2 costs (Eq. 3).

$$\min \; C_{inv} + C_{op} \tag{1}$$

$$C_{inv} = \sum_i [CRF_i (C_i \, G_i)] + \; C_{DHN} y \qquad \forall i \tag{2}$$

$$C_{\mathrm{op}} = \sum_{t=1}^{8760} \left(\frac{Q_{t,i} p_{t,i}}{\eta_i} - I_{\mathrm{grid,exp},t} p_{\mathrm{grid,exp},t} + I_{\mathrm{grid},t} p_{\mathrm{grid},t} + \; p_{\mathrm{CO_2}} \dot{m}_{\mathrm{CO_2},t} \right) \cdot \Delta_t \qquad \forall i \tag{3}$$

Where i is the technology index, $t \in \{1, \dots, 8760\}$ is the time step index, Δ_t is the length of time step in hours, $Q_{t,i}$ the power deployed in kW, $p_{t,i}$ the price of the energy carrier in EUR/kWh, η_i the conversion efficiency, $p_{grid,exp,t}$ and $p_{grid,t}$ the exporting and importing price of grid electrical power in EUR/kWh, and p_{CO_2} is the CO_2 cost in EUR/kg CO_2 eq.

The primary constraint is the satisfaction of all heating and electricity demands for each hour of the year. Additionally, power can only be exported ($I_{grid,exp,t}$) or imported ($I_{grid,t}$) to the grid in each time step. The model includes a ramping up and down rate limitation of technology i (Equation 4).

$$R_{down,i} G_i \leq P_{t,i} - P_{t-1,i} \leq R_{up,i} G_i \tag{4}$$

Where $P_{t,i}$ is the delivered power in kW, $R_{down,i}$ and $R_{up,i}$ are possible rates of change in delivered power w.r.t. the total installed power.

2.2. Framework

Assessing and addressing uncertainty in ESOMs requires quantifying and characterizing possible uncertainty ranges of model inputs and analyzing model outcomes. Mavromatidis et al. proposed a framework for distributed energy systems [4]. Firstly, model parameter values are characterized by defining empirical probability distributions. Secondly, the impact of these uncertain parameter distributions on model outcomes is analyzed. Then, the sensitivity of the model outputs to specific input parameters is analyzed to identify the most relevant uncertainty sources. We apply and expand this framework with an additional step, where the most impactful uncertainty sources are integrated into a model to derive robust decisions through optimization under uncertainty (OUU) (Figure 1) [5].

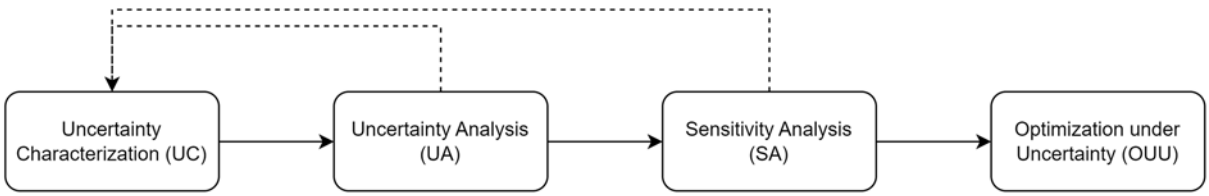

Figure 1. Overview of the framework to assess and optimize an energy system under uncertainty. Adapted from [4].

2.2.1. Uncertainty Characterization

Parameter uncertainty must be characterized by assigning value ranges and probability distributions to the model input parameters [4,6,7]. For ESOMs, these parameters generally include six broad categories: energy carrier prices, greenhouse gas emission factors, investment costs, technological parameters such as efficiencies and lifetime, energy demand, and weather patterns.

The characterization process generally starts with listing all parameters, then assigning probability distributions and uncertainty ranges through a specific methodology or assumptions, such as [6]. Moret et al. and Usher et al. assumed independent and uniform probability distributions over time [6,8]. However, other authors use less methodical approaches to characterize uncertainty or use more complex probability models of the parameters. For example, [4] used independent probabilities but included half-normal, normal, discrete uniform, and uniform distributions. [7] correlates gas and electricity prices for the Monte-Carlo simulations of the ESOM.

Another concern for ESOMs is the characterization of time series data uncertainty. The approaches vary from using different reference years to derive multiple time series for radiation and energy demands for the model [4] to scale the energy demands with a factor [6]. Ultimately, the spatial and temporal resolution should be investigated within the uncertainty assessment [8,9]. This paper assumes independent and uniform probability distributions for all parameters, and time series are multiplied by a factor to consider weather uncertainty.

2.2.2. Uncertainty Assessment

An assessment of the impacts of input uncertainty on the model output is performed after the initial characterization. Monte Carlo (MC) simulations are a widespread technique to compute it by repeatedly sampling from the defined probability density functions [10]. The basic procedure of MC is to sample randomly N_{runs} times from the probability distributions, collect the model outputs, and evaluate them using statistical techniques [5]. With a very large N_{runs}, the output uncertainty can be empirically measured with high confidence. However, in ESOMs, high computational requirements are a limiting factor; hence other sampling techniques with better space-filling properties can be used to limit the number of required model runs [4]. This procedure is known as quasi-Monte Carlo (qMC) simulation. Literature differs on the number of required runs to assess the effects of uncertainty. Petkov et al. run each MC 300 times and then test for output convergence [7]. Mavromatidis et al. set a high number of runs at 5000 [4]. Some publications run the model "several hundred" times, and it is considered sufficient [5,7]. Other authors use formulas, such as Morgan's and Wilkins', and a desired model output confidence to determine the required N_{runs}. This publication applies a modified Sobol sequence to generate a quasi-random, low-discrepancy sequence of samples [11].

2.2.3. Sensitivity Analysis

If the previous uncertainty assessment reveals significant deviations in the model outcomes, a sensitivity analysis (SA) is conducted to apportion different sources of uncertainty in the model input to the output uncertainty [12]. A SA is global if the whole input uncertainty space is covered. The number of necessary model evaluations varies depending on the applied method. GSA with large data requirements are variance-based techniques such as the Sobol SA, which needs N(k + 2) model runs [12]. In contrast, an elementary effects method requires fewer model runs to assess the model [12]. This feature makes them often used in ESOMs to perform GSA [4,8].

In this work, the Morris Method, a semi-quantitative, elementary effects GSA method well suited for models with large amounts of input parameters (up to hundreds) and expensive model evaluations, is applied [12]. It provides an interval scale ranking of factors, which measures the importance of input factors for output uncertainty. In essence, it calculates the average of derivatives over the space of factors, discretized into a p-level grid. The measure of influence is μ^*, the mean the of absolute elementary effects [8]. It can be applied to sets or groups of factors, simplifying the analysis when appropriate. A disadvantage of the method is that it does not extract higher-order interaction effects of parameters.

2.2.4. Optimization under Uncertainty

There are several possible approaches to optimize a problem under uncertainty. Yue et al. review four different methods in their review paper: Monte Carlo (MC), stochastic programming (SP), robust optimization (RO), and modeling to generate alternatives [5]. Each has strengths and weaknesses and is therefore suited for different problem formulations and uncertainty sources.

This work uses a two-stage stochastic programming formulation to integrate uncertainty within the optimization formulation due to its simplicity and widespread use. The optimization objective is modified to minimize the first stage investment costs ("here-and-now", C_{inv}) as well as the expected second stage costs ("wait-and-see", $\mathbb{E}[C_{\text{op},s}]$) (Eq. 5) [13]. The here-and-now decision is made before uncertainty is revealed, while the wait-and-see decision is made afterward. The objective can be approximated through $s \in \mathrm{S}$ scenarios (Eq. 6) with a given probability π_s to solve the generally intractable expectation function. Several alternative approaches are available to construct these scenarios, including sample average approximation and expert opinion. This paper uses the latter.

$$\min \ C_{\text{inv}} + \mathbb{E}\left[C_{\text{op},s}\right] \tag{5}$$

$$\min \ C_{\text{inv}} + \sum_{s \in \mathrm{S}} \left(\pi_s \cdot C_{\text{op},s}\right) \tag{6}$$

3. CASE STUDY

3.1. Pre-processing

The energy system to meet the calculated residential heating and power demand of a small city in southern Germany with around a thousand residents and 300 buildings is computed as an example application. Various GIS data with LoD1 and LoD2 resolution are unified and processed to extract area, building height, and envelope volume of all buildings within the studied district. Then, an age category is assigned to each building, given its age distribution information within a 100x100 m raster provided by the building census "Zensus2011" dataset [14]. Then, a TABULA category [15], i.e., building typology, is assigned with the closest building type by dimensions, assuming the building has never been renovated. Lastly, a typical weather year (TWY) from the nearest meteorological weather station is selected [16]. The process output is a shapefile with

building dimensions and type for each residential building within the district. The process uses PostgreSQL and Python except for the LoD2 data handling, calculated with FME[1].

The input data is used to compute heating and electricity demands with the Python-based, open-source software City Energy Analyst (CEA) through a stochastic demand calculation model for each building [17]. The energy balances include solar radiation, occupancy, warm water consumption, building thermal properties, and installed heating systems. The resulting time series for heating and electricity demands are aggregated into a single hourly time series, a yearly building energy demand, and a building peak demand. This data is used as input for the DHN cost estimation and the MILP problem.

3.2. Energy System

The energy system structure is defined as shown in Figure 2. The are four primary energy sources: biomass, geothermal, natural gas, and solar radiation. These can be converted to heat and electricity with boilers, combined heat and power, heat pumps, and photovoltaic panels to cover the district's demands. Ramping up and down constraints were applied to deep hydrothermal geothermal sources because centrifugal submersible pumps used to transport hot water from depth to the surface need to be operated as constantly as possible. The MILP is formulated with pyomo and solved with a solver like GLPK or Gurobi.

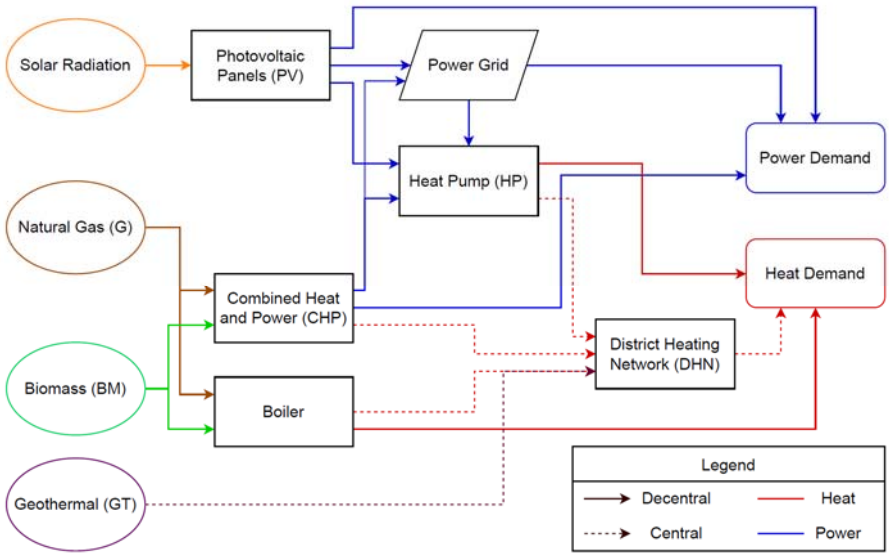

Figure 2. Energy system structure of the case study.

3.3. Uncertainty Characterization

The baseline cost and technical parameters are collected from the literature. Several cost databases were used for operational (Table 1), investment costs (

Table **2**), and uncertainty their uncertainty range determination [18–21]. A DHN investment cost of $7.81 \cdot 10^6$ EUR and 10 % transmission losses are computed through a MILP optimization with the open-source software THERMOS [22] (Table 1). Lastly, several parameters were grouped into sets to reduce the required optimization runs (Table 3). All uncertainty distribution ranges are assumed uniform in this case study.

Table 1. Lower and upper ranges of energy carrier and DHN costs.

Item	Unit	Lower bound	Upper bound	Reference
p_{pellets}	EUR/MWh	20	120	[19]
p_{chips}	EUR/MWh	15	100	Assumption
p_{gas}	EUR/MWh	30	500	[21]
p_{grid}	EUR/MWh	200	800	[23]
$p_{\text{grid,exp}}$	EUR/MWh	5	100	Assumption
p_{CO_2}	EUR/t	10	750	[24]
C_{DHN}	EUR	250000	$1 \cdot 10^8$	Assumption, [22]
$R_{\text{loss,DHN}}$	-	0.01	0.3	Assumption, [22]

[1] Commercial FME by Safe Software available at: https://fme.safe.com/.

Table 2. Nominal technology costs and technical parameters for central (c) and decentral (dec) units.

Technology	Description	Investment	CO_2-Factor	η_{power}	η_{heat}	Lifetime
Unit		EUR/kW or EUR	g CO_2 eq./kWh	-	-	y
PV	Photovoltaic panels	1200	40	1	0	20
$B_{G,c}$	Gas boiler	107	246	0	0.95	25
$B_{G,dec}$	Gas boiler	318	251	0	0.93	20
$B_{BM,c}$	Biomass boiler, pellet	586	55	0	0.96	28
$B_{BM,dec}$	Biomass boiler, wood chips	335	76	0	0.7	17.5
$CHP_{G,c}$	CHP gas	660	253	0.46	0.46	15
$CHP_{BM,c}$	CHP biomass, pellet	902	65	0.14	0.82	28
HP_{dec}	Heat pump, air-water	700	0	-0.33	1	18
HP_c	Heat pump, air 5 MWth	609	0	-0.28	1	15
GT_c	Deep hydrothermal geothermal	1500	0	-0.05	1	30

Table 3. Factors applied to upper and lower bounds of parameter sets.

Parameter set	Lower bound	Upper bound
Investment costs	0.5	1.5
Heat efficiency	0.9	1.1
Electrical efficiency	0.9	1.1
Battery discharge rate	0.1	5
Heat demand	0.1	2
Power demand	0.1	2
Lifetime generation	0.8	1.5
Lifetime storage	0.8	1.5

3.4. Uncertainty Analysis

Based on the defined uniform probability distributions, a quasi-Monte Carlo Simulation with Sobol's sampling scheme of the open-source Python package SAlib is used [25]. Twenty-three parameters and parameter sets are sampled, resulting in 1536 required optimization runs. Significant variability in objective function values was observed, with a mean of $2.71 \cdot 10^6$, a 25% quantile of $6.03 \cdot 10^5$, and a 75% quantile of $3.81 \cdot 10^6$. The optimization runs show a large variability in comparison to the baseline deterministic model value of $1.21 \cdot 10^6$. The generation and storage investment variables also show deviation from the deterministic value and a significant variability, as shown in Figure 3. Individual runs with substantial variations in the energy demand alongside cheap energy carrier costs cause outliers in installed capacities. A sensitivity analysis is needed to apportion this uncertainty to uncertain input parameters.

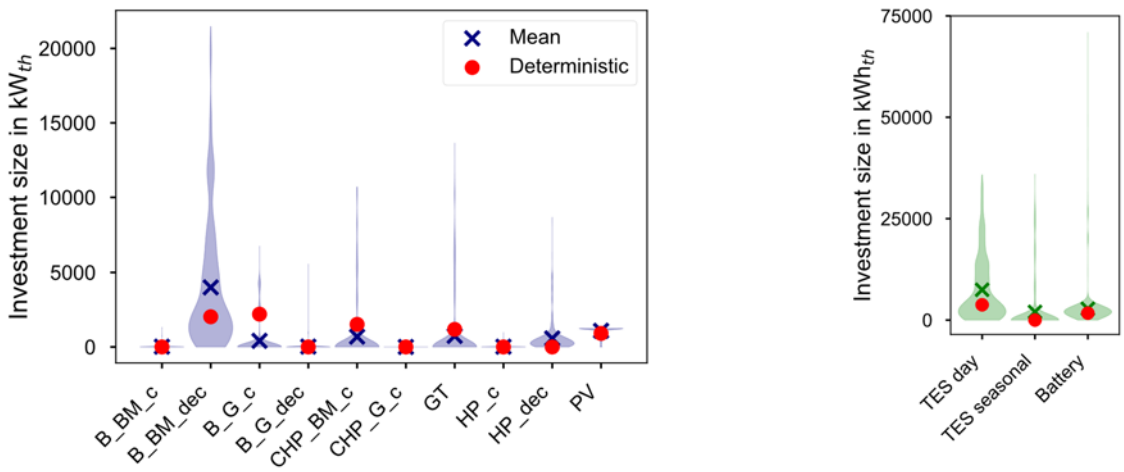

Figure 3. Violin plot of optimal investment sizes of energy-producing units (left) and storage (right), compared to their mean and deterministic baseline value.

3.5. Global Sensitivity Analysis

The method of Morris with Campolongo's enhancements, as implemented in SAlib, is used to test the influence of individual parameters and parameter sets in the significant objective value uncertainty [25]. Three additional parameters are varied with respect to the q-MC simulation to test the influence of these optimization parameters: the initial and final energy storage levels in kWh and the curtailment costs of excess energy. Therefore, 405 optimization runs with 15 optimal trajectories are required to analyze the 26 defined parameters and parameter groups.

Based on Morris' method, the most impactful parameters are ranked by their elementary effects (Figure 4). A small number of parameters have the largest impact on the objective function: heating and cooling demands, carbon tax price, financial parameters such as the internal rate of return, and storage efficiency. The latter could be an effect of the cheap and steady supply of geothermal energy, making storage efficiency more impactful than in other districts. Other commonly included parameters in stochastic and robust energy system optimization, such as energy carrier prices, are less impactful.

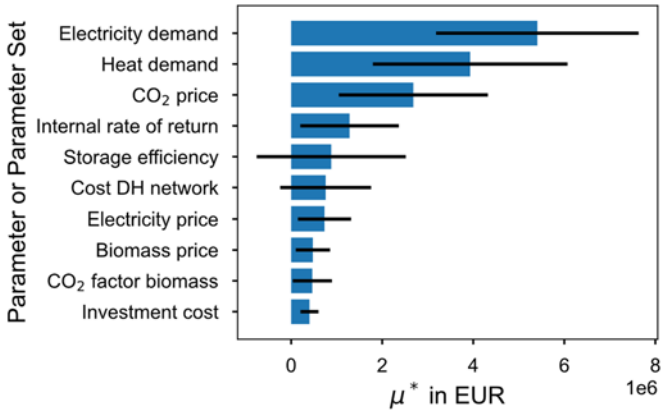

Figure 4. Bar plot of the mean absolute elementary effects of the ten most impactful parameters as calculated by the Morris method.

3.6. Optimization under Uncertainty

The two-stage SP problem is formulated with the Python package mpi-sppy [26]. Nine scenarios with equal probability are defined: past, current, and very high prices, including energy carrier and carbon prices with low, medium, and high demands. The problem was solved in around 4 hours with AMD Ryzen 5 PRO 4650U CPU, 16 GB of RAM, and the Gurobi solver. The results depicted in Figure 5 shows that the energy system is diversified to hedge against price and demand uncertainty. The deterministic "Base Case" and CO_2 minimization optimization models with baseline costs (

Table **2**) are not robust against demand fluctuations and cannot deliver energy demands for all cases. Total system costs are the lowest for the Base Case ($1.21 \cdot 10^6$ EUR/y) and are highest for CO_2 minimization ($2.28 \cdot 10^6$ EUR/y). The SP version is robust against several uncertainty scenarios, including higher carbon prices, with an associated moderate increase in total costs ($1.6 \cdot 10^6$ EUR/y, 32 % more than the base case).

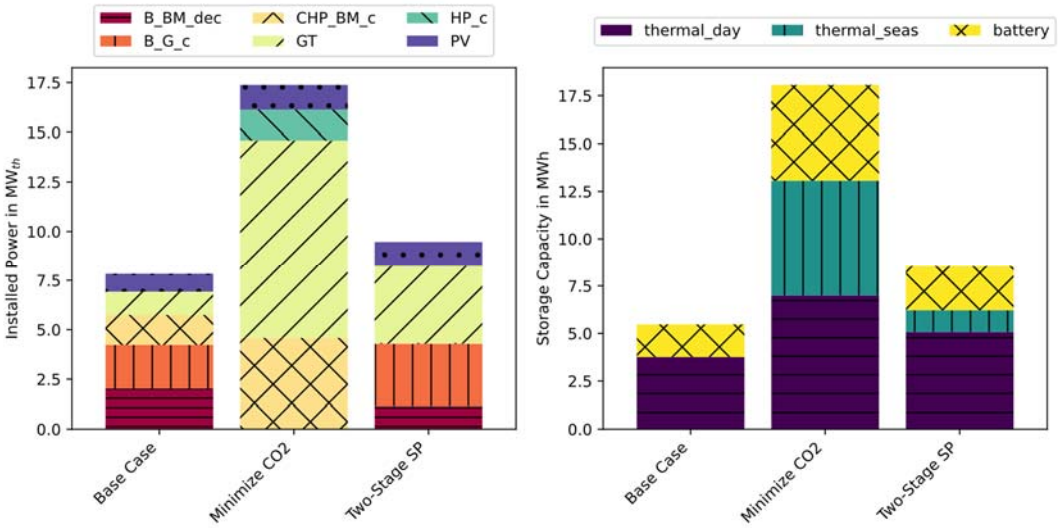

Figure 5. Optimal first-stage variables of generation (left) and storage (right) for the deterministic base case and CO_2 minimization, and the two-stage stochastic programming.

In all system configurations, renewable energy generation units have the largest share in installed energy generation capacity due to high carbon costs and competitive renewable energy costs, which are currently cheaper to operate than the natural gas-based system. However, these systems also must balance expensive upfront investment costs, which rely heavily on the assumption that technology lifetime and internal rate of return are constant throughout the whole plant lifetime. Uncertainty in the first stage is not included in this SP problem formulation.

3.7. Discussion

The applied framework successfully evaluates parameter uncertainty in the optimization of energy systems. The uncertainty characterization provides ranges and uniform probability distributions. For example, CO_2 price bounds are set to the maximal economic cost of climate change at 750 EUR/t CO_2 eq. [24], which pushes all carbon-related impacts to high values (see Figure 4). A possible approach to mitigate the effects of uncertainty distributions on the results is robust optimization. However, RO suffers from drawbacks such as complex model formulations and custom solution algorithms [27]. A hybrid between stochastic and robust optimization is distributionally robust optimization (DRO). Few papers with custom solution algorithms have been implemented [28]. The authors in [28] compare DRO, RO, and SP for an ESOM of the Swiss energy system and found that choosing uniform or normal probability distributions affects the model outcome.

The main limiting factors of the framework are high computational costs and the exclusion of parameter correlations in the MC and GSA. Increasing computing power or reducing model detail for some aspects, like electricity import or export, can help mitigate high computational costs. Regarding the second identified challenge, some authors have used correlations in their models [7]. Still, the overall trend in the literature is unclear on whether these correlations are appropriate, especially since detailed energy system-related data is generally difficult to collect or unavailable.

4. CONCLUSION

The presented framework allows planning energy systems at the district level, accounting for uncertainties in all input parameters. In this way, the designed energy system can be shown more transparently to planners and includes a holistic evaluation of the effects of uncertainty on the results. Additionally, the system is robust against the most impactful parameter changes, mainly energy demand and commodity prices. The limitations of the presented framework are expensive but feasible computational requirements and complex uncertainty characterization of the input parameters due to unavailable energy system data. Further work should focus on testing proposed alternative optimization techniques such as RO and DRO and including investment cost uncertainty. Nevertheless, the presented framework can be applied to plan sustainable, renewable, and robust energy systems at the urban district and regional scale, as well as to other related systems optimization problems with high computational demand.

ACKNOWLEDGEMENT

This work is funded by the German Ministry for Economic Affairs and Climate Action with funding reference number 03EN3055A.

REFERENCES

[1] S. Pfenninger, A. Hawkes, J. Keirstead, Energy systems modeling for twenty-first century energy challenges, Renewable and Sustainable Energy Reviews 33 (2014) 74–86. https://doi.org/10.1016/j.rser.2014.02.003.

[2] O. Edenhofer, K. Lessmann, C. Kemfert, M. Grubb, J. Kohler, Induced Technological Change: Exploring its Implications for the Economics of Atmospheric Stabilization: Synthesis Report from the Innovation Modeling Comparison Project, EJ SI2006 (2006). https://doi.org/10.5547/ISSN0195-6574-EJ-VolSI2006-NoSI1-3.

[3] M. Sameti, F. Haghighat, Optimization approaches in district heating and cooling thermal network, Energy and Buildings 140 (2017) 121–130. https://doi.org/10.1016/j.enbuild.2017.01.062.

[4] G. Mavromatidis, K. Orehounig, J. Carmeliet, Uncertainty and global sensitivity analysis for the optimal design of distributed energy systems, Applied Energy 214 (2018) 219–238. https://doi.org/10.1016/j.apenergy.2018.01.062.

[5] X. Yue, S. Pye, J. DeCarolis, F.G. Li, F. Rogan, B.Ó. Gallachóir, A review of approaches to uncertainty assessment in energy system optimization models, Energy Strategy Reviews 21 (2018) 204–217. https://doi.org/10.1016/j.esr.2018.06.003.

[6] S. Moret, V. Codina Gironès, M. Bierlaire, F. Maréchal, Characterization of input uncertainties in strategic energy planning models, Applied Energy 202 (2017) 597–617. https://doi.org/10.1016/j.apenergy.2017.05.106.

[7] I. Petkov, P. Gabrielli, Power-to-hydrogen as seasonal energy storage: an uncertainty analysis for optimal design of low-carbon multi-energy systems, Applied Energy 274 (2020) 115197. https://doi.org/10.1016/j.apenergy.2020.115197.

[8] W. Usher, T. Barnes, N. Moksnes, T. Niet, Global sensitivity analysis to enhance the transparency and rigour of energy

system optimisation modelling, Open Res Europe 3 (2023) 30. https://doi.org/10.12688/openreseurope.15461.1.

[9] M.I. Yliruka, S. Moret, F. Jalil-Vega, A.D. Hawkes, N. Shah, The Trade-Off between Spatial Resolution and Uncertainty in Energy System Modelling, in: 14th International Symposium on Process Systems Engineering, Elsevier, 2022, pp. 2035–2040.

[10] R.L. Harrison, Introduction To Monte Carlo Simulation, AIP conference proceedings 1204 (2010) 17–21. https://doi.org/10.1063/1.3295638.

[11] A. Saltelli, Making best use of model evaluations to compute sensitivity indices, Computer Physics Communications 145 (2002) 280–297. https://doi.org/10.1016/S0010-4655(02)00280-1.

[12] Global Sensitivity Analysis: The Primer, John Wiley & Sons, New York, NY, 2008.

[13] A. Shapiro, A. Philpott, A tutorial on stochastic programming, Manuscript. Available at www2. isye. gatech. edu/ashapiro/publications. html 17 (2007).

[14] Statistisches Bundesamt, ZENSUS2011 - Bevölkerungs- und Wohnungszählung 2011, 2011, https://www.zensus2011.de/DE/Home/home_node.html, accessed 31 May 2023.

[15] T. Loga, B. Stein, N. Diefenbach, TABULA building typologies in 20 European countries—Making energy-related features of residential building stocks comparable, Energy and Buildings 132 (2016) 4–12. https://doi.org/10.1016/j.enbuild.2016.06.094.

[16] L.K. Lawrie, D.B. Crawley, Development of global typical meteorological years (TMYx) (2019).

[17] J.A. Fonseca, T.-A. Nguyen, A. Schlueter, F. Marechal, City Energy Analyst (CEA): Integrated framework for analysis and optimization of building energy systems in neighborhoods and city districts, Energy and Buildings 113 (2016) 202–226. https://doi.org/10.1016/j.enbuild.2015.11.055.

[18] Danish Energy Agency, Technology Data, 2018, https://ens.dk/en/our-services/projections-and-models/technology-data, accessed 2 November 2022.

[19] Deutsches Pelletinstitut GmbH, DEPI - Pelletpreis/Wirtschaftlichkeit, 2022, https://www.depi.de/pelletpreis-wirtschaftlichkeit, accessed 3 November 2022.

[20] KEA Klimaschutz- und Energieagentur Baden-Württemberg GmbH, Technikkatalog zur kommunalen Wärmeplanung in Baden-Württemberg, 2022, https://www.kea-bw.de/waermewende/wissensportal/kommunale-waermeplanung/technikkatalog#c5088-content-5, accessed 2 November 2022.

[21] European Energy Exchange AG, EEX Market Data, 2022, https://www.eex.com/en/, accessed 2 November 2022.

[22] THERMOS project partners, THERMOS (Thermal Energy Resource Modelling and OptimisationSystem) project, https://www.thermos-project.eu/home/, accessed 2 August 2022.

[23] Eurostat, Energy statistics - an overview, 2022, https://ec.europa.eu/eurostat/statistics-explained/index.php?title=Energy_statistics_-_an_overview#Final_energy_consumption, accessed 13 September 2022.

[24] Umweltbundesamt, Gesellschaftliche Kosten von Umweltbelastungen, 2021, https://www.umweltbundesamt.de/daten/umwelt-wirtschaft/gesellschaftliche-kosten-von-umweltbelastungen#gesamtwirtschaftliche-bedeutung-der-umweltkosten, accessed 3 November 2022.

[25] J. Herman, W. Usher, SALib: An open-source Python library for Sensitivity Analysis, JOSS 2 (2017) 97. https://doi.org/10.21105/joss.00097.

[26] B. Knueven, D. Mildebrath, C. Muir, J.D. Siirola, J.-P. Watson, D.L. Woodruff, A parallel hub-and-spoke system for large-scale scenario-based optimization under uncertainty, Preprint (2020) 11–8088.

[27] S. Moret, F. Babonneau, M. Bierlaire, F. Maréchal, Decision support for strategic energy planning: A robust optimization framework, European Journal of Operational Research 280 (2020) 539–554. https://doi.org/10.1016/j.ejor.2019.06.015.

[28] E. Guevara, F. Babonneau, T. Homem-de-Mello, S. Moret, A machine learning and distributionally robust optimization framework for strategic energy planning under uncertainty, Applied Energy 271 (2020) 115005. https://doi.org/10.1016/j.apenergy.2020.115005.

The 18th International Symposium on District Heating and Cooling, September 3–6, 2023, Beijing, China

RESEARCH ON SOURCE-STORAGE DYNAMIC PROCEDURE-ORIENTED OPERATION AND CONFIGURATION OPTIMIZATION OF DISTRICT HEATING SYSTEM

Xuran Ma[a,b], Peng Wang[a,b*], Yifei Zhang[a,b*]

[a] *School of Architecture, Harbin Institute of Technology, 2651#, the 2nd Campus of Harbin Institute of Technology, 73 Huanghe Road, Nangang, Harbin, Heilongjiang 150090, China*

[b] *Key Laboratory of Cold Region Urban and Rural Human Settlement Environment Science and Technology, Ministry of Industry and Information Technology, Harbin, Heilongjiang, 150001, China*

[*] *Corresponding author. cahnburg@hit.edu.cn (P. Wang), 29598757@qq.com (Y. Zhang)*

ABSTRACT

The digitization and intelligence of district heating system will become an inevitable step to promote low and hence zero carbon energy utilization. This paper proposes a two-stage operational and configurational dynamic optimization model that considers the variations in physical parameters. Subsequently, the paper illustrates the optimal operational strategy of the system and the discrepancy between the dynamic and static models through a case study in North China. The results show that the dynamic models can detect changes in physical measurements such as indoor temperature, which can be referred to by DHS for operational control, and the contribution of heat storage equipment varies with the characteristics of peak and valley tariffs.

Keywords: District heating system, Source and storage capacity configuration, Operational optimization, Dynamic procedure-oriented model

1. INTRODUCTION

Energy systems are undergoing a series of revolutions with the global carbon neutrality target[1]. Within this trend, the digitization and intelligence of district heating system (DHS) will become an inevitable step to promote the low and hence zero carbon energy utilization[2]. Reasonable optimization model is the essential prerequisite for cost-efficient operation of heating systems. In the optimization process of all types of energy systems, the procedure-oriented principle[3] has been widely adopted as an important method. This method focuses on the thermal, electrical, and hydraulic processes of the system and describe the situation of system by modelling the inputs and outputs of the various components. This research method is commonly utilized in the optimization problems of energy hub[4], integrated energy system (IES)[5] , distributed energy system[6] and DHS[7].

Static procedures dominate the early optimization models. Kopanos et al.[8] consider the variable generation efficiency of combined heat and power (CHP) plants at different load rates and propose an operation strategy for minimum operational cost of a distributed micro CHP system with shared community heat storage and gas boiler. Jarmo et al. [9] propose a mixed integer linear programming (MILP)model to determine the heating network topology as well as the source and storage capacity of a distributed heating system with a pre-defined consumer and potential source storage location. Andreas et al. [10] propose a storage configurational MILP model with the consideration of the start/stop loss of CHP plants and illustrate the economic benefits after introducing storage equipment. Likewise, Gebremedhin et al. [11] analyze the energy structure and carbon reduction performance after introducing biomass CHP in a Nordic region with different heating demand scales. In the early stage of DHS optimization research, the static procedure-oriented source, network, load and storage input-output models are established with operation intervals, fixed or predicted heating load[12], procedure losses and other parameters, simplifying the dynamic or time-series variation characteristics of the input-output relationship in the system.

However, in the fourth-generation heating concept[13], which requires higher digitalization and intelligence level, the static optimization model can hardly reflect the detailed operating characteristics such as changes in heat pump COP caused by time-varying low-grade heat source conditions and dynamic indoor temperature, let alone real-time assessment and optimization for DHS. Therefore, dynamic procedure-oriented simulation models for DHS are essential in today's optimization modelling process[14]. Ghilardi et al.[15] take the dynamic heating regulation and the thermal comfort management process into consideration. The operational condition of DHS is reflected by dynamic supply temperature and indoor temperature, and the advantage of dynamic optimization is indicated. Similarly, Nguyen et al.[16] also adopt the building thermal process particle model reflecting building heat capacity in the DHS modelling process. Gu et al. [17] also

consider the building thermal process and dynamic network transmission loss when solving the problem of optimal system scheduling for the combined operation of CHP and wind power. In addition to the dynamic process of network and heating load, dynamic operational characteristics of source and storage such as frosting and defrosting of air source heat pump (ASHP)[18], the charging capacity of ice cooling storage influenced by the ice thickness[19], and the water and phase change material coupled thermal storage system[20] are also beneficial to be considered.

The two-stage optimization approach has been widely utilized in field of energy system. Guo et al. [21] present a configuration-operation two-stage optimization algorithm to to simultaneously minimize a hospital micro-CHP system's life cycle investment and carbon emission. Luo et al.[22] and Zhou et al.[23] also adopt this approach to reflect the design-operation logic process of energy systems. In addition, Zhang et al.[24] optimize the scheduling of source and storage facilities in DHS with a day-ahead and intra-day two-stage algorithm to ensure that the system can accommodate more wind power and reduce operational costs. Similarly, the two-stage approach is also applied to solve the problem of robust optimal scheduling of IES[25]. Therefore, the two-stage optimization model can better capture the chronological and logical character of the system's life cycle.

The above dynamic models aim to give the optimal design and operation of a system with a pre-defined heat source type for a specific region, but the heat source model is usually built with an operating interval constraint, which ignores the dynamic changes in operation COP of the heat pump facilities. And the analysis is often based on typical days in each season, and the different operational characteristics at different outdoor temperatures during the same season are often ignored. Therefore, this paper establishes the HP models considering the regional resource endowment conditions and presents a novel dynamic configuration-operation two-stage optimization model orienting the dynamic building, network, and source processes. Besides, the storage resources will be compared in this research with different sensitivity factors.

2. OPTIMIZATION MODEL

2.1. Planning problem statement

The framework of the proposed two-stage optimization process for the DHS is illustrated in **Figure 1**. The interrelated thermal process of DHS is described in terms of dynamic changes of physical variables such as indoor air and supply water temperature. The thermal process is adopted as a constraint in both stages' optimization model. The objective of the first stage is to minimize the initial investment of DHS, determining the capacity of equipment and minimizing the annual investment, while in the second stage, determining the final capacity optimal scheduling of DHS. The equipment operation interval constraints in the second stage are based on the optimization results in the first stage. After that, this paper analyzes the impact of the source-storage combination and peak-valley tariff factors on the optimization results.

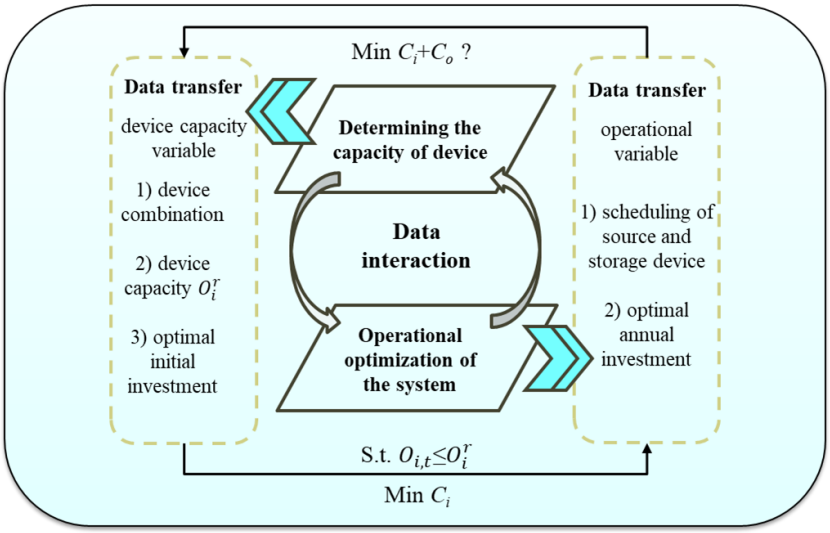

Figure 1. Framework of two-stage optimization process of the DHS

2.2. Objective function

As shown in Eq.(1), the minimum annual investment C_1 is adopted as the final objective function for economic optimization, where C_i donates the annual initial investment of facilities, C_o donates the annual operational cost, r donates the benchmark yield, and lc donates the life cycle of the system.

$$\min C_i \frac{r(1+r)^{lc}}{(1+r)^{lc}-1} + C_o \tag{1}$$

The objective function C_i for the first stage can be expressed as a function of the capacity of the equipment in Eq.(1). C_o includes the interaction with municipal electricity and gas in Eq.(2)-(3). Each F denotes the unit price for facility or energy purchase, E denotes the electricity generated, purchased and sold, Q denotes heat supply, while V denotes gas consumption.

$$\min C_i = E_{GT}^r F_{GT} + Q_{GB}^r F_{GB} + Q_{WHB}^r F_{WHB} + Q_{WSHP}^r F_{WSHP} + Q_{ASHP}^r F_{ASHP} + S_{HST}^r F_{HST} \tag{2}$$

$$C_o = \sum_{t=1}^{N} \left(E_{b,t} F_{E,b,t} - E_{s,t} F_{E,s,t} + V_{b,t} F_{V,b,t} \right) \tag{3}$$

2.3. Constraints

2.3.1. Process constraints

(1) Heat source

Heat sources include gas turbine (GT), waste heat boiler (combined operation with GT for heat recovery, WHB), gas boiler (GB), wastewater source heat pump (WSHP) and air source heat pump (ASHP), the generic input-output model is shown in Eq.(4), where O_i^r denotes the rated output of heat or electricity, $O_{i,t}$ and $I_{i,t}$ denotes the output and input at time t, $\eta_{i,t}$ denotes the energy conversion efficiency, $\alpha_{i,min}$ denotes the minimum load rate and binary variable $\varepsilon_{i,t}$ denotes the start/stop status of the i-th unit.

$$\alpha_{i\,min} O_i^r \varepsilon_{i,t} \le O_{i,t} = \eta_{i,t} I_{i,t} \le O_i^r \varepsilon_{i,t} \tag{4}$$

(2) Thermal energy storage

The thermal energy storage (TES) model has been developed with both insulation and blending heat losses in Eq.(5), where $\eta_{loss,s}$ denotes the insulation loss and $\eta_{loss,ch/dis}$ denotes the blending loss when charging and discharging. The rated charge/discharge capacity $Q_{ch/dis,max}$ of HST is determined by its maximum storage capacity S_{max} in Eq.(6) [26]. Finally, the HST operation status is limited in the interval in Eq.(7).

$$S_t = (1-\eta_{loss,s}) S_{t-1} + (1-\eta_{loss,ch}) Q_{ch,t} - \frac{Q_{dis,t}}{1-\eta_{loss,dis}} \tag{5}$$

$$S_t = (1-\eta_{loss,s}) S_{t-1} + (1-\eta_{loss,ch}) Q_{ch,t} - \frac{Q_{dis,t}}{1-\eta_{loss,dis}} \tag{6}$$

$$0 \le Q_{ch/dis,t} \le Q_{ch/dis,max} \tag{7}$$

(3) Building thermal process

Heat load in static models is usually calculated at a set room temperature (usually 18°C) or predicted from available data set, both of which ignore the potential for load shifting due to the thermal inertia of the building. As shown in **Figure 2**, after considering the thermal inertia of the building envelope and the internal entities, the heat load model is replaced by the building heat transfer model, according to the concept of thermal comfort management[27].

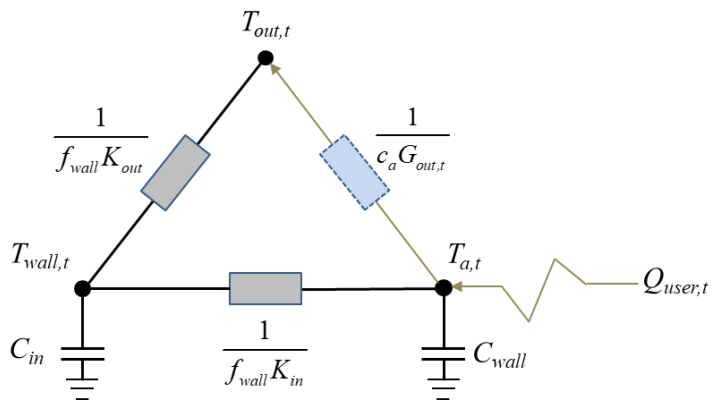

Figure 2. Simplified thermal resistance network diagram of building thermal process

The entire building envelope is equated to the same thermal mass, where the dynamics of $T_{wall,t}$ is influenced by the indoor air at $T_{a,t}$℃ and the outdoor convection and radiation effects, indicated as solar-air temperature at $T_{sa,t}$℃, as shown in Eq. (8)-(9).

$$T_{wall,t+1} = T_{wall,t} + \frac{f_{wall}K_{in}(T_{a,t} - T_{wall,t}) + f_{wall}K_{out}\left(T_{sa,t} - T_{wall,t}\right)}{C_{wall}} \tag{8}$$

$$T_{sa,t} = T_{out,t} + \frac{\rho_s I_t}{K_{out}} \tag{9}$$

Ignoring the storage effect of indoor heating equipment, they can be equivalent to the same indoor heat disturbance $Q_{user,t}$. Consider that the indoor air temperature field is uniformly distributed, and then all indoor objects and structures with heat storage characteristics can be equivalent to a comprehensive thermal mass. The thermal mass with the heat capacity of C_{in} receives heat from indoor heat disturbance, building envelope and cold air infiltration, shown in Eq.(10). In Eq.(11), the indoor temperature is limited to the comfort zone in accordance with Chinese GB50736-2012 and ASHRAE Standard 55[28].

$$T_{a,t+1} - T_{a,t} = \frac{Q_{user,t} + K_{in} f_{in}\left(T_{wall,t} - T_{a,t}\right) + c_a G_{out,t}\left(T_{out,t} - T_{a,t}\right)}{C_{in}} \tag{10}$$

$$18 \le T_{a,t} \le 26 \tag{11}$$

(4) Hydraulic and thermal model of heating network

The quasi-dynamic model of the heat network consists of both hydraulic and thermal sections. The hydraulic section can be expressed in the form of a matrix Eq.(12). The elements Δh_i in vector $\boldsymbol{\Delta H}$ can be determined by impedance s_i and flow rate g_i in Eq.(13).

$$\begin{cases} \boldsymbol{A}_H \boldsymbol{G} = \boldsymbol{Q} \\ \boldsymbol{B}_f \boldsymbol{\Delta H} = \boldsymbol{0} \end{cases} \tag{12}$$

$$\Delta h_i = s_i g_i^2 \tag{13}$$

For the thermal section, the characteristics are mainly characterized by heat transmission loss $\eta_{loss,net}$ and transmission delay Δt, shown in Eq.(14) -(15), where the heat loss is estimated according to the maximum heat dissipation value q_j specified in Chinese GB/T 4272-2015 and the information of j-th pipeline such as pipe diameter d_j, pipe length l_j and supply and return water temperature τ_g, τ_h. The transmission delay of branch network is determined by the heat load in each pipeline $Q_{j,t}^{source}$. The relationship between the heat supply from the heat source and the indoor heat disturbance can be expressed as Eq.(16).

$$\eta_{loss,net} = \frac{4000 q_j \sum l_j}{c_w \rho_w d_j v_j \left(\tau_g - \tau_h\right)} \tag{14}$$

$$\Delta t = \sum_{j=1}^{n} t_j = \sum_{j=1}^{n} \frac{4 l_j Q_{j,t}^{source}}{\pi \rho_w c_w d_j^2 \left(\tau_g - \tau_h\right)} \tag{15}$$

$$Q_t^{user} = \left(1 - \eta_{loss,net}\right) Q_{t-\Delta t}^{source} \tag{16}$$

2.4. Other constraints

2.4.1. Supply-demand balance constraints

The supply-demand balance constraints include the heat, electricity and gas balance in Eq.(17)-(19), where the subscript b is for buy and s for sell.

$$Q_t^{source} = Q_{WHB,t} + Q_{GB,t} + Q_{WSHP,t} + Q_{ASHP,t} + Q_{dis,t} - Q_{ch,t} \tag{17}$$

$$E_{b,t} + E_{GT,t} = E_{HP,t} + E_{s,t} \tag{18}$$

$$V_{GT,t} + V_{GB,t} = V_{b,t} \tag{19}$$

2.4.2. External purchase constraints

The purchasing and sale of energy is subject to restrictions in accordance with local policy, as Eq. (20)-(21).

$$V_{b.min} \le V_{b.t} \le V_{b.max} \tag{20}$$

$$E_{b/s,min} \le E_{b/s,t} \le E_{b/s,max} \tag{21}$$

3. CASE MODEL

An urban residential district in North China is selected as the case study, and the suitable combination of heat sources is selected based on the local resource endowment conditions to study the source storage capacity configuration and storage operational characteristics.

3.1. General information

The case area consists of 633,000m^2 residential buildings and 427,000m^2 school buildings. According to the resource endowment of the existing urban wastewater and gas network, the heat source is limited to the location shown in Figure 3. Considering the high price of electricity sales, GT is adopted as heat source to interact with the urban grid, while GB is introduced as a comparison to GT. Accordingly, the heating demand of the district is shown in **Figure 4**.

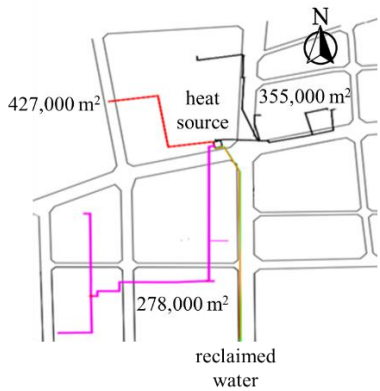

Figure 3. Layout of heat source and network

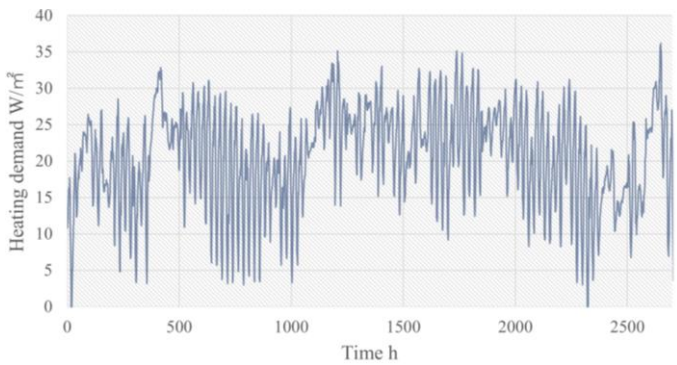

Figure 4. Hourly heating demand of the district

3.2. Variable efficiency of heat source units

As shown in **Figure 5**, the power generation efficiency of the gas turbine under part load conditions is given with literature research[29] and the operational power generation efficiency curve of the gas turbine is linearized in steps of 25% load factor *r*.

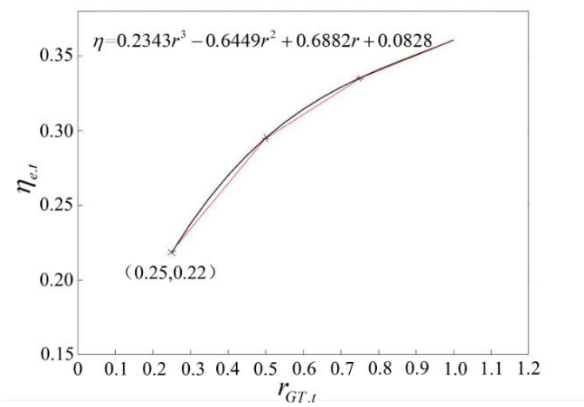

Figure 5. Variable efficiency and linearization of GT

The two types of heat pump shown in **Figure 6** are obtained from the corresponding resource endowment conditions of wastewater reclaimed water temperature and outdoor ambient temperature during the heating season.

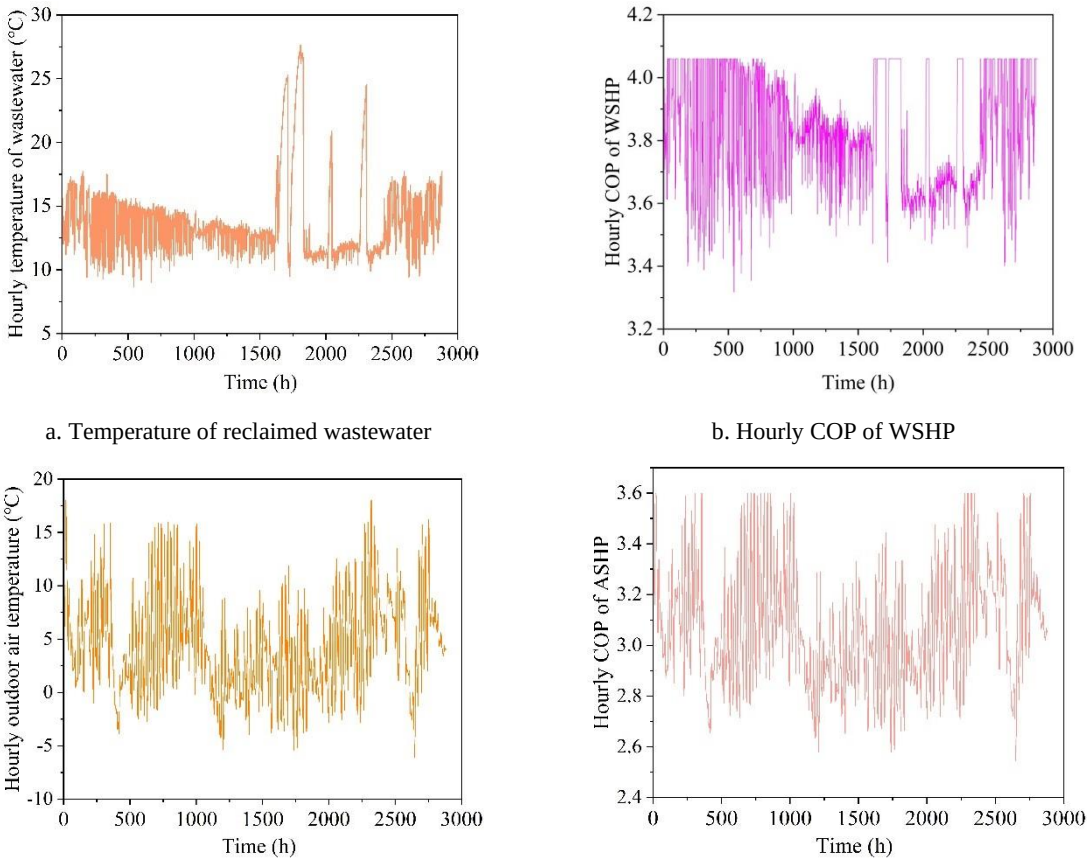

a. Temperature of reclaimed wastewater

b. Hourly COP of WSHP

c. Hourly outdoor temperature

d. Hourly COP of ASHP

Figure 6. Operational COP of heat pumps and their resource endowment during the heating season

3.3. Main parameters

Table 1 shows the unit price of each heat source equipment and other parameters obtained from market research while the energy price includes the peak-valley electricity price shown in **Figure 7** and the price 2.77 CNY/ m^3 for NG. The two-stage MILP model can be solved with the benders-dual cutting plane algorithm[30] in the Python environment.

Table 1. Operational and economic parameters of the energy supply units

Equipment	Rated efficiency and loss rate	Minimum load rate	Investment （CNY/kW）
GT	$\eta^r_{GT,e} = 0.25$ $\eta_{loss} = 0.07$	$\alpha_{GT\min} = 0.25$	$F_{GT} = 7900$
GB	$\eta_{GB} = 0.90$	$\alpha_{GB\min} = 0$	$F_{GB} = 850$
WHB	$\eta_{WHB} = 0.89$	$\alpha_{WHB\min} = 0$	$F_{WHB} = 1200$
ASHP	$COP^r_{ASHP} = 3.60$	$\alpha_{ASHP\min} = 0$	$F_{ASHP} = 1000$
WSHP	$COP^r_{WSHP} = 4.06$	$\alpha_{WSHP\min} = 0$	$F_{WSHP} = 1600$
HST	$\eta_{loss,s} = 0.01$ $\eta_{loss,ch} = 0.05$ $\eta_s = 0.05$	/	$F_{HST} = 110$ CNY/kWh

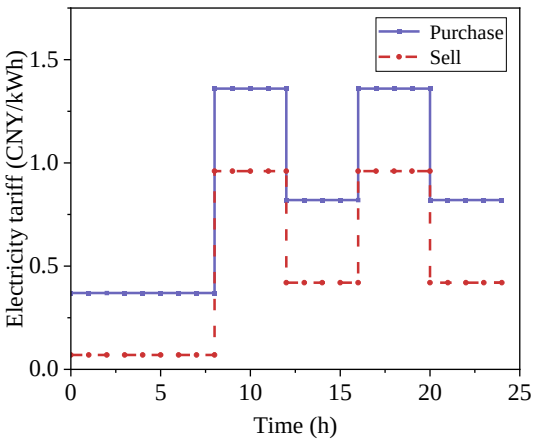

Figure 7. Electricity tariff signal

4. RESULTS

This section analyses the scheduling of source storage resources and the results of configuration results during different period of the heating season. Operational priorities and operating strategies for the heat source units are presented in this section, as well as the difference in operation and configuration results with the change of tariff peak-valley characteristics.

4.1. Operational results of dynamic optimization model

The results of typical system operational optimization results during the heating season are shown in **Figure 8**. The beginning/end and during the peak period of the heating season for 72 hours were intercepted respectively. 7**a** and 7**b** show the output of source and storage with the fluctuation of indoor temperature and indicate that the invocation of heat storage in buildings is directly related to the outdoor temperature. At the beginning/end of heating season, the indoor temperature fluctuates between 18 and 20.9°C. While during the peak period, the indoor temperature is fixed at 18°C. But HST still dominate absolutely compared to building heat storage resources.

The interaction between the DHS and the urban grid is shown in **Figure 8c** and 8**d**. The operational priority of heat source is mainly affected by peak-valley tariff. The priority can be summarized as: valley (WSHP>ASHP>WHB), flat (cooperation of WSHP and WHB > ASHP), peak (WHB > WSHP > ASHP). The priority indicates the order in which the units are switched on during operation period. Besides, the system purchases power during valley periods, avoids interacting with the grid during flat periods and sells power significantly during peak periods.

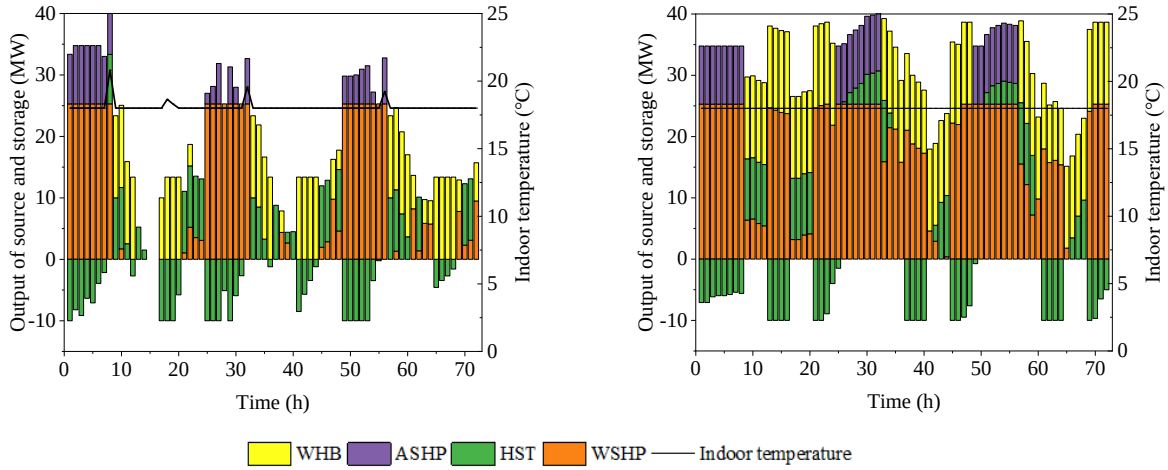

a. Output at the beginning/end period **b.** Output during the peak period

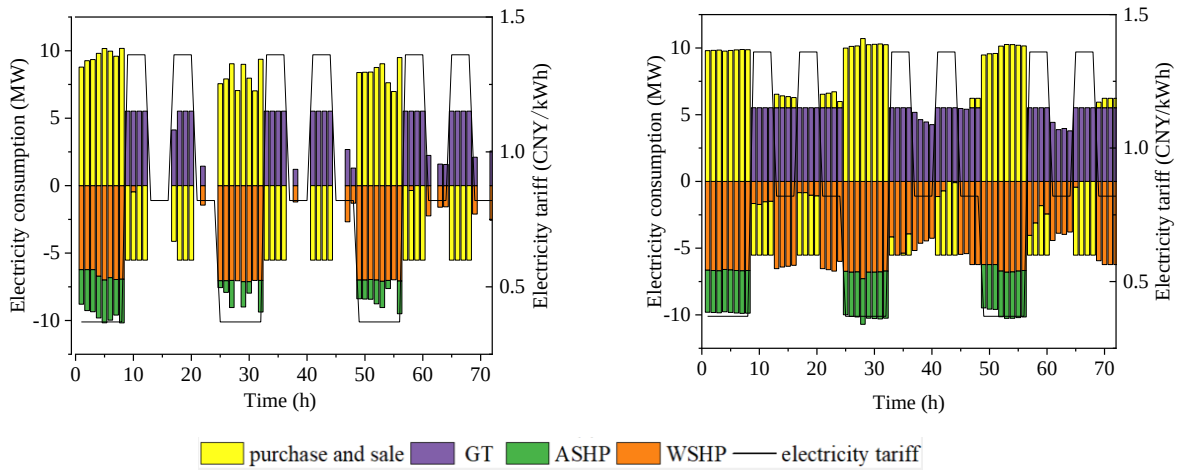

c. Electricity balance at the beginning/end period **d.** Electricity balance during the peak period

Figure 8. Operational optimization results

4.2. Analysis of storage resources

The energy storage resources of the DHS in the dynamic model include both HST and building thermal storage, both of which, especially HST, have an important role in the DHS. Even during the day when the room temperature reaches the peak, the HST still takes up 96.5% of the total heat storage (shown in **Figure 8a**).

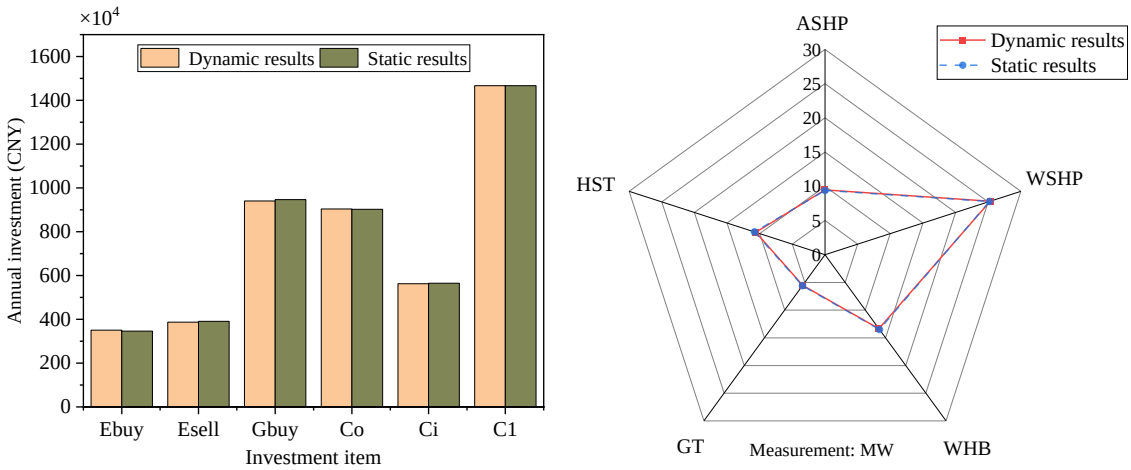

a. Economic optimization results **b.** Configuration results

Figure 9. Dynamic and static optimization results

As shown in **Figure 9**, only subtle differences between in the dynamic and static optimization results occurred, with the most significant impact on the configuration results for HST, which increased by only 2% in the static model. Therefore, the main advantage of dynamic optimization under the current peak-valley tariff policy is the ability to observe real-time changes in physical measurements such as indoor temperature, which can be adopted as the basis for system regulation for practical engineering optimization movements.

4.3. Analysis of peak-valley tariff policy

From the analysis in section 4.1, the peak-valley tariff is the key factor affecting the operation strategy of DHS. The optimal system operation strategy after increasing and decreasing the peak-valley difference in tariffs is shown in **Figure 10**. The operation strategy during the peak period is similar to that in section 4.1 and will not be discussed in detail. Restructuring peak tariff from 1.66 times the flat tariff to 2 times, with a same-proportion increase in the price of sale price, the optimization results are shown in **Figure 10a**. In this case, the role of the storage resources includes, in addition heat storage during the valley period, absorbing the excess heat generated when the sale of electricity movement occurs, which is not reflected in the original case.

As shown in **Figure 10b**, when the peak-valley ratio is 1, the storage resources are not invoked at the beginning and end of heating season, and the function of them is simply peak-shaving to obtain a smaller heat source capacity.

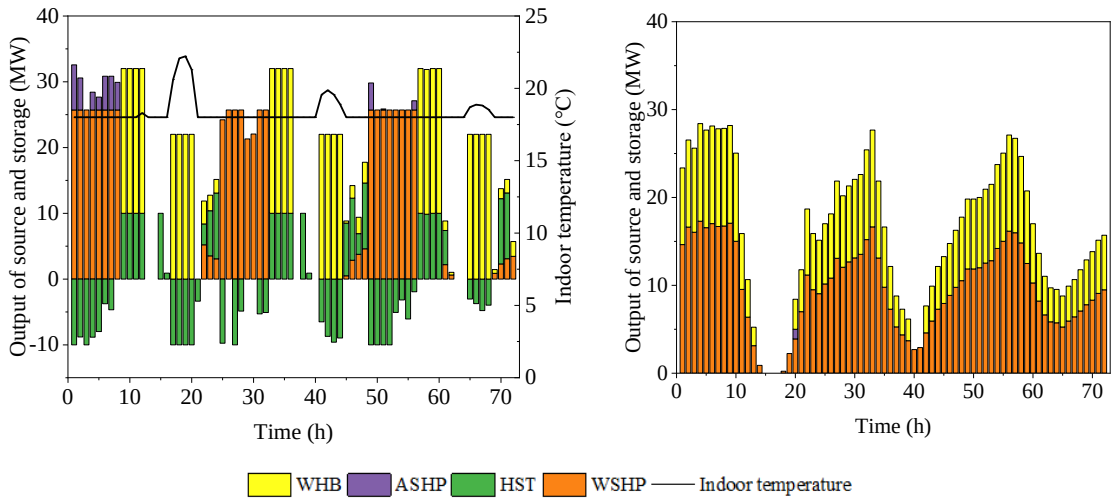

a. Output at the beginning/end period (p-v ratio=2) **b.** Output at the beginning/end period (p-v ratio=1)

Figure 10. Operational optimization results with different peak-load ratio

5. CONCLUSION

In this paper, with reference to the dynamic characteristics in DHS, a dynamic process-oriented optimization model is established, and the operation characteristics of thermal storage resources invocation and peak-valley tariff are analyzed with a case study. The conclusions can be summarized as follows.

(1) HST still takes over 96.5% of the total heat storage during the heating season and the building thermal storage only brings a 2% decrease of HST capacity.

(2) Although the dynamic and static models are very close in terms of capacity configuration results, the dynamic model can be adopted as a reference to judge the rationality of DHS through measurable variables e.g. indoor temperature.

(3) The contribution of heat storage equipment varies with the characteristics of peak and valley tariffs, as evidenced by the fact that when peak-valley ratio varies from 1 to 2, the contribution goes through peak shaving to reduce heat source capacity, load shifting to reduce electricity purchase costs and absorbing excess heat generated by the frequent electricity sales actions.

ACKNOWLEDGEMENT

This work was supported by the National Key R&D Program of China (No. 2021YFE0116100).

REFERENCES

[1] Liu Z, Deng Z, He G, Wang H, Zhang X, Lin J, et al. Challenges and opportunities for carbon neutrality in China. Nature Reviews Earth & Environment. 2022;3:141-55.
[2] Wang C, Lv C, Li P, Song G, Li S, Xu X, et al. Modeling and optimal operation of community integrated energy systems: A case study from China. Applied Energy. 2018;230:1242-54.
[3] Wegner P. Concepts and paradigms of object-oriented programming. ACM Sigplan Oops Messenger. 1990;1:7-87.
[4] Lu X, Liu Z, Ma L, Wang L, Zhou K, Feng N. A robust optimization approach for optimal load dispatch of community energy hub. Applied Energy. 2020;259.
[5] Jiang XS, Jing ZX, Li YZ, Wu QH, Tang WH. Modelling and operation optimization of an integrated energy based direct district water-heating system. Energy. 2014;64:375-88.
[6] Di Somma M, Yan B, Bianco N, Graditi G, Luh PB, Mongibello L, et al. Operation optimization of a distributed energy system considering energy costs and exergy efficiency. Energy Conversion and Management. 2015;103:739-51.
[7] Zhang R, Wang D, Liu Y, Chen Y, Fan J, Song C, et al. Economic optimization of auxiliary heat source for centralized solar district heating system in Tibetan Plateau, China. Energy Conversion and Management. 2021;243.
[8] Kopanos GM, Georgiadis MC, Pistikopoulos EN. Energy production planning of a network of micro combined heat and power generators. Applied Energy. 2013;102:1522-34.
[9] Söderman J, Pettersson F. Structural and operational optimisation of distributed energy systems. Applied Thermal Engineering. 2006;26:1400-8.
[10] Christidis A, Koch C, Pottel L, Tsatsaronis G. The contribution of heat storage to the profitable operation of combined heat and power plants in liberalized electricity markets. Energy. 2012;41:75-82.
[11] Gebremedhin A. Introducing District Heating in a Norwegian town – Potential for reduced Local and Global Emissions. Applied Energy. 2012;95:300-4.
[12] Dotzauer E. Simple model for prediction of loads in district-heating systems. Applied Energy. 2002;73:277-84.
[13] Lund H, Østergaard PA, Nielsen TB, Werner S, Thorsen JE, Gudmundsson O, et al. Perspectives on fourth and fifth generation district heating. Energy. 2021;227:120520.

[14] Schweiger G, Larsson P-O, Magnusson F, Lauenburg P, Velut S. District heating and cooling systems – Framework for Modelica-based simulation and dynamic optimization. Energy. 2017;137:566-78.
[15] Ghilardi LMP, Castelli AF, Moretti L, Morini M, Martelli E. Co-optimization of multi-energy system operation, district heating/cooling network and thermal comfort management for buildings. Applied Energy. 2021;302.
[16] Nguyen DT, Le LB. Joint optimization of electric vehicle and home energy scheduling considering user comfort preference. IEEE Transactions on Smart Grid. 2013;5:188-99.
[17] Gu W, Wang J, Lu S, Luo Z, Wu C. Optimal operation for integrated energy system considering thermal inertia of district heating network and buildings. Applied energy. 2017;199:234-46.
[18] Hu W, Song M, Jiang Y, Yao Y, Gao Y. A modeling study on the heat storage and release characteristics of a phase change material based double-spiral coiled heat exchanger in an air source heat pump for defrosting. Applied Energy. 2019;236:877-92.
[19] Jia L, Liu J, Chong A, Dai X. Deep learning and physics-based modeling for the optimization of ice-based thermal energy systems in cooling plants. Applied Energy. 2022;322.
[20] Lamrani B, Belcaid A, Lebrouhi BE, Khodadadi JM, El Rhafiki T. Dynamic thermal analysis of a coupled solar water heaters-thermal storage tank for solar powered district heating networks. Journal of Energy Storage. 2023;61.
[21] Guo L, Liu W, Cai J, Hong B, Wang C. A two-stage optimal planning and design method for combined cooling, heat and power microgrid system. Energy Conversion and Management. 2013;74:433-45.
[22] Luo XJ, Oyedele LO, Akinade OO, Ajayi AO. Two-stage capacity optimization approach of multi-energy system considering its optimal operation. Energy and AI. 2020;1.
[23] Zhou Z, Zhang J, Liu P, Li Z, Georgiadis MC, Pistikopoulos EN. A two-stage stochastic programming model for the optimal design of distributed energy systems. Applied Energy. 2013;103:135-44.
[24] Zhang M, Wu Q, Wen J, Pan B, Qi S. Two-stage stochastic optimal operation of integrated electricity and heat system considering reserve of flexible devices and spatial-temporal correlation of wind power. Applied Energy. 2020;275.
[25] Li P, Wang Z, Wang J, Yang W, Guo T, Yin Y. Two-stage optimal operation of integrated energy system considering multiple uncertainties and integrated demand response. Energy. 2021;225.
[26] Energy AD. Technology data for energy plants. 2012.
[27] Wang P, Ju Y, Liu S, Wang W, Lei C. Reduction analysis of building thermal models for simulation of heating accidents. Building Simulation. 2020;13:1249-58.
[28] Stevenson WJ. Using artificial neural nets to predict building energy parameters. Conference: 1994 American Society of Heating, Refrigerating, and Air Conditioning Engineers (ASHRAE) annual meeting, Orlando, FL (United States), 25-29 Jun 1994; Other Information: PBD: 1994; Related Information: Is Part Of ASHRAE transactions 1994: Technical and symposium papers Volume 100, Part 2; PB: 1372 p. United States: American Society of Heating, Refrigerating and Air-Conditioning Engineers, Inc., Atlanta, GA (United States); 1994. p. Medium: X; Size: pp. 1081-7.
[29] Lee JH, Kim TS, Kim E-h. Prediction of power generation capacity of a gas turbine combined cycle cogeneration plant. Energy. 2017;124:187-97.
[30] Zeng B, Zhao L. Solving two-stage robust optimization problems using a column-and-constraint generation method. Operations Research Letters. 2013;41:457-61.

The 18th International Symposium on District Heating and Cooling, September 3–6, 2023, Beijing, China

PRODUCTION OPTIMIZATION OF AN EXISTING DISTRICT HEATING NETWORK WITH MULTIPLE HEAT PRODUCERS

Theda Zoschke [a] */, Lukas Schmidt-Engelbertz [b] **, Christian Wolff [a], Armin Nurkanović [b], Clara Pineau [a], Quentin Lyons [a], Lilli Frison [a], Gregor Rohbogner [c], Daniel Weiß [c], Moritz Diehl [b], Axel Oliva [a]**

[a] *Fraunhofer Institute for Solar Energy Systems, Freiburg, 79110, Germany*
[b] *University of Freiburg, Freiburg, 79110, Germany*
[c] *HBG GmbH, Zell/Wiesental, 79669, Germany*
* *Corresponding author. theda.zoschke@ise.fraunhofer.de*
** *Equal contributors*

ABSTRACT

A Mixed Integer Linear Programming (MILP) optimization problem is formulated to optimize the power production of several heat production units and a storage tank in a district heating network in Weil am Rhein, Germany. This implementation is the first step in the development of a Model Predictive Control (MPC) methodology in the research project WOpS to operate networks with decentralized heat producers. Historical demand data and producer specifications of the existing network are used for the analysis. The operation is simulated for a winter and a summer day. It is shown that the methodology is successfully implemented, even though more constraints should be considered in future developments to include dynamic effects more realistically.

Keywords: MPC, MILP, District heating

1. INTRODUCTION

District heating networks (DHN) play a crucial role in implementing an emission-free heat supply, as they enable the optimal utilization of diverse renewable heat sources and industrial waste heat. However, as district heating networks grow larger and more diverse, and as decentralized feed-in points are integrated, the networks control and efficient production planning becomes increasingly challenging. This is especially true when heat production units cannot generate heat on demand, storage capacities exist and the temporal and local discrepancy between supply and demand must be compensated.

Under the framework of the German-funded Project WOpS, Model Predictive Control (MPC) will be integrated into several existing district heating networks to optimize the operation of all heat production units in an economically efficient manner. For an existing medium-sized district heating system in the city of Weil am Rhein, Germany, a Mixed Integer Linear Programming (MILP) optimization problem is formulated to optimize the production of the five main heat production units: a biomass boiler, a Combined Heat and Power (CHP) unit, an oil boiler as well as two gas boilers. Additionally, a 115 m³ thermal energy storage (TES) is integrated. In the current conventional strategy, the CHP unit provides the base load, followed by the biomass boiler while the fossil fuel boilers cover peak load demands. Energy prices, storage dispatch, operational constraints and the evaluation demand data are not considered. The novel optimization routine is implemented in a MPC framework using a simple heating network model.

In this contribution, we explain the software implementation of the algorithm and show first simulation results. While mixed-integer linear MPC or linear MPC has been used frequently in district heating production optimization [1–3], this work shows how to practically implement this approach on the example of an existing DHN with multiple heat producers and discusses the advantage to the current control strategy as well as the gap that is left with this approach to control networks with even more decentralized consumers. Future work involves implementing the MPC strategy into the actual network operation, the investigation of the challenges in practical implementation as well as the extension of the algorithm to include more dynamic effects.

2. METHODOLOGY

2.1. Formulation of Optimization Problem

This chapter summarizes the formulation of the optimization problem. The algorithm is implemented in Python using the open-source software package CasADi [4]. It consists of linear constraints and a linear objective function, with both binary and continuous variables, and is therefore classified as a MILP problem. For solving the optimization problem, the open-source solver SCIP [5] is used.

The overall aim is to minimize the objective function while considering several constraints that include the characteristics of the heat production units, the thermal energy storage and the behavior of the network. Consequently, all heat flows $\dot{Q}$ of the production units are used as decision variables of the objective function. For the modeling of heat production units, the constraints include maximum and minimum power outputs, ramping rate limits as well as minimum up- and down-times of operation. Additional decision variables needed here are the on/off and switch-on / switch-off binary variables as well as the charging/discharging power and stored heat of the TES that are introduced in the following paragraphs.

2.1.1. Objective Function

We aim at determining the production trajectory of each producer that minimizes the operational costs of the DHN. Consequently, the objective function C is modeled as

$$C(\dot{Q}) = \sum_{j=1}^{N_{TU}} \sum_{t=0}^{N_T} \left(\dot{Q}_j(t) c_j(t) + S_j^{up}(t)\, c_j^p \right) + \sum_{m=1}^{N_{TES}} \sum_{t=0}^{N_T} H_m(t)\, c_m^p \,, \tag{1}$$

where $\dot{Q}_j(t)$ is the generated heat of thermal unit *j* at time step *t*. The parameter $c_j(t)$ is the respective cost of generating one unit of heat in thermal unit *j* at time step *t*. This includes the cost of fuel and emissions. Depending on the type of heat generation, different parameters must be considered and consequently adapted for the formulation of the heat generation cost $c_j(t)$. For the scope of our optimization, we distinguish between boilers that only produce heat and CHP generation that also includes the selling of electricity. In addition, penalty costs c^p for the start-up of production units $S_j^{up}(t) = 1$ and the storage of heat in TES $H_m(t)$ are included to counteract a frequent start-up and shut-down of the producers and a high filling level of the storage. The number of heat production units in the set of all units in the network $\mathcal{J}$ is defined by N_{TU}, the number of all heat storages is N_{TES} and N_T is the number of time steps in the optimization horizon $\mathcal{T} = \{1, \dots, N_T\}$.

2.1.2. Constraints for switching binaries

To include the switch-on/switch-off process in the optimization problem, switching binaries are introduced. The binary variable $y_j(t)$ captures whether the respective unit is operating or not (on = 1 and off = 0) at time step t. The variables S_j^{up} (up) and S_j^{do} (down) aim at capturing the time of switch-on and switch-off. The switching binaries are related through the following two constraints [6],

$$y_j(t) - y_j(t-1) = S_j^{\mathrm{up}}(t) - S_j^{\mathrm{do}}(t), \qquad \text{for all } j \in \mathcal{J}, t \in \mathcal{T} \setminus \{1\}, \tag{2}$$

$$S_j^{\mathrm{up}}(t) + S_j^{\mathrm{do}}(t) \leq 1, \qquad \text{for all } j \in \mathcal{J}, t \in \mathcal{T}. \tag{3}$$

Equation (2) links the switch variables to the variable $y_j(t)$ that the units can only be switched on or off if the unit is not or is operating the timestep before. The case where both switch variables take the value one is prevented by equation (3). The initial state of the production unit $y_j(1)$ is set and does not need to be constrained by Equation (2).

2.1.3. Constraints for minimum and maximum capacity

The upper and lower bounds of the produced heat $\dot{Q}_j(t)$ depend on the maximum and minimum capacity of each production unit, the start-up and shutdown times, the power ramp-up and ramp-down rates, as well as the current output. The start-up limitations are implemented as the time of start-up t_j^{SU} until the producer reaches the minimum power $\dot{Q}_j^{min}$ that needs to be multiplied by the size of the optimization time step length Δt. The shut-down limitation is implemented as the time of shut-down t_j^{SD} until the producer is switched off. Ramp-up RU_j and ramp-down RD_j describe the process for the producer to get from minimum to maximum capacity and vice versa.

The upper bound is expressed by the following equations based on [7],

$$\dot{Q}_j(t) \leq \dot{Q}_j^{max}\left(y_j(t) - S_j^{\mathrm{do}}(t+1)\right) + \frac{\dot{Q}_j^{max}\Delta t}{t_j^{SD}} S_j^{\mathrm{do}}(t+1), \qquad \text{for all } j \in \mathcal{J}, t \in \mathcal{T} \setminus \{N_T\}, \tag{4}$$

$$\dot{Q}_j(t) - \dot{Q}_j(t-1) \leq RU_j\, \Delta t\, y_j(t-1) + \frac{\dot{Q}_j^{min}\Delta t}{t_j^{SU}} S_j^{\mathrm{up}}(t), \qquad \text{for all } j \in \mathcal{J}, t \in \mathcal{T} \setminus \{1\}, \tag{5}$$

where Equation (4) ensures that the produced heat $\dot{Q}_j(t)$ is less than the maximum possible power $\dot{Q}_j^{max}$ or the shutdown power in case the unit is switched off at the next time step. Equation (5) regulates the limit of the power change in two cases. The first case is when the unit remains operating, the power change must be less than the ramp RU. In the second case, the unit is switched on and cannot reach more power than the start-up time to reach minimum power allows.

Similarly, the lower bound is defined by the following two constraints, also based on [7],

$$\dot{Q}_j(t) \geq \dot{Q}_j^{min} y_j(t), \qquad \text{for all } j \in \mathcal{J}, t \in \mathcal{T}, \tag{6}$$

$$\dot{Q}_j(t-1) - \dot{Q}_j(t) \leq RD_j\, \Delta t\, y_j(t) + \frac{\dot{Q}_j^{max}\Delta t}{t_j^{SD}} S_j^{\mathrm{do}}(t), \qquad \text{for all } j \in \mathcal{J}, t \in \mathcal{T} \setminus \{1\}, \tag{7}$$

where Equation (6) ensures that if the unit is operating, the produced heat will not fall below its minimum capacity. Like Equation (5), Equation (7) checks that the difference between the power at time step $t-1$ and time step t does not exceed the ramp-down rate or the shutdown limits.

2.1.4. Constraints for minimum up- and down-time

A common technical feature of power generation units are the minimum up- and down-time constraints. They capture the effect that once a supply unit is turned on or off, it may need to stay in that state for a certain amount of time to prevent frequent switching. The following constraints specify the minimum up-time [7],

$$\sum_{k=1}^{L_j^{\mathrm{up}}} \left(1 - y_j(k)\right) = 0, \qquad \text{for all } t = \{1, \ldots, L_j^{\mathrm{up}}\}, j \in \mathcal{J}, \tag{8}$$

$$\sum_{k=t}^{t+UT_j-1} y_j(k) \geq UT_j\, S_j^{\mathrm{up}}(t), \qquad \text{for all } t = \{L_j^{\mathrm{up}}+1, \ldots, N_T - UT_j + 1\}, j \in \mathcal{J}, \tag{9}$$

$$\sum_{k=t}^{N_T} \left(y_j(k) - S_j^{\mathrm{up}}(t)\right) \geq 0, \qquad \text{for all } t = \{N_T - UT_j + 2, \ldots, N_T\}, j \in \mathcal{J}. \tag{10}$$

Equation (8) describes the status of the production units $y_j(k)$ in the first time step of the horizon. Here, the unit must operate for L_j^{up} further time steps if it is in operation at time step 0. L_j^{up} is calculated from the minimum up time UT_j in time steps of the production unit minus the time steps the unit was already operating at time step zero UT_j^0. Equation (9) forces the unit to continue generating power for the next $UT_j - 1$ time steps, if it gets turned on at time step t. It covers the middle range of the horizon. The end of the horizon, which is not covered by Equation (8) and Equation (9) is handled by Equation (10). It handles the up-time constraint when the producer is switched on at the end of the horizon with fewer remaining time steps than the minimum up-time UT_j. There it ensures that the producer stays in operation until the end of the horizon. The minimum down-time constraints can be implemented identically to constraints (8) to (10) simply by substituting the appropriate downtime parameters and variables, and by replacing $y_j(k)$ with $1 - y_j(k)$.

2.1.5. Thermal energy storage

A thermal energy storage (TES) unit is defined by its evolution of the stored heat H_m. This can be modelled as follows,

$$H_m(t+1) = H_m(t) + \Delta t \dot{Q}_m^{\mathrm{ch}}(t), \qquad \text{for all } t \in \mathcal{T} \setminus \{N_T\}, m \in \mathcal{M}. \tag{11}$$

$$H_m(t) \leq H_m^{max}, \qquad \text{for all } t \in \mathcal{T}, m \in \mathcal{M} \tag{12}$$

where m is a TES of the set of TES in the network $\mathcal{M}$. The variable $\dot{Q}_m^{\mathrm{ch}}$ describes the balance of incoming (positive) and outgoing (negative) heat flows in the TES. Equation (12) limits the stored heat to the maximum storage capacity H_m^{max}.

2.1.6. Energy conservation

The network enables the transport of generated heat to consumers and TES. In this process, heat can be injected or extracted at nodes $n \in \mathcal{N}$ of the network. Nodes are connected to each other with pipes and can exchange a heat flow through the pipes $\dot{Q}_p$. To define the equation of energy conservation for each node we have to sum up the incoming and outgoing heat flows at the specific node k for each connected producer, consumer, storage or pipe [1, 8], described by

$$\sum_j \dot{Q}_{j,n}(t) - \sum_m \dot{Q}_{m,n}^{ch}(t) - \sum_c d_{c,n}(t) + \sum_p \dot{Q}_{p,n}(t) = 0, \tag{13}$$
$$\text{for all } t \in \mathcal{T}, j \in \mathcal{J}, m \in \mathcal{M}, c \in \mathcal{C}, p \in \mathcal{P}, n \in \mathcal{N}.$$

The variable $d_{c,n}(t)$ is the heat demand of consumer c in the set of consumers $\mathcal{C}$ at node n. It must be noted that the heat flow of the pipes $\dot{Q}_p$ and the TES $\dot{Q}_m$ can be negative or positive depending on the energy conservation of each node. At the moment, power restrictions between the nodes are not enabled, but the introduced node structure allows to consider this in future analyses.

2.2. Model Predictive Control

The optimization described above is optimizing the heat production for a given prediction horizon. The horizon was chosen to be 24 hours and the sampling time step is 15 minutes. In the MPC setting, a new problem is solved in every step. A schematic block diagram of the MPC approach can be seen in Figure 1.

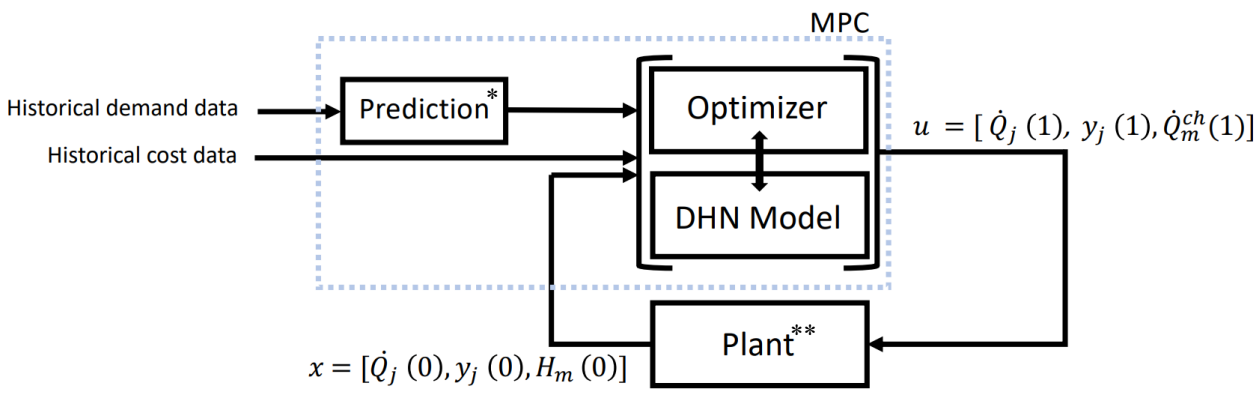

Figure 1: Block diagram of MPC approach.
* The prediction is represented by a randomization of historical data
** The plant is represented by a simple model that automatically transfers the control values u to the state values x

The power specifications u for the production units and thermal storage units resulting from the first time step of the optimization are forwarded to the control technology of the plants in the network, resulting in a Model Predictive Control (MPC) approach. A new optimization is then carried out for the next time step, shifting the horizon by the corresponding time step. At present, the control input u is used directly to determine the state x of the plants for the next MPC step. This simple approach is used to model the behavior of the units during offline testing. Other inputs to the control logic are the extracted demand data, fuel cost data, and an electricity selling price. Since the MPC is currently tested in historical periods where demand data is known, no prediction is required. To replicate the uncertainties of a forecast, the historical demand data is randomized in a range of +-20% for each MPC step.

2.3. Metadata Extraction

The reference system for the here described optimization methodology is a medium sized district heating network in Weil am Rhein located in the South-West of Germany. It consists of currently 75 consumers and 5 production units as well as a storage tank. Figure 2 shows the overall layout of the DHN on the city map of Weil am Rhein. To simplify the description of the network in the optimization formulation, it is reduced to 10 nodes according to Figure 3.

Figure 2: Map of Weil am Rhein including structure of the reference network

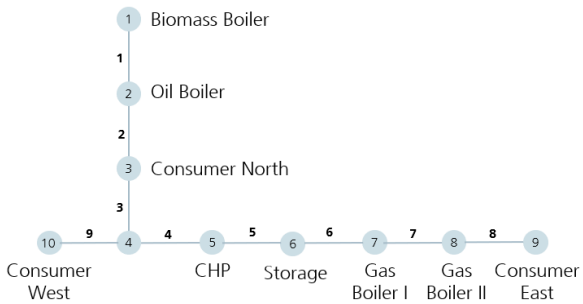

Figure 3: Simplified node structure of the reference network

The overall consumer mix predominantly consists of smaller and medium-sized customers, which are mostly single- and multi-family residential buildings. Most of the larger consumers are schools, care facilities or large multi-family houses. Consumer demand data of all substations is available in 15-minute increments. For this analysis, historical data for 2022 is used, with aggregated consumers in the northern, eastern, and western subnetworks and assigned to the respective nodes. Currently, 5 main active heat production units as well as the storage tank are located in the northern and eastern part of the network. Several additional heat production units are in construction and will be considered in future analyses. The DHN operates at temperature levels of approximately 75 - 105 °C supply and 45 - 55 °C return temperature, depending on season and ambient temperature. The input parameters for the formulation of the optimization problem can be found in Table 1. The maximum storage capacity that was assigned to the 115 m³ tank is 6 MWh. It can be reached if the temperature difference in the tank is about 45 K. The current control strategy for production optimization includes a simple hierarchical ordering of the main biomass boiler and CHP plant producers and a storage level dependent control for the fossil peak load boilers.

Table 1: Technical details of the main heat suppliers in the DHN

Production unit	**Unit**	**Biomass boiler**	**Oil boiler**	**CHP**	**Gas boiler I**	**Gas boiler II**
Subnetwork		*North*	*North*	*East*	*East*	*East*
Maximum capacity	*MW*	2.0	1.6	0.87	1.16	1.16
Minimum capacity	*MW*	0.7	1.2	0.43	0.29	0.29
Ramp-up/ Ramp-down	*MW/h*	0.2	26.1	1.32	26.1	26.1
Start-up time	*min*	15	15	15	15	15
Minimum runtime	*h*	350	0.25	1	0.25	0.25

To make computational analysis of the network possible, geographical data regarding the local property lots as well as the location of main and connection pipes is made available by the network operator, HBG. Based on this data, a code framework is established that links raw geographical datapoints to enable the following analyses:

- Selective mapping of network elements with a high resolution (e.g. single pipe segments / heat exchangers)
- Aggregation of consumers into subnetworks
- Provide input data and parameter sets for dynamic simulation of (sub-)networks
- Inclusion of addresses makes it possible to link consumption data to single consumers/nodes

Figure 4 shows the network structure that is derived from the data analysis. The light green dots represent the heat production units and storage, while the purple dots represent the consumers, where the marker size is scaled according to their consumption in 2022. The producers with the highest demand are located in the northern and eastern subnetwork, close to the main heat production units and storage.

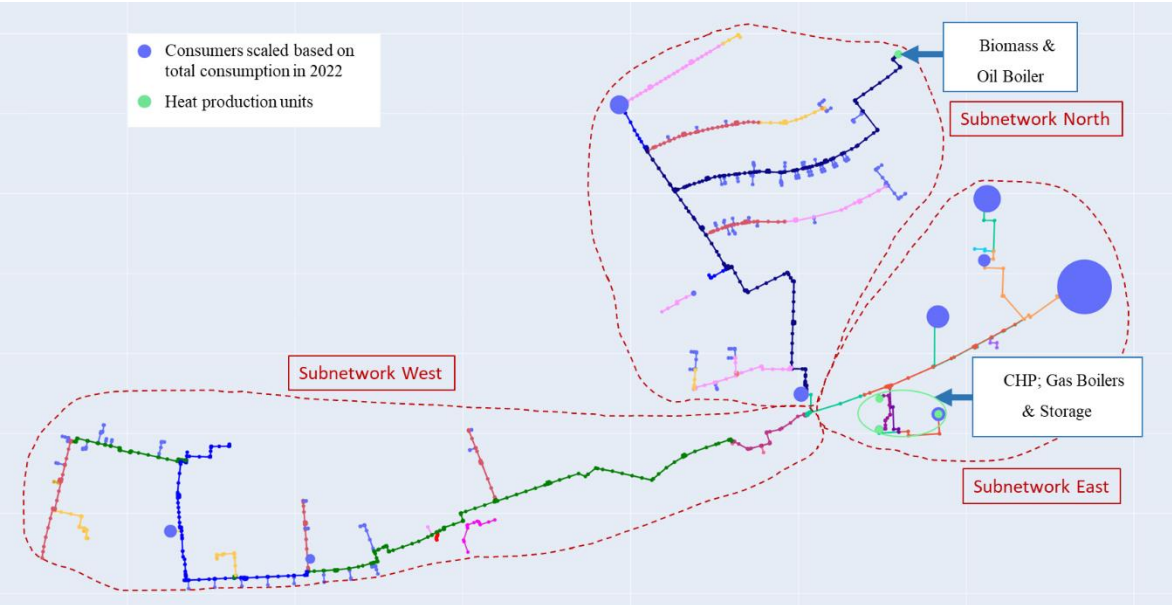

Figure 4: Representation of DHN based on geodata

2.4. Cost Assumptions

Beside the demand data as well as network and producer metadata, the cost data according to Table 2 is used as input into the optimization problem. This cost data is based on the DHN operator's real prices in 2022. To simplify the model, the data is assumed to be constant.

Table 2: Cost data

		Biomass	Gas	Oil	Electricity Selling Price	Carbon Emission Price
Cost	*€/MWh*	18	45	64	124	
	€/t_{CO2}					30.0

3. RESULTS

The optimization using the MPC approach is performed for a day in December with particularly high heat demand and a day in summer with low heat demand with a sampling time step of 15 minutes and a prediction horizon of 24 hours.

Figure 5 shows the results for a chosen winter day in December. There, the CHP plant is always prioritized as it has the lowest energy costs due to the ability to sell electricity. (orange line). Secondly the biomass boiler is used as it shows the second least energy costs (blue solid line). In the very beginning of the simulation the oil boiler is used, as the start-up and ramp-up of the biomass boiler and CHP plant take several time steps (purple solid line). The gas boilers are also used several times when the ramp-up of the CHP and biomass boiler does not match the rate of change of demand data between two MPC steps (red and green solid line). It is also easy to see that before peak loads (black solid line) the storage is charged (blue dashed line) to reduce the demand from fossil fuel generators.

The summer day, on the other hand, in Figure 6 shows a much lower heat demand (black line). As a result, only one producer needs to be turned on to meet the demand while simultaneously charging the storage tank. Equally as in winter, the CHP plant is addressed first because of the lowest production cost (orange line), mostly at its minimum capacity. When it is in operation, the storage gets charged (dashed blue line) as the demand is lower than the CHP plants minimum capacity. During the time the CHP plant is not running, the storage covers the demand of the consumers.

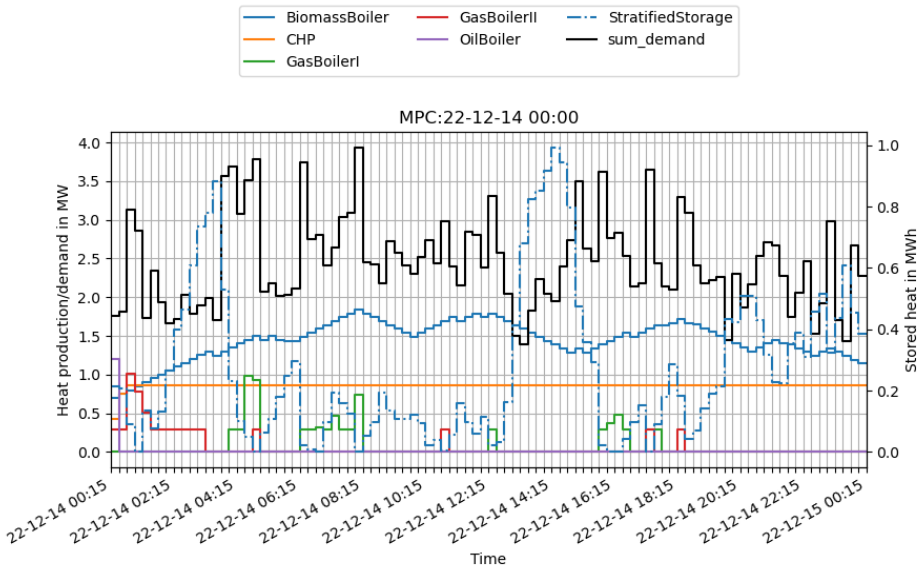

Figure 5: Model predictive control of producer power for reference network in Weil am Rhein for one day in December in 15 minutes time steps and prediction horizon of 24 hours

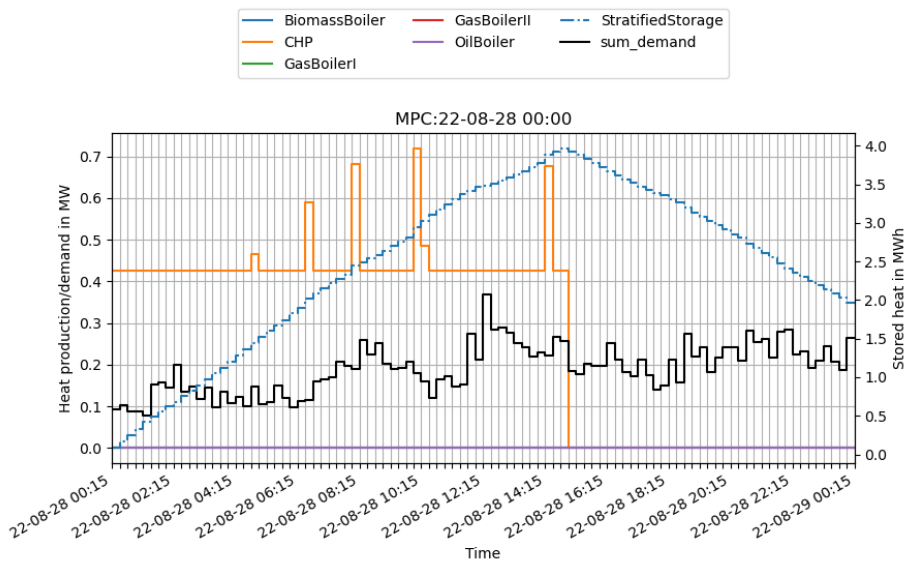

Figure 6: Model predictive control of producer power for reference network in Weil am Rhein for one day in August in 15 minutes time steps and prediction horizon of 24 hours

4. DISCUSSION

The implemented MPC controller allows the cost-optimized and automized control of various heat producers, taking into account the individual start-up and shut-down dynamics. Compared to the previous strategy no manual decisions need to be taken by the operator and varying demand and cost data can be processed automatically by considering it for a given time horizon. Furthermore, the integration of additional heat producers in the network is facilitated, since the cost-optimal balancing of the individual start-up and shut-down behavior becomes increasingly complex as the number increases.

The winter day example shows that the base load of the DHN can be covered by the CHP and the biomass boiler. Here, the remaining producers and the TES are used for load peaks or large rates of change between actual and randomly varied demand in two MPC steps. The low use of the TES is striking. To account for unforeseen demand changes, forecasting errors and uncertainties, the model should be adjusted, so more load peaks are covered by the TES alone, and oil and gas boiler operation is avoided. In addition, the model is based on simplified assumptions and it must be assumed that the heat demand is varying in real operation due to losses as well as flow and power restrictions in the DHN. For this reason, the model must be extended in the future to include more of these dynamics.

The evaluation of the summer day shows that the CHP plant alone can provide the heat needed to cover the hot water demand of the consumers. This is consistent with the operator's observations of network behavior. Also, the CHP should be turned off and on as little as possible due to increased wear and TES charging should be distinct. This is reflected in the evaluation as the CHP unit is only switched on once.

5. CONCLUSION AND OUTLOOK

The implementation of this linear mixed-integer optimization and MPC methodology is the first step in the research project WOpS. The results show that it is possible to optimize the production in an easy and efficient manner. This MPC will soon be implemented in the existing plant in Weil am Rhein and monitored in the upcoming winter season. The MPC controller will define the mass flow set point of the plant, while differential pressure, flow and temperature restrictions of the DHN from superordinate control loops as well as self-protection of production units will still be maintained. It is suspected that the impact of supply temperature variations and the coordination of different pumps in systems with even more decentralized producers will become increasingly challenging, as all these aspects influence the efficiency. Interactions between the different effects can hardly be foreseen and included in classic control loops. Therefore, it will be assessed, how the optimization routine needs to be extended to include more constraints like flow restrictions, transport delays, heat losses as well as supply temperature and pump speed optimization, which may lead to a non-linear optimization problem. The impact of different MPC routines on the control of DHNs with decentralized producers will be evaluated and demonstrated if they show to be successful in the theoretic analysis.

ACKNOWLEDGEMENT

This work was funded by the BMWK (German Federal Ministry of Economic Affairs and Climate Action) under grant 03EN3054A („WOpS - Wärmefluss-Optimierung zur Sektorenkopplung in Fernwärmenetzen mitttels MPC unter Berücksichtigung eines strommarktorientierten Betriebs“).

Bundesministerium für Wirtschaft und Klimaschutz

REFERENCES

[1] F. Verrilli *et al.,* “Model Predictive Control-Based Optimal Operations of District Heating System With Thermal Energy Storage and Flexible Loads,” *IEEE Trans. Automat. Sci. Eng.*, vol. 14, no. 2, pp. 547–557, 2017, doi: 10.1109/TASE.2016.2618948.

[2] G. Gambino *et al.,* “Optimal operation of a district heating power plant with thermal energy storage,” in *2016 American Control Conference (ACC)*, Boston, MA, USA, 2016, pp. 2334–2339.

[3] D. Quaggiotto, J. Vivian, and A. Zarrella, “Management of a district heating network using model predictive control with and without thermal storage,” *Optim Eng*, vol. 22, no. 3, pp. 1897–1919, 2021, doi: 10.1007/s11081-021-09644-w.

[4] J. A. E. Andersson, J. Gillis, G. Horn, J. B. Rawlings, and M. Diehl, “CasADi: a software framework for nonlinear optimization and optimal control,” *Math. Prog. Comp.*, vol. 11, no. 1, pp. 1–36, 2019, doi: 10.1007/s12532-018-0139-4.

[5] K. Bestuzheva *et al.,* “The SCIP Optimization Suite 8.0,” Technical Report, Optimization Online, 2021. [Online]. Available: http://www.optimization-online.org/DB_HTML/2021/12/8728.html

[6] L. L. Garver, “Power Generation Scheduling by Integer Programming-Development of Theory,” *Trans. AIEE, Part III: Power Appar. Syst.*, vol. 81, no. 3, pp. 730–734, 1962, doi: 10.1109/AIEEPAS.1962.4501405.

[7] J. M. Arroyo and A. J. Conejo, “Optimal response of a thermal unit to an electricity spot market,” *IEEE Trans. Power Syst.*, vol. 15, no. 3, pp. 1098–1104, 2000, doi: 10.1109/59.871739.

[8] J. Dorfner and T. Hamacher, “Large-Scale District Heating Network Optimization,” *IEEE Trans. Smart Grid*, vol. 5, no. 4, pp. 1884–1891, 2014, doi: 10.1109/TSG.2013.2295856.

The 18th International Symposium on District Heating and Cooling,
September 3-6, 2023, Beijing, China

Analysis of the energy consumption characteristics of the heating system of a mega airport terminal building: the example of a large airport in Beijing

Guan Dongya, Chen Chao*, Pan Song, Yang Yi, Qiao Peng, Sun Yongxiang

Department of Building Environment and Energy Application Engineering, Faculty of Urban Construction, Beijing University of Technology, Beijing 100124, China)
** Corresponding author. corresponding.chenchao@bjut.edu.cn.*

Abstract

Large airport terminals are transportation hubs and logistics centers in cities, with tall and complex buildings, large heating systems, and high energy consumption. This study focuses on a large airport terminal in Beijing and investigates the characteristics of its HVAC system composition and power consumption, along with the corresponding data on passenger flow during the three heating seasons spanning from January 2020 to February 2023. On-site measurement research, along with K-means cluster analysis and other methods, are employed to study the impact of terminal building scale, passenger flow, and outdoor meteorological parameters on the heating load and energy consumption characteristics of the heating system. The objective is to develop efficient, low-cost solutions that reduce carbon emissions and optimize the operation of the airport's heating energy system. This study provides a methodological reference and comprehensive data set for the effective energy management of such systems.

Keywords: Terminal building; Heating system; Load and energy consumption characteristics; Energy saving and low carbon

Heat Pump & Heat Exchanger

The 18th International Symposium on District Heating and Cooling, September 3–6, 2023, Beijing, China

THERMOPHYSICAL PROPERTY MODELS OF LUBRICANT OILS AND THEIR MIXTURES WITH REFRIGERANTS FOR COMPREHENSIVE HEAT PUMP ANALYSIS

Xiaoxian Yang[a*], Christian Hanzelmann[b], Steffen Feja[b], J.P. Martin Trusler[c], Markus Richter[a*]

[a] *Applied Thermodynamics, Chemnitz University of Technology, Chemnitz, 09107, Germany*
[b] *ILK Dresden: Institut für Luft- und Kältetechnik gemeinnützige Gesellschaft mbH, Dresden, 01309, Germany*
[c] *Department of Chemical Engineering, Imperial College London, SW7 2AZ, London, United Kingdom*
[*] *Corresponding author. xiaoxian.yang@mb.tu-chemnitz.de and m.richter@mb.tu-chemnitz.de*

ABSTRACT

Lubricant, as a key component in compressors, plays an important role in heat pump (HP) systems. Reliable knowledge of thermophysical properties of lubricants is essential, for example, to investigate the impact on the thermo-economic performance of a HP system when working fluids (typically refrigerants) are mixed with lubricants. Modelling all the required thermophysical properties (mainly: density, phase behavior, heat capacity, entropy, enthalpy, viscosity and thermal conductivity) of a lubricant and the lubricant + refrigerant mixtures in a HP system remains a key challenge. To tackle this challenge, we propose a novel approach based on treating the lubricant as a quasi-pure fluid, setting up a model set for all the required properties of the lubricant, and developing a parameter fitting procedure using the least amount of experiments. This model set includes the Patel-Teja-Valderrama equation of state, a simple expression for the ideal gas isobaric heat capacity as a linear function of temperature, and residual entropy scaling relations for viscosity and thermal conductivity. For parameter fittings, two extra models are required: Raoult's law of boiling point elevation and the modified Rackett equation. As a result, less than 20 experimental points are needed to fit all the parameters of a lubricant, and one experimental point is required to enable predictions for a binary lubricant + refrigerant mixture. For quasi-pure lubricants, in the liquid phase and not in the vicinity of the critical point, this modelling approach has an estimated uncertainty of 7 % for viscosity and 3 % for all other properties. Similar results are obtained for less asymmetric binary systems. For asymmetric binary systems, except for viscosity, the modelling approach still yield good prediction, typically within 10 %. With the developed modelling approach, the impact on the thermo-economic performance of a HP system when working fluids are mixed with lubricants are investigated.

Keywords: Lubricant, Refrigerant, Thermophysical Property Model, Heat Pump

1. INTRODUCTION

A lubricant reduces the friction and the heat generated when two contacting surfaces move over each other. Lubricant products are used in many applications world-wide, such as in internal combustion engines. Tens of million tons of lubricants are consumed all over the world each year [1]. Being key components in compressors, lubricants play an important role in many energy systems, such as heat pumps (HP) and organic Rankine cycles. Reliable knowledge of thermophysical properties of lubricants is essential, e.g. to investigate the thermo-economic performance of a HP system when working fluids are mixed with lubricants. However, lubricants are generally composed of a base oil plus a variety of additives to impart desirable characteristics. The components and composition of a lubricant product are difficult to determine accurately and often not disclosed by manufacturers. Traditional accurate thermophysical property modelling approaches, e.g., multi-parameter reference equations of state (EoS), cannot be used for lubricant products, because these approaches are generally developed for pure fluids or mixtures with known components and composition. Moreover, fluid thermophysical properties required in a system analysis might include density, phase behavior, heat capacity, entropy, enthalpy, viscosity and thermal conductivity. No single model can consider all these properties simultaneously; instead, a set of thermodynamic- and transport-property models is needed. Typically, an EoS is necessary for density and phase behavior, and together with an equation for the ideal gas isobaric heat capacity $c_p^o(T)$, heat capacity, entropy increments and enthalpy increments can be calculated. Then, additional models are required for the calculation of viscosity and thermal conductivity. A model set composed entirely of empirical equations for each property fitted to experimental data is not preferable as it gives rise to thermodynamic inconsistencies and some properties, such as entropy increments, are difficult to measure accurately. In this context, calculations of all needed thermophysical properties of lubricants and lubricant + working fluid (typically a pure refrigerant or refrigerant blend) mixtures in a system analysis remains a key challenge.

To tackle this challenge, we proposes a novel modelling approach to calculate all the important thermophysical properties of lubricants and their mixtures with other fluids. In this approach, a lubricant product is considered as a quasi-pure fluid and only a very small amount of experimental data is required to fit its parameters (e.g., critical temperature, critical pressure, acentric factor, etc). This endeavor is part of the Subproject 3 within the KETEC (Research Platform Refrigeration and Energy Technology) project [2]. The core part of the current research **will be** been published as a peer-reviewed article [3] .

2. METHODOLOGY

2.1. The Fluid Models and Parameters

For the calculation of all needed thermophysical properties of a quasi-pure lubricant in a HP system analysis, a model set was chosen. It included: Patel-Teja-Valderrama (PTV) [4] EoS, a correlation of the ideal-gas isobaric heat capacity as a linear function of temperature (linear-$c_p^o(T)$), residual entropy scaling for viscosity (RES-μ) and thermal conductivity (RES-λ). For a specific lubricant, to fit some of its parameters in this model set, two extra models are required: Raoult's law of boiling point elevation and modified Rackett equation. Within this model set, all parameters of a specific quasi-pure lubricant to be determined include: molar mass M, critical temperature T_c, critical density ρ_c, critical pressure p_c, acentric factor ω, two parameters k_0, k_1 in the linear-$c_p^o(T)$ and RES fitted parameters for viscosity $n_{\mu k}$ (k = 1,2,3,4) and thermal conductivity $n_{\lambda k}$ (k = 1,2,3,4). All these models, which are more or less 'textbook' knowledge, are described as detailed as necessary in the journal paper [3] and its supporting information. Here in this paper, only the key information and the parameter fitting method are presented. This model set can be easily extended for mixture calculations using simple mixing rules [3].

Raoult's law of boiling point elevation for molar mass**.** At a pressure for a pure solvent with a mass $m_{solvent}$, the boiling temperature is fixed at $T_{solvent}$. Added with a small mass of solute m_{solute}, the boiling temperature of the solution at the same pressure becomes $T_{solution}$. The molality b_{solute} of solute can then be calculated with:

$$b_{\text{solute}} = (T_{\text{solution}} - T_{\text{solvent}})/K_{\text{b}} \tag{1}$$

Here, K_b is a boiling point elevation constant, which depends to the solvent and pressure, and is independent to the solute. Later, the mole n_{solute} (=$b_{solute}\cdot m_{solvent}$) and average molar mass M_{solute} (=m_{solute}/n_{solute}) of the solute can be calculated. An example to calculate the value of K_b is given in the journal paper [3].

Modified Rackett Equation for critical point. A modified Rackett equation (mRE) was proposed here:

$$\rho_{\text{atm}} = \rho_{\text{c}} Z_{\text{c}}^{-(1-T/T_{\text{c}})^{2/7}} \tag{2}$$

where ρ_{atm} is liquid density at atmospheric pressure ($p \approx 0.10$ MPa), and ρ_c, T_c and Z_c are density, temperature and compressibility factor at the critical point respectively. Instead of ρ_{atm}, the original Rackett equation [5] uses saturated liquid density, which however is very difficult to measure as the saturated pressure of lubricant is very low (typically less than 1.0 Pa). Three density measurements at three different temperatures at 0.1 MPa (p = 0.1 MPa, T, ρ) are enough to fit the critical point information: ρ_c, T_c and Z_c. However, the fitted value of Z_c is generally unphysical [3]. Therefore a fixed value (e.g, 0.2563 as recommended for esters [5]) should be given to Z_c, and only two (p = 0.1 MPa, T, ρ) points are enough to determine ρ_c and T_c. Here four (p = 0.1 MPa, T, ρ) points are recommended in order to yield higher accuracy and to be in line with viscosity and thermal conductivity as discussed later. According to the definition of Z_c and the fitted M, ρ_c and T_c, the critical pressure p_c can be calculated.

PTV EoS for acentric factor. With critical point information known, the PTV EoS [4] can be adopted to fit ω using the same density measurements (p = 0.1 MPa, T, ρ) as in the critical point fitting. Here six different cubic EoS were tested: Soave-Redlich-Kwong (SRK) [6,7], Peng-Robinson (PR) [8], Peng-Robinson-Stryjek-Vera (PRSV) [9], Wilson-Redlich-Kwong (WRK) [10], PTV [4] and Redlich-Kwong (RK) [11]. However, except for the PTV EoS, all other EoS generally yield unreasonable ω. The success of the PTV EoS is attributed to its more accurate calculation of liquid density.

Linear-$c_p^o(T)$ for ideal gas. A correlation of ideal-gas isobaric heat capacity c_p^o as a linear function of temperature is:

$$c_{\text{p}}^{\text{o}} = k_1 \frac{(T - T_0)}{T_{\text{c}}} + k_0 \tag{3}$$

where k_0 is the value of c_p^o at T_0 = 298.15 K, and k_1/T_c is the gradient of c_p^o at T_0. The other ideal gas properties can then be calculated with a chosen reference state. Two c_p^o measurements at two different temperatures at 0.1 MPa (p = 0.1 MPa, T, c_p) are enough to fit parameters k_0 and k_1. Nonetheless, similar to density measurements, four measurements of (p = 0.1 MPa, T, c_p) are recommended. Please note, residual properties can be calculated with the PTV EoS.

RES for transport properties**.** The RES approach developed by Yang et al. [12–14] was used. The viscosity of pure fluids is:

$$\mu = \mu_{\rho \to 0} + \mu^{\text{r}} \tag{4}$$

Here the dilute gas viscosity $\mu_{\rho\to 0}$ of a pure fluid is a function of temperature, mass of one molecule m, collision diameter σ and pair-potential energy ε of the Lennard-Jones (L-J) particle. The L-J parameters can be estimated according to Chung et al. [15]: $\varepsilon/k_B = T_c/1.2593$ and $\sigma^3 = 0.3189/\rho_c$. The residual part of viscosity μ^r can be calculated with:

$$\mu^{\mathrm{r}} = \frac{\mu^{\mathrm{r}+}\rho_{\mathrm{N}}^{2/3}\sqrt{mk_BT}}{(s^+)^{2/3}} \tag{5}$$

$$\ln(\mu^{\mathrm{r}+}+1) = n_{\mu 1}\cdot(s^+) + n_{\mu 2}\cdot(s^+)^{1.5} + n_{\mu 3}\cdot(s^+)^2 + n_{\mu 4}\cdot(s^+)^{2.5} \tag{6}$$

$$s^+ = -s^{\mathrm{r}}/R \tag{7}$$

Here, ρ_N is the number density, k_B is the Boltzmann constant and s^r is residual entropy. The ρ_N and s^r can be calculated with the PTV EoS. Four viscosity measurements (p = 0.1 MPa, T, μ) are needed to fit the four parameters $n_{\mu k}$ (k = 1,2,3,4).

Thermal conductivity is calculated with:

$$\lambda = \lambda_{\rho\to 0} + \lambda^{\mathrm{r}} + \lambda_{\mathrm{C}} \tag{8}$$

Here, according to Chichester and Huber [16], the dilute gas thermal conductivity $\lambda_{\rho\to 0}$ is a function of $\mu_{\rho\to 0}$ and c_p^o; and according to the RES approach of Yang et al. [13], the residual part λ^r can be calculated with:

$$\lambda^{\mathrm{r}} = \frac{\lambda^{\mathrm{r}+}k_B\rho_{\mathrm{N}}^{2/3}\sqrt{k_BT/m}}{(s^+)^{2/3}} \tag{9}$$

$$\lambda^{\mathrm{r}+} = n_{\lambda 1}\cdot(s^+) + n_{\lambda 2}\cdot(s^+)^{1.5} + n_{\lambda 3}\cdot(s^+)^2 + n_{\lambda 4}\cdot(s^+)^{2.5} \tag{10}$$

The critical enhancement term λ_C can be set zero as a lubricant is normally used at conditions far away from its critical point. Four thermal conductivity measurements (p = 0.1 MPa, T, μ) are needed to fit the four parameters $n_{\lambda k}$ (k = 1,2,3,4).

Binary mixtures. According to all the mixing rules presented in the journal paper [3], only one parameter, *i.e.* the binary interaction parameter k_{ij}, needs to be determined to enable calculations of a binary system. The k_{ij} is a parameter in the van der Waals mixing rule used for the cubic EoS, therefore, suitable properties to fit k_{ij} are density and phase behavior. As will be discussed in section 3.2, vapor pressure (a phase behavior property, also named bubble point pressure) is much more sensitive to k_{ij} than density. Therefore, one vapor pressure point of a binary system should be measured to fit the k_{ij}. If no experimental vapor pressure is available for a binary system, k_{ij} could be set zero.

2.2. Heat pump analysis model

A schematic of a recuperative HP and its typical pressure-enthalpy (p-h) diagram are shown in Figure 1. The working fluid absorbs heat in the evaporator, is compressed to a higher pressure in the compressor, releases heat in the condenser, goes through a valve and continues to enter the evaporator. An internal heat exchanger is included to recover heat from the working fluid exiting the condenser to heat up the working fluid exiting the evaporator. The coefficient of performance (COP) is defined as $(h_5 - h_2)/(h_5 - h_{4r})$; subscripts refer to the state given in Figure 1.

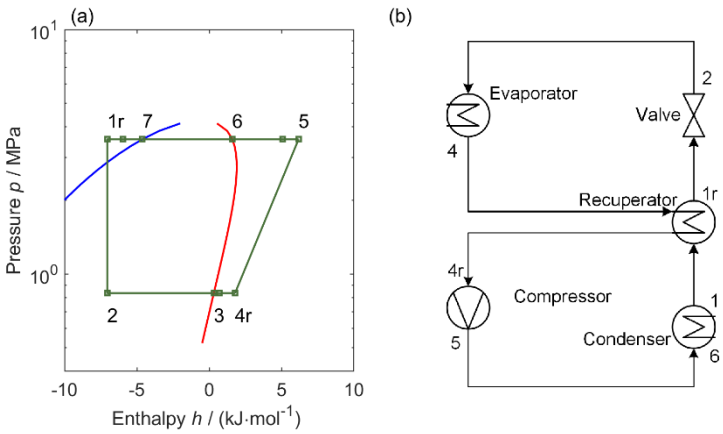

Figure 1. The (a) pressure-enthalpy (p-h) diagram and (b) schematic of a heat pump system.

3. RESULTS

3.1. Feasibility study

The parameter fitting method described in section 2.1 was determined with a feasibility study using well-studied pure fluids. Except for those with strong association force (heavy water, water and ethylene glycol), all pure fluids in the NIST's

REFPROP database version 10.0 [17] as well as in the NIST report 8263 [18] which are in the liquid phase at pressure p = 0.1 MPa and temperature T = (278.15 to 368.15) K were selected for the feasibility study. These fluids were chosen because most of lubricants have a similar feature and the needed experiments for parameter fittings are in the similar T-p range.

The feasibility study was carried out by (1) calculating 'experimental' values with REFPROP 10.0 [17], (2) adding bias to these calculated values to imitate experimental expanded (k = 2) uncertainties U_{exp} (relatively $U_{r,exp}$ 0.8 %, 4.0 %, 4.0 %, 4.0 % for density, heat capacity, viscosity and thermal conductivity, respectively, considering quick measurement techniques), and then (3) fitting the parameters of each fluid in the models. With the fitted parameters, the predicting capability of the model set was tested by calculating ρ, c_p, μ, λ, entropy increment Δs and enthalpy increment Δh of these pure fluids in a larger temperature range (223.15 to 473.15 K) and pressure range (up to 5.0 MPa), and compared to the REFPROP models. The comparison results are summarized in Figure 2. According to this figure, the systematic offset (corresponds to the average of relative deviation, ARD) of the model set from the REFPROP models are less than the measurement uncertainty U_{exp} and the scattering (corresponds to the average of the absolute value of relative deviation, AARD) is more or less at the same level of U_{exp}. The model set was estimated to have an uncertainty less than 7 % for viscosity and less than 3 % for all other properties. Viscosity has a higher uncertainty mainly because it shows a strong exponential relation to temperature, while other properties show more or less linear relations.

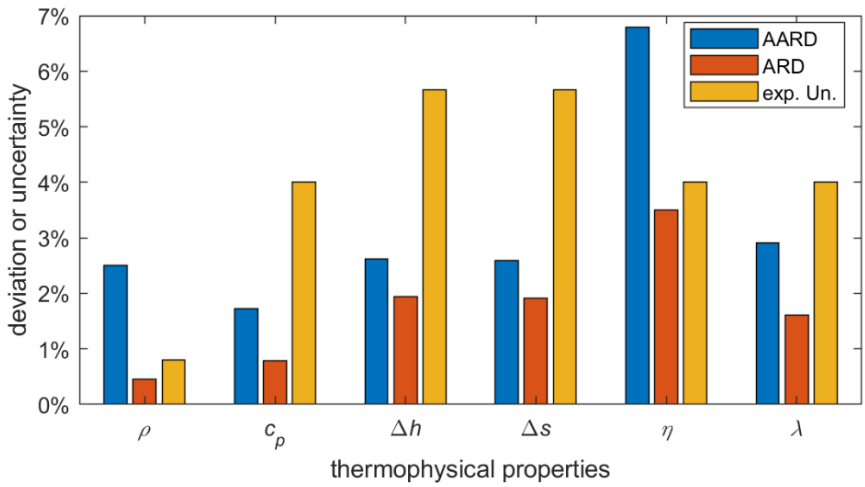

Figure 2. Average of the absolute value of relative deviation (AARD) and average relative deviation (ARD) from the model set [3].

3.2. Applied to Real Lubricants

One example of applying this modelling approach to lubricants and their mixtures is given here; more exampled is given in the journal paper [3]. Vapor pressure, density, heat capacity, viscosity and thermal conductivity measurements of PAG68 and PAG68 + propane mixtures (an asymmetric binary system) were carried out at ILK Dresden, Germany. Information of the experiment setups are summarized in Table 1 and the measurement results are given in the journal paper [3]. The PAG68 can be considered as a quasi-pure lubricant, which is a commercially available refrigeration lubricant. According to the confidentiality agreement with the manufacturer, no further information about PAG68 can be provided here. Please note, in the PAG68 measurements, pressure was typically at atmosphere pressure or slightly higher; while in the PAG68 + propane measurements, except for vapor pressure measurement, pressure was slightly higher than the vapor pressure (i.e., bubble point pressure) to keep the mixtures in liquid phase. No measurement efforts were carried out to obtain the average mole mass of PAG68; here we roughly choose a value of M_{PAG68} = 200 g/mol. Furthermore, although PAG is not an ester, its Z_c value was still fixed at 0.2563 (recommended for esters in [5]). Such a rough-estimated Z_c value can already yield good results as shown in the follows.

Table 1. Experimental setups for the PAG68 and PAG68 + propane measurements [a]

Property	Technique and reference	Uncertainty (k = 2)
Vapor pressure	Direct method (self-developed, ILK Dresden) [19]	0.15 bar or ± 1 %
Density	Vibrating tube densimeter (DMA HPM, Anton Paar) [19]	0.05 kg·m^{-3}
Heat capacity	Differential scanning calorimetry (stepwise method, µDSC 7 evo, Setaram) [20]	± 3 %
Viscosity	Oscillating piston (VISCOpro 2000, Cambridge Viscosity) [19]	± 10 %
Thermal conductivity	Ring-gap apparatus (self-developed, ILK Dresden)[21]	± 5 %

[a] This table is taken, unmodified from the journal paper [3].

Three points of density, four points of heat capacity and viscosity at different temperatures, and six points of thermal conductivity at three different temperatures of PAG68 were adopted to fit the parameters of PAG68; the fitted parameters are listed in Table 2. Together with the remaining data of PAG68, the relative deviations of the measured data from the model predictions are shown in Figure 3 (where data used for fitting are highlighted). The relative deviations for density, isobaric heat capacity, viscosity and thermal conductivity are generally within 2.0%, 0.5%, 4.0% and 1.0%, which is excessively good. Changing the value of M_{PAG68} resulted in the change of some fitted parameters, mainly critical pressure, but did not obviously affect the prediction performance for the quasi-pure PAG68, i.e., Figure 3 stayed almost the same.

Table 2. Parameters of PAG68 [a]

Property	M/ g·mol^{-1}	Z_c	T_c/ K	p_c/ MPa	ω	k_0/J·mol^{-1}·K^{-1}	k_1/J·mol^{-1}·K^{-1}	
value	200.000	0.2563	750.688	2.43500	0.7157	286.940	457.802	
Property	$n_{\mu1}$	$n_{\mu2}$	$n_{\mu3}$	$n_{\mu4}$	$n_{\lambda1}$	$n_{\lambda2}$	$n_{\lambda3}$	$n_{\lambda4}$
value	1.0000	0.1271	-0.2248	0.0433	32.5579	7.6460	-9.3029	1.5942

[a] Information in this table was taken from the journal paper [3].

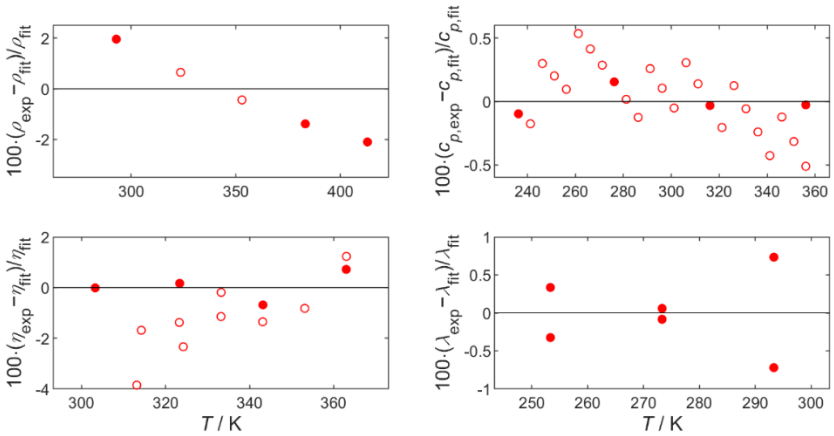

Figure 3. Relative deviation of the measured data of quasi-pure PAG68 to predictions of the model set. Data in full symbol are used to fit the parameters of PAG68. This figure is taken, unmodified from the journal paper [3].

For the calculations of the PAG68 + propane mixtures, the needed parameters of propane were obtained from REFPROP 10.0, and the binary interaction parameter k_{ij} = 0.0381 of the PAG68 + propane was fitted using one randomly picked vapor pressure point. The vapor pressure rather than density was used for k_{ij} fitting because vapor pressure is much more sensitive to k_{ij} than density. As shown in Figure 4, in the range of k_{ij} = (0.030 to 0.046), the root-mean-square (RMS) of the relative deviation of experimental densities to calculated values barely changes, but change significantly for vapor pressures.

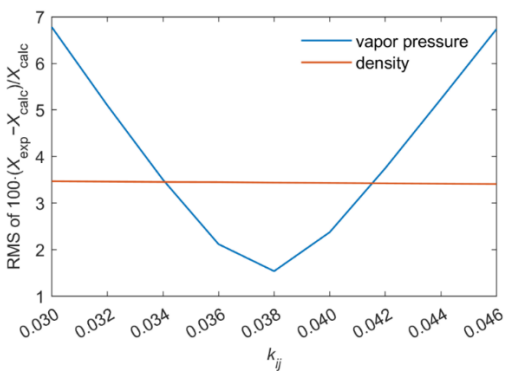

Figure 4. Sensitivity of the properties of the PAG68 + propane mixtures to the binary interaction parameter k_{ij}. RMS refers to root mean square. X refers to density and vapor pressure respectively. This figure is taken, unmodified from the journal paper [3].

Relative deviations of the experimental PAG68 + propane data from the model prediction are illustrated in Figure 5. Changing the value of M_{PAG68} resulted in the change of the fitted k_{ij}, but won't obviously affect the prediction performance for the mixtures as well. For such an asymmetric system, the relative deviation for vapor pressure, density and thermal conductivity are quite good: generally within 5 %, 5 %, and 10 %, respectively. However for viscosity, the deviation is as high as 700 %. The bad viscosity prediction for asymmetric systems is attributed to the strong exponential relation of viscosity with temperature, and there is no proper mixing rules for asymmetric systems within the RES-μ approach available.

Improvement in the viscosity prediction of asymmetric binary systems using the RES approach is challenging and is one of our future work within KETEC project. It is interested to note that, for density prediction of pure propane, the relative deviation is as high as 14 %, while for the PAG68 + propane mixture, the relative deviation is only up to 5 %.

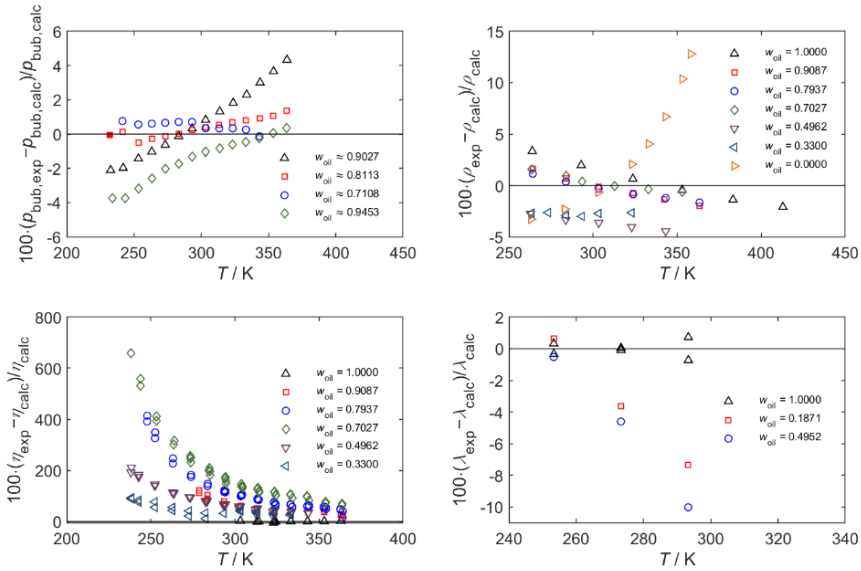

Figure 5. Relative deviations of the measured data of the PAG68 + propane mixtures from the predictions of the model set. Only one data (the one in full symbol in top left subfigure) is used to fit the binary interaction parameters, *w* refers to mass fraction. This figure is taken, unmodified from the journal paper [3].

3.3. Heat pump analysis

The pressure-enthalpy (*p-h*) and temperature-entropy (*T-s*) diagrams of a HP running with pure propane and propane mixed with 2 mol-% of PAG68 (~8,5 wt% oil) are plotted in Figure 6. The calculations were carried out at fixed condensation and evaporation pressures (3.5580 MPa and 0.8349 MPa respectively, which corresponds to saturated temperatures of pure propane at 359.89 K and 293.15 K respectively). The superheated and subcooled temperatures were both 5 K. The recuperative effectiveness, defined as $(T_1 - T_4)/(T_1 - T_{1r})$, was set as 0.1; and the compressor efficiency, defined as $(h_{5s} - h_{4r})/(h_5 - h_{4r})$, was set as 0.75.

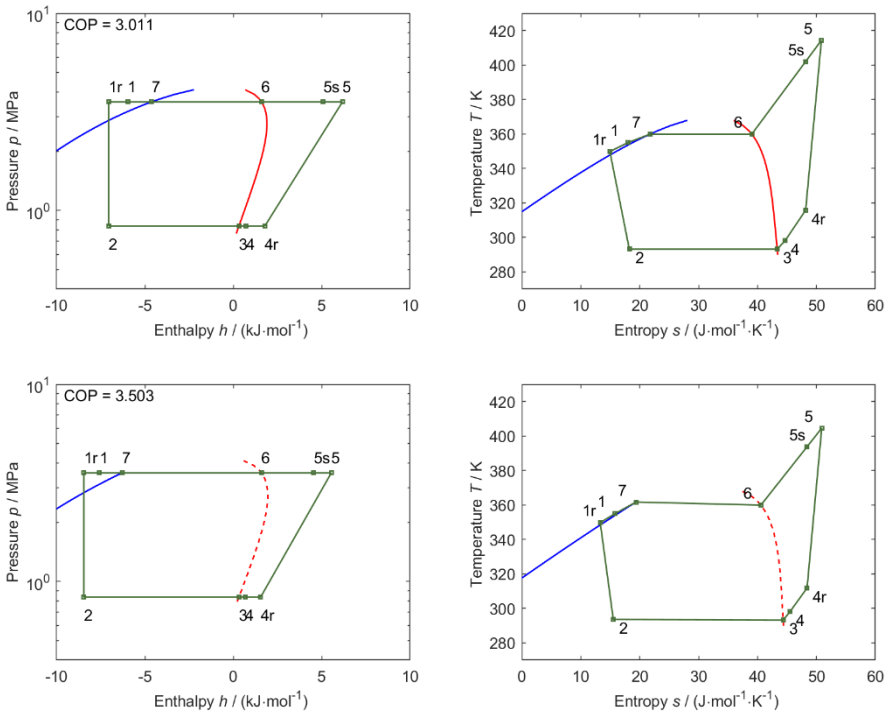

Figure 6. The pressure-enthalpy (*p-h*) and temperature-entropy (*T-s*) diagrams of a heat pump. Top figures: pure propane; bottom figures: propane mixed with 2 mol-% of PAG 68. The points (1,2,..7) are explained in Figure 1.

The dew-point of the propane + PAG68 mixture was unable to be calculated as the dew-point pressure is too low. Therefore no dew-point line of this mixture is shown in Figure 6, instead that of pure propane is presented (the dashed red curves in Figure 6). This assumption needs to be verified in the future work. As compared to pure propane, in the *p-h* diagram, the bubble-point line (the blue line in Figure 6) of the PAG68 + propane mixture obviously shifted towards lower enthalpy. This implies that more heat needs to be taken away to reach the saturated liquid state in the condenser and more heat needs to be adsorbed in the evaporator. This is the major reason that, the COP of the HP running with propane + PAG68 mixture (COP = 3.503) is higher than that with pure propane (COP = 3.011). In the *T-s* diagram, bubble-point line (blue line in Figure 6) shifted towards higher temperature; this agree with the Raoult's law of boiling point elevation. Besides, one can notice from the *T-s* diagrams that the temperature in the two-phase region of the PAG68 + propane mixture is no long a fixed value; it increased when running through the condenser. This might result in the condenser not running at the optimal status as designed.

More complicated analysis are yet to be carried in the future. For example, the viscosity of the working fluid will increase when mixed with oil. This might yield a pressure drop in the tubes and the heat exchangers that is high enough and can no longer be ignored. Besides, thermal conductivity of the working fluids will also change which might result in the machine not running at the designed optimal conditions. The fixed compressor efficiency is also no long reasonable as the oil will definitely affect the efficiency; analysis of which required detail modelling of the compressor and the two phase flows in the compressor.

4. CONCLUSION

Modelling all the important thermophysical properties (mainly including: density, phase behavior, heat capacity, entropy, enthalpy, viscosity and thermal conductivity) of a lubricant oil remains a key challenge nowadays. To tackle this challenge, we propose a novel modelling approach, with which, a lubricant oil is considered as a quasi-pure fluid, a simple model set is used for property calculations, and a procedure should be followed to fit the needed parameters using very small amount of experiments. This simple model set includes: Patel-Teja-Valderrama equation of state, ideal gas isobaric heat capacity as a linear function of temperature, and residual entropy scaling for viscosity and thermal conductivity. All needed parameters to be fitted include: molar mass, critical temperature, critical density, critical pressure, acentric factor, two parameters for heat capacity, and four parameters each for viscosity and thermal conductivity. To fit the molar mass, Raoult's law of boiling point elevation could be used, and to fit the critical point, a modified Rackett equation was proposed in this work. When the experimental technique for the molar mass fitting is not available, an approximate molar mass value can be given to a lubricant, effect of which to the performance of the modelling approach is very small. As a result, less than 20 experimental points (a minimal of 12) are needed to fit all the parameters of a pure or quasi-pure component, and one experimental point is required to enable a binary system prediction. It is important to note here, six cubic EoS candidates were studied, but only the PTV EoS yielded reasonable results because it can predict liquid densities more accurately than others.

The performance of the proposed modelling approach (the model set and the parameter fitting procedure) was first tested by calculating the well-studied pure fluids in enlarged temperature and pressure ranges, and comparing to REFPROP 10.0 calculations. Then, the modelling approach was further tested by being applied to real cases of lubricants and their mixtures with other fluids: an asymmetric propane + PAG68 binary system. As a result, in the liquid phase and not in the vicinity of the critical points, for pure fluids, this modelling approach has an estimated uncertainty of less than 7 % for viscosity and less than 3 % for all other properties. For asymmetric binary system, except for viscosity, the modelling approach still yield good prediction, typically within 10 %. The higher uncertainty in viscosity prediction is attributed to the strong exponential relation of viscosity with temperature; meanwhile, there are no proper mixing rules for asymmetric binary systems using the RES approach for viscosity.

This fluid modelling approach was applied to calculate COP of a simple heat pump system, with working fluid being propane mixed with 2 mol-% of PAG68. As compared to pure propane, the bubble-point line in the *p-h* diagram obviously shifted towards lower enthalpy; this eventually contribute significantly to the increase of COP. Meanwhile, the bubble-point line shifted towards higher temperature, which result in the condenser not running at the optimal status as designed. More complicated analysis are yet to be carried in the future.

ACKNOWLEDGEMENT

The realization of the project and the scientific work was supported by the German Federal Ministry of Education and Research on the basis of a decision by the German Bundestag (funding code 03SF0623A). The authors gratefully acknowledge this support and carry the full responsibility for the content of this paper.

REFERENCES

[1] Bartels T, Bock W, Braun J, Busch C, Buss W, Dresel W, et al. Lubricants and Lubrication. Ullmann's Encyclopedia of Industrial Chemistry, John Wiley & Sons, Ltd; 2003. https://doi.org/10.1002/14356007.a15_423.

[2] Urbaneck T, Matthes M, Richter M, Hempel O, Safarik M, Franzke U, et al. Research Platform Refrigeration and Energy Technology (KETEC) 2022. www.ketec.online (accessed April 25, 2023).

[3] Yang X, Hanzelmann C, Feja S, Trusler JPM, Richter M. Thermophysical property modelling of lubricant oils and their mixtures with refrigerants using least amount of experiments. Industrial & Engineering Chemistry 2023:(submitted).

[4] Patel NC, Teja AS. A new cubic equation of state for fluids and fluid mixtures. Chem Eng Sci 1982;37:463–73. https://doi.org/10.1016/0009-2509(82)80099-7.

[5] Vetere A. Again the Rackett equation. The Chemical Engineering Journal 1992;49:27–33. https://doi.org/10.1016/0300-9467(92)85021-Z.

[6] Soave G. Equilibrium constants from a modified Redlich-Kwong equation of state. Chemical Engineering Science 1972;27:1197–203. https://doi.org/10.1016/0009-2509(72)80096-4.

[7] Yang F, Liu Q, Duan Y, Yang Z. On the temperature dependence of the A function in the cubic equation of state. Chemical Engineering Science 2018;192:565–75. https://doi.org/10.1016/j.ces.2018.08.014.

[8] Peng D-Y, Robinson DB. A new two-constant equation of state. Ind Eng Chem Fundam 1976;15:59–64. https://doi.org/10.1021/i160057a011.

[9] Stryjek R, Vera JH. PRSV: An improved Peng—Robinson equation of state for pure compounds and mixtures. The Canadian Journal of Chemical Engineering 1986;64:323–33.

[10] Wilson GM. Vapor-liquid equilibria, correlation by means of a modified Redlich-Kwong equation of state. Advances in Cryogenic Engineering, Springer; 1964, p. 168–76.

[11] Redlich O, Kwong JNS. On the thermodynamics of solutions. V. An equation of state. Fugacities of gaseous solutions. Chem Rev 1949;44:233–44.

[12] Yang X, Xiao X, May EF, Bell IH. Entropy Scaling of Viscosity—III: Application to Refrigerants and Their Mixtures. J Chem Eng Data 2021;66:1385–98. https://doi.org/10.1021/acs.jced.0c01009.

[13] Yang X, Kim D, May EF, Bell IH. Entropy Scaling of Thermal Conductivity: Application to Refrigerants and Their Mixtures. Ind Eng Chem Res 2021;60:13052–70. https://doi.org/10.1021/acs.iecr.1c02154.

[14] Yang X, Xiao X, Thol M, Richter M, Bell IH. Linking Viscosity to Equations of State Using Residual Entropy Scaling Theory. Int J Thermophys 2022;43:183. https://doi.org/10.1007/s10765-022-03096-9.

[15] Chung TH, Lee LL, Starling KE. Applications of kinetic gas theories and multiparameter correlation for prediction of dilute gas viscosity and thermal conductivity. Ind Eng Chem Fund 1984;23:8–13. https://doi.org/10.1021/i100013a002.

[16] Chichester JC, Huber ML. Documentation and assessment of the transport property model for mixtures implemented in NIST REFPROP (Version 8.0). National Institute of Standards and Technology; 2008.

[17] Lemmon EW, Bell IH, Huber ML, McLinden MO. NIST Standard Reference Database 23: Reference Fluid Thermodynamic and Transport Properties-REFPROP, Version 10.0, National Institute of Standards and Technology. 2018. https://doi.org/10.18434/T4/1502528.

[18] Bruno TJ, Fortin T, Huber ML, Laesecke AD, Lemmon E, Mansfield E, et al. Thermophysical Properties of Polyol Ester Lubricants, NIST Interagency/Internal Report (NISTIR). National Institute of Standards and Technology, Gaithersburg, MD 2019. https://doi.org/10.6028/NIST.IR.8263.

[19] Feja S, Hanzelmann C. Experimental studies of thermodynamic properties of R744-oil-mixtures up to 140 °C and 150 bar. International Journal of Refrigeration 2015;60:135–41. https://doi.org/10.1016/j.ijrefrig.2015.07.018.

[20] Setaram. Technical Note 149: Determination of Heat Capacity from DSC or Calorimetry measurements. n.d.

[21] Ehle A, Feja S, Buschmann MH. Temperature Dependency of Ceramic Nanofluids Shows Classical Behavior. Journal of Thermophysics and Heat Transfer 2011;25:378–85. https://doi.org/10.2514/1.T3634.

The 18th International Symposium on District Heating and Cooling,
September 3-6, 2023, Beijing, China

ANALYSIS OF THREE-STAGE HYBRID ABSORPTION-COMPRESSION HEAT PUMP CYCLES WITH LARGE TEMPERATURE LIFT

Xi Zhang[a b], Zhenyuan Xu[a b*]

[a] *Institute of Refrigeration and Cryogenics, Shanghai Jiao Tong University, Shanghai 200240, China*
[b] *Engineering Research Center of Solar Power and Refrigeration, MOE, China*
[*] *Corresponding author. xuzhy@sjtu.edu.cn*

Abstract

Heat pumps, particularly air-source systems, have been recognized as a promising technology for deep decarbonization of heating supply, but their industrial application is severely limited by their low temperature lift and rapid performance degradation with increasing temperature lift. In this paper, three-stage hybrid absorption-compression heat pump cycles coupling an absorption heat transformer (AHT) and a cascade vapor compression heat pump (VCHP) are proposed to achieve large temperature lift. Different internal heat recovery configurations, where the condenser heat emitted from the AHT is recovered to the low-temperature stage or medium-temperature stage of the VCHP, are designed to increase the coefficient of performance (COP) under enlarged temperature lift. Thermodynamic comparison of the two configurations is performed using the Engineering Equation Solver software. The first configuration has lower refrigerant pressure ratios, while the second configuration can reach higher temperature lift of 140 °C with a COP above 1.2. The COP and temperature lift of the three-stage cycles are higher than those of the two-stage cycle, indicating great potential for realizing air-source heat pumps with ultra-high temperature output.

Keywords: High temperature; temperature lift; heat pump; hybrid

The 18th International Symposium on District Heating and Cooling, September 3–6, 2023, Beijing, China

Process Heat Supply By Heat Pumps And District Heating

Haochen Wang[a], Dimitri Nefodov[a], Markus Richter[a], Thorsten Urbaneck[a*]

[a] *Chemnitz University of Technology, 09107 Chemnitz, Germany*
[*] *Corresponding author. thorsten.urbaneck@mb.tu-chemnitz.de*

ABSTRACT

In recent years, the use of industrial waste heat as a heat source for high-temperature heat pumps has become increasingly important [1], [2]. In order to analyze further applications in the district heating sector, this paper deals with a parameter study.

In the district heating sector, the flow and return temperatures in existing networks are gradually lowered, e.g., to reduce heat losses. District heating systems cannot then supply consumers with higher temperatures (e.g., above 120 °C). The possibility of using the flow or return flow as a heat source also offers potential for high-temperature heat pumps. District heating operators can then take over the assignment of process heat supply or develop new customers.

Numerous influencing variables (such as different refrigerants, circuits, heat source temperatures) affect the heating capacity or efficiency of high-temperature heat pumps. Therefore, it is important to find an optimal heat pump solution for the respective boundary conditions.

To solve this problem, various refrigerants have been investigated, including natural refrigerants (R600, R601a, R744), HFO refrigerants (R1234ze(E), R1336mzz(Z), and HCFO refrigerants (R1224yd(Z), R1233zd(E)). Furthermore, improvements in the process can be achieved by modified circuits (e.g., internal heat exchanger, two-stage compression and intercooling with two-stage expansion). The heat pump inlet temperature on the source side is 50 to 100 °C. The target temperature of the heat supply is 140 °C (e.g., steam supply). All systems were modeled and simulated using the EBSILON®Professional program [3]. In the investigations, the COP was determined as an essential parameter. This in turn allows an optimal preselection of heat pumps. These systematic investigations show the functional progression of the COP, which promotes a better understanding of the problem. The results provide information for the district heating sector and industry to promote the use of high temperature heat pumps in district heating areas.

Keywords: Process heat, heat pump, district heating, simulation, parameter study

1. INTRODUCTION

New district and local heating systems are designed with the lowest possible supply and return temperatures. Operators also strive to lower temperatures in existing networks. These efforts are primarily aimed at minimizing heat losses. As a result, direct supply of process heat to customers (e.g., above 120 °C) is no longer feasible.

This problem can be solved by using high-temperature heat pumps (HTHP). In principle, the supply or return flow can be utilized as a heat source, allowing individual consumers in the network area to be supplied with heat at temperatures above 120 °C (superheated water or steam). This could form the basis for an interesting business model if low heat production cost can be achieved. In that case, district heating operators could attract new customers and increase sales.

The Coefficient of Performance for Heating (COP) ε_H (energy efficiency of process) and heating capacity of HTHP are influenced by various factors. The choice of refrigerant (ODP = 0, GWP < 5), the circuits, and the heat source temperatures play an important role [4] - [6]. Therefore, it is crucial to find an optimal heat pump solution tailored to the specific boundary conditions. To gain a comprehensive understanding of the problem, systematic simulations and analyses were conducted using EBSILON®Professional [3].

In this article, Section 2.1 introduces the configurations of the researched the circuits, while Section 2.2 presents the chosen refrigerants. Furthermore, Section 2.3 explains the boundary conditions of the simulations. The simulation results are focus on the Coefficient of Performance for Heating, Compression ratio and Heat production cost, which are presented and evaluated in Sections 3.1 to 3.3.

2. MODELS AND INVESTIGATIONS

2.1. Circuit

Figure 1 shows the three investigated heat pump circuits. These circuits were chosen due to their wide prevalence in practice. Figure 1 a) shows the basic circuit of a heat pump (referred to as the basic heat pump model), which consists of four main components: the compressor, condenser, expansion valve, and evaporator. The second circuit (Figure 1 b), referred to as single-stage compression with an internal heat exchanger (IHX)) extends upon the basic heat pump model and includes an additional internal heat exchanger. The internal heat exchanger can improve the COP by further cooling the refrigerant before it enters the expansion device, thereby increasing the suction temperature of the refrigerant. In the third circuit (Figure 1 c), referred to as two-stage compression and intercooling with two-stage expansion of the refrigerant), two compressors (low- and high-pressure stage) are used. Phase separation occurs in an intermediate cooler (flash tank) [2], [7].

All the above-mentioned circuits were modeled and then simulated using the EBSILON®Professional software. A specific control code (EbsScript) is used to handle the parameter variations. The code varies specific parameters (such as the inlet temperature on the heat source side, $T_{\mathrm{so,in}}$, and the suction superheat, T_{SH}), and then initiates the simulation. Subsequently, a MATLAB script verifies the data again to filter out results that do not comply with the simulation boundary conditions (as described in Section 2.3). This allows for the determination of results under the given boundary conditions.

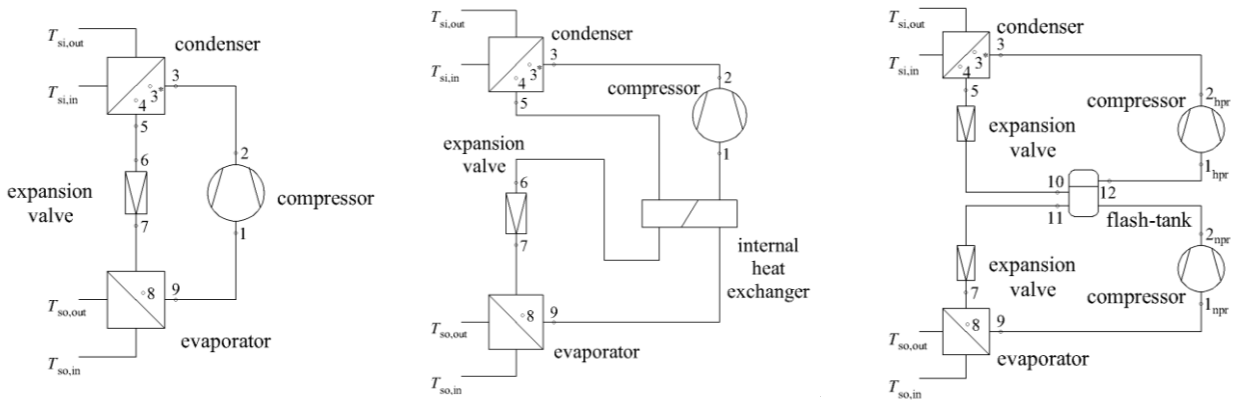

Figure 1. Investigated heat pump circuits; a) basic heat pump model, b) single-stage compression with an internal heat exchanger (IHX), c) two-stage compression and intercooling with two-stage expansion of the refrigerant

2.2. Refrigerants

Within this study, seven refrigerants, R600, R601a, R744, R1224yd(Z), R1233zd(E), R1234ze(E), and R1336mzz(Z), are investigated. Table 1 summarizes the main properties of the refrigerants. Nowadays, natural refrigerants are gaining attention due to environmental and economic concerns. Therefore, natural refrigerants are compared to synthetic refrigerants (hydrofluoroolefins (HFOs), and hydrochlorofluoroolefin (HCFOs)) within the scope of this study. The selected refrigerants have different safety classifications ranging from A1 to A3, thus covering a broad range of current and future refrigerants. All the refrigerants have an Ozone Depletion Potential (ODP) of zero and a Global Warming Potential (GWP) of less than five, thus complying with applicable policy regulations. Additionally, all the selected refrigerants (except R744) have critical temperatures above 150 °C, indicating that they can operate with subcritical state changes. Only the HTHP using R744 operates in the supercritical range. In this case, a very large temperature difference in the gas cooler is required to achieve high COP. Therefore, the HTHP using R744 is a special case.

Table 1. categorization and properties of the investigated refrigerants [1]

Refrigerants	Substance group	Chemical formula	T_0 (1 bar) [°C]	T_{crit} [°C]	p_{crit} [bar]	ODP	GWP	SG
R600	alkane	$CH_3CH_2CH_2CH_3$	-0.5	152.0	38.0	0	4	A3
R601a	alkane	$(CH_3)_2CHCH_2CH_3$	27.8	187.2	33.8	0	3	A3
R744	nature regfrigerant	CO_2	-78.5	31.0	73.8	0	1	A1
R1224yd(Z)	HCFO	$CF_3CF{=}CHCl(Z)$	14.0	155.5	33.3	0	< 1	A1
R1233zd(E)	HCFO	$CF_3CH{=}CHCl(E)$	14.0	166.5	36.2	0	1	A1
R1234ze(Z)	HFO	$CF_3CH{=}CHF(Z)$	9.8	150.1	35.3	0	< 1	A2L
R1336mzz(Z)	HFO	$CF_3CH{=}CHCF_3(Z)$	33.4	171.3	29.0	0	2	A1

2.3. Boundary conditions

In the simulation, except for the R744 heat pump operating in the supercritical range, the condensing pressure p_c and the evaporating pressure p_0 can be calculated using the condensing temperature T_c and the evaporating temperature T_0. The compressor discharge temperatures T_2 can be determined for the respective pressures. Similarly, the inlet temperature on the heat source side, $T_{so,in}$, was determined in the range of 50 to 100 °C. The temperature difference between the inlet and outlet on the heat source side is 5 K.

The superheating range of the suction gas is defined from 5 to 20 K [2]. In this study, the lowest possible superheat has been selected for refrigerants and circuits (except for R744). In circuit a) and circuit c), the superheating is 5 K for the refrigerants (R600, R1224yd(Z), R1233zd(E), R1234ze(Z)). This ensures that the compressor suction gas remains in a gaseous state. For refrigerants R601a and R1336mzz(Z), the authors set a superheating of 20 K to ensure that the compressor does not enter the two-phase region of the refrigerant during operation.

For the circuit b), the refrigerant first passes through the internal heat exchanger before entering the compressor. Compared to circuits a), this increases the superheating of the refrigerant before it enters the compressor. If the condensing pressure p_c remains constant, the compressor discharge temperature T_2 increases. To ensure that the compressor discharge temperature T_2 remains within a reasonable range (T_2 < 150 °C), a superheating of 0 K was chosen for refrigerants R600, R1224yd(Z), R1233zd(E), and R1234ze(Z), and a superheating of 15 K was chosen for refrigerants R601a and R1336mzz(Z).

The control of the R744 heat pump model is determined based on the compressor discharge pressure p_2. To ensure better comparability, the authors of this study choose a discharge pressure p_2 below 150 bar and a compressor discharge temperature T_2 in the same range (T_2 < 150 °C) for all simulations, as mentioned above.

Based on the study [8], the isentropic efficiency η_{is} is set to 0.7 for all simulations. The project *Research Platform for Refrigeration and Energy Technology KETEC* Subproject 10 [9] focuses on the storage and provision of process heat. Therefore, the inlet temperature on the heat sink side $T_{si,in}$ is set to 120 °C, and the outlet temperature of the heat sink side $T_{si,out}$ is set to 140 °C (condenser). To achieve comparable COPs, the inlet temperature of the heat sink side $T_{si.in}$ is set to 10 °C for the R744 heat pump (exception due to the substance properties).

In an early phase of the work, the generation of superheated water and superheated steam in the condenser was investigated. However, the simulation results showed that the influence of both variants on the COPs is negligibly small. Therefore, the following discussion is based on the case of superheated water production.

3. RESULTS AND DISCUSSION

3.1. Coefficient of Performance for Heating

The energetic efficiency of the HTHP is to be evaluated solely based on the Coefficient of Performance for Heating (COP) ε_H. Figure 2 a) shows an example of the COPs achievable with refrigerant R1224yd(Z) using the three circuits at different heat source temperatures. According to the COPs, circuit c) demonstrates a clear advantage over the other two variants. Circuit a) is the least advantageous. Figure 2 b) illustrates the relative increase in COPs for circuit b) and circuit c) compared to circuit a). On average, the relative increase is 13% (circuit b)) and 33% (circuit c)). It can be observed that the improvement in COPs due to the change in circuits has a greater impact at lower heat source temperatures. However, as the heat source temperature increases, the improvement in COPs gradually decreases.

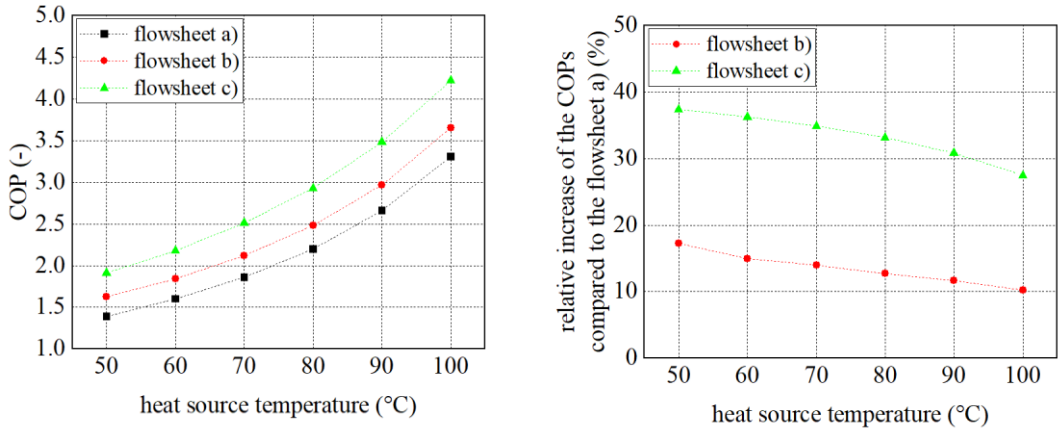

a) b)

Figure 2. Simulation results for the refrigerant R1224yd(Z), a) Dependence of the COP on the source temperature and the circuits according to Figure 1, b) Relative increase of the COPs compared to the circuit a)

R1224yd(Z) is a representative example to demonstrate the trend of the COPs for the different circuits and heat source temperatures. Among the remaining five refrigerants (except for R744) introduced at the beginning of the article, the simulation results show the same trend as with R1224yd(Z). The results can be seen in Figure 3 to Figure 5.

It should be noted that due to the limited boundary conditions, the seven refrigerants in this study cannot cover all heat source temperatures for all the three circuits. These limitations are also visible in Figure 3 to Figure 5. For example, in circuit c) with refrigerants R601a and R1336mzz(Z), the compression process of the high-pressure stage enters the two-phase region. Therefore, these two refrigerants are not included in Figure 5. When the heat source temperature is 50 °C, the points (R601a, circuit a); R1336mzz(Z), circuit a) and circuit b)) are not present in Figure 3 and Figure 4. This is because the corresponding evaporating pressure is below 1 bar.

R744 stands out among the seven refrigerants, primarily due to its low critical temperature (Table 1). As a result, the process operation must be in the supercritical range. This allows for higher COPs at low heat source temperatures compared to the other refrigerants. However, due to the limited boundary conditions, the COPs for R744 reach a limit of approximately three as the heat source temperature increases. For circuit c), R744 is also unsuitable due to its lower critical temperature. Therefore, no simulation results for R744 are not shown in Figure 5.

Based on Figure 3 and Figure 4, it can be observed that R744 achieves the highest COPs with circuit a) and circuit b) at heat source temperatures between 50 °C and 90 °C. R1233zd(E) achieves the highest COPs with circuit c). If R744 is not considered for circuit a) and circuit b), R1233zd(E) can achieve the highest COPs.

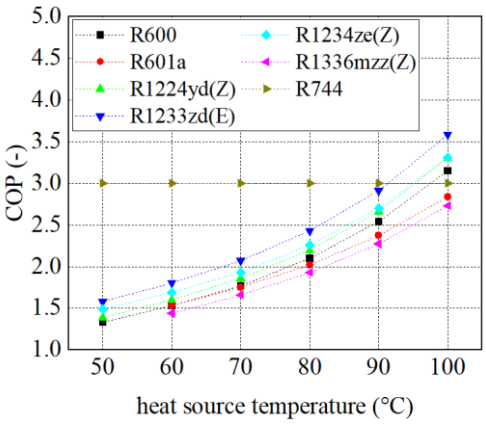

Figure 3. Dependence of the COP on the source temperature and the refrigerants for the circuit a)

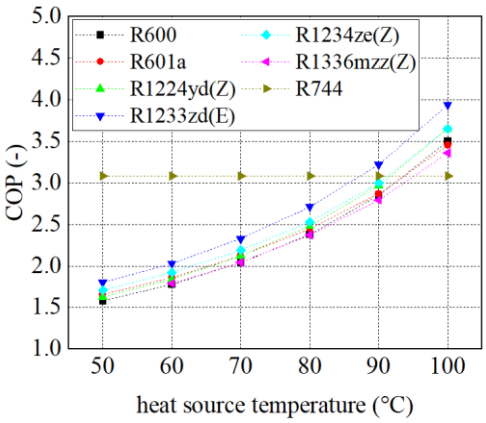

Figure 4. Dependence of the COP on the source temperature and the refrigerants for the circuit b)

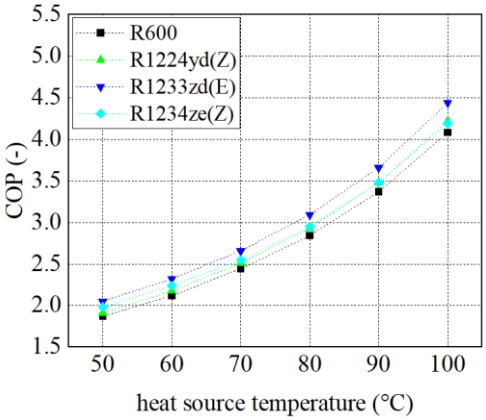

Figure 5. Dependence of the COP on the source temperature and the refrigerants for the circuit c)

3.2. Compression ratio

Compression is an important process in heat pumps, and reducing the compression effort is crucial. Without going into the actual implementation (such as the use of a compressor), this section aims to complement the results shown above and provide a better understanding of the operating ranges.

Figure 6 illustrates the functional relationship between compression ratios and heat source temperatures for various refrigerants. This figure is based on circuit a), where the condensing temperature remains constant. A lower compression ratio implies that the compressor can perform less work.

Figure 7 shows the pressure difference between the inlet and outlet of the compressor. Although R744 has the lowest compression ratio among all refrigerants, it still has the highest-pressure difference. For the other refrigerants, R1336mzz(Z) and R601a, the compression ratio is relatively high. However, the pressure difference remains below 30 bar.

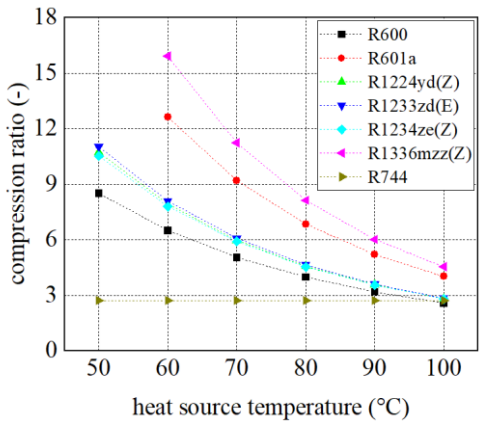

Figure 6. Dependence of the compression ratio on the source temperature and the refrigerants for the circuit a)

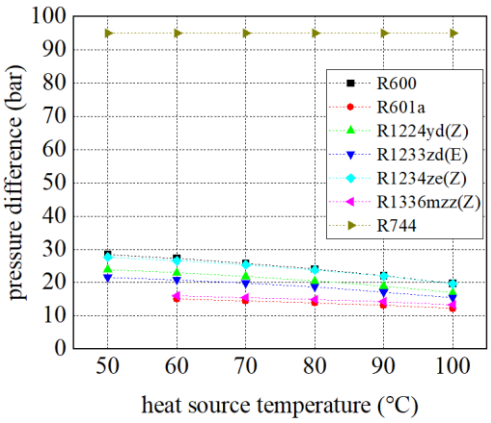

Figure 7. Dependence of the pressure difference on the source temperature and the refrigerants for the circuit a)

3.3. Heat production cost

The cost of heat production is a good way to assess or estimate economic feasibility in the sense of marginal cost analysis. At the same time, the results of different heat pump circuits with different refrigerants can be better compared. This means that only operating cost are considered, while other costs (such as investment cost) are not taken into account. In the past years (2017-2021), it has been observed that the use of zero-emissions electricity may have higher purchase cost compared to conventionally generated electricity [10]. However, due to increasing prices for conventional energy supply and decreasing prices for e.g., PV systems, the situation may be reversed in the present and upcoming years.

Figure 8 presents the results of an investigation of heat production cost. The two sub-figures differ in terms of the selected COPs (Figure 8 a): ε_H: 2.05; Figure 8 b): ε_H: 4.44). They indicate the lowest and highest COPs for circuit c) (refrigerant: R1233zd(E)).

To calculate the cost of heat production, the electricity purchase cost was varied from 0.00 €/kWh to 1.00 €/kWh and the heat purchase cost (district heating return flow) was varied from 0.00 €/kWh to 1.00 €/kWh as well. The red dashed lines in the figures represent the cost of heat production, with a price difference of 0.10 €/kWh between each two lines. In this calculation method, the COP of the heat pump is the only factor considered. Therefore, the slope of the red dashed lines (iso-lines of heat production cost) becomes steeper as the COP increases. This behavior can be clearly seen in Figure 8. With the help of Figure 8, the district heating supplier or customer can quickly estimate the marginal cost.

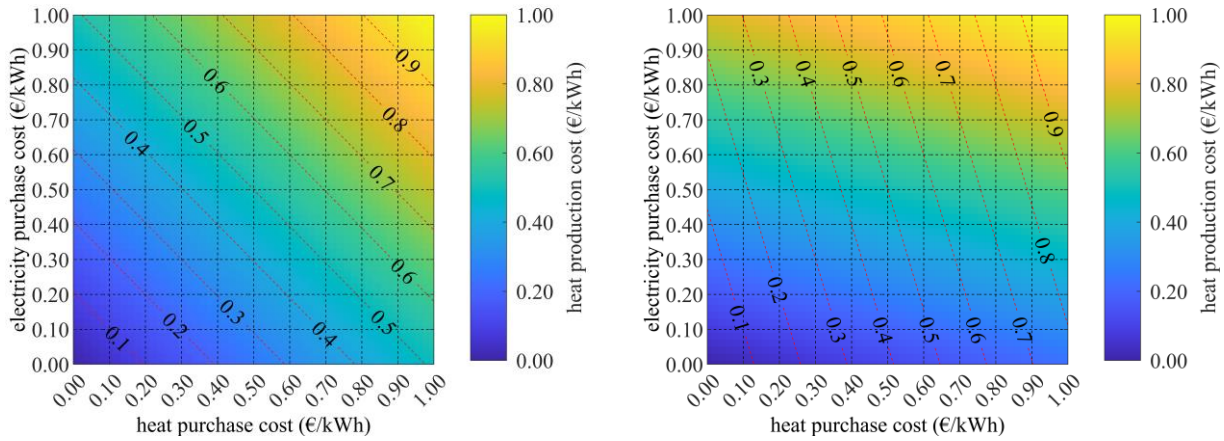

Figure 8. Dependence of the heat production cost on the electricity purchase cost and heat purchase cost (a) ε_H: 2,05, R1233zd(E); b) ε_H: 4,44, R1233zd(E))

Figure 9 is derived from Figure 8. The pink and blue dashed lines represent the cost of heat production at 0.10 €/kWh for the two COPs (ε_H: 2.05 and ε_H: 4.44). The shaded areas below these lines indicate the cost of heat production below 0.10 €/kWh. The shaded area increases as the COP increases (only the case with COP > 2 was considered). For the operator, a larger shaded area means greater flexibility in response to changes in electricity and heat purchase cost. The heat production cost lines intersect under the same cost (but different COPs). Connecting all the intersection points results in the red dashed line in Figure 9.

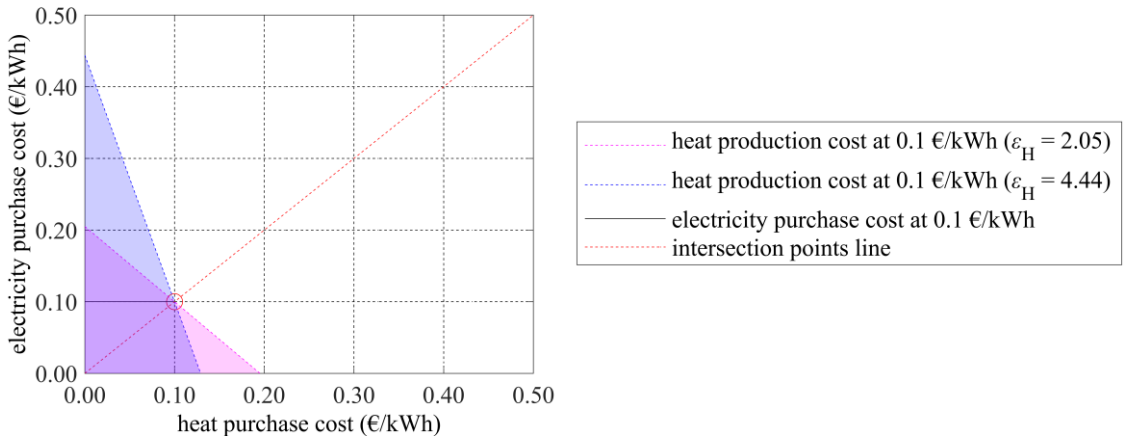

Figure 9. Comparison of the heat production cost using different COPs

4. CONCLUSION

In total, three heat pump circuits and seven refrigerants were analyzed for heat supply at 140 °C (superheated water or steam) in this study. A fictitious district heating system (supply or return flow) served as the heat source. Circuit c) yielded the highest COPs. However, specific considerations need to be made regarding the refrigerants. Using circuits a) and b), R744 achieved the highest COPs at lower heat source temperatures (T_{so}: 50...80 °C). The other refrigerants showcased their advantages at higher heat source temperatures (T_{so}: 100 °C). In circuit c), R1233zd(E) achieved the highest COPs, reaching a maximum value of 4.44. As a competing technology, direct electric heating (expected cost of heat production at 0.10 €/kWh) can be considered. To remain competitive, a higher COP allows for a wider acceptable range of electricity and heat purchase cost. In the present example, to achieve a heat production cost below 0.10 €/kWh with an ε_H of 4.44 (R1233zd(E)), the electricity purchase cost would have to be below approximately 0.45 €/kWh and the heat purchase cost would have to below approximately 0.12 €/kWh. Therefore, high COPs are critical to achieving the expected low cost of heat production.

All the circuits were modeled, simulated, and systematically analyzed using EBSILON®Professional software to select suitable heat pump solutions. The results provide fundamental insights and functional relationships for the district heating and industrial sectors. The aim is to expand the application potential of high-temperature heat pumps and replace conventional solutions with greenhouse gas emissions and high costs. The marginal cost analysis revealed a cost range of heat production below 0.10 €/kWh. Further efforts are required to offer process heat affordably, securely, and in an environmentally friendly manner. In subproject 10 of the *KETEC* research project, this is a central focus area. Thermal energy storage systems are envisaged to compensate for fluctuating energy supply and variable heat demand over time. The authors see considerable development and application potential here.

LIST OF SYMBOLS

Latin letters	
p	pressure [bar]
T	temperature [°C]
Greek letters	
ε_H	Coefficient of Performance for Heating [-]
η	efficiency [-]
Indexes and abbreviations	
0	evaporation
c	Condensation
COP	Coefficient of Performance for Heating
crit	critical
GWP	Global Warming Potential
HCFO	hydrochlorofluoroolefin
HFO	hydrofluoroolefins
hpr	high pressure
HTHP	high-temperature heat pump
in	inlet
is	isentropic
lpr	low pressure
ODP	Ozone Depletion Potential

out	outlet
SG	safety group based on SN EN 378-1: 2017 und ASHRAE Standard 34
SH	superheating
si	heat sink
so	heat source

ACKNOWLEDGEMENT

The research work is funded by the Federal Ministry of Education and Research (BMBF) under the reference 03SF0623A/B/C on the basis of a resolution of the German Bundestag. Project management is provided by Projektträger Jülich (PtJ). The authors would like to express their gratitude for the funding, support and cooperation.

REFERENCES

[1] Arpagaus, C. Hochtemperatur-Wärmepumpen Marktübersicht; Stand der Technik und Anwendungspotenziale. VDE Verlag GmbH, Berlin, Offenbach, 2019. - ISBN 978-3-8007-4550-0.

[2] Höges, C., Roskosch, D., Brach, J., Vering, C., Venzik, V., Müller, D. Investigation of the Interactions between Refrigerant. Energy Technol. Vol. 11 (2023). - https://doi.org/10.1002/ente.202201295

[3] Iqony Solutions GmbH. EBSILON®Professional 16 P1, 2023.

[4] Ozone Secretariat, United Nations Environment Programme. The Montreal Protocol on Substances that Deplete the Ozone Layer. Montreal, 1987. URL: https://ozone.unep.org/treaties/montreal-protocol [access: 05.05.2023].

[5] European Parliament. Regulation (EU) No 517/2014 of the European Parliament and of the Council of 16 April 2014 on fluorinated greenhouse gases and repealing Regulation (EC) No 842/2006, 2014.

[6] United Nations Treaty Collection. CHAPTER XXVII ENVIRONMENT.2.f. The Montreal Protocol on Substances that Deplete the Ozone Layer, Kigali, 2016. URL: https://treaties.un.org/Pages/ViewDetails.aspx?src=IND&mtdsg_no=XXVII-2-f&chapter=27&clang=_en [access: 05.05.2023].

[7] Bruno, F., Belusko, M., Halawa, E. CO2 Refrigeration and Heat Pump Systems - A Comprehensive Review. Energies (2019).

[8] Wang, J., Belusko, M., Liu, M., Evans, M., Alemu, A., Bruno, F. Preliminary Study On A Novel Transcritical CO2 High-Temperature Heat Pump. Proceedings of the 6th International Seminar on ORC Power Systems, Technical University of Munich, 2021.

[9] Urbaneck, T., Matthes, M., Richter, M., Hempel, O., Safarik, M., Franzke, U., Noack, R., Honke, M., Müller, M., Henninger, S., Schossig, P., Henning, H.-M., de Oliveira, H. T., Morgenstern, A., Nienborg, B., Gschwander, S., Engelmann, P., Benndorf, G. www.ketec.online. Website of the joint project, 30.05.2023.

[10] Nefodov, D, Xiao, S., Richter, M., Urbaneck, T. Nutzung eines Fernwärme-Rücklaufs als Wärmequelle zur Versorgung eines Nahwärmenetzes mit Wärmepumpen – Teil 2. HLH Lüftung/Klima Heizung/Sanitär Gebäudetechnik VDI Fachmedien 72. (2021) Vol. 6, pp. 59-63, ISSN 1436-5103.

Energy Storage

The 18th International Symposium on District Heating and Cooling,
September 3–6, 2023, Beijing, China

IRREVERSIBILITY EVALUATION OF HEAT TRANSPORT IN SEASONAL THERMAL ENERGY STORAGE UNITS FOR DISTRICT HEATING APPLICATIONS

Tianhao Xu, Xiaoyun Xie*, Yi Jiang

Building Energy Research Center, Tsinghua University, Beijing 100084, China
** Corresponding author. xiexiaoyun@tsinghua.edu.cn*

ABSTRACT

Seasonal thermal energy storage (STES) is an indispensable technology to correct temporal mismatch between supply and demand of carbon-free heat source throughout a year, for district heating systems. Existing STES technologies, such as pit thermal energy storage (PTES), tank thermal energy storage (TTES), borehole thermal energy storage (BTES), and aquifer thermal energy storage (ATES) have been utilized worldwide in varying scales, and there are a number of review studies summarizing the geometric and heat exchangers designs of the STES units as well as the key technical and economic performance indicators. Although such reviews provide explicit categorization for the existing STES systems almost all based on sensible heat storage, there is a lack of perspective differentiating the essential mechanisms of heat storage in view of heat transport irreversibility. For instance, the heat storage principle of thermocline hot water storage (THWS), including PTES and TTES, is based on vertical displacement of fluids to deliver stored hot water for later use, while BTES relies on heat conduction to raise the temperature of soil field. Such differences lead to varying characteristics of heat transport irreversibility, reflected in vastly different needs for re-boosting the temperature level of stored heat upon retrieval in practical terms. Therefore, this paper brings forward an analytical framework and entransy-dissipation models to evaluate the degree of irreversibility for THWS and BTES technologies. The results show that THWS is featured with a lower degree of irreversibility given that the mixing intensity across thermocline is maintained below a certain threshold. Demonstrating in-depth irreversibility evaluation of the existing STES technologies, this paper provides insight for selecting and designing STES pathways for low-carbon transition of district heating systems.

Keywords: seasonal thermal energy storage, irreversibility analysis, heat transfer, district heating

1. INTRODUCTION

Low-carbon transition of global energy systems is urgently needed. For district heating systems, integrating seasonable thermal energy storage (STES) devices is regarded as an effective pathway to replace fossil fuel demands by solar heat and industrial surplus heat stored throughout the year. Some European countries widely using urban district heating systems have built pilot STES projects with varying technologies and scales. For instance, Denmark has built nearly ten large-scale pit thermal energy storage (PTES) systems, each for one municipal district heating system, and the largest unit built in the town of Vojens has a total hot water storage volume of around 200,000 m^3. In Sweden, borehole thermal energy storage (BTES) systems are more common, and one of the largest units in the world is Emmaboda with a bore storage field of 200,000 m^3. German has built many solar communities (such as Chemnitz and Eggenstein) where PTES and tank thermal energy storage (TTES) devices are included in the centralized heating systems, and the storage volume varies in the range of hundreds to around ten thousand cubic meters. There are also several high-temperature aquifer thermal energy storage (ATES) projects in German, such as Neubrandenburg, in which heat is injected and retrieved through wells with aquifers of 1,200 meter deep. District heating systems are widely spread over the northern urban areas of China, where the total annual space heating demand is around 5 billion GJ. In the Chifeng City, the world's largest BTES system of 500,000 m^3 storage volume has been built and running, and there are several PTES installations of thousand to tens of thousand cubic meters in storage volume. In the prospected carbon-neutral urban heating systems of Northern China, even larger STES systems (up to ten million cubic meter of water storage volume equivalent) are needed because typical northern towns are more densely populated than typical European towns, and thus much higher total demand of heat storage is needed.

Although there is a variety of technological options for storing heat in seasonal cycles, operational results of many listed STES systems show that, as a common problem, heat pumping is often required upon heat discharging process because the output temperature level from storage is inadequate for indoor comfort heating or less than the forward temperature required of the district heating networks. For BTES, the Emmaboda system can only output 10-15% of its stored heat directly

to the hot water radiator heating system until an electric heat pump booster was installed in 2018. Afterwards, the discharged heat of 30-40ºC was directed to the heat pump evaporator and boosted to up to 55ºC, and the total amount of discharged heat available for heating increased by 3.5 times [1]. To solve a similar problem, an absorption heat pump system is proposed to lift the output temperature of discharged heat from the Chifeng BTES system, in demand of high-temperature steam as input [2]. For PTES, the monitoring data of, e.g., the Dronninglund [3] and Gram [4] systems show that output temperature lifting by an electrical heat pump is needed for the majority of the discharging periods. Furthermore, there are a number of STES systems (e.g., the Drake Landing Solar Community BTES system [5] and Neubrandenburg ATES system [6]) deploying boilers on the forward line of heat distribution systems for the same purpose. All such evidences point to the problem of STES systems that the useful temperature level is lost over annual cycles. An evident cause would be heat loss from storage to the ambient, while another important but often overlooked cause should be heat transport irreversibility across heat exchangers and within the storage media when heat loss is not considered.

Certainly, different STES designs and operational strategies lead to different characteristics in transient heat transfer, and several performance indicators have been used to characterize the level of irreversibility in literature. The principal parameter is exergy efficiency defined based on the second law of thermodynamics, which is widely used to evaluate not only heat storage but also thermal cycles involving heat-work conversion. In an ideal example for illustration [7], Dincer and Rosen introduce two thermal energy storage cycles with an equal energy efficiency but a significantly different exergy efficiency: both cycles are charged with the same hot stream with an inlet temperature of 85ºC and an outlet temperature of 25ºC, while in the first cycle heat is discharged with a 25ºC-inlet cold stream of a flow rate five times than that in the second cycle, so that the output temperature of the first cycle is only 35ºC (exergy efficiency is 27%) as compared with 75ºC of the second cycle (exergy efficiency is 73%), when the reference state is set as 20ºC. The first cycle is an example with larger irreversibility and the exergy efficiency quantifies the effect.

However, there seems to lack a generic study comparing BTES, PTES, ATES and STES other technologies regarding on exergy efficiency, and it could be incorrect to extract exergy efficiency data from individual studies to make inter comparison, because the selection of the reference state would affect the calculation results of exergy efficiency. Annually average ground temperature [8] or ambient air temperature [9] could be selected as dead state for evaluating BTES systems, while for TTES systems the dead state could be the inlet fluid temperature for discharging [10-12] or ambient air temperature [13]. Furthermore, the operational temperature range could be smaller for BTES and ATES than TTES and PTES, which might further complicate the comparison.

With calculation results from an assumed illustrative example, Figure 1 plots the variation of exergy efficiency with various conditions of degraded levels of output temperature (dT), reference state temperature (T_0) and operational temperature range (ΔT). With reference temperature of 0ºC (~ambient air temperature during winter), 10ºC (~annually average ground temperature), 20ºC (~water inlet temperature), the exergy efficiency significantly differs when ΔT is low. It can happen when the case of dT=15 K and T_0=0 ºC has a higher exergy efficiency than the case of dT=5 K and T_0=20 ºC, when ΔT is around 25 K. Therefore, exergy efficiency for characterizing and comparing irreversibility may present some limitations with respect to variation of reference state. For thermocline hot water storage systems, parameters characterizing thermal stratification, such as MIX number [14] and Recovery efficiency [15], are defined and used to present the level of mixing in stratified fluids, which can be also interpreted as measure of how much heat transports from the hot to cold parts of the storage media irreversibly. However, such parameters cannot be used for evaluating BTES systems. In a nutshell, we need an appropriate performance indicator which can reflect irreversibility of heat transport in a universal manner for existing STES technologies. Since STES cycles have long timespan and transient thermal performance, it is also required that such parameter should include the dimension of time and reflect transient heat transfer conditions in STES systems.

This paper presents a novel evaluation framework of heat transport irreversibility in STES units, based on the entransy dissipation theory first developed by Guo et al. [16]. The analytical solutions of the total entransy dissipation across a certain period of charging, namely accumulative entransy dissipation, are given for the first time in the paper for ideally simplified one-dimensional heat transfer models of thermocline hot water storage systems (applicable for both PTES and TTES) and BTES systems. Based on entransy dissipation concept, the heat transfer characteristics and heat storage mechanisms of PTES and BTES systems are revisited, and the essential difference in irreversibility between the two technologies is discussed. The paper aims at providing a new prospective for evaluating thermal performance of STES systems and insights for selecting and designing STES pathways for future district heating systems.

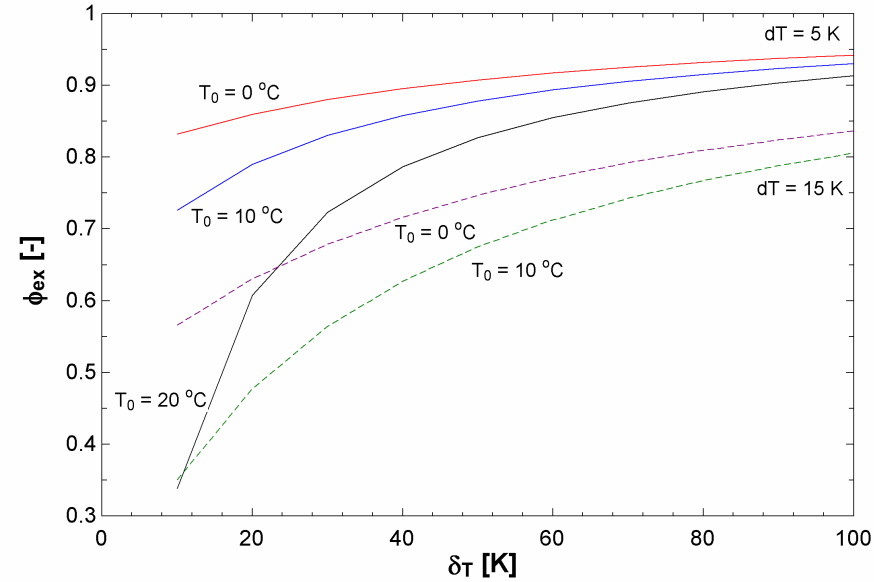

Figure 1. Comparison of exergy efficiency of two degraded levels of output temperature: dT=5 K (solid lines) and 15 K (dashed lines) over different selection of dead state (T_0=0, 10, 20°C), when operational temperature range (ΔT) varies in the range of 10 to 100 K.

This paper presents a novel evaluation framework of heat transport irreversibility in STES units, based on the entransy dissipation theory first developed by Guo et al. [16]. The analytical solutions of the total entransy dissipation across a certain period of charging, namely accumulative entransy dissipation, are given for the first time in the paper for ideally simplified one-dimensional heat transfer models of thermocline hot water storage systems (applicable for both PTES and TTES) and BTES systems. Based on entransy dissipation concept, the heat transfer characteristics and heat storage mechanisms of PTES and BTES systems are revisited, and the essential difference in irreversibility between the two technologies is discussed. The paper aims at providing a new prospective for evaluating thermal performance of STES systems and insights for selecting and designing STES pathways for future district heating systems.

2. METHODOLOGY

2.1. Analytical Framework

Entransy dissipation is originally defined as the loss of thermal potential caused by molecular thermal diffusion through thermally resistive materials, and so it can measure the degree of heat transport irreversibility. According to the entransy balance equation [16], the local rate of entransy dissipation can be expressed as $En = -q \cdot \nabla T$ (unit: $W{\cdot}K/m^3$). For three-dimensional STES systems in which heat transfer and entransy dissipation are transient, the integral forms of the local rate of entransy dissipation can be written as Eq. (1), considering thermal conduction as the heat transfer mechanism. ΔEn is defined as accumulative entransy dissipation with a unit of $J{\cdot}K$.

$$\Delta En = \int_{t1}^{t2} En dt = \int_{t1}^{t2} \iiint_V q \cdot (-\nabla T) dV dt = \int_{t1}^{t2} \iiint_V k \cdot (\nabla T)^2 dV dt \tag{1}$$

Besides entransy dissipation, change of entransy can occur with entransy flux and internal heat source. In practical terms, it can be perceived that, when considering the entire STES unit as a whole, the heat loss from the storage to the ambient leads to entransy change outside the boundary, and heat conduction within storage material from hot to cold parts, i.e., heat transport inside the boundary, causes entransy dissipation and leads to lowered useful temperature level of stored heat. Figure 2 illustrates a seasonal thermal energy storage cycle where heat is delivered from the source to the STES unit during charging and subsequently delivered to the sink during discharging. Across the source and sink heat exchangers, useful temperature level is lost despite negligible heat loss, which is a fundamental feature of all actual heat exchangers, and heat loss from the storage unit occurs throughout the cycle leading to temperature drops in storage media as well. Therefore, there are three main mechanisms resulting in change of entransy of the STES system: (1) heat transport across source and sink boundary heat exchangers; (2) heat loss to the ambient; (3) thermal conduction within storage material. The first two factors are common for any practical STES systems in spite of the technological option, while the last factor differs significantly between THWS and BTES units, as well as other thermal energy storage technologies such as ATES and latent heat thermal energy storage.

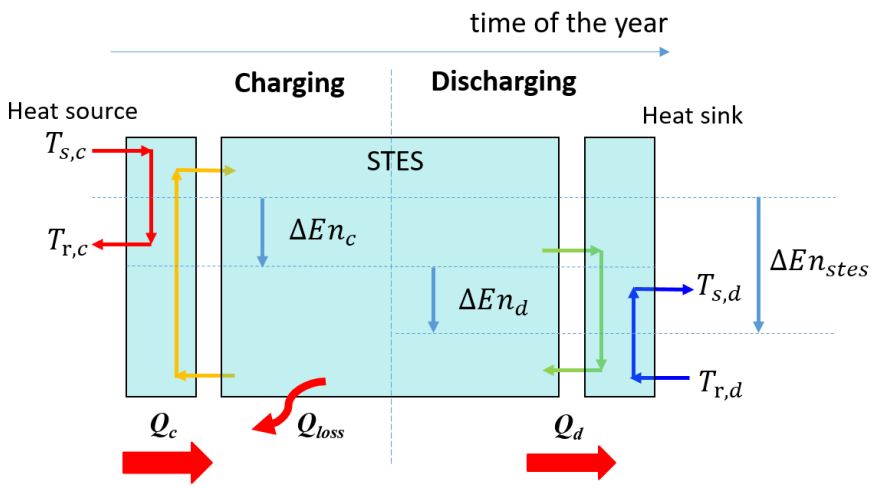

Figure 2. Entransy dissipation over a seasonal thermal energy storage cycle including charging and discharging processes

To analyze the entransy dissipation system by element and to stress the fundamental entransy dissipation process caused by heat storage mechanism, an analytical framework for heat transport irreversibility is proposed with a hierarchical structure, as shown in Table 1. In the first level, ideal charging/discharging processes where only one-dimensional heat transport within the storage media is considered. In the next levels, practical conditions in the heat storage cycle are gradually added to the scope of consideration, with the overall heat transfer and entransy dissipation models approaching the real picture.

Table 1 Ideal and practical charging process under the entransy dissipation evaluation framework

Level of heat transport irreversibility	**THWS**	**BTES**	**Heat transfer model descriptions**
Fundamental heat storage mechanism, ideal case	Flow only in gravitational direction, only axial heat conduction, no convective mixing and no heat loss	Only radial temperature gradient and heat conduction, no consideration of thermal resistance of components in a single borehole exchanger	One-dimensional heat equations
Practical internal heat transfer conditions	Consider mixing effects from turbulent mixing, flow entrainment, and natural convection	Consider temperature gradient in longitudinal direction, effects from buried length and neighboring boreholes also considered	Two- or three-dimensional heat transfer models
STES systems with heat source and sink heat exchangers	Consider temperature drop in the heat source and sink heat exchangers separating the STES unit and forward loops	Consider thermal resistance in the borehole heat exchangers and source/sink heat exchangers	Inclusion of heat transfer through heat exchangers
Heat loss to the surrounding environment	Heat loss to the ambient air and the ground field		Inclusion of heat loss modelling of the storage

As this paper aims at establishing the irreversibility analysis framework and illuminate different irreversibility characteristics between THWS and BTES units, the analytical solutions of entransy dissipation and performance comparisons are given for the first level introduced in Table 1. The charging process is specifically analyzed, since charging and discharging processes are symmetric to an extent.

2.2. Deduction of Accumulative Entransy Dissipation

For an ideal THWS unit, a one-dimensional advection-diffusion equation can be written for the axial direction, see Eq. (2).

$$\rho_w c_{p_w}(\frac{\partial T_w}{\partial t} + u_z \frac{\partial T_w}{\partial z}) = k_w \frac{\partial^2 T_w}{\partial z^2} \tag{2}$$

where u_z stands for the flow speed along the gravitational direction, which can be also understood as the rate of fluid displacement; ρ_w, c_{p_w}, and k_w are the density, specific heat, and thermal conductivity of water, which are assumed to be constant in the ideal case. Assuming that the hot and cold fluids, separated by the thermocline, can be regarded as two individual semi-infinite bodies, the water temperature in the thermocline region can be written as Eq. (3), where z_0 stands for the distance between the centerline of hot and cold fluids and the point of interest. Here, $\Delta T_s = T_{h,in} - T_{c,ini}$ and $T_{avg} = (T_{h,in} + T_{c,ini})/2$; $T_{h,in}$ is the constant inlet temperature of the hot water and $T_{c,ini}$ is the homogeneous initial temperature in the storage unit. α_w is the thermal diffusivity of water and erf stands for the error function.

$$T_w = \frac{1}{2}\Delta T_s \, erf(\frac{z_0}{2\sqrt{\alpha_w t}}) + T_{avg} \tag{3}$$

With Eq. (1) and Eq. (3), the accumulative entransy dissipation throughout the thermocline region can be deduced and written as Eq. (4). ΔEn_{thws} is a function of the geometric mean of the thermal conductivity and volumetric thermal capacity, and the parameters of time and temperature difference are also included.

$$\Delta En_{thws} = \frac{\Delta T_s^2 k_w}{\sqrt{\frac{\pi \alpha_w}{2t}}} = \Delta T_s^2 k_w \sqrt{\frac{2t}{\pi \alpha_w}} = \Delta T_s^2 \rho_w c_{p_w} \sqrt{\frac{2}{\pi}\alpha_w t} = \Delta T_s^2 \sqrt{\frac{2}{\pi} k_w \rho_w c_{p_w} t} \tag{4}$$

For an ideal BTES unit with a single vertical borehole, the infinite line source (ILS) model can be applied to analytically calculate the radial temperature distribution of the surrounding ground in a cylindrical coordinate. The heat equation can be written as Eq. (5).

$$\rho_g c_{p_g} \frac{\partial T_g}{\partial t} = k_g(\frac{\partial^2 T_g}{\partial r^2} + \frac{1}{r}\frac{\partial T_g}{\partial r}) \tag{5}$$

With the heat injection rate per meter of the borehole represented as q' (W/m), in the ILS model the ground temperature (T_g) can be expressed with a function of undisturbed ground temperature T_{g0}, q' , and an exponential integral, and then through Laplace Transformation, Eq. (6) can be used for calculating T_g with satisfactory accuracy, using the Euler–Mascheroni costant ($\gamma \approx 0.577$). ρ_g, c_{p_g}, k_g, and α_g are the thermo-physical properties of the ground.

$$T_g = T_{g0} + \frac{q'}{4\pi k_g} Ei\left(\frac{r^2}{4\alpha_g t}\right) = T_{g0} + \frac{q'}{4\pi k_g}[\ln\left(\frac{4\alpha_g t}{r^2}\right) - \gamma] \tag{6}$$

Based on Eq. (1) and Eq. (6), the accumulative entransy dissipation of the ground field can be deduced as Eq. (7), where r_{field} and r_{bh} represent the thermal penetration radius and borehole radius, respectively. It is reasonable to estimate the thermal penetration radius as $r_{field} = 3\sqrt{\alpha_g t_c}$ [17, 18], and r_{bh} is the borehole radius.

$$\Delta \mathrm{En}_{btes} = \int_0^t \int_{r_{bh}}^{r_{field}} k \cdot 2\pi r H_{bh} \frac{dT}{dr} \cdot \frac{dT}{dr} dr dt = \frac{q'^2 ln \frac{r_{field}}{r_{bh}} t_c}{2k_g \pi} \tag{7}$$

For clarity, the equivalent dissipative temperature difference (δT) is defined as the accumulative entransy dissipation divided by amount of heat storage capacity along the charging period, see Eq. (8).

$$\delta T = \frac{\Delta \mathrm{En}}{Q} = \begin{cases} \dfrac{\Delta T^2 \rho_w c_{p_w} \sqrt{\frac{2}{\pi}\alpha_w t}}{\Delta T \rho_w c_{p_w} u t} = \dfrac{\Delta T}{u}\sqrt{\dfrac{2\alpha_w}{\pi t}} & for\ THWS\ units \\ \dfrac{\dfrac{q'^2 ln \frac{r_{field}}{r_{bh}} t_c}{2k_g \pi}}{q' t_c} = \dfrac{q' ln \frac{3\sqrt{\alpha_g t}}{r_{bh}}}{2k_g \pi} & for\ BTES\ units \end{cases} \tag{8}$$

2.3 Parametric Analysis

In view of the abovementioned entransy dissipation models, the following design parameters of the STES systems would affect the amount of entransy dissipation in the ideal cases:

- Thermo-physical properties: for BTES units, type of the ground and its properties would largely influence thermal

conduction rate and entransy dissipation;

- Geometry of the storage units: for THWS units, the aspect ratio would affect the axial flow speed given the same total storage volume. For BTES units, typical borehole depth ranges between 10 to 150 m, and it is designed according to various parameters including the heat injection rate (q'), which directly influences the accumulative entransy dissipation.

We intend to use a comparative case study, where a simplified charging process of a seasonal thermal energy storage cycle is assumed, to compare the degree heat transport irreversibility between THWS and BTES technologies. For fair comparison, the primary principle is to assure the same amount of heat storage capacity can be achieved over the same period of charging. Secondly, although for BTES systems the heat transfer boundary condition is normally assumed to be the second type, there is an upper limit of the input temperature determined by the heat source. Therefore, another key boundary is that the ultimate input temperature allowing heat input to the BTES unit is assumed equal to the hot fluid temperature ($T_{h,in}$) enter the THWS units, which means the eventual temperature difference of BTES is set the same as the persistent temperature difference of THWS ($\Delta T^{t=t_c} = T_{g_{r=r_{bh}}}^{t=t_c} - T_{g0} = T_{h,in} - T_{c,ini}$). Based on these conditions, Table 2 lists the relevant parameters and the varying ranges in case studies. For BTES, the ground type varies between soil (e.g., clay and sand) to rock (e.g., limestone, granites, sandstone) having diverse thermo-physical properties, and typical values of the main ground types are selected for case study.

Table 2 Design and operational parameters of THWS and BTES for the comparative case study

	THWS	BTES			
Common design and operational parameters	Temperature: $T_{h,in} = T_{g_{r=r_{bh}}}^{t=t_c} = 90\,℃$; $T_{c,ini} = T_{g0} = 20\,℃$; $\Delta T^{t=t_c} = 70\,K$ Total theoretical thermal storage capacity: $Q_{tes} = 4500\,GJ$; Charging period: $t_c = 180\,d$				
Specific design parameters	Total hot water storage volume: $V_{thws} = 1.54 \times 10^4\,m^3$	Borehole depth: $L_{bh} = 1.7 \times 10^3\,m$ Heat injection rate: $q' = \frac{Q_{tes}}{L_{bh} \cdot t_c} = 233\,W/m$			
Parameters as variables for case study	Height of storage container: $H_{thws} = 10, 20, 50, 100\,m$ Aspect ratio of 0.12 to 3.9	Ground type	Thermal conductivity [W/(m·K)]	Volumetric heat capacity [MJ/(m^3·K)]	Thermal diffusivity [10^6 m^2/s]
Thermo-physical properties of storage material	Water: Thermal conductivity: 0.6 W/(m·K) Volumetric heat capacity: 4.18 MJ/(m^3·K) Thermal diffusivity: $1.43\times 10^{-7}\,m^2/s$	clay	1.7	3.4	0.5
		sand	2.4	2.9	0.83
		limestone	2.8	2.4	1.17
		granite	3.4	3	1.13
		sandstone	2.3	2.8	0.82

3. RESULTS AND DISCUSSION

Based on the analytical solutions provided in Section 2.2 and design parameters listed in Table 2, equivalent dissipative temperature difference (δT) is calculated for THWS and BTES along the charging process and plotted in Figure 3. The solid lines representing δT of THWS with different heights of the storage volume (i.e., different axial flow speeds u_z) all show a decreasing trend, while the dashed lines representing δT of BTES with different ground types, show an increasing trend. This is because, in the ideal case, the heat travels in the thermocline region only by molecular diffusion, which is featured with a penetration distance scaled as $\sqrt{t}$, see Eq. (8), while the fluid displacement effect of cold water by hot water in a perfectly stratified environment, which results in heat storage in the container, is a linear process with time. As a result, δT_{thws} is proportional to $t^{-1/2}$; in pratical terms, it can be understood as the molecular diffusion of heat penetrates slower than linear flow displacement with a constant speed in one-dimensional space, so that with a longer time, the effect of heat conduction leading to entransy dissipation gets gradually more insignificant compared with the increasing amount of heat along time. In contrast, δT_{btes} increases from around 25 K to 40 K from the beginning to the end of the charging process, mainly because the temperature at the borehole wall (i.e., the temperature in contact with the wall $T_{g_{r=r_{bh}}}$), which can be interpreted as the boundary temperature for heat injection, increases from about 58 to 90ºC. Thus, δT_{btes} can be regarded as a mean driving temperature difference for the overall radial heat distribution in the ground field. Unlike in ideal THWS units where heat conduction is only a 'by-product' of the flow displacement activity,

heat conduction itself is the effective mechanism for heat storage raising the ground temperature for BTES systems. Therefore, the heat storage mechanism is essentially different between THWS and BTES, and so the developing trends of δT are also different.

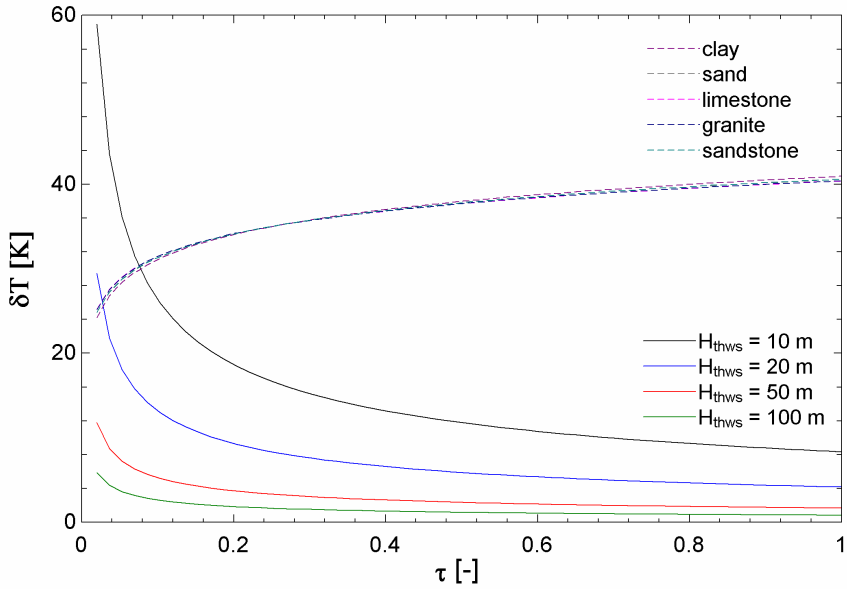

Figure 3 Comparison of equivalent dissipative temperature difference (δT) between BTES (dashed lines) and THWS (solid lines) under various design conditions; τ is the dimensional time.

It can be also observed from Figure 3, that the height of THWS units (H_{thws}) significantly affects δT_{thws}, as a higher but thinner storage unit (e.g., $H_{thws} = 100\ m$) leads to a lower level of δT_{thws} compared with a shorter but flatter one (e.g., $H_{thws} = 10\ m$) given the same storage volume. This is because entransy dissipation is only caused by thermal conduction across cross-sectional areas in the ideal case. Although THWS units of the same volume store the same amount of heat, the higher but thinner one has smaller cross-sectional areas for heat conduction to result in entransy dissipation and thus has lower δT_{thws}. For BTES, the five different ground types studied and shown in Figure 3 have different thermal conductivities and diffusivities, but their δT_{btes}-curves overlap well. This indicates that the ground properties are not the determinative factor of heat transport irreversibility in the ideal BTES systems. Overall, the comparative case study conducted for ideal charging process shows that THWS units have smaller equivalent dissipative temperature difference than BTES units. The primary cause for such difference is the heat storage mechanism of fluid displacement does not produce entransy dissipation itself, while the mechanism of heat conduction results in dissipation as long as there is temperature difference and thermal resistance.

In practice, STES systems with higher equivalent dissipative temperature difference presents a higher degree of heat transport irreversibility, which means the retrieved heat would be of less useful temperature level for the heating purpose. This is similar as the comparative case of exergy efficiency provided in the introductory section, as a lower exergy efficiency also reflects a higher degree of heat transport irreversibility. Although the ideal case study illustrates the fundamental difference between the displacement-based STES device and conduction-based STES device, many practical factors must be considered when comparing real STES systems, such as mixing phenomena in stratified water accelerating internal heat transport from the hot to cold parts of fluids, and borehole heat exchangers with thermal resistance of the borehole wall, tubes, and filling materials. The buried length of borehole and neighboring effects must also be considered. Considering the mixing effects leading to higher entransy dissipation, Figure 4 plots calculation results of the threshold value of axial flow speed (u_0), which is the minimum value of u_z for δT_{thws} to become lower than δT_{btes}, under various degree of mixing expressed by N_{mix} of 5-100. The analytical solution of u_0 is given in Eq. (9). N_{mix} is defined as the effective diffusion coefficient describing the ratio of the eddy thermal diffusivity (α_e), a parameter widely used in turbulent studies to quantify the phenomenological diffusion rate, to the molecular thermal diffusivity of water: $\alpha_e = N_{mix}\alpha_w$. As mixing effects strengthen, the threshold velocity should be higher to compensate the higher level of entransy dissipation caused by mixing.

$$u_0 = \left(ln\frac{2\sqrt{\alpha_g t}}{r_{bh}} - \frac{\gamma}{2}\right)\sqrt{\frac{2\alpha_w N_{mix}}{\pi t_c}} \Big/ ln\frac{3\sqrt{\alpha_g t}}{r_{bh}} \tag{9}$$

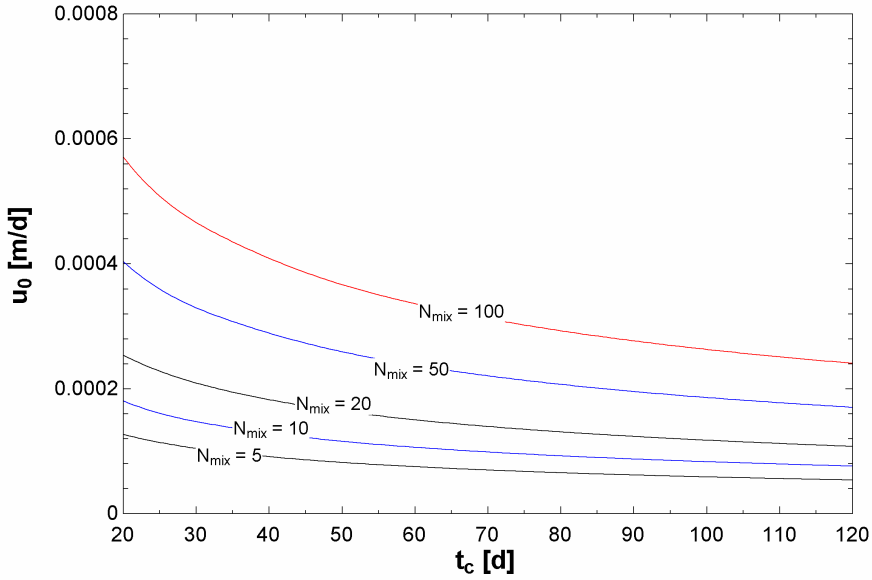

Figure 4 threshold value of axial flow speed (u_0) allowing THES to achieve lower equivalent dissipative temperature difference than BTES.

Despite the simplification and idealization, the analytical framework of heat transport irreversibility provides a theoretical tool for choosing and designing STES systems with lower loss in useful temperature levels for heating. It should be however noted that, concluding heat storage THWS units such as PTES and TTES. In other words, constraining mixing in the stratified fluid body is one of the most important premises for implementing THWS systems in practice, because such measures can reduce temperature re-boosting demands in the energy supply systems, which are usually provided by the heat pumps or boilers in the forward lines of the districting heating network.

4. CONCLUSION

In consideration of the limitation of exergy efficiency for evaluating the heat transport irreversibility in STES systems, this work establishes an entransy dissipation-based theoretical framework to evaluate the irreversibility for THWS (including PTES and TTES) and BTES systems. The analytical solutions of the accumulative entransy dissipation and equivalent dissipative temperature difference are provided for ideal charging process with the two types of technologies. Comparisons show that THWS mostly exhibits a lower level of entransy dissipation than BTES in ideal charging processes, because the heat storage mechanism of the former is fluid displacement, by which entransy dissipation only occurs within thermocline region due to limited heat conduction, while the latter entirely relies on heat conduction to achieve storage of heat. Furthermore, parametric analyses are conducted for THWS units regarding the height of storage container and for BTES regarding the ground properties. Calculation results show that the axial flow speed in THWS units, which can be also interpreted as the rate of fluid displacement, should be kept high for reducing the equivalent dissipative temperature difference, and a higher degree of mixing in stratified flow leads to a higher threshold value of axial flow speed for THWS units to reach less entransy dissipation than BTES units.

This work discloses the underlying relation between the heat storage mechanism and heat transport irreversibility through analytical solutions and case studies. As implication for practical STES systems, we tend to recommend THWS for district heating applications over BTES systems as long as mixing can be well refrained in stratified water. However, future studies are needed to concretely draw such conclusions for actual STES systems, by analyzing all segments of heat transport irreversibility listed in Table 1.

REFERENCES

[1] L. R. Olof Andersson, Niklas Håkansson. (2021) Heat Pump System Improved High-Temperature Borehole Thermal Energy Storage Efficiency. *HPT MAGAZINE*.
[2] F. Guo, X. Zhu, P. Li, and X. Yang, "Low-grade industrial waste heat utilization in urban district heating: Simulation-based performance assessment of a seasonal thermal energy storage system," *Energy,* vol. 239, p. 122345, 2022/01/15/ 2022, doi: https://doi.org/10.1016/j.energy.2021.122345.
[3] I. Sifnaios, G. Gauthier, D. Trier, J. Fan, and A. R. Jensen, "Dronninglund water pit thermal energy storage dataset," *Solar Energy,* vol. 251, pp. 68-76, 2023/02/01/ 2023, doi: https://doi.org/10.1016/j.solener.2022.12.046.
[4] C. Winterscheid and T. Schmidt, "Gram district heating monitoring data evaluation for the years 2016-2017," *Solites*

(Steinbeis Research Institute for Solar and Sustainable Thermal Energy Systems), 2019.
[5] L. Mesquita, D. McClenahan, J. Thornton, J. Carriere, and B. Wong, "Drake Landing Solar Community: 10 Years of Operation," 2017.
[6] F. Kabus *et al.*, "Aquifer Thermal Energy Storage in Neubrandenburg - Monitoring Throughout Three Years of Regular Operation," 11/21 2021.
[7] I. Dincer and M. A. Rosen, *Thermal energy storage: systems and applications*. John Wiley & Sons, 2021.
[8] H. Esen, M. Inalli, M. Esen, and K. Pihtili, "Energy and exergy analysis of a ground-coupled heat pump system with two horizontal ground heat exchangers," *Building and Environment,* vol. 42, no. 10, pp. 3606-3615, 2007/10/01/ 2007, doi: http://dx.doi.org/10.1016/j.buildenv.2006.10.014.
[9] O. Ozgener and A. Hepbasli, "Modeling and performance evaluation of ground source (geothermal) heat pump systems," *Energy and Buildings,* vol. 39, no. 1, pp. 66-75, 1// 2007, doi: http://dx.doi.org/10.1016/j.enbuild.2006.04.019.
[10] L. J. Shah and S. Furbo, "Entrance effects in solar storage tanks," *Solar energy,* vol. 75, no. 4, pp. 337-348, 2003.
[11] M. Y. Haller, C. A. Cruickshank, W. Streicher, S. J. Harrison, E. Andersen, and S. Furbo, "Methods to determine stratification efficiency of thermal energy storage processes – Review and theoretical comparison," *Solar Energy,* vol. 83, no. 10, pp. 1847-1860, 2009, doi: 10.1016/j.solener.2009.06.019.
[12] A. Mawire, M. McPherson, R. R. J. v. d. Heetkamp, and S. J. P. Mlatho, "Simulated performance of storage materials for pebble bed thermal energy storage (TES) systems," *Applied Energy,* vol. 86, no. 7, pp. 1246-1252, 2009/07/01/ 2009, doi: https://doi.org/10.1016/j.apenergy.2008.09.009.
[13] A. Lake and B. Rezaie, "Energy and exergy efficiencies assessment for a stratified cold thermal energy storage," *Applied Energy,* vol. 220, pp. 605-615, 2018/06/15/ 2018, doi: https://doi.org/10.1016/j.apenergy.2018.03.145.
[14] J. H. Davidson, D. A. Adams, and J. A. Miller, "A Coefficient to Characterize Mixing in Solar Water Storage Tanks," *Journal of Solar Energy Engineering,* vol. 116, no. 2, pp. 94-99, 1994, doi: 10.1115/1.2930504.
[15] H. A. Sheldon, A. Wilkins, and C. P. Green, "Recovery efficiency in high-temperature aquifer thermal energy storage systems," *Geothermics,* vol. 96, p. 102173, 2021/11/01/ 2021, doi: https://doi.org/10.1016/j.geothermics.2021.102173.
[16] Z.-Y. Guo, H.-Y. Zhu, and X.-G. Liang, "Entransy—A physical quantity describing heat transfer ability," *International Journal of Heat and Mass Transfer,* vol. 50, no. 13, pp. 2545-2556, 2007/07/01/ 2007, doi: https://doi.org/10.1016/j.ijheatmasstransfer.2006.11.034.
[17] P. Eskilson, "Thermal analysis of heat extraction boreholes," 1987.
[18] P. Eskilson and J. Claesson, "Simulation Model for Thermally Interacting Heat Extraction Boreholes," *Numerical Heat Transfer,* vol. 13, no. 2, pp. 149-165, 1988/03/01 1988, doi: 10.1080/10407788808913609.

The 18th International Symposium on District Heating and Cooling, September 3–6, 2023, Beijing, China

SIMULATIVE INVESTIGATIONS OF A HYBRID STORAGE CONCEPT FOR INDUSTRIAL STEAM HEAT SUPPLY

Dimitri Nefodov[a], Haochen Wang[a], Markus Richter[a], Robin Berlin[a], Thorsten Urbaneck[a]*

[a] *Professorship Applied Thermodynamics, Department of Mechanical Engineering, Chemnitz University of Technology, 09107 Chemnitz, Germany*

[*] *Corresponding author: thorsten.urbaneck@mb.tu-chemnitz.de*

ABSTRACT

Steam is a common heat transfer medium in industrial systems, which requires a significant amount of energy to generate. Within the current project KETEC (Research Platform Refrigeration and Energy Technology) concepts for the realization of the highly available, low-emission and energy-efficient supply of steam for industrial processes are fundamentally investigated. The solution approach provides for the use of a heat pump storage system. Steam generation is provided by a high-temperature heat pump using the low-GWP refrigerant R1336mzz(Z). The produced steam is buffered in a storage system to increase flexibility in steam generation and supply, with a minimum steam temperature of 140 °C. The heat pumps can currently only achieve good performance coefficients with low steam temperatures and high heat source temperatures. This limits the usable temperature difference, which has a negative effect on the Ruths steam storage. To increase the storage capacity in the small temperature range, steam storage can be combined with phase change materials (PCM).

This paper deals with the concept and possible implementation variants of a hybrid storage system based on a Ruths storage and a PCM when a steam generator with relatively low supply temperatures is used. The simulation of the system is performed with the software EBSILON®Professional.

The results confirm that the combination of the Ruths steam storage with the PCM is expedient. The usage of PCM increases the storage heat capacity and allows a larger amount of steam to be withdrawn from the Ruths storage. Consequently, the steam storage volume can be dimensioned smaller. The use of heat pumps allows the use of waste heat from other processes to increase overall efficiency.

Keywords: Heat pump, Ruths Steam Storage, PCM, Simulation, EBSILON®Professional

1. INTRODUCTION

In industrial process heat supply, steam is often used as the heat transfer medium. However, their production requires a relatively large amount of energy [1]. For example, in 2019, process heat accounted for approximately 66.7% of the energy consumption of German industry [2]. With the European Union aiming to reduce annual greenhouse gas emissions by 55% by 2030 and Europe aiming to be carbon neutral by 2050, the supply of process heat to industry must be given greater attention. Within the framework of the KETEC project (Research Platform for Refrigeration and Energy Technology) [3], concepts for the realisation of the highly available, low-emission and energy-efficient provision of steam for industrial processes based on heat pump-storage systems, among other things, are being fundamentally investigated.

Gradient pressure storages in steam supply systems are particularly suitable for storing (e. g. Ruths storages). During loading, steam is injected into the hot water in the storage tank. This injection causes an intensive heat and mass transfer, whereby the injected steam condenses and the hot water fill rate increases. At the same time, the storage tank temperature and pressure increase. The vapor and liquid phases are approximately in equilibrium. During discharge, steam is taken from the upper part of the storage. The pressure drops, thus the hot water evaporates. During the discharge process, the storage tank temperature decreases. However, a relatively small usable temperature difference leads to a larger required storage volume (e. g. 10 to 40 K).

To increase the storage capacity, especially in small temperature ranges, storage can in principle be equipped with phase change materials (PCM)[1]. Such approaches are known as hybrid storage in the literature. PCMs with different melting temperatures or ranges can be used for this purpose.

[1]Phase change materials (PCM) here are storage materials that perform the solid-liquid phase change and vice versa. I.e., steam storages do not classify as PCM storages.

The underlying research was able to identify three combination variants of the Ruths storage with PCM (Figure 1). These variants can be described as follows:

- V1) Use of a macro-encapsulated PCM within the Ruths storage,
- V2) Combination of the Ruths storage with external PCM storage,
- V3) Ruths storage with external PCM storage and internal heat exchanger.

Buschle et al. [4], [5] present different concepts of hybrid storage especially for the concrete industry (PROSPER project). In the given temperature range of 100 to 210 °C, the use of different PCMs (e.g. technical salts, organic PCMs) is possible. Thermal conductivity is mentioned as an important criterion. This parameter is decisive for the provision of the required heat output and for the design of the heat transfer surface. The thermal conductivity is relatively low for many PCMs. For this reason, *Buschle* et al. propose two possible solutions: increasing the heat transfer surface, e.g. through the use of macro-encapsulated PCMs (variant V1, Figure 1) as well as increasing the effective thermal conductivity, e.g. through the integration of layers with high thermal conductivity or the creation of composite materials with PCM. An externally located PCM storage (variant V2, Figure 1) is also considered beneficial.

Hofmann et al. [6] (HyStEPs project) presents investigations on the optimisation of hybrid storage systems in which PCM is placed on the outer shell of Ruths storage (variant V3, Figure 1). As a conclusion, the authors state that proposed hybrid storage could have lower costs compared to the Ruths storage (under assumptions made). However, the process requirements (charging and discharging times) have a strong influence on the possible cost savings through the use of hybrid storage compared to Ruths storage. In relation to the investment costs (storage only), there was a reduction of around 20% compared to the reference design without PCM storage.

Niknam et al. [7] have attempted to provide a comprehensive evaluation of the technical and economic aspects of hybrid thermal energy storage for industrial applications. The PCM in the reference system (variant V3) is located on the shell of the steam storage. The use of PCMs is very effective in extending the discharge time. The investment costs of a system with this hybrid storage were 5% less expensive than a conventional steam storage. This solution reduces the steam production costs (investment and operating costs) [7] of industrial systems.

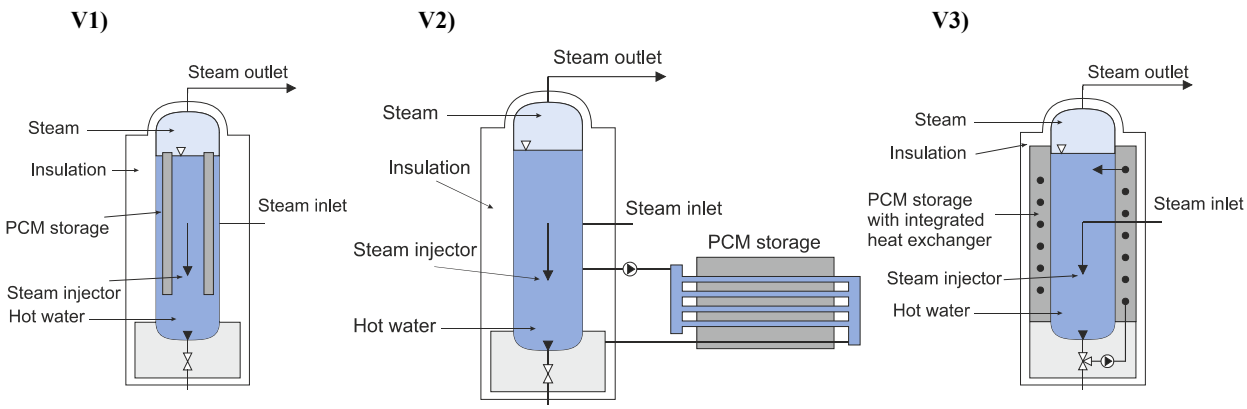

Figure 1. hybrid storages, V1) Use of the macro-encapsulated PCM within a Ruths storage tank, V2) Combination of the Ruths storage with external PCM storage, V3) Ruths storage with external PCM storage and internal heat exchanger (modified according to [4], [5], [6], [7])

Each of the above variants of hybrid storage (V1 to V3) has certain advantages and disadvantages. These are summarized in Table 1. The use of PCM creates limitations in the delivery of heating output, which are due to low thermal conductivity.

Table 1. Comparison of different approaches of hybrid storages for the supply of process steam

Variant	Ruths storage	V1	V2	V3
Advantages	high discharge capacity, fast availability for operation	low space requirement	spatial separation between PCM and Ruths storage, thus high degree of freedom in design	low space requirement
		higher specific heat capacity, lower investment and operating costs according to literature data		
Disadvantages	high space requirement, high pressures	displacement of hot water	high space requirement	
		sluggish behavior or reduced operational readiness, additional or higher costs due to further tanks, heat exchanger, PCM		

2. MODELING AND BOUNDARY CONDITIONS

2.1. System

In this paper, a hybrid storage system is investigated on the basis of variant V2. The Ruths storage unit with the externally arranged PCM storage unit supplies a sterilization process from the food industry as an example. The simulations are realised with the software EBSILON®Professional [8]. A high-temperature heat pump with a relatively low supply temperature of 140 °C serves as the steam generator. The heat pump operates with the low-GWP refrigerant R1336mzz(Z). A system without a storage tank (designation: R-WP) and a system with a Ruths storage tank (designation: R-RS) are defined as references. The use of a heat pump-storage system allows the avoidance of pollutant emissions. This applies in particular if power is supplied from renewable energy sources (e.g. photovoltaics). Furthermore, the return flow of a district heating network or industrial waste heat can be considered as a heat source.

2.2. Boundary conditions and reference systems

A batch sterilization process from the food industry is used as a heat sink. For example, in the process should be handled cans of tomato soup. According to assumptions, 4000 doses fit into the autoclave with a chamber volume of 2.2 m³. The autoclave with a starting temperature of 20 °C is supplied with steam for approx. 160 minutes (theoretical assumption) until the target temperature (mean temperature) of around 121 °C is reached. The temperature must be maintained for a period of 10 to 20 minutes to kill all microorganisms (Figure 2) [9]. The EBSILON component 165 is used to model the autoclave. Selected data for the simulation are summarized in Table 2.

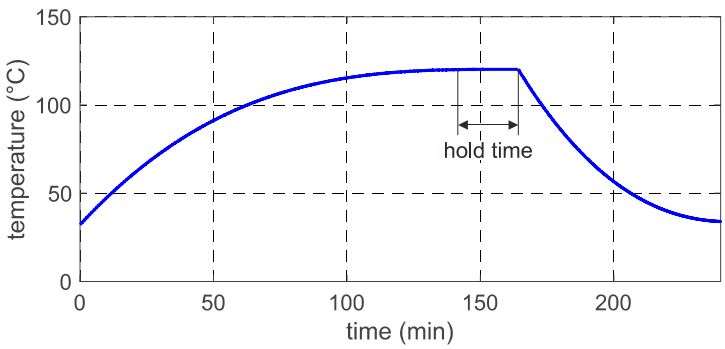

Figure 2. Exemplary temperature curve of a batch sterilization process (modified according to [9])

Figure 3 shows the schematic representation of the reference systems with and without Ruths storage. The investigations on the heat pump are not the subject of this paper, so that the heat supply is only taken into account with marginal values (component 1). Steam is supplied at a delivery temperature of 140 °C and a pressure of 3.6 bar. The Ruths storage tank (component 160) with a storage volume of 25 m³ is used to store thermal energy. The reference data shows Table 2.

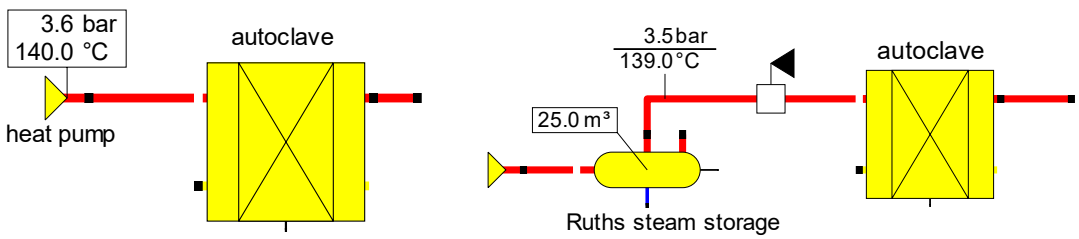

a) Reference model R-WP b) Reference model R-RS

Figure 3. Reference models (EBSILON-modeling), a) use of heat pump, b) use of a heat pump and a Ruths storage tank

Table 2. Reference model, selected parameters

System section	Heat pump	Ruths storage	Autoclave
Component (EBSILON)	1	160	165
Supply temperature (°C)	140	-	-
Heat transfer fluid	steam		
Storage medium	-	water/steam	tin cans with tomato soup
Storage volume (m³)	-	25	2.2
Storage mass (kg)		1253 (construction)	1868 (filled tin cans)
Total storage mass (kg)		23946	3759
Insulation thickness (m)	-	0.3	0.3
Thermal conductivity of insulation (W/mK)	-	0.04	

2.3. Hybrid storage system

The model with the hybrid storage is shown in Figure 4a). A parameter study (Figure 4 b)) was carried out for dimensioning the system R-PCM with the software EBSILON®Professional. Possible combinations of PCM storage mass and Ruths storage volume, which fulfil the target criteria according to section 2.2, are marked in blue. For further examinations, interpretation according to Table 3 (Figure 4 b), Point L) applies.

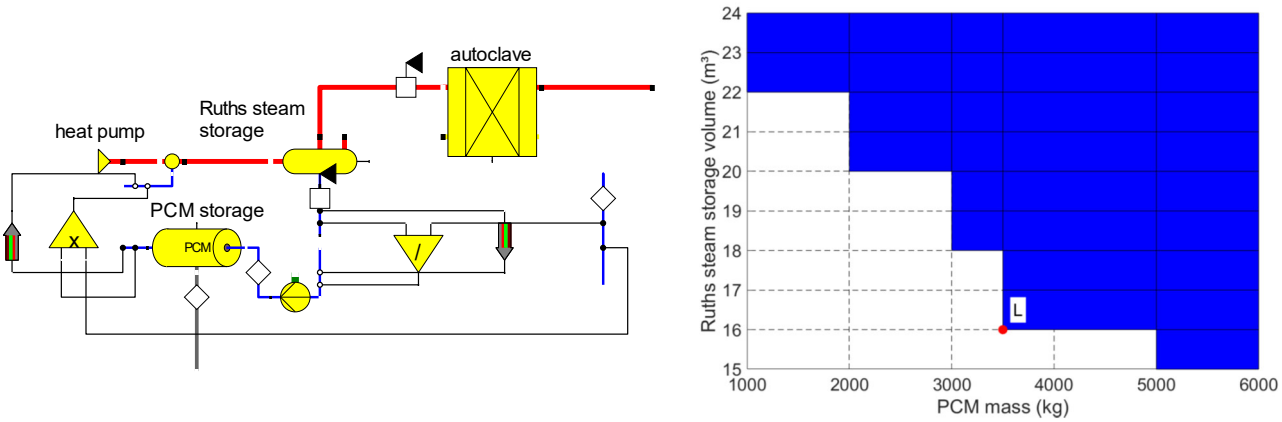

a) b)

Figure 4: a) Hybrid storage system R-PCM (EBSILON model), b) Results of the parameter study for the dimensioning of the hybrid storage (EBSILON simulation)

The PCM storage is modeled with the component 166. Initially, a fictitious PCM is used as the PCM. The material data were derived from the PCM RT80HC [8] data available in the EBSILON®Professional and adjusted for the melting point of 130 °C. The fictitious PCM has a density of 1500 kg/m³, a specific heat storage capacity of 1.9156 kJ/(kg K) at 25 °C as well as a thermal conductivity of 0.6 W/(m K). The data for the calculation of the specific heat capacity over temperature are considered in the form of a characteristic curve (Figure 5 a)). According to the assumptions, the PCM is located in a container in which there are several pipes through which steam flows. In the model, it is initially not useful to reproduce the entire PCM storage. Instead, a part of the pipe (l = 1 m, d = 0.009 m) with surrounding PCM (D = 0.047 m, m_{PCM} = 3.196 kg) is modelled as a representative volume element (Figure 5b)). Consequently, scaling of the mass flow is required.

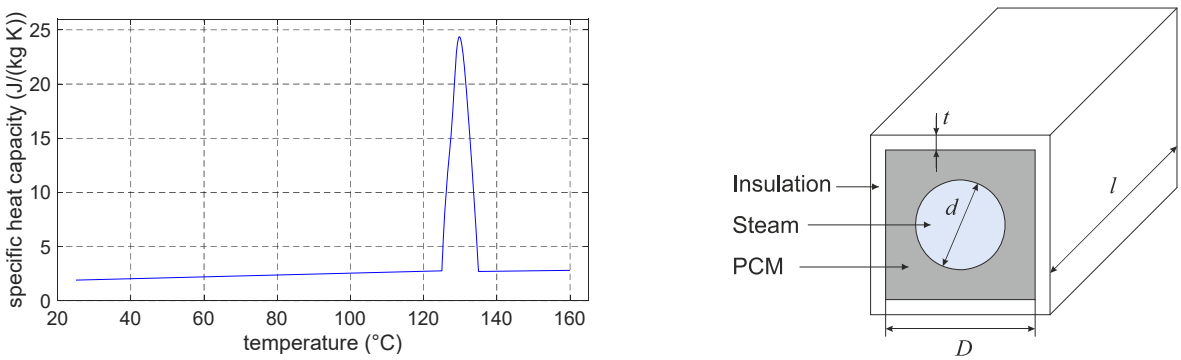

a) b)

Figure 5. a) Specific heat capacity of the fictive PCM over temperature, b) Schematic illustration of the representative volume element of the PCM storage

By using the PCM storage with a PCM mass of around 3500 kg, the volume of the Ruths storage can be reduced[2] from 25 m³ to 16 m³. The selected parameters for the model with the hybrid storage (variant R-PCM) are summarised in Table 3.

Table 3. Reference system R-PCM, selected parameters

System section	Ruths storage	PCM storage
Component (EBSILON)	160	166
Heat transfer medium	steam	steam
Storage medium	water/steam	imaginary PCM based on RT80HC
Storage volume (m³)	16	-
Fluid mass in the storage (kg)	13814 (water/steam)	3500 (PCM)
Total storage mass (kg)	14745	4444

3. RESULTS

First of all, the heating process of the autoclave is of interest. In order to better illustrate a difference to steam production with a storage tank, the initial state (model according to variant R-WP without storage tank) is to be simulated. The investigation provides a variation of the steam mass flow from 0.010 to 1.000 kg/s. The course of the average autoclave temperature over time for different loading mass flows is shown in Figure 6. According to the assumptions in section 2.2, the heating process should take approx. 160 minutes to achieve an even temperature distribution in the autoclave. At maximum heat pump steam mass flow of 1.000 kg/s, the target temperature of 121 °C is reached in about 34 minutes. Steam mass flows below 0.050 kg/s are not sufficient to reach the target temperature in the specified time. At a steam mass flow of 0.075 kg/s, the target temperature is reached in 148 minutes. Thus, this mass flow is initially considered as the reference value.

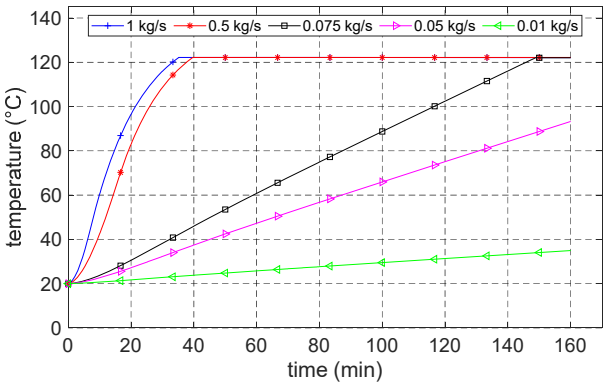

Figure 6. Curves of the average autoclave temperature for different steam mass flows during the sterilization process (variant R-WP)

During preliminary investigations, it was determined that the Ruths storage tank should have a volume of 25 m³ and a liquid level of approx. 98% in order to be able to supply the process. The Ruths storage (starting temperature of 139 °C, steam discharge mass flow of 0.078 kg/s) enabled the process to reach the sterilisation temperature of 121 °C in 160 minutes (Figure 7). The liquid level has decreased by 4.7% in the process. In addition, Figure 7 shows the temperature inside the autoclave ($T_{\mathrm{Autoklav,100}}$). The temperature rises sharply from the 55th to the 72th minute to the temperature of around 131 °C. Then the temperature in the autoclave follows the steam temperature from the Ruths storage tank.

[2] Data based on current parameter study.

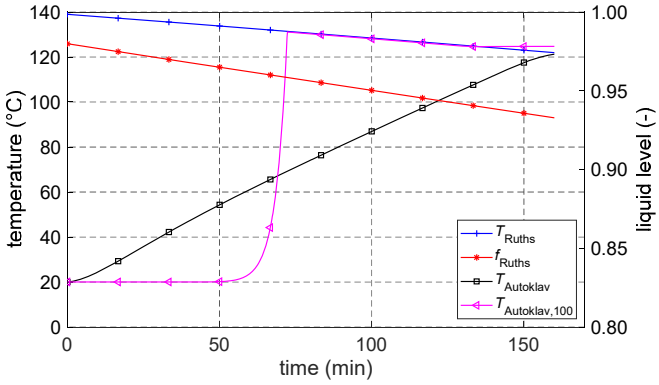

Figure 7. Temperature and level curve during discharging of the hybrid storage system and sterilisation process (variant R-RS)

The simulation results for the hybrid storage system are shown in Figure 8. The autoclave reaches the target temperature of 121 °C in 159 minutes. The liquid level in the Ruth storage tank drops by 5.87%. It is noticeable that the average temperature in the Ruths storage tank remains relatively high at the end of the charging process at approx. 127 °C. Lower temperatures can probably be achieved through further optimization of the operation.

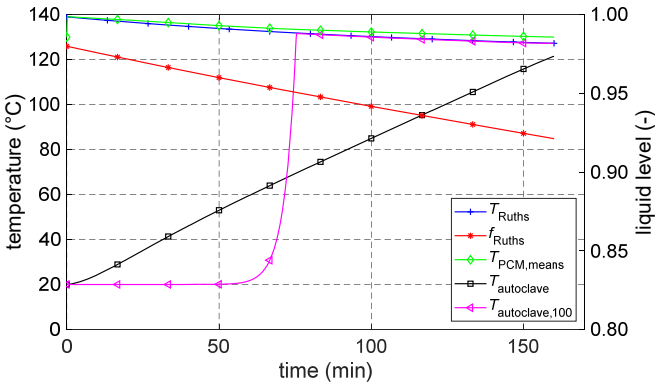

Figure 8. Temperature and level curve during discharging of the hybrid storage system and sterilisation process (variant R-PCM)

Figure 9 shows the loading time for the Ruths storage system (R-RS variant) and the hybrid storage system (R-PCM). The assumption is that the heat pump can only deliver a limited mass flow of steam of 0.070 kg/s. With the system according to variant R-RS (Figure 3 b)) the Ruths storage tank is heated from 121 °C to 139 °C in around 185 minutes. The liquid level increases by 4.85% (variant R-RS) or 26.58% (variant R-PCM). In the R-PCM variant (Figure 4a)), the phase change of the PCM as well as the relatively low thermal conductivity impairs the loading process. The loading time here is around 572 minutes (significantly longer than R-RS variant). The PCM temperature remains up to 2.4 K below the average temperature of the Ruths storage because of the heat exchanger.

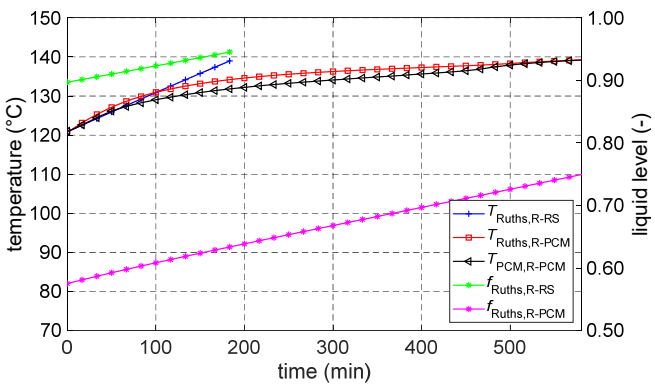

Figure 9. Curve of temperatures and liquid level during storage loading for variant R-RS and variant R-PCM

4. DISCUSSION

For the current investigations, the heating process of the autoclave as well as the considerations regarding the storage systems were of interest. When combining a high-temperature heat pump with renewable energies (e.g. photovoltaics), pollutant

emissions can be avoided, e.g. compared to natural gas firing. The disadvantages arise from the fact that the power supplied is often fluctuating (a. o. weather dependent). In order to improve the flexibility of operation and to decouple steam generation from steam consumption, the use of thermal energy storage systems is an obvious and effective solution.

In this paper, two systems with steam storages (variant R-RS and R-PCM) for supplying a batch process from the food industry were presented. The unloading mass flow of steam (in each case Ruths storage) remained constant at 0.700 kg/s. By using a PCM storage to expand the storage capacity in the small temperature range (125 to 135 °C), it was possible to reduce the required volume of the Ruths storage in the R-PCM variant by 36% compared to the R-RS variant. In the present case, the hot water was circulated between the Ruths and PCM storages. Compared to the use of steam, this has the advantage that the connecting pipes between the storages can be smaller. During storage discharge, the liquid level in the Ruths storage tank dropped by 4.70% (variant R-RS) or by 5.87% in the hybrid storage tank (variant R-PCM). It should be noted that the Ruths storage was cooled to around 122 °C for variant R-RS and to around 127 °C for variant R-PCM. Further operation optimization could reduce the value for the filling level even further and improve the use of the storage tank.

As expected, a decisive disadvantage occurs when loading the hybrid storage system. While a single Ruths storage (variant R-RS) requires approx. 185 minutes for a complete loading (from 121 °C to 139 °C), the loading of the hybrid storage unit requires approx. 572 minutes if the boundary conditions remain the same. In the process, the liquid level of the Ruths storage tank (variant R-PCM) increases by about 26.58%. In order to increase the rate of storage loading, further operational optimization or modifications to the storage design are required (e. g. use of ribs or additional particles for better heat transfer). Table 4 shows the advantages and disadvantages of variant R-PCM compared with variant R-RS.

Table 4. Comparison of variant R-PCM versus variant R-RS

Advantages	Disadvantages
Reduction of Ruths storage volume	More complicated operating strategy
Variable PCM storage shape possible	Electrical load for circulation pump
Deeper discharge of Ruths storage	Complicated design
	Significantly longer charging time

5. CONCLUSION

It is possible to produce the steam by using a high-temperature heat pump and store it for further purposes. Ruths storage tanks and hybrid storage systems (combination of Ruths and PCM storage) are suitable for steam storage. Such heat pump-storage systems can be used in various industries, such as the food industry.

In this paper, the heating process with a heat pump storage system in a sterilization process from the food industry was investigated. The EBSILON®Professional was used for modeling and simulation. This software is suitable in principle for the analysis of hybrid storage systems. Due to the internal software settings, it does not make sense to model the entire PCM storage. In the present investigations, a representative volume element consisting of pipeline as well as surrounding PCM was modeled and the results were subsequently scaled.

Due to the fact that the heat pumps can currently supply only relatively low steam temperatures, the usable temperature difference on the side of the Ruths storage tank and thus its storage capacity is limited. An additional PCM storage expands the storage capacity in this small temperature range and allows to take a larger amount of steam out of the Ruths storage. One disadvantage of the Ruths storage is that as discharge progresses, the storage tank temperature sinks. Next, the data from a real PCM will be used in the simulation. The disadvantages are to be minimised by optimising the operation as well as the design of the PCM storages. The authors work on this on this topic in sub-project 10 of the joint project KETEC Research Platform for Refrigeration and Energy Technology [3]. Further optimizations of the steam supply are planned here.

ACKNOWLEDGEMENT

The research work is funded by the Federal Ministry of Education and Research (BMBF) under the reference 03SF0623A/B/C on the basis of a resolution of the German Bundestag. Project management is provided by Projektträger Jülich (PtJ). The authors would like to express their gratitude for the funding, support and cooperation.

REFERENCES

[1] Bazzanella, M., Ausfelder, F. Low carbon energy and feedstock for the European chemical industry. Technologische Studie, DECHEMA Gesellschaft für Chemische Technik und Biotechnologie e.V., Frankfurt am Main, 2017.

[2] Federal Ministry for Economic Affairs and Climate Action. Energieeffizienz in Zahlen. Entwicklungen und Trends in

Deutschland 2021. https://www.bmwk.de/Redaktion/DE/Publikationen/Energie/energieeffizienz-in-zahlen-entwicklungen-und-trends-in-deutschland-2021.pdf?__blob=publicationFile&v=6 [accessed: 22.02.2023].

[3] Urbaneck, T., Matthes, M., Richter, M., Hempel, O., Safarik, M., Franzke, U., Noack, R., Honke, M., Müller, M., Henninger, S., Schossig, P., Henning, H.-M., de Oliveira, H. T., Morgenstern, A., Nienborg, B., Gschwander, S., Engelmann, P., Benndorf, G. www.ketec.online. Website of the joint project, 2023 [accessed: 03.06.2023].

[4] Buschle, J., Steinmann, W. D., Tamme, R. Latent heat storage for process heat applications. 10th International Conference on thermal Energy Storage ECOSTOCK 2006. New Jersey, USA, 2006.

[5] Buschle, J., Steinmann, W. D., Tamme, R. Latent Heat Storage for Process Heat Applications. DLR – German Aerospace Center. The Tenth International Conference on Thermal Energy Storage, Atlantic City, 2006.

[6] Hofmann, R., Dusek, S., Gruber, S., Drexler-Schmid, G. Design Optimization of a Hybrid Steam-PCM Thermal Energy Storage for Industrial Applications. Energies, 12 (2019) 5, p. 898. - ISSN 1996-1073.

[7] Niknam, P. H., Sciacovelli, A. Hybrid PCM-steam thermal energy storage for industrial processes – Link between thermal phenomena and techno-economic performance through dynamic modelling. Applied Energy, 331 (2023), p. 120358. - ISSN 03062619.

[8] Iqony Solutions GmbH. EBSILON®Professional 16 P1, 2023.

[9] Bender, B., Göhlich, D. (Ed.). Dubbel Taschenbuch für den Maschinenbau 3: Maschinen und Systeme. Berlin, Heidelberg: Springer Berlin Heidelberg, 2020. - ISBN 978-3-662-59714-9.

The 18th International Symposium on District Heating and Cooling, September 3–6, 2023, Beijing, China

Seasonal thermal energy storage using natural structures: GIS-based potential assessment for Northern China

Yichi Zhang[a,b*], Jianjun Xia[c]

[a] *Chalmers University of Technology, Gothenburg 412 96, Sweden*
[b] *Midea Building Technology, Midea, Foshan 528311, China*
[c] *Building Energy Research Center, Tsinghua University, Beijing 100084, China*
[*] *Corresponding author. yichi@chalmers.se*

ABSTRACT

Seasonal thermal energy storage (STES) allows storing heat for long-term and thus promotes the shifting of waste heat resources from summer to winter to decarbonize the district heating (DH) systems. Large-scale STES for urban regions is lacking due to the relatively high initial investment and extensive land use. To close the gap, this study assesses the potentials of using two naturally available structures for STES, namely valley and ground pit sites. Based on geographical information system (GIS) methods, the available locations are searched from digital elevation model and selected considering several criteria from land uses and construction difficulties. The costs of dams to impound the reservoir and the yielded storage capacities are then quantified to guide the choice of suitable sites. The assessment is conducted for the Northern China where DH systems and significant seasonal differences of energy demand exist. In total, 2,273 valley sites and 75 ground pit sites are finally identified with the energy storage capacity of 15.2 billion GJ, which is much larger than the existing DH demand. The results also prove that 682 valley sites can be achieved with a dam cost lower than 20 CNY/m^3.

Keywords: Seasonal thermal energy storage, Geographical information system, District heating, water reservoir

1. INTRODUCTION

In 2021, the energy consumption of the Chinese building accounts to 21% in the whole country, equaling to 22% of the entire society's carbon emission [1]. Within the building sector, around 19% of the energy is used for the space heating demand in Northern China during winter [2,3], making it an important factor in the plans towards carbon neutrality. The seasonal thermal energy storage (STES) technology can coordinate the temporal differences between the heating and electricity sectors in an efficient and cost-effective manner [4]. By storing and shifting excess energy in the form of hot water over a long term, the STES reduces the fossil fuels needed by the DH and improves the utilization of renewable energy. Besides, great potentials of industrial surplus heat are found in Northern China [5]. A major obstacle in utilizing such resources is the unmatching of excess heat in summer and DH demand in winter, which can also be solved by STES. Thereby, the STES can facilitate the decarbonization of energy sectors using the existing grid and facilities.

STES is mostly utilized in a small community with water storage capacity between 1,000 m^3 to 50,000 m^3 to increase renewable energy integrations [6]. However, such configuration is far less than the seasonal demand differences presented in large cities, whose heated floor area are normally over millions of m^2. A major reason for the lack of large-scale STES is the limitations in available sites. Considerations from geo-hydrological conditions, climate, and construction works are needed [7]. Besides, the huge investment for constructing large-scale STES also slows down the application. It is concluded that the cost of STES still needs to be reduced by half in order to be economically competitive on the heating market [6].

Recently, most studies on the improvement of STES are placed on the artificial one that is completely built from scratch [8]. Indeed, there are naturally available terrain structures such as ground pits or valleys that can be reformed into large hot water reservoirs for STES. Compared with manually built STES, a great amount of construction works can be saved. Besides, natural structures save the extensive land uses, which is a critical issue for manually excavated sites in urban regions. Similar idea of using natural structures have been developed in hydrology and power systems but is still missing for STES.

With the aim of identifying available locations and storage capacities of prospective STES, a GIS-based methodology is developed in this study, including site searching from digital elevation model (DEM) and selection procedures for integration into DH systems. The geometries and construction difficulties for STES based on two natural geo-structures, namely valley and ground pit, are analyzed. The assessment is applied for the Northern China where DH systems and significant seasonal differences of energy demand exist.

2. METHODOLOGY

2.1. Valley sites

A typical example of a valley site that is transformed into a water reservoir is shown in Figure 1. Through the construction of a dam along the virtual river network, the valley is closed, which is capable of impounding a certain amount of water. The entire land that holds all possible flowing water is called the watershed. The impounded area becomes the potential water reservoir, whose size is largely depending on the height of the dam.

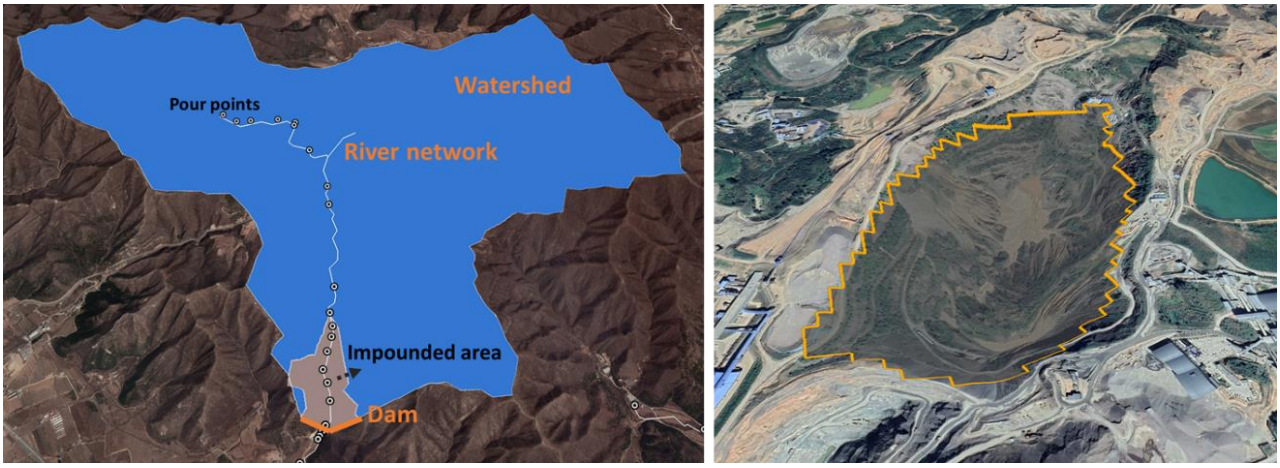

Figure 1. Typical examples of valley (left) and ground pit (right) sites.

The main input data is DEM, which represents the topographic surface of the Earth. 1 arc-second data from the shuttle radar topography mission with the resolution of approximately 30 m is used. The searching procedures for potential valley, see Figure 2, are based on the hydrology toolset in ArcGIS Pro. The drainage line is a channel where surface water naturally flows and is regarded as the valley line, generated by the flow accumulation and flow direction tools. Then, the pour points are created along the drainage lines with an interval of 10 m in altitude. These points are the locations where water flows out of the basin, which are also potential sites for the dams to impound water.

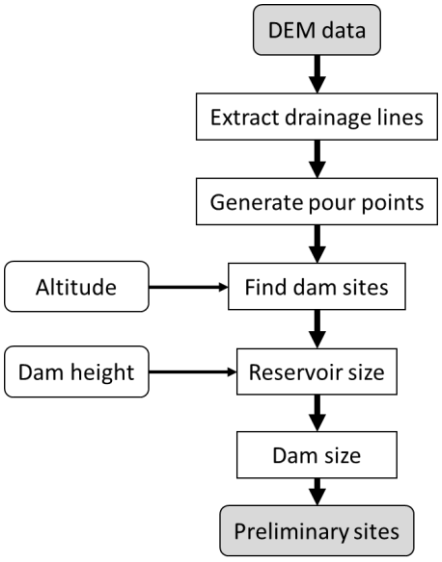

Figure 2. Flowchart for searching valley sites.

The design static water pressure for DH systems is commonly smaller than 1.5 MPa (equaling to around 150 m water head), considering the safety of pipes and valves. In this study, the average ground altitudes of all urban regions in Northern China are analyzed based on DEM data. The pour points with relative elevations of smaller than 30 m are selected as potential sites to build dams and STES units, based on pressure safety and pumping energy cost concerns. For each potential dam site, a watershed is created by the hydrology toolbox and the shape of the reservoir is generated by selecting rasters within the watershed that have lower altitude than the water surface. With the help of 3D Analyst tool, the area and volume of the potential reservoir are calculated.

A simplified structure of a concrete dam is considered in this study, as shown in Figure 3. The dam height is designed as 60 m considering the practical issues with constructions. The crest width is designed as 10 m to accommodate a road. The base width is set the same as the dam height, which is a common practice for concrete dam. The dam construction cost calculated

with the empirical functions from investigations of 80 large dams in Australia [9], as shown in Equation (1). The original cost data is in Australian Dollar and is converted to Chinese Yuan (CNY) considering an average exchange rate of 4.6.

$$Cost = \frac{4.6 \times 0.0039 \times 10^6 \times height^{1.5681} \times length^{0.6148}}{V_{water}} \tag{1}$$

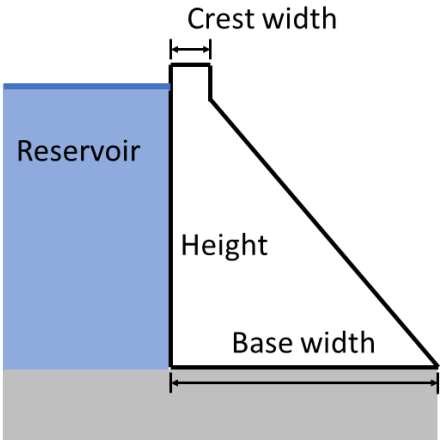

Figure 3. Simplified structure of a concrete dam.

2.2. Ground pit sites

Ground pits can be created by natural causes and human activities. Utilizing these pits for STES would save the construction cost while having little impact on the environment and landscape. A typical example of a desolated surface mining pit (latitude 40.06, longitude 118.54) with an average depth of 10 m below ground is shown in Figure 1. To locate ground pits, the lidar package developed by Qiusheng Wu [10] is applied. Based on level-set method, it is capable of delineating the nested hierarchy of surface depressions (pits) in DEMs and can be performed with Python or ArcGIS software. Similar as the searching procedures for valley sites, a minimum surface area of 10,000 m^2 and a maximum volume of 50 million m^3 are set. As the ground pits STES are designed to be connected with DH systems, limitations of elevations to nearby urban region is also effective.

2.3. Site selection

The identified preliminary valley sites are selected using several levels of criteria (see Table 1) to find the feasible ones for STES. To prevent redundant reservoirs that might even intersect with each other, a searching radius of 2 km is set. Within this area, the reservoir with the largest depth and its corresponding site is selected, to ensure a low thermal loss and lowest possible construction cost. The searching criterion assumes that the distance between two distinctive drainage lines (valleys) is generally larger than 2 km. Thereby, for every valley, one site is selected.

To avoid the negative impact on the environment, the reservoir cannot be built in natural reservations designated by the Ministry of Ecology and Environment. Built-up areas, roads, and railways, derived from the most recent data (2022) in OpenStreetMap, indicate intensive land uses and are not suitable for STES.

For valley site reservoirs, the construction of dam makes up a significant part in the overall project cost. The dam with construction cost higher than 150 CNY/m^3 is also excluded. This threshold refers to the currently lowest cost for artificially building a pit STES from scratch.

Table 1. Selection criteria for valley sites.

Criteria	Valley
Searching radius for redundant sites	2 km
Infeasible areas	Natural reservations
	Built-up area
	Roads and railways
Dam cost	≤ 150 CNY/m^3
Pipeline through mountains	Elevation changes along the route ≤ 50 m
Distance to urban regions	≤ 20 km

The STES cannot be built on the hilltop due to the issues with large elevation and water pressures. Nevertheless, even with a small elevation, the STES located in the valley surrounded by mountains is still not an attractive option because the pipeline to the urban region goes through mountains, which requires huge investment and construction works. This study uses an alternative method to determine if the STES site is within the mountains. For every reservoir site, the nearest urban region is found and connected with a straight line. Then, several observation points with the interval of 200 m are created along the line. The altitude of these points is compared with the altitude of the reservoir. If the relative elevation changes are smaller than 50 m, it can be assumed that there are no obvious obstacles along the route and the reservoir is selected.

This study uses the location of the municipal building as the representation of the urban center. The STES sites located within 20 km from the urban center are selected because the current DH networks can be easily expanded to reach that distance. According to experience from Chinese DH networks and long-distance transportation projects, a longer distance would require specially designed pipeline and systems.

For the finally selected reservoirs, the energy storage capacity is calculated using a temperature difference of 75 °C to maximize the storage benefit with a certain water volume. To achieve that, the return water temperature shall be reduced to around 20 °C.

3. RESULTS

3.1. Characteristics of valley sites

Using the GIS-based searching methodology, a total of 402,363 preliminary valley sites are identified in Northern China. After several steps of selection procedures, 2,273 sites that can be developed into STES units are included in the final set, as shown in Table 2. These potential sites would not interrupt the land use status and are located within 20 km from nearby urban regions. The geographical distributions of the final valley sites are presented in Figure 4, based on the map provided by ESRI ArcGIS.

Table 2. *Searching procedures and the numbers of selected valley sites*.

Procedures	No. of sites
Step 1: GIS-based searching	402363
Step 2: Remove redundant points	155634
Step 3: Area and volume requirement	85788
Step 4: Exclusion of reservations, built-up area	46801
Step 5: Dam size and construction cost	29815
Step 6: Pipeline through mountains	6095
Step 7: Distance to urban region ≤ 20 km	2273

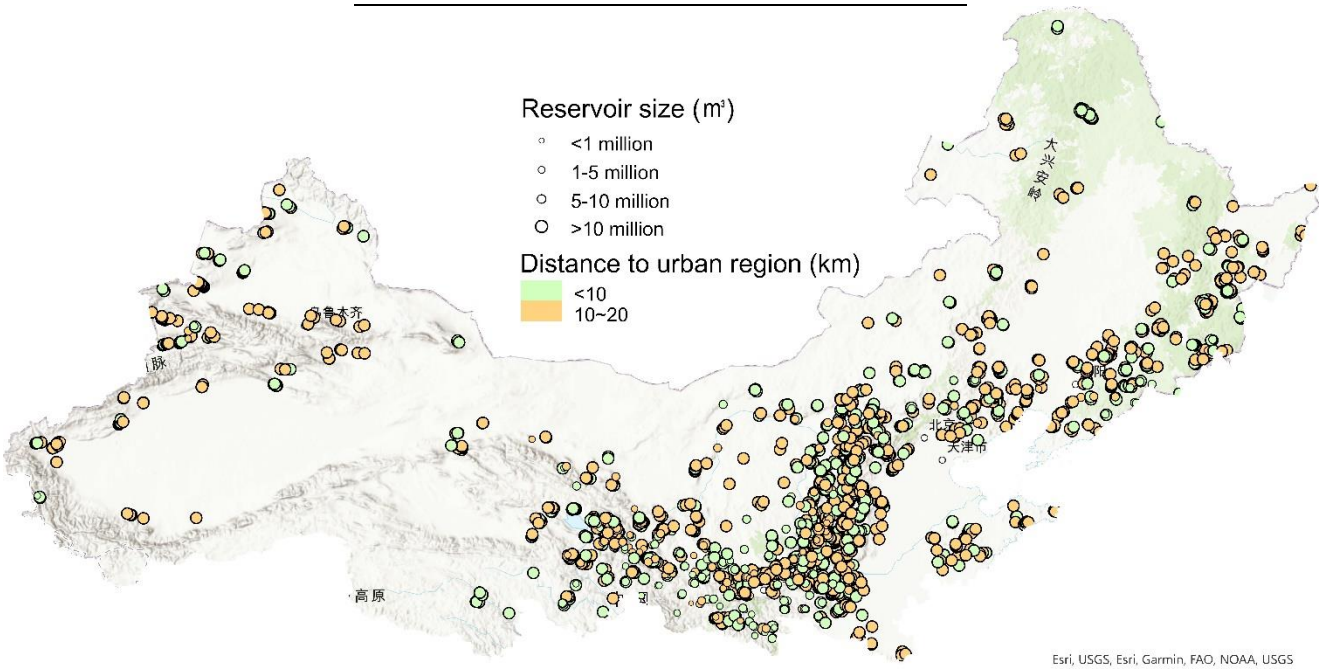

Figure 4. Selected valley sites in Northern China, classified by the reservoir size and distance to the nearest urban region.

Due to their specific geo-structures, the valley sites are gathered around major mountains in Northern China. It is seen that a large number of valley sites are distributed in the middle, around Qinling Mountains and Taihang Mountains. Although the

Northwestern part of China is famous for having huge mountains, only limited numbers of potential sites are found. The main reason is that there are few cities in this area while the searched sites are located far from urban regions. In contrary, the Eastern part of Northern China, including Henan, Shandong and Hebei provinces, have dense populations and numerous cities. The available STES sites in this region are also rare due to flat terrain features.

A general description of the main characteristics of selected sites is provided in Figure 5. The reservoirs have an average water storage capacity of around 21 million m^3, which is much larger than the currently common storage unit used in small communities. By transforming these reservoirs into STES units, a total water volume of 47.8 billion m^3 is achieved, with the energy storage capacity of 15.1 billion GJ. This aggregated value is already larger than the total DH demand of Northern China (around 5.4 billion GJ). The distribution of volumes also reveals that more than half of the potential sites have water capacity larger than 10 million m^3, while only 152 reservoirs are smaller than 5 million m^3.

The average cost of the dams is 29.3 CNY/m^3. According to the previous estimation about large-scale STES [11], the costs for geotechnical works, excavation and cover are the three most important parts in the project investment. Since the STES sites investigated in this study are built from natural structures that save excavation costs, the overall expenditure of the proposed STES is still attractive compared to the current practices of STES that usually cost more than 200 CNY/m^3.

The design dam height of 60 m defines the maximum depth of the reservoir, while the average depth, also known as the characteristic length, is 24.5 m. Considering an average water surface area of around 870,000 m^2, the impounded reservoir has a flat and shallow shape. Such shape brings new challenges such as the thermal loss and temperature stratification issues during practical operation. In order to maintain a good thermal storage performance, more research works from bottom-level design and optimization aspects are needed.

To further highlight the most promising sites within the selected data set, the ones with the least dam cost and shortest distance to urban regions are summarized in Table 3. It can be seen that there are still 57 sites located within 5 km radius with dam costs lower than 20 CNY/m^3. By slightly increasing the tolerance of distance to 10 km, 125 more sites are found.

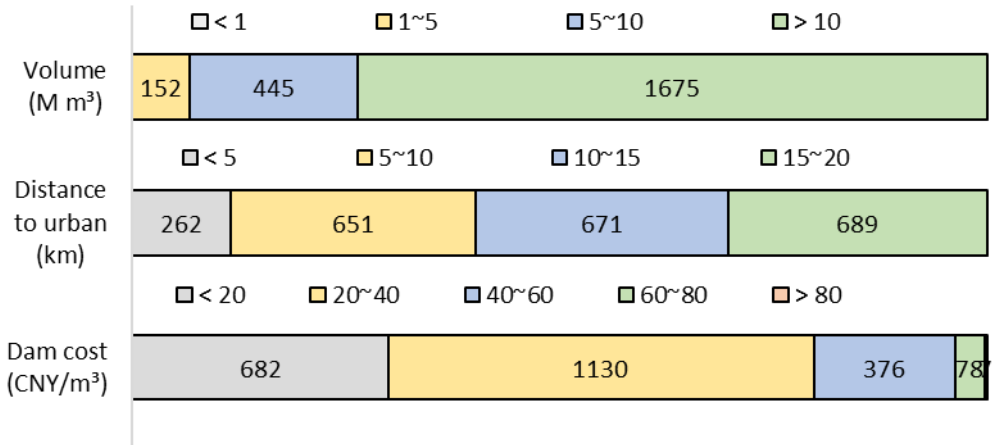

Figure 5. Distributions of storage volume, distance to urban regions, and investment in the selected valley sites.

Table 3. *Summary of promising valley sites considering criteria of dam cost and distance.*

	Criteria	No. of sites	Volume (billion m^3)	Storage capacity (billion GJ)
(1)	Dam cost ≤ 20 CNY/m^3 Distance ≤ 5 km	57	1.68	0.53
(2)	Dam cost ≤ 20 CNY/m^3 5 km < Distance ≤ 10 km	182	5.89	1.85
(3)	Dam cost ≤ 40 CNY/m^3 Distance ≤ 10 km	696	15.56	4.90

3.2. Characteristics of ground pit sites

Compared to valley sites, less ground pit sites are identified by the GIS-based searching procedure. The main reason is that pit sites are more demanding for terrain structures that shall naturally impound a certain area of water. In contrary, the valley sites rely on the constructions of dams to create reservoirs. Due to the same reason with structures, the dams and associated costs are not analyzed for pit sites. After several steps of selections, as shown in Table 4, only 75 sites remained as potential STES units. The geographically distributions of these sites are presented in Figure 6.

Table 4. *Searching procedures and the numbers of selected ground pit sites.*

Procedures	No. of sites
Step 1: GIS-based searching	64030
Step 2: Area and volume requirement	59465
Step 3: Exclusion of reservations, built-up area	44948
Step 4: Sink size, shape	25106
Step 5: Elevation requirement	11043
Step 6: Pipeline through mountains	3156
Step 7: Distance to urban region ≤ 20 km	75

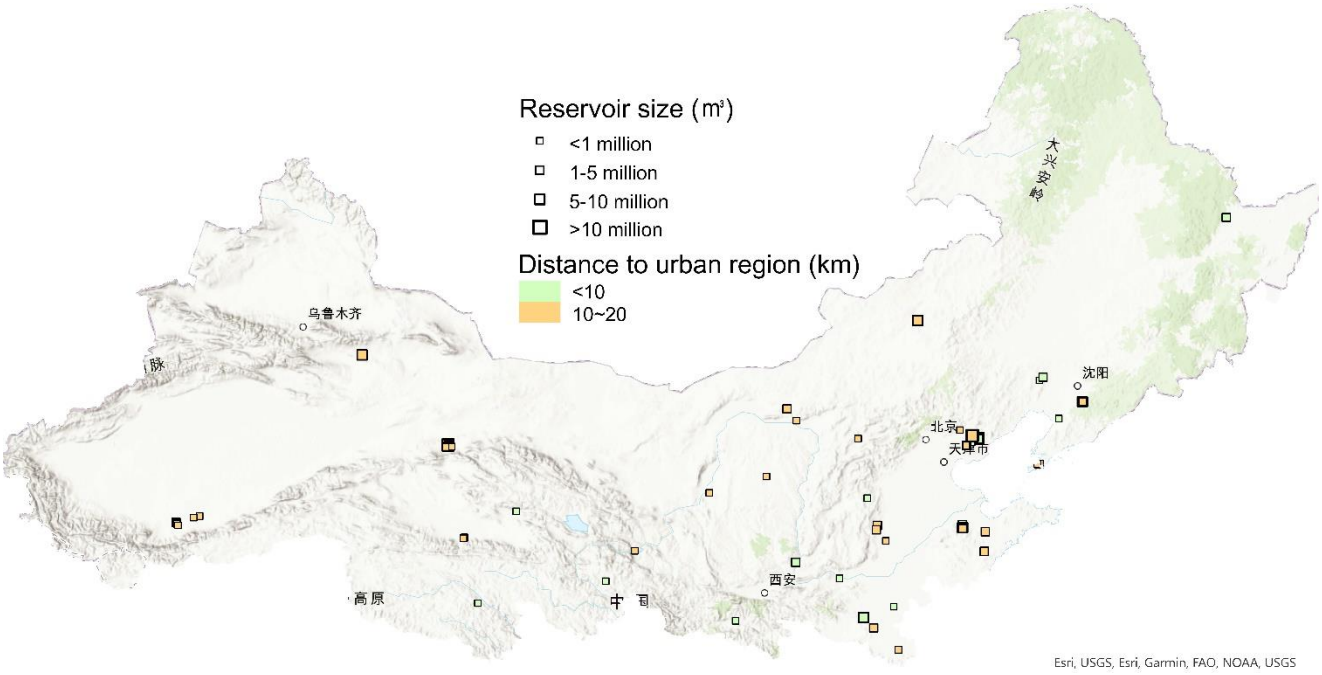

Figure 6. Selected ground pit sites in Northern China, classified by the reservoir size and distance to the nearest urban region.

The main characteristics of the selected pit sites are generally described in Figure 7. In total, the water storage volume of all 75 sites is 0.166 billion m^3, corresponding to an energy storage capacity of 52.4 million GJ. The average volume is 2.2 million m^3, which is also significantly smaller than the valley sites. As is shown in Figure 7, 46 pit sites have volumes smaller than 1 million m^3. From the perspective of practical construction, the STES based on pit sites are more easily achieved compared to those larger reservoirs impounded in valleys.

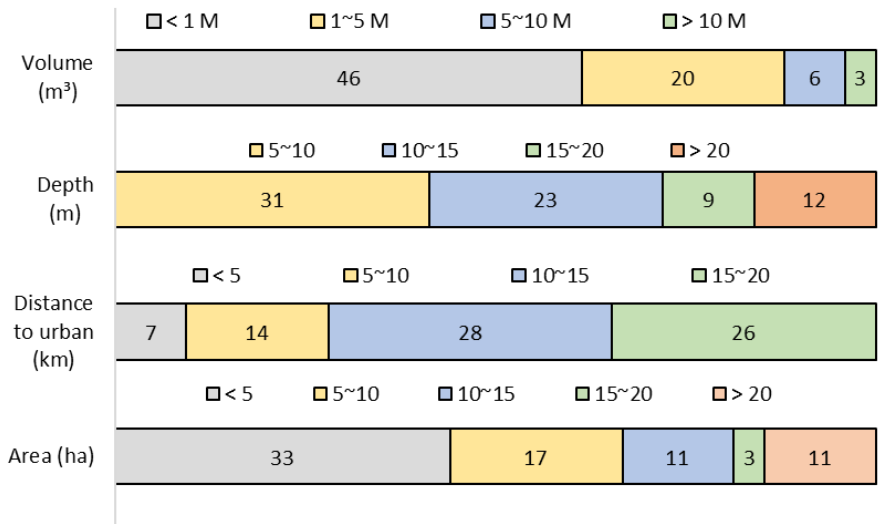

Figure 7. Distributions of storage volume, depth, distance to urban regions, and water surface area in the selected ground pit sites.

The average depth of the pit sites is 14.2 m, which is close to the current practices of manually built pit STES. The deepest pit is found in an open coal mine near Qian'an city, whose depth is around 70 m. As for the water surface area, an average value of 11 ha (110,000 m^2) is found. Considering these parameters, the shape of pit-based reservoir is less shallow than the valley-based reservoir.

4. DISCUSSION

The huge seasonal differences of DH demand in Northern China and extensive waste heat resources call for effective and economic energy storage solutions that can be applied in urban regions. From the scope of top-level planning, the findings of this study have identified the potentials of large-scale STES. However, to effectively put the idea into reality, more research works from bottom-level implementation stage are needed. The identified valley and pit reservoirs have shallow shapes that would create huge thermal losses to the environment. As the cost of insulation is an important factor in the overall project cost, economic solutions from material and structural design perspectives are needed. Besides, innovative measures such as diffusers and vertical partitions are also required to preserve the hot water for a seasonal period.

As for the utilization of STES, the reservoirs are prioritized for using in urban regions, so a distance limit of 20 km is set. This design is based on the availability of existing DH networks. However, there are flexible ways of connections between the heat source, STES, and the urban DH demand. A longer pipeline can be built to transport the waste heat into urban regions, as demonstrated by several projects in China [12,13]. This increases the freedom of choices for STES sites but requires more detailed evaluations on the project costs. Moreover, the STES can also be integrated with waste heat sources to improve the overall energy efficiency of industrial regions. Considering various application scenarios of STES, the combined planning of large-scale STES with energy supply and demand locations is an interesting topic to facilitate the co-decarbonization of multiple sectors.

5. CONCLUSION

This study identifies the locations and potentials of large-scale STES developed from two natural structures including the valley and ground pit, using a GIS-based searching methodology in Northern China. The most promising sites are selected considering various criteria from dam construction, land reservation, and reservoir sizes.

With the dam height of 60 m and elevations smaller than 30 m, 2,273 valley sites and 75 pit sites are finally identified, which in total has the energy storage capacity of 15.2 billion GJ. The reservoirs built from valley sites contribute most of the yielded capacity and have generally larger sizes than the pit reservoirs. The typical characteristics of identified sites including dam size, reservoir size, and average depth are analyzed. 682 valley sites are found to be achieved with a dam cost lower than 20 CNY/m^3. Based on the average depth and water surface area, the reservoirs are depicted as shallow shapes.

REFERENCES

[1] Building Energy Conservation Research Center. Annual report on China building energy efficiency 2023. Beijing: Architecture and Building Press; 2023.

[2] Su C, Madani H, Palm B. Heating solutions for residential buildings in China: Current status and future outlook. Energy Convers Manag 2018;177:493–510. https://doi.org/10.1016/j.enconman.2018.10.005.

[3] Zhang Y, Xia J, Fang H, Jiang Y, Liang Z. Field tests on the operational energy consumption of Chinese district heating systems and evaluation of typical associated problems. Energy Build 2020;224:110269. https://doi.org/10.1016/j.enbuild.2020.110269.

[4] Mahon H, O'Connor D, Friedrich D, Hughes B. A review of thermal energy storage technologies for seasonal loops. Energy 2022;239:122207. https://doi.org/10.1016/j.energy.2021.122207.

[5] Zheng W, Zhang Y, Xia J, Jiang Y. Cleaner heating in Northern China: potentials and regional balances. Resour Conserv Recycl 2020;160:104897.

[6] Yang T, Liu W, Kramer GJ, Sun Q. Seasonal thermal energy storage: A techno-economic literature review. Renew Sustain Energy Rev 2021;139:110732. https://doi.org/10.1016/j.rser.2021.110732.

[7] Zhou X, Xu Y, Zhang X, Xu D, Linghu Y, Guo H, et al. Large scale underground seasonal thermal energy storage in China. J Energy Storage 2021;33:102026. https://doi.org/10.1016/j.est.2020.102026.

[8] Xiang Y, Xie Z, Furbo S, Wang D, Gao M, Fan J. A comprehensive review on pit thermal energy storage: Technical elements, numerical approaches and recent applications. J Energy Storage 2022;55:105716. https://doi.org/10.1016/j.est.2022.105716.

[9] Petheram C, McMahon TA. Dams, dam costs and damnable cost overruns. J Hydrol X 2019;3:100026. https://doi.org/10.1016/j.hydroa.2019.100026.

[10] Wu Q. lidar: A Python package for delineating nested surface depressions from digital elevation data. J Open Source Softw 2021;6:2965. https://doi.org/10.21105/joss.02965.

[11] Ochs F, Dahash A, Tosatto A, Bianchi Janetti M. Techno-economic planning and construction of cost-effective large-scale hot water thermal energy storage for Renewable District heating systems. Renew Energy 2020;150:1165–77. https://doi.org/10.1016/j.renene.2019.11.017.
[12] Li Y, Chang S, Fu L, Zhang S. A technology review on recovering waste heat from the condensers of large turbine units in China. Renew Sustain Energy Rev 2016;58:287–96. https://doi.org/10.1016/j.rser.2015.12.059.
[13] Chen J, Zheng W, Kong Y, Yang X, Liu Z, Xia J. Case study on combined heat and water system for nuclear district heating in Jiaodong Peninsula. Energy 2021;218:119546. https://doi.org/10.1016/j.energy.2020.119546.

The 18th International Symposium on District Heating and Cooling,
September 3–6, 2023, Beijing, China

Swirl Loading of Hot Water Tanks – Detailed Simulation of the Flow in the Diffuser and Storage

Felix Oestreich[a], Thorsten Urbaneck[a*]

[a] *Professorship Applied Thermodynamics, Department of Mechanical Engineering, Chemnitz University of Technology, 09111 Chemnitz, Germany*
[*] *Corresponding author. thorsten.urbaneck@mb.tu-chemnitz.de*

ABSTRACT

Thermal energy storage systems contribute, among other things, to increasing the security of supply in the district heating system and to improving the efficiency of the district heating system (e.g., making the generators more flexible, storing waste heat, better hydraulic operation). Pressure vessels, so-called slim hot water storage tanks (storage type b1) are suitable for this purpose. The above mentioned advantages require efficient storage operation (low internal and external storage losses). This paper deals with the minimization of internal losses by improving the thermal stratification behavior. Thermal stratification with a thermocline between hot and cold zone as narrow as possible is an indicator of low mixing processes during loading. Minimizing these mixing processes during loading takes a key role in minimizing internal storage losses. *Lohse* and *Brähmer* investigated loading with conventional radial diffuser in slim hot water storage tanks with numerical flow simulation. The work identifies adverse flow effects due to the slim tank shape, such as a wall jet. This wall jet stimulates mixing processes and thus increases the internal storage losses. To overcome this flow problem, *Findeisen* et al. proposes swirl loading. The investigations of *Oestreich* et al. showed the flow behavior in the diffuser and in the storage, the effects on the thermal stratification as well as the advantageousness. This paper aims to provide a more detailed description of the flow processes. This knowledge is essential to better understanding the causes and effects of swirl loading and the structure of thermal stratification. Modeling and simulation of the diffuser and storage, respectively, are performed using *Ansys CFX*. *Large eddy simulation* (LES) is applied to resolve turbulent structures. This paper presents for the first time the vortex structures in the diffuser with internal elements for swirl generation. The storage flow exhibits similar behavior to known density flows (e.g., head and nose formation, instabilities in the free shear layers), which was previously unknown. High *Peclet* numbers (high advection currents) in the storage model lead to numerical instability of the simulation and therefore require increased discretization efforts.

Keywords: **thermal energy storage, charging, radial diffuser, swirl, large eddy simulation**

1. INTRODUCTION

The use of thermal energy storage enables, among other things, the flexibilisation of the generation fleet, the increase of supply security as well as the increase of system efficiency through e.g. waste heat utilisation. In district heating, these functions are performed by slim hot water storage tanks (storage type b2 in [1]). An example is shown in Figure 1. The pressure vessels have a so-called dished bottom according to DIN EN 28011 [2]. The operating range is at temperatures up to 200 °C and pressures up to 20 bar. Large system volumes can be achieved by setting up a storage cascade (series connection). The schematic structure is shown in Figure 2 a). The storage system is connected via the flow and return, e.g. with the district heating network. Efficient storage operation requires low internal and external losses. This article pursues the reduction of mixing effects during loading and an improvement of thermal stratification. A narrow transition layer between cold and warm zone is an indicator for good thermal stratification. Radial diffusers are typically used to achieve the lowest possible mixing effect during loading (Figure 2 b)). These realise a radial velocity reduction and a relatively uniform radial inflow into the storage (cf. Figure 2 c)). Investigations for radial diffusers in hot water storage tanks (compact design) show their suitability in principle [3]. However, the situation in slim storage tanks with dished heads is fundamentally different. Due to the slim shape of the storage tank, there is only little space available for the radial diffuser (limited by the storage tank diameter of 4 m). As the diffuser radius decreases, the radial velocity decay also decreases. This leads to higher inlet velocities of the loading fluid into the storage. Investigations by *Lohse* [4] and *Brähmer* [5] with Ansys CFX show the formation of adverse flow effects such as a radial wall jet (high momentum, reflection at the storage wall, cf. Figure 2 c)).

This penetrates the storage at high speed and stimulates strong mixing effects. This is contrary to the above-mentioned goals. In order to overcome this flow problem, *Findeisen* et al. [6] propose swirl loading. The radial diffuser is equipped with curved internal elements, see Figure 2 d). These generate a swirling flow. The loading fluid enters the storage in rotation, see Figure 2 e). This reduces the momentum of the wall jet. Recent investigations by *Oestreich* et al. [7] prove the advantages (e. g. reduction of internal storage losses) compared to loading with an available radial diffuser (cf. Figure 2 b)) and identify hitherto unnoticed flow effects in the guiding channel and in the storage. So far, there is no information available on the flow effects of swirl loading, especially the behaviour of turbulent structures. This is where the present article comes in. This article presents the results of numerical flow simulations. By using the *Large Eddy Simulation* (LES), essential turbulent structures and flow effects during swirl loading in the guiding channel and in the slim storage with dished bottom are identified and the current state of knowledge is expanded.

Figure 1. Slim hot water storage tanks, four times nine storage tanks in series, Chemnitz (Germany) district heating supply, operator eins/inetz

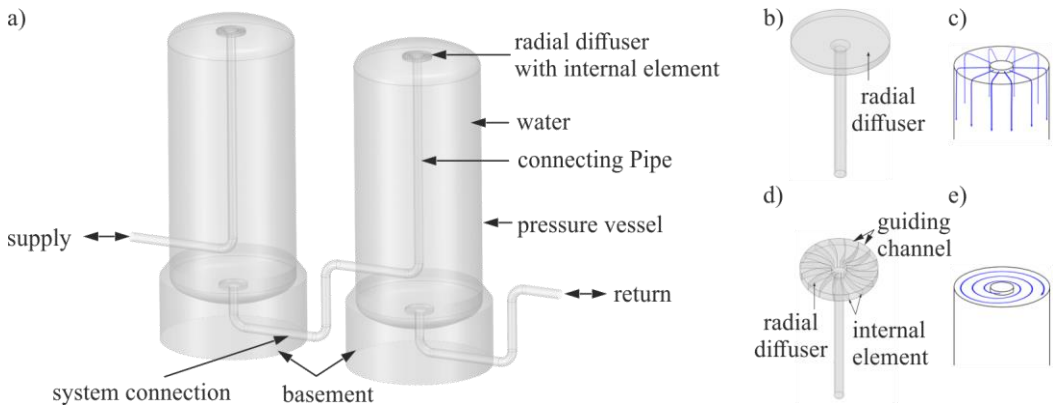

Figure 2. a) schematic diagram of a storage cascade with essential internals, b) schematic diagram of the radial diffuser without internals, c) simplified operating principle of radial loading, d) schematic diagram of the radial diffuser with internal elements, e) simplified diagram of the operating principle of loading with swirl

2. METHODOLOGY

Ansys CFX [8] is used to simulate the flow and heat transfer. The modelling includes a diffuser model as a 360° model with one of the connecting pipe (Figure 3 a)), with a single pipe (Figure 3 a), detailed view) and a storage model as a segment model (Figure 3 b)). Table 1 summarises the quantities for geometry and operation. The number of blades z indicates the number of internal elements. The swirl angle β includes the angle between the flow and the circle normal at the internal element. The storage model in Figure 3 b) corresponds to $h_{\mathrm{St}}/3$ with a spatial extension in the Z-direction of 2.8°. The rotational symmetry is exploited. The investigations in [7] prove the advantageousness of this approach. The storage has a dished bottom according to DIN EN 28011 [2] with the radius r_1 and r_2.

The modelling of the diffuser outlet or the fictitious outlet plane from the storage as an opening enables the consideration of recirculation (backflow into the diffuser or storage). The simulation is transient. Ideal boundary conditions are assumed. I.e. at the beginning of the loading the fluid is at rest ($U = 0\ \mathrm{m\ s^{-1}}$) with homogeneous temperature distribution (T_{St}). The loading takes place at constant temperature and with constant mass flow. In the storage simulation, the velocity components are specified for a swirl angle of 50° at the inlet (cf. Figure 3 b)). The heat transfer at the walls is not considered (adiabatic

walls). For the temperature and pressure-dependent material data for water, the *IAPWS-IF 97* [9] implemented in Ansys is used. The turbulence modelling is carried out with LES (WALE) [10]. This approach offers a good resolution of the flow variables near the wall and in the free shear flows. In addition, LES enables the resolution of large turbulent structures, while small-scale effects are modelled via filter functions [11]. The correct setup of a LES simulation makes high demands on the spatial, temporal and numerical discretisation. Several recommendations exist for this [12]. The *turbulent integral length scale* according to Eq. (1) is used to estimate the size of the computational grid or the element size. The model constant C_μ is 0.09 [13]. For the calculation, a simulation of the diffuser and storage model with the k-ω-SST model [13] is first necessary in order to obtain the turbulent dissipation rate ε and turbulent kinetic energy k. Another important criterion for estimating the convergence behaviour is the *Courant number* Eq. (2) [14]. This index relates the velocity and the time step size to the grid spacing in the main flow direction. For $Cr < 0.3$, sufficiently accurate convergence exists according to [13]. The *Peclet number* according to Eq. (3) relates the advection to diffusion currents [14]. The thermal diffusivity α is very low in the operating range $(0.17 \cdot 10^{-6}\ \mathrm{m^2 s^{-1}})$ [9] with respect to the velocity U of order $10^{-1}\ \mathrm{m\ s^{-1}}$. The solutions are numerically stable if $Pe < 2$ holds [14]. For the discretisation of the advection currents when using the LES, Ansys recommends the Central Difference Scheme [13].
The so-called Q-criterion [15] according to Eq. (4) is used for the visualisation of vortex structures. It includes the vorticity Ω and the shear rate S. The model constant C_Q is 0.25 [13]. This definition is implemented in Ansys CFX-Post by default.

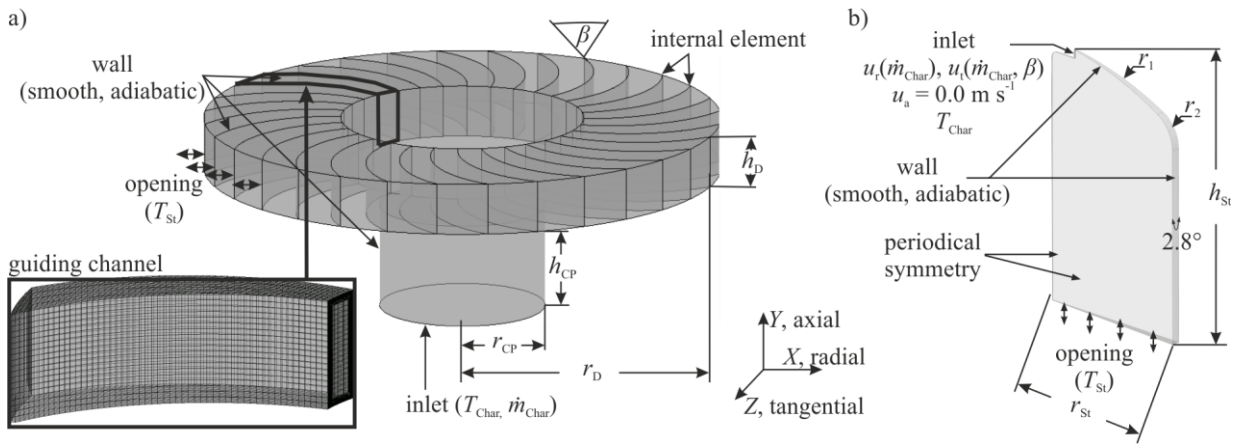

Figure 3. a) Diffuser model with boundary conditions and geometry sizes as well as detailed view of a representative guiding channel with computational grid, b) storage model with boundary conditions and geometry sizes

Table 1. Geometrical sizes of the storage and the radial diffuser and operating parameters

Quantity	Value	Quantity	Value	Quantity	Value
h_{St}	10.00 m	r_{CP}	0.16 m	T_{St}	50.0 °C
r_{St}	2.00 m	h_D	0.10 m	T_{Char}	125.0 °C
r_1	4.00 m	r_D	0.50 m	$\dot{m}_{Char}$	94.0 kg s^{-1}
r_2	0.40 m	β	50.00°		
h_{CP}	1.00 m	z	32.00		

$$l = C_\mu^{3/4} \frac{k^{3/2}}{\epsilon} \tag{1}$$

$$Cr = \frac{U \cdot \Delta t}{X} \tag{2}$$

$$Pe = \frac{U \cdot X}{\alpha_W} \tag{3}$$

$$Q = C_Q \cdot (\Omega^2 - S^2) \tag{4}$$

3. RESULTS

3.1. Discretisation

The simulation of the diffuser and storage model with the k-ω-SST model yields the turbulent integral length scale according to Eq. (1). The result is shown in Figure 4 a) for a guiding channel (compare with Figure 3 a) guiding channel).

This shows the element size of the computational grid. This enables the derivation of the element size of the computational grid according to the principle as small as possible and as large as necessary, taking into account the available computational resources. The maximum cell size in the guiding channel is set to 2 mm. This also enables the solution of small-scale effects. The boundary layer meshing is done with 21 prism layers and a growth factor of 1.3. This results in a cell number of approx. 500,000. The recommendation $Cr < 0.3$ is observed. This means that the simulation runs with only a few iteration steps, which reduces the overall computing time. The simulation of the guiding channel assumes isothermal conditions. Therefore, the Peclet number is not relevant. The central difference method is used [13]. The simulation duration is 6 s. After that, the flow course in the guiding channel no longer changes. The simulation of the storage model yields relatively large turbulent structures up to 10 cm (cf. Figure 4 b) red areas). The wall boundary layer is relatively finely interconnected with 18 prism layers. The number of cells in the circumferential direction is 12, which is relatively high but necessary due to the tangential flow. Both turbulent and laminar regimes are present in the storage. The position of the turbulent structures changes constantly over the loading duration (250 s), therefore the storage space is completely interconnected with a maximum cell size of 5 mm. The computational grid comprises 4 million cells. The time step size is relatively small at 10^{-4} s, but allows for low Courant numbers. At the beginning of loading, the temperature in the storage tank is relatively low (T_{St}) compared to the loading temperature (T_{Char}). Therefore, high advection currents occur. Because $Pe \gg 2$, the simulation is numerically unstable. The flow variables oscillate or take on non-physical values. This is a major drawback of the central difference method. Adjusting the computational grid with smaller cell spacing to achieve $Pe < 2$ leads to impractical sizes of the computational grid and is therefore not an option. Alternatively, the high resolution method is used [13]. It provides second-order accuracy. In addition, the computing time is acceptable and the physical limits are observed.

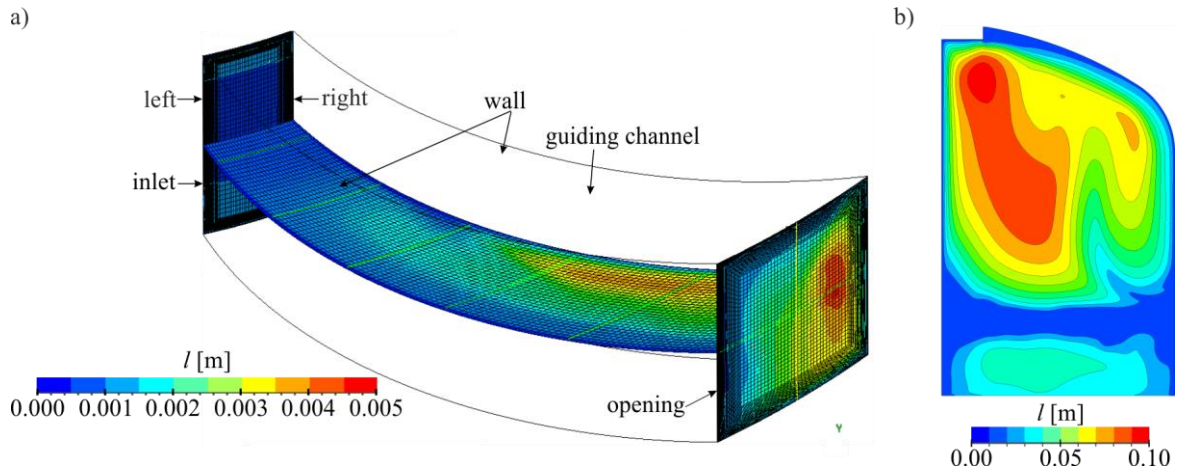

Figure 4. Turbulent integral length scale for a) single guiding channel with boundary conditions (cf. Figure 3 guiding channel), isometric representation, b) storage (centred on the *X*-axis)

3.2. Flow effects in the radial diffuser with internal elements

The flow in the radial diffuser with internal elements is shown in Figure 5. The colouring of the turbulent structures with $Q = 400\ \mathrm{s}^{-1}$ is relatively coarse and therefore gives a good overview of the situation in the diffuser and the guiding channels. The change from laminar to turbulent behaviour is triggered by the flow reversal at the upper diffuser plate. This is typical and known for LES simulations [16]. For this reason, the connecting pipe is not shown (no turbulent structures visible). Furthermore, this behaviour also explains the blue colouring in the middle of the diffuser (stagnation point and flow reversal). The detailed view of the guiding channel shows fluctuating velocities in the guiding channels, e.g., in Figure 5, bottom right. This is due to the statistical distribution of the flreow variables (LES character) [16]. The distribution of the vortex structures shows a complex, turbulent behaviour. The vortex strands are connected similar to a screw structure. For a differentiated observation and evaluation of the flow effects, the meshing and simulation of a single guiding channel is carried out (Figure 4 a)). The result is shown in Figure 6. The fluid flows from the inlet into the guiding channel. The effect of a centrifugal force causes the flow to be applied to the internal element. A centrifugal instability, the so-called Görtler vortex [17-19], forms in the boundary layer. The fluid near the wall is slowed down due to the wall adhesion condition. Faster fluid flows in from the outer boundary layer. Pressure gradients lead to balancing processes and roll up the Görtler vortex, G in Figure 6. A cross vortex forms inside the guiding channel due to the effect of a centrifugal force. This rotates across the cross-section of the guiding channel (cf. Q in Figure 6). The cross vortex runs on larger energy cascades than the Görtler vortex (higher kinetic energy of the main flow compared to the boundary layer flow). Approximately in the middle of the diffuser radius ($r_{\mathrm{D}}/2$), the cross vortex entrains the Görtler vortex. The Görtler vortex bursts and merges with the cross vortex. The cross vortex flows out of the guiding channel along the main flow direction. Due to the difference in velocity between the right and left side (Figure 4 a)), a pressure gradient forms along the main flow direction. This leads to recirculation and a radial longitudinal vortex (cf. L in Figure 6). The flow effects occur simultaneously and influence each other. This leads to

the formation of so-called screw structures. These are marked with HP in Figure 6.

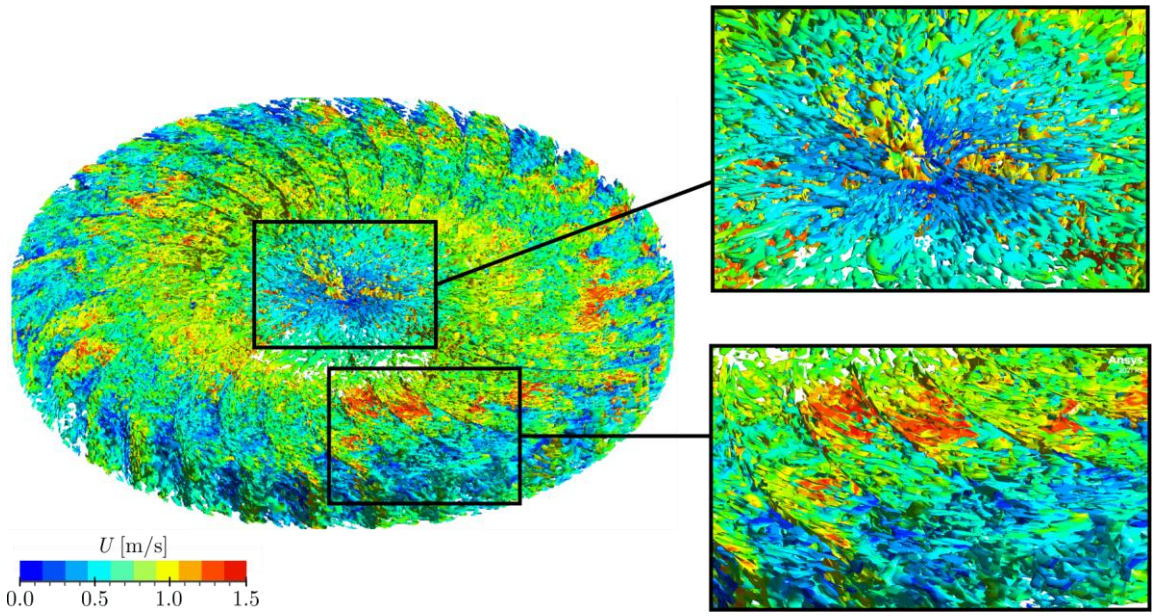

Figure 5. Flow effects in the radial diffuser with internal elements visualised with the Q-criterion ($400\ \mathrm{s}^{-2}$) and coloured according to the magnitude of the velocity (isometric view), detailed view top right: flow at the upper diffuser plate, bottom right: guiding channel with outflow

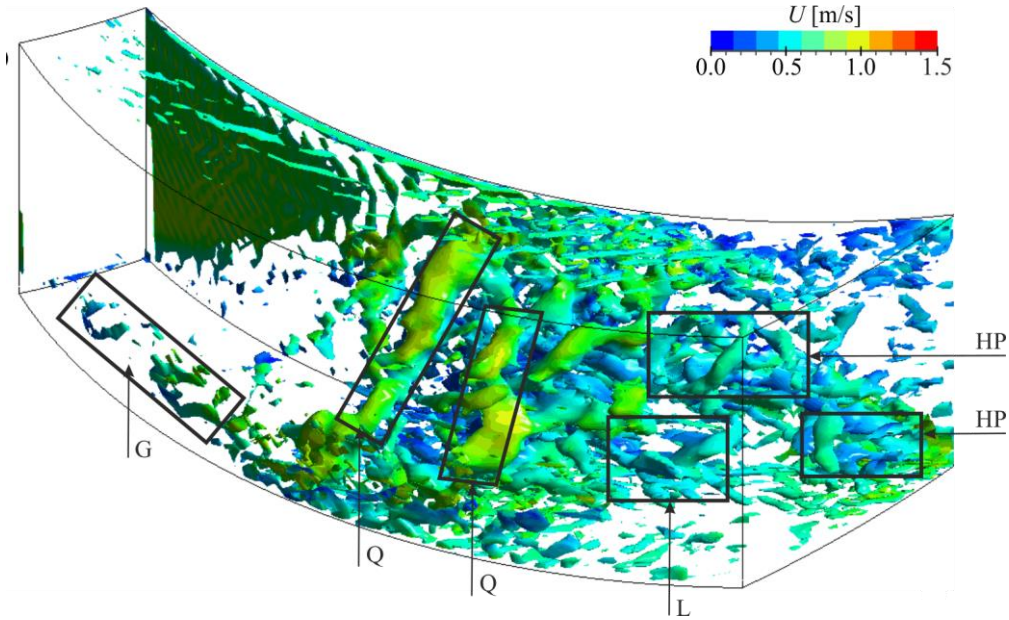

Figure 6. Flow effects in a representative guiding channel visualised with the Q-criterion ($Q = 1400\ \mathrm{s}^{-2}$) and coloured according to the magnitude of the velocity, significant flow effects are marked with G... Görtler vortex, Q... cross vortex, L...longitudinal vortex, HP... Helical Pairing

3.3. Flow effects in the slim tank with dished bottom

Figure 7 shows the flow in the storage. The storage fluid is introduced into the storage. Due to the density differences, the buoyancy forces act. As a result, the flow attaches itself to the ceiling of the storage. Due to the swirling flow, a red area forms over the diffuser height near the diffuser outlet (cf. Figure 7 a)). This is not the case with conventional radial diffusers. Vortices roll up at the layer boundary due to shear forces. The radial velocity component causes the flow to advance at the storage ceiling. There, a higher head is formed compared to the leading nose. This behaviour is known from density flows in cold water storages [20]. Here, the head-nose formation occurs in reverse (horizontally mirrored) to the density flow in flat-bottom tanks. The occurrence of the lobe-air structure cannot be clearly demonstrated. This is probably due to the high velocity of the wall jet, which closes the gap quickly. Shorter evaluation intervals in the simulation are necessary so that the proof can be successful. After 6 s, Kelvin-Helmholtz vortices are formed in the free shear layers (cf. Figure 7 b)). The resolution of these instabilities confirms the high quality of the computational grid. In the wake of the flow, further vortices

detach. The radial velocity component ensures a deep penetration of the flow into the storage space. In Figure 7 c), the flow comes to a standstill along the storage wall due to the buoyancy force. Then no vertically deeper penetration is possible. The loading fluid is deflected horizontally. Due to the temperature difference, it experiences a vertical acceleration. Then the flow penetrates into the centre of the storage. This process is associated with strong mixing effects. The intensity is shown in Figure 7 c), because in some cases heavier or colder areas lie above lighter, warmer areas. Wave movements are the result. With increasing operating variables (volume flow, temperature), the mixing effects or wave movements increase. At the end of this phase, the mixing area extends to the connection pipe (cf. Figure 7 d)). There, the reflection takes place again, combined with mixing effects. After 150 s an S-shaped transition layer is formed (cf. with Figure 7 e)). This is typical for swirl loading. When the rotation of the storage mass no longer has any influence, the transition layer flattens out into a straight line. More vortices form at the lower end of the boundary layer.

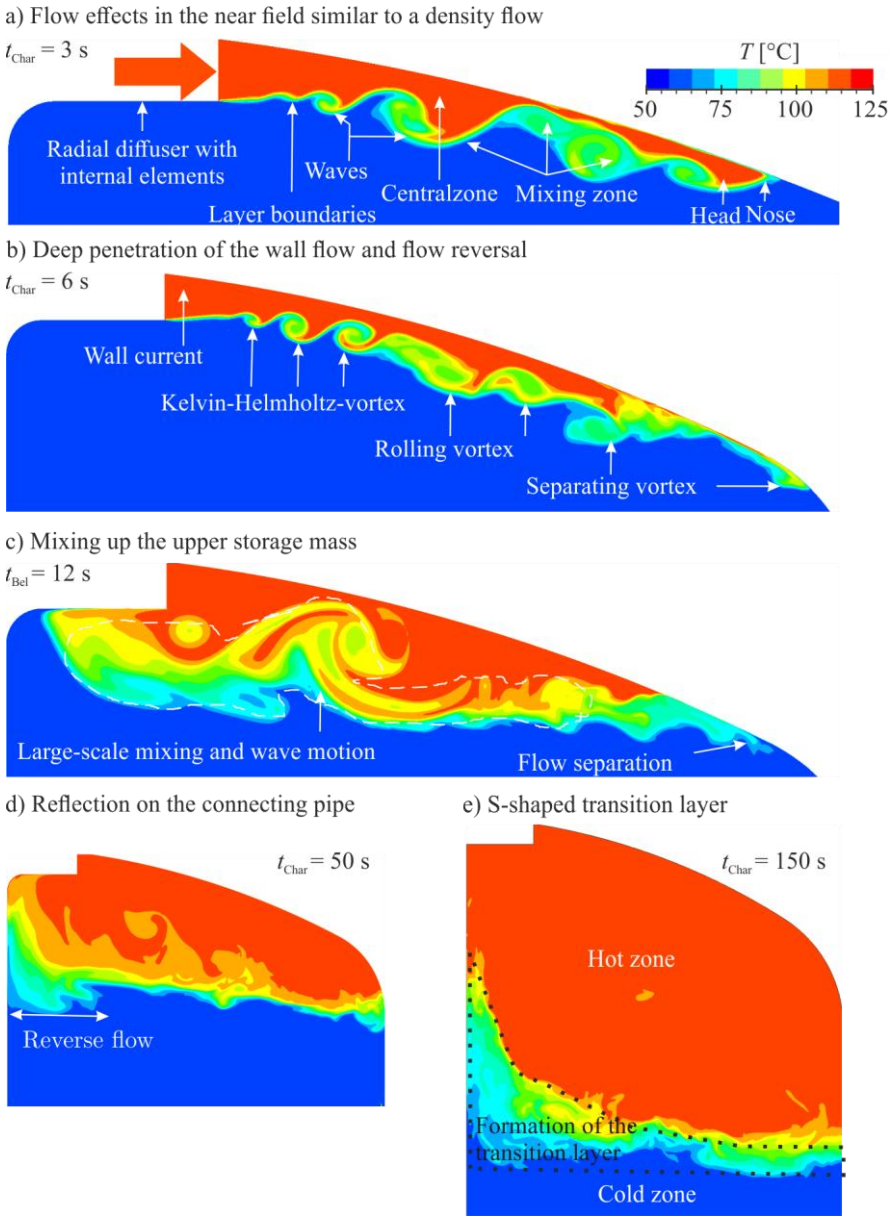

Figure 7. Flow effects during swirl loading in the slim hot water tank with dished bottom at different times with significant flow effects

4. CONCLUSION AND OUTLOOK

Slim hot water storage tanks with dished heads play a key role in increasing the efficiency of district heating networks. This requires high storage efficiency. This requires a narrow transition layer with low internal losses during loading. Oestreich et al [7] showed that swirl loading can make a significant contribution. So far, the detailed description of the flow effects of swirl loading in the radial diffuser with internal elements and in the storage remains unclear. This paper closes this gap.

The investigations are carried out with numerical flow simulation (CFD). Ansys CFX is used. A 360° diffuser model, a single guiding channel and a segment model of the storage are modelled and simulated. Turbulence modelling with LES

(WALE) resolves the vortex structures. Recommendations for the turbulent integral length scale, Courant and Peclet numbers are used for correct modelling. Observation of the diffuser model shows helically connected vortex structures. The simulation of a single guiding channel resolves the Görtler vortex as well as longitudinal and transverse vortices. Furthermore, the flow of a vortex can be reproduced from rolling up to bursting and transformation into a larger vortex. Due to the simultaneous character of the vortex effects, screw structures appear. These findings confirm the known flow effects from [7] and significantly expand the understanding. The discretisation of the storage model leads to numerical instability due to high Peclet numbers. The central difference method is not suitable in this case. Instead, the high resolution method is used. This problem could not be found in previous work [7] due to different turbulence modelling. For the first time, the simulation of the storage model shows in detail the flow effects in the development of thermal stratification during swirl loading. The flow behaves similar to a density flow with head and nose formation. Kelvin-Helmholtz vortices occur in the free shear layers. Future work will investigate the occurrence of a lapp-air structure. In addition, the transferability of the present findings to other operating and geometric sizes is being sought in order to be able to derive design recommendations for swirl loading.

ACKNOWLEDGEMENT

The underlying collaborative project is funded by the Federal Ministry of Education and Research (BMBF) under the number 03SF0623A/B/C on the basis of a resolution of the German Bundestag. Project management is carried out by the Project Management Organisation Jülich (PtJ). The responsibility for the content of this publication lies with the authors.

The authors gratefully acknowledge the GWK support for funding this project by providing computing time through the Center for Information Services and HPC (ZIH) at TU Dresden.

REFERENCES

[1] Urbaneck, T.: Water Tank Stores for Medium/Large Application. In: Reference Collection in Earth Systems and Environmental Sciences, Elsevier (2020). ISBN: 9780124095489.

[2] DIN 28011:2012-06: Gewölbte Böden - Klöpperform. Berlin. Beuth Verlag, 2012.

[3] Findeisen, F., Urbaneck, T., Platzer, B.: Radiale Diffusoren in Warmwasserspeichern- funktionale Untersuchung. Teil 3: Detaillierte Untersuchung des Beladeverhaltens. HLH Vol. 68, Issue 6 (2017), pp. 19–27. ISSN: 1436-5103.

[4] Lohse, R., Urbaneck, T., Brämer, C., Platzer, B. Effects during loading of hot water storages with a high aspect ratio EuroHeat&Power, English Edition VWEW Energieverlag Vol. 9, Issue 3 (2012). pp. 42–47. ISSN 1613-0200.

[5] Brähmer, C., Urbaneck, T., Lohse, R.: Influence of Geometry and Operation Parameters on Thermal Stratification. Euro Heat and Power 4 (2012), pp. 30–36. ISSN: 1630-0200.

[6] Findeisen, F. et al.: Beladesysteme für thermische Energiespeicher - neue konstruktive Ansätze. 25. Energie-Symposium Nutzung regenerativer Energiequellen und Wasserstofftechnik. T. Luschtinetz; J. Lehmann (Ed.). Stralsund, 2018, Proceedings, pp. 50–59. ISBN: 9783981774047.

[7] Oestreich, F., Urbaneck, T.: Loading Slim Hot Water Tanks With and Without Swirl Generation - First Results. 14th International Conference on Solar Energy and Buldings. Kassel (Deutschland), paper accepted.

[8] ANSYS, Inc.: ANSYS CFX 2019 R2. Canonsburg (USA), 2019.

[9] Wagner, W., Kretzschmar, H.: International Steam Tables - Properties of Water and Steam based on the Industrial Formulation IAPWS-IF97. Vol. 2nd, Springer Berlin, Heidelberg, 2008. ISBN: 978-3-540-74234-0. DOI: {10.1007/978-3-540-74234-0_3}.

[10] Nicoud, F., Ducros, F.: Subgrid-Scale Stress Modelling Based on the Square of the Velocity Gradient Tensor. Flow Turbulence and Combustion 62 (Sep.1999), pp. 183–200. DOI: 10.1023/A:1009995426001.

[11] Menter, F. et al.: An Overview of Hybrid RANS–LES Models Developed for Industrial CFD. Applied Sciences 11.6 (2021). ISSN: 2076-3417. DOI: 10.3390/app11062459. URL: https://www.mdpi.com/2076-3417/11/6/2459.

[12] Gerasimov, A. (ANSYS Sweden): Quick Guide to Setting Up LES-type Simulation. May 2016. URL: http://www.tfd.chalmers.se/~lada/comp_turb_model/postscript_files/Quick_Guide_to_Setting_Up_LES_version_1.4_for_Lars.pdf (23. 06. 2022).

[13] ANSYS, Inc.: ANSYS CFX-Solver Theory Guide. Release 14.0. 2011.

[14] Ferziger et al.: Computational Methods for Fluid Dynamics. 4th Edit. Springer, Cham, 2019. ISBN: 978-3-319-99693-6. DOI: https://doi.org/10.1007/978-3-319-99693-6.

[15] Jeong, J., Hussain, F.: On the identification of a vortex. In: Journal of Fluid Mechanics 285 (Feb. 1995), pp. 69–94. DOI: 10.1017/S0022112095000462.

[16] Fröhlich, J.: Large Eddy Simulation turbulenter Strömungen. Lehrbuch: Maschinenbau. Vieweg+Teubner Verlag, 2006. ISBN: 9783835101043.

[17] Görtler, H.: Über den Einfluss der Wandkrümmung auf die Entstehung der Turbulenz. Zeitschrift für Angewandte Mathematik und Mechanik, Vol. 20, Issue 3 (1940).

[18] Görtler, H.: Instabilität laminarer Grenzschichten an konkaven Wänden gegenüber gewissen dreidimensionalen Störungen. In: Zeitschrift für Angewandte Mathematik und Mechanik , Vol. 21, Issue 4 (1941).

[19] Saric, W. S.: Görtler Vortices. Annual Review of Fluid Mechanics 26:1, pp. 379–409 (1994).

[20] Urbaneck, T., Möller, H.; Kressner, T.; Platzer, B.: Kaltwasserspeicher mit radialen Diffusoren. Teil 2a: Schichtungsaufbau im Nahfeld - Grundlagen, Physik, Simulation. HLH Vol. 60, Issue 6 (2009), pp. 32 –36.

LIST OF SYMBOLS

Quantity	Symbol	Unit
Constant	C_Q	-
Constant	C_μ	-
Coordinate	X, Y, Z	m
Courant number	Cr	-
Height	h	m
Mass flow rate	$\dot{m}$	kg s^{-1}
Number of internal elements	z	-
Peclet number	Pe	-
Pressure	p	Pa
Q-criterion	Q	1 s^{-2}
Radius	r	m
Shear rate	S	1 s^{-1}
Swirl angle	β	°
Temperature	T	°C
Thermal conductivity	α	m² s^{-1}
Time	t	s
Turbulent dissipation rate	ε	m² s^{-2}
Turbulent kinetic energy	k	m² s^{-2}
Turbulent length scale	l	m
Velocity	U	m s^{-1}
Volume	V	m³
Vorticity	Ω	1 s^{-2}

Shortcut	Meaning
CFD	Computational Fluid Dynamics
Char	Charging
CP	Connecting pipe
D	Diffuser
G	Görtler vortex
HP	Helical-pairing
IAPWS-IF97	The International Association for the Properties of Water and Steam - Industrial Formulation 1997
L	Longitudinal vortex
LES	Large Eddy Simulation
Q	Cross vortex
St	Storage
W	Water

RESEARCH ON THE OPERATION STRATEGY OF THE DISTRICT HEATING AND COOLING INTEGRATED ENERGY SYSTEMS CONSIDERING ICE STORAGE AND LOAD DEMAND

Qu Tingting 1[a*], Wei Kaida 1[a], Li Wei 2[b], Han Jingxiao 2[b]

[a] *Beijing Jing Neng Thermal Development Co., Ltd. Hua yuan Branch1, Beijing 100124, China,*

[b] *Beijing District Heating Group Co., Ltd2, Beijing 100026, China,*

[*] *Corresponding author. 1443185646@qq.com.cn.*

ABSTRACT

The district heating and cooling integrated energy system (DHC-IES) is a complex system engineering that realizes multi-energy coupling and meets multiple loads on the demand side, and the coordinated and optimal operation of "source-load-storage" needs to be solved urgently. Given the problems of insufficient resource mobilization on the demand side of DHC-IES and the complex operation control of ice storage "peak shifting and valley filling", this paper takes a certain DHC-IES with ice storage that has been put into operation as the research object. Using the digital drive and mechanism modeling method, the demand side predicts the hourly heat load of user heat exchange station and the hourly cooling load of the user cooling exchange station and then studies the on-demand operation of the secondary return water temperature of the DHC-IES winter user heat exchange station considering the heat load prediction. The example shows that Set3 refers to the actual operation of the secondary return water temperature as the control target temperature, and the average error value of the secondary return water temperature prediction after considering the hourly heat load variable is 0.08°C. The multi-objective optimization model of the economy, energy consumption, and CO_2 emission of the DHC-IES summer energy station ice storage system is established based on the time-of-use electricity price, and the integrated demand response (IDR) of the cooling load of the energy station, the example shows that compared with scenario1 actual operation, scenario3 reduces daily operating costs by 13.5%, energy loss rate by 11.7%, and CO_2 emissions by 5.7%, while scenario4 reduces daily operating costs by 15.5%, energy loss rate by 9.8%, and CO_2 emissions by 3.8%.

Keywords: Ice storage; IDR; winter user heat exchange station; summer energy station;

1. INTRODUCTION

District heating and cooling integrated energy system (DHC-IES) is an energy system that coordinates energy production conversion, transmission and distribution, storage, consumption, and other links through the coupling utilization of multiple energy resources in the region, and under the premise of meeting the demand of cooling/heating loads, maximizes the comprehensive utilization efficiency of district heating and cooling, which has great significance for energy conservation and emission reduction. DHC-IES multi-energy coupling synergy and runtime economy improvement need energy storage to solve[1], ice storage, as a common form of cold storage, can assist power grid companies to "shift peaks and fill valleys", in DHC-IES plays an important role[2]. However, the operation control of ice storage is complex, which can easily cause inefficient equipment operation and waste of energy, and optimal control is the most ideal control strategy for ice storage operation[3-4]. In terms of single-objective optimization control with the economy as the goal, Henze et al.[5] established an optimization mathematical model and constraints for the annual operating cost of the ice storage district cooling system, and analyzed the operation optimization method. Zhang Feng et al.[6] took the minimization of operating costs as the objective function, and applied the operation optimization control strategy of the ice storage air conditioning system based on load forecasting, which could reduce the operating costs by 6.11%. In terms of multi-objective optimal control of the economy and energy consumption, Sun Yue et al.[7] constructed a multi-objective optimal operation control strategy for ice storage systems considering cost and energy consumption, to achieve the optimal comprehensive benefit. Ran Tong[8] analyzed the multi-objective optimization control of the ice storage system of an airport energy station with the lowest operating cost and the lowest energy consumption loss, saving the operating cost and energy consumption loss to varying degrees. In addition, the unified and optimal allocation of supply-side and demand-side resources can improve the performance of the DHC-IES system[9], and the establishment of accurate load forecasting models and the implementation of IDR are hot issues in the research of efficient and low-carbon operation of IES in parks. At present, the resource mobilization of the DHC-IES demand side is insufficient, and the management resources of the demand side are rarely used to improve the economic benefits of the system in the operation stage[10]. With the development of artificial intelligence, cooling/heating load demand forecasting provides conditions for demand response resources to participate in DHC-IES operations. without affecting the user experience, IDR improves the comprehensive utilization efficiency of DHC-IES and mobilizes demand-side management resources[11], which is a key technology to encourage the collaborative optimization of IES source-load-storage in the park[12]. At present, IDR's research in DHC-IES operation optimization focuses on electricity and heat demand response, Dong Dou[13] proposes a day-ahead optimization operation model considering peak and valley heat price and demand response, which

reduces operating costs. Xu Hang[14] established an integrated demand response strategy model of electricity and heat, which can further tap the potential of user control. Xu Fu Lu[15] constructed a collaborative optimization scheduling model of IDR for electric heating load, improving thermal power units' energy efficiency and flexibility.

In short, the optimal control of ice storage operation is based on the economic single goal or economic energy multiple goals, and with the proposal of carbon neutrality, multi-objective optimization needs to comprehensively consider CO_2 emissions. Cooling/heating load forecasting is an effective way to mobilize DHC-IES demand-side management resources and realize on-demand operation, and IDR contains relatively few cooling demand responses in DHC-IES operation optimization research. This paper combines data-driven and mechanism modeling methods and uses three machine learning algorithms on the demand side to predict the hourly heat load of the user heat exchange station and the hourly cooling load of the user cooling exchange station, and then the on-demand temperature operation strategy of DHC-IES winter user heat exchange station was studied considering the heat load forecast, and the multi-objective operation optimization strategy of economy, energy consumption and CO_2 emission of the ice storage system of the DHC-IES summer energy station was studied taking into account the time-of-use electricity price and cooling load forecast.

2. OVERVIEW OF DHC-IES WITH ICE STORAGE

2.1 Project Overview

The demand side of DHC-IES with ice storage provides heating for residential buildings in winter and commercial, office, and hotel buildings in summer, with 5 user heat exchange stations and 12 user cooling exchange stations; On the energy supply side, one energy station is operated, and the municipal electricity and municipal heat network are used to provide cool and heat sources for the user stations, realizing the coupling of "heat-electricity-cool". The energy station is equipped with energy conversion and storage equipment, and the winter heat supply converts the 130/70°C high-temperature hot water of the municipal heat network into 120/60°C hot water through the plate heat exchanger in the energy station to ensure the user's all-day heat load demand of the heat exchange station; Summer cooling adopts an external ice melting ice storage system connected in series upstream of the base load host in the energy station.

2.2 Main equipment modeling

Ignoring the pipeline transmission loss, this study mainly focuses on the "source-load-storage" modeling of energy conversion equipment, energy storage equipment, and load characteristics of user stations in energy stations.

2.2.1 Energy conversion equipment model

(1) Refrigeration host: mainly includes base load host and dual-condition host, and the equipment model is shown in Equation(1).

$$Q_{zl}(i) = COP_{zl} \times P_{zl}(i) \tag{1}$$

In the formula, $Q_{zl}(i)$ is the cooling capacity output of the refrigeration host in i period, kW ; COP_{zl} is the energy efficiency ratio of the refrigeration host; $P_{zl}(i)$ is input the electrical power of the refrigeration host in i period, kW .

(2) Cooling tower: a device that uses a motor to drive a fan to dissipate the waste heat of the ice storage system, and the approximate mathematical model is shown in Equation (2).

$$t_{lt}(i) = P_{zl}(i) + Q_{zl}(i) \tag{2}$$

In the formula, $t_{lt}(i)$ is the load-bearing load of the cooling tower in i period, kW .

(3) the plate heat(cool) exchanger: Using the phenomenon of heat transfer, heat is transferred from high (low) temperature fluid to low (high) temperature fluid to realize energy transfer and exchange, and the equipment model is shown in Equation(3).

$$Q_{hl}(i) = P_{hl}(i)\eta_{hl} \qquad Q_{hr}(i) = P_{hr}(i)\eta_{hr} \tag{3}$$

In the formula, $Q_{hl}(i)$ is the output power of the plate cool exchanger in i period, kW ; $P_{hl}(i)$ is the input power of the plate cool exchanger in i period, kW ; η_{hl} is the operating efficiency of the plate cool exchanger, kW ; $Q_{hr}(i)$ is the output power of the plate heat exchanger in i period, kW ; $P_{hr}(i)$ is the input power of the plate heat exchanger in i period, kW ; η_{hr} is the operating efficiency of the plate heat exchanger.

2.2.2 Energy storage device model

The energy storage equipment in the energy station is an external ice-melting ice storage tank, and the equation of the hourly cold storage capacity[16] is shown in Equation (4).

$$B_i = Q_{zb}(i) \times \sum_{k=1}^{4} PLR_{ik} \times \eta \tag{4}$$

In the formula, B_i is the dual-condition host's hourly ice storage during ice storage, RTh; $Q_{zb}(i)$ is dual-condition host rated cooling capacity under the ice in i period, RTh; PLR_{ik} is the k-deck dual-condition host produces the hourly load rate under ice; η is the dual-condition host conversion rate from cool to ice, with a value of 0.94.

2.2.3 User station load characteristic model

(1) The cooling load characteristics of the user cooling exchange station are shown in Equation (5).

$$(Q_{zl}(i)+Q_{ice}(i))(1-\lambda_l^{loss})(1-\eta_l^{uti})=\sum_{hl=1}^{12}Q_{hl}^{load}(i) \tag{5}$$

In the formula, $Q_{ice}(i)$ is the cooling capacity output of the ice storage tank in i period, RTh or kW ; λ_l^{loss} is the rate of loss of cooling energy; η_l^{uti} is the loss efficiency of the user's cooling station to the cooling energy; $Q_{hl}^{load}(i)$ is the cooling load demand of a user's cooling station in i period, RTh or kW .

(2) The heat load characteristics of the user heat exchange station are shown in Equation (6).

$$Q_{hr}(i)(1-\lambda_h^{\mathrm{loss}})(1-\eta_h^{\mathrm{uti}})=\sum_{hr=1}^{5}Q_{hr}^{load}(i) \tag{6}$$

In the formula, $\lambda_h^{\mathrm{loss}}$ is the thermal energy loss efficiency rate of the user heat exchange station; $Q_{hr}^{load}(i)$ is the heat load demand of a user's heat exchange station in i period, kW .

2.3 Energy station cooling energy consumption model

The energy consumption of the cooling operation of the energy station mainly occurs on the cooling side of the ice storage system, including the power consumption of the refrigeration host, cooling tower, and water pump, and the energy consumption of other equipment can be ignored.

2.3.1 Refrigeration host power consumption model

The relationship between cop and PLR of the refrigeration host is shown in Equation (7).

$$PLR(k)=\frac{Q_{zl}(i)x(k)}{Q_o(k)} \qquad COP_{zl}(k)=a_1+a_2\times PLR(k)+a_3\times PLR(k)^2 \tag{7}$$

The power consumption model of the refrigeration host is shown in Equation (8).

$$W_{zl}(i)=\sum_{k=1}^{m}\frac{Q_{zl}(i)x(k)}{COP_{zl}(k)} \qquad W_{zl}=\sum_{i=1}^{24}W_{zl}(i) \tag{8}$$

In the formula, $PLR(k)$ is the load rate of the k-th refrigeration host; $x(k)$ is the of the cooling load of the k-th refrigeration host to the total cooling load; $Q_o(k)$ is the rated power of the k-th refrigeration host, kW ; $COP_{zl}(k)$ is the energy efficiency ratio of the k-th refrigeration host; a_1 , a_2 , a_3 is the COP and PLR fitting coefficient of the refrigeration host; $W_{zl}(i)$ is m platform refrigeration hosts power consumption in i period, kWh; m is the number of refrigeration hosts; W_{zl} is the total daily power consumption of the refrigeration host, kWh.

2.3.2 Cooling tower power consumption model

Combined with practical engineering experience, the power consumption formula of the cooling tower is shown in Equation (9).

$$W_{lt}(i)=A\times t_{lt}(i) \qquad W_{lt}=\sum_{i=1}^{24}W_{lt}(i) \tag{9}$$

In the formula, $W_{lt}(i)$ is cooling towers consume electricity in i period, kWh; A is the fitting coefficient is 0.014 in combination with the actual fit of this project; $t_{lt}(i)$ is the load-bearing load of the cooling tower, kW ; W_{lt} is the total daily power consumption of the cooling tower, kWh.

2.3.3 Pump power consumption model

The power consumption of the water pump is the power consumption of the primary side pump, including the cooling water pump, ethylene glycol pump, and chilled water pump, and the power consumption model of the water pump is shown in Equation (10).

$$W_{p-l}=B\times P_lT_1+C\times P_yT_2+D\times P_dT_3 \tag{10}$$

In the formula, W_{p-l} is the total daily power consumption of the primary side pump, kWh; P_l is rated power for cooling water pumps, kW ; P_y is the rated power of the ethylene glycol pump, kW ; P_d is the rated power for chilled water pumps, kW ; B、C、D is the fitting coefficient between the running power and the rated power of the pump; T_1、 T_2、 T_3 is the working time of the cooling water pump, ethylene glycol pump, and chilled water pump throughout the day.

3. TEMPERATURE OPERATION STRATEGY OF WINTER USER HEAT EXCHANGE STATION CONSIDERING HEAT LOAD

The winter heating operation of DHC-IES with ice storage is that the control unit of the user heat exchange station supplies heating to residential buildings, and the operation strategy of the user heat exchange station mainly adopts the temperature operation with the secondary return water temperature as the control goal. Aiming at the problem of insufficient

resource mobilization on the demand side of DHC-IES winter heat supply, the control unit of Li xin Yi yuan user heat exchange station at the end of the winter heating system is selected as an example. Firstly, the hourly heat load of the user heat exchange station on the demand side is predicted based on BP, GA-BP, and GS-SVR models. Secondly, the hourly heat load prediction value is used as the characteristic variable of secondary return water temperature prediction, and the four prediction feature sets of secondary return water temperature are divided according to the actual operation. Finally, GRNN neural network was used to analyze the influence of hourly heat load variables on the temperature prediction of secondary return water, and the temperature operation strategy of the winter user heat exchange station was guided.

3.1 Example of hourly heat load prediction of user heat exchange station

Firstly, the original sample data of the Li Xin Yi yuan user heat exchange station from November 15, 2020, to March 15, 2021, with a total interval of 1 hour for 121 days, were collected for data preprocessing. secondly, the influencing variables of hourly heat load prediction were preliminarily screened as meteorological factors and historical heat load, through correlation analysis, eight influencing variables were selected as input variables of the t-hour cooling load prediction, there is the outdoor temperature at time t (prediction), the outdoor temperature at time t-1 (prediction), the outdoor temperature at time t-2 (prediction), relative humidity at time t (prediction), heat load at time t of the previous day ~ four days before the previous day. Finally, 2808 sets of hourly data will be collected to divide the dataset, of which 2112 sets of data are the training set and 696 sets of data are the test verification set. the prediction error results of the Li xin Yi yuan user heat exchange station from February 15, 2021, to March 15, 2021, of three heat load prediction models based on BP, GA-BP, and GS-SVR are shown in Table 1.The average relative error of the predicted hourly heat load based on the GS-SVR model is 3.04%, which can meet the requirements of DHC-IES winter heating operation according to engineering experience.

Table 1 Construction of three heat load prediction models and prediction error results

Model name	Build model parameters	Maximum relative error	Minimum relative error	Average relative error
BP	The learning rate of the 8-6-1BP neural network model is 0.015, and the error target value is 0.0000001.	43%	0.06%	7.22%
GA-BP	The 8-6-1GA-BP neural network model has 54 weights, 7 thresholds, 61 coding lengths, 50 population sizes, 0.8 Cross, 0.2 Mutation, 18 iterations, and 0.026 training accuracy.	36.6%	0.03%	6.86%
GS-SVR	The input and output variables are the same as above, when the time step is 0.5, the penalty parameter C is 0.7 and the kernel function variance g is 5.6.	25.8%	0.01%	3.04%

3.2 Prediction example of secondary return water temperature of winter user heat exchange station

Firstly, the outdoor temperature and historical operation data of the Lai sin Yi yuan user heat exchange station from November 15, 2020, to March 15, 2021, with a total interval of 1 hour for 121 days, were collected as sample data for data preprocessing. secondly, Outdoor temperature and historical operating data have a certain influence on the secondary return water temperature, through correlation analysis, the outdoor temperature at t time (T outdoor), the outdoor temperature at t+1 time (T+1 outdoor), the outdoor temperature at t+2 time (T+2 outdoor), the outdoor temperature at t+3 time (T+3 outdoor), the primary supply water temperature at t time (T1 supply), primary return water temperature at t time (T1 return), primary flow at t time (F1 supply), the secondary supply water temperature at t time (T2 supply), secondary flow at t time (F2 supply), hourly heat load (G demand), 10 characteristic variables are the characteristic variables predicted by the secondary return water temperature (T2 return). Then, to simulate the heating system's operation and explore the influence of hourly heat load characteristic variables on the secondary return water temperature, the 10 characteristic variables selected were divided into four feature sets, as shown in Table 2. Set1 is the 10 characteristic variables containing G demand, Set2 is the 9 characteristic variables except for G demand, Set3 refers to the actual operation with the secondary return water temperature as the control target temperature, including characteristic variables such as G demand, and Set4 strips the G demand from Set3. Finally, according to the four prediction feature sets, the collected 2904 sets of hourly data of the Lai Sun Yi yuan user heat exchange station are divided into data sets, of which 2208 sets of data are substituted as the training set and 696 sets of data are substituted into the GRNN neural network model training as the test verification set, and obtain the prediction error results of second return water temperature from February 15, 2021, to March 15, 2021, as shown in Table 3. Based on the characteristic set Set3, the average error value of the secondary return water temperature prediction is 0.08°C, and the operation management personnel can manage the temperature operation of the user's heat exchange station.

Table 2 Four feature sets for prediction of secondary return water temperature

Feature set	Enter the feature variables	Number	output
Set1	T1 supply, T1 return, F1 supply, T2 supply, F2 supply, T outdoor, T+1 outdoor, T+2 outdoor, T+3 outdoor, G demand	10	T2 return
Set2	T1 supply, T1 return, F1 supply, T2 supply, F2 supply, T outdoor, T+1 outdoor, T+2 outdoor, T+3 outdoor,	9	T2 return
Set3	T1 supply, F1 supply, T2 supply, T outdoor, T+1 outdoor, T+2 outdoor, T+3 outdoor, G demand	8	T2 return
Set4	T1 supply, F1 supply, T2 supply, T outdoor, T+1 outdoor, T+2 outdoor, T+3 outdoor,	7	T2 return

Table 3 Prediction error of secondary return water temperature in four feature sets

Feature set	Average relative error	Average error value （℃）
Set1	0.16%	0.06℃
Set2	0.19%	0.07℃
Set3	0.20%	0.08℃
Set4	0.29%	0.12℃

4. OPTIMIZATION OF SUMMER ENERGY STATION OPERATION CONSIDERING ICE STORAGE AND COOLING LOAD

DHC-IES with ice storage summer cooling is mainly the operation optimization of the ice storage system of the energy station, and the multi-objective optimization control is the key to the cooling operation control of the ice storage system of the energy station. The ice storage system of the energy station adopts a dual-condition host store ice and the base load host cooling as shown in Figure 1, or dual-condition host store ice and ice storage tank cooling as shown in Figure 2. When the electricity price is cheap at night, turn on the dual-condition host to store ice, and the base load host cooling to meet the cooling load demand at night. When the nighttime load is low and the PLR of base load host cooling is low, the nighttime cooling load demand can be provided by ice storage tank cooling.

At present, DHC-IES only provides cooling for hotel buildings at night, and the load demand is relatively small, such as the use of base load host cooling resulting in the low PLR, the use of ice storage tank cooling will increase the duration and amount of ice storage at night. Therefore, it is necessary to optimize the night ice storage duration and cooling mode of the energy station. Firstly, the hourly cooling load of the user cooling exchange station on the demand side is predicted based on BP, GA-BP, and GS-SVR models. Secondly, based on the time-of-use electricity price and the hourly cooling load demand of the energy station integrated demand response (the hourly cooling load demand of the energy station is equal to the sum of the predicted hourly cooling load of the user cooling exchange station operating at the same time). Finally, the NSGAII algorithm is used to optimize and solve the ice storage duration and cooling operation strategy of the ice storage system of the energy station is optimized in different scenarios at night with the goal are the lowest daily operating cost, the smallest energy loss rate, and the lowest CO_2 emissions.

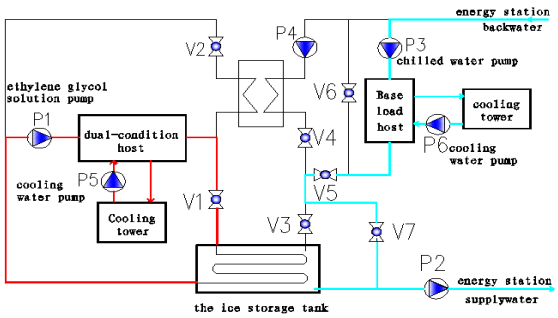

Figure 1 Diagram of the nighttime base load host cooling system

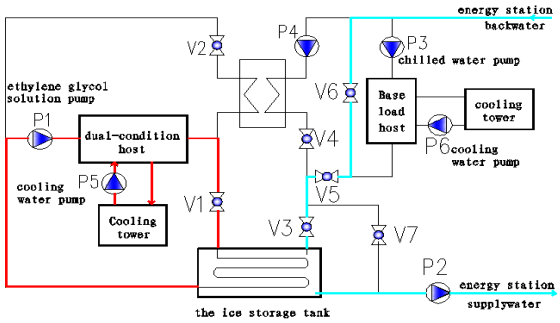

Figure 2 Diagram of the nighttime the ice storage tank cooling system

4.1 Multi-objective optimization of summer energy station cooling

4.1.1 Multi-objective function model for cooling operation

Taking 24 hours as the cooling operation cycle, the multi-objective function model of the ice storage system of the summer energy station is constructed with the lowest daily operating cost, the lowest energy loss rate, and the lowest CO_2 emission as the multi-objective:

(1)Daily running cost model:

$$f_1 = \min \cos t = \sum_{i=1}^{24} \left\{ \left[W_{zl}(i) + W_{lt}(i) + W_{p-l}(i) \right] \times e(i) \right\} \tag{11}$$

In the formula, $\cos t$ is total daily running costs, million yuan/day; $W_{zl}(i)$ is the refrigeration host consumes electricity in i period, kWh; $W_{lt}(i)$ is cooling towers consume electricity in i period, kWh; $W_{p-l}(i)$ is the total daily power consumption of the primary side pump in i period, kWh; $e(i)$ is the price of electricity in i period, Yuan/kWh.

(2)Energy loss rate model:

$$f_2 = \min per = \frac{W_{if}}{W_{ice}} = \frac{\sum_{i=1}^{n} (1-\eta)\left[W_{zl}(i) + W_{lt}(i) + W_{p-l}(i) \right]}{W_{zl} + W_{lt} + W_{p-l}} \tag{12}$$

In the formula, per is the dual-condition host's energy loss rate during nighttime ice making, %; W_{ice} is the total daily power consumption of the ice storage system; W_{if} is dual-condition host energy loss during nighttime ice making; n is the length of time to store ice for the night; η is the conversion rate of the cool energy into ice under the ice condition of the main mechanism of the double working condition is 0.94.

(3)Daily CO_2 emission model: $$f_3 = \min emission = \sum_{i=1}^{24} \left\{ \left[W_{zl}(i) + W_{lt}(i) + W_{p-l}(i) \right] \times E_{co_2} \right\} \tag{13}$$

In the formula, $emission$ is the daily CO_2 emissions, g; E_{co_2} is CO_2 equivalent coefficient per unit of electricity consumption in i period,604 g/kWh.

4.1.2 Constraints for cooling operation

(1) The total amount of ice storage at night is not greater than the maximum capacity of the ice storage tank; The daytime ice melting and cooling capacity of the ice storage tank in the cooling cycle is less than or equal to the total amount of ice storage at night, and to ensure the utilization efficiency of the ice storage tank, it should be greater than or equal to 95% of the total ice storage at night [16].

$$S = \sum_{i=1}^{n} B_i \le M \qquad S_1 = \sum_{i=n+1}^{T} Q_{ice}(i) \qquad 0.95S \le S_1 \le S \tag{14}$$

In the formula, S is the total amount of ice stored at night, RTh; B_i is dual-condition host's ice storage per hour, RTh; M is for the maximum capacity of the ice storage tank, RTh; n is ice storage time for the night, h; S_1 is the amount of ice melted during the day in the cooling cycle, RTh; T is cooling time for melting ice during the day, h; $Q_{ice}(i)$ is the amount of ice melt cooling supply of the ice storage tank, RTh.

(2) The sum of the main engine cooling (base load host and dual-condition host) and ice storage tank cooling should meet the cooling load demand of the energy station.

$$Q_{zl}(i) + Q_{ice}(i) = \sum_{hl=1}^{t} Q_{hl}^{load}(i) = Q_{nl}^{load}(i) \tag{15}$$

In the formula, $Q_{zl}(i)$ is the sum of the cooling capacity of the refrigeration host (base load host and dual-condition host) in i period, RTh; $Q_{hl}^{load}(i)$ is the cooling load demand of a user's cooling station, RTh; t is the number of user cooling exchange station in i period; $Q_{nl}^{load}(i)$ is energy station cooling load demand, RTh.

4.2 Example of hourly cooling load prediction of user cooling exchange station

The Longhu Tianjie user cooling exchange station that supplies cooling for commercial buildings was selected as an example for hourly cooling load forecasting. Firstly, the original sample data of the Longhu Tianjie user cooling exchange station from May 10, 2021, to September 14, 2021, with a total interval of 128 days at 13:00, were collected for data preprocessing. secondly, the influencing variables of hourly cooling load prediction were preliminarily screened as meteorological factors and historical cooling load, through correlation analysis, ten influencing variables were selected as input variables of the t-hour cooling load prediction. there is the outdoor temperature at time t (prediction), the outdoor temperature at time t-1 (prediction), the outdoor temperature at time t-2 (prediction), the relative humidity at time t (prediction), the relative humidity at time t-1 (prediction), the relative humidity at time t-2 (prediction), cooling load at time t of the previous day ~ four days before the previous day. Finally, 124 sets of hourly data at 13:00 will be collected to divide the dataset, of which 90 sets of data are the training set and 34 sets of data are the test verification set. the prediction error results of the Longhu Tianjie user cooling exchange station at 13:00 from June 21, 2021, to July 10, 2021, of three heat load prediction models based on BP, GA-BP, and GS-SVR are shown in Table 4. The average relative error of the predicted hourly cooling load based on the GA-BP model is 4.7%, which can meet the requirements of DHC-IES summer cooling operation according to engineering experience.

Table 4 Construction of three cooling load prediction models and prediction error results

Model name	Build model parameters	Maximum relative error	Minimum relative error	Average relative error
BP	The learning rate of the 10-4-1BP neural network model is 0.015, and the error target value is 0.0000001.	14.6%	0.6%	5.54%
GA-BP	The 10-4-1GA-BP neural network model has 44 weights, 5 thresholds, 49 coding lengths, 50 population sizes, 0.9Cross, 0.1 Mutation, 12 iterations, and 0.00873 training accuracy.	9%	0.3%	4.7%
GS-SVR	The input and output variables are the same as above when the time step is 0.1, the penalty parameter C is 194.01 and the kernel function variance g is 0.0118.	15.8%	0.4%	6.12%

4.3 Multi-objective optimization control example

This study takes the time-of-use electricity price and hourly cooling load prediction simulation values of an energy station in the summer of July 10, 2021, as an example, as shown in Table 5 and Table 6. The actual operation at night adopts scenario1 ice storage for 10 hours (21:00-23:00 in the flat section, 23:00-7:00 in the valley section) ice storage tank cooling, to compare and analyze the impact of different ice storage durations and cooling modes on the multi-objective optimal operation of cooling supply. In this study, different scenarios were designed, such as scenario2 ice storage for 10 hours of base load host cooling (21:00-23:00 in the flat section, 23:00-7:00 in the valley section), scenario3 ice storage for 8 hours of

ice storage tank cooling (23:00-7:00 in the valley section), and scenario4 ice storage for 8 hours base load host cooling (23:00-7:00 in the valley section). The NSGA-II algorithm was used to solve the Pareto optimal solution set of multi-objective optimization problems in different scenarios, and three target optimal solutions and night ice storage were screened out from the Pareto optimal solution set.

Table 5 Time-of-use electrovalency for energy station

Time	Time	Electrovalency （Yuan / kWh）
Peak segment	10:00-15：00；18:00-21：00	1.2710
Flat segment	7:00-10：00；15:00-18：00；21:00-23：00	0.7523
Valley segment	23:00-7：00	0.2849

Table 6 Hourly cooling load of energy station as of July 10, 2021

Time	0:00	1:00	2:00	3:00	4:00	5:00	6:00	7:00
Cooling load（RTh）	219	422	540	601	686	433	1707	6575
Time	8:00	9:00	10:00	11:00	12:00	13:00	14:00	15:00
Cooling load（RTh）	6093	6387	6110	5924	5758	6050	5965	6104
Time	16:00	17:00	18:00	19:00	20:00	21:00	22:00	23:00
Cooling load（RTh）	6407	4313	3600	2683	1782	1123	596	213

The multi-objective optimization control strategy using the NSGA-II algorithm is: During the night, according to the time-of-use electricity price, the dual-condition host started to store ice, and the base load host or ice storage tank cooling; During the day, the ice storage tank cooling and refrigeration host are used to jointly provide cooling load, ice storage tank cooling is used during peak hours of electricity consumption. and the refrigeration host is not opened, such as opening the refrigeration host to turn on the base load host first, followed by the dual-condition host. The refrigeration host should try to ensure that it operates in the energy-efficient stage (night duplex host >0.6, except for the night base load host cooling, the base load host >0.5) to ensure that the ice storage capacity of a cooling cycle is melted according to the operating constraints of 4.2.2. The NSGAII algorithm is used to solve the Pareto optimal solution set of multi-objective optimization problems in four different scenarios of the summer energy station ice storage system, as shown in Figure 3~Figure 6, corresponding to the three target optimal solutions and the amount of ice storage at night, as shown in Table 7. Compared with scenario1, scenario2 increases the daily operating cost by 0.5%, the energy loss rate is increased by 1.7%, and the CO_2 emission is increased by 0.8%. Compared with scenario1, scenario3 reduces daily operating costs by 13.5%, energy loss rate by 11.7%, and CO_2 emissions by 5.7%, while scenario4 reduces daily operating costs by 15.5%, energy loss rate by 9.8%, and CO_2 emissions by 3.8%. Therefore, scenario3 or scenario4 can be selected for optimal control in the actual operation control.

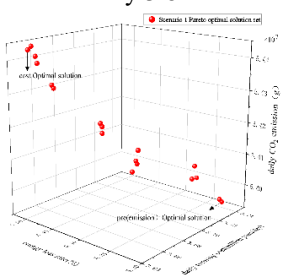

Figure 3: Scenario1 Pareto optimal solution set

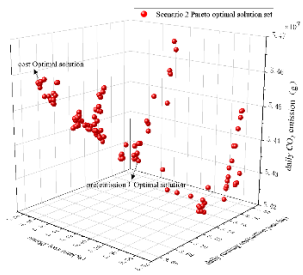

Figure 4: Scenario2 Pareto optimal solution set

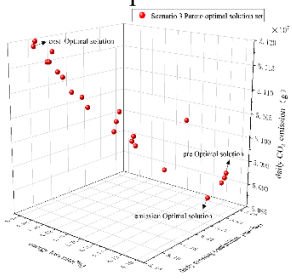

Figure 5: Scenario3 Pareto optimal solution set

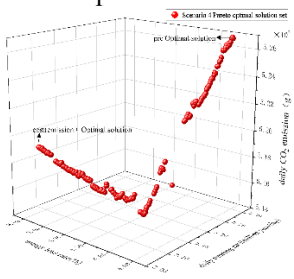

Figure6: Scenario4 Pareto optimal solution set

Table 7 Three optimal solutions and nighttime ice storage in four scenarios

	Pareto solution	Multi-objective optimization	Daily operating cost（million yuan/tian）	Energy loss rate（%）	CO_2 emission（g）	Amount of ice storage（RTh）
Scenario 1	18	$Cost$ Optimal solution	3.650	5.508	5.443×10^7	71008
		Optimal solution	3.737	5.320	5.395×10^7	67093
		$emission$ Optimal solution	3.737	5.320	5.395×10^7	67093
Scenario 2	89	$Cost$ Optimal solution	3.669	5.489	5.456×10^7	64021
		per Optimal solution	3.724	5.411	5.435×10^7	62349
		$emission$ Optimal solution	3.724	5.411	5.435×10^7	62349
Scenario 3	22	$Cost$ Optimal solution	3.157	4.876	5.119×10^7	59797
		per Optimal solution	3.253	4.705	5.093×10^7	56575
		$emission$ Optimal solution	3.241	4.718	5.088×10^7	56833
Scenario 4	333	$Cost$ Optimal solution	3.086	5.048	5.190×10^7	58327
		per Optimal solution	3.296	4.805	5.268×10^7	52901
		$emission$ Optimal solution	3.086	5.048	5.190×10^7	58327

5. CONCLUSION

DHC-IES is deeply integrated with information technology, and the supply-side and demand-side linkage response accelerates the process of China's "30·60" carbon peaking and carbon neutrality goals. This paper aims to solve the practical problems of DHC-IES engineering through digital transformation and provide useful guidance for the coordinated and optimal operation of the same type of DHC-IES. The main conclusions are as follows:

(1) the average relative error of hourly heat load prediction of user heat exchange stations based on the GS-SVR model is 3.04%, which can meet the requirements of DHC-IES winter heating operation according to engineering experience. through the calculation of four predicted feature sets of the secondary return water temperature of the user's heat exchange station, Set3 refers to the actual operation with the secondary return water temperature as the control target temperature and the average error value of the secondary return water temperature prediction is 0.08°C, and the operation management personnel can carry out the temperature operation management of the user's heat exchange station.

(2) The average relative error of hourly cooling load prediction of user cooling exchange stations based on GA-BP neural network is 4.7%, which can meet the requirements of DHC-IES summer cooling operation according to engineering experience. taking the time-of-use electricity price and hourly cooling load of the energy station on July 10, 2021, as examples, the NSGA-II algorithm is used to solve the multi-objective optimization Pareto optimal solution set for four different scenarios. The results showed that compared with scenario1 actual operation, scenario2 increases the daily operating cost by 0.5%, the energy loss rate is increased by 1.7%, and the CO_2 emission is increased by 0.8%. Compared with scenario 1, scenario3 reduces daily operating costs by 13.5%, energy loss rate by 11.7%, and CO_2 emissions by 5.7%, while scenario4 reduces daily operating costs by 15.5%, energy loss rate by 9.8%, and CO_2 emissions by 3.8%. Therefore, scenario3 or scenario4 can be selected for optimal control in the actual operation control.

REFERENCES

[1]ZHAO Yongqiang, HAO Jiacheng, ZHAO Na, et al. Energy storage demand, function and function mode of energy storage in energy Internet[J].Advanced Technology of Electrical Engineering and Energy,2018,37(02):68-75.

[2]Wang X K. Research and application of DHC-IES optimization operation with implicit cool/heat[D].Tianjin University of Technology, 2021.

[3]Lozano M A, Ramos J C, Serra L M. Cost optimization of the design of CHCP (combined heat, cooling, and power) systems under legal constraints[J].Energy,2010, 35(2):794-805.

[4]Tong Wei, Yan Xiuying, Jie Jun. Research on optimal control strategy and real-time control of ice storage system[J].Building Energy Efficiency,2007,35(200):1-3.

[5]Hengze, G. Evaluation of optimal control of active and passive building heat storage [J] International Journal of Thermology, 2004, 43 (2):173-183.

[6]ZHANG Feng, HOU Zhankui, LUO Yizhen. Optimal operation strategy of ice storage air conditioning system based on load forecasting[J]. Refrigeration and Air Conditioning,2020,20(09):65-70.

[7]SUN Yue, WU Qiong, LI Qifen, et al. Multi-objective operation optimization of ice storage system considering cost and energy consumption[J].Low Temperature and Superconductivity.2021,49(08):58-65.

[8]Ran Tong. Research on load prediction and energy-saving optimization of ice storage air conditioning system of an airport energy station[D].Xi'an University of Architecture and Technology, 2021.

[9]Li Ruiwen. Research on operation optimization of regionally integrated energy systems considering demand response[D].North China Electric Power University,2020.

[10]ZHENG Yang. Research on multi-time scale optimal operation of integrated energy system considering demand-side management[D].Beijing Jiaotong University, 2020.

[11]SUN Peng,GUAN Qi,FAN Yuanliang. Review of multi-energy system dispatching considering comprehensive demand response[J].Energy Conservation Technology,2019,37(217):476-480.

[12]Dergegieff. Research on source-load-storage collaborative optimization and benefit evaluation model of the integrated energy system in the park[D].North China Electric Power University,2020.

[13]Dong Dou. Optimal operation of regionally integrated energy system considering comprehensive demand response[D]. North China Electric Power University,2020.

[14]Xu Hang. Research on integrated response strategy in integrated energy system[D].Zhejiang University, 2019.

[15]Xu Fulu. Research on DHC-IES collaborative optimization considering electric heat demand response[D].Changsha University of Science and Technology, 2019.

[16]DUAN Xiaojian. Research on optimal control of district cooling system based on ice storage[D].South China University of Technology,2020.

The 18th International Symposium on District Heating and Cooling, September 3–6, 2023, Beijing, China

A new semi-analytic method for buoyancy-induced thermal stratification in hot water tanks

Chenghao Li[a*], Yunfei Bai[a], Wei He[b], Jihong Wang[a*]

[a] *School of Engineering, University of Warwick, Coventry, CV4 7AL, United Kingdom*
[b] *Department of Engineering, King's College London, London, WC2R 2LS, United Kingdom*
[*] *Corresponding author. jihong.wang@warwick.ac.uk*

ABSTRACT

Heat provision quality and thermal performance of a domestic hot water tank are closely linked to the degree of thermal stratification within stored water. Buoyancy-induced thermal stratification is dominant when a hot water tank is on standby cooling. Numerical approaches yield detailed yet accurate approximation on temperature evolution. However, these solvers estimate the temperature at a concerned location and time with known information of its neighbouring location and preceding time. This inherent nature of implicit iteration posts restrictions to wider applications of these numerical solvers in optimal study (like linear programming problems). This study bridges the gap by developing a semi-analytic method to estimate thermal stratification induced by buoyancy of hot water tanks without iterations. An explicit expression of water temperature as a function of standby time and tank height is analytically derived. By analogising natural convection as heat conduction that propagates from the tank bottom, the intractable nonlinear partial derivative equation (PDE) is decomposed into a linear PDE with convective boundary and an ordinary partial derivative equation, such that they can be easily solved stepwise. The compromised accuracy aroused from such an analogy is effectively compensated by synthetic thermal conductivity which is determined from validated numerical results. Results show the semi-analytic method satisfactorily approximates thermal stratification at different standby cooling durations. The effect of height-to-diameter ratios of tanks on stratification characteristics is numerically investigated and discussed. It is found that a constant synthetic thermal conductivity produces relatively accurate estimation when the geometry of a tank changes. Slight estimation discrepancies are shown at the lower part of the tank which can be further overcome by applying time-varying synthetic thermal conductivity. The developed semi-analytic method can efficiently estimate thermal stratification of hot water tanks in daily and seasonal applications, and its non-iteration feature enables a promising prospect in optimal research.

Keywords: Analytic method, Thermal stratification, Buoyancy, CFD

1. INTRODUCTION

Hot water tanks are one of the most commonly used sensible thermal energy storage technologies in water heating systems across domestic, industrial, and commercial sectors [1]. They serve to conserve heat and meet the heat demands in times of low supply. Hot water tanks can effectively facilitate the accommodation of renewable energy for the decarbonisation of the current heating system [2].

Water temperature is of great significance to performance evaluation for a domestic hot water tank as thermal comfort of users must be prioritised. When the water temperature is lower than the set point due to heat loss, auxiliary heaters (electric heating coil in most cases) must be switched on for temperature elevation. Moreover, lowered water temperature would also give rise to problems like bacteria growth [3]. It is therefore crucial to study the temperature evolution mechanism of hot water tanks. Uneven temperature distribution in a tank is constantly created caused by water circulation (injection and draw-off), and natural convection when the tank is on standby. Compared to warm water, cooled water is denser and tends to move downward driven by buoyancy force. The hot water tank is consequently thermally stratified. Thermal stratification describes the temperature gradient in storage medium, it acts as a barrier to hinder fierce cold-hot water mixing. This phenomenon is desirable when the availability of heat source is limited. For instance, in solar-assisted hot water production systems, freshly prepared hot water from the solar collector is injected to the top for a better stratification. Analysis shows that a well-stratified tank can improve energy efficiency of a heating system by 20% over a non-stratified tank [4]. Stratification can be artificially enhanced by structural specifications like diffusors and baffles, it also can be maintained by careful operations like reduced flow rates.

Thermal stratification modelling enables one to predict temperature conditions of a hot water tank. Circulation-induced stratification caused by fast perturbations like hot water injection is an advection-dominant process. Theoretical and experimental studies have confirmed that an apparent hot front can be well maintained in most flow conditions [5], [6].

Buoyancy-induced thermal stratification is, on the other hand, a slower process where heat conduction and convection play a non-negligible role [7]. When the tank is on standby, water near the tank walls emits heat to the environment because of imperfect insulation. Temperature drop gradually propagates inwards and causes small eddy flows by which the cooled water travels downwards and absorbs heat from the adjacent hot water [8]. Extensive research has been carried out to understand and mathematically describe the process. Fan et.al studied the water flow patterns due to standby cooling and correlated the relationship between flow velocities and temperature gradients [9]. Their follow-up research found out the correlation between heat flows with temperature gradients under various tank geometries [10]. Baeten et al developed and experimentally validated a one-dimensional model to approximate buoyancy-induced thermal stratification. The idea is to extract water from different layers with a prescribed distribution, to mix it with incoming water and re-enter the tank [11]. The distribution is derived from pre-validated numerical results and formulated with dimensionless numbers. A similar work done by Lago et.al focused on extending the application to other linear programming tools of such a method via smoothing the temperature distribution [12]. Other scholars studied in depth the boundary layers adjacent to side walls of a tank to describe the natural convection [7]. However, most of these numerical approaches are based on finite element method (FEM) in which the temperature at any point needs information of its neighboring points and preceding times. Despite higher accuracy in estimation results, the implicit iteration procedure associated with FEM-based models makes them difficult to incorporate with deterministic optimisers like linear programming. As a result, optimisation studies must idealise hot water tanks as either perfectly stratified or well-mixed. Prominent discrepancies in optimal results may arise if different degrees of stratification are assumed [13]. Non-iterative modelling approaches while keeping adequate accuracy require further investigations.

Analytic methods give exact solutions to the concerned equations governing the physical phenomenon. However, the complex interaction of convection and conduction relating to buoyancy flows makes it challenging to analytically solve the temperature function. In this work, a semi-analytic method is proposed to give an explicit expression of temperatures in the function of tank height and time. The nonlinear convection term is simplified as conduction with convective boundary conditions. Estimation accuracy is compensated by synthetic heat conductivity of water which is determined by validated numerical simulation results. Effects of tank geometry on temperature distribution are discussed and theoretically discussed.

2. METHODOLOGY

2.1. Problem description and its mathematical formulations

The semi-analytic method studies the temperature gradient in one direction, which has been justified to be accurate enough and computational lightweight over multi-dimensional models [14]. The cross sectoral schematic of the physical model of a hot water tank is shown in Fig. 1. Initially the tank is filled with hot water at temperature of T_i, heat loss occurs at the side wall and the bottom wall. Water omits less heat through top walls than other two parts and therefore the top surface is considered as adiabatic herein [9]. By assuming constant thermophysical properties of water, one-dimensional energy equation writes as follows:

$$\rho c_p \left(\frac{\partial T}{\partial t} + u \frac{\partial T}{\partial x} \right) = k \frac{\partial^2 T}{\partial x^2} - q_l \tag{1}$$

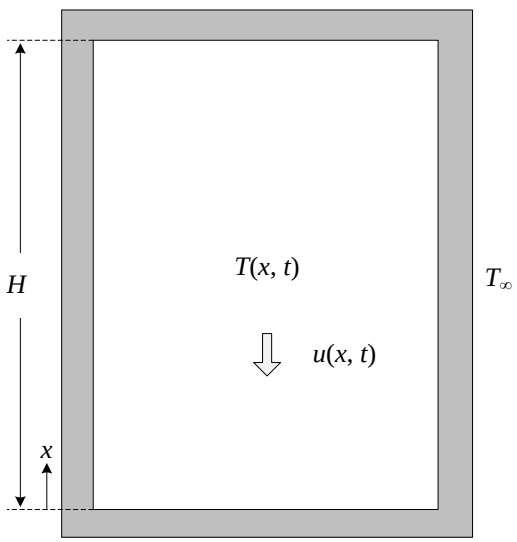

Fig. 1 Schematics of the physical model of a vertical hot water tank.

Where ρ is mass density, [kg/m^3], T is water temperature, [K], u is flow velocity, [m/s], c_p is heat capacity, [J/kg K], k is thermal conductivity, [W/m K], q_l is heat loss per unit volume, [W/m^3]. Eq.(1) is a second-order nonlinear partial derivative equation (PDE) in which velocity u varies with time and space. Such an equation is difficult to find out exact solutions. Here the equation is solved in two steps for an approximation solution.

2.2. A two-step semi-analytic solution to thermal stratification.

If the nonlinear term in Eq.(1) is omitted the PDE becomes a linear nonhomogeneous PDE, as referred in Eq.(2).

$$\rho c_p \frac{\partial T}{\partial t} = k_{syn} \frac{\partial^2 T}{\partial x^2} - q_l \tag{2}$$

Now the original problem is linearised if the coefficient is independent of time and space. The effect of convection is compensated by the coefficient k_{syn}, which in this study is called synthetic thermal conductivity. It has greater value than the material thermal conductivity because convection is stronger than particle movements. By this means, synthetic thermal conductivity is no longer a material property. The determination of k_{syn} is discussed later in section 3.2.

Eq.(2) is solved in two steps where heat loss through bottom wall and side wall are separately accounted for. The first step is to analogise natural convection as heat conduction with a cooling boundary (bottom). The second step is to account for heat loss through side walls using lumped capacitance method.

2.1.2. Step 1: Solution to heat conduction with convective boundary condition at the tank bottom

By considering heat loss through the tank bottom, the problem is rewritten as a second-order homogeneous PDE with convective boundary and initial conditions.

$$\begin{aligned} &\frac{\partial T}{\partial t} = \frac{k_{syn}}{\rho c_p} \frac{\partial^2 T}{\partial x^2} \text{ for } 0 < x < H, t > 0 \\ &\begin{cases} T(x,0) - T_i \\ h_b \left[T(0,t) - T_\infty \right] = -k_{syn} \dfrac{\partial T}{\partial x} \end{cases} \end{aligned} \tag{3}$$

Where h_b represents convective heat coefficient, [W/m^2 K], T_∞, T_i are ambient, initial temperature [K]. The solution of such problem is worked out in detail by Schneider [15], which writes as follows.

$$\frac{\theta(x,t) - T_i}{T_\infty - T_i} = 1 - \operatorname{erf}(X) - \left[\exp\left(\frac{h_b x}{k_{syn}} + \frac{h_b^2 \alpha t}{k_{syn}^2} \right) \right] \left[1 - \operatorname{erf}\left(X + \frac{h_b \sqrt{\alpha t}}{k_{syn}} \right) \right] \tag{4}$$

where $\theta(x,t)$ is the water temperature at position x and time t in step 1, [K]. α is the thermal diffusivity, [m^2/s]. $X = x \big/ \left(2\sqrt{\alpha t} \right)$, erf is the error function, $\operatorname{erf}(z) = \frac{2}{\sqrt{\pi}} \int_0^z e^{-t^2} \mathrm{d}t$ [16].

2.1.3. Step 2: Solution to heat loss through side walls using lumped capacitance method

In the second step, the heat loss through side walls is addressed by regarding the bulk water as a lumped capacitance. The problem is written as an ordinary derivative equation.

$$\frac{\mathrm{d}T}{\mathrm{d}t} = \frac{h_s A}{\rho c_p V} (T_\infty - T) \tag{5}$$

where h_s is the convective heat transfer coefficient, [W/m^2 K]. A is the surface area of the side wall, [m^2]. V is water volume inside the tank, [m^3]. The solution is obtained by applying separation of variables, and it is expressed as follows.

$$\frac{T(t) - T_\infty}{\theta(t) - T_\infty} = \exp\left(-\frac{h_s A \Delta t}{\rho c_p V} \right) \tag{6}$$

where Δt is the standby time, [s]. Here the water temperature obtained in step 1 substitutes the initial state in the solution in step 2.

2.1.4. Final solution

The mathematically intractable PDE as Eq.(2) has been decomposed step-wise, each of which is analytically derived. The final solution to water temperature is obtained by superposition of Eq.(4) and (6), which gives as follows.

$$T(x,t)=(T_i-T_\infty)\left\{1-\mathrm{erf}(X)-\left[\exp\left(\frac{h_b x}{k_{syn}}+\frac{h_b^2\alpha t}{k_{syn}^2}\right)\right]\left[1-\mathrm{erf}\left(X+\frac{h_b\sqrt{\alpha t}}{k_{syn}}\right)\right]\right\}\exp\left(-\frac{h_s A\Delta t}{\rho c_p V}\right)+T_\infty \tag{7}$$

Here two variables are introduced, $\varphi=1-\mathrm{erf}(X)-\left[\exp\left(h_b x/k_{syn}+h_b^2\alpha t/k_{syn}^2\right)\right]\left[1-\mathrm{erf}\left(X+h_b\sqrt{\alpha t}/k_{syn}\right)\right]$, and $\psi=\exp\left(-h_s A\Delta t/\rho c_p V\right)$. Rearranging Eq. (7), it gives the following concise form.

$$T(x,t)=\psi(t)\left\{\left[\left(1-\varphi(x,t)\right)\right]\cdot\left[T_i(x)-T_\infty\right]\right\}+T_\infty \tag{8}$$

Graphical interpretation of the two-step analytic method is shown in Fig. 2. The tank is at a uniform initial temperature, step 1 addresses heat conduction with negative heat flux imposed at the bottom consequently temperature profile bends at the bottom end. φ therefore denotes as the bending factor. Step 2 regards a lumped capacitance of the water in the tank that bears heat loss through the side wall. It shifts the temperature profile leftwards without changing its shape. So ψ is called the decay factor.

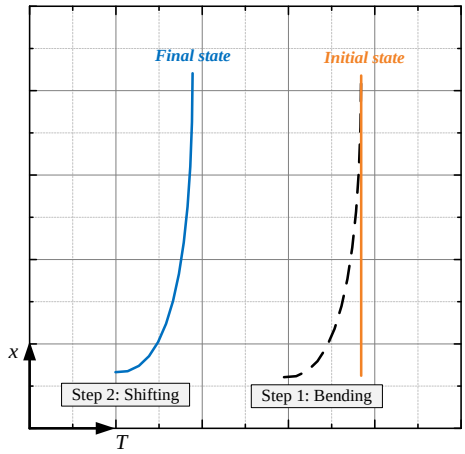

Fig. 2 Graphical interpretation of temperature evolution by the two-step analytic method.

With Eq.(8) one can explicitly get water temperature at any point and time with given information of tank geometry and external conditions. It greatly simplifies the calculation process compared to numerical solvers that rely on iterations and suffer from convergence issues. However, the accuracy of the two-step analytic method is compromised as temperature change caused by convection is represented by a single parameter. In an attempt to improve the accuracy of the analytic method, a numerical study is performed for identification of synthetic thermal conductivity.

2.2. Identification of synthetic thermal conductivity based on Computational Fluid Dynamics (CFD).

CFD is an effective and reliable tool to deal with sophisticated phenomena when experimental study is economically or technically infeasible. In the present work, CFD is used to identify synthetic thermal conductivity for the given cases. Numerical results are firstly validated against experiments from existing publications, and thereafter numerical results serve as trustworthy benchmark for parameter identification.

2.2.1. Problem description and simulation settings

A vertical hot water cylinder is studied here. Subsidiary parts other than water domain are neglected for convenience. Schematics of physical geometry of the tank is shown in Fig. 3 which is displayed in 2D axisymmetric coordinates. The volume of the tank is fixed at 150 l. The height-to-diameter ratio (called aspect ratio hereafter) is the main geometric feature that varies for different volumes. It is set as 5 in this section, its effect is discussed in detail in section 3.2.

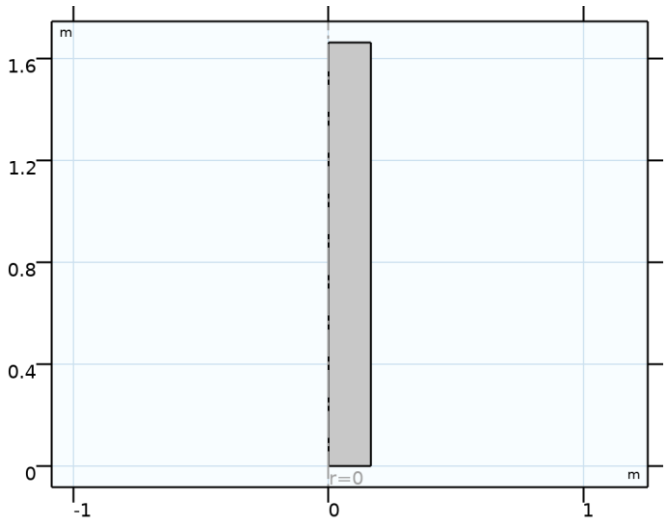

Fig. 3 2D axisymmetric geometry of 1 150-l hot water tank with aspect ratio of 5.

Reasonable assumptions are made to simplify the simulations. (1) Water is impressible; (2) laminar flow in the water domain; (3) no viscous dissipation; (4) constant heat capacity of water. Mathematical equations that govern the conservation of mass, momentum, and energy in the sense of transience are written as follows.

$$\frac{\partial \rho}{\partial t}+\frac{\partial(\rho u)}{\partial z}+\frac{1}{r}\frac{\partial(\rho r v)}{\partial r}=0 \tag{9}$$

$$\begin{aligned}\frac{\partial(\rho u)}{\partial t}+\frac{\partial(\rho u u)}{\partial z}+\frac{\partial(\rho v u)}{\partial r}&=-\frac{\partial p}{\partial z}+\mu\left(\frac{\partial^2 u}{\partial z^2}+\frac{1}{r}\frac{\partial u}{\partial r}+\frac{\partial^2 u}{\partial r^2}\right)+\rho g\\ \frac{\partial(\rho v)}{\partial t}+\frac{\partial(\rho u v)}{\partial z}+\frac{\partial(\rho v v)}{\partial r}&=-\frac{\partial p}{\partial z}+\mu\left(\frac{\partial^2 u}{\partial z^2}+\frac{1}{r}\frac{\partial v}{\partial r}+\frac{\partial^2 v}{\partial r^2}-\frac{v}{r^2}\right)\end{aligned} \tag{10}$$

$$c_p\left[\frac{\partial(\rho T)}{\partial t}+\frac{\partial(\rho u T)}{\partial z}+\frac{\partial(\rho v T)}{\partial r}\right]=k\left(\frac{\partial^2 T}{\partial z^2}+\frac{1}{r}\frac{\partial T}{\partial r}+\frac{\partial^2 T}{\partial r^2}\right) \tag{11}$$

Thermal insulation boundary condition is set at the top surface of the tank. Convective heat transfer condition is imposed at the side wall, the bottom and top wall, which are expressed in Eqs. (12) and (13)).

$$-k\frac{\partial T}{\partial z}=h_b\left(T_\infty-T\right) \tag{12}$$

$$-k\frac{\partial T}{\partial r}=h_s\left(T_\infty-T\right) \tag{13}$$

Heat transfer coefficients vary with insulation conditions, external environment, coefficients for the top, bottom, and side walls are set as 0.81, 1.52, and 1.81 W/(m^2·K), which is derived from experiments [9]. The described problem is implemented and solved using COMSOL Multiphysics. Other parameters used in the simulations are listed in Table 1. Independence of mesh and timestep is studied and the main results are presented in Table 1.

Table 1 Parameters used in the COMSOL Multiphysics 6.0.

Parameter [Unit]	**Value**
Initial temperature [°C]	80
Ambient temperature [°C]	15
Iteration tolerance [-]	10^{-4}
Number of elements [-]	16095
Timestep [s]	2
Simulation horizon [h]	24

3. RESULTS AND DISCUSSIONS

3.1. Validation of CFD results against experiment data

The buoyancy-induced thermal stratification is experimentally investigated on a 150l water tank with the aspect ratio of 5 in [9]. Water temperatures were measured with thermocouples placed along the height direction. In this section, the experimental measurements are used to validate the numerical results. Fig. 4 illustrates the comparison of numerical results and experiment data at different standby durations. Clear thermal stratifications in both experiments and simulations are observed where water close to the bottom is cooler than that near the top. Thermocline, referring to the location at which the steepest temperature gradient occurs, gradually moves upwards with the proceeding of standby. Moreover, the entire water domain bears heat loss. The simulation results generally have good alignment with the experimental measurements with the maximum relative error of 5.6%. The simulations slightly overestimate the water temperature near the bottom as stratification builds up. This parallels the issue observed in other research in which the authors' conjectures this is caused by variable ambient temperature, mains water leakage, etc. [9]. The experimental validation justifies that numerical simulations are accountable to reproduce thermal stratification caused by buoyant force during standby cooling. Numerical simulations are therefore served as benchmark for the later parameter identification.

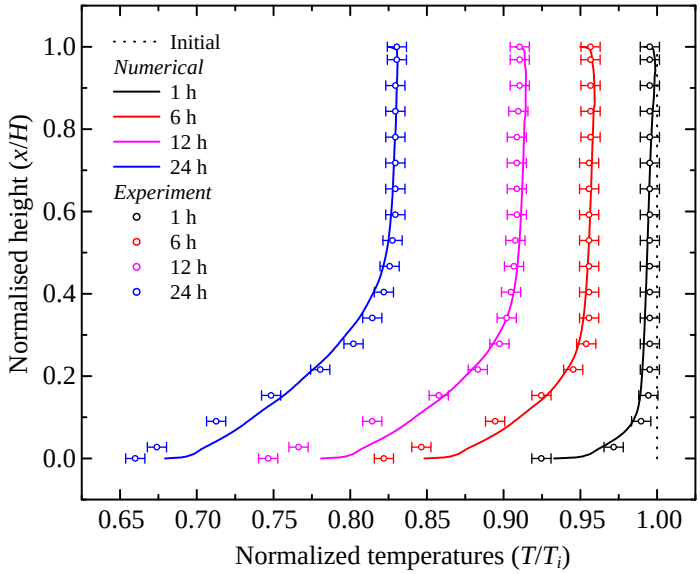

Fig. 4 Validation of CFD results against experimental measurements at different standby durations. The aspect ratio of the tank is 5. Measurement uncertainty is 0.5 K.

3.2. Synthetic thermal conductivities under different aspect ratios.

Unlike thermal conductivity that reflects the ability of a material to conduct heat due to particle vibrations and movements, synthetic thermal conductivity also includes the effect of natural convection. It is physically counterintuitive, however mathematically valid. Synthetic thermal conductivity is a critical component that influences the estimation accuracy of the two-step analytic method. In this section identification of synthetic thermal conductivity is performed.

Although the intensity of convection is susceptible to a number of factors, existing research has pointed out that aspect ratios of the tank is primarily influential to the degree of stratification [7], [17]. Conclusions drawn from the research reveal that the greater the aspect ratio, the more evident the stratification. As suggested in [6], stratification becomes less affected by aspect ratio when it is lesser than 3. Therefore in the study aspect ratios of 3 and 5 are investigated. The rest geometry parameters are in line with those in the previous section. Synthetic thermal conductivity is identified using trial and error until the best agreement is reached.

Fig. 5 shows the analytic solutions and simulation results of a 150-l tank after standby cooling of 6,12, 18, and 24 hours. It is seen that the two-step analytic method can well describe the degree of thermal stratification and heat loss during a standby cooling process. The temperature gradient is greater as the cooling continues, and the thermocline gradually moves to the upper part of the tank. When the aspect ratio decreases, it is found that the temperature profile becomes flatter, in other words, the water is less thermally stratified. This phenomenon coincides with existing findings from the cited literature [7], [17]. Such an effect can be theoretically explained by Grashof number, which is a dimensionless ratio of buoyant to viscous force in natural convection. In the case of vertical plates, it writes as $Gr = g\beta\Delta TL^3/\nu^2$. As such, the intensity of buoyant force is positively proportionate to length of the cooling surface, referring to the tank height here. For a slim and tall tank, the natural convection is therefore more intense, and thermal stratification is more prominent.

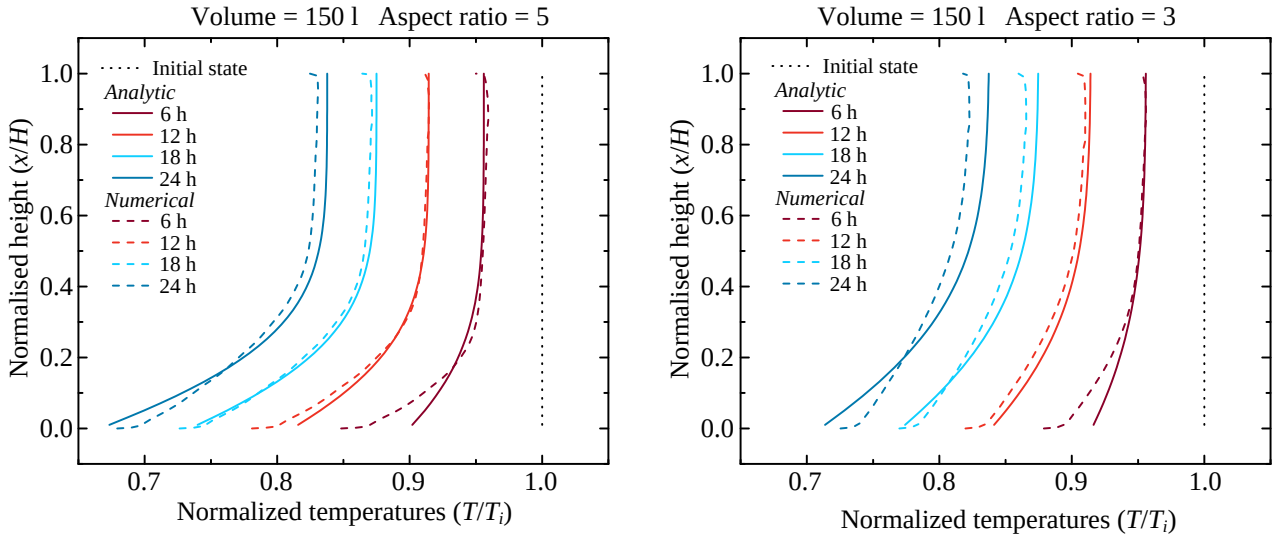

Fig. 5 Comparison of the analytic solutions and simulation results in the case of aspect ratio being 5 (left) and 3 (right). The synthetic thermal conductivity is set as 20 W/m/K in both cases.

The synthetic thermal conductivity is manually set as 20 W/(m·K) for the best approximation. Though the analytic method in general yields satisfactory precision at the upper body of the tank, estimation discrepancies are observed near the bottom especially for the 6-hour curve. This is because the strength of natural convection changes over time at the bottom region. Fig. 6 presents the streamline patterns on the axisymmetric plane after standby cooling of 6, 12, 18, 24 hours. The color palette indicates flow velocities. It is implied from the streamline density that the intensity of natural convection at the upper part of the tank is constant throughout the standby whereas convection near the bottom is weaker as the standby goes on. This explains the discrepancies by applying a time-independent synthetic thermal conductivity to the two-step analytic method.

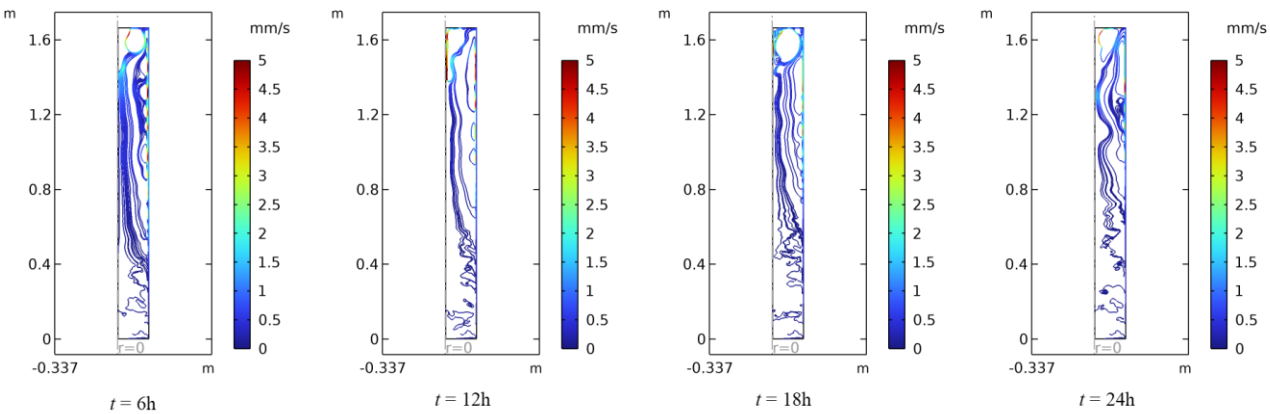

Fig. 6 Streamline patterns on the axisymmetric plane at time of 6, 12, 18, 24 hours (from the left to right). The aspect ratio of the tank is 5. Color rendering implies the flow velocities.

4. CONCLUSION

Hot water tanks are gradually thermally stratified when they are on standby for a certain time. In the context of domestic heating, the resultant temperature degradation jeopardies heat provision quality and maybe leads to other health and safety issues. There is a lack of modelling approach to give realistic thermal stratification without iterations. In summary, this work presents a semi-analytic method to bridge this gap where an explicit expression of water temperature is derived analytically. Natural convection caused by buoyancy is regarded as heat conduction developing from tank bottom as a physical analogy. Synthetic thermal conductivity is introduced and determined with numerical simulations for improved estimation accuracy. The developed method yields adequately accurate temperatures at any height and duration of standby cooling without iterations, it creates a notable opportunity to improve computation efficiency and optimisation quality for energy systems where buoyancy-induced thermal stratification in hot water tanks is significant. Further work needs to be conducted in terms of estimation robustness in different conditions, and the application in deterministic optimisation,

ACKNOWLEDGEMENT

This research was supported by the Engineering and Physical Sciences Research Council (EPSRC) of United Kingdom [grant number EP/W027372/1]. The authors would also like to acknowledge the support from the Chancellor's International Scholarship, University of Warwick.

REFERENCES

[1] Fayaz Hussain, M. Zillur Rahman, Ashvini Nair Sivasengaran, M. Hasanuzzaman. Energy storage technologies, in *Energy for Sustainable Development: Demand, Supply, Conversion and Management*, Elsevier Inc., 2019, 125–165.

[2] G. Barone *et al.* Solar Hot Water Heating Systems. *Compr. Renew. Energy, Second Ed. Vol. 1-9* 2022; 1–3:463–500.

[3] Yichi Zhang, Pär Johansson, Angela Sasic Kalagasidis. Applicability of thermal energy storage in future low-temperature district heating systems – Case study using multi-scenario analysis. *Energy Convers. Manag.* 2021; 244:, May:

[4] N K Ghaddar. STRATIFIED STORAGE TANK INFLUENCE ON PERFORMANCE OF SOLAR WATER HEATING SYSTEM TESTED IN BEIRUT. *Renew. energy* 1994; 4:, 8:911–925.

[5] Y. M. Han, R. Z. Wang, Y. J. Dai. Thermal stratification within the water tank. *Renew. Sustain. Energy Rev.* 2009; 13:, 5:1014–1026.

[6] Zalman Lavan, James Thompson. Experimental study of thermally stratified hot water storage tanks. *Sol. Energy* 1977; 19:, 5:519–524.

[7] Yakai Bai, Ming Yang, Zhifeng Wang, Xiaoxia Li, Longfei Chen. Thermal stratification in a cylindrical tank due to heat losses while in standby mode. *Sol. Energy* 2019; 185:, December 2018:222–234.

[8] Yogender Pal Chandra, Tomas Matuska. Stratification analysis of domestic hot water storage tanks: A comprehensive review. *Energy Build.* 2019; 187:110–131.

[9] Jianhua Fan, Simon Furbo. Buoyancy driven flow in a hot water tank due to standby heat loss. *Sol. Energy* 2012; 86:, 11:3338–3349.

[10] Jianhua Fan, Simon Furbo. Thermal stratification in a hot water tank established by heat loss from the tank. *Sol. Energy* 2012; 86:, 11:3460–3469.

[11] Brecht Baeten, Thomas Confrey, Sébastien Pecceu, Frederik Rogiers, Lieve Helsen. A validated model for mixing and buoyancy in stratified hot water storage tanks for use in building energy simulations. *Appl. Energy* 2016; 172:217–229.

[12] Jesus Lago, Fjo De Ridder, Wiet Mazairac, Bart De Schutter. A 1-dimensional continuous and smooth model for thermally stratified storage tanks including mixing and buoyancy. *Appl. Energy* 2019; 248:, October 2018:640–655.

[13] A. Campos Celador, M. Odriozola, J. M. Sala. Implications of the modelling of stratified hot water storage tanks in the simulation of CHP plants. *Energy Convers. Manag.* 2011; 52:, 8–9:3018–3026.

[14] Eberhard Markus Kleinbach, W. A. BECKMA, S. A. KLEIN. Performance Study of One-Dimensional Models for Stratified Thermal Storage Tank. *Sol. Energy* 1993; 50:, 2:155–166..

[15] P.J.Schneider. *Conduction Heat Transfer*. Reading, MA: Addison-Wesley Publishing Company, 1955.

[16] L C Andrews. *Special Functions of Mathematics for Engineers*. SPIE Optical Engineering Press, 1998. [Online]. Available: https://books.google.co.uk/books?id=2CAqsF-RebgC

[17] Burak Kurşun, Korhan Ökten. Effect of rectangular hot water tank position and aspect ratio on thermal stratification enhancement. *Renew. Energy* 2018; 116:639–646.

Optimization Study of Solar Heating System with Coupling of Water and PCM Thermal Storage

Q Q Gu[a], J L Zhao[a*]

[a] *Dalian University of Technology, Dalian, 116024, China*
[*] *J L Zhao. zhaojinling@dlut.edu.cn*

ABSTRACT

In view of the common problems of low heat storage density and serious heat loss in existing solar heating systems with seasonal heat storage based on apparent heat storage, a new type solar heating system with coupling of water and PCM thermal storage (SHS-WPTS) is proposed. The system uses long-term water pit thermal storage and short-term phase change water tank to realize coupled heat storage, and two system forms are set up in series and parallel according to the connection method of the thermal storage device; based on the TRNSYS platform, a numerical model of the system's annual operating performance is established, and the correctness of the numerical model is verified by actual measurement and experimental data. The changes in the heat storage temperature are obtained through simulation. In addition, a solar heating system that uses long-term water pit thermal storage and short-term water tank is set up as a control group for comparative analysis, and the advantages of phase change water storage tank in SHS-WPTS in terms of enhanced heating stability and efficient use of solar energy are verified. The annual solar collector efficiency, heat storage efficiency and solar fraction of the series system have increased by 1.52%, 3.52%, 5.46%.Finally, comparing and analyzing the series and parallel systems, it is concluded that the series system has the best performance. The research results provide theoretical and technical reference for the application of solar heating system with seasonal thermal storage.

Keywords: Seasonal heat storage, phase change heat storage, solar heating, TRNSYS simulation

1. INTRODUCTION

Solar energy is a kind of renewable and clean energy, which has the advantages of rich reserves, pollution-free and universality, but it also has the problems of low energy flow density and uneven seasonal distribution. To solve this problem, research on solar heating systems using seasonal heat storage technology has been carried out at home and abroad. Most of the large-scale projects in operation use water as the heat storage medium in the form of apparent heat storage [1]-[4]. The principle of apparent heat storage is simple, but there are disadvantages such as low energy storage density and large temperature fluctuations. Its volume and footprint are large, and the heat loss is also large, and there are certain requirements for building pressure [5]. The heat storage efficiency, heat collection efficiency, and solar fraction of the operating system all have room for further improvement [6].Compared with apparent heat storage, phase change heat storage has high energy density and small temperature fluctuations. It can reduce the volume and heat dissipation loss of the heat storage device, which is conducive to the stable operation of the heating system. Therefore, many researchers use phase change heat storage instead of water tank heat storage [7]-[11].However, due to the low thermal conductivity, low phase transition enthalpy and flammability of phase change materials, as well as the insufficient long-term thermal stability of phase change materials due to corrosion, supercooling and phase segregation [12], practical applications are limited. At present, large-scale and long-term latent heat storage is still in the experimental stage, and existing applied research is mainly used for short-term storage [13].

In this study, a new type of solar heating system with coupling of water and PCM thermal storage (SHS-WPTS) is proposed. The system uses a seasonal water pit and a short-term phase change water tank to realize coupled heat storage. According to the connection method of the phase change water tank and the water tank, it is divided into two system forms: series and parallel. According to their respective hot water storage temperature, they cooperate with each other to adjust. Taking an actual building as an example, the TRNSYS software simulates the operation and verifies the operating characteristics of the new system, and at the same time verifies that the addition of the phase change water tank is conducive to improving the stability of the system and the energy efficiency of the system.

2. METHODOLOGY

2.1. SHS-WPTS system form

The structure of SHS-WPTS is divided into solar collecting subsystem, heat storage subsystem, heat supply subsystem and heat consumption subsystem. The solar collecting subsystem includes a collector part; The heat storage subsystem includes a short-term phase change heat storage tank and a long-term water pit. According to the different connection forms of the components of the heat storage subsystem, two distinctive design schemes of series and parallel are provided. The heating

subsystem is divided into three parts according to the different outlet temperature, including the direct heating part, the heat exchanger part, and the water source heat pump auxiliary heating part. Figure 1 show the design diagrams of the two systems.

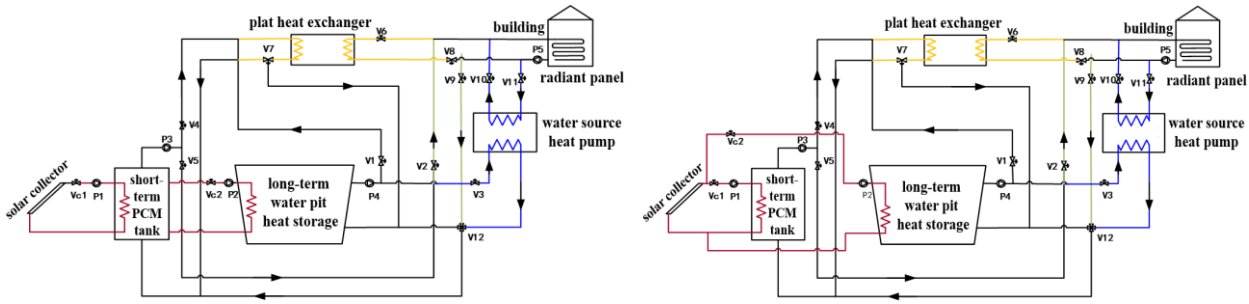

(a) Series SHS-WPTS (b) Parallel SHS-WPTS

Figure 1. Schematic diagram of SHS-WPTS

2.2. Design of the operating modes and adjustment methods of system

According to the designed series SHS-WPTS and parallel SHS-WPTS, the control modes of heat storage and heating operation are set separately. Through the electric valve V_{c1} and the hot water collection pump P_1, the phase change water tank heat storage mode is opened and closed, and the water tank heat storage mode is opened and closed through the electric valve V_{c2} and the water tank hot water collection pump P_2.For parallel SHS-WPTS, since the two heat storage devices are connected in parallel, the heat collection cycle does not affect each other, and can be controlled separately. The water temperature T_H at the outlet of the collector is controlled, and T_H is divided into three temperature intervals: high temperature, medium temperature and low temperature. The temperature range of the medium temperature range is calculated according to the phase change temperature of the phase change material. The opening of the phase change water tank and the pool heat storage mode is divided into two situations according to the heating period and the non-heating period: in the non-heating period, when the high temperature and low temperature periods meet the heat storage conditions, the pool will give priority to heat collection; in the medium temperature period and the heat storage conditions are met, the phase change water tank will give priority to heat collection; during the heating period, the heat collected by the collector is only stored in the short-term phase change hot water storage tank.

References to system operation adjustment methods[14],[15].Set up 3 different heating modes, choose 40℃~60℃ as the outlet temperature range of the heat source for direct heating. When T_g is higher than 60℃, a plate heat exchanger is used for cooling; when T_g is lower than 40℃, a water source heat pump is used to assist in heating.

2.3. Construction of TRNSYS model of SHS-WPTS

The main feature of TRNSYS simulation program is modular instantaneous dynamic simulation. The new system proposed in this paper mainly includes solar heat collection module, heat storage module, terminal heating module, valve module, control module, etc. The output end of the module is successively connected with the input end of another module according to the system composition. The TRNSYS simulation platform of series and parallel SHS-WPTS is constructed. Figure 2 shows the simulation model of parallel SHS-WPTS.

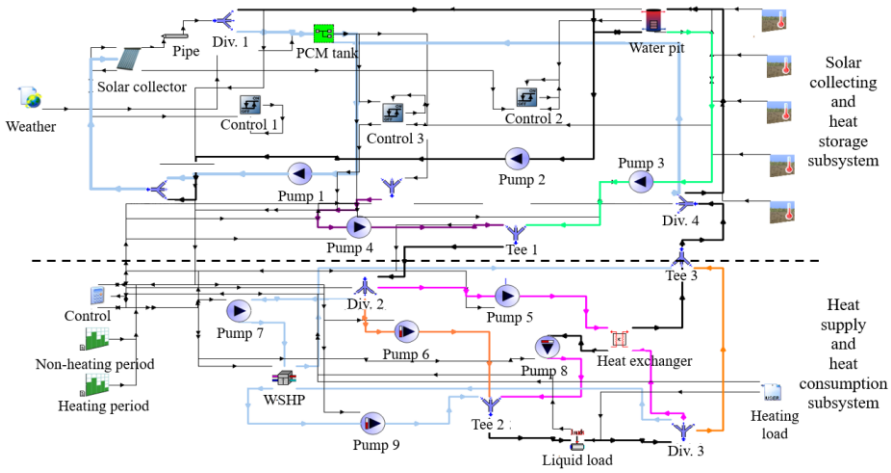

Figure 2. TRNSYS simulation system of the new parallel SHS-WPTS

2.4. Verification of the simulation model of SHS-WPTS

Because there is no practical project using SHS-WPTS at home and abroad, the acquisition of measured and experimental data has limitations. To verify the correctness of the system construction and module setting of the TRNSYS model. For the long-term and short-term heat storage devices of the new system, a solar heating system with seasonal pit storage and a phase change heat storage system are constructed respectively to verify the two systems. The measured and experimental data in relevant literatures are compared with the simulation results, and the relative deviation is used as the analysis index. The relevant calculation is shown in the following formula.

For SHS-WPTS, the measured object is a club in Shandong Province in the literature [16]. The system form is consistent with the form of the series solar cross-season heating system in this study. According to the literature, the relevant parameters of the collector, water tank, sink and other components are set, and the measured system is compared with the numerical simulation model. The simulation results in Figure 3 can better reflect the changes in the water temperature of the seasonal pool of key heat storage components in the actual project. The measured data are more consistent with the trend of the simulation results, and the values are relatively similar. The maximum relative deviation is 11:00 on December 1st, the simulated temperature is 27.49℃, the measured data is 26.15℃, and the maximum relative deviation is 5.13%.The average difference within three days was 0.82℃, and the average relative deviation was 3.14%.Secondly, during the simulation verification process, no errors in the water temperature, heat, flow rate, etc. output of each loop were found, and the simulation results were in line with the actual engineering laws. Since the pipeline loss in the model is ignored, there are also differences between the actual system operation mode and the model, which is the main reason for the deviation.

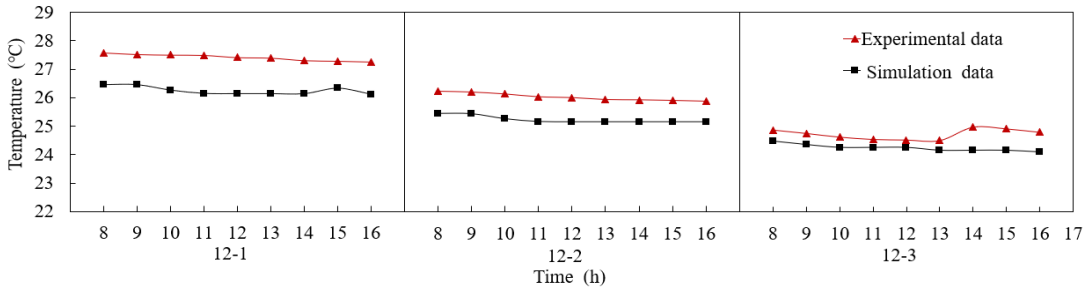

Figure 3. Comparison of simulated and measured mean temperature of the water pit

For the phase change water tank heat storage and exothermic system, the experimental object in the literature [17] is a cylindrical barrel design with built-in phase change material. The water flows through the heat transfer coil and the phase change material for heat transfer, which is consistent with the structure of the existing Type1334 phase change module in this study. Construct a TRNSYS model consistent with the experimental system, set the heat storage condition to 83℃, 1.4m^3/h, and the exothermic condition to 35℃, 1.3m^3/h, and obtain the simulation results of the heat storage process and the exothermic process to compare with the experimental results as shown in Figure 4.This simulation is more consistent with the trend of TRNSYS simulation results. The maximum difference between the two in the heat storage process is 2.03℃, the average difference is 0.49℃, the maximum relative deviation is 2.10%, and the average relative deviation is 0.69%.The maximum difference between the two in the exothermic process is 4.40℃, the average difference is 2.06℃, the maximum relative deviation is 5.34%, and the average relative deviation is 3.32%.There is a certain deviation between the average temperature simulation of the phase transition water tank during the heat storage and exothermic processes and the measured data. The analysis reasons are as follows: the heat transfer loss to the environment is ignored in the model, and the maximum relative deviation of the heat storage and exothermic processes numerically is within the maximum allowable deviation range.

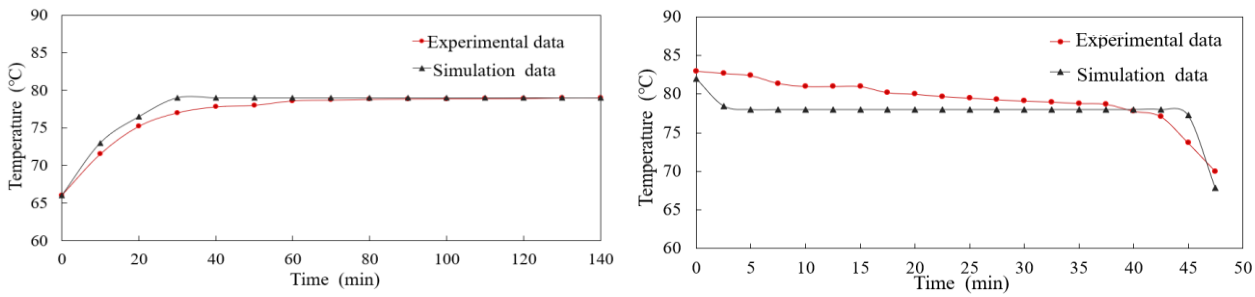

(a) Charging process (b) Discharging process

Figure 4. Comparison of simulated and measured temperature of PCM tank in different process

In summary, the accuracy of the constructed models of seasonal water storage heating system and phase change tank heat

storage and heat release system is verified. The results prove to a certain extent that the system construction and control strategies of the TRNSYS simulation model established in this study are reasonable and dependable.

3. CASE STUDY

The research object of this paper is a residential community in Dalian City, which has twelve buildings with a total heating area of 24,360m^2[18]. The heating period is from November 5 of the current year to April 5 of the next year, 152 days in total. The DeST-H is used to simulate the heat load of the continuous heating system, and the detailed climate data for the simulation comes from the typical meteorological year data of Meteonorm 8 [19]. The simulation results show that the maximum heat load is 860.84kW, and the total heat load during the heating period is 3.95×10^{3}GJ. The outdoor temperature range is [-13℃, 22℃].

Based on the simulated heat load results and the design basis of component parameters in the literature [14], the initial parameters of SHS-WPTS in series and parallel in a cell in Dalian are calculated, which are listed in Table 1.

Table 1. SHS-WPTS initial parameter design table

Component	Design parameter unit	Design parameter	value
	Intercept efficiency	%	70
Collector	Collector area	m^2	3270
	Water tank volume	m^3	1200.00
	PCM volume ratio	%	20.00
PCM tank	Melting temperature	℃	45.00
	Enthalpy of PCM	kJ/kg	220.00
	Volume	m^3	15000.00
Water pit	Height	m	10.00
Heat exchanger	Heat transfer coefficient	kW/（m^2·℃）	3.00

4. RESULTS AND DISCUSSION

To better analyze the effectiveness of the series and parallel solar heating system, which uses water pit and water tank for heat storage (SHS-PTTS) is set as the control group. The data of heat collection, heat storage, heat supply and water supply temperature of the above series-parallel system are compared and analyzed, and the advantages of the new system in enhancing heat supply stability and utilizing solar energy efficiently due to the use of phase change heat storage tank are verified.

4.1. Analysis of the operation characteristics of the system

Figure 5 is a diagram of the annual outlet temperature change of the heat storage device of the series system. During the heat storage period, the average temperature of the long-term hot water pit rose from the initial 10℃ to 66.63℃. At the beginning of the heat storage season from April 5th to June 5th, the temperature of the PCM tank failed to reach the phase change point. The phase change material is solid. Due to the heat storage effect of the PCM tank, the temperature of the water body began to rise to 45℃, and the liquid phase rate of the phase change material reached 1 on June 16th. Liquid distribution. During the heating period, with the reduction of effective heat collection and the increase of heat load demand, the temperature of the PCM tank gradually decreases, and the temperature drops to 59.47℃ by the end of the heating period. Among them, in February and March, due to the large heat load demand, the outlet temperature of the long-term water tank does not meet the heating conditions. The heating is provided by the short-term PCM tank. The temperature of the device drops rapidly to the lowest point of 38.29℃, and the phase change material below the freezing point begins to phase transition and is distributed in a two-phase state. Finally, at the end of the heating, the demand for heating decreases, and the temperature of the PCM tank rises and is distributed in a liquid state.

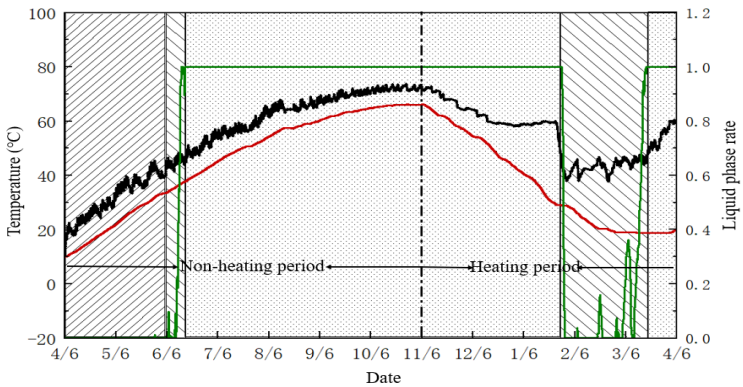

PCM tank temperature Water pit temperature Liquid phase rate
PCM solid state PCM two-phase state PCM liquid state

Figure 5. The outlet temperature of the series SHS-WPTS heat storage device changes throughout the year

Figure 6 shows the change of the annual outlet temperature of the parallel system and the parallel heat storage device throughout the year. During the heat storage period, the temperature of the pool continues to rise to 68.98℃. During the heating period, the temperature of the pool continues to drop to 23.40℃ at the end. The heat storage of the PCM tank is only carried out in the medium temperature range [48℃, 50℃] in the late non-heating period. The heat storage is carried out from October 6th to November 5th, and the heat storage begins until October 14th. The PCM tank is in significant heat storage, so the temperature rises relatively quickly. After 118h, the temperature of the PCM tank begins to rise to 45℃, the phase change material is in the two-phase zone, and the average temperature rises very slowly, basically around the melting point of the phase transition. After that, on February 3, the average temperature of the PCM tank began to rise rapidly. At this time, the latent heat storage ended and the liquid phase apparent heat storage stage was entered. The average temperature of the PCM tank reached the highest value of 59.78℃.Then it enters the heating period, and at the beginning, the liquid phase is also pyro thermic, and the PCM temperature drops faster. It can be seen from the slope of the curve that the heat release process is faster than the heat storage process. The latent heat release stage was only maintained for 44h, and the change was not obvious. Then the temperature of the phase transition water tank began to drop sharply again, and it entered the stage of significant heat exothermic. Finally, on February 16, the temperature of the phase transition water tank dropped to 30.71℃, and the heating conditions were not met. Heat storage began, until the temperature at the end of the heating rose to 67.83℃.

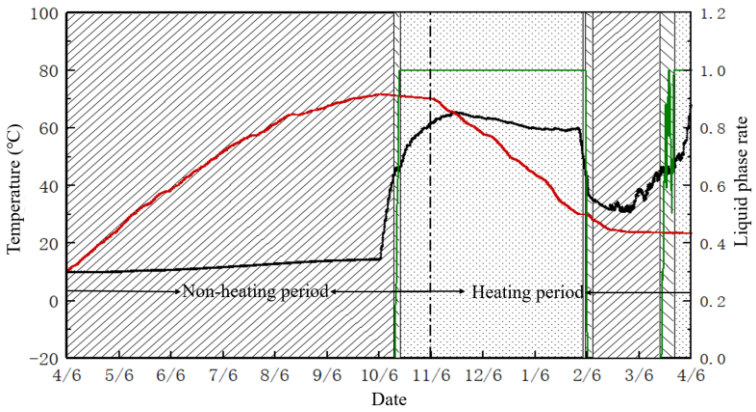

PCM tank temperature Water pit temperature Liquid phase rate
PCM solid state PCM two-phase state PCM liquid state

Figure 6. The outlet temperature of the parallel SHS-WPTS heat storage device changes throughout the year

4.2. Comparative analysis of the annual operation results of SHS-WPTS and SHS-PTTS

The data in Table 2 show that the heat storage of the PCM tank and the pool in the series display dual storage system has increased by 334.36GJ and 108.73GJ respectively compared to the series display dual storage system. If the same heat is stored as the PCM tank, the volume of the ordinary water tank will need to be increased by 1137m^3; if the series display dual storage system needs to obtain the same heat storage as the pool added to the PCM tank system, calculated based on a temperature rise of 70℃, the volume of the pool needs to be increased by 369m^3, and the initial investment in the corresponding series display system will cost more. 1.035 million yuan. The cumulative total heat collection and heat supply of the series latent dual storage system also increased by 81.65GJ and 156.46GJ respectively compared to the ordinary water storage system, and the total power consumption was reduced by 9.71% compared to the ordinary water tank.

Table 2. Statistics on heat collection, heat storage, heat supply and power consumption of series systems

System	Serial SHS-WPTS		Serial SHS-PTTS	
	PCM tank	Water pit	Water tank	Water pit
Total heat collection (GJ)	5441.01		5359.36	
Total heat storage (GJ)	4747.39	3892.55	4413.03	3783.82
Total heat supply (GJ)	663.97	2802.51	595.83	2714.19
Total power consumption	986.22		1081.99	

In the parallel system, as shown in the data in Table 3, the cumulative heat storage and heat supply of the apparent dual storage system is 121.90GJ and 207.59GJ more than that of the apparent dual storage system. The corresponding temperature rise is calculated at 70℃. The water tank and pool of the parallel display system need to be increased by 43m^3 and 372m^3, and the initial investment will cost 182,000 yuan more. Due to the addition of the PCM tank system, the operation is more stable, the start and stop of the heat pump is reduced, and the power consumption is reduced by 45GJ.Compared with the

series apparent latent dual storage system, taking into account the fact that the PCM tank of the parallel apparent latent dual storage system stores heat in a significant heat manner during the non-heating period, the advantages of latent heat storage are not fully utilized, and the heat storage in the water tank is stopped during the non-heating period, and the surrounding environment will produce heat loss. The cumulative heat storage and cumulative heat supply of the parallel system in parallel are reduced by 4.76% and 4.28% respectively compared with the series.

Table 3. Statistics on heat collection, heat storage, heat supply and power consumption of parallel systems

System	Parallel SHS-WPTS		Parallel SHS-PTTS	
	PCM tank	Water pit	Water tank	Water pit
Total heat collection (GJ)	5578.15		5490.64	
Total heat storage (GJ)	1092.15	3439.50	1079.73	3330.02
Total heat supply (GJ)	619.82	2526.81	576.23	2362.81
Total power consumption	1472.88		1517.88	

The water supply temperature of the series and parallel apparent potential and apparent dual storage system is compared and analyzed. The heating period is selected from March 14-26 of the following year. The heating source is a PCM tank. Figure 6 shows the change of the water supply temperature on the user side over time when two different heat storage systems are adopted. According to the analysis, the water supply temperature fluctuation range of series and parallel display double storage system is large, and the variation range is 5-10 ℃. Because the phase change heat storage measures are adopted, the start and stop times of the latent double storage solar heating system are reduced a lot, the water supply temperature is stable at 50℃, and the heating is more stable. The PCM tank can play a buffer role between the unit and the heating users, reduce the frequency of unit start and stop, and eliminate the insufficient heating phenomenon in individual cold weather through heat storage.

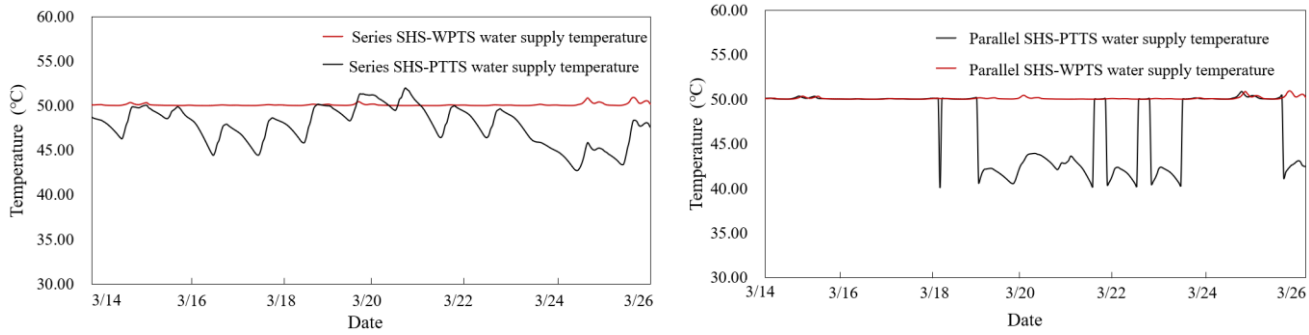

(a) Series system (b) Parallel system

Figure 7. Variation of water supply temperature in SHS-WPTS and SHS-PTTS

To verify the effectiveness of the new SHS-WPTS performance improvement, based on the system energy balance equation, choose the evaluation index of energy efficiency that they are selected for solar collector efficiency η_c, heat storage efficiency η_s and solar fraction f[20], the related calculation formula as shown in 2-4, respectively represent the heating subsystem, the efficiency of heat storage subsystem and the whole system.

$$\eta_c = \left|\frac{Q_C}{Q_{sr}}\right| \times 100\% \tag{1}$$

$$\eta_S = \left|\frac{Q_S}{Q_C}\right| \times 100\% \tag{2}$$

$$f = \left|\frac{Q_h}{Q_g}\right| \times 100\% \tag{3}$$

Where, Q_C is the effective heat collection by the collector, $Q_{sr}$is the total amount of incident solar radiation, Q_S is the effective heat storage of heat storage device, Q_h is the effective heat provided by solar energy, Q_g is the heat load of the building.

According to the simulation results, the heat collection efficiency of the series and parallel display dual storage systems and the series and parallel display dual storage systems are respectively 33.57%,34.42 %,33.07%,33.88%.The series and parallel systems using PCM tanks heat up slowly during the heat storage period compared to the system using ordinary water tanks. The temperature of the heat storage device is slower than that of the system using ordinary water tanks, and the outlet temperature of the collector is larger, which is conducive to heat collection. The heat collection efficiency of the series and parallel systems added to the PCM tank increased by 1.52% and 1.59%.

The average annual heat storage efficiency of series and parallel display dual storage and series and parallel display dual

storage systems is 86.78%,82.29%,83.83%,82.90%. In view of the control strategy of the parallel system during the non-heating period, phase change heat storage is carried out in the medium temperature range, and most of the heat is stored in water pit. During the non-heating period, the series system reduces the heat loss from long-term cross-season heat storage to the surrounding environment, so the heat storage efficiency of the series system is higher.

The monthly solar fraction of the series and parallel display dual storage systems is higher than that of the display dual storage system. The annual average solar fraction of the series and parallel display dual storage systems and the series and parallel display dual storage systems is 87.84%,79.74%,83.88%,74.48%. The solar fraction of the series and parallel apparent dual storage systems is 5.46% higher and 1.12% higher than that of the apparent dual storage system. The solar fraction of the parallel system is lower than that of the series system. This is mainly due to the short heating time of the water tank. During this period, the heat storage capacity of the water tank was not fully utilized. Therefore, the system can be optimized by adjusting the volume of the PCM tank or increasing the range of the heat storage medium temperature interval, and rationally arranging the heating time.

Through the comparative analysis of the energy efficiency of the above-mentioned different structural forms of system operation, it can be concluded that the addition of PCM tanks has played a positive role in improving the performance of the series and parallel cross-season heat storage and heating systems throughout the year.

4.3. Comparative analysis of energy efficiency of series and parallel SHS-WPTS

According to the simulation results of the operating characteristics of the SHS-WPTS system mentioned earlier, the heating capacity and heating time of the series and parallel SHS-WPTS under three typical operating conditions are compared. The comparison results are shown in Table 4.The data in the table show that the heat collection efficiency of the parallel SHS-WPTS system is 34.42%, which is 3.04% higher than that of the series system. Since the parallel system is based on the heat storage of the pool in the early stage of the non-heating period in the parallel system, the volume of the pool is larger, and the temperature rise is slower than that of the PCM tank used in the series system for heat storage, and the inlet temperature of the collector is also reduced. Therefore, it is conducive to the collector to collect heat, and the effective heat collection is 137GJ more than that of the series system, so the efficiency of the solar collector is relatively high.

Table 4. Heating time, capacity, and power consumption under three typical operating conditions of SHS-WPTS

Series SHS-WPTS	Indirect heating	Direct heating	Water source heat pump auxiliary heating
Heating time (h)	533.00	2379.00	736.00
Heat supply (GJ)	532.92	2237.60	1175.77
Power consumption (GJ)		986.22	
Parallel SHS-WPTS	Indirect heating	Direct heating	Water source heat pump auxiliary heating
Heating time (h)	664.00	1917.00	1067.00
Heat supply (GJ)	697.51	1887.54	1361.13
Power consumption (GJ)		1472.88	

Table 5 shows the comparison results of the energy efficiency indicators of the series and parallel SHS-WPTS systems. The heat storage efficiency of the series and parallel SHS-WPTS are 86.78% and 83.83%, respectively. The parallel heat collection of the parallel system is higher than that of the series system. However, because the parallel control strategy of the parallel system during the non-heating period performs phase change heat storage in the medium temperature range, and the heat storage is mostly in the pool. During the non-heating period, the thermal insulation effect of the water tank in the series system is better than that of the pool, and the temperature of the pool in the series system is 3-4℃ lower than that of the parallel pool in the parallel system, to avoid the heat loss to the surrounding environment caused by the cross-season storage of the pool is reduced, so the heat storage efficiency of the series system is higher. The highest solar fraction of the series system is 87.84%, which is 3.15% higher than that of the parallel system. The reason is mainly because in the series system, the time for direct heating using the water tank has been extended, which reduces the equipment loss caused by the heat exchanger and the water source heat pump during heating.

Table 5. Series and parallel SHS-WPTS energy efficiency indicators

System	Heat collection efficiency (%)	Heat storage efficiency (%)	Solar fraction (%)
Series SHS-WPTS	33.57	86.78	87.84
Parallel SHS-WPTS	34.42	83.83	79.74

5 CONCLUSION

This paper proposes a new type of solar heating system with water storage pit and phase change material storage tank. Research analyzed the difference of operating characteristics between the systems through TRNSYS simulation. The system without PCM tank is set as the control group to verify the effect of phase change heat storage system on system performance improvement.

1) The numerical model is set up by SHS-WPTS, phase change collection hot water tank system effect, the heat storage, heating time and heating has a certain amount of ascension, the average temperature of the heat storage device is low, reduce the heat loss with the surrounding environment, phase transition water tank is a good way to unit to act as a buffer between the heating users, stable water supply temperature. Research verified the advantages of the new system using phase change heat storage in enhancing the stability of heat supply and utilizing solar energy efficiently.

2) Compare the three performance indicators of the system: solar collector efficiency, heat storage efficiency and solar fraction and verify the effectiveness of adding a new system to improve the performance of the phase change tank. Compared the energy efficiency of the parallel system and the series system. The results show that the heat storage efficiency and solar fraction of the series system are 3.04% and 10.06% higher than that of the parallel system, respectively, but the solar collector efficiency of the parallel system is significantly higher than that of the series system.

REFERENCES

[1] Mo C, Park J U, Yoon H K. Simulation of a central solar heating system with seasonal storage in Korea [J]. Solar Energy, 1998, 64(4/6):163-178.

[2] Tao T, Zhang F, Zhang W, et al. Low Cost and Marketable Operational Experiences for a Solar Heating System with Seasonal Thermal Energy Storage (SHSSTES) in Hebei (China)[J]. Energy Procedia, 2015, 70:267-274.

[3] Bauer D, Marx R. German central solar heating plants with seasonal heat storage [J]. Solar Energy, 2010, 84: 612–623.

[4] Xu L, Torrens J I, Guo F. Application of large underground seasonal thermal energy storage in district heating system: A model-based energy performance assessment of a pilot system in Chifeng, China[J]. Applied Thermal Engineering, 2018, 137(3): 319–328.

[5] XU J, WANG R Z, LI Y. A review of available technologies for seasonal thermal energy storage [J]. Solar Energy, 2014, 103(7): 610-638.

[6] XIANG Y T, XIE Z C, FURBO S, et al. A comprehensive review on pit thermal energy storage: Technical elements, numerical approaches and recent applications [J]. JOURNAL OF ENERGY STORAGE, 2022, 55(4); 21-27.

[7] H. MEHLING, L.F. CABEZA, S. HIPPELI, et al. PCM-module to improve hot water heat stores with stratification [J]. Renewable energy, 2003, 28(5): 699-711.

[8] NAGHIBI Z, CARRIVEAU R, TING D S K. Improving clean energy greenhouse heating with solar thermal energy storage and phase change materials[J]. ENERGY STORAGE, 2020, 2(1):5-14.

[9] AGHBALOU F, BADIA F, ILLA J. Exergetic optimization of solar collector and thermal energy storage system [J]. International Journal of Heat and Mass Transfer, 2006, 49(7): 1255-1263.

[10] KAYGUSUZ K, AYHAN T. Experimental and theoretical investigation of combined solar heat pump system for residential heating [J]. Energy Conversion and Management, 1999, 40(13): 1377-1396.

[11] SHEN, YONGLIANG, LIU, SHULI, MAZHAR, ABDUR REHMAN, et al. A review of solar-driven short-term low temperature heat storage systems [J]. Renewable & sustainable energy reviews, 2021, 141(5):1-20.

[12] ANAND A, SHUKLA A, KUMAR A, et al. Cycle test stability and corrosion evaluation of phase change materials used in thermal energy storage systems [J]. JOURNAL OF ENERGY STORAGE, 2021, 39(2): 11-16.

[13] ENGLMAIR G, KONG W, BRINKØ BERG J, et al. Demonstration of a solar combi-system utilizing stab. supercooling of sodium acetate trihydrate for heat storage[J]. Applied Thermal Engineering, 2020, 166(10): 3-10.

[14] ZHAO J, LYU L, LI X. Numerical analysis of the operation regulation in a solar heating system with seasonal water pool thermal storage [J]. Renewable Energy, 2020, 150(8): 1118-1126.

[15] Marx R, Bauer D, Drueck H. Energy Efficient Integration of Heat Pumps into Solar District Heating Systems with Seasonal Thermal Energy Storage[M]//Lentz A, Renne D. Energy Procedia. 2014, 34(3):2706-2715.

[16] Measham L. Optimization of parameters of solar heating system for cross-season pool heat storage. Dalian University of Technology Thesis, 2015, 102(2): 56–107.

[17] Jing Y. Numerical calculation and experimental research on heat storage and exothermic properties of new phase change materials. Tianjin University of Commerce, 2008, 45(5): 80-93.

[18] Zhao Jinling, Lu Lianyi. Analysis of the operation and adjustment of the solar heating system for cross-season pool heat storage [J].District heating, 2016, 185(6): 62-67.

[19] KAPLANIS S, KUMAR J, KAPLANI E. On a universal model for the prediction of the daily global solar radiation[J].

RENEWABLE ENERGY, 2016, 91(7): 178-188.
[20] Lizhen Wang, Donglin Zheng, Guang Cheng. An adaptability evaluation of large-scale solar energy for hot water application based on energy-economic-environment consideration: A case study of city-residential buildings in China [J]. Journal of Cleaner Production, 2021, 296, 126585.

The 18th International Symposium on District Heating and Cooling, September 3–6, 2023, Beijing, China

AMMONIA-BASED SORPTION THERMAL BATTERY FOR EFFICIENT HEAT SUPPLY

L. Jiang[a,*], Y. Huang[a], W.Y. Zhang[a], Abel Mehari[a], X. J. Zhang[a]

[a] *Key Laboratory of Clean Energy and Carbon Neutrality of Zhejiang Province, Institute of Refrigeration and Cryogenics, Zhejiang University, Hangzhou, Zhejiang 310027, China*

[*] *Corresponding author. Email: jianglong@zju.edu.cn*

ABSTRACT

Ammonia-based sorption thermal battery (STB) is gathering momentum due to the advantage of high energy storage density and strong operation flexibility. To further improve the system adaptability to cold region, compression-assisted sorption thermal battery (CSTB) is inclined to reach a required heat release temperature by adjusting internal reaction pressure difference. However, the role of compression process in CSTB and its performance limiting factors under dynamic operating conditions remains unclear. This paper investigates the performance of CSTB by matching continuous compression processes under different working conditions. The results indicate that an average heat output power per kg $MnCl_2$ adsorbent ranges from 0.042 kW to 0.26 kW when ambient temperature increases from -10°C to -10°C. Heat storage efficiency in an hour varies from 8% to 60%, and energy storage density (ESD) varies from 150 kJ·kg^{-1} to 950 kJ·kg^{-1}. Besides, for the comparison between CSTB and STB, it demonstrates that under the condition of 40°C heat release temperature and 10°C ambient temperature, ESD of STB is a bit larger than that of CSTB by 47 kJ·kg^{-1}. When ambient temperature drops to 0°C, ESD of STB decreases to 310 kJ·kg^{-1}, which is 50% lower than that of CSTB. It reveals that the compression process is key to CSTB at lower ambient temperature, and expected to have a desirable performance by regulating sorption kinetics in real application.

Keywords: sorption, thermal battery, compression process, heat supply

Nomenclature

Ar	Sorption kinetic constant
c	Specific heat capacity (J·kg^{-1}·K^{-1})
CSTB	Compression-assisted sorption thermal battery
E	Energy (J)
E_0	Activation energy (J·mol^{-1})
ENG	Expanded natural graphite
ESD	Energy storage density (kJ·kg^{-1})
h	Specific enthalpy (J·kg^{-1})
HTS	High temperature salt
LHS	Latent heat storage
LTS	Low temperature salt
$MnCl_2$	Manganese chloride
m	Mass (kg)
mr	Sorption kinetic constant
n	Amount of substance (mol)
Q	Heat (J)
R	Gas constant (J·mol^{-1}·K^{-1})
$SrCl_2$	Strontium chloride
STB	Sorption thermal battery
P	Pressure (Pa)
S	Entropy (J·mol^{-1}·K^{-1})
SHS	Sensible heat storage
T	Temperature (K)
t	Time (s)
u	Specific internal energy (J·kg^{-1})
V	Volume (m^3)
W	Work (J)
x	Global conversion rate

Greek letters

ΔH	Reaction enthalpy of sorbent (J·mol^{-1})

ΔS	Reaction entropy of sorbent ($J \cdot mol^{-1} \cdot K^{-1}$)
η	Efficiency

Subscripts

ad	Adsorption
amb	Ambient
comp	Compressor
de	Desorption
eq	Equilibrium
H	High temperature salt
in	Inlet
out	Outlet
tot	Total

1. INTRODUCTION

To achieve the goal of carbon peak and carbon neutrality, low-carbon energy technologies would play a significant role to address the issues of high energy consumption and environmental pollution [1, 2]. A remarkable fact is that different decarbonized technologies cannot be well fulfilled with available energy resources due to the mismatch between energy generation and consumption in terms of time-scale and space-scale [3, 4]. As a branch of energy storage technologies, thermal energy storage (TES) has attracted burgeoning attention in the past decades since it can be used as a supplementary way to store the heat through energy conversion [5, 6]. Based on the working mechanism, sensible heat storage (SHS) technologies have been most widely investigated, e.g., hot water storage tank [7, 8]. With the increased requirement of system compactness, latent heat storage (LHS) is gradually playing a leading role due to its relatively high energy storage density (ESD) that is round 2-4 times higher than that of SHS [8-10]. Compared with SHS and LHS, thermochemical heat storage (THS) takes the advantage of the highest ESD and the minimum heat loss for the long-term energy storage, which tends to attract more attention in recent years [11-13].

It is acknowledged that THS can be classified into chemical reaction and sorption type [11, 14]. The basic working principle is to store the heat through chemical or physical working processes [15, 16]. Since thermal battery is analogous to electric battery, sorption thermal energy storage (STES) is also termed as sorption thermal battery (STB) [17, 18]. Thermal energy is transferred into sorption reaction enthalpy during the charging process while the heat is released during heat release process [19]. When compared with other sorbates, e.g., water and methanol, ammonia-based STB is highly attractive due to its versatility in working conditions, especially for the applications like power generation and freezing. A new barrier for ammonia-based STB by using chemisorption working pairs is that it cannot perform under some severe working conditions according to Clausius–Clapeyron equation [20]. For example, during the heat charging process, it is difficult to operate if ambient temperature in summer is higher than 40oC. Also, when ambient temperature is lower than 0oC, heat release process may not happen [21, 22]. This is mainly because the driving force of chemisorption working pairs are determined by pressure difference. The working process is limited if temperature difference cannot meet the requirement. Under this scenario, compression-assisted sorption thermal battery (CSTB) is proposed to meet a required heat release temperature by adjusting internal pressure difference of 1-2 bar [23, 24]. In comparison with configuration of STB, a compressor is integrated into common sorption and resorption systems, i.e., between reactor and evaporator or between high temperature salt (HTS) reactor and low temperature salt (LTS) reactor [14, 25]. Thus, one remarkable fact is that CATB could have more flexibility to extend temperature adaptability of up to 80oC. Besides, CSTB has a high system ESD and a low initial cost when compared with two-stage STB, which is used to break through the original temperature limit of STB by using two or more groups of sorption working pairs [15, 26].

Researches on STB and CSTB mainly lie in the fields of the advanced material development, experimental investigation and thermodynamic simulation [27, 28]. The simulation study is generally divided into steady-state analysis and dynamic analysis. For the steady-state thermal analysis, most of researches concentrate on the thermal performance of heat input and heat supply based on an equilibrium chemisorption reaction process. Due to the monovariant characteristics of chemisorption process, temperature is only determined by working pressure. This method is suitable to analyze thermal cycle performance or the overall heat supply of solid sorption systems [29, 30]. Li et al. [31] presented an innovative dual-mode thermochemical sorption energy storage for the seasonal TES utilization. The analysis results indicated that ESD of the proposed thermal cycle could be higher than 1000 kJ·kgadsorebent-1(For simplification, the expression of kJ·kgadsorebent-1 is replaced with kJ·kg-1 in the rest of paper). Yan et al. [32] investigated a thermochemical sorption heat storage cycle for the low-grade heat recovery. Results indicated that thermal energy temperature was upgraded from 81 °C to 170 °C based on a STB cycle. Besides, Bao et al. [33] proposed an integrated chemisorption cycle for the ultra-low grade heat recovery and thermo-electric energy storage. The overall thermal efficiency and exergy efficiency of the hybrid cycles ranged from 47% to 100% and from 62% to 93%, respectively. Our previous work explored the working performance of using CSTB for heat supply in cold region. The analysis results revealed that CSTB could have a high energy storage efficiency when compared with

current two-stage STB [34]. Also, CSTB was proposed to be integrated with solar energy. The high energy utilization efficiency was predicted to be improved by up to 25% [23]. For the simulation of dynamic working processes, Ma et al. [35] numerically studied a solar seasonal STB for the domestic heating in UK. The results indicated that with a 30.5 m2 solar collector, STB could cover about 57.4% of space heating for a dwelling. Thinsurat et al. [36] studied the performance of a CSTB system with a solar photovoltaic-thermal collector to support the domestic space heating. The achieved ESD was around 0.6 GJ·m-3 and the storage efficiency was 0.88 with the net electricity consumption of 180 kWh. But the main point is that the compression process is not fully evaluated, which may lead to a relatively high heat output when compared to real performance of CSTB without a good match among various components of the systems.

It is demonstrated that current researches mainly focus on thermal cycle analysis or the steady-state simulation to predict the overall performance of STB and CSTB [37, 38]. The dynamic simulation process of CSTB, especially for resorption conjugating compression process is rarely reported. However, the instantaneous working process could have more insights when predicting the numerical performance of CSTB for efficient heat supply. It may pose some more challenges, e.g., (1) Considering CSTB using resorption working pair, pressure of HTS reactor and LTS reactor continuously change in sorption and desorption processes. This is quite different from the analysis of thermal cycle, i.e., pressure of HTS and LTS reactor is assumed as constant during the working process. Heat input and heat release time would be different from that of steady-state simulation. (2) The pressurization process of the compressor for CSTB need to be adjusted rather than keeping as constant pressure ratio from a thermodynamic perspective, which would have more flexibility of the compressor for CSTB. In this case, desorption or adsorption would be hindered if pressure difference is not enough to drive the working processes. Also compression may assist the heat charging and heat release processes if temperature difference is enough for the driving force.

To address the above challenges, the resorption conjugating compression process of CSTB is initially investigated to present a holistic system performance in terms of global conversion rate, ESD and energy storage efficiency. The compressor model is based on the previous research of an oscillating diaphragm compressor through a detailed dynamic modelling and generic simulation methods, which is validated by the related experiment [39]. Various heat charge and release temperature are adopted to explore the performance under various working conditions, e.g., severe cold region, which is expected to bring more insights on the dynamic working performance of CSTB. The framework of this paper is illustrated as follows. Concept of CSTB and working pairs are indicated in Section 2. Methodologies for sorption reactor and compressor of CSTB are elaborated in Section 3. Results and discussions are indicated in Section 4, followed by conclusions in Section 5.

2. CONCEPT OF CSTB SYSTEM

The basic configuration of a CSTB system by using resorption working pair is indicated in Figure 1. The main components include a HTS reactor, a LTS reactor and an oscillating diaphragm compressor. The common shell and finned sorption reactors are used in this work. The reactors are filled with composite sorbents that are developed using metal chlorides and expanded natural graphite (ENG) for an improved heat and mass transfer performance. The sorption stability of composite sorbent could be ensured without swelling and agglomeration [40]. Considering suitable working temperature ranges, composite manganese chloride ($MnCl_2$) and strontium chloride ($SrCl_2$) with a consolidation density of 500 $kg \cdot m^{-3}$ and mass ratio of 80% [41] are selected for HTS and LTS reactors, respectively. Chemical reactions of $MnCl_2$ and $SrCl_2$ with ammonia are indicated as shown in Equations 1 and 2. The reaction processes involve the reaction of $MnCl_2$ ammoniate with ammonia from 2 moles to 6 moles, and $SrCl_2$ ammoniate with ammonia from 1 mole to 8 moles. A reciprocating compressor, with the advantages of high adaptability and strong corrosion resistance, is adopted for the continuous compression working processes of CSTB. The working processes of the compressor include compression, discharge, expansion and suction. It consists of two isobaric stages and two polytrophic stages.

$$MnCl_2 \cdot 2NH_3 + 4NH_3 \leftrightarrow MnCl_2 \cdot 6NH_3 + 4\Delta H_{MnCl_2} \quad (1)$$

$$SrCl_2 \cdot NH_3 + 7NH_3 \leftrightarrow SrCl_2 \cdot 8NH_3 + 7\Delta H_{SrCl_2} \quad (2)$$

Compared with SHS or LHS, the proposed CSTB is used for long-term or seasonal energy storage. Thermal energy, such as solar energy, is used during the heat charging process to heat the HTS reactor for desorption. The desorbed ammonia is then adsorbed by the LTS reactor, and the sorption heat can be discharged to an environmental heat sink. From the equilibrium chemisorption process, the compression process is required when temperature difference cannot drive the desorption process. The chemical reaction enthalpy of sorption working pairs stores thermal energy. Desorption of LTS cannot occur during the release process when the ambient temperature is too low, which is common in high latitudes during the winter. In this case, the compressor can be powered by electricity to increase refrigerant pressure. Then, sorption heat can be released at the required output temperature by using a small amount of off-grid electricity.

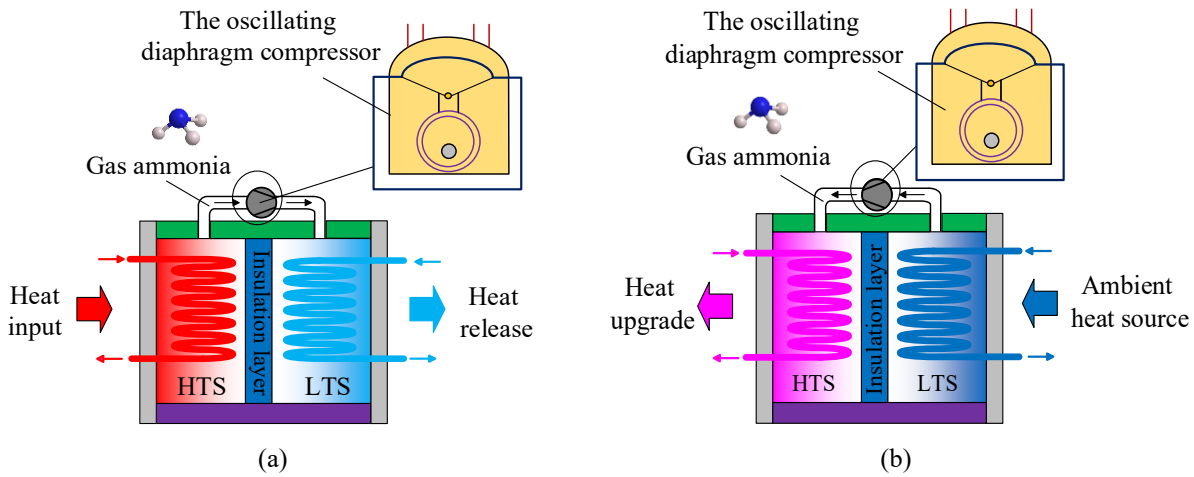

Figure 1. Schematic diagram of CSTB by using resorption working pair (a) heat charging process; (b) heat release process.

3. METHODOLOGY

To analyze the dynamic performance of CSTB, detailed evaluations are carried out through simulation. This section introduces the analysis methodology, which includes assumptions, parameter definitions, thermophysical property computations, and model validation. During the heat charging process, heat source temperature is selected from 60°C to 100°C while ambient temperature is in the range of 20-40°C. Temperature ranges of heat source are within the range of low-grade heat utilization, e.g., solar energy. During the heat release process, ambient temperature is selected from -10°C to 10°C, and the output temperature ranges from 40°C to 80°C when considering the application of cold region.

To evaluate the performance of CSTB, a numerical model of CSTB is developed. The numerical model consists of two finned-tube sorption reactors, a diaphragm compressor and the void space between the reactors and the compressor. The lumped parameter method is adopted in each simulation area. The finned-tube sorption reactor model is developed with the following simplified assumptions.

1. The heat conduction of composite sorbent in the axial direction is neglected.

2. The packing density of the composite sorbent inside the unit tube is uniform.

3. Heat loss from sorption reactor and tube is ignored.

4. The non-equilibrium chemisorption is evaluated at an equilibrium pressure drop of 1.0 bar.

5. The mass transfer limitation is ignored in the chemisorption process.

The Clausius–Clapeyron equation for chemisorption working pairs is expressed as Equation 3 [42].

$$\ln(P_{eq})=-\frac{\Delta H}{RT}+\frac{\Delta S}{R} \tag{3}$$

where P_{eq} is the equilibrium pressure; ΔH is reaction enthalpy of NH_3; ΔS is reaction entropy of NH_3; R is gas constant and T is temperature.

The values of ΔH and ΔS for $SrCl_2$ and $MnCl_2$ reacted with the ammonia are obtained from Ref. [43, 44], as shown in Table 1.

Table 1. Reaction enthalpy and entropy of sorption for $SrCl_2$ and $MnCl_2$.

	$SrCl_2/NH_3$ 1-7 [43]	$MnCl_2/NH_3$ 2-6 [44]
ΔH ($J\cdot mol^{-1}$)	41432	47416
ΔS ($J\cdot mol^{-1}\cdot K^{-1}$)	132.9	228.07

In the reactors, adsorption and desorption rates are evaluated through reaction pressure, reaction temperature and reaction degree. The chemisorption kinetic equations are used in terms of adsorption and desorption processes, which could be expressed as Equations 4 and 5, respectively.

$$\frac{dx}{dt}=Ar_{ad}(1-x)^{mr_{ad}}\frac{P-P_{eq}(T)}{P}\exp\left(\frac{-E_0}{RT}\right) \tag{4}$$

$$\frac{dx}{dt}=Ar_{de}x^{mr_{de}}\frac{P_c-P_{eq}(T)}{P}\exp(\frac{-E_0}{RT}) \tag{5}$$

where x is the global conversion rate that represents the degree of conversion of the chemisorption, Ar and mr are the constant parameters, P is the working pressure, P_{eq} is the equilibrium pressure, and E_0 is the activation energy.

The values of Ar, mr and E_0 for $SrCl_2$ and $MnCl_2$ reacted with the ammonia are obtained from Ref. [45, 46], as shown in Table 2.

Table 2. The kinetic parameters of $SrCl_2$ and $MnCl_2$ reacted with the ammonia.

	$SrCl_2/NH_3$ 1-7 [45]		$MnCl_2/NH_3$ 2-6 [46]	
	Adsorption	Desorption	Adsorption	Desorption
Ar	0.019	0.125	0.00174	0.00902
mr	2.96	3.02	0.4	0.63
E_0	6921	9000	0	0

The global conversion rate x is defined as the ratio of adsorbed molar amount of ammonia and the total molar amount of ammonia, as shown in Equation 6.

$$x=\frac{n_{ad}}{n_{tot}} \tag{6}$$

The kinetic model of sorption reactor is widely adopted in chemisorption numerical study, the parameters of which are obtained through experimental fitting. The fitting results are highly consistent with experimental results. Hence, the kinetic model is adopted in this study to simulate adsorption and desorption processes of the reactor.

The dynamic model of a diaphragm compressor developed by Najjaran et al. [39] is adopted in the simulation of CSTB. The operating cycle of the compressor consists of suction process, compression process, discharge process and expansion process. The quasi-steady assumption is adopted in the compressor simulation. During suction process, the cylinder pressure is assumed equal to desorption pressure. During heat release process, cylinder pressure is assumed equal to adsorption pressure. The operating cycle of the compressor follows the first law of thermodynamics in an open system, and energy equation of gas in the cylinder is defined as Equation 7.

$$\frac{d(mu)}{dt}=\dot{Q}+\dot{m}_{in}h_{in}-\dot{m}_{out}h_{out}-P\frac{dV}{dt} \tag{7}$$

where m is the mass of gas in cylinder, u is the specific internal energy, $\dot{Q}$ is heat loss, P is pressure in the cylinder, V is cylinder volume, $\dot{m}_{in}$ and $\dot{m}_{out}$ are the mass flow rate of the inlet and outlet, h_{in} and h_{out} are the specific enthalpy of the inlet gas and outlet gas. The variation of cylinder volume with rotation angle is illustrated in Ref. [39], and the change rate of cylinder volume can be obtained from the rotation speed of the compressor.

The compressor model has been validated by the experimental data and manufacture data in Ref. [39]. The maximum deviation between simulation data and manufacture data is 19%, and the maximum deviation between simulation data and experimental data is 30%. At an inlet pressure of 1 bar and the outlet pressure of 6 bar, the simulation results of the current compressor model are compared with the simulation results in Ref. [39], as shown in Figure 2. The inlet and outlet mass flow rates are well consistent with the reference results, which indicates the accuracy of the compressor model.

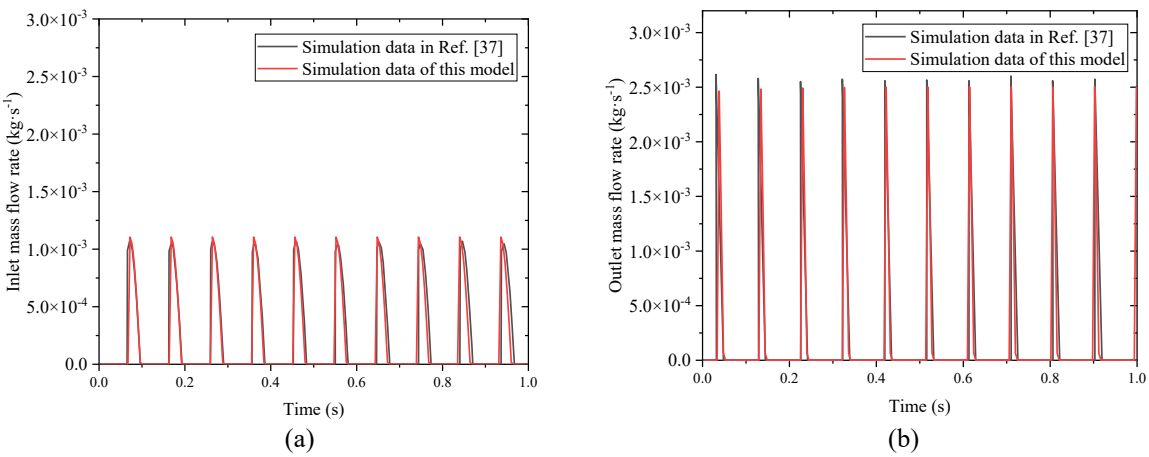

Figure 2. Validation of the compressor model (a) the inlet mass flow rate; (b) the outlet mass flow rate.

In the void space between the compressor and the reactor, the state of the gas is calculated by Equation 8.

$$\frac{d(mu)}{dt}=\dot{m}_{in}h_{in}-\dot{m}_{out}h_{out} \tag{8}$$

For void space upstream of the compressor, the inlet gas comes from the desorption reactor, and the outlet gas flows to the compressor. For void space downstream of the compressor, the inlet gas comes from the compressor, while the outlet gas is outputted to the adsorption reactor. The pressure in void space is assumed to be reaction pressure, indicating the state in void space has a significant impact on adsorption and desorption processes. In the absence of compression-assisted operation, the inlet gas comes from the desorption reactor, and the outlet gas goes to the adsorption reactor.

The heat input during heat charging process is calculated by Equation 9.

$$Q_{in}=\Delta n_{NH_3,de}\Delta H+c_{MnCl_2}m_{MnCl_2}(T_H-T_{amb}) \tag{9}$$

where $\Delta n_{NH3,de}$ is the molar amount adsorbed NH_3 in HTS, c_{MnCl2} is the specific heat capacity of $MnCl_2$, m_{MnCl2} is the mass of $MnCl_2$, T_H is the temperature in HTS, T_{amb} is ambient temperature.

The heat output of CSTB could be calculated by Equation 10.

$$Q_{out}=\Delta n_{NH_3,ad}\Delta H-c_{MnCl_2}m_{MnCl_2}(T_H-T_{amb}) \tag{10}$$

where $\Delta n_{NH3,ad}$ is the molar amount of the adsorbed NH_3 in HTS. While the sorption heat is less than the sensible heat of $MnCl_2$, CSTB is unable to output the heat, and Q_{out} is assumed as zero under this circumstance.

Compression work for CSTB is calculated by Equation 11. P is the pressure of cylinder, and the variation rate of cylinder volume with rotation angle is obtained from Ref. [39]. The rotation speed is defined as 1500 rpm in this study. Compression work for CSTB is calculated by integrating Equation 11 throughout the entire simulation time.

$$W_{comp}=\int -PdV=\int -P\frac{dV}{d\theta}\frac{d\theta}{dt}dt \tag{11}$$

Energy input for CSTB during the heat charging process is calculated by Equation 12.

$$E_{in}=Q_{in}+W_{comp} \tag{12}$$

The net energy output of CSTB is calculated by Equation 13.

$$E_{out}=Q_{out}-W_{comp} \tag{13}$$

Energy storage efficiency of CSTB is calculated by Equation 14.

$$\eta_{storage}=\frac{E_{out}}{E_{in}} \tag{14}$$

Energy storage density in terms of mass of salt can be defined as Equation 15.

$$ESD_{salt}=\frac{Q_{out}}{m_{salt}} \tag{15}$$

4. RESULT AND DISCUSSION

In this section, the charging and heat release dynamic characteristics are presented by considering various working temperatures and compression process, which significantly influence the working pressure, global conversion rate, and energy density. Then, the performance of STB with and without a compressor is compared. When heat exchanging flow rate of heat source and cold source is large enough, the temperature inside the reactor will be close to the temperature of the source. Since the main purpose of this study is to investigate the heat charging and heat release performance of CSTB with a continuous compression processes, all investigations are conducted at certain desorption and adsorption temperatures. In the charging process, desorption temperature is considered as heat source temperature while adsorption temperature is considered as ambient temperature. During heat release process, the desorption temperature is considered as ambient temperature while the adsorption temperature is considered as heat release temperature.

4.1 Heat charging process

Figure 3 indicates the working pressure of HTS and LTS reactor for CSTB under the conditions of 60-100°C heat source temperature and 20-40°C ambient temperature during the heat charging process. As shown in Figure 3a, the desorption pressure of HTS increases with the increase of working time. The desorption temperature is the main source to determine the working pressure rather than the temperature difference between heat source and environment. The desorption pressure

ranges from 0.2 bar to 1.8 bar. For the adsorption pressure of LTS shown in Figure 3b, the value is much higher than that of the desorption pressure of HTS since the adsorption rate of LTS is lower than the desorption rate of HTS. The gas is accumulated downstream of the compressor until the adsorption pressure reaches a sufficiently high value, which makes the adsorption rate close to the desorption rate.

Since the adsorbent cannot be completely reacted with adsorbate in real application, the global conversion rate is used to reflect the reaction extent of sorption working pairs. Figure 4 indicates the global conversion rate of CSTB under the conditions of 60-100°C heat source temperature and 20-40°C ambient temperature during the heat charging process. The global conversion rate increases with the increase in working time. It is positively related to heat source temperature because the higher temperature usually leads to the larger desorption rate, the lower equilibrium adsorption capacity and the higher equilibrium pressure. For the operating conditions at low heat source temperatures, the global conversion rate is lower at higher ambient temperatures because the equilibrium pressure of LTS reactor increases. The hindrance of adsorption caused by ambient temperature is especially evident at 60°C heat source temperature. Adsorption pressure is low at low desorption temperatures, and the effect of equilibrium pressure on adsorption rate is more evident at the lower adsorption pressure. Therefore, it is necessary to provide a relatively high-temperature heat source for HTS to create enough driving force when ambient temperature is high.

At high heat source temperatures, adsorption pressure is much higher than the equilibrium reaction pressure of LTS. The role of the equilibrium pressure on the global conversion rate is relatively small, which can be explained by Equation 5. Therefore, the hindrance of adsorption caused by ambient temperature is not evident at high heat source temperatures. At 70°C heat source temperature, the global conversion rate at 30°C ambient temperature eventually catches up with that at 20°C ambient temperature, which could reach 64% in an hour. At 80°C heat source temperature, the global conversion rate of the CSTB at ambient temperatures of 20°C and 30°C almost coincide. When heat source temperatures are 90°C and 100°C, the global conversion rates of CSTB at high ambient temperatures gradually exceed those at lower ambient temperatures when sorption process proceeds. The global conversion rate of CSTB at high heat source temperatures increases around 1% and 0.5% when ambient temperature increases from 20°C to 30°C and from 30°C to 40°C, respectively. It is mainly because higher temperatures not only increase the equilibrium pressure but also increases the last term of Equation 5. According to Arrhenius equation, chemical reaction rate increases at higher temperatures. Adsorption pressure becomes higher during the adsorption process of LTS, and the effect of equilibrium pressure continuously declines. If adsorption pressure reaches a sufficient value, such as around 10 bar at 90°C heat source temperature, the higher chemical reaction rate at higher temperatures dominates adsorption rate of LTS. At high heat source temperatures, the global conversion rate of CSTB becomes higher with the increase of ambient temperature. The maximum global conversion rate of CSTB in an hour is 68.6% at 100°C heat source temperature and 40°C ambient temperature. In comparison, the lowest global CSTB conversion rate in an hour is 53.3% at 60°C heat source temperature and 40°C ambient temperature.

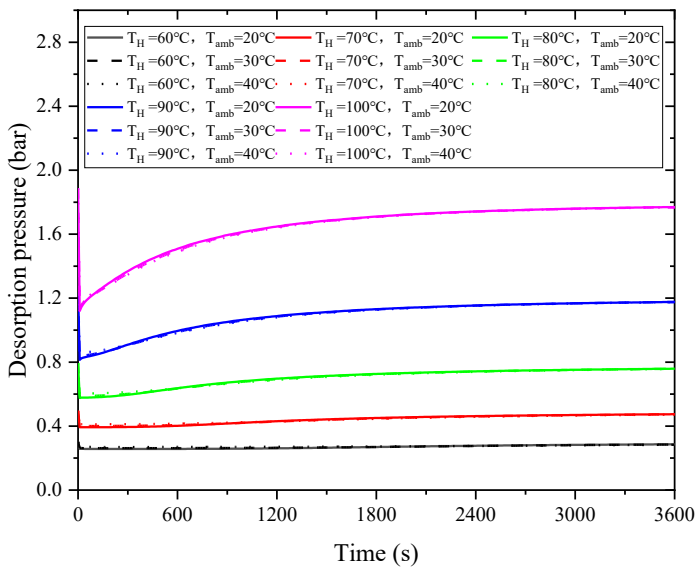

(a)

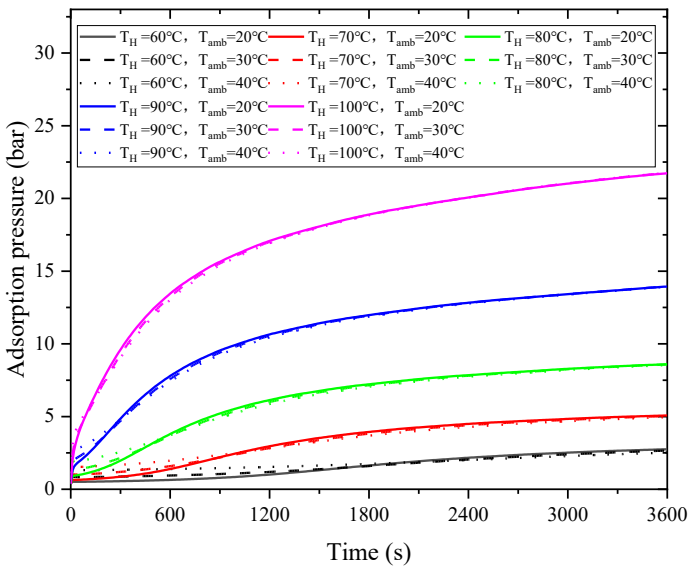

(b)

Figure 3. Pressure variation of CSTB vs. the working time under the conditions of 60-100°C heat source temperature and 20-40°C ambient temperature (a) HTS; (b) LTS.

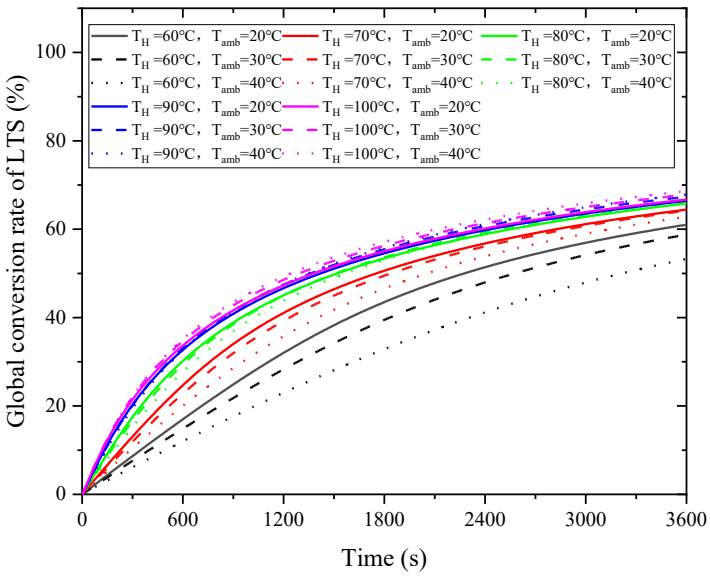

Figure 4. The global conversion rate of CSTB vs. the working time under the conditions of 60-100°C heat source temperature and 20-40°C ambient temperature.

Heat input during the charging process consists of the sensible heat of adsorbent and reaction heat stored by adsorbent, as illustrated in Equation 12. Figure 5 indicates the heat input for CSTB under the conditions of 60-100°C heat source temperature and 20-40°C ambient temperature during heat charging process. The initial heat input is the sensible heat of adsorbent, and it can be found that the sensible heat of adsorbent only accounts for a small portion of total heat input. Heat storage process is quicker at higher heat source temperatures because high temperature increases both desorption rate and the equilibrium pressure. Heat input is reduced at higher ambient temperatures when the heat source temperature is low. It is mainly because desorption rate of CSTB is related to adsorption rate. When the adsorption rate is low, gas accumulates downstream of the compressor, and the gas in HTS is difficult to flow into LTS, which causes desorption pressure to rise. Simultaneously, the temperature difference between HTS and environment is lower, and the sensible heat for HTS decreases. However, heat input is slightly higher at higher ambient temperatures when the heat source temperature is high. Hence, adsorption in LTS can promote desorption in HTS, and the effect of ambient temperature on heat stored is similar to that on LTS global conversion rate. The maximum heat input in an hour of heat storage process is around 1550 kJ at 100°C heat source temperature and 40°C ambient temperature, while the minimum heat input is around 1000 kJ at 60°C heat source temperature and 40°C ambient temperature.

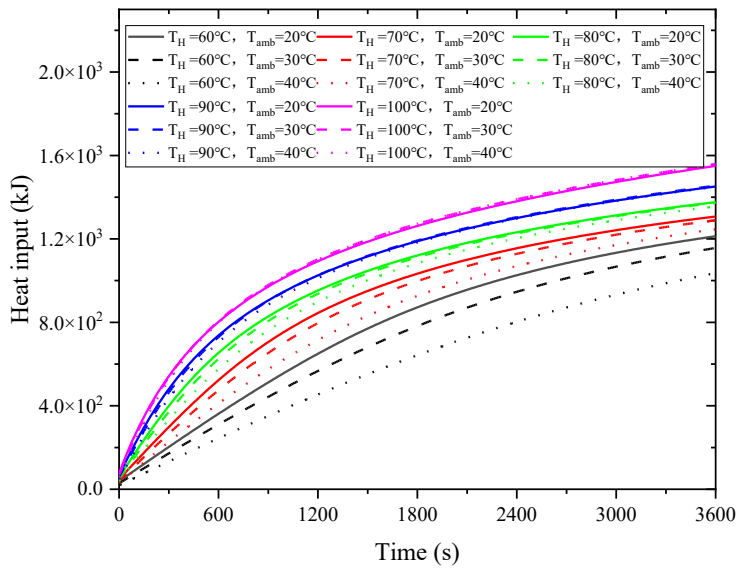

Figure 5. Heat input of CSTB vs. the working time under the conditions of 60-100°C heat source temperature and 20-40°C ambient temperature.

Heat charging process ends when all of the ammonia in HTS is desorbed and adsorbed by LTS. Figure 6 indicates the heat input and compression work of a complete heat charging process under the conditions of 60-100°C heat source temperature and 20-40°C ambient temperature. It is indicated that heat input is larger when the temperature difference between heat source and environment is higher because of the sensible heat of HTS. When the heat source temperature is higher and the ambient temperature is lower, the compression work is reduced. This is mainly because the spontaneity of adsorption process is greater under these conditions, and the compressor consumes less work. Because of the increase in heat input, total energy input increases with heat source temperature. Total energy input increases with the increase of ambient temperature when heat source temperature is lower than 80°C, and the input decreases with the increase of ambient temperature when heat source temperature is higher than 80°C. This is because the enhancement of compression work is larger than the reduction of heat input as ambient temperature increases at low heat source temperature, and a reverse situation could happen at high heat source temperature. The minimum total energy input is 2007 kJ, obtained at 60°C heat source temperature and 20°C ambient temperature; the maximum total energy input is 2054 kJ, obtained at 100°C heat source temperature and 20°C ambient temperature. At 60°C heat source temperature and 20°C ambient temperature, the minimum total energy input is 2007 kJ, while the maximum total energy input is 2054 kJ at 100°C heat source temperature and 20°C ambient temperature.

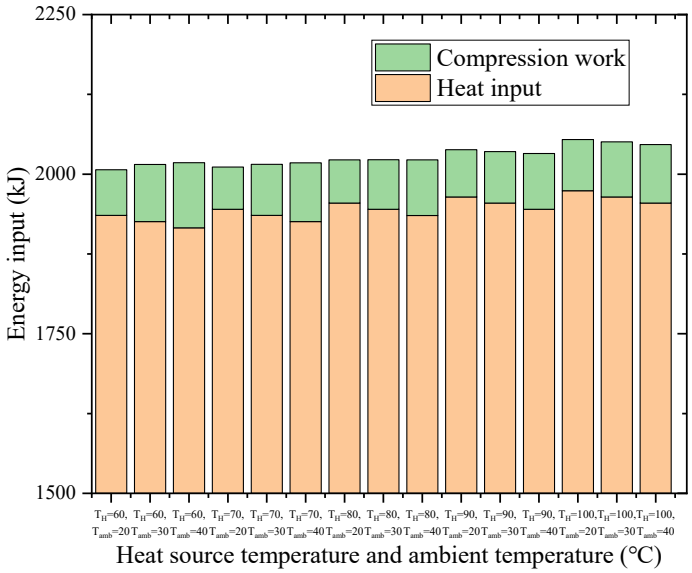

Figure 6. Energy input of CSTB under the conditions of 60-100°C heat source temperature and 20-40°C ambient temperature.

4.2 Heat release process

Figure 7 indicates the working pressure of HTS and LTS reactor for CSTB under the conditions of 40-60°C heat release temperature and -10-10°C ambient temperature during heat release process in winter. As shown in Figure 7a, the desorption pressure of LTS drops with the increase in working time. The desorption temperature is the main source to producing the

working pressure rather than the temperature difference during heat release process. The initial value of desorption pressure at 10°C ambient temperature is high but rapidly decreases while the desorption pressure stabilizes at approximately 0.05 bar at -10°C ambient temperature. When the ambient temperature is relatively high, the desorption process is accelerated, and the desorption rate decreases due to the consumption of stored ammonia. Figure 7b indicates that the adsorption pressure in HTS maintains relatively stable. As mentioned above, the reaction kinetics of HTS is superior to that of LTS. Because the gas in HTS is rapidly adsorbed, the adsorption pressure will not rise as quickly as the heat charging process.

Figure 8 indicates the global conversion rate of CSTB under the conditions of 40-60°C heat release temperature and -10-10°C ambient temperature during heat release process. The conversion rate of CSTB is faster at higher ambient temperatures and lower heat release temperatures. It is because the pressure difference between LTS and HTS decreases as ambient temperature and heat release temperature rise. Ambient temperature has a stronger impact on sorption process than heat release temperature. At 10°C ambient temperature, the global conversion rate of CSTB increases from 55% to 80% in an hour, which is dependent on heat release temperature while the global conversion rate increases from 20% to 50% at 0°C ambient temperature. When ambient temperature is -10°C, the conversion rate is less than 35% in an hour, and sorption cannot proceed at 80°C heat release temperature. The sorption process appears to be hampered at low ambient temperatures. Even with a compression-assisted process, sorption cannot occur if the temperature difference between LTS and HTS is too large. The heat release temperature should be reasonably chosen at a low ambient temperature. Otherwise, hindrance of sorption process is high, which would have a significant impact on the performance during heat release process.

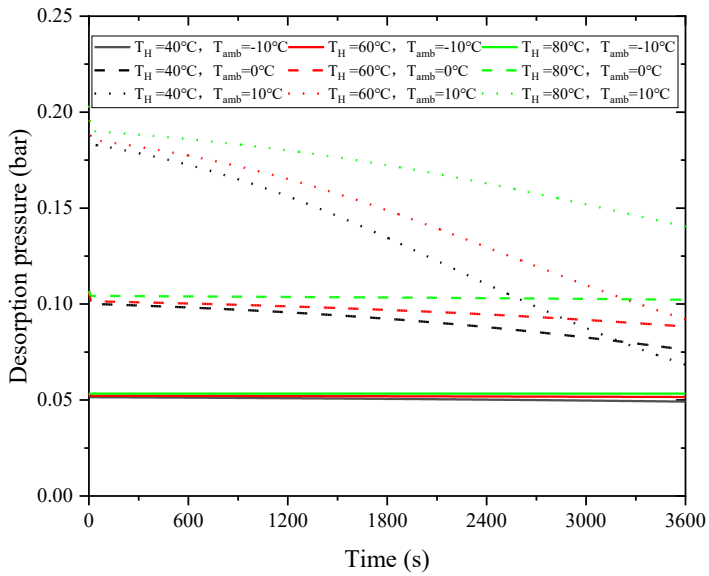

(a)

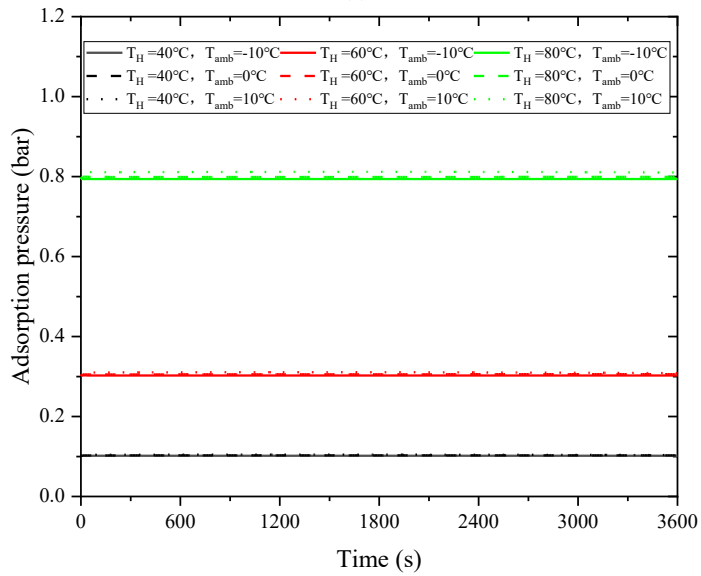

(b)

Figure 7. Desorption and adsorption pressure of CSTB under the conditions of 40-60°C heat release temperature and -10-10°C ambient temperature (a) LTS; (b) HTS.

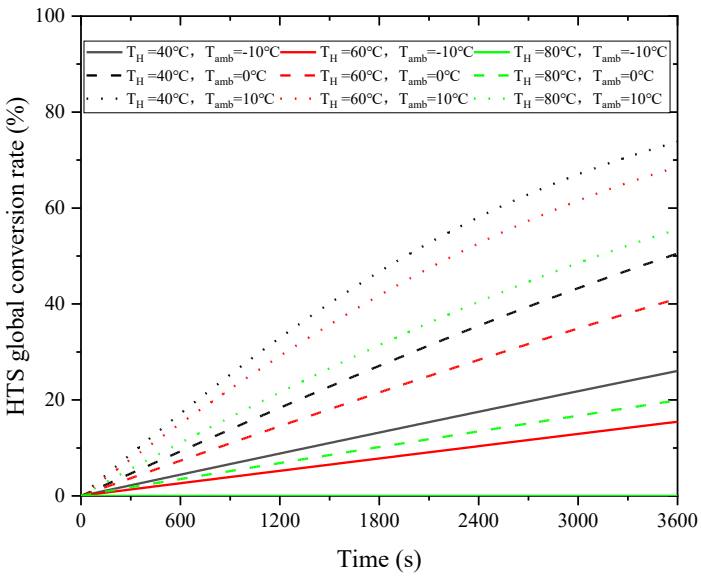

Figure 8. The global conversion rate of CSTB vs. the working time under the conditions of 40-60°C heat release temperature and -10-10°C ambient temperature.

Figure 9 shows heat output of CSTB during the heat release process. Heat output is evaluated by ammonia adsorption heat and sensible heat of HTS. Initially, adsorption heat is used for heating HTS to reach heat release temperature, and no heat output power can be found. Preheating time depends on both the global conversion rate and temperature difference between heat supply and environment. The shorter preheating time is obtained at lower heat release temperatures and higher ambient temperatures. At low heat release temperatures and high ambient temperatures, the global conversion rate of CSTB is higher and sensible heat of HTS is lower, which could reduce the preheating time. The shortest preheating time is 61 s at 40°C heat release temperature and 10°C heat release temperature, while the longest preheating time is around 1000 s at 60°C heat release temperature and -10°C heat release temperature. CSTB can provide a useful heat output after preheating process. Heat output is larger when ambient temperature is higher. Also, the higher heat output power can be obtained by decreasing heat release temperature. It is noted that low heat release temperature should be selected at extremely low ambient temperature to ensure sufficient heat output power. According to the heat output curves of 10°C ambient temperature, heat output power drops in the later stage of heat release process. It is because the desorption rate decreases with the increase of the global conversion rate, as illustrated in Equation 5.

Figure 10 shows ESD of CSTB during heat release process, which is defined as heat output per kilogram of adsorbent. The maximum heat output in an hour is 950 $kJ \cdot kg^{-1}$ at 40°C heat release temperature and 10°C ambient temperature while the minimum heat output in an hour is 150 $kJ \cdot kg^{-1}$ under the condition of 60°C heat release temperature and -10°C ambient temperature. It is indicated that the average heating power of 1 kg $MnCl_2$ adsorbent is as high as 0.26 kW at 10°C ambient temperature and 40°C heat release temperature, which demonstrates good heating performance. In severe cold environment of -10°C, 1 kg $MnCl_2$ adsorbent can provide 0.042 kW heating power at 60°C heat release temperature. As power density is low under severe cold environment, sufficient HTS is required for heat supply to meet the requirements of heating power. Another choice is to decrease heat release temperature to ensure heating power. When heat release temperature decreases to 40°C, heating power of 1 kg $MnCl_2$ rises to 0.85 kW. Although power density is low in severe cold regions, heat supply time is extended. It can be concluded that different design strategies of CSTB should be adopted in different working environments. When ambient temperature is extremely low in winter, the reactor should be designed large enough to load sufficient HTS to ensure heating power. Similarly, the reactor should be designed smaller when ambient temperature is relatively high in winter. As heat supply time is shorter at higher ambient temperatures, more reactors should be established for the continuous heat supply.

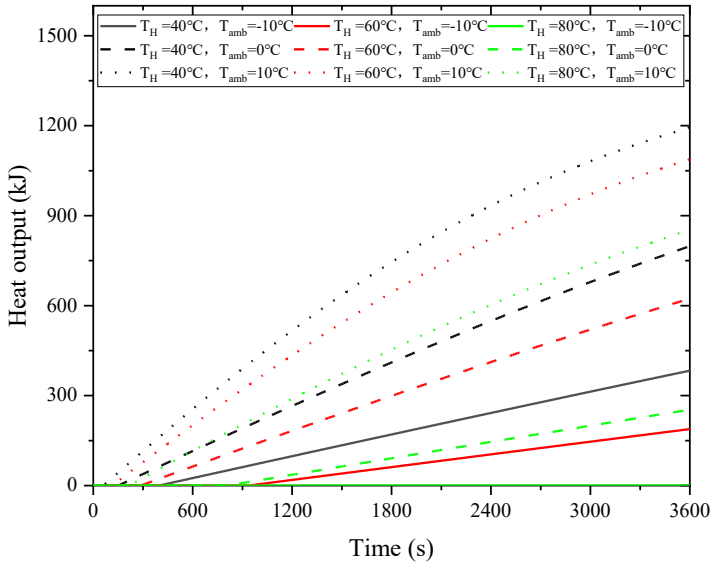

Figure 9. Heat output of CSTB vs. the working time under the conditions of 40-60°C heat release temperature and -10-10°C ambient temperature.

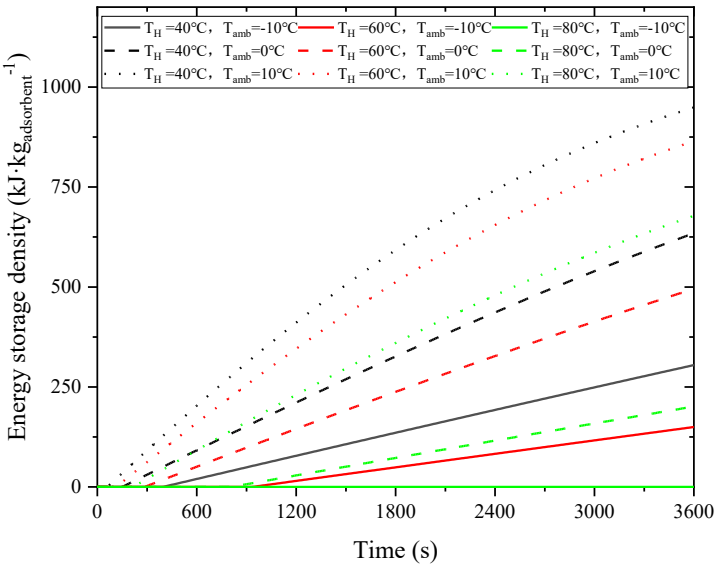

Figure 10. Energy storage density of CSTB vs. the working time under the conditions of 40-60°C heat release temperature and -10-10°C ambient temperature.

Figure 11 indicates energy storage efficiency of CSTB under the conditions of 40-80°C heat release temperature and -10-10°C ambient temperature during heat release process. Energy storage efficiency reaches a higher value at lower heat release temperatures and higher ambient temperatures. This is mainly because the global conversion rate and heat output are larger. Simultaneously, compression work declines at lower pressure difference between HTS and LTS, which further increases net energy output. At 40°C heat release temperature and 10°C ambient temperature, almost 60% of the input energy is consumed in an hour, which shows good energy utilization efficiency. Under the condition of 60°C heat release temperature and -10°C ambient temperature, energy storage efficiency only reaches around 8% in an hour. It is indicated that the energy storage efficiency can reach a high value at high ambient temperatures and low heat release temperatures. Due to the slow heat output process at the extreme cold of -10°C, long heat supply times of several hours are needed for good heat storage efficiency.

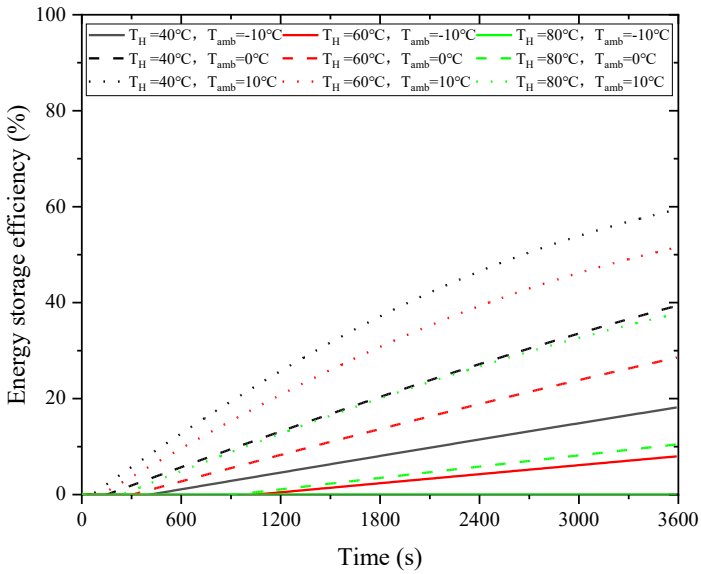

Figure 11. Energy storage efficiency of CSTB vs. the working time under the conditions of 40-60°C heat release temperature and -10-10°C ambient temperature.

5. CONCLUSION

Conclusion may include advantages, limitations, and possible applications.A CSTB using $MnCl_2$ and $SrCl_2$ as working pairs with a reciprocating compressor is investigated to present the dynamic working performance when considering the continuous compression process. After the detailed description of the system and dynamic model, the dynamic behaviour of CSTB under varying operating conditions is examined to reveal the transient characteristics of different parameters (adsorption/desorption pressure and global conversion rate) and performance indices (ESD and energy storage efficiency). Besides, the overall performance of the CSTB is compared to those of STB, and the performance-limiting factors of the compression process are identified in the charging and heat release processes. The main conclusions are yielded as follows:

1. During the heat charging process, both adsorption pressure and desorption pressure decrease with the increase in working time. Higher global conversion rates are obtained at higher heat source temperatures. During heat charging process, the maximum heat input of 1558 kJ in an hour is obtained at 100°C heat source temperature and 40°C ambient temperature. Considering heat input and compression work, energy input during the heat charging process is lower at lower heat source temperatures. The minimum total energy input is 2054 kJ, which is obtained at 60°C heat source temperature and 20°C ambient temperature. During heat release process, desorption pressure decreases with the increase of working time while adsorption pressure almost keeps constant. The global conversion rate is higher at lower heat release temperatures and higher ambient temperatures. At 10°C ambient temperature, heat output in an hour is about 950 $kJ \cdot kg^{-1}$, with an average output power of up to 0.26 kW. In severe cold environment of -10°C ambient temperature, heat output power per kg adsorbent is as low as 0.042 kW. Heat storage efficiency in an hour varies from 8% to 60%, depending on ambient temperature and temperature difference between HTS and environment.

2. Compared to STB without compression-assisted process, CSTB shows the preferable performance at low ambient temperature. Heat charging process of CSTB can proceed under some conditions that sorption process of STB cannot occur. During heat release process, sorption process of STB cannot occur at extremely low ambient temperatures and high heat release temperatures, while CSTB can supply heat under most circumstances. The conversion rate, energy storage density, and energy storage efficiency of CSTB are higher than that of STB, except under the conditions of high ambient temperatures and low heat release temperatures. At 40°C heat release temperature and 10°C ambient temperature, energy storage density of STB is 47 $kJ \cdot kg^{-1}$ larger than that of CSTB, and energy storage efficiency of STB is 3% higher than that of CSTB. When ambient temperature drops to 0°C, ESD of STB decreases to 310 $kJ \cdot kg^{-1}$, which is 50% lower than that of CSTB.

The decarbonised heating would play a more important role in the next few decades. CSTB could be considered as a method to solve the problem for seasonal energy storage and utilization. With compression-assisted process, heat charging and release processes could be accelerated with a higher thermal performance and system flexibility. Future work of CSTB should lie in the accurate control of the compressor, thermal design of sorption reactor and effective match among the components in real testing conditions.

ACKNOWLEDGEMENT

This research was supported by National Natural Science Foundation of China (No. 52276022) and supported by the Basic

Research Funds for the Central Government 'Innovative Team of Zhejiang University' under contract number (2022FZZX01-09).

REFERENCES

[1] An GL, Wu SF, Wang LW, Zhang C, Zhang B. Comparative investigations of sorption/resorption/cascading cycles for long-term thermal energy storage. Applied Energy. 2022;306:117991.

[2] Jiang L, Liu W, Wang RQ, Gonzalez-Diaz A, Rojas-Michaga MF, Michailos S, et al. Sorption direct air capture with CO2 utilization. Progress in Energy and Combustion Science. 2023;95:101069.

[3] Pisciotta M, Pilorgé H, Feldmann J, Jacobson R, Davids J, Swett S, et al. Current state of industrial heating and opportunities for decarbonization. Progress in Energy and Combustion Science. 2022;91:100982.

[4] Rashidi S, Karimi N, Sunden B, Kim KC, Olabi AG, Mahian O. Progress and challenges on the thermal management of electrochemical energy conversion and storage technologies: Fuel cells, electrolysers, and supercapacitors. Progress in Energy and Combustion Science. 2022;88:100966.

[5] Liu L, Wang R, Wang Y, Li W, Sun J, Guo Y, et al. Comprehensive analysis and optimization of combined cooling heating and power system integrated with solar thermal energy and thermal energy storage. Energy Conversion and Management. 2023;275:116464.

[6] Song Y, Xu Q, Liu X, Xuan Y, Ding Y. High-performance thermal energy storage and thermal management via starch-derived porous ceramics-based phase change devices. International Journal of Heat and Mass Transfer. 2022;197:123337.

[7] Gautam A, Saini RP. A review on sensible heat based packed bed solar thermal energy storage system for low temperature applications. Solar Energy. 2020;207:937-56.

[8] Zhang Z, Zhang J, Yuan H, Zheng X, Mei N. Design and experimental analysis of energy-saving and heat storage of a hot water tank based on the source-sink matching principle. Case Studies in Thermal Engineering. 2023;41:102672.

[9] Hu N, Li Z-R, Xu Z-W, Fan L-W. Rapid charging for latent heat thermal energy storage: A state-of-the-art review of close-contact melting. Renewable and Sustainable Energy Reviews. 2022;155:111918.

[10] Tan S, Zhang X. Progress of research on phase change energy storage materials in their thermal conductivity. Journal of Energy Storage. 2023;61:106772.

[11] Chen X, Zhang Z, Qi C, Ling X, Peng H. State of the art on the high-temperature thermochemical energy storage systems. Energy Conversion and Management. 2018;177:792-815.

[12] Hua W, Yan H, Zhang X, Xu X, Zhang L, Shi Y. Review of salt hydrates-based thermochemical adsorption thermal storage technologies. Journal of Energy Storage. 2022;56:106158.

[13] Crespo A, Frazzica A, Fernández C, de Gracia Á. Optimizing the discharge process of a seasonal sorption storage system by means of design and control approach. Journal of Energy Storage. 2023;60:106652.

[14] Ding Z, Wu W. Type II absorption thermal battery for temperature upgrading: Energy storage heat transformer. Applied Energy. 2022;324:119748.

[15] Ding Z, Wu W. A novel double-effect compression-assisted absorption thermal battery with high storage performance for thermal energy storage. Renewable Energy. 2022;191:902-18.

[16] Zhang Y, Palomba V, Frazzica A. Understanding the effect of materials, design criteria and operational parameters on the adsorption desalination performance – A review. Energy Conversion and Management. 2022;269:116072.

[17] Ding Z, Wu W. Dynamic discharging characteristics of absorption thermal battery under different capacity regulation strategies. Energy and Built Environment. 2022; 4:341-353.

[18] Palomba V, Brancato V, Frazzica A. Thermal performance of a latent thermal energy storage for exploitation of renewables and waste heat: An experimental investigation based on an asymmetric plate heat exchanger. Energy Conversion and Management. 2019;200:112121.

[19] Yu YQ, Zhang P, Wu JY, Wang RZ. Energy upgrading by solid–gas reaction heat transformer: A critical review. Renewable and Sustainable Energy Reviews. 2008;12:1302-24.

[20] Wu S-F, Wang L-W, An G-L, Zhang B. Excellent ammonia sorption enabled by metal-organic framework nanocomposites for seasonal thermal battery. Energy Storage Materials. 2023;54:822-35.

[21] Gao P, Wang LW, Zhu FQ. A novel hybrid solid sorption-compression refrigeration technology for refrigerated transportation and storage. International Journal of Refrigeration. 2021;122:1-10.

[22] Gao P, Wei X, Wang L, Zhu F. Compression-assisted decomposition thermochemical sorption energy storage system for deep engine exhaust waste heat recovery. Energy. 2022;244:123215.

[23] Jiang L, Liu W, Lin YC, Wang RQ, Zhang XJ, Hu MK. Hybrid thermochemical sorption seasonal storage for ultra-low temperature solar energy utilization. Energy. 2022;239:122068.

[24] Ding Z, Wu W, Huang S-M, Huang H, Bai Y, He Z. A novel compression-assisted energy storage heat transformer for low-grade renewable energy utilization. Energy. 2023;263:125681.

[25] Jiang L, Roskilly AP, Wang RZ, Wang LW, Lu YJ. Analysis on innovative modular sorption and resorption thermal cell for cold and heat cogeneration. Applied Energy. 2017;204:767-79.

[26] Jiang L, Wang RZ, Wang LW, Roskilly AP. Investigation on an innovative resorption system for seasonal thermal energy storage. Energy Conversion and Management. 2017;149:129-39.
[27] Jiang L, Roskilly AP. Thermal conductivity, permeability and reaction characteristic enhancement of ammonia solid sorbents: A review. International Journal of Heat and Mass Transfer. 2019;130:1206-25.
[28] Li W, Jaromír Klemeš J, Wang Q, Zeng M. Efficient thermal management strategy of Li-ion battery pack based on sorption heat storage. Energy Conversion and Management. 2022;256:115383.
[29] Godefroy A, Perier-Muzet M, Mazet N. Thermodynamic analyses on hybrid sorption cycles for low-grade heat storage and cogeneration of power and refrigeration. Applied Energy. 2019;255:113751.
[30] Godefroy A, Perier-Muzet M, Neveu P, Mazet N. Hybrid thermochemical cycles for low-grade heat storage and conversion into cold and/or power. Energy Conversion and Management. 2020;225:113347.
[31] Li T, Wang R, Kiplagat JK, Kang Y. Performance analysis of an integrated energy storage and energy upgrade thermochemical solid–gas sorption system for seasonal storage of solar thermal energy. Energy. 2013;50:454-67.
[32] Yan T, Wang CY, Li D. Performance analysis of a solid-gas thermochemical composite sorption system for thermal energy storage and energy upgrade. Applied Thermal Engineering. 2019;150:512-21.
[33] Bao H, Ma Z, Roskilly AP. Integrated chemisorption cycles for ultra-low grade heat recovery and thermo-electric energy storage and exploitation. Applied Energy. 2016;164:228-36.
[34] Jiang L, Li S, Wang RQ, Fan YB, Zhang XJ, Roskilly AP. Performance analysis on a hybrid compression-assisted sorption thermal battery for seasonal heat storage in severe cold region. Renewable Energy. 2021;180:398-409.
[35] Ma Z, Bao H, Roskilly AP. Seasonal solar thermal energy storage using thermochemical sorption in domestic dwellings in the UK. Energy. 2019;166:213-22.
[36] Thinsurat K, Ma Z, Roskilly AP, Bao H. Compressor-assisted thermochemical sorption integrated with solar photovoltaic-thermal collector for seasonal solar thermal energy storage. Energy Conversion and Management: X. 2022;15:100248.
[37] Hu H, Han Y, Gao P, Zhang W, Wu W, Yang Q, et al. Chemisorption heat pump governed by asynchronous start-stop method for stable heat output. Energy Conversion and Management. 2023;277:116681.
[38] Gao P, Hu H, Jin S, Wang S, Chen Y, Wu W, et al. Solar-driven compression-assisted desorption chemisorption refrigeration/cold energy storage system. Energy Conversion and Management. 2022;258:115474.
[39] Najjaran A, Meibodi S, Ma Z, Bao H, Roskilly T. Experimentally Validated Modelling of an Oscillating Diaphragm Compressor for Chemisorption Energy Technology Applications. Energies. 2023;16:489.
[40] Jiang L, Wang LW, Jin ZQ, Wang RZ, Dai YJ. Effective thermal conductivity and permeability of compact compound ammoniated salts in the adsorption/desorption process. International Journal of Thermal Sciences. 2013;71:103-10.
[41] Jiang L, Wang LW, Wang RZ. Investigation on thermal conductive consolidated composite CaCl2 for adsorption refrigeration. International Journal of Thermal Sciences. 2014;81:68-75.
[42] Wang R, Wang L, Wu J. Adsorption Refrigeration Technology: Theory and Application. Wiley. 2014.
[43] Fitó J, Coronas A, Mauran S, Mazet N, Perier-Muzet M, Stitou D. Hybrid system combining mechanical compression and thermochemical storage of ammonia vapor for cold production. Energy Conversion and Management. 2019;180: 709-723.
[44] An GL, Wang LW, Gao J, Wang RZ. A review on the solid sorption mechanism and kinetic models of metal halide-ammonia working pairs. Renewable and Sustainable Energy Reviews. 2018;91: 783-792.
[45] Huang H-J, Wu G-B, Yang J, Dai Y-C, Yuan W-K, Lu H-B. Modeling of gas–solid chemisorption in chemical heat pumps. Separation and Purification Technology. 2004;34:191-200.
[46] An G, Li Y, Wang L, Gao J. Wide applicability of analogical models coupled with hysteresis effect for halide/ammonia working pairs. Chemical Engineering Journal. 2020;394:125020.

The 18th International Symposium on District Heating and Cooling, September 3–6, 2023, Beijing, China

Thermochemical energy storage for heating applications – An experimental study

Mingxi Ji*, Abdalqader Ahmad, Hongkun Ma, Yulong Ding*

Birmingham Centre for Energy Storage, School of Chemical Engineering, University of Birmingham, Birmingham, B15 2TT, UK
** Corresponding authors. mxj164@studnet.bham.ac.uk (Mingxi Ji), y.ding@bham.ac.uk (Yulong Ding)*

ABSTRACT

The critical role of thermal energy storage (TES) in the net-zero energy transition future has been widely recognised, particularly for addressing challenges associated with variable renewable energy generation, waste heat utilisation, and energy supply and demand mismatches. There are mainly three types of TES technologies (sensible, latent and thermochemical), this work is concerned with thermochemical energy storage (TCES). The TCES is commonly regarded as a long-duration energy storage technology, but it can also be used for short- and medium-term applications. This work studies a packed bed-based TCES system, with a specific focus on district/domestic space and water heating applications. The work experimentally investigated the performance of a 7.5 kWh TCES system using both a pure sorbent (silica gel) and a salt hydrated based composite thermochemical material (CTCM) named BCES-CTCM-130. The temperature profiles at different locations in the system were monitored and the effects of charging/discharging flow rates and temperatures on the system performance were examined. The charging/discharging efficiency and system Coefficient of Performance (COP) are evaluated. The results showed a temperature lift of ~30 °C is achievable and the outlet temperature remained above 35 °C for more than 7 hours. Also, the CTCM has charging and discharging efficiencies of ~56% and ~71%, respectively, with an overall COP of 0.39. The COP would increase to 0.58 if the exhaust heat in the charging process could be utilised. Compared to pure thermochemical material, the BCES-CTCM-130 showed a higher temperature lift and a higher efficiency.

Keywords: Thermochemical energy storage, Sorption based heating system, Solid-gas system, Packed bed reactor

Nomenclature

General		W	Humidity ratio in kg_{water}/kg_{da}
C_1...,C_6	Calculation constants	∅	Relative humidity in %
h	Specific enthalpy in kJ/kg	*Subscripts*	
$\dot{m}$	Air mass flowrate in kg/s	bed	Packed bed reactor
P	Total barometric pressure in Pa	cha	Charging
$P_{F,C}$	Axial fan energy consumption during charging in kW	dis	Discharging
$P_{F,D}$	Axial fan energy consumption during discharging in kW	da	Dry air
P_w	Water vapour pressure in Pa	g	Saturated water vapour
P_{ws}	Water vapour saturation pressure in Pa	heater	Inline heater
Q_{des}	Total energy stored by the TCM during the charging in kJ	in	Inlet
Q_{ads}	Total energy released during the discharging in kJ	out	Outlet
$Q_{t,in}$	Total energy consumption for one specific charging and discharging cycle in kJ	t	Total
Q_{heater}	Total energy consumed by the inline heater in kJ	*Greek symbols*	
T	Dry bulb temperature in K	η	Thermal efficiency

1. INTRODUCTION

In recent years, there has been a notable increase in energy consumption, resulting in a corresponding rise in the use of conventional fossil fuels. Unfortunately, this trend has led to elevated greenhouse gas emissions, posing more risks due to global warming [1]. Between 1990 and 2021, the world's annual carbon dioxide (CO_2) emissions, raised from 22.7 billion tonnes to 37.1 billion tonnes. This upward trend highlights the alarming growth in emissions over the past three decades which required an urgent solution [2]. The International Energy Agency [3] indicates that 40% of global total energy consumption took up by building applications which results in 24% of global CO_2 emissions. Looking into the building sector, energy consumption was mainly used for space heating and hot water generation for the residents. In line with carbon neutralisation objectives, renewable energy sources are projected to take an increasing share of the global energy production

landscape. However, one of the challenges faced by renewable energy sources is the mismatches in time, space and energy grade between energy supply and demand, hampering their deployment compared to conventional fossil fuels [4]. According to Gong et al. [5], the current district heating system experiences the fourth generation which utilised the integration of renewable energy or low-grade waste heat sources for heat provision. To overcome the issues related to the intermittent nature of renewable energy and low-grade waste heat sources, the dependence on specific time, space and grade availabilities, and the flexibility in energy end use, thermal energy storage (TES) has a pivotal role to play [6]. TES can also help facilitating sector coupling and decarbonising the next generation district heating and cooling systems [7]. Integrated TES in district heating systems provides means to store excess energy generated during periods of high production and release it when demand is greater or when energy sources are not actively generating energy [8]. Therefore, the discontinuity of energy supply can be mitigated, and shifting the load to off-peak times to reduce the CO_2 emissions, leads to a more reliable and flexible energy system [9].

TES can be categorized into three main types: sensible energy storage, latent energy storage, and thermochemical energy storage. The sensible TES involves storing and releasing the energy in the form of temperature difference of a storage medium by heating or cooling it. The latent TES stores energy through the phase change of a storage medium, which can be a solid-liquid or a liquid-gas phase transition, allowing for a high storage capacity than the sensible heat storage and more stable charging and discharging process [10]. Thermochemical energy storage (TCES) utilizes reversible sorption and/or chemical reactions to store and release energy [11]. TCES is considered the most suitable seasonal storage method compared to the sensible and latent TES due to its high energy density and minimal energy losses during the storage stage [12]. **Figure 1** illustrates the basic principle of the TCES technology.

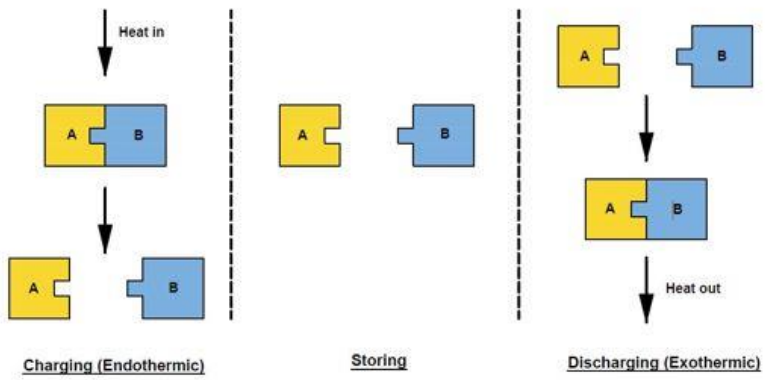

Figure 1. Thermochemical energy storage concept [13]

During the charging process, heat is supplied to alter chemical bonds between reactants and/or sorption pairs (A and B) through an endothermic reaction. As a result, the thermochemical materials (TCM) undergo dissociation, and the separated components can be stored independently at the ambient temperature. In the discharging process, the separately stored reactants and/or sorbent pairs recombine to produce the chemical bonds (AB), releasing stored thermal energy due to exothermic reaction. This reversible process allows for efficient storage and retrieval of thermal energy in TCES systems [14]. Contemporary TCES systems are still suffering from a number of drawbacks, including system complexity, materials durability/cyclability and low system-level performance.

This study reports an experimental study on a solid-gas packed bed based TCES system using sorption pairs as the thermochemical materials. A comparison of the pure sorbent and composite sorbents is made to illustrates the advantages of the use of composite TCM. Both process efficiencies (charging and discharging) and the system-level performance in the form of the so-called Coefficient of Performance (COP) are evaluated for domestic heating applications though the conclusions are also expected to be applicable to some industrial applications. Fundamentally, the work also seeks to understand the potential use of the TCES system to district/domestic heating applications.

2. METHODOLOGIES

This section covers the used methodology to build and test a TCM based thermal energy storage system that be used for heating applications, which includes the materials selection and preparation, test rig configuration, experimental procedure and corresponding efficiencies evaluation were presented.

2.1. Materials selection and preparation

Among all solid-gas TCM, salt hydrates offer several advantages of suitable exothermic temperature, high energy storage

density and cheap that make them attractive for various applications, particularly in district/domestic heating [17]. N'Tsoukpoe et al. [18] systematically investigated 45 pre-selected salt hydrates, strontium bromide ($SrBr_2$) emerged as the most promising candidate from the thermodynamic perspective and cyclability. While salt hydrates offer several advantages, it is essential to address some of the associated drawbacks. These include slow thermodynamics and kinetics, issues with agglomeration and swelling, as well as limitations in mass transfer due to permeability and porosity concerns [19],[20]. To overcome the limitations, the concept of using composite materials has been proposed such as preventing salt agglomeration and swelling and improving the thermal conductivity of the reactor bed [21]. During experiments, composite thermochemical materials (CTCM) was a combination of salt hydrate embedded within a porous matrix. The high molar reaction enthalpy, good revisability, well cyclability and well performance in mass transfer make it a potential candidate as thermochemical material [22]. Therefore, salt hydrated was selected as the thermochemical material in this work and porous host matrix structure could support the materials and enlarger the adsorption surface area as well as improve the heat and mass transfer over cycles [23]. The other was pure sorbent (silica gel, brought from Brownell limited) which runs as a reference for the comparison to investigate the performance improvement of the CTCM as shown in **Figure 2**.

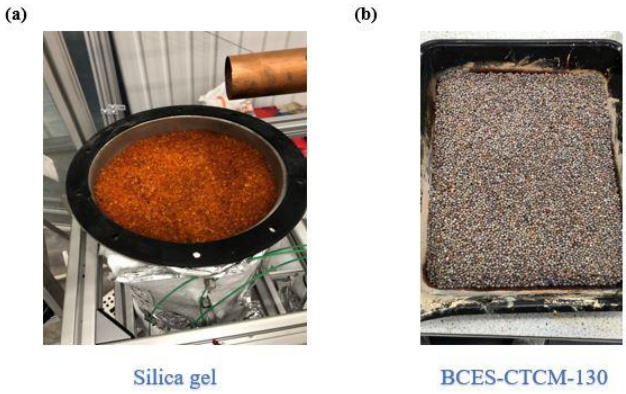

Figure 2.Pure sorbent silica gel and composite thermochemical materials used in packed bed reactor

2.2. Experiment test rig setup

As aforementioned, the TCES technology remains at a low technology readiness level. Therefore, a prototype TCES system (with a designed capacity of 7.5 kWh) was designed, constructed, and commissioned to test the system-level performance. **Figure 3** is the schematic diagram of the preliminary TCES system. The system configuration includes a packed bed reactor an axial fan that provided working fluid air, an inline heater as an energy source during the charging process, a humidification unit that provided water vapour during the discharging process and a heat exchanger with cold water tank for heat recovery. To further access the temperature profile within the reactor bed, six thermocouples were installed and named T1 to T6 from the bottom to the top layer with 100 mm gap. Additional thermocouples, humidity sensors and a flowmeter were fitted at different locations in the system to measure the operating parameters of the system.

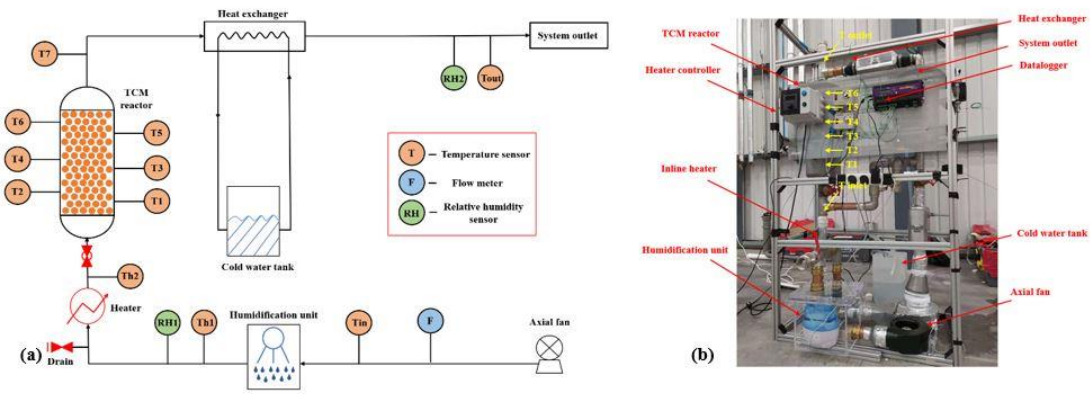

Figure 3. TCES system (a) Schematic diagram (b) Lab test rig setup

2.3. Experimental procedure

The experimental procedure was composed of three steps: charging, storage, and discharging. The charging (desorption) process was done by introducing hot air through the bed to remove the adsorbate (water). The inlet airflow was from a blower at ambient temperature, heated to 130 °C using inline heater element before entering the reactor bed. During the storing step, the system was cool down to ambient temperature and waited for further utilisation. The discharging (adsorption) process

was done by passing moist air through the bed, enabling the thermochemical reaction to take place. The stored heat was released from the materials and provided a temperature lift for the system outlet.

2.4. TCES system performance analysis

To examine the thermal efficiency of the TCES system during the charging process, a ratio of total desorption energy in the reactor to the total energy consumption of the system was used and as shown in equation (1).

$$\eta_{cha} = \frac{Q_{des}}{Q_{heater} + P_{F,c}} = \frac{\dot{m}\left(h_{out,bed,cha} - h_{in,bed,cha}\right)}{\dot{m}\left(h_{out,heater} - h_{in,heater}\right) + P_{F,c}} \tag{1}$$

Where Q_{des} is the total energy required for the charging (desorption) process and it was calculated using the enthalpy difference of air at the reactor inlet and outlet in kJ, considering that 5 - 10 % of this energy can be lost to the environment. Q_{heater} is the total energy consumption by the inline heater which is calculated using the enthalpy difference of air at the heater inlet and outlet in kJ. $P_{F,c}$ is the energy consumption by the axial fan given by the manufacturer in kJ, $\dot{m}$ is the air mass flowrate in kg/s and h is the specific enthalpy in kJ/kg.

The discharging thermal efficiency of the system is defined as a ratio of the total energy released by TCM through adsorption to the total energy consumption during the discharging process, shown in the following equation (2).

$$\eta_{dis} = \frac{Q_{ads}}{Q_{des} + P_{F,d}} = \frac{\dot{m}\left(h_{out,bed,dis} - h_{in,bed,dis}\right)}{\dot{m}\left(h_{out,bed,cha} - h_{in,bed,cha}\right) + P_{F,d}} \tag{2}$$

Where Q_{ads} is the total energy released during the discharging (adsorption) process and it was using the enthalpy difference of air at the reactor inlet and outlet in kJ. While the total energy consumption is consisting of the total amount of energy required for the charging process, Q_{des} and the power consumed by the axial fan, $P_{F,d}$ given by the manufacturer in kJ.

The Coefficient of Performance (COP) was estimated to assess the overall system performance. It could be defined by the ratio of the total energy released during adsorption to the total energy consumption of the TCES system in both charging and discharging, according to Equation (3)

$$COP = \frac{Heating\ effect}{Total\ energy\ comsumption} = \frac{Q_{ads}}{Q_{t,in}} = \frac{Q_{ads}}{Q_{heater} + P_{F,c} + P_{F,d}} \tag{3}$$

where $Q_{t,in}$ is the total energy consumption for one specific charging and discharging cycle, including total energy consumption by the inline heater and power consumption of the axial fan in both charging and discharging. From abovementioned, efficiencies calculation included the specific enthalpy of the moist air which can be expressed by the summation of individual partial enthalpies from [24].

$$h_t = h_{da} + W \cdot h_g \tag{4}$$

$$W = 0.62198 \times \frac{P_w}{P - P_w} \tag{5}$$

Where h_t is the total enthalpy of the mixture, h_{da} is the specific enthalpy of dry air, h_g is the specific enthalpy of saturated water vapour, W is the humidity ratio given, P is the total barometric pressure and P_w is the water vapour pressure which could be calculated as follows in Equation (6).

$$P_w = \emptyset \times P_{ws} \tag{6}$$

Where $\emptyset$ is the relative humidity and P_{ws} is water vapor saturation pressure shown in Equation (7).

$$P_{ws} = e^{\frac{C1}{T} + C2 + C3T + C4T^2 + C5T^3 + C6In(T)} \tag{7}$$

Where T is the dry bulb temperature in Kelvin, $C_1 \ldots C_6$ are the constants as shown in **Table 1**.

Table 1. Constants for water vapor saturation pressure calculation [24].

Constants	Values	Constants	Values
C_1	-5.8×10^3	C_4	4.17610^{-5}
C_2	1.3915	C_5	-1.44510^{-8}
C_3	-4.86410^{-2}	C_6	6.545

3. RESULTS AND DISCUSSION

Figure 4 illustrates the charging process result for pure sorbent silica gel and CTCM. The red and orange curves are the inlet temperature and outlet temperature of the reactor, respectively. The remaining curves are the temperature sensors inside the reactor with a 100mm distance from bottom to top (T1 to T6). For the charging process, the temperature increases rapidly and reaches the first peak at the first 20 minutes in all positions then slowly drops down. The theory behind this phenomenon is the latent heat of water evaporation during TCM dehydration (desorption process) led to a reduction in temperature. The first layer has the shortest period for breaking the bonded energy between water and TCM itself as its position is close to the inlet air at the bottom. Oppositely, the top layer has the longest period due to its position at the top layer within the reactor bed. Finally, once the TCM became unsaturated, the temperature of the materials will increase again until it reaches the full charge mode. In terms of operating parameters, they experienced the same conditions during experiments which included a regeneration temperature of 130°C and an air flowrate of 1650 L/min. It could be seen from the figures, the charging process temperature for both TCMs was nearly identical, the difference in the comparison was the water evaporation stage. Due to materials properties, salt hydrated with porous matrix undergo a thermochemical reaction (chemisorption) which is different from the physisorption of silica gel. The CTCM has a faster dehydration kinetic, and reduced duration of full charge. Therefore, the charging duration of CTCM is 3.75 hours which is slightly shorter compared to 4 hours of silica gel.

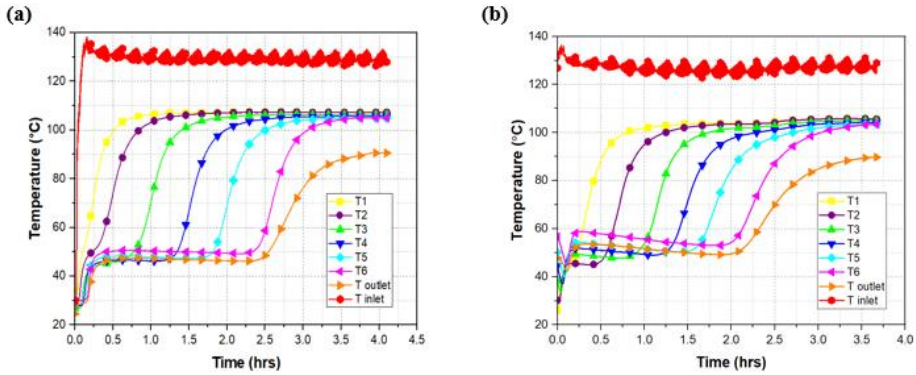

Figure 4. Experiment results of charging process for (a) silica gel (b) CTCM

Regarding discharging process, the temperature dramatically increases in the first half-hour due to water vapour in moist air reacting with TCM to allow the thermochemical reaction to take place (adsorption process). After TCM reached a peak temperature for a while and declines gradually one by one to its stable temperature. This means that the thermal energy stored during the charging process was released by the exothermic reaction. Normally, there are two criteria to examine the feasibility of TCM in further applications. One is the ability to rise the system outlet temperature (temperature lift), and the other is the potential to provide a sufficient duration of hot outlet temperature to the end users.

Figure 5 presents the discharging process of both the pure sorbent silica gel and the CTCM. Similarly, the blue and orange curves are the inlet temperature and outlet temperature of the reactor, respectively. The rest of the temperature curve represents the sensors inside the reactor. The same conditions were applied to both candidates during experiments which included an inlet temperature of 17 °C, air flowrate of 1450 L/min and inlet relative humidity of 60%. Unlike the charging process, the discharging process significantly indicated differentiation. Firstly, CTCM performed a higher peak temperature of 56°C compared to 45°C for silica gel resulting in a higher temperature lift of ~ 30°C. The CTCM effectively increase the maximum adsorption temperature and have a faster decreasing rate of outlet temperature than silica gel. This difference can be attributed to the varying reaction kinetics between the two materials. CTCM demonstrated a faster chemisorption phenomenon, leading to a more rapid and efficient adsorption process.

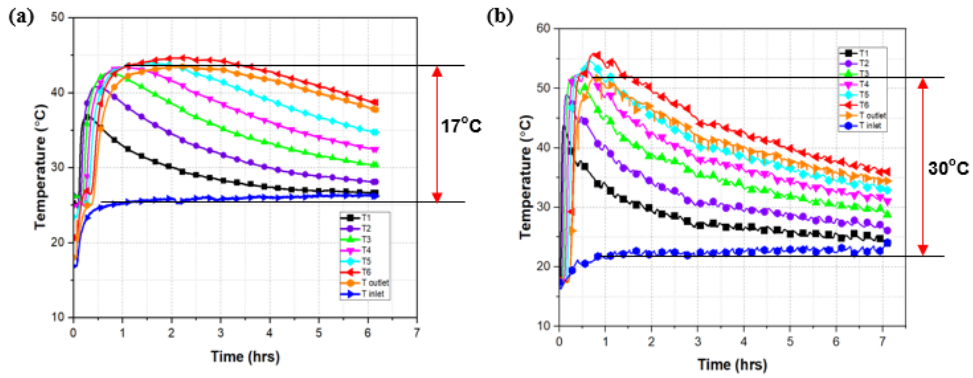

Figure 5. Experiment results of discharging process for (a) silica gel (b) CTCM

Following the above methodology, the charging/discharging efficiency and COP of both silica gel and CTCM experimental results were evaluated as shown in **Table 2**. Under the same operating conditions, CTCM experimental result performs higher efficiencies in charging, discharging and COPs, respectively. However, the difference is not significant for charging efficiency. This may be due to the shorter charging duration of CTCM which reduces the energy consumption of the axial fan and less heat losses to surrendering. The other is in the discharging process, a larger temperature lift of CTCM indicates more thermal energy releasing and higher discharging efficiency. Therefore, the thermal performance of CTCM would be better than the results of silica gel and further experimental investigation will focus on the CTCM.

Table 2. Efficiencies calculation for both TCMs

Efficiencies	**Charging (%)**	**Discharging (%)**	**COP (-)**
Pure sorbent – silica gel	48.32	42.00	0.358
BCES-CTCM-130	50.69	47.61	0.416

A lower COP is calculated compared to the values from the literature, there could be two reasons. One is the outlet air from the reactor during the charging process was vented to the ambient directly. Instead of wasting the high temperature from the reactor outlet, a heat exchanger could help to recover that part of the thermal energy by connecting the outlet to the inlet of the reactor in order to preheat the cold air from the axial fan. The other is the energy generated by the TCES is underestimated due to the part of the heat that will continuously generate beyond the discharging duration. Thus, it should consider that portion of heat during the calculation of the overall system efficiency. Moreover, systematic experiments should be done to acquire optimal operating conditions for maximum COPs including setting temperature, relative humidity, and air flowrate. Thus, the effect of inlet air flowrate during discharging process was explored to optimise the COP as shown in **Figure 6**.

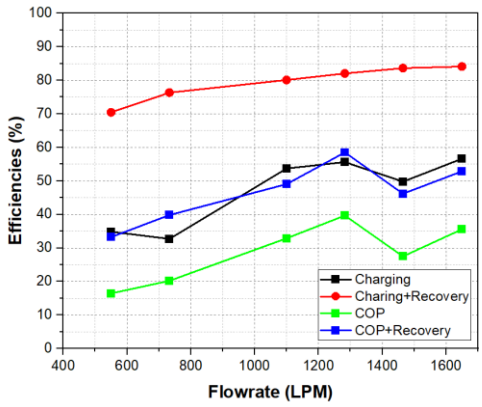

Figure 6. Efficiencies and COP variation under different flowrate

Originally, a higher COP was expected to be experienced at a higher flowrate. However, the highest discharging efficiency and COP are 71.31% and 0.39, respectively at a flowrate of 1283 L/min from **Figure 6**. This is possibly due to the high flowrate allowing more water vapour to enter the reactor bed, which speeds up the thermochemical reaction. Nevertheless, an overly high flowrate reduced the residence time of the surface adsorption reaction and the discharging duration also declined. Apart from normal charging efficiency and COP in **Figure 6**, a recovery part was added which under calculation

of an extra preheating heat exchanger installed. Although the enhancement is not yet finished, the prospect of improving COP is achievable.

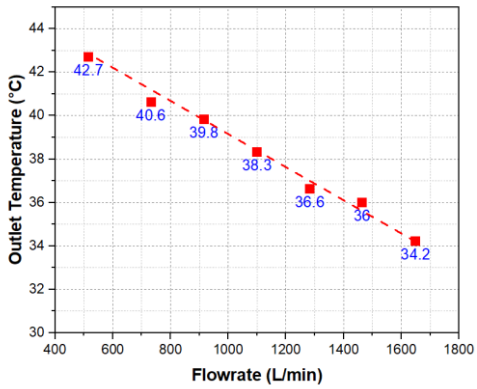

Figure 7. Outlet temperature after 7 hours discharging under different flowrate

Also, a comparison of outlet temperature between experiments was plotted as presented in **Figure 7**. A higher flowrate resulted in a lower outlet temperature during the discharging process. Although the amount of heat stored in TCM was constant since the full charge completed, the rate of heat released would increase due to the high flowrate within the bed. Consequently, a lower outlet temperature was observed for the same discharging duration and an optimal flowrate of around 1283 L/min is recommended for further systematic study in terms of efficiencies. Lastly, BCES-CTCM-130 would be advocated for heating applications which performs higher temperature lift and higher efficiencies.

4. CONCLUSION

The feasibility of applying TES in domestic heating applications has been experimentally investigated in this work, where a packed bed based system with a capacity of 7.5 kWh has been built and tested. Two types of thermochemical materials were applied for comparison, pure sorbent silica gel and the other is composite of salt hydrated embedded in the porous matrix. The results indicate that the BCES-CTCM-130 exhibit promising potential for district and domestic heating applications due to their ability to achieve an outlet temperature of 35°C following discharging process, along with an impressive temperature lift of 30°C. In terms of system-level efficiencies, the comprehensive performance of CTCM surpasses that of pure sorbent. Also, the experimental study of CTCM achieved its highest coefficient of performance (COP) value of 0.39 at an air flowrate of 1283 L/min. However, the COP evaluated in this study was lower compared to values reported in other literature. This is due to the huge energy consumption in the charging process. One potential solution is to install a preheat heat exchanger which harnesses the hot air from the outlet to recover thermal energy. As a result, the system COP could be increased to 0.58 theoretically. Future investigations will primarily concentrate on altering additional operating parameters such as inlet temperature and inlet relative humidity to optimise the thermal performance of the TCES system.

ACKNOWLEDGEMENT

This is work is partially funded by the UK Engineering and Physical Sciences Research Council (EPSRC) under Grants EP/P003605/1, EP/V012053/1, EP/T022981/1 and EP/S0326221/1.

REFERENCES

[1] Li W, Klemeš JJ, Wang Q, Zeng M. Salt hydrate–based gas-solid thermochemical energy storage: Current progress, challenges, and perspectives. Renew Sustain Energy Rev 2022;154.
[2] Ritchie H, Max R. CO2 emissions - Our World in Data. Our World Data 2017, https://ourworldindata.org/co2-emissions; [Accessed May 16, 2023].
[3] IEA. Greenhouse Gas Emissions from Energy - Data product – IEA, https//www.Iea.org/data-and-statistics/data-product/greenhouse-gas-emissions-from-energy; [Accessed May 16, 2023]
[4] Marín PE, Milian Y, Ushak S, Cabeza LF, Grágeda M, Shire GSF. Lithium compounds for thermochemical energy storage: A state-of-the-art review and future trends. Renew Sustain Energy Rev 2021;149.
[5] Gong Y, Ma G, Jiang Y, Wang L. Research progress on the fifth-generation district heating system based on heat pump technology. J Build Eng 2023;71:106533.

[6] Kuznik F, Johannes K, Obrecht C, David D. A review on recent developments in physisorption thermal energy storage for building applications. Renew Sustain Energy Rev 2018;94:576–86.
[7] Angelidis O, Ioannou A, Friedrich D, Thomson A, Falcone G. District heating and cooling networks with decentralised energy substations: Opportunities and barriers for holistic energy system decarbonisation. Energy 2023;269:126740
[8] Buffa S, Cozzini M, D'antoni M, Baratieri M, Fedrizzi R. 5th generation district heating and cooling systems: A review of existing cases in Europe. Renew Sustain Energy Rev 2019;104:504-22.
[9] Groppi D, Pfeifer A, Garcia DA, Krajačić G, Duić N. A review on energy storage and demand side management solutions in smart energy islands. Renew Sustain Energy Rev 2021;135:110183.
[10] Abedin AH. A Critical Review of Thermochemical Energy Storage Systems. Open Renew Energy J 2011;4:42–6.
[11] Aydin D, Casey SP, Riffat S. The latest advancements on thermochemical heat storage systems. Renew Sustain Energy Rev 2015;41:356–67.
[12] Clark RJ, Mehrabadi A, Farid M. State of the art on salt hydrate thermochemical energy storage systems for use in building applications. J Energy Storage 2020;27:101145.
[13] Desai F, Sunku Prasad J, Muthukumar P, Rahman MM. Thermochemical energy storage system for cooling and process heating applications: A review. Energy Convers Manag 2021;229:113617.
[14] Pan ZH, Zhao CY. Gas–solid thermochemical heat storage reactors for high-temperature applications. Energy 2017;130:155–73.
[15] Hongois S, Kuznik F, Stevens P, Roux JJ. Development and characterisation of a new MgSO4-zeolite composite for long-term thermal energy storage. Sol Energy Mater Sol Cells 2011;95(7):1831-37
[16] N'Tsoukpoe KE, Schmidt T, Rammelberg HU, Watts BA, Ruck WKL. A systematic multi-step screening of numerous salt hydrates for low temperature thermochemical energy storage. Appl Energy 2014;124:1–16.
[17] Richter M, Habermann EM, Siebecke E, Linder M. A systematic screening of salt hydrates as materials for a thermochemical heat transformer. Thermochim Acta 2018;659:136–50.
[18] Michel B, Neveu P, Mazet N. Comparison of closed and open thermochemical processes, for long-term thermal energy storage applications. Energy 2014;72:702–16.
[20] Gordeeva LG, Aristov YI. Composites "salt inside porous matrix" for adsorption heat transformation: A current state-of-the-art and new trends. Int J Low-Carbon Technol 2012;7:288–302.
[21] Scapino L, Zondag HA, Van Bael J, Diriken J, Rindt CCM. Sorption heat storage for long-term low-temperature applications: A review on the advancements at material and prototype scale. Appl Energy 2017;190:920–948.
[22] Li W, Guo H, Zeng M, Wang Q. Performance of SrBr2·6H2O based seasonal thermochemical heat storage in a novel multilayered sieve reactor. Energy Convers Manag 2019;198.
[23] Rui J, Luo Y, Wang M, Peng J, She X. Design and performance evaluation of an innovative salt hydrates-based reactor for thermochemical energy storage. J Energy Storage 2022;55:2352–152.
[24] ASHRAE, F. ASHRAE handbook SI Editions. Georgia, USA: American Society of Heating, Refrigerating and Air-Conditioning Engineers; 2005.

The 18th International Symposium on District Heating and Cooling,
September 3-6, 2023, Beijing, China

Research and Application of Heat Storage in District Heating Network of Heating Plant

Zhiwei tang[a*], Tao Lu[a], Yanfei Zhu[b]

[a] *Beijing University of Technology, Beijing, 100124, China*
[b] *Beijing Thermal Engineering Design Co. Ltd. Beijing, 100000, China*
[*] *Zhiwei Tang. tangzhiw@263.net l. china*

Abstract

Effectively utilizing the inherent heat storage capacity of the district heating network (DHN) is equivalent to applying a heat storage tank in the heating network system. By adjusting the operation of the heating network system, when the heat demand of the heat user is low, the heat is stored in the network system. When the heat demand of the heat user is high, the excess heat in the network system is released to the heat user. The "heat storage tank" can improve the flexibility of heat output from regional boiler rooms and thermal power plants. This paper theoretically analyzes the dynamic heat storage and release process of the heating network system, defines the heat storage capacity of the heating network system as "the difference between the heat storage amount in the heating network system under heat storage adjustment operating conditions and under actual operating conditions", and defines temperature-increasing type, flow-increasing type and comprehensive heat storage adjustment The theoretical heat storage capacity of the heating network system under regulation; and takes the Yongtai Heating Plant heating network system in Beijing as a research target for case analysis. The results show that when using temperature-increasing type heat storage regulation, there is a large difference in heat storage capacity between early/late cold periods and severe cold periods in heating network systems, but their trends are consistent and decrease with increasing relative heating load ratio; when using flow-increasing type heat storage regulation , The heat storage capacity of the heating network system is small, with a maximum heat storage capacity of 3.09MWh, and its trend is different from that of temperature-increasing type heat storage regulation. The heat storage capacity of this regulation method increases with increasing relative heating load ratio; when using comprehensive heat storage regulation , Release this part of stored heat to users under this regulation method, which can maintain heating time from 0.33h to 4.71h, and as relative heating load ratio increases, this part of stored heat can maintain heating time decreases accordingly.

Keywords: District Heating Network; Short-Term Heat Storage; Thermal Inertia

Biographical Note(s):
Zhiwei Tang, Faculty of Environment and Life, Beijing University of Technology, main research direction: research on enhanced heat transfer and process energy conservation.
Tao Lu, Faculty of Environment and Life, Beijing University of Technology, main research direction: District Heating Network system energy storage
Yanfei Zhu, Beijing Thermal Engineering Design Co., Ltd, main research direction: Design of *District Heating Network* system.

1. INTRODUCTION

The thermoelectric coupling characteristics of cogeneration units limit the flexibility of the system. Because the utilization

of renewable energy has time periodicity, this characteristic is not conducive to the utilization of renewable energy and the large-scale development of renewable energy. Therefore, it is of great significance to realize the thermoelectric decoupling of cogeneration units[1]. At present, there are three ways to improve the peak shaving capacity of thermoelectric units[2,3]: one is to add electric boilers, heat storage tanks, large heat pumps and other thermal electrolytic coupling equipment[4-7] ; the second is to repair the structure of the thermoelectric unit itself, such as compensation heating and deep peak shaving technology[8,9] ; the third is to develop the system 's peaking capacity in depth, use the thermal inertia of the heating pipe network system and the building to store heat, and relieve the constraint of the " heat-determined electricity " mechanism.[10-13] The core idea of this technology is to use the continuously expanding heating area of urban heating network systems and their intricate branches represent a huge water capacity in the network. In practical applications, this part of the water capacity can be regarded as a ready-made “heat storage tank”. By adjusting the operation of the heating network system, when the heat demand of the heat user is low, the heat is stored in the heating network system. When the heat demand of the heat user is high, the excess heat in the heating network system is released to the heat user. The “heat storage tank” can improve the flexibility of heat output from the heating network system. With the country vigorously promoting “Internet + heating” technology, most heating companies in China have completed the transition from manual operation to automated operation. The informatization, digitalization and intelligent heating platform are gradually being built, creating a feasible objective environment for precise monitoring and heat storage regulation of urban heating network systems[14-16].

This paper theoretically analyzes the dynamic heat storage and release process of the heating network system, defines the heat storage capacity of the heating network system as “the difference between the heat storage amount in the heating network system under heat storage adjustment operating conditions and under actual operating conditions”, and defines temperature-increasing type, flow-increasing type and comprehensive heat storage adjustment The theoretical heat storage capacity of the heating network system under regulation; and takes the Yongtai Heating Plant heating network system in Beijing as a research target for case analysis.

2. METHODOLOGY

2.1. heat storage regulation principle of DHN

Large-scale regional heating systems have a considerable water capacity in their fluid transmission and distribution networks, and have great potential for participating in system heat storage and release. The heating delay characteristics of heating network systems also provide adjustment space for system heat storage and release. The principle of heat storage regulation in urban heating network systems is shown in Figure 1.

In the process of heat storage and release in the heating network system, it is set that when the indoor temperature is high or the relative heating load ratio of the heat user is low during the day, it is the heat storage period; when the outdoor temperature is low or the relative heating load ratio of the heat user is high during the day, it is the heat release period to achieve “peak shifting and valley filling” of heat load for heat users.

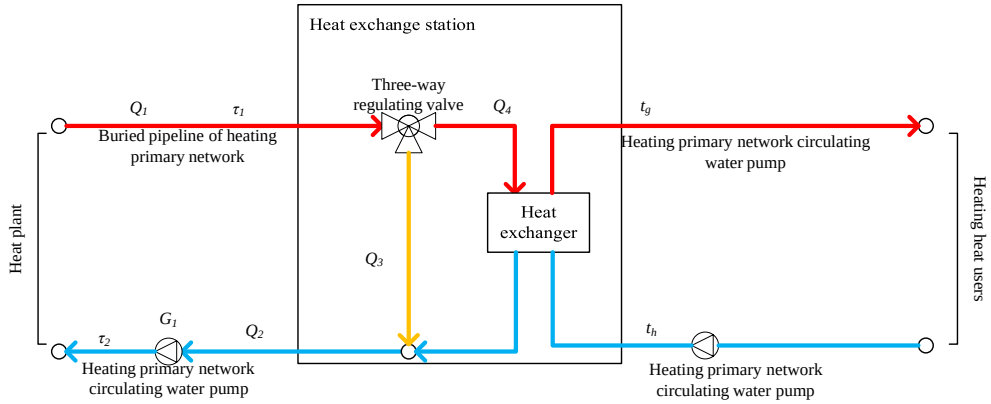

Figure 1. Heat storage regulation flow chart of urban heating network system

By using the delay characteristics and water capacity of the heating network system for heat storage and release, during the heat storage period, the heat output Q_1 of the heat source is increased by increasing the supply and return temperature τ_1 of the primary heating network or increasing the flow rate G_1 of the circulating water pump of the primary heating network. The three-way regulating valve on the heat side of the heat exchange station is controlled accordingly to enable the heat required by the heat user Q_4 to exchange heat with the cold side fluid through the heat exchanger in the heat exchange station, always keeping the supply water temperature t_h of the secondary heating network at a set temperature. The excess heat Q_3 is combined with the heated hot water through the return water pipe after heat exchange. The return water temperature τ_2 of the primary heating network rises, and excess heat is stored in the primary network through this

adjustment method, ultimately improving the heat output of the heat source during the heat storage period and improving the heat output of the heat source when indoor temperature is high or relative heating load ratio of heat users is low during day.

During the heat release period, restore to original centralized heating operation adjustment method. Since part of heat was stored in return water pipe of heating network system during heat storage period, without using high heat output from heat source, supply water pipe of heating network system can reach set operating conditions under original centralized heating operation adjustment method. Ultimately reduce heat output from heat source during release period and reduce its output when outdoor temperature is low or relative heating load ratio of users is high during day.

2.2. heat storage capacity analysis of DHN

The heat storage capacity of the pipe network is defined in this article as "the difference between the heat storage capacity of the heating pipe network system under the heat storage regulation operating conditions and the actual operating process under the reference operating conditions." The heating pipe network system can adjust its heat storage capacity through certain heat storage operations (increasing the supply water temperature of the primary heating network or increasing the circulation flow rate of the primary heating network). When the supply water temperature of the primary heating network and the circulation flow rate of the primary heating network reach their maximum values, the maximum heat storage capacity of the heating pipe network system is reached.

From a macro perspective, when the adjusted heat supply from the heat source is higher than the heat demand of each heat user, the excess heat supply is stored in the heating water, and the heat storage capacity of the heating pipe network system increases. This part of the heat storage can be released when it is necessary to reduce the heat output of the heat source. While ensuring the quality of heating for heat users, it reduces the heat supply from the heat source.

As mentioned earlier, pipe network heat storage and release ultimately manifest as changes in the average temperature of thermal media within the pipe network. Under normal operating adjustment modes for heating systems, thermal conditions in pipe networks are close to steady state and do not participate in system heat storage and release. Dynamic adjustment of supply water temperature from a heat source or changing circulation flow rate in a primary network can actively utilize pipe network heat storage capacity. Therefore, during calculation of heat storage capacity for a heating pipe network system, as in Equation (1).

$$Q_{xr} = C_p \cdot M \cdot \Delta T \tag{1}$$

In the formula: Q_{xr} is the heat storage capacity of the heating network system，in kJ；C_p is the specific heat capacity of water at constant pressure in the heating network system in J/(kg·K); M is the water capacity of the heating network system，in kg；ΔT is the increase in temperature of the buried pipes in the heating network system due to heat storage regulation，in K。

3. RESULTS

3.1. thermal condition of temperature rising heat storage adjustment

Under temperature-increasing heat storage regulation, the heating pipe network system increases the supply water temperature of the primary heating network during the heat storage period and restores the increased supply water temperature of the primary heating network to the reference temperature during the heat release period. The trend of supply and return water temperature changes and heat storage and release under this heat storage regulation mode of the heating pipe network system is shown in Figure 2.

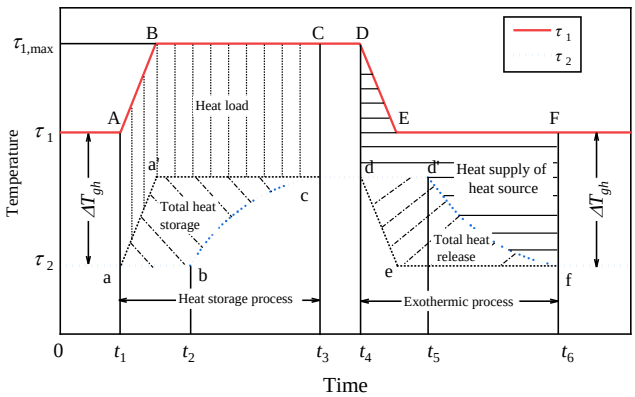

Figure 2. Dynamic thermal conditions of DHN under temperature-increasing heat storage regulation

Figure 2 shows the dynamic heat storage and release process of the primary heating network under changes in heat source supply water temperature. During the heat storage process, the heat source starts to supply excess heat from time t_1. After a period of time, the supply water temperature of the primary heating network rises from the reference value τ_1 to the upper limit of pipe network transmission temperature $\tau_{1,max}$. After high-temperature water reaches each heat exchange station, excess heat is returned to the return water pipe network through three-way regulation. The high-temperature water with the shortest circulation cycle returns to the heat source at time t_2, causing changes in the return water temperature of the primary heating network at the heat source. At time t_3, high-temperature water with the longest circulation cycle returns to the heat source, and the temperature distribution of thermal media in the return water pipe network reaches a new steady state. Since the supply water temperature and circulation flow rate of the heating pipe network system remain unchanged, during time t_2-t_3, excess heat supplied by the heat source gradually decreases and returns to baseline heating state at time t_3. During heat storage process, polygon A-a-a'-c-C-B-A characterizes system's actual thermal load; polygon A-a-b-c-C-B-A characterizes actual heat supply from heat source; therefore polygon a-a'-c-b-a characterizes total heat storage capacity of pipe network.

Similar to heat storage process, during heat release process of heating pipe network system, return water temperature of primary heating network also exhibits certain time lag. Heat source's supply water temperature begins to decrease at time t_4; return water temperature of heating pipe network system responds at time t_5. When return water temperature of primary heating network at heat source decreases to reference value τ_1, pipe network's heat release process ends. During time t_5-t_6, heat supply from heat source continues to increase and returns to reference value at time t_6.

Based on comparison between baseline operating conditions and maximum heat storage conditions shown in Figure 2 for primary heating network, calculation process for theoretical heat storage capacity under temperature-increasing heat storage regulation mode is as in Equation (2).

$$CAP_t = c_p \cdot M_{\text{dhn}} \cdot \left(\tau_{1,max} - \tau_1\right) \quad (2)$$

In the formula: CAP_t is the theoretical heat storage capacity of the primary heating network under temperature-increasing heat storage regulation, in J; $\tau_{1,max}$ is the maximum temperature that the medium in the primary heating network can withstand, in ℃; τ_1 is the reference supply water temperature of the primary heating network, in ℃; M_{dhn} is the total water capacity of the primary heating network, in kg.

From Equation (2), it can be concluded that under temperature-increasing heat storage regulation mode, heat storage capacity of urban heating pipe network system is related to highest medium temperature that heating pipe network system can withstand and reference supply water temperature of primary heating network. Increasing highest medium temperature that pipe network can withstand can significantly increase theoretical heat storage capacity of primary heating network under temperature-increasing heat storage regulation mode.

3.2. thermal condition of increasing flow heat storage adjustment

Under increased flow rate heat storage regulation, heating pipe network system increases circulation pump flow rate of primary heating network during heat storage period and restores increased circulation pump flow rate of primary heating network to reference circulation flow rate during heat release period. The theoretical dynamic thermal power of supply and return water temperature and circulation pump flow rate under increased flow rate heat storage regulation mode for this heating pipe network system is shown in Figure 3.

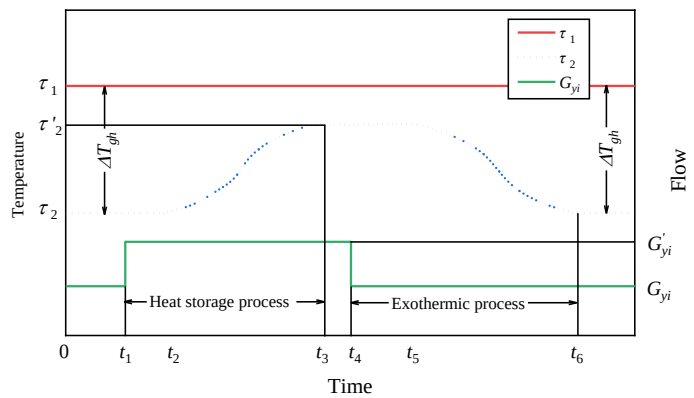

Figure 3. Dynamic thermodynamic process of DHN under increasing flow heat storage regulation

Figure 3 shows dynamic heat storage and release process of primary heating network under increased flow rate heat storage regulation mode. Similar to temperature-increasing heat storage regulation mode, total circulation flow rate of primary heating network increases from reference value G_{yi} to G'_{yi} at time t_1. To maintain constant supply water

temperature, heat source needs to supply excess heat. This part of excess heat returns to return water pipe network of primary heating network through three-way regulating valve. High-temperature water with shortest circulation cycle returns to heat source at time t_2, causing changes in return water temperature of primary heating network at heat source. At time t_3, high-temperature water with longest circulation cycle returns to heat source, temperature distribution of thermal media in return water pipe network reaches new steady state, heat storage process of return water pipe network ends and heat supply from heat source returns to reference value.

For heat release process of primary heating network, system circulation flow rate decreases to reference value G_{yi} at time t_4. Due to high return water temperature at heat source, in order to maintain constant supply water temperature, heat source reduces its heat output operation. At this time, return water pipe network is in heat release state. After return water temperature at heat source returns to reference value at time t_6, pipe network's heat release process ends.

Based on comparison between baseline operating conditions and maximum heat storage conditions shown in Figure 3 for primary heating network, calculation process for theoretical heat storage capacity under increased flow rate regulation mode is as in Equation (3).

$$CAP_g = c_p(\tau_1 - \tau_2)\left(1 - \frac{G_{yi}}{G'_{yi}}\right)M_{dhn} \quad (3)$$

In the formula: CAP_g is the theoretical heat storage capacity of the primary heating network under increased flow rate heat storage regulation, in J; τ_2 is the reference return water temperature of the primary heating network, in ℃; G_{yi} is the reference circulation flow rate of the primary heating network, in t/h; G'_{yi} is the increased circulation flow rate of the primary heating network, in t/h.

From Equation (3), it can be concluded that under increased flow rate heat storage regulation mode for primary heating network of urban heating pipe network system, its heat storage capacity is related to increased circulation flow rate of primary heating network and reference supply and return water temperature difference of primary heating network. Increasing increased circulation flow rate of primary heating network can significantly increase theoretical heat storage capacity of primary heating network under increased flow rate heat storage regulation mode.

3.3. comprehensive heat storage regulation thermal conditions

Increasing both heat source supply water temperature and primary network circulation flow rate can achieve greater pipe network heat storage capacity. Figure 4 shows change curve of heat source supply and return water temperature and circulation pump flow rate during comprehensive heat storage process of primary heating network.

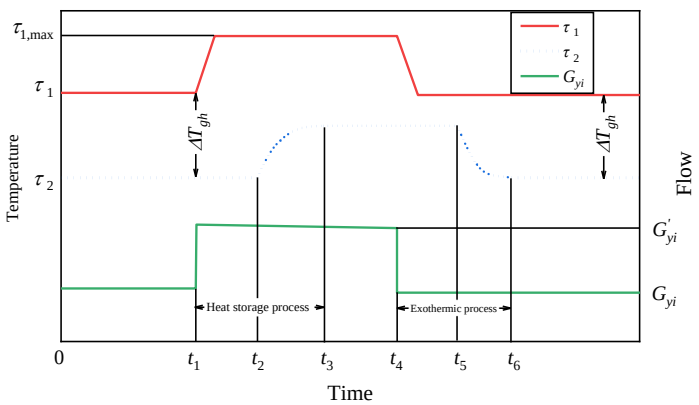

Figure 4. dynamic thermal condition of DHN under comprehensive heat storage regulation mode

Figure 4 shows dynamic heat storage and release process of primary heating network under comprehensive heat storage regulation mode. At time t_1, heat source increases supply water temperature to upper limit of pipe network transmission temperature $\tau_{1,max}$, while circulation pump flow rate of primary heating network increases to G'_{yi}. This part of excess heat returns to return water pipe network of primary heating network through three-way regulating valve. High-temperature water with shortest circulation cycle returns to heat source at time t_2, causing changes in return water temperature of primary heating network at heat source. This part of heat is stored in supply and return water pipes of primary heating network. At time t_3, return water temperature at heat source stabilizes and completes heat storage process of primary heating network.

For heat release process of primary heating network, at time t_4, supply water temperature of primary heating network gradually decreases from upper limit of pipe network transmission temperature $\tau_{1,max}$ to reference supply water

temperature τ_1 of primary heating network. At the same time, circulation pump flow rate of primary heating network decreases from G'_{yi} to G_{yi}. Due to high return water temperature at heat source, in order to maintain constant supply water temperature, heat source reduces its output operation. At this time, return water pipe network is in heat release state. After return water temperature at heat source returns to reference value at time t_6, pipe network's heat release process ends.

Based on comparison between baseline operating conditions and maximum heat storage conditions shown in Figure 4 for primary heating network, calculation process for theoretical heat storage capacity under temperature-increasing heat storage regulation mode is as in Equation (4).

$$CAP_{total} = CAP_t + CAP_g. \quad (4)$$

In the formula: CAP_{total} is the heat storage capacity of the heating primary network under the comprehensive heat storage regulation, in J.

According to Equations (2) to (4), comprehensive theoretical heat storage capacity of primary heating network is related to highest medium temperature that pipe network can withstand, reference supply and return water temperatures and maximum circulation flow rate from heat source. Increasing highest medium temperature that pipe network can withstand and increased circulation flow rate of primary heating network can significantly increase heat storage capacity of primary heating network. In addition, reference supply and return water temperature difference from heat source also directly affects size of heat storage capacity for primary heating network.

4. DISCUSSION

4.1 heating plant configuration

The urban heating network system used for case study in this paper is located in Haidian District, Beijing. The heat source is provided by Yongtai Heating Plant. The heating area is about 1.2419 million m^2 and the heating radius is about 1.1km. According to the theoretical heat storage capacity calculation formula of the heating network system in Section 4.3, the relevant values are summarized as shown in Table 1. To evaluate the theoretical heat storage capacity of Yongtai Heating Plant's heating network system and to ensure the hydraulic balance during the operation of the heating network system, the increased primary network flow rate of heating is set to not exceed 1.5 times the reference flow rate of the primary network of heating.

Table 1 Parameter values of theoretical heat storage capacity calculation case of DHN

Name of style	**Appearance**
Parameters Primary network design supply and return water temperature	80/50 ℃
Secondary network design supply and return water temperature /	65/45 ℃
Maximum supply water temperature that the primary network can withstand /	150 ℃
Primary network design circulating water pump flow rate	1450 t/h
Maximum circulating water pump flow rate of the primary network	1820 t/h
Total water capacity of the primary network	2.626×10^6 kg

4.2 case analysis

In order to distinguish between the operating conditions of the heating network system in early and late cold periods and severe cold periods, this paper sets that when the relative heating load ratio of heat users is below 0.5 (including 0.5), the heating network system is in early and late cold periods; when the relative heating load ratio of heat users is above 0.5, the heating network system is in severe cold period.

In order to discuss the thermal conditions and heat storage capacity of different heat storage adjustments under the actual operation adjustment mode of Yongtai Heating Plant, this section carries out temperature-increasing heat storage, flow-increasing heat storage and comprehensive heat storage under the actual operation adjustment of Yongtai Heating Plant. The comparison of thermal conditions is shown in Figures 5 to 7 respectively, and the comparison of heat storage capacity and heat storage time that can maintain heating under comprehensive heat storage adjustment is shown in Figure 8.

As shown in Figure 5, under the actual operation adjustment benchmark of Yongtai Heating Plant, before using temperature-increasing heat storage adjustment, the supply water temperature of primary network for heating in early and late cold periods was 66°C, and return water temperature was maintained between 51°C-63°C. The average temperature difference between supply and return water was maintained; during severe cold period, supply water temperature was 80°C and return water temperature was maintained between 50°C-62°C.

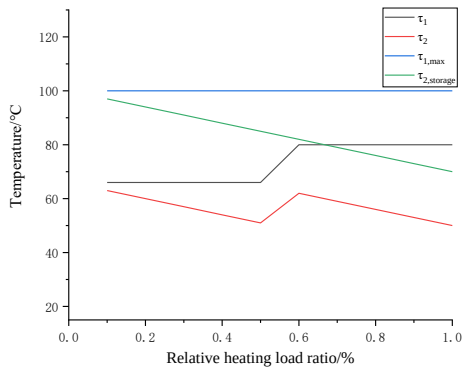

Figure 5. Comparison of thermal conditions of the system with increasing temperature heat storage

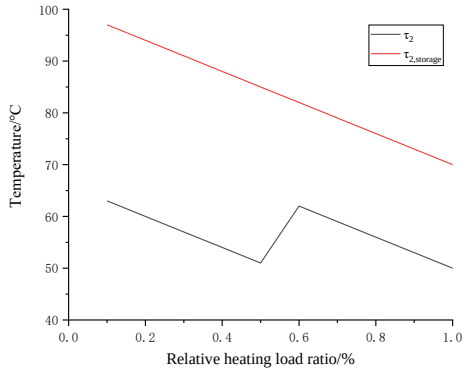

Figure 6. Comparison of thermal conditions of increasing flow heat storage system

When using temperature-increasing heat storage adjustment, set supply water temperature of primary network for heating to 100°C. After reaching steady state, return water temperature of primary network for heating in early and late cold periods increased accordingly to 85°C-97°C; return water temperature of primary network for heating during severe cold period increased accordingly to 70°C-82°C; greatly increased average temperature difference between supply and return water of primary network for heating system, i.e., stored excess heating capacity in heating network system.

As shown in Figure 6, when using flow-increasing heat storage adjustment, set circulation pump flow rate of primary network for heating to 1820m3/h and not exceeding 1.5 times reference circulation pump flow rate. After reaching steady state, return water temperature of primary network for heating during early and late cold periods increased accordingly to 55.03°C-63.80°C; return water temperature of primary network for heating during severe cold period increased accordingly to 58.04-66.84°C; increased temperature of return water pipeline of primary network for heating; i.e., stored excess heating capacity in heating network system.

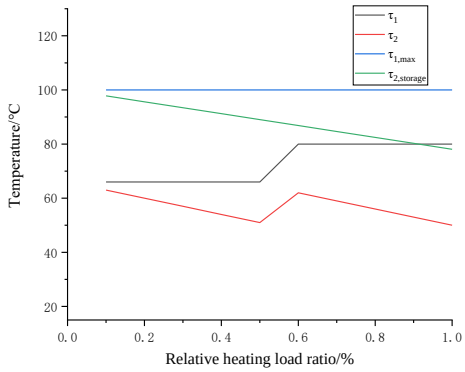

Figure 7. Comparison of thermal conditions of integrated heat storage system

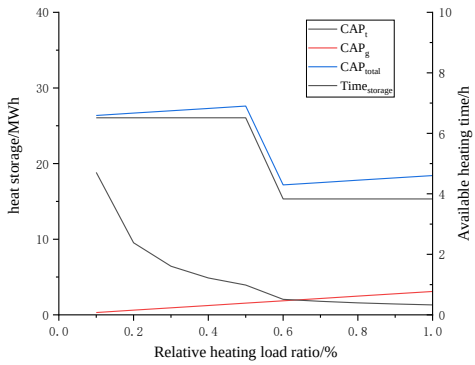

Figure 8. Comparison of heat storage capacity under actual operation regulation

As shown in Figure 7, when using temperature-increasing heat storage adjustment, set supply water temperature of primary network for heating to 100°C and set circulation pump flow rate of primary network for heating to 1820m3/h without exceeding 1.5 times reference circulation pump flow rate. After reaching steady state, return water temperature of primary network for heating during early and late cold periods increased accordingly to 89.03°C-97.81°C; return water temperature of primary network for heating during severe cold period increased accordingly to 78.06-86.84°C; i.e., stored excess heating capacity in heating network system.

As shown in Figure 8, when using temperature-increasing heat storage adjustment mode, there is a big difference between early/late cold period and severe cold period in terms of heat storage capacity of heating network system. In early/late cold period, maximum heat storage capacity was 27.60MWh; while during severe cold period maximum heat storage capacity was 18.41MWh.

5. CONCLUSION

In order to analyze the heat storage capacity of the heating network system, this paper first summarizes the dynamic heat storage and release characteristics and basic heat storage and release modes of the primary network to obtain the thermal conditions and theoretical heat storage capacity of the heating network system under various heat storage and release operation adjustment modes. Then, based on the theoretical heat storage and release modes of the heating network system, numerical simulation calculation is carried out on the Yongtai Boiler Room heating network system. The main conclusions are as follows:

(1) Based on the changes in temperature and flow rate of the heating network system, the heat storage adjustment modes of the heating network system are summarized as temperature-increasing, flow-increasing and comprehensive heat storage adjustment modes. The theoretical dynamic thermal conditions of primary network for heating system under these three heat storage adjustment conditions are given.

(2) The heat storage capacity of the heating network system is defined as "the difference between the heat storage capacity of the heating network system under heat storage adjustment operation conditions and that under reference operation conditions during actual operation". The theoretical heat storage capacity of primary network for heating under temperature-increasing, flow-increasing and comprehensive heat storage adjustment is defined.

(3) When using temperature-increasing heat storage adjustment mode, there is a big difference between early/late cold period and severe cold period in terms of heat storage capacity of heating network system. However, their changing trend is consistent and decreases with increasing relative heating load ratio.

(4) When using flow-increasing heat storage adjustment mode, heat storage capacity of heating network system is small with maximum heat storage capacity being 3.09MWh. The changing trend is different from that of temperature-increasing heat storage adjustment mode. Heat storage capacity increases with increasing relative heating load ratio.

(5) When using comprehensive heat storage adjustment mode, releasing heat stored in heating network system to heat users can maintain heating time for 0.33h to 4.71h. With increasing relative heating load ratio, this part of stored heat can maintain heating time accordingly decreases.

ACKNOWLEDGEMENT

We would like to extend our sincere thanks to Beijing Heat Supply Engineering Design Company. for their assistance and cooperation. Their contributions have been instrumental in the success of this work.

REFERENCES

[1] Yingfei Gong, Xuan Yang, Jingkun Xu, et al, Optimal operation of integrated energy system considering virtual heating energy storage[J], Energy Reports,2021,7(1): 419-425.
[2] SHEN R R, XUAN W Y, ZHANG J, et al, Review of Retrofitting Methods for Decoupling Heat and Electricity Generation to Promote the Power System Flexibility[J], Energy of China,2021,43(05):51-59. (in Chinese)
[3] AN N, YE P, GUAN D J, et al, Review of Electric-Thermal Coupling for Thermoelectric Units[J], Journal of Shenyang Institute of Engineering(Natural Science) , 2019, 15(04): 354-359+372. (in Chinese)
[4] FAN Q W, JV W P, HUANG J S, et al, Research on Decoupling of Heat and Power of Industrial Steam Supply Unit Based on Heat Storage Process[J], Turbine Technology, 2019,61(03): 221-223+188. (in Chinese)
[5] LI J J, HU L X, Research on Accommodation Scheme of Curtailed Wnd Power Based on Peak-Shaving Electric Boiler in Secondary Heat Supply[J], Power System Technology, 2015,39(11): 3286-3291. (in Chinese)
[6]]Xiaochn Yang, Svend Svendsen, Improving the district heating operation by innovative layout and control strategy of the hot water storage tank[J], Energy and Buildings, 2020，224(1):110273.
[7] Fabian Levihn, CHP and heat pumps to balance renewable power production: Lessons from the district heating network in Stockholm [J], Energy, 2017137(15):670-678.
[8] Xu T, ZHOU Y, WANG X L, Research on Peak Regulation Capability of 300-MW Combined Heat and Power plant[J], Electric Power,2014,47(09):35-41. (in Chinese)
[9] Yang Y , Kai W , Long H , et al. Integrated electricity and heating demand-side management for wind power integration in China[J]. Energy, 2014, 78(15):235-246.
[10] BI Q S, LV X Y, LI D X, et al, Research on the Capacity of In-depth Peak Regulation of Large-scale Heat Supply Unit Based on Characteristics of Thermal Storage of Heat Supply Network and Buildings[J], Turbine Technology, 2014,56(02): 141-144. (in Chinese)
[11] XIE H B, Research on Wind Accommodation Method by Source-network-load Coordination of Combined Heat and Power System Considering Pipe Network Heat Storage[D], Harbin Institute of Technology, 2019. (in Chinese)
[12] Hennessy J , Li H , Wallin F , et al. Flexibility in thermal grids: a review of short-term storage in district heating distribution networks[J]. Energy Procedia, 2019,158(02):2430-2434.
[13] ZHANG Y G, ZHANG Z P, LI D F, Discussion on the application of heat storage technology of long-distance pipeline network in thermo-electrolysis coupling [J], District Heating, 2020,39(04):22-30. (in Chinese)
[14] WANG J D, ZHOU Z G, ZHAO J N, et al, Heat storage mode and capacity evaluation of district heating network[J], Heating Ventilating & Air Conditioning, 2019, 49(01) :46-51+88. (in Chinese)
[15] Wang D, Heat Storage analysis of central heating pipe network[J], District Heating, 2021,40(06):97-102. (in Chinese)
[16] CHENG T C, Energy-saving operation regulation of primary heat pipe network system based on heat storage[D]. Beijing University of Civil Engineering and Architecture,2017. (in Chinese)

The 18th International Symposium on District Heating and Cooling,
September 3-6, 2023, Beijing, China

RESEARCH AND APPLICATION OF GRAPHITE THERMAL HEAT STORAGE UNIT IN THE CORE AREA OF BEIJING

Li Zhongbo[a]，Zhang Lianxin[b]，Zhang Mingming[b]，Qin Yuan[a]，Hao Wei[a]，Li Zhi[b*]

[a] *Beijing District Heating Group Co.，LTD, Beijing, 100028, China*
[b] *Beijing Thermal Equipment Manufacturing Co., Ltd, Beijing, 100176 , China*
[*] *Corresponding author. haooydogqq@126.com*

Abstract

As a material with high heat storage density and high thermal conductivity, graphite has certain advantages in dealing with limited limitation. In this paper, the graphite heat storage heating system is adopted in the four oil boiler rooms in Dongcheng and Xicheng District of Beijing Heating Group. Because the boiler room is located in the core area of Beijing and is limited by the floor area and power increase capacity, a cascade heat storage strategy according to different peak and valley peacetime periods is proposed. According to the analysis of heating in Beigang boiler room, the wide temperature area reaches 250℃, the heat storage reaches more than 800 kWh, and the maximum heat storage replacement throughout the day reaches 1400 kWh. At the same time, the heat release performance in cold weather is tested, and the results show that more than 75% of the supply temperature is within the set range, and a good heating temperature range is obtained. Through the economic evaluation, the energy consumption of the original oil-fired boiler is more than 40%, and it has certain economy after the transformation. After the transformation, the carbon dioxide emission is reduced by about 150t compared with the primary fuel oil boiler, which is a green and clean heating scheme that can effectively reduce the carbon emission.

Keywords: Graphite heat storage; Cascade heat storage; Green carbon reduction

Biographical Note(s):
Study the principle of the graphite as a high heat storage material,and bulit a batch of heating demonstration applications.

1. INTRODUCTION

At present, global climate deterioration has become a major problem common to mankind. The Special Report on Global Temperature Rise of 1.5°C (IPCC SR1.5) released in 2018 pointed out that[1] when the global average temperature exceeds 1.5°C relative to pre-industrial times, the Earth's climate will undergo irreversible catastrophic changes. Between 3% and 29% of terrestrial species will be at very high risk of extinction [2-3]. In order to solve environmental problems, clean and low-carbon energy with renewable energy as the main body is becoming a strategic energy. The International Energy Agency IRENA predicts that the share of renewable energy will increase to 86% by 2050 [4]. Renewable energy is characterized by randomness and discontinuity. In the construction of low-carbon, efficient and clean energy system, heat storage technology plays an important role in the fields of peak cutting and valley filling, consumption of renewable energy and industrial waste heat recovery [5]-[6].

The oil boiler room in the core area of Beijing does not have the conditions for grid-connected transformation, so the oil boiler is still retained as a heat source and the tail denitrification device is installed, but there are still large safety and environmental protection risks in the actual operation of these boiler rooms, and the comprehensive operation cost is high. Therefore, a graphite sensible heat storage heating system is built to replace the heat source of the oil-fired boiler and realize the peak cutting and valley filling of electricity. The working principle and control strategy of the heat storage heating system are introduced, and the heat release performance and heating effect of the graphite sensible heat storage heating system are analyzed, and the benefits of the graphite sensible heat storage heating system are analyzed.

2. BACKGROUND AND CURRENT SITUATION

In accordance with the requirements of Beijing Municipal Government to vigorously promote the optimization and adjustment of energy structure and promote the emission reduction of pollutants at source, the boiler room of Dongcheng Beigang was cleaned and reformed. The station has a construction area of 3734 m^2, the design heat index of the unit construction area is 64 W/ m^2, and the heating period is 24 hours a day from November 15 to March 15. A 0.5MW oil-fired boiler was originally configured as a heat source. Due to the location of the boiler room in the core area of East City of Beijing, limited by the floor area and electric capacity of the boiler room, this demonstration project uses the site of the original oil-fired boiler room to arrange the heat storage body, the primary system of the heat storage side, the secondary heating system, the heat storage distribution box, and the low-voltage cabinet of electric capacity increase in the boiler room. With the graphite steam generator as the only heat source and the partial heat storage strategy, the electric heat storage of oil-fired boiler is replaced.

In the design, the installed capacity of the graphite steam generator is 238kW, the size of the graphite body is 2.5m×2.2m ×0.9m, and the operating wide temperature zone is 500℃−250℃ during the operation stage, and the energy storage density reaches 0.62GJ/m^3. Figure 1 is the physical diagram of the graphite heat storage heating system in the boiler room of Beigang.

Figure 1 Beigang graphite heat storage heating system

3. PRINCIPLE AND ANALYSIS

3.1 heating supply system

The heating system is divided into a primary circulation system, a secondary circulation system and a water refill system, and its system diagram is shown in Figure 2. The graphite steam generating device uses resistance heating, strengthens heat transfer through an embedded heat exchange tube, and realizes heat transfer to the working medium, in which the working medium in the tube is water-water vapor.

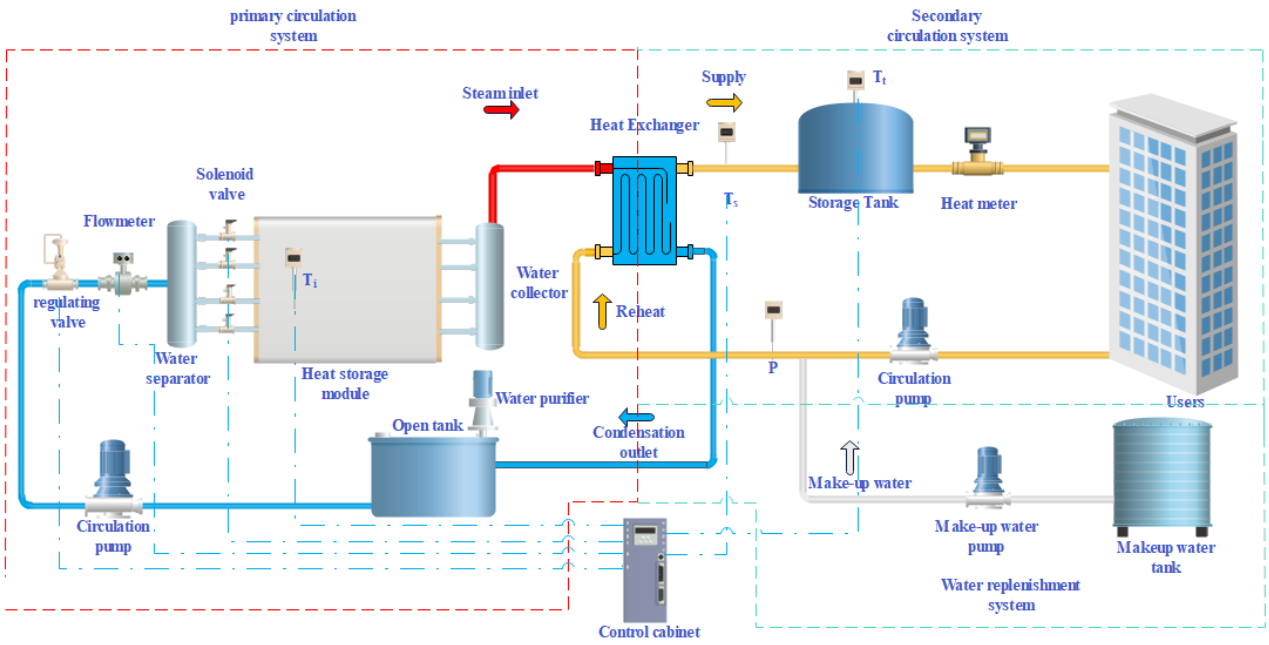

Figure 2 Graphite heat storage heating system diagram

The primary circulation system is an open system. After the plate heat exchanger, the primary condensate enters the open pure water tank, which is powered by the circulation pump. After the flow adjustment by the regulating valve and the flow meter, the inlet water distributor enters the inlet water distributor.

The secondary circulation system is a closed system. Different from the traditional secondary heating system, it is equipped with a water storage tank for temperature regulation. The secondary heating load is controlled jointly by the secondary temperature supply Ts and the secondary water storage tank temperature Tt to achieve a balance between supply and demand.

The water replenishment system is a constant pressure water supply system of the water pump. The pressure P is collected by the pressure transmitter of the secondary cycle for feedback control to maintain the constant pressure of the system.

According to the secondary temperature supply T_s, the temperature of the secondary water storage tank T_t and the temperature of the heat accumulator T_i, the heat exchange area of the heat exchange tube and the flow rate of the working medium in the heat exchange tube are adjusted jointly by the electromagnetic valve, the flowmeter and the regulating valve to achieve the balance of supply and demand.

3.2 Step heat storage strategy

Table 1 shows the peak and valley of Beijing. Due to the limited site and the large load fluctuation of the envelope structure during the heating season, the investment of adopting total heat storage based on the design load is larger. According to the time period in Table 1, the step heat storage strategy can reduce the initial investment of the equipment, but increase the operation cost of the equipment. The operation strategy is as follows:

Table 1 Beijing peak , Valley and Flat section

Period	Time
Peak power period	10:00～15:00 18:00～21:00
Valley power period	23:00～7:00
Flat power period	7:00～10:00 15:00～18:00 21:00～23:00

3.2.1 From 23:00 to 7:00

This time period is in heat release mode while charging. Under this condition, the graphite is stored by electric heating rod, and the graphite steam generating device releases heating heat according to demand. During this period, the graphite is heated from the lowest and lowest temperature to the upper temperature and maintains a high temperature state.

3.2.2 From 7:00 to 10:00

Since the heating load of the entire heating season is affected by outdoor temperature and wind speed, the variation range is large, so considering the economic maximization, this time period is divided into two working conditions according to whether the heat stored by the graphite meets the heat consumption of the peak electricity in the following period:

1） When the heating load is large, the heat storage cannot meet the peak heat supply of the following peak power period, and the operation strategy of this period is to open the heating mode of charging and discharging while maintaining the heat stored by the valley power to meet the peak heat release for the following 5 hours and achieve the maximum economy.

2） When the heating load is small, the heat storage can meet the peak heat supply of the next period, then the graphite is cooled to meet the set temperature of the current heating load, and the heating is maintained at this temperature for this period, and the valley electricity replaces part of the flat electricity to achieve economic maximization.

3.2.3 From 10:00 to 15:00

During this period, the heating is stopped, and the corresponding lower limit heating temperature of the graphite is determined based on the actual load. After the temperature of the thermal storage medium decreases to the lowest limit temperature, the graphite maintains that temperature for heating. When there is a high heat load, it is also necessary to partially activate peak electricity to maintain the temperature of the thermal storage medium and ensure the heating quality. During this stage, the thermal energy stored in the graphite is released to ensure that the graphite reaches the minimum temperature required for heating quality. The graphite has a wide temperature range of 250℃, with a mass of 8300 kg and an average specific heat capacity of 1.43 kJ/kgK. The released thermal energy from the graphite is 820 kWh.

3.2.4 From 15:00 to 18:00

During this period, the graphite is heated to a specific temperature to meet the energy requirements for peak electricity in the next three hours. This stage operates in a simultaneous charging and discharging mode, where the overall temperature of the graphite steadily increases and then remains at a specific temperature.

3.2.5 From 18:00 to 21:00

During this stage, the thermal energy stored during the previous period of regular electricity usage is utilized. In extremely cold weather conditions, where the heating load is approximately 200 kW or higher, this stage can consume more than 600 kWh of stored thermal energy. This allows for the substitution of peak electricity with regular electricity, resulting in certain economic benefits.

3.2.6 From 21:00 to 23:00

During this period, it is the stage of simultaneous heating and releasing heat. The graphite temperature is maintained within a specific low temperature range to provide heating without utilizing the thermal energy stored during off-peak electricity periods. This approach aims to preserve the stored thermal energy for optimal economic efficiency.

The graphite thermal storage heating system in the Beigang Boiler Room adopts a cascading thermal storage strategy. During off-peak electricity periods, it is possible to substitute more than 800 kWh of peak electricity with off-peak electricity. Similarly, during regular electricity periods, it is possible to substitute more than 600 kWh of peak electricity with regular electricity. The system has a maximum thermal storage capacity of over 1400 kWh throughout the day.

4. RESULTS AND ANALYSIS

4.1 Heating Performance

The graphite thermal storage replacement project in the fuel oil boiler room commenced operation on November 7, 2022, and completed one heating season until March 15, 2023.

Figure 3 illustrates the supply and return temperature curves of the graphite thermal storage heating system on January 23, 2023, under the condition of -13°C. The test duration was 2 hours, with the primary side representing stable atmospheric saturated steam. The set upper limit for the secondary supply temperature was 56 degrees, while the lower limit was 53 degrees. Based on the data, it is evident that over 75% of the supply temperatures remained within the designated range, with a maximum supply temperature of 57°C and a minimum supply temperature of 52.7°C. The supply temperature

remained relatively stable. The return temperature fluctuated within the range of 48.2°C to 50.5°C, exhibiting steady fluctuations. The average heat release power was approximately 175 kW, achieving stable heating performance under cold weather conditions in Beijing

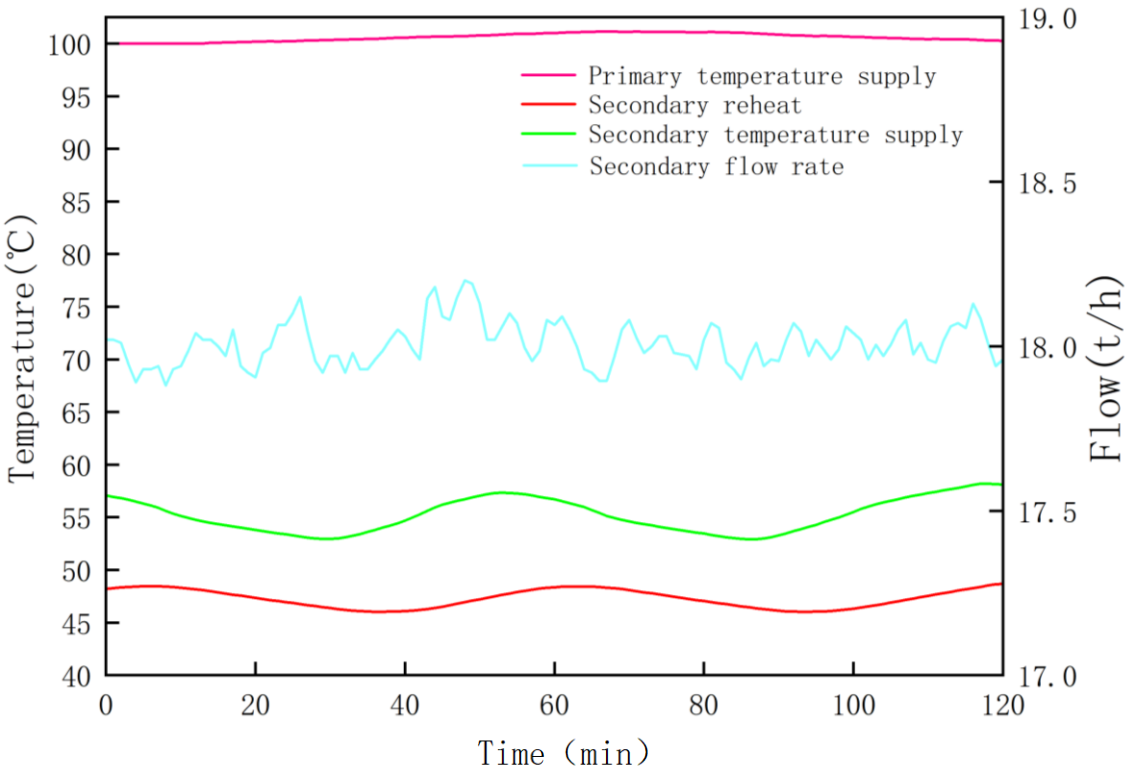

Figure 3: Supply Temperature Curve of the Graphite Thermal Storage Heating System

4.2 Operational Analysis

By employing a partial thermal storage strategy, the proportion of peak, Valley and Flat power usage over a single heating season is shown in Figure 4. The percentages for peak, Valley and Flat power are 9.6%, 47.2%, and 43.2%, respectively. This indicates that the system meets the requirements of substituting electric thermal storage in boiler rooms with limited area in the core region while also achieving a certain peak shifting and valley filling effect.

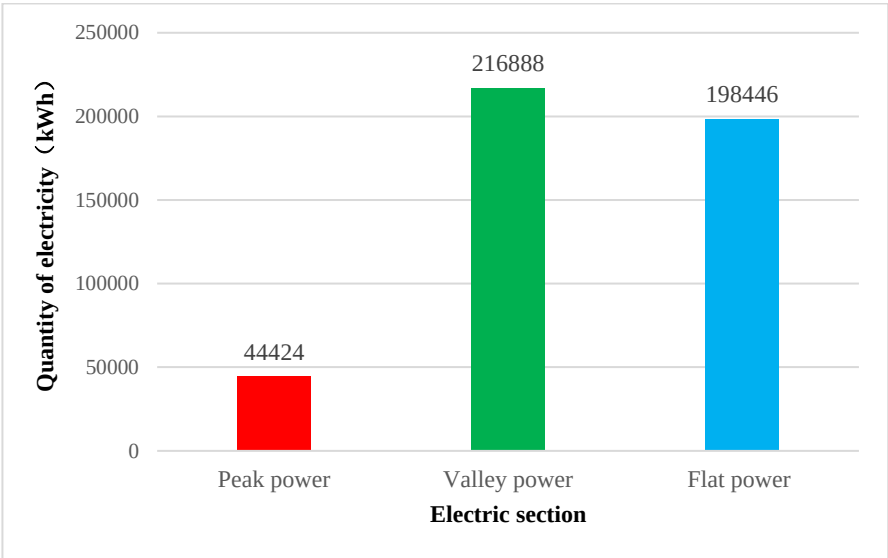

Figure 4: Proportion of Peak, Valley and Flat power Usage in the Heating Season for the Graphite Thermal Storage Heating System.

5. BENEFITS AND ANALYSIS

5.1Economic Benefits

The economic comparison between the original fuel oil boiler and the graphite thermal storage heating system is presented

in Table 2. The heat supply provided by both sources is similar. However, due to a significant increase in electricity prices for off-peak and regular electricity during the 2023 heating season, the energy cost of the graphite thermal storage system is reduced by approximately 21.5% compared to the fuel oil boiler, resulting in an overall saving of 44.5%. When considering the peak, off-peak, and regular electricity prices from 2022, the graphite thermal storage system achieves an energy cost reduction of around 33.14% and an overall saving of 54.2%.

These figures demonstrate that the graphite thermal storage heating system offers superior economic performance compared to the original fuel oil boiler. It significantly reduces energy costs and provides substantial overall savings. The system's economic viability is further enhanced by its ability to capitalize on off-peak and regular electricity, thereby reducing dependence on expensive peak electricity.

Table 2: Economic Comparison between the Graphite Thermal Storage Heating System and the Fuel Oil Boiler

Heating Sources	Seasonal Heat Value (GJ)	Energy Cost (thousand yuan)	Expenses for Exhaust Gas, Ash Removal, Labor, Maintenance, etc. (ten thousand yuan)	Overall Saving (ten thousand yuan)	Overall Saving (%)
Graphite Thermal Storage Heating System	1649	33.34	0.8	27.4	44.5
Fuel Oil Boile	1687	42.46	19.1		

5.2 Social Benefits

The demonstration project, which replaced the fuel oil boiler and changed the heating method, has reduced the emissions of pollutants such as carbon dioxide and sulfur dioxide caused by combustion. The original fuel oil boiler consumed 51.15 tons of diesel fuel, but after the transformation, the carbon dioxide emissions have been reduced by approximately 150 tons or more, resulting in certain social benefits.

6.CONCLUSION

This project serves as the first demonstration application of a graphite thermal storage heating system. Due to constraints such as boiler room space and electricity capacity, a strategy was adopted with full-time thermal storage using off-peak electricity, partial thermal storage using mid-peak electricity, and no thermal storage during peak electricity periods. After operating for one heating season, the system has generally met the design requirements. However, there are areas that require further improvement in the future.

1) In the future, it is recommended to gradually increase the upper limit temperature of the thermal storage medium, expand the temperature range, and reach the initial design upper limit of 620 degrees. This will enhance the thermal storage density and further reduce the heating costs.

2) During operation, it is important to adjust the heating load and thermal storage parameters of the graphite steam generation device based on changes in the heating load. This will result in energy savings and improved utilization of off-peak and mid-peak electricity, thereby optimizing the system's performance.

3) The economic viability of thermal storage systems is greatly influenced by peak, off-peak, and mid-peak electricity pricing policies. Corresponding green energy policies can also significantly impact the development and adoption of thermal storage technologies.

7 REFERENCES

[1] IPCC. Global Warming of 1.5°C [R]. 2018.

[2] Kuang, S., Zhou, Z., Liang, M., Gao, X., Cao, Y. (2022). Interpretation of the IPCC Sixth Assessment Report Working Group II. Environmental Protection, 50(09), 71-75.

[3] Jiang, T., Zhai, J., Luo, Y., Su, B., Chao, Q., Wang, Y., Wang, G., Huang, J., Xu, R., Gao, M., Miao, L. (2022). Progress in Climate Change Impact, Adaptation, and Vulnerability Assessment: New Insights from IPCC AR5 to AR6. Journal of Atmospheric Sciences, 45(04), 502-511.

[4] International Renewable Energy Agency. Innovation outlook: Thermal energy storage [R]. 2020.

[5] Hu, Y., Ma, X., Lei, B., Li, Y., Zhang, W., Guo, X., Lei, J. (2018). Feasibility Study on Promoting New Energy Consumption in Southern Power Grid with Energy Storage. Southern Power System Technology, 12(09), 53-61.

[6] Yang, L., Cao, Y., Wei, W., et al. (2020). Configuration Method of Energy Storage for Wind Farms Considering Wind Power Uncertainty and Wind Curtailment Constraint. Automation of Electric Power Systems, 44(16), 45-52..

The 18th International Symposium on District Heating and Cooling,
September 3–6, 2023, Beijing, China

ANALYSIS ON THERMOELECTRIC COOPERATIVE PEAK SHAVING USING ELECTRIC BOILER AND HEAT STORAGE

Jianbo Han[a], Haichao Wang[a*]

[a] *Dalian University of Technology, Dalian , 116024, China*
[*] *Haichao Wang. haichaowang@dlut.edu.cn. China*

ABSTRACT

Cogeneration is the main way of heating in northern China. It is subject to the operation strategy of "determining electricity by heat" and the instability of renewable energy, which limits the flexible operation of regional energy system and leads to serious wind curtailment. In order to respond to the goal of "carbon peak and carbon neutrality" and increase the flexibility of thermal and power system operation, The system scheme of using electric boiler and heat accumulator to realize thermoelectric cooperative peak shaving is proposed, and the operation strategy of the system is reasonably optimized considering the system operation benefit and new equipment cost. Matlab software was used to model the optimal scheduling, YALMIP and CPLEX were used to solve the model, and the optimal heat storage capacity and the optimal power of the electric boiler suitable for the example of cooperative peak shaming in the thermal power plant were obtained. When equipped with 100MW electric boiler and 20000m³ heat accumulator, compared with the original system, the wind power consumption capacity of the thermal power plant can be increased by 30.6%, and the coal consumption can be reduced by 9.11%, which effectively improves the revenue of the thermal power plant and reduces energy consumption.

Keywords: electric boiler; wind power absorption ;combined heat and power transformation; heat storage

1. INTRODUCTION

At present, a large amount of fossil energy consumption and increasing environmental pollution have seriously affected the sustainable development of China's economy and ecology. The 14th Five-Year Plan points out that our country will achieve carbon peak by 2030 and carbon neutrality by 2060. Energy conservation, emission reduction and full utilization of renewable energy is one of the important ways to achieve the "carbon peak and carbon neutrality" goal[1]. As China's installed wind power capacity continues to increase, it is expected to exceed 1 billion kW in 2050[2]. There is a problem of mismatch between heat and electricity in winter heating in northern China, which squeeches the space of wind power online and causes serious wind curtailment.

In the past few years, thermal storage technology has received widespread attention in the application of intelligent heating network (fourth generation district heating system).[3] Large-scale heat storage devices have been applied to the transformation of thermal power plants, in addition to large heat pumps, renewable energy sources etc., which can improve the system wind power consumption capacity to a certain extent. It is also necessary to consider the economic cost of system operation and select the appropriate auxiliary equipment capacity to formulate the best operation strategy, otherwise it will only increase the initial investment of system transformation and affect the normal operation of the system[4-5].

Cogeneration units equipped with electric boilers directly consumes wind power for auxiliary heating, which can effectively improve the flexible peak shaving capacity of thermoelectric units, reduce the thermal output of thermoelectric units, and provide a certain space for wind power online. In this paper, the use of electric boiler and heat accumulator to transform the thermal power plant, through software simulation analysis of the optimal capacity of auxiliary equipment, rational use of renewable energy, reduce unit operation energy consumption, improve the system wind power consumption capacity, and then realize the maximum operation benefit of the thermal power plant.

2. ANALYSIS OF SYSTEM OPERATION MECHANISM

Electric boiler has the advantages of fast heating and high efficiency. The cogeneration unit is equipped with electric boiler. When the user's heat load is small before and after heating period, the electric boiler can be directly used for heating. In the middle of the heating period, when the user's heat load is high, the electric boiler bears part of the heat load, which reduces electrical output while meeting the user's heat demand, and the system obtains a downward peak regulation capacity. However, how to coordinate the operation of the thermoelectric unit and the electric boiler is the basis of economic analysis[6].

The electric boiler is used to directly consume wind power to heat the return water of the heat network[7], and then the return water is heated by plate heat exchanger to the specified temperature, and the user is heated. During the night when the electric load is low, the heat generated by the electric boiler is stored in the heat accumulator, and during the day when the electric load is peak, the heat accumulator emits heat for auxiliary heating. The system can effectively reduce the thermal output of the thermoelectric unit, improve the flexibility of the operation of the thermoelectric unit, and provide Internet space for wind power. The operating principle of the system is shown in Figure 1.

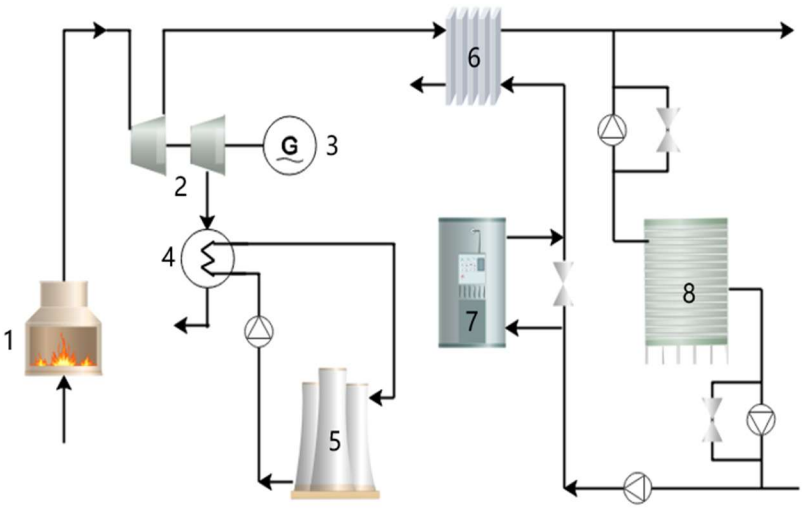

1 coal-fired boiler; 2 steam turbine; 3 generator; 4 condenser; 5 condensation tower;

6 heat exchanger; 7 electric boiler; 8 heat accumulator

Figure 1. Schematic diagram of system operation

3. SYSTEM OPTIMIZATION SCHEDULING MODEL

3.1. Objective function

Considering the system operation cost and the income obtained from heat sales, electricity sales and wind power consumption, the objective function of the system is expressed as follows:

$$\text{Max f(x)} = F_{e,sale} + F_{h,sale} + F_{w,sale} - F_{cost} \tag{1}$$

Where $F_{e,sale}$ is revenue from electricity sales of thermoelectric units and pure condensing units in heating season, ten thousand yuan / year; $F_{h,sale}$ is heating season heat sales revenue, ten thousand yuan / year; $F_{w,sale}$ is heating monsoon power revenue, ten thousand yuan / year; F_{cost} is operating cost of heating season system thermoelectric unit, pure condensing unit and electric boiler, ten thousand yuan / year.

$$F_{e,sale} = C_e \times \sum_{t=1}^{T_{max}} \sum_{i=1}^{I} P_i^{CHP}(t) + C_e \times \sum_{t=1}^{T_{max}} \sum_{j=1}^{J} P_j^{CON}(t) \tag{2}$$

$$F_{h,sale} = C_h \times Q_D(t) \tag{3}$$

$$F_{w,sale} = C_w \times \sum_{t=1}^{T_{max}} P_w(t) \tag{4}$$

$$F_{cost} = \sum_{t=1}^{T_{max}} \sum_{i=1}^{I} F_i^{CHP}(t) + \sum_{t=1}^{T_{max}} \sum_{j=1}^{J} F_j^{CON}(t) \tag{5}$$

Where C_e、C_h、C_w is electricity price, heat price and wind power price, this paper takes 373.1 yuan /MWh, 21.5 yuan /GJ and 570 yuan /MWh; $P_i^{CHP}(t)$、$P_j^{Con}(t)$ is electrical output of the ith thermoelectric unit and the j pure condensing unit at time t, MW; $Q_D(t)$ is system thermal load at time t, MW; $P_w(t)$ is wind power at time t, MW; $F_i^{CHP}(t)$、$F_j^{CON}(t)$ is operating cost of the ith thermoelectric unit, the pure condensing unit and the electric boiler at time t, ten thousand yuan.

3.2. Condition of constraint

(1) Electric power balance constraint

$$E_D(t) + P_{EB}(t) = \sum_{i=1}^{I} P_i^{CHP}(t) + \sum_{j=1}^{J} P_j^{CON}(t) + P_w(t) \tag{6}$$

Where $E_D(t)$ is system electrical load at time t, MW; $P_{EB}(t)$ is electricity consumption of the electric boiler at time t, MW.

(2) Thermal balance constraint

$$Q_D(t) = \sum_{i=1}^{I} Q_i^{CHP}(t) + Q_{EB}(t) + Q_{TES,S}(t) - \eta_{TES,r} \times Q_{TES,R}(t) \tag{7}$$

Where $Q_D(t)$ is system thermal load at time t, MW; $Q_i^{CHP}(t)$ is heat generation of thermoelectric unit i at time t, MW; $Q_{EB}(t)$ is heat production of electric boiler at time t, MW; $Q_{TES,S}(t)$、$Q_{TES,R}(t)$ are heat storage and heat release of the heat accumulator at time t, MW; $\eta_{TES,r}$ is heat release efficiency of heat accumulator, %.

(3) Combined heat and power generation unit

Operating range constraints:

$$175 \le P_i^{CHP}(t) \le 383 \tag{8}$$

$$0 \le Q_i^{CHP}(t) \le 448 \tag{9}$$

Unit climbing constraints:

$$\left|P_i^{CHP}(t) - P_i^{CHP}(t-1)\right| \le 80 \tag{10}$$

(4) Pure condensing thermal power unit

$$100 \le P_j^{CON}(t) \le 200 \tag{11}$$

Unit climbing constraints:

$$\left|P_j^{CON}(t) - P_j^{CON}(t-1)\right| \le 70 \tag{12}$$

(5) Electric boiler

The cogeneration unit bears the main load, which is supplemented by an electric boiler and a heat accumulator when the peak regulation capacity of the unit is insufficient.

$$Q_{EB}(t) = \eta_{EB} \times P_{EB}(t) \tag{13}$$

$$0 \le P_{EB}(t) \le P_{EB,max} \tag{14}$$

Where $Q_{EB}(t)$、$P_{EB}(t)$ are heating power and electric power of electric boiler at time t, MW; $P_{EB,max}$ is maximum electric power of electric boiler, MW; η_{EB} is the thermoelectric conversion efficiency of electric boiler is 0.98 [8].

(6) Wind farm

The amount of wind power online is less than the predicted value of wind power:

$$0 \le P_w(t) \le P_{w,pore}(t) \tag{15}$$

Where $P_{w,pore}(t)$ is the value of wind forecast, MW.

(7) Heat storage tank

Heat storage equation at time t:

$$Q_{TES}(t) - Q_{TES}(t-1) = \eta_{TES,s} \times Q_{TES,S}(t) - Q_{TES,R}(t) \tag{16}$$

Heat storage capacity constraints:

$$0 \le Q_{TES,S}(t) \le Q_{MAX} \tag{17}$$

The heat storage tank runs for one cycle, ending at the same time as the beginning of the heat storage:

$$Q_{TES}(0) = Q_{TES}(T_{max}) = 0 \tag{18}$$

Heat storage and release power constraints:

$$0 \le Q_{TES,S}(t) \le Q_{S,max} \tag{19}$$

$$0 \le Q_{TES,R}(t) \le Q_{R,max} \tag{20}$$

Where $Q_{TES,S}(t)$、$Q_{TES,R}(t)$ are Heat storage and heat release power of heat storage tank at time t; $Q_{S,max}$、$Q_{R,max}$ is Maximum heat storage and heat release power of heat storage tank.

4. Case study

In order to study the effect of using electric boiler and heat accumulator to realize thermoelectric decoupling, in the previous section, the operation modeling of cogeneration system is completed, and the mathematical model of electric boiler and heat accumulator participating in system peak regulation is established. In this section, a thermal power plant in Changchun City, Jilin Province will be used as an example for simulation to analyze the role of the scheme in improving the ability of the thermal power unit to adapt to wind power and reducing the energy consumption of the unit.

The heating season of Changchun City in 2016 was selected for simulation analysis, and the heating time was from October 15 to April 15 of the next year, a total of 183 days, to explore the impact of this scheme on wind power consumption and operating costs. Wind power forecast, electric load and heat load data are shown in Figure 2, where there is an obvious peak and valley period for heat load in the heating season, and the distribution of electric load is relatively uniform.

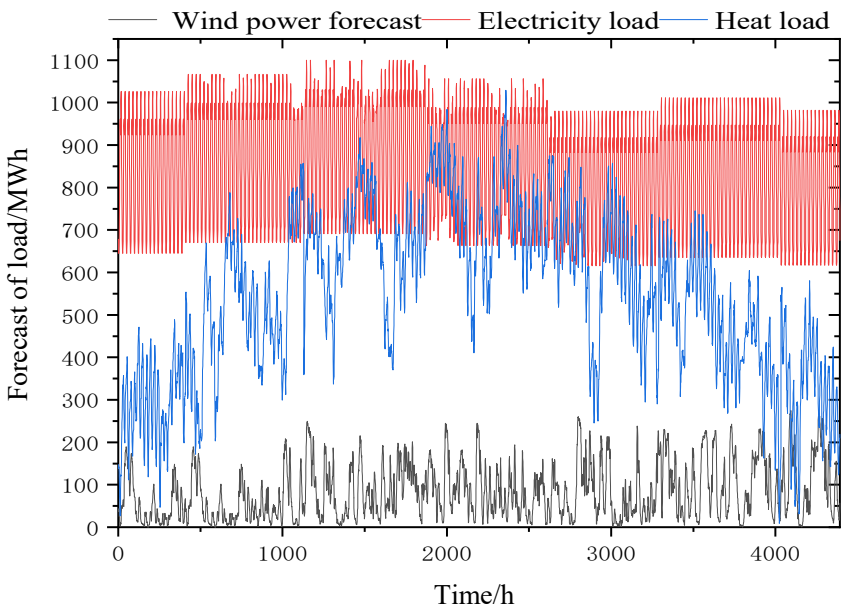

Figure 2. Wind power forecast, electric load and thermal load data

The base load data of the heating season is put into the system model for calculation, and the influence of the configuration of electric boilers and heat accumulators with different capacities on the overall operation of the system is analyzed, and the operation results of the original system are compared to analyze the economy and applicability of the transformation scheme.

In this paper, the capacity of electric boiler is 80-120MW, the calculation interval is 10MW, and the heat accumulator volume is 10000-50000m³, and the calculation interval is 10000m³. The transformation costs of cogeneration are respectively: electric boiler cost 750,000 yuan /MW, heat accumulator cost 3000 yuan /m³[9]. The simulation results are shown in Figure 3. When the heat accumulator volume is the same, and the electric boiler with different capacity is equipped with, the net income of the overall operation of the system has a similar change law. The net income of the system increases first and then decreases. When the power of the electric boiler is 100MW, the net income reaches the peak; When the heat accumulator volume is 20000m³, the system net benefit is the largest. As shown in Figure 3, due to the influence of the initial investment of equipment, there is a phenomenon that the net income of system operation decreases when the equipment capacity increases, so the volume of the heat accumulator needs to be calculated accurately.

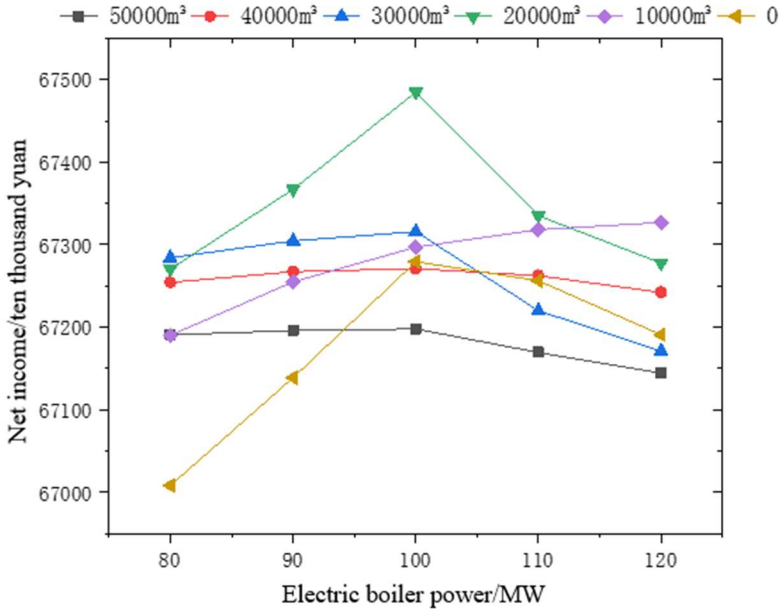

Figure 3. Results of simulation

As shown in Figure 4, the effect of the scheme equipped with electric boiler and heat accumulator at the same time is better than that of the scheme equipped with electric boiler only. The wind curtailment rate of different schemes decreases with the increase of the capacity of new equipment, and the combination of electric boiler and heat accumulator can effectively reduce the waste of wind power.

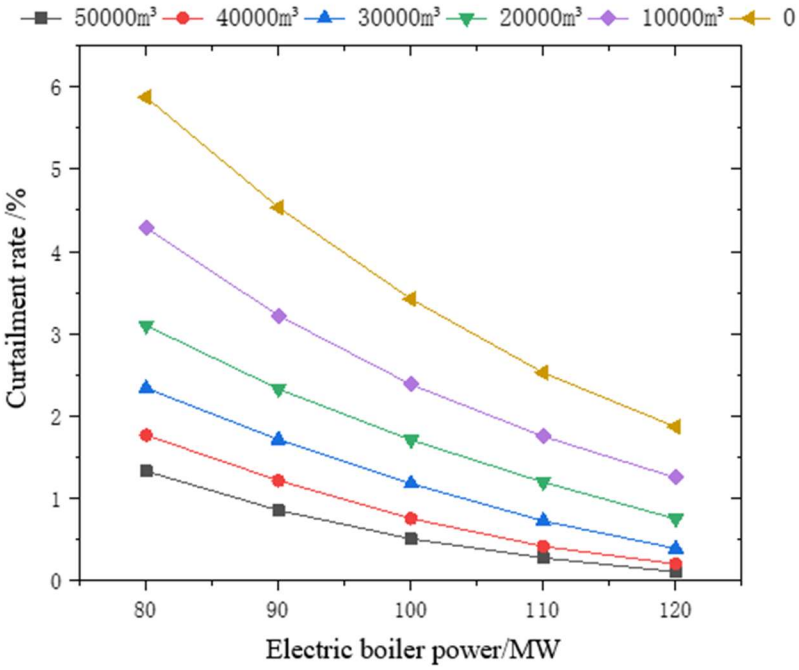

Figure 4. Wind curtailment rate of different schemes

The addition of auxiliary equipment electric boiler and heat accumulator to realize the "thermoelectric decoupling" of the cogeneration unit is conducive to improving the wind power consumption capacity of the system. As shown in Figure 5, with the continuous increase of electric boiler capacity, the wind power consumption capacity of the system gradually decreases, but the growth rate of wind power consumption capacity slows down; The heat accumulator volume is also positively related to the level of wind power consumption. With the increase of the capacity of electric boiler, the increase of the volume of heat accumulator has a smaller improvement on the wind power consumption capacity of thermal power plant.

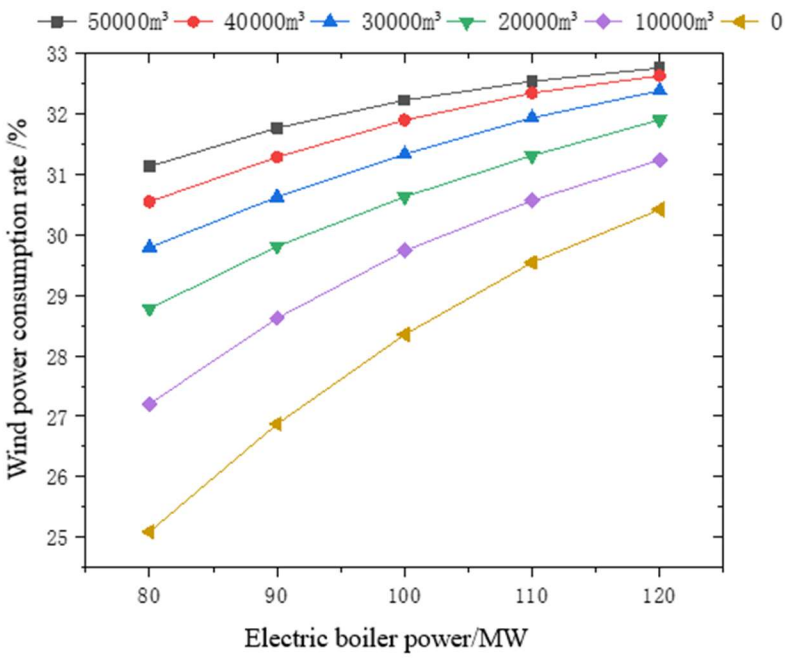

Figure 5. Wind power consumption capacity of different schemes

The wind power online capacity of the transformation scheme is significantly increased compared with the original system, but the growth rate slows down with the increase of equipment capacity. When the capacity of the electric boiler is 100MW and the capacity of the heat accumulator is 20000m ³, 84704.63MWh of wind power can be absorbed, and the wind power consumption capacity of the thermal power plant can be increased by 30.6%. The relationship between the amount of wind power connected in different schemes and the predicted amount of wind power connected in the original system is shown in Figure 6.

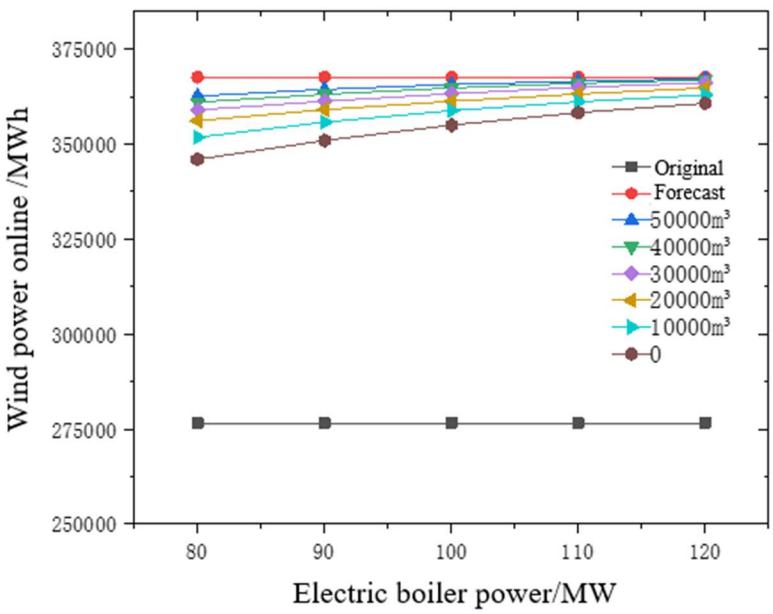

Figure 6. Comparison of wind power online capacity and wind power forecast capacity of different schemes with the original system online capacity

Equipped with electric boiler and heat accumulator, the wind power consumption capacity of the thermal power plant can be improved at the same time. It can also effectively reduce the operation energy consumption of thermal power plants. The coal consumption cost coefficients of thermal power units and pure condensing thermal power units of thermal power plants are shown in Table 1.

Table 1. Operating coal consumption cost coefficient of cogeneration units and pure condensing thermal power units[9]

Name	a $t/(MW^2 \cdot h)$	b $t/(MW \cdot h)$	c t/h
Thermoelectric unit	0.000072	0.2292	14.618
Pure condensing unit	0.000171	0.2705	11.537

Coal consumption in operation of cogeneration units and pure condensing thermal power units:

$$B_{CHP} = \sum_{i=1}^{I} a_{CHP} \cdot (P_{CHP})^2 + b_{CHP} \cdot P_{CHP} + c_{CHP} \tag{21}$$

$$B_{CON} = \sum_{i=1}^{I} a_{CON} \cdot (P_{CON})^2 + b_{CON} \cdot P_{CON} + c_{CON} \tag{22}$$

In the thermal power plant, only the cogeneration unit and the pure condensing thermal power unit consume coal, and the electric boiler directly consumes electricity for auxiliary heating. According to the above formula, the coal consumption required by the operation of the thermal power plant in a heating season is calculated. The coal consumption of different schemes and the coal saving rate compared with the original system are shown in Figure 7.

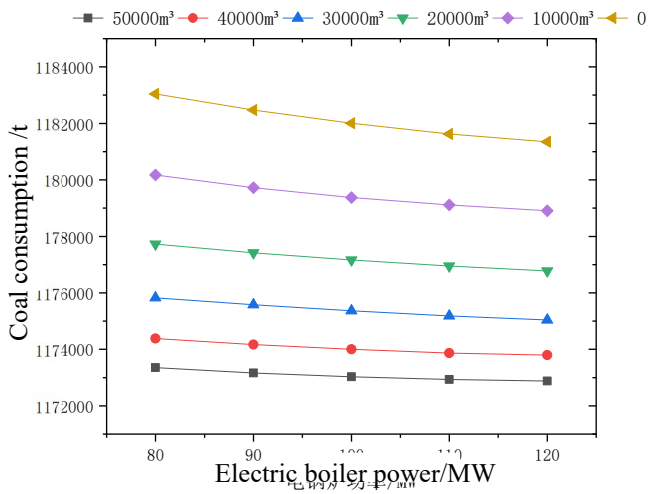

a. Coal consumption

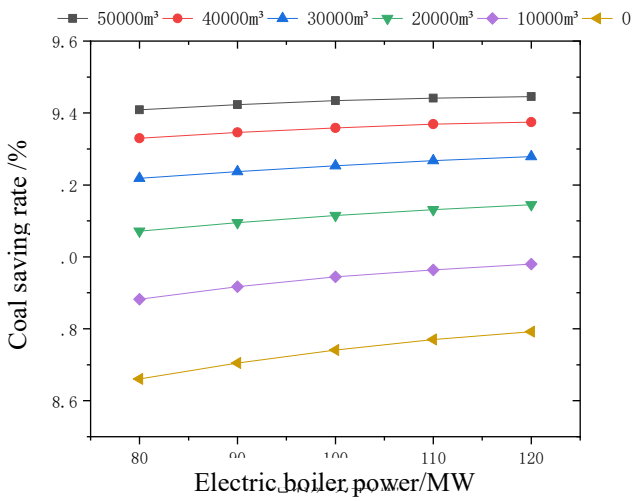

b. Coal saving rate

Figure 7. Coal consumption and coal saving rate of different schemes

As shown in the figure, equipped with electric boilers and heat accumulators can effectively reduce the coal consumption of system operation, improve the efficiency of thermal power plants and reduce carbon emissions. After the transformation of the thermal power plant, the operating coal consumption of the system is inversely correlated with the capacity of the electric boiler and the capacity of the heat accumulator. The larger the capacity of the new equipment is, the better the coal saving effect is, but with the increase of the capacity of the regenerator, the influence of the capacity of the electric boiler on the coal saving rate of the system gradually reduced. When the capacity of the electric boiler is 100MW and the capacity of the heat accumulator is 20000m³, the operating profit of the system is the largest, and the coal consumption can be reduced by 9.11% compared with the original system.

5. CONCLUSION

In this paper, the technical scheme of thermoelectric transformation of thermal power plant using electric boiler and heat accumulator is analyzed, and considering the cost of new equipment, Matlab software is used for system modeling, and the mathematical model of maximum net income of thermal power plant is established. YALMIP and CPLEX are used to solve the model, and the operation characteristics of thermal power unit before and after transformation are analyzed. By analyzing the influence of different equipment capacities on the net income of the thermal power plant, it is determined that the optimal capacity of the new equipment is 100MW for the electric boiler and 20000m³ for the heat accumulator, which can maximize the net income of the thermal power plant during the heating season, reduce the operating coal consumption of the system by 9.11%, and reduce the carbon emissions of the system. In terms of wind power consumption, the addition of auxiliary equipment can increase the wind power consumption capacity of thermal power plants by 30.6%, which can effectively reduce wind curtailment and alleviate the problem of insufficient peak regulation capacity of cogeneration units.

ACKNOWLEDGEMENT

This paper is derived from the Key project of International Scientific and Technological Innovation Cooperation between the governments of the Ministry of Science and Technology "Development of the digital-twin for a district heating system and the smart control based on dynamic simulation towards a low-carbon energy sector" (No. 2021YFE0116200).

REFERENCES

[1] P. Xu, J. Chen, J. Zhang, Optimization strategy of electrode boiler cogeneration combined heating system for CSP power station considering carbon trading, Modern Electronics Technique 2023;46(3):136-142.
[2] N. Wang, C. Zhang, X. He, Y. Yang, L. Chen, H. Liu, C. Wang, X. Jiang, C. Ye, . Optimization of active heat storage in heat network based on wind curtailment consumption, Electric Power 2023;56(2):114-122.
[3] W. Xia, From "District Heating" to "Multi-Energy Supply" -- Introducing the Fourth Generation of "District Energy Supply System" in Europe, Building Energy EFFICIENCY 2018;46(3):142-143.
[4] J. Wang, Research on residential heating model based on energy consumption simulation, Urban Architecture Space 2022;29(8):246-247.
[5] W. Long, Carbon Neutral Urban Building Energy Systems (4): Energy Storage, Heating Ventilating & Air Conditioning 2022;52(11):1-12.
[6] Q. Lv, S. Du, L. Liu, N. Zhang, H. Wang, R. Liu, Economic analysis of configured electric boiler peak regulation in thermal power plants in Northeast auxiliary service market, Automation of Electric Power Systems 2019;43(20):49-56.
[7] X. Pang, X. Zhang, L. Lv, S. Shi, X. Cui, G. Pei, Improved artificial bee colony optimization scheduling method for cogeneration system with heat storage device, Science Technology and Engineering 2022, 27(22):12006-12015.
[8] G. Sun, W. Zhang, J. Zhou, H. Liu, Optimal allocation of electric boilers and heat storage in thermal power plants based on Cournot model, Electric Drive 2023;53(3):56-63.
[9] R. Zhang, Research and optimization of integrated technology of thermoelectric peak regulation in coal-fired thermal power plant to promote the consumption of wind power, Dalian University of Technology 2020, pp. 105.

Policy & Market

The 18th International Symposium on District Heating and Cooling, September 3–6, 2023, Beijing, China

A Comparative Study of Low-Carbon Heating Pathways in China, Japan and Korea

Zihan Zhu[a], Dexi Sun[a], Seul-Ye Lim[b], Rong Liu[c], Jianjun Xia[a*]

[a] *Building Energy Research Center, School of Architecture, Tsinghua University, Beijing, 100084, China*
[b] *Korea District Heating Corporation, Seoul, 01811, Korea*
[c] *China District Heating Association, Beijing, 100028, China*
[*] *Corresponding author. xiajianjun@tsinghua.edu.cn*

ABSTRACT

The Paris Agreement proposed to control global temperature rise, and Asian countries announced carbon neutrality strategies in response. The energy and building sectors are the main sources of carbon emissions, with heating accounting for a significant portion. Therefore, formulating a low-carbon development path for heating according to local conditions is central to achieving carbon neutrality in Asia. This paper focuses on the research and prediction of heating load and clean heating resources in China, Japan and Korea. On this basis, the heating mode and low-carbon heating pathways are planned and compared. At present, China mainly develops district heating in northern regions, and Korea and Japan mainly develop decentralized heating. All three countries have a large amount of available waste heat from thermal power, nuclear power, industrial production and data centers. Compared with decentralized heating, district heating in Japan and Korea can make better use of the above-mentioned waste heat, reduce additional energy input, and have advantages in terms of economy and pollutant emissions. For the three countries, completing energy-saving renovation of buildings on the demand side as soon as possible, preferentially using clean heat sources for heating on the supply side, and using renewable electricity to supplement heat are important measures on the low-carbon heating pathway.

Keywords: Carbon neutrality, Heating load, Clean heating resources, Low-carbon heating routes, District heating

1. INTRODUCTION

To control the current increase in global temperature, several Asian countries have proposed carbon-neutrality policies, with Korea and Japan proposing to achieve carbon neutrality by 2050 and China proposing to achieve carbon neutrality by 2060. The building and energy sectors produce a large proportion of total carbon emissions, making them key focus areas for achieving carbon neutrality. District heating (DH) is closely related to both sectors. Therefore, Asian countries should develop clean and low-carbon DH solutions and take concrete actions to achieve their carbon neutrality targets.

To identify suitable research methods and future low-carbon heating paths, a literature review was conducted for countries with similar latitudes and climatic conditions in Europe and Asia. In response to the future energy crisis and sustainable development goals, European countries have carried out a significant amount of research on heating routes. Some researchers[1]-[5] studied various aspects of heating resource forecasting, heating demand forecasting, heating sources and demand distribution, clean heating route in Europe. Previous research has focused on possible heating pathways in China[6],[7]. Focusing on Northern China, the researchers conducted surveys and made predictions on the heating load, heating potential and their future development potential. Subsequently, they designed various clean heating routes. Finally, an optimal clean heating scheme was selected by comparing many aspects. Research has also been conducted on Korea's national clean heating resources[8],[9]. In Japan, most existing studies in this field have focused on integrating waste heat into the DH system[10]-[12]. These studies have examined the heating load and clean energy heating capacity throughout Japan, and compared energy efficiency and economics under different scenarios as a means to identify the best development pathway.

Based on the available literature, in comparison to the relatively mature research on low-carbon heating paths in Europe, research in Asia has some shortcomings. First, with respect to supply and demand, existing research lacks general, national-scale applicability, requiring greater synthesis of the available clean heating resources as well as a focus on future heating load and heat source requirements. As an exception, one recent study provides a forecast of heating in China's northern regions, which could be expanded to other Asian countries[13]. Secondly, regarding low-carbon heat-supply pathways, research in China is relatively well developed and serves as a useful reference. In Japan and Korea, however, existing studies are focused on a single clean heat source and do not comprehensively consider their integrated use. In addition, there is a current lack of analysis and comparison of heating routes between different countries. Hence, further research on low-carbon heat-supply routes in Asia is urgently required.

Having similar latitudes and climates, China, Japan, and Korea were selected for further comparison of low-carbon heating development pathways. The selected time horizons were 2022 (the status quo), 2035 (mid-term scenario), and 2050 (long-term scenario). Firstly, the supply and demand sides of heating were considered to establish both current and future scenarios in Sections 2. Based on this, in Sections 3 and 4, supply and demand were then matched, and different low-carbon heating pathways were designed for each country. Optimal pathways were then evaluated based on energy consumption, pollutants, economics, and other aspects. The most suitable heating modes for each country were identified according to their respective resource endowment. Lastly, the conclusions are presented in Sections 5.

2. METHODS

2.1. Building heating load forecasting methods

Building heating loads for China, Korea, and Japan (CKJ) were calculated according to building area and the building heat consumption index, as Eq. (1).

$$\text{Building heating loads} = \text{Building area} \times \text{Building heat consumption index}$$
$$(\text{Building area} = \text{Population} \times \text{Number of buildings per capita}) \quad (1)$$

2.1.1. Building area

The results in China in this section primarily refer to the data presented by Zheng[7]. The urban floor area in Northern China was 15.2 billion m^2 in 2018 and is projected to reach 20.5 billion m^2 by 2035 and 21.8 billion m^2 by 2050.

Population data for Korea were obtained from the Korea Statistics Bureau. Per capita building area under the current scenario was calculated based on the statistical data available for the administrative divisions of the Korea Statistics Bureau. The projected building area in Korea between 2035 and 2050 is presented in Table 1.

Population data for Japan were obtained from the Bureau of Statistics of Japan. Future population projections are available from the Japan Population Research Institute. The current per capita building area in Japan was based on the data available from the Japan Bureau of Statistics. Based on a relatively stable trend, building area projections for 2035 and 2050 are presented in Table 2.

Table 1. Korea building area forecast

	2018	2035	2050
Population (1,000 people)	51826.1	50868.7	47358.5
Building area per capita (m^2/person)	43.8	45.7	48.0
Total building area (100 million m^2)	22.7	23.3	23.8

Table 2. Japan building area forecasts

	2018	2035	2050
Population (1,000 people)	126749.0	114726.5	101880.0
Building area per capita (m2/person)	26.0	30.0	35.2
Total building area (100 million m2)	32.9	34.4	35.8

2.1.2. Building heating load index

Considering the convenience of comparison with the available data for China, the speed of building renovation was divided into three modes: slow (according to status quo), medium (as completed by 2050), and rapid (as completed by 2035). Based on Zheng[7], the heating load of urban buildings in Northern China was 3.87 billion GJ in 2018, growing to 3.54 billion GJ by 2035 and 3.68 billion GJ by 2050.

According to the Korean Building Energy Efficiency Grade Standard, the primary energy consumption per unit area of each grade of building is divided into 10 classes. Jung[14] calculated that the building heating load in Korea accounted for 17.8% of the total annual energy consumption. In the case of centralized heating, energy consumption during transportation and other energy loss should be considered. Therefore, the heating load index of buildings was calculated as Eq. (2). The current and projected future building heating load indicators for Korea are presented in Table 3.

$$\text{Building heating load index} = \text{Building energy efficiency grade index} \times 17.8\% \times \text{Decentralized heating ratio}$$
$$+\text{District heat supply heating load index} \times \text{District heating ratio} \quad (2)$$

According to the Japanese Building Standard 1999[15], from north to south, eight regional areas were distinguished based on their different heating load indicators. The Japanese building heating load index was also calculated using Eq. (2). The data selection for the building energy efficiency grade index and DH load index differed according to the three transformation modes, and the current (2018) and future projected building heating load indicators for Japan are presented in Table 4.

Table 3. Building energy efficiency rating index forecasts

Table 4. Predictions of building energy efficiency level

for Korea

MJ /m²/year	2018	2035	2050
Rapid mode	117	75	75
Medium mode	117	82	75
Slow mode	117	98	83

indicators in Japan

MJ /m²/year		2018	2035	2050
Decentralized heating	Rapid mode	112	97	97
	Medium mode	112	100	97
	Slow mode	112	105	100
District heating	Rapid mode	254	169	169
	Medium mode	254	180	169
	Slow mode	254	197	180

2.2. Clean heating resources forecasting methods

The clean heating resources discussed in this section are the waste heat of power plants (thermal power plants and nuclear power plants), IWH (industrial waste heat), biomass resources, waste resources, and data center waste heat. Among them, power plants waste heat and IWH are clean heating resources because they are waste heat originally discarded in their production process, and no pollution emissions are generated in the process of utilization. Based on the status quo and national policy, industrial development and other aspects were considered to derive future scenarios. As Zheng[7] already provided forecasts for Northern China (except for data centers), new forecasts were not developed for this region.

2.2.1. Waste heat from power plants

The total installed capacity of thermal power plants in China is 15,300 MW. Projecting the future thermal power plant size and heating potential, the total installed capacity of coal-fired and gas-fired thermal power in Northern China is 499,000 MW when only the units above 600 MW are retained. Combining the projections of installed coal-fired and gas-fired thermal power and nuclear power, the total surplus heat from power plants in Northern China is expected to be 5,136 million GJ in 2050.

Data for Korean power plants were obtained from the IEA and Korea Statistics Bureau. In 2020, the installed capacity of thermal power was 24,000 MW, and the installed capacity of nuclear power was 11,000 MW. Projected power plant waste heat was based on future power generation structure[16], as shown in Figure 1. Based on this, a projection of waste heat from power plants in 2050 assumes a thermal power installed capacity of 12,000 MW, and a nuclear power installed capacity of 10,000 MW. The total waste heat from these power plants (by 2050) is 26,000 MW.

Data for Japanese power plants were obtained from the IEA and the Japan Statistics Bureau. In 2020, the thermal power installed capacity was 85,000 MW, and the nuclear power installed capacity was 11,000 MW. Based on the Japanese 2050 target[17], projected changes in the power generation structure are shown in Figure 2. Based on this, the predicted status of power plant waste heat in 2050 assumes an installed thermal power capacity of 63,000 MW, and an installed nuclear power capacity of 8,000 MW. The total projected waste heat from power plant (by 2050) is 64,000 MW.

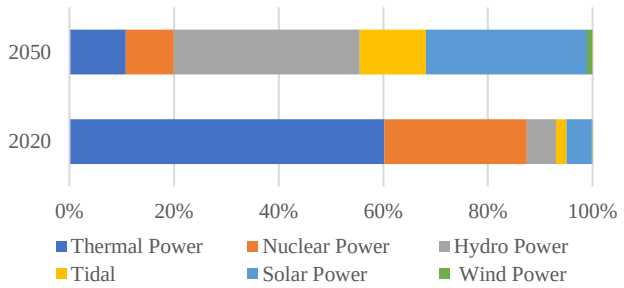

Figure 1. Current and future forecasted power generation structure in Korea

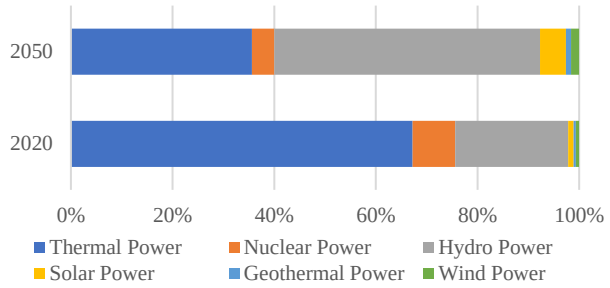

Figure 2. Current and future forecasted power generation structure in Japan

2.2.2. Industrial waste heat

IWH is divided into ferrous metal smelting waste heat, non-ferrous metal smelting waste heat, chemical waste heat, petroleum processing waste heat, and other IWH. Some calculation methods in this section refer to the previous study of Zheng[7]. The predictions of IWH potential were made with reference to the expected trends in industrial output obtained from the literature[18],[19].

By 2050, the total utilization potential of IWH in Northern China is 1,406 million GJ, and total waste heat is projected to drop to 919 million GJ.

According to the IEA "Korea 2020 Energy Policy Review"[20], and data from the Korea Industrial Park Corporation and Korea Statistics Bureau, in 2020, Korean steel and copper output was 70.9 million tons and 848,000 tons, respectively. Based on these values, the current IWH potential in Korea is approximately 386 million GJ. The projected IWH potential of Korea based on industrial output is 258 million GJ by 2050, of which petrochemical waste heat and ferrous metal (primarily steel) smelting waste heat still account for the largest proportion (48% and 44%, respectively).

Based on the data from the IEA, METI, Statistics Bureau of Japan, and the Japan Ministry of Economy, Trade, and Industry, steel output was 69.494 million tons and copper output was 773,000 tons in 2020. Based on this, the current IWH potential of Japan is 286 million GJ. Projected IWH potential based on industrial output is 225 million GJ by 2050, of which the waste heat from ferrous metal (iron and steel) smelting still accounts for the largest share (58%) of the total.

2.2.3. Biomass resources

The total annual amount of crop straw production in Northern China is 488 million tons, and the potential for gas production from livestock manure is 223 million GJ. Based on these data, the total amount of heat from biomass resources is 5.3 billion GJ. In 2050, 701 districts and counties are projected to have surplus biomass, with a total heat-supply potential of 3.058 billion GJ. Excluding rural self-use, the expected available heat in cities and towns from biomass is 1.8 billion GJ.

Data on biomass resources in Korea were obtained from the statistics of the Korea Statistics Bureau. The production of rice and beans and the number of pigs, cattle, and sheep in Korea were studied, from which the total biomass resource was determined. Based on these calculations, the potential distribution of biomass resources in Korea is 60 million GJ by 2050.

Data on Japanese biomass resources were obtained from the Japan Bureau of Statistics. Based on the production of rice, wheat, and beans and the number of pigs, cattle, and sheep, the projected distribution of biomass potential in Japan is 110 million GJ by 2050.

2.2.4. Waste resources

The heat from urban waste is closely related to population size, with each person generating 367.95 g of waste per day. According to population forecasts in 2.1.1, the current waste heat resource potential in Northern China is totaling 249 million GJ, 16 million GJ in Korea, 90 million GJ in Japan.

2.2.5. Data center waste heat

According to a Greenpeace report[21], the total electricity consumption of data centers in China was 160.9 billion kWh in 2018. The "Data Center White Paper"[22] collected the data of 49.9% racks above large size in China by 2017. The "China Data Center Energy Use Report"[23] provides data on the total electricity consumption of data centers based on power usage efficiency (PUE) and indicates that the associated total available waste heat in Northern China is ~322 million GJ. Based on current trends, this is expected to increase to 1.89 billion GJ by 2050.

According to the "2020–2023 Korea Data Center Report"[24], since 2000, Korean data centers have grown at an annual rate of 5.9%. In 2019, there were 158 data centers in Korea, 57% of which were private data centers. Between 2000 and 2019, the annual electricity consumption of private data centers increased from 9,360 to 20,026 kW. According to the total power consumption of these data centers, the associated waste heat is approximately 128 million GJ, and based on current trends, it is expected to reach 250 million GJ by 2050.

Based on current IT equipment power consumption and the "Current Status and Future Prospects for Power Consumption of IT Equipment"[25], power consumption by data centers in Japan was 15 TWh in 2005, growing to 47 TWh in 2020. According to strategic calculations, Japanese PUE was 1.9 in 2005, 1.3 in 2025, and 1.1 in 2050. Based on the total power consumption of data centers, the current total amount of waste heat available from data centers is ~220 million GJ and is expected to increase to 440 million GJ by 2050 based on current trends.

3. RESULTS

3.1. Building heating load forecast results

According to the projected building area and building heating load indicators for CKJ, heating loads under the current and future scenarios are presented in Table 5. A comparison of the heating load per unit area of buildings in CKJ is shown in Figure 3. Compared to that of Japan, China and Korea have higher heat consumption per unit of floor area, and there is more room for energy saving. This is largely because Japan began implementing building energy conservation measures earlier, launching the "Residential Energy Saving Benchmark" in 1980 with revisions in 1992 and 1999.

Table 5. Predictions of heating loads for under different models in CKJ

billion GJ	Status quo	Rapid mode	
	2018	2035	2050
China	3.87	3.54	3.68
Korea	0.48	0.40	0.41
Japan	0.57	0.54	0.56

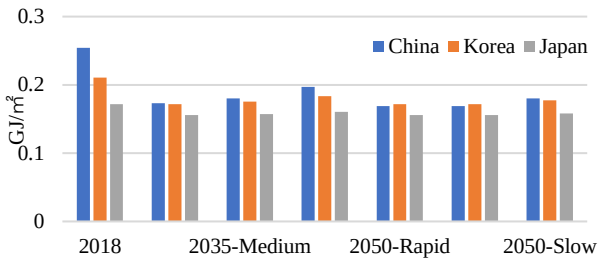

Figure 3. Schematic of the research methodology used to compare district heating pathways for China, Japan, and Korea

3.2. *Clean heating resources forecast results*

Based on statistical projections, the clean heating potential of CKJ by 2050 will be approximately 8.21, 1.38, and 2.88 billion GJ, respectively, with expected proportions of clean heat sources shown in Figure 4. The major clean heating resource in Northern China is power plant waste heat, and Korea and Japan have a relatively large share of waste heat from power plants. In addition, waste heat from data centers in Japan and Korea and IWH in Korea has high potential for utilization.

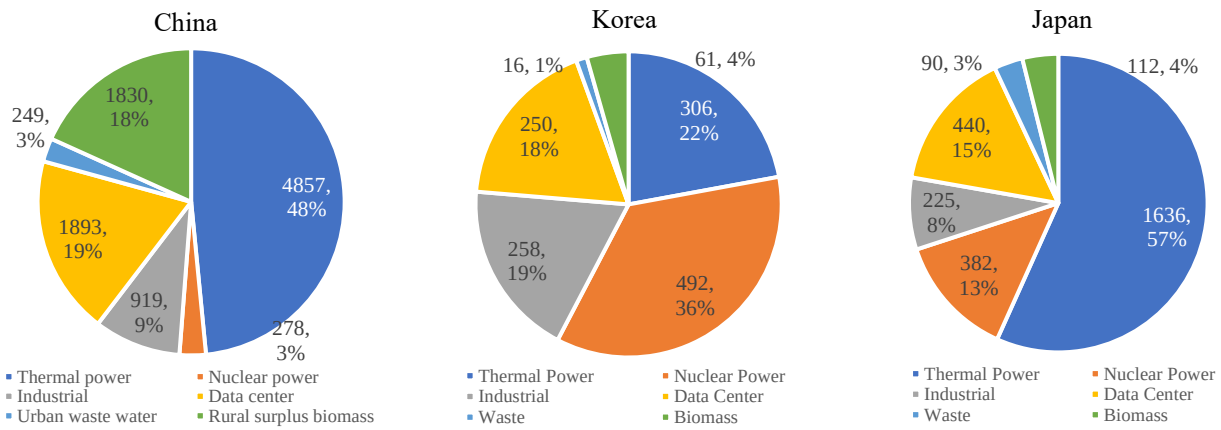

Figure 4. Clean heating resources in CKJ by 2050 (million GJ)

3.3. *Matching analysis*

Comparing the supply-side heating capacity with the demand-side heating load in 2050, the heating capacity of CKJ can meet the overall heating demand. However, considering the difficulties and poor economics of long-distance transportation of waste heat resources, further regional analysis is required. Due to the inconsistent distribution of waste heat resources and heat demand, there are shortages in clean heat sources in CKJ by region. Based on Figure 5, there is a projected load shortage of 218 million GJ based on the clean heating resources in Northern China, 91 million GJ in Korea, and 186 million GJ in Japan.

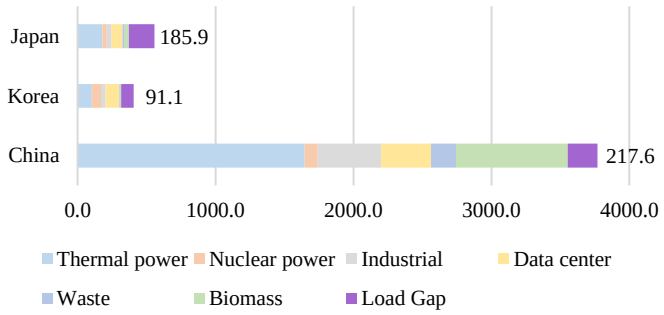

Figure 5: Planning for the rapid renovation of heating structure: heat supply in 2050 (million GJ)

4. DISCUSSION

4.1. *Heating mode analysis*

Zhang[6] suggested that qualitative analyses of whether to adopt centralized heating in a region can be conducted based on regional resource endowments. Based on national policies or research calculations, DH is a better choice for urban areas in

Northern China, where it is the main means of heating in winter. According to the China District Heating Association, the DH area in Northern China accounts for approximately 88.2% of the total urban heating area; in Korea, urban DH currently accounts for ~17% of the total area, and in Japan, where decentralized heading is the dominant mode, this figure is only 0.4%. In Korea and Japan, there is still much waste heat that can potentially be used as a DH source, indicating considerable scope for development.

Projections for Korea and Japan are shown in Figure 6 and Figure 7, in which the following clean heating resources are considered suitable for DH: waste heat from power plants, IWH, and waste heat from data centers. The utilization of waste and biomass resources is suitable for decentralized heating. The use of gas or renewable electricity suitable for decentralized heating can supplement the heat source deficit. The projected proportion of DH by 2050 in Korea is 82.24% and in Japan is 83.69%, both significantly higher than the current proportions. At present, most areas in Korea and Japan use decentralized heating, and a large amount of waste heat from thermal power, nuclear power, industry, and data centers is not utilized. Moreover, the centralized heating facilities in these countries are suboptimal, and further analyses are needed to determine whether such a large scale of centralized heating should be adopted.

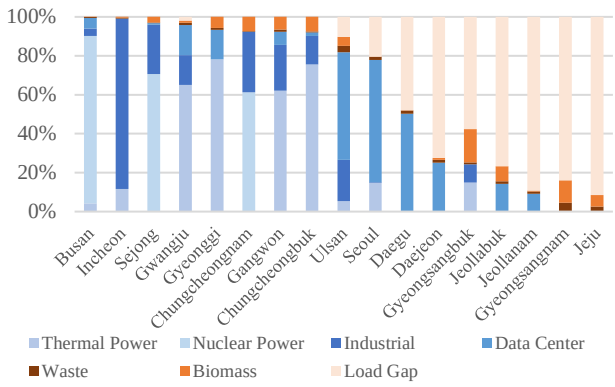

Figure 6: Korean resource endowment by region in 2050

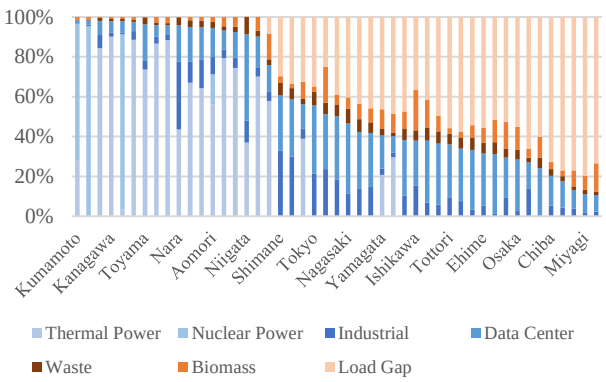

Figure 7: Japanese resource endowment by region in 2050

4.2. Design and comparison of district heating schemes

Based on the previous analyses, the heat-supply models were divided into centralized heat supply (assuming the same proportion as the status quo) and large-scale centralized heat supply. Because there is a shortage of clean energy for heating on the supply side, Zheng[7] proposed the use of gas or renewable electricity to make up for this shortfall. Adding the three retrofit rates to the demand side, 12 medium scenarios were devised for comparison.

(1) Energy consumption

The heating load increases after the adoption of large-scale centralized heating, and the energy consumption of centralized heating is higher than that of decentralized heating. However, the utilization of waste heat itself does not increase the energy consumption of the production process. Therefore, considering only the consumption of supplementary energy, the energy consumption of centralized heating is considerably less than that of decentralized heating. Based on these projections, in 2050, the minimum gas consumption in Korea is 4.2 billion Nm^3, and the consumption of renewable electricity is 13.3 billion kWh. In comparison, the minimum gas consumption in Japan is 5.0 billion Nm^3, and the consumption of renewable electricity is 15.8 billion kWh. Decentralized heating consumes approximately twice as much gas and renewable electricity as DH.

2) Pollutant emissions

Considering the main pollutants (NO_x, SO_2, dust, etc.) emitted by residential heating schemes in Japan and Korea, after the adoption of large-scale DH, the use of power plants and IWH for heating increases. As the use of waste heat does not increase pollutant emissions, only the pollutants emitted by supplementing the heating load deficit were considered, and the large-scale adoption of centralized heating would lead to lower levels of pollutant emissions than that at the status quo. The emissions of dust are similar when gas and electricity are used on the supply side to make up the heating load gap for the same heating mode. However, for NO_x and SO_2, emissions are low when using renewable electricity. Demand-side building retrofits would lead to low emissions of all pollutants under the rapid-mode scenario.

(3) Economic feasibility

The economic feasibility of residential heating in Korea and Japan were assessed. DH increases transportation energy consumption, while decentralized heating cannot use waste heat, energy consumption considerably increases. If electric-

driven heat pumps are used, DH costs slightly more than decentralized heating. If gas is used for supplemental heating, decentralized heating is more expensive than DH. Assuming the same heating mode, the use of renewable electricity is more economical than using gas when making up for the heating load gap. In the long term, a is better comparing only the annual operating costs, the rapid retrofit pathway is the economical option.

4.3. Summary

By comparing several aspects, for CKJ, heating solutions on the supply and demand sides become clear. The supply side should preferentially use clean heat sources for heating; when the heating is insufficient, renewable electricity should be used to supplement the heating gap. Furthermore, the energy-saving renovation of buildings on the demand side should be completed as soon as possible.

With respect to heating modes, the government has made it clear that DH will be adopted in urban areas in Northern China, and decentralized heating will be adopted in rural areas and Southern China. The advantage of centralized heating over decentralized heating is that the waste heat generated from the production processes of power plants and industries can be used without the need for dedicated energy consumption for heating. Therefore, only the waste heat utilization process and the supplementary heat production and utilization process need to be considered in the comparison. By studying the heating models in Korea and Japan, centralized heating is more economical in the long run; there is little difference between centralized heating and decentralized heating in terms of pollutant emissions; and centralized heating has a clear advantage in terms of primary energy consumption. Overall, centralized heating is the better choice.

Table 6: Comparison of future heating schemes in China, Korea, and Japan

		Energy consumption	**Emissions**	**Economy**
Heating mode (Korean, Japanese)	District heating	More	**Less**	**Better**
	Decentralized heating	**Less**	More	Worse
Supply side (Chinese, Korean, Japanese)	Renewable electric supplementary heating	**Less**	**Less**	**Better**
	Gas supplementary heat	More	More	Worse
Demand side (Chinese, Korean, Japanese)	Rapid retrofit	**Less**	**Less**	**Better**
	Medium Retrofit	Medium	Medium	Medium
	Slow retrofit	More	More	Worse

5. CONCLUSION

Based on the current status of heat supply, heat demand, and clean heat sources, pathways have been presented for matching heat supply and demand to support low-carbon development in Asia, focusing on China, Korea, and Japan. The building and energy sectors account for a large proportion of total carbon emissions in Asia, and heat supplies are closely related to both of these sectors. Thus, clean and low-carbon heat supplies are central to achieving carbon neutrality.

The heating load in Korea is projected to fall to 390.7 billion MJ by 2050 through rapid building renovation or increase to 616.9 billion MJ if large-scale centralized heating is adopted. The heating load in Japan is projected to fall to 390.9 billion MJ by 2050 through rapid building renovation or increase to 609.4 billion MJ if large-scale DH is adopted. According to clean heat source projections, the clean heat supply potential will be approximately 53,000 MW in Korea and 131,000 MW in Japan by 2050. In Korea, waste heat from power plants, industrial sites, and data centers accounts for 95% of the total available clean heat sources for centralized heating. Waste heat from power plants and data centers in Japan also account for a large proportion, reaching 88%. In contrast, biomass in China is relatively abundant and is primarily distributed in rural areas, providing abundant heat source resources for decentralized heating in rural areas in Northern China.

Finally, under a low-carbon heating pathway, clean heat sources are preferentially used to heat the supply side, supplemented with renewable electricity when supply is insufficient. On the demand side, energy-saving building renovations should be completed as soon as possible. With respect to heating modes, the use of large-scale DH can make full use of waste heat generated by power plants, industrial production, and data centers. It is estimated that by 2050, the minimum annual cost of such a pathway will be 3,395 billion won in Korea 388 billion yen in Japan. Notably, the DH mode in urban areas in Northern China can provide a useful reference for the development of DH in Korea and Japan.

ACKNOWLEDGEMENT

This work was supported by IEA DHC Project "District Heating Schemes for Carbon Neutrality in Asia: XIll-08", the 14th Five-Year National Key R&D Plan of China (Grant No.2022YFC3802401) and Ministry of Housing and Urban-Rural Development R&D Project of China (Grant No.K20220771).

REFERENCES

[1] Persson U, Moeller B, Werner S. Heat Roadmap Europe: Identifying strategic heat synergy regions. Energy Policy. 2014;74:663-81.
[2] Connolly D. Heat Roadmap Europe: Quantitative comparison between the electricity, heating, and cooling sectors for different European countries. Energy. 2017;139:580-93.
[3] Moeller B, Wiechers E, Persson U, Grundahl L, Connolly D. Heat Roadmap Europe: Identifying local heat demand and supply areas with a European thermal atlas. Energy. 2018;158:281-92.
[4] Connolly D, Lund H, Mathiesen BV, Werner S, Moller B, Persson U, et al. Heat Roadmap Europe: Combining district heating with heat savings to decarbonise the EU energy system. Energy Policy. 2014;65:475-89.
[5] Hansen K, Connolly D, Lund H, Drysdale D, Thellufsen JZ. Heat Roadmap Europe: Identifying the balance between saving heat and supplying heat. Energy. 2016;115:1663-71.
[6] Zheng W, Zhang Y, Xia J, Jiang Y. Cleaner heating in Northern China: potentials and regional balances. Resources Conservation and Recycling. 2020;160.
[7] Zheng W. Research on clean heating roadmap for Northern Chinese: potentials and regional balances [M.S.]. China: Tsinghua University, 2021.
[8] Bourtsalas AC, Seo Y, Alam MT, Seo Y-C. The status of waste management and waste to energy for district heating in South Korea. Waste Management. 2019;85:304-16.
[9] Lee J-Y. Current status of ground source heat pumps in Korea. Renewable & Sustainable Energy Reviews. 2009;13(6-7):1560-8.
[10] Fujii S, Furubayashi T, Nakata T. Design and Analysis of District Heating Systems Utilizing Excess Heat in Japan. Energies. 2019;12(7).
[11] Dou Y, Togawa T, Dong L, Fujii M, Ohnishi S, Tanikawa H, et al. Innovative planning and evaluation system for district heating using waste heat considering spatial configuration: A case in Fukushima, Japan. Resources Conservation and Recycling. 2018;128:406-16.
[12] Furubayashi T, Nakata T. Analysis of woody biomass utilization for heat, electricity, and CHP in a regional city of Japan. Journal of Cleaner Production. 2021;290.
[13] Zheng W, Xia J, Zuo H, Fang H. Investigation on clean heat sources and heat loads in northern regions. District Heating. 2019; 198(01):26-35+53.
[14] Jung Y, Kim J, Lee H. Multi-criteria evaluation of medium-sized residential building with micro-CHP system in South Korea. Energy and Buildings. 2019;193:201-15.
[15] Murakoshi C, Nakagami H, Nakamura M. New challenge for residential building energy efficiency standards in Japan: unify energy efficiency of envelope and housing appliances. Proceedings of the ECEEE 2007 Summer Study, 2007; 5:793-804.
[16] D'Ambrogio E, Chahri S. South Korea's pledge to achieve carbon neutrality by 2050. Members' Research Service, 2021; 690.693.
[17] D'Ambrogio E. Japan's 2050 goal: A carbon-neutral society. 2021.
[18] Kawase R, Matsuoka Y. Steel Production Estimation in Japan with Considering Global Market. Journal of Japan Society of Civil Engineers Ser G (Environmental Research). 2015; 71(5): 383-91.
[19] Ministry of Economy, Trade and Industry of Japan. Future Supply and Demand Trends of Petrochemical Products in the World, https://www.meti.go.jp/press/2019/10/20191017004/20191017004.html; 2019 [2022].
[20] IEA. Korea 2020 Energy Policy Review, https://www.iea.org/reports/korea-2020; 2020 [2022].
[21] Zhang W, Zhang S, Wang X, Qiao J, Zhang J, Kong W. Research on Energy Consumption and Renewable Energy Use Potential of Chinese Data Centers in Lighting Green Cloud. Beijing: Greenpeace; 2019, 54.
[22] China Academy of Information and Communications Technology & Open Data Center Committee. Data Center White Paper. Beijing; 2018, 36.
[23] LEED Data Center Advisory (China) Committee. China Data Center Energy Usage Report. Beijing; 2019, 39.
[24] Korea Data Center Council. Korea Data Center Market 2020-2023. Korea; 2019, 32.
[25] Japan Science and Technology Agency. Current Status and Future Prospects for Power Consumption of IT Equipment. Japan; 2019, 19.

The 18th International Symposium on District Heating and Cooling,
September 3-6, 2023, Beijing, China

Analysis and Forecast of Factors Influencing the Setting of Centralized Heat Supply Prices in Northern China's Cities and Towns

Li Junjie [a], Wang Chunlin[a, *], Fang Hao[b,a], Li Yanhe[b,a]

[a] *School of Resource Environment and Architectural Engineering, Chifeng University, Chifeng, 024000, China*
[b] *Inner Mongolia Fulong Heating Engineering Technology Co., Ltd. Chifeng, 024000, China*
[*] *Wang Chunlin，wangchunlin@cfxy.edu.cn，China*

Abstract

The setting of heat supply prices directly determines whether the heat supply industry can achieve a virtuous cycle. A high or low price set by the government will hinder the progress of heat supply reform, so a method needs to be found to establish a heat supply price that is acceptable to all parties in the game. Taking the centralised heat supply areas of northern towns as the subject of this study, the regulations governing heat supply in these areas were subjected to indicator distillation cluster analysis, analysis of the degree of correlation between relevant heat supply indicators and principal component analysis to predict the setting of heat prices in terms of GDP per capita, disposable income per capita and urbanisation rate. The development of heat supply prices should reflect a human-centred philosophy, adapt to social interests and consumer needs, provide new ideas for the development of the heat supply industry, and contribute to the high-quality development of the heat supply industry.
Keywords: urban central heating; hot price setting; PCA; neural network prediction

Supported by Natural Science Foundation of Inner Mongolia Autonomous Region of china（No.2023LHMS05013）

1. INTRODUCTION

Following the vision of the "carbon peak, carbon neutral" target, the relevant state departments have introduced a series of supporting policies and industrial plans centred on this target. As an important part of the energy industry's downstream chain, the urban heating industry plays an important role in the energy transition development strategy. Despite the rapid development of clean energy heating and heating in China's cities, there are still shortcomings, and in recent years, the state has increased subsidies for clean heating, which has contributed to the acceleration of the process[1]. However, most local governments have only been implementing policy subsidies for three years, and they are decreasing year on year. This suggests that heating subsidies are becoming a huge burden on the state. Using subsidies to modernise clean heating is not a long-term solution for large heating companies. Clean heating has also caused an increase in operating costs, making heating companies less enthusiastic about promoting clean heating at the same time as the company. Faced with pressure from the government and the public, if companies cannot afford it, it will spill over to customers and continue to lower the heating temperature or even stop supply, leaving them without heat. As a result of the government's concern for the affordability of users, only modest adjustments were made to heating charges, which may have led to some heating companies being upside down in terms of costs. In such circumstances, the various policies set by the government can have varying degrees of impact on various stakeholders, which match and constrain each other and work together.

In an era of heat reform, one of the challenges facing heating companies is to introduce heat supply mechanisms that can activate the heat market. In any industry, the most effective mechanism to stimulate market performance is a pricing mechanism and this study addresses the heat supply dilemma by introducing a new pricing mechanism for heat supply. The specific technical route is as follows:

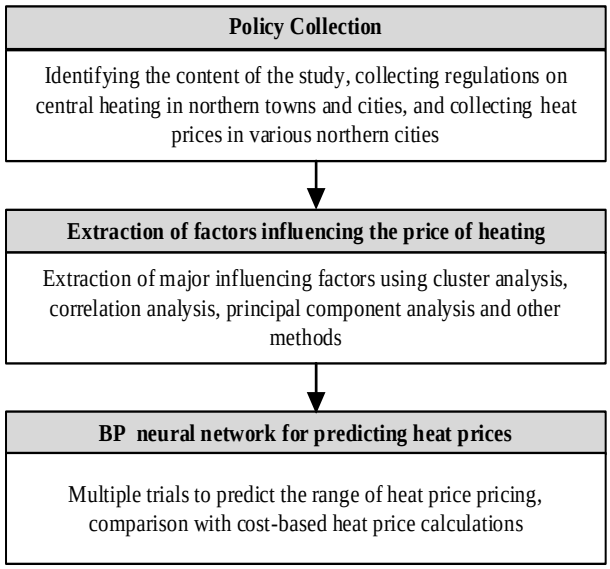

Figure 1. Technology Roadmap

2. Extraction of heat price impact indicators

2.1 Categorisation analysis of heat supply price impact indicators

Heat supply management regulations are formulated in order to regulate the management of heat supply and use in cities and towns, safeguard and protect the lawful rights and interests of both heat supply and heat use, in accordance with the relevant national laws and regulations, and in the light of the actual situation in the region. The regulations consist of the General Provisions, Planning and Construction, Heat Supply Guarantee, Heat Management, Facility Management, Legal Liability, By-laws and other parts.Translated with www.DeepL.com/Translator (free version)The clustering analysis of heating indicators was carried out with reference to the latest central heating regulations in each region against the research objectives of this topic of central heating tariffs in northern towns. The heating regulations have been in place since 2004 and the latest version is fully updated from 2021. It is feasible to conduct the analysis of heat supply price impact indicators in subsidised areas in accordance with the latest heat supply regulations. In this study, the latest heating regulations for central heating areas in northern cities and towns in nine provinces were collected, and the indicators refined were heating period, indoor temperature, charging system, refund for non-compliance with room temperature standards, refund rate for heat supply unit reasons for stopping heating, and refund rate for users stopping using heat. For convenience and analysis, the raw data is converted quantitatively according to reasonable rules, and the indicators are stratified and assigned on a scale of 1 to 6, naming the series in a specific order. The conversion criteria are listed in the table below:

Table1. Indicator assignment conversion criteria

Specific indicators	Assignment conversion criteria
Heating period	182=6；150=4；120=2；not known=1
Room temperature	Room temperature of 18°C or more throughout the day = 6; Bedroom and living room (hall) temperature of not less than 18°C throughout the day = 4; Room temperature of bedroom and living room (hall) meets the temperature requirements of the national code = 2; not known = 1
Charges	Two-part heat price = 6; users with heat metering charges pay the full amount of heat charges in advance to the heating unit according to the area, and after the heating period, settle the heat charges according to the actual measurement, with more refunds and less compensation[2] = 4; users with heat metering are charged according to the amount of heat used; those who do not have the conditions for separate heat metering are charged according to the heating area = 2; not known = 1
Room temperature not up to standard	Refund of heat charges in accordance with relevant regulations = 6; Reduction in heat charges due to heating companies causing substandard indoor temperatures = 5. If the room temperature does not reach the standard for more than 48 consecutive hours, the heat charge will be reduced by 4; if the indoor temperature is lower than 18°C (excluding 18°C) or higher than 14°C (including 14°C), the heat charge will be reduced by half on a daily basis; if the indoor temperature is lower than 14°C (excluding 14°C), the heat charge will be waived on a daily basis [3]= 3; If the room temperature is below 18°C and above 16°C (including

	16°C), 30% of the user's daily standard heat bill will be refunded on a daily basis; if the room temperature is below 16°C and above 14°C (including 14°C), 50% of the user's daily standard heat bill will be refunded on a daily basis; if the room temperature is below 14°C, 100% of the user's daily standard heat bill will be refunded on a daily basis=2; not known=1
Heat supply unit reasons for stopping the heat	If the heat is stopped for more than 48h, the heat charge will be refunded double by the day = 6, and the corresponding heating charge will be refunded according to the regulations and mutual agreement = 5; if the heat is stopped for more than 24h continuously, the heat charge will be refunded to the heat user by the day from the day the heat is stopped = 4. Reduction of the heat charge according to the duration of the suspension[4] = 3; if the heat is suspended for more than 24h continuously, the heat charge shall be refunded double on a daily basis, the total amount of the refund shall not exceed the heat charge paid by the user for the current period = 2, not known = 1
Heat cessation refund	Payment of a basic fee for the operation of the heating facility = 6; payment of a basic heat fee, which may not be higher than 20% of the total heat fee paid according to the heating area = 5; collection of a basic fee for operation, but not higher than 15% of the total heat fee paid according to the heating area = 4; payment of a basic fee = 3; payment of a heat loss compensation fee = 2; not known = 1

The results of the cluster analysis are as follows:

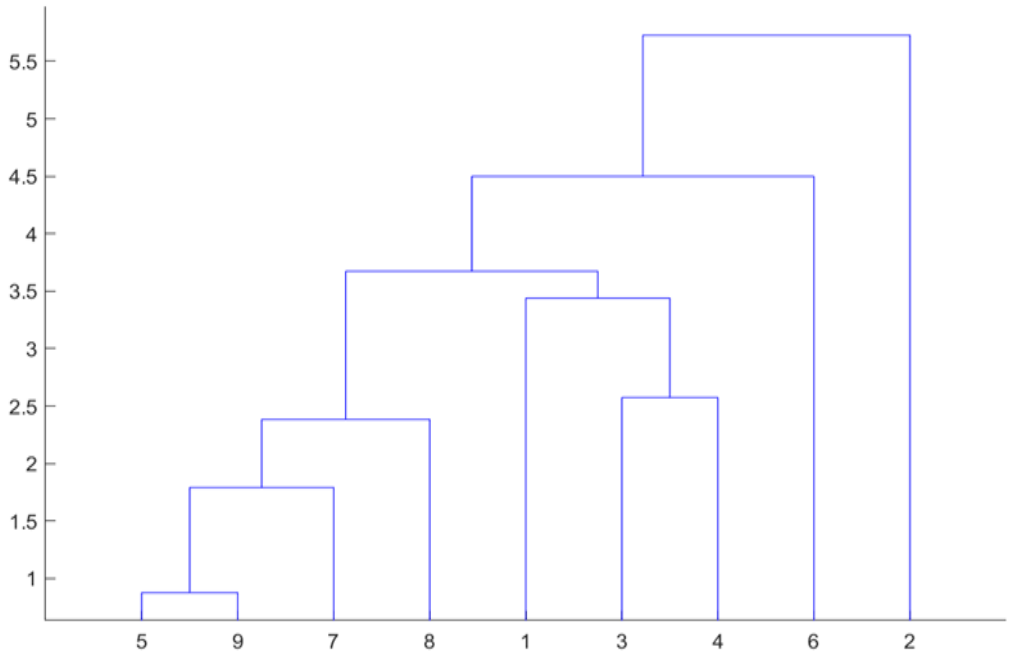

Figure 2. Cluster analysis of heating regulations in nine provinces and municipalities

As can be seen from the chart, the nine provincial administrative regions can be divided into three categories: the first category is Hebei Province (5), Henan Province (9), Tianjin (7) and Shandong Province (8); the second category is Heilongjiang Province (1), Liaoning Province (3), Inner Mongolia Province (4) and Beijing (6); and the third category is Jilin Province (2).

2.2 Preliminary analysis of basic heat supply price indicators

GDP per capita, aging rate, resident population, central heating area, heating days, cogeneration heating price, cogeneration heating price, gas boiler heating price, coal-fired boiler heating price, base price, metering price of northern cities have correlation analysis of variable factors with relevance, correlation analysis refers to the analysis of two or more variables with correlation of the elements, so as to measure the two factors' Correlation is used to measure the linear correlation between two variables X and Y. The value is between -1 and 1. The larger the absolute value, the stronger the correlation.

From the results, the factors with very strong and strong correlation are filtered out and categorised in terms of urban metrics, economic indicators, heat supply indicators, and other aspects, as shown in the table below.

Table2. Degree of correlation of relevant variables

Classification	Related variable elements	Correlation coefficient	Degree of relevance
Urban metrics and heat prices	Urbanisation rate and base price	0.9578	Extremely strong correlation
	Ageing rates and the price of heating from coal-fired boilers	0.9466	Extremely strong correlation
	Urbanisation rate and the price of heating with gas boilers	0.7661	Strongly related
	Urbanisation rate and the price of heating from coal-fired boilers	-0.7917	Strongly related
	GDP per capita and gas boiler heating prices	0.9836	Extremely strong correlation
	Per capita disposable and gas boiler heating prices	0.9394	Extremely strong correlation
Economic indicators and heat prices	GDP per capita and CHP heating prices	0.6678	Strongly related
	GDP per capita and CHP heating prices	0.6678	Strongly related
	GDP per capita and base prices	0.6816	Strongly related
	Disposable income per capita and base prices	0.7443	Strongly related
	Per capita disposable and CHP heating prices	0.6395	Strongly related
Heat Indicators and Heat Prices	Central heating area and metering price	0.8141	Extremely strong correlation
	Number of heating days and metering price	0.9117	Extremely strong correlation
Other	Resident population and central heating area	0.9333	Extremely strong correlation
	GDP per capita and urbanisation rate	0.7916	Strongly related

From the analysis results graph for filtering and categorisation, the absolute value of the relative coefficient between each two indicators is greater than 0.60, and the degree of correlation between GDP per capita and heating price of coal-fired boilers, ageing rate and heating price of coal-fired boilers, and urbanisation rate and heating price of coal-fired boilers is the greatest, indicating that GDP per capita, ageing rate, urbanisation rate and disposable income of urban residents can be used as the development and evaluation of heating price setting The correlation between per capita GDP, ageing rate, urbanisation rate and urban residents' disposable income is the highest.

2.3 Extraction of key heat supply price impact indicators

The correlation coefficient indicates the degree of correlation between different indicators, with a higher absolute value indicating a higher degree of correlation. As there is a certain amount of overlapping information between variables with high correlation and this overlap has a great impact on the objectivity of the estimation results, the need for principal component analysis can be demonstrated by analysing the correlation matrix. Therefore, principal component analysis was conducted on GDP per capita, ageing rate, urbanisation rate and disposable income of urban residents.

A principal component analysis of the data on GDP per capita, disposable income of urban residents, urbanisation rate, centralised heating area and ageing rate for 59 cities in the north was conducted and the results of the eigenvalues and contribution values were calculated as follows:

Table3. Calculation of eigenvalues and contribution rates

Principal Component Number	Eigenvalue λ	Contribution %	Cumulative contribution %
1	2.806	56.117	56.117
2	1.075	21.504	77.622
3	0.595	11.891	89.512
4	0.406	8.121	97.634
5	0.118	2.366	100.000

Normally, principal components with eigenvalues greater than 1 are retained and those with eigenvalues less than 1 are discarded, so that the final number of principal components is less than the number of indicators n. It is also possible to reach a certain cumulative contribution rate according to the size of the contribution, using different criteria, such as above 70%, above 85% or others. Here, the indicators with a cumulative contribution rate exceeding to above 85%, GDP per capita, urban disposable income and urbanisation rate, are chosen for the next step of analysis.

2.4 Heat price assessment method based on BP neural network prediction

BP neural network is one of the most commonly used neural network models today. It does not need to define a mathematical equation in advance to show the relationship between input and output, but only needs to learn some rules through its own training to get the closest result to the desired output for a given input, and its output is a continuous quantity from 0 to 1. It can also learn and store a large number of matching relationships between input and output data without first analyzing the mathematical equation describing the matching relationship[5] .

Importing the dataset, there are 3 features that will affect the setting of the heat price, namely GDP per capita, urban disposable income per capita and urbanisation rate, so the data related to these 3 features are statistically collated as the feature data (input data) for the prediction model, the data from the training set and the test set are read, and the input and output values are divided, the data from the training set are normalised in the second step, and the data are normalised to (between -1,1), and the third step builds a BP neural network. As the actual problem may consist of several competing metrics, the solution to the problem usually does not include a single optimal solution, but rather a set of non-inferior solutions, which usually cannot be solved by traditional multi-objective optimisation methods. It is therefore analysed together with a particle swarm algorithm, where particles continuously change state in a multidimensional search space until equilibrium or an optimum is reached or the computational limit is exceeded[6]. In the fourth step the optimal initial threshold weights optimised by the genetic algorithm are given to the network for prediction; in the sixth step, once all parameters have been set, BP training can be performed and finally the prediction results are back-normalised to obtain the true value of the prediction and to evaluate the error.

In order to more intuitively evaluate the law of heat tariff setting combined with the heat supply management regulations cluster analysis results collected in the last three years in Hebei Province, Henan Province, Tianjin City, Shandong Province contains 25 cities per capita GDP, urban residents disposable income, urbanisation rate, a total of 60 sets of data for neural network prediction.

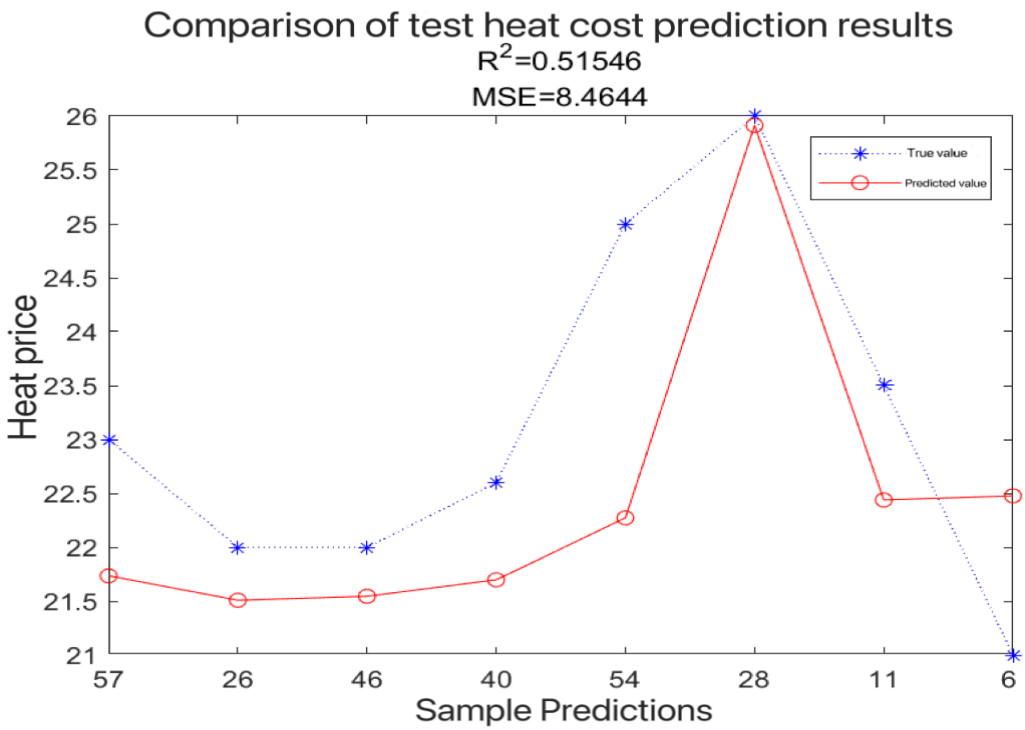

Figure 3. Comparison of tested heat costs with predicted results

2.5 Judgement of predictive models

The closer the mean squared error is to zero, the better the predictive ability of the model. If there is only one output, you can run it to see how much the predicted result differs from the output as a judgement of the validity of the result.

From the comparison graphs of the test heat cost prediction results with the smallest mean square error filtered from the randomly generated training samples, it appears that the predicted values are similar to the actual heat values but do not converge exactly to 0. The reasons for this are the small amount of data and the difficulty in collecting data, some of which is not reflected in the China Statistical Yearbook and can only be estimated by Baidu. In order to avoid these causes of bias, several training sessions can be carried out to find the average value and calculate the standard error to give a range of heat price setting.

2.6 Typical calculation examples

Zhang Shensheng has set a heat price of 27.75 RMB / m^2 for Shenyang based on a costing method[7]. In order to make a comparison, this paper selects Shenyang City for heat price neural network prediction, predicts future chargeable heat prices based on known data such as local per capita GDP, urban residents' disposable income and urbanisation rate, and uses a pricing mechanism that links heating charges and heat energy consumption to encourage consumers to take the initiative to regulate and achieve Efficient allocation of resources to achieve energy savings [8].

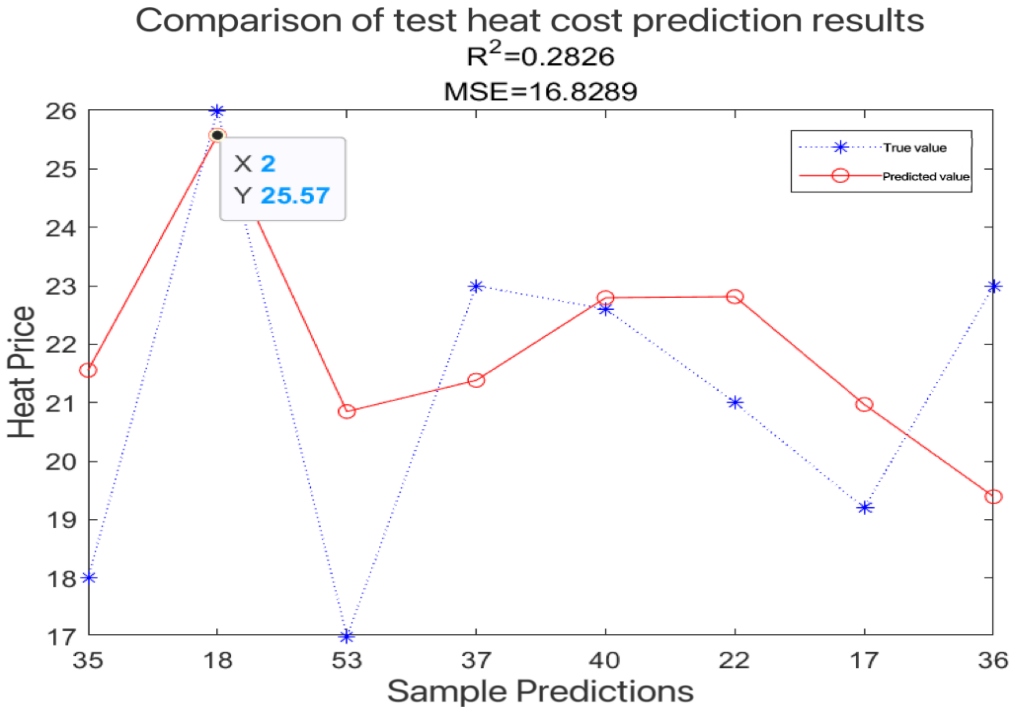

Figure 4. Comparison of test heat bill results in Shenyang

The horizontal coordinate 18 in the figure shows the comparison of the predicted results of the test heat cost in Shenyang, where the local heat price is 26 RMB/m^2, and the predicted result of the BP neural network yields a heat price of 25.57 RMB/m^2 in Shenyang. by running the neural network several times, the following relevant data are obtained:

Table4. Results of 25 neural network forecasts in Shenyang

Number of times (times)	Average value (RMB/$m^{2)}$	Standard error	Predicted value
25	25.11	0.32	25.11±0.32

The above table shows that the predicted heat price in Shenyang is 25.11±0.32 RMB/m^2. and the standard error is taken once for every 5 sets of data interval for the experimental results, and the error law is shown in the following table:

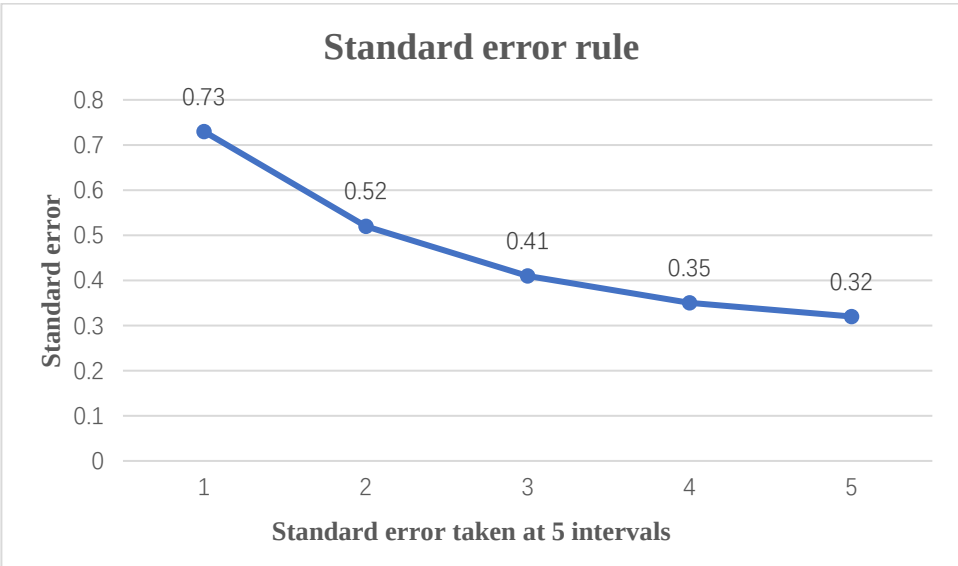

Figure 5. Standard error rule

The graph shows that the error decreases with the number of tests, the more tests, the smoother the change in value, so the smaller the standard error can be achieved through multiple tests, making the pricing range smaller and giving the government a reasonable choice of price range for pricing.

2.7 Analysis of calculation results

Error accuracy level:

The actual heat price in Shenyang is RMB 26/m^2 and the heat price obtained from the bp neural network is RMB 25.11/m^2, a difference of RMB 0.89/m^2 from the actual heat price. it can be seen that the prediction of heat price by bp neural network has a certain reasonableness. Therefore, the standard deviation of the mean and the arithmetic mean can be obtained by predicting the heat price several times, so that the error and accuracy are within a certain range, and thus the heat price of a city can be predicted in a reasonable range.

The impact of different factors on heat prices:

At present, China's heating price system there are many controversies: heating price management is not standardised, the Government, although the implementation of strict control, but the lack of supervision of the production costs of heating enterprises, the lack of pricing cost norms and accounting standards, the lack of pricing of the scientific nature. At present, China's heating costs and heating prices lack of "linkage" mechanism, energy prices, labour costs and other factors of production prices market-oriented decision, rising seriously, the local GDP per capita to reflect the local economic strength and people's standard of living, the higher the prices, the higher the GDP, the price of heat should be higher, but the government out of social sustainability considerations. However, due to social affordability considerations, the government has not increased heat prices in line with rising prices or the rate of change has been very small, resulting in serious losses for heat supply enterprises. According to the disposable income of urban residents to adjust the price of heat, the people's energy-saving incentives will also be stronger, after energy saving, effective use of energy, the price increased, some people with high incomes, for the price is not sensitive to, may not care about, how much more to burn it doesn't matter, hope that the side of the home is particularly hot, then more spending more money, the price-sensitive people, through the economical use of his to ensure that his budget will not be increased and there are May be reduced; heating companies can use the price increase that part of the income to compensate for the loss of the heating company, so that everyone can choose according to their own needs, to achieve heat on demand, in order to obtain the support of the masses, it is necessary to consider the majority of heat users to benefit, so as to mobilise their enthusiasm. Urbanisation rate refers to the proportion of the resident population of a region's cities and towns to the total population of the region, which is an important indicator for measuring the level of urbanisation and reflecting the process of urbanisation. With the continuous development of the economy, the acceleration of the urbanisation process, and the gradual improvement of the living standards of the people, the urban heating industry is developing rapidly, the heating area of cities and towns is constantly growing, and the demand for centralised heating in the city is increasing, which promotes the rapid development of China's urban heating The rapid development of the industry, the urbanisation rate has also become one of the factors affecting the price of heat supply, with the increase in the urbanisation rate, the increase in urban job opportunities, wage income may also be increased accordingly, which will make the heat users have more money to save, the residents of the heat comfort has a higher demand for heat, it will increase the demand for heat, and will successively affect the change of the price of heat.

Positive effects:

There are differences in the demands of the various actors in the reform of the heating price charging mechanism, which makes it difficult to reach cooperation. All actors are playing for their own interests, so how to get a coordinated and symbiotic result requires the government to think holistically and systematically when introducing policies. According to the analysis of the factors affecting the price of heat to predict the price of heat and adjust the price appropriately, the government through the local economic strength and people's living standards, the development of appropriate heat prices, so that the heating enterprises can make a profit, so that the heat users can heat on demand, users have the incentive to reduce their own unnecessary energy consumption, so that the various actors can be widely participated in, in order to improve the price policy of centralised heating; to strengthen the cost of heat supply enterprises and the The establishment of a good price regulation mechanism can help the heating system to achieve a balance between supply and demand, which is conducive to helping heating enterprises to improve the technical efficiency of all aspects of the heating system, screening out inefficient enterprises, and promoting the benign development of the heating market.

3. CONCLUSION

The various policies set by the government can have different degrees of impact on various stakeholders, and they match and constrain each other to work together. High or low heat prices set by the government can hinder the progress of heat supply reform, so there is a need to find a way to establish heat prices that are acceptable to all parties involved in the game. In order to achieve a 'win-win' situation for both the heating company and the customer, or even a 'win-win' situation for the government and society, this study combines cluster analysis, correlation analysis, and the use of a 'win-win' approach.

This study combines cluster analysis, correlation analysis, principal component analysis and neural network prediction methods to forecast heat costs. By analysing the shortcomings of the existing heat supply mechanism, a set of three main influencing factors, such as local GDP per capita, disposable income of urban residents and urbanisation rate, was designed to predict the heat supply price level through the basic data of social development in the past three years,a difference of RMB 0.89/m^2 from the actual heat price, which has some pricing reference value.

The known data predicts the future price of chargeable heat supply and facilitates the adjustment of behaviour patterns of stakeholders while promoting the interests of various interest actors to be safeguarded. Such a heat pricing mechanism will

not only increase the satisfaction of heat users with their usage and make their heat bills reasonable, but also allow heat supply companies to make more profits, thus promoting a virtuous cycle in the heat supply industry. Most importantly, by incentivising consumers to use energy more economically, energy consumption can be reduced, which has an important positive effect on both the energy transition and the promotion of clean energy.

REFERENCES

[1] General Office of the Ministry of Finance, General Office of the Ministry of Housing, Urban and Rural Development, General Office of the Ministry of Ecology and the Environment, General Department of the National Energy Administration, Notice on the Organization of Declaring Clean Heating Projects in Northern Areas in Winter 2022 [J]. Circular of the Ministry of Finance of the People's Republic of China,2022(05):31-38.

[2] Heilongjiang Urban Heat Supply Regulations [N]. Heilongjiang Daily,2011-08-24(013).

[3] Trial Measures for the Management of Centralized Heat Supply in Henan Province [J]. Henan Provincial People's Government Gazette,2018(06):3-7.

[4] Liaoning Urban Heat Supply Regulations [N]. Liaoning Daily News,2022-10-02(003).

[5] Chen, Wing-Hui, Hu, Chou-Ming. Study on task pricing model optimization strategy for mobile crowdsourcing platform[J]. Science and Technology Management Research,2022,42(01):149-155.

[6] Zhang Mingming. Research on the design of reverse logistics network for end-of-life vehicle recycling [D]. North China Electric Power University (Beijing), 2020.

[7] Zhang Shensheng, Gao Ming, Zhang Xuejiao. Study on the management mode of heat metering and charging in Liaoning Province[J]. Construction Economics,2010(01):61-64.

[8] Su Hong, Liu Chunsheng. Reflections on the design of a mechanism based on heating metering charges [J].District heating,2021(01):38-43.

The 18th International Symposium on District Heating and Cooling,
September 3–6, 2023, Beijing, China

Comparative Analysis of Heat and Power Supply System in China and Nordic Countries

Shunyong Yin, Dexi Sun, Xu Luo, Jiayang Chen, Jianjun Xia*
Building Energy Research Center, Tsinghua University, Beijing, 100084, China
** Corresponding author. xiajianjun@tsinghua.edu.cn*

ABSTRACT

The four Nordic countries are at the forefront of the world in developing low-carbon energy supply systems and have put forward the goal of building a 100% renewable energy system. The study of their energy supply systems has important implications for China in achieving carbon peaking and carbon neutrality goals. This paper focuses on a comparative analysis of the energy supply systems of China and the four Nordic countries, with the aim of quantifying the similarities and differences between them. Firstly, this paper defines the demand and supply heat-to-power ratio of the energy system, calculates and analyses their classification and characteristics, and proposes a method for matching the supply and demand of energy systems based on heat-to-power ratios through theoretical derivation. This method can be used to quantitatively calculate, analyze and compare different regional energy systems in terms of total energy, time dimension and spatial dimension. Next, the energy supply systems of the four Nordic countries and Northern China are quantitatively analyzed in three dimensions respectively. The similarities and differences between China and the Nordic countries are demonstrated. Afterwards, combining with the findings of the comparative analysis, the optimization for the design of the energy supply system in Northern China is conducted. The optimized design reduces fossil energy use and carbon emissions by more than 50% in Northern China. Finally, a summary and outlook of the above research is presented. In the light of the comparative analysis of the energy supply systems in Northern China and Nordic countries, recommendations are made for the construction of energy supply systems in Northern China, based on the principle of "learn fully and avoid following blindly".

Keywords: Heat-to-power ratio; Comparative analysis of China and the four Nordic countries; Energy supply system; Urban heating in Northern China

1. INTRODUCTION

In response to climate change and global warming, the four Nordic countries (FNCs) have set a goal of building a 100% renewable energy system and are pioneers of zero-carbon energy systems. China has also set a goal of peaking CO_2 emissions by 2030 and achieving carbon neutrality by 2060. In the future, fossil energy fuels will be gradually reduced and the energy supply system will be dominated by heat and power supply systems. However, China's current energy structure, still dominated by fossil energy, has high total carbon emissions, and its low-carbon development faces many challenges and problems: (a) China has the same per capita land area as Denmark. Can China directly replicate the way of building energy supply systems in Denmark and other Nordic countries, and achieve the carbon reduction goals through a 100% renewable energy system? (b) China has more fossil energy thermal power units. What is the appropriate development orientation and retention ratio of the units? (c) What are the key technologies needed to achieve decarbonization and synergy of heat and power in China's energy supply system with a high proportion of renewable energy systems?

A literature review of European energy system studies has been conducted. For 100% renewable energy systems, a systematic review has been conducted by Hansen et al [1]. For the European power system, research has covered various aspects such as power plant flexibility retrofit [2], energy storage [3], power markets, and grid construction [4]. For the European heating system, the studies focused on the fourth generation district heating (4GDH) technology with low-temperature [5], seasonal thermal energy storage () [6], and heating development routes [7]. It can be observed that low-temperature heating, STES and spatially planned matching of various heating resources are the main trends. However, the differences in resource endowments between China and Europe are large, and the development path of Northern Europe cannot be replicated in China as a whole.

Some studies have also been conducted by Chinese scholars to address the above issues. Research on the development prospect of fossil-energy thermal power in China focuses on two aspects: first, fossil-energy thermal power still needs to leave a certain amount of capacity in the future [8][9]; second, thermal power needs to cooperate with carbon capture, utilization and storage (CCUS) technology to achieve zero carbon emission [10]. The key technology research of low-carbon heat and power synergistic supply system in China mainly involves power plant flexibility retrofit [11], heat and power synergistic retrofit of thermal power plants[12], auxiliary power peak regulation market [13], nuclear power heating [14] and

STES [15]. However, the above technologies lack more detailed studies in terms of specific implementation paths, spatial and temporal distribution and matching of supply and demand.

In energy supply systems, heat-to-power ratio (HPR) is an important parameter that can quantitatively portray the heat and power supply-demand matching relationship, and scholars have widely applied it in various studies. These include energy supply- demand matching characteristics [16], heat and power coupling [17], building energy supply [18][19], and combined system studies of wind/solar and thermal power plants [20]. However, the definitions and calculations of HPRs in the above studies are different and need to be clearly defined when used.

Based on the above studies, this paper will further investigate the previous issues. In Section 2, a method of energy system supply-demand matching analysis based on HPR is proposed, and an overview of energy data from China and Europe is presented. Section 3 carries out a quantitative comparison analysis of the energy supply systems of the FNCs and China in terms of total energy, time dimension and spatial dimension. Section 4 adopts the above methods and comparative results to optimize the design of energy supply systems in northern China and quantitatively evaluate their effectiveness in reducing fossil energy consumption and carbon emissions. Finally, Section 5 concludes the full study.

2. METHODOLOGY AND DATA

2.1 Matching supply and demand in energy systems based on heat-to-power ratio

On the demand side of a heat and power energy system, the demand-side heat-to-power ratio (DHPR) R for an area is defined as the ratio of the demand for heating load H to the demand for power load E, expressing the relative magnitude of the heating and power loads in the heat and power system:

$$R = \frac{H}{E} \tag{1}$$

Since heating and power loads are time-dependent variables, DHPRs are accordingly classified into hourly, daily, monthly and yearly DHPRs. The DHPR is an objective property of a region, representing the heat and power demand characteristics of a region under natural and socio-economic influences. It can play an important role in the quantitative planning and application of energy storage systems in the region by reflecting seasonal and hourly differences with different calculation time dimensions.

The supply side of the heat and power energy system in a region is the various energy supply equipment, including heat sources and power sources. In this paper, the supply-side heat-to-power ratio (SHPR) r_i of the energy supply equipment i in the area is defined as the ratio of the heat output h_i to the power output e_i, which represents the relative magnitude of the heat supply and power supply capacity of the energy supply equipment:

$$r_i = \frac{h_i}{e_i} \tag{2}$$

Thereby, the calculation of the overall HPR r, overall heating output h, and overall power output e on the supply side of the heat and power energy system in the area can be derived from the SHPR r_i, heating output h_i, power supply output e_i, heating output share x_i, and power output share y_i for each type of energy supply equipment as follows:

$$x_i = \frac{h_i}{h_1 + h_2 + \cdots \ldots + h_n} = \frac{h_i}{\sum_{j=1}^{n} h_j} \tag{3}$$

$$y_i = \frac{e_i}{e_1 + e_2 + \cdots \ldots + e_n} = \frac{e_i}{\sum_{j=1}^{n} e_j} \tag{4}$$

$$r = \frac{h}{e} = \frac{\sum_{i=1}^{n} h_i}{\sum_{i=1}^{n} e_i} = \frac{\sum_{i=1}^{n} h_i}{\sum_{i=1}^{n} \frac{h_i}{r_i}} = \frac{1}{\sum_{i=1}^{n} \frac{1}{r_i} \times \frac{h_i}{\sum_{i=1}^{n} h_i}} = \frac{1}{\sum_{i=1}^{n} \frac{x_i}{r_i}} \tag{5}$$

$$r = \frac{h}{e} = \frac{\sum_{i=1}^{n} h_i}{\sum_{i=1}^{n} e_i} = \frac{\sum_{i=1}^{n} e_i \times r_i}{\sum_{i=1}^{n} e_i} = \sum_{i=1}^{n} \frac{e_i}{\sum_{i=1}^{n} e_i} \times r_i = \sum_{i=1}^{n} y_i \times r_i \tag{6}$$

According to the value of e_i, the SHPR of the energy supply equipment can be divided into the following categories: (a) When e_i=0, it means that such energy supply equipment only provides heat and does not consume or produce electricity. In this case, the SHPR r_i is $+\infty$. This type of energy supply equipment can be combined with others to improve the overall SHPR. (b) When e_i<0, it means that this type of energy supply device consumes electricity and produces heat, in which case the SHPR is negative, i.e. r_i<0. This mode can increase the overall SHPR in combination with other energy supply devices with positive SHPRs. (c) When e_i>0, this means that such a supply device can produce both electricity and heat,

such as cogeneration, in which case r_i>0.

The maximum SHPR is an important parameter in matching energy supply and demand. The maximum SHPR for eight typical energy supply equipment is shown in Table 1.

To match energy supply and demand in a region, the DHPR is an objective property of the region, i.e., the objective function of supply-demand matching, while the SHPR is a technical means that can be subjectively adjusted in a region, i.e., the variable function of supply-demand matching. As a result, a generic equation (7) for energy system supply-demand matching can be obtained:

$$\frac{H}{E} = R = f(r_i, h_i, e_i) = \frac{\sum_i r_i e_i + \sum_j h_j}{\sum_i e_i} \tag{7}$$

The equation can be applied to the calculation of supply-demand matching in a region at various time scales, and can be used both for the balance check of the status quo matching and the identification of existing energy supply problems, and for optimal design in the planning of regional energy supply systems.

Table 1. Maximum supply heat-to-power ratio for each type of energy supply equipment

Energy supply equipment	Maximum supply heat-to-power ratio
Heating-only equipment (boilers and industrial waste heat)	+∞
Biomass cogeneration and garbage cogeneration	2.3~3
Coal-fired cogeneration unit with waste heat recovery	1.8~2
Coal-fired cogeneration unit without waste heat recovery	1.5~1.7
Gas-fired cogeneration unit with waste heat recovery	0.8~1
Gas-fired cogeneration unit without waste heat recovery	0.6~0.7
Power-only equipment (thermal power, wind, solar, hydropower, nuclear power)	0
Electric boiler	-1
Electric heat pump	-4~-3

2.2 Source of energy data in China and Europe

Energy system research data can be divided into direct data and indirect data: direct data are direct values of energy demand and supply at different time scales, such as electricity/heat consumption, power and heat output of energy supply equipment, etc. Direct data can be directly used to calculate the demand and supply HPR of the energy system. Indirect data are data through which the demand and supply of the energy system can be calculated and estimated or can reflect the changes in the

Table 2. Source of energy data in China and Europe

Item		Data source
Heat supply – direct data	Annual/ monthly heat consumption; Heating load curve; Heat source mix/ energy consumption; Output curve of heating equipment	IEA-National data, Heat Roadmap Europe 4 National report, Nordic Council of Ministers Heating and Cooling, ODYSSEE-MURE Database-Residential&Service, data from national statistical bureaus & energy bureaus, reports & statements from heating companies, Carbon Emission Accounts & Datasets (CEADs) provincial energy inventories, China Energy Statistical Yearbook, China Urban & Rural Construction Statistical Yearbook, Annual Report on China Building Energy Efficiency, Report on China District Heating Development, Test data from actual engineering projects, typical curves from academic papers, technical reports & equipment system data from heating companies
Power supply – direct data	Annual/ monthly electricity consumption; Power load curve; Power generation data; Power import and export	IEA- National data, ENTSO-E transparency Platform, ENTSO-E national member companies, NORD POOL-power system consumption, China Energy Statistical Yearbook, Compilation of Electric Power Industry Statistics, China Electric Power Yearbook, National Development and Reform Commission-Typical Electricity Load Curves for Provincial Power Grids, National Bureau of Statistics
Heat supply – indirect data	Building area	ODYSSEE-MURE Database-Residential&Service, China Urban & Rural Construction Statistical Yearbook, Annual Report on China Building Energy Efficiency
	Meteorological data	Ladybug Tools, DeST meteorological data module, Meteonorm meteorological database
Power supply – indirect data	Grid electricity price	ENTSO-E national member companies, NORD POOL and other grid trading platforms
Industrial data – indirect data	Industrial energy use	IEA-World Energy Balance Database, China Energy Statistics Yearbook, CEADs provincial energy inventories

supply and demand of the energy system, for example, through the heating area of buildings, meteorological data, grid electricity prices, industrial energy use, etc.

The Chinese and European energy system data sources involved in this paper are shown in Table 2.

3. COMPARATIVE ANALYSIS

3.1 Analysis of energy supply systems in four Nordic countries

An analysis of the primary energy supply mix of the FNCs, Sweden, Finland, Norway and Denmark, is shown in Figure X. The share of coal in the overall energy mix of the FNCs is only 6%. The share of oil, biomass, hydro energy, nuclear energy and other forms of energy is even, and the share of renewable energy is large.

The electricity and heat supply systems of the FNCs are basically self-sufficient. 380.2 TWh of electricity was consumed by the FNCs in 2019. The electricity transmission among the FNCs is frequent, but the FNCs as a whole only carried out cross-border electricity import and export transmission with the power systems of six European countries, with an annual cumulative import of 17.1 TWh and export of 17.5 TWh. The ratio of total imports, total exports and net imports to electricity consumption in the FNCs is less than 10% in 92% of the 8760h of the year, and the largest instantaneous import or export ratio is only about 16%. As for heat, the heat-using units that adopt decentralized heating methods, which heat locally by burning fuel or consuming electricity, do not have heat import and export; and those who adopt centralized heating, which pursue low water supply temperature and low pipeline network transmission and distribution losses under the development trend of 4GDH systems, also do not have long distance cross-country heat transportation.

The energy supply systems of the FNCs are analyzed in terms of both total energy amount and time dimensions to match supply and demand. On the demand side, the FNCs have a total annual heat demand of 495.5 TWh and a total electricity demand of 380.2 TWh, with an overall annual DHPR of 1.30. 33.2% of the electricity demand is for residential use, 23.0% for public buildings, totally more than half (56.2%) for the building sector. Of the heat demand, urban space heating accounts for the largest share of heat use, with 55%. On the supply side, hydropower accounts for 46.1% of the total installed power capacity of 104 million kW in the FNCs, mainly concentrated in Norway and Sweden; the overall power generation hours of non-fossil energy sources are 4259 h, much higher than the overall power generation hours of fossil energy sources at 1439 h, which further increases the power generation ratio of non-fossil energy sources to 91.4% with the original installed power capacity ratio of 78.3%. For heat sources, biomass fuel accounts for 38.8% of the overall heating fuel structure, and non-fossil energy sources account for no less than 64%, with a high level of green and low-carbon heat supply rate. Applying the general Equation (7) of energy system supply and demand matching, all functional modes are classified into coupled supply of heat and power, power supply only, and heat supply only. The results show that 181.1 TWh of heat generation in the heating systems of the FNCs is coupled with the power system, accounting for 36.6% of the total heat supply, i.e., the heat supply system has a heat-power coupling rate of 36.6%. Similarly, 33.1 TWh of the electricity generated in the power supply system is coupled with the heat system, which means the heat-power coupling rate of the power supply system is 8.7%. Among them, the coupled heat mainly comes from electric direct heating and electric heat pumps, and all the coupled electricity comes from combined heat and power (CHP) of various fuel types. The heat-power coupling for each type of energy supply is shown in Figure X.

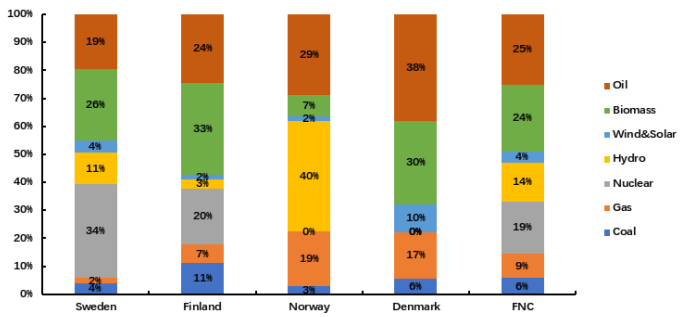

Figure 1. Primary energy supply in the FNCs in 2019

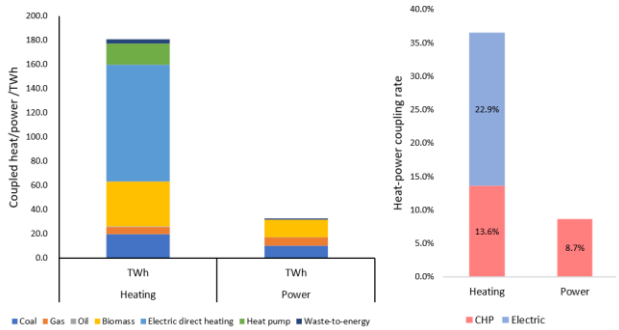

Figure 2. Overall heat-power coupling supply in the FNCs

From the time dimension, the trends of heat and power loads and SHPR are consistent on a monthly and daily scale, showing a "U" shape of high in heating season and low in non-heating season. The heating load varies along with the difference between indoor and outdoor temperatures, showing a great seasonal imbalance, which also leads to the seasonal imbalance of power load and SHPR. The daily electricity load shows a "weekend effect", where electricity consumption is significantly lower on Saturdays and Sundays than in the middle of the week. A monthly time step is sufficient to reflect the overall seasonal pattern. When considering seasonal power supply and demand matching, power sources are divided into five categories: non-adjustable renewable power, nuclear power, adjustable renewable power, fossil-fired power, and

import/export power. As shown in Figure 3, the seasonal peak regulation of power system is dominated by hydropower, assisted by fossil energy thermal power, and a small amount of import/export power to make up for the power balance problem. The seasonal peak regulation of the heating system mainly relies on biomass combustion and other heat-only energy supply methods. Cogeneration units are mainly involved in seasonal peak regulation of the power system, while taking into account the seasonal peak regulation of heating systems during the heating season. However, due to the power structure in Northern Europe, the cogeneration units are limited in the proportion of heat supply they can undertake. Considering intra-day hourly peak regulation, the power system adopts a peak regulating method with hydropower as the main source and import/export power as a supplement. The heating system has very small intra-day heating load fluctuations. The heat-only heat source and electric heating can be flexibly adjusted, and the CHP is equipped with short-period heat storage tanks to ensure heat supply by storing the excess heat generated during the peak power period until the low power load period.

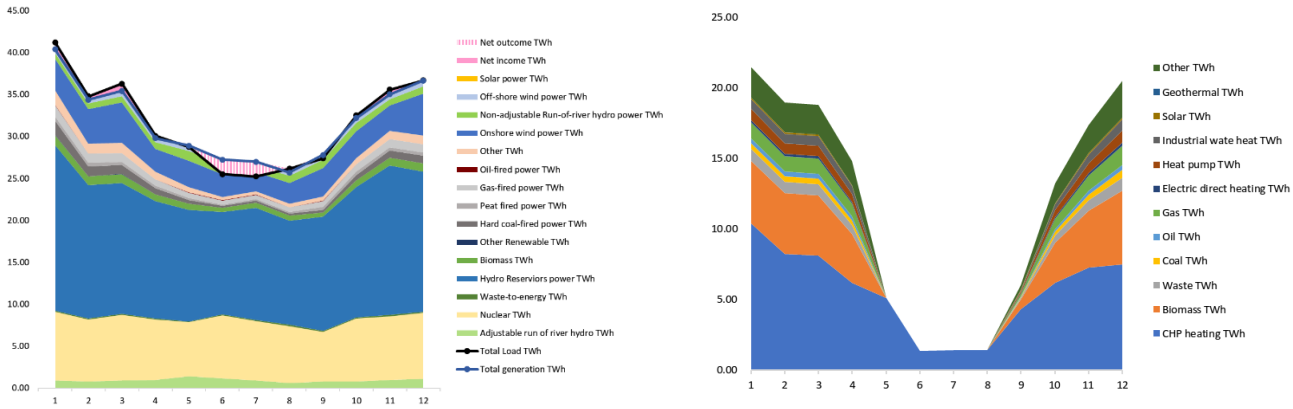

(a) Power (b) Heat

Figure 3. Regulation mode of heat and power supply system in FNCs

3.2 Comparison of Chinese and Nordic energy supply systems

In 2019, the net export of electricity in mainland China was 17.342 billion kWh, accounting for only 0.2% of the total electricity consumption; There is no thermal power input and output with other countries. Therefore, like the FNCs as a whole, mainland China is basically self-sufficient in thermal and electric energy.

The total annual consumption of electricity in mainland China is 7.2 trillion kWh, and the total annual consumption of heat is 44.34 billion GJ, that is, the overall heat-to-power ratio demand of energy supply system in mainland China is 1.70, which is close to 1.30 in the FNCs. However, the structure of heat demand in northern Europe and China is quite different. 87.3% of China's heat demand is concentrated in industrial production, which is absolutely dominant. The demand for urban space heating only accounts for 10.2%. In this study, the industrial heat will be deducted from the process industrial heat, and only the non process industrial heat will be considered, that is, papermaking, textile, biopharmaceutical, food, rubber, mechanical and electrical products and other industries with hot water and steam as the main process heat source, which can effectively participate in the heat and power energy system. In terms of geographical scope, only 15 provinces and cities in northern China are considered. Most of them adopt district heating system and have high space heating demand. After limiting the analysis scope, the heat consumption structure in northern China is similar to that in the FNCs, with urban space heating accounting for 57.7% of the total heat demand.

From the perspective of total supply and demand matching, the power consumption per capita of the f FNCs (14000 kWh/person) is 2.5 times that of northern China (5724 kWh/person). The power consumption in northern China is mainly concentrated in the secondary industry, especially the high energy consuming process industry. The main power source in northern China is fossil energy thermal power units, which account for more than 75% of power production. The proportion of non-fossil energy installed capacity (78.3%) and non-fossil energy power generation (93.4%) in the FNCs are much higher than those in northern China (36.8%, 22.4%). In terms of thermal power, for the industrial processes, northern China mainly relies on industrial steam and coal combustion from cogeneration, while the FNCs mainly use direct combustion. For space heating, district heating is generally used in northern China, and the district heating rate can reach 84.5%; While the district heating in the FNCs is relatively market-oriented and commercialized, and the district heating rate is only 41.8%. In China, coal-fired fuels account for 80.9% of the fuel structure of district heating sources, of which more than 60% are coal-fired cogeneration; In the FNCs, renewable energy is the main fuel (accounting for 49.1%), of which 96% is biomass. Considering all kinds of thermal uses, the proportion of non-fossil energy heating in the thermal supply system in northern China is only 25%, while the proportion of biomass resources and renewable electricity heating in the FNCs has reached 64%. In terms of power supply and heating systems, China's thermal power coupling rate is higher than that of the FNCs, because China's thermal power and its cogeneration play a leading role in the thermal power energy supply system.

From the time dimension, the seasonal differences of power supply structure between northern China and Northern Europe are shown in Table 3. Thermal power is the main power source in northern China. Seasonal fluctuations correspond to power demand, with double peaks in winter and summer; Hydropower is the main power generation in the FNCs, and it is mainly reservoir power generation, so it is also the main body of seasonal peak shaving, which is consistent with the change of power demand, and the output peak occurs in winter. For thermal supply, northern China and the FNCs have large seasonal differences in thermal demand. At present, northern China mainly relies on thermal power plants and various boilers for seasonal peak shaving, while the FNCs mainly use various boilers and electric heating for peak shaving, while thermal power plants focus on electric peak shaving, taking into account thermal peak shaving. China and the FNCs can adopt STES to use the heat wasted in non-heating seasons. The difference is that the FNCs focus on solar energy, while the northern China mainly uses a large amount of waste heat generated by process industry.

Table 3. Seasonal regulation difference of power system

Power supply		Northern China	Nordic countries
Thermal power	Proportion	80.30%	8.90%
	Monthly fluctuation	24.00%	69.70%
	Peak period	Summer & winter	Winter
Hydropower	Proportion	5.50%	53.10%
	Monthly fluctuation	60.60%	34.80%
	Peak period	Summer	Winter
Nuclear power	Proportion	1.50%	22.90%
	Peak period	Stable	Stable
Wind power	Proportion	8.40%	12.20%
	Monthly fluctuation	39.40%	53.00%
	Peak period	Spring & winter	Spring & winter
Solar power	Proportion	4.30%	0.30%
	Monthly fluctuation	38.80%	91.90%
	Peak period	Spring & Autumn	Summer

From the spatial dimension, northern China has a vast territory and spans a variety of terrain and climate regions. There are differences in the geographical distribution of the supply and demand matching of energy supply systems in different regions. The overall HPR in northern China is 0.65, the lowest is 0.20 and the highest is 1.87 among provinces and cities, with great differences. The overall HPR of the FNCs is 1.30, the highest is 2.14 in Denmark, and the lowest is 0.56 in Norway. On the whole, it is higher than the provinces and cities in the northern region, and the spatial difference is relatively small. According to the analysis of HPR and the characteristics of energy supply and demand, northern China can be divided into three categories: first, consumption regions, whose power consumption is dominated by tertiary industry, and the proportion of industrial power consumption is relatively small. The monthly fluctuation of the ratio of demand to heat and power in such areas is obvious, and has a high ratio of heat and power, with Beijing as a typical representative; The second is severe cold regions, which have a large demand for heat during the heating season, resulting in a generally high HPR. Heilongjiang is a typical region; The third is the industrial production-oriented regions, in which the power consumption structure is dominated by the second generation, and the industrial power consumption accounts for a large proportion. Such areas generally have a low thermal power ratio, represented by Inner Mongolia and Qinghai.

4. APPLICATION IN THE OPTIMIZATION OF ENERGY SUPPLY SYSTEMS

4.1 Optimization for Beijing, Heilongjiang, Inner Mongolia and Qinghai

For the typical provinces in the three types of regions of consumption type, severe cold type and industrial type, the energy supply and demand matching method based on thermal power ratio is applied to analyze the existing problems of the energy supply system, and optimize the design according to the local resource endowment. Because the direct combustion of fossil fuel heating is an urgent problem to be solved in the near future in the low-carbon construction of northern China, only the urban space heating part with the strongest heat-power coupling is considered in the heat demand, and the optimization design is carried out based on the existing power supply structure; The optimal design scale mainly focuses on the optimal matching of the total amount dimension and the seasonal month by month dimension in the time dimension of the provincial region. The main conclusions are shown in Table 4.

Beijing is a typical consumption region. Using the general formula of energy system supply and demand matching (7), the monthly supply and demand matching balance of the optimized energy supply system in Beijing heating season is analyzed.

Table 4. Optimization Results for Beijing, Heilongjiang, Inner Mongolia, and Qinghai

Region	Types	Overall DHPR	Overall SHPR	Current situation		Optimized heat source situation			
				The proportion of non-fossil fuels in power generation	The proportion of non-fossil fuels in district heating	Industrial waste heat	Power plant	Electric heat pump	Bio-mass
Beijing	Consumption	1.34	~1.00	0.073	0.137	52%	33%	12%	3%
Heilongjiang	Severe cold	2.01	1.50~20	0.24	0.14	20%	50%	0%	30%
Inner Mongolia	Industrial	0.32	0.10~0.50	0.17	0.22	29%	68%	2%	1%
Qinghai	Industrial	0.28	0.10~0.39	0.82	0.025	22%	19%	26%	33%

4.2 Overall optimization design in northern China

Based on the characteristics of the above regions, the fossil energy combustion heating in the energy supply system of the northern provinces and cities is optimized and replaced. The comparison of the overall urban heating system structure before and after the design is shown in Figure 4. The optimized heat source structure makes full use of industrial waste heat, reflecting Chinese characteristics, and combines with other low-carbon heat sources to make the heat source structure more diversified. Unlike the current pattern of excessive reliance on fossil energy such as coal and gas, it is not only more low-carbon, but also more energy efficient.

Table 5 shows the effect of the optimized design. The optimized design scheme can increase the proportion of non-fossil energy in the urban heating system in northern China by 48.7%, reduce fossil energy consumption by 56%, and reduce overall carbon emissions by 52%, which is of great significance to the low-carbon construction of the overall energy supply system in northern China and the realization of the dual carbon goal.

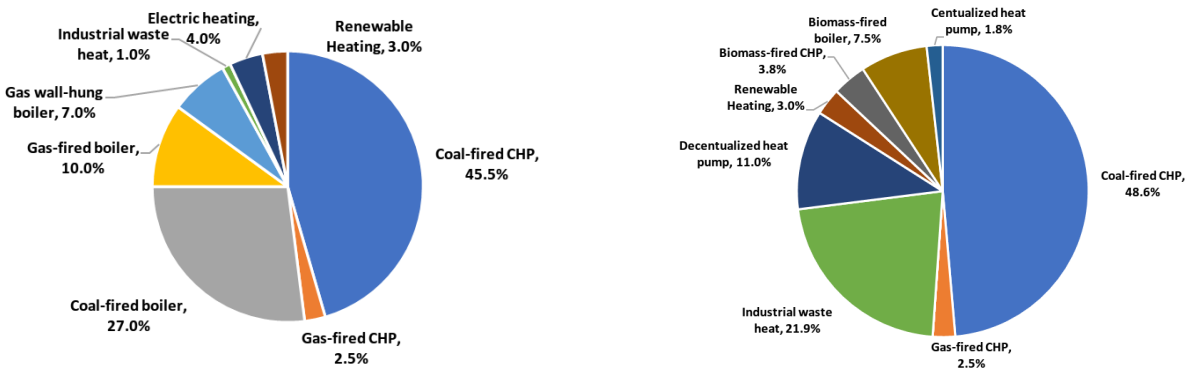

(a) Current situation (b) Optimized design

Figure 4. District heating structure in northern China

Table 5. Comparison of current situation and optimal design of district heating in northern China

	Proportion of non-fossil energy	Total fossil energy consumption	Total carbon emissions	Unit fossil energy consumption	Unit carbon emission
	%	100 million tce	100 million tCO2	kgce/GJ	kgCO2/GJ
Current situation	0.131	1.35	3.4	29.66	74.86
Optimized design	0.618	0.59	1.62	13.02	35.62

5. CONCLUSION

This paper focuses on a comparative analysis of the energy supply systems in China and Nordic Countries, with the aim of exploring the similarities and differences between China and the FNCs and providing references for the construction of low carbon energy supply systems in Northern China. Compared to the FNCs, the overall heat to power ratio in northern China is lower, but the seasonal differences and spatial imbalances are more obvious. The non-fossil energy resources in northern China are less well-endowed than those in the FNCs, and the main non-fossil energy sources in the future are wind and solar power, which are more volatile, so fossil thermal power will still take on the important task of peak regulation.

Applying the method of matching supply and demand in energy systems based on HPR, the energy supply systems of the FNCs and Northern China are quantified in terms of total energy, time dimension and spatial dimension respectively. Based on the existing electricity structure for the three typical provinces and the overall urban heating heat source in northern China, the optimal design can increase the overall non-fossil energy share to 62%, reducing fossil energy use by 56% and carbon emissions by 52%.

The construction of energy supply systems in Northern China must not directly copy the construction ideas of the FNCs. It should insist on the main role of thermal power in peak regulation and develop key technologies for the synergy of heat and power system; vigorously develop industrial waste heat supply and combine it with seasonal heat storage; and make full use of large pipe network infrastructure to develop district heating.

ACKNOWLEDGEMENT

This work was supported by the 14th Five-Year National Key R&D Plan of China (Grant No.2022YFC3802401) and Ministry of Housing and Urban-Rural Development R&D Project of China (Grant No. K20220771).

REFERENCES

[1] Hansen K, Breyer C, Lund H. Status and perspectives on 100% renewable energy systems. Energy, 2019.
[2] VGB Powertech. Flexibility toolbox compilation of measures for the flexible operation of coal-fired power plants. 2018. [2020-04-20]. https://www.vgb.org/flexibility_toolbox.html?dfid=90943.
[3] Lund H, Østergaard P A, Connolly D, et al. Energy storage and smart energy systems. International Journal of Sustainable Energy Planning and Management, 2016, 11: 3-14.
[4] Pfluger B, Wietschel M. Impact of renewable energies on conventional power generation technologies and infrastructures from a long-term least-cost perspective. EEM2012–9th international conference on the European energy market (2012).
[5] Lund H, Werner S, Wiltshire R, et al. 4th Generation District Heating (4GDH). Energy, 2014, 68(4):1-11.
[6] Tian Z, Zhang S, Deng J, et al. Large-scale solar district heating plants in Danish smart thermal grid: Developments and recent trends. Energy conversion and management, 2019, 189: 67-80
[7] Persson U, Möller B, Werner S. Heat Roadmap Europe: Identifying strategic heat synergy regions. Energy Policy, 2014, 74: 663-681.
[8] Jiang Y. The future and transformation path of China's low carbon energy system. [2022-07-27]. https://mp.weixin.qq.com/s/eJmuy7S5L35q8hXKlAOv8Q (In Chinese)
[9] Shu Y, Zhang L, Zhang Y, et al. Carbon Peak and Carbon Neutrality Path for China's Power Industry. Strategic Study of Chinese Academy of Engineering, 2021,23(06):1-14. (In Chinese)
[10] Liu S, Li H, Zhang K, et al. Techno-economic analysis of using carbon capture and storage (CCS) in decarbonizing China's coal-fired power plants. Journal of Cleaner Production, 2022, 351: 131384. (In Chinese)
[11] Pan E, Tian X, Xu T, et al. Status, Critical Problems and Prospects of Flexibility Retrofit of Thermal Power in China. Electric Power Construction,2020,41(09):58-68. (In Chinese)
[12] Wu Y. Research on Parameter Configuration and Operation Regulation of Centralized Heating Based on Heat-Power Cooperation. Tsinghua University. 2018. (In Chinese)
[13] Yuan J, Xi X. The Current Situation and Problems of the Construction of China's Electric Power Auxiliary Service Market. China Power Enterprise Management,2020(07):34-38. (In Chinese)
[14] Pan W. Seawater desalination and water heat co production and co transport technology. Tsinghua University. 2019.
[15] Guo F. Research on the Application of Industrial Waste Heat Solar Energy Cross season Heat Storage in Urban Centralized heating system. Tsinghua University. 2019. (In Chinese)
[16] Liu L. Optimized operation of regional comprehensive energy system with adjustable heat to power ratio. North China Electric Power University, 2020. (In Chinese)
[17] Men J. Research on optimal scheduling of thermal and electrolytic coupling in integrated energy system. Liaoning Technical University, 2022. (In Chinese)
[18] Liso V, Zhao Y, Brandon N, et al. Analysis of the impact of heat-to-power ratio for a SOFC-based mCHP system for residential application under different climate regions in Europe. International Journal of Hydrogen Energy, 2011, 36(21):13715-137262010.
[19] Lamas J, Shimizu H, Matsumura E, et al. Fuel consumption analysis of a residential cogeneration system using a solid oxide fuel cell with regulation of heat to power ratio. International Journal of Hydrogen Energy, 2013, 38(36):16338-16343.
[20] Lan L. Analysis of Characteristics and Economic for New Energy Power Generation [D]. North China Electric Power University,2014.

IEA DHC Annex TS4 Digitalisation of district heating

The 18th International Symposium on District Heating and Cooling, September 3–6, 2023, Beijing, China

DIGITALISATION IN DISTRICT HEATING – WITH DATA TO OPTIMISED SYSTEMS AND NEW BUSINESS OPPORTUNITIES

D. Schmidt[a*], M. Tunzi[b], E. Widl[c], M. Blesl[d], D. Vanhoudt[e]

[a] *Fraunhofer Institute for Energy Economics and Energy System Technology IEE, 34119 Kassel, Germany*
[b] *Technical University of Denmark (DTU), 2800 Kgs. Lyngby, Denmark*
[c] *Austrian Institute of Technology GmbH (AIT), 1210 Vienna, Austria*
[d] *Technical University of Stuttgart, 70565 Stuttgart, Germany*
[e] *VITO - Flemish Institute for Technological Research NV / EnergyVille, 3600 Genk, Belgium*
[*] *Corresponding author: dietrich.schmidt@iee.fraunhofer.de*

ABSTRACT

District heating and cooling (DHC) networks are often run with a small number of sensors and actuators to provide the necessary supply and to maximize economics based on a predetermined high ecologic performance. With better knowledge of the demand and flexibility options, it is feasible to optimize heat generation and network functioning overall. Improved network management based on real-time measurement data and the incorporation of new digital business processes are made possible by a greater deployment of information and communication technology. Clarifying the role of digitalization for various components within district heating and cooling systems is necessary for ongoing growth, as is promoting opportunities for the integration of digital processes into DHC systems. Digital technologies are expected to improve the efficiency and system integration of additional renewable sources while also making the entire energy system smarter, more reliable, and efficient. Future district energy systems could be able to completely optimize their plant and network functioning while empowering the end user thanks to digital applications. However, there are still more difficulties to be overcome, including issues with data privacy and security as well as issues with data ownership. The research findings from the IEA DHC Annex TS4 on "Digitalization of District Heating Systems – Optimized Operation and Maintenance of District Heating and Cooling Systems via Digital Process Management" are presented and discussed in this publication.

https://www.iea-dhc.org/the-research/annexes/2018-2024-annex-ts4

Keywords: Digitalization of district heating; operation and maintenance; business processes and models

1. INTRODUCTION

It is thought that the widespread adoption of digital technology would make our energy systems smarter, more efficient, and more reliable. The utilization of cutting-edge digital technology and procedures also creates new commercial opportunities and is predicted to result in a considerably higher integration of renewable energy sources into the systems [1]. The DHC Annex TS4 initiative is aimed to promote the possibilities of integrating digital processes into DHC schemes in this context. This necessitates a clarification of the function of digitalization for various aspects of the district heating and cooling system's operation and maintenance. Additionally, these technologies' application are shown in close collaboration with a number of industrial partners. Additionally, issues including data privacy and security, as well as queries regarding data ownership, are addressed [2]. The overall structure of the internationally cooperative work of Annex TS4 within the Technology cooperation program on District Heating and Cooling (DHC) of the International Energy Agency (IEA) is given in this article. The initiative offers a forum for the sharing of research findings from both national and international activities. In this approach, information on the digitalization of district heating and cooling systems is gathered, compiled, and presented.

2. CURRENT SITUATION IN DISTRICT HEATING

In order to ensure the necessary supply task and to maximize economic and ecological performance, district heating and cooling (DHC) networks are often run with a small number of controls (like the regulation of the supply temperatures or the network pressure). In the traditional network operation, there is no detailed information about the supply and utilization structures (such as heat plant characteristics, power demand, or time profiles) [2].

With increased knowledge of the demand and flexibility options (storages), peak shaving and the reduction of pricey peak boiler usage are achievable, as well as an efficient heat generation and overall network functioning. In these systems, projects that have previously been completed demonstrate a broader integration of varying heat sources, such as solar

thermal energy and power-to-heat applications functioning on the electricity markets. As in many other sectors, greater use of information and communication technology opens doors for improved network management based on real-time measurement data and the incorporation of new business models. In this context, an increasing number of businesses are providing products and services, such as smart meters or digital analysis platforms.

3. THE RISING ROLE OF DIGITALIZATION IN DISTRICT HEATING

Modern DHC system design and management are becoming increasingly sophisticated. This is brought on by various interrelated factors [2]:

- An growing proportion of dispersed, renewable, or waste heat sources are replacing the old strategy of depending on a single, programmed, large heat or CHP plant.
- The adoption of smart heat meters makes it possible to automatically gather large consumption data sets with fine precision, opening the way for the evolution of the customer's role in the end-to-end system but also forcing us to think about GDPR-related issues.
- The DHC systems are becoming important balancing actors in the multi-energy system's journey to decarbonization as a result of the integration of many energy sectors, but at the expense of having to respond to more unpredictable energy (and capacity) costs.

District heating suppliers are facing both possibilities and threats as a result of the current changes and advancements in the operating environment. The changing business climate is anticipated to be the primary impact of the integration of digital technology and procedures for district heating providers. New services and products will join the market, and existing business models will shift as a result of these new technology. On the other hand, the demand for alternative heating options from customers and the greater energy efficiency of the building stock have an impact on the current business models. Here, digitization will introduce new ways to interact with various client groups and address evolving customer wants [3].

The particular significance of digitalization in district heating systems arises from the fact that it is a need for cutting-edge low temperature, or "4th generation," heat networks [4,5] that incorporate variable and renewable heat sources. Therefore, digitalization has the potential to make heat networks more efficient, dependable, better suited for the integration of lower temperatures, such as through the optimal use of heat pumps or CHP units, and more profitable, such as through the reduction of expensive fossil fuel consumption or through the reduction of transmission losses.

Digitalization in district heating systems are demanding a

- Large number of sensors present in the network,
- An automated recording, transfer and storage of data
- Automated analyses of data
- The use of analyses beyond automated billing to optimize the network operation.

4. THE INTERNATIONAL COOPERATION INITIATIVE IEA DHC ANNEX TS4

The project DHC Annex TS4 aims to raise awareness of the potential for incorporating digital technology into district heating and cooling systems. The project's primary areas of attention include new business model potential based on digital technology and the legal environment for using things like data, for example. Additionally, a description of how digitalization affects many aspects of system operation and maintenance is provided. A tight partnership between industry and research teams demonstrates how these technologies and procedures are implemented.

The initiative aims to provide insights and information on how the district heating sector and system suppliers are impacted by digitization. It emphasizes the state of the art, points out obstacles, and offers goals, targets, and suggestions for each of the district heating systems' targeted levels:

- Level of sector coupling or integration of numerous sources of production
- Building and consumption levels
- distribution level
- Legal level
- Economic and business level

The project considers the full energy chain, from production/generation through distribution to end usage and particularly consumer (secondary side systems).

The main objectives of DHC Annex TS4 are to:

- Raise awareness among the various stakeholders and users of the benefits of implementing digital processes; and
- Provide a current overview of the digitalization of district heating schemes in terms of R&D projects, demonstrators, and case studies.
- Consider non-technical factors such as business models, legal considerations, and policy instruments when evaluating barriers and enablers to digitalization processes in district heating and cooling schemes.

5. WORKING STRUCTURE OF ANNEX TS4

Three interconnected primary emphasis areas have been established in order to achieve the activity's aforementioned objectives. The work on district heating's digitization measures should center on the firsthand implementation of the optimization of the real-time operation of heating grids in order to focus on the primary interest area of the district heating branch. Second, on improving the use of digital planning tools, and third, on putting digital business procedures into place in the businesses that offer district heating services.

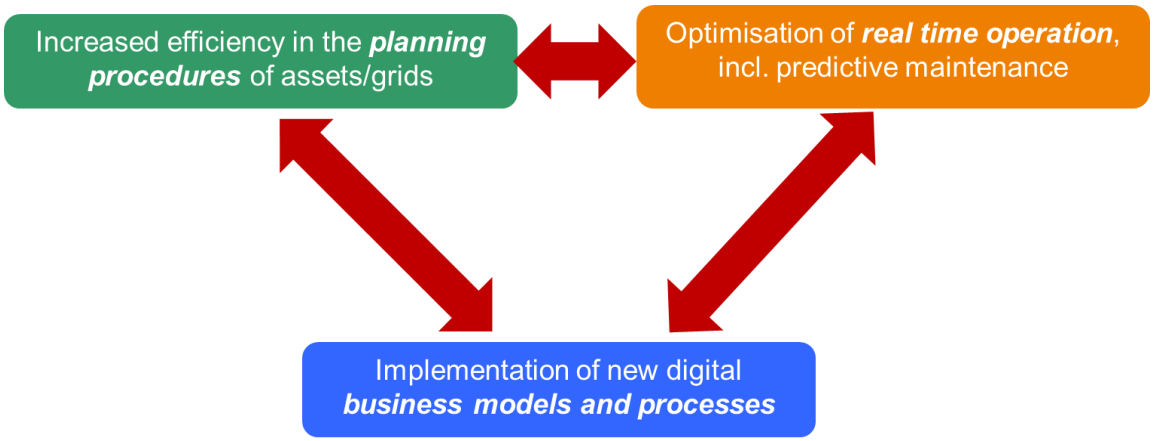

Figure 1. Principal areas of work for IEA-DHC Annex TS4

All research efforts that are the focus of this activity are organized into so-called subtasks in order to achieve the goals outlined above.

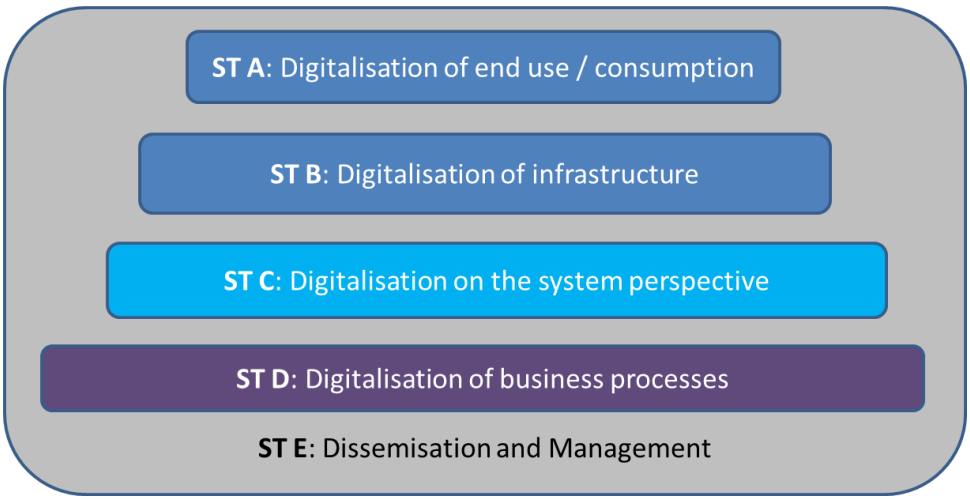

Figure 2. Working structure of the IEA-DHC Annex TS4

Within the group of participants from industrial partners and from research organizations, main interest areas for the digitization of district heating systems were identified, and this working structure is built on those areas. The following provides a more thorough description of various working groups.

5.1. Digitalization of end use / consumption

This working item's goal is to create and demonstrate techniques for improving the operation of heating systems in buildings in order to lower supply and return temperatures as well as the peak load. These approaches are based on data from energy meters.

Heat cost allocators on radiators, space heating sub-energy meters, household hot water systems, and the main energy meter on the district heating supply to individual buildings are all migrating to digital and wireless technology. Therefore, in addition to the yearly data used for the heating bills, they may also give hourly data on the actual functioning of the heating systems in buildings.

This new circumstance serves as the foundation for the creation of approaches that will lower the operating temperatures of heating systems and boost the overall efficiency of the heating supply.

The following are sample illustrations of work that has to be done on specific buildings:

- Usage the heating power of the radiators and the relationship between measured total energy usage for space heating and external temperature on a daily basis to determine the ideal supply temperature curve for the weather compensation control unit. This shows a potential lower supply temperature.
- Identify individual radiators with inadequate heating capacity caused by thermostatic radiator valve malfunctions or air entrapment in the radiator. In order to use the ideal low supply temperature and provide comfort temperatures in all rooms, this can make it simple to maintain the heating system.
- To combine the heating of cold water with the provision of circulation heat loss, choose the best heating power for heating home hot water tanks. In DHW-systems with tanks and circulation systems, this can lower the return temperature as well as the peak load power.

By completing these action items, methods are presented for achieving improved overall network efficiency through lower system temperatures, which may be attained by putting digital measurements into place.

5.2. Digitalization of infrastructure

This working item considers the infrastructure viewpoint for district heating systems' digitization procedures. In order to increase system performance and assist the planning procedures for system extensions, etc., the modeling of the complete supply and network system is particularly important. Application of digital twins for DHC networks is crucial in this situation. It is also necessary to handle benefits and use cases from a system viewpoint, at the component level, and as controller-in-the-loop/hardware-in-the-loop. Focus is placed on reviewing current implementations of digital twins in district heating networks in terms of tangible benefits, real-world experiences, and lessons learned, as well as the techniques and data employed. Additionally, the methods for creating digital twins are categorized according to the system boundaries that have been selected, the level of detail or time interval, and the model features as physical / data driven model or static / dynamic. Focusing on methodologies and needs is the main challenge in this work using digital twins for simulation-related objectives. Questions such as:

- How to create a digital twin?
- What data sources are accessible or necessary?
- Which interfaces ought to be employed?

shall be responded to.

5.3. Digitalization on the System Perspective

Here, the emphasis is on the digitalization of district heating from a systems perspective, i.e., how digitalization can be used to improve the sustainability and efficiency of district heating networks as a whole, as well as how district heating networks can benefit the overall energy system. Operational optimization and analytics are the main areas of attention in this work item:

- Operational optimization is here defined as active interaction with the network, i.e. real interventions in the operation of the network. Think of modifying the control of temperatures or flow rates in the network in order to achieve a certain objective on the network or energy system scale (e.g. peak shaving or increasing the share of renewable energy in the energy system). These interventions could happen on the supply side as e.g. control of storage (small, large, seasonal), sector coupling through CHPs, HPs or production portfolio management. Active interaction with the network, or genuine interventions in network functioning, is referred to here as operational optimization. Consider changing the network's control of temperatures or flow rates to accomplish a specific goal

at the network or energy system scale (such as peak shaving or raising the proportion of renewable energy in the system). These interventions might take the form of production portfolio management, sector coupling via CHPs or HPs, or regulation of storage (small, big, or seasonal).

- The analytics tasks do not seek to actively interfere with the network's normal operation. However, these tasks involve analyzing network performance in order to increase the network's effectiveness and sustainability. The assessments from the supply side are concentrating on the super guarding of the heat supply infrastructure or on the predictive maintenance of the heat supply infrastructure. Leak identification, load distribution analysis for future extensions, undesired bypass detection, heat loss distribution, material and component degradation, or water quality analysis are the main areas of interest from the distribution side. On the demand side, the analytics are focused on end-user empowerment through energy-saving suggestions, substation fault detection, undesired bypass detection, leak detection, heat supply contract conformance, user behavior and efficiency analysis, and substation fault detection.

5.4. Digitalization of business processes

It is well acknowledged that digitalization is a vital technology for developing low temperature district heating networks with a large proportion of renewable energy sources. Examining the commercial worth of digitalized district heating systems and calculating their economic potential and return on investment are the goals here. Digitalization can handle the escalating complexity brought by, for example, by sector coupling, by having an influence on the whole district heating and cooling value chain from manufacturing and distribution to buildings and end-users. Digitalization can also help the new economic models that district heating will need to become more appealing than individual heat sources. Issues with data security and other legal obligations will be taken into consideration.

The research provided answers to the following important questions:

- How can deploying digital twins, allowing the system operate closer to its technological boundaries, or strengthening troubleshooting processes help digitalization enhance daily operations?
- How may digitalization help with asset management, design, and planning, as well as investment targeting?
- How might digitization enable innovative, user-friendly business models?
- What skills are required to achieve this business value?
- What legal considerations apply to the rights to utilize end-user consumption data as a driving force behind the digitization process?

Examining the cost factors for running and maintaining a district heating and cooling network and assessing the economic possibilities for improvements based on the tools and insights made available by digitization are the key concerns in this work item. Examples of best practices are used to support and validate the expected return on investment. Additionally, suggestions for novel possible business models that digitization may permit are gathered. The energy supplier may do this by providing services to the consumer, ranging from monitoring the district heating substations in the associated buildings to finally selling 21 degrees in the living room rather than kWh of energy. Demand response and heat storage capabilities in buildings may also be factors in business strategies.

5.5. Knowledge Transfer, Dissemination, Management

This work item has been focused on gathering and disseminating data on ongoing and completed activities within this activity. This has involved things like creating an information portal and planning a ton of lectures and workshops.

- The initiation of demonstration projects and the creation of novel activity forms between academia and industry.
- Examples of recommended practices documented.
- Informational materials, a website, and several workshops/seminars.
- Creation of a practitioner's guidebook as the final report

The collaborative action in this work item requires input from the outcomes of the previous work items. The outcomes of the assignment and the information gathered have been distributed through various methods. Information is disseminated through a web-based platform, numerous public seminars, and widely read scientific publications. In order to facilitate public access to and use of the results, the findings of Annex TS4 activities have been summarized.

The major product of this IEA DHC Annex project will be presented at a final conference in November 2023 and will be a guidebook that compiles the results of the work completed within this activity. Nine nations contributed constantly to the initiative via industry and research partners.

6. CONCLUSION

With readily available and quickly evolving digital solutions that can utilize data from the field and from multiple sources (market pricing, weather predictions, etc.) to accomplish effective design and efficient operations, digitalization is the key to managing the ensuing complexity successfully. Therefore, an important strategy to enable the decarbonization of the energy system is district heating and cooling. However, DHC systems have to be changed in order to realize its potential since it has grown increasingly complicated as a result of a variety of production methods, remote sources, and sector coupling. When the value chain is considered as a whole, high performance is attained. Particularly, the economic potential of buildings and consumers has not yet been completely realized [1]. The challenges of data security and privacy, as well as concerns about data ownership, must be addressed, and solutions must be developed, in order for digital processes to be more widely integrated. So that the necessary rapid transformation has real-world business models, products, and services that are ready for the market. The strong communication between the scientific community and system producers, utilities, and service providers is the project's greatest asset [7].

ACKNOWLEDGEMENT

The outline of the IEA DHC Annex TS4 work that is being provided here was developed collaboratively by all participants from a variety of nations. The authors and all participants would like to express their gratitude to the several national funding organizations and business partners that supported this study.

REFERENCES

[1] Pozzi, M. et al., “Digitalisation in District Heating and Cooling Systems – a Tangible Perspective to Upgrade Performance”, DHC+ Platform c/o Euroheat & Power, Brussels, 2023.

[2] Schmidt, D., “Digitalization of District Heating and Cooling Systems”, Proceedings of the 17th International Symposium on District Heating and Cooling, 06-09 September 2021, Nottingham, United Kingdom, 2021.

[3] Männistö, J. and Grönberg, A., “The Impact of Digitalisation in District Heating”, Deloitte and Touche Oy, Group of Companies, 2016.

[4] Schmidt, D. and Kallert, A. (Ed.), “Low Temperature District Heating Design Guidebook”. Final report of IEA DHC Annex TS1 Low Temperature District Heating for Future Energy Systems, AGFW-Project Company, Frankfurt/M., 2017.

[5] Lund, H., Wiltshire, R., Svendsen, S., Thorsen, J.E., Hvelplund, F., Mathiesen, B., “4th Generation district heating (4GDH) integrating smart thermal grids into future sustainable energy systems, Energy, 68 (2014), pages 1-11.

[6] AGFW, “Bringing Focus into Digitalisation in District Heating” (in German), AGFW AGFW-Project Company, Frankfurt/M., 2019.

[7] Schmidt, D., “Digitalisation of District Heating”, In: EUROHEAT&POWER international, Brussels, Belgium, Vol. 2020, no. 2, (2020), pages 28-30.

The 18th International Symposium on District Heating and Cooling, September 3-6, 2023, Beijing, China

DIGITAL TRANSFORMATION IN DISTRICT HEATING SYSTEMS: A SCOPING REVIEW

Zheng Grace Ma[a*], Bo Nørregaard Jørgensen[a]

[a] *SDU Center for Energy Informatics, The Maersk Mc-Kinney Moller Institute, The Faculty of Engineering, University of Southern Denmark, Odense, 5230, Denmark*
[*] *zma@mmmi.sdu.dk*

Abstract

The application of digital technologies provides the potential to optimize district heating system operations. However, there are also several challenges to realizing the full potential of digitalization in district heating systems. Therefore, this paper conducts a scoping review of thirty articles with thematic analysis and qualitative synthesis. The analysis result reveals that six district heating segments have been discussed in the literature: district heating network, buildings, district heating substations, combined heat and power, renewable energy sources, and district heating underground pipes. District heating networks and buildings are the two main focuses. However, the integration of thermal storage into the district heating system and sector coupling between electricity grids and district heating networks are rarely discussed. Furthermore, Artificial Intelligence techniques, especially Machine Learning, are popularly applied in the literature for heat load/demand forecasting, operation schedule prediction, dataset creation, prediction model improvement, fault detection, evaluation and optimization, and digital twin development. Heat load/demand forecasting is the main focus and different ML methods have been applied, e.g., Regression algorithms, Decision Tree Algorithms, Artificial Neural Networks, and Support vector machines.

Keywords: District heating; digitalization; Artificial intelligence

The 18th International Symposium on District Heating and Cooling,
September 3–6, 2023, Beijing, China

Exploiting Synergies of Data-Driven and Model-Based Approaches for Leakage Localization in District Heating Networks

Dennis Pierl[a*], Kai Vahldiek[b], Julia Koltermann[c], Bernd Rüger[d], Kai Michels[a], Frank Klawonn[b], Andreas Nürnberger[c]

[a] *Institute of Automation Technology, University of Bremen, Otto-Hahn-Allee 1, 28359 Bremen, Germany*
[b] *Institute for Information Engineering, Ostfalia University of Applied Sciences, Salzdahlumer Str. 46/48, 38302 Wolfenbüttel, Germany*
[c] *Institute for Technical and Business Information Systems, Otto von Guericke University, Universitätsplatz 2, 39106 Magdeburg, Germany*
[d] *SWM Services GmbH, Emmy-Noether-Str. 2, 80992 München, Germany*
[*] *Corresponding author. dpierl@iat.uni-bremen.de*

ABSTRACT

Leakages in District Heating Networks (DHN) can significantly disrupt network operation and supply reliability depending on their extent. In case of large medium losses, a complete shutdown may be inevitable to protect the infrastructure from secondary damage (e.g., to pumps). In this case, customers are cut off from the heat supply resulting in both economic and energy losses. To prevent this, the damaged network parts can be separated by use of remote-controlled valves and thus the operation of the remaining network can be maintained. However, this requires a fast detection and an accurate localization of the leakage. For this purpose, three different leakage localization approaches have been developed, which are based on existing measurement data (such as pressure and flow rate) that are relevant for network operation. A first data-driven approach evaluates the pressure wave that occurs in case of leakages and propagates through the network at speed of sound. In the second, also purely data-driven approach, leakages are to be localized using machine learning methods. The last approach is based on a numerical-analytical network model to estimate the network state (i.e. all pressures and mass flows) and subsequently localize the leakage. The three approaches can also exchange data and interim results with each other. In context of this paper, measurement data from real leakage events of a DHN are analyzed to evaluate the three approaches' individual performance. Since these approaches have different advantages and disadvantages, exploitation of synergies is a promising strategy. Therefore, the individual results are shared among the different approaches to narrow down the possible leakage locations and reduce the search space. With this additional information, the leakage localization is performed again to quantify the improvement on the overall leakage localization performance.

Keywords: Leakage Localization, Pressure Wave Evaluation, Machine Learning, Numerical-Analytical Network Model

1. INTRODUCTION

The detection and localization of leakages in District Heating Networks (DHN) is a crucial yet challenging task for the network operator in order to maintain network operation. Both economic and environmental aspects are of importance in this context. The refilling of the transport medium lost due to the leakage and the interruption of the heat supply to the consumers lead to significantly increased costs in energy provision and a reduction in energy efficiency. Furthermore, the emerging, hot, and pressurized transport medium can harm people and environment. Therefore, a fast and reliable detection and localization of the damaged network part is mandatory in order to take immediate countermeasures and mitigate the impacts of the leakage. For this reason, the development of methods for leakage detection and localization is often part of research and there already exist a wide range of data and/or model-based approaches and proposed solutions.

A large part of literature deals with the development of methods for leakage localization in Water Distribution Networks (WDN) or other transport pipelines like gas or oil pipelines, a considerably smaller part deals explicitly with leakages in the domain of district heating. In district heating, one of the first relevant papers is a review paper by Zhou et al. [1], that presents different technologies for leakage detection, including model-based, data-driven, and infrared thermography methods. Differences to WDN and other pipe networks are also discussed. Xue et al. [2] use a hydraulic model in combination with machine learning methods to localize leakages within a rather small network. The usage of a network model to detect and localize leakages is as well proposed by Bahlawan et al. [3], where both single and multiple leakages are successfully identified by means of a Digital Twin of the DHN of University of Parma. The localization of leakages by evaluating the pressure wave caused by the leakage has as well been part of research work. Valinčius et al. published several papers on that

topic. In their most recent work [4], numerical methods and tools were used to model various pipe burst scenarios. This was done to study the limitations of such pressure wave-based leakage localization approaches. The method was as well applied to a real DHN to verify their results. Increasingly, machine learning is also being used to diagnose leakages. In Zhou et al. [5], neural networks were trained and used to localize leakages in two different laboratory DHNs with high success rates. A very recent review paper by van Dreven et al. [6] gives a good overview of intelligent approaches and especially highlights the importance of machine learning techniques and increasing number of studies that use artificial neural networks (ANN).

As there are similarities between different kinds of piped networks, some methods may be adapted across fields. Especially for WDNs, there exists a large variety of techniques for leakage localization. Many model- and data-based leakage localization methods are based on pressure residuals, comparing measured pressure values of the leakage-free and leaky scenarios like in Ferrandez-Gamot et al. [7], Soldevila et al. [8] or Ferreira et al. [9]. In the latter, other frequently used model-based approaches are presented briefly and compared to each other. These are nodal pressure sensitivities, inverse analysis and a technique based on classifiers. The pressure residual approach is adapted by Sophocleous et al. [10], which consists of two stages. The first step is to reduce the search space by excluding non-pipe nodes of the network model from the localization procedure. Subsequently, the leakage localization is carried out by solving an optimization problem to find the best fitting leakage locations of all possible leakage scenarios. Guan et al. [11] propose a pressure-driven background leakage model to improve the accuracy of traditional hydraulic model-based approaches. Both the model parameterization and the leakage localization are performed applying direct optimization techniques, in this particular case genetic algorithms. For leakage localization in other pipe networks, machine learning has as well become an increasingly common part of research in the recent years. Zadkarami et al. [12] were one of the first to use multi-layer perceptrons (MLP) for hydrocarbon pipelines, but rather for leakage diagnosis than for localization. For WDNs, Quiñones-Grueiro et al. [13] compared different classifiers for localization and concluded that there is no significant difference in performances under various uncertainty scenarios. In this context, van der Walt et al. [14] conclude that the performance of support vector machines and ANNs depends also on available measurement data. Mashhadi et al. [15] found that ANNs, logistic regression and random forest classifiers perform well for leakage localization, but also mention that both flow and pressure data is necessary. In summary, the performance of classifiers in most studies is hardly evaluated under real conditions and depends highly on the setup and available training data.

The leakage localization approaches and the obtained results presented here have been developed within the scope of a joint research project and were already discussed and examined in several previous publications. In Rüger et al. [16], the application of a prototype for both leakage detection and localization based on the evaluation of the leakage-induced negative pressure wave is presented. Historical measurement data of a refilling process were used to examine the prototype's practicability and performance. In a following publication by Vahldiek et al. [17], a new pressure wave-based approach for leakage localization is proposed and a quality assessment of several real events is performed. In Vahldiek et al. [18], new algorithms for the detection of the pressure drop time points (PDTP) in not equidistantly sampled pressure measurement data have been developed and presented. These new approaches have been compared to already existing algorithms. Using the pressure wave-based approach, a possible method for optimal sensor positioning was suggested by Vahldiek et al. [19],[20]. In this method, the sensor combination for the DHN is determined either iteratively or in a single step, for which leakages can be localized with the highest, local resolution. It was shown that both strategies lead to the same result. In addition to this method based on time series of pressure measurement data, two other approaches have been developed which use steady-state measurement data of all available pressure, flow, and temperature sensors of the DHN. This is a model-based as well as a purely data-driven, machine learning approach. In Pierl et al. [21], the impact of random measurement errors on the performance and reliability of these three approaches was examined on the basis of a simulation study. In another publication by Vahldiek et al. [22], the results obtained by applying these three methods to two real events in a DHN of the project partner Stadtwerke München were presented. It was demonstrated that each of the approaches is generally capable to correctly localize leakages under real conditions.

In the majority of contributions to leakage localization, individual model-based or purely data-driven methods are developed and applied in isolation. In some cases, different approaches are indeed already combined, such as the use of a hydraulic network model to generate a data base for the application of clustering or pattern recognition techniques. But the resulting method is still principally based on the same type or set of data. Due to the fact that different approaches may not be applicable for all practical use cases or may not provide any results at all, a combination of a variety of methods could be a way to address these challenges. The aim of the joint research project was the development of a combined detection and localization approach that maximizes detection rate, localization accuracy, and reliability in general. To this end, synergy effects between the three individual approaches are identified and exploited. The purpose of this paper is to quantify the improvements resulting from combining these approaches.

2. METHODOLOGY

The three individual approaches developed for leakages localization in DHNs are in part applied in different phases of a leakage (initial reaction, new steady state) and therefore they do not rely on the same measurement data. Due to the methodologies, each of the individual approaches shows particular advantages and disadvantages, making it optimal for certain situations while infeasible for others. These three individual approaches are pressure wave detection (PWD), model-based state estimation (MBSE) and machine learning (ML), which are briefly described below. Subsequently, potential synergy effects between them and the resulting combined approach are outlined.

2.1. Individual Localization Approaches

If there is a large spontaneous leakage, a pressure wave will propagate through the entire DHN at the speed of sound. Each sensor is reached by that pressure wave at a different point in time. The PWD approach evaluates the resulting effects by determining the PDTPs at all pressure sensors distributed throughout the network. Subsequently, these PDTPs are used to localize the leakage. It is necessary that a fully developed pressure wave is present to apply this method. The approach consists of two steps: The first one is the determination of the PDTPs for each sensor. The second one is the attribution to the possibly affected exclusion area (EA) by evaluation of the PDTPs.

The basis of the MBSE approach is a hydraulic model of the underlying DHN, which, in addition to the pipe equations, considers all relevant active and passive elements of the network, such as measurement devices, pumps or valves. The network model is used within the scope of a constrained optimization problem to estimate the network state (i.e. all pressures and pipe flows) that best fits the available measurement data and valve states. The constraints of the optimization problem vary depending on the current status of the network: normal operation or leakage case. During normal operation, the MBSE approach attempts to approximate the current consumption quantities. In case of a leakage, the most recently estimated consumptions are instead kept constant and the leakage amount is distributed throughout the DHN model. The result of the computations is a ranking list of all EAs, which are sorted in descending order according to their leakage probability (LP). This represents the ratio of the leakage amount attributed to an EA by the algorithm in relation to the total leakage amount and ranges from 0 to 100 %. The LP, in combination with EA ranking, indicates the reliability of this approach.

The ML approach builds on a large number of simulated leakages generated with the hydraulic network model used by the MBSE approach to create a classification model that predicts the EA affected by a leakage. The same set of available sensor data can be used to predict the EA during a real event. In the past, methods like Decision Tree Ensembles, Support Vector Machines or Naïve Bayes were used [21],[22], but further investigations have shown that especially simple neural networks deliver good results for the localization of real events where the training takes considerably less time compared to the previous favorite, the support vector machine. Thus, a MLP with one hidden layer of 30 neurons that compresses the sensor data is implemented for this paper, where a multiclass model is used for predictions without synergies and combined binary models are applied when there is a preselection of EAs. The output of these models will be a probability for each EA that it is affected by the leakage, which is combined into a ranking of all EAs or preselected EAs, respectively. Due to the random nature of the MLP and the issue that the network and operational states of the training data does not fit those of the real events, high fluctuations in predictions for real data are expected and will be quantified in the results. Since this paper addresses the impact of using synergy effects, these problems can be neglected for now.

2.2. Combined Synergistic Approach

Because of the individual requirements regarding quality and quantity of the measurement data used in the three approaches, different optimal use cases arise for each. However, the objective is to develop a universally applicable method for leakage localization that works reliably independent of the nature of the leakage occurrence. To achieve this goal, the three approaches are combined and can exchange data and intermediate results with each other. This is intended to compensate individual weaknesses and to emphasize the approaches' strengths. Figure 1 shows exemplarily the refill mass flow $\dot{m}_L$ in case of a leakage and illustrates both the time range of application as well as the data exchanged between the individual approaches, including data flow directions.

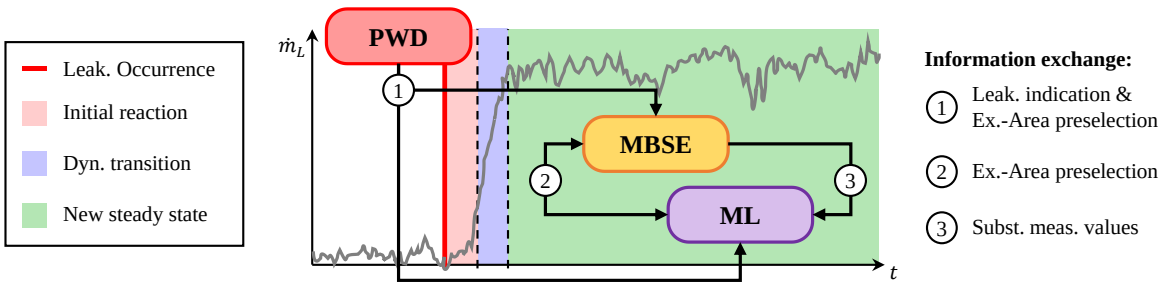

Figure 1. Information exchange and chronological schedule in the application of the individual approaches in case of a leakage

Due to the uniqueness and the temporal limitation of pressure waves, PWD might only be applied immediately after leakage occurrence during the initial reaction phase. Consequently, for PWD only one data set per leakage event is available for evaluation and localization. Both MBSE and ML, on the other hand, are applied to the new steady state after all oscillation resulting from the leakage have settled. At this point, the first results by PWD are already available and can be provided to these two approaches. This is a preselection of potentially affected EAs. With this additional information, the MBSE can a priori narrow down the solution space when computing the hydraulic network state. ML can only be applied directly if valid measurement data is available for all sensors that were also used during its trainings process. If this is not the case, the missing data is substituted by simulated values generated by MBSE previously. Furthermore, since the new steady state persists as long as the leakage is present, MBSE and ML may be applied repeatedly while exchanging localization results. In the context of this paper, the two information exchange strategies (IES) ① and ③ as shown in Figure 1 are used.

3. RESULTS

3.1. Case Study

In order to be able to evaluate the performance of the three individual approaches and the resulting improvement achieved by their combination and use of the described synergies, measurement data from a total of 18 different events in a real DHN are investigated. Most of these events are refill processes, which have similar effects on the DHN as leakages. The topology of the DHN with an accumulated pipe length of approx. 190 km, which is subdivided into 28 EAs, is shown in Figure 1. Each EA may be separated from the rest of the DHN by a set of associated valves. A total of 104 pressure, 11 flow and 42 temperature sensors are distributed along the DHN, whose continuously record measurement values form the data base for leakage localization. The events differ both in damage location, leakage amount $\dot{m}_L$, and rate (gradient) $\Delta\dot{m}_L/\Delta t$ of the leakage [15]. The locations of all events are indicated in the network topology in Figure 1. The information on leakage amount and rate of each event can be found in Table 1. In order to perform the leakage localization with MBSE, an estimation of the non-measured consumption quantities must be performed during normal operation prior to the event. In practice, this is done cyclically at certain time intervals. Here, the consumption estimation is carried out three times in time intervals of five minutes until immediately before the occurrence of the event. The leakage localization then takes place at least one minute after the event has been detected. This is necessary because all event-related transient processes in the hydraulic states must have subsided.

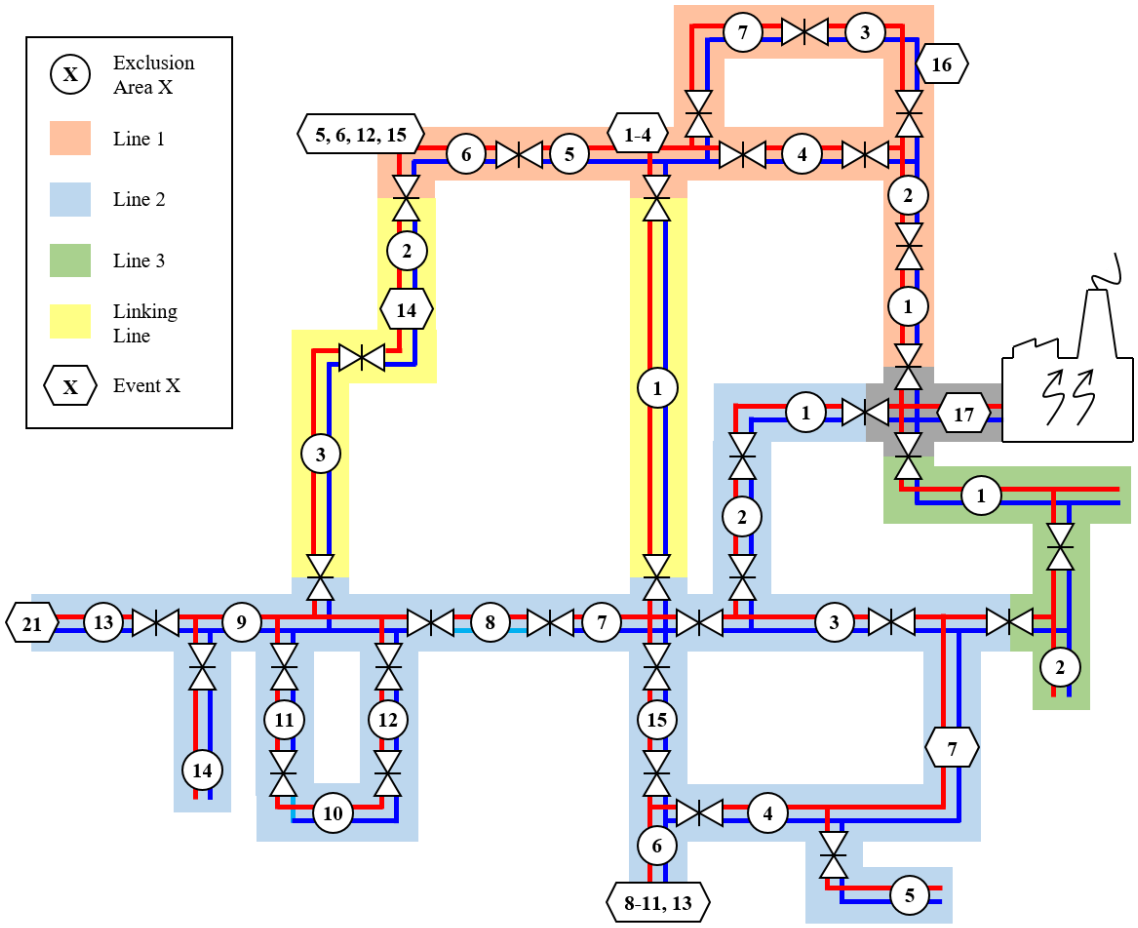

Figure 2. Overview of the topology of the DHN under investigation including indications for the locations of all leakage events

The case study presented here consists of two parts. In the first step, the available measurement data of all events are evaluated by the three individual approaches independently, if possible. Each approach hereby generates an EA ranking list from which a performance criterion (PC) can be derived. This PC depends on the ranking of the actually affected EA in the ranking list and is defined as follows:

$$PC = \frac{N - r}{N - 1} \cdot 100\ \% \tag{1}$$

Where r is the ranking of the actually affected EA and N is the total number of EAs, here $N = 28,$ of the underlying DHN. The PC ranges from 100.0 % (first place in the ranking) to 0.0 % (last place in the ranking). Based on these results, the performance of the individual approaches may first be assessed. Then, according to the IES as shown in Figure 1, interim results are shared among the approaches. Here, the top five ranks of the EA ranking of PWD are handed over to the other approaches. The second IES used is the generation of simulated substitute measurement values by MBSE for ML. Subsequently, the leakage localization is carried out again using this additional information. Finally, for the localization results obtained from this combined, synergistic approach, the PC is computed according to Equation (1) and compared to those of the individual approaches.

3.2. Individual Results

The results obtained by the PWD approach shown in Table 1 have already been presented in another publication by Vahldiek et al. [17]. Here, the method MoFoDatEv was applied to a total of 22 events. The PC used in that publication was as well based on the ranking of the affected EA within the resulting ranking list and originally ranged from 100.0 % (first place in the ranking) to 3.6 % (last place in the ranking). For comparability of the three approaches presented, the PC for PWD was recalculated according to Equation (1). Furthermore, the events 18 to 20 and 22 were removed, as no evaluation was possible for them with the other two methods MBSE and ML. For event 17, the affected EA was not contained in the training data, so this was also excluded for the ML approach. With an average value of 74.3 % over all events, suitable leakage localization results were achieved. The approach ranked the affected EA for only one event on the last place. In contrast, for three events the affected EA was on the first place with 100.0 %. Furthermore, for eight events, the right EA is on the first three places in the ranking (PC $\geq$ 92.6 %). Since in almost half of all events the correct exclusion area is ranked on the first three places, the method is very suitable for a practical application to localize the leakage as quickly and, above all, correctly as possible.

The results obtained by only using MBSE for the single events vary significantly in terms of both placements in the EA ranking as well as LPs. For five of the 18 events investigated, the actually affected EA is placed first in the ranking. In ten cases, the damaged EA is at least still ranked among the top five places. In three cases, namely events 5, 9 and 13, MBSE does not find the actually affected EA at all, thus achieving a PC of 0.0 %. Overall, the performance of the approach varies relatively widely, from very good results to a few results without any significant value. As the MBSE approach does not analyze the transient behavior resulting from the occurrence of a leakage, the gradient of the leakage mass flow with respect to time $\Delta\dot{m}_L/\Delta t$ is most likely not of importance. But it would be reasonable to assume that the absolute leakage amount $\dot{m}_L$ has an influence on the results. However, this assumption cannot be validated in the basis of the results shown here. On the one hand, MBSE localizes the correct EA at comparatively low leakage amounts, such as for the events 6 or 8. But on the other side, the approach partially fails for very large leakage amounts, as in event 13.

For the ML approach, the whole process of randomly splitting data and fitting the model with randomly initialized weights was repeated 50 times to quantify fluctuations. The results vary from a mean PC of 20.4 % to a maximum of around 94.7 % with high standard deviations of 17.4 % in average. For 15 events, the ML approach is either outperformed by the PWD or MBSE approach. In one case, namely event 9, the PC was significantly higher than with the other approaches, but still the model is not practically applicable with such a high level of uncertainty. Furthermore, there is no clear pattern to be seen when comparing the individual results with the other approaches' individual results, i.e. a good performance in, for example, MBSE, does not necessarily result in a good performance of the ML approach.

3.3. Combined Approach Results

Since usually only one distinct pressure wave is emitted and present within a short time frame when a leakage occurs, a multiple or repeated application of PWD is not possible or does not yield any further information. In addition, the pressure wave, hence the application time for PWD, occurs chronologically before MBSE and ML can be applied at all. For these reasons, PWD cannot benefit from synergy effects from the other two approaches. On the other hand, however, the localization result of PWD is available promptly after leakage occurrence that both MBSE and ML can use this result for their own evaluations in any case. This corresponds to IES ① shown in Figure 1. Finally, the ML approach can also benefit from the results of MBSE. For MBSE, Table 1 shows the combined localization results from using the preliminary results from PWD. For ML, missing or invalid measurement values have been substituted by simulation results from MBSE and as well preliminary results from PWD have been used.

Comparing the results of MBSE in the individual and combined application case, a significantly higher PC value is achieved for almost each of the events. For 13 out of the 18 events, the ranking of the actually affected EA has either improved or at least remains the same. Moreover, in just as many cases, the affected EA is on the first three places in the ranking (PC $\geq$ 92.6 %). However, for the two events 14 and 21, the MBSE approach using synergy does not yield any viable result. In the case of the events 7 and 8, the combined localization results actually deteriorated. In order to quantitatively indicate the improvement of the localization results overall, the mean of the PC over all valid computations is referred. For MBSE, this value increases from previously approx. 73 % with 18 valid results to over 78 % with 16 valid results for the combined application. This corresponds to an improvement of the PC of almost 8 %.

Table 1. Comparison of the localization results of 18 events in a real DHN applying the individual approaches and using synergies

#	$\dot{m}_L$ [m³/h]	$\Delta\dot{m}_L/\Delta t$ [m³/h/min]	PWD (PC) individual	MBSE (PC) individual	MBSE (PC) combined	ML (ØPC ± STD) individual	ML (ØPC ± STD) combined
1	78.0	36.3	92.6 %	63.0 %	92.6 %	68.8 ± 14.7 %	95.1 ± 4.1 %
2	146.1	39.0	92.6 %	81.5 %	96.3 %	72.1 ± 18.2 %	95.9 ± 3.0 %
3	221.4	100.3	92.6 %	74.1 %	96.3 %	75.3 ± 17.0 %	96.2 ± 3.6 %
4	251.9	40.8	96.3 %	96.3 %	96.3 %	77.5 ± 14.8 %	94.9 ± 3.9 %
5	94.0	16.7	100.0 %	0.0 %	92.6 %	51.8 ± 17.0 %	89.3 ± 4.1 %
6	113.5	9.0	88.9 %	100.0 %	100.0 %	49.0 ± 15.1 %	89.6 ± 3.7 %
7	100.0	35.2	77.8 %	88.9 %	0.0 %	33.3 ± 18.8 %	-
8	50.0	25.7	96.3 %	88.9 %	0.0 %	20.4 ± 16.7 %	95.3 ± 4.3 %
9	100.0	27.0	3.7 %	0.0 %	0.0 %	25.3 ± 18.9 %	-
10	124.0	68.6	0.0 %	85.2 %	96.3 %	25.9 ± 18.8 %	-
11	158.0	56.7	88.9 %	100.0 %	100.0 %	33.6 ± 26.7 %	96.3 ± 3.8 %
12	140.0	32.9	100.0 %	100.0 %	100.0 %	94.7 ± 8.9 %	94.7 ± 2.4 %
13	231.7	155.6	100.0 %	0.0 %	96.3 %	23.7 ± 18.2 %	94.4 ± 4.0 %
14	76.9	10.6	22.2 %	70.4 %	-	66.1 ± 16.7 %	-
15	195.6	65.7	85.2 %	96.3 %	96.3 %	44.9 ± 17.8 %	89.4 ± 3.2 %
16	158.4	122.6	88.9 %	100.0 %	100.0 %	93.7 ± 11.0 %	95.4 ± 2.8 %
17	421.3	3530.0	77.8 %	100.0 %	100.0 %	-	-
21	133.0	234.5	33.3 %	74.1 %	-	74.2 ± 25.9 %	-
Ø			**74.3 %**	**73.3 %**	**78.9%**	**55.3 ± 17.4 %**	**93.9 ± 3.6 %**

To obtain statistical measures from the ML approach, the procedure of preparing data, modeling, and predicting was repeated 50 times. Combined results could only be obtained for events where the right EA was part of the preselection. In all those cases, significant improvements can be observed in mean as well as standard deviation values. The mean PC now ranges from 89.3 % to 96.3 % with an average standard deviation of 3.6 %.

4. DISCUSSION

Below, the results presented in sections 3.2. and 3.3. and in Table 1 are discussed and critically analyzed. Referring to the mean PC values, a significant improvement is achieved overall when synergies are used. For both MBSE and ML, the PC values also increase for almost every single event. Only a few cases, where either no result found or the PC deteriorated, need to investigated in more detail.

For MBSE, these are events 7 to 9 and 14 and 21, as for these the PC either decreased drastically or no evaluation was possible at all. However, the outcome for the two events 14 and 21 are not surprising on closer examination. The numerical process of state estimation did not converge and therefore did not provide any valid results. This is likely due to the fact that in these two cases the PWD approach already had a very low PC. Therefore, the actually affected EA was totally excluded by MBSE. This result is nevertheless useful, since in such a case it could at least be recognized than an incorrect prediction has been made. More of interest are events 7 to 9, as in these cases the PC is 0.0 %. For event 9, it was not possible to make any statement about the affected EA without using synergies. As expected, this does not change with the information provided by PWD, which also was unable to successfully localize the leakage. For event 8, the algorithm without using synergies localizes the correct EA with very low LP on fourth place in the EA ranking. Although a correct prediction was made by PWD, using synergies here lead to a PC of 0.0 %. A more detailed analysis of the simulation results shows that

instead of the actually affected EA 6 in line 2, the directly neighboring EA 4 is ranked first with a very high LP of over 99.0 % (cf. Figure 2). Thus, it can be said that the approach works correctly in principle, but in this case maybe not sufficiently accurate. A result not yet completely clear is found for event 7. Without synergies, a good PC of about 89.0 % is achieved. As the damaged EA is not ranked on the top five places by PWD (PC $<$ 85.2 %), MBSE excludes this EA from the localization process. Hence, there should be no result like for events 14 and 21. But in this case, the solver converged to a PC of 0.0 %. At this point, further research is necessary, possibly by means of a simulation study under comparable conditions.

For ML, the PC is highly improved by using synergies. This must be viewed critically since the number of options is strongly limited and a PC of less than 85.2 % is not possible in the evaluated cases. But from a practical perspective the applicability is improved. The average PC of 93.9 % implies that the correct EA is located between ranks 2 and 3 in most cases. Another issue arises from the fact, that results were only evaluable for preselections containing the correct EA, which was not the case for the events 7, 9, 10, 14 and 21. When applying this method online during operation, it is not known if the ranking really contains the affected EA. Therefore, this has to be assessed via probabilities or other quality measures, either from the single models or from the PWD or MBSE approach. Furthermore, the training data was not tailored to the events' network and operational states, so the individual results could be improved further this way. The same fact can explain the inconsistent results over the events and the differing performance compared to the other approaches.

5. CONCLUSION

In this paper, three different approaches for leakage localization and their application to measurement data on 18 leakage or refilling events in a real DHN are presented. Furthermore, possible synergy effects between the individual methods and their use to increase the accuracy and reliability of leakage localization are discussed. A combined approach is developed exploiting these synergies, which is as well applied to the available measurement data of the 18 events. The results obtained from the application of the individual approaches and the combined, synergistic approach are compared with each other and the achieved improvement is assessed.

With PWD, the actually affected EA is already in the top five of the EA ranking for two-third of the events investigated. In the other cases, the pressure wave resulting from the leakage was presumably not detectable distinctly enough in the available pressure measurement data. Application of MBSE leads to good results for ten out of the 18 events, where the actually affected EA is among the five highest ranked EAs. Individual results of the ML approach show a poor performance, but a preselection improved the predictions significantly, although there are less options to make wrong predictions.

When combining PWD, MBSE and ML using synergies, the correct leakage allocation rate according to the defined PC improves overall. This applies both to the mean PC values for MBSE and PWD as well as to the majority of the single events. For MBSE, the mean PC increases from approx. 73 % for the individual application to almost 79 %. For ML, in addition to an increase in the mean PC value from 55 % to over 93 %, there is also a significantly reduction in the standard deviation of the results. This indicates that the combination of the approaches based on different measurement data respectively effects of leakages is a rewarding strategy.

The results presented here are already promising, yet there is still potential for improvement both in the individual approaches as well as in the use of the synergies. To improve the PWD approach, the determination of PDTPs can be enhanced. Therefore, the used method MoFoDatEv can be extended to find the pressure drop more precisely within the data. Currently, only events with a large and clear pressure drop lead to a high PC value. In the long term, the approach should also be able to evaluate small, creeping leakages. The procedure on which the MBSE approach is based can be further improved by extending it to include the computation of the thermal state variable temperature and by more precise calibration of the underlying network model. Furthermore, there is great potential for this approach in the advancing use of smart meters to determine current consumption quantities. This is due to the very inaccurate estimation of a large number of non-measured customer consumptions. For ML, to address the problem of quantifying the probability of having the correct EA in the preselection, quality measures from all approaches could be taken as a further synergy. For explaining the variations across the events, similarity measures between different network or operational states could be computed. A further step would be to generate event-tailored training data. Further concepts include integration of information about the network topology into the training process and transforming the classification problem into a regression problem to predict distances to an EA instead of the EA itself. In general, algorithms for the recognition of false detections or localizations need to be developed. These could be based, e.g., on the analysis of the individual results of the three approaches or on their metrics such as the objective function or constraint violation values of MBSE. There is still much potential regarding the IES by passing the EA rankings. Instead of a hard decision for the top ranks, a probability-based list could be used. This way, faulty localizations through one of the approaches would not have such a strong negative impact on the overall result. In addition, IES ② is currently still unused. Here, the rankings could be exchanged iteratively between MBSE and ML until the ranking list no longer alters. All these measures have great potential to significantly improve the localization performance. But still, further research is necessary.

ACKNOWLEDGEMENT

We would like to thank the Federal Ministry of Economic Affairs and Climate Actions (BMWK) and the Project Management Jülich (PtJ) for funding this research and development project as part of the Federal Government's 6th Energy Research Program (funding code: 03ET1624 A – D). Furthermore, we would like to thank Mr. Christian Lukas (Development Office for Physical Technology) for his dedicated and competent support in network modelling in STANET as well as Mr. Friedrich Fischer-Uhrig (Engineering Office Fischer-Uhrig) for providing STANET for academic purpose.

Supported by:

Federal Ministry for Economic Affairs and Climate Action

on the basis of a decision by the German Bundestag

REFERENCES

[1] S. Zhou, Z. O'Neill, C. O'Neill. A review of leakage detection methods for district heating networks. Applied Thermal Engineering 2018; 137: 567 – 574.

[2] P. Xue, Y. Jiang, Z. Zhou, X. Chen, X. Fang, J. Liu. Machine learning-based leakage fault detection for district heating networks. Energy and Buildings 2020; 223: 110161.

[3] H. Bahlawan, N. Ferraro, A. Gambarotta, E. Losi, L. Manservigi, M. Morini, C. Saletti, P. R. Spina, M. Venturini. Detection and identification of faults in a District Heating Network. Energy Conversion and Management 2022; 266: 115837.

[4] M. Valinčius, M. Vaišnoras, A. Kaliatka. Study and demonstration of pressure wave-based leak detection in a district heating network. Structure and Infrastructure Engineering 2018; 14(2): 151 – 162.

[5] S. Zhou, C. Liu, Y. Zhao, G. Zhang, Y. Zhang. Leakage diagnosis of heating pipe-network based on BP neural network. Sustainable Energy, Grids and Networks 2022; 32: 100869.

[6] J. van Dreven, V. Boeva, S. Abghari, H. Grahn, J. Al Koussa, E. Motoasca. Intelligent Approaches to Fault Detection and Diagnosis in District Heating: Current Trends, Challenges, and Opportunities. Electronics 2023; 12: 1448.

[7] L. Ferrandez-Gamot, P. Busson, J. Blesa, S. Tornil-Sin, V. Puig, E. Duviella, A. Soldevila. Leak Localization in Water Distribution Networks using Pressure Residuals and Classifiers. IFAC-PapersOnLine 2015; 48(21): 220 – 225.

[8] A. Soldevila, J. Blesa, S. Tornil-Sin, E. Duviella, R. M. Fernandez-Canti, V. Puig. Leak localization in water distribution networks using a mixed model-based/data-driven approach. Control Engineering Practice 2016; 55: 162–173.

[9] B. Ferreira, A. Antunes, N. Carriço, D. Covas. Comparison of model-based techniques for pipe burst location in water distribution networks. IOP Conference Series: Earth and Environmental Science 2023; 1136(1): 012039.

[10] S. Sophocleous, D. Savić, Z. Kapelan. Leak Localization in a Real Water Distribution Network based on Search-Space Reduction. Journal of Water Resources Planning and Management 2019; 145(7): 04019024.

[11] Y. Guan, M. Lv, S. Dong. Pressure-driven Background Leakage Models and their Application for Leak Localization Using a Multi-population Genetic Algorithm. Water Resources Management 2023; 37: 359 – 373.

[12] M. Zadkarami, M. Shahbazian, K. Salahshoor. Pipeline leakage detection and isolation: An integrated approach of statistical and wavelet feature extraction with multi-layer perceptron neural network (MLPNN). Journal of Loss Prevention in the Process Industries 2016; 43: 479 – 487.

[13] M. Quiñones-Grueiro, J. M. Bernal-de Lázaro, C. Verde, A. Prieto-Moreno, O. Llanes-Santiago. Comparison of Classifiers for Leak Location in Water Distribution Networks. IFAC-PapersOnLine 2018; 51(24): 407 – 413.

[14] N. van der Walt, P. S. Heyns, D. N. Wilke. Pipe network leak detection: comparison between statistical and machine learning techniques. Urban Water Journal 2019; 15(10): 953 – 960.

[15] N. Mashhadi, I. Shahrour, N. Attoue, J. El Khattabi, A. Aljer. Use of Machine Learning for Leak Detection and Localization in Water Distribution Systems. Smart Cities 2021; 4: 1293 – 1315.

[16] B. Rüger, D. Pierl, M. Guber, J. Yin, M. Baur, H. Eberhard, F. Klawonn, K. Michels. Online Leakage Attribution to Exclusion Areas: Prototype Application. Energy Procedia 2018; 149: 575 – 584.

[17] K. Vahldiek, B. Rüger, F. Klawonn. Leakages in District Heating Networks – Model-Based Data Set Quality Assessment and Localization. Sensors 2022; 22(14): 5300.

[18] K. Vahldiek, Y. Yao, B. Rüger, F. Klawonn. Application and Optimization of Algorithms for Pressure Wave Evaluation Based on Measurement Data. Applied Sciences 2022; 12(9): 4192.

[19] K. Vahldiek, B. Rüger, D. Pierl, F. Klawonn. Optimal Sensor Placement for Pressure Wave Detection for Leakage Localization in a District Heating Network. Energy Reports 2021; 7(4): 499 – 507.

[20] K. Vahldiek, B. Rüger, F. Klawonn. Optimal Sensor Placement and Influence of Noise on Pressure Wave Evaluation for Leakage Localization in a District Heating Network. Sustainable Energy, Grids and Networks 2022; 30: 100672.

[21] D. Pierl, K. Vahldiek, J. Koltermann, B. Rüger, K. Michels, F. Klawonn, A. Nürnberger. Online Model- and Data-Based Leakage Localization in District Heating Networks - Impact of Random Measurement Errors. IEEE International Conference on Systems, Man, and Cybernetics (SMC) 2020, Toronto (Canada): 2331 – 2338.

[22] K. Vahldiek, J. Koltermann, D. Pierl, B. Rüger, A. Nürnberger, K. Michels, F. Klawonn. Leakage Localization in District Heating Networks Based on Real Network and Measurement Data. Energy Reports 2021; 7(4): 508 – 516.

Sino-Danish Perspectives on Green District Energy

The 18th International Symposium on DH and Cooling,
September 3–6, 2023, Beijing, China

INSPIRATIONAL LESSONS OF DENMARK'S HEAT PLANNING FOR CLEAN HEATING IN CHINA

Lipeng Zhang[a*], Noémi Schneider[b], Toke Liengaard[b], Allan Bertelsen[c]

[a] *Sino-Danish Clean and Renewable Heating Cooperation Center, Beijing, 100027, China*
[b] *Centre for Global Cooperation, Danish Energy Agency, Carsten Niebuhrs Gade 43,1577 Copenhagen V, Denmark*
[c] *Embassy of the Kingdom of Denmark in Beijing, 1 Dong Wu Jie, San Li Tun 100600, Beijing China*

[*] *lipengzhang_dh@outlook.com*

ABSTRACT

Heat planning is a systematic methodology that utilizes locally available waste and renewable energy sources, maximizes the benefits of district heating, and establishes connections with other industries and sectors, considering cost-effectiveness, socio-economic factors, and environmental benefits. Denmark has effectively employed heat planning during its green transition since the energy crisis in the 1970s. The lessons learned from Denmark's experience can serve as a reference for China to achieve its energy and climate goals. This paper aims to explore the similarities and differences between heat planning in Denmark and China, including the policy frameworks, methodologies, planning procedures, and stakeholders involved. By examining the Danish approach and its effects during the energy transition, we can draw conclusions and provide suggestions to tackle the challenges facing China's clean heating sector using scientifically guided heat planning.

Keywords: Heat planning, district heating, Denmark and China

1. INTRODUCTION

Climate change has become a global issue that cannot be ignored, and the primary driver of climate change is greenhouse gas (GHG) emissions. There are four main GHGs: carbon dioxide (CO_2), methane (CH_4), nitrous oxide (N_2O), and fluorinated gases (f-gases). According to the United Nations Climate Change 2015 report [1], human activities have significantly contributed to the increase in GHG concentrations in the atmosphere since the mid-20th century, leading to climate change. In 2020, global atmospheric CO_2 concentrations reached their highest levels in over 3 million years [2].

To address this challenge, all countries and industries must work together to reduce GHG emissions. The UN's Global Status Report for Buildings in 2020 [3] highlighted that the buildings sector accounted for approximately 35% of total final energy consumption and GHG emissions, making it the highest-emitting sector. Furthermore, domestic heating alone contributes to more than 50% of buildings' energy consumption and GHG emissions.

According to a report by the United Nations Environment Programme (UNEP) [4], district energy systems, including district heating (DH), are cost-effective and efficient solutions for reducing GHG emissions and primary energy demand. The World Bank[5] also emphasizes the importance of improving efficiency and modernizing DH with clean energy technologies to achieve energy security and air pollution control. Denmark's success in utilizing DH to overcome the energy crisis of the 1970s and becoming almost energy self-sufficient in Europe [6] demonstrates the significance of DH.

China has set ambitious targets to peak CO_2 emissions by 2030 and achieve carbon neutrality by [7]. These targets will accelerate the transition to non-fossil energy sources. However, China's annual energy consumption has consistently increased in the past two decades, from 1.56 billion tons of standard coal in 2001 to 5.24 billion tons in 2021, nearly a 2.35-fold increase[8]. Fossil fuels such as coal, oil, and natural gas still dominate China's energy profile, as shown in Figure 1. Notably, coal consumption for heating purposes increased from 85.9 million tons in 2001 to 369.3 million tons in 2020[9]. Moreover, China's heating sector has undergone rapid development, with the urban northern regions having a heating floor area of 15.2 billion m^2 by the end of 2019, of which 13.1 billion m^2 relies on DH, accounting for 85% of the total heating floor area in urban areas of northern China. Over the past decade, the DH area has grown by 10% annually. In 2019, the total CO_2 emissions from heating in northern cities and towns were approximately 550 million tons, accounting for 26% of the CO_2 emissions related to building energy consumption nationwide, with CO_2 emissions per unit area reaching 36kg CO_2/m^2 [10].

Data reveals that coal remains the primary fuel for China's DH system, indicating that the transition from fossil fuels to green energy sources in the heating sector still has a long way to go. The importance of international cooperation in the energy sector is emphasized in China's 14th Five-Year Plan[11]. I In this article, Denmark is chosen as the benchmark country due to its similar climate to northern China and the substantial utilization of DH in both countries. Denmark's success in overcoming the energy crisis of the 1970s and achieving a green and low-carbon energy transformation serves as an inspirational example for China.

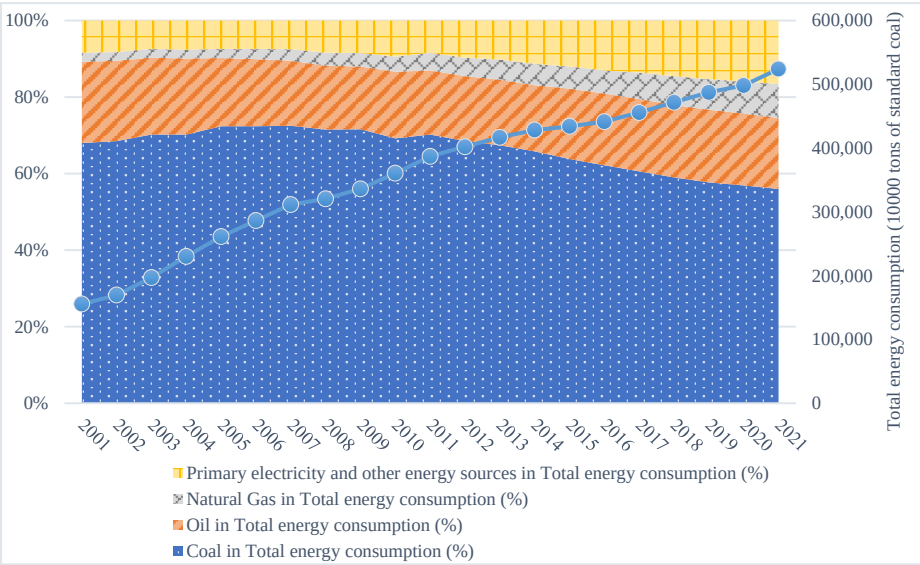

Figure 1. 2001~2021 Yearly energy consumption constitution in China

Denmark's DH system is now recognized as one of the most efficient globally, with approximately two-thirds of Danish households connected to it[12]. Motivated by the energy crisis, Denmark underwent an energy transformation from fossil fuels to green sources. Between 1990 and 2019, the country achieved a decoupling of economic growth from GHG emissions and energy consumption. Denmark's GDP increased by around 70%, while gross energy consumption and GHG emissions decreased by approximately 20% and 40%, respectively[13]. Low-carbon energy sources, such as DH from clean and sustainable sources, combined heat and power (CHP), and renewable energy systems, played a significant role in Denmark's pursuit of energy efficiency and self-sufficiency. Figure 2 illustrates Denmark's fuel consumption for DH production from 1980 to 2020. The analysis reveals that the increased adoption of CHP and DH in Denmark resulted in a 60% reduction in CO_2 emissions in the heating sector, decreasing from 25kg CO_2/m^2 of heated floor space in 1980 to 10kg CO_2/m^2 in 2020[14].

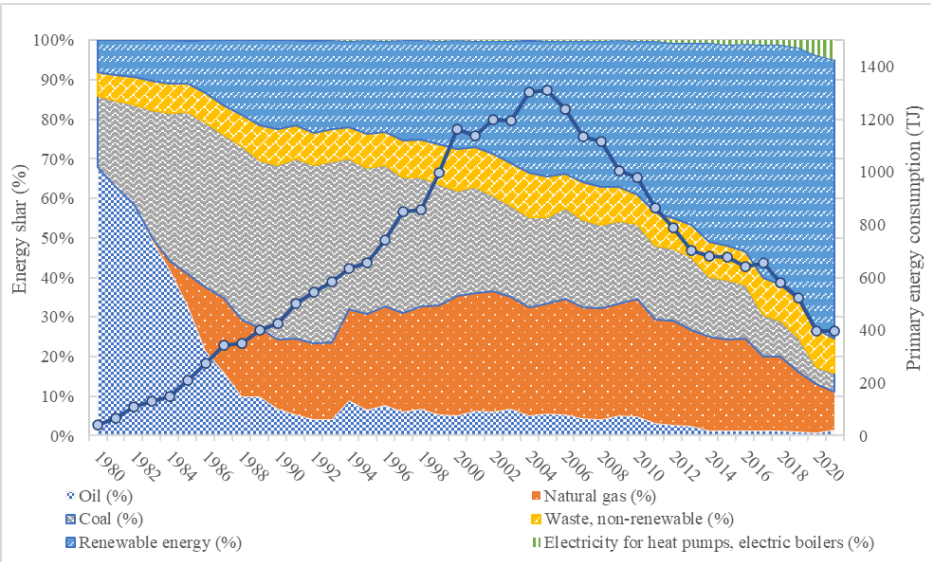

Figure 2. 1980-2021 Fuel consumption for district heating production and primary energy consumption in Denmark

During this period, heat planning emerged as a crucial component of Danish energy planning. Heat planning is a structured methodology that forms the foundation of modern DH systems. It focuses on utilizing waste heat, harnessing locally available renewable energy sources, and ensuring the cost-effectiveness of urban infrastructure operations while considering environmental preservation. Municipal heat plans, initially mandated by national law in 1979, have been instrumental in

providing a policy and regulatory framework that promotes the sustained growth of Danish DH[15].

2. METHODOLOGY

This study adopts a methodology that involves analyzing and comparing the development of heat planning in Denmark and China. By examining the policy frameworks, illustrating heat planning methodologies, comparing the procedures involved, and analyzing the roles of relevant stakeholders in both countries' heat planning processes (as shown in Figure 3), the study aims to identify differences and refine key elements from Denmark's experience that China can draw inspiration from when pursuing low-carbon DH solutions.

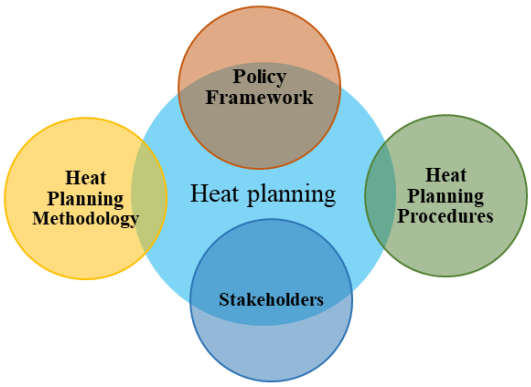

Figure 3. Key elements of heat planning

3. COMPARISON, ANALYSIS, AND DISCUSSION

Denmark's district heating planning model, which emphasizes the efficient use of locally available clean energy and fosters cost-effectiveness and environmental benefits, differs from China's traditional heat planning model. Denmark has established a green and highly efficient energy system with DH and combined heat planning as its cornerstones.

3.1 Policy Framework of Heat Planning

3.1.1 Denmark

During the 1970s, Denmark faced significant disruptions due to international oil crises. In response, the country formulated an energy policy aimed at enhancing supply security and reducing reliance on oil. In 1976, Denmark launched its first energy plan called "Energy Policy 1976," [16] seeking to decrease oil dependency by promoting the utilization of natural gas. Additionally, coal and renewable energy were seen as means to reduce reliance on oil, leading to a significant shift to coal-based energy production initially.

To fulfill the objectives outlined in the energy policy, Denmark began developing the Heat Supply Act. This act, established in 1979, aimed to promote the most socioeconomically beneficial energy usage for space heating while decreasing oil dependency through the expansion of DH and natural gas utilization. Over the years, Denmark's heat planning has evolved on the foundation of policies and governmental decisions formulated several decades ago. It has continuously been strengthened through the implementation of new legislation, addressing varied motivations such as improving energy efficiency, enhancing energy security, addressing climate impact, and fostering the development of renewable energy sources.

Presently, the Danish government has set a clear climate target: Denmark aims to achieve climate neutrality by 2045, and GHG emissions must be reduced by 70% by 2030 compared to 1990 levels [17]. Energy policy plays a crucial role in providing comprehensive legislation and guidelines for heat planning in Denmark. The Heat Supply Act, encompassing regulations concerning the structure and content of heat planning, serves as the regulatory foundation for nearly all aspects of the Danish heating sector. Effective heat planning has paved the way for a new era in public DH, which still persists today.

3.1.2 China

In China, heat planning is typically incorporated into urban master plans, which are developed based on population and building area growth projections for the next 5, 10, or 15 years. National policies serve as the general basis for heat planning and have evolved over time. Different developmental stages in the heating industry have been characterized by policies focused on slow growth, rapid development, commercialization and energy conservation, and more recently, clean and renewable heating, see Figure 4. It could say for each stage; it is the result of national policy-oriented. For instance, in 2003, "Guiding Opinions on the Pilot Work of Reforming the Urban Heating System" was released, and in 2005, "Opinions on Further Promoting the Reform of the Urban Heating System" followed. The policies were regarded as the beginning of the

heating reform, which aimed at realizing heat metering and billing according to actual consumption. Subsequently, 116 of 125 northern cities had established a metering and charging system by the end of this stage, and the renovated building area for energy savings was 22 million m^2 before 2012[18]. Currently, China's top national energy policy is to strive for carbon neutrality by 2060, which necessitates transforming the economy and energy system.

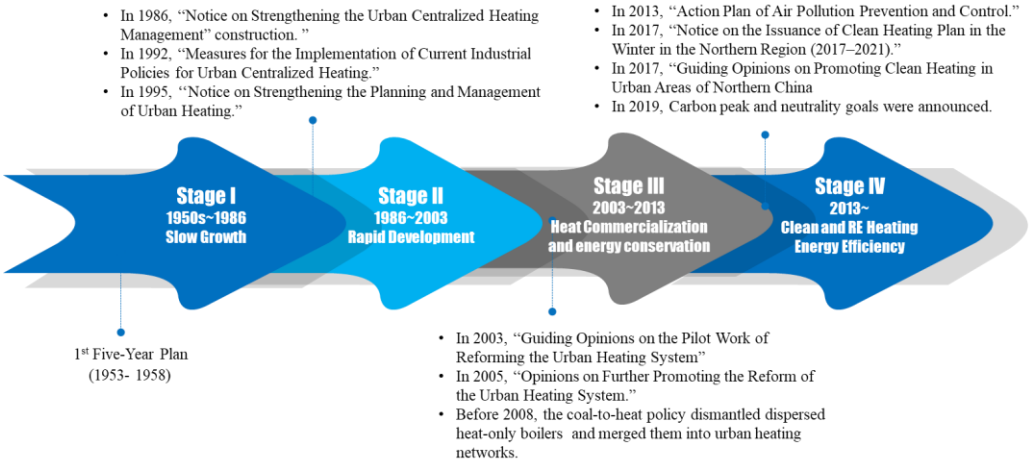

Figure 4. Four development stages and policy orientation of China' heating Industry

While China has successfully implemented management regulations for various fields, such as urban gas, road lighting, drainage, and water supply, state-level regulation for heating still requires further development. To establish a clean, efficient, safe, and modern heating system, it is essential to include upper-level laws that regulate the heating market, respond to policy and standard changes, and provide a political foundation.

3.2 Heat Planning methodology used in Denmark and China

3.2.1 Denmark

Denmark's energy model places an emphasis on DH as a foundational concept. It highlights the benefits of utilizing diverse energy sources locally while giving equal importance to improving energy system efficiency and promoting clean, low-carbon usage. Most importantly, the Danish energy model focuses on the interactions and synergies among sectors and systems rather than solely focusing on individual components and concepts. For example, the integration of the electricity market with DH has played a significant role in Denmark's success. By closely connecting these two systems, energy efficiency is maximized, and different energy sources are effectively utilized. A comprehensive energy planning approach that considers short and long-term goals is crucial. Aligning the design and impact assessments with national energy objectives ensures a coherent and strategic approach.

Moreover, Denmark employs methodologies such as Levelized Cost of Energy (LCOE), feasibility studies, and socio-economic calculations in their heat planning evaluation. The LCOE calculation is done within the DH company, and it is a useful tool for DH company to compare different investments[19]. Cost-effectiveness and socio-economic assessments are crucial in Danish heat planning. The analysis considers a wide range of costs and benefits, including taxes and externalities such as emissions costs.

Levelized Cost of Energy Calculation

In the Danish heat planning proposal, the LCOE methodology is used to determine the costs and revenues associated with a project, discounting them to their net present value equivalent to the average expected price for consumers. This aids in assessing project feasibility. The LCOE calculates how much money must be made per unit of energy to recoup the lifetime costs of the system, including capital investment, maintenance costs, fuel expenses, operational costs, and interest rates. It simplifies the analysis by combining fixed and variable costs into a single measurement. Feasibility studies in Denmark follow standard cost-benefit analysis evaluation methods, which involve comparing projected costs and benefits to determine project viability.

Feasibility Study

In Danish heat planning, feasibility studies follow the standard cost-benefit analysis evaluation method. This decision-making tool compares the projected costs and benefits of a project to determine its viability from a business perspective. The analysis involves assessing all project costs and subtracting them from the projected benefits. The results help determine the feasibility of a decision.

Danish buildings can be heated through DH or individual heating. The feasibility study method considers the operational and investment costs of individual technologies and the conversion of individual heating supplies to DH. Users can choose DH technologies and determine the proportion of individual supply to be converted.

Socio-Economic Calculation

Energy policies in the 1980s emphasized the importance of comprehensive accounting for costs and benefits in energy projects. In 1990, the Danish government issued an energy plan highlighting the role of socio-economic accounting in energy project planning [20]. Since then, assessing the cost-effectiveness of heat supply options and conducting socio-economic cost-benefit analyses have become crucial in Danish heat planning.

Through socio-economic analysis, projects that provide the most significant net benefit to society are prioritized. This analysis considers a wide range of societal and externality costs, including emissions costs. Project alternatives are evaluated over their expected technical lifetimes, typically 20 years. The analysis relies on methodologies and data provided by institutions like the Danish Energy Agency or other relevant institutions.

3.2.2 China

China's heating planning, according to standards set by the China DH Association in 2021 [21], includes various aspects such as resource mapping, heating demand prediction, heating energy sources, methods, scale of heat sources, network system layout, investment estimation, energy conservation, environmental protection analysis, and implementation measures.

While the Chinese standards mention investment estimation and environmental protection analysis, there are limited descriptions of the relevant content and methods. It is essential to have a solid foundation of reasonable data to apply cost-effectiveness or socio-economic methods effectively.

3.3 ***Heat Planning Procedures***

3.3.1 Denmark

In Denmark, heat planning follows a step-by-step approach. Local municipalities first map existing heat demand and supply methods, as well as the energy sources used. They also estimate future heat demand and supply possibilities. Regional heat supply overviews are then created based on the information provided by municipalities. In the second step, cities prepare options for future heat supply while local authorities prepare regional summaries. Finally, the DH plans are developed, identifying heat supply options and the locations for future heat supply units and networks.

In the 1990s, heat planning in Denmark shifted from national planning to a project-based approach. The timeline for heat planning projects can vary depending on local conditions and circumstances, and the usual timeline is shown in Figure 5. Initially, DH companies develop plans for new projects based on their own economic interests, such as reducing costs or ensuring a reliable supply. Once a specific project is identified, advisors make final calculations and formalize them in a project proposal. This proposal is then submitted to the municipality for approval, which is based on a socioeconomic assessment. Once approved, the project is carried out, and price regulation ensures that the DH company can cover its costs.

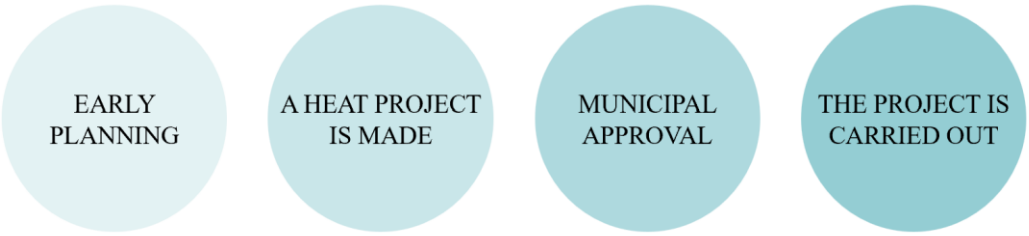

Figure 5. Usual timeline of heat planning based on the project approach

Overall, the project-based approach allows for flexibility in heat planning, taking into account local conditions and stakeholder interests. The various steps, from initial planning to implementation, involve careful evaluation, financial support, and collaboration between different parties to ensure an effective and efficient heat supply.

3.3.2 China

The general procedure and framework for China's heat planning typically involve funding, bidding, designing, evaluating, and implementation, as shown in Figure 6. The local government allocates funds from the local Finance Bureau to support the consulting fees for heat planning. After funding approval, the government organizes a bidding process, and qualified design institutes or consulting agencies participate. During the design phase, the winning bidder conducts site visits and engages with local stakeholders in accordance with relevant national, provincial, and local policies. After finalizing the heat

planning design proposal, the government entrusts a third party to evaluate it, often involving domestic professionals and experts. During the implementation stage, government bodies provide guidance, supervision, and management of heat supply and use at the provincial and city levels, with the heating company playing a primary role.

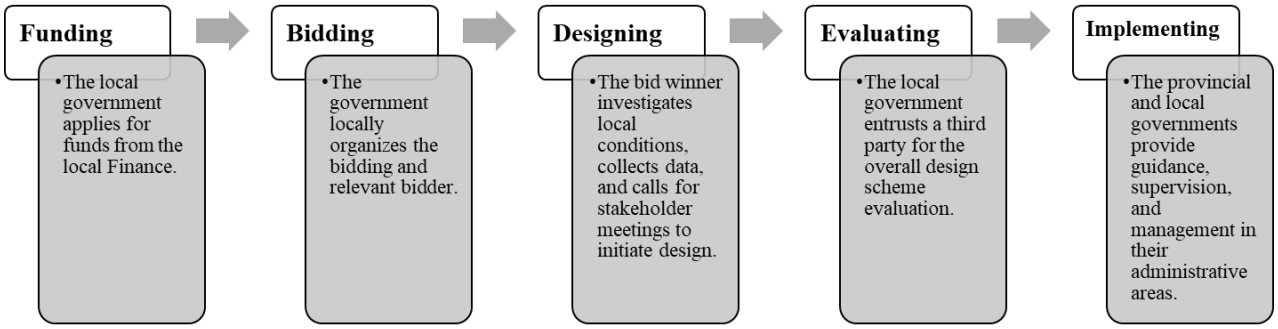

Figure 6. The heat planning procedures applied in China

3.4 Stakeholders

3.4.1 Denmark

In Denmark, the development of green and efficient DH systems involves various stakeholders, ranging from planning to operation. These stakeholders include the European Union (EU), the Danish national government, municipalities, DH companies, and individual heat consumers. The relationships among them are characterized by top-down policies and bottom-up power, as depicted in Figure 7. Over the past decades, their roles have been adjusted to optimize their powers and responsibilities.

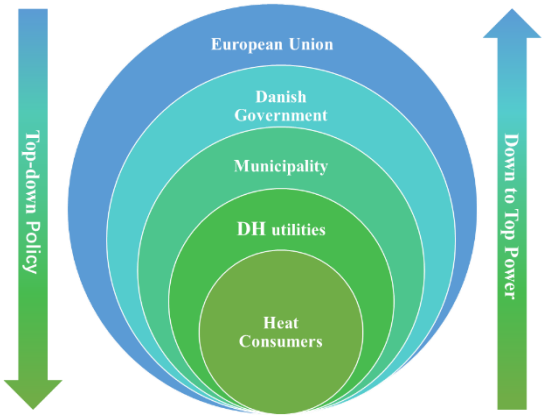

Figure 7. Stakeholders in Danish Heat Planning

European Union (EU): Denmark adheres to European energy goals and regulations as a member state of the EU.

Danish Government: The Danish Energy Agency (DEA) and the Danish Utility Regulator (DUR) are vital entities responsible for energy policy-making and regulation within the Danish government. The DEA's responsibilities span from energy production to end-user consumption. In the DH sector, the DEA aims to promote increased use of renewable energy sources and enhance overall system flexibility. The Danish Utility Regulator oversees the DH sector and ensures compliance with various aspects of Danish utility regulations, particularly pricing.

Municipalities: In Denmark, municipalities are responsible for developing and updating municipal heat plans and approving heat projects. They act as local regulators overseeing the activities of DH companies within their jurisdiction.

DH utilities: Danish DH companies typically collaborate closely with municipal governments. These companies are either municipally-owned or privately owned by the customers themselves. Rather than distributing profits to shareholders, the profits of Danish DH companies are returned to customers through reduced heat prices. These companies meticulously handle changes in fixed costs in heat prices, taking into account the interests of heat consumers while ensuring compliance with regulatory scrutiny.

Heat consumers: The needs of heat consumers play a significant role in local decision-making processes and the cost-benefit analysis of heat projects. Heat consumers have confidence in the regulation and scrutiny of prices and investments, knowing

that they will receive reliable and reasonable pricing.

Overall, the collaboration and synergy among these various stakeholders ensure the development of green and efficient DH systems in Denmark. Its success in the introduction of a business model that benefits multiple parties involved, fostering cooperation and shared benefits. The Danish government formulates policies and regulations, and the importance of the municipality was emphasized at the national level, recognizing their role in sustainable development. DH companies operate and comply with regulations, and heat consumers' interests are considered throughout the decision-making process. This integrated approach ensures a reliable and sustainable heat supply for Danish communities.

3.4.2 China

In China, the administration framework related to heating involves several critical national administrations such as the National Energy Administration (NEA), the Ministry of Housing and Urban-Rural Development (MoHURD), and the National Development and Reform Commission (NDRC). These administrations are responsible for overseeing clean energy sources, buildings, and pricing mechanisms within the heating sector, respectively. Unlike Denmark, there is no single core government department dedicated solely to the heating industry in China. Since 2013, more policies related to clean heating have been jointly released, involving multiple authorities and ministries in the administrative framework of the heating sector. Additionally, individual heat consumers in China typically pay fixed heating fees based on the heating area, while state-owned heating companies receive heating subsidies from local financial departments to compensate for financial losses incurred by adhering to the area-based charging system. Municipal authorities manage heating companies in accordance with local heating management regulations.

CONCLUSIONS

The implementation of national policies in Denmark has been supported by legislative guarantees, which have played a significant role in the transformation of DH from black to green. In China, however, there is a need for stronger support at the national level, as the current heating regulations are not as comprehensive. This calls for the introduction of national regulations in the heating field, which will help align heating management norms at all levels, clarify the focus of heating management work, and support the country's 3060 goals in the heating sector.

Adopting a holistic approach to heat planning in China is crucial to address the policy and technical challenges. This approach involves identifying local resources and heat demands, enabling decision-makers to make informed choices in transitioning to a clean heating system. Heat planning strategies should also incorporate broader energy planning and sector integration, taking into account the potential of renewable energy sources and thermal storage. In the northern regions of China, the lack of overall heat planning has resulted in an unclear understanding of locally available heat sources, hindering the practical implementation of clean or renewable energy in the heating sector. This has also led to issues such as imbalanced heat demand and supply, as well as suboptimal designs that make regional optimization challenging.

Denmark employs specific methodologies in heat planning, such as the calculation of the levelized cost of energy (LCOE), which determines the amount of money required per unit of heating to recover the lifetime costs of the system. The cost-benefit analysis evaluation method is used to assess the projected costs and benefits associated with a project decision, facilitating sound business decision-making. Moreover, socio-economic analysis ensures that all societal and externality costs are considered when evaluating heating projects. Successful implementation of these methodologies relies on robust data collected through the digitalization, automation, and intelligence of DH systems. Therefore, the data statistics and management in China's heating industry and the automation upgrade of the sector will contribute to practical heat planning implementation.

This study highlights areas for future work, including analyzing the policy framework and its support for heating regulations, conducting in-depth research on socio-economic calculation methods and cost-benefit analysis methods used in Danish heating planning, improving the database for China's heating planning, clarifying the elements to be enhanced throughout the heating planning process, and considering carbon emissions in the lifecycle of heating systems during planning. Additionally, understanding the roles and responsibilities of multiple stakeholders in China's heating reform and exploring multi-stakeholder cooperation models inspired by Danish practices can contribute to efficient, green, and safe heating development in China.

References

[1] “https://www.un.org/en/climate change,” UN and Climate Change, 2020.
[2] World Meteorological Organization (WMO), “State of the Globe Climate 2020,” 2021. Accessed: Jun. 05, 2023. [Online]. Available: https://library.wmo.int/
[3] UNEP, “2020 Global Status Report for Buildings and Construction Towards a zero-emissions, efficient and resilient Buildings and Construction sector,” 2020. [Online]. Available: www.globalabc.org.

[4] UNEP, "District Energy in Cities: Unlocking the Potential of Energy Efficiency and Renewable Energy," 2015
[5] World Bank, "Building Energy-efficient Homes for Low-carbon Cities in China," 2011. http://www.worldbank.org/
[6] Dansk Fjernvarme, "Danish district heating association." http://www.fjernvarmen.dk/
[7] S. Zhang and W. Chen, "Assessing the energy transition in China towards carbon neutrality with a probabilistic framework," Nat Commun, vol. 13, no. 1, Dec. 2022, doi: 10.1038/s41467-021-27671-0.
[8] "National Bureau of Statistics," http://www.stats.gov.cn/.
[9] China Tsinghua University Building Energy Research Center, 2021 Annual Report on China Building Energy Efficiency. Beijing: China Architecture & Building Press, 2021.
[10] China District Heating Association, "China Urban Heating Annual Report 2021," 2021.
[11] "14th Five-Year Plan of China (2021-2025)," https://www.gov.cn/, 2021.
[12] DEA, "Energistatistik," https://ens.dk/service/statistik-data-noegletal-og-kort/maanedlig-og-aarlig-energistatistik.
[13] E. and U. Danish Ministry of Climate, "Denmark's Fourth Biennial Report," 2021.
[14] European Environment Agency, "CO2 emissions per m^2 for space heating," https://www.eea.europa.eu/.
[15] Danish Energy Agency, "Regulation and planning of district heating in Denmark Contents," 2017.
[16] S. Biegaa et al., "Alternative Danish energy planning," 1990.
[17] Danish Energy Agency, "Energy in Denmark 2021," 2021. [Online]. Available: www.ens.dk
[18] B. Zhu, C. Liu, and C. Wei, "Urban residential heating policy in China: A review," Energy Build, vol. 253, p. 111547, Dec. 2021, doi: 10.1016/j.enbuild.2021.111547.
[19] Danish Energy Agency, "District Heating Assessment Tool," 2017. [Online]. Available: www.ens.dk/en
[20] J. Munksgaard and A. Larsen, "Energy Policy in Denmark and the Danish Affiliate."
[21] China District Heating Association (CDHA), Standard for heating supply planning. China, 2021.

ACKNOWLEDGEMENT

This article thanks for the support from the Sino-Danish Clean and Renewable Heating Cooperation Program. Implementing the program in China has enabled the research in this paper to be carried out. The research in this paper benefits from the expertise of other co-authors in heating planning, and be thankful for their contributions.

The 18th International Symposium on District Heating and Cooling, September 3–6, 2023, Beijing, China

CAPTURING INSIGHTS FOR DISTRICT HEATING FROM POWER SYSTEM MODELLING IN CHINA

Francesco Lovat [a*], Susana Paardekooper [a], Noémi Schneider [a], Jie Xu [a], Phil Swisher [b], Lipeng Zhang [c], Allan Bertelsen [d], Lars Bregnbaek[b]

[a] *Danish Energy Agency, Carsten Niebuhrs Gade 43, 1577, Copenhagen, Denmark*
[b] *Ea Energianalyse A/S, Gammeltorv 8, 6. Sal, 1457 Copenhagen, Denmark*
[c] *Danish Energy Agency (external consultant) 1#Guozixiang, Xicheng District, Beijing China 100052*
[d] *Embassy of the Kingdom of Denmark in Beijing, 1 Dong Wu Jie, San Li Tun 100600, Beijing China*
[d]

[*] *Corresponding author. fmla@ens.dk*

ABSTRACT

District heating in China is currently provided primarily by coal, and associated with air pollution and inefficiency in heat supply. However, there is increasing evidence that district heating has an important role to play in future energy systems. This paper investigates the potential for district heating to contribute to the decarbonization and pathway towards energy transformation. It takes the perspective of several global trends and their applications in the field of district heating as a technology, to address widespread concerns like energy security, green growth, energy efficiency and carbon reductions. It then investigates the applicability of these trends for China, and couples these insights with the energy system and power sector modelling performed in support of the China Energy Transformation Outlook.

Based on this, the paper argues that there is a strong reason to further investigate the potential of district heating to further and support the aim of a flexible, clean, and secure energy system that can actively deliver on China's 2030 and 2060 objectives. The use of district heating allows for the integration of several forms of clean and renewable sources available to China, including future types of excess heat from new technologies like electrolysis. Sector coupling between the electricity and heating sectors provides more flexibility, especially in light of thermal storage. These results show the value of combining quantitative energy system modelling with trends and developments in district heating, and highlight the potential role of district heating in achieving the development strategy for China towards 2060.

Keywords: District Heating, Sector Coupling, Electrification, Energy System Analysis, Energy Transformation

1. INTRODUCTION

With the statement from President Xi Jinping at the General Debate of the 76th Session of the United Nations General Assembly in September 2021, China confirmed that its commitment to tackle climate change under the terms of the Paris Agreement [1] will see it peak its carbon dioxide (CO_2) emissions before 2030 and achieve net-zero emissions before 2060. This calls for an acceleration of the transformation of the energy sector in China, where fossil fuels are still dominant in the national energy profile. The heating sector is one of the key elements to ensure those targets are reached. In 2019, the total CO_2 emissions of heating in northern cities and towns were about 550 million tons, accounting for 26% of the CO_2 emissions related to the energy consumption of buildings in the country [2]. District heating (DH) accounts for 85% of the total heating urban areas in Northern China, making it the world's largest DH system [2]. Furthermore, coal is still the main fuel for DH supply in China, with more than a quarter being supplied by coal-fired boilers directly, and 45% of district heating being supplied through coal-fired cogeneration plants [2].

Although DH systems in China have been well studied and there is renewed interest in research in this area, especially since the central government issued the Clean Winter Heating Plan in Northern China (2017-2021), the focus has largely been on technologies and operation of the systems. Some studies consider the role of DH in the energy system, but they remain rare. For example, previous research reviewed the potential for DH system [3] or analyzed clean heating in Northern China [4], [5] [6]. In 2015, Xiong et al. performed a quantitative study to analyze the future heat strategy for China for 2030 [7]. However, to the authors' knowledge, no study has been carried out since to support the decarbonization of the whole heating sector in China by comprehensively quantifying available heat sources and potential savings combined with an energy system analysis.

The purpose of this paper is to combine quantitative energy system modelling with qualitative analysis of the role of district heating in achieving the decarbonization targets and in addressing other concerns such as energy security and energy

efficiency. This gives a foundation to a better understanding of the challenges that district heating development in China will face in the future and of the key technologies enabling a flexible, clean and secure not only district heating system but also overall energy system that is necessary to achieve China's climate targets. It can also identify future areas of development for modelling of energy systems, informed by global trends such as increased energy system integration and sector coupling.

This paper is structured to give an insight and discussion on the results of the power sector modelling, specifically the EDO model as employed in China Energy Transformation Outlook 2022 (CETO 22) [8], on the district heating sector. The following section explains the methodology of the study and presents the models and data used to carry out the quantitative energy system modelling. Then the results are presented and discussed in Section 3, leading to a conclusion in Section 4.

2. METHODOLOGY

The methodology utilized in this study is based on an analysis of the results from quantitative energy system modelling. The analysis takes the perspective of several global trends in the energy field such as increased electrification of the energy system, sector coupling, development of efficient buildings, etc. and their applications in the field of district heating as a technology. These insights are then used to analyze how district heating can contribute to address widespread concerns like energy security, green growth, energy efficiency and carbon reductions.

By examining how the trends could apply to China using the results of the energy and power modelling, the study aims to capture insights for the modelling and development of a clean, secure and efficient district heating system in China and to figure out the role of district heating as a technology in achieving China's climate targets.

2.1. Model used

The EDO (Electricity and District heating Optimisation) model is a fundamental model of power and district heating systems built on the Balmorel model [9]. It is a partial equilibrium model which essentially finds the least-cost economical dispatch and capacity expansion solution for the represented energy system. The model is represented at the provincial level, considering the integrated coupling between district heating sector and power sector, as well as resource constrains. The model includes thermal power (including combined heat and power (CHP)), wind, solar (including concentrating solar-thermal power (CSP)), hydro, power storage, heat-only boilers, heat storages, heat pumps, etc.

2.2 Technology overview

The EDO model provides a comprehensive representation of the district heating sector, as depicted in Figure 1. It offers various technological options for each specific heating area, encompassing urban, county level, towns, townships, and even industrial district heating consumption.

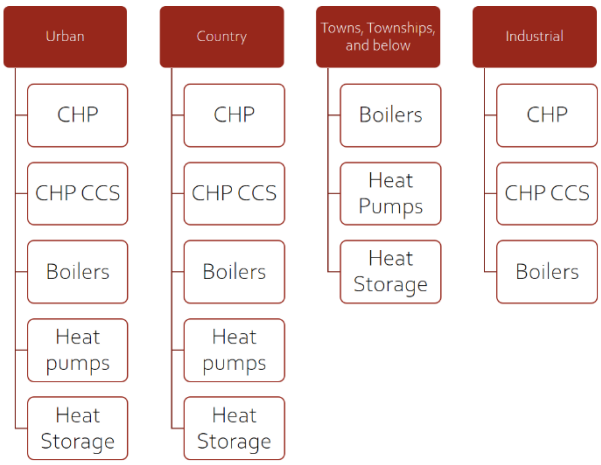

Figure 1. Representation of the heating sector in the EDO model

One notable feature of the EDO model is its flexibility in accommodating different energy sources and conversion technologies (feedstocks) for heating processes. This means that the model includes a diverse range of boiler types, such as those fired by wood, straw, coal, natural gas, or electricity. Similarly, the model incorporates CHP plants that operate with different fuel sources. In addition to boilers and CHP plants, the EDO model takes into account the utilization of heat pumps, which play a crucial role in the heating sector. These heat pumps contribute to efficient and sustainable heating solutions. Furthermore, the model adequately represents industrial heat, considering its unique characteristics and requirements.

Overall, the EDO model's comprehensive technological representation encompasses various heating areas and incorporates multiple options for different technologies, fuel sources, and heat generation methods, making it a valuable tool for analyzing and optimizing heating systems.

2.3 Data inputs

The EDO model relies on various data inputs to ensure accurate and up-to-date analysis. The primary sources of data include publicly available information from China Energy Transformation Outlook 2022 (CETO 22) [8] as well as data from China energy statistical yearbook [10], China urban,-rural and regional development statistical yearbook [11] and the China Energy Council (CEC) Statistics.

The future electricity and heat demand trajectories presented here are based on the scenario design process conducted for the CETO 22. These trajectories follow the narrative of the Carbon Neutral Scenario (CNS), which is an accelerated transition scenario aiming to achieve the "before 30-60" goal. In this study, a more stringent assumption was included to ensure that the energy system becomes carbon neutral by 2050 at the latest.

2.3.1 Base year district heating demand data

The base year district heating demand includes three parts: 1) industrial district heating demand, taken from China energy statistical yearbook 2021 [10] (table 5-2 Energy Balance of China, industry sector) , 2) district heating for space heating in buildings, taken from China energy statistical yearbook 2021 [10] (table 5-2 Energy Balance of China, table 5-2 Energy Balance of China, aggregating districting data from 'Wholesale and Retail Trades, Hotels and Catering Services', ' Residential 'and 'others'), supplemented with 3) the data from China urban-rural construction statistical yearbook 2020 [11].

2.3.2 Future district heating demand and underlying assumptions

CETO 22 examines future district heating demand, encompassing both industrial and space heating in buildings. To analyze building-related heating, important factors considered are floor area, energy intensity, and technology share.

Floor area

The future projection of residential floor area, as shown in Figure 2, is determined by factors such as population growth, urbanization rates, and per capita dwelling areas. On the other hand, the projection for public and commercial buildings involves additional factors like GDP growth, industrial structure, and the number of service industry practitioners. According to CETO 22, it is expected that the total floor area will reach 81.2 billion square meters by 2060. This includes 45.2 billion square meters for urban residential buildings, 11.3 billion square meters for rural residential buildings, and 24.7 billion square meters for commercial and public buildings.

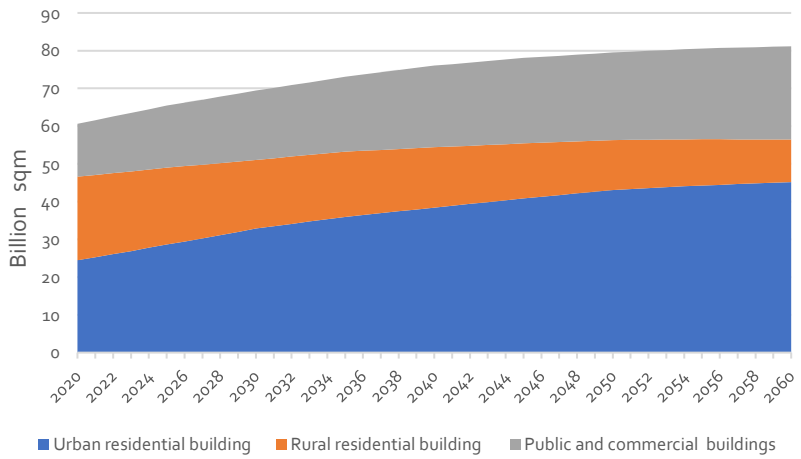

Figure 2. Future floor area

Space heating intensity

The CNS sets ambitious targets for building retrofits and energy codes detailed in Figure 3. By 2030, all existing urban residential buildings are expected to meet energy saving code 75, followed by existing public and commercial buildings by 2035. Newly-built urban residential and public/commercial buildings will adhere to the more stringent energy saving code 85. By 2040, all existing rural buildings will be retrofitted to meet energy saving code 75. Additionally, passive building adoption is projected to reach 80% for newly-built urban residential buildings and 100% for newly constructed public and commercial buildings by 2040.

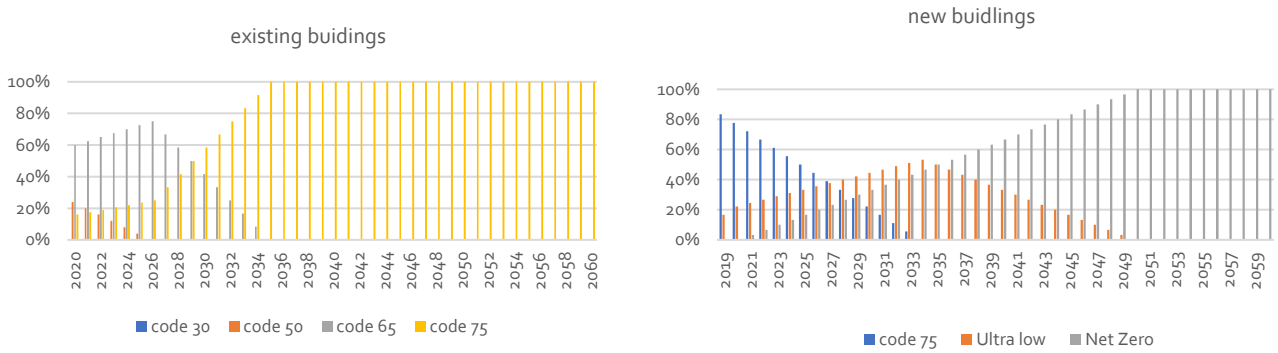

Figure 3. Future building codes in both existing and new buildings

The adoption of these measures will result in a notable decrease in heating intensity for all buildings, as shown in Figure 4. Specifically, for northern residential buildings, it is projected that the average heating intensity will decrease to 60 kWh per square meter by 2035 and further decrease to 47 kWh per square meter.

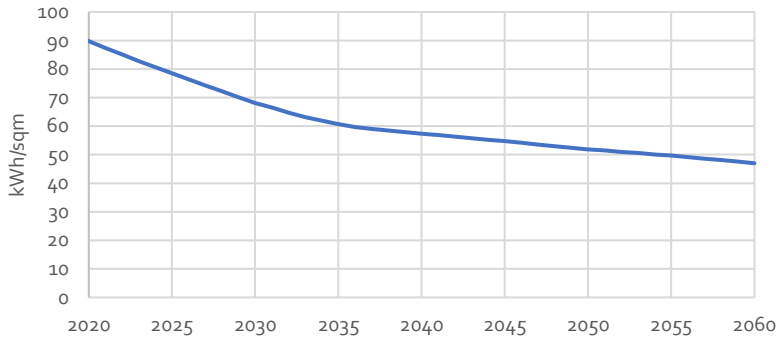

Figure 4. Average heating intensity in north residential buildings.

District heating demand

Space heating supply is a key factor in achieving energy conservation in the building sector, primarily through district heating and improved building insulation. Figure 5 shows that the total demand for district heating is projected to peak at 3010 TWh around 2050, followed by a decline to 2900 TWh by 2060. This decline can be attributed to the reduced space heating demand resulting from the implementation of more efficient buildings.

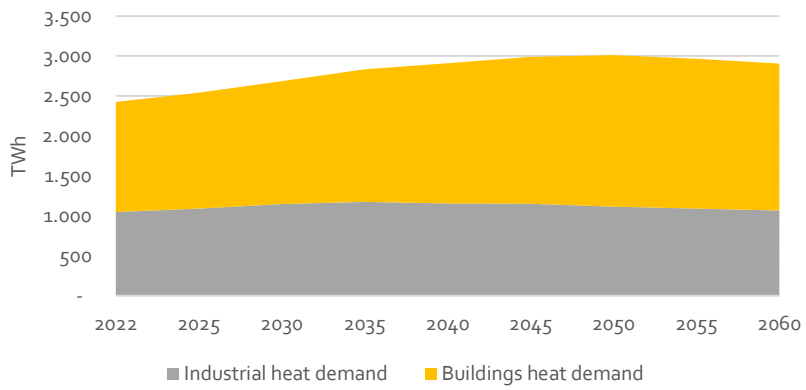

Figure 5. District heating demand projection until 2060 following the CETO 22 CNS scenario.

2.3.3 Other Relevant Data

In addition to heat demand data, other relevant information for the heating sector is sourced from various reputable sources. MoHURD, for instance, provides valuable insights into policy frameworks, regulations, and regional planning initiatives related to heating. This data plays an important role in contextualizing the analysis and ensuring alignment with national and regional energy strategies. Furthermore, the EDO model incorporates data from the CEC Statistics. This data source provides essential information on the capacity of CHP systems and boilers, allowing the model to accurately represent the existing infrastructure and its potential impact on the heating sector.

To enhance the accuracy and comprehensiveness of the model, additional data inputs are obtained from the CETO 22 report [8]. This publicly available report offers techno-economic parameters for the various technologies included in the EDO model. These parameters encompass factors such as capital costs, operational efficiencies, emissions profiles, and other relevant economic and technical characteristics. The utilization of this comprehensive dataset strengthens the model's ability to evaluate and compare different technology options effectively.

By leveraging these diverse data sources, the EDO model ensures a robust and informed analysis of the heating sector. It captures crucial aspects such as heat demand, infrastructure capacity, policy frameworks, and techno-economic parameters. Through the integration of these data inputs, the model provides valuable insights for policymakers, researchers, and stakeholders in shaping efficient and sustainable heating strategies.

3. RESULTS AND DISCUSSION

This results section shows some of the main outcomes of the power system modelling that relate to the (district) heating sector. They are used to describe in some more detail the mechanisms that can be observed in the district heating sector as within a **Carbon Neutral Scenario and a "before 30-60" scenario.**

3.1 Heat generation and production

In regards of district heating generation, model outputs per technology group are shown in Figure 6 and Figure 7. Several transitions can be observed, that are all largely driven by the carbon constraint in the model to achieve neutrality by 2050.

The first is the changing energy mix in the sector. There is a clear phase out of solid fossil fuels and fossil fuel capacity in the district heating sector, especially after the carbon peaking in 2030, which is largely replaced by large-scale heat pumps. It is relevant to note the efficiency of large scale heat pumps, since their contribution in terms of energy supply is relatively large compared to the installed capacity. Thermal energy storage also dramatically increases after 2030, to play a significant role in the heat supply mix. As soon as large-scale heat pumps and electric boilers are cheap enough to absorb the excess electricity production from variable renewable energy sources, more heat storage is needed in the system too, see Figure 6. Heat storage become crucial buffers to allow this.

Additionally, there is relatively direct replacement from heat only (fuel) boilers to electric boilers. Here it is relevant to note that while the absolute volume of heat generated in boilers increases, the relative reliance of the district heating sector on boilers as a means of heat production decreases. Furthermore, there remains capacity for heat only (fuel) boilers longer even until 2060, but this is not used for heat production. The capacity is retained largely because it has already been built and does not require further investments, and it can continue to serve as back-up. This both testifies to the speed of the transition that is required to decarbonize the district heating sector, but also that the future system can provide the reliability and security to provide heat, so the back-up is not required.

There are several reasons, why we may observe a relatively high share of electric boilers in the CNS. The first to recall is that district heating in China typically does not include domestic hot water provision. This in and of itself is an interesting characteristic for further analysis [12], but also means that there are relatively fewer hours for the district heating system to operate, so the full-load hours will be less. This then gives rise to preference of the technologies with lower investment costs, but higher marginal costs, such as electric boiler, compared to large-scale heat pump which has higher up-front investment costs, but due to its efficient conversion of electricity into heat, much lower marginal costs. The second reason for this result could be that the dynamics, which are driven by changes in the relative marginal costs of heat and electricity, are magnified since large-scale heat pumps and electric boilers together represent the majority of the installed production capacity. Since the model does not currently represent a diverse supply mix (see also discussion of possible future district heating sources to consider below), the optimization model magnifies dynamics and changes to the energy system architecture that may alter the way that boilers and heat pumps play relative roles in terms of absorbing intermittent renewable electricity and providing flexibility services to the energy system.

The second observation is an increase in heat generation in the district heating and industrial sectors, even though Section 2 outlines a decrease in residential and service sector demands. This is largely due to the application of district heating in industry, including new industries like power-to-X and direct air carbon capture processes, leading to an increasing demand, and consequently generation, from the year 2045 onwards. These types of future industries are represented in the power sector modelling in EDO, since they are expected to start to play an important role in fully decarbonized energy systems.

Because some of the processes related around this can be strongly endo- or exothermic, it can both be useful to include district heating as an option to supply them in the future, and useful to consider them as a potential source of industrial excess heat for district heating, alongside other sources of industrial excess heat, even in the future. Further exploring different types of district heating sources could also including looking at excess heat from power generation, and explore the role of cogeneration plants in more detail than has been done here. A better understanding of biomass scarcity, and the flexibility of

back-pressure and condensing modes in power plants to explore the potential for district heating to contribute to efficiency and flexibility in the energy system. This can also include the exploration of excess heat from nuclear power plants [13] [14], which has been studied specifically for the Chinese context. Finally, exploring the application of direct renewables, in the form of geothermal and solar thermal district heating, is also likely to contribute to a fuller and broader perspective on what district heating could look like in the future, and how it can support the implementation of the 2060 carbon neutrality goals.

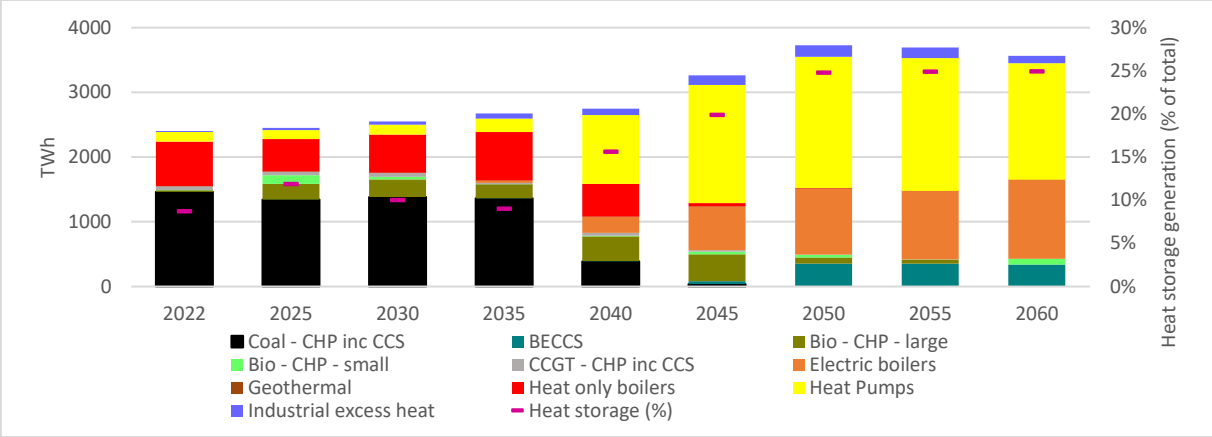

Figure 6. Heat generation in TWh by technology group up to 2060 except for heat storage generation, which is represented as its share of the total heat generation in a year in the secondary vertical axis.

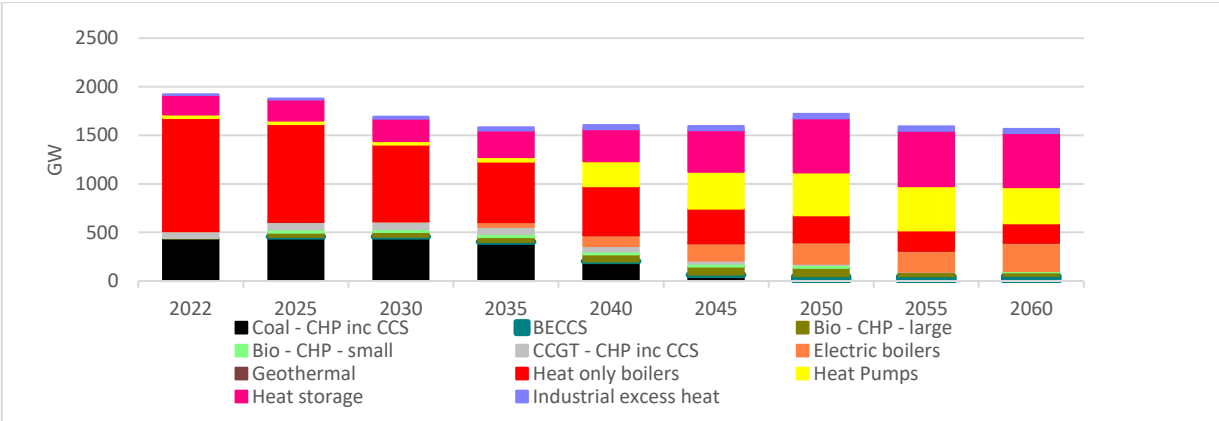

Figure 7. Installed capacity for heating technologies up to 2060.

3.2 Weekly dispatch

Figure 8 illustrates an hourly heating generation dispatch for a full week in summer and Figure 9 the hourly electricity generation from variable renewable energy sources and the consequent marginal electricity costs. It illustrates that the heating-electricity coupling allows for the utilization of excess renewable electricity during periods of high production (central hours of the day), which can be redirected to meet the heating demands of buildings and industrial processes. Abundant renewable energy available, leading to high electricity production from these sources. However, as renewable energy generation is inherently intermittent and subject to fluctuations, there will be periods of surplus electricity that may exceed the immediate demand, leading to lower marginal electricity costs, as shown in Figure 9.

The model approach is to employ electric heat pumps and electric boilers to fill up short-term heat storages which would in their turn release the stored heat during night hours. Ultimately, this process would convert the surplus electricity into heat and support further electrification. Moreover, Figure 8 shows that the coupling is enhanced with the integration of the short-term thermal energy storage systems present in EDO. These storage systems can store excess heat generated from renewable electricity, allowing for its utilization at a later time when renewable energy production is insufficient. This is represented by the pink line in the graph, having negative values to represent the charging of the storage and positive values when discharging. In the model only short term thermal storage is represented including insulated tanks.

During a week with high penetration of variable renewables, the behavior of the energy system would involve a dynamic interplay between electricity generation, consumption, and the heating sector. With the availability of excess renewable electricity, the flexible sources mentioned earlier, including energy storage systems, vehicle-to-grid (V2G) technologies, load shifting, and electric vehicle (EV) charging, play a vital role in balancing the electricity grid. These flexible sources can absorb surplus electricity during periods of high production and release it back to the grid when demand exceeds renewable

energy supply. Furthermore, the increased penetration of variable renewables would likely lead to a higher reliance on demand response mechanisms. Demand response involves adjusting electricity consumption patterns in response to fluctuations in supply or electricity prices. For example, during periods of high renewable energy generation, electricity prices may be lower as shown in Figure 9, incentivizing consumers to shift their electricity consumption to these times. This load shifting behavior helps to align electricity demand with the variable renewable energy supply, thereby reducing the need for fossil fuel-based power plants to meet peak demand.

In summary, with a high penetration of variable renewable sources, the coupling of electricity and heating generation becomes crucial for optimizing the operation of the energy system. By utilizing excess renewable electricity for heating purposes through technologies like heat pumps and thermal energy storage, the variability of renewable production can be effectively managed. Additionally, the integration of flexible sources and demand response mechanisms allows for better balancing of the electricity grid, ensuring a reliable and sustainable energy supply.

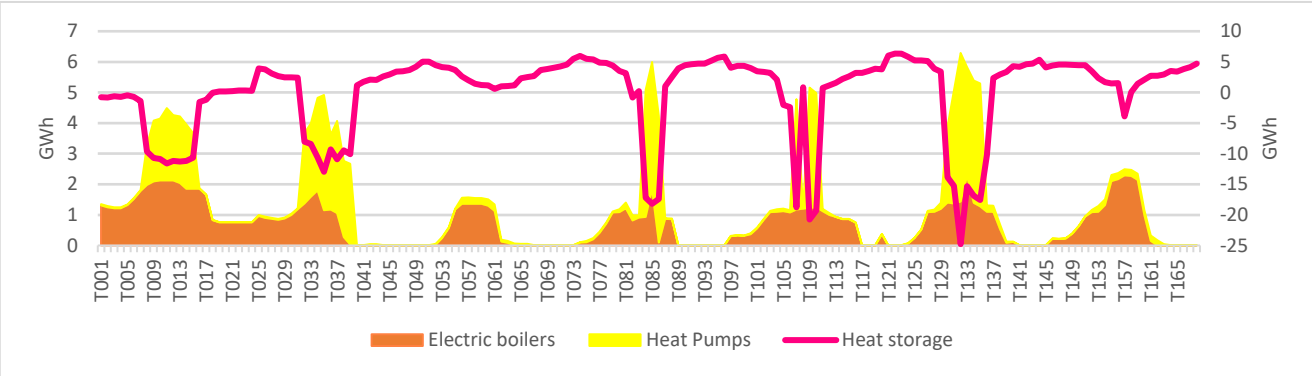

Figure 8. Hourly heat dispatch for selected technologies during a summer week for the model year 2030. Electric boilers and heat pumps are primary vertical axis. Heat storage values correspond to the secondary vertical axis.

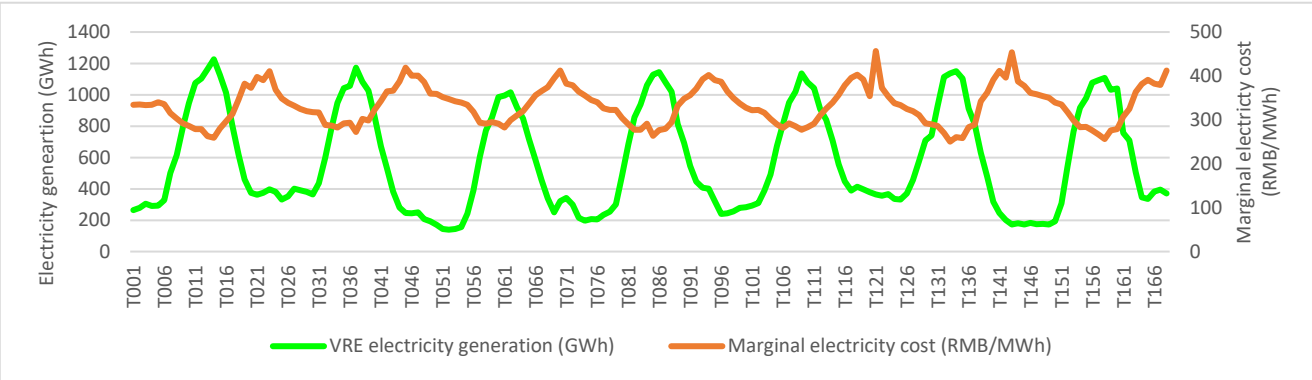

Figure 9. Electricity generation from variable renewable energy sources (wind, solar) and marginal electricity cost in RMB/MWh for a summer week of the model year 2030.

4. CONCLUSION

Transforming China's energy system to achieve carbon neutrality by 2060 is not possible without transforming the heating system. Heating is a key sector that requires attention in the decarbonization pathways, both in the demand and supply side. DH is a part of the solution, if it phases out fossil fuels for more diverse energy sources and shift away from heat only production to sector coupling and better connection with power and industry sectors. Transforming the heating sector can support the further transformation of the power sector and energy system through increased efficiency, flexibility and diversification.

These transitions are characterized by several trends. The first is increasing sector integration between the power and thermal sectors, through electrification. This is clearly well-represented in the combination of power and heat sector modelling. This trend is observed very clearly in the case for the large-scale heat pumps, which have relatively high investment costs, but can efficiently convert electricity to heat, and electric boilers, which have lower investment costs and can absorb large amounts of (otherwise excess) electricity. As shown, this represents a highly flexible link with the electricity sector, since it both allows for the efficient use of electricity to create heat, when electricity is scarce, and the (cheap) absorption of electricity when it is especially abundant. This if even further supported by the use of thermal storage.

The second trend is the seeking of more integration of different sources. The EDO model has strong capacities to model the DH sector, but the modelling for CETO 22 has not put analytical focus on the inclusion of industrial excess heat, solar

thermal, or geothermal energy. These technologies are expected to a strong point of leverage for increasing the renewable share of heating, and being able to access renewable and energy efficient sources that would otherwise be wasted [15], [16]. In doing so they are expected to support the role of district heating more broadly. Also for China, there is emerging evidence that these have the potential to be relevant resources to support the transformation of the heating (and broader energy) sector [14], [17], [18]. Strengthening the data sources and analytical capabilities of the scenario development to reflect this trend on including more sources, could give good insight to how the district heating sector could further support the integration of efficient and renewable sources to provide clean and secure heating and deep decarbonization.

Exploring these trends is only possible by combining power sector modelling with quantitative energy system modelling of the district heating system. This paper gives a perspective on better understanding and modelling the role that district heating development in China can play in the future and how it can enable a flexible, clean and secure not only district heating system but also overall energy system that is necessary to achieve China's climate targets.

ACKNOWLEDGEMENT

The research presented in this paper is supported by the Danish Energy Partnership Program and the Sino-Danish Strategic Sector Cooperation for Clean Heating in China. The responsibility for the contents lies solely with the authors, and should not be attributed to the affiliated organizations.

REFERENCES

[1] United Nations, Paris Agreement, 2015. [Online]. Available: https://unfccc.int/sites/default/files/english_paris_agreement.pdf.
[2] China District Heating Association, China Urban Heating Annual Report 2021, 2021.
[3] L. Zhang, Y. Li, H. Zhang, X. Xu, Z. Yang og W. Xu, A review of the potential of district heating system in Northern China, *Applied Thermal Engineering,* vol. 188, 2021.
[4] Z. Zhang, Y. Zhou, N. Zhao, H. Li, B. Tohniyaz, P. Mperejekumana, Q. Hong, R. Wu, G. Li, M. Sultan, A. M. I. Zayan, J. Cao, R. Ahmad og R. Dong, Clean heating during winter season in Northern China: A review, *Renewable and Sustainable Energy Reviews,* vol. 149, 2021.
[5] C. Su, H. Madani og B. Palm, Heating solutions for residential buildings in China: Current status and future outlook, *Energy Conversion and Management,* vol. 177, 2018.
[6] Y. Zhang, W. Zheng, H. Fang og J. Xia, Clean heating in Northern China: Regional investigations and roadmap studies for urban area towards 2050, *Journal of Cleaner Production,* vol. 334, 2022.
[7] W. Xiong, Y. Wang, B. V. Mathiesen, H. Lund og X. Zhang, Heat roadmap China: New heat strategy to reduce energy consumption towards 2030, *Energy,* vol. 81, 2015.
[8] China Energy Transformation Program, China Energy Transformation Outlook 2022, 2022. [Online]. Available: https://www.cet.energy/2022/06/28/ceto_2022/.
[9] Balmorel Energy System Model, The Balmorel Open Source Project, [Online]. Available: http://www.balmorel.com/.
[10] National Bureau of Statistics of China, China Energy Statistical Yearbook, China Statistics Press, Beijing, 2021.
[11] National Bureau of Staistics of China, China urban, rural and regional development statistical yearbook, China Statistics Press, Beijing, 2020.
[12] L. Zhang, O. Gudmundsson, J. E. Thorsen, H. Li og S. Svendsen, Optimization of China's Centralized Domestic Hot Water system by Applying Danish Elements, *Energy Procedia,* vol. 61, 2014.
[13] Y. Li, W. Pan, J. Xia og Y. Jiang, Combined heat and water system for long-distance heat transportation, *Energy,* vol. 172, 2019.
[14] J. Chen, W. Zheng, Y. Kong, X. Yang, Z. Liu og J. Xia, Case study on combined heat and water system for nuclear district heating in Jiaodong Peninsula, *Energy,* vol. 218, 2021.
[15] H. Lund, S. Werner, R. Wiltshire, S. Svendsen, J. E. Thorsen, F. Hvelplund og B. V. Mathiesen, 4th Generation District Heating (4GDH): Integrating smart thermal grids into future sustainable energy systems, *Energy,* vol. 68, 2014.
[16] S. Paardekooper, H. Lund, J. Zinck Thellufsen, N. Bertelsen og B. V. Mathiesen, Heat Roadmap Europe: strategic heating transition typology as a basis for policy recommendations, *Energy Efficiency,* vol. 15, 2022.
[17] J. Huang, J. Fan og S. Furbo, Feasibility study on solar district heating in China, *Renewable and Sustainable Energy Reviews,* vol. 108, 2019.
[18] F. Sun, B. Hao, L. Fu, H. Wu, Y. Xie og H. Wu, New medium-low temperature hydrothermal geothermal district heating system based on distributed electric compression heat pumps and a centralized absorption heat transformer, *Energy,* . 232, 2021.

Renewable energy in district heating systems in China: Status and perspectives

Meng Yuan[a*], Brian Vad Mathiesen[a], Noémi Schneider[b], Jianjun Xia[c], Wen Zheng[c], Lipeng Zhang[d]

[a] *Department of Planning, Aalborg University, Rendsburggade 14, 9000 Aalborg, Denmark*
[b] *Centre for Global Cooperation, Danish Energy Agency, Carsten Niebuhrs Gade 43, 1577 Copenhagen V, Denmark*
[c] *Building Energy Research Center, School of Architecture, Tsinghua University, Beijing, 100084, China*
[d] *Danish Energy Agency (External consultant), 1# Guozixiang, Xicheng District, Beijing, 100052, China*

[*] *Corresponding author. mengy@plan.aau.dk*

Abstract

In the fight against climate change, China's aim is to ensure that the CO_2 emissions peak before 2030 and to reach carbon neutrality by 2060. The heating sector is one of the key elements to ensure those targets are reached. Today around 95% of heating is based on coal, natural gas and oil. With energy efficiency and renewable energy changes using district heating and smart energy systems, this transition can be more cost efficient. Currently, district heating has covered approx.85% of the total heating areas in Northern China, however a deeper understanding is required to unlock the full potential of this infrastructure. In this paper we illustrate that a combination of energy refurbishment of buildings, energy efficiency using waste heat, and renewable energy sources from geothermal, bioenergy and solar thermal, can decarbonize the buildings using district heating in China. By using lower temperature 4th generation district heating, thermal energy storage and large-scale heat pumps, such systems can help integrating more renewable energy. In international and Chinese scientific literature there is a lack of research and knowledge within smart energy systems, low temperature district heating and unconventional waste heat sources. Although the sources and main infrastructures needed in the form of district heating pipe network and electricity grids exist, a deeper understanding is needed in response to the challenges regarding the geographical separation between renewable sources and demanding area as well as the potential for deeper renovation of buildings and further expansion of district heating. Such knowledge is required to support the early signs of policies changing towards stronger focuses on energy efficiency and renewable energy.

Keywords: District Heating; Renewable Energy; Waste heat; 4th generation district heating; Smart Energy Systems; China